RIKEN Accelerator Progress Report

2020

Vol. 54

国立研究開発法人理化学研究所　仁科加速器科学研究センター
RIKEN Nishina Center for Accelerator-Based Science

RIKEN Accelerator Progress Report 2020

Vol. **54**

国立研究開発法人理化学研究所　仁科加速器科学研究センター
RIKEN Nishina Center for Accelerator-Based Science
Wako, Saitama, 351-0198 JAPAN

RIKEN Accelerator Progress Report 2020 Vol. 54

This is an unabridged version of the 54th volume of RIKEN Accelerator Progress Report (hereinafter referred to as APR), the official annual report of the Nishina Center for Accelerator-Based Science.

A PDF version of APR can be downloaded from our website.
http://www.nishina.riken.jp/researcher/APR/index_e.html

Published by
RIKEN Nishina Center for Accelerator-Based Science
2-1 Hirosawa, Wako-shi, Saitama 351-0198 JAPAN

Director of RIKEN Nishina Center for Acclerator-Based Science
Hiroyoshi Sakurai

Contact
Progress@ribf.riken.jp

RIKEN Nishina Center for Accelerator-Based Science, September 2021

PREFACE

The RIKEN Accelerator Progress Report is the annual report of all the research activities conducted at the RIKEN Nishina Center for Accelerator-Based Science (RNC). This volume, No. 54, covers the activities conducted during the Japanese fiscal year of 2020 (i.e., April 2020 to March 2021).

Last December, the news of the sad demise of Prof. Dr. Akito Arima, who passed away on December 6, 2020, became widespread worldwide. As many people know, he was a distinguished physicist of the nuclear structure theory. As one of the top administrators of universities and institutes, he contributed toward the promotion of academic activities in the field of science and technology; he was also a politician of the House of Councilors and ministers of the government. He was the President of RIKEN from 1993 to 1998; during this period, he launched three major research activities at the current RNC: realizing the RI Beam Factory (RIBF) project, and establishing the RAL branch office for muon sciences and the RIKEN BNL Research Center (RBRC) for high-energy nuclear physics. Following the commencement of its operation in 2007, the RIBF has become one of the best facilities worldwide for low-energy nuclear physics. I was incredibly happy to present him with the achievements of the RIBF at the conference in Shanghai in 2018, as a celebration of his 88^{th} birthday. Furthermore, he also encouraged international relationships with Asian countries, especially China and Vietnam, and significantly improved research collaboration. At the RNC Monthly Meeting held on December 9, 2020, all the RNC members offered a silent prayer in view of his considerable achievements and contributions. As a person, he was known for his firm philosophy and humanity; he loved nature, physics, and the youth. At this occasion, I would like to offer my deepest condolences and also express my sincere respect for his guidance across a wide range of fields.

In 2020, the world was affected by the COVID-19 pandemic. Consequently, given that the coronavirus is carried and spread by people, people's activities have been severely restricted. Nevertheless, personal relationships remained intact owing to advances in the Internet. As a result, many discoveries pertaining to human communication through various online/virtual activities have been reported. For instance, all the PAC meetings in FY2020 were organized remotely. Furthermore, certain symposia and workshops were conducted in a hybrid style combining in-person and online communications.

Onsite activities, where people and things/facilities interact, form the essence of technological development and experimental research. It is, therefore, considerably important to implement measures for preventing the spread of the coronavirus. At the RIBF, we were able to avoid a divide between people and things/facilities, while sustaining the research activities. Local and domestic staff members realized achievements in terms of developing facilities and conducting experiments. One such achievement is the upgrade of the RILAC (SRILAC) and the complete installation of GARIS-III; this represents the completion of the preparation for moving forward with novel research. Furthermore, we succeeded in increasing the ^{70}Zn and ^{238}U beam intensities at the SRC, thus realizing a high-intensity beam for the HiCARI campaign using "tracking" germanium detectors and the mass measurement of many unknown nuclei during the MR-TOF experiment performed in parallel.

However, onsite research activities were still stagnant, given the restrictions on people traveling across borders and overseas. This resulted in a divide between people and things/facilities at the overseas research facilities of the RHIC and RAL and the joint international research at the RIBF.

Seventeen press releases were issued in FY2020, and selected achievements of 2020 are compiled in the "Highlights of the Year" section of this volume. These indicate the growing multi-disciplinary activities at the RNC for science, technology, and innovation. It should be noted that these achievements were made not only by in-

house researchers and engineers at the RNC but also by collaborating users at the RIBF, RBRC, and RAL. The paper titled "Surface localization of the dineutron in ^{11}Li," which was published in Physical Review Letters, is a result of the first spectroscopy with fully completed kinematics measurements conducted at SAMURAI in order to demonstrate the dineutron component in ^{11}Li. With regard to heavy-ion beam breading, the paper titled "Improvement of rotifer as the new food item in larviculture" had a significant impact on the society, and the results were featured as "Godzilla the rotifer" in the Economist magazine issued January 23, 2021.

Awards were also presented to the colleagues of the RNC. Takahiro Nishi was presented with the 17$^{\text{th}}$ Annual Meeting Award of the Particle Accelerator Society of Japan, and Takashi Ichihara was presented with the 2020 JPCERT/CC Certificate of Gratitude, JPCERT Coordination Center. Furthermore, the Nishina Memorial Prize was awarded to Kazuma Nakazawa, a visiting scientist at the Strangeness Nuclear Physics Laboratory.

With regard to the organization of the RNC, Hiroyuki Ichida and Masanori Kidera were appointed as the Team Leaders of the Plant Genome Evolution Research Team and the Infrastructure Management Team, respectively, as of October 2020.

The coronavirus crisis is expected to continue even after 2021. Nevertheless, we are extremely grateful to be blessed with an environment that allows us to continue with our research. Hence, it is vital that we acknowledge the mission of RIKEN and aggressively accept new challenges in research and development activities.

Hiroyoshi Sakurai
Director
RIKEN Nishina Center for Accelerator-Based Science

C O N T E N T S

Ⅱ. RESEARCH ACTIVITIES I (Nuclear, Particle and Astro-Physics)

1. Nuclear Physics

2. Nuclear Physics (Theory)

3. Nuclear Data

4. Hadron Physics

5. Hadron Physics (Theory)

6. Particle Physics

7. Astrophysics and Astro-Glaciology

8. Accelerator

9. Instrumentation

Ⅲ. RESEARCH ACTIVITIES II (Material Science and Biology)

1. Atomic and Solid State Physics (Ion)

2. Atomic and Solid State Physics (Muon)

3. Radiochemistry and Nuclear Chemistry

4. Radiation Chemistry and Biology

Ⅳ. OPERATION RECORDS

Ⅴ. EVENTS

Ⅵ. ORGANIZATION AND ACTIVITIES OF RIKEN NISHINA CENTER (Activities, Members, Publications & Presentations)

ACCELERATOR PROGRESS REPORT

FEATURE ARTICLE

SRILAC is Go!

Photo : Superconducting acceleration cavity for SRILAC

First Beam from SRILAC

RILAC upgrade project—Background and overview

The synthesis and naming of the 113th element, nihonium, is one of RIKEN's most noteworthy achievements; further, it has had a social impact in that the new element from Japan was added to the periodic table of elements.[1–3] This element was produced by the RIKEN heavy-ion linac (RILAC),[4] which has been in operation since 1980 as an injector to the RIKEN ring cyclotron (RRC) and for stand-alone applications such as those in atomic physics. In 1996, RILAC was upgraded to increase the beam intensity in RRC,[5–7] and in 2001, a booster linac[8] was installed as part of the RI Beam Factory (RIBF) project[9] under financial support from CNS, the University of Tokyo. This final step allowed nuclear physics experiments to be conducted in the RILAC facility.

Following the success of nihonium, research collaborations led by RIKEN scientists have set the next project of synthesizing new elements of atomic numbers greater than 118. To this end, metal ion beams such as vanadium and chromium need to be accelerated. However, the production cross section is expected to drop to less than a quarter of that for producing nihonium, and therefore, beam intensities need to be increased. In addition, it was estimated that the acceleration energy will need to be increased. Therefore, we need to increase the acceleration voltage of RILAC and beam intensity to initiate the project of synthesizing the new element.

Large accelerator facilities have contributed to society in the recent year in addition to promoting basic science such as research on super heavy element (SHE). At RIBF, several efforts have been invested in producing and distributing radioisotopes for research. One of the most popular isotopes is ^{211}At, and its production using AVF cyclotrons is being actively pursued for future medical applications.[10] ^{211}At has a short half-life of approximately 7 h, and a high-intensity beam of particles is essential for mass production. However, the technology for the mass production of ^{211}At has not been established. Therefore, the establishment of a technology for the mass production of useful isotopes has been added to the objectives of the RILAC upgrade plan.

The RILAC upgrade project (Fig. 1), which aims to synthesize new elements and develop technology for the mass production of useful radioisotopes, was approved with a supplementary budget in FY2016. Indeed, this enhancement plan will lead to a considerably higher intensity of the beam to the RRC, especially the metal ion beam, compared to that before.

The target performance expected in this upgrade program is to accelerate ions with $M/q = 6$ to $E = 6.5$ MeV/nucleon at more than 2.5 particle μA. To achieve this goal, we first built a new ion source. The structure of the ion source is almost identical to the

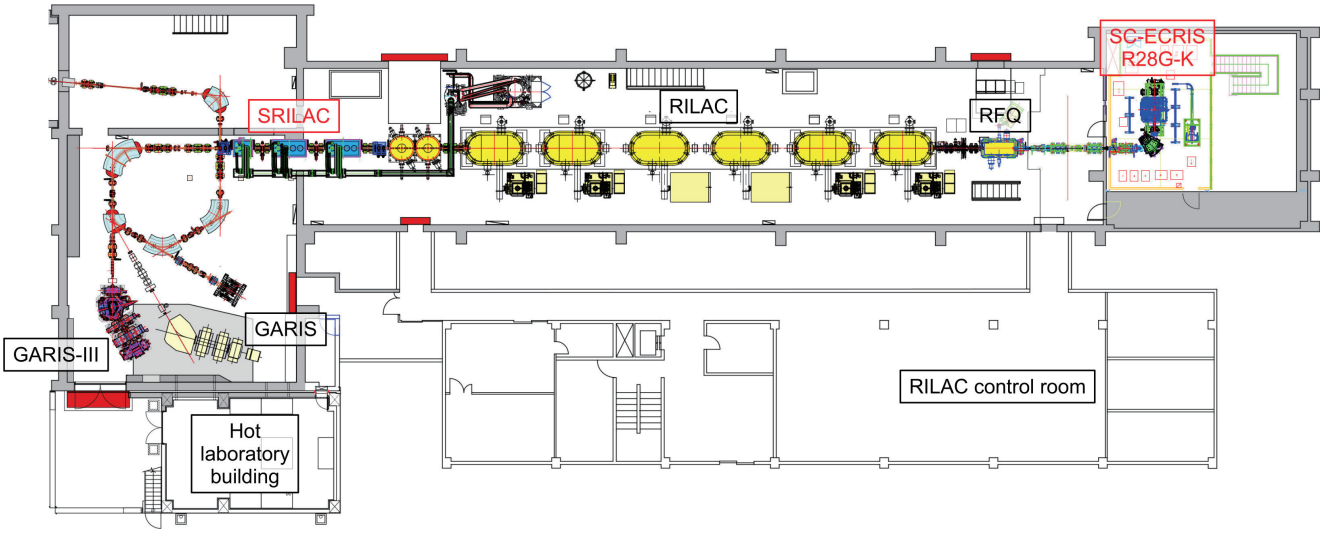

Fig. 1. Overview of RILAC upgrade project. 18-GHz ECRIS was replaced by R28G-K, and a downstream part of RILAC was replaced by SRILAC.

28-GHz superconducting electron cyclotron resonance ion source (SC-ECRIS) that has been operational since 2010.[11] There is a risk of damage to SC cavities in the downstream caused by the high-intensity beams. Therefore, we decided to limit the emittance in the low energy beam transport (LEBT) section up to the radio frequency quadrupole (RFQ) by measuring the beam emittance effectively.

Second, we replaced the last four normal conducting cavities in the RILAC booster with ten SC cavities to increase acceleration energy. Quarter-wavelength resonators (QWRs) were used as the SC cavities. A frequency of 73.0 MHz, which is four times the fundamental frequency of the RIBF, was selected for the SC cavities. This frequency is selected considering its future application as an RIBF injector. For the SC-QWR, we developed a 75.5 MHz QWR that cooperates with KEK under the ImPACT program since FY2014.[12] This experience has been of great help in the upgrade project.

In addition to the ion source, SC cavities, and refrigerator, test facilities of the cavities and a new hot laboratory building for processing radioisotopes were constructed. Further, a gas-filled recoil ion separator (GARIS) -II was moved from the RILAC facility to the E6 room in the Nishina Memorial Building to start the SHE experiments as soon as possible.[13] Meanwhile, the RRC resonator was modified to solve the problem of insufficient voltage at the RRC,[14] which had been a bottleneck in increasing beam intensity. This modification greatly contributed to the large increase in the uranium beam intensity for the BigRIPS experiments.

The construction of the ion source completed in March 2018 and the installation of the SC cavity in March 2019; this was followed by the construction of the control system of the SC cavities and the commissioning of the refrigerator in September 2019. The first beam was delivered on January 28, 2020 and the facility inspection was conducted on March 30, 2020, which marked the completion of the construction plan on schedule and within budget. This project could not have been accomplished without the help of the related manufacturers, KEK for the collaborative research, administrative staff for the many orders, and the management of the Nishina Center. We thank everyone who supported this project.

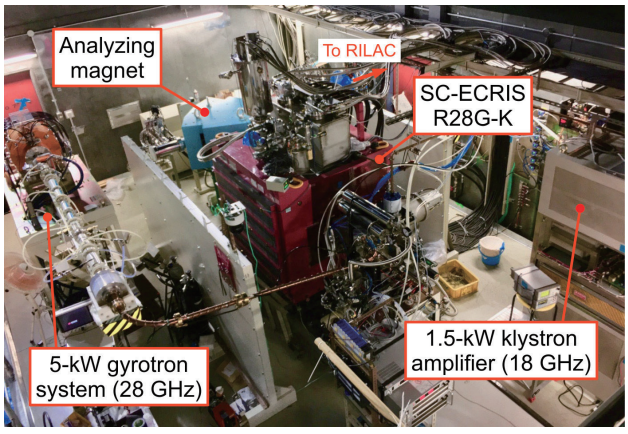

Fig. 2. Photograph of R28G-K and microwave generators (18-GHz klystron amplifier and 28-GHz gyrotron system). Extracted ion beams are analyzed by the dipole magnet and transported to the accelerator cavities of RILAC.

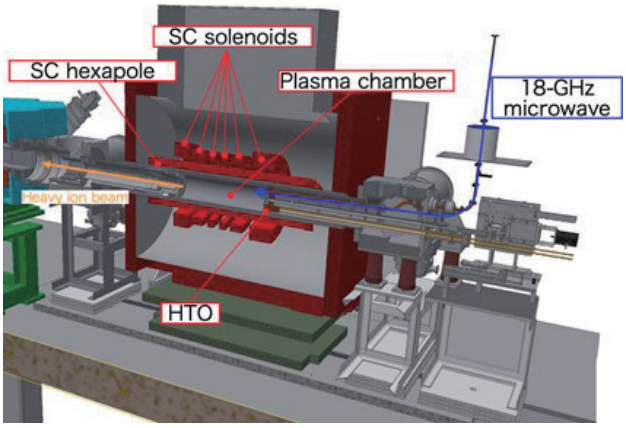

Fig. 3. Schematic cross section of the R28G-K. The large volume plasma chamber is surrounded by six SC solenoidal and one SC hexapole magnets. Both the 18- and 28-GHz microwaves are injected from the right side of the plasma chamber. The HTO is mounted on the injection side of the plasma chamber.

28-GHz Superconducting ECR Ion Source for RILAC

We constructed a 28-GHz SC-ECRIS as an essential part of the RILAC upgrade that began in FY2016. An ECRIS confines a hot electron plasma in which electrons are heated by microwaves through the ECR in a "magnetic field well." That is, a "magnetic mirror field" created by a combination of solenoidal and hexapole magnets known as the minimum-B configuration.[15] Multiple charged heavy ions are created by countless collisions of ions with sufficiently high-energy electrons in plasma. In the next projects at RILAC such as the search for new SHE with atomic number $Z > 118$ and RI production, it is necessary to provide unprecedented high-intensity ion beams. This means that it is necessary to confine the electron plasma, which has a higher density and a higher temperature than the plasma generated in the ECRIS used in RILAC, in a stable manner. Therefore, as shown in Fig. 2, new SC-ECRIS named RIKEN 28-GHz SC-ECRIS "KURENAI" (R28G-K) equipped with fully SC magnets and a high-power microwave generator system was launched in 2018.

R28G-K is equipped with six SC solenoidal magnets and a SC hexapole magnet as shown in Fig. 3. The arrangement of the SC magnets was set by the Ion source team of RIKEN Nishina center[11,16] based on previous research.[17–19] The SC coils are fabricated from Nb-Ti alloy and immersed in liquid He (more than 300 L) maintained in a high-power cryostat system combined with two 10-K GM (RDK-408S, SHI ltd.) and one 4-K GM (RDK-408D2, SHI ltd.) cryocoolers. Further, a GM-JT cryocooler (4 W at 4 K, SHI ltd.) is used to remove the excess heat induced by the large amounts of highly energetic X-ray radiation from the plasma. The maximum magnetic field of microwave injection side (B_{inj}), beam extraction side (B_{ext}), and radial magnetic field at the plasma chamber surface (B_{r}) are 3.8, 2.4, and 2.1 T, respectively. Otherwise, the bottom of the "field well" B_{min} changes from 0.5 T to 1.0 T, which makes the microwaves with both frequencies of 18 GHz and 28 GHz available to induce ECR with suitable mirror ratios such as $B_{\mathrm{inj}}/B_{\mathrm{min}} \sim 4$, $B_{\mathrm{ext}}/B_{\mathrm{min}} \sim 2$–3, and $B_{\mathrm{r}}/B_{\mathrm{min}} \sim 2$–3. Further, the shape of the mirror field around the B_{min} area can be changed arbitrarily by using the six solenoidal magnets. In other words, the field gradient and size of the ECR region can be changed to study the effects on the ECR plasma to optimize the beam intensity with a higher charge state. Since the SC magnets can generate a strong and large mirror field, the plasma chamber is a large-capacity cylinder with an inner diameter of 150 mm and a length of 575 mm. A total of 10 L/min or more of cooling water flows through the chamber wall. The large volume of the plasma chamber increases not only the volume of plasma but also the confinement time of the ions in the plasma to achieve a higher charge state.

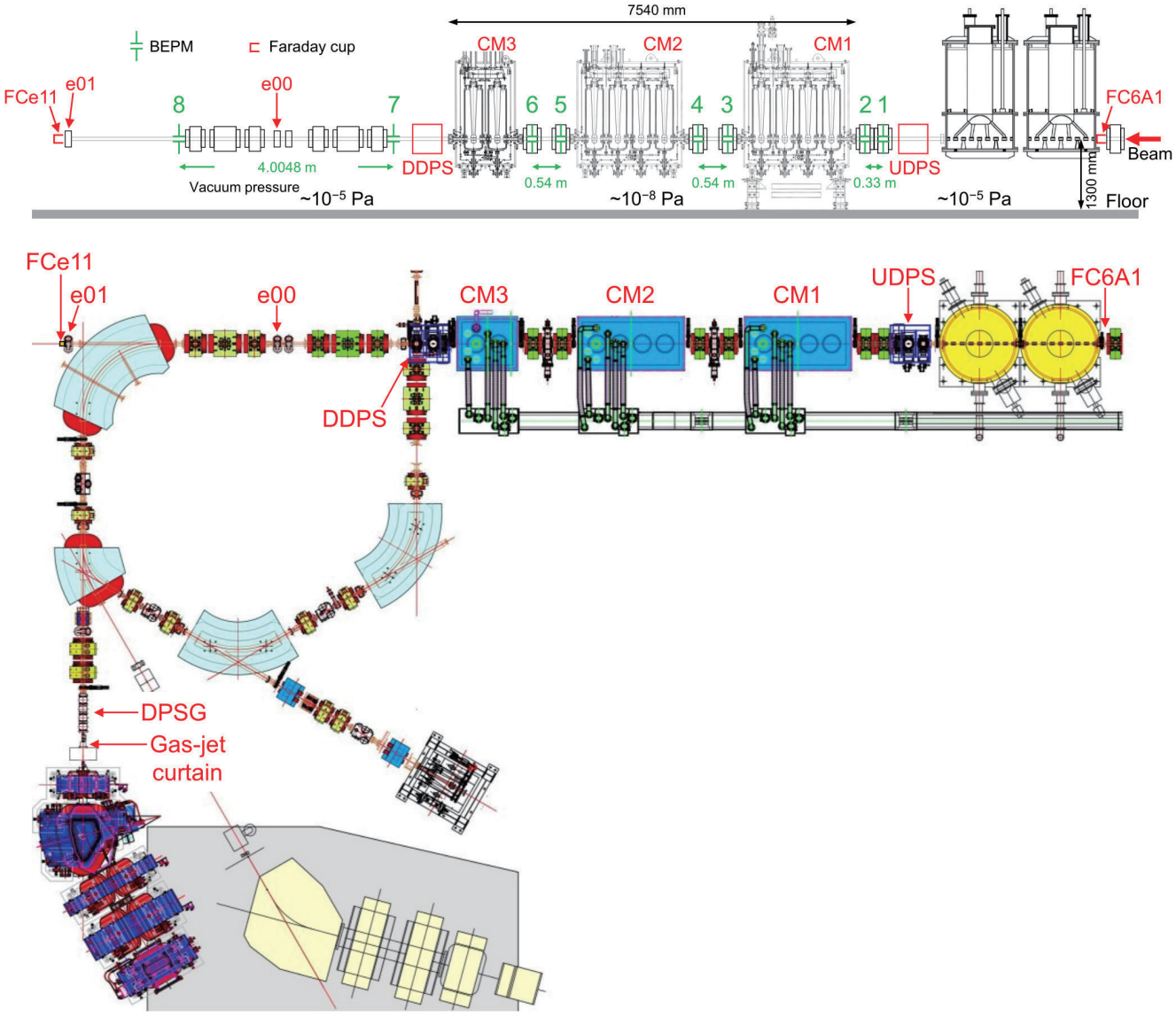

Fig. 4. Side and top views of the layout of SRILAC. Apparatuses described in the text are labeled.

The high-power microwave system contains a 1.5-kW klystron amplifier and 5-kW gyrotron for microwaves with frequencies of 18 GHz and 28 GHz, respectively. The high-power microwaves heat the electron in the plasma to remove the electrons bound deep inside the atoms or ions.

Recently, we have been developing a method to evaporate a solid material with a high melting point such as vanadium or calcium oxide using the high temperature oven (HTO).[20] The tungsten crucible of the HTO is heated to 2,000 K by the Joule heat caused by the high DC current of 700 A. For supplying the vanadium beam to search for the new SHE, the experiment lasted for about a month; therefore, we modified R28G-K so that two ovens could be used as described in the progress report this year.

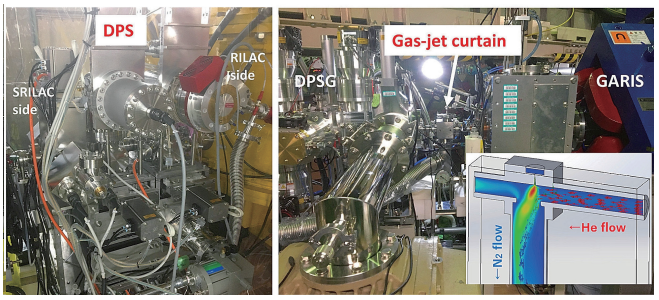

Fig. 5. Photographs of DPS (Left) and gas-jet curtain (Right).

Overview of SRILAC

The superconducting-RILAC (SRILAC) comprises three cryomodules (CM1, CM2, and CM3, see "SRILAC cryomodule" for detail), with room-temperature medium energy beam transport (MEBT) between them as shown in Fig. 4. The CMs contain neither SC magnets nor cold diagnostic devices. For the beam transport line connecting the CMs, the so-called MEBT, a newly designed beam energy position monitor (BEPM) is employed instead of traditional wire scanners and Faraday cups to avoid the generation of particulates that cause the degradation of the cavity performance (See "Beam energy position monitoring system for SRILAC" for detail). Further, to prevent the contamination of the SC parts where the vacuum pressure level is 1×10^{-8} Pa, it is important to have an isolation system between the existing room-temperature part where the vacuum pressure level is several 10^{-5} Pa and the SRILAC (See "Compact particle-removal differential-pumping system and N_2 gas-jet curtain for SRILAC" for detail).

Compact particle-removal differential-pumping system and N_2 gas-jet curtain for SRILAC

A compact non-evaporable getter-based differential pumping system (DPS) with electrostatic particle suppressors[21] has been developed to mitigate the large difference in the vacuum and clean conditions between the SRILAC and existing old RILAC with beamlines built almost four decades ago. The three-stage DPS was designed to achieve a pressure reduction from the existing beamline vacuum (10^{-6}–10^{-5} Pa) to an ultra-high vacuum of less than 10^{-8} Pa in SC cavities within a very limited length of only 75 cm, which ensures a beam aperture greater than 40 mm. All components (chambers, pumps, valves, vacuum gauges, etc.) were cleaned and assembled in an ISO class-1 clean room. The installation of the DPSs (UDPS and DDPS, See Figs. 4 and 5) was completed in December 2019. In operations during the past year, we confirmed that the DPSs achieved the desired pressure reductions in a stable manner without serious problems such as field emission problems.

During operations with GARIS-III for SHE research, He leakages to the SRILAC became an issue although a four-stage large DPS upstream of the GARIS (DPSG) was used for the windowless accumulation of He gas up to ∼70 Pa. The pressure of DDPS is increased to $\sim 10^{-7}$ Pa with the gas-filled GARIS-III when we use the narrow orifices of ϕ15 mm in the DPSG, which makes it difficult to transport high-intensity heavy-ion beams.

We introduced a N_2 gas-jet curtain downstream of DPSG (Figs. 4 and 5). The gas-jet curtain method is a new method introduced in the DPS of the He gas stripper.[22] This method suppresses the leakage of He gas by hitting a N_2-gas jet perpendicular to the He gas flow, and it converts the leaked gas into N_2 gas, which can be evacuated effectively with the DPS.

The gas-jet curtain system has a beam aperture with the diameter of ϕ25 mm. The nozzle is a two-dimensional Laval nozzle designed to generate an N_2-gas jet with a Mach number of 3.5 by optimizing with CFD calculations (Fig. 5).

In the tests with the GARIS team, we confirmed that there was no serious backflow of N_2 gas to the GARIS-III when the gas-jet curtain was under our operating conditions using a quadrupole mass analyzer. The effect of charge exchanges and energy losses of the injected beams by N_2 gas jet were confirmed to be negligible.

The installation of the gas-jet curtain was finished in September 2020. The leakage of He gas was significantly reduced with the N_2 gas-jet curtain and the pressure of the DDPS was $\sim 10^{-8}$ Pa even with larger orifices greater than ϕ25 mm in DPSG, which reduced the difficulties with high-intensity beam transport to the GARIS-III.

Table 1. Design parameters of SC-QWRs for SRILAC. The surface resistance is conservatively assumed to be 22.4 nΩ in the calculation.

Item	Value
Operating temperature	4.5 K
Frequency at 4.5 K	73.0 MHz
Duty	100%
E_{inj}	3.6 MeV/nucleon
E_{out}	6.5 MeV/nucleon
Maximum gap voltage	2.4 MV
Cavity type	QWR (TEM)
No. of SC cavities	10
Synchronous phase	$-25°$
β_{opt}	0.078
TTF	0.9
Aperture	ϕ40 mm
G	22.4 Ω
R_{sh}/Q_0	579 Ω
Target Q_0	1.0×10^9
Q_{ext}	$(1.0\text{–}4.5) \times 10^6$
P_0	8 W
E_{acc}	6.8 MV/m
V_{acc} at $E_{\mathrm{acc}} = 6.8$ MV/m, $\beta = 0.078$	2.16 MV
$E_{\mathrm{peak}}/E_{\mathrm{acc}}$	6.2
$B_{\mathrm{peak}}/E_{\mathrm{acc}}$	9.6 mT/(MV/m)
Amplifier output	7.5 kW
Beam current	∼100 electric μA

SRILAC cryomodule

The SRILAC comprises three CMs that contain a total of ten SC cavities.[23,24] CM1 and CM2 each contain four SC cavities, and CM3 contains two SC cavities (Fig. 4). The SC cavity of SRILAC is based on a coaxial QWR made of pure niobium. The resonant frequency is 73.0 MHz and the cavity is operated at 4.5 K cooled by liquid helium. The SC-QWR is fabricated using 3.5 mm and 4 mm pure niobium plates pressed together to make the top plate, stem, outer conductor, and bottom plate, and these are then assembled by electron beam welding. This is the first actual QWR made of pure niobium in Japan. Each QWR is designed to provide an acceleration voltage of 2.4 MV or higher at 8 W per unit. The design parameters of the cavity are summarized in Table 1.

Cross-sectional views of the QWR and CM are shown in Fig. 6. A pure titanium jacket is attached outside the cavity to store liquid helium. Permalloy is inserted into the space between the cavity and titanium jacket for magnetic shielding. The resonant frequency shifts because of external disturbances such as fluctuations in the liquid helium pressure. The tuner slightly pushes and deforms the cavity's beam port, which changes its capacitance and tunes its frequency to compensate for the slow shift. However, the frequency adjustment range of this tuner is 14 kHz towards lowering the resonant frequency, and therefore, the frequency variation is reduced by fine tuning the stem of each cavity and the total length of the outer conductor during assembly.[25]

The inner surface of the cavity was chemically polished to 110 μm after assembly, annealed at 750°C, and then chemically polished to 20 μm to maximize the performance of the SC cavity. The cavity was then high-pressure washed with ultrapure water from each port and vacuum sealed in an ISO class-1 clean room. After vacuum sealing, it was baked at 120°C, and performance tests were conducted on the single unit. As shown in Ref. 24), all ten actual cavities fabricated exceeded the target Q_0 value of 1×10^9 in the test. The cavity must be operated in compliance with the High

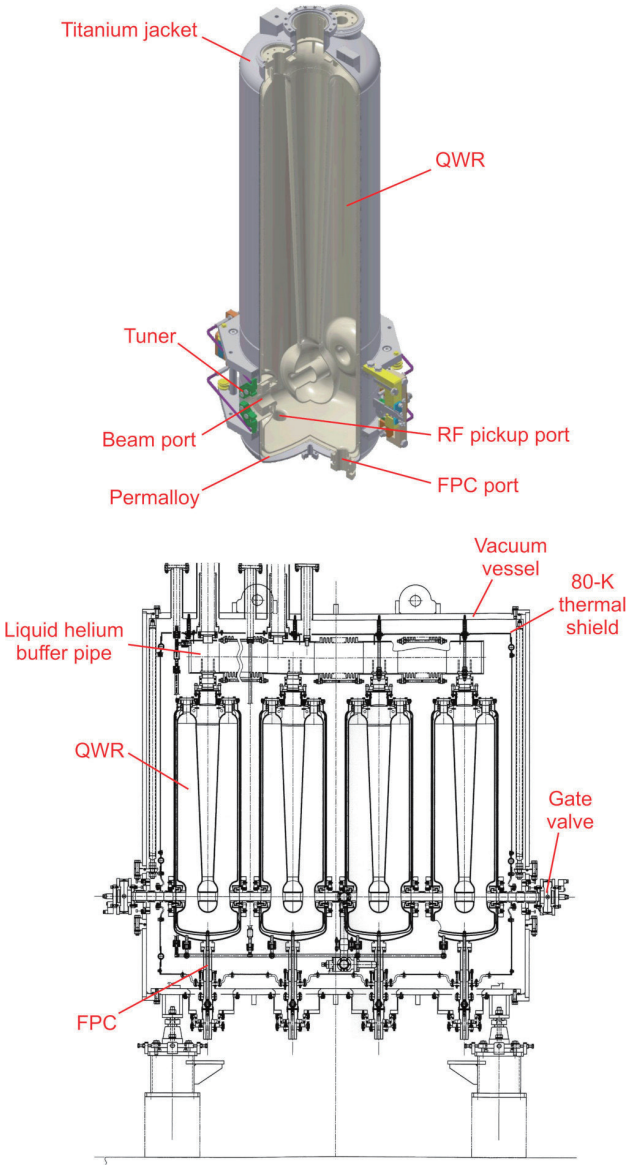

Fig. 6. Cross-sectional views of SC-QWR (top) and cryomodule that contains four SC-QWRs (bottom).

Pressure Gas Safety Act in Japan, and therefore, it was fabricated after preliminary evaluation and then commissioned for inspection.

A fundamental power coupler (FPC) and RF pickup are mounted on the bottom plate of the cavity. The FPC is a coaxial capacitively coupled type, vacuum sealed with a single ceramic window in the normal temperature section; it can handle the RF input power of 5 kW or more.[26] The FPC inner conductor is fabricated from oxygen-free copper, and the outer conductor from stainless steel with a copper plating on the inner surface. The thickness of the copper plating was determined by balancing heat penetration with the heat transfer to the low temperature side and heat generation caused by RF power.

The vacuum vessel of the CM is made of steel and divided into the top plate, top box, middle box, bottom box, and bottom plate. Electroless nickel plating was applied to prevent corrosion. The cavity is built with four glass-epoxy pillars on the bottom plate. One support is fixed in place, while the other three slide horizontally to allow for repositioning during cooling. Liquid helium buffer pipe is installed at the top of the cavity to control the liquid level for stable cooling. An aluminum plate is used for the 80-K thermal shield, which is cooled by liquid nitrogen flowing in series through three CMs. Cernox sensors are used as thermo sensors for the cavity, Pt-Co for the 4.5 K region, and Pt100 for the 80 K region. The heat load of the CM is estimated to be about 18 W for heat intrusion and about 32 W for RF loss in the cavity during steady state operation in a module containing four cavities. However, a heat load of 100 W per CM was set as the design standard value for operation during performance degradation.

The first step in assembling the CM is to move the bottom plate with the cavity and the middle box into the clean room and to fasten the cavity and beam pipe to seal their vacuum so that no dust can enter the cavity. Then, helium piping, liquid nitrogen piping, tuners, thermal shields, super insulators, etc. were installed, and the upper and lower boxes were covered after moving to the installation site (Fig. 7).

Fig. 7. Photographs of cryomodule. (Left) After assembling and sealing the cavities and beam pipes in the clean room. (Right) After alignment at the installation site.

Table 2. Requirements from cryomodules for SRILAC.

Item	Value
No. of SC cavities	10
No. of cryomodules	$2+1$
Temperature of SC cavities	4.5 K
Temperature of thermal shield	80 K
Weight of cold mass	1475 kg
Heat load to 4.5 K cold mass	
Dynamic	120 W
Static	30 W
Heat load to thermal shield	120 W
Cooling power	$\geq$500 W
Inventory	313 L
Design pressure of the He vessel	0.125 MPa(A)
Allowable pressure fluctuation	4.0×10^{-4} MPa

A total of ten sets of digital low-level RF (LLRF) circuits and 7.5 kW transistor amplifiers were introduced to excite the cavities. A digital low-level circuit is equipped with an FPGA that stabilizes the RF voltage and phase by PID control and obtains the tuning phase from the directional coupler signal. Internal parameters of the digital low-level circuit can be set remotely from a programmable logic controller (PLC). Transistor amplifiers can operate with full output reflection, and they are equipped with five 1.5 kW output units with built-in isolators to continue operation in the event of unit failure. A control system using the PLC is provided for each CM to control these RF equipment.

Cryogenic system for SRILAC

The requirements from CMs for the SRILAC are summarized in Table 2. SC cavities work at 4.5 K. The thermal shield is designed to be cooled down by liquid nitrogen, and the total weight of the cold mass is 1.5 ton. Heat load to 4.5 K and 80 K are 150 and 120 W, respectively. The inventory of liquid helium is 313 L and the allowable fluctuation of pressure in the SC cavities is as small as 4 hPa because a change in pressure can change the resonance frequency of the SC cavities. The design pressure of the vessel is as low as 0.125 MPa(A) because the cavity has bellow, which cannot sustain higher pressure.

The cryogenic system was designed to have a cooling power of 500 W at 4.5 K. This system comprises a helium compressor, refrigerator, and buffer tank. The cooling power is four times that of the heat load because we like to have a big margin to ensure contin-

uous operation even if the condition of the surface on the cavities is not so good that the cavities need considerably more cooling power. Figure 8 shows a cooling diagram of the cryogenic system. The compressed helium gas is introduced to a cold box and liquefied. Liquid helium is then supplied to the three headers in the CMs from the top. The evaporated cold helium gas is returned to the cold box and the helium compressor via heat exchangers. During pre-cooling, helium gas is supplied from the bottom to cool down the cavities efficiently. Green lines are used for liquid nitrogen supplied for shield cooling. A backup compressor for the superconducting ring cyclotron (SRC) was used for this cryogenic system to reduce the total cost. The required pressure fluctuation of 4 hPa looks tight; however, from experience, it is possible by control return pressure by the return valve with a precise pressure gauge. The Air Liquide company supplied devices for the cryogenic system other than the compressor. Radiation-resistant valve positioners were adopted because we install the refrigerator in the accelerator room.

The stand-alone operation of the helium refrigerator demonstrated a cooling capacity of 700 W at 4.5 K before the first cooling of the SRILAC. Figure 9 shows the cooling down curves. The cold mass was successfully cooled down to liquid helium temperature in four days although pre-cooling was halted because of the trouble in the thermal insulation vacuum system for half a day. The heat load was estimated from the heater in the helium refrigerator to be 150 W for $2+1$ CMs. The pressure fluctuation was hit within 4 hPa.

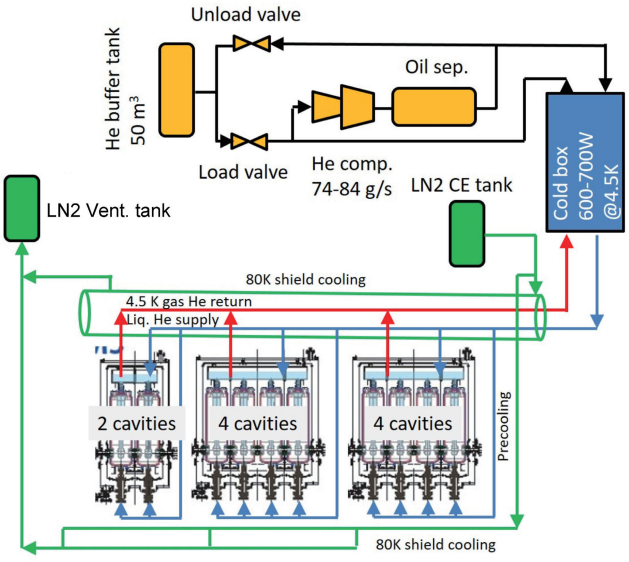

Fig. 8. Cooling diagram for SRILAC.

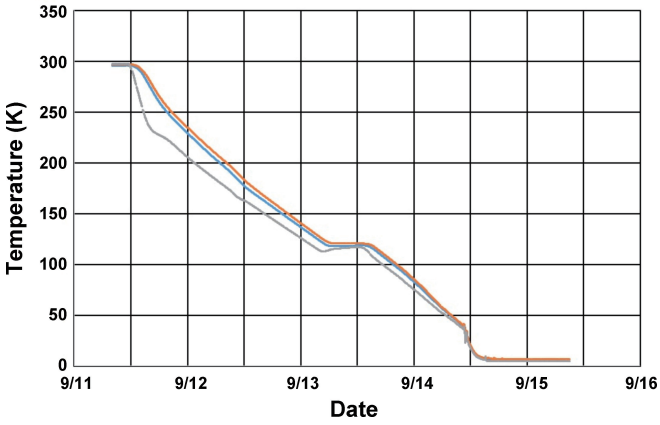

Fig. 9. Temperature of cold masses in the three CMs in the first cooling down.

Beam energy position monitoring system for SRILAC

It is crucial to monitor a beam to accelerate it stable manner. When the SRILAC beam is accelerated, beam loss must be reduced to under 1 W/m. Furthermore, destructive monitors generate outgassing; if they are used, it becomes difficult to maintain the Q-value and surface resistance of the SC cavities over a long period of time. Therefore, we developed a new BEPM system that can simultaneously measure the beam position and energy by measuring the time-of-flight (TOF) to continuously monitor the beam nondestructively. A great advantage of this system is that it can handle a time-chopped beam by synchronizing the measurement system with the beam-chopping signal. At the start of commissioning, the beam was chopped to several percent duty cycle to protect the SC cavity from beam loss. Although the beam intensity was 20 electric nA, we measured the beam position and energy to accuracies of ± 0.1 mm and several 10^{-4} precision, respectively.

Depending on the installation location, three types of BEPMs (Types I, II, and III) were designed and 11 BEPMs were fabricated. The BEPMs are installed in the centers of the quadrupole magnets located between the CMs. Photographs of three types of BEPMs and a cross section of a BEPM are shown in Fig. 10. The ideal linear response of the quadrupole moments is realized by using a parabolic design while maintaining good linear position sensitivity.

A block diagram of the BEPMs and data-acquisition (DAQ) system is shown in Fig. 11. The DAQ system can synchronize the RF reference with a beam chopper signal. The amplified pickup signals are transmitted through coaxial cables to the signal processing devices. The upstream and downstream signals are switched by multiplexers and digitized by digitizers (PXIe-5160). Although the sampling speed is 1.25 GS/s, a consider-

ably higher sampling speed of 50 GS/s can be achieved by using the random interleave mode under the condition that the signal is repeating continuously. Thus, highly accurate TOF measurements can be realized. All modules are integrated into a PXI express chassis. The signal process procedures are controlled by the LabVIEW 2019 graphical programming language, and module drivers are supported by the National Instruments Corporation. The obtained data are shared using the CA Lab that is a user-friendly, lightweight, and high-performance interface between the LabVIEW program language and EPICS-based control system. It allows easy reading and writing of EPICS process variables (PV). Measurement results are displayed on a remote desktop. Further, once these data are saved, the Control System Studio (CSS), which is an Eclipse-based tool to operate a large-scale control system, can display the results anywhere in the control room.

The first $^{40}Ar^{13+}$ beam acceleration commissioning was conducted using nine SC cavities. Figure 12 shows the displayed results of the BEPM measurements immediately after the beam was successfully accelerated to 6.2 MeV/nucleon (2020/01/28 21:02). The waveforms, beam positions, and beam energies at each station are displayed; the value circled in red indicates the final accelerated energy.

The BEPM system worked extremely well when determining phases of SC cavities and confirming beam energies and positions, which enabled stable beam acceleration. The measured beam energy is plotted in Fig. 13 as a function of the phase of the final SC cavity. In the focusing region, the lower energy beam gains

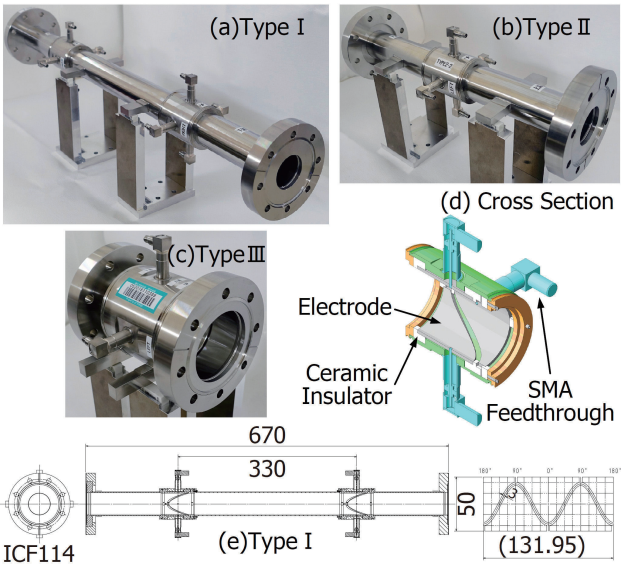

Fig. 10. Photographs of the three types of BEPMs: (a) Type I, (b) Type II, and (c) Type III. (d) Cross section drawing of a BEPM. (e) Schematic of Type I.[27]

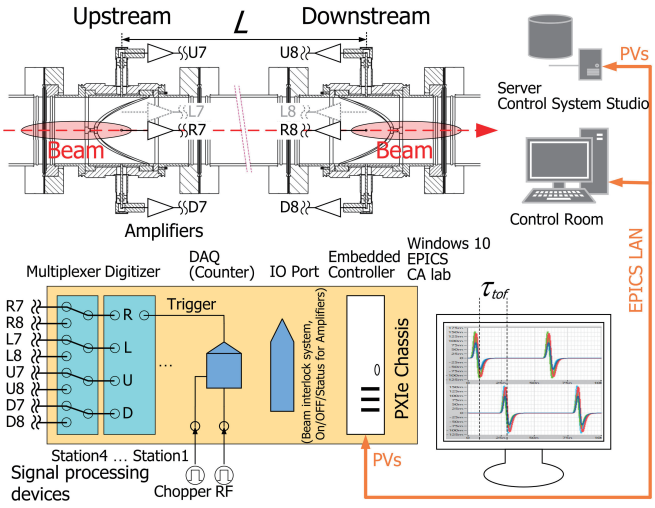

Fig. 11. Block diagram of BEPMs and DAQ system.[27]

energy, whereas in the defocusing region, the lower energy beam loses energy. This measurement clearly shows us the region we should select to accelerate the beam stably. The phases of SC cavities are currently set to −25°. Each phase of the SC cavity was measured and set in sequence from upstream to downstream (See "Beam Commissioning of SRILAC" for detail).

Overview of Control System for SRILAC Project

A distributed control system that uses Experimental Physics and Industrial Control System (EPICS) should be adopted as in RIBF to operate the SRILAC project efficiently, and a higher-level application protocol needs to be integrated to the EPICS Channel Access (CA) protocol. Further, the SRILAC control system requires corrections and upgrades to the shortcomings of previous RILAC control system, for example control protocol for an electromagnet power supply and a machine protection system.

In this project, the R28G-K was installed at the frontend of RILAC to increase the beam intensity. The new SC-ECRIS control system consists of PLCs embedded with EPICS.[28] The ion source control system differs from other control systems in that control stations with digital and analogue modules need to be installed on the high-voltage stage. At RIBF, a reliability of the conventional SC-ECRIS control system is not so high because interlock signals are exchanged via TCP/IP between the safety system and control stations on the high-voltage stage. The new SC-ECRIS control system uses two different types of CPUs (sequence CPU and Linux CPU) in the main PLC station, and it was connected to five PLC substations with a star-topology field bus communication using optical fibers for insulation. As a result, the interlock signal

exchanges the control station on the high-voltage stage through field bus communication on the optical fiber; system reliability was improved compared with the system that uses the TCP/IP-based interlock signal.

With this SRILAC project, the layout of the beamline has changed and new electromagnet power supplies have been introduced for the LEBT electromagnet. Old electromagnet power supplies were utilized for MEBT electromagnets. These electromagnet power supplies control used GPIB as the communication protocol, and their performance was relatively low compared with the modern protocol. Therefore, we upgraded the power supplies to replace the GPIB communication with the standard method of RIBF control system such as FA-M3 PLC and NIO.[29] In beam commissioning, approximately 30 modified electromagnet power supplies were controlled via EPICS CA protocol without problems.

With the installation of the SRILAC downstream of the normal conducting RILAC, a machine protection system has become necessary. For the previous RILAC control system, the machine protection system, which comprises a simple electromagnetic relay circuit has been implemented. The machine protection system is called the Beam Interlock System (BIS) at RIBF; further, we newly developed and implemented BIS for SRILAC. The BIS has a mechanism that activates the beam chopper for a signal triggered by an error from the control equipment and stops the beam. The speed at which the trigger signal is transmitted to the CPU is improved compared with that of the conventional BIS by adopting the field bus connection for inter-station communication. In addition, by adopting a ring-topology, we designed it to increase redundancy.

In the previous RILAC control system, hard-wired

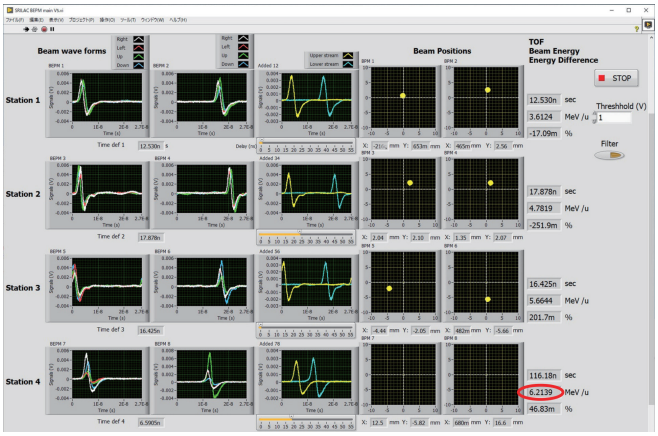

Fig. 12. Displayed BEPM measurement results immediately after the $^{40}Ar^{13+}$ beam was successfully accelerated to 6.2 MeV/nucleon (2020/01/28 21:02). Positions at station 4 were off scale, and it was corrected after the first trial acceleration.[27]

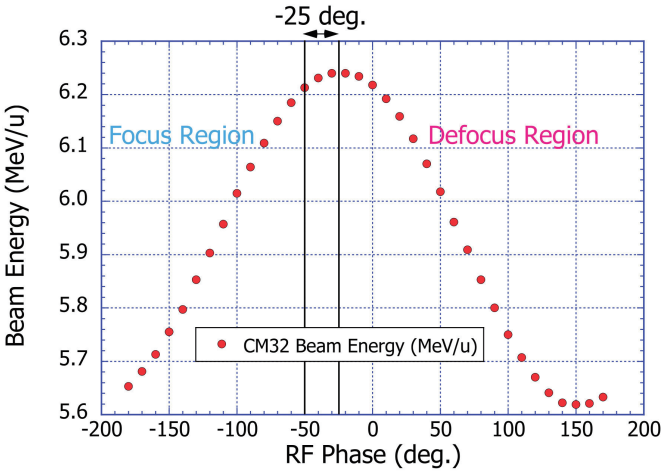

Fig. 13. Measured beam energy plotted as a function of the phase of the final SC cavity.[27]

control that directly connects the accelerator room and control room with a wire was already replaced and all operations were based on remote control. However, various systems such as data collection and RF control were not integrated with the EPICS CA protocol, and these were stand-alone systems. When the control system was updated in the SRILAC project, all control protocols for the higher-level application were integrated in the EPICS CA protocol. For example, BEPM was a LabVIEW-based system using National Instrument PXI, and by introducing CA Lab in the middle layer, we succeeded to operate it using the EPICS CA client.[27]

Since we succeeded to access to almost all control equipment including the above-mentioned electromagnet power supply, BIS, BEPM, and RF using the EPICS CA protocol, it had become possible to unify the development method of the operator interface (OPI) and realize various OPIs using CSS (Fig. 14). In addition, the Archiver Appliance has been newly introduced as the EPICS-based data archive system; it has become possible to store nearly 10,000 signal points as data at a cycle of 10 Hz or higher.[30] This system has the ability to search for arbitrary data by the timestamp and visualize the data on a Web-based application. During SRILAC beam commissioning, the Archiver Appliance was very useful for clarifying the behavior of SC cavity and the cause of troubles, and it is currently one of the essential tools for SRILAC beam tuning. In the RILAC control room (Fig. 1), consoles for hard-wired control system have been removed and new consoles ideal for the remote-control system have been introduced (Fig. 15).

In the near future, we plan to improve the performance of BIS and implement another type of machine protection system driven by the behavior of electri-

cal current for the electromagnet[31] because of the increase in the beam intensity from SRILAC.

Beam Commissioning of SRILAC

The design parameters of the SRILAC are listed in Table 1, and its layout is shown in Fig. 4. The TEM cavities for the SRILAC are designed to operate in the CW mode. The gap length of the cavity is optimized for $\beta = 0.078$ particles with a transit time factor of 0.9. The maximum gap voltage is 2.4 MV, which corresponds to an acceleration gradient E_{acc} of 6.8 MV/m with a synchronous phase of $-25°$.

The FPC is designed with a tunable coupling so that a Q_{ext} range from 1×10^6 to 4.5×10^6 can be achieved by changing the insertion distance of its antenna. The maximum beam current is about 100 electric μA for the SHE synthesis experiments; therefore, beam loading is negligible. A low Q_{ext} as small as 10^6 was selected to broaden the resonance curve with a ± 60 Hz operational-frequency-range achieved by an RF input power of 7.5 kW. In October 2019, the first RF test with an operational temperature of 4.5 K was performed without significant trouble, except SC05 encountered a vacuum leakage from the ceramic window of the coupler. During the RF test, amplitude feedback and phase-lock loop parameters of the newly developed digital LLRF were optimized and a stable RF-field was successfully obtained.

After a successful RF test, in January 2020, the beam acceleration test was conducted for the first time. An ^{40}Ar beam was accelerated based on the requirement for SHE synthesis experiments. However, one of the SC-QWRs (SC05) was not available; therefore, the acceleration energy was lowered to 6.2 MeV/nucleon from the designed energy of 6.5 MeV/nucleon.

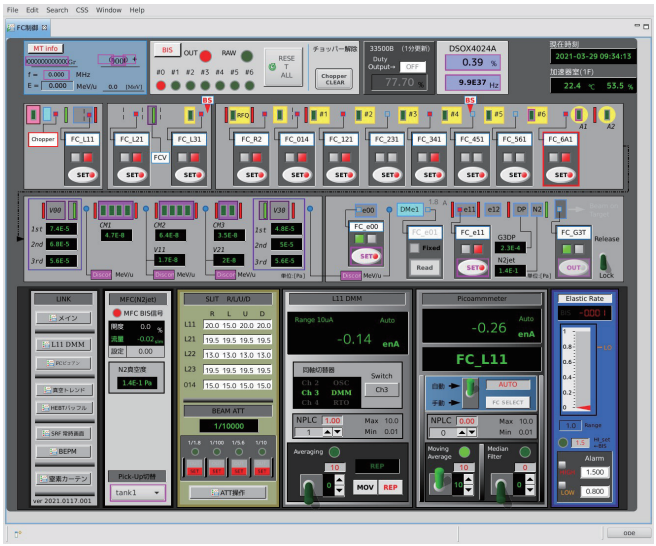

Fig. 14. Screenshot of CSS-based OPI for Faraday cup operation.

Fig. 15. New consoles for remote operation in the RILAC control room.

The $^{40}Ar^{13+}$ beam with an intensity of approximately 23 electric nA (duty 3%, chopper frequency 1 kHz) was accelerated to 6.2 MeV/nucleon with a gap voltage of 1.13 MV. For the SC-linac tuning, SC-QWRs were energized one-by-one and the beam energy was measured with a systematic variation of the RF-field phase (Fig. 16). The beam energy was precisely obtained by a TOF measurement with a pair of BEPMs with a low beam current as described above. The phase-scan plot, where E_{out} is plotted as a function of the RF-field phase for each cavity, is shown in Fig. 16. The synchronous phase $\phi_{\mathrm{s}} = -25°$ was obtained by shifting the RF-field phase from the zero acceleration/bunching phase by 65° towards the top of the sine curve. The beam position remained almost at the center of beam aperture during the phase scan because of the geometrical correction caused by the steering effect of the QWR cavity.[23] The accelerated beam energy successfully reached 6.2 MeV/nucleon at 9 PM on January 28, 2020.

After elaborate tuning, the transmission efficiency from FC6A1 to FCe11 in Fig. 4 reached 100% with a beam current of 6.11 electric μA. The vertical and horizontal beam positions monitored by BEPM were centralized and the beam loss which occurred at the MEBT was minimized keeping the deterioration of the vacuum pressure below 1×10^{-7} Pa.

A $^{51}V^{13+}$ beam with an energy from 4.2 MeV/nucleon to 6.3 MeV/nucleon was delivered for a user service time. To achieve a beam current of 10 particle μA, the transmission efficiency of the low-energy part of the RILAC and optimization of the beam transport of the SRILAC are currently being analyzed. The data archive system[30] for many accelerator parameters in-

cluding not only the RF-field of the RF cavities, but also the excitation current of the magnets, vacuum, temperature of the cooling water, and BEPMs, is very helpful to understand what occurs during beam tuning. Each cavity achieved the acceleration gradient of 5.7 MV/m that accelerates ions with M/q of 5.4 to 6.5 MeV/nucleon with ten cavities. The newly developed digital LLRF will be adopted to each RF system of the RT-DTLs, RFQ, and bunchers to improve the stability of their RF-field.

Beam transport optimization from SRILAC to GARIS-III

This section reports on beam transport. Heavy-ion beams accelerated to approximately 6 MeV/nucleon by SRILAC are transported to GARIS-III through the transport line called the high energy beam transport (HEBT) line. The configuration of the beam line is TQ–TQ–D–SQ–SQ–DQ (TQ = Triplet Quadrupole, D = Dipole, SQ = Singlet Quadrupole, DQ = Doublet Quadrupole) as shown in Fig. 4. Further, there is one dipole magnet between the second SQ and DQ, but this is not excited when the beam is transported to GARIS-III. The duct diameter is 60 mm in most places; however, it is narrowed to 15–25 mm just before the target because of DPSG.

The requirements for the beam transport of the HEBT line are (A) beam loss less than a few percent and (B) the adjustability of beam spot shape on the GARIS-III target depending on the experimental conditions. The first requirement is important for maintaining the outside radiation dose. Since the side wall of GARIS-III is relatively thin, it is necessary to measure and confirm the dose while optimizing beam transport. For the second requirement, a horizontal ellipse is desired in the production run to prevent the local depletion of the rotating target, while a large circle shape is desired in the calibration run. To satisfy these requirements, the beam envelope should be narrower just before the target, where there is a relatively smaller acceptance, and it should be wider at the target.

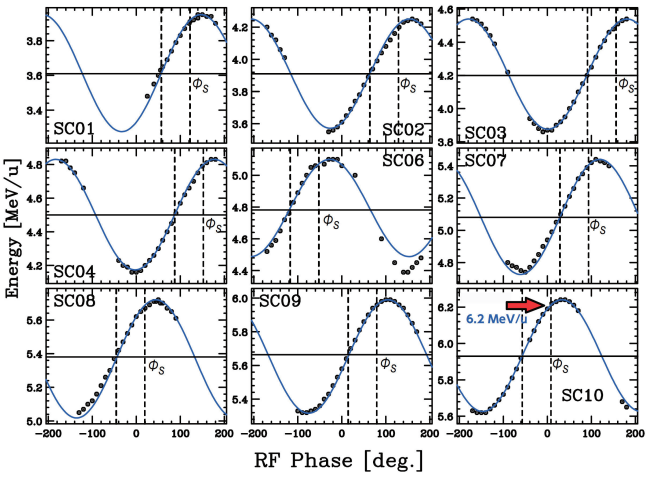

Fig. 16. Phase scan plot for first ^{40}Ar 6.2 MeV/nucleon acceleration test.

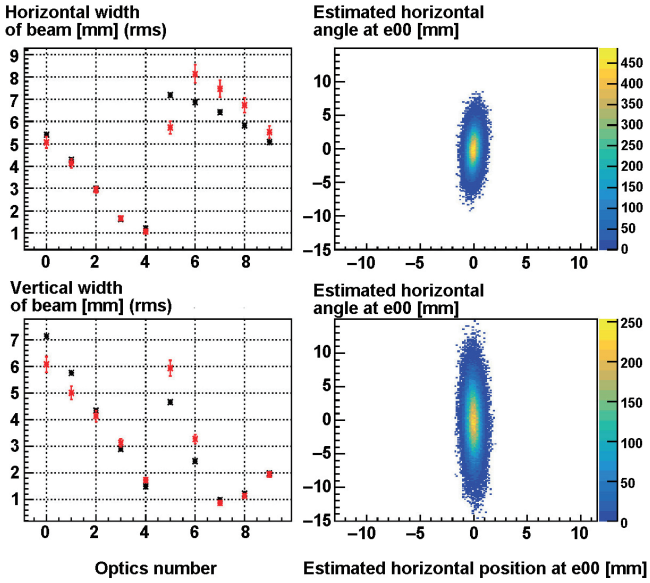

Fig. 17. Data of emittance measurement after phase-ellipse adjustment at an object point e00. (Left) Measured values (red dots) and fit results (black dots) of beam widths at the point denoted as e01. (Right) Phase ellipse estimated by fitting results. Top and bottom figures correspond to horizontal and vertical directions, respectively.

Detailed optical calculation is required according to the phase ellipse of the beam at that time to realize the ideal optics with a limited number of optical elements. The optics are adjusted in the following three steps. First, the phase ellipse of the beam at e00, which is defined as the object point in the optical design, is measured using the wire scanners at e00 and e01 (Fig. 4). The beam width at e01 is measured with several optics between e00 to e01 by changing the TQ magnets. Comparing the obtained widths and transfer matrices, the phase ellipse at e00 is estimated. Second, the phase ellipse at e00 is adjusted to be upright by the TQ upstream of e00 based on an optical calculation. Third, the optics from the object point to GARIS-III are tuned using optical simulation[32] based on an adjusted phase ellipse at e00 and an experimental requirement for beam spot shape. In the default optics, the position magnifications from e00 to GARIS-III are 1.0 in both of the horizontal and vertical directions. Based on the measured phase ellipse and experimental requirements, position magnifications are adjusted while suppressing the beam envelope in the entire beam line. Finally, the optical system is optimized with a few particle μA beam by fine-tuning the quadrupole magnets

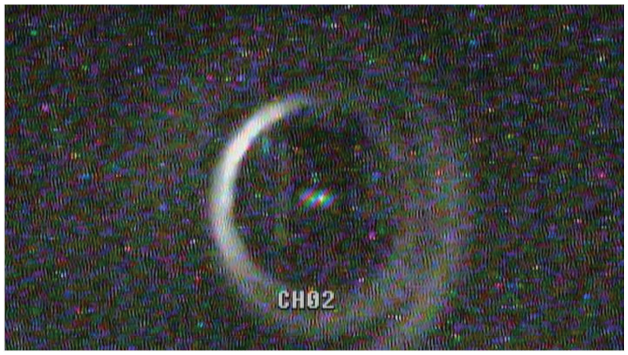

Fig. 18. Beam spot picture on viewer at GARIS-III target taken by CCD camera. The beam spot shape is a horizontal ellipse as expected.

and steerers based on the baffle inside the differential pumping system and viewer on the target.

Figure 17 shows an example of the estimated e00 phase ellipse after step 2, which causes the phase ellipse to be upright. This measurement was performed in a commissioning run in June 2020, in which Ar^{11+} accelerated to 5 MeV/nucleon with intensity of 30 electric nA was utilized. The graphs shown on the left represent the beam widths (rms) measured by the e01 wire scanner in each optics, the red dots represent the measurements, and black dots represent fit results. The contour plots shown on the right are phase ellipses at e00 estimated from the fit results. Here, the phase ellipses are assumed to be two-dimensional Gaussian distributions. As shown in the figures, the phase ellipses were adjusted to be upright as calculated. The horizontal 4 rms emittance was $\epsilon_{\rm h} = 3.1$ (πmm·mrad), and the vertical 4 rms emittance was $\epsilon_{\rm v} = 6.5$ (πmm·mrad), respectively. These values were consistent within 20% with the values before the phase-ellipse adjustment. The measurement and adjustment of the phase ellipses are almost automated except for the data acquisition by the wire scanners; they are completed in about an hour.

After the phase-ellipse adjustment, the optics from e00 to the GARIS-III target were optimized. As shown in Fig. 18, the beam spot on the target was tuned to be a horizontal ellipse, as expected for the rotation target. It was confirmed using Faraday cups that the beam loss was controlled within a few percent. Also leakage radiation was within the allowable range. In these adjustments, the calculation of optics and the application of calculated currents to magnets were automated; the optics optimization was completed in a few hours including the fine adjustment of the steerers.

Optics in the HEBT line was optimized as expected based on the phase ellipse measurement and optical simulation. A new method to estimate the phase ellipse with non-destructive detector BPEMs[33] is under development.

References

1) K. Morita *et al.*, J. Phys. Soc. Jpn. **81**, 103201 (2012).
2) P. J. Karol *et al.*, Pure Appl. Chem. **88**, 139 (2016).
3) `http://iupac.org/iupac-is-naming-the-four-new-elements-nihonium-moscovium-tennessine-and-oganesson/`.
4) M. Odera *et al.*, Nucl. Instrum. Methods Phys. Res. A **227**, 187 (1984).
5) A. Goto *et al.*, RIKEN Accel. Prog. Rep. **28**, 163 (1995).
6) T. Nakagawa *et al.*, Rev. Sci. Instrum. **71**, 637 (2000).
7) O. Kamigaito *et al.*, Rev. Sci. Instrum. **70**, 4523 (1999).
8) O. Kamigaito *et al.*, Rev. Sci. Instrum. **76**, 013306 (2005).
9) Y. Yano, Nucl. Instrum. Methods Phys. Res. B **261**, 1009 (2007).
10) Y. Wang *et al.*, RIKEN Accel. Prog. Rep. **53**, 192 (2020).
11) T. Nakagawa *et al.*, Rev. Sci. Instrum. **81**, 02A320 (2010).
12) N. Sakamoto *et al.*, Proc. 18th International Conference on RF Superconductivity (SRF2017), 681 (2017).
13) Y. Watanabe *et al.*, RIKEN Accel. Prog. Rep. **51**, 132 (2018).
14) K. Yamada *et al.*, RIKEN Accel. Prog. Rep. **52**, 13 (2019).
15) R. Geller, in *Electron Cyclotron Resonance Ion Sources and ECR Plasmas*, (IOP Publishing, Bristol, 1996) p. 121.
16) Y. Higurashi *et al.*, Rev. Sci. Instrum. **85**, 02A953 (2014).
17) G. D. Alton *et al.*, Rev. Sci. Instrum. **65**, 775 (1994).
18) M. A. Leitner *et al.*, Phys. Scr. **T92**, 171 (2001).
19) D. Hitz *et al.*, Rev. Sci. Instrum. **73**, 509 (2002).
20) J. Ohnishi, Proc. 23rd International Workshop on ECR Ion Source (ECRIS2018), 180 (2018).
21) H. Imao *et al.*, RIKEN Accel. Prog. Rep. **53**, 10 (2020).
22) H. Imao *et al.*, RIKEN Accel. Prog. Rep. **52**, 14 (2019).
23) N. Sakamoto *et al.*, Proc. 29th Linear Accelerator Conference (LINAC18), 620 (2018).
24) K. Yamada *et al.*, Proc. 19th International Conference on RF Superconductivity (SRF2019), 502 (2019).
25) K. Suda *et al.*, Proc. 19th International Conference on RF Superconductivity (SRF2019), 182 (2019).
26) K. Ozeki *et al.*, RIKEN Accel. Prog. Rep. **52**, 106 (2019).
27) T. Watanabe *et al.*, Proc. 9th International Beam Instrumentation Conference (IBIC2020), 295 (2020).
28) A. Uchiyama *et al.*, Rev. Sci. Instrum. **91**, 025101 (2020).
29) A. Uchiyama *et al.*, Proc. 16th Annu. Meet. Part. Accel. Soc. Jpn. (PASJ), 869 (2019).
30) A. Uchiyama *et al.*, Proc. 17th Annu. Meet. Part. Accel. Soc. Jpn. (PASJ), 739 (2020).
31) K. Kumagai *et al.*, RIKEN Accel. Prog. Rep. **52**, 115 (2019).
32) `https://web-docs.gsi.de/~weick/gicosy/`.
33) T. Watanabe *et al.*, Proc. 8th International Beam Instrumentation Conference (IBIC2019), 526 (2019).

I. HIGHLIGHTS OF THE YEAR

<< Selection process of highlights >>

Highlights are selected by a two-step process. In the first step, a referee who reviews a manuscript decides whether she/he would recommend it as one of the highlights.
Members of the editorial board then make additional recommendations if they think an important contribution has not been recommended by the referee.

The second step involves the editor-in-chief proposing a list of highlights based on the recommendation given above to the editorial board. After discussing the scientific merits and uniqueness of the manuscripts from viewpoints of experts/non-experts, the editorial board makes the final decision.

Oblate shapes and metastable states of ^{92,94}Se†

P. -A. Söderström,[*1,*2,*3,*4] C. Lizarazo,[*1,*2] V. Werner,[*1] N. Pietralla,[*1] P. M. Walker,[*5] G. X. Dong,[*6] F. R. Xu,[*7] T. R. Rodríguez,[*8] F. Browne,[*9] P. Doornenbal,[*3] S. Nishimura,[*3] C. R. Niță,[*10] and A. Obertelli[*1,*3,*11] for the SEASTAR2015 collaboration

The main goal of the second SEASTAR campaign[1] performed at the RIBF was the exploration of the nuclear structure evolution in the region of a possible onset of deformation and shape transition between the two corner-stone nuclei ^{78}Ni[2] and ^{110}Zr.[3] As this region is known for the large abundance of nuclear isomers,[4] the EURICA decay setup[5,6] was installed at the end of the ZeroDegree spectrometer in addition to the SEASTAR instrumentation. Thus, complementary to the in-beam spectroscopy data of the Se chain,[7] it was possible to observe internal isomeric decay using high-resolution γ-ray spectroscopy.[8]

The type of metastable configurations observed in deformed atomic nuclei, whereby two quasiparticle states are formed by breaking pairs of nucleons close to the Fermi level, significantly changing the angular momentum projection on the symmetry axis is known as K isomers. These typically originate from deformed Nilsson orbitals coming up from lower-lying shells in well deformed prolate nuclei. Analogously, the typical downsloping of these orbitals on the oblate side opens up the possibility for a new region of K isomers at low Z and oblate deformation for exotic nuclei, involving the same orbitals from higher-lying shells as within the prolate deformed $Z \sim 72$ region.

In Ref. 8), we report on the observation of such states for ^{92,94}Se from EURICA during the SEASTAR campaign, see Fig. 1, as well as the impact of their decay pattern on the discussion of shape evolution at $N = 60$. Potential energy surface calculations suggest oblate $K^\pi = 7^-$ ($\nu 11/2^-[505] \otimes \nu 3/2^+[402]$) and $K^\pi = 9^-$ ($\nu 11/2^-[505] \otimes \nu 7/2^+[404]$) configurations for the negative-parity states in ^{92}Se, and $K^\pi = 7^-$ ($\nu 11/2^-[505] \otimes \nu 3/2^+[411]$) for the isomer of ^{94}Se. For ^{94}Se, this leads to a hindrance factor of $F_W = 2.49 \times 10^8$ and a reduced hindrance $f_\nu \sim 25$. Characteristic values for $E1$ K-trap decays with $\nu = 6$ are within $27 \lesssim f_\nu \lesssim 42$.[9,10]

Also, the observed $J^\pi = 7^-$ states have very different decay paths for the two isotopes. The decay properties can partially be explained considering that the collective wave functions predicted by the SCCM method for ^{92}Se[7] are relatively soft, implying that K is not a good quantum number due to the lack of well-defined rigid axial symmetry. For ^{94}Se, however, the SCCM method proposes a rigid oblate ground state and a rigid prolate yrare band, increasing the wave-function overlap between an oblate isomer and the oblate ground state relative to the prolate yrare band.

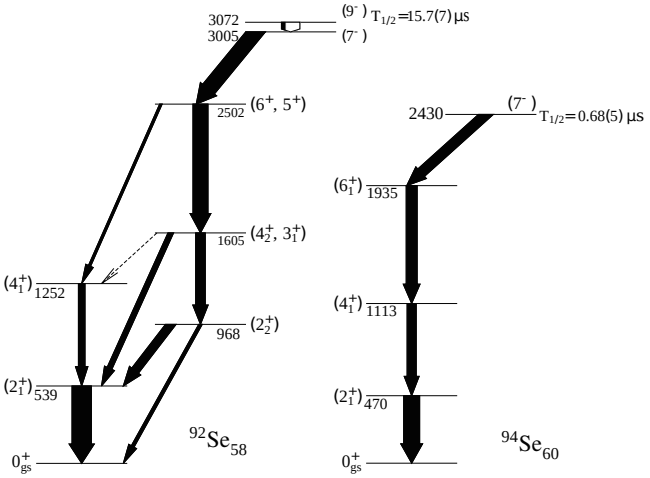

Fig. 1. Level schemes constructed for ^{92,94}Se. The arrow width of each transition indicates its intensity.

This work presents the observation and interpretation of ^{92,94}Se isomeric states. The different isomeric decay paths of each isotope contrast the relatively smooth systematics of the ground-state and $K = 2$ excited bands observed from in-beam spectroscopy.[7] Also, a similar 32 ns isomer was recently observed for ^{94}Kr at the ALTO facility of the IPN Orsay with the ν-Ball array,[11] allowing the systematic evaluation of the 7^- and 9^- states along $N = 58$.

† Condensed from the article in Phys. Rev. Lett. **124**, 222501 (2020)

*1 Institut für Kernphysik, Technische Universität Darmstadt
*2 GSI Helmholtzzentrum für Schwerionenforschung GmbH
*3 RIKEN Nishina Center
*4 ELI-NP, IFIN-HH
*5 Department of Physics, University of Surrey
*6 School of Science, Huzhou University
*7 State Key Laboratory of Nuclear Physics and Technology, Peking University
*8 Departamento de Física Teórica, Universidad Autónoma de Madrid
*9 School of Computing Engineering and Mathematics, University of Brighton
*10 DFN, IFIN-HH
*11 IRFU, CEA, Université Paris-Saclay

References

1) P. Doornenbal *et al.*, RIKEN Accel. Prog. Rep. **49**, 35 (2016).
2) R. Taniuchi *et al.*, Nature **569**, 53 (2019).
3) N. Paul *et al.*, Phys. Rev. Lett. **118**, 032501 (2017).
4) D. Kameda *et al.*, Phys. Rev. C **86**, 054319 (2012).
5) S. Nishimura, Prog. Theor. Exp. Phys. **2012**, 03C006 (2012).
6) P. -A. Söderström *et al.*, Nucl. Instrum. Methods Phys. Res. B **317**, 649 (2013).
7) S. Chen *et al.*, Phys. Rev. C **95**, 041302(R) (2017).
8) C. Lizarazo *et al.*, Phys. Rev. Lett. **124**, 222501 (2020).
9) G. D. Dracoulis *et al.*, Rep. Prog. Phys. **79**, 076301 (2016).
10) Z. Patel *et al.*, Phys. Rev. C **96**, 034305 (2017).
11) R. -B. Gerst *et al.*, Phys. Rev. C **102**, 064323 (2020).

Properties of ^{187}Ta revealed through isomeric decay†

P. M. Walker,[*1] Y. Hirayama,[*2] G. J. Lane,[*3] H. Watanabe,[*4,*5] G. D. Dracoulis,[*3] M. Ahmed,[*2,*6] M. Brunet,[*1] T. Hashimoto,[*7] S. Ishizawa,[*5,*8,*2] F. G. Kondev,[*9] Yu. A. Litvinov,[*10] H. Miyatake,[*2] J. Y. Moon,[*7] M. Mukai,[*6,*2,*5] T. Niwase,[*2,*5,*11] J. H. Park,[*7] Zs. Podolyák,[*1] M. Rosenbusch,[*2] P. Schury,[*2] M. Wada,[*2,*6] X. Y. Watanabe,[*2] W. Y. Liang,[*12] and F. R. Xu[*12]

We report results from the production and separation of a low-energy beam of the neutron-rich tantalum isotope, $^{187}Ta_{114}$, together with its high-spin isomeric state. The production process exploits multi-nucleon transfer (MNT) reactions which have been shown to be effective for making neutron-rich nuclei.[1] The large angular momentum transfer in MNT reactions is a key aspect for the formation of high-spin isomers.

The experiment was performed at the RIKEN Nishina Center with the recently commissioned KEK Isotope Separation System (KISS) facility.[2] This is the first facility of its kind, capable of stopping heavy-ion reaction products in a high-pressure (80 kPa) argon gas cell, performing laser resonant ionization for element (Z) selectivity, and achieving mass (A) separation of the electrostatically extracted, singly charged, 20 keV ions in a dipole magnet with a resolving power $A/\Delta A = 900$.

The ^{187}Ta ions were produced by MNT reactions of a 50 particle-nA beam of ^{136}Xe at 7.2 MeV/nucleon, delivered by the RIKEN Ring Cyclotron. The beam was incident on a 5 μm thick natural tungsten target at the entrance to the argon gas cell.

The 20 keV secondary beam of laser-ionized tantalum was mass separated (1.5 ions/s of ^{187}Ta) and transported to a moving-tape collection point, surrounded by a low-background, 32-element gas proportional counter with 80% of 4π solid angle for β particles and conversion electrons[3] and four Super Clover germanium γ-ray detectors with a total absolute full-energy-peak efficiency of 15% at 150 keV. The tape transport was operated with equal beam-on/beam-off periods, with the radioactivity moved to a shielded location at the end of each cycle. The chosen beam-on periods were 30 s, 300 s and 1800 s, with five days of data taking.

An isomer in ^{187}Ta at 1789(13) keV had been identified in the Experimental Storage Ring at GSI,[4] but without observation of the decay radiations. Details of the excited-state structure of ^{187}Ta have now been revealed by the isomeric γ-ray emissions, as illustrated in Fig. 1. The isomer is found to have an excitation energy of 1778(1) keV, with a half-life of 7.3(9) s.

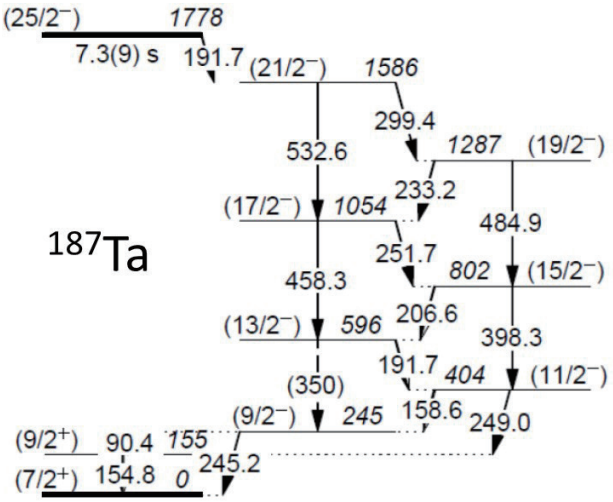

Fig. 1. Level scheme for ^{187}Ta based on γ-ray transitions observed following the decay of a $T_{1/2} = 7.3(9)$ s isomer.

Despite the proximity to $N = 116$, which is predicted to be the critical point for a ground-state prolate-oblate shape transition, the reduced hindrance for the 191.7 keV, E2 isomeric decay remains substantial, with $f_\nu = 27(1)$, indicating that K is approximately conserved, and therefore that axial symmetry is not strongly violated. Nevertheless, weak violation of axial symmetry is indicated by the observed irregularity in the 9/2[514] rotational band that is populated through the isomer decay. Comparison with the rhenium isotone, ^{189}Re, supports calculations showing that axial symmetry is better conserved for the lower-Z nuclei, through the $N \approx 116$ shape transition region.

The new capability to produce low-energy beams of neutron-rich tantalum isotopes and isomers demonstrates the power of the gas-stopping technique for nuclear structure studies of exotic neutron-rich nuclei, even with refractory elements. This marks a milestone on the way to the exploration of nuclei predicted to have well-deformed oblate ground states.

† Condensed from the article in Phys. Rev. Lett. **125**, 192505 (2020)

*1 Department of Physics, Surrey University
*2 Wako Nuclear Science Center (WNSC), IPNS, KEK
*3 Department of Nuclear Physics, ANU
*4 School of Physics, Beihang University
*5 RIKEN Nishina Center
*6 Graduate School of Science and Engineering, Tsukuba University
*7 Rare Isotope Science Project, Institute for Basic Science (IBS)
*8 Graduate School of Science and Engineering, Yamagata University
*9 Physics Division, ANL
*10 GSI Helmholtzzentrum für Schwerionenforschung GmbH
*11 Department of Physics, Kyushu University
*12 School of Physics, Peking University

References

1) Y. X. Watanabe *et al.*, Phys. Rev. Lett. **115**, 172503 (2015).
2) Y. Hirayama *et al.*, Nucl. Instrum. Methods Phys. Res. B **463**, 425 (2020).
3) M. Mukai *et al.*, Nucl. Instrum. Methods Phys. Res. B **463**, 421 (2020).
4) M. W. Reed *et al.*, Phys. Rev. Lett. **105**, 172501 (2010).

In-gas-cell laser resonance ionization spectroscopy of ^{196,197,198}Ir†

M. Mukai,[*1,*2,*3] Y. Hirayama,[*3] Y. X. Watanabe,[*3] S. Schiffmann,[*4,*5] J. Ekman,[*6] M. Godefroid,[*5] P. Schury,[*3] Y. Kakiguchi,[*3] M. Oyaizu,[*3] M. Wada,[*3] S. C. Jeong,[*7] J. Y. Moon,[*7] J. H. Park,[*7] H. Ishiyama,[*1] S. Kimura,[*1] H. Ueno,[*1] M. Ahmed,[*2] A. Ozawa,[*2] H. Watanabe,[*8] S. Kanaya,[*9] and H. Miyatake[*3]

The experimentally measured nuclear quadrupole deformation parameters of mercury, gold, platinum, and iridium approach the value for the spherical shape with increasing neutron number.[1)] However, for iridium isotopes, the finite-range droplet model (FRDM)[2)] predicts a shape transition from prolate ($A \leqq 196$) to oblate ($A \geqq 197$) at $A = 197$. We have investigated the evolution of nuclear structure of iridium isotopes, $^{196\text{–}198}$Ir ($Z = 77$, $N = 119$–121), with in-gas-cell laser ionization spectroscopy as the first step of a systematic study of nuclear structures for nuclei around $N = 126$ at the KEK Isotope Separation System (KISS).[3)] In the present work, we report the magnetic dipole moments (μ), mean-square charge radii, and nuclear quadrupole deformation parameters (β_2), as determined from hyperfine structure (HFS) measurements.

Neutron-rich iridium isotopes were produced using multi-nucleon transfer reactions of a ^{198}Pt target (12.5 mg/cm^2) and ^{136}Xe beam (9.4 MeV/nucleon, 50 particle-nA).[4)] The target-like fragments were thermalized and neutralized in a gas cell filled with purified Ar gas of ∼1 atm[3)] and re-ionized element-selectively by using a laser resonance ionization technique at the exit of the gas cell. The excitation transition of $5d^76s^2\ {}^4F_{9/2} \rightarrow 9/2^\circ$ ($\lambda_1 = 247.587$ nm) was chosen for the spectroscopy, and the excitation laser was produced by a dye laser pumped by an excimer laser. The mass number was chosen using a dipole magnet with a mass resolving power of $A/\Delta A \sim 900$. The mass-analyzed ions were transported to a decay station, which consists of a tape transport device, a multi-segmented proportional gas counter, and four clover-type germanium detectors.

The extraction of each nucleus was confirmed through the measurement of β-decay half-life. The HFS spectra were measured by counting β-rays as a function of excitation laser frequency, as shown in Fig. 1. The measured spectra were fitted using the Voigt function for each transition between HFSs of ground and excited states to determine the μ and isotope shift values.

The μ value of ^{197}Ir ($I^\pi = 3/2^+$) was determined to be

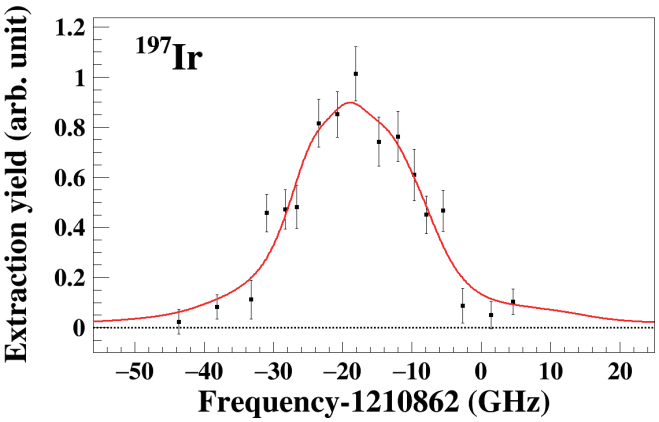

Fig. 1. Spectrum of ^{197}Ir ion counts as a function of the excitation laser frequency with the best fit (red solid line). The black dotted line indicates the fitted background level. The spectrum was measured at an argon gas pressure of 74 kPa.

$+0.27^{+0.10}_{-0.03}$ μ_N. In the case of the unknown spin nuclei ^{196}Ir ($I^\pi = (0^-)$) and ^{198}Ir, the results of chi-square fitting strongly indicate that their nuclear spin are $I > 0$ with fitted μ values of +(0.31–0.36) μ_N ($I = 1$–3) for ^{196}Ir and +(0.13–0.26) μ_N ($I = 1$–3) for ^{198}Ir.

The quadrupole deformation parameter was deduced from the measured isotope shifts while assuming an axial-deformed nuclear charge distribution and theoretical electronic factor of the excitation transition from large-scale atomic calculations.[5)] The deduced $|\beta_2|$ values were 0.06(2) and 0.07(2) for ^{197}Ir and ^{198}Ir, respectively.

The experimental μ values were compared with calculated μ values based on the strong coupling model.[6,7)] The comparison shows good agreement in the μ value for ^{197}Ir with the assumption of prolate deformation and suggests $I = 1^-$ or 2^- for ^{196}Ir and $I = 2^-$ for ^{198}Ir.

† Condensed from the article in Phys. Rev. C **102**, 054307 (2020)

*1 RIKEN Nishina Center
*2 Graduate School of Sciences and Technology, University of Tsukuba
*3 Wako Nuclear Science Center (WNSC), Institute of Particle and Nuclear Studies (IPNS), High Energy Accelerator Research Organization (KEK)
*4 Department of Physics, Lund University
*5 Spectroscopy, Quantum Chemistry and Atmospheric Remote Sensing (SQUARES), Université libre de Bruxelles
*6 Materials Science and Applied Mathematics, Malmö University
*7 Rare Isotope Science Project, Institute for Basic Science
*8 International Research Center for Nuclei and Particles in the Cosmos, Beihang University
*9 Department of Physics, Osaka University

References

1) D. Verney *et al.*, Eur. Phys. J. A **30**, 489 (2006); G. Ulm *et al.*, Z. Phys. A **325**, 247 (1986); K. Wallmeroth *et al.*, Nucl. Phys. A **493**, 224 (1989); Th. Hilberath *et al.*, Z. Phys. A **342**, 1 (1992).
2) P. Möller *et al.*, At. Data Nucl. Data Tables **59**, 185 (1995).
3) Y. Hirayama *et al.*, Nucl. Instrum. Methods Phys. Res. B **353**, 4 (2015); Y. Hirayama *et al.*, Nucl. Instrum. Methods Phys. Res. B **412**, 11 (2017).
4) Y. X. Watanabe *et al.*, Phys. Rev. Lett. **115**, 172503 (2015).
5) S. Schiffmann, M. Godefroid, J. Quant. Spectrosc. Radiat. Transf. **258**, 107332 (2020).
6) I. Hamamoto, Phys. Rev. C **99**, 024319 (2019).
7) A. Bohr, B. R. Mottelson, Mat. Fys. Medd. K. Dan. Vidensk. Selsk. **27**, 16 (1953).

Fragmentation of single-particle strength around the doubly-magic nucleus ^{132}Sn and the position of the $0f_{5/2}$ proton-hole state in ^{131}In†

V. Vaquero,[*1] A. Jungclaus,[*1] T. Aumann,[*2,*3] J. Tscheuschner,[*2] E. V. Litvinova,[*4] J. A. Tostevin,[*5] H. Baba,[*6] D. S. Ahn,[*6] R. Avigo,[*7,*8] K. Boretzky,[*3] A. Bracco,[*7,*8] C. Caesar,[*2,*3] F. Camera,[*7,*8] S. Chen,[*9,*6] V. Derya,[*10] P. Doornenbal,[*6] J. Endres,[*10] N. Fukuda,[*6] U. Garg,[*11] A. Giaz,[*7] M. N. Harakeh,[*3,*12] M. Heil,[*3] A. Horvat,[*2] K. Ieki,[*13,*6] N. Imai,[*14] N. Inabe,[*6] N. Kalantar-Nayestanaki,[*12] N. Kobayashi,[*14,*6] Y. Kondo,[*15,*6] S. Koyama,[*14,*6] T. Kubo,[*6] I. Martel,[*16] M. Matsushita,[*17] B. Million,[*8] T. Motobayashi,[*6] T. Nakamura,[*15,*6] N. Nakatsuka,[*6,*2] M. Nishimura,[*6] S. Nishimura,[*6] S. Ota,[*17] H. Otsu,[*6] T. Ozaki,[*15,*6] M. Petri,[*2] R. Reifarth,[*18] J. L. Rodríguez-Sánchez,[*19,*3] D. Rossi,[*2] A. T. Saito,[*15,*6] H. Sakurai,[*6,*14] D. Savran,[*3] H. Scheit,[*2] F. Schindler,[*2,*3] P. Schrock,[*2] D. Semmler,[*2] Y. Shiga,[*13,*6] M. Shikata,[*15,*6] Y. Shimizu,[*6] H. Simon,[*3] D. Steppenbeck,[*6] H. Suzuki,[*6] T. Sumikama,[*6] D. Symochko,[*2] I. Syndikus,[*2] H. Takeda,[*6] S. Takeuchi,[*6] R. Taniuchi,[*14,*6] Y. Togano,[*15,*6] J. Tsubota,[*15,*6] H. Wang,[*6] O. Wieland,[*8] K. Yoneda,[*6] J. Zenihiro,[*6] and A. Zilges[*10]

The neutron-hole and proton-hole nuclei ^{131}Sn and ^{131}In were studied using one-nucleon removal reactions from doubly-magic ^{132}Sn at relativistic energies. In ^{131}In, a 2910(50)-keV γ ray was observed for the first time, see Fig. 1, mainly thanks to the good energy and time resolution of the eight $LaBr_3$ detectors employed in this experiment. This high-energy γ ray was tentatively assigned to the decay of the $0f_{5/2}$ proton-hole state to the known $1/2^-$ level at 365 keV. Thus, the excitation energy of the last so far unknown proton-hole state in ^{132}Sn was fixed to 3275(50) keV. From the absolute intensities of the observed γ rays, the spectroscopic factors for the $1d_{5/2}$ and $0g_{7/2}$ neutron-hole states in ^{131}Sn and the $1p_{3/2}$ and $0f_{5/2}$ proton-hole states in ^{131}In were determined. They nicely agree with those of the analog states with quantum numbers $n(\ell+1)_{j+1}$ in ^{207}Pb and ^{207}Tl indicating that the close resemblance between the shell structures around the doubly-magic nuclei ^{132}Sn and ^{208}Pb established since long also holds for the spectroscopic factors. To investigate the origin of the strong fragmentation of single-particle strength state-of-the-art calculations based on the relativistic particle-vibration coupling model were performed. While the coupling to the first excited 3^- states in the core nuclei ^{132}Sn and ^{208}Pb was identified as the main origin for the reduced spectroscopic factors measured for the $1d_{5/2}/1f_{7/2}$ single-particle states in ^{131}Sn/^{207}Pb and the $1p_{3/2}/1d_{5/2}$ levels in ^{131}In/^{207}Tl, clearly more complex coupling scenarios are responsible for the strong fragmentation and the small measured spectroscopic factors in the case of the $0g_{7/2}/0h_{9/2}$ states in ^{131}Sn/^{207}Pb and the $0f_{5/2}/0g_{7/2}$ levels in ^{131}In/^{207}Tl.

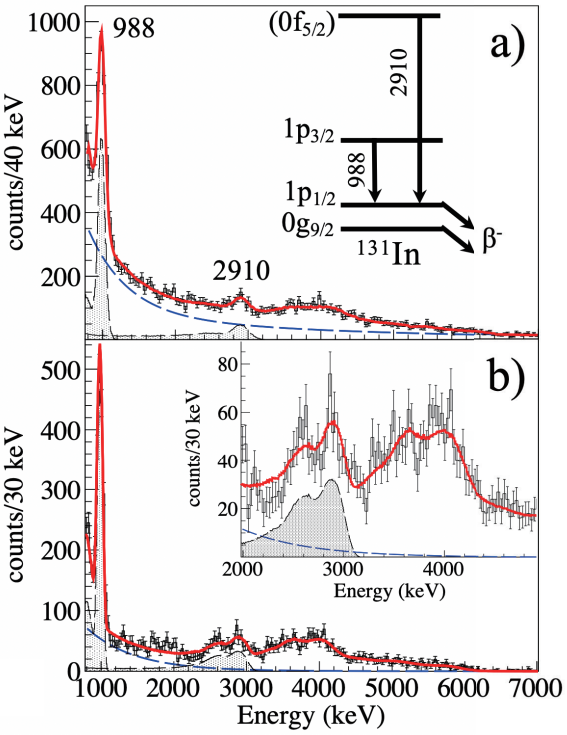

Fig. 1. Doppler-corrected γ-ray spectra of ^{131}In populated via one-proton removal from ^{132}Sn measured with a) 96 NaI crystals of DALI2 covering polar angles in the range $\theta = 50$–150° and b) eight $LaBr_3$ detectors placed at $\theta = 30^\circ$ (adopted from Fig. 1 of the original article).

† Condensed from the article in Phys. Rev. Lett. **124**, 022501 (2020)

*1 Instituto de Estructura de la Materia, CSIC
*2 Institut für Kernphysik, TU Darmstadt
*3 GSI Helmholtzzentrum für Schwerionenforschung GmbH
*4 Department of Physics, Western Michigan University
*5 Department of Physics, University of Surrey
*6 RIKEN Nishina Center
*7 Dipartimento di Fisica dell'Università degli Studi di Milano
*8 INFN, Sezione di Milano
*9 School of Physics and State Key Laboratory of Nuclear Physics and Technology, Peking University
*10 Institut für Kernphysik, Universität zu Köln
*11 Department of Physics, University of Notre Dame
*12 KVI-CART
*13 Department of Physics, Rikkyo University
*14 Department of Physics, The University of Tokyo
*15 Department of Physics, Tokyo Institute of Technology
*16 Departamento de Fsica Aplicada, Universidad de Huelva
*17 Center for Nuclear Study, The University of Tokyo
*18 Institut für Kernphysik, Goethe University Frankfurt
*19 Universidad de Santiago de Compostela

Experimental studies of the two-step scheme with an intense radioactive ^{132}Sn beam for next-generation production of very neutron-rich nuclei†

H. Suzuki,[*1] K. Yoshida,[*1] N. Fukuda,[*1] H. Takeda,[*1] Y. Shimizu,[*1] D. S. Ahn,[*1] T. Sumikama,[*1] N. Inabe,[*1] T. Komatsubara,[*1] H. Sato,[*1] Z. Korkulu,[*1] K. Kusaka,[*1] Y. Yanagisawa,[*1] M. Ohtake,[*1] H. Ueno,[*1] T. Kubo,[*1] S. Michimasa,[*2] N. Kitamura,[*2] K. Kawata,[*2] N. Imai,[*2] O. B. Tarasov,[*3,*1] D. P. Bazin,[*3,*1] J. Nolen,[*4,*1] and W. F. Henning[*4,*5,*1]

The usefulness of a two-step scheme with a ^{132}Sn beam proposed[1] for the efficient production of mid-heavy very-neutron-rich RIs was investigated, as an alternate method for the in-flight fission of a ^{238}U beam (one-step scheme). The two-step scheme is a combination of an isotope-separation online (ISOL) system with a thick U target and a high-intensity proton beam as the first step, and the projectile fragmentation of re-accelerated RI beams (*e.g.*, ^{132}Sn) as the second step. We measured production cross sections beyond ^{125}Pd, up to which the cross sections had already been measured at GSI together with the neighboring RIs,[2] to evaluate the yields of RIs using the two-step scheme with a ^{132}Sn beam. The 278-MeV/nucleon ^{132}Sn beam was supplied from BigRIPS, and the very neutron-rich RIs around the neutron number $N = 82$ were produced in the ZeroDegree spectrometer with a 5.97-mm Be target. Yields obtained by the two-step and one-step schemes were estimated based on the measured cross sections, and we examined whether and to what extent the two-step scheme at future 1-MW beam facilities can reach further into the neutron-rich region.

Figure 1 shows the production yields of Pd isotopes obtained using the two-step scheme with a ^{132}Sn beam and the one-step scheme with 1-MW beam powers. The two-step yields (Y_{2step}) decrease more slowly with neutron numbers than the one-step yields (Y_{1step}), and Y_{2step} becomes larger than Y_{1step} beyond ^{124}Pd. The ratio of Y_{2step}/Y_{1step} around the $N = 82$ region is shown in Fig. 2. This ratio systematically increases, as moving away from the stability line. Thus, the two-step scheme is more favorable than the one-step scheme to yield more neutron-rich region beyond our results, especially for the region of the supernova r-process path. The calculated Y_{2step} with a cross-section formula COFRA[4] indicated by black lines reproduces the experimental results well.

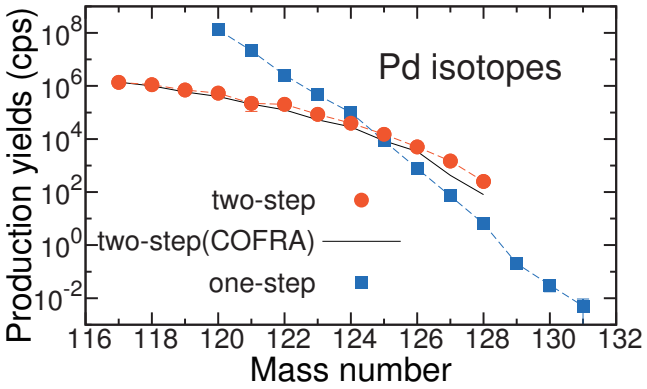

Fig. 1. Yield comparison between the two-step scheme with a ^{132}Sn beam (orange circles) and the one-step in-flight fission of a ^{238}U beam (blue squares) for Pd isotopes.

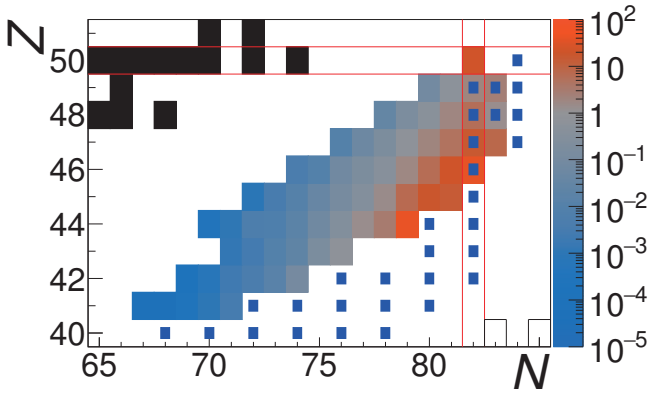

Fig. 2. Ratios of the Y_{2step} with a ^{132}Sn beam to the Y_{1step}. Orange and blue regions indicate that the two- and one-step schemes are more useful than the other, respectively. Dark-blue square dots represent the supernova r-process path.

ISOL systems can provide various RIs over the nuclear chart; thus, a wide region of very neutron-rich RI beams can be produced by the two-step scheme. By using the ISOLDE yield database[3] and the cross-section formula COFRA, the Y_{2step} in the whole region was estimated. The Y_{2step} was expected to be larger than the Y_{1step} around the neutron-rich $N = 50$, 60, 82, and 90, including the supernova r-process path. The two-step scheme is considered a powerful tool to open a new window into the unknown region of mid-mass to heavy, very neutron-rich nuclei.

† Condensed from the article in Phys. Rev. C **102**, 064615 (2020)

*1 RIKEN Nishina Center
*2 Center for Nuclear Study, University of Tokyo
*3 National Superconducting Cyclotron Laboratory, Michigan State University
*4 Division of Physics, Argonne National Laboratory
*5 Physik Department, Technische Universität München

References

1) K. Helariutta *et al.*, Eur. Phys. J. A **17**, 181 (2003).
2) D. Pérez-Loureiro *et al.*, Phys. Lett. B **703**, 552 (2011).
3) ISOLDE Yield Database web page, `http://isoyields-classic.web.cern.ch`.
4) COFRA web page, `http://www.usc.es/genp/cofra`.

On-line commissioning of the new SLOWRI/ZD-MRTOF system

M. Rosenbusch,[*1] S. Chen,[*2] Y. Hirayama,[*1] D. S. Hou,[*3] S. Iimura,[*4,*5] H. Ishiyama,[*4] Y. Ito,[*6] S. Kimura,[*4] J. Liu,[*3] S. Michimasa,[*7] H. Miyatake,[*1] S. Naimi,[*4] S. Nishimura,[*4] T. Niwase,[*8,*1,*4] P. Schury,[*1] A. Takamine,[*4] M. Wada,[*1] Y. X. Watanabe,[*1] H. Wollnik,[*9] W. Xian,[*2] and S. Yan[*10]

The new combined gas cell and MRTOF spectrograph developed for high-precision atomic mass measurements at BigRIPS has been finalized and transported to the F11 position behind the ZeroDegree spectrometer of RIBF. The combination of the new cryogenic gas cell[1] with the MRTOF system was initially tested in October 2020, where stable $^{39}K^{+}$ ions were extracted from the gas cell and detected at the system's downstream TOF detector. The system was ready to operate on-line just before the start of the 2020 HiCARI campaign, which enabled the first on-line commissioning of the new setup. The commissioning run took place in parasitic on-line operation during the HiCARI experiments (see HiCARI APR publications in this volume). After passing the HiCARI target and detectors, the reaction products were transported through the ZeroDegree spectrometer and stopped in the new cryogenic gas cell. Energy degraders were used to reduce the beam energy to match the He gas cell's stopping power. The stopped reaction products were extracted mostly as singly-charged ions and transported to the MRTOF setup[2] where their masses were determined with high precision and accuracy. The 2020 HiCARI campaign lasted throughout the month of November with five separate experiments, and another two experiments took place in December. During our commissioning, mass measurements covering four different regions in the nuclide chart have been carried out (see Fig. 1). Total system efficiencies, determined by comparing the incoming rate from F11 at the PID system with the detected rate after MRTOF, varied according to the presence of contaminants in the helium gas. While some of the radioactive species were dispersed across molecular sidebands (*e.g.* $^{55}ScOH^{+}$), very reasonable ion transport could be reached for many other species, *e.g.* $^{85}As^{+}$ with 0.16% and $^{137}Te^{+}$ with 1.3% total efficiency. In sum, the commissioning campaign was highly successful with more than 70 atomic masses measured during the HiCARI campaign. Notable results have been achieved in four different regions. Around neutron-rich Ti and V isotopes, our results include isotopes from Ca to Fe with ^{55}Sc, ^{58}Ti, and ^{59}V being the most exotic, which improve nuclear masses very recently measured using the TOF-Bρ method at NSCL[3] and RIBF[4] denoting the front line of nuclear mass studies in this region. In the neutron-rich region above Ni, nuclides have been studied reaching from Ga to Kr with ^{84}Ga, ^{86}Ge, ^{89}As, and ^{91}Se as most exotic isotopes. In this group the isotopes $^{88,89}As$ have been measured for the first time while three other isotopes provide a significant improvement of the previously performed measurements. Another region addressed with success is from Mo to Rh isotopes including the first mass measurement of ^{112}Mo. In the fourth region addressed, *i.e.* near ^{132}Sn, we have demonstrated the isomeric mass separtion of $^{134g,m}Sb$ (W. Xian, APR same volume). In total, three isotope masses have been measured for the first time and eleven other isotope masses improve the present uncertainty significantly. By performing this first on-line commissioning of a gas stopper connected to BigRIPS in a parasitic mode, we were able to efficiently identify and resolve issues that could not be studied offline. This will allow for a very rapid improvement in performance going forward. In March 2021, the next commissioning run takes place, wherein the neutron-rich Ni region will be addressed by HiCARI group. Furthermore, two different beam times with the ZD-MRTOF system as main experiment have been approved for 2021.

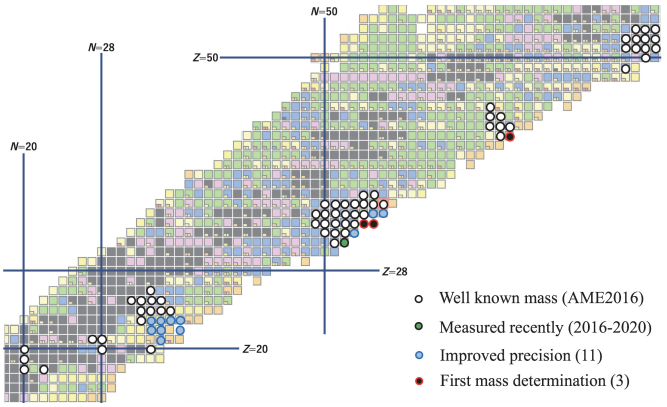

Fig. 1. Nuclear mass measurements during the HiCARI campaign and the results by the ZD-MRTOF system. Background color code illustrates the measured precision from AME2016 (see Nucleus-win for reference).

*1 Wako Nuclear Science Center (WNSC), IPNS, KEK
*2 Department of Physics, the University of Hong Kong
*3 IMP Lanzhou
*4 RIKEN Nishina Center
*5 Department of Physics, Osaka University
*6 Advanced Science Research Center, JAEA Ibaraki
*7 Center for Nuclear Study, the University of Tokyo
*8 Department of Physics, Kyushu University
*9 Dep. of Chem. and Biochem., New Mexico State University
*10 Jinan University

References
1) A. Takamine *et al.*, RIKEN Accel. Prog. Rep. **53** (2018).
2) M. Rosenbusch *et al.*, Nucl. Instrum. Methods Phys. Res. B **463**, 184 (2020).
3) Z. Meisel *et al.*, Phys. Rev. C **101**, 052801(R) (2020).
4) S. Michimasa *et al.*, Phys. Rev. Lett. **125**, 122501 (2020).

Mapping of a new deformation region around ^{62}Ti†

S. Michimasa,[*1] M. Kobayashi,[*1] Y. Kiyokawa,[*1] S. Ota,[*1] R. Yokoyama,[*2] D. Nishimura,[*3] D. S. Ahn,[*4] H. Baba,[*4] G. P. A. Berg,[*5] M. Dozono,[*1] N. Fukuda,[*4] T. Furuno,[*6] E. Ideguchi,[*7] N. Inabe,[*4] T. Kawabata,[*6] S. Kawase,[*8] K. Kisamori,[*1] K. Kobayashi,[*9] T. Kubo,[*10,*11] Y. Kubota,[*4] C. S. Lee,[*1] M. Matsushita,[*1] H. Miya,[*1] A. Mizukami,[*12] H. Nagakura,[*9] H. Oikawa,[*12] H. Sakai,[*4] Y. Shimizu,[*4] A. Stolz,[*11] H. Suzuki,[*4] M. Takaki,[*1] H. Takeda,[*4] S. Takeuchi,[*13] H. Tokieda,[*1] T. Uesaka,[*6] K. Yako,[*1] Y. Yamaguchi,[*1] Y. Yanagisawa,[*4] K. Yoshida,[*2] and S. Shimoura[*1]

The mass of atomic nuclei is a fundamental quantity as it reflects the sum of all interactions within the nucleus, which is a quantum many-body system comprised of two kinds of fermions, protons and neutrons. Changes in the shell structures of nuclei far from stability can be directly probed by mass measurements.

In the neutron-rich Cr and Ti region, the shell evolution around the ls-closed neutron number of 40 has attracted considerable attention in recent years. The onset of island of inversion (IoI), which was discovered around ^{32}Mg[1] for the first time, was theoretically predicted along the $N = 40$ isotones.[2] The IoI is well characterized by the emergence of the Jahn-Teller (JT) stabilization,[3,4] which is promoted by configuration mixing on the Fermi surface. The goal of the present experiment was to confirm the presence or absence of this effect through the first mass measurements of neutron-rich Ti isotopes around $N = 40$.

The experiment was performed at the RI Beam Factory (RIBF) at RIKEN, which is operated by RIKEN Nishina Center and Center for Nuclear Study, University of Tokyo. The masses were measured directly by using the TOF-$B\rho$ technique. Neutron-rich isotopes were produced by fragmentation of a ^{70}Zn primary beam at 345 MeV/nucleon in a ^{9}Be target. The fragments were separated by the BigRIPS separator,[5] and transported in the High-Resolution Beamline to the SHARAQ spectrometer.[6]

Figure 1 shows the present results of the two-neutron separation energy (S_{2n}) of Sc, Ti, and V isotopes, together with theoretical S_{2n} systematics obtained from the macroscopic-microscopic Weizsäcker-Skyrme-type formula with treatments of two radial basis functions corrections (LZU).[9] This model largely reproduces the S_{2n} trends including the present results. However, it is obvious that the model underestimates the S_{2n} values in ^{61,62}Ti isotopes. The results, therefore, confirm that ^{62}Ti becomes very stable.

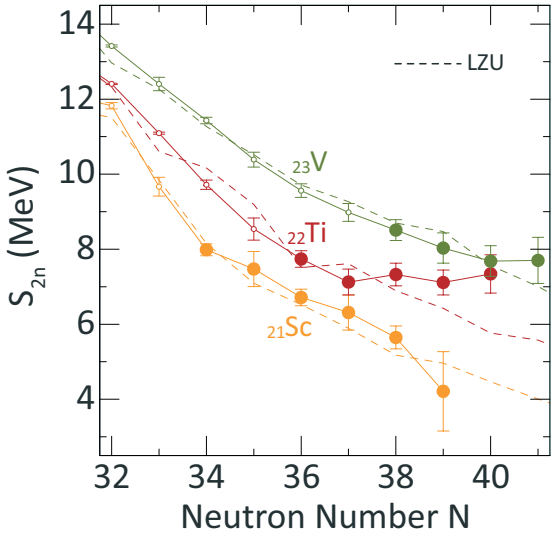

Fig. 1. Two-neutron separation energies (S_{2n}) of Sc, Ti, and V isotopes around $N = 40$. Closed symbols indicate values determined from the present experimental masses, and open symbols are literature values.[7,8] Solid lines connect isotopes, and dashed lines show theoretical predictions by the LZU model.[9]

Since the behavior of the mass surface is similar to that in the $N = 20$ IoI, it is reasonably demonstrated that the JT stabilization arises in the vicinity of ^{62}Ti. The theory[4] suggests that this enhancement of the JT stabilization around ^{62}Ti is caused by configuration mixing among neutron $fpgd$ orbitals enhanced by the degeneracy of the neutron orbitals.

† Condensed from the article in Phys. Rev. Lett. **125**, 122501 (2020)

*1 Center for Nuclear Study, The University of Tokyo
*2 Dept. of Physics & Astronomy, University of Tennessee
*3 Dept. of Physics, Tokyo City University
*4 RIKEN Nishina Center
*5 Dept. of Physics, University of Notre Dame
*6 Dept. of Physics, Kyoto University
*7 RCNP, Osaka University
*8 Dept. of Advanced Energy Engineering Sciences, Kyushu University
*9 Dept. of Physics, Rikkyo University
*10 FRIB, MSU
*11 NSCL, MSU
*12 Dept. of Physics, Tokyo University of Science
*13 Dept. of Physics, Tokyo Institute of Technology

References

1) E. K. Warburton, J. A. Becker, B. A. Brown, Phys. Rev. C **41**, 1147 (1990).
2) B. A. Brown, Prog. Part. Nucl. Phys. **47**, 517 (2001).
3) H. A. Jahn, E. Teller, Proc. Poy. Soc. **A161**, 220 (1937).
4) P. -G. Reinhard, E. W. Otten, Nucl. Phys. **A420**, 173 (1984).
5) T. Kubo, Nucl. Instrum. Methods Phys. Res. B **204**, 97 (2003).
6) T. Uesaka *et al.*, Prog. Theor. Exp. Phys. **2012**, 03C007 (2012).
7) M. Wang *et al.*, Chin. Phys. C **41**, 030003 (2017).
8) Z. Meisel *et al.*, Phys. Rev. C **101**, 052801(R) (2020).
9) N. -N. Ma *et al.*, Chin. Phys. C **43**, 044105 (2019).

Surface localization of the dineutron in ^{11}Li†

Y. Kubota,[*1,*2] A. Corsi,[*3] G. Authelet,[*3] H. Baba,[*1] C. Caesar,[*4] D. Calvet,[*3] A. Delbart,[*3] M. Dozono,[*2] J. Feng,[*5] F. Flavigny,[*6] J. -M. Gheller,[*3] J. Gibelin,[*7] A. Giganon,[*3] A. Gillibert,[*3] K. Hasegawa,[*8] T. Isobe,[*1] Y. Kanaya,[*9] S. Kawakami,[*9] D. Kim,[*14] Y. Kikuchi,[*10,*1,*11] Y. Kiyokawa,[*2] M. Kobayashi,[*2] N. Kobayashi,[*12] T. Kobayashi,[*8] Y. Kondo,[*13] Z. Korkulu,[*14,*15] S. Koyama,[*12] V. Lapoux,[*3] Y. Maeda,[*9] F. M. Marqués,[*7] T. Motobayashi,[*1] T. Miyazaki,[*12] T. Nakamura,[*13] N. Nakatsuka,[*16] Y. Nishio,[*17] A. Obertelli,[*3] K. Ogata,[*18,*11] A. Ohkura,[*17] N. A. Orr,[*7] S. Ota,[*2] H. Otsu,[*1] T. Ozaki,[*13] V. Panin,[*1] S. Paschalis,[*4] E. C. Pollacco,[*3] S. Reichert,[*19] J. -Y. Roussé,[*3] A. T. Saito,[*13] S. Sakaguchi,[*17] M. Sako,[*1] C. Santamaria,[*3] M. Sasano,[*1] H. Sato,[*1] M. Shikata,[*13] Y. Shimizu,[*1] Y. Shindo,[*17] L. Stuhl,[*14,*1] T. Sumikama,[*8] Y. L. Sun,[*3] M. Tabata,[*17] Y. Togano,[*13] J. Tsubota,[*13] Z. H. Yang,[*1] J. Yasuda,[*17] K. Yoneda,[*1] J. Zenihiro,[*1] T. Uesaka[*1]

A unique aspect of nuclei with respect to other fermionic many-body systems is the emergence of a spatially compact two-neutron pair, *dineutron*,[1] which is completely different from the Bardeen-Cooper-Schrieffer-(BCS)-like pairings that appear in momentum space. The dineutron correlation is presumed to be important for elucidating the stabilities and exotic structures of neutron drip-line nuclei, as well as the infinite nuclear matter. Studies on the dineutron formation and the density dependence of ^{11}Li are crucial because it has a halo structure: the matter density gradually varies from the saturated core to the very low-density tail where only valence neutrons exist. It allows the study of the density-dependent properties of the dineutron correlation.

The quasifree (p, pn) reaction was employed to probe the entire volume of ^{11}Li with the least effect of absorption. The measurement was performed at RIBF using the SAMURAI spectrometer,[2] combined with the 15-cm-thick liquid hydrogen target MINOS[3] and dedicated (p, pn) setup.

The strength of the dineutron in ^{11}Li was evaluated by using the correlation angle θ_{nf}, which is the angle between the momentum vectors of two valence neutrons. The spatially compact dineutron should have an angle larger than 90°. Figure 1 shows that the mean value of

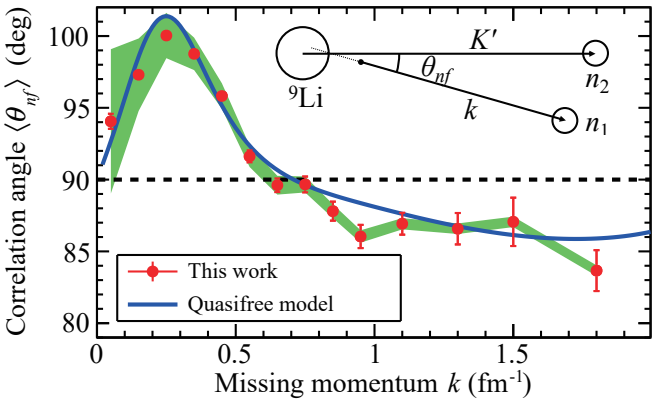

Fig. 1. Mean values of the correlation angle. Black dashed line shows the expected $\langle\theta_{nf}\rangle$ value for the two uncorrelated neutrons. Inset shows a schematic of θ_{nf} in ^{11}Li.

θ_{nf} clearly depends on the missing momentum k, which is the measure of the radial position of the two neutrons in ^{11}Li. The peak structure of $\langle\theta_{nf}\rangle$ at $k \sim 0.3$ fm^{-1} can be interpreted as the localization of the dineutron, which is maximized at $r \sim 3.6$ fm from the center of the ^{9}Li core. The quasi-free model[4] well reproduces the experimental data.

The result implies that the dineutron correlation is prominent only around the ^{9}Li core surface where the density is $10^{-3} \lesssim \rho/\rho_0 \lesssim 10^{-2}$, and it becomes weaker at the tail of the halo, where the density is extremely low. It is consistent with the Hartree-Fock-Bogoliubov calculation[5] for infinite nuclear matter. If this is a universal characteristic of the dineutron correlation, it should appear at the low-density surface of any neutron-rich nuclei. Future (p, pn) experiments should investigate the nature of the dineutron correlation in nuclei of interest, such as ^{6}He, ^{16}C, and ^{24}O.

† Condensed from the article in Phys. Rev. Lett. **125**, 252501 (2020)

*1 RIKEN Nishina Center
*2 Center for Nuclear Study, University of Tokyo
*3 Département de Physique Nucléaire, IRFU, CEA, Université Paris-Saclay
*4 Department of Physics, Technische Universität Darmstadt
*5 Department of Physics, Peking University
*6 IPN Orsay, Université Paris Sud
*7 LPC Caen, ENSICAEN, Université de Caen Normandie
*8 Department of Physics, Tohoku University
*9 Department of Applied Physics, University of Miyazaki
*10 Tokuyama College, National Institute of Technology
*11 Department of Physics, Osaka City University
*12 Department of Physics, University of Tokyo
*13 Department of Physics, Tokyo Institute of Technology
*14 Center for Exotic Nuclear Studies, Institute for Basic Science
*15 Institute for Nuclear Research, Hungarian Academy of Sciences
*16 Department of Physics, Kyoto University
*17 Department of Physics, Kyushu University
*18 Research Center for Nuclear Physics, Osaka University
*19 Department of Physics, Technische Universität München

References

1) A. B. Migdal, Soviet J. Nucl. Phys. **16**, 238 (1973).
2) T. Kobayashi *et al.*, Nucl. Instrum. Methods Phys. Res. B **317**, 294 (2013).
3) A. Obertelli *et al.*, Eur. Phys. J. A **50**, 8 (2014).
4) Y. Kikuchi *et al.*, Prog. Theor. Exp. Phys. **2016**, 103D03 (2016).
5) M. Matsuo, Phys. Rev. C **73**, 044309 (2006).

Probing alpha clusters in the low-density region of the nuclear surface†

J. Tanaka,[*1] Z. H. Yang,[*2] S. Typel,[*3,*4] and T. Uesaka[*1] for the RCNP $(p, p\alpha)$ Collaboration

The formation of alpha clusters in the ground state of heavy nuclei has been unclear for many years, both theoretically and experimentally. Although the existence of preformed alpha particles in alpha-decay nuclei is an essential element in the theory of alpha decay,[1] it was challenging to explain the appearance of alpha clusters with the conventional mean-field models. In recent years, theoretical research based on the generalized density functional made progress and predicted that alpha clusters can exist in the low-density region of the nuclear surface.[2] It was shown that the formation amplitudes of alpha clusters on the nuclear surface of tin isotopes decrease monotonically with increasing neutron excess, and the formation amplitude of ^{124}Sn is approximately half that of ^{112}Sn.[3] To directly prove the existence of alpha clusters in the surface of nuclei, the quasi-free alpha knockout reaction is appropriate.

Our group performed an experiment at the Research Center for Nuclear Physics of Osaka University. A proton beam at 392 MeV generated at the cyclotron facility bombarded stable tin targets (^{112}Sn, ^{116}Sn, ^{120}Sn, ^{124}Sn) with an intensity of 100 nA. To achieve the high-precision measurement of knocked-out alpha particles, we used double-arm spectrometers. The experimental setup is shown in Fig. 1. A proton beam impinges on a tin target (red arrow from the left). Following a $^{A}\mathrm{Sn}(p, p\alpha)^{A-4}\mathrm{Cd}$ reaction (emphasized in the inset),

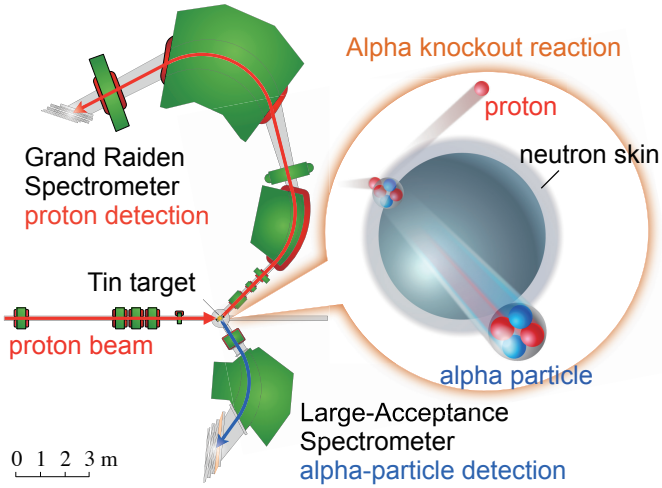

Fig. 1. Schematic illustration of the experimental setup.

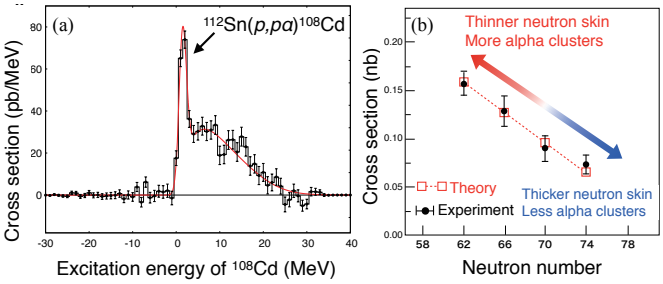

Fig. 2. (a) Missing-mass spectrum of the $^{112}\mathrm{Sn}(p, p\alpha)^{108}\mathrm{Cd}$ reaction. (b) Neutron-number dependence of the $(p, p\alpha)$ reaction cross sections.

a scattered proton is analyzed by the Grand Raiden spectrometer at an angle of 45.3°. A knocked-out alpha particle is analyzed by the LAS spectrometer at an angle of 60.0°.

The momenta of scattered protons and knocked-out alpha particles were analyzed with the Grand Raiden spectrometer[4] and a large acceptance spectrometer, respectively. The missing-mass spectra of $\mathrm{Sn}(p, p\alpha)\mathrm{Cd}$ reactions were constructed from these momenta, and strong transitions from the ground state of Sn to the vicinity of the ground state of Cd were observed. Figure 2 shows (a) the missing-mass spectrum of $^{112}\mathrm{Sn}(p, p\alpha)^{108}\mathrm{Cd}$. The peak indicated by the arrow is the transition from the ground state of ^{112}Sn to the vicinity of the ground state of ^{108}Cd. Figure 2(b) shows the isotope dependence of cross sections.[5] The black filled circles indicate experimental data, and the red open squares indicate theoretical predictions, where the theoretical alpha-cluster formation probabilities were converted to the $(p, p\alpha)$ cross sections using nuclear reaction calculations based on the distorted wave impulse approximation. A good agreement with the theoretical conjecture is observed.

The theoretical study further suggested not only the control of the formation of alpha clusters by neutron skins, but also the suppression of neutron skins by the appearance of alpha clusters. The series of experimental studies of surface alpha clusters have the potential to revise the parameters correlated with the neutron-skin thickness in the nuclear equation of state in the future.

† Condensed from the article in Science **371**, 260 (2021)
*1 RIKEN Nishina Center
*2 Research Center of Nuclear Physics, Osaka University
*3 Technische Universität Darmstadt, Fachbereich Physik, Institut für Kernphysik
*4 GSI Helmholtzzentrum für Schwerionenforschung GmbH

References

1) G. Gamow, Z. Phys. **51**, 204 (1928).
2) S. Typel *et al.*, Phys. Rev. C **81**, 015803 (2010).
3) S. Typel, Phys. Rev. C **89**, 064321 (2014).
4) M. Fujiwara *et al.*, Nucl. Instrum. Methods Phys. Res. A **422**, 484 (1999).
5) J. Tanaka *et al.*, Science **371**, 260 (2021).

Reaction cross sections on a deuteron as a probe of nuclear radii†

W. Horiuchi,[*1] Y. Suzuki,[*2,*3] T. Uesaka,[*3,*4] and M. Miwa[*3,*4]

Total reaction or interaction cross section measurement has been used as a standard tool to determine the nuclear radii of unstable nuclei. The total reaction cross section of a proton target is known to exhibit strong incident energy dependence that can be used to deduce both the neutron and proton radii.[1,2] A neutron target may also be useful for the structual study of the unstable nuclei as it has a different sensitivity compared to that of the proton target but no neutron target exists. Since the deuteron is composed of neutrons and protons, the total reaction cross section on a deuteron target must include both information on the nucleus-neutron and the nucleus-proton scattering profiles.

To describe high-energy nucleus-deuteron reactions, we employ the Glauber model,[3] wherein the nucleus-nucleon total reaction cross section σ_N $(N = n, p)$ can be obtained by $\sigma_N = \int d\boldsymbol{b}\ (1 - \left|e^{i\chi_N^P(\boldsymbol{b})}\right|^2)$. Under the optical-limit approximation, the optical phase-shift function $e^{i\chi_N^P(\boldsymbol{b})}$ at the impact parameter vector $\boldsymbol{b}$ can be evaluated using the projectile's density and nucleon-nucleon (NN) scattering profiles. A unique advantage of the deuteron target is that one can calculate the phase-shift function accurately using its ground-state wave function $\phi_d(\boldsymbol{r})$. The nucleus-deuteron total reaction cross section $\sigma_d = \int d\boldsymbol{b}\,(1 - P_d(\boldsymbol{b}))$, and it can be obtained with

$$P_d(\boldsymbol{b}) = \left| \int d\boldsymbol{r}\,|\phi_d(\boldsymbol{r})|^2 e^{i\chi_p^P(\boldsymbol{b}+\frac{1}{2}\boldsymbol{s})+i\chi_n^P(\boldsymbol{b}-\frac{1}{2}\boldsymbol{s})} \right|^2, \quad (1)$$

where $\boldsymbol{r} = (\boldsymbol{s}, z)$ with z being the beam direction.

In most measurements, the interaction cross section $\sigma_{d:I}$ is observed but not σ_d. Since σ_d includes all inelastic cross sections, $\sigma_d > \sigma_{d:I}$ always holds. However, a calculation of $\sigma_{d:I}$ demands all bound-state wave functions of the projectile, which is difficult in general. For the deuteron target, provided the projectile has only one bound state, *i.e.*, its ground state, one can evaluate $\sigma_d - \sigma_{d:I}$ with the same inputs required to evaluate σ_d as $\Delta_0\sigma = \int d\boldsymbol{b}\,(P_0(\boldsymbol{b}) - P_d(\boldsymbol{b}))$ with

$$P_0(\boldsymbol{b}) = \int d\boldsymbol{r}\,|\phi_d(\boldsymbol{r})|^2 \left| e^{i\chi_p^P(\boldsymbol{b}+\frac{1}{2}\boldsymbol{s})+i\chi_n^P(\boldsymbol{b}-\frac{1}{2}\boldsymbol{s})} \right|^2. \quad (2)$$

If the projectile has more than one bound state, $\Delta_0\sigma$ gives the lower bound of $\sigma_d - \sigma_{d:I}$.

Figure 1 displays σ_d, σ_p, and σ_n for ^{30}Ne as a function of incident energy. σ_d is always significantly smaller than $\sigma_p + \sigma_n$ by about 70–90% of $\sigma_p + \sigma_n$ due to the "eclipse" of the constituent neutron and proton.[3] The energy dependence of these cross sections follows that of the NN total cross section. The information of the nucleus-neutron scattering profile is included in σ_d. As already mentioned, the deuteron target has the advantages that the upper bound of the interaction cross section can be evaluated reliably using the deuteron wave function. Further, Fig. 1 displays the upper bound of the interaction cross section $\sigma_{d:I}$ and $\Delta_0\sigma$ for ^{30}Ne. $\Delta_0\sigma$ has at maximum 60–70 mb at around 80 MeV/nucleon, which is about 6% of σ_d. In addition, $\Delta_0\sigma$ decreases with increasing incident energy. The ratio $\Delta_0\sigma/\sigma_d$ becomes at most few percent beyond 300 MeV/nucleon. For the unstable nuclei near the dripline that has only one bound state, a reliable interaction cross section can be obtained, and this greatly improves the accuracy of the radius extraction. We conclude that measuring the total reaction cross sections on both deuteron and proton targets is the most unambiguous and promising approach to determine the neutron and proton radii of unstable nuclei.

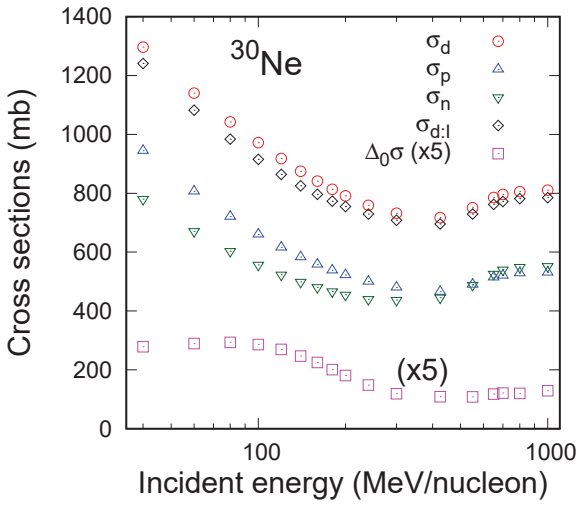

Fig. 1. Various cross sections for ^{30}Ne adopted from the original paper. See text for details.

References

1) W. Horiuchi, Y. Suzuki, T. Inakura, Phys. Rev. C **89**, 011601(R) (2014).
2) W. Horiuchi, S. Hatakeyama, S. Ebata, Y. Suzuki, Phys. Rev. C **93**, 044611 (2016).
3) R. J. Glauber, *Lectures in Theoretical Physics*, edited by W. E. Brittin, L. G. Dunham (Interscience, New York, 1959), Vol. 1, p. 315.

† Condensed from the article in Phys. Rev. C **102**, 054601 (2020)

*1 Department of Physics, Hokkaido University
*2 Department of Physics, Niigata University
*3 RIKEN Nishina Center
*4 Department of Physics, Saitama University

Mean-square radius of the neutron distribution and skin thickness derived from electron scattering†

H. Kurasawa,[*1] T. Suda,[*2,*3] and T. Suzuki[*2]

To the authors' knowledge, this is the first study to deduce the neutron distribution from electron scattering data in the history of nuclear physics.[1)]

The question how neutrons are distributed in nuclei has been a longstanding problem. Although it is one of the most fundamental problems in nuclear physics, the neutron distribution has not been well determined yet, because there is no simple and reliable method to explore it experimentally.[2)] In contrast to the neutron distribution, the proton distribution has been widely investigated through the nuclear charge density deduced from electron scattering.[3)] Electron scattering is an unambiguous and unique tool to examine the charge distribution, because the electromagnetic interaction is well understood and allows reactions that do not disturb the nuclear ground-state properties.[4)]

So far, electron scattering has been believed to be useful for the study of the only proton distribution and has not been discussed in the context of the neutron distribution in nuclei.[4)] The SCRIT in RIKEN[5)] also constructed with the primary objective of exploring the proton distribution in unstable nuclei, although the neutron distribution plays a crucial role in the stability of neutron-rich nuclei. Such dogma is based on the fact that the neutron charge density is approximately 1% of the total nuclear charge density and oscillates as a function of the nuclear coordinate, yielding zero integrated charge.

Recently, the precise expressions for the moments of the nuclear charge density were derived according to relativistic quantum mechanics.[6)] It has been shown that the second-order moment of the nuclear charge density(R_c^2) is dominated by the mean-square radius (msr) of the point proton distribution (R_p^2), while the nth (≥ 4)-order moment depends on the (n-2)th-order moment of the point neutron distribution also. For example, the fourth-order moment (Q_c^4) of the charge density depends on the msr of the point neutron distribution (R_n^2). The contribution of R_n^2 to Q_c^4 is dominated by the number of excess neutrons.

The present authors have analyzed experimental data of R_c^2 and Q_c^4 deduced from the electron scattering off ^{40}Ca, ^{48}Ca, and ^{208}Pb, which are available at present.[3)] First, using relativistic and non-relativistic mean field models accumulated over the last 50 years in nuclear physics, the linear relationship between the various moments are explored with the use of the least-squares method. Next, from the intersection of the predicted least-square lines and the lines of the experimental value for R_c^2 or Q_c^4 , the values of R_n^2 together with R_p^2 of those nuclei have been estimated. They are obtained within 1% accuracy, including both experimental error and the standard deviation of the least-square lines.[1)]

This paper opens a new possibility of electron scattering as a clean and practical probe to extract neutron density information. As the contributions from the neutron density to the charge density are expected to increase in neutron-rich nuclei, the new electron scattering facilities in the world[5)] which are led by the SCRIT[7)] would make the forthcoming study of unstable nuclei more efficient and stimulating, both experimentally and theoretically.

References

1) H. Kurasawa, T. Suda, T. Suzuki, Prog. Theor. Exp. Phys. **2021**, 013D02 (2021).
2) M. Thiel *et al.*, J. Phys. G **46**, 093003 (2019).
3) H. De Vries, C. W. De Jager, C. De Vries, Atom. Data Nucl. Data Tables **36**, 495 (1987).
4) T. deForest, J. D. Walecka, Adv. Phys. **15**, 1 (1966).
5) T. Suda, H. Simon, Prog. Part. Nucl. Phys. **96**, 1 (2017).
6) H. Kurasawa, T. Suzuki, Prog. Theor. Exp. Phys. **2019**, 113D01 (2019).
7) K. Tsukada *et al.*, Phys. Rev. Lett. **118**, 262501 (2017).

† Condensed from the article in Prog. Theor. Exp. Phys. **2021**, 013D02 (2021)

*1 Department of Physics, Chiba University
*2 Research Center for Electron-Photon Science, Tohoku University
*3 RIKEN Nishina Center

Isotopic production of high-radiotoxic nuclide ^{90}Sr via proton- and deuteron-induced reactions†

R. Matsumura,[*1,*2] H. Otsu,[*1] H. Wang,[*1] N. Chiga,[*1] S. Kawase,[*3] K. Nakano,[*3] H. Sakurai,[*1,*4] M. Shikata,[*5] S. Takeuchi,[*5] and Y. Togano[*5] for the ImPACT-RIBF Collaboration

The processing of spent fuels from nuclear power plants is a worldwide problem. The by-products of the reprocessing of spent fuels are high-level radioactive wastes, which contain minor actinides and fission products. In this study, we focus on ^{90}Sr, which is the most radiotoxic nuclide in fission products.[1] There is a strong desire to develop nuclear transmutation technology using accelerator facilities to reduce these harmful nuclides. The simplest method is to irradiate the radioactive waste with a neutron beam. However, it is not well known how much and into which nuclide ^{90}Sr is transmuted in this reaction. Therefore, it is essential to study the reaction cross sections to each nuclide from ^{90}Sr in advance. From this perspective, the inverse kinematics, *i.e.*, incident ^{90}Sr beam on light-particle targets, is an effective method for identifying reaction products in the forward direction.

The experiment was performed at RIBF. A secondary beam including ^{90}Sr was produced by the in-flight fission of ^{238}U at 345 MeV/nucleon on a 3-mm-thick ^{9}Be production target, selected and identified event-by-event using the TOF-$B\rho$-ΔE method.[2] Beam particles at 104 MeV/nucleon bombarded CH_2, CD_2, and C reaction targets placed at the entrance of ZDS. The residual nuclei produced in reactions were identified in ZDS with the same method as BigRIPS. Because the momentum acceptance of ZDS is limited to ±3%, the experiment was conducted using five different momentum settings ($\Delta(B\rho)/B\rho = -9$, -6, -3, 0, and $+3$%) for each target to accept a wide range of the mass-to-charge ratio A/Q. The reaction cross sections were deduced from the number of incident ^{90}Sr nuclides, the number of residual particles of each species, and the thickness of the target. The backgrounds of carbon from CH_2 and CD_2 targets and beam-line materials were subtracted using empty and carbon target runs.

The data points above 1 mb were obtained with good statistics. These were compared with the calculations using the Particle and Heavy Ion Transport code System (PHITS),[3] as shown in Fig. 1. The Liége Intranuclear Cascade model (INCL4.6) and the Generalized Evaporation Model (GEM) were employed in the calculations. It is observed that the calculation results were overestimated around the mass number of the projectile. Few-

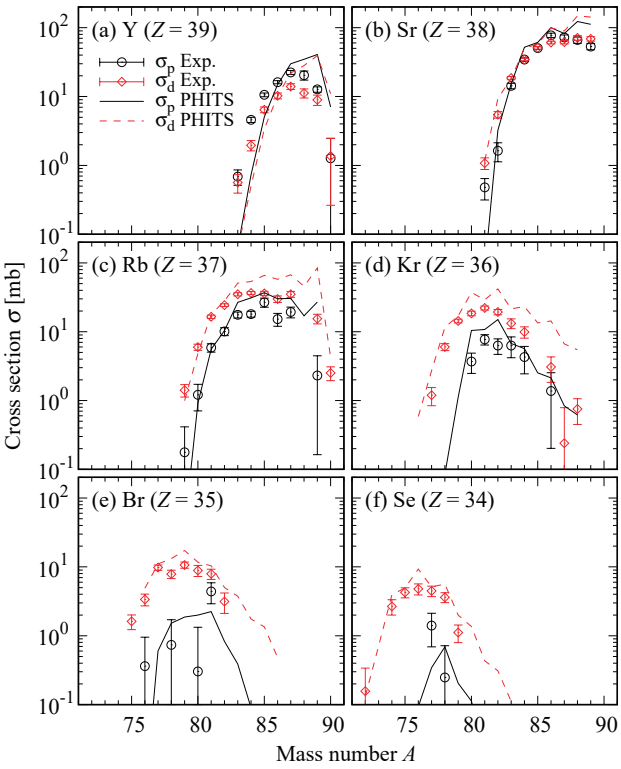

Fig. 1. Isotopic-production cross sections of proton- (circles) and deuteron-induced (diamonds) reactions and those obtained from the PHITS calculations (proton for solid and deuteron for dotted lines).

nucleon removal reactions are not interpreted properly in INCL because momentum distributions of the nuclear surface are treated in a semiclassical way.[4] In addition, even-odd staggering effects appeared excessively for nuclides produced by emitting many nucleons. This may be controlled to some extent by considering the competition between particle and γ-ray emissions, as well as the discrete energy levels, in the GEM.

In the lower energy deuteron-induced reaction, it has been observed that the initial reaction mechanism changes drastically due to the breakup into proton and neutron during the reaction.[5] Thus, we would also like to obtain the reaction data for ^{90}Sr in the near future.

† Condensed from the proceedings in JAEA-Conf 2021-001
*1 RIKEN Nishina Center
*2 Department of Physics, Saitama University
*3 Department of Advanced Energy Engineering Science, Kyushu University
*4 Department of Physics, The University of Tokyo
*5 Department of Physics, Tokyo Institute of Technology

References

1) K. Nishihara, JAEA-Data/Code **2010-012** (2010).
2) N. Fukuda *et al.*, Nucl. Instrum. Methods Phys. Res. B **317**, 323 (2013).
3) T. Sato *et al.*, J. Nucl. Sci. Technol. **55**, 684 (2018).
4) D. Mancusi *et al.*, Phys. Rev. C **91**, 034602 (2015).
5) H. Wang *et al.*, Commun. Phys. **2**, 78 (2019).

CP-odd gluonic operators in QCD spin physics†

Y. Hatta*1,*2

The explanation of matter-antimatter asymmetry of the universe requires new origins of CP-violation beyond the Standard Model (BSM). One of the interesting CP-violating operators that can be induced in the QCD Lagrangian due to BSM physics is the Weinberg operator.[1] In this report I point out a novel relation between the hadronic matrix element of the Weinberg operator and a certain twist-four correction in polarized Deep Inelastic Scattering (DIS). Such a relation suggests an exciting possibility that polarized DIS experiments can provide useful information to the physics of the nucleon electric dipole moment (EDM), or more generally, BSM-origins of hadronic CP violations.

The Weinberg operator is a dimension-six purely gluonic operator

$$\mathcal{O}_W = g f_{abc} \tilde{F}^a_{\mu\nu} F^{\mu\alpha}_b F^{\nu}_{c\alpha}. \tag{1}$$

This operator violates CP and can be induced in the QCD Lagrangian by physics beyond the Standard Model. It is considered as one of the candidate operators to generate a large EDM of the nucleons and nuclei.

The key observation is the following exact operator identity

$$\begin{aligned} \mathcal{O}_W &= -\partial^\mu (\tilde{F}_{\mu\nu} \overleftrightarrow{D}_\alpha F^{\nu\alpha}) - \frac{1}{2} \tilde{F}_{\mu\nu} \overleftrightarrow{D}^2 F^{\mu\nu} \\ &\equiv \mathcal{O}_4 + \mathcal{O}_D, \end{aligned} \tag{2}$$

Eq. (2) shows that one can choose $\mathcal{O}_W$ and $\mathcal{O}_4$ as the independent basis of operators and study their mixing. Due to the equation of motion, one can write

$$\mathcal{O}_4 \approx \partial^\mu (\bar{\psi} g \tilde{F}_{\mu\nu} \gamma^\nu \psi), \tag{3}$$

to linear order in partial derivative ∂^μ. Such mixing is usually neglected in the literature because $\mathcal{O}_4$ is a total derivative and hence does not contribute to the CP-violating effective action $\int d^4x \mathcal{O}_4 = 0$. However, when it comes to hadronic matrix elements, mixing becomes crucial because only the nonforward matrix element is nonvanishing. Specifically, their RG equation takes the form

$$\frac{d}{d\ln\mu^2} \begin{pmatrix} \mathcal{O}_W \\ \mathcal{O}_4 \end{pmatrix} = -\frac{\alpha_s}{4\pi} \begin{pmatrix} \gamma_W & \gamma_{12} \\ 0 & \gamma_4 \end{pmatrix} \begin{pmatrix} \mathcal{O}_W \\ \mathcal{O}_4 \end{pmatrix} \tag{4}$$

where

$$\gamma_W = \frac{7}{3} N_c + \frac{2}{3} n_f \tag{5}$$

is the anomalous dimension of the Weinberg operator.[2] The anomalous dimension of $\mathcal{O}_4$ is the same as that of the undifferentiated, twist-four operator $\bar{\psi} g \tilde{F}^{\mu\nu} \gamma_\nu \psi$ and is known to be[3]

$$\gamma_4 = \frac{8}{3} C_F + \frac{2}{3} n_f. \tag{6}$$

To determine the off-diagonal component γ_{12}, I evaluate the following three-point Green's function

$$\langle 0 | \mathrm{T}\{\psi(-k) A^\rho_a(q) \bar{\psi}(p) \mathcal{O}_W\} | 0 \rangle \tag{7}$$

with off-shell momenta and nonzero momentum transfer $\Delta = k - p - q \neq 0$. The result is

$$\gamma_{12} = -3N_c. \tag{8}$$

It immediately follows that the following linear combination is the eigenstate of the RG evolution

$$\mathcal{O}_W + \frac{\gamma_{12}}{\gamma_W - \gamma_4} \mathcal{O}_4 = \mathcal{O}_W - \frac{9N_c^2}{3N_c^2 + 4} \mathcal{O}_4. \tag{9}$$

Since this operator has a rather large anomalous dimension $\gamma_W \sim 10$, in particular larger than γ_4 by a factor of about 2, at high enough renormalization scales μ^2 one has

$$\langle \mathcal{O}_W \rangle \approx \frac{9N_c^2}{3N_c^2 + 4} \langle \mathcal{O}_4 \rangle \approx 2.61 \langle \mathcal{O}_4 \rangle, \tag{10}$$

In terms of the nucleon matrix elements

$$\langle P | \bar{\psi} g \tilde{F}^{\mu\nu} \gamma_\nu \psi | P \rangle = -2 f_0 M^2 S^\mu \tag{11}$$

$$\frac{1}{M^3} \langle P' | g f^{abc} \tilde{F}^a_{\mu\nu} F^{\mu\sigma}_b F^{\nu}_{c\sigma} | P \rangle = 4E \bar{u}' i\gamma_5 u. \tag{12}$$

I get

$$E \approx \frac{9N_c^2}{2(3N_c^2 + 4)} f_0 \approx 1.3 f_0. \tag{13}$$

Therefore, one can evaluate the matrix element E of the Weinberg operator through the measurement of the f_0 parameter relevant to the twist-four corrections in polarized DIS.[4,5] f_0 can be extracted from the $g_1(x)$ structure function measured at the future Electron-Ion Collider (EIC) in the U.S. This is a new connection between the EIC and physics beyond the Standard Model. It will demonstrate the EIC's unique capability to address low-energy nucleon observables in a high energy collider.

† Condensed from the article in Phys. Rev. D **102**, 094004 (2020)

*1 RIKEN Nishina Center
*2 Physics Department, Brookhaven National Laboratory

References
1) S. Weinberg, Phys. Rev. Lett. **63**, 2333 (1989).
2) A. Y. Morozov, Sov. J. Nucl. Phys. **40**, 505 (1984).
3) E. V. Shuryak, A. I. Vainshtein, Nucl. Phys. B **199**, 451 (1982).
4) E. V. Shuryak, A. I. Vainshtein, Nucl. Phys. B **201**, 141 (1982).
5) X. D. Ji, P. Unrau, Phys. Lett. B **333**, 228 (1994).

Start the operation of AVF-BIS and its performance evaluation as a successor system to BIS

M. Komiyama,[*1] A. Uchiyama,[*1] M. Fujimaki,[*1] M. Hamanaka,[*2] T. Nakamura,[*2] and N. Fukunishi[*1]

The beam interlock system (BIS) for machine protection began operation in 2006 along with the beam commissioning of RIBF.[1)] The BIS is still under stable operation; however, its maintenance has become gradually difficult because some of the modules used in the system are discontinued and cannot be replaced. In addition, another problem is the declining performance of the system because of the increase in the number of inputs to the system during its 14 years of operation. Measurements performed in summer 2020 show that the average response time of BIS, the time from when the system receives the interlock signal to when the beam is stopped, is approximately 18 ms, which is greater than the system design value of 10 ms. To operate higher-power beams in the future more safely, a response speed of 10 ms or less is required. Therefore, we have been developing a successor system to the BIS for a few years, and we applied the prototype to the AVF cyclotron and its low-energy experimental facility as AVF-BIS in summer 2020. We will report its operation status and performance evaluation.

The hardware constitution and process flow of the prototype are shown in Fig. 1; the details are reported in Ref. 2). One new advantage of the prototype is that it has a multi-central processing unit (CPU) configuration that can shorten the response time of the system by using different CPUs according to the speed required by each process such as stopping the beam after receiving the interlock signal and parameter setting of the system. We set up the prototype comprising two programmable logic controller (PLC) stations: one with a Linux-based CPU and a sequence CPU was installed in the vault for the polarized ion source, and the other with a sequence CPU was installed in vault C for the power supplies for the magnets. The communication between the two stations was performed through FL-net (an open network protocol used for interconnection between controllers) using dedicated wiring; the signal setting and monitoring are performed by the terminal in the control room via the Ethernet. In AVF-BIS, 25 digital inputs and 24 analog inputs are used as the interlock signals; 5 digital outputs are used to stop a beam in total.

As a result of the oscilloscope-measured signal transmission speed in the AVF-BIS, the observed response time averaged 2 ms and 5.7 ms, respectively, within one station and with both stations. The average response time is 1.4 ms and 3.8 ms for the operation within one station and using two stations, respectively, in the test prior to the introduction of the prototype as AVF-BIS. The difference between the two measurements is attributed to the difference in the length of the ladder program executed on the sequence CPU: the ladder program became longer as a result of the repeated program modifications when operating the prototype as the AVF-BIS. However, it is sufficient as the performance of the AVF-BIS. When deploying the AVF-BIS in the same scale as the BIS that consists of 5 PLC stations with roughly 400 signals, the response time is estimated to be almost 10 ms. The basis for the estimation is as follows: increase the number of total signals and the time required for the signal transmission via FL-net increases depending on the number of PLC stations.

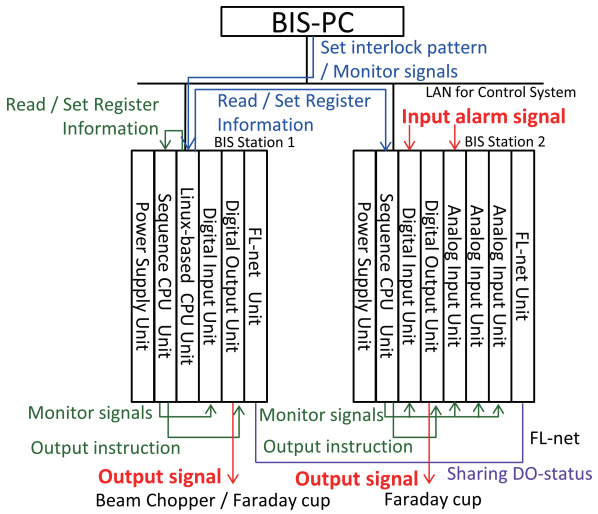

Fig. 1. Hardware constitution and process flow in the prototype. Blue lines represent communication via Ethernet, green lines represent communication via PLC bus, and purple lines represent communication via FL-net.

The above result shows that it is possible to achieve half the response time of the existing BIS by expanding the prototype to the successor system of the BIS; however, simultaneously, it shows that it limits the performance of the system. In a system with insufficient performance, it may not be possible to maintain the increase in the number of signals required to be monitored by the BIS in the future when a higher-power beam accelerated by RIBF, and another higher performance system may be required again. To avoid such a scenario, we have started to study a system with a field-programmable gate array (FPGA). The process that requires high speed is executed on the FPGA while the system is designed based on PLC. The system aims to reduce the response time to digital input signals to less than 1 ms.

*1 RIKEN Nishina Center
*2 SHI Accelerator Service Ltd.

References

1) M. Komiyama *et al.*, RIKEN Accel. Prog. Rep. **39**, 239 (2006).
2) M. Komiyama *et al.*, Proc. ICALEPCS2019, 2019-10, pp. 384–387.

HiCARI: High-resolution Cluster Array at RIBF

K. Wimmer,[*1,*2] P. Doornenbal,[*2] N. Aoi,[*3] H. Baba,[*2] F. Browne,[*2] C. Campbell,[*4] H. Crawford,[*4] H. De Witte,[*5] C. Fransen,[*6] H. Hess,[*6] S. Iwazaki,[*3] J. Kim,[*2] A. Kohda,[*3] T. Koiwai,[*7,*2] B. Mauss,[*2] B. Moon,[*2] T. Parry,[*8] P. Reiter,[*6] D. Suzuki,[*2] R. Taniuchi,[*9,*2] S. Thiel,[*6] and Y. Yamamoto[*3]

The RIKEN Nishina Center and the RIBF have been conducting in-beam γ-ray spectroscopy experiments at the forefront of nuclear structure research. Studies on exotic nuclei have focused on experiments employing beams with the largest possible isospin asymmetry. Low beam intensities require thick secondary reaction targets to achieve reasonable luminosity for measurements as well as a high efficiency γ-ray detector. The NaI(Tl) detector array DALI2[1)] features a very high detection efficiency, $\sim$20% for 1 MeV γ rays, but it has very limited resolution for the transition energies (approximately 10% FWHM for typical in-beam experiments). This detector is ideally suited for first spectroscopy experiments for nuclei at the limits of the known nuclear chart, as well as for studies featuring low level densities or selective population of states such as magic nuclei or Coulomb excitation. The detailed spectroscopy of complex level schemes and measurements of excited state lifetimes are not possible with the DALI2 array.

To overcome these limitation for in-beam γ-ray spectroscopy experiments at the RIBF, the HiCARI project was initiated. The HiCARI array comprises segmented high-purity germanium detectors. This provides excellent energy resolution to in-beam experiments by improving both the intrinsic energy resolution of the detector material itself and the position resolution for the interaction points of the γ ray with the detector material, which is required for the Doppler reconstruction of transition energies. The high resolution also allows determining the lifetimes of excited states by analyzing the shape of the peak in the Doppler reconstructed spectrum. For the HiCARI array, eight Miniball triple cluster detectors,[2)] 8(4)-fold segmented Clover detectors from IBS Korea (two clusters) and IMP China (four clusters), the RCNP quad-type 36-fold segmented tracking detector, and a triple segmented tracking detector P3 from LBNL Berkeley, which is also 36-fold segmented, are available. The final array installed at the F8 focus for experiments employing the ZeroDegree spectrometer comprises six Miniball triples, four Clovers, and the two tracking detector modules; it is shown in Fig. 1.

The readout electronics is based on the digital data acquisition of the GRETINA array.[3)] The signals of each central contact and segment electrode are digitized with a 100 MHz sampling rate and recorded. The energy is derived using a trapezoidal filter algorithm. For the tracking detectors, the energy and three-dimensional position information of individual interaction points within the segments is derived from the GRETINA signal decomposition analysis.

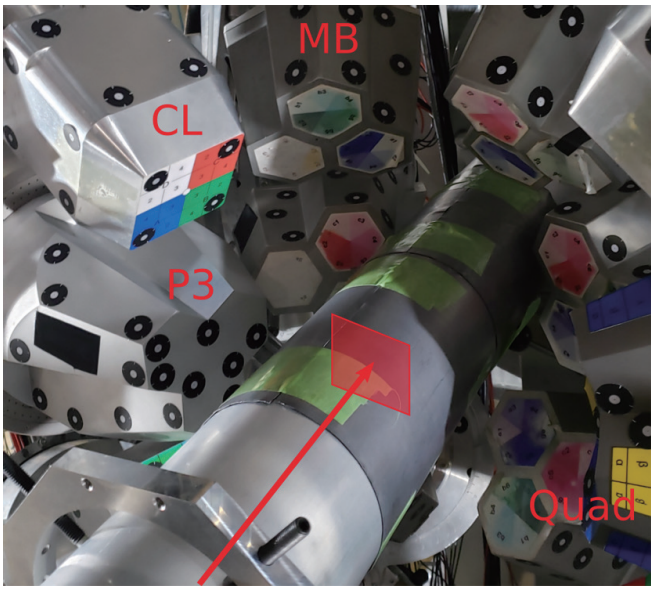

Fig. 1. HiCARI array located at the F8 focus. The beam enters through the beam pipe from the left. The forward ring ($\theta_{\rm lab} \sim 22$–55°) comprises six Miniball detector modules (MB). The tracking detectors (P3 and Quad) are located in the horizontal plane, with the Clover detectors (CL) arranged on top and bottom of the $\theta_{\rm lab} \sim 60$–85° ring.

Before the experimental campaign (for details on individual experiments, see contributions in this volume), a series of characterization and commissioning measurements was performed. In-beam measurements using an intense ^{82}Ge beam of approximately 260 MeV/nucleon impinging on Be and Au targets of various thicknesses were used to characterize the in-beam efficiency and resolution of the HiCARI array. The response to the high-intensity, low-energy radiation from atomic processes in the collision of beam and target was also investigated, and the effect of different shielding materials was explored.

*1 IEM-CSIC
*2 RIKEN Nishina Center
*3 RCNP, Osaka University
*4 Nuclear Science Division, Lawrence Berkeley National Laboratory
*5 Instituut voor Kern- en Stralingsfysica, KU Leuven
*6 Institut für Kernphysik, Universität zu Köln
*7 Department of Physics, University of Tokyo
*8 Department of Physics, University of Surrey
*9 Department of Physics, University of York

References

1) S. Takeuchi *et al.*, Nucl. Instrum. Methods Phys. Res. A **763**, 596 (2014).
2) N. Warr *et al.*, Eur. Phys. J. A **49**, 40 (2013).
3) S. Paschalis *et al.*, Nucl. Instrum. Methods Phys. Res. A **709**, 44 (2013).

Removing non-isobaric ions from an MRTOF-MS by periodic electric pulses

S. X. Yan,[*1,*2] M. Rosenbusch,[*2] W. D. Xian,[*3,*2] S. D. Chen,[*3,*2] Y. Hirayama,[*2] D. S. Hou,[*4,*2] S. Iimura,[*5,*6] H. Ishiyama,[*5] Y. Ito,[*7] S. Kimura,[*5] J. J. Liu,[*3,*2] H. Miyatake,[*2] S. Nishimura,[*5] T. Niwase,[*8,*5,*2] P. Schury,[*2] A. Takamine,[*5] M. Wada,[*2] Y. X. Watanabe,[*2] and H. Wollnik[*9]

In the recent SLOWRI/ZD-MRTOF[1] commissioning run, radioactive ions were extracted with stable molecular ions spanning a wide mass range from impurities in the helium gas cell. Owing to the periodic nature of an MRTOF mass spectrometer (MRTOF-MS), this leads to an overlapping of ions with ions of varying A/q performing different numbers of laps in the TOF spectra. Unwanted stable molecular ions with higher abundance than the ions of interest prevented the identification of exotic isotopes from BigRIPS. Thus, it was necessary to devise a new purification method to remove contaminant ions as much as possible in our online measurement. An in-trap mass separation system for the ZD-MRTOF system was not yet installed during commissioning runs. Such systems are scheduled for the future based on existing knowledge, *e.g.*, selection methods called in-trap potential lift technique[2] and in-trap deflector technique.[3] Both techniques apply electric pulses to eject unwanted ions, where a single pulse on the order of a kilovolt is used at the moment of ion ejection (only applicable for isobaric ion separation) in the first method, and periodic low-voltage pulses are applied to a deflector inside the MRTOF device for the wideband ejection of ions in the second method. Here, we implement a new mass filter method based on periodic 600 V pulses of 2–4 μs duration using mirror electrodes that were on the ground potential previously. This periodic rectangular pulse is applied to injection-side mirror electrodes 5–8 (see graphic and simulated potentials in Fig. 1).

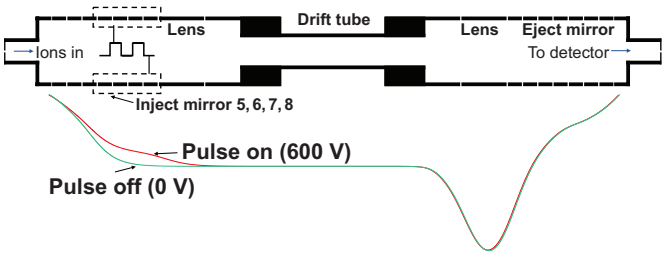

Fig. 1. Schematic of cleaning mode and potential distribution along the axis in MRTOF-MS.

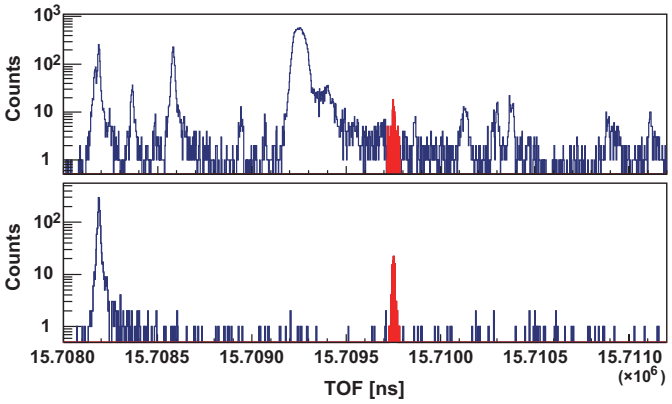

Fig. 2. Measured TOF spectrum without and with the cleaning mode; spectral peak marked in red is ^{82}Ge.

The flight time depends on the mass-to-charge ratio $t \propto \sqrt{(A/q)}$ of the ions. Different ion species of equal initial energy separate during flight in the MRTOF analyzer according to their A/q. The "on"/"off" stage of the pulses is synchronized with the wanted A/q value, and therefore, it is ensured that the ions of interest always experience the "off" stage when crossing the pulsed electrodes. In turn, the unwanted A/q ions are not synchronized, and they cross the pulsed region randomly in time. Being affected by the pulses once or several times changes their kinetic energy and additionally scatters the ions in a radial direction, which leads to unstable trajectories and ejection of ions. This ejection scheme was first tested in a simulation, and then applied in the experiment. After about 100–200 laps, ions of undesirable A/q crossed this region several times, and they could mostly be removed from the system. In our online experiments, the cleaning mode was applied; a comparison without and with the cleaning is shown in Fig. 2. Only the selected mass range is retained, and other mass areas are considerably clean in the spectrum. Although a very slight peak shift may occur due to the fluctuation of mirror potentials, this can be measured and corrected in the mass analysis. The new cleaning method was successful and enabled our first online measurements to determine low count rate nuclides.

*1 Institute of Mass Spectrometry and Atmospheric Environment, Jinan University
*2 Wako Nuclear Science Center(WNSC), IPNS, KEK
*3 Department of Physics, The University of Hong Kong
*4 Institute of Modern Physics, Chinese Academy of Science
*5 RIKEN Nishina Center
*6 Department of Physics, Osaka University
*7 Advanced Science Research Center, JAEA Ibaraki
*8 Department of Physics, Kyushu University
*9 Department of Chemistry and Biochemistry, New Mexico State University

References

1) M. Rosenbusch *et al.*, Nucl. Instrum. Methods Phys. Res. B, **463**, 184 (2020).
2) F. Wienholtz *et al.*, Int. J. Mass. Spectrom., **421**, 285 (2017).
3) P. Fischer *et al.*, Rev. Sci. Instrum. **91**, 023201 (2020).

Development of the gaseous Xe scintillation detector for heavy RI beams

Y. Hijikata,[*1] J. Zenihiro,[*1] H. Baba,[*2] M. Dozono,[*3] S. Enyo,[*1] N. Fukuda,[*2] T. Harada,[*2,*4] Y. Matsuda,[*5] S. Michimasa,[*3] D. Nishimura,[*6] S. Nishimura,[*2] S. Ota,[*3] H. Sakaguchi,[*7] H. Sato,[*2] Y. Shimizu,[*2] S. Sugawara,[*6] H. Suzuki,[*2] H. Takahashi,[*6] H. Takeda,[*2] S. Takeshige,[*8] J. Tanaka,[*2] S. Terashima,[*9] R. Tsuji,[*1] T. Uesaka,[*2] S. Yamamura,[*10] and K. Yoshida[*2]

In this contribution, we briefly report on the performance test of the gaseous Xe scintillation detector installed in the F7 vacuum chamber of BigRIPS. In this test, we use the detector for the particle identification of heavy RI beams up to the atomic number $Z \sim 90$ for the first time. At present, RIBF is the best facility for the generation of high-intensity and high-energy RI beams in the world. However, the use of high-intensity RI beams is now limited because of radiation damage and/or the slow responses of the standard detectors of BigRIPS.[1] As machine time is also limited because of the hogh cost of electric power, failure to use the high-intensity RI beams would be a significant loss.

Therefore, we proposed a new detector using scintillation photons from Xe gas. Because the average energy expended per scintillation photon is very small (<20 eV) and its lifetime is relatively short (5 ns and 100 ns),[2] the detector is expected to have a good energy resolution and a fast response time. The Xe detector is promising for the ΔE measurements of high-intensity RI beams (>100 kcps), where the ion chamber (IC) cannot work because of the slow response. To replace the IC with the Xe detector, we must first compare its energy resolution

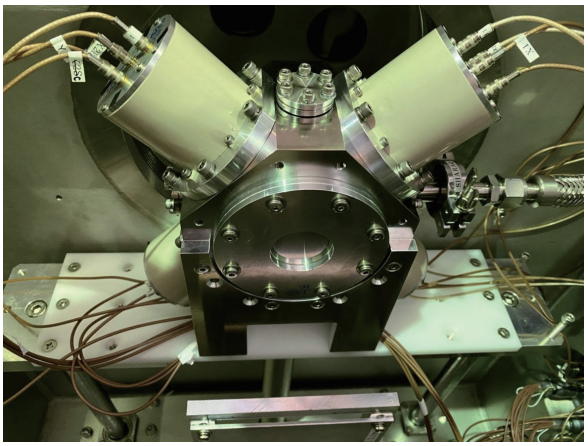

Fig. 1. Photograph of the new version of the gaseous Xe scintillation detector. Four 2-inch-ϕ PMTs (Hamamatsu, R6041-406) were attached to the corners.

*1 Department of Physics, Kyoto University
*2 RIKEN Nishina Center
*3 CNS, University of Tokyo
*4 Department of Physics, Toho University
*5 CYRIC, Tohoku University
*6 Department of Natural Sciences, Tokyo City University
*7 RCNP, Osaka University
*8 Department of Physics, Rikkyo University
*9 School of Physics, Beihang University
*10 Department of Physics, University of Tokyo

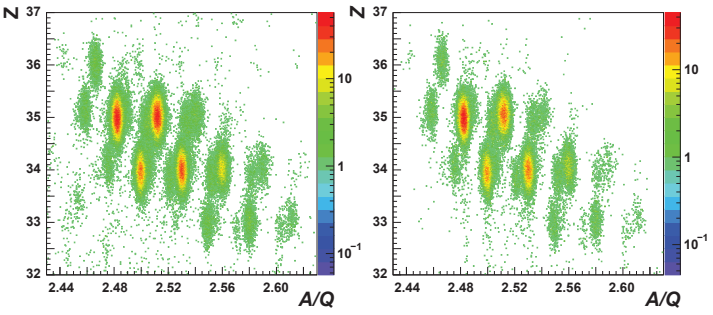

Fig. 2. Z obtained using the IC (left) and the Xe detector (right) vs. A/Q spectra with the Ge setting.

to that of the IC. A prototype of the detector was tested using a cocktail secondary beam at 300 MeV/nucleon up to $Z = 55$ at HIMAC, QST in Chiba. An rms resolution of $\Delta Z = 0.2$ around $Z = 55$ in sigma was achieved.[3] However, it is difficult to install the prototype in the vacuum chambers at the focal planes in the BigRIPS beamline owing to the thick detector material, which consists of 4-atm and 12-cm-thick Xe gas and 2-mm-thick Al windows. We recently built a new version of the Xe detector with 2-atm and 9-cm-thick Xe gas and 125-μm-thick Kapton windows, as shown in Fig. 1. The material thickness is approximately 100 mg/cm^2, which is comparable to that of the IC.

In November 2020, we installed the new detector in the F7 vacuum chamber for the first time and performed a test experiment by using several heavy RI and primary beam settings such as Ge, Sb, Er, Th, and U. We successfully acquired data of particles of different Z and different beam intensities. For the readout circuits, flash ADC (CAEN V1730) have been used in addition to the conventional QDC and TDC modules to check the high-rate torelance. Figure 2 shows the obtained two-dimensional PI spectra with the Ge setting. To deduce Z and A/Q values, the energy loss ΔE of the IC and the Xe detector as well as time of flight between the F3 and F7 plastic scintillators are used. The rms resolution of $\Delta Z \sim 0.22$ determined from the ΔE in the Xe detector is very close to that of the IC. Although the analysis is ongoing, the preliminary spectra show that the Xe detector will be helpful under high-intensity beam conditions.

References

1) T. Kubo *et al.*, Nucl. Instrm. Methods Phys. Res. B **204**, 97 (2003).
2) M. Mimura *et al.*, Jpn. J. Appl. Phys. **48**, 076501 (2009).
3) J. Zenihiro *et al.*, RIKEN Accel. Prog. Rep. **51**, 156 (2018).

μSR study of slightly pressurized organic superconductor κ-$(ET)_4Hg_{2.89}Br_8$

D. P. Sari,[*1,*2] Y. Ishii,[*1] I. Watanabe,[*2] and H. Taniguchi[*3]

Organic superconductors are single-band system, similar to high-critical-temperature (high-T_c) cuprates superconductors. A distinct difference can be observed in their lattice, *i.e.*, squared cuprates and triangular organics. In the case of squared cuprates, the Mott insulating state has an antiferromagnetic (AF) ground state in the 1/2-filled band case, while the anisotropic triangular ($t = t'$) organics also exhibit AF state. Here, t and t' are the nearest and next nearest transfer integral between sites, respectively. For a triangular lattice Mott insulator, owing to geometrical frustration ($t \sim t'$), the system cannot be magnetically ordered down to the mili-Kelvin order, *i.e.*, a spin liquid state. Owing to hole doping, it should also become metallic and superconducting (SC). However, the realistic candidate material was limited until the discovery of hole-doped organic superconductor κ-$(ET)_4Hg_{2.89}Br_8$ (κ-HgBr). In metallic state, resistivity exhibits the linear-temperature dependence, $\rho \propto T$, which is not a Fermi-liquid behavior. The susceptibility from 300 to 2 K is nearly perfectly scaled to that of a non-doped spin liquid organic insulator κ-$(ET)_2Cu(CN)_3$.[1)] By pressure, this non-Fermi-liquid behavior turns into conventional Fermi-liquid behavior at the $P_c = 0.5$ GPa, where T_c is also the highest (~7 K) in the pressure-temperature phase diagram.[2)] The non-Fermi-liquid behavior at low-pressure region is similar to the metallic state of high-T_c cuprates or low-pressure range of multi-band heavy fermion $CeCoIn_5$, and it is referred to as a strange metallic region.[1,2)] Because κ-HgBr exhibits similarities with other strongly correlated electron systems, it is interesting to determine the type of Cooper pairing that occurs in κ-HgBr.

We aim to determine the pairing symmetry in κ-HgBr by μSR. We performed μSR measurement down to 0.3 K on the ARGUS spectrometer at the RIKEN-RAL muon facility with HELIOX cryostat and fly-path setup. We developed a technique for applying a decent pressure on κ-HgBr crystals because at ambient pressure, the SC state of κ-HgBr is not bulky due to the inhomogeneous state.[3)] Approximately 130 mg crystals were carefully aligned and stuck together using diluted polymer glue. This strategy was effective for applying enough pressure on the sample as we conducted magnetization measurement using SQUID with a similar sample setup. Figures 1(a) and (b) show the result of SQUID measurement. The demagnetization effect due to sample shape was treated for all analyses. The temperature dependence of susceptibility determined $T_c = 4.6(2)$ K whereas the field dependence of magnetization (MH-curve) was measured at several temperatures; the SC volume fractions were estimated at each temperature. Consequently, the estimated SC volume fraction at 2 K was found to be approximately 90%, as shown in Fig. 1(a). Comparing this with the referred result obtained from ac-susceptibility measurement,[3)] a pressure of at least 0.3 GPa was applied to the sample. This expectation was confirmed by the estimation of the lower-critical field, H_{c1}, by SQUID, resulting in the absolute value of H_{c1} at 0 K, *i.e.*, 27 Oe. The result is consistent with the measurement performed using zero-filed (ZF) μSR at 0.3 K. H_{c1} was estimated as follows. The sample was ZF-cooled to 0.3 K. Transverse-field (TF) was applied for approximately 10 min to destroy the shielding field. After cutting off the TF, the ZF-relaxation rate was measured. At TF = 25 Oe, the relaxation rate started to increase. Therefore, we concluded that the sample was in bulk condition and a slight pressure, $P \gtrsim 0.3$ GPa, was applied. Using these results, we measured the ZF-μSR relaxation rate in κ-HgBr down to 0.3 K. The temperature independence of ZF-relaxation rate was observed, indicating that spontaneous internal fields do not appear in the superconducting state. This result is consistent with that in Ref. 4), in which the measurement was performed down to 1.5 K and at ambient pressure. Thus, the possibility of spin triplet and $d+id$-wave symmetry in κ-HgBr due to the expected triangular lattice in κ-HgBr becomes very low. The temperature dependence of London penetration depth measurement using TF-μSR is necessary for determining the SC gap symmetry, which will be discussed in the future work.

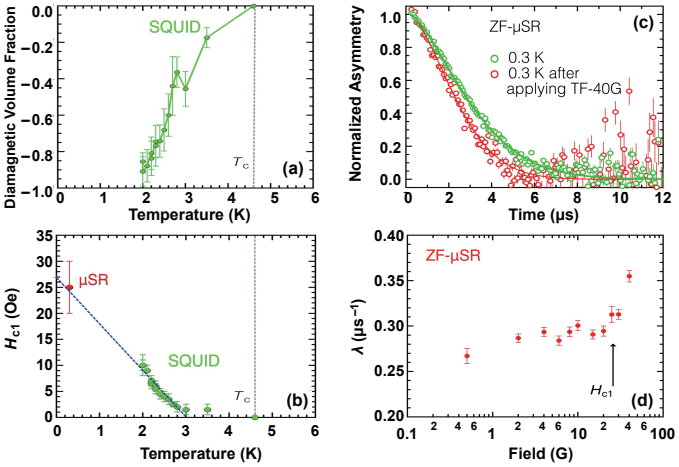

Fig. 1. (a) Temperature dependence of SC volume fraction measured by SQUID. (b) Temperature dependence of H_{c1} measured by SQUID down to 2 K compared with μSR measurement. (c) ZF-μSR time spectra before and after applying TF of 40 G. The solid lines are the exponential decay fitting lines. (d) Relaxation rate of ZF-μSR time spectra after applying several TF, from 2 to 40 G.

*1 College of Engineering, Shibaura Institute of Technology
*2 RIKEN Nishina Center
*3 Department of Physics, Saitama University

References
1) H. Oike *et al.*, Nat. Commun. **8**, 756 (2017).
2) H. Taniguchi *et al.*, J. Phys. Soc. Jpn. **76**, 113709 (2007).
3) H. Oike *et al.*, Phys. Rev. Lett. **114**, 067002 (2015).
4) K. Satoh *et al.*, Physica B 404, 597 (2009).

Targeted alpha therapy of cancer: Evaluation of [^{211}At] AAMT targeting LAT1†

K. Kaneda-Nakashima,[*1,*2] Z. Zhang,[*2] Y. Manabe,[*1,*2] A. Shimoyama,[*1,*2] K. Kabayama,[*1,*2] T. Watabe,[*1,*2] Y. Kanai,[*1,*3] K. Ooe,[*1,*3] A. Toyoshima,[*1,*2] Y. Shirakami,[*1,*2,*3] T. Yoshimura,[*1] M. Fukuda,[*2,*4] J. Hatazawa,[*1,*3] T. Nakano,[*2,*4] K. Fukase,[*1,*2] and A. Shinohara[*1,*2]

L-type amino acid transporter 1 (LAT1) is an isoform of the system L, which is Na^+-independent neutral amino acid transport agency. LAT1 is expressed in primary human cancers originating in various organs such as the brain, lung, thymus, and skin, it is a well-known specific cancer marker. Amino acid tracers containing radioactive halogen have attracted attention for use as probes in single photon emission computed tomography (SPECT) and positron emission tomography (PET). L-3-[^{18}F]- α-methyl-tyrosine (^{18}F-FAMT) has higher potential for tumor specificity than 2-deoxy-2-[^{18}F] fluoroglucose (^{18}F-FDG), which is widely employed as a PET probe for cancer staging. Further FDG has the potential for false-positive accumulation within inflammation related to high glucose metabolism in macrophages or neutrophils, whereas ^{18}F-FAMT accumulates in tumors via LAT1, which is expressed only in cancer cells.[1] In contrast, ^{18}F-FAMT is not transported by other isoforms of the system L (*e.g.*, LAT2, LAT3, and LAT4), that are expressed in normal tissues.[2,3] Therefore, our L-3-[^{211}At] - α-methyl-tyrosine (^{211}At-AAMT) is expected to exhibit LAT1 specificity and to have the potential to be used as a targeting alpha therapy (TAT) treatment.

Methods

The ^{209}Bi$(\alpha, 2n)^{211}$At reaction using the AVF Cyclotron at the Research Center for Nuclear Physics, Osaka University (Ibaraki, Japan) was used to produce ^{211}At.[4] Further ^{211}At was produced with the same nuclear reaction at the Nishina Center for Accelerator-Based Science, RIKEN, and it was then transported to the Osaka University.

PANC-1 cells were cultured at 37°C in D-MEM containing 10% fetal bovine serum and 1% antibiotics in a humidified incubator with 5% CO2. Cultured cells were washed in PBS (-) and harvested with trypsin. Tumor xenograft models were established by the subcutaneous injection of 1×10^7 cells in 0.2 mL of serum-free medium and Matrigel (1:1) into female BALB/c-nu/nu mice. PANC-1 xenograft mice (10 weeks old; body weight = 19.3 ± 1.4 g) were used when the tumor size reached approximately 50 mm^3 on average.

The mice were divided into two groups according to the injected dose [0.4 MBq ($n = 4$, 4.0 ± 0.2 MBq/mL); control ($n = 4$)]. The control group only received solvents.

Tumor sizes and body weights were measured three times per week. Mice were sacrificed when the tumor size reached more than 10% of the total weight. The mice were observed for 40 days. Uptakes were normalized by the injected dose (MBq) and body weight (g).

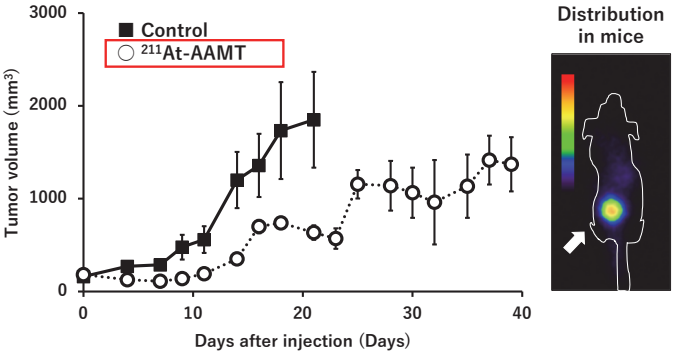

Fig. 1. Efficacy of ^{211}At-AAMT using the PANC-1 xenograft model. Tumor growth inhibition by ^{211}At-AAMT (Left). Coronal images of ^{211}At-AAMT in tumor-bearing model (Right).

Results

In the PANC-1 model, the control mice were injected only with solvents (0.2 w/v% AcOH and 1 w/v% ascorbic acid solution) and the ^{211}At-AAMT treatment group received i.v. injections of the 0.4 MBq/mouse ^{211}At-AAMT solution. No inflammation or abnormalities were observed around the injection site. In the ^{211}At-AAMT treatment group, the tumor growth was clearly inhibited and the body weight was not significantly decreased compared to the control group (Fig. 1).

Conclusion

^{211}At-AAMT may be considered a novel anti-cancer drug. While ^{211}At-AAMT could inhibit tumor growth with a single treatment, the tumor was not completely abolished, and therefore, a single injection was insufficient to decrease the tumor size continuously. Multiple doses may be necessary to exploit the high anti-tumor effect of ^{211}At-AAMT. In conclusion, ^{211}At-AAMT may be an effective anti-cancer drug when administered multiple times or in combination with existing anti-cancer drugs.

References
1) A. Achmad *et al.*, BMC Med. Imaging **17**, 66 (2017).
2) L. Wei *et al.*, J. Pharmacol. Sci. **130**, 101 (2016).
3) L. Wei *et al.*, Cancer Sci. **107**, 347 (2016).
4) T. Watabe *et al.*, J. Nucl. Med. **60**, 1301 (2019).

† Condensed from the article Cancer Sci. **112**(3), 1132 (2021)
*1 Institute for Radiation Sciences, Osaka University
*2 Graduate School of Science, Osaka University
*3 Graduate School of Medicine, Osaka University
*4 Research Center for Nuclear Physics, Osaka University

Influence of antibody stabilization with sodium ascorbate on radioimmunotherapy with an ^{211}At-conjugated anti-tissue factor antibody†

H. Takashima,[*1,*2] Y. Koga,[*1,*2] S. Manabe,[*3,*4,*5] K. Ohnuki,[*6] R. Tsumura,[*1] T. Anzai,[*1] N. Iwata,[*1] Y. Wang,[*2] T. Yokokita,[*2] Y. Komori,[*2] D. Mori,[*2] H. Haba,[*2] H. Fujii,[*6] Y. Matsumura,[*7] and M. Yasunaga[*1]

Alpha radiation is characterized by higher linear transfer compared to other types of ionizing radiation and a range of 50–100 μm in tissue. Therefore, the selective tumor accumulation of alpha emitters exerts potent antitumor effects without serious toxicity against normal cells adjacent to the tumor. Astatine-211 (^{211}At) is an alpha emitter, its high production yield is sufficient to prepare ^{211}At-labeled radiopharmaceuticals for administration at clinical doses.

Tissue factor (TF), a transmembrane glycoprotein initiating the extrinsic blood coagulation cascade, is overexpressed in tumors such as gastric cancer, pancreatic cancer, and malignant gliomas.[1,2)]

Immunoglobulin G (IgG) selectively accumulate in tumor via the enhanced permeability and retention (EPR) effect.[3)] In addition, the antigen-antibody reaction enhances the tumor accumulation of antibodies.[2)] Therefore, we focused on applying anti-TF monoclonal antibodies (mAbs) established by us to armed antibodies such as antibody-drug conjugate (ADC)[4–6)] and antibody labeled with therapeutic radionuclides.

We synthesized ^{211}At in the ^{209}Bi(α, $2n$)^{211}At reaction using the RIKEN azimuthally varying field (AVF) cyclotron, and we labeled an anti-TF mAb with the radionuclide as previously reported.[7)]

To evaluate ^{211}At-conjugaed anti-TF mAb, we performed sodium dodecyl sulfate-polyacrylamide gel electrophoresis (SDS-PAGE) and flow cytometry analyses. In the SDS-PAGE analysis, ^{211}At-conjugated anti-TF mAb was smeared, which was in contrast to band patterns in ^{211}At-unlabeled anti-TF mAbs. Consequently, flow cytometry analysis revealed that the binding activity of the astatinated mAb was disturbed compared with ^{211}At-unlabeled mAbs. These findings suggest that anti-TF mAb was denatured by the ^{211}At-induced radiochemical reaction. Then, to protect anti-TF mAb from denaturation, we purified astatinated mAbs using an elution buffer containing sodium ascorbate (SA), which is a free radical scavenger. In the SDS-PAGE analysis, band patterns were demonstrated in ^{211}At-conjugated anti-TF mAbs eluted in phosphate-buffered saline (PBS) containing 0.6 or 1.2% SA and ^{211}At-unlabeled mAbs. Consequently, the binding activities of the astatinated anti-TF mAbs in the SA solution were comparable to those of ^{211}At-unlabeled mAbs.

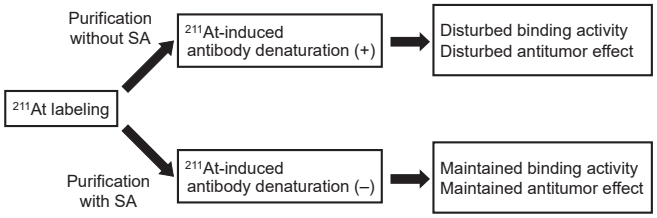

Fig. 1. Summary of ^{211}At-induced antibody denaturation and protective effect of sodium ascorbate.

^{211}At-conjugated anti-TF mAbs stabilized with SA exerted greater cytocidal effects on gastric cancer cells than the astatinated mAb eluted in PBS. Similar to ADC, the cytotoxicities of the stabilized immunoconjugates depended on the level of TF in the cancer cell.

To evaluate *in vivo* toxicities, we observed the body weight loss in mice administered SA, ^{211}At-conjugated anti-TF mAb, or free ^{211}At. Although body weight loss was observed in mice administered PBS containing 1.2% SA, the loss was transient and the radioprotectant seemed tolerable. Body weight loss after the administration of the astatinated anti-TF mAb in PBS containing 1.2% SA was milder than free ^{211}At dissolved in 1.2% SA solution.

^{211}At-conjugated anti-TF mAb eluted in PBS containing 1.2% SA showed significantly greater antitumor effects in a high TF-expressing gastric cancer xenograft model than the non-stabilized immunoconjugate. Similar to ADC, the antitumor effect of the astatinated anti-TF mAb in 1.2% SA soution depended on the TF expression on the cell membrane of cancer cells.

In summary, SA protected the astatinated anti-TF mAb from ^{211}At-induced antibody denaturation, which resulted in the maintained binding and antitumor activities of the immunoconjugate (Fig. 1). Without intolerable side effects, ^{211}At-conjugated anti-TF mAb eluted in PBS containing 1.2% SA showed potent antitumor effects in gastric cancer xenograft models dependent on the level of TF on the cancer cell membrane.

† Condensed from the article in Cancer Sci. **112**, 1975 (2021)

*1 Developmental Therapeutics, EPOC, National Cancer Center
*2 RIKEN Nishina Center
*3 Laboratory of Functional Molecule Chemistry, Pharmaceutical Department and Institute of Medicinal Chemistry, Hoshi University
*4 Research Center for Pharmaceutical Development, Tohoku University
*5 Glycometabolic Biochemistry Laboratory, RIKEN
*6 Division of Functional Imaging, EPOC, National Cancer Center
*7 Department of Immune Medicine, National Cancer Center Research Institute, National Cancer Center

References

1) Y. W. van den Berg *et al.*, Blood **119**, 924 (2012).
2) H. Takashima *et al.*, Sci. Rep. **7**, 12341 (2017).
3) Y. Matsumura *et al.*, Cancer Res. **46**, 6387 (1986).
4) Y. Koga *et al.*, Int. J. Cancer **137**, 1457 (2015).
5) R. Tsumura *et al.*, J. Control. Release **284**, 49 (2018).
6) R. Tsumura *et al.*, Oncol. Rep. **45**, 329 (2021).
7) H. Takashima *et al.*, RIKEN Accel. Prog. Rep. **53**, 172 (2020).

Kinetics of Rad51 foci in G2 phase after heavy-ion irradiation in mammalian cells

M. Izumi*1 and T. Abe*1

DNA double-strand breaks (DSBs) are the most lethal type of damage caused by ionizing irradiation and are repaired mainly by non-homologous end joining (NHEJ) or homologous recombination (HR) in mammalian cells; alternative NHEJ and/or single-strand annealing work only when both NHEJ and HR are impaired. Accelerated heavy-ion particles with high linear energy transfer (LET) induce complex and fragmented DNA damage affecting the pathway choice and the efficiency of DSB repair.

Several published results of survival assay using Chinese hamster mutant cell lines deficient in NHEJ or HR suggest that NHEJ is inhibited after heavy-ion irradiation.[1,2] In contrast, studies using inhibitors and mouse mutant cell lines suggest that NHEJ is a major repair pathway after heavy-ion irradiation, although HR is more important for higher-LET radiation.[3,4] It is also reported that clustered DNA damage enhances end resection, which could promote HR, alt-NHEJ, and SSA.[5,6] Therefore, the DNA repair mechanism after heavy-ion irradiation is still controversial in higher eukaryotes.

Our previous study using human fibroblast and a specific inhibitor against NHEJ or HR suggests that NHEJ and HR work competitively and compensate for each other after X-irradiation.[7] On the other hand, NHEJ is the major repair pathway after heavy-ion irradiation, and HR does not seem to compensate for NHEJ. However, it is unknown whether HR efficiently repairs DSBs caused by heavy ions or whether the DNA damage checkpoint delays the entry into the S/G2 phase, where HR occurs.

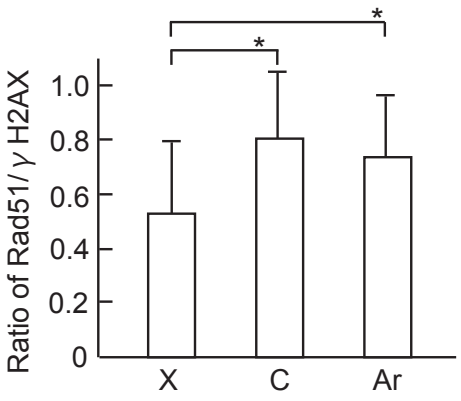

Fig. 1. Ratio of Rad51/phosphorylated histone H2AX (γH2AX) foci 1 h after irradiation in HeLa cells. Aphidicolin (10 μM) was added 30 min before irradiation, and cells were irradiated with 2 Gy of X-rays, carbon ions (LET = 80 keV/μm), or argon ions (LET = 300 keV/μm) and incubated in the presence of aphidicolin for 1 h after irradiation. The foci formation of Rad51 and γH2AX was detected by immunostaining. Student't t test: $^*P < 0.01$. Error bars represent SD.

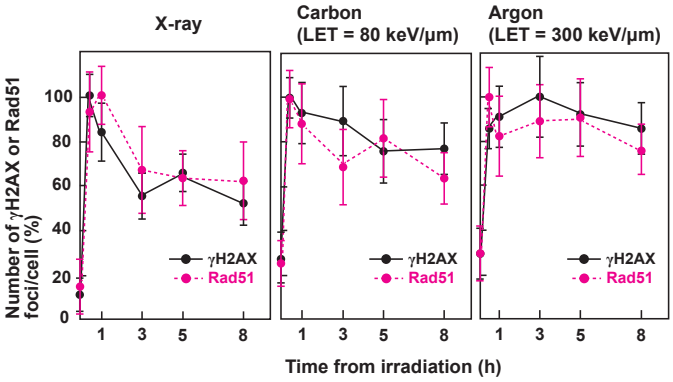

Fig. 2. Time course of phosphorylated histone H2AX (γH2AX) and Rad51 foci after irradiation in G2 cells. The percentage of foci per cell was plotted by normalizing the numbers at the maximum time point as 100% after irradiation.

In this study, we examined the DNA repair kinetics as well as the repair pathway usage in the G2 phase. Exponentially growing HeLa cells were irradiated with X-rays, carbon ions, or argon ions and incubated in the presence of aphidicolin to arrest S-phase progression and inhibit transition from the S to the G2 phase. The repair efficiency and pathway usage were estimated by the kinetics of the phosphorylated histone H2AX foci and Rad51 foci, which reflect the DSBs and HR, respectively. S-phase cells were identified by the pan-nucleic staining of the phosphorylated histone H2AX and excluded from analysis.

The ratio of Rad51/phosphorylated histone H2AX foci induced by heavy-ion irradiation was higher than that induced by X-rays (Fig. 1). The number of Rad51 foci decreased more slowly after heavy-ion irradiation than after X-ray irradiation, with the kinetics similar to those of phosphorylated histone H2AX (Fig. 2). These results suggest that HR is favored after heavy-ion irradiation, although HR repairs DSBs less efficiently after heavy-ion irradiation.

*1 RIKEN Nishina Center

References

1) H. Wang *et al.*, DNA Repair **7**, 725 (2008).
2) S. C. Genet *et al.*, Oncol. Rep. **28**, 1591 (2012).
3) H. Ma *et al.*, Radiat. Oncol. **10**, 225 (2015).
4) A. Gerelchuluun *et al.*, Rad. Res. **183**, 345 (2015).
5) H. Yajima *et al.*, DNA Repair 12, 936 (2013).
6) A. Shibata *et al.*, EMBO J. **30**, 1079 (2011).
7) M. Izumi, T. Abe, RIKEN Accel. Prog. Rep. **53**, 24 (2020).

Improvement of rotifer as the new food item in larviculture†

K. Tsuneizumi,*1 M. Yamada,*1 K. Ichinose,*1 H. Ichida,*1 and T. Abe*1

In larviculture, rotifers (*Brachionus plicatilis* sense strict) are generally used as the initial food source.[1] The lorica length of rotifers is distributed in the range of 170–320 μm in individuals carrying amictic eggs. The next food item *Artemia* nauplii has a body length of 400–1,000 μm. Although the proper management of feed size and density associated with fish larval growth is needed,[2] there is a size gap between rotifers and *Artemia* nauplii. No feed items to bridge the size gap of 320–400 μm have been developed in the food scheme of fish larvae.

To improve the mass mortality and abnormal development of fish larvae during the period of growth corresponding to the size gap, this study applied carbon and argon heavy-ion-beam irradiation in mutation breeding[3,4] to select rotifer mutants with larger lorica sizes.

In our previous study, the Notojima strain, known as the largest rotifer strain in Japan, was irradiated with carbon (C) and argon (Ar) ion beams at different doses. We developed a screening method with the lorica length as an indicator and established 56 large mutants (Table 1).[5] In this study, we measured the population growth rate as the parameter of good bait. The population growth rate of each large mutant line was observed with 5-mL cultures. For each line, every five individuals were inoculated into 6 wells containing 5 mL of fresh culture medium (18 practical salinity units) with Chlorella. The total number of rotifers in each well was counted after 5 days. The population growth rate of each well was calculated with the following equation: population growth rate = ln (total population/5 individuals)/5 days). The average values of each large mutant line were calculated using data obtained with six replications and standardized using the control group.

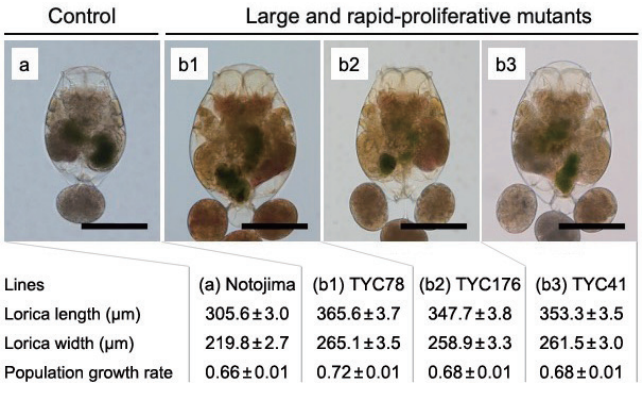

Fig. 1. Photograph of rotifer lines with proliferative difference and the control. (a) Control rotifer. (b1-3) Large and proliferative mutants with higher population growth rates than the control. Values are mean ± standard errors, and images of rotifer lines are of individuals with the average lorica lengths. Scale bars represent 200 μm.

Table 1. Frequency of large and rapid-proliferative mutants

Heavy ion	Dose (Gy)	Irradiated rotifer (No.)	Active proliferation		Large mutants		Rapid proliferation	
			Lines (No.)	Frequency (%)	Lines (No.)	Frequency (%)	Lines (No.)	Frequency (%)
C ion	100	240	195	81.3	10	5.1	3	1.5
	150	250	183	76.3	6	3.3	2	1.1
	200	504	391	77.6	13	3.3	6	1.5
	300	504	321	63.7	13	4.0	2	0.6
	400	240	98	40.8	9	9.2	1	1.0
	600	240	60	25.0	1	1.7	0	0.0
Ar ion	25	216	197	91.2	1	0.5	0	0.0
	50	216	145	67.1	2	1.4	1	0.7
	75	216	140	64.8	1	0.7	0	0.0
	100	216	84	38.9	0	0.0	0	0.0
	150	216	17	7.9	0	0.0	0	0.0
Total		3048	1831	60.1	56	3.1	15	0.8

The following 3 mutant lines showed a significantly higher population growth rate than the control: TYA41 (Steel's multiple comparison tests, $P < 0.05$), TYC78, and TYC176 ($P < 0.01$) (Fig. 1). The large mutant lines showed an equal or higher growth rate than the control are categorized as the rapid proliferation in Table 1. The frequency of appearance was calculated using the mutant lines showing active proliferation after irradiation: mutant frequency (%) = (number of rapid proliferation)/(number of active proliferation) × 100. The highest frequency was observed at 100 and 200 Gy with the C-ion beam. For TYC78 produced at 200 Gy, we decided that a C-ion beam of 200 Gy was the optimal irradiation condition to establish a large rotifer. Similarly, the highest frequency was observed at 50 Gy with the Ar-ion beam, and TYA41 was selected from the same condition. This was also determined to be the optimum irradiation dose. Thus, these three mutants are suitable to solve the feed-size gap between rotifers and *Artemia* nauplii and should improve the marine fish larviculture system.

Food shortages due to population growth and increased consumption are a major global concern, and countries around the world are searching for ways to increase food production. The enlarged rotifers obtained in this study could potentially provide a stable supply of larger rotifers at low cost, enhancing aquaculture.

† Condensed from the article in Biosci. Biotech. and Biochem. (DOI: 10.1093/bbb/zbaa094) (2021)

*1 RIKEN Nishina Center

References

1) S. Mills *et al.*, Hydrobiologia **796**, 39 (2017).
2) T. Kotani *et al.*, J. World Aquac. Soc. **40**, 383 (2009).
3) T. Abe *et al.*, in *Plant Mutation Breeding and Biotechnology*, edited by Q. Y. Shu *et al.* (CABI, Oxfordshire, 2012), p. 99.
4) A. Tanaka *et al.*, J. Radiat. Res. **51**, 223 (2010).
5) K. Tsuneizumi *et al.*, RIKEN Accel. Prog. Rep. **53**, 213 (2020).

II. RESEARCH ACTIVITIES I
(Nuclear, Particle and Astro-Physics)

1. Nuclear Physics

RI beam production at BigRIPS in 2020

H. Takeda,[*1] N. Fukuda,[*1] H. Suzuki,[*1] Y. Shimizu,[*1] N. Inabe,[*1] K. Kusaka,[*1] M. Ohtake,[*1] Y. Yanagisawa,[*1] H. Sato,[*1] K. Yoshida,[*1] and T. Uesaka[*1]

The radioactive isotope (RI) beam production at the BigRIPS fragment separator[1] in 2020 is presented here. Table 1 summarizes the experimental programs that involved the use of the BigRIPS separator in this period and the RI beams produced for each experiment. All the experiments originally scheduled for the spring beamtime were postponed owing to the COVID-19 pandemic. In the autumn beamtime, ^{238}U and ^{70}Zn primary beams were provided.

The ^{238}U beam campaign started in October. During a tuning phase of BigRIPS at startup, an auto-focusing and auto-centering system was tested with a ^{82}Ge beam for the first time at RIBF.[2] After the BigRIPS tuning phase followed by the commissioning of HiCARI, a PALIS experiment was performed with an RI beam around ^{191}Bi to evaluate the extraction efficiency using alpha emitters in the ^{191}Bi region.

Five HiCARI experiments were subsequently performed with the ZeroDegree spectrometer. A cocktail beam of ^{84}Ge/^{83}Ga/^{82}Zn was produced to study neutron intruder states and collectivity. ^{86}Se/^{84}Ge, ^{88}Se/^{86}Ge, and ^{90}Se beams were produced to explore quadrupole and octupole collectivity. A cocktail ^{111}Nb/^{112}Mo/^{113}Tc beam was produced to perform high-resolution spectroscopy and lifetime measurements. A ^{130}Cd beam was produced to study single-particle states in ^{129}Ag. A ^{136}Te beam was produced to characterize a strongly Coulomb-excited state above 4 MeV in ^{136}Te. During these HiCARI experiments, mass measurements with a multi-reflection time-of-flight mass spectrometer (MRTOF-MS) located downstream of the ZeroDegree spectrometer were performed symbiotically. Subsequently, a machine study for the Rare RI Ring was performed with a ^{75}Ga beam.

At the end of the ^{238}U beam campaign, a machine study for a high-purity Th-beam development including performance evaluations of beamline detectors for a high-Z, high-rate RI beam was performed using a ^{220}Th beam.[3]

After switching to the ^{70}Zn primary beam, two HiCARI experiments were conducted with the ZeroDegree spectrometer. ^{56}Ti and ^{58}Ti beams were produced to study the evolution of collectivity in Ti isotopes. ^{36}Ca, ^{38}Ca, ^{48}Ca, and ^{54}Ca beams were produced to investigate systematically the reduction factor for the deduced spectroscopic factors. A symbiotic MRTOF experiment was performed again.

A new isotope search experiment was conducted around the ^{45}Si region at the end of the ^{70}Zn beam campaign.[4]

The RI beam production at BigRIPS from the start of operation in March 2007 is summarized in our database.[5] At first, you will be redirected to the welcome page. Follow the links "Database of RI Beams Produced at BigRIPS" → "List of Experiments" → "Summary" to reach the summary page; you can reach the page in subsequent attempts.

References
1) T. Kubo, Nucl. Instrum. Methods Phys. Res. B **204**, 97 (2003).
2) Y. Shimizu *et al.*, in this report.
3) N. Fukuda *et al.*, in this report.
4) H. Suzuki *et al.*, in this report.
5) Y. Shimizu *et al.*, Nucl. Instrum. Methods Phys. Res. B, **463**, 158 (2020). Available at `https://ribeam.riken.jp/`.

Table 1. List of experimental programs together with RI beams produced at the BigRIPS separator in 2020.

Primary beam (Period)	Exp. Prog. No.	Spokesperson	Course	RI beams
^{238}U 345 MeV/nucleon (Oct. 25–Nov. 24)	NP1712-RIBF166-03	T. Sonoda	PALIS	^{191}Bi
	NP1912-RIBF196-01	F. Flavigny	ZeroDegree	^{84}Ge/^{83}Ga/^{82}Zn
	NP1912-RIBF190-01	F. Browne	ZeroDegree	^{86}Se/^{84}Ge, ^{88}Se/^{86}Ge, ^{90}Se
	NP1912-RIBF187-01	W. Korten	ZeroDegree	^{111}Nb/^{112}Mo/^{113}Tc
	NP1912-RIBF189-02	Z. Podolyak	ZeroDegree	^{130}Cd
	NP1912-RIBF193-01	A. Jungclaus	ZeroDegree	^{136}Te
	PE19-02 / PE20-01	M. Wada	ZeroDegree	(symbiotic)
	MS-EXP20-04	Y. Yamaguchi	Rare RI Ring	^{75}Ga
	MS-EXP20-02	N. Fukuda	ZeroDegree	^{220}Th
^{70}Zn 345 MeV/nucleon (Dec. 2–Dec. 13)	NP1912-RIBF142R1-01	T. Koiwai	ZeroDegree	^{56}Ti, ^{58}Ti
	NP1912-RIBF170R1-01	H. Crawford	ZeroDegree	^{36}Ca, ^{38}Ca, ^{48}Ca, ^{54}Ca
	PE20-02	M. Wada	ZeroDegree	(symbiotic)
	DA20-03	H. Suzuki	BigRIPS	^{45}Si

*1 RIKEN Nishina Center

Production cross-section measurement and new-isotope search for very-neutron-rich RIs produced from ^{70}Zn beam at 345 MeV/nucleaon by BigRIPS separator

H. Suzuki,[*1] M. Yoshimoto,[*2] N. Fukuda,[*1] H. Takeda,[*1] Y. Shimizu,[*1] Y. Yanagisawa,[*1] H. Sato,[*1] and K. Yoshida[*1]

We performed production cross-section measurements and a new-isotope search in the neutron-rich region with the atomic numbers Z = 12–19, located southeast of ^{48}Ca in the nuclear chart. The neutron-rich radioactive isotopes (RIs) were produced by the projectile fragmentation of a 600-particle-nA ^{70}Zn beam at 345 MeV/nucleon impinged on a 10-mm-thick Be target in the BigRIPS separator. Particle identification based on the TOF-$B\rho$-ΔE method[1] was performed in the second stage of BigRIPS. Three BigRIPS settings were used with ^{45}S, ^{43}Si, and ^{45}Si as centeral particles. The former two settings were for the cross-section measurements, and the last one was for the new-isotope search. The production cross sections were deduced from the measured production rates and their transmission efficiencies in BigRIPS, which were simulated with LISE^{++} calculations.[2] In the simulation, parameters that control the momentum and angular distribution[2,3] are not changed from the default values in the current preliminary analysis.

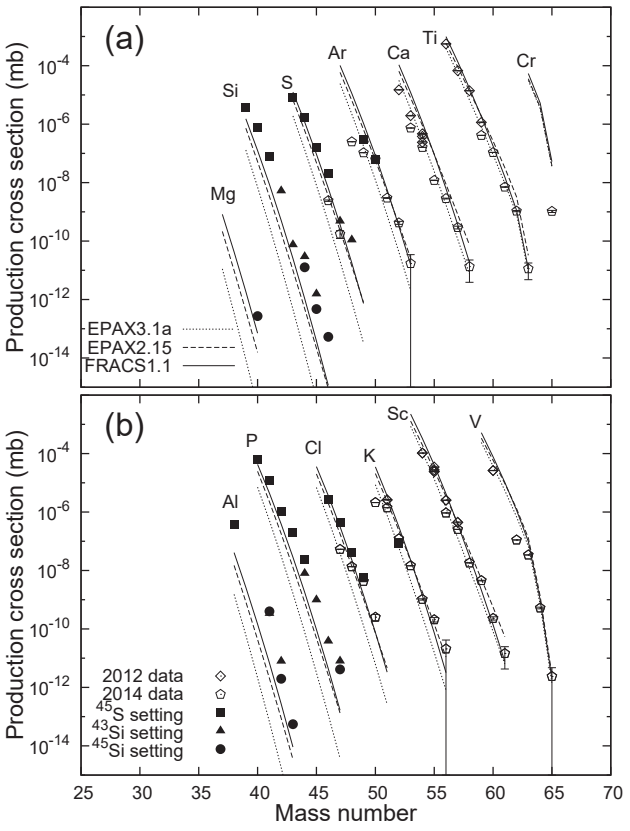

Fig. 1. Measured production cross sections of RIs produced in the ^{70}Zn + Be reaction at 345 MeV/nucleon with semi-empirical cross-section formulae. (a) Results for even-Z isotopes. (b) Results for odd-Z isotopes.

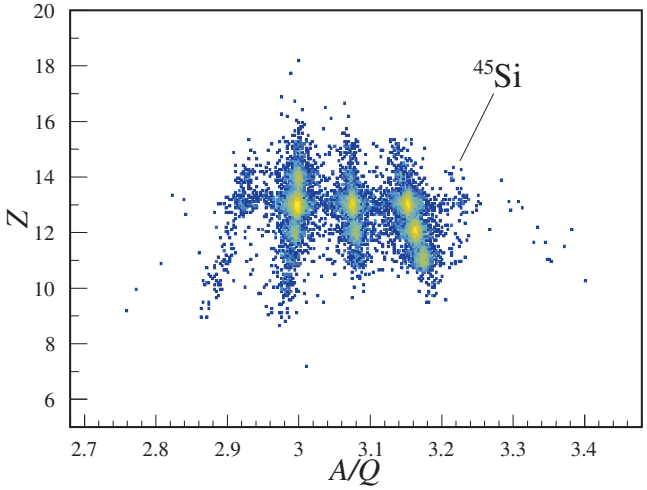

Fig. 2. PID plots obtained in the ^{45}Si setting. Events of a new isotope, ^{45}Si, were clearly observed.

Figure 1 shows the production cross sections of RIs obtained in this work (filled symbols), together with measurements in 2012 and 2014 (open symbols). The solid, dashed, and dotted lines show the cross sections predicted by the semi-empirical formula FRACS1.1,[4] EPAX2.15,[5] and EPAX3.1a.[6] Overall, FRACS1.1 best reproduces the measured cross sections among these formulae; however, around the very-neutron-rich region, the discrepancy between the measured and predicted cross sections becomes larger. A new isotope, ^{45}Si, was discovered in this work, as shown in Fig. 2. One event was also observed at the location of ^{46}Si, although more elaborate analysis, such as background removal, is needed for confirmation as a new isotope. The detailed analysis is currently in progress.

*1 RIKEN Nishina Center
*2 Department of Physics, Gifu University

References

1) N. Fukuda *et al.*, Nucl. Instrum. Methods Phys. Res. B **317**, 323 (2013).
2) O. B. Tarasov, D. Bazin, LISE^{++} site, `http://lise.nscl.edu,MichiganStateUniversity`.
3) H. Suzuki *et al.*, Nucl. Instrum. Methods Phys. Res. B **317**, 756 (2013).
4) B. Mei, Phys. Rev. C **95**, 034608 (2017).
5) K. Sümmerer, B. Blank, Phys. Rev. C **61**, 034607 (2000).
6) K. Sümmerer, Phys. Rev. C **86**, 014601 (2012).

$N = 32$ shell closure below calcium: Low-lying structure of ^{50}Ar†

M. L. Cortés,[*1,*2] W. Rodriguez,[*3,*1,*4] P. Doornenbal,[*1] A. Obertelli,[*5,*6] J. D. Holt,[*7,*8] J. Menéndez,[*9,*10] K. Ogata,[*11,*12] A. Schwenk,[*6,*13,*14] N. Shimizu,[*9] J. Simonis,[*15] Y. Utsuno,[*16,*9] K. Yoshida,[*16] and the SEASTAR2017 Collaboration

An interesting region to study shell evolution is around Ca isotopes, where the development of shell closures for $N = 32$ and $N = 34$ has been suggested. The $N = 32$ sub-shell closure was evidenced by its relatively high $E(2^+)$ energy,[1] and confirmed by two-proton knockout cross sections[2] and mass measurements.[3] For the $N = 34$ shell closure, evidence was provided by $E(2^+)$,[4] systematic mass measurements,[5] and neutron-knockout cross sections.[6] The preservation of the $N = 32$ shell closure has been determined in Ti and Cr via spectroscopy, reduced transition probabilities, and precision mass measurements, while for $N = 34$, it has been suggested to disappear above Ca. In contrast, the recent measurement of the $E(2^+)$ of ^{52}Ar suggests the conservation of the $N = 34$ shell closure for $Z = 18$.[7] The first spectroscopy of ^{50}Ar showed a relatively high $E(2^+)$,[8] hinting at the conservation of the $N = 32$ shell closure below Ca. A candidate for the 4^+ state was also reported. No further spectroscopic information is available for this very exotic nucleus. This work reports low-lying states in ^{50}Ar.

A beam of ^{70}Zn with an average intensity of 240 particle nA was fragmented on a Be target. Isotopes were identified using BigRIPS[9] and delivered to the 151.3(13)-mm-long liquid hydrogen target of MINOS[10] placed in front of the SAMURAI magnet. Outgoing fragments were identified using SAMURAI and associated detectors.[11] The DALI2$^+$ array,[12,13] composed of 226 NaI(Tl) detectors, was used to detect the emitted γ-rays. Doppler-corrected γ-ray spectra were obtained using the reaction vertex and the velocity of the fragment reconstructed with MINOS.

Based on the spectra and $\gamma\gamma$ analysis of the proton- and neutron-knockout, inelastic-scattering, and multinucleon-removal reactions, the level scheme shown in Fig. 1 was constructed. The two previously reported transitions and five new ones were identified. Theoretical level energies and spectroscopic factors for the proton- and neutron-knockout reactions were obtained with shell-model calculations using the SDPF-MU interaction, as well as with *ab initio* calculations using the VS-IMSRG approach. Tentative spin assignments were made based on the comparison of the calculations and the experimental results. In both calculations, states with $J^\pi = 2^+$ are preferably populated by the reactions, as shown in the figure. In addition, a (3^-) state is suggested to be populated following the proton inelastic scattering. Both theoretical calculations provide consistent results and a relatively good agreement with the experimental data, emphasizing the subshell closure at $N = 32$ and strengthening our understanding of shell evolution in this region.

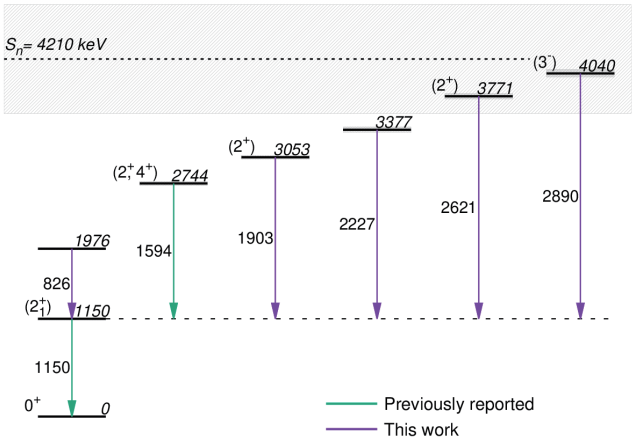

Fig. 1. Experimental level scheme of ^{50}Ar.

† Condensed from Phys. Rev. C. **102**, 064320 (2020)
*1 RIKEN Nishina Center
*2 INFN-Legnaro
*3 Departamento de Física, Universidad Nacional de Colombia
*4 Departamento de Física, Pontificia Universidad Javeriana
*5 IRFU, CEA, Université Paris-Saclay
*6 Institut für Kernphysik, Technische Universität Darmstadt
*7 TRIUMF
*8 Department of Physics, McGill University
*9 Center for Nuclear Study, The University of Tokyo
*10 Departament de Física Quàntica i Astrofísica, Universitat de Barcelona
*11 RCNP, Osaka University
*12 Department of Physics, Osaka City University
*13 ExtreMe Matter Institute (EMMI)
*14 Max-Planck-Institut für Kernphysik
*15 Institut für Kernphysik and PRISMA Cluster of Excellence, Johannes Gutenberg-Universität
*16 Advanced Science Research Center, JAEA

References
1) A. Huck *et al.*, Phys. Rev. C **31**, 2226 (1985).
2) A. Gade *et al.*, Phys. Rev. C **74**, 021302 (2006).
3) F. Wienholtz *et al.*, Nature **498**, 346 (2013).
4) D. Steppenbeck *et al.*, Nature **502**, 207 (2013).
5) S. Michimasa *et al.*, Phys. Rev. Lett. **121**, 022506 (2018).
6) S. Chen *et al.*, Phys. Rev. Lett. **123**, 142501 (2019).
7) H. N. Liu *et al.*, Phys. Rev. Lett. **122**, 072502 (2019).
8) D. Steppenbeck *et al.*, Phys. Rev. Lett. **114**, 252501 (2015).
9) T. Kubo *et al.*, Prog. Theor. Exp. Phys. **2012**, 03C003 (2012).
10) A. Obertelli *et al.*, Eur. Phys. J. A **50**, 8 (2014).
11) T. Kobayashi *et al.*, Nucl. Instrum. Methods Phys. Res. B **317**, 294 (2013).
12) S. Takeuchi *et al.*, Nucl. Instrum. Methods Phys. Res. A **763**, 596 (2014).
13) I. Murray *et al.*, RIKEN Accel. Prog. Rep. **51**, 158 (2017).

Proton removal and lifetimes in the Ca isotopes: Spectroscopy and reaction studies

H. L. Crawford,[*1] S. Paschalis,[*2] and M. Petri[*2] for the RIBF170R1 Collaboration

Nucleon knockout reactions are an essential and powerful tool to study the single-particle structure of nuclei far from stability. Through comparison of measured ($\sigma_{\rm exp}$) and theoretical ($\sigma_{\rm th}$) inclusive and exclusive cross-sections they provide a method to assign specific single-particle configurations and occupancies of states in nuclei. However, the theoretical description of knockout reactions is challenging, requiring both a treatment of the reaction dynamics and the nuclear structure of initial and final states.

The ratio $R = \sigma_{\rm exp}/\sigma_{\rm th}$ has been found, in stable nuclei and specifically for $(e, e'p)$ and single-nucleon transfer reactions[1,2] to be consistently less than 1 ($R \sim 0.6$), a reduction attributed to short and long-range correlations not captured in the shell-model. However, moving away from β-stability, a study by Tostevin and Gade[3] using available one-nucleon removal data on unstable isotopes performed at intermediate energies (∼100 MeV/nucleon) shows a dependence of R on the difference in the proton and neutron separation energies of the initial system. This dependence is in contrast to both transfer reaction data taken at lower energies and to new data reported recently by the R^{3}B collaboration[4] and RIBF[5] for quasi-free one-proton knockout at higher energies.

Given the important implications of disentangling the reaction and structure effects related to the origin of the ΔS dependence of R observed in knockout reactions, we have performed an experiment to directly explore the isospin dependence of proton knockout on both C and H targets at RIBF energies. In addition to the reaction cross-sections, we were also able to take advantage of the opportunity presented by the HiCARI high-resolution γ-ray array[6] at RIBF to simultaneously explore lifetimes in the neutron-rich Ca isotopes, which provide an important testing ground for interactions derived from chiral Effective Field Theory and many-body methods.

The experiment was performed in December 2020 at the RIBF as part of the HiCARI campaign. A ^{70}Zn primary beam was accelerated to 345 MeV/nucleon and fragmented on a ^{9}Be primary target to produce secondary beams centered on ^{38,48,54}Ca. Fragments were separated and identified within BigRIPS using the standard ΔE-TOF-ΔE method. The secondary beam impinged on 1 g/cm^2 thick C and 1.2 g/cm^2 thick CH_2 targets at the F8 focal plane, which induced knockout reactions. The reaction residues were identified in the ZeroDegree spectrometer. The preliminary particle identification plots for the setting on ^{54}Ca are shown in Fig. 1. De-excitation γ-rays were detected within the HiCARI array.

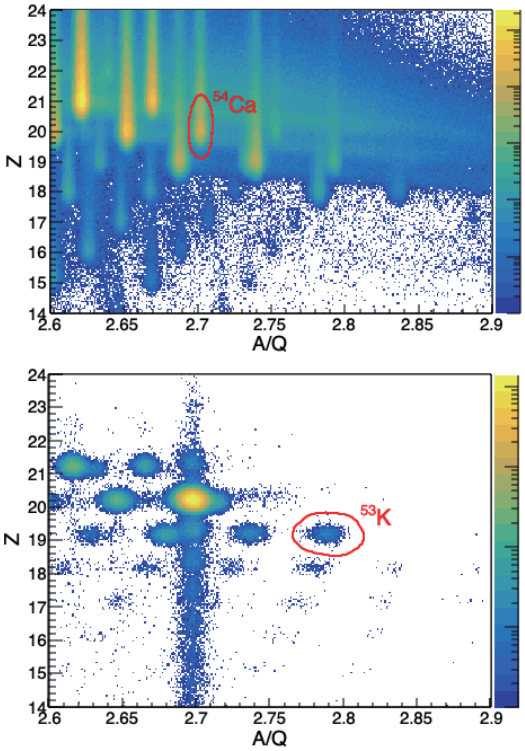

Fig. 1. (Top) Particle identification plot for incoming beam particles in BigRIPS for the setting of ^{54}Ca. (Bottom) Reaction residue particle identification in the ZeroDegree spectrometer, gated on incoming ^{54}Ca particles.

Currently, the proton removal inclusive and exclusive cross-sections from ^{38,48,54}Ca to final states in ^{37,47,53}K are under analysis. In addition, γ-ray spectra in the most neutron-rich Ca isotopes, namely ^{53,54}Ca are being carefully analyzed. Preliminary energy spectra show evidence for lifetimes within the sensitivity range for line-shape analysis, which will be pursued in the next stages of analysis.

*1 Nuclear Science Division, Lawrence Berkeley National Lab
*2 Department of Physics, University of York

References
1) B. P. Kay *et al.*, Phys. Rev. Lett. **111**, 042502 (2013).
2) G. Kramer *et al.*, Nucl. Phys. A **679**, 267 (2001).
3) J. A. Tostevin, A. Gade, Phys. Rev. C **90**, 057602 (2014).
4) L. Atar *et al.*, Phys. Rev. Lett. **120**, 052501 (2018).
5) S. Kawase *et al.*, Prog. Theor. Exp. Phys. **2018**, 021 D01 (2018).
6) K. Wimmer *et al.*, in this report.

Evolution of collectivity in Ti isotopes towards the $N = 40$ island of inversion

T. Koiwai[*1,*2] and K. Wimmer[*3,*2] for the RIBF142R1 Collaboration

Over the past decade, significant efforts on both the experimental and theoretical fronts have focused on the development of nuclear collectivity in exotic isotopes around $N = 40$. It was revealed that the new island of inversion, where the intruder configuration is strongly favored in the ground state, at $N = 40$ is centered around ^{64}Cr.[1,2] It is then interesting to question whether this enhanced collectivity established in the region around the Fe and Cr isotopes presents itself in exotic systems with fewer protons, namely, Ti isotopes. Several theoretical calculations[2–6] show the difference in the reduced transition rates, $B(E2; 0^+ \rightarrow 2^+)$ values, for neutron-rich Ti isotopes beyond ^{56}Ti when considering different model spaces. Although the energies for the first 2^+ state are consistent and agree with experimental data, the $B(E2)$ values differ, depending on whether the *gd* shell is included in the calculations. This suggests that the boundary of the island of inversion is located between ^{56}Ti and ^{58}Ti. To answer these questions, the Coulomb excitation of ^{56,58}Ti was measured.

The experiment was conducted at the RIBF as a part of the HiCARI campaign. A ^{70}Zn primary beam with a maximum intensity of 600 particle nA was accelerated to 345 MeV/nucleon and impinged on a 11-mm-thick ^{9}Be primary target to produce a secondary beam for ^{56,58}Ti. The beam fragments were separated and identified by the BigRIPS using the standard $\Delta E-$TOF$-B\rho$ method. The secondary beam impinged on a 1-mm-thick Au target to induce a Coulomb excitation reaction. A 3-mm-thick Be target was also used to determine the nuclear contribution to the excitation. The reaction residuals were identified by the ZeroDegree spectrometer. De-excitation γ rays were detected by the HiCARI array[7] at the F8 focal plane. The preliminary particle identification plots are shown in Fig. 1. Tails will be removed by further analysis.

Currently, the data are under analysis. The preliminary Doppler-corrected energy spectra show the clear transition peaks at known energies of the first 2^+ state in both ^{56,58}Ti. Moreover, candidates of peaks are found in coincidence with the one-neutron knockout channel from ^{56,58}Ti, which will reveal the configuration of the ground-state wave function of these nuclei.

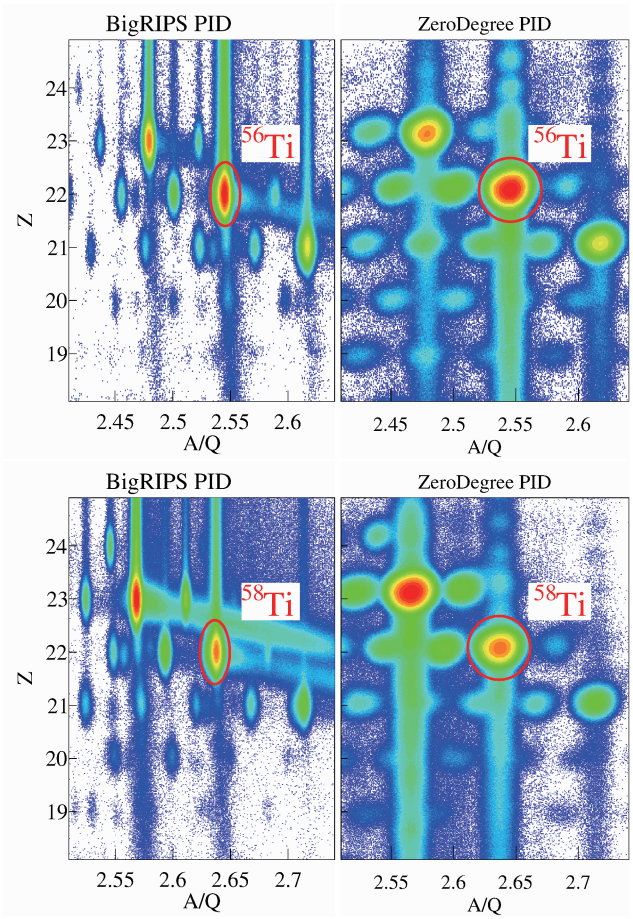

Fig. 1. Particle identification plots for both the incoming beam and outgoing residuals. The top panel shows the ^{56}Ti setting and the bottom the ^{58}Ti setting.

References

1) H. L. Crawford *et al.*, Phys. Rev. Lett. **110**, 242701 (2013).
2) S. M. Lenzi, F. Nowacki, A. Poves, K. Sieja, Phys. Rev. C **82**, 054301 (2010).
3) A. Poves, J. Sánchez-Solano, E. Caurier, F. Nowacki, Nucl. Phys. A **694**, 157 (2001).
4) M. Honma, T. Otsuka, B. A. Brown, T. Mizusaki, Eur. Phys. J. A **25**, s01, 499 (2005).
5) Y. Tsunoda *et al.*, Phys. Rev. C **89**, 031301(R) (2014).
6) L. Coraggio, A. Covello, A. Gargano, N. Itaco, Phys. Rev. C **89**, 024319 (2014).
7) K. Wimmer *et al.*, in this report.

*1 Department of Physics, University of Tokyo
*2 RIKEN Nishina Center
*3 IEM-CSIC

RIBF190: Exploring collectivity beyond ^{78}Ni

F. Browne*1 and V. Werner*2 for the RIBF 190 Collaboration

Recently, it has been indicated that the doubly magic ^{78}Ni has competing low-lying spherical and prolate-deformed states.[1] In its north-east quadrant, measurements of $E(2_1^+)$ and $E(4_1^+)$ of the $N = 52, 54$ Zn isotopes show deformation of ground-states becomes prominent beyond $N = 50$.[2] Shell model[3,4] and interacting boson model calculations[5] that reproduce the available spectroscopic information of $N > 50$ Se and Ge isotopes predict them as transitioning from their $N = 50$ sphericity to collective structures. In the case of the Ge isotopes this takes the form of soft and rigid triaxiality, while the Se isotopes start to exhibit prolate-oblate shape coexistence. Initial spectroscopy seems to agree with the models that predict these interesting features.[6,7] In addition to the quadrupole degrees of freedom, octupole collectivity may be expected to be enhanced in the neutron-rich Ge/Se region due to their proximity to the "doubly octupole magic" numbers, $N = 56$ and $Z = 34$

An experiment was performed over 4 days with three BigRIPS settings to extract the reduced transition probabilities of low-lying states in ^{84,86}Ge and ^{86,88,90}Se in order to clarify the quadrupole and octupole collectivity of the region. Exotic nuclei were produced from the in-flight fission of a ^{238}U beam which was accelerated to 345 MeV/nucleon. Following fission, the isotopes of interest were selected in the first stage of BigRIPS using the $B\rho$-ΔE-$B\rho$ technique and identified with the second stage using their $B\rho$, ΔE, and time-of-flight (TOF) values. The BigRIPS particle-identification plots for the three settings of the experiment are shown in Fig. 1. Secondary targets of Be (3.8-mm-thick) and Bi (1.1 mm-thick) were situated at the F8 focal plane to induce nuclear and Coulomb excitations, respectively. Gamma rays emitted from excited states were detected with the HiCARI array[8] which surrounded F8. The trajectory of incoming and outgoing ions with respect to the target was measured with PPACs. Following the reaction targets, ions were transported through the ZeroDegree spectrometer where they were identified, again using their $B\rho$, ΔE, and TOF values. Finally, the ions were stopped in a gas cell and their masses recorded using a MR-TOF setup.

While off-line data analysis is yet to begin, the on-line γ-ray spectra show clearly that the main objectives of the experiment are attainable. In addition to the Coulomb excitation to the 2_1^+ states being observed in all objective nuclei, some nuclei show 2_2^+ excitations on the heavy target.

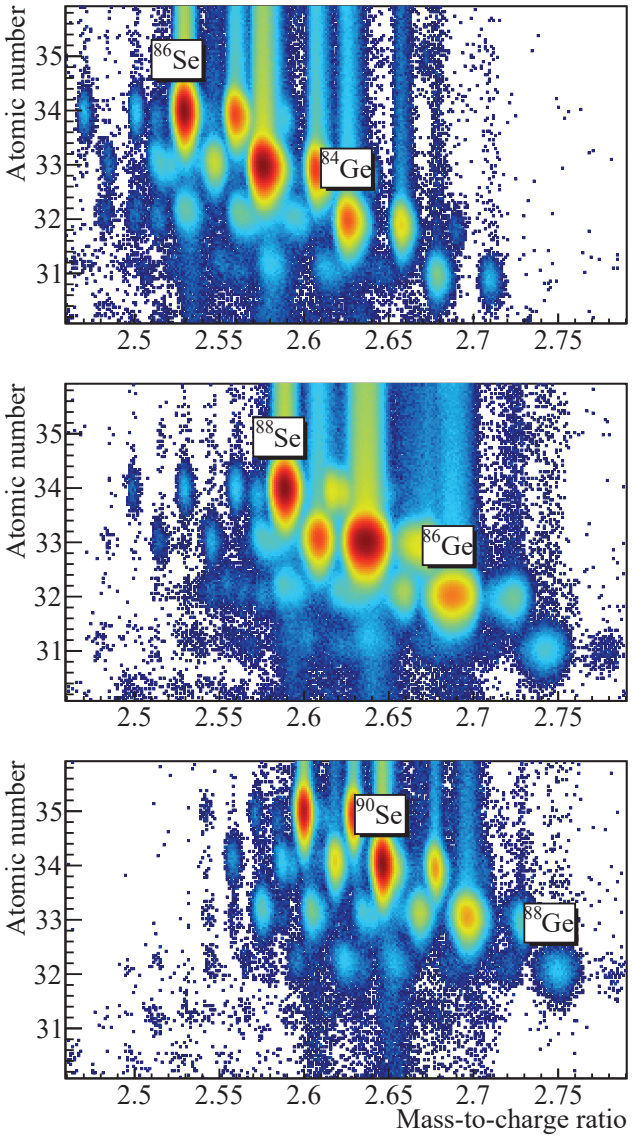

Fig. 1. On-line particle identification plots for the three BigRIPS settings employed during the experiment. Labels refer to the identified ions below them.

*1 RIKEN Nishina Center
*2 IKP, TU Darmstadt

References

1) R. Taniuchi *et al.*, Nature (London) **569**, 53 (2019).
2) C. Shand *et al.*, Phys. Lett. B **773**, 492 (2017).
3) K. Sieja, T. R. Rodríguez, K. Koloz, D. Verney, Phys. Rev. C **88**, 034327 (2013).
4) K. Sieja, Private communication (2019).
5) K. Nomura, R. Rodríguez-Guzmán, L. M. Robledo, Phys. Rev. C **95**, 064310 (2017).
6) M. Lettmann *et al.*, Phys. Rev. C **96**, 011301(R) (2017).
7) S. Chen *et al.*, Phys. Rev. C **95**, 041302(R) (2017).
8) K. Wimmer *et al.*, in this report.

Neutron intruder states and collectivity beyond $N = 50$ towards ^{78}Ni

F. Flavigny,[*1] M. Górska,[*2] and Zs. Podolyák[*3] for the RIBF196 and HiCARI Collaborations

The recent spectroscopy of ^{78}Ni,[1] together with the identification of shape coexistence just below the $N = 50$ shell closure for ^{80}Ge[2] and ^{79}Zn,[3] indicates that deformed intruder configurations could play a crucial role in low-energy structure properties in this region and towards the limits of the nuclear chart. Such configurations are predicted to originate from multiparticle-multihole excitations[4] above the $N = 50$ and $Z = 28$ shell gaps pushed down in energy due to neutron-proton correlations, which enhance quadrupole collectivity. Quantifying how collectivity develops near ^{78}Ni is crucial because it influences binding energies and the drip-line location[5] with consequences for nucleosynthesis calculations relying on these inputs. Because these states involve many-particle excitations, their theoretical description is challenging, and identifying them experimentally is, thus, of prime interest to constrain models. So far, very few experimental indications of these configurations have been obtained in ^{80}Ge and ^{79}Zn, but no direct evidence of these configurations exist for $N = 50$ or above in more exotic species.

During the RIBF196 experiment in November 2020, we sought to identify and characterize for the first time such 2p-1h intruder states in ^{83}Ge and ^{81}Zn which are the last two odd-even $N = 51$ isotones above ^{79}Ni. To do so, we used neutron knockout from ^{84}Ge and ^{82}Zn, both having two neutrons in the $s_{1/2}d_{5/2}$ valence space above $N = 50$. This direct reaction allows the removal of one of the neutrons from the quasi-full $g_{9/2}$ orbital below $N = 50$ to selectively populate $9/2^+$ intruder states based on a $\nu(g_{9/2})^{-1}(s_{1/2}d_{5/2})^{+2}$ configuration and extract their spectroscopic factors.

In addition, the first spectroscopy of low-lying levels in ^{82,84}Zn[6] recently indicated that magicity was strictly confined to $N = 50$ in ^{80}Zn with the onset of deformation developing towards heavier Zn isotopes. To reproduce these findings, it was demonstrated that state-of-the-art shell model calculations needed to include sufficient valence orbitals above $N = 50$ (full *gds* valence space) and to allow the breaking of the ^{78}Ni core. Simultaneously to the study of the intruder states mentioned above, these low-lying states in ^{82}Zn were populated using proton removal from ^{83}Ga, and their lifetimes will be studied by line-shape analysis.

To reach these scientific goals, we performed an experiment in which a primary beam of ^{238}U with a mean intensity of 60 particle nA at 345 MeV/nucleon collided with a 4-mm thick ^{9}Be primary target at the object point of the BigRIPS separator. The secondary beam was purified using Al degraders at the F1 and F5 dispersive planes (8- and 2-mm thick). The secondary cocktail beam containing approximately 61%, 7.4% and 0.2% of ^{84}Ge,^{83}Ga and ^{82}Zn, respectively, at averaged rates of approximately 6100, 740, and 20 s^{-1} impinged for 2.5 days on a 6-mm-thick ^{9}Be target at 253, 248, and 242 MeV/nucleon. Event-by-event identification of projectiles and reaction residues in terms of the atomic number (Z) and mass-to-charge ratio (A/Q) was achieved using the TOF-$B\rho$-ΔE method in both the BigRIPS and ZeroDegree spectrometers. A preliminary particle identification plot in BigRIPS without higher-order optical corrections is shown in Fig. 1. De-excitation γ-rays of the neutron and proton knockout residues ^{83}Ge,^{82}Zn and ^{81}Zn were detected using the HiCARI germanium array (described separately[7]) surrounding the secondary reaction target. A 0.5-mm-thick lead shield was placed around the beam pipe surrounding the target to reduce the rate of low-energy atomic background in the detectors. Known and unknown transitions in ^{83}Ge were clearly identified online. The statistics obtained in this neutron-knockout channel will allow clear identification of the states populated and their possible intruder character after careful analysis of the feeding pattern.

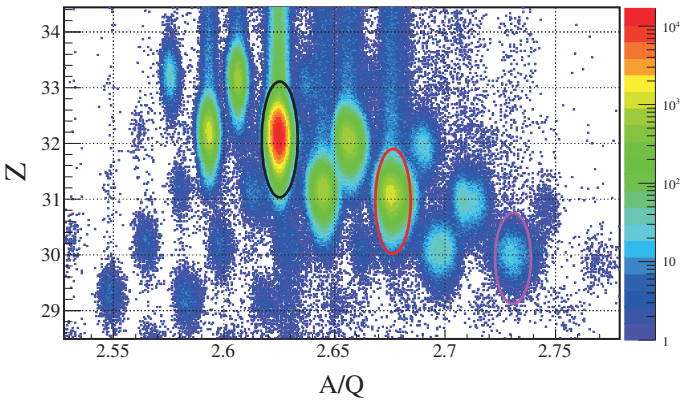

Fig. 1. Preliminary particle identification of the secondary beam in BigRIPS. Black, red and purple ellipsoids indicate ^{84}Ge, ^{83}Ga, ^{82}Zn respectively, see text for details.

*1 LPC Caen, CNRS/IN2P3
*2 GSI Helmholtzzentrum für Schwerionenforschung GmbH
*3 Department of Physics, University of York

References
1) R. Taniuchi *et al.*, Nature **569**, 53 (2019).
2) A. Gottardo *et al.*, Phys. Rev. Lett. **116**, 182501 (2016).
3) X. F. Yang *et al.*, Phys. Rev. Lett. **116**, 219901 (2016).
4) K. Heyde, J. L. Wood, Rev. Mod. Phys. **83**, 1467 (2011).
5) J. Erler *et al.*, Nature **486**, 509 (2012).
6) C. Shand *et al.*, Phys. Lett. B **773**, 492 (2017).
7) K. Wimmer *et al.*, in this report.

High-resolution spectroscopy and lifetime measurements in neutron-rich Zr and Mo isotopes

W. Korten,[*1] B. Moon,[*2,*3] and K. Wimmer[*4,*3] for the RIBF187 Collaboration

One of the most interesting cases of shape evolution in nuclei is encountered along the semi-magic ($Z = 40$) Zr isotopes. While ^{90}Zr, at neutron number $N = 50$, shows properties of a doubly-magic nucleus, neutron-deficient Zr isotopes become well-deformed towards ^{80}Zr. On the neutron-rich side, a sudden onset of deformation is also indicated by the dramatic lowering of the first excited 2^+ state from ^{98}Zr to ^{100}Zr.

When going towards even more neutron-rich isotopes the question about the further shape evolution arises since the theoretical predictions diverge. Many theoretical calculations have been performed for ^{110}Zr since it combines the magic numbers $Z = 40$ and $N = 70$ of the harmonic oscillator potential and could be another quasi doubly-magic nucleus. This question was answered in a previous SEASTAR experiment at the RIBF,[1] which measured the first excited states of ^{110}Zr and showed that this isotope is rather well deformed. However, several questions remain open, such as the possibility of shape coexistence or triaxial deformation at $Z = 40$, $N = 70$ as predicted by different theoretical models.[3–5]

We performed high-resolution spectroscopy of nuclei around ^{110}Zr in an experiment with the HiCARI array[2] in order to measure lifetimes of their (first) excited states . The high-resolution γ-ray detectors from HiCARI will allow to resolve level schemes by measuring γ rays from ∼100 keV, and to measure lifetimes of excited states between ∼20 ps and 1 ns. The results will also allow to confirm the level scheme of ^{110}Zr and to measure decay branching ratios of states beyond the 2_1^+ for the first time.

The nuclei of interest were populated by proton-removal reactions from projectiles around ^{112}Mo, produced from a primary ^{238}U beam, impinging on a secondary Be target. Particle identification of the radioactive beams for selecting the proper reaction channel was performed with the BigRIPS and the ZeroDegree spectrometers. Examples of the particle identification plots are shown in Fig. 1. Average intensities and purities of the projectiles of interest amounted to 81 and 3000 pps and 0.8% and 34% for ^{111}Nb and ^{113}Tc, respectively. Additionally, ^{112}Mo was transmitted at a high rate as well. ^{110}Zr was populated through proton removal reactions from ^{111}Nb and ^{112}Mo. The high intensity of ^{113}Tc allowed to obtain significantly more statistics for ^{112}Mo than in the previous experiment.[1] Additionally, the neighbouring even-even nuclei, ^{108}Zr and ^{110}Mo, have been populated strongly to allow for a detailed lifetime analysis.

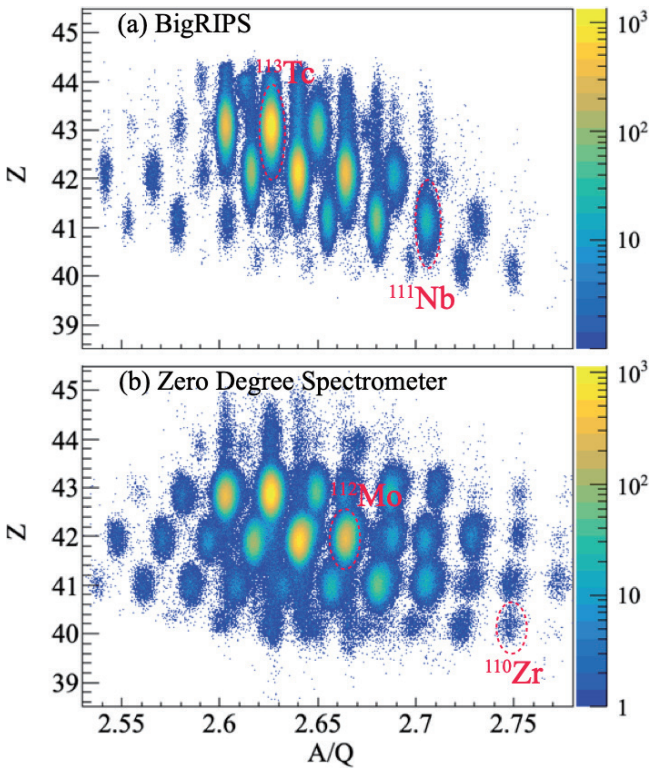

Fig. 1. Preliminary particle Identification (PID) for BigRIPS (top) and ZeroDegree (ZD) spectrometer (bottom).

In order to optimize the experiment for the long lifetimes of the 2^+ states, expected to be several hundred ps, the Be target was positioned 10 cm upstream of the center of HiCARI. Lifetimes will be extracted using the line-shape method[6] and will give access to the collective properties. The experiment will allow to distinguish between predictions of different nuclear models concerning the shape of ^{110}Zr, the key isotope for the evolution of collective properties along the $N = 70$ isotones.

*1 IRFU, CEA Paris-Saclay
*2 CENS, IBS
*3 RIKEN Nishina Center
*4 IEM-CSIC

References
1) N. Paul *et al.*, Phys. Rev. Lett. **118**, 032501 (2017).
2) K. Wimmer *et al.*, in this report.
3) M. Borrajo *et al.*, Phys. Lett. B **746**, 341 (2015).
4) J. Libert, Phys. Rev. C **60**, 1 (1999).
5) T. Togashi *et al.*, Phys. Rev. Lett. **117**, 172502 (2016).
6) P. Doornenbal *et al.*, Nucl. Instrum. Methods Phys. Res. A **613**, 218 (2010).

Single particle structure of semi-magic $^{129}Ag_{82}$

T. Parry,[*1] Zs. Podolyák,[*1] M. Górska,[*2] M. Armstrong,[*2] and A. Yaneva[*2] for the RIBF189 Collaboration

The shell structure is one of the fundamental ingredients in the understanding of mesoscopic systems, which includes the atomic nucleus. One crucial question in nuclear physics is how the quantum orbitals evolve as the number of protons and neutrons change. The ordering of the nuclear orbitals can change drastically in neutron-rich nuclei. In extreme cases, traditional magic numbers can disappear and new ones can emerge. Such changes were already observed for light nuclei, and are predicted for middle-mass ones. The evolution of orbitals and shell gap has obvious consequences on the r-process nucleosynthesis, which is responsible for the production of half of the nuclei heavier than iron. The abundances of nuclei with magic neutron numbers are enhanced due to their lower neutron capture probabilities. Thus the $A \sim 130$ r-process abundance peak is the consequence of the $N = 82$ neutron shell closure. The unknown evolution of the shell structure in this region is one of the main sources of nuclear physics uncertainty in r-process calculations. One has to rely on theoretical models whose predictions for regions far off stability diverge significantly.

^{129}Ag is a singly magic $N = 82$ nucleus. With three protons holes below ^{132}Sn it is neutron-rich, and any experimental information to be obtained on its structure is directly applicable for the understanding of the influence of the $N = 82$ nuclei on the r-process path. Using proton knockout from ^{130}Cd single proton states in ^{129}Ag can be populated.

The experiment was performed in November 2020. For an approximate length of 3 days a 345 MeV/nucleon beam of ^{238}U with an average intensity of around 60 particle nA impinged on a 4 mm ^{9}Be target. Fission fragments were separated and identified in flight with the BigRIPS separator centred on ^{130}Cd. Identification was achieved by using the $B\rho$-ΔE-$B\rho$ technique on an individual particle basis. A preliminary BigRIPS particle identification plot is shown in Fig. 1. This secondary radioactive beam impinged on another target of 6 mm ^{9}Be located at F8. The new germanium HiCARI array[1)] was located around this second beryllium target and used to detect the emitted γ rays with high resolution. The reaction products were identified in the ZeroDegree spectrometer, centred on ^{129}Ag, using the same methods as in BigRIPS.

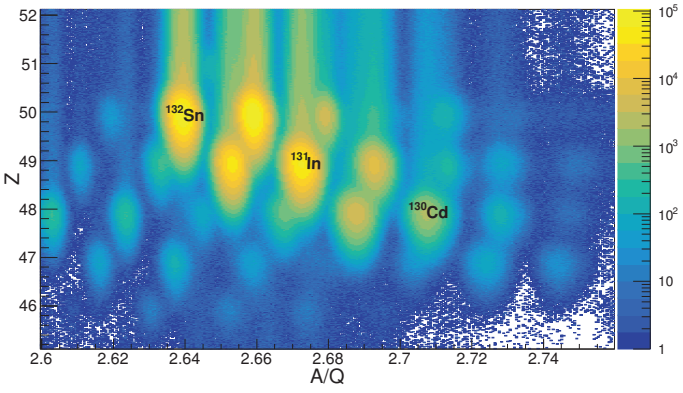

Fig. 1. Particle identification in BigRIPS with $N = 82$ nuclei including ^{130}Cd required for the main expected production channel of ^{129}Ag.

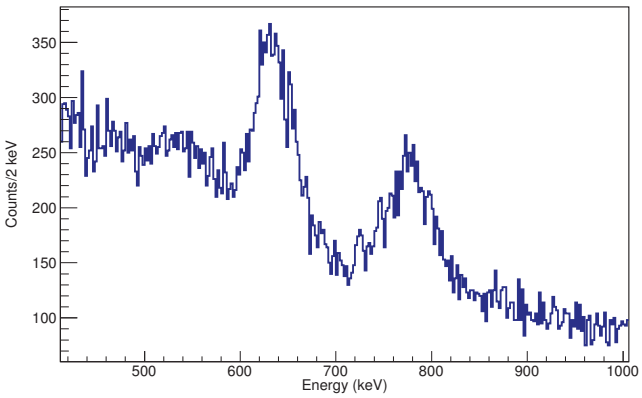

Fig. 2. Doppler corrected γ-ray spectrum of ^{128}Cd as measured by the full HiCARI. Clearly visible are the known[2)] 646 keV 2^+ to 0^+ and 785 keV 4^+ to 2^+ transitions.

The obtained data set is under analysis. As an early indication of the ability of the HiCARI array to achieve in-flight gamma-ray spectroscopy the isotope ^{128}Cd was selected to confirm the array was functioning as intended. ^{128}Cd was selected due to its high yield and its known structure.[2)] A preliminary Doppler corrected γ-ray spectrum of ^{128}Cd populated in one-proton removal from ^{131}In showing the 4^+ and 2^+ gamma rays is presented in Fig. 2. Note that using β values determined for individual particles, as well as updated calibrations, will result in a much better improved energy resolution.

*1 Department of Physics, University of Surrey
*2 GSI Helmholtzzentrum für Schwerionenforschung GmbH

References

1) K. Wimmer *et al.* (HiCARI Collaboration), in this report.
2) A. Scherillo *et al.*, Phys. Rev. C **70**, 054318 (2004).

Characterization of a strongly Coulomb-excited state at an excitation energy above 4 MeV in ^{136}Te

A. Jungclaus*1 and P. Doornenbal*2 for the NP1912-RIBF193 Collaboration

In April 2015, the experiment NP1306-RIBF98R1 was performed aiming for a methodical study of the systematic uncertainties inherent to the analysis of Coulomb excitation experiments at relativistic energies, using ^{136}Te as a high-statistics test case. The analysis of the obtained data is finished and the results are published.[1–3] In that experiment, besides the known 607-keV, $2_1^+ \rightarrow 0_1^+$ transition, additional γ strength in the range 3.0–4.5 MeV was observed in the inelastic excitation of ^{136}Te on a gold target.[4] The experimental spectra are nicely described assuming that two γ rays are detected, whereas the bump at high energy is too broad to be described by one single transition. However, due to the limited in-beam energy resolution of the DALI2 spectrometer, the individual γ-ray energies can only be determined with rather large uncertainties. The intensity ratio between the two lines clearly depends on the γ-ray multiplicity of the event. The line at higher energy has a higher yield when only one γ ray is detected, while the one at lower energy is more intense for events with γ-ray multiplicity two. From this observation, it can be concluded that the γ ray with higher energy is emitted in cascades with lower multiplicity. Unfortunately, however, due to random coincidences with background γ rays, it is not possible to go beyond this qualitative statement. Based on the available experimental information it is not possible to determine whether the two transitions populate the 4_1^+ and 2_1^+ or the 2_1^+ and 0_1^+ states of ^{136}Te.

The large cross section measured for the excitation of a state above 4 MeV in a heavy nucleus such as ^{136}Te in the inelastic scattering on a gold target is difficult to explain. Whatever the spin of the newly identified state is, the corresponding transition probability is exceptionally large. Theoretical studies suggest that the new excited state in ^{136}Te may be related to the existence of loosely-bound neutrons outside the ^{132}Sn core. It is therefore of utmost interest to better characterize this unusual state.

The availability of the HiCARI array at RIKEN in 2020 offered the unique opportunity to further investigate this interesting case. The superb position resolution of the tracking detectors translates into a very good in-beam energy resolution for high-energy γ rays. Therefore, the inelastic excitation of ^{136}Te on a gold target was measured again with the goal to determine the energies of the two high-energy γ rays emitted in the decay of the new state with sufficient precision in order to establish to which low-lying levels of ^{136}Te the decay proceeds. In addition, also the inelastic excitation on a Be target was studied in order to allow for a determination of the nuclear deformation length from the measured cross section. The aim of this part of the experiment was to obtain further information with respect to the spin of the new state above 4 MeV in ^{136}Te.

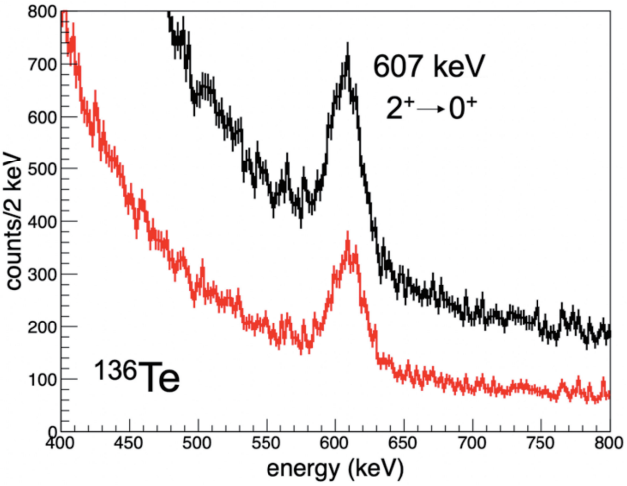

Fig. 1. HiCARI γ-ray spectrum of ^{136}Te populated via inelastic excitation on a gold target, considering either all γ-ray multiplicities (black) or $M_\gamma = 1$ (red).

The experiment NP1912-RIBF193 was performed during the HiCARI campaign in November 2020. For both the Au and Be targets the expected counting statistics was accumulated and the taken data in the experiment is currently under analysis. The selection of the reaction channel was achieved via event-by-event ion identification in the BigRIPS and ZeroDegree spectrometers. A preliminary γ-ray spectrum of ^{136}Te in the region around the known $2_1^+ \rightarrow 0_1^+$ transition, taken with the HiCARI array following the inelastic excitation on a gold target, is shown in Fig. 1.

*1 IEM-CSIC, Madrid
*2 RIKEN Nishina Center

References

1) V. Vaquero *et al.*, Phys. Rev. Lett. **118**, 202502 (2017).
2) V. Vaquero *et al.*, Phys. Lett. B **795**, 356 (2019).
3) V. Vaquero *et al.*, Phys. Rev. C **99**, 034306 (2019).
4) V. Vaquero, PhD thesis, Universidád Autónoma de Madrid, 2018.

Study of the ^{9}C proton breakup reaction

A. I. Chilug,[*1,*2,*3] V. Panin,[*4] L. Trache,[*1] D. State,[*1,*2] I. C. Stefanescu,[*1,*2] J. Tanaka,[*3] H. Otsu,[*3] T. Motobayashi,[*3] A. Spiridon,[*1] and T. Uesaka[*3] for HI-p Collaboration

The ^{9}C proton breakup reaction was studied during the SAMURAI29 experiment at RIKEN. The reaction was studied by two methods: Coulomb dissociation and nuclear breakup. The physics goal of the experiment was to evaluate the astrophysical S_{18}-factor of the inverse process, the ^{8}B$(p,\gamma)^{9}$C, at energies relevant for astrophysics.

The SAMURAI29 experiment is the first performed among a series of 4 experiments with proton-rich secondary beams and was carried out with a 160-MeV/nucleon ^{9}C beam produced from an ^{18}O primary beam, at the F13 focal plane using the SAMURAI magnetic spectrometer. The whole experimental setup is detailed in Ref. 1) and in Ref. 2). The detection system was prepared to ensure the inclusive and exclusive measurements of the ^{9}C breakup reaction. Therefore, a silicon GLAST-type detector system and a set of two new drift chambers (PDC1 and PDC2) were used to detect the protons produced in the breakup. Both systems were used for the first time during the experiment.

The silicon detectors, the signals of which were processed using a combination of HINP16 electronics and the new Dual-Gain Preamplifiers developed by the RIKEN-ATOMKI collaboration,[3)] enabled the simultaneous detection of the proton and ^{8}B from the reaction. Therefore, they cover a large dynamic energy range, as shown in Fig. 1. Having these tracking detectors together with other SAMURAI standard detectors enabled

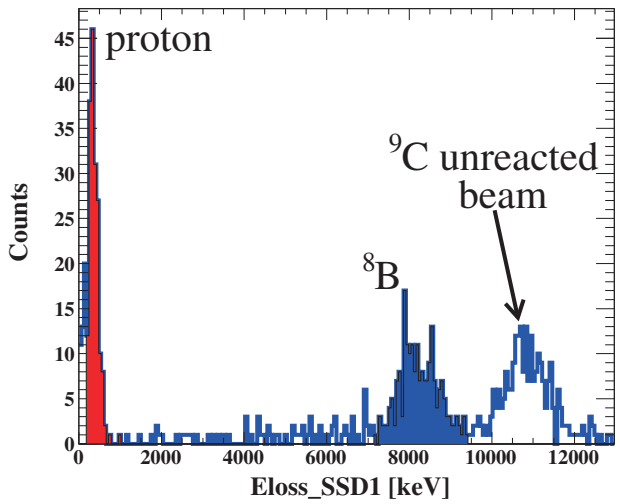

Fig. 1. Energy deposited by the proton and ^{8}B recorded simultaneously in the first layer of the silicon detector.

*1 Department of Nuclear Physics, IFIN-HH
*2 Doctoral School of Physics, University of Bucharest
*3 RIKEN Nishina Center
*4 GSI Helmholtzzentrum fur Schwerionenforschung GmbH

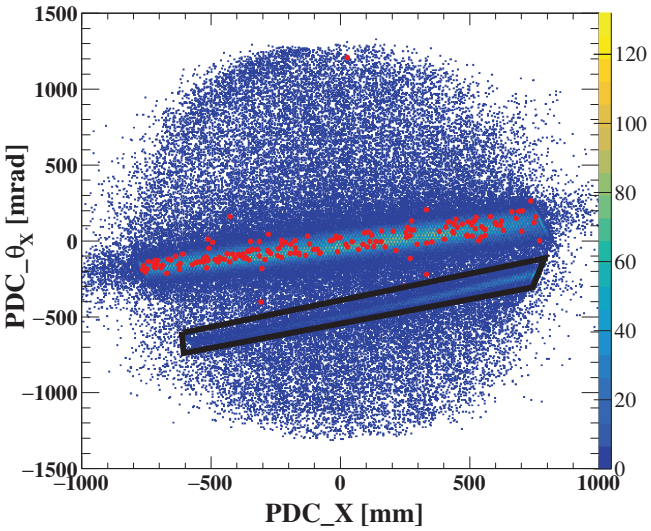

Fig. 2. Protons tracked in the proton drift chambers (PDCs).

the reconstruction of the proton momentum distribution, which provides information on the shell occupied by the removed proton in ^{9}C.

A serious complication in the analysis is the background from the interaction of the beam particles with the experimental detectors, which must be excluded from the events. One example is the protons produced in the plastic scintillator bars of the HODF, which were detected in the PDCs. In Fig. 2, the red dots indicate the protons produced in the target with the condition of coincident proton signals in the silicon detectors, whereas the events marked with the black box area in the figure are protons produced in the HODF detector.

The following steps have been achieved so far in the data analysis.

(1) The one-proton removal channel from ^{9}C nucleus is clearly separated in the data.
(2) With the tracked positions in the silicon detectors placed after the target, it was possible to reconstruct the reaction vertex.
(3) The proton and ^{8}B momentum distributions were determined.
(4) The Coulomb dissociation yield of the ^{9}C breakup as a function of the relative energy between the proton and ^{8}B was obtained.

Further analysis of the experimental data is in progress.

References

1) A. I. Chilug *et al.*, RIKEN Accel. Prog. Rep. **52**, 27 (2019).
2) A. I. Chilug *et al.*, AIP. Conf. Proc. **2076**, 060001 (2019).
3) V. Panin *et al.*, RIKEN Accel. Prog. Rep. **51**, 148 (2018).

Gamow-Teller giant resonance in ^{11}Li neutron drip-line nucleus

L. Stuhl,[*1,*2,*3] M. Sasano,[*3] J. Gao,[*3,*4] Y. Hirai,[*5] K. Yako,[*2] T. Wakasa,[*5] D. S. Ahn,[*3] H. Baba,[*3] A. I. Chilug,[*6,*3] S. Franchoo,[*7] Y. Fujino,[*8] J. Gibelin,[*9] I. S. Hahn,[*1,*10] Z. Halász,[*11] T. Harada,[*12] M. N. Harakeh,[*13,*14] D. Inomoto,[*5] T. Isobe,[*3] H. Kasahara,[*5] D. Kim,[*1,*15] G. G. Kiss,[*11] T. Kobayashi,[*16] Y. Kondo,[*17] Z. Korkulu,[*1,*3] S. Koyama,[*18] Y. Kubota,[*3] A. Kurihara,[*17] H. N. Liu,[*19] M. Matsumoto,[*17] S. Michimasa,[*2] H. Miki,[*17] M. Miwa,[*20] T. Motobayashi,[*3] T. Nakamura,[*17] M. Nishimura,[*3] H. Otsu,[*3] V. Panin,[*3] S. Park,[*10] A. T. Saito,[*17] H. Sakai,[*3] H. Sato,[*3] T. Shimada,[*17] Y. Shimizu,[*3] S. Shimoura,[*2] A. Spiridon,[*6] I. C. Stefanescu,[*6] X. Sun,[*3,*4] Y. L. Sun,[*19] H. Suzuki,[*3] E. Takada,[*21] Y. Togano,[*8] T. Tomai,[*17,*3] L. Trache,[*6] D. Tudor,[*6,*3] T. Uesaka,[*3] H. Yamada,[*17] M. Yasuda,[*17] K. Yoneda,[*3] K. Yoshida,[*3] J. Zenihiro,[*3] and N. Zhang[*22,*2]

Recent nuclear physics studies are increasingly focused on the region far from the valley of stability, thereby leading to an increase in the intensity of available exotic isotopes. We started a program[1] at the RIKEN Radioactive Isotope Beam Factory with the objective of measuring the spin-isospin responses of light nuclei along the neutron drip line. There are no available data on nuclear collectivity (giant resonances) on any drip-line nucleus.

In the SAMURAI30 experiment, we studied the most basic nuclear collectivity, the Gamow-Teller (GT) giant resonance, in ^{11}Li (at 181 MeV/nucleon) and ^{14}Be (at 198 MeV/nucleon) nuclei. The charge-exchange (CE) (p, n) reactions in inverse kinematics are efficient tools for extracting the B(GT) strengths of unstable isotopes, up to high excitation energies, without Q-value limitation.[2] The uniqe setup of the Particle Analyzer Neutron Detector Of Real-time Acquisition (PANDORA)[3] low-energy neutron counter + SAMURAI magnetic spectrometer,[4] together with a thick liquid hydrogen target allowed us to perform such measurements with high luminosity and low background. In our previous study on ^{132}Sn, we verified that with this setup, we can extract the strength distribution of isovector spin-flip giant resonances in unstable nuclei with quality comparable to those on stable nuclei.[5]

In the ^{11}Li$(p, n)^{11}$Be reaction, we identified clear kinematical correlations[6] between the neutron energy and laboratory scattering angle for more than ten different decay channels of ^{11}Be: $^{10}\mathrm{Be}+n$, $^{9}\mathrm{Be}+2n$, $^{9}\mathrm{Li}+p+n$, $^{8}\mathrm{Li}+p+2n$, $^{9}\mathrm{Li}+d$, $^{8}\mathrm{Li}+t$, $^{8}\mathrm{Li}+d+n$, $^{7}\mathrm{Li}+t+n$, $^{7}\mathrm{Li}+d+2n$, $^{6}\mathrm{Li}+t+2n$, $\alpha+{}^{6}\mathrm{He}+n$ and $2\alpha+3n$.

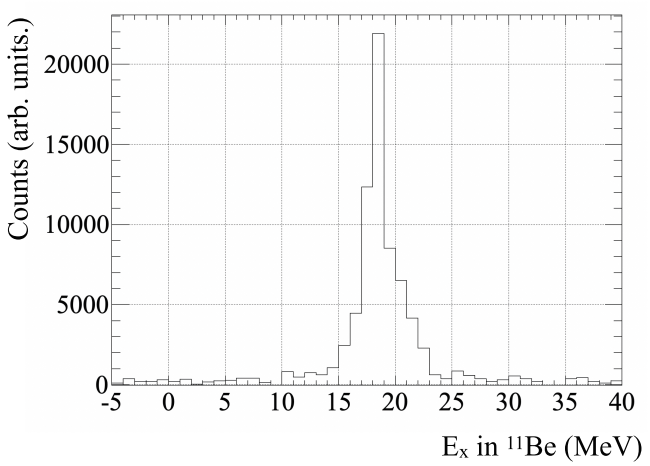

Fig. 1. Excitation energy spectrum in the 6°–8° center-of-mass system for $^{8}\mathrm{Li}+\mathrm{t}$.

The excitation-energy spectra up to approximately 40 MeV have been reconstructed. The background subtraction and acceptance correction are performed. As an example, Fig. 1 presents the excitation energy spectrum in the daughter nucleus ^{11}Be for the $^{8}\mathrm{Li}+t$ decay channel for $\theta_{\mathrm{C.M.}} = 6°$–$8°$. A forward scattering peak in the 0°–10° center-of-mass system indicates a strong GT transition in all decay channles at approximately 19 MeV, below the Isobaric analogue state,[7] which agrees well with previous beta-decay studies.[8]

*1 Center for Exotic Nuclear Studies, Institute for Basic Science (IBS)
*2 Center for Nuclear Study, University of Tokyo
*3 RIKEN Nishina Center
*4 School of Physics, Peking University
*5 Department of Physics, Kyushu University
*6 Horia Hulubei Nat. Inst. of Phys. and Nucl. Eng.
*7 Inst. de Physique Nuclaire, Univ. Paris-Saclay
*8 Department of Physics, Rikkyo University
*9 LPC CAEN
*10 Department of Physics, Ewha Womans University
*11 ATOMKI, Institute for Nuclear Research, HAS
*12 Department of Physics, Toho University
*13 University of Groningen
*14 GSI Helmholtzzentrum für Schwerionenforschung GmbH
*15 Department of Physics, Korea University
*16 Department of Physics, Tohoku University
*17 Dept. of Physics, Tokyo Institute of Technology
*18 Department of Physics, University of Tokyo
*19 Dépt. Physique Nucl., CEA, Univ. Paris-Saclay
*20 Dept. of Physics, Saitama University, Saitama
*21 National Institute of Radiological Sciences (NIRS)
*22 Institute of Modern Physics, Chinese Acad. of Sci.

References

1) L. Stuhl *et al.*, RIKEN Accel. Prog. Rep. **48**, 54 (2015).
2) M. Sasano *et al.*, Phys. Rev. Lett. **107**, 202501 (2011).
3) L. Stuhl *et al.*, Nucl. Instrum. Methods Phys. Res. A **866**, 164 (2017).
4) T. Kobayashi *et al.*, Nucl. Instrum. Methods Phys. Res. B **317**, 294 (2013).
5) J. Yasuda *et al.*, Phys. Rev. Lett. **121**, 132501 (2018).
6) L. Stuhl *et al.*, Nucl. Instrum. Methods Phys. Res. B **463**, 189 (2020).
7) T. Teranishi *et al.*, Phys. Lett. B **407**, 110 (1997).
8) R. Raabe *et al.*, Phys. Rev. Lett. **101**, 212501 (2008).

One proton removal cross section of ^{25}F with a carbon target

Y. Yoshitome,[*1,*2] Y. Kondo,[*1,*2] T. Nakamura,[*1,*2] J. A. Tostevin,[*3] R. Tanaka,[*1,*2] R. Minakata,[*1,*2] S. Ogoshi,[*1,*2] N. A. Orr,[*4] N. L. Achouri,[*4] T. Aumann,[*5,*6] H. Baba,[*2] F. Delaunay,[*4] P. Doornenbal,[*2] N. Fukuda,[*2] J. Gibelin,[*4] J. W. Hwang,[*7] N. Inabe,[*2] T. Isobe,[*2] D. Kameda,[*2] D. Kanno,[*1,*2] S. Kim,[*7] N. Kobayashi,[*1,*2] T. Kobayashi,[*8,*2] T. Kubo,[*3] S. Leblond,[*4] J. Lee,[*2] F. M. Marqués,[*4] T. Motobayashi,[*2] D. Murai,[*9] T. Murakami,[*10] K. Muto,[*8] T. Nakashima,[*1,*2] N. Nakatsuka,[*10,*2] A. Navin,[*11,*14] S. Nishi,[*1,*2] H. Otsu,[*2] H. Sato,[*2] Y. Satou,[*7] Y. Shimizu,[*2] H. Suzuki,[*2] K. Takahashi,[*8] H. Takeda,[*2] S. Takeuchi,[*2] Y. Togano,[*9] A. G. Tuff,[*12] M. Vandebrouck,[*13] and K. Yoneda[*2]

Experimental one-proton (neutron) removal cross sections σ_{-1p} (σ_{-1n}) with light target nuclei (Be and C) at intermediate energies have been shown to be hindered with respect to the corresponding theoretical values. Their ratio $R_s = \sigma_{\rm exp}/\sigma_{\rm th}$ (reduction factor) shows a strong linear dependence on the difference between the $1p$ and $1n$ separation energies, $\Delta S = S_p - S_n$ ($S_n - S_p$).[1,2] This dependence has been recognized as a key to understand correlations beyond the shell-model-based picture of atomic nuclei. The theoretical cross sections are evaluated using shell-model spectroscopic factors C^2S combined with an established reaction theory at intermediate energies, such as eikonal and impulse approximation. The reduction factor depends on the reaction used and the reduction mechanisms are yet to be clarified.[3]

We report a preliminary result of the one-proton removal cross section of ^{25}F with a carbon target at 218 MeV/nucleon. This data point is a useful addition to the systematics of the one-nucleon removal cross sections. It should be noted that ^{25}F has one proton more than doubly-magic ^{24}O. Accordingly, we expect that the spectroscopic factor for proton removal from ^{25}F is close to unity. However, the recent ^{25}F$(p,2p)$ measurement at SHARAQ at RIBF[4] obtained a much-reduced value of 0.36(13) from ^{25}F to the bound ^{24}O. We also note that the ΔS value of 10.17(24) MeV for ^{25}F lies between those of the stable nuclei ($|\Delta S| < 8$ MeV) and drip-line nuclei ($|\Delta S| = 15$–30 MeV). As such, the one-nucleon removal cross section from ^{25}F on the carbon target is a valuable addition.

The ^{25}F$(-p)$ removal cross section on the carbon target was measured using the SAMURAI device at RIBF, as a by-product of the measurement of the one-proton removal of ^{26}F and ^{27}F into ^{25}O and ^{26}O, respectively.[5] For details of the experimental setup and method, see Ref. 5). The ^{25}F secondary beam was produced by the projectile-fragmentation of ^{48}Ca at 345 MeV/nucleon with a thick beryllium target. The beam intensity of ^{25}F reached 1.1×10^3 particles/s with a purity of 3.4%. The ^{25}F projectile then impinged on the carbon target with a thickness of 1.8 g/cm^2. The mean energy at the middle of the target was 218 MeV/nucleon, with momentum acceptance of $|\Delta P/P| \leq 0.6\%$. The particle identification (PID) for ^{25}F was obtained by the standard method at the BigRIPS.[5] The PID of the ^{24}O residue was made by the measurements of the time of flight (TOF), and energy loss ΔE at the hodoscope (HODF), with the magnetic rigidity ($B\rho$) obtained by the tracking with the two multi-wire drift chambers, FDC1 and FDC2, at the entrance and exit of the SAMURAI superconducting magnet, respectively.[5,6] The central field of the magnet was 3.0 T.

The ^{25}F$(-p)$ removal cross section was extracted using the ratio of the counts of the outgoing ^{24}O to those of ^{25}F, where the background events measured with the empty target were subtracted. The effect of reaction loss in the thick target was incorporated using the procedure in Ref. 7). The obtained preliminary value of the one-proton removal cross section of ^{25}F is 7.1(8) mb. USDB-interaction shell- and eikonal-model calculations give the theoretical cross section 14.9 mb, resulting in the reduction factor $R_s = 0.48(5)$. Further evaluation of nucleon removal cross sections in neighboring neutron-rich isotopes is in progress.

*1 Department of Physics, Tokyo Institute of Technology
*2 RIKEN Nishina Center
*3 Department of Physics, University of Surrey
*4 LPC-Caen, ENSICAEN, Université de Caen, CNRS/IN2P3
*5 Institut für Kernphysik, Technische Universität Darmstadt
*6 ExtreMe Matter Institute (EMMI) and Research Division, GSI
*7 Department of Physics and Astronomy, Seoul National University
*8 Department of Physics, Tohoku University
*9 Department of Physics, Rikkyo University
*10 Department of Physics, Kyoto University
*11 GANIL, CEA/DSM-CNRS/IN2P3
*12 Department of Physics, University of York
*13 Institut de Physique Nucléaire, Université Paris-Sud, IN2P3-CNRS
*14 Present address: GANIL CEA/DRF-CNRSI/N2P3

References

1) A. Gade *et al.*, Phys. Rev. C **77**, 044306 (2008).
2) J. A. Tostevin, A. Gade, Phys. Rev. C **90**, 057602 (2014).
3) T. Aumann *et al.*, Prog. Part. Nucl. Phys., in press.
4) T. L. Tang *et al.*, Phys. Rev. Lett. **124**, 212502 (2020).
5) Y. Kondo *et al.*, Phys. Rev. Lett. **116**, 102503 (2016).
6) T. Kobayashi *et al.*, Nucl. Instrum. Methods Phys. Res. B **317**, 294 (2013).
7) N. Kobayashi *et al.*, Phys. Rev. C **86**, 054604 (2012).

Particle identification of SAMURAI11 experiment

J. Gao,[*1,*3] M. Sasano,[*1] L. Stuhl,[*6,*2] Y. Hirai,[*4] T. Wakasa,[*4] D. S. Ahn,[*1] J. K. Ahn,[*13] H. Baba,[*1] K. Chae,[*20] A. Chilug,[*5,*1] K. Cook,[*15] Y. Fujino,[*7] N. Fukuda,[*1] B. Gao,[*19] S. Goto,[*4] I. S. Hahn,[*6,*8] Y. Hamano,[*4] Z. Halász,[*9] T. Harada,[*10] S. Hong,[*20] S. Huang,[*1,*3] N. Inabe,[*1] D. Inomoto,[*4] T. Isobe,[*1] H. Kasahara,[*4] D. Kim,[*6,*8] T. Kobayashi,[*14] Y. Kondo,[*15] Z. Korkulu,[*6,*1] A. J. Krasznahorkay,[*9] H. Miki,[*15] K. Miki,[*14] S. Mitsumoto,[*4] M. Miwa,[*18] T. Motobayashi,[*1] T. Nakamura,[*15] M. Nishimura,[*1] H. Oshiro,[*4] H. Otsu,[*1] V. Panin,[*1] S. Sakaguchi,[*4] D. Sakai,[*14] H. Sakai,[*1] S. Sakaki,[*4] H. Sato,[*1] T. Shimada,[*15] Y. Shimizu,[*1] B. Sun,[*21] X. Sun,[*1,*3] H. Suzuki,[*1] J. Tanaka,[*1] Y. Togano,[*7] T. Tomai,[*15,*1] T. Uesaka,[*1] Y. Utsuki,[*14] H. Wang,[*15] X. Xu,[*19] K. Yako,[*2] A. Yasuda,[*15] K. Yoneda,[*1] K. Yoshida,[*1] Y. Yoshitome,[*15] and J. Zenihiro[*1]

In this report, we present the particle identification (PID) results of the decay fragments from the ^{48}Cr$(p,n)^{48}$Mn reaction in the SAMURAI11 experiment.[1)]

The charge number Z and mass to charge ratio A/Z are used to identify particles, where Z is calculated using the energy loss ΔE and time-of-flight measured in the hodoscope and A/Z is calculated using the rigidity and flight path from the simulation and the time-of-flight. With the position and angle information from the drift chambers before and after the SAMURAI magnet, the rigidity and trajectory of the particle could be extracted by simulation. The simulation program uses a 4th-order Runge-Kutta method to simulate the trajectory and it iterates several times to determine the rigidity that reproduces the position and angle measured in the drift chambers.

Our hodoscope detector consists of seven bars. The size of each bar is 1200 mm(H) × 100 mm(W) × 10 mm(T). The PID in one hodoscope bar is shown in Fig. 1. Because the position on the PID plot of one particle could be slightly shifted in different bars, we evaluate the resolution on one bar only. The resolution of the charge number Z is $\sigma_{Z,^{48}\mathrm{Cr}} = 0.20$ and $\sigma_{Z,^{46}\mathrm{V}} = 0.19$, corresponding to 5.0σ separation for $Z = 23$ and $Z = 24$. The resolution of the mass to charge ratio A/Z is $\sigma_{A/Z,^{46}\mathrm{V}} = 0.0099$ and $\sigma_{A/Z,^{47}\mathrm{V}} = 0.0083$, corresponding to 4.3σ separation.

This work was funded by the China Scholarship Council, KAKENHI project 16H06716, the Japan Society for the Promotion of Science, and Kurata Grant from the Kurata Memorial Hitachi Science and Technology Foundation.

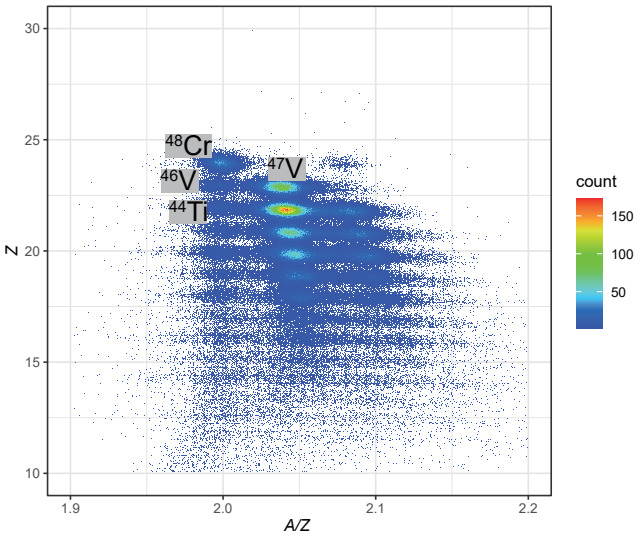

Fig. 1. PID in one bar of hodoscope. This bar is the one next to the bar hitting by beam particles, on the higher rigidity side. Some particles are labeled on the figure.

*1 RIKEN Nishina Center
*2 Center for Nuclear Study, University of Tokyo
*3 School of Physics, Peking University
*4 Department of Physics, Kyushu University
*5 Horia Hulubei Nat. Inst. of Phys. and Nucl. Eng.
*6 Center for Exotic Nuclear Studies, Institute for Basic Science
*7 Department of Physics, Rikkyo University
*8 Department of Physics, Ewha Womans University
*9 ATOMKI, Institute for Nuclear Research
*10 Department of Physics, Toho University
*11 KVI - CART, University of Groningen
*12 GSI Helmholtzzentrum für Schwerionenforschung GmbH
*13 Department of Physics, Korea University
*14 Department of Physics, Tohoku University
*15 Dept. of Physics, Tokyo Institute of Technology
*16 Department of Physics, University of Tokyo
*18 Dept. of Physics, Saitama University
*19 Institute of Modern Physics, Chinese Acad. of Sci.
*20 Department of Physics, Sungkyunkwan University
*21 School of Physics and Nuclear Engineering, Beihang University

Reference
1) M. Sasano *et al.*, RIKEN Accel. Prog. Rep. **53**, 40 (2019).

Symmetry energy investigation with pion production from Sn + Sn systems†

G. Jhang,[*1,*2,*3] J. Estee,[*1,*2,*3] J. Barney,[*1,*2,*3] G. Cerizza,[*1,*2,*3] M. Kaneko,[*1,*4] J. W. Lee,[*1,*5] W. G. Lynch,[*2,*3] T. Isobe,[*1] M. Kurata-Nishimura,[*1] T. Murakami,[*1,*4] C. Y. Tsang,[*2,*3] M. B. Tsang,[*2,*3] R. Wang,[*2] H. Baba,[*1] N. Fukuda,[*1] B. Hong,[*5] T. Kobayashi,[*6] P. Lasko,[*7] J. Łukasik,[*7] A. B. McIntosh,[*8] H. Otsu,[*1] P. Pawłowski,[*7] H. Sakurai,[*1] C. Santamaria,[*1,*2] R. Shane,[*2] D. Suzuki,[*1] S. Tangwancharoen,[*2] Z. G. Xiao,[*9] S. J. Yennello,[*8,*10] Y. Zhang[*9] for the SπRIT Collaboration
and
M. Colonna,[*11] P. Danielewicz,[*2,*3] C.-M. Ko,[*8,*12] A. Ono,[*6] H. Wolter[*13] for the TMEP collaboration

In the last couple of decades, pions produced in the high density regions of heavy ion collisions have been considered to be one of sensitive probes to investigate the symmetry energy term in the nuclear equation of state at high densities, a key property to understand neutron stars. In our new experiment designed to study the symmetry energy, the multiplicities of negatively and positively charged pions have been measured with high accuracy for central ^{132}Sn + ^{124}Sn, ^{112}Sn + ^{124}Sn, and ^{108}Sn + ^{112}Sn collisions at $E/A = 270$ MeV with the SπRIT Time Projection Chamber[2,3] placed inside the SAMURAI spectrometer[4] at RIBF. While individual pion multiplicities are measured to 4% accuracy, those of the charged pion multiplicity ratios are measured to 2% accuracy. We compare these data to predictions from seven major transport models which have taken part in the Transport Model Evaluation Project (TMEP).[5–7] The calculations reproduce qualitatively the dependence of the multiplicities and their ratios on the total neutron and proton number in the colliding systems.

As shown in Fig. 1, however, the predictions of the transport models from different codes differ too much to allow extraction of reliable constraints on the symmetry energy from the data even using the double pion ratio. This finding may explain previous contradictory conclusions on symmetry energy constraints obtained from pion data in Au + Au system.[8–12] These new results call for still better understanding of the differences among transport codes, and new observables that are more sensitive to the density dependence of the symmetry energy.

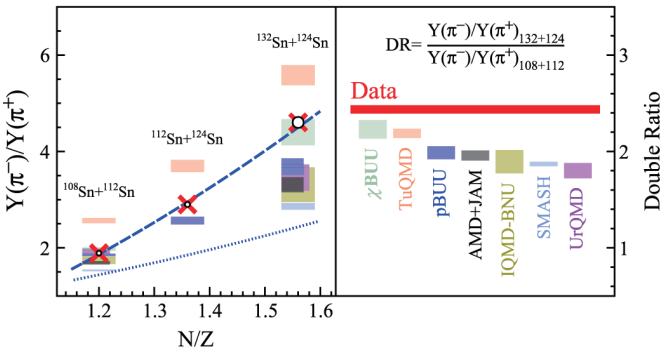

Fig. 1. (Left panel) Experimental charged pion yield ratios as a function of N/Z together with the results of seven transport-model predictions for the soft and stiff symmetry energies (the difference of predictions are presented by the height of colored boxes). The dashed blue line is a power-law fit with the function $(N/Z)^{3.6}$, while the dotted blue line represents $(N/Z)^2$ of the system. (Right panel) Double pion yield ratios for ^{132}Sn + ^{124}Sn and ^{108}Sn + ^{112}Sn. The data and their uncertainty are given by the red horizontal bar and the results of the transport models are shown by the colored boxes, in a similar way as in the left panel. Taken from Ref. 1).

† Condensed from the article in Phys. Lett. B **813**, 136016 (2021)[1)]

*1 RIKEN Nishina Center
*2 National Superconducting Cyclotron Laboratory, Michigan State University
*3 Department of Physics, Michigan State University
*4 Department of Physics, Kyoto University
*5 Department of Physics, Korea University
*6 Department of Physics, Tohoku University
*7 Institute of Nuclear Physics PAN
*8 Cyclotron Institute, Texas A&M University
*9 Department of Physics, Tsinghua University
*10 Department of Chemistry, Texas A&M University
*11 INFN-LNS, Laboratori Nazionali del Sud
*12 Department of Physics and Astronomy, Texas A&M University
*13 Faculty of Physics, Ludwig-Maximilians-University of Munich

References

1) G. Jhang *et al.*, Phys. Lett. B **813**, 136016 (2021).
2) J. Barney *et al.*, arXiv:2005.10806.
3) R. Shane *et al.*, Nucl. Instrum. Methods Phys. Res. A **784**, 513 (2015).
4) H. Otsu *et al.*, Nucl. Instrum. Methods Phys. Res. B **376**, 175 (2016).
5) A. Ono *et al.*, Phys. Rev. C **100**, 044617 (2019).
6) J. Xu *et al.*, Phys. Rev. C **93**, 044609 (2016).
7) Y.-X. Zhang *et al.*, Phys. Rev. C **97**, 034625 (2018).
8) J. Hong, P. Danielewicz, Phys. Rev. C **90**, 024605 (2014).
9) B. -A. Li, Phys. Rev. Lett. **88**, 192701 (2002).
10) Z. -Q. Feng, G .-M. Jin, Phys. Lett. B **683**, 140 (2010).
11) Z. Xiao *et al.*, Phys. Rev. Lett. **102**, 062502 (2009).
12) W. -J. Xie, J. Su, L. Zhu, F. -S. Zhang, Phys. Lett. B **718**, 1510 (2013).

Proton efficiency function for high-multiplicity events in the SπRIT-TPC investigated by the embedding technique

M. Kaneko,[*1,*2] J. Barney,[*2,*3] G. Cerizza,[*2,*3] J. Estee,[*2,*3] T. Isobe,[*2] G. Jhang,[*2,*3] M. Kurata-Nishimura,[*2] P. Lasko,[*5,*2] J. W. Lee,[*4,*2] J. Łukasik,[*5] W. G. Lynch,[*3] T. Murakami,[*1,*2] P. Pawłowski,[*5,*2] C. Santamaria,[*2,*7] C. Y. Tsang,[*2,*3] M. B. Tsang[*3] for the SπRIT Collaboration

The SπRIT-time projection chamber (TPC)[1] project aims to constrain the high-density nuclear symmetry energy by using heavy-ion collisions. We measured light charged particles emitted from central Sn + Sn collisions at 270 MeV/nucleon, which have been predicted to provide sensitive probes of the symmetry energy at supra-saturation densities.[2] In this report, we describe the reconstruction efficiency of protons in central ^{132}Sn + ^{124}Sn collisions.

The Sn target is placed approximately 1 cm upstream from the TPC; hence, the charged particles emitted in forward angles are mainly observed. In central Sn + Sn collisions producing high charged-particle multiplicity, signals induced by charged particles can interfere with each other, causing the tracks to be merged and/or broken. As it would be difficult to fully simulate realistic situations, the embedding technique[3] is applied. The digitized signal of a single proton traversing the TPC is generated based on a Monte Carlo simulation. Subsequently, the generated signal is embedded into real events, which are analyzed by the same track reconstruction algorithm as for the physical tracks. The proton's reconstruction efficiency with a given track multiplicity can be estimated by comparing the embedded tracks and the reconstructed tracks.

The spectrum of transverse momentum p_{T} vs. scaled rapidity $y_0 = y/y_{\mathrm{NN}}^{\mathrm{c.m.}} - 1$ of protons is corrected by the following procedure, where y and $y_{\mathrm{NN}}^{\mathrm{c.m.}}$ are the rapidity of the detected proton and the center-of-mass rapidity of the nucleon-nucleon system, respectively. It is noted that the momentum resolution of the TPC can distort the measured spectrum. To consider this bin-smearing effect in the efficiency calculation, the distribution of embedded protons needs to be properly weighted. First, the measured p_{T}-y_0 spectrum is used as the weighting factor. The efficiency as a function of p_{T}-y_0 is obtained as the ratio of reconstructed protons to embedded ones. Subsequently, the corrected p_{T}-y_0 spectrum of protons is obtained as the raw spectrum divided by the efficiency. In the next iteration, the corrected spectrum is used as the weighting factor. This process is iterated until the correction converges.

As shown in Fig. 1, the correction converged after two iterations. Since we limited the azimuthal angle of tracks to $-30° \leq \phi \leq 20°$ in the analysis, which is expected to be the efficient region of the TPC, the reconstruction efficiency of protons is estimated to be approximately 90%. The efficiency exceeds 100% at $y_0 > 1.8$ because the original statistics of protons is quite low at such a high y_0 and overcounting occurs owing to the smearing of the proton rapidity at a lower y_0. In addtion to protons, the p_{T}-y_0 spectra of deuterons and tritons are also corrected, which are being compared with theoretical predictions to extract physics statements for publications in the future.

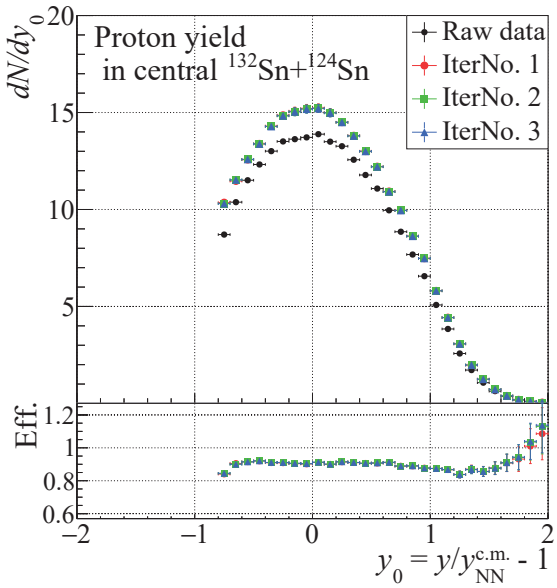

Fig. 1. The top panel shows p_{T}-integrated dN/dy_0 spectra of protons in central ^{132}Sn + ^{124}Sn collisions with and without efficiency corrections (colored and black markers, respectively). The bottom panel shows the efficiency obtained with respect to their ratios.

This work is supported by the Japanese MEXT KAKENHI under grant No. 24105004; the U.S. DOE under Grant Nos. DE-SC0004835, DE-SC0014530, and DE-NA0002923; the U.S. NSF under Grant No. PHY-1565546; and the Polish NSC under Grant Nos. UMO-2013/09/B/ST2/04064 and UMO-2013/10/M/ST2/00624. The computing resources were provided by the HOKUSAI system at RIKEN.

*1 Department of Physics, Kyoto University
*2 RIKEN Nishina Center
*3 NSCL and Dept. of Phys. & Ast., Michigan State University
*4 Department of Physics, Korea University
*5 Institute of Nuclear Physics, PAN, Kraków
*6 Department of Physics, Tsinghua University
*7 Lawrence Berkeley National Laboratory, UC Berkeley

References

1) R. Shane *et al.*, Nucl. Instrum. Methods Phys. Res. A **784**, 513 (2015).
2) M. B. Tsang *et al.*, Phys. Rev. C **95**, 044614 (2017).
3) M. Anderson *et al.*, Nucl. Instrum. Methods Phys. Res. A **499**, 659 (2003).

Observation of anisotropic collective flow of charged particles and neutrons in heavy-ion collisions at beam energies of 400 MeV/nucleon

S. Yamamura,[*1,*2] S. Nishimura,[*2] T. Isobe,[*2] V. H. Phong,[*2] M. Kaneko,[*2,*3] T. Murakami,[*3] Y. Nakai,[*2] D. Nishimura,[*4] M. Nishimura,[*2] N. Chiga,[*2] and E. Takada[*5]

The anisotropic collective flow of protons and neutrons in heavy-ion collisions is expected to provide experimental information on the equation of state (EOS) of high-density and neutron-rich nuclear matters because it reflects the symmetry energy at the high-density region.[1] The anisotropy is expressed by the distribution function of particle emissions observed from the reaction plane as

$$\frac{dN}{d\varphi} = \frac{N_0}{2\pi}\left(1 + 2\sum_n v_n \cos n\varphi\right), \quad (1)$$

where φ, N_0 and v_n represent the emission angle of the particles observed from the reaction plane, normalization constant, and the anisotropic strength, respectively. The difference between the v_1 (directed flow) of neutrons and of protons is theoretically expected to be highly sensitive to EOS around target rapidity[2] even though only a few experimental data are available.

A pilot experiment (H355) was conducted at HIMAC by impinging 400 MeV/nucleon ^{132}Xe beam on a CsI target (500 mg/cm^2) at a high intensity of 10^6 particles/spill to measure the proton and neutron flows precisely. In this experiment, 32 plastic scintillators (EJ299-33, $30 \times 55 \times 127$ mm^3) were used to identify neutrons using pulse-shape discrimination. The detectors were placed parallel to the beam axis and in a cylindrical configuration to detect particles at target rapidity. Charged and neutral particles can be identified by combining these detectors called NiGIRI (Neutron, ion, and γ-ray identification for radioactive isotope beam) and charged particle veto scintillators. Figure 1 shows the prototype NiGIRI array.[3] Energies of the detected particles are deduced from the time-of-flight between the CsI target and NiGIRI detectors. Another set of 32 plastic scintillators called the Kyoto-array were used to cover the mid-rapidity region. The emitted angles of the charged particles were measured for determining the reaction plane. The plane was determined by the beam axis and $\boldsymbol{Q}$ vector obtained using

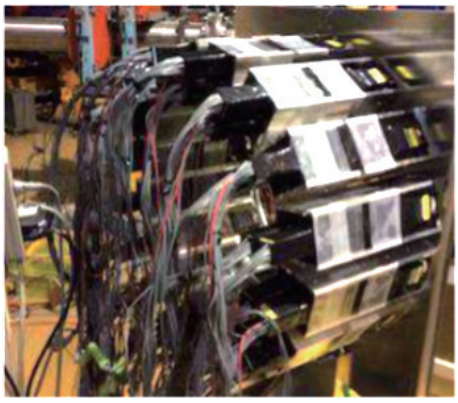

Fig. 1. NiGIRI detectors[3] (16 arrays 2 layers).

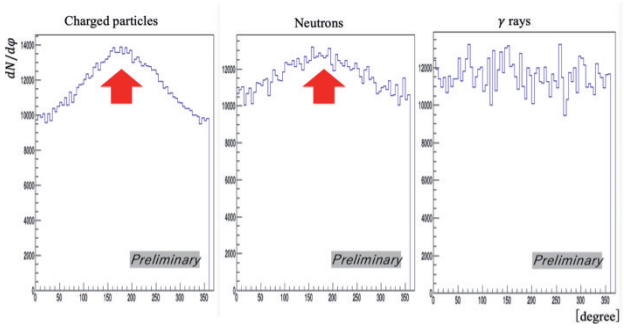

Fig. 2. Measured distribution functions dN/φ of charged particles (left), neutrons (center), and γ rays (right). The spectra were integrated over momentum and impact parameter.

$$\boldsymbol{Q} = \sum_k \begin{pmatrix} \cos\theta_k \\ \sin\theta_k \end{pmatrix}, \quad (2)$$

where θ_k denotes a hit angle of Kyoto-array; the summation is taken over the number of detected particles. The cross-talk events observed in the Kyoto-array were mostly rejected in the $\boldsymbol{Q}$-vector determination to minimize the detector bias.

Emission angles of charged particles, neutrons, and γ rays with respect to the angle of $\boldsymbol{Q}$ vector were studied at target rapidity using the data of NiGIRI. Figure 2 shows the measured distribution functions ($dN/d\varphi$) of the charged particles, neutrons, and γ rays. The results indicate a clear anisotropy for charged particles and neutrons, and show flatter distribution for γ rays; the results are expected to indicate collective flow, particularly v_1, and therefore a pressure gradient is observed in the high-density region in heavy-ion collisions.

To the best of the author's knowledge, this experiment prooves for the first time that it is possible to directly compare the collective flow among light charged ions and neutrons around target rapidity. An upgraded experiment with a higher resolution of the reaction plane detector arrays will be performed at HIMAC and possibly RIBF in the future.

*1 Department of Physics, University of Tokyo
*2 RIKEN Nishina Center
*3 Department of Physics, Kyoto University
*4 Department of Natural Science, Tokyo City University
*5 NIRS

References

1) B. A. Li, *et al.*, Phys. Rep. **464**, 113 (2008).
2) Z. Q. Feng, Phys. Rev. C **85**, 014604 (2012).
3) H. Matsuzawa *et al.*, RIKEN Accel. Prog. Rep. **48**, 212 (2015).

Measurement of proton elastic scattering from ^{132}Sn at 300 MeV/nucleon in inverse kinematics

T. Harada,[*1,*2] J. Zenihiro,[*3] Y. Matsuda,[*4] S. Terashima,[*5] H. Sakaguchi,[*6] N. Aoi,[*6] H. Baba,[*2] M. Dozono,[*7] F. Endo,[*7] S. Enyo,[*3] Y. Fujikawa,[*3] S. Hanai,[*7] S. Hayakawa,[*7] Y. Hijikata,[*3] J. W. Hwang,[*7] N. Imai,[*7] K. Inaba,[*3] S. Ishida,[*4] T. Isobe,[*2] T. Kawabata,[*8] S. Kiyotake,[*9] A. Kohda,[*6] H. Kurosawa,[*4] R. Kojima,[*7] R. Maeda,[*4] Y. Maeda,[*9] S. Y. Matsumoto,[*3] R. Matsumura,[*1,*2] B. Mauss,[*2] S. Michimasa,[*7] T. Murakami,[*3] D. Nishimura,[*10] T. Nishimura,[*9] K. Nosaka,[*3] S. Ota,[*7] K. Sakanashi,[*3] H. Shimizu,[*7] D. Suzuki,[*2] J. Tanaka,[*2] R. Tsunoda,[*7] T. Uesaka,[*2] and K. Yamamoto[*4]

The equation of state (EOS) of nuclear matter is expressed as the EOS of the symmetric nuclear matter and the symmetry energy. Particularly, the symmetry energy is important for understanding astrophysical phenomena, such as neutron stars. The EOS of symmetric nuclear matter is understood from previous experiments on stable nuclei, however there is much less understanding of the the symmetry energy. From many theoretical studies, it is known that the slope parameter of the symmetry energy is strongly correlated with neutron skin thickness, which is defined as the difference between the neutron and proton root-mean-square radii. In neutron-rich nuclei, the excess neutrons form a neutron skin structure. It is expected that this symmetry energy can be constrained by determining the neutron skin thickness from the neutron and proton density distributions.

We employed proton elastic scattering to extract neutron and proton density distributions. For stable nuclei, we have established a method to extract the proton and neutron density distributions using proton elastic scattering.[1] To employ this method to unstable nuclei with large asymmetry, we started a new project to measure the elastic scattering of protons with RI beams (ESPRI) in inverse kinematics. We developed a recoil proton spectrometer (RPS), which consists of a 1-millimeter-thick solid hydrogen target (SHT[2]), two multi-wire drift chambers (MWDCs), two plastic scintillators, and fourteen NaI rods. We measure the angle and energy of the recoil protons from the SHT using the RPS. We successfully performed ESPRI measurements for several light unstable nuclei.[3]

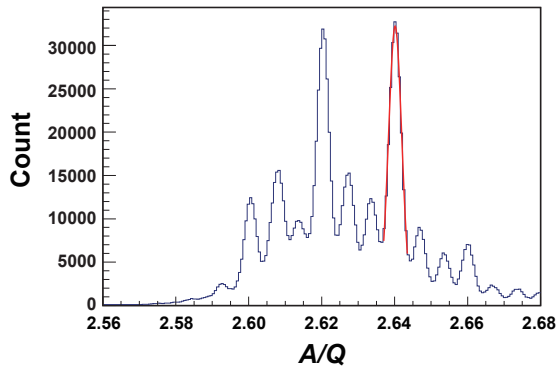

Fig. 1. A/Q spectrum of secondary beam including ^{132}Sn deduced from position and time-of-flight information at BigRIPS. The peak of ^{132}Sn is located at $A/Q = 2.64$ shown in red. The A/Q resolution in r.m.s is 0.058%.

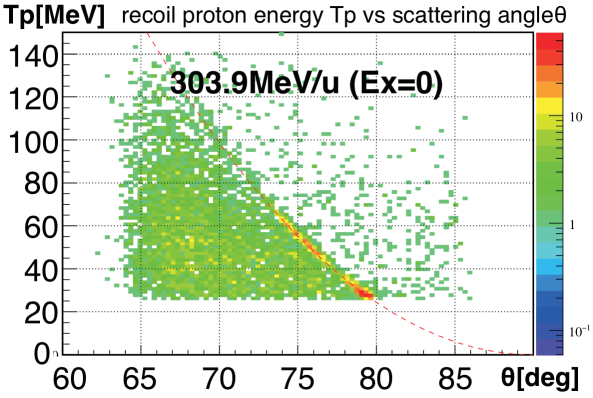

Fig. 2. Kinematical correlations of ^{132}Sn between scattering angles θ and kinematic energies of scattered protons T_p. The red dotted line indicates elastic scattering events between ^{132}Sn at 303.9 MeV/nucleon and protons.

^{132}Sn has a larger isospin asymmetry than ^{208}Pb, and is expected to have a thicker neutron skin thickness. In Novenver 2019, we performed proton elastic scattering from ^{132}Sn at 300 MeV/nucleon at the F12 area.[4] The total beam rate was up to 600 kcps, and the purity of ^{132}Sn was 20%. The A/Q spectrum of the secondary beam including ^{132}Sn under high intensity is shown in Fig. 1. We identified elastic events of ^{132}Sn from the correlation of the kinematic energies and recoil angles of the scattered protons with NaI rods and MWDCs as shown in Fig. 2. Data analysis for deducing the excitation energy spectrum of ^{132}Sn and the angular distribution of the cross section is now in progress.

*1 Department of Physics, Toho University
*2 RIKEN Nishina Center
*3 Department of Physics, Kyoto University
*4 CYRIC, Tohoku University
*5 School of Physics, Beihang University
*6 RCNP, Osaka University
*7 CNS, University of Tokyo
*8 Department of Physics, Osaka University
*9 Department of Applied Physics, Miyazaki University
*10 Department of Natural Sciences, Tokyo City University

References

1) H. Sakaguchi *et al.*, Prog. Part. Nucl. Phys. **97**, 1 (2017).
2) Y. Matsuda *et al.*, Nucl. Instrum. Methods Phys. Res. A **643**, 6 (2011).
3) Y. Matsuda *et al.*, Phys. Rev. C **87**, 034614 (2013).
4) J. Zenihiro *et al.*, RIKEN Accel. Prog. Rep. **53**, 44 (2019).

Results on the β decay of ^{60}Ge and ^{62}Ge measured at RIBF

S. E. A. Orrigo,[*1] B. Rubio,[*1] W. Gelletly,[*1,*2] P. Aguilera,[*1,*3] A. Algora,[*1,*4] A. I. Morales,[*1] J. Agramunt,[*1] D. S. Ahn,[*5] P. Ascher,[*6] B. Blank,[*6] C. Borcea,[*7] A. Boso,[*8] R. B. Cakirli,[*9] J. Chiba,[*10] G. de Angelis,[*11] G. de France,[*12] F. Diel,[*13] P. Doornenbal,[*5] Y. Fujita,[*14] N. Fukuda,[*5] E. Ganioğlu,[*9] M. Gerbaux,[*6] J. Giovinazzo,[*6] S. Go,[*15] T. Goigoux,[*6] S. Grévy,[*6] V. Guadilla,[*1] N. Inabe,[*5] G. G. Kiss,[*4,*5] T. Kubo,[*5] S. Kubono,[*5] T. Kurtukian-Nieto,[*6] D. Lubos,[*16] C. Magron,[*6] F. Molina,[*3] A. Montaner-Pizá,[*1] D. Napoli,[*11] D. Nishimura,[*17] S. Nishimura,[*5] H. Oikawa,[*10] V. H. Phong,[*5,*18] H. Sakurai,[*5,*19] Y. Shimizu,[*5] C. Sidong,[*5] P. -A. Söderström,[*5] T. Sumikama,[*5] H. Suzuki,[*5] H. Takeda,[*5] Y. Takei,[*10] M. Tanaka,[*14] J. Wu,[*5] S. Yagi[*10]

The investigation of the structure of nuclei close to the limits of stability is a topic of paramount importance in modern nuclear physics. The $T_z = -2$, ^{60}Ge nucleus is a semi-magic, $N = 28$ isotone whose decay is almost unknown. An exotic feature seen in other $T_z = -2$ nuclei[1,2] is the competition between the γ de-excitation and the (isospin-forbidden) proton emission from the $T = 2$ isobaric analog state populated by β decay in the daughter nucleus. Little was known about the decay of the $T_z = -1$, ^{62}Ge nucleus. In other $T_z = -1$ nuclei a suppression of isoscalar γ transitions between $J^\pi = 1^+$, $T = 0$ states (Warburton and Weneser *quasi-rule*[3,4]) has been observed.[5]

Heavy proton-rich nuclei can be produced with unprecedented statistics at the Radioactive Isotope Beam Factory (RIBF) of the RIKEN Nishina Center. In the NP1112-RIBF82 experiment, 1.5×10^4 ^{60}Ge and 2.1×10^6 ^{62}Ge ions were recorded. They were produced by fragmenting a ^{78}Kr primary beam (345 MeV/nucleon and intensity up to 250 particle nA) on a Be target. The fragments were selected and identified by the BigRIPS separator by means of the $B\rho$-ΔE-ToF method. They were then implanted in the WAS3ABi setup, consisting of three 1-mm-thick double-sided Si strip detectors of a 6×4 cm^2 area. The EURICA array, arranged in 12 clusters containing 7 high-purity Ge crystals each, was used for γ detection.

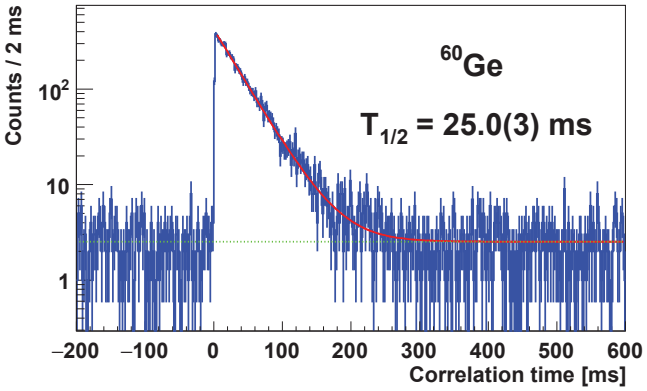

Fig. 1. Time correlations between ^{60}Ge implants in WAS3ABi and subsequent β-delayed protons ($E_p > 1$ MeV) detected in the same pixel of WAS3ABi.

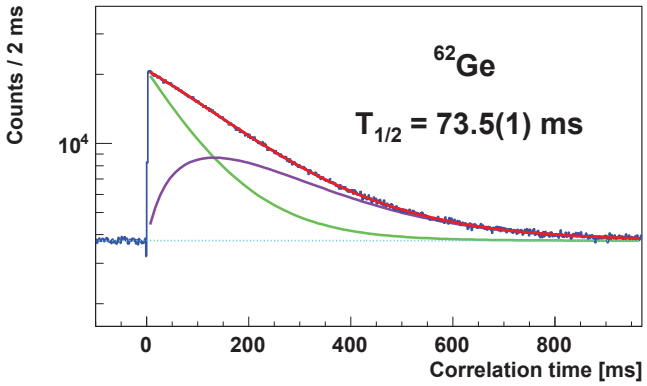

Fig. 2. Time correlations between implanted ^{62}Ge ions and β decays in the same or adjacent pixel of WAS3ABi.

For ^{60}Ge, the first experimental information on both the β-delayed proton and γ emissions has been extracted. By gating on the β-delayed proton emission, a half-life value of 25.0(3) ms has been obtained for ^{60}Ge (Fig. 1). For ^{62}Ge, new information on the β-delayed γ emission has been obtained, indicating the persistence of the *quasi-rule*.[3,4] A half-life value of 73.5(1) ms has been extracted for ^{62}Ge (Fig. 2). The precision on both ^{60}Ge and ^{62}Ge half-lives has been improved in comparison with values in the literature.

*1 IFIC, CSIC-Univ. Valencia
*2 Department of Physics, Surrey University
*3 Chilean Nuclear Energy Commision
*4 MTA ATOMKI
*5 RIKEN Nishina Center
*6 CEN Bordeaux Gradignan
*7 National Institute for Physics and Nuclear Engineering, IFIN-HH
*8 INFN Sezione di Padova
*9 Department of Physics, Istanbul University
*10 Department of Physics, Tokyo University of Science
*11 INFN Laboratori Nazionali di Legnaro
*12 GANIL
*13 Institute of Nuclear Physics, University of Cologne
*14 Department of Physics, Osaka University
*15 Dept. of Physics and Astronomy, University of Tennessee
*16 Physik Department E12, Technische Universität München
*17 Department of Natural Sciences, Tokyo City University
*18 Faculty of Physics, VNU University of Science
*19 Department of Physics, University of Tokyo

References

1) S. E. A. Orrigo *et al.*, Phys. Rev. Lett. **112**, 222501 (2014).
2) S. E. A. Orrigo *et al.*, Phys. Rev. C **93**, 044336 (2016).
3) G. Morpurgo, Phys. Rev. **110**, 721 (1958).
4) D. H. Wilkinson, *Isospin in Nuclear Physics*, (Elsevier Science Publishing Co Inc.,U.S., 1969).
5) F. Molina *et al.*, Phys. Rev. C **91**, 014301 (2015).

On the β-decay of ^{70}Kr

A. Vitéz-Sveiczer,[*1,*2,*3] A. Algora,[*1,*2] A. I. Morales,[*1] B. Rubio,[*1] G. Kiss,[*2] J. Agramunt,[*1] V. Guadilla,[*1] A. Montaner-Pizá,[*1] S. E. A. Orrigo,[*1] A. Horváth,[*3] G. de Angelis,[*4] D. Napoli,[*4] F. Recchia,[*5] S. Lenzi,[*5]A. Boso,[*5] S. Nishimura,[*6] V. H. Phong,[*6] J. Wu,[*6] P. -A. Söderström,[*6] T. Sumikama,[*6] H. Suzuki,[*6] H. Takeda,[*6] D. S. Ahn,[*6] H. Baba,[*6] P. Doornebal,[*6] N. Fukuda,[*6] N. Inabe,[*6] T. Isobe,[*6] T. Kubo,[*6] S. Kubono,[*6] H. Sakurai,[*6] Y. Shimizu,[*6] C. Sidong,[*6] B. Blank,[*7] P. Ascher,[*7] M. Gerbaux,[*7] T. Goigoux,[*7]J. Giovinazzo,[*7] S. Grévy,[*7] T. Kurtukián Nieto,[*7] C. Magron,[*7] W. Gelletly,[*1,*8] Zs. Dombrádi,[*7] Y. Fujita,[*9] M. Tanaka,[*9] P. Aguilera,[*10] F. Molina,[*10] J. Eberth,[*11] F. Diel,[*11] D. Lubos,[*12] C. Borcea,[*13] E. Ganioglu,[*14] D. Nishimura,[*15] H. Oikawa,[*15] Y. Takei,[*15] S. Yagi,[*15] W. Korten,[*16] G. de France,[*17] P. Davies,[*18] J. Liu,[*19] J. Lee,[*19] T. Lokotko,[*19] I. Kojouharov,[*20] N. Kurz,[*20] and H. Shaffner[*20]

In this contribution, we present preliminary results of the analysis of the β-decay of ^{70}Kr from the experiment NP1112-RIBF93. The main goal of the experiment was to study isospin-related effects and p-n pairing signatures in the region of $A \sim 70$ using the information obtained from the β-decays of ^{70,71}Kr.

To produce the isotopes of interest the fragmentation of a ^{78}Kr primary beam with an energy of 345 MeV/nucleon was used. Average beam currents of 40 particle nA were provided by the RIKEN Nishina Center accelerator complex. The ^{78}Kr primary beam impinged on a 5 mm thick ^{9}Be target to produce a cocktail radioactive beam. The fragments produced were then separated and selected using the BigRIPS separator. The ions were then implanted in the WAS3ABi active stopper, surrounded by the EURICA γ-ray spectrometer[1] for the study of their β decay.

Gamma rays associated to the de-excitation of states populated in the daughter nucleus ^{70}Br were identified using conventional β-γ and β-γ-γ coincidence techniques similarly to the procedure followed in Ref. 2). For more details see Refs. 3, 4). The analysis has also allowed us to improve the precision of the deduced β-decay half-life and construct the level scheme of states populated in the decay, which extends up to 3.3 MeV excitation energy in ^{70}Br.

In Fig. 1 we present the deduced Gamow-Teller β strength in the daughter nucleus compared to the predictions of the *pn* quasiparticle random-phase approximation (pnQRPA) calculations for two possible deformation minima in ^{70}Kr.[5] The calculations presented here are based on the SLy4 force, which is a well tested force throughout the whole nuclear chart. Alternative theoretical calculations are also performed using a pseudo-LS model.[6] We are presently working in the final details of a publication[7] based on this study.

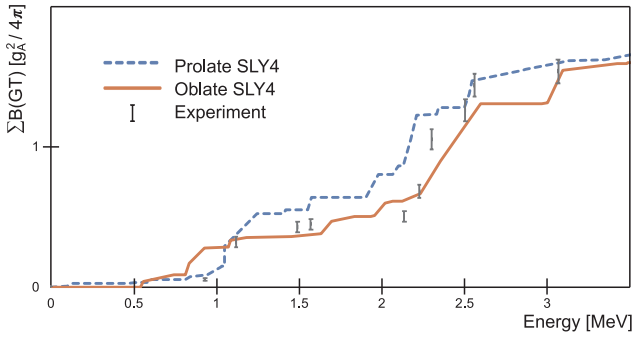

Fig. 1. Preliminary comparison of the experimental (black) and calculated accumulated B(GT) values for the ^{70}Kr $\rightarrow$ ^{70}Br β decay.[5] The experimental B(GT) uncertainties are determined by the feeding error of the levels and the error of the half-life. The orange solid line corresponds to the values calculated for the oblate minimum, the blue dashed line corresponds to the prolate minimum of the ground state of ^{70}Kr.

*1 IFIC, CSIC-Univ. Valencia
*2 MTA ATOMKI
*3 ELTE TTK Fizikai Intézet
*4 INFN Laboratori Nazionali di Legnaro
*5 INFN Sezione di Padova
*6 RIKEN Nishina Center
*7 CEN Bordeaux-Gradignan
*8 Department of Physics, Surrey University
*9 Department of Physics, Osaka University
*10 Comisión Chilena de Energía Nuclear (CCHEN)
*11 Institut für Kernphysik, Universität zu Köln
*12 Physik Department, Technische Universität München
*13 National Institute for Physics and Nuclear Engineering, IFIN-HH
*14 Department of Physics, University of Istanbul
*15 Department of Physics, Tokyo University of Science
*16 IRFU, CEA, Université Paris-Saclay
*17 GANIL
*18 Department of Physics, York University
*19 Department of Physics, University of Hong Kong
*20 GSI Helmholtzzentrum für Schwerionenforschung GmbH

References

1) S. Nishimura, Prog. Theor. Exp. Phys. **2012**, 03C006 (2012).
2) A. I. Morales *et al.*, Phys. Rev. C **95**, 064327 (2017).
3) A. Vitéz-Sveiczer *et al.*, RIKEN Accel. Prog. Rep. **53**, 28 (2019).
4) A. Vitéz-Sveiczer *et al.*, Acta Phys. Pol. B **51**, 587 (2020).
5) P. Sarriguren, private communication.
6) P. Van Isacker, private communication.
7) A. Vitéz-Sveiczer *et al.*, in preparation.

Measuring β-decay strength distribution in the ^{78}Ni region using VANDLE

M. Singh,[*1] R. Yokoyama,[*1] R. K. Grzywacz,[*1,*2] T. King,[*2] S. Nishimura,[*3] N. T. Brewer,[*1,*2] P. Brionnet,[*3] J. Bundgaard,[*1] I. Cox,[*1]A. Fijalkowska,[*4] L. Fraile,[*5] S. Go,[*6] A. Gottardo,[*7] M. Karny,[*4] A. Keeler,[*1] A. Korgul,[*4] M. Madurga,[*1] K. Miernik,[*4] S. Neupane,[*1] M. Niikura,[*8] M. Pfutzner,[*4] M. Piersa,[*4] M. Rajabali,[*9] B. C. Rasco,[*2] K. P. Rykaczewski,[*2] M. Silkowski,[*4] M. Stepaniuk,[*4] J. L. Tain,[*10] A. Tolosa,[*10] M. Wolinska-Cichocka,[*4] and Z. Xu[*1] for the VANDLE Collaboration

The properties of nuclei away from the line of stability, revealed in the β-decay of the neutron-rich side, are crucial in understanding nuclear structure evolution and providing inputs for r-process simulations. Measurements of half-lives, one- and two-neutron emission probabilities ($P_{n,2n}$), and neutron energy spectra provide information on the β-decay strength distribution (S_β). The S_β measurement for Ga with $N > 50$, ^{83,84}Ga showed that the decay properties of the r-process isotopes near ^{78}Ni are dominated by the Gamow-Teller decay of the ^{78}Ni-core states.[1)] Through their work on ^{86,87}Ga using BRIKEN,[3)] R. Yokoyama *et al.*,[2)] demonstrated a need to consider the competition between one- and multi-neutron emissions to predict branching ratios of r-process nuclei. It also strengthened the argument for the necessity of neutron energy measurements for understanding the details of the neutron emission process. The Versatile Array of Neutron Detector at Low Energy (VANDLE)[4)] experiment at RIBF RIKEN aims to provide measurements of S_β for the decay of ^{78}Ni and neighboring nuclei using time-of-flight (ToF) based neutron spectroscopy. The isotopes of interest were produced from a 345 MeV/nucleon ∼46-particle-nA ^{238}U beam impinged on 4-mm-thick Be target by projectile fragmentation. The nuclei identified by the BigRIPS[5)] facility were supplied to the F11 focal plane, where they were implanted in a segmented-YSO based implantation detector[6)] for ∼4 days. A YSO detector consists of a segmented YSO crystal ($75 \times 75 \times 5$ mm^3) coupled to a position-sensitive photo-multiplier tube. YSO is used to establish ion-beta correlations and provides the start time of the ToF. VANDLE, consisting of EJ200 scintillator bars coupled at both ends to PMTs, provides the stop time of neutron ToF. A set of 48 medium ($3 \times 6 \times 120$ cm^3) VANDLE bars were arranged in a 100-cm radius circle with YSO at the center, as shown in Fig. 1. In addition, two HPGe clovers and (ten 3" × 3" and two 2" × 2") $LaBr_3$ were set up in a close geometry around the YSO detector to record γ-transitions from the decays. All the signals were read using XIA Pixie-16 revF digitizers at 250 MHz and 12-bit digitization.[7)] Neutron spectra were measured for $^{78-81}$Cu isotopes to establish the role of the $N = 50$ shell gap on the β-decay properties. We show the first measurement of the neutron energy spectrum of $^{81}Cu_{52}$ decay in Fig. 2. The spectrum indicates that neutrons with energies of 0.4–3 MeV were emitted from excited states in ^{81}Zn.

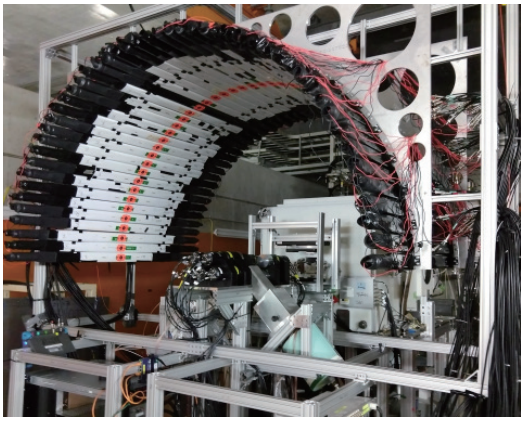

Fig. 1. VANDLE setup at the F11 focal plane of ZDS.

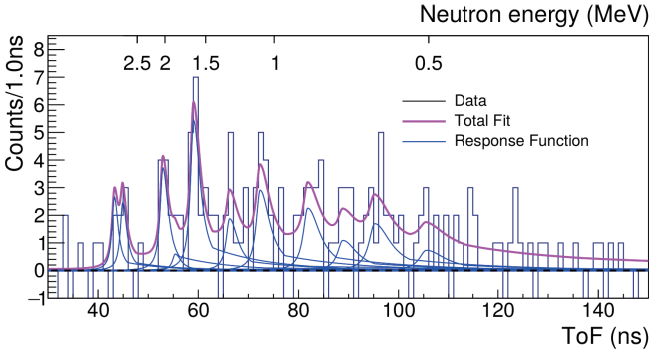

Fig. 2. Neutron energy spectrum of ^{81}Cu measured by VANDLE.

*1 Dept. of Physics and Astronomy, University of Tennessee
*2 Physics Division, Oak Ridge National Laboratory
*3 RIKEN Nishina Center
*4 Faculty of Physics, University of Warsaw
*5 Grupo de Física Nuclear IPARCOS, Universidad Complutense de Madrid
*6 Department of Physics, Kyushu University
*7 INFN-LNL
*8 Department of Physics, University of Tokyo
*9 Department of Physics, Tennessee Tech University
*10 IFIC, CSIC-Universitat de Valencia

References
1) M. Madurga *et al.*, Phys. Rev. Lett. **117**, 092502 (2016).
2) R. Yokoyama *et al.*, Phys. Rev. C **100**, 031302 (2019).
3) A. Tarifeño-Saldivia *et al.*, J. Instrum. **12**, P04006 (2017).
4) W. A. Peters *et al.*, Nucl. Instrum. Methods Phys. Res. A **836**, 122 (2016).
5) N. Fukuda *et al.*, Nucl. Instrum. Methods Phys. Res. B **317**, 323 (2003).
6) R. Yokoyama *et al.*, Nucl. Instrum. Methods Phys. Res. A **937**, 93 (2019).
7) S. V. Paulauskas *et al.*, Nucl. Instrum. Methods Phys. Res. A **737**, 22 (2014).

Constraining multi-neutron emission models with spectroscopy of neutron-rich Ga isotopes using BRIKEN array

R. Yokoyama,[*1] R. Grzywacz,[*1,*2] B. C. Rasco,[*1,*2] N. T. Brewer,[*1,*2] K. P. Rykaczewski,[*2] I. Dillmann,[*3] J. L. Tain,[*4] S. Nishimura,[*5] and the BRIKEN collaboration

As we move further from the line of β-stability towards the neutron drip line, Q_β values become larger than the two-neutron separation energy (S_{2n}), which allows multi-neutron emissions after β-decay. In the neutron-rich nuclei along the astrophysical r-process path, multi-neutron emissions are considered to be dominant decay modes.[1)] The numbers of neutrons emitted in the β-decays of exotic nuclei modify the decay path back to stability and affect the final abundance calculation. However, experimental data that enable the evaluation of multi-neutron emissions for the r-process nuclei are almost non-existent. Until quite recently, theoretical predictions of the neutron emission branching ratio (P_n) were based on a cut-off model that assumes only the higher-multiplicity neutron emission prevails in the energy regions open to multiple neutron-emission channels. In order to include the competition of one-neutron emission from the states above S_{2n}, Kawano *et al.* developed a Hauser-Feshbach statistical model calculation.[2)]

We studied neutron-rich Ga isotopes by means of β-n-γ spectroscopy at RIBF using the high-efficiency neutron counter array BRIKEN,[3–5)] with two Ge clover detectors. The result that one-neutron emission is dominant for all the four Ga isotopes was interpreted as competition in one-neutron emission among two-neutron unbound states, and we demonstrated that the inclusion of the statistical model reproduces the branching ratio better than the cut-off model.[6)]

Recently, we analyzed γ-ray spectra of the decay of $^{84-87}$Ga. Figure 1 shows γ spectra gated by the neutron multiplicity of the BRIKEN array for the decay of ^{86}Ga. γ rays from ^{84,85,86}Ge are clearly identified in the $2n$, $1n$, and $0n$ gated spectra. The $2^+ \rightarrow 0^+$ γ ray from ^{84}Ge in the two-neutron branches was observed at 624 keV. The intensity of the 624-keV γ ray per 100 two-neutron decays was 37(8)%. We performed our Hauser-Feshbach statistical model calculation by using the strength distribution and level densities from shell-model calculations. This model was used to validate the measurement of the neutron spectra in the decay of ^{83,84}Ga.[7)] The shell model produced less states below S_{2n} than the number of the default levels generated by the statistical model using the Gilbert-Cameron formula. When known, the low-lying states in the decay daughters calculated by the shell model were replaced with experimental data. Compared with the feeding of the experimental 624-keV state in ^{84}Ge, the statistical model predicted the γ intensity as 33%, which is in good agreement with the experimental value we measured. The statistical model also reproduced the γ branching ratio of other γ rays in the decay. The detailed β-n-γ analysis of other neutron-rich Ga isotopes is in progress.

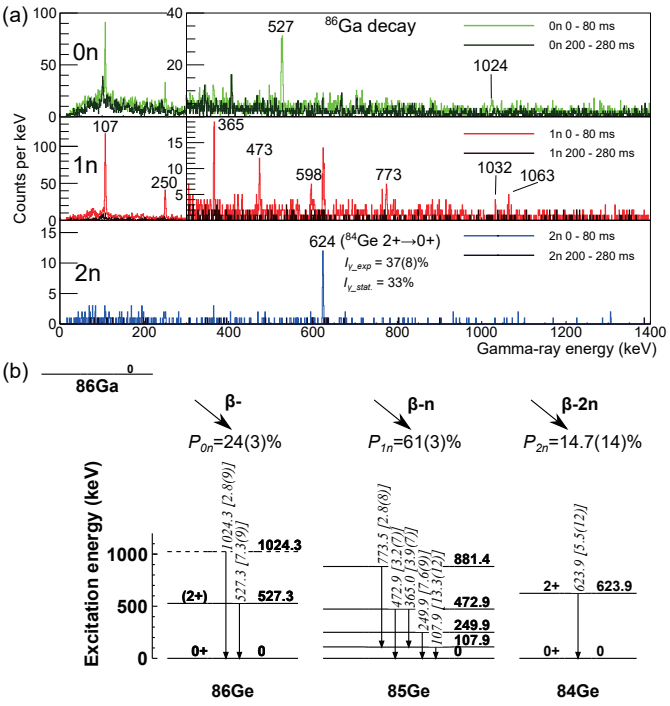

Fig. 1. (a) γ-ray spectra of the decay of ^{86}Ga gated by neutron multiplicities in the BRIKEN array. (b) Decay scheme. γ branching per 100 decays is shown in the square brackets.

*1 Department of Physics and Astronomy, the University of Tennessee, Knoxville
*2 Physics Division, Oak Ridge National Laboratory
*3 TRIUMF
*4 IFIC, CSIC-Universitat de Valencia
*5 RIKEN Nishina Center

References

1) P. Möller *et al.*, At. Data Nucl. Data Tables **125**, 1 (2019).
2) T. Kawano *et al.*, Nucl. Phys. A **913**, 51 (2013).
3) A. Tarifeño-Saldivia *et al.*, J. Instrum. **12**, P04006 (2017).
4) A. Tolosa-Delgado *et al.*, Nucl. Instrum. Methods Phys. Res. A **925**, 133 (2019).
5) B. C. Rasco *et al.*, Nucl. Instrum. Methods Phys. Res. A **911**, 79 (2018).
6) R. Yokoyama *et al.*, Phys. Rev. C **100**, 031302(R) (2019).
7) M. Madurga *et al.*, Phys. Rev. Lett. **117**, 092502 (2016).

Spectroscopy of ^{99}Cd and ^{101}In from β decays of ^{99}In and ^{101}Sn†

J. Park,[*1] R. Krücken,[*2] D. Lubos,[*3] R. Gernhäuser,[*3] M. Lewitowicz,[*4] S. Nishimura,[*5] and H. Sakurai[*6], for the EURICA Collaboration

Experimental knowledge in the doubly magic ^{100}Sn region, relevant for tests of nuclear shell models (SM), proton-neutron interactions in $N \approx Z \approx 50$ nuclei and the end of the rapid proton-capture process (*rp*-process) in nuclear astrophysics, has been expanded through a β-decay spectroscopy campaign at RIBF.[1)] The literature on β decays of ^{99}In and ^{101}Sn has been either nonexistent or contentious due to low statistics, but subsequent analyses of the β-delayed γ-ray spectroscopy data from the RIBF9 experiment revealed new states in ^{99}Cd and addressed the ambiguity concerning the level scheme of ^{101}In.

Using WAS3ABi[2)] and EURICA[3)] detectors which were deployed at the end of the ZeroDegree spectrometer, decay events following ^{99}In and ^{101}Sn ion implantations were correlated. 30 new γ rays belonging to ^{99}Cd were observed, and a subset of γ rays previously assigned to ^{101}In has been confirmed in this measurement. Two new high-energy γ rays were assigned to ^{101}In in this work. The available γ-γ coincidence data was analyzed to build on the level scheme of ^{99}Cd, as shown in Fig. 1. Alternatively, the experimental energies and intensities of the γ rays were compared with the SM calculations based on the SR88MHJM[4)] interaction, in a model space of $\pi(2p_{1/2}, 1g_{9/2})$ and $\nu(1g_{7/2}, 2d_{5/2}, 2d_{3/2}, 3s_{1/2}, 1h_{11/2})$ orbitals above the ^{88}Sr core. The effect of varying effective charges and theoretical transition energies on the branching ratios of γ rays was assessed. Tentative assignments of new excited states were made for both ^{99}Cd and ^{101}In, where a good agreement was found within theoretical uncertainties. No significant inconsistencies in the intensities of γ rays were found between the experiment and theory in a γ-ray energy range of 0–2500 keV.

β-delayed proton emission events from the decay of ^{101}Sn were recorded and incorporated in the γ-ray intensity analysis. The competition between branching ratios of protons versus γ rays from high-energy states in ^{101}In was evaluated using a semi-empirical theory on proton emission.[5)] The two competing hypotheses concerning the ground-state spin of ^{101}Sn, being either the $5/2^+$ based on the $2d_{5/2}$ single-neutron configuration or the $7/2^+$ based on the $1g_{7/2}$ configuration, were examined by comparing the experimental γ-ray intensities and the integrated β-delayed proton emission branching ratio to theoretical values. Due to the imprecise knowledge of the proton separation energy of ^{101}In and low experimental γ-ray statistics, there was insufficient circumstantial evidence for an unambiguous spin assignment of the ground state of ^{101}Sn. Determining the single-particle energies of the $N = 51$ isotones, ^{99}Cd and ^{101}Sn, would result in an enhanced systematic review of the $N = 50$ shell evolution in the proton-rich nuclei close to ^{100}Sn.

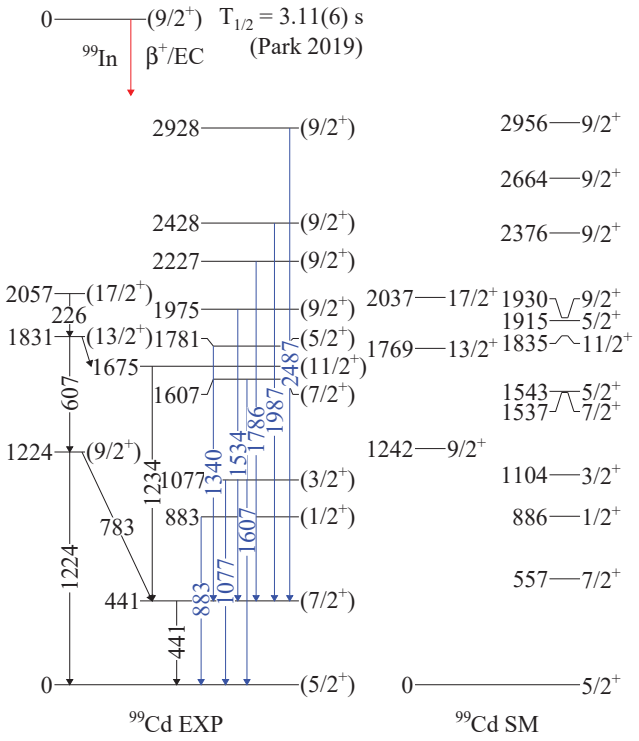

Fig. 1. Experimental level scheme of ^{99}Cd, compared to SM calculations. Only the states revealed by the β decay of ^{99}In are shown. The blue arrows indicate new γ rays observed in this work.

References
1) J. Park *et al.*, Phys. Rev. C **99**, 034313 (2019).
2) S. Nishimura, Prog. Theor. Exp. Phys. **2012**, 03C006 (2012).
3) P. -A. Söderström *et al.*, Nucl. Instrum. Methods Phys. Res. B **317**, 649 (2013).
4) D. T. Yordanov *et al.*, Phys. Rev. C **98**, 011303(R) (2018).
5) D. S. Delion, R. J. Liotta, R. Wyss, Phys. Rep. **424**, 113 (2006).

† Condensed from the article in Phys. Rev. C. **102**, 014304 (2020)

*1 Center for Exotic Nuclear Studies, Institute for Basic Science
*2 TRIUMF
*3 Physik Department, Technische Universität München
*4 Grand Accélérateur National d'Ions Lourds (GANIL)
*5 RIKEN Nishina Center
*6 Department of Physics, University of Tokyo

Total absorption γ-spectroscopy study of the beta decay of ^{100}Sn

J. A. Victoria,[*1] A. Algora,[*1,*2] B. Rubio,[*1] J. L. Tain,[*1] A. Tolosa,[*1] J. Agramunt,[*1] E. Nacher,[*1] S. E. A. Orrigo,[*1] V. Guadilla,[*3] G. Kiss,[*2] D. Sohler,[*2] I. Kuti,[*2] T. Davinson,[*4] O. B. Hall,[*4] D. M. Kahl,[*4] C. G. Bruno,[*4] C. J. Appleton,[*4] P. J. Woods,[*4] S. Nishimura,[*5] N. Fukuda,[*5] H. Suzuki,[*5] D. S. Ahn,[*5] H. Baba,[*5] Y. Shimizu,[*5] H. Takeda,[*5] D. Nishimura,[*5] T. Isobe,[*5] M. Kaneko,[*5] S. Kubono,[*5] H. Sakurai,[*5] H. Shimizu,[*5] T. Sumikama,[*5] P. Doornenbal,[*5] M. L. Cortes,[*6] Zs. Podolyak,[*7] W. Gelletly,[*7] E. Ganioglu,[*8] Y. Fujita,[*9] F. Molina,[*10] J. Liu,[*11] J. Lee,[*11] K. P. Rykaczewski,[*12] M. Wolinska-Cichocka,[*13] M. Labiche,[*14] C. J. Griffin,[*15] S. Bae,[*16] J. Ha,[*16] and Y. Litvinov[*17]

In this report we are presenting the progress on the analysis of the NP1612-RIBF147 experiment. The goal of this experiment was to study the beta decay of ^{100}Sn and neighbouring nuclei using the total absorption technique. In our measurement the total absorption spectrometer DTAS[1)] was used in combination with the implantation detector AIDA.[2)] Details of the experiment can be found in Ref. 3).

One key aspect of the work performed was to improve the signal to background ratio of the coincident data as much as possible. The sorting conditions of the data and the number of parameters available for the analysis makes this task daunting without proper quantification of the code optimisations. For that reason we introduced a figure of merit. The figure quantifies the improvements

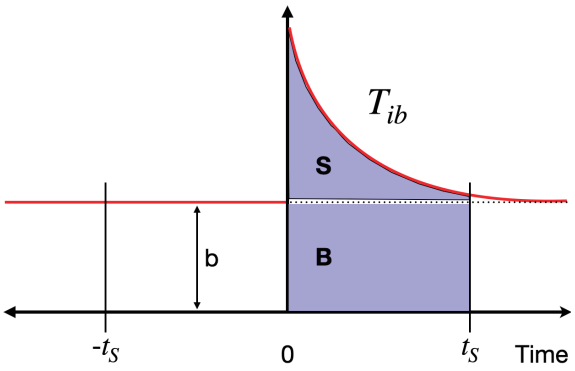

Fig. 1. Parameters employed in the definition of the figure of merit for the time distribution of the β particles. The area S stands for signal, B for background, b is the high of the background. B is estimated using the backward correlation time interval $[-t_s, 0]$. T_{ib} stands for implant-β time.

*1 IFIC, CSIC-Univ. of Valencia
*2 MTA ATOMKI
*3 Subatech/Ecole des Mines, CNRS/IN2P3, Université de Nantes
*4 School of Physics and Astronomy, University of Edinburgh
*5 RIKEN Nishina Center
*6 INFN Laboratori Nazionali di Legnaro
*7 Department of Physics, Surrey University
*8 Department of Physics, University of Istanbul
*9 Department of Physics, Osaka University
*10 Comisión Chilena de Energía Nuclear (CCHEN)
*11 Department of Physics, University of Hong Kong
*12 Physics Division, Oak Ridge National Laboratory
*13 Heavy Ion Laboratory, Warsaw University
*14 STFC Daresbury Laboratory
*15 Physical Sciences Division, TRIUMF
*16 Dept. of Physics and Astronomy, Seoul National University
*17 GSI Helmholtzzentrum für Schwerionenforschung GmbH

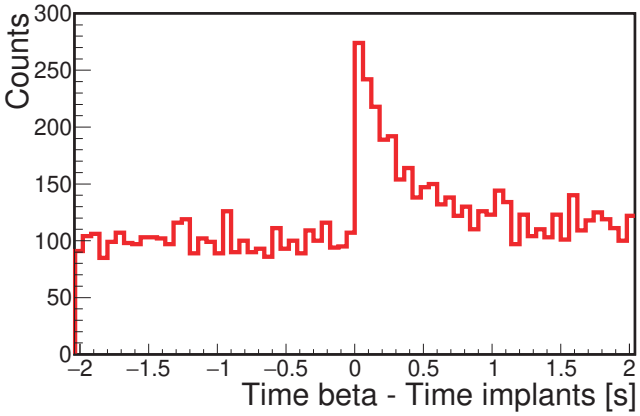

Fig. 2. Time distribution of the β particles emitted after the decay of ^{100}Sn in coincidence with DTAS.

made by the changes in the analysis code looking for the reduction of the accidental correlations associated to the decay of ^{100}Sn. In our study we changed several sorting parameters and compared the area of the true correlations (S) with the area of the background (B) (see Fig. 1. for an schematic view). The optimisation consisted in looking for conditions that increase the S to B ratio. Note that the correlation time window (t_s) is related to the decay half-life of the implanted nucleus of interest. Some improvements on the AIDA sorting code were also necessary.[4)]

In Fig. 2 we show the present status of the implant-β time correlation (gated with the condition on the DTAS firing) after implementing all cleaning conditions for the ^{100}Sn. Thanks to the procedures applied, an increase of the signal to background ratio of the order of 20% was achieved, improving the DTAS gamma correlated data. In the near future we will refine the calibration of the detectors and calculate the response function of the setup, which is mandatory for the total absorption spectrum analysis. Due to technical problems during our run we were only able to take data for 4 days from a total of 10 approved days. The continuation of the experiment is expected to occur in 2021.

References

1) J. L. Tain *et al.*, Nucl. Instrum. Methods Phys. Res. A **803**, 36 (2015).
2) C. J. Griffin *et al.*, Proc. XIII Nuclei in the Cosmos 1., 97 (2014).
3) A. Algora *et al.*, RIKEN Accel. Prog. Rep. **53**, 30 (2019).
4) O. B. Hall, private communication.

Shape evolution of ^{106,108,110}Mo in the triaxial degree of freedom†

J. Ha,[*1,*2] T. Sumikama,[*2,*3] F. Browne,[*2,*4] N. Hinohara,[*5] A. M. Bruce,[*4] S. Choi,[*1] I. Nishizuka,[*3] S. Nishimura,[*2] P. Doornenbal,[*2] G. Lorusso,[*2,*6,*7] P. -A. Söderström,[*2] H. Watanabe,[*2,*8] R. Daido,[*9] Z. Patel,[*2,*6] S. Rice,[*2,*6] L. Sinclair,[*2,*10] J. Wu,[*2,*11] Z. Y. Xu,[*12,*13] A. Yagi,[*9] H. Baba,[*2] N. Chiga,[*2,*3] R. Carroll,[*6] F. Didierjean,[*14] Y. Fang,[*9] N. Fukuda,[*2] G. Gey,[*15,*16] E. Ideguchi,[*9] N. Inabe,[*2] T. Isobe,[*2] D. Kameda,[*2] I. Kojouharov,[*17] N. Kurz,[*17] T. Kubo,[*2] S. Lalkovski,[*18] Z. Li,[*11] R. Lozeva,[*14,*19] H. Nishibata,[*9] A. Odahara,[*9] Zs. Podolyák,[*6] P. H. Regan,[*6,*7] O. J. Roberts,[*4] H. Sakurai,[*2] H. Schaffner,[*17] G. S. Simpson,[*15] H. Suzuki,[*2] H. Takeda,[*2] M. Tanaka,[*9] J. Taprogge,[*2,*20,*21] V. Werner,[*22,*23] and O. Wieland[*24]

The properties of the 2_2^+ band in even-even nuclei are closely connected with the triaxial motion in the direction of the γ degree of freedom, such as the γ-vibration, rigid triaxial rotor,[1] or γ-unstable rotor.[2] The lowering of the known 2_2^+-state energy in neutron-rich molybdenum isotopes ($Z = 42$) is interpreted as the development of these triaxial motions associated with the ground-state shape. We studied the neutron-rich ^{106,108,110}Mo isotopes with higher statistics by measuring the β-delayed γ rays.

A neutron-rich cocktail beam was produced from the fragmentation of a 345-MeV/nucleon $^{238}U^{86+}$ beam. The nuclides were separated and identified on the BigRIPS separator and delivered to F11. The ions and β particles were detected by the WAS3ABi active stopper. A high-purity Ge array, EURICA,[3] and fast-timing $LaBr_3$(Ce) array were used to measure the energy and time of γ rays.

Figure 1 shows $B(E2)$ determined from the lifetime measurement of the 2_1^+ states using the $LaBr_3$(Ce) array. The quadrupole deformation parameters β_2 of ^{106,108,110}Mo were deduced to be 0.349(13), 0.327(10), and 0.305(7), respectively. The results were compared with beyond-mean-field calculations using SLy4 and SLy5+T interactions, for which the predicted ground-state shapes were oblate and prolate, respectively. The prolate shape was indicated because the calculation with the SLy5+T interaction reproduces both $B(E2)$ and the energies of the ground-state band.

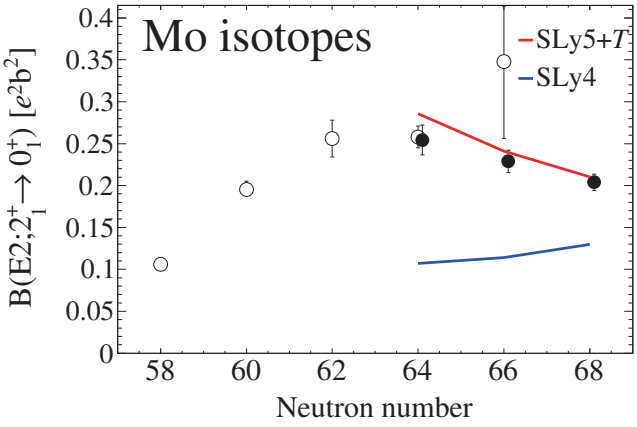

Fig. 1. $B(E2; 2_1^+ \rightarrow 0_1^+)$ of the neutron-rich Mo isotopes. The theoretical results calculated with SLy4 and SLy5+T interactions are shown.

The 2_2^+ band in ^{110}Mo was extended up to the 7^+ state. The energy staggerings of the 2_2^+ bands in ^{106,108,110}Mo are close to that of the axially symmetric rotor of the γ-vibrational state, rather than Davydov's rigid-triaxial rotor model or Wilets-Jean model for γ-unstable nuclei. A candidate of the two-phonon γ vibrational band with $K^\pi = 4^+$, which has not been well established yet, was found in ^{110}Mo. The $K^\pi = 4^+$ band decays only to the γ-vibrational band, and the energy of the $K^\pi = 4^+$ state is 2.5 times larger than that of the 2_2^+ state. Moreover, new 0_2^+ states were assigned in ^{108}Mo and ^{110}Mo.

The spin and parity of parent nuclei were assigned from the $\log ft$ values to be 4^- and 2^- for the ground state in ^{106}Nb and ^{108}Nb, respectively. Two β-decaying states were identified in ^{110}Nb, and their spin-parities were asigned as 2^- and 6^-.

† Condensed from the article in Phys. Rev. C **101**, 044311 (2020)

*1 Department of Physics and Astronomy, Seoul National University
*2 RIKEN Nishina Center
*3 Department of Physics, Tohoku University
*4 School of Computing, Engineering, and Mathematics, University of Brighton
*5 Center for Computational Sciences, University of Tsukuba
*6 Department of Physics, University of Surrey
*7 National Physical Laboratory
*8 IRCNPC, School of Physics and Nuclear Energy Engineering, Beihang University
*9 Department of Physics, Osaka University
*10 Department of Physics, University of York
*11 Department of Physics, Peking University
*12 Department of Physics, University of Tokyo
*13 Department of Physics, University of Hong Kong
*14 IPHC, CNRS/IN2P3, Université de Strasbourg
*15 LPSC, Université Grenoble-Alpes
*16 ILL
*17 GSI Helmholtzzentrum für Schwerionenforschung GmbH
*18 Department of Physics, University of Sofia
*19 CSNSM, CNRS/IN2P3, Université Paris-Sud
*20 Departamento de Física Teórica, Universidad Autónoma de Madrid
*21 Instituto de Estructura de la Materia, CSIC
*22 A.W. Wright Nuclear Structure Laboratory, Yale University
*23 Institut für Kernphysik, Technische Universität Darmstadt
*24 INFN Sezione di Milano

References
1) A. S. Davydov, G. F. Filippov, Nucl. Phys. **8**, 237 (1958).
2) L. Wilets, M. Jean, Phys. Rev. **102**, 788 (1956).
3) P. -A. Söderström *et al.*, Nucl. Instrum. Methods Phys. Res. B **317**, 649 (2013).

Evolution of proton single-particle states in neutron-rich Sb isotopes beyond $N = 82$[†]

A. Jungclaus,[*1] J. M. Keatings,[*2] G. S. Simpson,[*3] H. Naïdja,[*4] A. Gargano,[*5] S. Nishimura,[*6] P. Doornenbal,[*6] G. Gey,[*3,*7,*6] G. Lorusso,[*6] P. -A. Söderström,[*6] T. Sumikama,[*8] J. Taprogge,[*1,*9,*6] Z. Y. Xu,[*6] H. Baba,[*6] F. Browne,[*10,*6] N. Fukuda,[*6] N. Inabe,[*6] T. Isobe,[*6] H. S. Jung,[*11] D. Kameda,[*6] G. D. Kim,[*12] Y. -K. Kim,[*12,*13] I. Kojouharov,[*14] T. Kubo,[*6] N. Kurz,[*14] Y. K. Kwon,[*12] Z. Li,[*15] H. Sakurai,[*6,*16] H. Schaffner,[*14] Y. Shimizu,[*6] H. Suzuki,[*6] H. Takeda,[*6] Z. Vajta,[*17] H. Watanabe,[*6] J. Wu,[*15,*6] A. Yagi,[*18] K. Yoshinaga,[*19] S. Bönig,[*20] J. -M. Daugas,[*21] R. Gernhäuser,[*22] S. Ilieva,[*20] T. Kröll,[*20] A. Montaner-Piza,[*23] K. Moschner,[*24] D. Mücher,[*22] H. Nishibata,[*18] A. Odahara,[*18] R. Orlandi,[*25] M. Scheck,[*26] K. Steiger,[*22] and A. Wendt[*24]

The chain of Sb isotopes, with a single proton outside the closed $Z = 50$ proton shell, has attracted for many years a special interest since it offers the unique possibility to study the evolution of the proton single-particle states in the $Z = 50$–82 major shell over a wide range of neutron number. Prior to this work, excited-state information was available from the very neutron-deficient isotope ^{105}Sb, close to the presumably doubly-magic ^{100}Sn, up to the neutron-rich isotope ^{135}Sb. Above the $N = 82$ neutron shell gap, when the neutrons start filling the $1f_{7/2}$ orbital, a dramatic decrease of the energy of the $5/2^+_1$ state from 962 keV in ^{133}Sb to 281 keV in ^{135}Sb was observed.[1,2)]

The present work aimed for an extension of the experimental information towards more neutron-rich Sb isotopes. Excited states in ^{136,137,138}Sb, populated in the β decay of the semi-magic Sn isotopes ^{136,137,138}Sn, were studied within the EURICA campaign. The clean ion identification and high γ-ray detection efficiency allowed to observe for the first time the decay of excited states in the $N = 86$ isotope ^{137}Sb, which is considered as one of the key nuclei to pin down the evolution of the single-particle structure beyond $N = 82$. As shown in Fig. 1, the experimental energy of the $5/2^+_1$ state, $E_x = 84$ keV, lies in the middle between the results of shell-model calculations performed using two different realistic effective interactions, labeled Napoli and N3LOP. Together with a similar comparison for ^{136,138}Sb, the new experimental information thus allows to trace the evolution of the single-particle energies above the $N = 82$ shell closure.

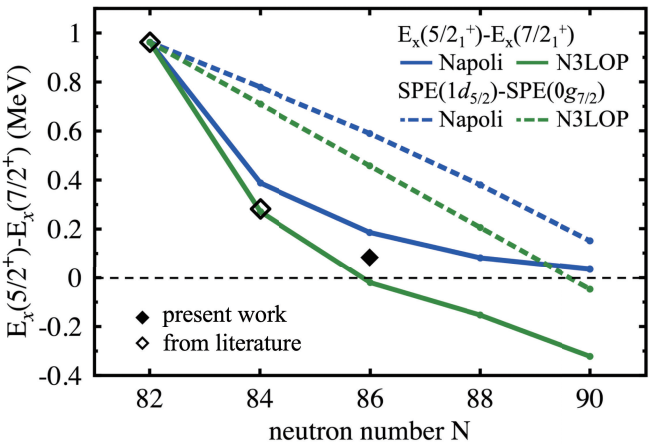

Fig. 1. Excitation energy difference between the $5/2^+_1$ and $7/2^+_1$ states in the odd Sb isotopes. Experimental values are shown as open (literature) and filled (present work) diamonds while solid blue (green) lines represent the results of SM calculations employing the Napoli (N3LOP) interactions. The differences between the effective SPE of the $1d_{5/2}$ and $0g_{7/2}$ orbitals are shown by dashed lines (adopted from Fig. 7 of the original article).

† Condensed from the article in Phys. Rev. C **102**, 034324 (2020)

*1 IEM-CSIC
*2 School of Computing, Engineering, and Physical Sciences, University of the West of Scotland
*3 LPSC, Université Joseph Fourier Grenoble 1, CNRS/IN2P3, Institut National Polytechnique de Grenoble
*4 Laboratoire de Physique Mathematique et Subatomique, Constantine University
*5 INFN Sezione di Napoli
*6 RIKEN Nishina Center
*7 Institut Laue-Langevin
*8 Department of Physics, Tohoku University
*9 Departamento de Física Teórica, Universidad Autónoma de Madrid
*10 School of Computing, Engineering and Mathematics, University of Brighton
*11 Department of Physics, Chung-Ang University
*12 Rare Isotope Science Project, Institute for Basic Science (IBS)
*13 Department of Nuclear Engineering, Hanyang University
*14 GSI Helmholtzzentrum für Schwerionenforschung GmbH
*15 School of Physics and State key Laboratory of Nuclear Physics and Technology, Peking University
*16 Department of Physics, University of Tokyo
*17 Atomki
*18 Department of Physics, Osaka University
*19 Department of Physics, Faculty of Science and Technology, Tokyo University of Science
*20 Institut für Kernphysik, Technische Universität Darmstadt
*21 CEA, DAM
*22 Physik Department E12, Technische Universität München
*23 IFIC, CSIC-Univ. Valencia
*24 IKP, University of Cologne
*25 Advanced Science Research Center, Japan Atomic Energy Agency
*26 School of Engineering, University of the West of Scotland

References

1) M. Sanchez-Vega *et al.*, Phys. Rev. C **60**, 024303 (1999).
2) J. Shergur *et al.*, Phys. Rev. C **71**, 064321 (2005).

BRIKEN measurements of P_n-values and half-lives for understanding the formation of the r-process rare-earth peak: progress on the Ce to Nd region

A. Tarifeño-Saldivia,[*1] G. G. Kiss,[*2] J. L. Tain,[*3] A. Estrade,[*4] S. Nishimura,[*5] J. Agramunt,[*3] A. Algora,[*3] N. T. Brewer,[*6] R. Caballero-Folch,[*7] F. Calvino,[*1] T. Davinson,[*8] I. Dillmann,[*7] N. Fukuda,[*5] R. K. Grzywacz,[*9] O. Hall,[*6] N. Mont-Geli,[*1] A. I. Morales,[*3] A. Navarro,[*1] N. Nepal,[*5] M. Pallàs,[*1] B. C. Rasco,[*6] K. P. Rykaczewski,[*6] N. T. Szegedi,[*2] A. Vitz-Sveiczer,[*2] A. Tolosa-Delgado,[*3] P. Vi,[*10] R. Yokoyama,[*9] M. Wolinska-Cichocka,[*11] and P. Woods[*8] for the BRIKEN Collaboration[*12]

The Rare-Earth Peak (REP) is a distinctive local maximum observed around mass $A \sim 160$ in the elemental abundance distribution of the rapid-neutron capture process (r-process). Because the REP is formed after neutron exhaustion,[1] it provides a unique probe for studying the late-time environmental conditions of the r-process site.[2] According to theoretical models, β-decay rates ($T_{1/2}$) and delayed neutron emission probabilities (P_n-values) play important roles in the formation of the REP.[3] The region of nuclei with the most significant impact on the formation of the REP has been determined via sensitivity studies.[4] Most of the $T_{1/2}$ on this region have already been measured by the EURICA collaboration.[7] However, the experimental determination of P_n-values is yet to be achieved.

The NP1612-RIBF148 experiment exploits the unique capabilities of the BRIKEN setup[5,6] for the measurement of β-delayed neutrons. This experiment attemps to study P_n-values and $T_{1/2}$ for the nuclei which are important to REP formation.[4] In the 2018 experimental run, a 60-particle-nA ^{238}U beam, with 345 MeV/nucleon, hitting a 4 mm thick Be target was used to produce the secondary radioactive beam. The neutron-rich fragments were filtered out by the BigRIPS fragment separator and the ZeroDegree spectrometer. The beam setting was centered on ^{165}Pm.

Here, we report preliminary results from the 2018 experimental run. Figure 1 shows the measured beta-decay half-lives in the region from Ce to Nd isotopes. The experimental results are compared with previous measurements performed by the EURICA collaboration,[7] and with FRDM + QRPA theoretical calculations.[8,9] The BRIKEN experimental data agree well with the previous measurements. In addition, our results exhibit an improved precision for the heavier nuclei region. Based on the current status of the data analysis for this experiment, we expect to obtain at least one new $T_{1/2}$ per atomic number on the heavier isotopes from the Ce to Nd region. These results will be reported in the future.

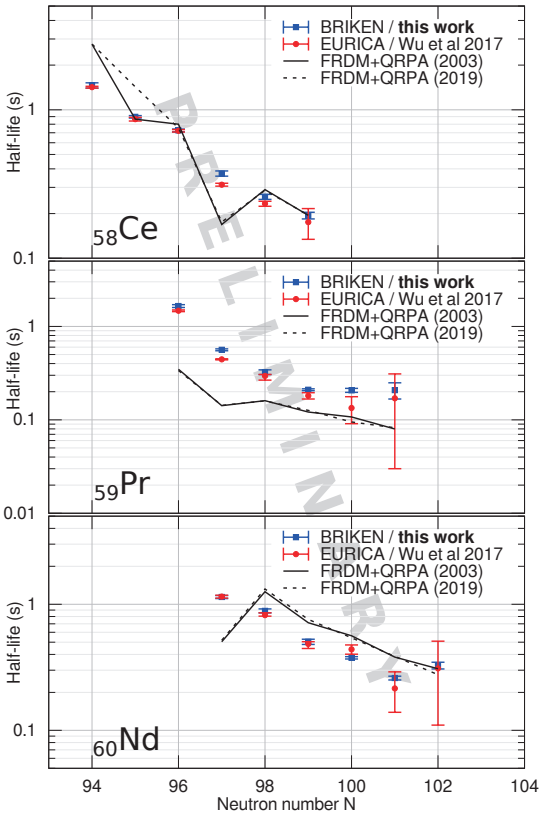

Fig. 1. Systematic trends in BRIKEN results of β-decay half-lifes (blue) compared with previous measurements (red),[7] and theoretical calculations.[8,9]

*1 Universitat Politècnica de Catalunya (UPC)
*2 Institute for Nuclear Research (Atomki)
*3 Instituto de Física Corpuscular (IFIC)
*4 University College of Science and Engineering, CMU
*5 RIKEN Nishina Center
*6 Physics Division, Oak Ridge National Laboratory
*7 Physical Sciences Division, TRIUMF
*8 School of Physics and Astronomy, University of Edinburgh
*9 Department of Physics and Astronomy, University of Tennessee
*10 Faculty of Physics, VNU University of Science
*11 HIL, University of Warsaw
*12 www.wiki.edu.ac.uk/display/BRIKEN/Home

References
1) R. Surman *et al.*, Phys. Rev. Lett. **79**, 1809 (1997).
2) M. R. Mumpower *et al.*, Astrophys. J. **752**, 117 (2012).
3) A. Arcones *et al.*, Phys. Rev. C **83**, 045809 (2011).
4) M. R. Mumpower *et al.*, Phys. Rev. C **85**, 04580 (2012).
5) I. Dillmann *et al.*, Nucl. Phys. News **28**, 28 (2018).
6) A. Tolosa-Delgado *et al.*, Nucl. Instrum. Methods Phys. Res. A **925**, 133 (2019).
7) J. Wu *et al.*, Phys. Rev. Lett. **118**, 072701 (2017).
8) P. Möller *et al.*, Phys. Rev. C **67**, 055802 (2003).
9) P. Möller *et al.*, At. Data Nucl. Data Tables **125**, 1 (2019).

Precision measurement of ground-state electric quardrupole moment for neutron-rich ^{21}O

A. Gladkov,[*1] H. Yamazaki,[*1] Y. Ichikawa,[*1] A. Takamine,[*1] H. Nishibata,[*2] K. Asahi,[*1] K. Kawata,[*1,*3] K. Imamura,[*1] M. Tajima,[*1] K. Tsubura,[*1] and H. Ueno[*1]

The anomalous nuclear properties had been experimentally indicated for the neutron-rich ^{23}O isotope, such as the formation of halo structure[1] and the presence of the new neutron magic number at neutron number[2] $N = 16$. This originates the interest in the shell evolution in this region of neutron-rich oxygen isotopes. Such information can be directly provided by the knowledge about the nuclear properties of neighboring isotopes, such as ^{21}O.

Previously, we have conducted the measurements of the electromagnetic moments of ^{21}O[3] and the ground-state magnetic moment has been successfully determined. However, due to RF tank circuit limitations, the obtained spectrum for the quadrupole moment (Q-moment) measurement was insufficient to make firm conclusions and required further study. Since then, the experimental setup was improved and the Q-moment has been successfully measured.

The present experiment was carried out using the RIPS separator at the RIBF facility. A spin-polarized beam of neutron-rich ^{21}O was produced in the projectile fragmentation reaction of a ^{22}Ne beam at 70 MeV/nucleon on a 185-mg/cm^2 Be target. To ensure polarization, the momentum window and emission angle of the secondary fragments were selected to be $p_F = p_0 \times (0.97 \pm 0.03)$ and $\theta_F > 1.5°$, respectively. Here, p_0 is the fragment momentum corresponding to the projectile velocity. The secondary beam of ^{21}O was then purified by the momentum and momentum-loss analyses and delivered to the β-ray detected nuclear magnetic resonance (β-NMR) apparatus installed downstream the beam line. The well-established method of β-NMR[4] in combination with adiabatic fast passage technique[5] was applied to measure quadrupole moment.

The obtained nuclear quadrupole resonance (NQR) spectra are shown on Fig. 1. It consists of the two series of measurements. The black circles represent the measurement with ±44 kHz modulation of quadrupole coupling constant $\nu_Q = eqQ/h$, where q, Q and h denote the electric field gradient of the stopper material, the Q-moment and the Planck's constant, respectively. The spectra are plotted with $A_\beta P$ values measured as a function of deviation from the peak frequency $\nu_Q^{\rm peak}$, where $A_\beta P$ is the β-decay asymmetry parameter, and P the ^{21}O nuclear spin polarization. A resonant peak formed by the β rays emitted from ^{21}O stopped at the substitution site of TiO_2 is clearly identified in Fig. 1. Due to the improvement in polarization detection, the signal-to-noise ratio was greatly increased and a less pronounced additional NQR effect was detected at a lower Q-moment region.

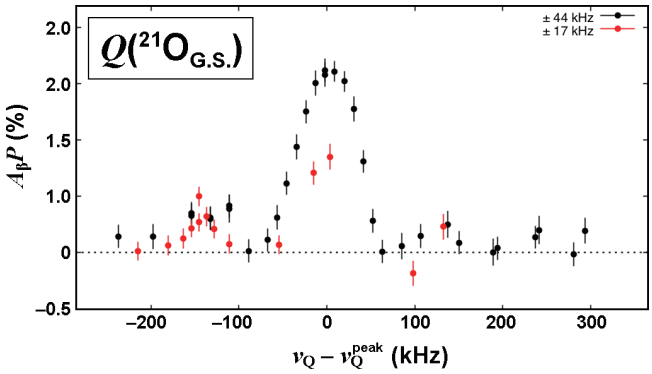

Fig. 1. β-NQR spectra of ^{21}O in TiO_2 single crystal. The figure shows the results of two series of measurements with ν_Q modulation of ±44 kHz (black circles) and ±17 kHz (red circles) are shown.

In order to investigate this minor peak in more detail, a measurement with narrower scan width of ±17 kHz was conducted. The result of this measurement is represented on Fig. 1 by the red solid circles. The centroid position of the small peak is consistent with the previous nuclear quadrupole resonance (NQR) measurement of ^{21}O at RIPS in 2016.[3] The origin of the additional lower-amplitude peak is under analysis. In overall, the two NQR measurements confirmed the existence of a major peak at higher Q-moment region that could not be detected in 2016 due to several experimental limitations. The Q-moment value of ^{21}O can be then firmly assigned based on the obtained results. The uncertainty assignment based on the peak shape analysis and the discussion of the results in terms of ^{21}O nuclear structure are work-in-progress.

*1 RIKEN Nishina Center
*2 Department of Physics, Kyushu University
*3 Center for Nuclear Study, The University of Tokyo

References
1) C. Nociforo *et al.*, Phys. Lett. B **605**, 79 (2005).
2) D. Cortina-Gil *et al.*, Phys. Rev. Lett. **93**, 062501 (2004).
3) A. Gladkov *et al.*, RIKEN Accel. Prog. Rep. **51**, 74 (2018).
4) D. Nagae *et al.*, Nucl. Instrum. Methods Phys. Res. B **266**, 4612 (2008).
5) A. Abragam, *The Principles of Nuclear Magnetism* (Springer, Oxford, 1961).

Investigations of magnetic moments in Coulomb fission

G. Häfner,[*1,*2] R. Lozeva,[*1] M. Si,[*1] Y. Ichikawa,[*3,*4] H. Ueno,[*3] D. S. Ahn,[*3] K. Asahi,[*3] T. Asakawa,[*3,*5] H. Baba,[*3] A. Esmaylzadeh,[*2] N. Fukuda,[*3] A. Gladkov,[*3] K. Imamura,[*3] N. Inabe,[*3] K. Kawata,[*3,*6] L. Knafla,[*2] A. Kusoglu,[*7] M. Niikura,[*8] Y. Sasaki,[*3,*5] H. Sato,[*3] Y. Shimizu,[*3] H. Suzuki,[*3] M. Tajima,[*3] A. Takamine,[*3] H. Takeda,[*3] Y. Takeuchi,[*3,*5] Y. Yanagisawa,[*3] H. Yamazaki,[*3] and K. Yoshida[*3]

Magnetic moments present an important tool to study the single-particle character of excited states. They are directly related to the g factor and provide a crucial test for the wave functions of particular states predicted by theoretical models. One experimental requirement for the measurement of g factors is the spin alignment of the nuclear ensemble that is obtained in the reaction populating a nucleus of interest. In this experiment, Coulomb fission is used to produce the nuclear alignment, and the magnetic moments of isomeric states are investigated.

The region around the doubly magic ^{132}Sn has been of prime interest in the past decades owing to its importance from the perspectives of astrophysics and nuclear structure. The investigation of nuclei with few valence particles is interesting because several isomeric structures emerge in them. For example, the three-proton-hole $Z = 47$ isotopes ^{124,125}Ag have isomers based on the unique parity orbitals $\pi(0g_{9/2})$ and $\nu(0h_{11/2})$.[1)]

The experiment is performed at the RIBF using the BigRIPS spectrometer. A primary ^{238}U beam at an energy of 345 MeV/nucleon impinged on a thin ^{184}W production target with an average beam intensity of approximately 100 particle nA. The momentum distribution is selected with slits at the F1 focal plane. The nuclei of interest are separated and identified using the BigRIPS separator.[2)] The secondary ions are stopped in a 3-mm-thick Cu host at the F8 focal point. The detection setup consisted of four high-purity Ge (HPGe) and two $LaBr_3$(Ce) detectors, arranged with each detector type at 90° with respect to each other. To measure the magnetic moments, the TDPAD method is used; it has been applied successfully at the RIBF.[3–5)]

In the experiment, approximately $5{\cdot}10^6$ ions of ^{124}Ag and approximately $3{\cdot}10^6$ ions of ^{125}Ag are identified in each of the experimental settings. The particle identification (PID) of these secondary ions is achieved after the identification and tracking detectors are fully calibrated offline. The spectroscopy could be performed after calibration and various corrections of the γ-ray detectors in energy and time. Figure 1 shows the delayed γ-ray energy spectrum of all Ge detectors with a PID gate for the ^{125}Ag ions. All transitions below the known $(17/2^-)$ isomer can be identified. For the TDPAD analysis, a good in-beam time resolution is essential. The setup is optimized using ^{60}Co and ^{152}Eu sources, with a typical resolution of 8(1) ns (FWHM) achieved by the detectors in the range of interest. This corresponds to a resolution of 12(1) ns in-beam for the same detector, *e.g.*, for the 670 keV transition in ^{125}Ag. As an example, the inset of Fig. 1 shows the time-resolution spectrum for one of the HPGe detectors, demonstrating the capabilities of this setup. The analysis of the magnetic moment from the oscillation pattern is currently in progress. Therefore, it is necessary to have spin alignment, which will be shown by measuring the magnetic moment of a known calibration case.

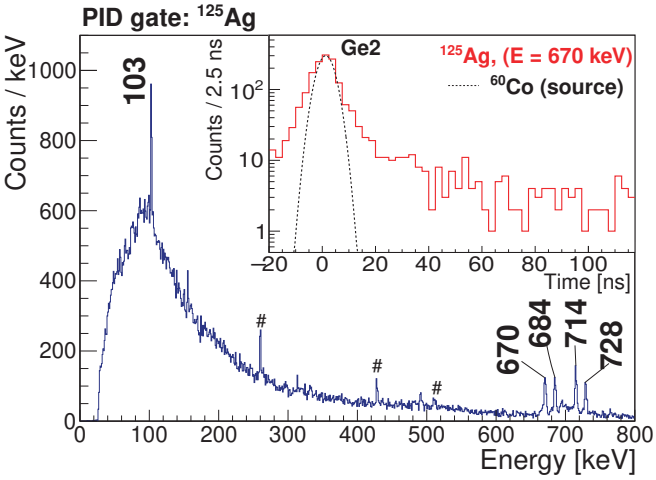

Fig. 1. Delayed HPGe energy spectrum for the ^{125}Ag ions. Background transitions are labelled with "#." The inset shows the time-resolution spectrum of one detector for a source and in-beam measurement.

*1 Université Paris-Saclay, CNRS/IN2P3, IJCLab
*2 IKP, University of Cologne
*3 RIKEN Nishina Center
*4 Department of Physics, Kyushu University
*5 Department of Advanced Sciences, Hosei University
*6 Center for Nuclear Study, University of Tokyo
*7 Department of Physics, Istanbul University
*8 Department of Physics, University of Tokyo

References
1) S. Lalkovski *et al.*, Phys. Rev. C **87**, 034308 (2013).
2) T. Kubo *et al.*, Nucl. Instrum. Methods Phys. Res. B **204**, 97 (2003).
3) Y. Ichikawa *et al.*, Nat. Phys. **8**, 918 (2012).
4) Y. Ichikawa *et al.*, Nat. Phys. **15**, 321 (2019).
5) F. Boulay *et al.*, Phys. Rev. Lett. **124**, 112501 (2020).

Re-measurement of the ^{4}He(^{8}He, ^{8}Be) reaction

S. Masuoka,[*1,*2] S. Shimoura,[*1] M. Takaki,[*1] S. Ota,[*1] S. Michimasa,[*1] M. Dozono,[*1] C. Iwamoto,[*1] K. Kawata,[*1] N. Kitamura,[*1] M. Kobayashi,[*1] R. Nakajima,[*1] H. Tokieda,[*1] R. Yokoyama,[*1] D. S. Ahn,[*2] H. Baba,[*2] N. Fukuda,[*2] T. Harada,[*3] E. Ideguchi,[*4] N. Imai,[*1] N. Inabe,[*2] Y. Kondo,[*5] T. Kubo,[*2] Y. Maeda,[*6] F. M. Marqués,[*7] M. Matsushita,[*1] T. Nakamura,[*5] N. Orr,[*7] H. Sakai,[*2] H. Sato,[*2] P. Schrock,[*1] L. Stuhl,[*1,*2] T. Sumikama,[*2] H. Suzuki,[*2] H. Takeda,[*2] K. Taniue,[*6] T. Uesaka,[*2] K. Wimmer,[*8] K. Yako,[*1] Y. Yamaguchi,[*1] Y. Yanagisawa,[*2] K. Yoshida,[*2] and J. Zenihiro[*2]

In our previous study, the candidate resonance of the $4n$ system (tetra-neutron) was determined using the ^{4}He(^{8}He, ^{8}Be)$4n$ reaction with a 186 MeV/nucleon ^{8}He beam.[1)] A new measurement with better statistics and better accuracy was performed to confirm the existence of the tetra-neutron system.[2)]

The intensity of the ^{8}He beam was 3.5×10^6 particles per second at the liquid helium target, and approximately twice compared to that of the previous experiment. Low pressure multi-wire drift chambers (LP-MWDCs) were installed at the focal planes F3, F6, and F-H10(S0), to measure the trajectory and momentum of the beam. The time reference to determine the drift time in LP-MWDCs was obtained from a plastic scintillator at F3.

We present the analysis of the LP-MWDCs developed to eliminate accidental coincidence events induced by the high intensity beam. The ^{8}He beam from the SRC had a bunch structure with a periodic cycle of 73 ns. There are two cases of accidental coincidence as illustrated in Fig. 1(a) and (b). The filled circles represent the particle, which triggered the data acquisition. The other particle in the next bunch (open circle) hits in (a), whereas two particles together hit in the same bunch in (b). In the analysis, we carefully treated these events, which created multiple hits within the maximum drift time of 120 ns in the LP-MWDCs. The events of Fig. 1(a) were successfully identified by selecting the drift-time region of the LP-MWDC and the total traveling time from F3 to S2 focus corresponding to the beam energy.

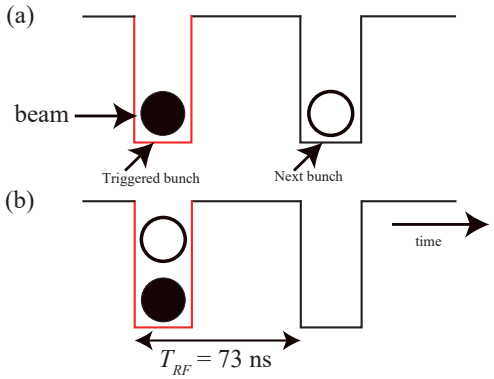

Fig. 1. Time structure of the beam bunch. The solid circles show particles triggering data acquisition, and the open circles are accidental particles. (a) Beam contains both the 'Triggered bunch' and 'Next bunch.' (b) Two particles are in the triggered bunch.

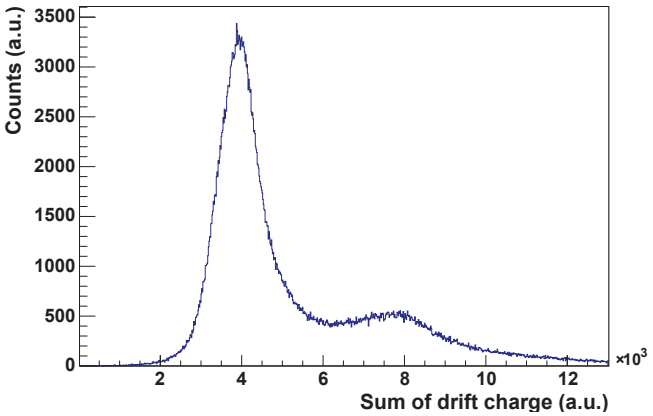

Fig. 2. Energy distribution of LP-MWDC.

In the case of Fig. 1(b), we simply eliminated such events because the triggered beam particle and accidental particle in the same bunch cannot be distinguished. To identify such cases, we estimated the total energy spectrum obtained by using the Time-Over-Threshold data of its signal. Figure 2 shows the total energy distributions measured at LP-MWDC; two peaks are visible. The peak at higher energies results from multiple-hit events, and 75% of the multiple hit events were rejected by selecting energies below 6,000. This value is consistent with the probability of an occurrence of pile up events.

After the treatment, the tracking efficiency of the beam was 95%. In the present experiment, one of the LP-MWDCs installed at F-H10 was damaged under the intense irradiation of the ^{8}He beam and operated with a low efficiency of 48%. The overall tracking efficiency of the ^{8}He beam is therefore 80%, which still ensures better statistics than the previous experiment.

Data analysis is in progress toward the final result.

*1 Center for Nuclear Study, the University of Tokyo
*2 RIKEN Nishina Center
*3 Department of Physics, Toho University
*4 Research Center for Nuclear Physics, Osaka University
*5 Department of Physics, Tokyo Institute of Technology
*6 Faculry of Engineering, Univ. of Miyazaki
*7 Laboratorie de Physique Corpusculaire, IN2P3-CNRS, ENSICAEN et Université de Caen
*8 Department of Physics, the University of Tokyo

References

1) K. Kisamori *et al.*, Phys. Rev. Lett. **116**, 052501 (2016).
2) S. Masuoka *et al.*, RIKEN Accel. Prog. Rep. **50**, 198 (2017).

Alpha-decay correlated mass measurement of ^{206,207}Ra using an MRTOF-MS system equipped with an α-TOF detector

T. Niwase,[*1,*2,*3] M. Wada,[*3] P. Schury,[*3] P. Brionnet,[*2] S. D. Chen,[*4,*3] T. Hashimoto,[*5] H. Haba,[*2] Y. Hirayama,[*3] D. S. Hou,[*6,*7,*8] S. Iimura,[*9,*2,*3] H. Ishiyama,[*2] S. Ishizawa,[*10,*2] Y. Ito,[*11] D. Kaji,[*2] S. Kimura,[*2] J. Liu,[*4,*3] H. Miyatake,[*3] J. Y. Moon,[*5] K. Morimoto,[*2] K. Morita,[*1,*2] D. Nagae,[*1] M. Rosenbusch,[*3] A. Takamine,[*2] T. Tanaka,[*12] Y. X. Watanabe,[*3] H. Wollnik,[*13] W. Xian,[*4,*3] and S. X. Yan[*14]

Toward the precise mass measurement of heavy and superheavy nuclides, the SHE-Mass-II facility[1] was constructed with a multi-reflection time-of-flight mass spectrograph (MRTOF-MS)[2] coupled with the gas-filled recoil ion separator GARIS-II.[3] We installed an α-TOF[4] detector, which simultaneously records the time-of-flight (TOF) signal and subsequent α-decay. In order to demonstrate the α-TOF detector, an experiment was performed using the ^{51}V + ^{159}Tb reaction. A ^{51}V beam was accelerated to 6.0 MeV/nucleon by the RIKEN Ring Cyclotron (RRC). The beam energy on the target was reduced by an aluminum degrader to 4.8 MeV/nucleon. The beam impinged upon 460 μg/cm^2-thick ^{159}Tb targets with a 3 μm Ti backing, mounted in a rotating target wheel.

The fusion evaporation residues (ERs) were separated from the primary beam and transported using GARIS-II. After decelerating ERs using a Mylar foil, the ERs were stopped in a cryogenic helium gas catcher, and the thermalized ions were extracted by a radio frequency (RF) carpet and transported to the MRTOF-MS via multiple RF ion traps.

We observed ERs, ^{206,207}Fr, and ^{206,207}Ra as doubly charged ions. The subsequent α-decays were additionally detected by the α-TOF detector. Using ^{206,207}Fr as the isobaric references, the masses of ^{206,207}Ra were directly determined. The mass excess of ^{206}Ra was 3540(54) keV, which agrees with the values reported in AME2016.[5]

The TOF spectrum for the A/q = 103.5 region is shown in Fig. 1. The singles events and ^{207}Ra decay-correlated events are plotted. In the case of the ground state of ^{207}Ra, the correlated events of the TOF and the α-decay could not be observed, because the incoming rate was higher than the decay rate, while the decay-correlated events were observed in the isomeric state ^{207m}Ra owing to its short half-life. The energies of the α-decay were selected as higher than 7.32 MeV, 2σ apart from the centroid of ^{207g}Ra, to avoid contamination from ^{207g}Ra.

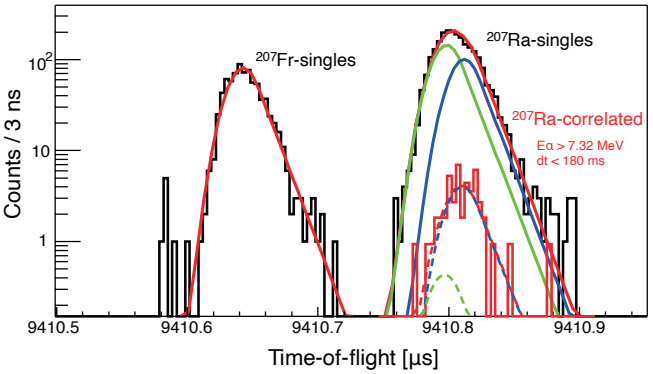

Fig. 1. Time-of-flight spectrum around the ^{207}Ra^{2+} region. The red histogram indicates the decay-correlated events. The green and blue lines show the fitting of the ground and isomeric states of the singles (solid lines) and decay-correlated events (dot lines).

The peaks of singles $^{207g/m}$Ra^{2+} and decay-correlated ^{207m}Ra^{2+} were fitted. The shape of the peak was determined by ^{207}Fr^{2+}. The mass excess of ^{207g}Ra was determined to be 3538(15) keV, and the excitation energy of ^{207m}Ra was $E_{\rm ex}$ = 552(42) keV from the α-decay correlated TOF spectrum. These values are consistent with those evaluated by α-decay spectroscopy.[5]

The alpha branching ratio of ^{207m}Ra was determined from the counting of TOF and α-decay events. The spin parity was expected to be 13/2$^+$ based on its single-particle level energy and the analogous reduced alpha width to the neighboring nuclei.

*1 Department of Physics, Kyushu University
*2 RIKEN Nishina Center
*3 Wako Nuclear Science Center (WNSC), KEK
*4 Department of Physics, The University of Hong Kong
*5 Institute for Basic Science, Rare Isotope Science Project
*6 Institute of Modern Physics, Chinese Academy of Science
*7 University of Chinese Academy of Science
*8 School of Nuclear Science and Technology, Lanzhou University
*9 Department of Physics, Osaka University.
*10 Graduate School of Science and Engineering, Yamagata University
*11 Japan Atomic Energy Agency
*12 Department of Nuclear Physics, The Australian National University
*13 Department of Chemistry and Biochemistry, New Mexico State University
*14 Institute of Mass Spectrometer and Atmospheric Environment, Jinan University

References

1) M. Wada *et al.*, RIKEN Accl. Prog. Rep. **52**, 136 (2019).
2) P. Schury *et al.*, Nucl. Instrum. Methods Phys. Res. B **335**, 39 (2014).
3) D. Kaji *et al.*, Nucl. Instrum. Methods Phys. Res. B **317**, 311 (2013).
4) T. Niwase *et al.*, Nucl. Instrum. Methods Phys. Res. A **953**, 163198 (2020).
5) M. Wang *et al.*, Chin. Phys. C **41**, 030003 (2017).

First high-precision direct determination of the atomic mass of a superheavy nuclide

P Schury,[*1] T. Niwase,[*1,*2,*3] M. Wada,[*1] P. Brionnet,[*2] S. Chen,[*4] T. Hashimoto,[*5] H. Haba,[*2] Y. Hirayama,[*1] D. S. Hou,[*6,*7,*8] S. Iimura,[*9,*2,*1] H. Ishiyama,[*2] S. Ishizawa,[*10,*2] Y. Ito,[11,*2,*1] D. Kaji,[*2] S. Kimura,[*2] H. Koura,[*11] J. J. Liu,[*4,*1] H. Miyatake,[*1] J. -Y. Moon,[*5] K. Morimoto,[*2] K. Morita,[*12,*13] D. Nagae,[*13] M. Rosenbusch,[*1] A. Takamine,[*2] Y. X. Watanabe,[*1] H. Wollnik,[*14] W. Xian,[*4,*1] and S. X. Yan[*15]

We present the first direct measurement of the atomic mass of a superheavy nuclide. Atoms of ^{257}Db ($Z = 105$) were produced online at the RIKEN Nishina Center for Accelerator-Based Science using the fusion-evaporation reaction ^{208}Pb(^{51}V, $2n$)^{257}Db. The gas-filled recoil ion separator GARIS-II was used to suppress both the unreacted primary beam and some transfer products, prior to delivering the energetic beam of ^{257}Db ions to a helium gas-filled ion stopping cell wherein they were thermalized. Thermalized ^{257}Db^{3+} ions were then transferred to a multi-reflection time-of-flight mass spectrograph for mass analysis. An alpha particle detector embedded in the ion time-of-flight detector allowed disambiguation of the rare ^{257}Db^{3+} time-of-flight detection events from background by means of correlation with characteristic α-decays (see also T. Niwase in this issue). The extreme sensitivity of this technique allowed a precision atomic mass determination from 11 events. The mass excess was determined to be $100\,063(231)_{\rm stat}(72)_{\rm sys}$ keV/c^2.

In recent experience, elements with a second ionization potential below 24 eV have been near uniformly extracted from the gas cell as doubly charged ions. Surprisingly, no counts were seen for ^{257}Db^{2+}, while ^{257}Db^{3+} was observed with the rate which, based on cross-section, target thickness, and primary beam intensity, indicated it constituted the preponderance of ^{257}Db ions. The rate of ^{257}Db^{3+} extracted from the gas cell was roughly 4 per day. These ions were analyzed by the MRTOF-MS with the α-TOF detector,[1] which allowed us to correlate ToF events with subsequent α-decays. Such correlations allowed removal of even low-intensity backgrounds and confirm that we were truly measuring ^{257}Db^{3+}.

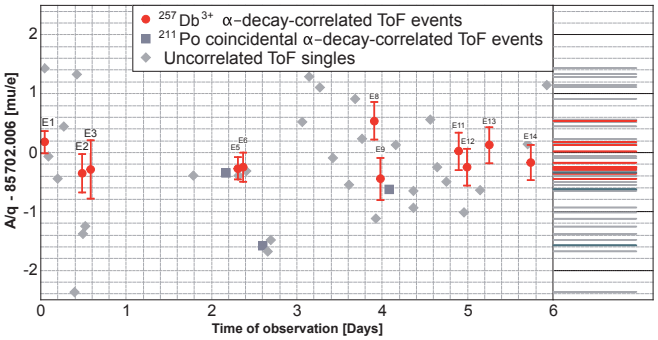

Fig. 1. Apparent A/q evaluated for each ToF single near the expected position of ^{257}Db^{3+}. The data are plotted in terms of deviation from the A/q for ^{257}Db^{3+} as determined from AME16.[2] Statistical uncertainties are only evaluated for α-decay correlated ToF events.

Figure 1 shows the data measured over 105 hours of beam on target. As the MRTOF was operated with a resolving power of $R_{\rm m} \approx 300\,000$, the A/q range presented is about 10-FWHM. The red points represent events where the ToF signal was followed within 120 s by an α decay event with energy $E_\alpha \geq 7.0$ MeV to encompass all possible α-decays from ^{257}Db and its decay products; some α-decay-correlated ToF events within this gate were attributed to the α-decay of ^{211}Po.

Based on the 11 alpha decay correlated ToF events, the mass of ^{257}Db could be determined with a precision of 231 keV/c^2 (82 μu/e). The value is in agreement with indirect measurements.[2,3] Unfortunately, the mass resolution of the MRTOF and the energy resolution of the α-TOF were insufficient to resolve isomeric states. With recent improvements in the mass resolving power (See S. Yan in this issue) we should be able to resolve the isomer and ground state provided the isomer has excitation energy above 250 keV/c^2. A followup effort to determine the state order via MRTOF mass analysis is planned for FY2021.

*1 Wako Nuclear Science Center (WNSC), IPNS, KEK
*2 RIKEN Nishina Center
*3 Department of Physics, Kyushu University
*4 Department of Physics, The University of Hong Kong
*5 Institute for Basic Science
*6 Institute of Modern Physics
*7 University of Chinese Academy of Sciences
*8 School of Nuclear Science and Technology
*9 Department of Physics, Osaka University
*10 Graduate School of Science and Engineering, Yamagata University
*11 Advanced Science Research Center, Japan Atomic Energy Agency
*12 Department of Physics, Kyushu University
*13 Research Center for SuperHeavy Elements, Kyushu University
*14 New Mexico State University
*15 Institute of Mass Spectrometer and Atmospheric Environment, Jinan University

References
1) T. Niwase *et al.*, Nucl. Instrum. Methods Phys. Res. A, **953**, 163198 (2020).
2) M. Wang *et al.*, Chin. Phys. C, **41** 030003 (2017).
3) Y. Ito *et al.*, Phys. Rev. Lett. **120**, 152501 (2020).

β-decay spectroscopy of ^{187}Ta

M. Mukai,[*1] Y. Hirayama,[*2] Y. X. Watanabe,[*2] S. C. Jeong,[*2] H. Miyatake,[*2] S. Ishizawa,[*1,*2,*3] T. Niwase,[*1,*2,*4] M. Rosenbusch,[*2] P. Schury,[*2] M. Wada,[*2] H. Watanabe,[*1,*5] M. Brunet,[*6] F. G. Kondev,[*7] G. J. Lane,[*8] Yu. A. Litvinov,[*9] Zs. Podolyák,[*6] and P. M. Walker[*6]

The nuclear data of neutron-rich nuclei around $N = 126$, such as the nuclear mass, decay half-life, and decay scheme, are key for understanding the formation of the third peak around $A = 195$ through the r-process in explosive stellar environments, and the data are required to be investigated experimentally. Furthermore, the neutron-rich region around $Z = 75$ is not only a transition region of nuclear deformation, but also expected to contain high-energy long-lived isomers. Owing to the astrophysical and nuclear physics interests in this nuclear region, nuclear spectroscopy has been performed at the KEK Isotope Separation System (KISS) [1,2] installed in the Radioactive Isotope Beam Factory (RIBF), RIKEN.

The isomeric states of ^{187}Ta ($Z = 73$, $N = 114$) were first observed in the Experimental Storage Ring (ESR) at GSI.[3] In that study, the half-lives and excited energies were determined to be 2.3(6) min for the ground state (gs), 22(9) s for the first isomeric state (m1) at the excitation energy $E_x = 1789(13)$ keV, and >5 min for the second isomeric state (m2) at $E_x = 2935(14)$ keV.[3] We performed the β- and γ-decay spectroscopy of ^{187}Ta to investigate the nuclear structure of the ground and two isomeric states at KISS. They are predicted to have nuclear spins of $25/2^-$ and $41/2^+$ for the m1 and m2 states, respectively. The results of successful experiments on the m1 isomer were reported in Ref. 4). The present report describes the progress of the analysis investigating the unknown β-decays of $^{187gs,\,m1,\,m2}$Ta.

$^{187gs,\,m1,\,m2}$Ta were produced using multi-nucleon transfer reactions of a natural tungsten target (5 μm thick) and ^{136}Xe beam (7.2 MeV/nucleon, 50 particle-nA). The target-like fragments were thermalized and neutralized in a gas cell filled with purified Ar gas of $\sim$1 atm[2] and re-ionized element-selectively by using a laser resonance ionization technique[5] at the exit of the gas cell. Subsequently, the mass number was chosen by using a dipole magnet with a mass resolving power of $A/\Delta A \sim 900$. The mass-analyzed ions were transported to the decay station, which consists of a tape transport device, a multi-segmented proportional gas counter,[6] and four clover-type germanium detectors.

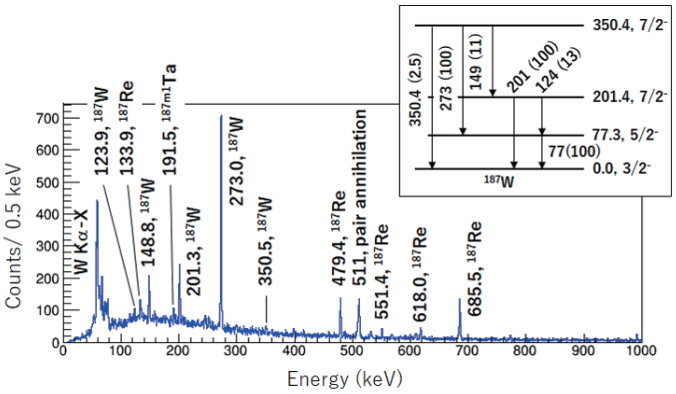

Fig. 1. Energy spectrum of γ-rays associated with the β-decay of ^{187}Ta and ^{187}W, as well as some of the internal transitions of ^{187m1}Ta. The labels indicate the energy (keV) and possible origin of the observed γ-rays. The inset shows a part of the low-energy level scheme in ^{187}W. The values in parentheses are the relative intensities of transitions.[7]

Figure 1 shows the γ-ray energy spectrum in coincidence with events of the gas counter telescope, which are sensitive to electron energies of >100 keV.[6] The measurement was performed with the time sequence of beam-on/off = 1800/1800 sec. We observed γ-rays originating from β-decays of ^{187}Ta as well as ^{187}W ($T_{1/2}$ = 24.0 h), which is the daughter nucleus of ^{187}Ta, and from the internal decay of ^{187m1}Ta ($T_{1/2} = 7.3(9)$ sec)[4] emitting high-energy (>100 keV) conversion electrons. The γ-ray transitions were assigned not only through comparison with previously reported transition energies,[7] but also by checking the half-lives from the energy-gated time spectra for each gamma peak. Consequently, all of the observed γ-rays emitted from ^{187}W were identified (upper right scheme in Fig. 1). The observed γ-rays emitted from ^{187}Re agree with those measured in previous decay studies.

Further analysis to determine the decay branch from the three states of ^{187}Ta is ongoing.

*1 RIKEN Nishina Center
*2 Wako Nuclear Science Center (WNSC), Institute of Particle and Nuclear Studies (IPNS), High Energy Accelerator Research Organization (KEK)
*3 Graduate School of Science and Engineering, Yamagata University
*4 Department of Physics, Kyushu University
*5 International Research Center for Nuclei and Particles in the Cosmos, Beihang University
*6 Department of Physics, University of Surrey
*7 Physics Division, Argonne National Laboratory
*8 Department of Nuclear Physics, Australian National University
*9 GSI Helmholtzzentrum für Schwerionenforschung GmbH

References

1) Y. Hirayama *et al.*, Nucl. Instrum. Methods Phys. Res. B **353**, 4 (2015).
2) Y. Hirayama *et al.*, Nucl. Instrum. Methods Phys. Res. B **412**, 11 (2017).
3) M. W. Reed *et al.*, Phys. Rev. C **86**, 054321 (2012).
4) P. M. Walker *et al.*, Phys. Rev. Lett. **125**, 192505 (2020).
5) Y. Hirayama *et al.*, Rev. Sci. Instrum. **90**, 115104 (2019).
6) M. Mukai *et al.*, Nucl. Instrum. Methods Phys. Res. A **884**, 1 (2018).
7) V. Bondarenko *et al.*, Nucl. Phys. A **811**, 28 (2008).

β-γ Spectroscopy of ^{192}Re

H. Watanabe,[*1,*2,*3] Y. X. Watanabe,[*3] Y. Hirayama,[*3] A. N. Andreyev,[*4,*5] T. Hashimoto,[*6] F. G. Kondev,[*7] G. J. Lane,[*8] Yu. A. Litvinov,[*9] J. J. Liu,[*10] H. Miyatake,[*3] J. Y. Moon,[*6] A. I. Morales,[*11] M. Mukai,[*2,*3,*12] S. Nishimura,[*2] T. Niwase,[*2,*13] M. Rosenbusch,[*3] P. Schury,[*3] M. Wada,[*3] and P. M. Walker[*14]

Decay spectroscopy of ^{192}Re has been carried out using the KEK Isotope Separation System (KISS).[1–3] A RI beam of ^{192}Re was produced via multi-nucleon transfer between a 50-particle-nA projectile of ^{136}Xe and a natural Pt target with a thickness of 10.7 mg/cm^2. The 10.75-MeV/nucleon primary beam from the RIKEN Ring Cyclotron was decelerated to 8.8 MeV/nucleon after passing through Ti degraders placed in front of the Pt target. The reaction products were thermalized and neutralized in a doughnut-shaped gas cell filled with 80-kPa gaseous argon, and then transported by a gas flow to the cell outlet, where a two-color, two-step resonant laser ionization technique was applied for an unambiguous selection of a single element. The singly charged ^{192}Re$^+$ ions were extracted through the RF ion guides and reaccelerated at 20 keV, followed by mass separation using the KISS spectrometer.

During 4.2 days of data run, about 1.5×10^5 ^{192}Re nuclides were collected with an average intensity of 0.3 particles/s on a 12-μm-thick aluminized mylar tape at the end of the KISS beamline. The decay measurements were carried out with three different beam-on/off conditions of 90/180, 24/48, and 45/15 s in order to accommodate decays both from the ground state ($T_{1/2}$ = 16(1) s[4]) and from a previously reported long-lived isomer ($T_{1/2} = 61^{+40}_{-20}$ s[5]) in ^{192}Re. The implantation position was surrounded by a multi-segmented proportional gas counter (MSPGC) that covered 80% of the 4π solid angle with two layers of 16 counters.[6] The MSPGC was surrounded by four large-volume Clover-type HPGe detectors in a close geometry, having a γ-ray add-backed full-energy peak efficiency of 7.8% at 1 MeV.

Figure 1 shows an example of the β-delayed γ-ray coincidence spectrum and the decay scheme of ^{192}Re obtained in the present work. More details about the experimental results and physics discussion are described in Ref. 7).

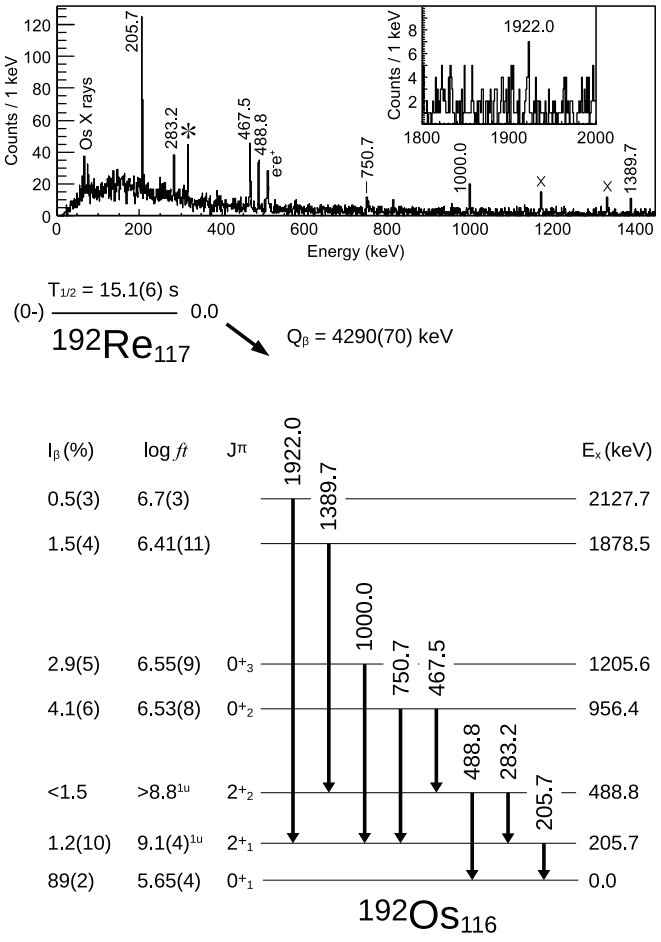

Fig. 1. Top: γ-ray energy spectrum measured in coincidence with MSPGC following implantation of ^{192}Re. Transitions in ^{192}Os are labeled with their energy values, while γ-ray peaks that originate from the room background and beam contaminants are marked with crosses and asterisk, respectively. The inset magnifies a high-energy region. Bottom: Level scheme of ^{192}Os populated in the β decay of ^{192}Re. The observed γ rays are consistent with those reported in Ref. 4). The superscript "1u" indicates first-forbidden unique β decay.

*1 School of Physics, Beihang University
*2 RIKEN Nishina Center
*3 Wako Nuclear Science Center (WNSC), IPNS, KEK
*4 Department of Physics, University of York
*5 Advanced Science Research Center, Japan Atomic Energy Agency (JAEA)
*6 Rare Isotope Science Project, Institute for Basic Science (IBS)
*7 Physics Division, Argonne National Laboratory
*8 Department of Nuclear Physics, Australian National University
*9 GSI Helmholtzzentrum für Schwerionenforschung
*10 Department of Physics, the University of Hong Kong
*11 Instituto de Fisica Corpuscular (CSIC-Universitat de Valencia)
*12 Graduate School of Sciences and Technology, University of Tsukuba
*13 Department of Physics, Kyushu University
*14 Department of Physics, University of Surrey

References

1) Y. Hirayama *et al.*, Nucl. Instrum. Methods Phys. Res. B **353**, 4 (2015).
2) Y. Hirayama *et al.*, Nucl. Instrum. Methods Phys. Res. B **376**, 52 (2016).
3) Y. Hirayama *et al.*, Nucl. Instrum. Methods Phys. Res. B **412**, 11 (2017).
4) C. M. Baglin, Nucl. Data Sheets **113**, 1871 (2012).
5) M. W. Reed *et al.*, Phys. Rev. C **86**, 054321 (2012).
6) M. Mukai *et al.*, Nucl. Instrum. Methods Phys. Res. A **884**, 1 (2018).
7) H. Watanabe *et al.*, Phys. Lett. B **814**, 136088 (2021).

Insight into the reaction dynamics of proton drip-line nuclear system ^{17}F + ^{58}Ni at near-barrier energies†

L. Yang,[*1] C. J. Lin,[*1,*16] H. Yamaguchi,[*2,*3] J. Lei,[*4] P. W. Wen,[*1] M. Mazzocco,[*5,*6] N. R. Ma,[*1] L. J. Sun,[*1] D. X. Wang,[*1] G. X. Zhang,[*7] K. Abe,[*2] S. M. Cha,[*8] K. Y. Chae,[*8] A. Diaz-Torres,[*9] J. L. Ferreira,[*10] S. Hayakawa,[*2] H. M. Jia,[*1] D. Kahl,[*1] A. Kim,[*11] M. S. Kwag,[*8] M. La Commara,[*12] R. Navarro Pérez,[*13] C. Parascandolo,[*14] D. Pierroutsakou,[*14] J. Rangel,[*10] Y. Sakaguchi,[*2] C. Signorini,[*5,*6] E. Strano,[*5,*6] X. X. Xu,[*1] F. Yang,[*1] Y. Y. Yang,[*15] G. L. Zhang,[*7] F. P. Zhong,[*1,*16] and J. Lubian[*10]

In recent times, the availability of high-quality radioactive beams has greatly increased our ability to study the reactions induced by exotic nuclei.[1] In contrast to neutron-halo projectiles, reactions induced by weakly bound proton-rich nuclei, especially those with proton-halo or valence-proton structures, present distinctive properties. Both the core and valence proton have long-range Coulomb interaction with the target; thus, the dynamic Coulomb polarization effect is of particular importance.[2] So far, research on reactions with proton drip-line nuclei is still in its infancy, and the reaction mechanism is not yet clear.

^{17}F can be treated properly with a two-body model as an inert ^{16}O core and a loosely bound proton.[3] In this report, we present the results of complete kinematics measurements to investigate the reaction mechanisms of ^{17}F interacting with ^{58}Ni at energies around the Coulomb barrier. The experiment was performed at the Center for Nuclear Study Radioactive Ion Beam separator (CRIB).[4] The Multi-layer Ionization-chamber Telescope Array (MITA)[5] was used to detect the reaction products over a large range of Z. Angular distributions of elastic scattering, exclusive and inclusive breakup, as well as the total fusion (TF) cross sections were derived simultaneously for the first time.

The excitation functions of the total reaction ($\sigma_{\rm R}$), inclusive ($\sigma_{\rm Inc.^{16}O}$) and exclusive ($\sigma_{\rm Exc.^{16}O}$) ^{16}O, as well as the TF from evaporation protons are shown in Fig. 1. Fusion is dominant in the above-barrier region, and it reduces exponentially as the energy decreases. The $\sigma_{\rm Inc.^{16}O}$ and $\sigma_{\rm Exc.^{16}O}$, however, vary smoothly with the energy, and $\sigma_{\rm Inc.^{16}O}$ becomes the major component in the sub-barrier region. The behavior of the TF cross section can only be reproduced by the continuum-discretized coupled-channels (CDCC) calculation considering the couplings from the continuum states, indicating that the enhancement of TF at the sub-barrier energy is mainly due to the breakup coupling.

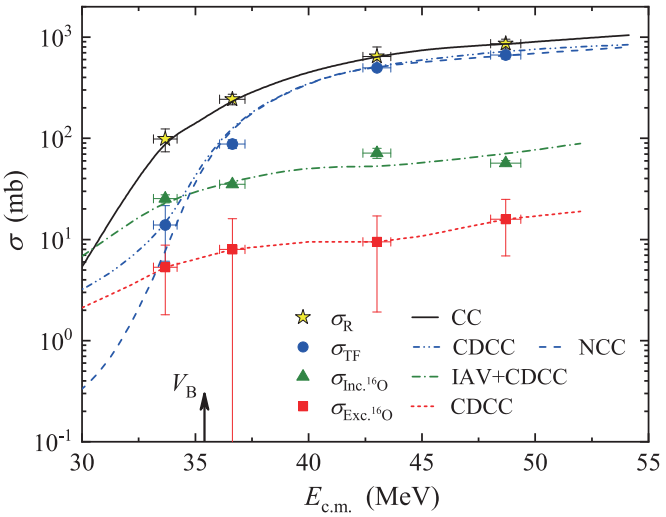

Fig. 1. Excitation functions of the total reaction (stars), exclusive (squares) and inclusive (triangles) breakups, and the TF (circles). The curves denote the corresponding theoretical results: the solid line denotes the coupled channel (CC) result; the dot-dot-dashed and dotted curves are the CDCC results for TF and elastic breakup, respectively; the dashed line shows the CDCC calculations performed by switching off the couplings from the continuum states (NCC); and the dot-dashed line is the result of the three-body model proposed by Ichimura, Austern, and Vincent[6] plus CDCC. The arrow indicates the nominal position of the Coulomb barrier.

† Condensed from the article in Phys. Lett. B **813**, 136045 (2021)

*1 Department of Nuclear Physics, China Institute of Atomic Energy
*2 Center for Nuclear Study, University of Tokyo
*3 National Astronomical Observatory of Japan
*4 Institute of Nuclear and Particle Physics, and Department of Physics and Astronomy, Ohio University
*5 Dipartimento di Fisica, Universita di Padova
*6 Istituto Nazionale di Fisica Nucleare-Sezione di Padova
*7 School of Physics, Beihang University
*8 Department of Physics, Sungkyunkwan University
*9 Department of Physics, University of Surrey
*10 Instituto de Física, Universidade Federal Fluminense
*11 Department of Science Education, Ewha Womans University
*12 Department of Pharmacy, University Federico II
*13 Department of Physics, San Diego State University
*14 Istituto Nazionale di Fisica Nucleare-Sezione di Napoli
*15 Institute of Modern Physics, Chinese Academy of Sciences
*16 Department of Physics, Guangxi Normal University

References

1) L. F. Canto *et al.*, Phys. Rep. **596**, 1 (2015).
2) M. Ito, K. Yabana, T. Nakatsukasa, M. Ueda, Nucl. Phys. A **787**, 267c (2007).
3) C. A. Bertulani, P. Danielewicz, Nucl. Phys. A **717**, 199 (2003).
4) Y. Yanagisawa *et al.*, Nucl. Instrum. Methods Phys. Res. A **539**, 74 (2005).
5) N. R. Ma *et al.*, Eur. Phys. J. A **55**, 87 (2019).
6) M. Ichimura *et al.*, Phys. Rev. C **32**, 431 (1985).

2. Nuclear Physics (Theory)

Dineutron and effective pairing forces in momentum space

M. Yamagami *1

The spatial two-neutron correlation, called dineutron correlation, is one of the unique features around the neutron drip line. The dineutron correlation has been discussed extensively in light-mass nuclei such as ^{11}Li,[1,2] but it is considered to be a universal phenomenon over all mass-number regions.[3]

We propose a new effective pairing force by focusing on the spatial structure of a neutron pair. First, we discuss the necessity by performing a three-body model calculation with the density-dependent zero-range force (DD $\delta(\boldsymbol{r})$-force),[1,2] $V_\delta(\boldsymbol{r}_1,\boldsymbol{r}_2) = V^{(0)}\{1-\eta[\rho(\boldsymbol{r}_1)/\rho_0]\}\,\delta(\boldsymbol{r}_1-\boldsymbol{r}_2)$. The DD $\delta(\boldsymbol{r})$-force is widely used in nuclear structure calculations.[1–3] It must be supplemented with a cutoff in the two-particle spectrum, $\varepsilon_1+\varepsilon_2 \le E_{\rm cut}$. The parameters $V^{(0)}$ and η are adjusted for each $E_{\rm cut}$ so as to reproduce the properties of low-energy neutron-neutron (nn) scattering and the two-neutron energy E_{2n} of finite nuclei. The parameter $\rho_0 = 0.16$ fm^{-3} is the saturation density.

In Fig. 1, the root-mean-square (rms) values $k_{\rm rel}$ and $q_{\rm cm}$ of the relative and center of mass (cm) momenta of paired neutrons in ^{11}Li and ^{12}Be are shown. $k_{\rm rel}$ converges, while $q_{\rm cm}$ diverges as a function of $E_{\rm cut}$ owing to undesirable coupling to high-momentum components of single-particle states in the continuum.

In order to overcome the difficulties, we consider a new effective pairing force in momentum space (k space) that has a non-local separable form (k-SEP force), $V_{\rm SEP} = -\frac{1}{2\pi^2}V_k^{(0)}g(\boldsymbol{k})g(\boldsymbol{k}')h(\boldsymbol{q})h(\boldsymbol{q}')$. Here, the Yamaguchi-type form factor $g(\boldsymbol{k}) = 1/(\boldsymbol{k}^2+\Lambda^2)$ and the Gaussian distribution $h(\boldsymbol{q}) = (\sqrt{\pi}q_0)^{-3}e^{-\boldsymbol{q}^2/q_0^2}$ for the relative momentum $\boldsymbol{k}$ and the cm momentum $\boldsymbol{q}$ of paired neutrons are adopted. The parameters $V_k^{(0)}$ and

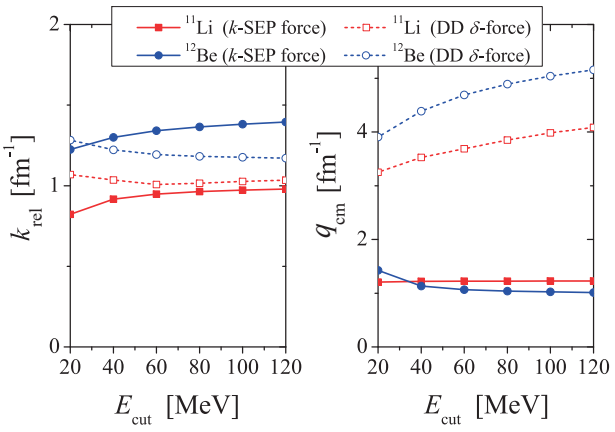

Fig. 1. Relative momentum $k_{\rm rel}$ and cm momentum $q_{\rm cm}$ of the neutron pair in ^{11}Li and ^{12}Be. The results using the k-SEP force and the DD $\delta(\boldsymbol{r})$-force are shown.

*1 Department of Computer Science and Engineering, University of Aizu

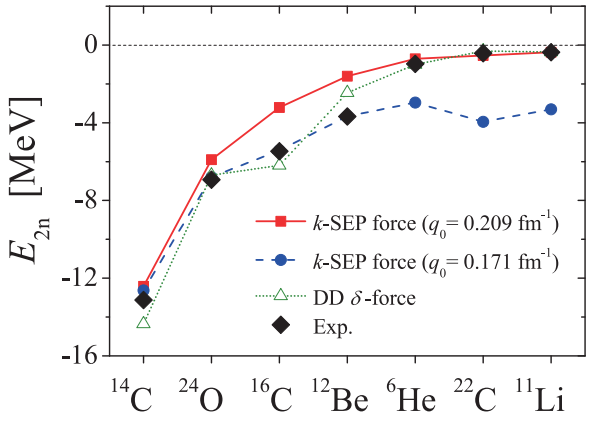

Fig. 2. Two-neutron energies E_{2n} obtained with the k-SEP force ($q_0 = 0.209$ and 0.171fm^{-1}) and the DD $\delta(\boldsymbol{r})$-force with fixed $E_{cut} = 40$ MeV and $\eta = 0.849$, in comparison with the experimental data.

Λ are fixed so as to reproduce the properties of low-energy nn scattering.[4] The parameter q_0 is fixed by the two-neutron energy E_{2n} of finite nuclei.

The $k_{\rm rel}$ and $q_{\rm cm}$ obtained with the k-SEP force are shown in Fig. 1. They converge well above $E_{\rm cut} = 100$ MeV. Here, the parameter $q_0 = 0.209$ fm^{-1} (0.171 fm^{-1}) is used for ^{11}Li (^{12}Be). The small cm momentum $q_{\rm cm}$ indicates that the pairing correlation occurs only around the nuclear surface region in real space. The relative momentum $k_{\rm rel}$ in ^{12}Be becomes larger than that in Borromean ^{11}Li owing to the high-momentum component in the bound $1p_{1/2}$ state.

The two-neutron energies E_{2n} of three-body systems can be classified into two categories as shown in Fig. 2. The Borromean nuclei (^{6}He, ^{22}C, ^{11}Li) are well described with $q_0 = 0.209$ fm^{-1}, while $q_0 = 0.171$ fm^{-1} for non Borromean nuclei. Because the parameter q_0 introduces a cutoff for correlations in the opening angle θ_k between $\boldsymbol{k}_1$ and $\boldsymbol{k}_2$ as $\cos\theta_k \lesssim q_0^2/(2k_1k_2)$ in $h(\boldsymbol{q})$, the pairing correlations have a more collective nature in calculation with a larger q_0.

In conclusion, we proposed a new effective pairing force that describes well the structure of the neutron pair. It is also easily utilizable in various frameworks such as the density functional theory in k space.[5]

References

1) G. F. Bertsch, H. Esbensen, Ann. Phys. (NY) **209**, 327 (1991).
2) H. Esbensen, G. F. Bertsch, K. Hencken, Phys. Rev. C **56**, 3054 (1997).
3) M. Matsuo, K. Mizuyama, Y. Serizawa, Phys. Rev. C **71**, 064326 (2005).
4) H. Tajima, T. Hatsuda, P. van Wyk, Y. Ohashi, Sci. Rep. **9**, 18477 (2019).
5) M. Yamagami, Phys. Rev. C **100**, 054302 (2019).

Structure of ^{12}C studied by the no-core Monte-Carlo shell model

T. Abe,[*1] P. Maris,[*2] T. Otsuka,[*1,*3] N. Shimizu,[*4] Y. Utsuno,[*5,*4] and J. P. Vary[*2]

Carbon-12 is of particular importance in our life. This nucleus is produced by the triple-α reactions through the second 0^+ state known as the Hoyle state. The properties of this state are still being investigated actively both in the experimental and theoretical ways. On the theoretical side, *ab initio* approaches for low-energy nuclear structure calculations have been developed rapidly in recent years, owing to recent computational and methodological developments. Here, we report the low-lying states of ^{12}C examined by the *ab initio* calculations in the no-core Monte Carlo shell model (MCSM).[1)]

We have performed the large-scale calculations in the no-core shell-model (NCSM) method,[2)] applying the MCSM technique for conventional shell-model calculations.[3–5)] The no-core MCSM calculations have been done with 100 basis states in the basis space of $N_{\rm shell} = 7$ with the harmonic-oscillator energy of $\hbar\omega = 20$ MeV. We have adopted the Daejeon16 NN interaction,[6)] which is based on an NN interaction from chiral effective field theory (χEFT).

Figure 1 shows preliminary results of the no-core MCSM calculations in comparison with the experimental data.[7)] In Fig. 1, the absolute energies and transition strengths for three low-lying states are shown. The no-core MCSM results with the Daejeon16 interaction provide a reasonable agreement with the experimental data for the ground 0^+ and the first-excited 2^+ states. The experimental ground-state energy is -92.16 MeV, while our result is -91.9 MeV and well reproduces the no-core full-configuration (NCFC, one of the other NCSM approaches) result with the same interaction of $-92.9(1)$ MeV.[6)] The point-proton radius for the ground state is $\sim$2.29 fm both in the no-core MCSM and the NCFC methods, corresponding to the experimental value of 2.33 fm. The excitation energy of the first-excited 2^+ state is 5.01 MeV in the no-core MCSM and 4.57(15) MeV in the NCFC. These energies are also comparable with the experimental value of 4.44 MeV. The electric quadrupole and monopole transition strengths are also in reasonable agreement with the experimental values.

The excitation energy of the second 0^+ state, however, is higher than the experimental value by $\sim$3 MeV and the point-proton radius is 2.60 fm, which is smaller than the values by the phenomenological calculations, typically larger than 3 fm (see, for example, Ref. 8) and references therein). It is because the Hoyle state is believed to have the loosely-bound three-α-cluster structure and is challenging to be described in the harmonic-oscillator basis at least with the basis space employed here. It is awaited to extrapolate our results obtained in the finite basis-space size into the infinite basis-space-size limit so as to compare with the experimental values and also the other theoretical calculations in more detail. Based on our preliminary calculations, the investigation of the intrinsic structure of ^{12}C is currently underway, aiming to elucidate the α-cluster structure in light-mass nuclear systems from first principles.

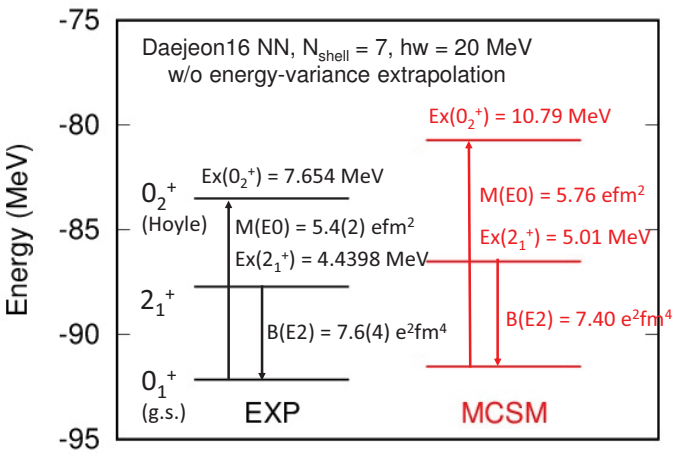

Fig. 1. Excitation spectra of ^{12}C. The right (left) side in the figure shows no-core MCSM results (experimental data) with the red (black) color. The energy levels of three low-lying states are shown by horizontal bars. The electric quadrupole and monopole transition strengths are denoted by arrows. The experimental data are taken from Ref. 7).

*1 RIKEN Nishina Center
*2 Department of Physics and Astronomy, Iowa State University
*3 Department of Physics, the University of Tokyo
*4 Center for Nuclear Study, the University of Tokyo
*5 Advanced Science Research Center, Japan Atomic Energy Agency

References
1) T. Abe, P. Maris, T. Otsuka, N. Shimizu, Y. Utsuno, J. P. Vary, Phys. Rev. C **86**, 054301 (2012).
2) B. R. Barrett, P. Navrátil, J. P. Vary, Prog. Part. Nucl. Phys. **69**, 131 (2013).
3) T. Otsuka, M. Honma, T. Mizusaki, N. Shimizu, Y. Utsuno, Prog. Part. Nucl. Phys. **47**, 319 (2001).
4) N. Shimizu, T. Abe, Y. Tsunoda, Y. Utsuno, T. Yoshida, T. Mizusaki, M. Honma, T. Otsuka, Prog. Theor. Exp. Phys. **2012**, 01A205 (2012).
5) N. Shimizu, T. Abe, M. Honma, T. Otsuka, T. Togashi, Y. Tsunoda, Y. Utsuno, T. Yoshida, Phys. Scr. **92**, 063001 (2017).
6) A. M. Shirokov, I. J. Shin, Y. Kim, M. Sosonkina, P. Maris, J. P. Vary, Phys. Lett. B**761**, 87 (2016).
7) F. Ajzenberg-Selove, Nucl. Phys. A **506**, 1 (1990).
8) M. Chernykh, H. Feldmeier, T. Neff, P. von Neumann-Cosel, A. Richter, Phys. Rev. Lett. **98**, 032501 (2007).

Double charge-exchange phonon states†

X. Roca-Maza,[*1,*2] H. Sagawa,[*3,*4] and G. Colò[*1,*2]

The possibility of inducing double charge-exchange (DCX) excitations by means of heavy-ion beams at intermediate energies has recently fostered interest in new collective excitations such as double isobaric analog states (DIAS) and double Gamow-Teller giant resonances (DGTR). A research program based on a new reaction, (^{12}C, ^{12}Be(0_2^+)), is planned at the RIKEN RIBF facility with high-intensity heavy-ion beams at the optimal energy of E_{lab} = 250 MeV/nucleon to excite the spin-isospin response.[1] A big advantage of this reaction is based on the fact that it is a $(2p, 2n)$-type DCX reaction, and one can use a neutron-rich target to excite DGTR strength. In this report, we present some formulas to evaluate different combinations of the average excitation energies of DIAS and DGTR by using commutator relations for the double isospin $\sum_{i,j=1}^{A} t_-(i)t_-(j)$ and spin-isospin operator $\sum_{i,j=1}^{A} \boldsymbol{\sigma}(i)t_-(i)\boldsymbol{\sigma}(j)t_-(j)$. Here, $\boldsymbol{t} = \boldsymbol{\tau}/2$, and $\boldsymbol{\sigma}$ and $\boldsymbol{\tau}$ denote the Pauli matrices in spin and isospin space, respectively. Specifically, we present formulas to estimate $E_{\rm DIAS} - 2E_{\rm IAS}$ from the most relevant isospin symmetry breaking (ISB) terms in the nuclear Hamiltonian and $E_{\rm DGTR} - E_{\rm DIAS} - 2(E_{\rm GTR} - E_{\rm IAS})$ from a simple albeit realistic Hamiltonian including separable residual interactions.

The expectation value for the energy of the DIAS is defined as

$$E_{\rm DIAS} \equiv \langle {\rm DIAS}|\mathcal{H}|{\rm DIAS}\rangle - \langle 0|\mathcal{H}|0\rangle \ , \qquad (1)$$

where $|0\rangle$ represents the ground state, and

$$|{\rm DIAS}\rangle \equiv \frac{T_-|{\rm IAS}\rangle}{\langle {\rm IAS}|T_+T_-|{\rm IAS}\rangle^{1/2}} \qquad (2)$$

is the definition of the DIAS state in terms of the IAS that, in turn, can be written as $|{\rm IAS}\rangle \equiv T_-|0\rangle/\langle 0|T_+T_-|0\rangle^{1/2}$, where $T_+ = \sum_i^A t_+(i)$ and $T_- = \sum_i^A t_-(i)$ are the isospin raising and lowering operators, respectively.

Starting from Eq. (1) and the definitions of DIAS and IAS previously given, one may write the excitation energy of DIAS as

$$E_{\rm DIAS} = \frac{\langle 0|[T_+^2,[\mathcal{H},T_-^2]]|0\rangle}{\langle 0|T_+^2T_-^2|0\rangle} \ , \qquad (3)$$

assuming that the ground state has good isospin; in other words, there is no isospin mixing, and $T_+|0\rangle = 0$. Remembering that the $E_{\rm IAS}$ is written as, within the same approximation (*i.e.*, no isospin mixing in the ground state), $E_{\rm IAS} = \langle {\rm IAS}|\mathcal{H}|{\rm IAS}\rangle - \langle 0|\mathcal{H}|0\rangle = \langle 0|[T_+,[\mathcal{H},T_-]]|0\rangle/\langle 0|T_+T_-|0\rangle$, one can eventually write

$$E_{\rm DIAS} = 2E_{\rm IAS} + \frac{\langle 0|[T_+,[T_+,[[\mathcal{H},T_-],T_-]]]|0\rangle}{2(N-Z)(N-Z-1)}. \qquad (4)$$

The energy of the double GT state can be defined in an analogous way to Eq. (3) as

$$E_{\rm DGTR} = \frac{\langle 0|[O_+^2,[\mathcal{H},O_-^2]]|0\rangle}{\langle 0|O_+^2O_-^2|0\rangle}, \qquad (5)$$

where the GT transition operators are $O_\pm = \sum_i^A \sigma_z(i)t_\pm(i)$. After some algebraic manpulations, we can rewrite the energy of DGTR (5) as

$$E_{\rm DGTR} = 2E_{\rm GT} + \frac{\langle 0|[O_+,[O_+,[[H,O_-],O_-]]]|0\rangle}{2(N-Z)(N-Z-1)} \ . \qquad (6)$$

Double GT and IAS average excitation energies have been determined for the first time using double and quartic commutator relations. In order to provide semi-quantitative theoretical estimates, we have adopted two approximations. First, an independent particle picture has been assumed. We have also provided expressions in which, by simplifying further, the neutron and proton distributions have been taken as hard spheres. This simplification has turned out to be very useful to capture the main terms dominating the calculated quantities.

In conclusion, within our approach, double IAS and GT resonance energies in neutron-rich nuclei are dominated by the same physics as their single counterparts because the main contribution is from $2E_{\rm IAS}$ and $2E_{\rm GTR}$, respectively. Hence, the effect of two-body Coulomb interaction has a decisive effect on the average energy $E_{\rm DIAS}$, while the spin-orbit and residual isospin and spin-isospin interactions play a substantial role in the average energy $E_{\rm DGTR} - E_{\rm DIAS}$. More specifically, we have found that the corrections due to quartic commutators follow the approximate laws $E_{\rm DIAS} - 2E_{\rm IAS} \approx \frac{3}{2}A^{-1/3}$ MeV (even the isospin mixing effects are accounted in $E_{\rm IAS}$) and $E_{\rm DGTR} - E_{\rm DIAS} - 2(E_{\rm GTR} - E_{\rm IAS}) \approx 16A^{-1}$ MeV.

† Condensed from the article in Phys. Rev. C. **101**, 014320 (2020)

*1 Dipartimento di Fisica, Università degli Studi di Milano
*2 INFN, Sezione di Milano
*3 RIKEN Nishina Center
*4 Center for Mathematics and Physics, the University of Aizu

Reference

1) M. Takaki *et al.*, Proposal for Nuclear Physics Experiment at RI Beam Factory, "Search for double Gamow-Teller giant resonances in $\beta\beta$-decay nuclei via the heavy-ion double charge exchange ^{48}Ca(^{12}C, ^{12}Be(0_2^+)) reaction."

Exotic nuclear shape due to cluster formation at high angular momentum†

Balaram Dey,[*1] Shan-Shan Wang,[*2] Deepak Pandit,[*3] Srijit Bhattacharya,[*4] Xi-Guang Cao,[*5] Wan-Bing He,[*6] Yu-Gang Ma,[*7] N. Quang Hung,[*8] and N. Dinh Dang,[*9]

It is now well established that clustering plays a very important role in self-conjugate light nuclei and is also associated with strongly deformed shapes of nuclei.[1,2] One of the probes to study this deformation experimentally at high temperature (T) and angular momentum (J) is the γ-decay from the giant dipole resonance (GDR) built on excited states.[1,2] The GDR lineshape gets fragmented in deformed nucleus providing crucial information about the nuclear deformation. As a matter of fact, it has been successfully employed experimentally to study the Jacobi shape transition, an abrupt change of shape from non-collective oblate to collective triaxial or prolate shape above a critical spin, in several light nuclei such as ^{31}P, ^{45}Sc, ^{46}Ti and ^{47}V.[1,2] However, when this shape transition is examined in self-conjugate nuclei ^{32}S[1] and ^{28}Si[2] through the reactions ^{20}Ne + ^{12}C and ^{16}O + ^{12}C, respectively, the GDR lineshape fragments into two prominent peaks at high $J(\sim 20\hbar)$ providing a direct evidence of the large deformation but, intriguingly, the shapes found are completely different from those seen from Jacobi shape transition (signature of which is a sharp peak at 10 MeV arises due to the Coriolis splitting of the GDR frequencies). Therefore, these observations clearly highlight that the clustering is not only important in mass $A < 20$ region but could also play major role in $A \sim 30$, which has not been studied enough.

Microscopic effects such as shell structure, pairing and isospin effects play important role in deciding the nuclear structures at low excitation energy. However, even after incorporating these effects, the experimental GDR lineshapes ($T \sim 2.0$ MeV and $J \sim 20\hbar$) could not be explained for ^{28}Si and ^{32}S nuclei.[3] In the present work, an extended quantum molecular dynamics (EQMD) model[4] has been carried out to understand the GDR lineshapes of ^{28}Si and ^{32}S nuclei, and to investigate how the exotic shapes due to cluster formation at high T and J are manifested through GDR strength function.

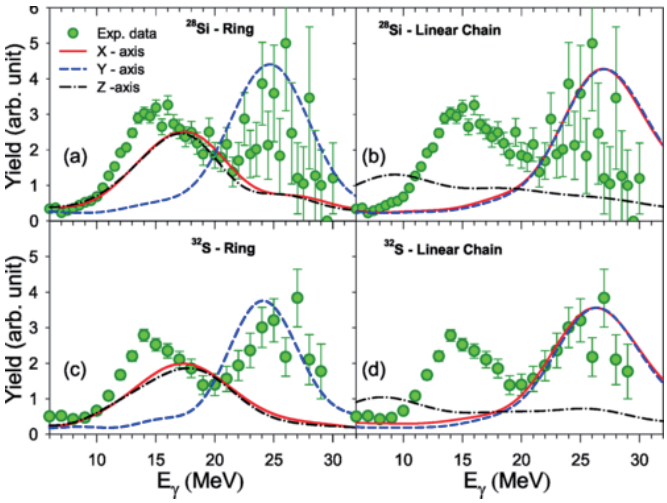

Fig. 1. EQMD calculations for both ^{32}S and ^{28}Si nuclei.

The results of EQMD calculation have been compared with the existing experimental data of ^{32}S and ^{28}Si as shown in Fig. 1. It should be mentioned that the alpha correlation is included in the EQMD model based on the fact that the many body nucleon-nucleon correlation is intrinsically embedded in all microscpic QMD type model and the details of EQMD results are discussed in Refs. 3, 4). It is found that the EQMD predicts the general trend of the experimental GDR strength functions for ^{32}S and ^{28}Si by considering the ring or toroidal configuration. Nevertheless, the peak around 25 MeV can only arrive due to cluster formation highlighting the existence of the α-clustering structure at such high T and J since this peak could not be predicted within the mean-field calculations. Interestingly, the rotation of these exotic shapes will not lead to the Coriolis splitting of the GDR strength function (due to larger moment of inertia leading to smaller angular frequency), which could be the reason for the absence of the Jacobi shape transition in ^{32}S and ^{28}Si. The present result highlights the role of α cluster states above the decay threshold, which is still an open field of investigation.

† Condensed from the article in Phys. Rev. C **102**, 031301(R) (2020)

*1 Bankura University
*2 Shanghai Institute of Applied Physics, Chinese Academy of Sciences
*3 Variable Energy Cyclotron Centre
*4 Dept. of Phys., Barasat Govt. College
*5 Shanghai Advanced Research Institute and Zhangjiang Laboratory
*6 Key Laboratory of Modern Physics and Ion-Beam application (MOE), Institute of Modern Physics, Fudan University
*7 Shanghai Institute of Applied Physics, Chinese Academy of Sciences, and Key Laboratory of Modern Physics and Ion-Beam application (MOE), Institute of Modern Physics, Fudan University
*8 Institute of Fundamental and Applied Sciences, Duy Tan University
*9 RIKEN Nishina Center

References

1) D. Pandit *et al.*, Phys. Rev. C **95**, 034301 (2017).
2) B. Dey *et al.*, Phys. Rev. C **97**, 014317 (2018).
3) B. Dey *et al.*, Phys. Rev. C **102**, 031301R (2020).
4) W. B. He *et al.*, Phys. Rev. Lett. **113**, 032506 (2014).

Probing dilute nuclear density by antiproton-nucleus scattering†

K. Makiguchi,*1 W. Horiuchi,*1 and A. Kohama*2

Nuclear density distributions are the basic properties of atomic nuclei. Traditionally, the charge density distributions have been measured using electron-nucleus scattering. Hadronic probes have been used to study matter density distributions, especially via proton-nucleus scattering. Recently, we proposed a practical approach to extract the nuclear surface diffuseness of unstable nuclei using proton-nucleus elastic scattering differential cross sections.[1,2] As a natural extension of the previous study, we investigated antiproton-nucleus scattering because it could provide a different sensitivity to the nuclear structure than the proton probe because the antiproton-nucleon ($\bar{p}N$) total cross sections are typically 3–4 times larger than those of NN at incident energies varying from a few hundreds to thousands MeV.

High-energy antiproton-nucleus reactions can be efficiently described by the Glauber model.[3] The total reaction and elastic scattering cross sections can be obtained by evaluating the optical phase-shift function $e^{i\chi(\boldsymbol{b})}$ as a function of the impact parameter vector $\boldsymbol{b}$. In optical limit approximation, we have $i\chi(\boldsymbol{b}) = -\int \rho_N(\boldsymbol{r}) \Gamma_{\bar{N}N}(\boldsymbol{b}-\boldsymbol{s})\, d\boldsymbol{r}$, where $\boldsymbol{r} = (\boldsymbol{s}, z)$ with z denoting the beam direction, nucleon (N) one-body density $\rho_N(\boldsymbol{r})$, and antinucleon-nucleon $\bar{N}N$ profile function $\Gamma_{\bar{N}N}(\boldsymbol{b})$. The parameters of the profile function were determined to reproduce the $\bar{p}N$ and $\bar{p}$-^{12}C cross-section data. The validity of the present model is demonstrated in Fig. 1. The theoretical cross sections were significantly consistent with the experimental data without any adjustable parameter using harmonic-oscillator type density distributions that reproduce the observed charge radii.

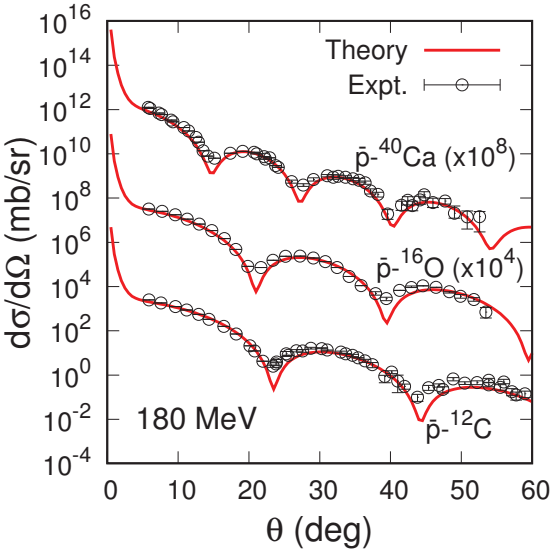

Fig. 1. Elastic scattering differential cross sections for antiproton-nucleus scattering at 180 MeV/nucleon adopted from the original paper.

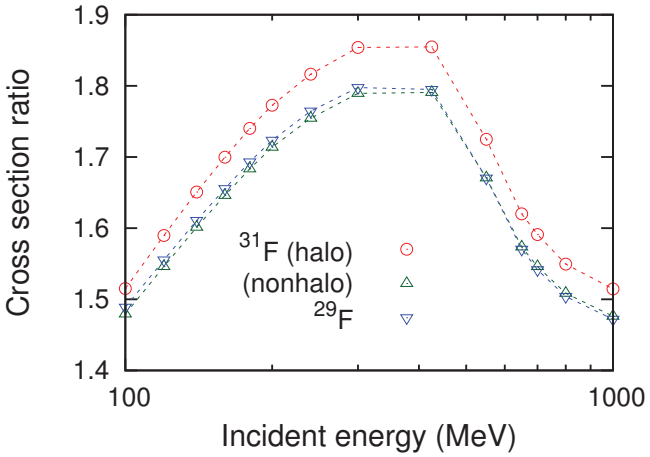

Fig. 2. Ratio of total reaction cross sections of ^{29,31}F for antiproton and proton scattering as a function of the incident energy adopted from the original paper.

We found that strong absorption occurs even beyond the nuclear radius owing to the large $\bar{p}N$ elementary cross sections, resulting in strong sensitivity in the nuclear tail. This sensitivity is quantified by taking an example of a possible halo nucleus ^{31}F, which is located at the fluorine dripline; however, the antiproton scattering on unstable nuclei is still not feasible. According to the investigations in Ref. 4) the shell gap between $0f_{7/2}$ and $1p_{3/2}$ orbits is essential and the dominance of the $(1p_{3/2})^2$ configuration forms the halo structure in ^{31}F. We considered these density distributions of ^{31}F with $(1p_{3/2})^2$ (halo) and $(0f_{7/2})^2$ (nonhalo) dominance from Ref. 4) and calculated the ratio of the total reaction cross sections of antiproton and proton scattering. Figure 2 displays the ratios of ^{31}F as a function of incident energy. The ratios of ^{29}F with harmonic-oscillator type density distributions are also plotted for comparison. ^{31}F with the halo tail yielded the largest ratios, while the non-halo density produced almost the same behavior as ^{29}F, *which demonstrates the advantage of antiproton scattering in the analysis of dilute density distribution.*

References
1) S. Hatakeyama, W. Horiuchi, A. Kohama, Phys. Rev. C **97**, 054607 (2018).
2) S. Hatakeyama, W. Horiuchi, A. Kohama, RIKEN Accel. Prog. Rep. **52**, 7 (2019).
3) R. J. Glauber, in *Lectures in Theoretical Physics*, edited by W. E. Brittin, L. G. Dunham (Interscience, New York, 1959).
4) H. Masui, W. Horiuchi, and M. Kimura, Phys. Rev. C **101**, 041303(R) (2020).

† Condensed from the article in Phys. Rev. C **102**, 034614 (2020)
*1 Department of Physics, Hokkaido University
*2 RIKEN Nishina Center

Nuclear charge radii with a trained feed-forward neural network†

D. Wu,[*1] C. L. Bai,[*1] H. Sagawa,[*2,*3] and H. Q. Zhang[*4]

During the last few decades, theoretical and experimental studies of the isotopic changes of ground- and low-lying states have been performed intensively to elucidate the evolution of the shell structure, shape coexistence phenomena, and shape transitions. In particular, charge radii and electromagnetic moments are very sensitive quantities from which precise information of the nuclear structure can be extracted.

Machine learning (ML) is one of the most popular algorithms for dealing with complex systems owing to its powerful and convenient inference abilities. The neural network, which is an algorithm of machine learning, has been widely used in different fields: artificial intelligence (AI), medical treatment, and physics of complex systems. In this work, we attempt to train a ML model for a description of the nuclear charge radii based directly on some experimental or quasi-experimental data, such as proton and neutron numbers, shell effect, and deformation. We search for any other physical quantities that are correlated to the charge radii.

To this end, we employ a standard fully connected feed-forward neural network (FNN), which can build a complex mapping between the input space and output space through multiple compounding of simple nonlinear functions. The FNN is a multilayer neural network with an input layer, hidden layers, and an output layer. The structure of the neural network is labelled as $[N_1, N_2, \ldots, N_n]$, where N_i denotes neuron numbers of the ith layer and $i = 1$ and n represent the input and output layer, respectively. In this study, we adopt the input layer $N_1 = 3$ and the output layer $N_n = 1$. The model is trained with the input data set of proton number Z, neutron number N, the excitation energy of the first 2^+ state $E_{2_1^+}$, and the symmetry energy. The deformation and shell effects on charge radius are included by the $E_{2_1^+}$ values. We adopt as the data set all the nuclei for which the experimental values of both $E_{2_1^+}$, and charge radii are available. The data set includes 347 nuclei in total. As the data set is not large enough, we must choose a small network structure, which includes 44 neurons and involves 201 parameters.

In the present ML study, all the charge radii of Ca, Sm, and Pb isotopes are included in the testing set to check the prediction power of models. The model reproduces well not only the slope of isotopic dependence, but also the kink of charge radii at the magic numbers $N = 82$ of Sm isotopes and $N = 126$ of Pb isotopes. The obtained charge radii of Ca isotopes with and without symmetry energy input are shown in Fig. 1. Experimental results taken from Refs. 1), 2) show a sharp kink structure at $N = 28$ and a peak between two closed shells at $N = 20$ and 28, followed by a rapid increase after $N = 28$. This figure indicates that the symmetry energy input is critical for the qualitative and quantitative description of the Ca isotopes.

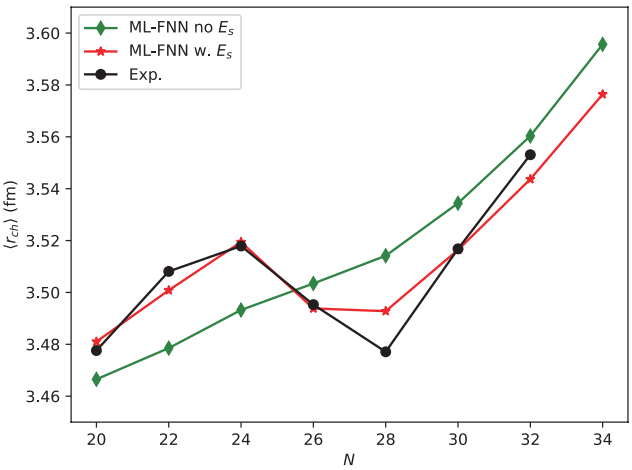

Fig. 1. Charge radii of Ca isotopes calculated by the model trained with and without taking the symmetry energy input into account. The ML results obtained with and without the symmetry energy input are labelled by the red stars and green diamonds, respectively. The experimental data taken from Refs. 1), 2) are labelled by the filled black circles.

We also perform Hartree-Fock-Bogolyubov (HFB) calculations for the radii of Ca isotopes. The HFB calculations show a clear correlation between the symmetry energy and charge radii in Ca isotopes as far as the absolute magnitude is concerned. Whereas the ML shows that the symmetry energy input has a remarkable effect on the precise descriptions of charge radii of Ca isotopes including the kink structure, the HFB calculation shows that the symmetry energy changes the absolute magnitude of charge radii, but the kink structure at $N = 28$ is not well reproduced. The physical implication of the present successful ML study remains an open question and needs to be studied in the future.

† Condensed from the article in Phys. Rev. C. **102**, 054323 (2020)

*1 College of Physics, Sichuan University
*2 RIKEN Nishina Center
*3 Center for Mathematics and Physics, University of Aizu
*4 China Institute of Atomic Energy

References

1) R. F. Garcia Ruiz *et al.*, Nat. Phys. **12**, 594 (2016).
2) I. Angeli, K. P. Marinova, At. Data Nucl. Data Tables **99**, 69 (2013).

Effects of finite nucleon size, vacuum polarization, and electromagnetic spin-orbit interaction on nuclear binding energies and radii in spherical nuclei†

T. Naito,[*1,*2] X. Roca-Maza,[*3,*4] G. Colò,[*3,*4] and H. Z. Liang[*1,*2]

In the density functional theory (DFT) for nuclear physics, the ground-state energy is usually given by $E_{\rm gs} = T_0 + E_{\rm nucl}\left[\rho_p, \rho_n\right] + E_{\rm Cd}\left[\rho_{\rm ch}\right] + E_{\rm Cx}\left[\rho_{\rm ch}\right]$, where T_0 is the Kohn-Sham kinetic energy and $E_{\rm nucl}$, $E_{\rm Cd}$, and $E_{\rm Cx}$ are the energy density functionals (EDFs) of the nuclear, Coulomb direct, and Coulomb exchange parts, respectively. Here, ρ_p and ρ_n are the ground-state density distributions of protons and neutrons, respectively, and $\rho_{\rm ch}$ is the charge density distribution.

The Coulomb EDF $E_{\rm C} = E_{\rm Cd} + E_{\rm Cx}$ is, in principle, written in terms of the charge density $\rho_{\rm ch}$ [1] because the Coulomb interaction involves the charge itself, instead of the point protons. Nevertheless, the protons and neutrons are assumed to be point particles, *i.e.*, $\rho_{\rm ch} \equiv \rho_p$, in most self-consistent nuclear DFT calculations. In this paper, the finite-size effects of nucleons are implemented to the self-consistent steps of the Skyrme Hartree-Fock calculation, where only the electric form factors of nucleons are considered. The Coulomb direct term $E_{\rm Cd}$ holds the conventional form, while the modified Perdew-Burke-Ernzerhof GGA Coulomb exchange functional [2,3] is used instead of the exact Fock term.

The charge density distribution $\rho_{\rm ch}$ is written in terms of ρ_p, ρ_n, and the electric form factors of protons and neutrons, $\tilde{G}_{{\rm E}p}$ and $\tilde{G}_{{\rm E}n}$, as $\tilde{\rho}_{\rm ch}\left(q\right) = \tilde{G}_{{\rm E}p}\left(q^2\right)\,\tilde{\rho}_p\left(q\right) + \tilde{G}_{{\rm E}n}\left(q^2\right)\,\tilde{\rho}_n\left(q\right)$, where the quantities with the tilde denote those in the momentum space. Once the finite-size effects are considered, *i.e.*, $\rho_{\rm ch} \not\equiv \rho_p$, the chain rule of the functional derivative should be applied to derive the effective potential of the nucleon τ, $V_{{\rm eff}\tau}\left(\boldsymbol{r}\right) = \frac{\delta E[\rho_p,\rho_n]}{\delta\rho_\tau(\boldsymbol{r})}$. Finally, the Coulomb potential for nucleons with the finite-size effects reads $V_{{\rm C}\tau}\left(r\right) = \left\{\mathcal{V}_{\rm C}\left[\rho_{\rm ch}\right] * G_{{\rm E}\tau}\right\}\left(r\right)$, where $\mathcal{V}_{\rm C}\left[\rho_{\rm ch}\right]$ is the conventional form of the Coulomb potential and $*$ denotes the convolution. The Coulomb potential for the neutrons does not vanish within the self-consistent finite-size effects, because $G_{{\rm E}n} \not\equiv 0$.

Other possible electromagnetic (EM) contributions, *i.e.*, the vacuum polarization and EM spin-orbit interaction, are also considered. We used effective one-body potential of the vacuum polarization for a charged particle under the Coulomb potential caused by $\rho_{\rm ch}$, known as the Uehling potential.[4] The EM spin-orbit interaction, which originates from the interaction between the nucleon spin and $V_{{\rm C}\tau}$, is also considered by using the first-order perturbation theory.

The isospin-symmetry breaking (ISB) terms of the nuclear force are also implemented to compare the contributions of the EM interaction with those of the ISB terms of nuclear force. The SAMi functional[5] is used for the nuclear EDF for most calculations, and the SAMi-ISB functional[6] is used instead when the ISB originating from $E_{\rm nucl}$ is considered explicitly.

The proton finite-size effect makes the nuclei more bound; for example, the nucleon finite-size effect decreases the binding energy by 8.2 MeV in ^{208}Pb. In contrast, the neutron finite-size effect makes the nuclei less bound, and its contribution is almost one order of magnitude smaller than the proton contribution, for example, by 1.2 MeV in ^{208}Pb, which is non-negligible in heavy nuclei. The contribution of the vacuum polarization to the total energy is also non-negligible, and it makes the nuclei less bound, for example, by 3.7 MeV in ^{208}Pb. The contribution of the electromagnetic spin-orbit interaction to the total energy is approximately 50 keV. Systematically, the contribution of the ISB terms of the nuclear force to the total energy is comparable to that of the proton finite-size effect in heavy nuclei, while the former is more significant than the latter in light nuclei. The neutron finite-size effect and vacuum polarization are also non-negligible. On the other hand, the contribution of the electromagnetic spin-orbit interaction to the total energy depends on the shell structure.

The mass difference between the mirror nuclei ^{48}Ca and ^{48}Ni was also calculated. All the corrections to the Coulomb functional with the SAMi-ISB functional cooperate to reproduce the mirror-nuclei mass difference within 300 keV accuracy, while the error is 1.5 MeV if the conventional Coulomb functional is used.

† Condensed from the article in Phys. Rev. C **101**, 064311 (2020)

*1 Department of Physics, The University of Tokyo
*2 RIKEN Nishina Center
*3 Dipartimento di Fisica, Università degli Studi di Milano
*4 INFN, Sezione di Milano

References

1) A. Bulgac, V. R. Shaginyan, Nucl. Phys. A **601**, 103 (1996).
2) J. P. Perdew, K. Burke, M. Ernzerhof, Phys. Rev. Lett. **77**, 3865 (1996).
3) T. Naito, X. Roca-Maza, G. Colò, H. Liang, Phys. Rev. C **99**, 024309 (2019).
4) E. A. Uehling, Phys. Rev. **48**, 55 (1935).
5) X. Roca-Maza, G. Colò, H. Sagawa, Phys. Rev. C **86**, 031306 (2012).
6) X. Roca-Maza, G. Colò, H. Sagawa, Phys. Rev. Lett. **120**, 202501 (2018).

Trajectory in 2D plot of IS and IV densities of ^{48}Ca and ^{208}Pb†

S. Yoshida,[*1] H. Sagawa,[*2,*3] J. Zenihiro,[*2,*4] and T. Uesaka[*2]

Recently, the neutron skin thicknesses of doubly closed shell nuclei $^{208}_{82}$Pb$_{126}$ and $^{48}_{20}$Ca$_{28}$ have been investigated intensively. Theoretical studies with modern energy density functionals (EDFs) indicate that the thickness of the neutron skin, $\Delta r_{np} \equiv r_n - r_p$, embodies the stability of pure neutron matter and provides important information on the symmetry energy of neutron matter equation of states (EoS), which is a sum of the well-known EoS of the symmetric nuclear matter and the symmetry energy. The two EoSs govern the formation of not only nuclei but also astrophysical phenomena such as neutron stars and supernova explosions.

In this paper, we propose a model to examine the details of the symmetry energy by using the isoscalar (IS) and isovector (IV) density distributions. The neutron skin is an integrated quantity extracted from neutron and proton density distributions. However, the radial density distributions will provide more information to elucidate quantitatively the EoS of both nuclear matter and neutron matter. To this end, it is essential to study the radial dependence of IS and IV densities, which can be extracted from neutron and proton densities.

The IS and IV densities are defined as $\rho_{\rm IS}(r) = \rho_n(r) + \rho_p(r)$ and $\rho_{\rm IV}(r) = \rho_n(r) - \rho_p(r)$, respectively. Experimental IS and IV densities of ^{48}Ca[1)] are plotted in Fig. 1. The solid black curve sandwiched by the dotted lines is the experimental trajectory of IS versus IV densities at different radii r. The equi-energy contour lines of HF EDF, $\varepsilon(\rho_n, \rho_p) = \varepsilon(\rho_{\rm IS}, \rho_{\rm IV}) =$ constant, are calculated using SAMi-J27 and plotted for the values from 3 MeV at $\rho_{\rm IS} = \rho_{\rm IV} \approx 0$ to -15 or -16 MeV at the saturation density $\rho_{\rm IS} \approx 0.16$ fm^{-3} with an energy step of 1 MeV.

The dashed lines correspond to the constant IV density line $\rho_{\rm IV} = \rho_{\rm IS}(N-Z)/A$ of the asymmetric nuclear matter. The experimental trajectory is above the constant density limit in the surface region. This feature suggests a strong IV pressure to push the IV density towards the surface region rather than the interior of nucleus. The Fermi liquid of a finite nucleus may fill the valley determined by EDF from the bottom at approximately $\rho_{\rm IS} = 0.16$ fm^{-3} to the top of valley at $\rho_{\rm IS} = \rho_{\rm IV} = 0.0$ fm^{-3}. The trajectory plots are started from the right-hand side at $r = 0$ fm and ends at the left corner at $r = 6$ fm. The dots on the solid line indicate different radius points with $r = 0, 1, 2, 3, \ldots$ fm from the right to the left. The positive IV density at $r = 0$ fm reflects a larger neutron density than that of protons at the central region corresponding to $r = 0$ fm. Keeping the $\rho_{\rm IS}$ almost constant, the experimental curve rises to the surface region at $r = 3$ fm, where the dots are separated largely because of a rapid change in the IV density. This can be understood qualitatively from a flat contour map around the IS density $\rho = 0.16$ fm^{-3} so that the IV density can have large freedom within the limit of the equi-energy contour line.

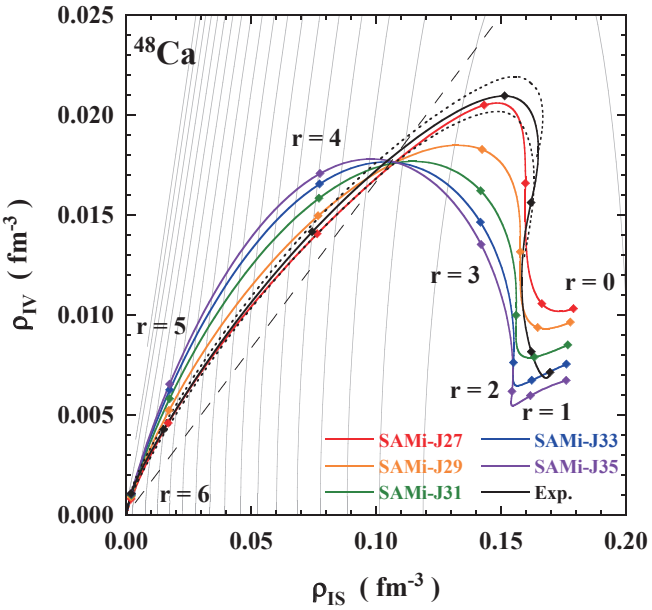

Fig. 1. Trajectories of isoscalar (IS) and isovector (IV) densities of ^{48}Ca. The experimental curve (black solid line) is compared with theoretical ones with Skyrme interactions. The equi-energy contour lines are calculated using the SAMi-J family. The equi-energy contour lines are plotted for SAMi-J27. See the text for details.

We can see a clear J-dependence for the enhancement of IV density at $r = 4$ fm; a larger J value yields a greater neutron density at the surface. Compared with the experimental data, SAMi-J27 shows the best agreement in the entire region of this plot.

In summary, we propose a new 2D plotting method of IS-IV densities to extract not only the empirical symmetry energy coefficients J, L, and $K_{\rm sym}$, but also the asymmetric isospin term K_τ in the nuclear incompressibility. We found strong correlations between the curvature of the 2D density at the density $\rho_{\rm IS} = 0.1$ fm^{-3} and the symmetry energy coefficients J, L, and K_τ. The optimal values are found to be $J = 27.2$ MeV, $L = 31.6$ MeV, $K_{\rm sym} = -154.7$ MeV, and $K_\tau = -300.6$ MeV for the SAMi-J EDF from the IS-IV density plots of ^{48}Ca and ^{208}Pb.

Reference

1) J. Zenihiro *et al.*, arXiv:1810.11796 (2018).

† Condensed from the article in Phys. Rev. C **102**, 064307 (2020)

*1 Science Research Center, Hosei University
*2 RIKEN Nishina Center
*3 Center for Mathematical Sciences, the University of Aizu
*4 Department of Physics, Kyoto University

Energy-weighted sum rule for Gamow-Teller giant resonances in high-spin isomeric states of $N = Z$ nuclei†

M. Sasano,[*1] H. Sagawa,[*1,*2] T. Suzuki,[*3,*4] and M. Honma[*2]

Among collective modes,[1] the Gamow-Teller (GT) giant resonance is an interesting excitation mode. It is a 0 $\hbar\omega$ excitation that is characterized by the quantum-number changes in the orbital angular momentum ($\Delta L = 0$), spin ($\Delta S = 1$), and isospin ($\Delta T = 1$). It is induced by the transition operator $\sigma\tau$.

Recently, an experimental project was proposed to measure the GT transitions from the ^{52}Fe(12^+) high-spin isomeric state provided as an RI beam.[2] Inspired by this, herein, we derived an energy-weighted sum rule (EWSR) to estimate the energies of GT giant resonances in high-spin isomeric (HSI) states in $N = Z$ nuclei and evaluated the spin and isospin residual interactions by comparing the EWSR with the shell model calculations.

The sum rules provide a reliable tool for evaluating the natures of giant resonances. In the calculations of sum rules, the contributions from all the final states are summed up. Therefore, the sum-rule values solely depend on the properties of the initial ground state and the Hamiltonian of the system, but they are not sensitive to the details of the final states. Roughly speaking, the non-energy-weighted sum rule (NEWSR) provides a criterion for the collectivity of the observed resonances, while the EWSR provides a measure of the interaction strength driving the oscillation.

By dividing EWSR with NEWSR, the average energy of the resonance can be derived. We found that, with the simple Bohr-Mottelson Hamiltonian,[3] the average energy relation is written as

$$E_{\mathrm{GT}}^{\nu=-1} - E_{\mathrm{M1}}^{\nu=-1} = 4\frac{\kappa_{\sigma\tau} - \kappa_{\sigma}}{A} \langle i\,|S_0|\,i\rangle\,. \qquad (1)$$

Here, $\kappa_{\sigma\tau}$ and κ_{σ} are the spin-isospin and spin coupling constants used in the hamiltonian. A is the mass number of the nucleus. $\langle i\,|S_0|\,i\rangle$, and $E_{\mathrm{GT}}^{\nu=-1}$ and $E_{\mathrm{M1}}^{\nu=-1}$ correspond to the expectation value of the spin excess along the elongation axis of the nucleus, the average energies of the GT and M1 transitions, respectively.

This relation is analogous to the average energy relation derived in Ref. 4) for $N > Z$ 0^+ nuclei. In the latter case, the left-hand side of the relation is the energy difference between the GT giant resonance and the isobaric analog state. $\langle i\,|S_0|\,i\rangle$ in the right-hand side is replaced with the neutron excess $N - Z$. Thus, instead of $\kappa_{\sigma\tau} - \kappa_{\sigma}$, $\kappa_{\sigma\tau} - \kappa_{\tau}$ appears. The GT energies in high-spin isomers with $N = Z$ have different sensitivies from those in $N > Z$ 0^+ nuclei. This is because these states have different symmetries in the spin and isospin space.

We used the newly derived energy relation to analyze the results of the shell model calculations for the GT transition from ^{52}Fe(12^+) and ^{94}Ag(21^+) $N = Z$ high spin isomers. In the shell-model calculations, the effective interactions, GXPF1J[5] and PIGD5G3[6] were used for Fe and Ag, respectively. From the analysis, $\kappa_{\sigma\tau} - \kappa_{\sigma}$ was derived as 20.4–20.5 MeV. By assuming a $\kappa_{\sigma\tau}$ value of 23 MeV, the strength of the spin residual interaction, κ_{σ} was deduced as 2.5 MeV. Thus, we demonstrated that the GT energies in high spin isomers are useful for evaluating the short-range part of the spin residual interaction, which is important to describe the onset of the pion condensation in nuclear matter.

We thank Haozhao Liang for the valuable discussions. This work was supported in part by JSPS KAKENHI (Grant Numbers JP19K03858 and JP19K03855).

References

1) M. N. Harakeh, A. M. van der Woude, *Giant Resonances*, (Oxford University Press, Oxford, 2001).
2) K. Yako *et al.*, private communications.
3) A. Bohr, B. R. Mottelson, *Nuclear Structure Single-Particle Motion*, Vol.I, (Benjamin, New York 1969).
4) T. Suzuki, Phys. Lett. B **104**, 92–94 (1981); T. Suzuki, Nucl. Phys. A **379**, 110–124 (1982).
5) M. Honma *et al.*, J. Phys. Conf. Series **20**, 002 (2005).
6) M. Honma *et al.*, RIKEN Accel. Prog. Rep. **48**, 77 (2015).

† Condensed from the article in Phys. Rev. C **103**, 014308 (2021)

*1 RIKEN Nishina Center
*2 Center for Mathematics and Physics, University of Aizu
*3 Department of Physics, College of Humanities and Science, Nihon University
*4 National Astronomical Observatory of Japan

A fully microscopic model of total level density in spherical nuclei†

N. Quang Hung,[*1,*2] N. Dinh Dang,[*3] L. Tan Phuc,[*1,*2] N. Ngoc Anh,[*4] T. Dong Xuan,[*1,*2] and T. V. Nhan Hao[5]

The nuclear level density (NLD) is one of important inputs for the calculations of low-energy nuclear reactions and astrophysics. It also contains various information on the internal structure of atomic nuclei such as single-particle levels, pairing correlations, spin distributions, collective (vibrational and/or rotational) excitations, nuclear thermodynamics, *etc.* Although many theoretical studies have been carried out during the last seven decades to find a reliable and fully microscopic model of NLD, there has still been lacking a fully microscopic NLD model. Recently, we have proposed a microscopic NLD model based on the exact pairing plus independent-particle model at finite temperature (EP+IPM).[1)] The latter, which has a very short computing time and contains no fitting parameters to the experimental NLD data, can describe quite well the NLDs and thermodynamic properties of several hot nuclei. Nevertheless, the EP+IPM still contains two shortcomings, which limit its fully microscopic foundation. These shortcomings come from the use of empirical formulas for the spin cut-off σ and collective enhancement factors. The latter is a multiplication of the vibrational $k_{\rm vib}$ and rotational $k_{\rm rot}$ enhancement factors.[1)]

In this paper, we develop a fully microscopic version of the EP+IPM, limited to spherical nuclei (rotational enhancement factor $k_{\rm rot} = 1$), in which three significant improvements are included. First, the single-particle spectra are taken from the Hartree-Fock mean field plus exact pairing (HF+EP) with an effective MSk3 interaction,[2)] instead of the Woods-Saxon potential in the original version of EP+IPM. Second, the spin cut-off parameter is directly calculated by using the statistically thermodynamic method $\sigma^2 = \frac{1}{2}\sum_k m_k^2 {\rm sech}^2\left(\frac{1}{2}E_k/T\right)$, where m_k is the single-particle spin projection (in the deformed basis) and E_k is the quasiparticle energy. Last, the vibrational enhancement of NLD is directly calculated based on the vibrational partition function $Z_{\rm vib}(T) = \sum_{\lambda,i}(2\lambda+1)e^{-E_i^\lambda/T}$, where E_i^λ are all the eigenvalues obtained by solving the self-consistent HF+EP+RPA (SC-HFEPRPA) equation[3)] for the corresponding multipolarity λ, which runs from 0 to 5. The total partition function of the system is then calculated by combining this vibrational partition function with that of the EP+IPM (without vibrational enhancement), namely $\ln Z'_{\rm total} = \ln Z'_{\rm EP+IPM} + \ln Z'_{\rm vib}$, where $Z'(T)$ is the excitation partition function.[1)]

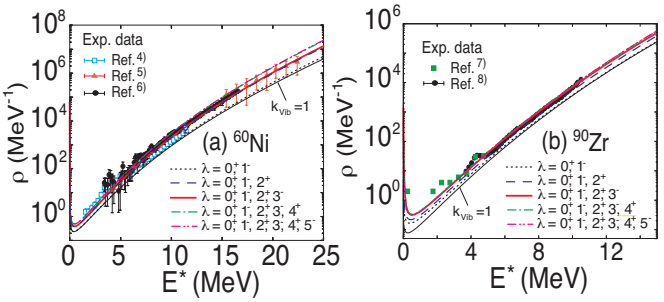

Fig. 1. Total NLDs obtained within the fully microscopic EP+IPM by gradually adding higher collective vibrational modes λ to the vibrational partition function versus the experimental data for ^{60}Ni (a) and ^{90}Zr (b). Experimental data are taken from Refs. 4–8).

The numerical tests for two spherical ^{60}Ni and ^{90}Zr nuclei (see Fig. 1) show that the monopole and dipole excitations ($\lambda = 0^+$ and 1^-) have little enhancement to the total NLD. By adding the quadrupole $\lambda = 2^+$ and octupole 3^- excitations, the EP+IPM NLDs are in excellent with the experimental data. However, adding higher hexadecapole $\lambda = 4^+$ and quintupole $\lambda = 5^-$ excitations enhances the NLD further but the results obtained slightly overestimate the experimental data because these states are always located at a very high-excitation energy, which goes beyond the vibrational excitation region. The results shown in Fig. 1 are of particular valuable as they are the first microscopic calculation, which confirms the important role of the quadrupole and octupole excitations in the description of NLD. We also found that the vibrational enhancement factor obtained within our fully microscopic approach is smaller than that calculated using the empirical and phenomenological formulas. In addition, the spin cut-off factor obtained within our microscopic approach are larger than that obtained by using the empirical formula.

† Condensed from the article in Phys. Lett. B **811**, 135858 (2020)

*1 Institute of Fundamental and Applied Sciences, Duy Tan University
*2 Faculty of Natural Sciences, Duy Tan University
*3 RIKEN Nishina Center
*4 Dalat Nuclear Research Institute, Vietnam Atomic Energy Institute
*5 Faculty of Physics, Hue University of Education

References

1) N. Q. Hung, N. D. Dang, L. T. Q. Huong, Phys. Rev. Lett. **118**, 022502 (2017).
2) L. T. Phuc, N. Q. Hung, N. D. Dang, Phys. Rev. C **97**, 024331 (2018).
3) L. T. Phuc, N. Q. Hung, N. D. Dang, Phys. Rev. C **99**, 064322 (2019).
4) A. V. Voinov *et al.*, Phys. Rev. C **76**, 044602 (2007).
5) J. R. Huizenga *et al.*, Phys. Rev. **182**, 1149 (1969).
6) A. V. Voinov *et al.*, EPJ Web Conf. **21**, 05001 (2012).
7) `https://www-nds.iaea.org/RIPL-3/`.
8) Y. Byun *et al.*, Phys. Rev. C **90**, 044303 (2014).

Isobaric analog state energy in deformed nuclei: A toy model†

X. Roca-Maza,[*1,*2] H. Sagawa,[*3,*4] and G. Colò[*1,*2]

The effects of deformation on the energy of the isobaric analog state (IAS) are studied through microscopic deformed Hartree-Fock-Bogolyubov calculations. A simple yet physical toy model is also presented to provide guidance when predicting unknown IAS energies of deformed nuclei. The deformed HFB calculations are performed for several neutron-deficient medium-mass and heavy nuclei to predict the IAS energies.

Isospin is one of the most important (approximate) symmetries in nuclei. The validity of isospin symmetry has been established by the experimental observation of IASs by charge-exchange reactions. Recently, these states have been investigated extensively in connection with the symmetry energy, particularly to determine the so-called slope parameter L. Thus far, theoretical studies of IAS have mainly focused on spherical nuclei such as ^{48}Ca, ^{90}Zr, and ^{208}Pb. However, a large number of deformed nuclei exist, but transparent information on the effects of deformation on IAS is still lacking. In this paper, we derive a general formula for the effects of deformation on the Coulomb direct contribution to the energy of the IAS and provide a simple albeit physical model. Then, we study several neutron-deficient medium-mass and heavy nuclei, which are now planned to be studied experimentally in RCNP, Osaka within the LUNESTAR project.

The IAS energy $E_{\rm IAS}$ can be defined as the energy difference between the analog state $|A\rangle$ and the parent state $|0\rangle$ as follows:

$$E_{\rm IAS} = \langle A|\mathcal{H}|A\rangle - \langle 0|\mathcal{H}|0\rangle = \frac{\langle 0|T_+[\mathcal{H},T_-]|0\rangle}{\langle 0|T_+T_-|0\rangle} \ , \quad (1)$$

where $T_\pm = \sum_i^A t_\pm(i)$ are the isospin raising/lowering operators. The direct Coulomb term of IAS energy for an axially symmetric nucleus can be evaluated as

$$E_{\rm IAS}^{\rm Cd} = E_{\rm IAS}^{\rm Cd,sph}\left[1 - \frac{\beta_{2n}\beta_{2p}}{4\pi} + \frac{(\beta_{2n}-\beta_{2p})(\beta_{2n}+\beta_{2p})}{4\pi} + \frac{(\beta_{2n}-\beta_{2p})^2}{4\pi}\right] , \quad (2)$$

where $\beta_{2n(2p)}$ is the quadrupole deformations for neutrons (protons). For $\beta_{2n} = \beta_{2p}$, this reduces to

$$E_{\rm IAS}^{\rm Cd} = E_{\rm IAS}^{\rm Cd,sph}\left[1 - \frac{\beta_2^2}{4\pi}\right] . \quad (3)$$

From Eq. (3), one should expect that a larger quadrupole deformation corresponds to a smaller IAS energy. For a qualitative understanding of the effect of deformation on the IAS energy, Eq. (3) predicts, for very deformed nuclei with $\beta_2 \approx 0.8$, a relative reduction in $E_{\rm IAS}$ of approximately 5% with respect to the spherical nucleus.

Table 1. Results of deformed HFB calculations with SAMi EDF.[1] All energies are in MeV. $E_{\rm IAS}^{\rm HFB}$ is the sum of the direct Coulomb, exchange Coulomb, and isospin mixing contributions. The deformation effect on IAS energy has been estimated from the HFB calculations, $\Delta E_{\rm IAS}^{\rm HFB} \equiv E_{\rm IAS}^{\rm HFB}(\beta_{2n},\beta_{2p}) - E_{\rm IAS}^{\rm HFB}(\beta_{2n}=0,\beta_{2p}=0)$.

Nucl.	β_{2n}	β_{2p}	$E_{\rm IAS}^{\rm HFB}$	$E_{\rm IAS}^{\rm exp}$ [2]	$\Delta E_{\rm IAS}^{\rm HFB}$
$^{102}_{46}$Pd	0.186	0.174	13.346		−0.162
$^{106}_{48}$Cd	0.255	0.256	13.810		−0.089
$^{112}_{50}$Sn	0.192	0.199	14.085	14.019	−0.001
$^{120}_{52}$Te	0.039	0.042	14.353		−0.001
$^{124}_{54}$Xe	0.000	0.000	14.749		0.000
$^{130}_{56}$Ba	0.000	0.000	15.114		0.000
$^{136}_{58}$Ce	0.126	0.158	15.352		−0.081
$^{138}_{58}$Ce	0.040	0.047	15.331		−0.010
$^{142}_{60}$Nd	0.000	0.000	15.509		0.000
$^{144}_{62}$Sm	0.000	0.000	15.950	16.075	0.000
$^{156}_{66}$Dy	0.201	0.225	16.755		−0.003
$^{158}_{66}$Dy	0.197	0.217	16.723		−0.028
$^{162}_{68}$Er	0.348	0.378	16.975	16.861	−0.112
$^{164}_{68}$Er	0.346	0.377	16.881	16.778	−0.110
$^{168}_{70}$Yb	0.385	0.413	17.171		−0.212
$^{174}_{72}$Hf	0.304	0.319	17.629		−0.091
$^{176}_{72}$Hf	0.267	0.276	17.538	17.388	−0.086
$^{180}_{74}$W	0.278	0.299	17.911		−0.101
$^{184}_{76}$Os	0.335	0.355	18.223		−0.171
$^{190}_{78}$Pt	−0.147	−0.141	18.649		−0.037
$^{196}_{80}$Hg	−0.180	−0.187	18.906		−0.070

Table 1 lists the results of deformed HFB calculations for several neutron-deficient nuclei as predicted by SAMi EDF. $E_{\rm IAS}^{\rm HFB}$ is the sum of the direct Coulomb, exchange Coulomb, and isospin mixing contributions. The deformation effect is also shown as $\Delta E_{\rm IAS}^{\rm HFB}$, and it varies from −212 keV in ^{168}Yb at the maximum to zero for no deformation cases.

The deformed HFB results reproduce well the experimentally known IAS energies within an error of approximately100 keV and previde a good guide for the experimental search for new IAS states of these neutron-deficient nuclei. In general, the deformation effect is small, but it might be important for the precise prediction of IAS energy within an accuracy of several tenths of keV.

† Condensed from the article in Phys. Rev. C**102**, 064303 (2020)

*1 Dipartimento di Fisica, Università degli Studi di Milano
*2 INFN, Sezione di Milano
*3 RIKEN Nishina Center
*4 Center for Mathematics and Physics, the University of Aizu

References
1) X. Roca-Maza, G. Colò, H. Sagawa, Phys. Rev. C **86**, 031306 (2012).
2) M. Antony, A. Pape, J. Britz, At. Data Nucl. Data Tables **66**, 1 (1997).

Parity-conserved self-consistent CHFB solution

K. Sugawara-Tanabe*1,*2 and K. Tanabe*3

We developed a new program for solving the constrained Hartree-Fock-Bogoliubov (CHFB) equation without parity mixing. In this scheme (CHFB5), we require five constraints, one each on the total angular-momentum I, proton number Z_+ in the + parity shell (p^+), proton number Z_- in the − parity shell (p^-), neutron number N_+ in the + parity shell (n^+), and neutron number N_- in the − parity shell (n^-). As an example, we choose ^{134}Nd with the same parameter set as that adopted in Ref. 1). Here, we solved the full CHFB equation[2] including all exchange terms (Fock terms), while Ref. 1). adopts only the Hartree terms. The values of (Z_+, Z_-, N_+, N_-) are selected in reference to the usual CHFB solutions with three constraints (CHFB3). The usual CHFB3 solutions show $(Z_+, Z_-, N_+, N_-) = (14.59, 17.41, 13.87, 10.13)$ at $I = 0$, while $(14.04, 17.96, 14.0, 10.0)$ at $I = 26$. Here, $(Z, N) = (32, 24)$ are numbers outside the closed core $(28, 50)$. Thus, we select $(14, 18, 14, 10)$ for the CHFB5 equation. The intrinsic difference between CHFB3 and CHFB5 solutions is in the quasi-particle (QP) energies. In Fig. 1, we compare the behavior of the lowest QP energies of Λ with its time-reversed energy $\tilde{\Lambda}$ vs. I. The equations for Λ and $\tilde{\Lambda}$ have been provided in Ref. 2). The degeneracy is lifted by the Coriolis anti-pairing effect with increasing I. Figure 1(A) shows the neutron shell, and (B) the proton shell. In both panels, $\pm$ specifies the $\pm$ shell; the filled symbols express $\tilde{\Lambda}$ and the open symbols Λ. Those in the abbreviation "with" denote CHFB5 solutions, while the others denote CHFB3 solutions. At low I, QP energies by CHFB3 and CHFB5 solutions coincide in the neutron shells (A); however, there is a considerable difference among the p^+ shell (B). The negative value of Λ in the n^+ shell is observed at $I = 10$ in both CHFB3 and CHFB5 solutions; this indicates the first backbending is caused by the $i_{13/2}$ level in the n^+ shell. There occur negative values of Λ in the n^+ and n^- shells around $I = 20$ to 26, and they correspond to decreasing Δ_n, *i.e.*, 0.00021 (CHFB3) and 0.00035 (CHFB5).

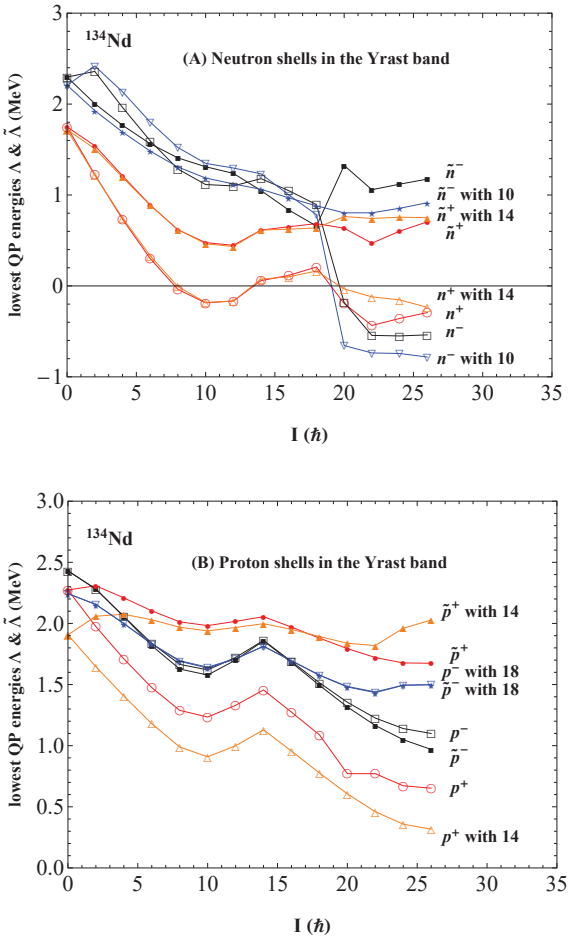

Fig. 1. (A) Lowest QP energies Λ and $\tilde{\Lambda}$ in the neutron shell as functions of angular momentum I. The red open-circles represent Λ, and the red filled-circles represent $\tilde{\Lambda}$ in the n^+ shell by the CHFB3 solutions; the orange open-triangles denote Λ, and the orange filled-triangles represent $\tilde{\Lambda}$ in the n^+ shell by the CHFB5 solutions. The open squares represent Λ, and the filled squares represent $\tilde{\Lambda}$ in the n^-shell by the CHFB3 solutions, while the blue open-triangles-down represent Λ, and the blue filled-triangles-down represent $\tilde{\Lambda}$ in the n^-shell by the CHFB5 solutions. (B) The lowest QP energies of Λ and $\tilde{\Lambda}$ in the proton shell as functions of I. The red open-circles represent Λ, and the red filled-circles represent $\tilde{\Lambda}$ in the p^+ shell by the CHFB3 solutions, while the orange open-triangles represent Λ, and the orange filled-triangles represent $\tilde{\Lambda}$ in the p^+ shell by the CHFB5 solutions. The open squares represent Λ, and the filled squares represent $\tilde{\Lambda}$ in the p^-shell by the CHFB3 solutions, while the blue open-triangles-down represent Λ and the blue filled-triangles-down represent $\tilde{\Lambda}$ in the p^-shell by the CHFB5 solutions.

References

1) K. Tanabe, K. Sugawara-Tanabe, Phys. Lett. **259B**, 12 (1991).
2) K. Sugawara-Tanabe, K. Tanabe, RIKEN Accel. Prog. Rep. **52**, 1148 (2019).

*1 RIKEN Nishina Center
*2 Department of Information Design, Otsuma Women's University
*3 Department of Physics, Saitama University

Role of exact treatment of thermal pairing in radiative strength functions of ^{161,163}Dy nuclei†

L. Tan Phuc,[*1,*2] N. Quang Hung,[*1,*2] N. Dinh Dang,[*3] L. T. Quynh Huong,[*4] N. Ngoc Anh,[*5] N. Ngoc Duy,[*6] L. Ngoc Uyen,[*7] and N. Nhu Le,[*8]

The photon or radiative strength function (RSF), defined as the average electromagnetic transition probability per unit of γ-ray energy E_γ,[1)] has an important role in the study of nuclear reaction properties such as γ-ray emission rate, reaction cross section, and/or nuclear astrophysical processes.[2)] Very recently, we have proposed a microscopic model to simultaneously describe the nuclear level density and RSF.[3)] For the RSF, we employed the phonon damping model (PDM),[4)] which consistently includes the exact thermal pairing (EP), in order to take into account both temperature-dependent giant dipole resonance (GDR) width (within the PDM) and thermal pairing (within the EP). The goal of the current work is to shed a light on the microscopic nature of the low-energy enhancement in the RSF data caused by the PDR (Pygmy Dipole Resonance). Three dysprosium isotopes ^{161,162,163}Dy are selected to do the calculations within the EP+PDM. The results will be compared with the phenomenological models (standard Lorentzian-SLO and generalized Lorentzian-GLO) and the other microscopic model (Quasiparticle random-phase approximation-QRPA). The RSF at each energy E_γ and temperature T is defined as follow

$$f_{E1}(E_\gamma,T) = \left(\frac{1}{3\pi^2\hbar^2c^2}\right)\frac{\pi}{2}\frac{\sigma_{E1}\Gamma_{E1}(E_\gamma,T)S_{E1}(E_\gamma,T)}{E_\gamma}, \quad (1)$$

where σ_{E1} is the GDR cross section which is obtained microscopically within the PDM, Γ_{E1} is the temperature-dependent GDR width, and S_{E1} is the GDR strength function.

Figure 1 depicts the total RSFs obtained within the PDM with and without EP the experimental data[5)] as well as those obtained within the microscopic D1M+QRPA ($E1$ and $E1+M1$) and phenomenological GLO-SLO models. The results obtained show that, due to the effect of EP, the EP+PDM can describe reasonably well the RSF data in both low and high-energy regions without adding any extra strength function. As a result, at least eight free parameters have been reduced within the EP+PDM calculations as compared to the description by the phenomenological GLO-SLO model.

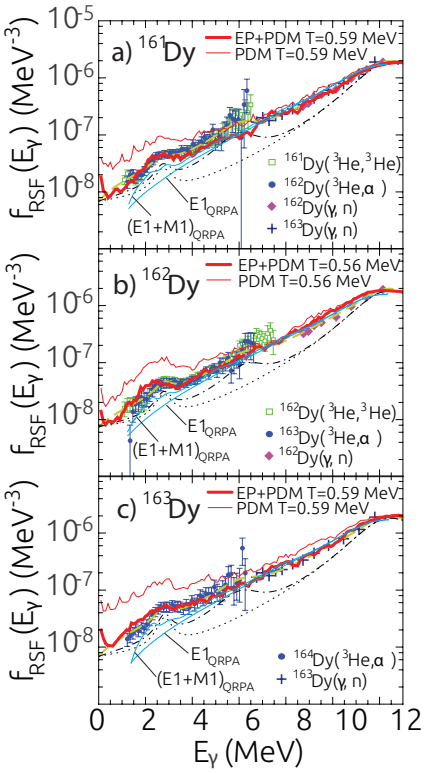

Fig. 1. Total RSFs obtained within the PDM (thin solid lines), EP+PDM (thick solid lines) versus the QRPA RSFs for the $E1$ and $E1+M1$ excitations and the experimental data[5)] for $^{161-163}$Dy. The dashed, dash-dotted, and dotted lines stand for the RSFs obtained within the phenomenological GLO-SLO models with 2 PDRs, 1 PDR, and without PDR, respectively.

Temperature is found to have a significant effect on the RSF at the low energy $E_\gamma \leq S_n$, whereas it does not change much the RSF in the high-energy one $E_\gamma > S_n$, questioning the validity of the Brink-Axel hypothesis. In addition, due to the effects of EP and couplings of all *ph*, *pp*, and *hh* configurations within the PDM, the EP+PDM can also partially reproduce the scissors resonance in $^{161-163}$Dy nucleus at low E_γ without adding a SR strength function in the RSF. These findings indicate the importance of EP and couplings to non-collective *pp* and *hh* configurations at finite temperature in the microscopic description of total RSF in excited nuclei.

† Condensed from the article in Phys. Rev. C **102**, 061302(R) (2020)

*1 Institute of Fundamental and Applied Sciences, Duy Tan University
*2 Faculty of Natural Sciences, Duy Tan University
*2 RIKEN Nishina Center
*3 Department of Natural Science and Technology, University of Khanh Hoa
*4 Dalat Nuclear Research Institute, Vietnam Atomic Energy Institute
*5 Department of Physics, Sungkyunkwan University
*6 Department of Engineering Science, University of Electro-Communications
*7 University of Education, Hue University

References

1) J. M. Blatt, V. F. Weisskopf, *Theoretical Nuclear Physics* (Wiley, New York, 1952).
2) J. Kopecky, M. Uhl, Phys. Rev. C **41**, 1941 (1990).
3) N. Q. Hung, N. D. Dang, L. T. Q. Huong, Phys. Rev. Lett **118**, 022502 (2017).
4) N. D. Dang, A. Arima, Phys. Rev. Lett. **80**, 4145 (1998).
5) `https://www.mn.uio.no/fysikk/english/research/about/infrastructure/ocl/nuclear-physics-research/compilation/`.

Non-relativistic expansion of Dirac equation by the reconstituted Foldy-Wouthuysen transformation†

Y. X. Guo*1,*2 and H. Z. Liang*2,*1

In the past few decades, the density functional theory (DFT) has been successfully applied in both the non-relativistic and relativistic frameworks to describe the ground-state and excited-state properties of thousands of nuclei in a microscopic and self-consistent manner. However, the connection between these two frameworks remains unclear. The non-relativistic expansion of the Dirac equation is considered to be a potential bridge connecting these two frameworks.[1,2)]

Recently, the reconstituted similarity renormalization group (SRG) method was proposed.[3)] Compared to conventional methods, the reconstituted SRG method not only showed a much faster convergence, but also yielded single-particle densities $\rho_v(\boldsymbol{r}) = \psi^\dagger(\boldsymbol{r})\psi(\boldsymbol{r})$ that are closer to the exact values. Moreover, for the single-particle scalar densities $\rho_s(\boldsymbol{r}) = \psi^\dagger(\boldsymbol{r})\gamma_0\psi(\boldsymbol{r})$, the γ_0 matrix should be transformed in the same manner as the Dirac Hamiltonian. However, the original Dirac Hamiltonian is operated with infinite steps of unitary transformations in both the conventional and reconstituted SRG methods. Therefore, the calculations of single-particle scalar densities are not trivial in SRG methods.

Meanwhile, with the consideration of the strong scalar potential, we further applied another well-known technique, the Foldy-Wouthuysen (FW) transformation, to the general cases in the covariant DFT and performed the corresponding expansion up to the $1/M^4$ order.[4)] With the present FW transformation, all the unitary transformations involved hold explicit forms. On this basis and with inspiration from the reconstituted SRG method, we developed the reconstituted FW transformation. By replacing the bare mass M with the Dirac mass M^* and defining the corresponding new operators, the contributions related to the higher powers of the quotient of the scalar potential and the bare mass are absorbed into the lower orders.

As a step forward, the so-called picture-change error,[5,6)] *i.e.*, the difference between the densities calculated in the Schrödinger picture and those obtained in the Dirac picture, has also been investigated through calculations starting from basic field operators. After considering such picture-change errors, *i.e.*, the relativistic corrections, both the single-particle vector and scalar densities become much closer to the exact results. In addition, the difference between ρ_v and ρ_s originates from the $1/M^{*2}$ order, as does the relativistic correction $\Delta\rho$. Therefore, the relativistic corrections also play a crucial role in the difference between the vector and scalar densities.

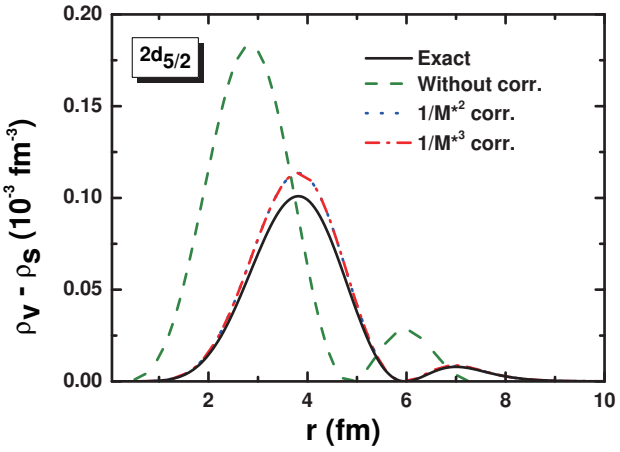

Fig. 1. Difference between the single-particle density and the single-particle scalar density for the neutron $2d_{5/2}$ state of nucleus ^{208}Pb.

By taking the $2d_{5/2}$ state of ^{208}Pb as an example, the difference between the single-particle density and the single-particle scalar density is shown with the black solid line in Fig. 1. The result without any relativistic correction is shown with the olive dashed line, while the results calculated with the consideration of relativistic corrections up to the $1/M^{*2}$ and $1/M^{*3}$ orders are shown with the blue dotted and red dash-dotted lines, respectively. It can be seen from Fig. 1 that the differences between the results without the relativistic corrections and the exact values are systematic. There are differences in the positions of peaks and nodes as well as the amplitudes. In contrast, the results with the relativistic corrections remarkably reproduce the behavior of the exact values, particularly in terms of the positions of peaks and nodes.

Based on the above discussions, the reconstituted FW transformation is a promising method to connect the relativistic and non-relativistic DFTs for future studies.

† Condensed from the article in Phys. Rev. C **101**, 024304 (2020)
*1 Department of Physics, The University of Tokyo
*2 RIKEN Nishina Center

References

1) P. G. Reinhard, Rep. Prog. Phys. **52**, 439 (1989).
2) M. Bender, P. H. Heenen, P. G. Reinhard, Rev. Mod. Phys. **75**, 121 (2003).
3) Y. X. Guo, H. Z. Liang, Phys. Rev. C **99**, 054324 (2019).
4) Y. X. Guo, H. Z. Liang, Chin. Phys. C **43**, 114105 (2019).
5) M. Douglas, N. M. Kroll, Ann. Phys. (N. Y.) **82**, 89 (1974).
6) B. A. Hess, Phys. Rev. A **33**, 3742 (1986).

On the role of three-particle interactions in nuclear matter†

W. Bentz*1 and I. C. Cloët*2

In a previous publication[1] we discussed an interesting relation between the skewness J of nuclear matter ($J = 27\rho^3 \left(\mathrm{d}^3E_A/\mathrm{d}\rho^3\right)$, where ρ is the baryon density and E_A the energy per nucleon in isospin symmetric nuclear matter) and the isoscalar three-particle interaction parameters. In this paper, we wish to discuss an equally interesting relation between the slope parameter L of the symmetry energy ($L = 3\rho\frac{\mathrm{d}a_s}{\mathrm{d}\rho}$, where $a_s \simeq 32$ MeV is the symmetry energy) and the isovector three-particle interaction parameters.

We extend Landau's basic formula[2] for the variation of the energy density of nuclear matter to include the third order term, which involves the spin-averaged three-particle forward scattering amplitude $h^{(\tau_1\tau_2\tau_3)}(\vec{k}_1, \vec{k}_2, \vec{k}_3)$. Here $\tau_i = (p, n)$, and h is symmetric under simultaneous interchanges of the momentum variables $\vec{k}_i$ and the isospin variables τ_i. Taking finally the isospin symmetric limit, we can derive the following relations for J and L in terms of the incompressibility K and the symmetry energy a_s:

$$J = -9K + \frac{9p_F^2}{M} \times \left[\left(-3+\frac{8}{3}\frac{M}{M^*}\right) - \frac{4}{3}\frac{Mp_F}{M^{*2}}\frac{\partial M^*}{\partial p_F} + \frac{M}{M^*}\left(H_0 - H_1\right)\right],$$

$$L = 3a_s - \frac{p_F^2}{2M} \times \left[\left(1-\frac{2}{3}\frac{M}{M^*}\right) + \mu\left(\frac{M}{M^*}\right)^2 - \frac{M}{M^*}\left(H_0' - \frac{1}{3}H_1\right)\right].$$

Here p_F is the Fermi momentum, M the free nucleon mass, M^* the Landau effective mass, $\frac{\partial M^*}{\partial p_F}$ refers to the momentum dependence of M^* at the Fermi surface, and $\mu = \rho\frac{\partial}{\partial\rho^{(3)}}\left(\frac{\Delta M^*}{M}\right)$ expresses the dependence of $\Delta M^* = M^{*(p)} - M^{*(n)}$ on the isovector density $\rho^{(3)} = \rho^{(p)} - \rho^{(n)}$. The dimensionless isoscalar and isovector three-particle interaction parameters

$$H_\ell = \left(\frac{2p_F M^*}{\pi^2}\rho\right) h_\ell\,, \quad H_\ell' = \left(\frac{2p_F M^*}{\pi^2}\rho\right) h_\ell'$$

are the $\ell = 0, 1$ moments of the isoscalar ($h_\ell = \frac{1}{4}(h_\ell^{(ppp)} + 3h_\ell^{(ppn)})$) and isovector ($h_\ell' = \frac{1}{4}(h_\ell^{(ppp)} - h_\ell^{(ppn)})$) combinations of the 3-particle forward scattering amplitude at the Fermi surface.

By using empirical information, it was shown in Ref. 1) that the above expression for J requires a large positive 3-particle term $\frac{M}{M^*}(H_0 - H_1) > 1.24$. On the other hand, if we use the canonical value $a_s = 32$ MeV together with $\mu \simeq 0.27$, which is the central value of the empirical range $\mu = 0.27 \pm 0.25$ reported in Ref. 3), the sum of the first two terms in $[\ldots]$ in the expression for L is ~ 0.6, almost independent of M^* within the empirical range $0.7 < M^*/M < 1$. The empirical range of the slope parameter[3] $L = 59 \pm 16$ MeV then implies that the 3-particle term $\frac{M}{M^*}\left(H_0' - \frac{1}{3}H_1\right)$ is negative, with a magnitude smaller than unity.

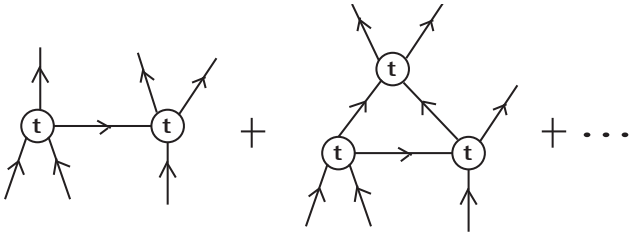

Fig. 1. First two terms in the Faddeev series. Circles represent two-body t-matrices.

Theoretically the three-particle amplitudes should be calculated from the Faddeev equation, which is illustrated by Fig. 1. The driving term, which we call the "2-particle correlation (2pc) term," can be easily estimated by using effective contact interactions of the Landau-Migdal type. Restricting the calculation to s-waves ($\ell = 0$) for simplicity gives the analytic results

$$H_0^{(2\mathrm{pc})} = \frac{\ln 2}{4}\left(F_0^2 + 3F_0'^2 + 3G_0^2 + 9G_0'^2\right),$$

$$H_0^{'(2\mathrm{pc})} = \frac{\ln 2}{4}\left(\frac{1}{3}F_0^2 + \frac{4}{3}F_0F_0' - \frac{1}{3}F_0'^2 + G_0^2 + 4G_0G_0' - G_0'^2\right).$$

Here F_0, F_0', G_0, G_0' are the dimensionless $\ell = 0$ two-particle Landau-Migdal parameters, as defined for example in Ref. 2). While the isoscalar $H_0^{(2\mathrm{pc})}$ is positive definite and of the order of unity or even larger, depending mainly on the magnitude of G_0', the isovector $H_0^{'(2\mathrm{pc})}$ is negative and small compared to unity for most of the published sets of Landau-Migdal parameters. Because the p-wave term H_1 is suppressed by large factors,[1] this simple estimate makes it plausible that the three-body interactions give a large positive contribution to J, and a small negative contribution to L. To obtain more quantitative results, it would be interesting to apply the Faddeev method in the framework of effective field theories for nuclear matter.

References
1) W. Bentz, I. C. Cloët, Phys. Rev. C **100**, 014303 (2019).
2) J. Negele, H. Orland, *Quantum Many-particle systems* (Springer, 1980).
3) B. -A. Li, B. -J. Cai, L. -W. Chen, J. Xu, Prog. Part. Nucl. Phys. **99**, 29 (2018).

† Condensed from an article by W. Bentz and I. C. Cloët, to be published in Phys. Rev. C (2021)

*1 Department of Physics, Tokai University
*2 Physics Division, Argonne National Laboratory

A3-Foresight theory collaboration for nuclear data library: A3LIB

K. Yoshida*1 for the A3LIB Collaboration

A quantitative understanding of the r-process nucleosynthesis requires nuclear data across the nuclear chart, including the vicinities of the neutron drip line, which are experimentally inaccessible. Thus the nuclear theory plays a decisive role to bridge between nuclear experiments at RI beam facilities and microscopic inputs of the r-process simulation.

The condition of the r-process is given by an astrophysical environment of explosive phenomena with some possible scenarios. Although nuclear physics that enters the reaction network may depend on the scenario, the most important nuclear data are the nuclear masses, β-decay properties, and neutron capture rates;[1,2] Given the neutron-number density, temperature, and entropy, the seed nuclei are formed through the nuclear statistical equilibrium. Here, the nuclear masses are a key nuclear physics quantity. When the temperature decreases in the order of 100 keV, various nuclear reactions take place, and the neutron-capture process generates neutron-rich nuclei. If the neutron-number density is high, it proceeds to the production of the heaviest nuclei, and fission occurs. In every process, competition with the β-decay should be considered. The β-decay and the β-delayed neutron emission play a role in shaping the final abundance distributions observed in nature.

The nuclear energy-density functional (EDF) approach is a possible theoretical model to describe the above-mentioned nuclear properties in a vast mass region of the nuclear chart in a single framework. Researchers in the A3 (Chine, Japan, and Korea) countries have developed the nuclear EDF method and computational techniques. It is natural to start collaboration on the construction of the nuclear data table necessary for the r-process modeling and the development of the associated nuclear many-body theory.

I briefly explain a rough plan of the theory collaboration. As shown in Fig. 1, the development of the theory and model for each nuclear property is strongly related. The key to success is the construction of the EDF. Given the EDF, the binding energy of a nucleus and the single-particle level density are obtained in a Kohn–Sham scheme. Parallel to an attempt at the microscopic construction of EDF from an inter-particle interaction, a phenomenological construction is planned in collaboration with the researchers in Korea. The KIDS functional was introduced to better describe the neutron-star equation of state. We apply the KIDS functional to open-shell nuclei, where the nucleonic superfluidity and shape deformation show up. Subsequently, the KIDS functional is improved for finite nuclei. We developed a novel method for describing odd mass nuclei for a systematic calculation of the nuclear mass. The implementation is performed in the KIDS code.

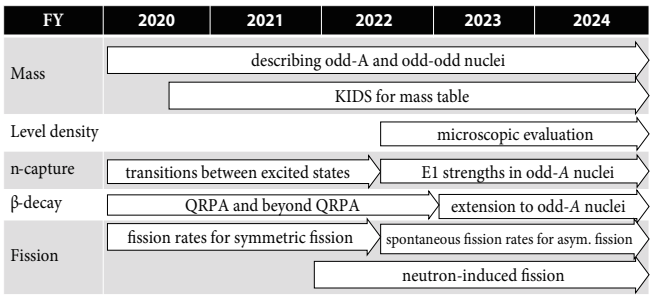

Fig. 1. Plan for the development of A3LIB.

To describe the neutron capture and β decay rates, we employ the EDF-based quasiparticle RPA (QRPA). In neutron-rich nuclei where the neutron separation energy is approximately a few MeV, the direct capture process dominates over the compound process. In such a case, the low-lying excited states and transitions are evaluated microscopically. The description of the transitions among excited states is in progress. For β decay, we take two approaches: a beyond QRPA method for magic nuclei to describe the spreading effect and the QRPA for deformed nuclei.

The microscopic calculation of the fission rate is a big challenge in nuclear theory. The mass parameters and potential energy in the collective (effective) Hamiltonian for fission are microscopically calculated in an EDF approach. The fission rate is then evaluated, *e.g.*, by WKB approximation. Hybrid modeling for the fission yield is planned, where the parameters of the phenomenological model, such as the Langevin approach, are evaluated by a microscopic EDF method.

Finally, the uncertainty quantification is essential in developing a new generation of the nuclear data table. The A3LIB is based on the EDF method; thus, all the calculated quantities are correlated through the coupling constants of EDF. We plan to perform the correlation analysis at each step of the calculation. The results will be provided in the existing data library online.

References
1) M. R. Mumpower *et al.*, Prog. Part. Nucl. Phys. **86**, 86 (2016).
2) T. Kajino *et al.*, Prog. Part. Nucl. Phys. **107**, 109 (2019).

*1 Department of Physics, Kyoto University

3. Nuclear Data

EXFOR compilation of RIBF data in 2020

T. Tada,[*1] M. Kimura,[*1,*3] M. Aikawa,[*2,*4] and N. Otuka[*4,*5]

Nuclear reaction data support the most essential part of nuclear technologies (power production, nuclear fuel cycles, environmental monitoring, dosimetry, radiation safety, radioisotope production, radiotherapy, and medical diagnostics, etc.) and sciences (nuclear physics, nuclear chemistry, geophysics, and astrophysics). Nuclear databases are compilations of measured reaction data, and they play a vital role in providing the best estimate for nuclear reactions to various science fields and related areas. One of the largest and globally used public nuclear reaction databases is the EXFOR library (EXchange FORmat for experimental nuclear reaction data).[1] The EXFOR library is a universal common repository for nuclear reactions established in 1967. The International Network of Nuclear Reaction Data Centres (NRDC) maintains the EXFOR library under the auspices of the International Atomic Energy Agency (IAEA).[2] The EXFOR library covers a wide range of nuclear reactions such as neutron-, charged-particle- and photon-induced reactions.

Our group, the Hokkaido University Nuclear Reaction Data Centre (JCPRG),[3] was founded in 1973 and joined the NRDC as the first member of the Asian countries in 1975. We are responsible for the compilation of the charged-particle- and photon-induced nuclear reactions measured in Japanese facilities.[4] Our contributions to the EXFOR database reaches approximately 10% of the total amount. The database compilation process involves the scanning of peer-reviewed journals for published papers within the EXFOR scope. A unique entry number is assigned to each selected paper to be compiled for the EXFOR library. We extract the information of the bibliography, experimental setup, measured physical quantities, measured numerical data and uncertainties. The information is input in a single entry of EXFOR. During this process, we contact the corresponding authors for questions on the contents of the papers and requests for numerical data.

JCPRG has been cooperating with the RIKEN Nishina Center for the compilation of data obtained by RIBF since 2010, which aims to enrich the availability of RIBF data. In 2020, we compiled 45 new articles produced at Japanese facilities and modified 18 old entries. This includes 17 articles from RIKEN, 15 new articles, and 2 old entries. The compiled data are accessible by entry numbers listed in Table 1. We thank the authors of these papers for their kind cooperation.

Table 1. Entry numbers with references compiled from RIBF data in 2020.

	Entries		
New	E2625[5]	E2626[6]	E2633[7]
	E2634[8]	E2641[9]	E2644[10]
	E2645[11]	E2646[12]	E2648[13]
	E2650[14]	E2652[15]	E2653[16]
	E2654[17]	E2655[18]	E2657[19]
Revised	E2557[20]	E2616[21]	
Total		17	

We acknowledge that collaboration with RIKEN is a great help for us to establish an effective procedure for the compilations. Most RIKEN data are very quickly compiled after publication and end-users can access it smoothly. We also thank all authors of RIKEN articles who kindly provided numerical data. This greatly helps increase the accuracy and quality of the database.

*1 Graduate School of Science, Hokkaido University
*2 Faculty of Science, Hokkaido University
*3 Research Center for Nuclear Physics (RCNP), Osaka University
*4 RIKEN Nishina Center
*5 NDS, IAEA

References

1) N. Otuka *et al.*, Nucl. Data Sheets **120**, 272 (2014).
2) `https://www-nds.iaea.org/`.
3) Hokkaido University Nuclear Reaction Data Centre, `http://www.jcprg.org/`.
4) M. Kimura, AAPPS Bulletin **28**, 24 (2018).
5) J. Yasuda *et al.*, Phys. Rev. Lett. **121**, 132501 (2018).
6) N. Paul *et al.*, Phys. Rev. Lett. **122**, 162503 (2019).
7) A. Corsi *et al.*, Phys. Lett. B **797**, 134843 (2019).
8) M. L. Cortes *et al.*, Phys. Lett. B **800**, 135071 (2020).
9) K. Nakano *et al.*, Phys. Rev. C **100**, 44605 (2019).
10) S. Chen *et al.*, Phys. Rev. Lett. **123**, 142501 (2019).
11) D. S. Ahn *et al.*, Phys. Rev. Lett. **123**, 212501 (2019).
12) V. Vaquero *et al.*, Phys. Rev. Lett. **124**, 22501 (2020).
13) Z. Tsoodol *et al.*, Appl. Radiat. Isot. **159**, 109095 (2020).
14) A. R. Usman *et al.*, Nucl. Instrum. Methods Phys. Res. B **469**, 42 (2020).
15) M. U. Khandaker *et al.*, Nucl. Instrum. Methods Phys. Res. B **470**, 1 (2020).
16) M. Sakaguchi *et al.*, Nucl. Instrum. Methods Phys. Res. B **472**, 59 (2020).
17) M. Saito *et al.*, Nucl. Instrum. Methods Phys. Res. B **471**, 13 (2020).
18) T. Lokotko *et al.*, Phys. Rev. C **101**, 34314 (2020).
19) K. Sugihara *et al.*, Nucl. Instrum. Methods Phys. Res. B **470**, 15 (2020).
20) V. Vaquero *et al.*, Phys. Rev. Lett. **118**, 202502 (2017).
21) X. H. Sun *et al.*, Phys. Rev. C **101**, 64623 (2020).

4. Hadron Physics

Transverse momentum dependence of forward neutron single spin asymmetries in polarized $p^{\uparrow}+p$ collisions at $\sqrt{s}=200$ GeV†

B. Mulilo*1,*2 for the PHENIX Collaboration

The PHENIX Collaboration has, for the first time, explicitly measured the transverse momentum (p_T)-dependent single spin asymmetries (A_N) for inclusive neutrons produced in the forward region of the PHENIX detector with $\eta > 6.8$ using 2015 data. During this time, a proton with transverse polarization collided with another proton at $\sqrt{s} = 200$ GeV. Owing to the limited acceptance and resolution of the detector, the measured quantities were considerably smeared. We, therefore, corrected for the smearing in the measured p_T and azimuth (ϕ) using unfolding.[1)]

As the physics of forward neutron production is not clearly understood, we performed detailed simulations using different event generators as input to a full GEANT3 simulation.[2)] The generators DPMJET3.1, PYTHIA6.1, and PYTHIA8.2 were used because diffractive processes are very differently handled. Another generator was an empirical distribution of forward neutrons in p_T, mimicking a one-pion exchange (OPE) model in which a pion balancing the momentum between the incoming proton and outgoing neutron collided with the other proton beam using PYTHIA 8. Ultra-peripheral collisions (UPCs) also play a role in forward neutron production.[3)] The distribution of photons was, therefore, simulated using the STARLIGHT[4)] generator, and the photons collided with the proton beam using PYTHIA 8. As all Monte Carlo (MC) generators were intrinsically spin independent, we simulated spin effects by re-weighting events as a function of the generated p_T ($p_{T,g}$) and azimuth (ϕ_g) with the spin states ($\uparrow$) and ($\downarrow$) randomly assigned. Furthermore, as the shape of p_T-dependent A_N is not precisely known, we used three weight forms to provide as much flexibility as possible. The weight (w) based on a polynomial of third order (Pol3), power law, and exponential forms is given by Eqs. (1), (2), and (3), respectively, with Pol3 being the most general one:

$$w = \left(a \cdot p_{T,g} + b \cdot p_{T,g}^2 + c \cdot p_{T,g}^3\right) \sin(\phi_g + \lambda \cdot \pi), \quad (1)$$

where λ (± 1) is the spin state and a, b, and c are free parameters. Accordingly, the power-law weight is,

$$w = \left(a \cdot p_{T,g}^b\right) \sin(\phi_g + \lambda \cdot \pi), \quad (2)$$

and the last parameterization is an exponential form, which eventually decays asymptotically as

$$w = a\left(1 - \mathrm{e}^{b \cdot p_{T,g}}\right) \sin(\phi_g + \lambda \cdot \pi). \quad (3)$$

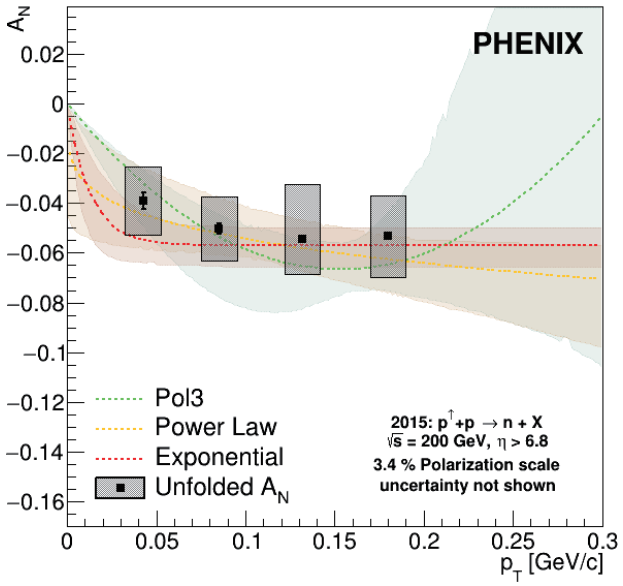

Fig. 1. Overall p_T-dependent A_N values shown as black solid square points averaged over all parameterizations, MC, and unfolding. Shaded boxes display total uncertainties from the unfolding, choice of MC, and functional form. Light-green, brown, and yellow shaded regions show χ^2 below 10 units for Pol3, power-law, and exponential forms, respectively, while the corresponding broken lines show the best matching parameterizations.

The performance of parameters, functional form, and MC generator in reproducing A_N values was evaluated by the minimum χ^2 between the measured MC and data asymmetries. The 2D spin-dependent neutron yields in p_T and ϕ were then unfolded using the TSVDUnfold class based on a singular value decomposition (SVD)[1)] of the smearing response matrix. Overall A_N values were finally calculated from the unfolded yields using the left-right A_N formula[5)] after fitting a sine modulation having magnitude and phase as free parameters. In Fig. 1, overall A_N values rapidly increase at low p_T ($\lesssim 0.1$ GeV/c) and slowly level off at high p_T. With this result, the first reliable tests of mechanisms producing these asymmetries can be performed.

† Condensed from article in Phys. Rev. D **103**, 032007 (2021)

*1 RIKEN Nishina Center
*2 Department of Physics, Korea University

References
1) A. Hocker *et al.*, Nucl. Instrum. Methods Phys. Res. A **372**, (1996).
2) A. Adare *et al.*, Phys. Rev. D **90**, 012006 (2014).
3) C. Aidala *et al.*, Phys. Rev. Lett. **120**, 022001 (2018).
4) S. R. Klein *et al.*, Comput. Phys. Com. **212**, (2017).
5) A. Adare *et al.*, Phys. Rev. D **88**, 032006 (2013).

Transverse single-spin asymmetry for very forward neutral pion production in polarized $p+p$ collisions at $\sqrt{s} = 510$ GeV†

M. H. Kim*1,*2 for the RHICf Collaboration

In high-energy polarized $p+p$ collision, the left-right cross section asymmetry, which is called as transverse single-spin asymmetry (A_N) of very forward ($\eta > 6$) particle production, plays an important role in understanding the spin-involved production mechanism from the view points of perturbative and nonperturbative interactions. The RHICf experiment[1] measured the A_N of very forward neutral pion in polarized $p+p$ collisions at $\sqrt{s} = 510$ GeV in June, 2017 at the Relativistic Heavy Ion Collider (RHIC).

The nonzero asymmetries of the neutral pion have been measured by many experiments[2,3] in the forward ($2 < \eta < 4$) kinematic range, and they have been explained only by quarks and gluons' degrees of freedom. However, a possible contribution from the nonperturbative interaction has been recently highlighted because larger asymmetries were observed in more isolated neutral pion events[4,5] that could be connected to nonperturbative event topology. A straightforward approach to studying the role of nonperturbative interaction is measuring the A_N of the neutral pion in the very forward kinematic area where the nonperturbative interaction is expected to dominate.

We installed an electromagnetic calorimeter (RHICf detector) at the zero-degree area 18 m away from the beam collision point at the STAR experiment. The RHICf detector consists of two sampling calorimeters with lateral dimensions of 20 mm × 20 mm and 40 mm × 40 mm, respectively. Both calorimeters are composed of 17 tungsten absorbers, 16 GSO plates for energy measurement, and 4 layers of GSO bars for position measurement. Since the radiation length of the detector is 44 X_0, the electromagnetic shower stops its development in the middle of the detector. The RHICf detector has an energy resolution of 2.5–3.5% for 100–250 GeV π^0s and the p_T resolution of 3.0–4.5% in $0.0 < p_T < 0.8$ GeV/c.

To the best of our knowledge, we observed large asymmetry in a very forward neutral pion production for the first time, which means a possible contribution from the nonperturbative interaction. Comparison between RHICf and previous forward neutral pion measurements are depicted in Fig. 1. At very low $p_T < 0.07$ GeV/c, the asymmetries are consistent with zero. However, as p_T increases, the asymmetries increase as a function of x_F, approximately showing the same magnitudes and tendency of the forward ones.

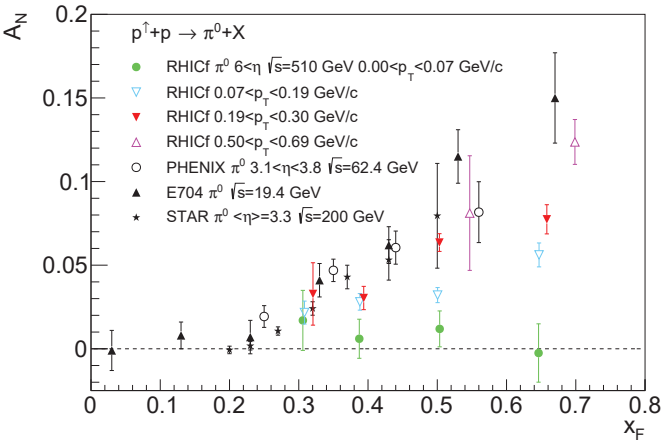

Fig. 1. Forward (black) and very forward (color) neutral pion asymmetries as a function of x_F in different p_T regions.

It may be necessary to consider nonperturbative interaction to understand both forward and very forward neutral pion asymmetries.

However, RHICf data can be affected by perturbative interaction in the low p_T region. The perturbative and nonperturbative interactions may make their own nonzero asymmetries respectively. Since the result of this report is the one analyzed inclusively, more detailed analysis is necessary to reduce the diverse possibilities.

We have started combined analysis with STAR. Signals in the STAR detectors will identify whether the neutral pions of the nonzero asymmetries come from perturbative or nonperturbative interaction. Further, we are preparing a series of follow-up experiments for developing a larger detector. In the near future, further analysis and experiments will provide a powerful input to understand the origin of both forward and very forward neutral pion asymmetries.

References
1) RHICf Collaboration, LOI, arXiv: 1409. 4860v1.
2) A. Adare *et al.* (PHENIX Collaboration), Phys. Rev. D **90**, 012006 (2014).
3) B. I. Abelev *et al.* (STAR Collaboration), Phys. Rev. Lett. **101**, 222001 (2008).
4) S. Heppelmann (STAR Collaboration), Proc. Sci. **191** (DIS2013), 240 (2013).
5) M. M. Mondal (STAR Collaboration), Proc. Sci. **203** (DIS2014), 216 (2014).

† Condensed from the article in Phys. Rev. Lett. **124**, 252501 (2020)

*1 RIKEN Nishina Center
*2 Department of Physics, Korea University

Transverse single spin asymmetry in charged pion production at midrapidity in polarized $p+p$ collisions at 200 GeV

J. H. Yoo*[1] for the PHENIX Collaboration

One of the main goals of the RHIC spin program is the determination of the transverse-spin structure of the proton, which can in turn provide some insight into the angular-momentum component of partons. For reaching the goal, we measure Transverse Single-Spin Asymmetries (TSSAs) which are left-right asymmetries of final stage particles produced in the transversely polarized $p+p$ collision.[1)] The TSSAs (A_N) of pion at midrapidity in $p+p$ collision is expected to be helpful to understand the transversity distributions of quark and gluons, the transverse intrinsic parton momentum, initial and final state effects. In PHENIX the charged pions at mid-rapidity can be measured by the central arm detectors that consist of the Electro-Magnetic Calorimeter (EMCal), Ring-Imaging Cherenkov Detec tor (RICH), Drift Chamber (DC), Pad Chamber (PC). Trigger fired if pions deposited energy over than 1.4 GeV on EMCal and we can detect charged pion's track and energy. In mid-rapidity charged pion measurement, the background is categorized into two sources which are hadron background(kaon and proton) and electron background(electron and positron). Pions with momentum above 5 GeV/c create Cherenkov light in the RICH but kaons and protons can't create Cherenkov light under

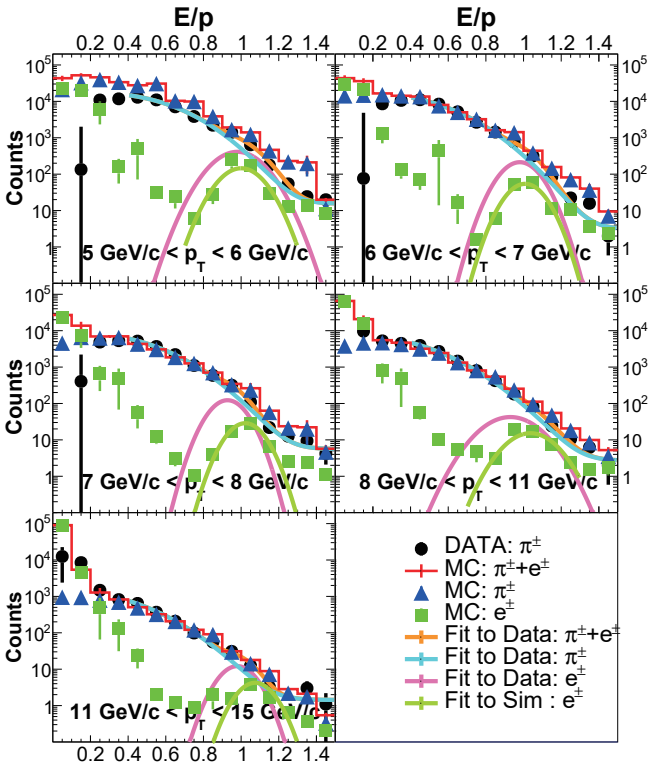

Fig. 1. E/p distribution in pion enhancement sample for five P_T bins.

Table 1. Background fraction of two samples.

particle	p_T bin (GeV/c)	$r_{\pi,e}$
$\pi^{\pm}$	5–6	0.0436
	6–7	0.0688
	7–8	0.1375
	8–11	0.1192
	11–15	0.2154
$e^{\pm}$	5–6	0.00652
	6–7	0.06569
	7–8	0.1646
	8–11	0.8560
	11–15	0.9178

16 GeV/c and 30 GeV/c, respectively. Only electron background remained an object to subtract. In EMCal, electrons lost most of their energy by electromagnetic interactions. Therefore, primary electron's energy/momentum (E/p) distributed around 1. A secondary electron track from photon conversion would be incorrectly reconstructed with large momentum. Therefore secondary electron's energy/momentum would be in the low area. because we can know only background fraction but we can't distinguish electron event from pion event, Eq. (1) is used for background correction of the asymmetries.[2)] By using Monte Carlo simulation, we calculated electron background fraction in both pion enhancement sample ($0.2 < E/p < 0.8$) and electron enhancement sample ($E/p < 0.2$ and $0.8 < E/p$).

$$A_N^{\pi} = \frac{A_N^{\pi,\mathrm{Sig}}(1+r_\pi) - A_N^{e,\mathrm{Sig}} r_\pi (1+r_e)}{1 - r_\pi r_e} \quad (1)$$

$$r_\pi \equiv \frac{N^{\pi,\mathrm{Bg}}}{N^{\pi,\mathrm{Sig}}} = \frac{A^e_{\mathrm{DATA}}}{A^e_{\mathrm{MC_{lumi\_scaled}}}} \times \frac{N^e_{\mathrm{MC_{lumi\_scaled}}}}{N^{\pi+e}_{\mathrm{DATA}}} \quad (2)$$

$A_N^{\pi,\mathrm{Sig}}$, $A_N^{e,\mathrm{Sig}}$ are asymmetry in the pion and electron enhanced sample, respectively. A^e_{DATA}, $A^e_{\mathrm{MC_{lumi\_scaled}}}$ are amplitude of the Gaussian centered at around one in the data and the luminosity scaled MC simulation, respectively. $N^{\pi,e}_{\mathrm{DATA}}$ and $N^{\pi,e}_{\mathrm{MC_{lumi\_scaled}}}$ are number of entries in the E/p distributions for the data and the luminosity scaled MC simulation in pion enhanced sample, respectively. Figure 1 shows E/p distribution of pion data and distributions of pion and electron in MC, respectively. Background fraction tended to increase with increasing p_T (Table 1). These values are used to calculate corrected A_N for charged pion.

*1 Department of Physics, Korea University

References
1) C. Aidala *et al.* (PHENIX Collaboration), Phys. Rev. D **95**, 112001 (2017).
2) T. B. Moon, Analysis Note No. 1268 in PHENIX Collaboration.

Improvement of the DCA resolution for PHENIX

G. Nukazuka,[*1] Y. Akiba,[*1] T. Hachiya,[*1,*2] and T. Todoroki[*3]

The PHENIX experiment accumulated data from the Relativistic Heavy Ion Collider at Brookhaven National Laboratory from 2001 to 2016 to study quark-gluon plasma and the spin structure of the nucleon.

The measurement of the distance of closest approach (DCA), which is the minimum distance from a beam collision point to the trajectory of a reconstructed particle, significantly suppress the background to heavy-flavor production measurements in a single electron channel. The vertex tracker (VTX)[1,2] consists of two layers with silicon pixel sensors and two layers with silicon strip sensors. The VTX in each of the west and east arms measures the trajectory, and the beam-beam counter determines the Z-coordinate of the beam collision point. DCA is calculated event by event using this information.

In 2016, PHENIX measured Au-Au collisions at the collision energy $\sqrt{s_{NN}} = 200$ GeV. One of the tasks needed to start the data summary tape production of the data is the alignment of the VTX detector. In the alignment process, we found strong linear correlations between DCA in the transverse direction with respect to the beam-axis and the residual in track fitting in the direction $s = r\Delta\phi$ (Fig. 1), where r is the distance from the beam axis and $\Delta\phi$ is the relative azimuth angle between hits and track projections on the VTX plane. The abscissa and ordinate axes represent the residual in the s direction and the transverse DCA, respectively. Only clusters with a transverse momentum p_T between 1.5 GeV/c and 2.0 GeV/c are shown in Fig. 1. Green points show average values over the DCA of a residual bin. A linear fitting shown with the red line estimates the correlation.

The correlation strength depends on p_T, the arm, and the VTX layer. The correlations can be used to correct the DCA value and to improve the DCA resolution. The corrected DCA distribution is narrower than the raw distribution (Fig. 2). The dark and light blue histograms represent the raw and corrected DCA distributions, respectively. Fittings with a Gaussian function to the raw DCA (red) and the corrected DCA (orange) yield DCA resolutions.

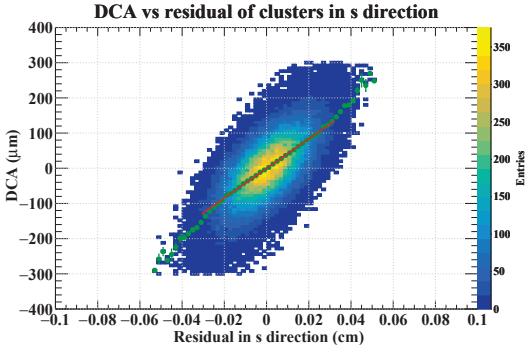

Fig. 1. Correlation between DCA and the cluster residual in the s direction in the innermost layer of the west arm with the selection $1.5 < p_T < 2.0$ GeV/c.

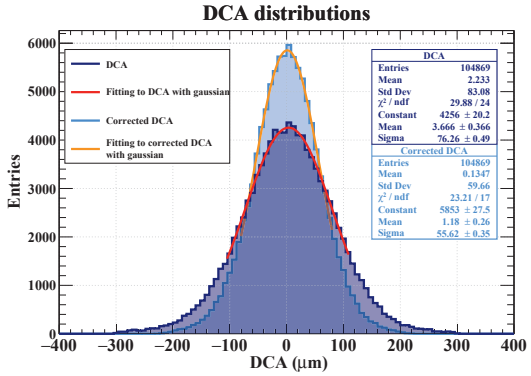

Fig. 2. DCA (dark black) and corrected DCA (light blue) distributions taken by the west arm with the selection $1.5 < p_T < 2.0$ GeV/c.

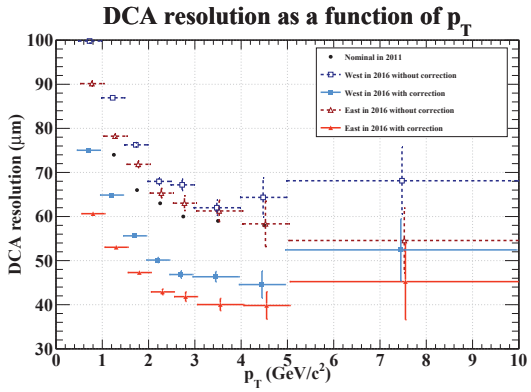

Fig. 3. DCA resolutions as a function of p_T. Points except black ones are slightly shifted for visibility.

Figure 3 shows DCA resolution as a function of p_T. The dark and light blue graphs are the raw and corrected DCA resolutions in the west arm, respectively, while the graphs in dark and light red are those in the east arm. The black points indicate the nominal DCA resolution for a run in 2011.[2] By applying all corrections, the resolution is improved by 15% to 35%.

In 2016, VTX was operated without one strip layer in the west arm owing to a beam accident in 2015. Under those severe conditions, a DCA resolution less than 50 μm was achieved in $p_T > 2.0$ GeV/c, while it was approximately 60 μm in 2011.[2]

This method may reduce background in the heavy flavor measurements because it is valid for data from other PHENIX runs, in principle.

*1 RIKEN Nishina Center
*2 Department of Mathematical and Physical Science, Nara Women's University
*3 Tomonaga Center for the History of the Universe, University of Tsukuba

References

1) K .Adcox *et al.*, Nucl. Instrum. Methods Phys. Res. A **499**, 469 (2003).
2) A. Adare *et al.*, Phys. Rev. C **93**, 034904 (2016).

Recent progress of polarized Drell–Yan experiment at Fermilab, SpinQuest (E1039)

K. Nagai,[*1] Y. Goto,[*2] Y. Miyachi,[*3] K. Nakano,[*2,*4] G. Nukazuka,[*2,*3] S. Sawada,[*2,*5] and T. -A. Shibata[*2,*6]

The SpinQuest (E1039) experiment aims to investigate the structure of the proton through the polarized fixed-target Drell–Yan process at Fermilab. In the Drell–Yan process, an antiquark ($\bar{q}$) in a hadron and a quark (q) in another hadron annihilate and decay into a lepton pair ($\ell + \bar{\ell}$) via a virtual photon (γ^*): $q + \bar{q} \to \gamma^* \to \ell + \bar{\ell}$. The Drell–Yan process is a suitable probe to study antiquarks in the proton because the antiquark is always involved in this process.

One of the most important unresolved puzzles of the proton is the "proton spin puzzle." The proton spin has been considered to be carried by the quark spins. However, the EMC experiment at CERN showed that the contributions of spins of quarks and antiquarks to the proton spin are much less than 100%.[1,2] Further experiments later confirmed that these contributions constitute only approximately 30% of the proton spin. Many possible contributions have been considered to solve this puzzle. One of them is the contribution of the orbital angular momenta (OAM) of quarks and antiquarks.

The Sivers function, which is a function of the Bjorken x and the transverse momentum of the quarks, can give some hints about the OAM contributions. The Sivers function is a kind of so-called transverse-momentum-dependent parton distribution function (TMD). It represents the correlation beween the transverse momentum of a quark and the spin of the parent hadron. If the Sivers functions of antiquarks are non-zero, then the contributions of the OAM of antiquarks to the proton spin are not zero. The Sivers function (f_{Sivers}) is proportional to the single-spin asymmtry (A_N): $f_{\mathrm{Sivers}} \propto A_N \propto (N_L - N_R)/(N_L + N_R)$, where N is the number of Drell–Yan dimuons and the subscripts L and R denote the direction of the virtual photon (left and right, respectively). Therefore, the Sivers functions can be experimentally accessed by measuring the single-spin asymmetry.

The semi-inclusive deep inelastic scattering (SIDIS) experiments have found the non-zero value of single-spin asymmetries of quarks. The contributions of quarks and antiquarks are not separated by SIDIS. The SpinQuest experiment will measure the single-spin asymmetry of $\bar{d}$ and $\bar{u}$ in the Drell–Yan process using a 120 GeV proton beam and polarized hydrogen and deuterium targets.

*1 High Energy Nuclear Physics, LANL
*2 RIKEN Nishina Center
*3 Faculty of Science, Yamagata University
*4 School of Science, Tokyo Institute of Technology
*5 Institute of Particle and Nuclear Studies, KEK
*6 College of Science and Technology, Nihon University

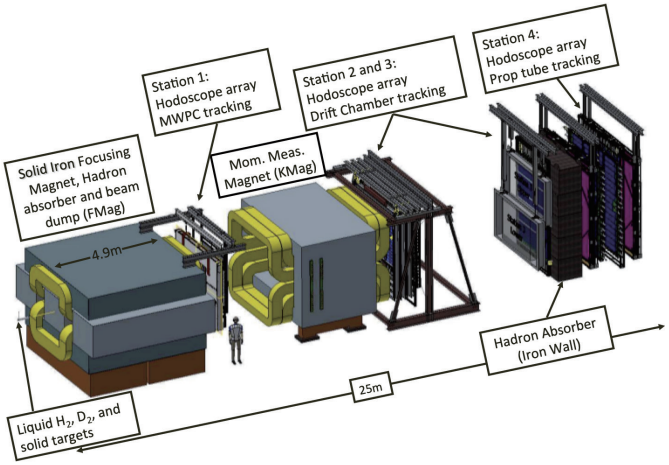

Fig. 1. The E906 spectrometer.[3] The target system has been renewed, and dark-photon hodoscopes are installed for SpinQuest.

The SpinQuest spectrometer is basically the same as the SeaQuest (E906) spectrometer[3] (Fig. 1). We are now updating it for the SpinQuest experiment. The major update is the installation of the polarized targets, as the E906 experiment used only unpolarized targets. The details have already been reported in the previous progress report.[4] We installed another set of hodoscope planes to detect potential dark photon events. Its optimization is underway.

The detectors are being repaired and updated. All the drift chambers for SpinQuest were used in the E906 experiment, but one of the drift chambers was damaged after the E906 experiment was completed. We have determined the cause of damage and have repaired the drift chamber. Some of the less efficient proportional tubes and hodoscopes have also been repaired. The optimization of their operation is now in progress.

The beam time is expected to begin in the middle of 2021. After two years of data aquisition, we expect to find an important piece in the proton spin puzzle.

References

1) J. Ashman *et al.* (EMC Collaboration), Phys. Lett. B **206**, 364 (1988).
2) J. Ashman *et al.* (EMC Collaboration), Nucl. Phys. B **328**, 1 (1989).
3) C. A. Aidala *et al.* (SeaQuest Collaboration), Nucl. Instrum. Methods Phys. Res. A **930**, 49 (2019).
4) Y. Miyachi *et al.*, RIKEN Accel. Prog. Rep. **53**, 81 (2020).

Measurement of J/ψ productions in $p+d$ and $p+p$ at SeaQuest

K. Nakano,[*1,*2] Y. Goto,[*2] Y. Miyachi,[*3] K. Nagai,[*4] S. Sawada,[*2,*5] and T. -A. Shibata[*2,*6]
for the E906/SeaQuest Collaboration

The partonic structure of the proton is one of the most vital topics in hadron physics. The SeaQuest (E906) experiment at the Fermi National Accelerator Lab (FNAL) in USA is aimed at measuring the flavor asymmetry of light antiquarks in the proton, $\bar{d}(x)/\bar{u}(x)$, at large Bjorken x ($\gtrsim 0.3$). It utilizes the 120-GeV proton beam from the FNAL Main Injector and targets of liquid hydrogen and liquid deuterium. The preliminary result of $\bar{d}(x)/\bar{u}(x)$ using the Drell–Yan process has been reported.[1)]

The data recorded by SeaQuest include J/ψ productions. The $p+d/p+p$ ratio of J/ψ cross sections is sensitive to distributions of both antiquarks and gluons through the $q\bar{q}$ annihilation ($q\bar{q} \to J/\psi$) and gluon fusion ($gg \to J/\psi$), as shown in Fig. 1. The $q\bar{q}$ annihilation dominates at large Feynman x ($x_F \gtrsim 0.4$) where SeaQuest can measure. Therefore, this measurement is expected to provide additional constraints on parton distribution functions (PDFs), particularly of antiquarks at the middle Bjorken x. The systematic uncertainties of the measurement are largely reduced by taking the ratio of the cross sections.

Muon pairs from J/ψ decays were detected by the SeaQuest spectrometer.[2)]

SeaQuest acquired physics data from 2013 to 2017 to record 1.4×10^{18} beam protons on targets. The first half of the recorded data were analyzed. Figure 2 shows the distributions of the invariant mass of muon pairs. The yield of J/ψ was evaluated based on the fraction of the J/ψ component in this fit. The detection efficiency of J/ψ was corrected by simulation. The beam intensity was measured with a secondary-electron emission monitor (SEM) for normalizing the $p+d$ and $p+p$ cross sections.

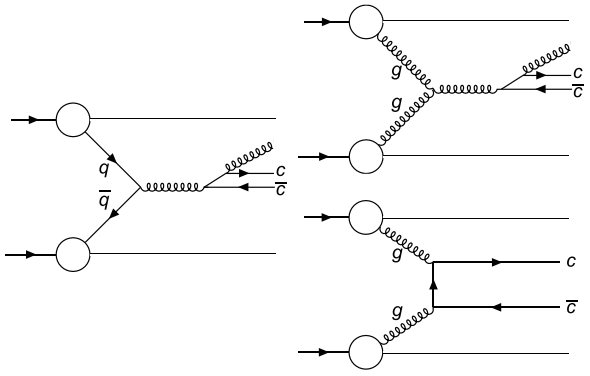

Fig. 1. Leading diagrams of J/ψ productions.

*1 School of Science, Tokyo Institute of Technology
*2 RIKEN Nishina Center
*3 Faculty of Science, Yamagata University
*4 High Energy Nuclear Physics, Los Alamos National Lab
*5 Institute of Particle and Nuclear Studies, KEK
*6 College of Science and Technology, Nihon University

Figure 3 shows the $p+d/p+p$ ratio of the J/ψ cross sections as a function of x_F. The systematic uncertainty of the SeaQuest result arises from the modeling of the combinatorial background and the relative luminosity normalization between targets. The experimental result is consistent with the two predictions as shown in the figure. The analysis including the latter half of the recorded data is underway.

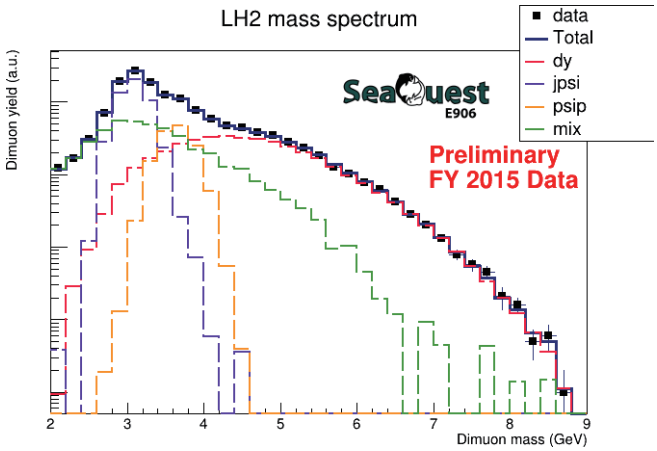

Fig. 2. Distributions of invariant mass of muon pairs. The points are experimental data obtained by SeaQuest. They were fitted by the components of the four processes, namely the Drell-Yan process, J/ψ production, ψ' production, and combinatorial background. The sum of the four components is represented by the thick line. :

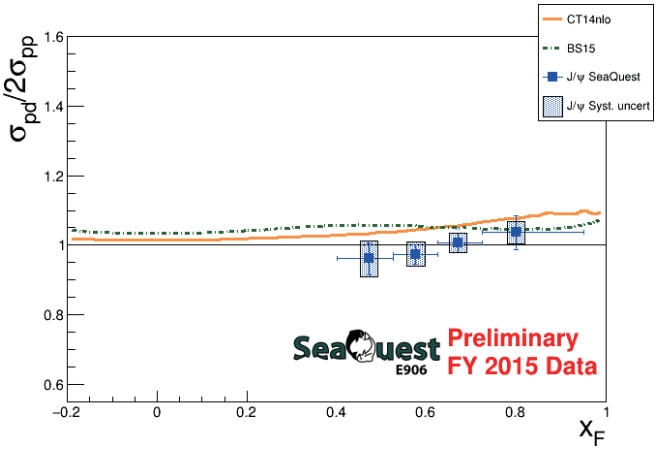

Fig. 3. Cross-section ratio vs. x_F. The points are experimental data obtained by SeaQuest. The two lines are predictions[3)] by the color evapolation model with different PDF sets.

References

1) K. Nagai *et al.*, RIKEN Accel. Prog. Rep. **52**, 86 (2019).
2) C. A. Aidala *et al.*, SeaQuest, Nucl. Instrum. Methods Phys. Res. A **930**, 49 (2019).
3) M. L. Mangano *et al.*, Nucl. Phys. B **405**, 507 (1993).

Expression of interest for EIC-Japan

Y. Goto,[*1] Y. Akiba,[*1] I. Nakagawa,[*1] and R. Seidl[*1] for the EIC-Japan Group

The Electron-Ion Collider (EIC) is a great research opportunity for Japan, and we are working to form a Japanese group (EIC-Japan). We will form a high-energy accelerator-based experimental group in the field of both nuclear and particle physics. In response to the "Call for Expressions of Interest (EOIs) for Potential Cooperation on the EIC Experimental Program" by BNL and JLab, we submitted an EOI by the EIC-Japan group in November, 2020. The EOI is non-binding, and its purpose is to guide expectations and better understand the potential EIC experimental equipment scope.

In Japan, the Science Council of Japan (SCJ) developed a master plan for large-scale research programs in academia (Master Plan 2020) in 2019–2020. The EIC was recognized as an important international collaborative research project with a long-term research plan by the Future Planning Committee of the Committee on Nuclear Physics, and it was proposed to the Master Plan. Consequently, the EIC was selected as an academic major research project although it was not yet selected as a priority project in the Master Plan 2020.

The EIC-Japan group plans to design and construct forward detectors of the EIC detector, especially calorimeters, to lead the study on forward and very forward physics. Forward detectors are one of the most important detectors for precisely reconstructing certain events of the deep inelastic scattering (DIS) process, which is the basis of all research at the EIC. We can precisely determine the spin and internal orbital motion of partons in the nucleon, which is still poorly understood, by measuring the forward and most forward jets, hadrons, photons, and electrons and by studying their correlations. In particular, the contribution of gluons, sea quarks, and orbital angular momentum to the proton spin remains a mystery. In addition, our understanding of the most forward events is expected to greatly enhance the development of QCD-based event generators. Further, this will greatly contribute to eliminating uncertainties in other high-energy particle experiments and cosmic ray observations.

We participated in the development of the forward hadron calorimeter,[1] which is essential for forward jet reconstruction and hadron energy measurements, as well as triggering. Designing and developing the calorimeter is a joint project with the EIC generic detector R&D group eRD1 and the STAR upgrade project. A prototype calorimeter developed as the STAR forward calorimeter comprises 38 layers of iron absorbers and plastic scintillator plates. A wavelength-shifting (WLS) plate provides uniform and efficient light collection from all scintillation tiles along the depth of the tower. The light from the WLS plate is measured with SiPMs. Since the energy resolution of this detector is $70\%/\sqrt{E(\mathrm{GeV})}$ with an additional constant term, the one for the EIC requires higher energy resolution.

We proposed the development of a zero-degree apparatus in the EIC experiment,[2] and it has been approved as eRD27 this year. Zero degree detectors serve critical roles for a number of important physics topics at the EIC. We study the requirements and technologies of zero-degree detectors, and we develop a position-sensitive zero-degree calorimeter (ZDC). In this program, we will conduct 1) a photon detector study at a low energy <300 MeV, cooperating with eRD1 for crystal and glass scintillators; 2) a prototype study of ZDC with position sensitivity, with the ALICE-FoCal technology and the LHC-ZDC technology with fused silica; and 3) a radiation hardness study of scintillators.

Subsequently, in addition to the proposals in the master plan, we have expanded our activities as a Japanese group to include a group interested in building a silicon tracking detector. The team is open to new collaborators. Heavy flavor quarks are highlighted at the EIC as the ideal probe to study open questions in QCD, such as mass and flavor dependence of energy loss, fragmentation and hadronization modification in a nuclear medium, nuclear parton distributions, and so on. Silicon sensor detectors are the key technology employed for heavy flavor detection by observing their decay vertex precisely. The performance of silicon sensors thus plays a crucial role in pursuing the research in heavy flavor physics at a satisfactory level. We propose to apply a silicon sensor based on silicon-on-insulator monolithic pixel (SOIPIX) detector technology[3] that has been developed by the KEK group. SOIPIX has demonstrated the world's best tracking resolution of 0.680 ± 0.006 μm in a silicon detector using 120 GeV FNAL's test beam. Further SOIPIX is employed as the inner vertex detector of 4π silicon hybrid detector proposed by ANL and BNL collaborators.

References

1) Y. Goto *et al.*, RIKEN Accel. Prog. Rep. **52**, 87 (2019).
2) Y. Goto *et al.*, RIKEN Accel. Prog. Rep. **53**, 82 (2020).
3) Y. Arai *et al.*, Nucl. Instrum. Methods Phys. Res. A **636**, S31–S36 (2011).

*1 RIKEN Nishina Center

Semi-inclusive deep inelastic scattering at the Electron Ion Collider

R. Seidl*1

The electron-ion collider, EIC, will be a newly build accelerator at Brookhaven National Laboratory to collide polarized electrons with polarized protons and light ions, as well as unpolarized heavier nuclei. It will be the perfect place to study the strong interaction with collision energies between $\sqrt{s} = 29$ to 141 GeV and luminosities that are expected to be three orders of magnitude higher than achieved at the HERA ring in Germany. In early 2020 the US DOE office of science acknowledged the EIC officially as a project that will be built in the next 10 years. A large community of more than 1000 members has already formed with interest in the EIC, organized as the EIC user group.[1] Within this group a call for a comprehensive Yellow report was formed that updates earlier publications on the physics goals[2,3] and closely looks at the technological options for EIC detectors to have in order to fulfill these physics goals. The main process at the EIC is deeply inelastic lepton-nucleon (or nucleus) scattering, DIS, in which only the scattered lepton is detected. The kinematic variables x, which is the momentum fraction of the nucleon a parton has, and the momentum transfer of the process Q^2 can be extracted. Typically scales of $Q^2 > 1$ GeV^2 are considered as in that case the extracted cross sections and spin asymmetries can be factorized into hard scattering processes between partons that can be described by perturbative QCD and nonperturbative parton distribution functions, PDFs. PDFs describe the distribution of quarks and gluons within the nucleon as a function of the momentum fraction x at a given scale Q^2. In semi-inclusive DIS at least one final state hadron is also detected and the type, charge, momentum fraction z and transverse momentum relative to the boson mediating the lepton-parton scattering informs on the flavor, spin and intrinsic transverse momentum of the struck parton with the help of fragmentation functions. These semi-inclusive DIS processes cover most of the main physics goals of the EIC. For example, the spin contribution by individual sea quark flavors to the total nucleon spin can be probed this way. Also the three-dimensional momentum picture of the nucleon can be obtained via SIDIS measurements and the closely related Sivers function and the tensor charges for quarks, sea-quarks and gluons (gluons only for the Sivers function).

As an example of the work by the SIDIS group of the yellow report, the four-dimensional coverage of SIDIS hadrons was studied at all envisioned collision energies taking into account a potential detector configuration ranging from $-3.5 < \eta < 3.5$ with varying particle identification (PID) ranges depending on suitable technologies. Figure 1 displays the coverage for pions. One can see that at intermediate x and Q^2 the maximum PID momentum of only 6 GeV limits the expected coverage while elsewhere the coverage is sufficient. This is caused by the fact that at central rapidities no compact PID detector can cover a larger momentum range. Using these detector coverages and realistic smearing, pseudo-data was created resembling actual measurements extrapolated to about 10 fb^{-1}, which corresponds to about a year of EIC running. This pseudo-data was then used in global fits by theorists to extract the impact on various physics goals of the EIC such as the tensor charges that potentially relates to physics beyond the standard model,[4] the Sivers function,[5] as well as the expected scale dependence of the functions that relate to the three-dimensional momentum picture of the nucleon. The Yellow Report is now publicly available[6] and provides the basis for the ongoing review process of the DOE.

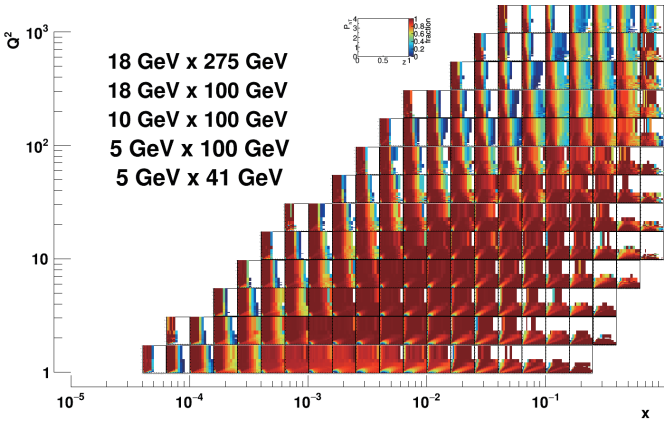

Fig. 1. Particle identification acceptance ratios for pions from semi-inclusive events at the EIC as a function of momentum fraction z and transverse momentum P_T, in bins of x and Q^2.

References

1) http://www.eicug.org/ .
2) A. Accardi *et al.*, Eur. Phys. J. A **52**, 268 (2016) (arXiv:1212.1701 [nucl-ex]).
3) D. Boer *et al.*, arXiv:1108.1713 [nucl-th].
4) L. Gamberg, Z. B. Kang, D. Pitonyak, A. Prokudin, N. Sato, R. Seidl, Phys. Lett. B **816**, 136255 (2021).
5) A. Vladimirov, R. Seidl, in preparation.
6) R. Abdul Khalek *et al.*, arXiv:2103.05419 [physics.ins-det].

*1 RIKEN Nishina Center

Bus-extender development for sPHENIX INTT detector

T. Hachiya,[*1,*4] Y. Akiba,[*1] D. Cacace,[*2] K. Cheng,[*3] S. Hasegawa,[*5] D. Imagawa,[*9] H. Imai,[*9] T. Kondo,[*6] C. Kuo,[*3] H. -S. Li,[*7] R. -S. Lu,[*8] E. Mannel,[*2] C. Miraval,[*2] M. Morita,[*4] I. Nakagawa,[*1] Y. Namimoto,[*4] S. Nishimori,[*4] R. Nouicer,[*2] G. Nukazuka,[*1] R. Pisani,[*2] M. Shibata,[*4] C. Shih,[*3] M. Stojanovic,[*7] W. -C. Tang,[*3] and X. Wei[*7]

sPHENIX is a major upgrade of the PHENIX experiment at RHIC, and it aims to study the properties of quark-gluon plasma by measuring jet and upsilon productions and their modifications. An intermediate tracker (INTT) is a silicon strip barrel detector for sPHENIX.[1)] A bus-extender is a special cable used for signal transfer between the INTT detector and read-out electronics placed at least 120 cm away from the INTT. The bus-extender has the following requirements: (1) flexibility, (2) length, (3) high-density signal line (128 lines/5 cm), and (4) high-speed signal transfer (by LVDS).

We developed a bus-extender in the past three years.[2)] We found that the prototype of our 120 cm-long bus-extender exhibits good electrical performance in terms of signal loss and reflection. Some issues were found in the prototype. The first issue is the formation of the through hole. The bus-extender comprises a four-layer flexible printed cuicuit, and the through hole is used to connect the signal lines between layers. We found that the through hole had a nodule structure, which can cause instability during long-term use. Figure 1 shows the layer structure of the bus-extender (left) and the cross section view of the through hole (middle); the nodule structure is formed in the through hole. We attempted the production procedure by changing the drilling methods and Cu-plating methods to remove the nodules; however, they still existed. We changed the glue used to laminate the multiple layers; this new glue works effectively. Figure 1 (right) shows the cross-section of the hole with the new glue.

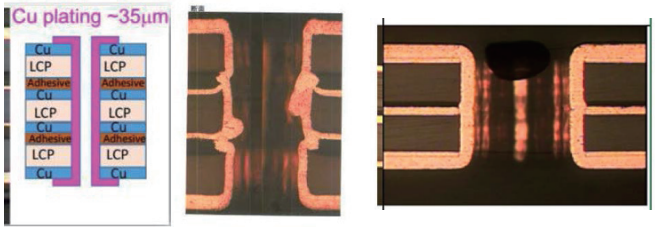

Fig. 1. (left) Layer structure of the bus-extender. (middle) Cross section of the through hole made by the original glue; nodules are formed. (right) Cross section of the hole with the new glue.

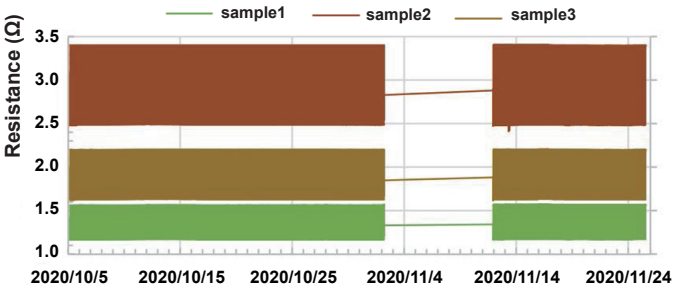

Fig. 2. Result of the thermal cycling test (1000 cycles in 50 days).

We performed a thermal cycling test to test its long-term stability. The test employs the application of high (75°C) and low (−15°C) temperatures for 30 min each; the temperature are changed at short time intervals (5 min). We repeated this test for 1000 cycles. We prepared three samples and measured the resistance of the through holes to evaluate the stability. These samples had 400, 600, and 1000 through holes that are daizy chained. During the test, the polymer of the sample expands and shrinks because of changes in temperature. This results in cracks in the through hole. If the through holes have cracks, the resistance becomes a large value. Figure 2 shows the result of the thermal cycling test. The resistances changes repeatedly within a valid range because of the changes in temperature for the entire periods. This indicates that the through hole has sufficent stability.

The second issue is that the peel strength of the prototype is about 4 N. This value is very small compared with the standard FPC (20 N). We found that the new glue improved the peel strength to 30–40 N. The results are summized in Ref. 3).

The radiation hardness and yield rate of the bus-extender are also studied. The current status of the studies are summarized in the Refs. 4, 5).

We successfully developed the bus-extender, and we plan to start mass production in 2021.

*1 RIKEN Nishina Center
*2 Physics Department, Brookhaven National Laboratory
*3 Department of Physics, National Central University
*4 Department of Mathematical and Physical Science, Nara Women's University
*5 Japan Atomic Energy Agency
*6 Tokyo Metropolitan Industrial Technology Research Institute
*7 Department of Physics and Astronomy, Purdue University
*8 Department of Physics, National Taiwan University
*9 Department of Physics, Rikkyo University

References

1) I. Nakagawa *et al.*, in this report.
2) T. Hachiya *et al.*, in this report.
3) M. Morita *et al.*, in this report.
4) H. Imai *et al.*, in this report.
5) D. Imagawa *et al.*, in this report.

5. Hadron Physics (Theory)

Non-global logarithms in hadron collisions at $N_c = 3$†

Y. Hatta*1,*2 and T. Ueda*3

Recently, there have been a lot of activities in developing Monte Carlo algorithms for simulating parton showers beyond the large-N_c (leading-N_c) approximation where $N_c = 3$ is the number of colors. Traditionally, in most event generators, the large-N_c approximation has been the only practical way to keep track of the color indices of many partons involved. Among other observables, the finite-N_c corrections are particularly important but difficult to quantify for the so-called non-global observables[1] which are sensitive to the wide-angle emission of soft gluons in restricted regions of phase space. In Ref. 2), we have developed a framework to resum non-global logarithms at $N_c = 3$ by improving and completing the earlier attempt.[3] Numerical results are so far available only for two observables in e^+e^- annihilation: interjet energy flow[2] and the hemisphere jet mass distribution.[4] In this work we demonstrate that our approach can be practically applied to hadron collisions where it is probably most useful. We do so by explicitly computing the rapidity gap survival (or 'veto') probabilities in Higgs plus dijet production $pp \to HjjX$. The relevant logarithms are of the form $(\alpha_s \ln Q/E_{out})^n$ where Q is the hard scale (Higgs mass or jet transverse momentum) and $E_{out} \ll Q$ is the veto scale.

Consider quark-quark scattering $q_i(p_1)q_j(p_2) \to q_k(p_3)q_l(p_4)H$ where $i,j,k,l = 1,2,3$ are color indices. The outgoing quarks with momenta p_3, p_4 are back-to-back and detected as two jets in the forward and backward directions. We are interested in the probability that the energy emitted in the central rapdiity region $\pi - \theta_{in} > \theta > \theta_{in}$ is less than E_{out}.

The leading-order amplitude can be written as

$$\mathcal{M}_{ijkl} = M_1 \delta_{ki}\delta_{lj} + M_8 t^a_{ki} t^a_{lj}. \tag{1}$$

where $M_{1,8}$ are amplitudes in the singlet and octet channel. We dress up (1) by attaching soft gluons to external legs in the eikonal approximation. We then square it and average over color indices to get the cross section

$$M_1^2 P^1_{qq} + \frac{N_c^2 - 1}{4N_c^2} M_8^2 P^8_{qq}. \tag{2}$$

$P^{1,8}$ are the gap survival probabilities in the singlet and octet channels.

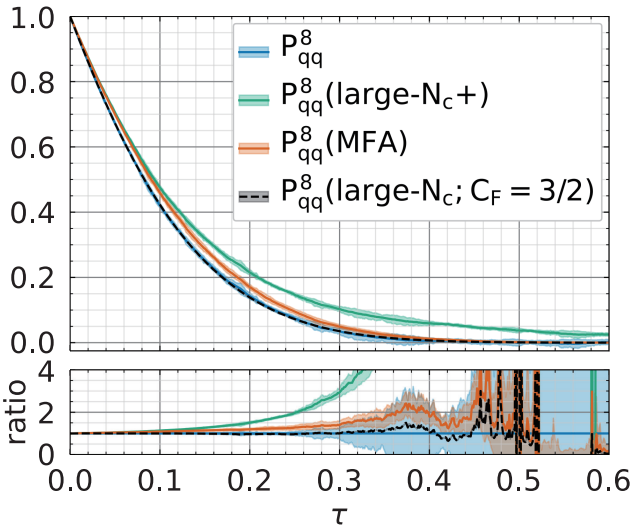

Fig. 1. Gap survival probability in $qq \to qqH$, color-octet channel.

$$P^1_{qq} = \frac{1}{N_c^2}\left\langle \mathrm{tr}(U_3 U_1^\dagger)\mathrm{tr}(U_4 U_2^\dagger)\right\rangle, \tag{3}$$

$$P^8_{qq} = \frac{\left\langle \mathrm{tr}(U_3 U_2^\dagger)\mathrm{tr}(U_4 U_1^\dagger) - \frac{\mathrm{tr}(U_3 U_1^\dagger)\mathrm{tr}(U_4 U_2^\dagger)}{N_c^2}\right\rangle}{N_c^2 - 1}, \tag{4}$$

where U_α is the fundamental Wilson line in the direction of α. We compute these probabilities as a function of

$$\tau = \frac{\alpha_s}{\pi} \ln \frac{P_T}{E_{out}}. \tag{5}$$

The result for P^8_{qq} for $\theta_{in} = \pi/3$ is shown in Fig. 1 together with its various approximations. Surprisingly, we find a very good agreement with the large-N_c approximation in which P is simply computed from the solution of the Banfi-Marchesini-Smye equation.[5] A similar conclusion is reached for other channels including gluons in the initial state. While we do not fully understand the reason of this agreement at the moment, if it turns out to be a robust feature, it is good news because one can approximately get full-N_c results in hadron collisions using the known large-N_c frameworks.[1,5]

References
1) M. Dasgupta, G. Salam, Phys. Lett. B **512**, 323 (2001).
2) Y. Hatta, T. Ueda, Nucl. Phys. B **874**, 808 (2013).
3) H. Weigert, Nucl. Phys. B **685**, 321 (2004).
4) Y. Hagiwara, Y. Hatta, T. Ueda, Phys. Lett. B **756**, 254 (2016).
5) A. Banfi, G. Marchesini, G. Smye, J. High Energy Phys. **08**, 006 (2002).

† Condensed from the article in Nucl. Phys. B **962**, 115273 (2021)

*1 RIKEN Nishina Center
*2 Physics Department, Brookhaven National Laboratory
*3 Faculty of Science and Technology, Seikei University

Verification of the QED tenth-order electron $g-2$: Diagrams without a fermion loop

A. Hirayama[*1,*2] and M. Nio[*1,*2]

A comparison between the measured value of the electron anomalous magnetic moment and its theoretical prediction is the most stringent test of the quantum electrodynamics (QED) and, hence, the standard model (SM) of elementary particles. The measurement was performed by trapping a single electron in a cylindrical Penning trap. The deviation of the g value of the electron from Dirac's prediction, $a_e = (g-2)/2$, was determined as[1)]

$$a_e[\text{expt.}] = 0.001\ 159\ 652\ 180\ 73\ (28)\ [0.24\ \text{ppb}]. \quad (1)$$

A new experiment aiming at a 20-fold improvement in the uncertainty is in progress.

To match the precision of measurement, theory must take into account small but non-negligible contributions from hadronic and electroweak interactions. The QED contribution is dominant and required up to the tenth order of perturbation theory because $(\alpha/\pi)^5 \sim 6.8\times10^{-14}$, where α is the fine-structure constant. By now, all terms up to the eighth order have been firmly established. The tenth-order term was obtained only by one group and has not yet been cross-checked.[2)] To theoretically predict a_e, a value of α is needed. Recently, two very precise values of α became available, both of which were determined using atom interferometry. The Cs[3)] and Rb[4)] atom experiments yielded

$$\alpha^{-1}(\text{Cs}) = 137.035\ 999\ 046\ (27) \quad [0.20\ \text{ppb}], \quad (2)$$
$$\alpha^{-1}(\text{Rb}) = 137.035\ 999\ 206\ (11) \quad [81\ \text{ppt}], \quad (3)$$

respectively. The difference is about $5.5\,\sigma$. A new Cs experiment has already started to reveal one more digit of α. We then have two SM predictions of a_e:

$$a_e[\text{theory} : \alpha(\text{Cs})] = 0.001\ 159\ 652\ 181\ 62\ (23), \quad (4)$$
$$a_e[\text{theory} : \alpha(\text{Rb})] = 0.001\ 159\ 652\ 180\ 265\ (94), \quad (5)$$

where the uncertainty is solely governed by that from α in both cases. Note that the discrepancy between measurement and theory is positive in sign for α(Cs), while it is negative for α(Rb).

Considering the accuracy required for future experiments, the tenth-order QED term must be carefully reexamined. A total of 12,672 Feynman vertex diagrams contributes to the tenth-order term. Among them, 6,354 diagrams without a fermion loop form a gauge-invariant set called Set V. This is the most difficult set to evaluate, and the uncertainty of the QED contribution to a_e entirely originates from Set V.

*1 RIKEN Nishina Center
*2 Department of Physics, Saitama University

So far, two independent numerical evaluations of Set V have been executed by two groups.[5,6)] There is, however, 4.8 σ tension between the results. The difference is still negligible for the current precision of a_e but will certainly become crucial in the near future.

In Ref. 5), numerical integration was performed on 389 self-energy-like diagrams each, which are concatenations of nine vertex diagrams via the Ward-Takahashi identity. In contrast, 3,213 integrals derived from vertex diagrams were evaluated in Ref. 6). Because the renormalization schemes used to construct integrands are different, the numerical result of one integral of the former does not coincide with the sum of the corresponding nine integrals of the latter. The direct comparison of numerical results of integrals is nontrivial.

The gap can be filled by calculating the difference in vertex renormalization constants, δL, of two renormalization schemes for every vertex diagram. The difference in numerical results of Set V integrals can be expressed in terms of these δL's and lower-order contributions of the anomalous magnetic moment.

We numerically computed all the necessary δL's that are derived from 1 second-, 4 fourth-, 28 sixth-, and 269 eighth-order vertex diagrams. The computation took approximately 120,000 hours in total. This is a small and quick calculation compared with the numerical evaluation of Set V integrals.

Diagram-by-diagram comparison was performed for the fourth-, sixth-, and eighth-order cases, and our verification method worked very well. For the tenth order, we examined numerical results representing the 2,232 Set V vertex diagrams that have no self-energy subdiagram and correspond to 135 integrals of self-energy-like diagrams. No inconsistency was found in any of the 135 integrals between Refs. 5) and 6). The investigation of the remaining 4,122 diagrams that have at least one self-energy subdiagram is in progress and will be completed soon.

We thank Prof. T. Aoyama and Prof. M. Hayakawa for useful discussions. This work is supported in part by JSPS KAKENHI 16K95338, 19K21872, and 20H05646. Numerical calculations were conducted on HOKUSAI-BigWaterfall of RIKEN.

References

1) D. Hanneke *et al.*, Phys. Rev. Lett. **100**, 120801 (2008).
2) T. Aoyama *et al.*, Phys. Rev. Lett. **109**, 111807 (2012).
3) R. H. Parker *et al.*, Science **360**, 191–195 (2018).
4) L. Morel *et al.*, Nature **588**, 61–65 (2020).
5) T. Aoyama *et al.*, Phys. Rev. D **97**, 036001 (2018).
6) S. Volkov, Phys. Rev. D **100**, 096004 (2019).

6. Particle Physics

Time development of conformal field theories associated with L_1 and L_{-1} operators†

T. Tada*1,*2

An unconventional time development of the two-dimensional conformal field theory (CFT) induced by the L_1 and L_{-1} operators was studied by employing the formalism previously developed in a study of sine-square deformation (SSD).[1] Consequently, we found that the retention of the Virasoro algebra naturally leads to the presence of a cut-off near the fixed points (shown as gray blobs in Fig. 1). The introduction of a scale by the cut-off may appear at odds with the conformal symmetry; however, it is essential to derive the formula for entanglement entropy.[2,3]

The SSD of two-dimensional CFT[4] has been explained with a formalism developed in Refs. 5, 6), in which unconventional time developments, other than the radial time development, were utilized to study CFTs. One such time development suited with the study of SSD was named "dipolar quantization." Further generalization was investigated by Wen, Ryu and Ludwig,[7] where the entanglement Hamiltonian and other interesting deformations of two-dimensional CFT were studied.

In this study, we visit the following particular time development, which was not studied in Ref. 6):

$$L_1 + L_{-1} + \bar{L}_1 + \bar{L}_{-1}, \tag{1}$$

instead of ordinary $L_0 + \bar{L}_0$. We found that this time-development corresponds to the entanglement Hamiltonian as discussed in Ref. 7).

The significance of the operator (1) can be understood in the following way. The L_0, L_1, and L_{-1} operators constitute $sl(2,\mathbf{R})$ algebra. A linear combination of these operators,

$$x^{(0)}L_0 + x^{(1)}L_1 + x^{(-1)}L_{-1}, \tag{2}$$

can be mapped to

$$x'^{(0)}L_0 + x'^{(1)}L_1 + x'^{(-1)}L_{-1}, \tag{3}$$

by the adjoint action of $sl(2,\mathbf{R})$; however, the following quadratic form of the coefficients, which is known as the quadratic Casimir element, remains the same:

$$c^{(2)} \equiv \left(x^{(0)}\right)^2 - 4x^{(1)}x^{(-1)}. \tag{4}$$

Using this $c^{(2)}$, the general linear combinations (2) can be categorized into three distinctive groups that are not accessible from each other by the $sl(2,\mathbf{R})$ action. Typical operators for each group are: L_0 represents $c^{(2)} > 0$, $L_0 - \frac{1}{2}(L_1 + L_{-1})$ represents $c^{(2)} = 0$, and $L_1 + L_{-1}$ represents $c^{(2)} < 0$. Thus, we could investigate the $L_1 + L_{-1}$ operator by applying the formalism developed in Refs. 5, 6) and demonstrate that the aforementioned three cases, including $L_1 + L_{-1}$, can be studied in a unified manner.

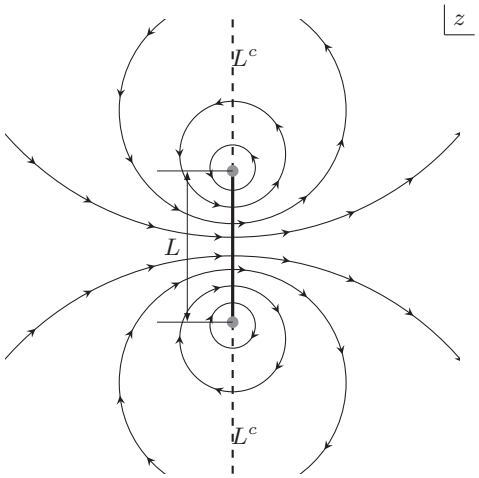

Fig. 1. Flow of time t can be considered to begin at a section of space with length L (solid line). The remaining space, including infinity, is depicted as a dashed line and denoted by L^c. The setup corresponds to the entanglement entropy for the segment with length L.

References
1) A. Gendiar, R. Krcmar, T. Nishino, Prog. Theor. Phys. **122**, 953 (2009), Erratum: [Prog. Theor. Phys. **123**, 393 (2010)].
2) C. Holzhey, F. Larsen, F. Wilczek, Nucl. Phys. B **424**, 443 (1994).
3) H. Casini, M. Huerta, R. C. Myers, J. High Energy Phys. **1105**, 036 (2011).
4) H. Katsura, J. Phys. A **45**, 115003 (2012).
5) N. Ishibashi, T. Tada, J. Phys. A **48**, 315402 (2015).
6) N. Ishibashi, T. Tada, Int. J. Mod. Phys. A **31**, 1650170 (2016).
7) X. Wen, S. Ryu, A. W. W. Ludwig, Phys. Rev. B **93**, 235119 (2016).

† Condensed from the article in J. Phys. A Math Theor. **53**, 255401 (2020)

*1 RIKEN Nishina Center
*2 RIKEN iTHEMS

Study of Lorentzian sine-square deformed CFT†

X. Liu[*1,*2] and T. Tada[*2,*3]

The concept of sine-square deformation (SSD) was first introduced into two-dimensional conformal field theory (2D CFT) in Ref. 1). In previous studies, we found that the introduction of SSD in 2D CFT defines a new time translation generated by the SSD Hamiltonian.[1)] The SSD CFT processes the Virasoro algebra with a continuum index.[2)] Further, inspired by the discovery in SSD CFT, we generalized this study to CFT using more general modular Hamiltonians, and found three different types of Virasoro algebra in the Euclidean CFT.[3)] In this study, we extend our analysis to Lorentzian CFT. To consider CFT in the Minkowski spacetime, the universal covering space of the Minkowski spacetime must be introduced. Generally, a spacetime is mapped to a Penrose diamond on the cylinder, which is the universal covering of the Penrose diamond. The time translation is defined on the universal covering using the Luscher-Mack Hamiltonian $\frac{\hat{P}_0+\hat{K}_0}{2}$.[4)] Consider the worldline for a particle in a Penrose diamond; if we perform a special conformal transformation, the worldline may cross the boundary of the Penrose diamond and move on to the next patch. This problem can be solved if the time translation for the CFT is defined to be confined in a single Penrose diamond, implying that the CFT becomes effectively non-compact under such time translations. This can be achieved by applying SSD in Lorentzian CFT; the non-compactness of CFT can be observed from the continuum index of the Virasoro Algebra.[5)] We performed similar analysis as that in the Euclidean signature.[2,3)] Next, we investigate the three different cases with Hamiltonians having plus, minus, and zero values in the quadratic Casimir element. We select three examples from the three cases:

- The Luscher Mack Hamiltonian $\frac{\hat{P}_0+\hat{K}_0}{2}$,
- The Rindler Hamiltonian $\hat{M}_{01}$,
- The Naive Hamiltonian $\hat{P}_0$.

We define different mode decompositions of the energy-stress tensor with 0th modes corresponding to each Hamiltonian in the three cases. By applying the commutation relation of the energy-stress tensor, we can obtain three types of Virasoro Algebra:

- Luscher Mack type: The Virasoro generators in this type must bear discrete indices; otherwise, ambiguities are observed in the generators.
- Rindler type: The Virasoro generators in this type must bear discrete indices to remove the ambiguities and preserve the local conformal symmetry. There is UV divergence in the central extensional term in the Virasoro Algebra.
- The Naive type: The Virasoro generators can have continuum indices. This corresponds to the SSD case, where the theory is effectively non-compact. Thus, the time translation is confined inside a single Penrose diagram. See Fig. 1.

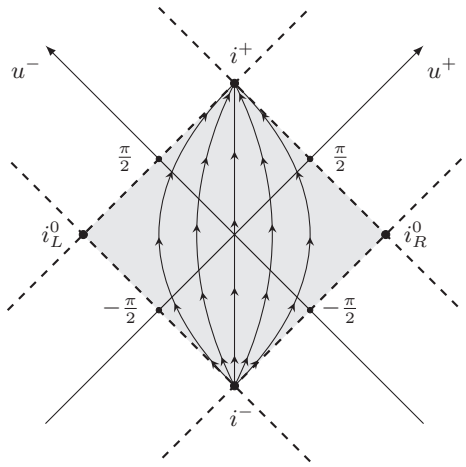

Fig. 1. The universal covering space of the Penrose diamond (shaded region) is charted by u^+ and u^-. While the conformal symmetry is represented using the entire covering space, the time flow by P_0 (arrowed line) is confined within a single Penrose diamond.

The conformal invariance requires the introduction of the universal covering space; moreover, occasionally, the Lorentzian CFT is considered to be unphysical owing to the existence of a closed time-like curve. In this study, our analysis ensured that there is no closed time-like curve if the Naive Hamiltonian is selected instead of the Luscher-Mack Hamiltonian.[5)]

References
1) H. Katsura, J. Phys. A **45**, 115003 (2012).
2) N. Ishibashi, T. Tada, J. Phys. A **48**, 315402 (2015).
3) T. Tada, J. Phys. A **53**, 255401 (2020).
4) M. Luscher, G. Mack, Commun. Math. Phys. **41**, 203 (1975).
5) X. Liu, T. Tada, Prog. Theor. Exp. Phys. **2020**, 061B01 (2020).

† Condensed from the article in Prog. Theor. Exp. Phys. **2020**, 061B01 (2020)

*1 Department of Physics, University of Tokyo
*2 RIKEN Nishina Center
*3 RIKEN iTHEMS

Empirical formulas for the standard-model parameters

Y. Akiba*1

We report empirical formulas for the parameters of the standard-model. Table 1 lists the formulas for the mass of the charged leptons (e, μ, τ), three neutrinos (ν_1, ν_2, ν_3), six quarks (u, c, t, d, s, b), and gauge bosons (W, Z), and Higgs boson (H). The formulas yield the masses in terms of the Planck mass

$$M_{pl} = 1.220910 \pm 0.000029 \times 10^{19} \text{ GeV}.$$

The last column of the table presents the relative difference $|m_p^c/m_p^m - 1|$ of the calculated value m_p^c and the measured value m_p^m for particle p. Table 2 compares the mass values from the formulas and neutrino oscillation data. Table 3 lists the formulas for the Cabibbo-Kobayashi-Maskawa quark mixing parameters. Table 4 lists the formulas for the neutrino-mixing angles. Table 5 lists the formulas for the fine structure constant α and the strong coupling constant α_s. These formulas yield 24 of 25 free parameters of the standard-model. The remaining one, the neutrino CP violation angle δ_{CP}, has not been measured. The values calculated from the formulas are in good agreement with the data. The one common constant in the mass formulas, $\epsilon_0 = 2 \times (6\pi)^{-48}$, which agrees with the Hubble constant H_0 times the Planck time $t_{\rm pl}$ ($\epsilon_0 \simeq H_0 \times t_{\rm pl}$) within the accuracy of H_0, suggests that the particle masses are related to the expansion of the universe. A model to explain these formulae is reported in the next article,[1] and implications to gravity and cosmology are reported in the article appearing after that.[2]

Table 1. Formulas for the masses of the SM particles.

p	formula ($\mu_p = m_p/M_{\rm pl}$)	$\lvert m_p^c/m_p^m - 1\rvert$
e	$\frac{1}{12\pi^2}\epsilon_0^{1/3}\left(1+\frac{1}{4}\frac{1}{(6\pi)^2}\right)^{-1}$	5.9×10^{-6}
μ	$\frac{3}{2}\epsilon_0^{1/3}\left(1-\frac{3}{6\pi}+\frac{27}{4}\frac{1}{(6\pi)^2}\right)^{-1}$	5.2×10^{-5}
τ	$9\pi\epsilon_0^{1/3}\left(1-\frac{3}{4}\frac{1}{6\pi}+\frac{5}{4}\frac{1}{(6\pi)^2}\right)^{-1}$	1.6×10^{-5}
ν_1	$\frac{2}{3}\epsilon_0^{1/2}\left(1+\frac{1}{6\pi}\right)^{-1}$	See Table 2
ν_2	$2\epsilon_0^{1/2}\left(1-\frac{1}{6\pi}\right)^{-1}$	See Table 2
ν_3	$4\pi\epsilon_0^{1/2}\left(1+\frac{1}{6\pi}\right)^{-1}$	See Table 2
t	$8(6\pi)^2\epsilon_0^{1/3}$	5.5×10^{-3}
c	$12\epsilon_0^{1/3}$	3.8×10^{-2}
u	$8(6\pi)^{-2}\epsilon_0^{1/3}$	3.9×10^{-3}
b	$3(6\pi)\epsilon_0^{1/3}\left(1+\frac{3}{2}\frac{1}{6\pi}+\frac{27}{4}\frac{1}{(6\pi)^2}\right)^{-1}$	5.6×10^{-3}
s	$\epsilon_0^{1/3}$	2.2×10^{-2}
d	$(6\pi)^{-1}\epsilon_0^{1/3}\left(1+\frac{1}{6\pi}\right)^{-1}$	1.6×10^{-2}
Z	$\frac{1}{(8\pi^2)}\epsilon_0^{1/4}\left(1+\frac{1}{12}\frac{1}{6\pi}+\frac{1}{12}\frac{1}{(6\pi)^2}\right)^{-1/2}$	1.5×10^{-5}
W	$\frac{2^{-1/4}}{(8\pi^2}\epsilon_0^{1/4}\left(1-\frac{3}{2}\frac{1}{6\pi}-\frac{9}{4}\frac{1}{(6\pi)^2}\right)^{-1/2}$	1.0×10^{-4}
H	$\frac{2^{1/2}}{8\pi^2}\epsilon_0^{1/4}\left(1+\frac{3}{2}\frac{1}{6\pi}-\frac{9}{2}\frac{1}{(6\pi)^2}\right)^{-1/2}$	3.4×10^{-4}

Table 2. Comparison of the calculated masses of neutrinos with the neutrino oscillation data.

Quantity	Calculated	Measured
$m_2^2 - m_1^2$	7.39×10^{-5} eV^2	$7.37^{+0.20}_{-0.15}\times10^{-5}$ eV^2
$m_3^2 - m_1^2$	2.58×10^{-3} eV^2	$2.56\pm0.04\times10^{-3}$ eV^2

*1 RIKEN Nishina Center

Table 3. Formulas of the CKM matrix elements.

	formula	calculated	measured
V_{us}	$\left(\frac{1}{6\pi}\left(1+\frac{1}{6\pi}\right)^{-1}\right)^{1/2}$	0.22445	0.22452 ± 0.0044
V_{cb}	$\left(\frac{2}{3}\right)^{1/2}\frac{1}{6\pi}$	0.04332	0.04214 ± 0.00076
V_{ub}	$\frac{4}{3}\frac{1}{(6\pi)^2}$	0.003753	0.00365 ± 0.00012
$\bar{\eta}$	$\left(1+\frac{3}{2}\frac{1}{6\pi}+\frac{27}{4}\frac{1}{(6\pi)^2}\right)\frac{1}{\pi}$	0.3497	$0.355^{+0.012}_{-0.011}$

Table 4. Formulas of the neutrino-mixing matrix.

	formula	calculated	measured
s_{12}	$\left(\frac{1}{3}\left(1-\frac{1}{6\pi}\right)\left(1+\frac{1}{6\pi}\right)^{-1}\right)^{1/2}$	0.547	0.545 ± 0.016
s_{23}	$\left(\frac{3}{2\pi}\left(1+\frac{1}{6\pi}\right)\left(1-\frac{1}{6\pi}\right)^{-1}\right)^{1/2}$	0.729	0.714 ± 0.053
s_{13}	$\left(\frac{1}{12\pi}\right)^{1/2}\left(1-\frac{1}{6\pi}\right)\left(1+\frac{1}{6\pi}\right)^{-1}$	0.146	0.147 ± 0.003

Table 5. Formulas of the coupling constants α and $\alpha_s(M_Z)$

	formula	calculated	rel. error
α^{-1}	$44\pi\left(1+\frac{1}{3}\frac{1}{6\pi}\right)^{-1/2}$	137.0238	8.9×10^{-5}
$\alpha_s(M_Z)$	$\frac{\sqrt{2}}{4\pi}\left(1+\frac{1}{6\pi}\right)$	0.11851	3.5×10^{-3}

References

1) Y. Akiba, in this report.
2) Y. Akiba, in this report.

Quarternion-spin-isospin model for the standard-model parameters

Y. Akiba *1

The standard model (SM) successully describes the nature, but it has at least 25 free parameters. In the preceding article[1)] we reported empirical formulas with no free parameter for 24 SM parameters: 15 particle masses, four Cabbibo-Kobayashi-Masukawa (CKM) quark mixing parameters, three neutrino mixing angles, the fine structure constant, and the strong coupling constant.

The pattern of the formulas suggests that there is an algebraic model underpinning them and that the numbers 6π and $\epsilon_0 = 2 \times (6\pi)^{-48}$ play key roles in this model. The fact that ϵ_0 agrees with the Hubble constant H_0 times the Planck time $t_{\rm pl}$, $\epsilon_0 \simeq H_0 t_{\rm pl}$, suggests that there is a relation between the mass of the SM particles and the metric of spacetime.

In this article, we introduce the quarternion-spin-isospin (QST) model, which explains these formulas and the relation $H_0 t_{pl} = \epsilon_0$. The QST model is so named because it is based on operators that are products of unit quarternions and operators of spin and weak isospin.

The QST model is based on the following 64 operators that are introduced here as normalized primordial action (NPA):

$$\left\{\frac{I^\mu\sigma^\nu\tau^a}{6\pi}, \frac{\varepsilon\tau^a}{6\pi}, \frac{\varepsilon i}{6\pi}, \frac{\varepsilon I^c\tau^c}{6\pi}, \frac{\varepsilon i\tau^3}{6\pi}, \frac{-\varepsilon I^c}{4\pi}, \frac{-\varepsilon i}{2\pi}, -\varepsilon, \varepsilon, i, 1\right\}.$$

The QST model has five primary ansatzes.

(A1) The Planck time $t_{\rm pl} = 5.3912 \times 10^{-44}$ s is the minimum duration of time in nature. The time t is an integer n in the unit of $t_{\rm pl}$, and the physics state at $t = n$ is represented as $|n\rangle$. $t_{\rm pl}$ is a fundamental constant of nature, as are the speed of light in vacuum c and the Planck constant $\hbar$.

(A2) The change of $|n\rangle$ for $t_{\rm pl}$ is represented by a set of 49 operators $\hat{\mathcal{L}}_p^{\rm EAD}$ we name as elementary action density (EAD). An EAD corresponds to a term of the SM Lagrangian.

(A3) An EAD is a sum of the equivalent vee product $P_{48}(S_{48}, \sigma)$ of 48 NPAs,

$$\hat{\mathcal{L}}_p^{\rm EAD} = \sum P_{48}(S_{48}^{NPA}, \sigma) = \sum \hat{\partial}_{\sigma(p_1)} \vee \cdots \vee \hat{\partial}_{\sigma(p_{48})},$$

where $S_{48}^{NPA} = \{\hat{\partial}_{p_1}, \cdots, \hat{\partial}_{p_{48}}\}$ is a set of 48 NPAs and σ is a permutation ($k \to \sigma(k), 1 \le k \le 48$).

(A4) All 49 EADs are invariant for the following permutations:

$$(I^1, I^2, I^3) \to (I^1, I^2, I^3), (I^2, I^3, I^1), (I^3, I^1, I^2),$$
$$(\sigma^1, \sigma^2, \sigma^3) \to (\sigma^1, \sigma^2, \sigma^3), (\sigma^2, \sigma^3, \sigma^1), (\sigma^3, \sigma^1, \sigma^2).$$

There are 12 EADs that are invariant for permutations:

$$(\tau^1, \tau^2, \tau^3) \to (\tau^1, \tau^2, \tau^3), (\tau^2, \tau^3, \tau^1), (\tau^3, \tau^1, \tau^2). \quad (1)$$

(A5) The SM emerges as a continuous approximation of the QST model as each EAD becomes a term of the SM Lagrangian in the limit of $t_{\rm pl} \to 0$.

We found 49 EADs that correspond to the elementary particles of the SM, which are summarized in Table 1. All of the 24 formulas of the parameters of the standard model can be derived from the 49 EADs in the table. The model also predicts that the CP violation in the neutrino sector is 100%. Thus, all of the 25 free parameters of the standard model are derived from the QST model. In additon, the model predicts that the Hubble constant times the Planck time is $H_0 t_{pl} = 2 \times (6\pi)^{-48}$. We discuss the implications for general relativity and cosmology in the next article.[2)]

Table 1. Values of elementary action densities.

	$(6\pi)^2\epsilon_0 i\tau^3$	$(6\pi)^2\epsilon_0 i$	$(6\pi)\epsilon_0 i\tau^3$	$(6\pi\epsilon_0 i)$	$(6\pi)\epsilon_0$	$\epsilon_0 i\tau^3$	$\epsilon_0 i$	ϵ_0
$\hat{\mathcal{L}}_{g_{3D}}$								3_a^*
$\hat{\mathcal{L}}_{g_{2D}}$								2_a
$\hat{\mathcal{L}}_{GG}$								24_a^*
$\hat{\mathcal{L}}_{uG}$								8_a
$\hat{\mathcal{L}}_{cG}$								24_b^*
$\hat{\mathcal{L}}_{tG}$								8_b
$\hat{\mathcal{L}}_B^m$							18_b	
e	4_a					1		3_b^*
μ	4_a		-12_a			27_a		3_c^*
τ	4_a		-3		3_a^*	$1+4$		
ν_1		12_a		12				2_b
ν_2		-4_a		4				2_b
ν_3		12_a		12	2			
ν_3'		12_a		12	-2			
U_{15}	-12_a					2_a		
U_{17}	$3 \times (-4)$		-12_b			2_b		
D	-12_a					1		
u	4_b							-8_a
c	$4_b + 4_c$							-24^*
t	4_c							-8_b
d	-12_a		-12_a		-3^*			
s	-12_b							3_d^*
b	4_d		6		3_b^*	27_b	18_a	
Z		12_b^*		1			1	
H		-4		-6			18_c	
W		12_b^*		-18^*			-27	

*1 RIKEN Nishina Center

References

1) Y. Akiba, in this report.
2) Y. Akiba, in this report.

$R = 12H_0^2$ and its implications to gravity and cosmology

Y. Akiba *1

In the preceding article,[1] I report a model (QST model) that can yield the formulas of the standard model (SM) parameters. The model implies that the product of the Hubble constant H_0 and the Planck time t_{pl} is $H_0 t_{pl} = 2 \times (6\pi)^{-48} = \epsilon_0$. This relation is derived as follows.

The spacetime metric of the Hubble expansion is

$$ds^2 = -dt^2 + e^{2H_0 t}(dx^2 + dy^2 + dz^2).$$

The Ricci scalar curvature R and $\sqrt{-g}$ of this metric are

$$\begin{aligned} R &= 12H_0^2, \\ \sqrt{-g} &= e^{3H_0 t}. \end{aligned}$$

For $t = t_{\rm pl}$, we have $\sqrt{-g} = e^{3H_0 t} \simeq 1 + 3H_0 t_{\rm pl}$. In the QST model, the correspondence relation is

$$\sqrt{-g} \leftrightarrow 1 + \hat{\mathcal{L}}_{g3D} = 1 + 3\epsilon_0.$$

Thus, we have $H_0 t_{pl} = \epsilon_0$. Because $H_0 = \epsilon_0 / t_{pl}$ is a constant, R is a constant. The QST model implies that $R = 12H_0^2$ (constant). We discuss the implication of this equation in general relativity and cosmology below.

We can generalize the metric to allow local changes of the scale with a constraint $R = 12H_0^2$:

$$ds^2 = -e^{2u(x,y,z)}dt^2 + e^{2H_0 t}(dx^2 + dy^2 + dz^2).$$

The R of this metric is

$$\begin{aligned} R &= -(2\Delta u + 3(\nabla u)^2)e^{-2H_0 t} + 12H_0^2 e^{-2u} \\ &= 12H_0^2. \end{aligned}$$

We can show that Coulomb gravity can be derived from this metric. When we take the approximation $H_0 \simeq 0$, we have

$$R = -2\Delta u - 3(\nabla u)^2 = 0.$$

If u is small, we can ignore the $(\nabla u)^2$ term, and we have $\Delta u = 0$. In general relativity, $g_{00} \simeq -1 - 2\phi_G$, where ϕ_G is the gravitational potential. As $e^{2u} = -g_{00}$ and $e^{2u} \simeq 1 + 2u$, $u \simeq \phi_G$. Therefore,

$$\Delta\phi_G \simeq \Delta u = 0.$$

Thus, the relation $R = 0$ implies Coulombic gravitational potential under the weak gravity approximation. If we take into account the fact that $H_0 \neq 0$, the potential equation for gravity becomes non-linear.

Next, we discuss the effect of $R = 12H_0^2$ for the motion of an astronomical object. Consider the following metric (Sp-metric):

$$ds^2 = -dt^2 + e^{2H_0 t}\left(\frac{dr^2}{1 - \frac{2r_s}{r}} + r^2(d\theta^2 + \sin^2\theta d\phi^2)\right).$$

One can show that the Ricci tensor $R_{\mu\nu}$ and the Ricci scalar curvature R of this metric are

$$\begin{aligned} R_t^t &= 3H_0^2, R_r^r = 3H_0^2 - \frac{2r_s}{r^3}e^{-2H_0 t}, \\ R_\theta^\theta &= R_\phi^\phi = 3H_0^2 + \frac{r_s}{r^3}e^{-2H_0 t}, \\ R &= R_t^t + R_r^r + R_\theta^\theta + R_\phi^\phi = 12H_0^2. \end{aligned}$$

This metric describes the spacetime metric outside a very large spherical mass, *e.g.*, a star or a planet. It is a metric with spherical symmetry, like the Schwartzchild metric, but with $R = 12H_0^2$. Note that $R_{\mu\nu} = 0$ and $R = 0$ for the Schwartzchild metic.

One can solve Keplerian moton in this metric. The solution implies that the radius r of a circular orbit of an object around the large mass at the origin increases with time as

$$\dot{r}/r = \sqrt{2}H_0 = 1.0104 \times 10^{-10}/\text{yr}.$$

The factor $\sqrt{2}$ arises from the fact that the Keplerian motion is a two dimensional motion. One can show that the scale expansion rate of two-dimensional radius ρ with $R = 12H_0^2$ is $\sqrt{2}H_0$.

This prediction agrees with the observed rate of expansion of the the Moon's orbit radius $r_{\rm Moon}$ around the Earth[2] within the uncertainty of the data.

$$\begin{aligned} \dot{r}_{\rm Moon} &= 3.82 \pm 0.07\text{cm/yr}, \\ \dot{r}_{\rm Moon}/r_{\rm Moon} &= (0.994 \pm 0.0182) \times 10^{-10}/\text{yr}. \end{aligned}$$

This good agreement indicates that the expansion of the lunar-orbit radius is due to Hubble expansion.

We found a few emprical formulas of cosmological parameters that are similar to those of the SM parameters. For CMB temperature, we found

$$T = \frac{1}{(6\pi)^2}{\epsilon_0}^{1/2}\left(1 + \frac{1}{4\pi} - \frac{1}{(6\pi)^2}\right)^{1/2}.$$

This formula yields $T_{\rm CMB}^{\rm calc} = 2.7249$ K, which agrees with the obsrved value $T_{\rm CMB} = 2.7255 \pm 0.0006$ K within the uncertainty of the data. The QST model can explain the emprical formula.

*1 RIKEN Nishina Center

References
1) Y. Akiba, in this report.
2) B. G. Bills, R. D. Ray, Geophys. Res. Lett. **26**, 3045 (1999).

7. Astrophysics and Astro-Glaciology

A novel high-resolution laser-melting sampler for discrete analyses of ion concentrations and stable water isotopic compositions in firn and ice cores

Y. Motizuki,[*1] Y. Nakai,[*1] K. Takahashi,[*1] J. Hirose,[*1] Y. V. Sahoo,[*1] Y. Yano,[*1] M. Yumoto,[*2] M. Maruyama,[*2] M. Sakashita,[*2] K. Kase,[*2] and S. Wada[*2]

Ice cores preserve past climatic changes and, in some cases, astronomical signals. Here we present a newly developed automated ice-core sampler that employs laser melting (see Fig. 1). In our system, a hole in an ice core approximately 3 mm in diameter is melted and heated well below the boiling point by laser irradiation, and the meltwater is simultaneously siphoned by a 2 mm diameter movable evacuation nozzle that also holds the laser fiber. The advantage of sampling by laser melting is that molecular ion concentrations and stable water isotope compositions in ice cores can be measured at high depth resolution, which is advantageous for ice cores with low accumulation rates, such as ice cores drilled around Dome Fuji station in Antarctica.

This device takes highly discrete samples from ice cores, attaining depth resolution as small as ∼3 mm with negligible cross contamination; the resolution can also be set at longer lengths suitable for validating longer-term profiles of various ionic and water isotopic constituents in ice cores.

The laser beam used to melt the ice is supplied through the wall of the freezer container by a continuous-wave operated Er-doped fiber laser (CEFL-TERA, Keopsys Inc.) through optical fibers (core/clad diameter = 200/220 μm). The laser wavelength is 1.55 μm (near infrared) and the maximum output power is 10 W. The 1.55-μm wavelength takes advantage of the strong absorption bands of ice and water from 1.4–1.6 μm. In addition, because 1.55-μm lasers are commonly used in optical communication technologies, suitable optical fibers are commercially available.

To check the stability of the sampler in the −20°C environment, we performed a continuous sampling test in which 100 vials were filled with a minimal volume (0.65 mL) of meltwater. In this test, the laser power was set at 1.9 W, the nozzle intrusion speed was 0.52 mm/s, the pumping speed was 5.5 mL/min, and the horizontal and vertical pitch of the nozzle was 2.5 mm. It took 8 hours 47 minutes to complete this test with no issues the ∼ −20°C environment. Figure 2 shows a dummy ice block made up from ultrapure water (Milli-Q water) after this stability test. We conclude that the sampling rate will not be a bottleneck during high-throughput isotopic and ionic ice-core analyses.

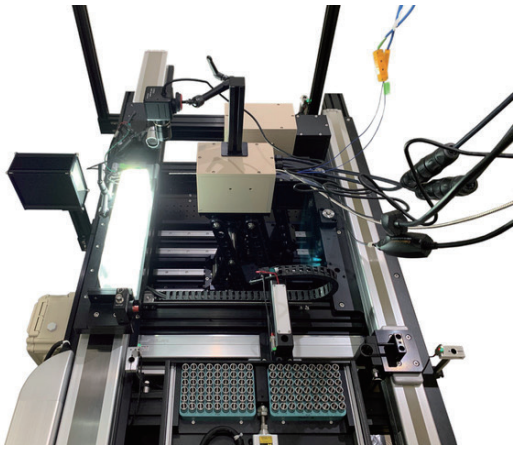

Fig. 1. Photo showing a newly-developed laser-melting ice core sampler.

Fig. 2. Photo showing an ice block after the continuous extraction of 100 meltwater samples in a stability test.

We also conducted experiments to check whether there was any leaching of ions from inner components and to check the degree by which samples mixed with each other during continuous sample collection. We found a 2.4% "memory effect," which is usually significantly less than the analytical accuracy (a few μg/L) of ion analyses by ion chromatography. We conclude that internal contamination and cross contamination are negligible with this sampler.

With this new sampler design, the analysis of the 2,000-year record embodied in the Dome Fuji firn core, which took us several years, could now be finished in about 30 working days by using two isotopic analyzers. For the first time, we can now realistically contemplate strategic plans for cores recovered from low-accumulation sites that include large numbers of repeated operations, such as compiling continuous 2,000-year profiles with annual resolution of ionic and water isotopic constituents. Finally, our sampler has the capability to profile ionic and isotopic constituents at monthly resolution to pursue intriguing transient signals, potentially by annual layer counting.

*1 RIKEN Nishina Center
*2 RIKEN Center for Advanced Photonics

Reference

1) Motizuki *et al.*, submitted to Cold Reg. Sci. Technol.

Annually resolved *d*-excess record from a shallow ice core (DFS10) near Dome Fuji station, East Antarctica

Y. V. Sahoo,[*1], Y. Motizuki,[*1], Y. Nakai,[*1], and K. Takahashi,[*1]

Ice cores are well preserved and utilized as proxies for past climates and temperature reconstruction. A second-order equation given by the deuterium excess[1] (referred to as *d*-excess), $d = \delta D - 8 \times \delta^{18}\mathrm{O}$, is defined from the Meteoric Water Line. Here, δD and $\delta^{18}\mathrm{O}$ are the isotopic water compositions given by δD or $\delta^{18}\mathrm{O}$ (‰) $= (R_{\mathrm{measured}} - R_{\mathrm{VSMOW}})/R_{\mathrm{VSMOW}}$, where R is the ratio $^{2}\mathrm{H}/^{1}\mathrm{H}$ or $^{18}\mathrm{O}/^{16}\mathrm{O}$, R_{VSMOW} is the reference standard, Vienna Standard Mean Ocean Water, and R_{measured} is the measured ratio of a sample.

The *d*-excess is primarily related to physical parameters such as relative humidity, air temperature, sea surface temperature of the oceanic source or precipitation at the site, and the trajectory of moisture source.[2] On a global scale, an annual average value of d is relatively constant around 10.

Vimeux *et al.*[3] demonstrated the *d*-excess changes during transition from the glacial and interglacial periods of Vostok deep ice core data; the changes were well characterized in the plot of *d*-excess versus δD, implicating changes in oceanic moisture sources as a result of changes in Earth's orbital obliquity. The *d*-excess records for the Dome Fuji site have been studied with daily snow precipitation[4,5] and a deep ice core spanning the past 360,000 years.[6] So far, moisture sources and climate changes have been studied for deep ice cores in Antarctica which span a long period; however, is it possible to determine the same tendency on short scales with annually-resolved *d*-excess data from shallow ice cores? Here, we briefly report the correlation of *d*-excess with $\delta^{18}\mathrm{O}$ in a shallow ice core.

The shallow ice core (DFS10) was drilled in 2010 from the site at 10 km south of Dome Fuji station, East Antarctica. The DFS10 site is located (77°40'S, 39°62'E) at 3,800 m above sea level. The ice core drilling project was conducted by Japanese Antarctic Research Expedition. The analyzed samples represent a temporal resolution of about one year ranging from 2 m to 60 m in depth (∼1300 years). All samples were analyzed using Liquid Water Isotope Analyzer (Los Gatos Research, Inc.) at RIKEN.

A linear relation between δD and $\delta^{18}\mathrm{O}$, with a slope of 7.77, $R^2 = 0.987$ for DFS10 was determined. This is close to the local meteoric water line. The *d*-excess shows no correlation with $\delta^{18}\mathrm{O}$ (δD) on an annual or short scale; however, simulation studies established a correlation on longer scales with other ice cores drilled in Antarctica. Fig. 1a shows a smoothed 50 data points running average of *d*-excess plotted against smoothed $\delta^{18}\mathrm{O}$, and clusters into groups are evident. This case shows hierarchal structures: For groups of ∼500 years, a general decrease in *d*-excess with time is observed, suggesting that the moisture source could have systematically changed through the years. Each group subdivided into shorter time scales (∼50 years) reveals smaller clusters of *d*-excess pattern changing with time (Fig. 1b). As seen here, the *d*-excess/$\delta^{18}\mathrm{O}$ small clusters follow a pattern with time. This pattern is not observed in a similar plot with the raw data ($R^2 = 0.04$, Pearson's $R = -0.19$).

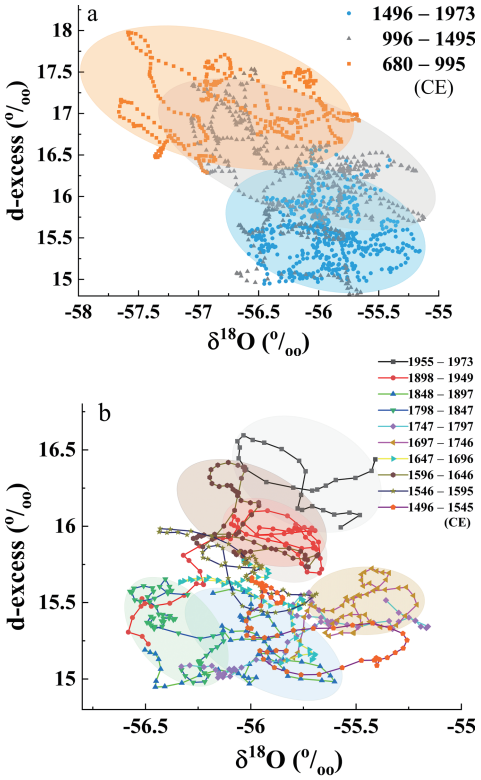

Fig. 1. (a) Deuterium excess versus $\delta^{18}\mathrm{O}$; the data are smoothed using 50 data points running average. The color highlights the bunched ∼500 years period to show the changes in *d*-excess. (b) The same, but for data points from 1496 to 1973 CE (blue highlight from a) are subdivided into ∼50 years period.

The *d*-excess variation depends on a number of factors and intensive simulation or modeling studies are necessary to provide an insight into climate change on a shorter scale, which needs to be assessed using shallow ice cores.

*1 RIKEN Nishina Center

References
1) W. Dansgaard, Tellus **16**, 436 (1964).
2) L. Merlivat, J. Jouzel, J. Geophys. Res. **84**, 5029 (1979).
3) F. Vimeux *et al.*, Nature **398**, 410 (1999); J. Geophy. Res. **106**(31), 863 (2001).
4) H. Motoyama *et al.*, J. Geophy. Res. **110**, D11106 (2005).
5) K. Fujita, O. Abe, Geophys. Res. Lett. **33**, L18503 (2006).
6) R. Uemura *et al.*, Clim. Past. **8**, 1109 (2012).

8. Accelerator

High-intensity vanadium-beam production to search for a new super-heavy element with $Z = 119$†

T. Nagatomo,[*1] Y. Higurashi,[*1] J. Ohnishi,[*1] T. Nakagawa,[*1] and O. Kamigaito[*1]

In March 2020, we successfully accelerated the first beam ($^{40}Ar^{13+}$) using several superconducting quarter-wavelength resonators (SC-QWRs)[2] installed in RIKEN heavy-ion linear accelerator (RILAC)[1] to achieve enough energy to synthesize new super-heavy elements (SHEs) with an atomic number greater than 118. To overcome the extremely small production cross section of SHE with $Z = 119$, it was necessary to provide a highly charged vanadium (V)-ion beam such as $^{51}V^{13+}$ with very high intensity. Thus, we constructed a superconducting electron cyclotron resonance ion source (SC-ECRIS) for RILAC, which was named RIKEN 28-GHz SC-ECEIS "KURENAI" (R28G-K).[3] R28G-K has essentially the same structure[4] as another SC-ECRIS that is the only source of heavy ions including uranium for RIBF, which is renamed RIKEN 28-GHz SC-ECEIS "SUI" (R28G-S).[5,6] When operating the SC-QWR, the particulate matter sputtered from the beam pipe irradiated by the beam is thought to significantly reduce the gap voltage by increasing the surface resistance of the cavity, thus we must suppress the beam loss as much as possible. For this purpose, we installed "slit triplet" in the low energy beam transport to limit the transverse emittance.[3] This indicates that only a portion of the beam extracted from R28G-K is available despite the demand for an unprecedented beam intensity. Therefore, we systematically studied the effects of the amount of the V vapor and power of the microwaves, which heat up the plasma in the ion source, on the beam intensity, and the optimal parameters that would allow long-term experiments with the highest possible beam intensity.

The upper figure in Fig. 1 shows the two high temperature ovens (HTOs)[7] installed in the ion source. The HTO was developed as an evaporator for high melting point materials such as vanadium. The V-vapor amount was equivalent to the sum of the consumption rates of the metallic V sample in each HTO crucible. The capacity of each crucible was approximately 2.2 gram of the granular metallic V. The $^{51}V^{13+}$-beam intensity extracted from R28G-S was obtained as a contour plot in the lower figure in Fig. 1 as a function of the consumption rate of the V metal and the total power of the 18- and 28-GHz microwaves. As a consequence of the contour plot, it was deduced that a 400-electric μA V^{13+}-beam can be produced at ~6-mg/h consumption and 2.5-kW microwaves. Because the total capacity of the two HTO crucibles is 4.4 gram, we can provide the high intense V beam for one month without interruption. Furthermore, at 24-mg/h consumption and 2.9-kW microwaves, we also obtained the V-ion beam with an intensity of 600 electric μA that is suitable for essential development, for example, target development.

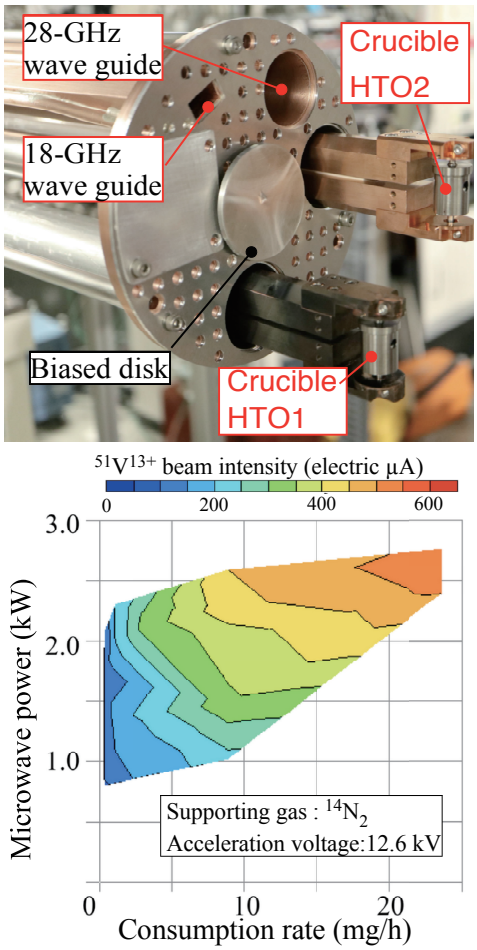

Fig. 1. Two HTO mounted on the injection flange of the plasma chamber of R28G-K (upper), and obtained contour plot of the $^{51}V^{13+}$ beam intensity as a function of the consumption rate and the microwave power (lower).

References
1) E. Ikezawa *et al.*, in Proc. HIAT2015, (Yokohama, Japan, 2015), p. 222.
2) N. Sakamoto *et al.*, Proc. SRF2019, (Dresden, Germany, 2019), p. WETEB1.
3) T. Nagatomo *et al.*, Rev. Sci. Instrum. **91**, 023318 (2020).
4) G. D. Alton *et al.*, Rev. Sci. Instrum. **65**, 775 (1994).
5) T. Nakagawa *et al.*, Rev. Sci. Instrum. **81**, 02A320 (2010).
6) Y. Higurashi *et al.*, Rev. Sci. Instrum. **85**, 02A953 (2014).
7) J. Ohnishi *et al.*, Proc. ECRIS2018, (Catania, Italy, 2018), p. 180.

† Condensed from the article in the Proc. of 24th Int. Workshop on ECR Ion Sources (ECRIS'20), East Lansing, USA, September 2020, in press

*1 RIKEN Nishina Center

R&D in AVF cyclotron

J. Ohnishi,[*1] A. Goto,[*2] and Y. Kotaka[*3]

We aim to increase the beam intensity and energy in the AVF cyclotron. In 2020, 7.25 MeV/nucleon He beams with intensity greater than 40 μA were stably supplied for RI-production experiments, and the maximum beam energy was successfully increased from 14 MeV to 30 MeV for protons. This paper describes the supply of a 30 MeV proton beam and the temperature-monitoring system in the deflector septum for extracting beams with an intensity greater than 1 kW.

Previously, the maximum energy of the AVF cyclotron for protons was 14 MeV; however, in the summer of 2017, the new central region was installed to accelerate beams with higher energies, for example, a 30 MeV proton (Harmonic $H = 1$ acceleration) and 14 MeV/nucleon deuteron.[1)] The shape of the old and new central regions, orbits of 30 MeV protons, and the central orbit of normal $H = 2$ operation are shown in Fig. 1. In February 2020, an acceleration test was conducted because the RI-production experiment using the 30 MeV proton beam was scheduled. The results of this test showed that a part of the beam in the second turn hit the phase slit, which was modified in 2019, and the shape of the slit was corrected in a hurry. As a result, a 30 MeV proton beam with a current of 10 μA was successfully accelerated and supplied for the user's experiment in June. The passing efficiency in the AVF cyclotron was approximately 7%.

To prevent the deflector septum from melting due to beam loss, a system was installed to monitor the temperature of the septum with thermocouples (TCs) and to stop the beam when an abnormal temperature rise is detected. Figure 2 shows a part of the deflector to which the TCs are attached. The septum is made of copper, and it has a thickness of 0.3 mm and a height of 12 mm. As shown in the figure, the septum has a notch with a length of 20 mm in the beam direction for dispersing beam loss. The two TCs were attached 6 mm above and below the tip of the septum notch. Figure 3 shows the time response of the temperatures at the tip of the septum notch (beam loss point) and the TC position calculated with ANSYS[2)] for a beam loss of 300 W (assuming a beam diameter of 2 mm). These calculation results show that the maximum temperature of the septum exceeds the melting point of copper (1085°C) within 1 s with a beam loss of approximately 370 W. Further, it is found that the temperature rise at the TC position was as small as one tenth of the maximum temperature and its response speed was slow. Therefore, we will stop the beam before the septum melts when the temperature rise for each 0.1 s measurement interval exceeds a predetermined value owing to any abnormal beam loss. The system will be used in 2021 when the permission limit on the radiation protection for the 7.25 MeV/nucleon He beams will be increased to 70 μA.

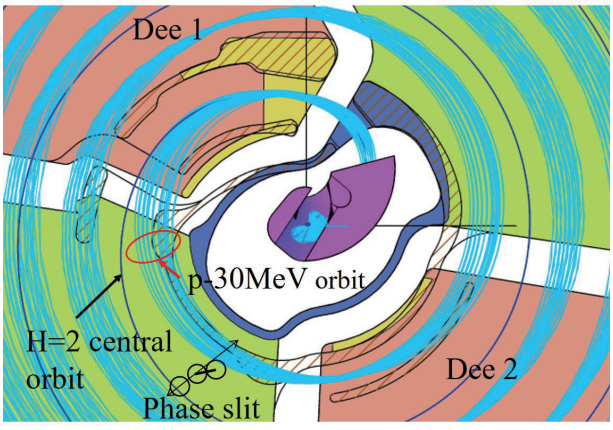

Fig. 1. New and old central region of the AVF Cyclotron. Hatched area indicates the old region. Beam orbits for 30 MeV protons and the central orbit of the normal $H = 2$ acceleration are also shown.

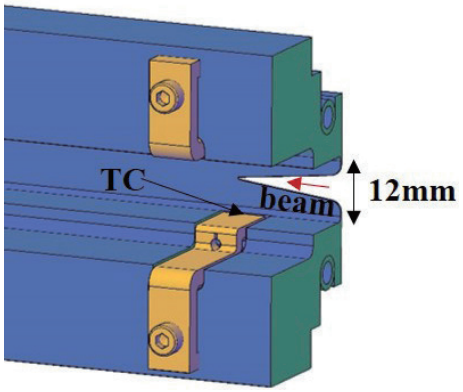

Fig. 2. Tip of the deflector septum to which thermocouples are attached.

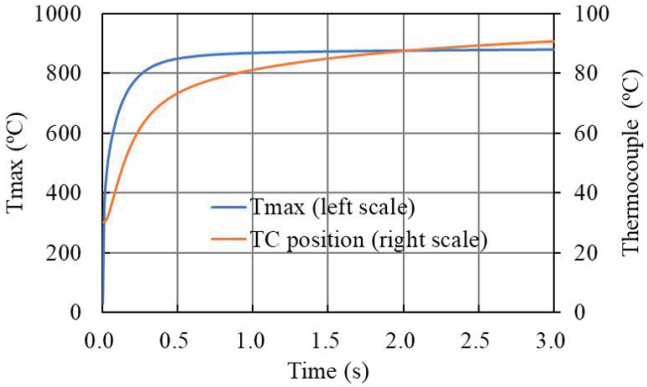

Fig. 3. Time response of temperatures on the septum calculated by ANSYS.

*1 RIKEN Nishina Center
*2 Institute of Materials Structure Science, KEK
*3 Center for Nuclear Study, University of Tokyo

References
1) J. Ohnishi *et al.*, RIKEN Accel. Prog. Rep. **51**, 137 (2018).
2) `https://www.ansys.com/`.

Charge stripper ring for RIKEN RI beam factory†

H. Imao*1

The use of charge strippers is almost inevitable for the efficient acceleration of particularly heavy ions such as uranium in heavy-ion accelerator complexes. At the RIKEN RI Beam Factory (RIBF), the total charge stripping efficiency of two strippers, He gas[1,2] and rotating graphite sheet disk strippers,[3] used for uranium acceleration is less than 5%, which creates a serious bottleneck for potential intensity upgrades in the near future. We have proposed the use of charge stripper rings (CSRs)[4,5] as a cost-effective method to achieve a 10-fold increase in the intensity of the ^{238}U beams at RIBF.

Figure 1 shows a design view of the CSR for the first stripper (CSR1), which is a compact isometric ring with the same design circumferences of 37.1953 m (15 times the distance interval of the beam bunches from the RIKEN Ring Cyclotron (RRC) at a frequency of 18.25 MHz) for all circulating uranium beams with eight different charge states from 59+ to 66+. CSR1 consists of gas strippers (He and nitrogen strippers), eight main bending magnets (BM1-8), two acceleration cavities, a re-buncher, four charge-dependent quadrupole stations, injection magnets (IBM and injector quadrupole triplets), extractor bending magnets (EBM1 and EBM2), steerers for closed-orbit distortion corrections, and diagnostic boxes involving beam diagnostics and vacuum pumps. In the CSR1, beams other than the selected U^{64+} beams reenter the stripper with a ring after recovering the energy lost in the stripper. The U^{35+} beams are injected simultaneously into the charge stripper ring using the charge exchange injection method. The recycling cycles are repeated, and only the U^{64+} beams are continuously extracted, using a magnetic deflection channel. The isometric ring is used to hold the bunch structure of beams to match the acceptance of the latter-stage cyclotrons.

The CSR1 lattice is a mirror-symmetric reversed lattice with the symmetry plane at the center of the stripper section. The high-density quadrupole stations equipped with a quadrupole doublet or triplet for all charge states will be used to control the optics for all charge states. The design of a compact quadrupole magnet is a key issue. We have already finished the calculations and are preparing to manufacture "hourglass-like" quadrupole magnets[6] as shown in Fig. 1.

We conducted some calculations for the key design issues of CSR1. A realistic lattice for 8 charge states circulating in CSR1 was derived. Possible sources of emittance growth with a new multi-stage stripper scheme were also investigated. We also performed calculations for the beam transport of U^{35+} from RRC to CSR1 and then those of U^{64+} from CSR1 to fRC. The effective charge stripping efficiency of CSR1 in the present calculation was approximately 60%, and further detailed calculations and optimizations were conducted.

References

1) H. Okuno *et al.*, Phys. Rev. ST Accel. Beams **14**, 033503 (2011).
2) H. Imao *et al.*, Phys. Rev. ST Accel. Beams **15**, 123501 (2012).
3) H. Hasebe *et al.*, EPJ Web Conf. **229**, 01004 (2020).
4) H. Imao *et al.*, Proc. CYC2016, Zurich, Switzerland, 2016, pp. 155–159.
5) H. Imao *et al.*, Proc. IPAC2018, Vancouver, Canada, 2018, pp. 41–46.
6) Patent application filed by RIKEN and HITACHI Engineering Co., Ltd. with the application number JP2020-056540 in Japan.

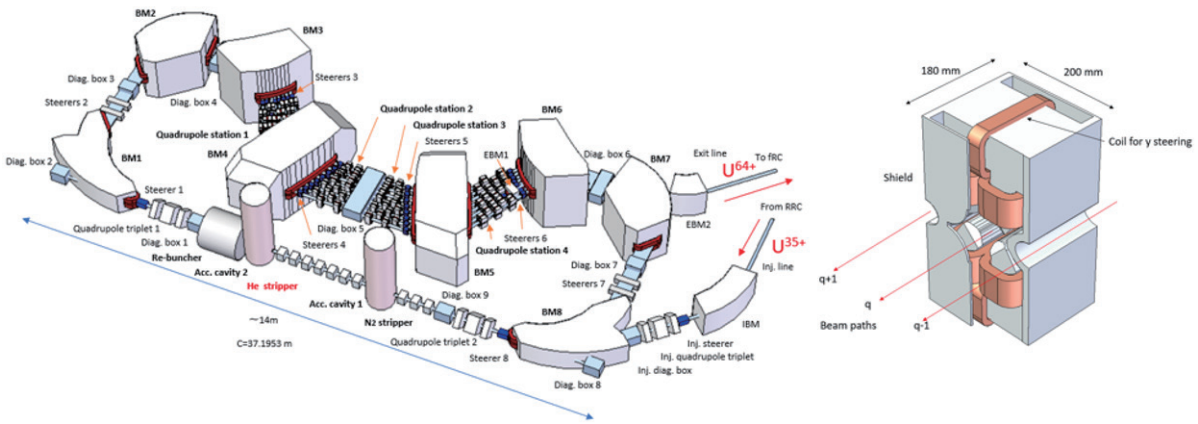

Fig. 1. Design view of the CSR1 (left) and "hourglass-like" quadrupole magnet (right).

† Condensed from the article in J. Instrm. **15**, P12036 (2020)
*1 RIKEN Nishina Center

2020 operational report for the Nishina RIBF water-cooling system

T. Maie,[*1] K. Kusaka,[*1] E. Ikezawa,[*1] Y. Watanabe,[*1] K. Kobayashi,[*2] J. Shibata,[*2] M. Oshima,[*3] H. Shiraki,[*3] and H. Hirai[*3]

Operation Condition

As the COVID-19 pandemic affected the operation of the cooling systems of Nishina and RIBF in FY2020, the RIBF operation planned for the H1 term was completely cancelled. In FY2020, RIBF's cooling systems were operated for approximately two and half months, and Nishina's cooling systems for AVF-standalone, AVF + RRC, AVF + RRC +IRC and RILAC2 + RRC + GARIS-II were operated for approximately five months. No significant troubles that could cause the long-term interruption of accelerator operation occurred, and the cooling systems operated stably, with the exception of some minor problems.

Trouble Report

In troubleshooting, the symptoms were fortunately minor. Therefore, instead of interrupting the machine time for repairs, while providing emergency measures, repairs such as the switching of beams or summer maintenance were performed during the long-term accelerator outage period. The typical examples of troubles that occurred in FY2020 are a water leak from the cooling plumbing joint and deterioration of cooling water purity due to water leakage, failure in the cooling water pump motor bearing, failure in the control instrumentation air compressor, and device outages caused by an instantaneous voltage drop due to a lightning strike (1–2 times a year).

Periodic Maintenance

Although the operation time was shorter overall because the COVID-19 pandemic, regular maintenance was conducted as planned. As we report it every year, we omit details about the periodic maintenance

Upgrades

The construction of cooling systems dedicated to the diagnostic device (named "New FC-G01") for high-intensity beams began this year, as planned. After the completion of the construction in March 2021, the construction of the power systems and control systems is planned to start in April 2021 with the goal of starting a comprehensive test run within FY2021. Furthermore, an actual load test using the beam of the equipment for enhancing the RRC cooling capacity, which was completed in 2019, is scheduled for March. If the measurement result is satisfactory, the cooling systems are planned to be used in the operation of RIBF from April 2021. The cooling systems are expected to contribute greatly to the mitigation of the fluctuations in the magnetic field due to temperature variations in the RRC cooling water, which has been the problem for many years.

References

1) T. Maie *et al.*, RIKEN Accel. Prog. Rep. **52**, (2018).
2) T. Maie *et al.*, RIKEN Accel. Prog. Rep. **59**, (2019).

*1 RIKEN Nishina Center
*2 SHI Accelerator Service Co., Ltd.
*3 Nippon Air Conditioning Service Co., Ltd.

Status of vacuum pumping systems in accelerator facilities

Y. Watanabe,[*1] E. Ikezawa,[*1] M. Fujimaki,[*1] S. Watanabe,[*1] K. Yamada,[*1] M. Nishida,[*2] K. Oyamada,[*2] J. Shibata,[*2] K. Yadomi,[*2] and A. Yusa[*2]

Vacuum pumping systems in accelerator facilities have the following two problems: vacuum leakage and update issue. The vacuum leakage is a malfunction of old accelerator facilities caused by age-related deterioration. The update issue is that almost all old vacuum pumps and accessories cannot be replaced with new units owing to a budget limitation. In this paper, we discuss the current status of vacuum pumping systems.[1,2)]

A vacuum pumping system in an accelerator facility[1)] comprises cryopump systems, turbomolecular pump (TMP) systems, rough pumping systems, additional chamber (AC) pumping systems, and subpumping systems (subvacuum of a resonator). Table 1 lists the number of vacuum pumping systems in accelerator facilities. Each ring cyclotron contains more than 80 sets of cryopump systems,[2)] more than 120 sets of TMP systems, and 2–8 sets of rough pumping, AC pumping, or sub-pumping systems. In addition, more than 160 module-type vacuum gauges (total pressure gauge controller) combined with Pirani and cold cathode gauges are used to monitor vacuum pressure and interlocking vacuum process control in accelerator facilities. Table 2 lists the number of malfunctions in the pumps and gauges from 2018 to 2020. In a year, three to nine malfunctions occur in each unit. The number of malfunctions may have been lower before 2017 because of the shutdown of the RILAC due to the SRILAC installation in 2017–2019 and the closure of the RIBF due to the COVID-19 pandemic in 2020.

Vacuum pumping systems have been in operation for 14–42 years.[2)] In particular, RRC cryopumps, large RILAC TMPs (5000 L/s), and large RRC TMPs (5000 L/s) were manufactured in 1985, 1978–1987, and 1985, respectively. In addition, the doses in the SRC, IRC, and AVF room are extremely high during beam irradiation. Therefore, the number of malfunctions caused by age-related deterioration and environmental radiation will increase further in the future. New spare units of vacuum pumping systems were purchased gradually, but these spare units are still not sufficient. The following requirements remain.

(1) All the existing RRC cryopump compressors have been discontinued by the manufacturer; therefore, at least six cryopump compressors must be replaced with new ones within a few years. Based on such measures, one cryopump system set of the IRC-NE valley cavity was relocated to the RRC-VS valley cavity in 2019, and two cryopump systems operate in the IRC-NE valley cavity. Six SRC cryopump compressors should be also replaced with new ones in the future.

(2) In the case of large TMPs, although one 5000 L/s TMP of the RRC was replaced with a new one in 2017 and one of the RILAC is scheduled to be updated, the other 5000 L/s TMPs are not yet scheduled for replacement. In addition, a few malfunctions of large rotary pumps (RPs) have been occurring in the rough pumping system of ring cyclotrons and have not been repaired. Therefore, these large RPs must be replaced with new units in the future, although their operating times are lower.

Table 2. Number of malfunctions from 2018 to 2020.

	2018	2019	2020
Cryopump[a]	4	6	7
Turbomolecular pump[b]	3	8	4
Rotary pump	5	3	7
Vacuum gauge[c]	4	6	9

[a] Includes a compressor. [b] Includes an attached power supply. [c] Includes a controller, Pirani gauge, and cold cathode gauge.

However, small TMPs and RPs as well as vacuum gauges have been repaired or updated, and these have been relatively stable. Oil leaks in small RPs were mainly repaired by replacing new O-rings and seals, and vacuum gauges were repaired by replacing some boards and parts.

Consequently, if more cryopumps or TMPs malfunction in a year, it will be difficult to operate accelerator facilities depending on the number of spare units. Therefore, the priority would be to purchase a sufficient number of spare units.

References

1) S. Yokouchi *et al.*, RIKEN Accel. Prog. Rep. **41**, 101 (2008).
2) Y. Watanabe *et al.*, RIKEN Accel. Prog. Rep. **50**, 154 (2016).

Table 1. Number of vacuum pumping systems in accelerator facilities.

	RILAC[a]	RILAC2[a]	AVF[a]	RRC	fRC	IRC	SRC	BT[a]
Cryopump system	11	8	2	14	6	14[b]	22	3[c]
TMP system (TMP + RP)	14	11	1	4	2	4[d]	4[d]	78
Rough pumping system (MDP[e] + RP)	–	–	–	2[d]	2	2	2	–
AC pumping system (TMP + RP)	–	–	–	4	–	4	–	–
Sub-pumping system (TMP + RP)	–	–	–	–	–	4	8	–
Module-type vacuum gauge	16	9	1	14	3	14	10	78

[a] Excludes ion sources, SRILAC, or charge strippers. [b] One set was relocated to RRC. [c] Includes a re-buncher and D6-BEA. [d] One is out of order or offline. [e] Mechanical booster pump.

*1 RIKEN Nishina Center
*2 SHI Accelerator Service Ltd.

9. Instrumentation

Development of ^{216}Th and ^{220}Th beams at the BigRIPS separator

N. Fukuda,[*1] H. Suzuki,[*1] Y. Shimizu,[*1] H. Takeda,[*1] J. Tanaka,[*1] and K. Yoshida[*1]

We report the status of the development of ^{216}Th and ^{220}Th beams that are to be used in the recently proposed nuclear-reaction experiment at SAMURAI. The goal of this development is to determine the BigRIPS separator settings that completely meet the requirements for the beams used in the experiment.

The Th (^{216}Th or ^{220}Th) beam is produced by means of the projectile fragmentation of a 345 MeV/nucleon ^{238}U beam and separated using the BigRIPS separator. The essential requirements for the beam are as follows:

(1) Th-beam rate $\geq 10^4$ Hz
(2) Total beam rate at BigRIPS-F7 $\leq 5 \times 10^4$ Hz
(3) Beam energy $\geq$250 MeV/nucleon

In order to meet the requirments of (1) and (2) simultaneously, the purity of the Th beam must be 20% or heigher. Meanwhile, to achieve a higher beam energy (requirement (3)), the thicknesses of the production target and degrader must be small, which could result in insufficient isotope separation and thereby make it difficult to obtain high purity. Another concern is the particle identification (PID) of heavy fragments. In BigRIPS, in-flight PID based on the TOF-$B\rho$-ΔE method[1] has successfully been performed for heavy fragments with Z = 82–90 and beam energies of approximately 200 MeV/nucleon.[2] However, for fragments with higher beam energy ($\geq$250 MeV/nucleon in the present case), PID might be more difficult because of the deterioration in Z resolution caused by possible energy-loss straggling due to charge-state fluctuations.[3]

A test of the Th-beam production was conducted as a machine study (MS-EXP20-02) in November 2020. In consideration of the limited beam time of 12 h, we focused on the evaluation of PID performance and the investigation of contaminants. The RI beams around ^{220}Th were produced by the projectile fragmentation of a ^{238}U beam impinging on a 1-mm-thick beryllium target. The setting of the BigRIPS separator was nearly optimized for the production of a ^{220}Th beam, in which the magnetic rigidity $B\rho$ values at D1, D2, and the second stage (D3–D6) of BigRIPS were tuned for He-like, H-like, and He-like ^{220}Th ions, respectively, to remove huge contaminants from large fission-fragment yields. A 1-mm-thick aluminum degrader was installed at F5, while there was no suitable (sufficiently thin) degrader installed at F1. Instead, the parallel-plate avalanche (PPAC) detector at F1 served as a charge-exchange foil to reduce the amount of contaminants.

Figure 1 shows the Z vs. A/Q PID plot for fragments produced (a) without and (b) with the F5 degrader. The A/Q values of the fragments were deduced under the assumption that the charge states of the ions did not change at F5. The relative A/Q resolution is evaluated to be 0.08% in 1σ. No significant amounts of contaminants were observed in either setting. In the presence of the F5 degrader, fragments in the region of Z = 85–95 were extracted as intended, showing that a thickness of 1 mm is sufficient for the aluminum degrader. The expected location of ^{220}Th^{88+} is indicated by the red solid circle, in which no blobs of isotopes are found in each setting. This is probably because most of the ions transmitted to F7 changed their charge state at F5, and consequently, their A/Q values could not be deduced correctly under the present assumption. Therefore, charge-state identification based on accurate $B\rho$ analysis is required to achieve correct PID. It should also be noted that the relative Z resolution is as poor as 0.69% (1σ). Elaborate data analysis is currently in progress.

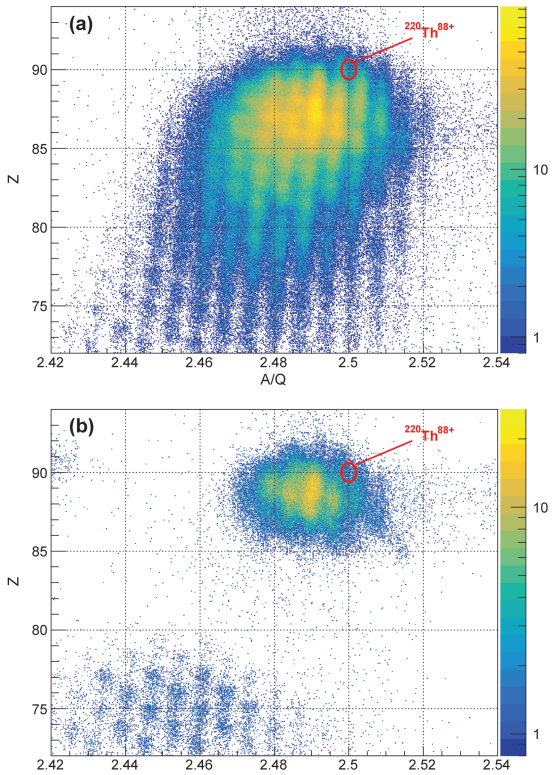

Fig. 1. Particle identification plot of Z vs. A/Q for fragments produced in the ^{238}U+Be reaction a) without energy degraders and b) with an energy degrader (1-mm-thick Al) was used at F5. The red solid circle indicates the expected location of ^{220}Th^{88+} (A/Q = 2.5, Z = 90).

*1 RIKEN Nishina Center

References
1) N. Fukuda *et al.*, Nucl. Instrum. Methods Phys. Res. B **317**, 323 (2013).
2) T. Sumikama *et al.*, Nucl. Instrum. Methods Phys. Res. B **463**, 237 (2020).
3) H. Weick *et al.*, Nucl. Instrum. Methods Phys. Res. B **168**, 164 (2000).

BYACO ecosystem for innovative online operation of BigRIPS experiments with seamless connection to comprehensive analysis

T. Sumikama,[*1] Y. Shimizu,[*1] and H. Baba[*1]

Device and detector settings can be optimized online by using information based on histograms created in an online analysis. The particle identification (PID) of a radioactive isotope (RI) beam is often necessary to check the detector response. PID analysis is one of the most important issues, especially for RI-beam tuning, to produce the required RI beams at the BigRIPS fragment separator.[1] RI-beam separation and PID are difficult for heavy or low-energy RI beams, since the charge state of the RI beam could be different from that of the fully-stripped ion and/or the accuracy of the energy-loss prediction may be insufficient. For the PID analysis of RI beams having different charge states from that of the main RI beam or occasionally having any charge states, comprehensive analyses including fine calibrations and consistency checks among different RI-beam settings were performed after the experiments.[2–4] In order to operate the BigRIPS separator for these types of RI beams, it is desirable to perform the comprehensive analysis online.

The BeYond Analysis, Control, or Operation alone (BYACO) ecosystem is being developed for the innovative online operation of BigRIPS experiments by connecting the comprehensive analyses seamlessly with other components such as device and detector controls and data acquisition systems. BYACO connects each component using REST and WebSocket application programming interfaces (APIs) by applying rapidly evolving web technologies, as shown in Fig. 1. The BYACO main server is built using Node.js[5] and distributes a single-page application in the web browser, which is written using the React JavaScript library.[6] The main server handles requests as the proxy server. Other servers return a response for the forwarded request and can generate an event-driven request to others. To share information in real time, push notifications are sent using WebSocket technology. A client or each server sends a list of interest to the main server. When each server detects updates, they are sent to requesting clients through the main server.

The data analysis is divided into real-time and comprehensive analyses, as shown in Fig. 1. The raw-data calibration and PID reconstruction are processed in the real-time analysis. The obtained variables including the raw data are stored as a TTree object in ROOT.[7] When waveform data are taken in the future, high-throughput processing will be necessary before the real-time PID reconstruction. For the comprehensive analysis, a ROOT-based graphical user interface (GUI) analyzer for the BigRIPS experiment

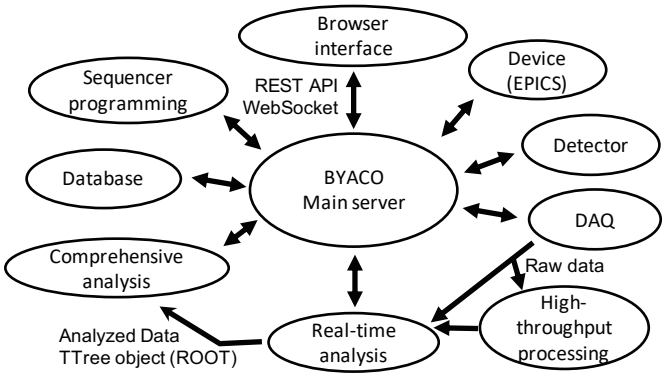

Fig. 1. Conceptual diagram of the BYACO ecosystem. The REST and WebSocket APIs are used for the communication. The sequencer programming is for sequential operations such as automatic RI-beam tuning.

(BigROOT) was developed. Macro programs used in the offline analysis are implemented as selectable tools working on PROOF-Lite in ROOT,[7] which provides functions for the event loop as well as histogram drawing and final analyses. The GUIs to perform simple curve fitting and to make projection and profile histograms have been implemented.

The sequential operation consisting of the data acquisition, analysis, device control, etc. needs to await a response or status change. At present, the sequence of these asynchronous tasks, which are performed by referring to many types of information, are managed using the Redux and Redux-Saga libraries[8,9] on Node.js. As the first application of the sequential operation, the automatic focusing and centering of RI beams were tested online in 2020 with great success.[10]

*1 RIKEN Nishina Center

References

1) N. Fukuda *et al.*, Nucl. Instrum. Methods Phys. Res. B **317**, 323 (2013).
2) N. Fukuda *et al.*, J. Phys. Soc. Jpn. **87**, 014202 (2018).
3) T. Sumikama *et al.*, Nucl. Instrum. Methods Phys. Res. B **463**, 237 (2020).
4) T. Sumikama *et al.*, Nucl. Instrum. Methods Phys. Res. A **986**, 164687 (2021).
5) Node.js, `https://nodejs.org/`.
6) React, `https://reactjs.org/`.
7) R. Brun, F. Rademakers, Nucl. Instrum. Methods Phys. Res. A **389**, 81 (1997), `https://root.cern.ch/`.
8) Redux, `https://redux.js.org/`.
9) Redux-Saga, `https://redux-saga.js.org/`.
10) Y. Shimizu *et al.*, in this report.

Development of auto-focusing and auto-centering system for the BigRIPS separator

Y. Shimizu,[*1] N. Fukuda,[*1] H. Takeda,[*1] H. Suzuki,[*1] T. Sumikama,[*1] T. Baba,[*1] and K. Yoshida[*1]

Various radioactive isotope (RI) beams have been produced by the superconducting in-flight separator BigRIPS since 2007.[1] We are developing the technologies of the RI-beam separation[2,3] and particle-identification analysis.[4] We developed efficient RI beam production, including a control system for the magnetic field with a feedback algorithm.[5] In the case of a ^{132}Sn beam, the production time was reduced by a factor of approximately 1/4 in the past decade. To further improve the efficiency of RI beam production, we are developing a fully automatic RI beam production system based on our technological developments and experiences. As the first step, auto-focusing and auto-centering systems were developed to automatically tune the STQs and dipole magnets on the BigRIPS separator.

In the auto-focusing and auto-centering systems, we used the BYACO (BeYond Analysis, Control, or Operation alone) ecosystem developed for online operation of the BigRIPS separator by connecting the comprehensive analyses seamlessly with others, such as devices and data acquisition (DAQ) systems.[6] The sequencer programming of the auto-focusing and auto-centering includes an automated loop, which consists of 7 steps

1. Start DAQ,
2. Start analysis,
3. Provide analyzed results,
4. Stop DAQ,
5. Evaluate new magnet currents,
6. Apply new magnet currents, and
7. Output the stability of the magnets.

The realtime analysis program is always running to convert raw data into analyzed data stored as a TTree object in ROOT.[7] Presently, when the step shifts from 5 to 6, one of the choices "APPLY TO TUNE," "NEXT FOCAL PLANE," and "FINISH" must be selected on the browser interface.

The system test of the auto-focusing and auto-centering system was conducted online for the ^{82}Ge-beam production required for HiCARI commissioning. The auto-centering was performed for each focal plane in the order of F2, F5, and F7. Subsequently, the auto-focusing was performed for each focal plane in the order of F1, F2, F3, F5, and F7. Figure 1 shows the positions and phase spaces at each focal plane after the auto-focusing and auto-centering. These auto-tunings were successfully demonstrated. Furthermore, the operation time became shorter than that of conventional manual tuning.

In future work, the simultaneous tuning of the STQs and dipole magnets will be continuously automated in the order of F1 to F7.

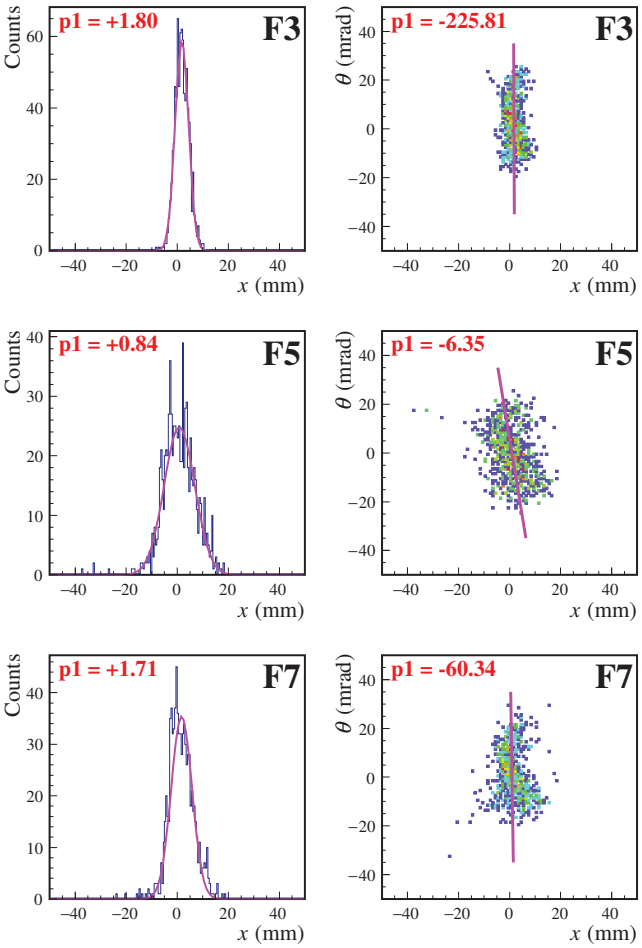

Fig. 1. Positions (left column) and phase spaces (right column) at each focal plane (F3, F5, and F7) after the auto-focusing and auto-centering. The pink curves and lines show the fitted functions of the Gaussian and 1st order polynomial, respectively. The p1 values show the fitted results.

*1 RIKEN Nishina Center

References

1) T. Kubo, Nucl. Instrum. Methods Phys. Res. B **204**, 97 (2003).
2) N. Fukuda *et al.*, J. Phys. Soc. Jpn. **87**, 014202 (2018).
3) T. Sumikama *et al.*, Nucl. Instrum. Methods Phys. Res. B **463**, 237 (2020).
4) N. Fukuda *et al.*, Nucl. Instrum. Methods Phys. Res. B **317**, 323 (2013).
5) Y. Shimizu *et al.*, RIKEN Accel. Prog. Rep. **50**, 206 (2017).
6) T. Sumikama *et al.*, in this report.
7) R. Brun, F. Rademakers, Nucl. Instrum. Methods Phys. Res. A **389**, 81 (1997).

Thermo-mechanical simulation of high-power rotating target for BigRIPS separator

K. Yoshida*1 and Y. Yanagisawa*1

Thermo-mechanical simulations have been performed for the high-power rotating target system[1,2] of the BigRIPS separator in order to evaluate the stability of the rotating target against high-power beam irradiation. A 2-mm-thick Be target rotating at 300 rpm is expected to heat up to 1230°C[3] with a ^{238}U beam at an energy of 345 MeV/nucleon and intensity of 1 particle μA, which meets the target beam intensity of RIBF. The Be target does not melt in the heat of the beam, because the melting point of Be is 1287°C. However, it is not clear whether the target is stable under thermal deformation or the destruction of the target at such a high temperature. Thus, the thermo-mechanical simulation of the rotating target was performed to check its stability.

Coupled transient thermal-structural finite-element analysis using the simulation code ANSYS[4] was utilized for the thermo-mechanical simulation. In the first step, the temperature distribution of the rotating target was obtained through a transient thermal calculation with the moving heat-source model described Ref. 3). The simulation model consisted of the Be target with a diameter of 300 mm and thicknesses of 2, 3, 4 mm and a cooling disk with a diameter of 240 mm and a thickness of 25 mm in which a cooling water channel was formed. The temperature dependence of thermal conductivity and heat capacity were taken into account in the calculation. Heat transfer coefficients of 10.5 and 3 kW/m^2 K were used for thermal contacts between the cooling water and cooling disk and between the cooling disk and Be target, respectively. The obtained time-dependent temperature distribution was then transferred to the transient structural calculation with ANSYS under elastic and plastic deformation. The deformation and stress caused by the thermal expansion of the target at the given temperature distribution were calculated in a time-dependent manner. The temperature dependence of the Young's modulus, strain-stress curve (bilinear hardening is assumed), and thermal expansion coefficient of the Be target were taken into account in the calculation.

Figure 1 shows the calculated results for a ^{238}U beam at 345 MeV/nucleon and 1 particle μA with a size of 1 mm^2 impinging on a 2-mm-thick Be target rotating at 300 rpm. In the figure, only half of the model is displayed in order to show the cross section of the target. In Fig. 1(a), the temperature distribution is mapped in color on the original model shape. The highest temperature is observed at the beam spot, and the high-temperature region is spread along the beam trajectory. The Von Mises stress due to the thermal expansion is mapped on the deformed model shape in Fig. 1(b). The deformation is magnified by a factor 50 and shown in Fig. 1(b). The Be target is enlarged by 0.6 mm in the radial direction and bent toward the cooling disk by 0.3 mm at the circumference. Thus, the deformation is very small compared with the 300-mm diameter of the rotating target. A small but finite plastic deformation is observed along the beam trajectory. This is why the von Mises stress at the beam trajectory decreases after the beam passes. A plastic expansion occurs at the beam spot, and the expanded shape is retained even when the temperature drops after the beam passes through.

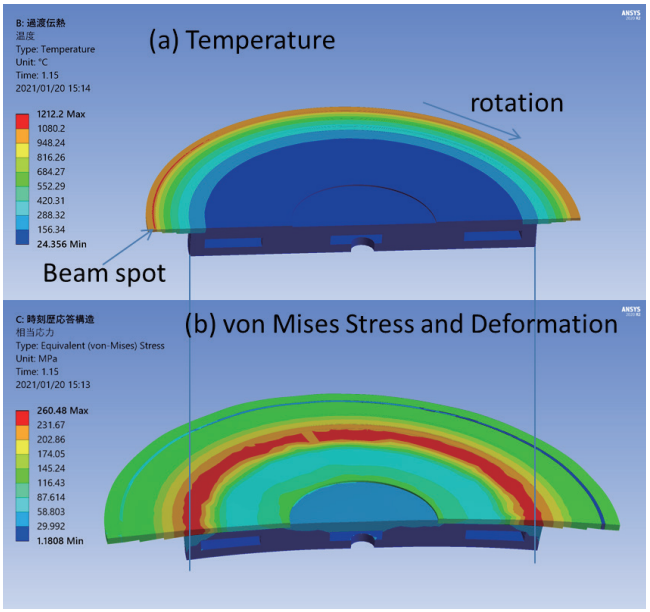

Fig. 1. Results of thermo-mechanical calculation of the rotating target. Only half of the simulation model is displayed in the figure to show the cross section of the target. (a) Temperature distribution of the target displayed in color on the original model shape (not deformed). (b) von Mises stress distribution displayed in color on the deformed shape. Deformation was magnified by a factor 50 so that the deformation can be viewed easily.

The maximum von Mises stress of 260 MPa appeared at the contact region between the target and cooling disk. The value is well below the ultimate tensile strength of 440 MPa. The calculation results show that the rotating target is stable under thermal deformation and destruction.

*1 RIKEN Nishina Center

References

1) A. Yoshida *et al.*, Nucl. Instrum. Methods Phys. Res. A **521**, 65 (2004).
2) A. Yoshida *et al.*, Nucl. Instrum. Methods Phys. Res. A **590**, 204 (2008).
3) K. Yoshida *et al.*, RIKEN Accel. Prog. Rep. **53**, 103 (2020).
4) ANSYS. Inc Product Release 20.

Incidents involving the DMT3 magnet in the beam transport line from SRC to BigRIPS

K. Kusaka,[*1] K. Yoshida,[*1] M. Ohtake,[*1] and Y. Yanagisawa[*1]

The DMT3 magnet in the "T-course" beamline is designed as a resistive-type magnet with saddle-shaped correction coils in addition to main coils. The correction coils are installed in the gap of the magnet and were originally excited with the main coils in series. The main coil has 72 turns and consists of 6 double pancakes, in which a 13.5×13.5 mm hollow conductor is wound 6 times in each layer. The correction coil, on the other hand, is a 12-turn double pancake. However, the layer isolation of the lower correction coil was damaged in an October 2017 incident.[1] Furthermore, the upper correction coil was found to be short-circuited in November 2019.[2] We then investigated the possible use of the DMT3 magnet without correction coils by increasing the energizing current.

As the maximum current of the original DMT3 power supply was 650 A, an additional auxiliary DC power supply was introduced in the DMT3 excitation circuit in a parallel connection. Water-cooled protection diodes were also used for safety.[2] At the end of the beam time in December 2019, we excited only the main coils in the DMT3 magnet using two power supplies with currents of 150 A and 563 A. We confirmed that the uranium beam focused on the BigRIPS target well and the main coils were well cooled with sufficient water flow. However, ramping the DMT3 power supply from 0 to 563 A with the simultaneous use of the auxiliary power supply with a current of 150 A caused instability; therefore, we were forced to ramp up in a stepwise manner to avoid instability.

In March 2020, we again tested power supplies for the operation of the DMT3 magnet without correction coils. Using the same excitation circuit, we energized the main coils while monitoring the voltage of each coil pancake. We found that the lower main coil was damaged.

Figure 1 shows the excitation voltage at each pancake of the DMT3 coils. Firstly, we energized the magnet by using the auxiliary power supply only with a current of 150 A. The voltages of all the pancakes coincided. We then further energized the magnet using the DMT3 power supply with a maximum current of 650 A. The total current was 800 A, which was larger than the current of 710 A used to transport uranium beams from SRC. The excitation voltages of the second and the fourth pancakes of the lower main coils decreased with time, while the voltage of other four pancakes increased because of the temperature rise of conductors. These unstable behaviors in excitation voltage indicate damage to the isolation between coil layers. We then decreased the current and re-energized with currents of 100 A and 610 A. The excitation voltage of all pancakes coincided in this case. We consider that the two pancakes are not critically damaged.

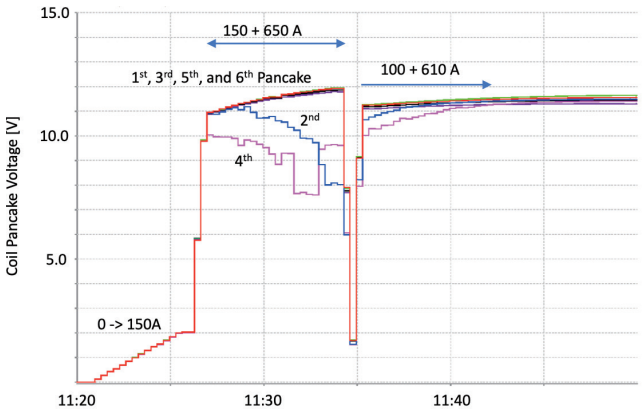

Fig. 1. Excitation voltage at each pancake of the DMT3 lower main coil.

Although the lower main coil of DMT3 was damaged, ^{238}U and ^{70}Zn beams were successfully transported from SRC to BigRIPS targets in 2020 beam time. We excited the DMT3 magnet with the main coils and undamaged lower correction coil, which was installed in 2018.

New main coils for the DMT3 magnet are now being designed and fabricated. The new main coil is designed so as to fit in the DMT3 iron pole and yoke. Furthermore, we increased the number of turns from 72 to 84 such that the original DMT3 power supply energizes the magnet without an auxiliary power supply. New main coils will be installed in early summer 2021.

References

1) K. Kusaka *et al.*, RIKEN Accel. Prog. Rep. **51**, 173 (2018).
2) K. Kusaka *et al.*, RIKEN Accel. Prog. Rep. **53**, 104 (2019).

*1 RIKEN Nishina Center

Trace-back method for dispersion matching conditions of primary beams at RIBF

A. Sakaue,[*1] D. S. Ahn,[*1] H. Baba,[*1] N. Fukuda,[*1] N. Fukunishi,[*1] N. Inabe,[*1] K. Itahashi,[*1] K. Kusaka,[*1] T. Nishi,[*1] Y. Shimizu,[*1] T. Sumikama,[*1] H. Suzuki,[*1] H. Takeda,[*1] T. Uesaka,[*1] Y. Yanagisawa,[*1] K. Yoshida,[*1] S. Y. Matsumoto,[*2,*3] R. Sekiya,[*2,*3] Y. K. Tanaka,[*3] K. Yako,[*4] and H. Geissel[*5]

We are preparing for an experiment to search for double Gamow-Teller giant resonance (RIBF-141R1, DGTGR) at RIBF. We use a part of BigRIPS, F0-F5, as a spectrometer;[1)] this is a common setup for spectroscopic experiments at the pionic Atom Factory (RIBF-135R1, piAF).

In these experiments, the energy spread of the primary beam has the largest contribution to the energy resolution. To remedy this situation, we are developing dispersion-matching optics, where the energy spread is canceled out under the condition that the dispersion at the target position F0 $(x|\delta)_{\mathrm{F0}}$ is 34.1 mm/% for DGTGR and 44.6 mm/% for piAF.

In order to satisfy these conditions with sufficient precision, we need to develop diagnostic methods of the phase distributions at F0 based on tracking information and the tuning method by using the optical elements in the upper stream. Owing to severe radiation conditions, detectors in the upstream sections require radiation hardening, and the information obtained in the section is limited. Here, we employ the trace-back method to obtain the phase distributions from distributions measured by tracking detectors at the F3, F5, and F7 planes. In this method, a set of the horizontal position x, angle a, and relative momentum deviation from the reference particle δ $(= \delta p/p)$ at F3 is converted to one at a certain plane by multiplying with a transfer matrix. The x and a at F3 are instantly obtained by measuring the trajectory of the beam using the tracking detectors. The δ is deduced from the horizontal positions x at F5 and F7, which are dispersive and achromatic focal planes, respectively.

We attempted to apply the method by analyzing data taken in June 2018 for study of the superconducting ring cyclotron-BigRIPS (SRC-BigRIPS) optical system. A primary beam of $^{18}O^{8+}$ with an energy of 230 MeV/nucleon was transported to F7. The beam trajectory was measured by parallel-plate avalanche counters (PPACs) at F3, F5, and F7 for different settings of optics between SRC and F0.

We obtained reconstructed phase distributions at F0 by using the trace-back method. Figure 1 shows the distributions at F0 for two different settings of optics, which are $(x|\delta)_{\mathrm{F0}} = 34.1$ mm/% for the upper panel and 44.6 mm/% for the lower panel. Each slope corresponds to the dispersion at F0, and the deduced values

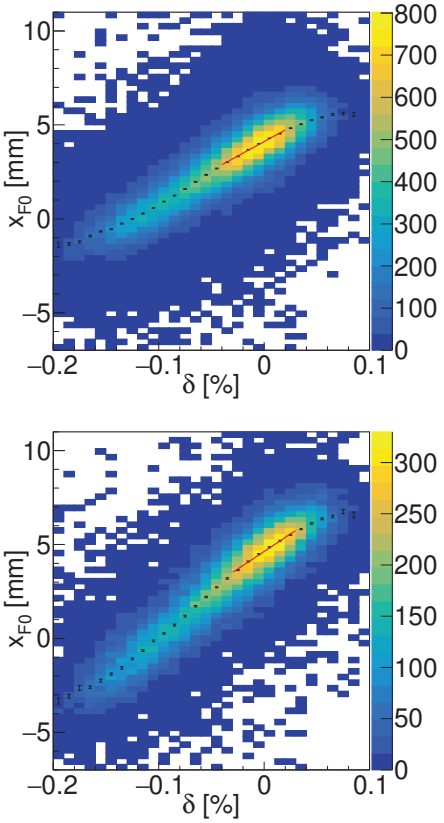

Fig. 1. Correlation between the deduced x and δ at F0 for two different settings: $(x|\delta)_{\mathrm{F0}} = 34.1$ mm/% (upper panel) and $(x|\delta)_{\mathrm{F0}} = 44.6$ mm/% (lower panel). Fitting results obtained using linear functions are shown with red lines. Each slope corresponds to the deduced dispersion.

are 30.8 mm/% and 37.3 mm/%, respectively. The fit region corresponds to the momentum spread for the well-tuned beam ($\sigma \sim 0.03\%$).[2)] The precision of determination of the dispersion at F0 is approximately 3 mm/%, which is sufficient as the experimental resolution. The absolute values of dispersion in this measurement were slightly different from the ideal values. By referring to the reconstructed distribution, we can tune the optics so as to cancel the difference. We are now refining the tuning method to provide an online feedback based on the diagnosis.

In summary, we have developed the trace-back method for tuning the dispersion at F0 so as to fulfill the matching condition. We are now working on an optimization of the tuning method for the beam time.

*1 RIKEN Nishina Center
*2 Department of Physics, Kyoto University
*3 RIKEN Cluster for Pioneering Research
*4 CNS, University of Tokyo
*5 GSI Helmholtzzentrum für Schwerionenforschung GmbH

References
1) T. Nishi *et al.*, Nucl. Instrum. Methods Phys. Res. B **317**, 290 (2013).
2) T. Nihsi, Doctoral Thesis, University of Tokyo (2015).

Conceptual design of a heavy ion storage ring RUNBA

M. Wakasugi,[*1,*2] T. Ohnishi,[*1] R. Ogawara,[*1,*2] S. Takagi,[*2] K. Kuze,[*2] and Y. Yamaguchi[*1]

We plan to construct a heavy ion storage ring, RUNBA (Recycled-Unstable-Nuclear Beam Accumulator) adjacent to the SCRIT facility in the E21 experimental room. RUNBA will be a research and development machine for developing and establishing a beam recycling technique in a storage ring for application to nuclear reaction studies for rare RI beam. This project is ongoing under the joint research program between ICR Kyoto University and RIKEN Nishina Center (RNC). In the last year, we transfered the storage ring (sLSR),[1] which was avandoned for more than ten years, from ICR to RNC. RUNBA is a rebuilt machine of sLSR and we are designing the lattice structure and machine layout in E21. Figure 1 shows a current floor plan of the RUNBA facility. RUNBA will be connected to ERIS, which is an ISOL system for SCRIT experiments.

Continuous singly-charged ion beams from ERIS are converted into a pulsed ion beam by FRAC and a highly-charged ion beam by RECB (Resonant Extraction Charge Breeder),[2] which is under development at ICR. A fully-stripped pulsed ion beam with 10 keV/nucleon is injected into RUNBA with a multi-turn injection method. Consequently, it can be accelerated up to 10 MeV/nucleon by repeating five times the acceleration process in which the ion velocity doubled by sweeping an RF frequency at the non-resonant ferrite cavity and synchronously ramping up the magnetic field.

The concept of beam recycling is that the energy loss, energy straggling, and transverse angular straggling produced when the beam passes through the internal target are corrected turn by turn and particle by particle, and beam circulation is stably maintained until nuclear reaction occurs at the target. Therefore, devices required to be equipped in RUNBA in addition to the fundamental optical elements include an internal target system, acceleration cavity, energy-dispersion corrector, and transverse emittance corrector. The fundamental properties in the current design of RUNBA are summarized in Table 1. The beta and dispersion functions over the whole ring are shown in Fig. 2. RUNBA optics is formed with 6 bending magnets, 3-family 12 quadrupole magnets, 2-family 4 sextupole magnets, and a triple-bend achromatic arc structure that is adopted to provide achromatic focus points for internal target insertion in the straight section. In another straight section, an energy-dispersion corrector will be installed and emittance correctors in the horizontal and vertical directions are placed at positions where the betatron phase advances are 0.75 from the target. The diffusion of energy spread would be suppressed by giving appropriate positive or negative energy gain determined from the difference in flight time from the target to energy-dispersion corrector. The emittance correctors transversely kick ions according to the transverse position measured at the target. These new feedback systems are now being developed at ICR.

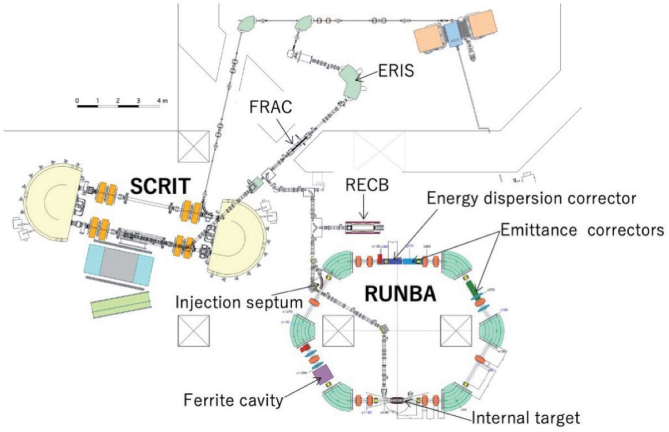

Fig. 1. A plane view of RUNBA facility.

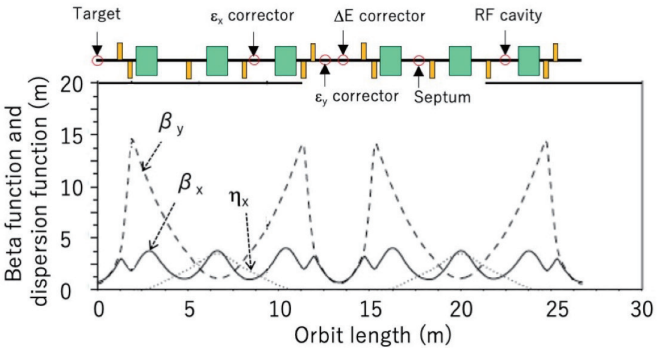

Fig. 2. Beta and dispersion functions of RUNBA.

Table 1. Lattice structure and properties of RUNBA.

Circumference (m)	26.557
Maximum Bρ (Tm)	1.05
Transition γ	1.855
Harmonics (10 keV/nucleon, 10 MeV/nucleon)	(32, 1)
RF frequency (MHz)	1.674–3.348
Tunes (ν_x, ν_y)	(2.368, 1.695)
Max. dispersion functions (η_x, η_y) (m) at focal point	(3.497, 0.0)
Beta functions (β_x, β_y) (m)	(0.697, 0.527)
Dispersion functions (η_x, η_y) (m)	(0.0, 0.0)

*1 RIKEN Nishina Center
*2 ICR, Kyoto University

References

1) A. Noda *et al.*, Proc. EPAC2006, 237 (2006).
2) R. Ogawara *et al.*, in this report.

Development of Resonant-Extraction Charge Breeder (RECB)

R. Ogawara,[*1,*2] S. Takagi,[*2] K. Tsukada,[*2] H. Tongu,[*2] Y. Kuriyama,[*2] and M. Wakasugi[*1,*2]

In the RUNBA project,[1] RI ions from ERIS[2] are accelerated in the storage ring (RUNBA) for nuclear reaction experiments. For efficient acceleration, RI ions should be a highly charged ion beam. Although an EBIT type charge breeder (CB) is widely used to increase the charge state, an efficiency of only 20% hase been achieved do far because of finite spread in charge state distribution.[3] We developed a prototype of a resonant-extraction charge breeder (RECB) to improve the efficiency, the RECB can selectable extract only the desired charge state ions.

In a RECB, a longitudinal electrostatic potential for ion trapping is designed as a quadratic shape on an electron beam axis (Fig. 1). The longitudinal motion of ions in the potential is a simple harmonic oscillation for which the frequency depends on the mass-to-charge ratio. Thus, the ion motion is excited by adding an oscillation to the electrostatic potential at the resonant frequency. Then, ions of a selected charge state are extracted from the trapping regions, and the others are left in the RECB. When we apply a time-dependent potential $V_{\mathrm{trap}}(z,t) = (a + b\sin(\omega t))z^2$ (z, ω, and a and b represent the position, frequency of the potential oscillation, and constants, respectively), the ion motion is described by Mathieu's differential equation.

As shown in Fig. 1, RECB consists of an electron gun, a solenoid coil, an electron beam collector, and 20 electrodes that form the trapping potential $V_{\mathrm{trap}}(z,t)$ using a DC power supply and a function generator. In the trapping region, the energy, current, and beam radius, of the electron beam were −32 keV, 10 mA, and 0.06 mm, respectively. Collection efficiency at the electron beam collector was more than 99.5% when the solenoid magnetic field was 0.13 T. Extracted ions with an energy of 10 keV/q from the RECB were separated by the analyzing magnet, and then, they were detected with a channeltron.

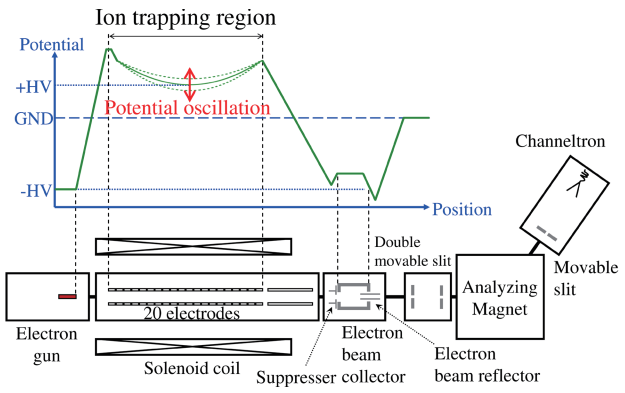

Fig. 1. The schematic diagram of the prototype RECB.

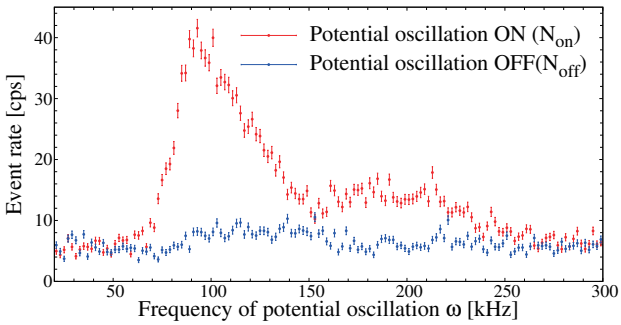

Fig. 2. Spetrum of extracted $^{12}C^{4+}$ ions.

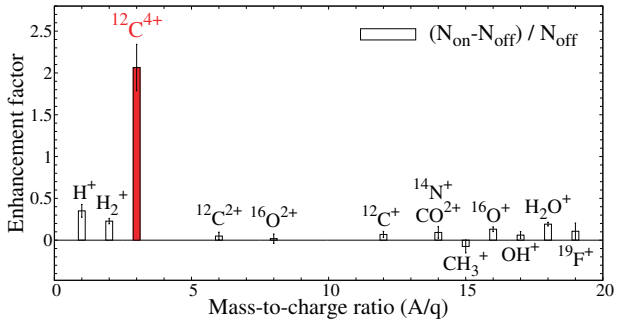

Fig. 3. Enhancement factors of extracted of $^{12}C^{4+}$ ions.

We evaluate the performance of the potential oscillation by measuring the extracted residual gas ions (vacuum pressure = 5×10^{-6} Pa). Figure 2 shows an example of a $^{12}C^{4+}$ ion extraction where the depth of the quadratic shape potential is 150 V and the function generator supplies a 1.0 V_{pp} sine wave for a short duration of 0.5 ms with a repetition rate of 500 Hz. The red and blue plots indicate the spectrum of the extracted $^{12}C^{4+}$ ions from the RECB with and without the potential oscillation (N_{on} and N_{off}), respectively. We confirmed that $^{12}C^{4+}$ ions were extracted at their fundamental frequency (90 kHz) and second order harmonic frequency (180 kHz). The spread of the spectrum was attributed to a distortion of the electrostatic potential produced by the space charge of trapped ions. Figure 3 shows the enhancement factor estimated by the event rate for ($N_{\mathrm{on}} - N_{\mathrm{off}}$) divided by that for N_{off} at a frequency of 90 kHz. The enhancements for the $^{12}C^{4+}$ ions were 30, 42, and 9.0 times greater than those for the $^{12}C^{+}$, $^{12}C^{2+}$, and H_2^+ (same A/q of $^{12}C^{6+}$) ions, respectively. In future work, we will optimize the electrostatic potential form to improve charge state selectivity for extraction.

*1 RIKEN Nishina Center
*2 Institute for Chemical Research, Kyoto University

References

1) M. Wakasugi *et al.*, in this report.
2) T. Ohnishi *et al.*, Nucl. Instrum. Methods Phys. Res. B, **317**, 357 (2013).
3) F. Wenander, J. Instrum. **5**, C10004 (2010).

Development of a forward detector for the measurement of the mean square radius of the neutron distribution of unstable nuclei by electron scattering

H. Wauke,[*1,*2] A. Enokizono,[*1] T. Suda,[*1,*2] K. Tsukada,[*1,*3] T. Ohnishi,[*1] M. Wakasugi,[*1,*3] M. Watanabe[*1]

In nuclear physics, the nucleon density distribution is an essential physical quantity because it directly reflects the wave function of nucleons. Electron scattering provides detailed information of the nucleus's charge density distribution, dominated by the proton distribution. However, it is difficult to determine the neutron distribution by electron scattering because its contribution to the charge density distribution is less than a few percent.

It was recently suggested that the mean square radius (msr) of the neutron distribution could be accessed by measuring the fourth–order moment of the charge density distribution.[1,2] The charge form factor deduced from elastic electron scattering at the low momentum transfer can be Taylor-expanded as $F(q) \sim 1 - \frac{<r^2>_c}{6}q^2 + \frac{<r^4>_c}{120}q^4 - \frac{<r^6>_c}{5040}q^6 \cdots$, where F is the form factor, q is the momentum transfer, and $< r^n >_c$ is the nth-order moments of the charge density distribution. Figure 1 shows the q^2 dependence of the ^{132}Xe form factor and the contribution of each term of the above equation. The msr of the neutron distribution measurement of unstable nuclei by electron scattering will be obtained in a region that covers the forward scattering angle (12–25° for the electron beam energy $E_e = 150$ MeV). In the low momentum transfer region (less than 0.09 fm^{-2} in the case of Xe isotopes), the form factor is sensitive almost to only the second- and fourth-order moments of the charge density distribution.

The study of the msr of the neutron distribution of Xe isotopes (stable : $^{124–136}$Xe, unstable : ^{138,140}Xe) by electron scattering is under consideration at the SCRIT facility.[3] A forward detector for measuring the fourth-order moment of the charge density distribution is under discussion. A series of background studies were performed using an alternative detector to investigate the number of background events at the new setup for the measurement in the low momentum transfer region. This is because it may not be possible for the forward detector to distinguish between the elastic scattered electrons signals from the target nuclei and the background signal if there are more or similar amounts of background events than the true one in the target region (length is 500 mm). The background study was performed with a calorimeter array of seven CsI crystals and two drift chambers, which covered a scattering angle of $18 \pm 1°$ from the center of the SCRIT device and measured the scattered electrons energy E'_e by summing energy deposits of CsIs.

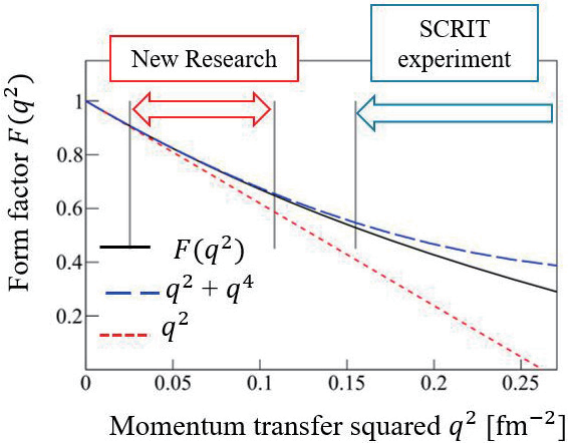

Fig. 1. q^2 dependence of the ^{132}Xe form factor obtained by the past experiment.[4] The black line shows the form factor for which all moments are calculated. The red and blue lines show the form factor up to the second- and fourth-order moment of the charge density distribution, respectively.

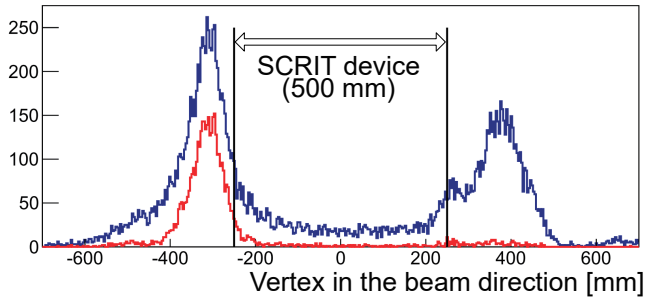

Fig. 2. Reconstructed vertex distribution of electron scattering events from the target region (blue line). The red line shows the events where the scattered electrons have kinetic energies higher than 100 MeV. The events at −450 to −200 mm are from the material upstream of the target region. The blue line shows events containing low energy.

Figure 2 shows the reconstructed vertex distribution of electron scattering events from the target region. The red line in Fig. 2 denotes those of $E'_e > 100$ MeV and is identified as the elastic events. These events at −450 to −200 mm are considered as the elastic scattering events of the electron beam halo from the material upstream of the target region. The forward detector cannot separate these events from the vertex distribution of the target nuclei. It needs to consider approaches to reduce background events, for example, by reducing the material around the SCRIT device.

*1 RIKEN Nishina Center
*2 ELPH, Tohoku University
*3 Institute for Chemical Research, Kyoto University

References

1) H. Kurasawa, T. Suzuki, Prog. Theor. Exp. Phys. **2019**, 113D01 (2019).
2) H. Kurasawa, T. Suda, T. Suzuki, in this report.
3) M. Wakasugi *et al.*, Nucl. Instrum. Methods Phys. Res. B **317**, 668 (2013).
4) K. Tsukada *et al.*, Phys. Rev. Lett. **118**, 262501 (2017).

Ion-beam-profile monitor using MCP at the SCRIT electron scattering facility

T. Ohnishi,[*1] S. Ichikawa,[*1] and M. Wakasugi[*1,*2]

At the SCRIT electron scattering facility,[1] ion-beam-profile monitors[2] are installed in the ion-beam transport line for injecting low-energy (∼10 keV) ions into the SCRIT device.[1] They are composed of a meshed Faraday cup, a CsI(Tl) scintillator, an optical prism, and a network-based CCD camera. Using these monitors, ion-beam tuning is performed in real time. However, it is difficult to apply them to a low-rate ion beam, such as a continuous beam with 10^7 ions/s or a pulsed beam with 10^6 ions/pulse, because the number of produced photons is considerably less than the expected value calculated using the conversion factor, 2×10^4 photons/MeV. One of the reasons for this suppression is that the low-energy ions stop near the surface of a CsI(Tl) scintillator and the number of involved CsI molecules is insufficient. Thus, a new ion-beam-profile monitor is required for real-time beam tuning with low-energy RI beams. This year, we tested a new monitor using a micro channel plate (MCP) and report out first results in this paper.

Figure 1 presents a schematic view and photograph of an ion-beam-profile monitor using an MCP. This monitor consists of two MCPs equipped with a phosphor screen (HAMAMATSU F2806 with P46), an optical prism, and a network-based CCD camera (Basler scA640-70gc). The horizontal and vertical dimensions of the effective area of the MCP are 45 mm and 35 mm, respectively. A collimator, which has a 28-mm diameter hole, is installed in front of the optical prism to define the effective detection area because the effective area of the MCP is larger than the entrance size of the optical prism, 30 mm^2. In the present setting, ion beams are directly observed with MCPs. The applied voltages of MCP-in, MCP-out, and Phos-in, which are electrodes shown in Fig. 1, are 0, 2, and 6 kV, respectively. The extracted electron cloud resulting from the beam encountering the MCP surface is converted to photons in the phosphor screen, which are transported to the CCD camera through the collimator and the optical prism. The exposure time of the CCD camera is set to 500 μs. Data from the CCD camera are monitored through a network in real time. With a pulsed beam, the trigger of the CCD camera is synchronized with the injection timing.

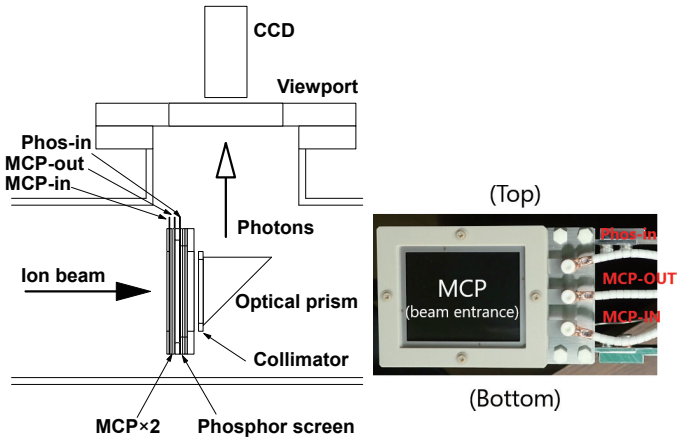

Fig. 1. Schematic view and photograph of the ion-beam-profile monitor. MCP-IN, MCP-OUT, and Phos-in represent electrodes of the monitor.

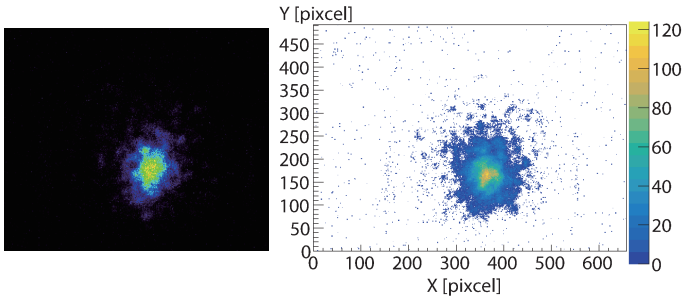

Fig. 2. Beam profile of 1 pulse with a 10^4 ions/pulse beam. Left figure is the image of the beam profile and right figure is its digital number distribution.

The commissioning of the new ion-beam-profile monitor was performed using a ^{138}Ba-ion beam of 6 keV. Figure 2 shows the measured beam profile of only 1 pulse using a 1-Hz pulsed beam with 10^4 ions/pulse. The number of ions with a low-intensity pulsed beam was estimated with the current of a continuous beam, 13 pA, measured at the Faraday cup installed in front of the ion-beam-profile monitor. Calibration was performed using a 0.3-nA continuous beam and a pulsed beam with 5×10^5 ions/pulse. Figure 2 shows an image of the beam profile (left) and its digital number distribution (right). More detailed analysis is being performed to estimate the number of injected ions using only the digital number distribution.

We tested the new ion-beam-profile monitor using an MCP with a low-intensity pulsed ion beam. The beam profile of a low-intensity pulsed ion beam was successfully measured in real time. In the case of RI beams using the present monitor, electrons corresponding to the decay of the RIs can cause background events. To avoid this problem, a thin foil is installed in front of the MCPs to stop RI beams, and electrons produced during the decay of RIs are used as an MCP signal. Next year, we will test a new setup using RI beams and evaluate its applicability considering the efficiency and position resolution.

*1 RIKEN Nishina Center
*2 ICR, Kyoto University

References

1) M. Wakasugi *et al.*, Nucl. Instrum. Methods Phys. Res. B **317**, 668 (2013).
2) M. Togasakai *et al.*, RIKEN Accel. Prog. Rep. **44**, 173 (2011).

Extraction test of stopped Bi isotopes in PALIS gas cell

T. Sonoda,[*1] I. Katayama,[*1] M. Wada,[*2] H. Ishiyama,[*1] V. Sonnenschein,[*3] H. Tomita,[*3] R. Terabayashi,[*3] K. Hattori,[*3] H. Iimura,[*4] S. Iimura,[*1] T. M. Kojima,[*1] M. Rosenbusch,[*2] A. Takamine,[*1] N. Fukuda,[*1] T. Kubo,[*1] S. Nishimura,[*1] Y. Shimizu,[*1] T. Sumikama,[*1] H. Suzuki,[*1] H. Takeda,[*1] M. Tanigaki,[*5] and K. Yoshida[*1]

We are developing a scheme of parasitic low-energy RI-beam production (PALIS)[1] in the second focal chamber (F2) of BigRIPS to effectively use rare isotopes and to perform comprehensive measurements of the physical properties of exotic nuclei.

In our previous experiment,[2] we confirmed the feasibility of a new gas-cell geometry that separates high- and low-radiation areas with a long gas tube. The current setup for the PALIS on-line examination evaluates RI extraction by detecting alpha rays via alpha-emitter decay, which results in enhanced sensitivity because of the extremely low background environment. While the alpha-emitter element should be available on resonant laser ionization in an off-line or on-line experiment. Therefore, we chose a bismuth (^{191}Bi) beam that can be produced by projectile fragmentation via a uranium beam and beryllium target. In a 12 hours online PALIS experiment, we focused on two objectives: 1) identify the stopped Bi isotope and 2) extract the stopped Bi isotope from the gas cell.

To achieve the first objective, we observed alpha rays created via decays from the alpha emitters that were stopped in the ΔE solid-state detector (SSD) placed in front of the gas cell by adjusting the energy degrader, as shown in Fig. 1. As the energy resolution was considerably low because of the high electrical background at F2, isotope identification by alpha energy (E_α) was impossible from this energy spectrum. However, we obtained other information from the timing chart by using a pulsed BigRIPS beam. The half-lives extrapolated by decay fitting to individual timing charts for specific energy ranges were 42.12 ± 4.66 s (5.4–6.1 MeV), 11.87 ± 0.73 s (6.1–6.6 MeV) and 7.7 ± 0.3 s (6.6–7.5 MeV). The tentative isotope candidates for these half-lives are ^{192}Bi ($T_{1/2} = 39.6$ s, $E_\alpha = 6060$ keV), ^{191}Bi ($T_{1/2} = 12.4$ s, $E_\alpha = 6309$ keV), and ^{190}Bi ($T_{1/2} = 6.4$ s, $E_\alpha = 6456$ keV).

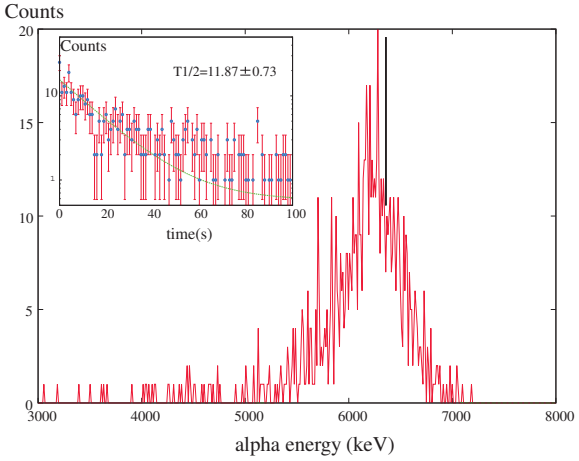

Fig. 1. Alpha spectrum observed using a ΔE Solid-state detector (SSD) placed in front of the gas cell. The inset shows the alpha counts versus time in the beam-off period in the energy range of 6.1–6.6 MeV in the alpha spectrum.

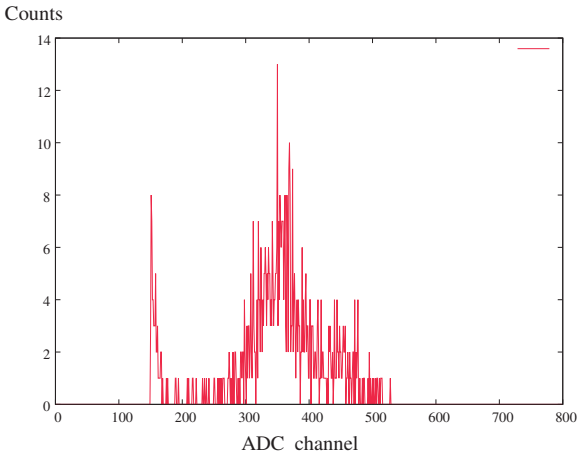

Fig. 2. Alpha spectrum observed using a silicon PIN diode placed after the gas-cell exit.

To achieve the second objective, we performed an extraction test of RIs that were stopped in argon gas (50 kPa) and transported to the gas-cell exit via a long gas tube by simple gas flow to finally impinge on a silicon PIN diode detector located after the gas-cell exit hole. We confirmed the extracted RIs from alpha spectra observed using the silicon PIN diode, as shown in Fig. 2. These extracted RIs included species of all charge states such as neutral and positive/negative ions. By comparison with the total number of alpha counts detected at the ΔE SSD, normalizing primary beam intensity, and considering the solid angle of the detector, we preliminarily evaluated the extraction efficiency as approximately 1%.

The extraction of stopped RIs out of the gas cell was confirmed. In the next beam time, we will apply laser ionization for producing low-energy RI beam.

*1 RIKEN Nishina Center
*2 Wako Nuclear Science Center (WNSC), IPNS, KEK
*3 Faculty of Engineering, Nagoya University
*4 Advanced Science Research Center, JAEA
*5 Institute for Integrated Radiation and Nuclear Science, Kyoto University

References

1) T. Sonoda *et al.*, Prog. Theor. Exp. Phys. **2019**, 113D02 (2019).
2) T. Sonoda *et al.*, RIKEN Accel. Prog. Rep. **53**, 105 (2019).

Improvement of evacuation time of RI from argon gas cell

T. Sonoda,[*1] M. Wada,[*2] K. Hattori,[*3] H. Iimura,[*4] S. Iimura,[*1] H. Ishiyama,[*1] I. Katayama,[*1] T. M. Kojima,[*1] M. Rosenbusch,[*2] V. Sonnenschein,[*3] R. Terabayashi,[*3] A. Takamine,[*1] and H. Tomita[*4]

An argon gas cell coupled to a resonant laser ionization is a powerful tool for the production of high-purity low-energy RI-beam. This method utilizes neutral RI transportation using simply a gas flow, until it reaches the location for laser ionization which is typically close to the exit of the gas cell. A feasible RI is restricted by its half-life, which should be longer than the evacuation time of the gas cell. The evacuation time can be determined from the conductance of a small exit aperture and gas cell volume. Under adiabatic expansion, the conductance depends only on the diameter of the exit aperture[1] as follows:

$$C = 0.14 \times \phi^2. \quad (1)$$

where the units are L/s for C and mm for ϕ. The gas is argon. The evacuation time of a gas cell of volume V can be written as:

$$t = \frac{V}{C}. \quad (2)$$

For example, when the gas cell volume is 100 cm^3 and the exit diameter is 1 mm, the evacuation time is 714 ms. This value makes it difficult to aim for very rare RI regions, where the half-lives are typically less than 100 ms.

In order to address a fast evacuation, two solutions can be considered: (1) using a small volume for the gas cell and (2) using a large exit aperture. However, these improvements are limited by the stopping efficiency for high-energy RIs, which require a large volume acceptance. They are also limited by the capability of differential pumping. Here we propose installation of an rf-carpet with a very small exit aperture in the initial differential pumping room while using a large aperture for the gas cell exit. Figure 1 shows a schematic layout. The rf-carpet is placed after the gas cell exit. The pressure in this room can be increased up to 1 kPa at which the ion extraction by the rf-carpet is still practical without a discharge problem. The ions move with a gas jet toward the rf-carpet after exiting the gas cell; subsequently they are guided by the rf- and dc-electric fields to the exit of the rf-carpet. Owing to the small exit aperture of the rf-carpet, the loads from the following differential pumping are suppressed. When the exit aperture of the gas cell is large, the total gas throughput becomes very high, leading to an extremely high gas consumption cost. However, by using a gas circulation system,[2] the gas consumption rate can be drastically saved.

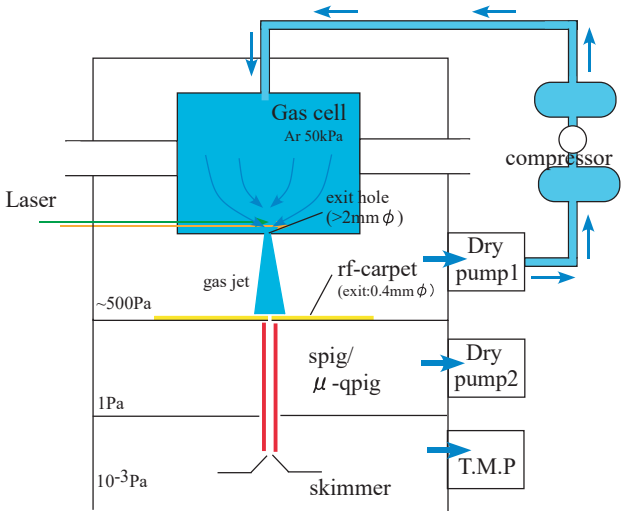

Fig. 1. Proposed gas cell and differential pumping layout in combination with rf-carpet.

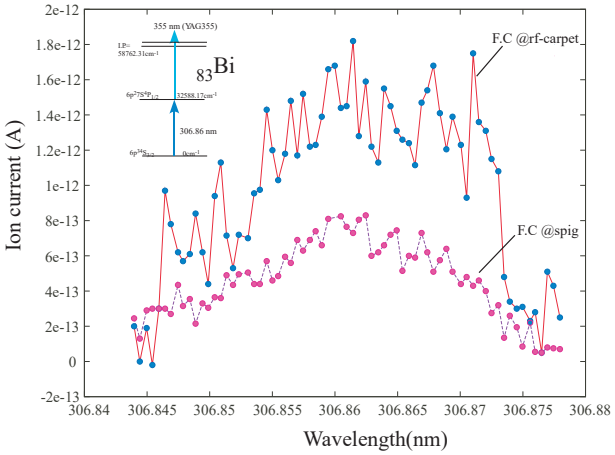

Fig. 2. Ionization spectrum by scanning first step excitation when rf-carpet/spig is used as Faraday cup.

A preliminary off-line experiment was conducted with a 0.4 mm rf-carpet aperture for photo-ionized Bi ions. The pressure at the rf-carpet was approximately 500 Pa. Bi atoms were produced inside the gas cell, and subsequently they were ionized by the laser and extracted from the gas cell exit (2 mmϕ). Figure 2 shows the result of the comparison when the ions are collected on the rf-carpet and on the spig rods placed next to the rf-carpet. We confirmed a reasonable extraction efficiency for the rf-carpet. The feasibility study is in progress.

*1 RIKEN Nishina Center
*2 Wako Nuclear Science Center (WNSC), IPNS, KEK
*3 Faculty of Engineering, Nagoya University
*4 Advanced Science Research Center, JAEA

References

1) A. Roth, *Vacuum Technology* (North-Holland, Amsterdam 1982).
2) T. Sonoda, *et al.*, Rev. Sci. Instrum. **87**, 065104 (2016).

Fourth report on offline tests for RF carpet transportation in RF ion guide gas cell at the SLOWRI facility

A. Takamine,[*1] S. Iimura,[*1,*2,*3] D. Hou,[*3,*4,*5] M. Wada,[*3] M. Rosenbusch,[*3] S. Chen,[*3,*6] W. Xian,[*3,*6] S. Yan,[*3,*7] P. Schury,[*3] Y. Ito,[*1,*8] T. M. Kojima,[*1] T. Sonoda,[*1] Y. X. Watanabe,[*3] H. Ueno,[*1] and H. Ishiyama[*1]

A new gutter structure RF ion guide gas cell[1] was developed at the SLOWRI facility. The gas cell comprises two RF carpet (RFC) stages. We previously reported on the transportation efficiencies of the 1st stage RFC for various gas pressures and various RF frequencies.[2,3] In this report, the transport efficiency including the 2nd stage RFC is presented.

The 2nd RFC comprises concentric ring electrodes with a pitch of 0.26 mm (electrode width of 0.1 mm and inter-electrode spacing of 0.16 mm); there is a ϕ0.65 mm exit hole at the center of the 2nd RFC. Ions are collected onto the 1st carpet and transported to the inner edges of the pair of the 1st RFCs. After they are pulled over the edge to the 2nd RFC by a DC field, they are delivered to the exit hole by the "ion surfing" transport technique that uses the combination of two-phases RF and four-phases audio-frequency (AF) fields[4] (Fig. 1). A segmented quadrupole ion beam guide (smQPIG) is placed behind the exit hole. The ions are transported to a high vacuum region by the smQPIG through differential pumping stages.

We recently investigated the transport efficiency including the 2nd RFC in offline tests. Cesium ions were produced from a surface ionization ion source at the inner wall of the gas cell. The entire setup has been described in Ref. 1). We measured the ion currents on the RFCs and subsequently on the smQPIG. The RFC transport efficiency was defined as the ratio of the two currents.

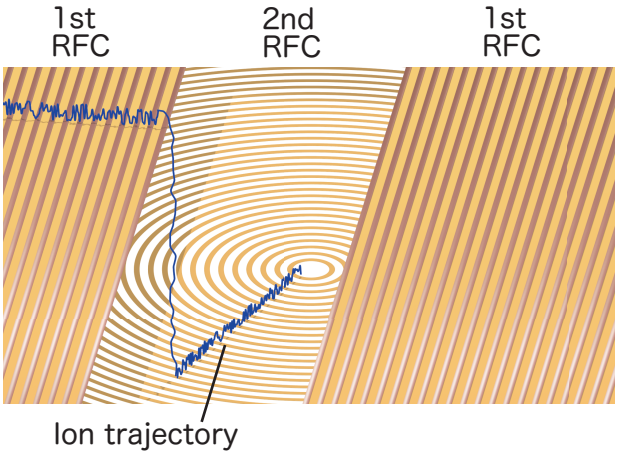

Fig. 1. Sketch of 1st RFC and 2nd RFCs around the exit hole with an ion trajectory in blue.

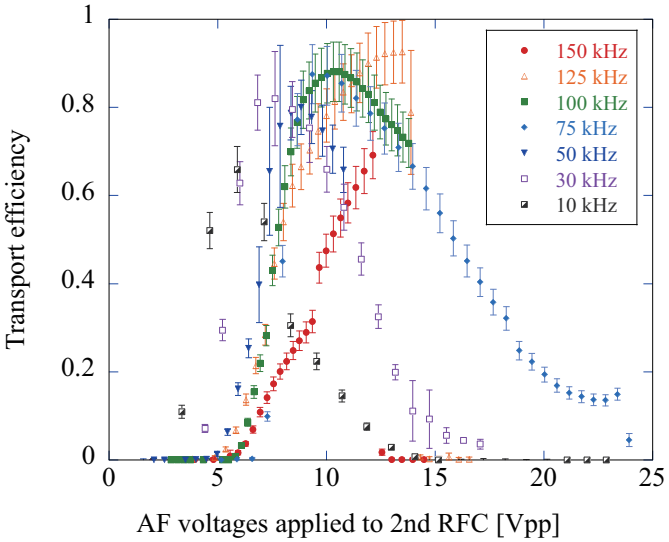

Fig. 2. Offline test results on the transport efficiency for Cs^+ as a function of AF voltages at various AF frequencies.

Figure 2 shows the test results in 133 mbar of room temeperature He gas as a function of the AF voltages for various AF frequencies. The RF voltages applied to the 1st and 2nd RFCs were 103 V_{pp} at 8.15 MHz and 111 V_{pp} at 10.06 MHz, respectively. The push DC field between the 1st and 2nd RFCs was ~40 V/cm. We achieved ~90% transport efficiency with an AF frequency of 125 kHz in this measurement. The plots show a sudden drop at 12–15 V_{pp} for AF frequencies $\geq$125 kHz, because the AF signals became highly distorted by the AF/RF coupling circuitry. An attempt to improve the circuit characteristics is afoot.

This gas cell was coupled to an MRTOF mass spectrograph for a parasitic experiment during the HiCARI campaign in 2020. The online experiment results about this gas cell are reported in other articles by S. Iimura and D. Hou in this issue.

*1 RIKEN Nishina Center
*2 Department of Physics, Osaka University
*3 Wako Nuclear Science Center (WNSC), IPNS, KEK
*4 Institute of Modern Physics, Chinese Academy of Sciences
*5 School of Nuclear Science and Technology, Lanzhou University
*6 Department of Physics, The University of Hong Kong
*7 Institute of Mass Spectrometry and Atmospheric Environment, Jinan University
*8 Advanced Science Research Center, JAEA

References

1) A. Takamine *et al.*, RIKEN Accel. Prog. Rep. **52**, 139 (2019).
2) S. Iimura *et al.*, RIKEN Accel. Prog. Rep. **53**, 107 (2020).
3) A. Takamine *et al.*, RIKEN Accel. Prog. Rep. **53**, 108 (2020).
4) G. Bollen, Int. J. Mass Spectrom. **299**, 131 (2011).

High mass resolving power and isomeric state separation at SLOWRI/ZD-MRTOF system

W. Xian,[*1,*2] M. Rosenbusch,[*2] S. Chen,[*1,*2] Y. Hirayama,[*2] D. Hou,[*3,*2] S. Iimura,[*5,*4] H. Ishiyama,[*4] Y. Ito,[*6] S. Kimura,[*4] J. Liu,[*3] H. Miyatake,[*2] S. Nishimura,[*4] T. Niwase,[*7,*4,*2] P. Schury,[*2] A. Takamine,[*4] M. Wada,[*2] Y. X. Watanabe,[*2] H. Wollnik,[*8] and S. Yan[*9]

With high precision and accuracy, as well as short measuring times, the multi-reflection time-of-flight mass spectrograph (MRTOF-MS) has become competitive with Penning traps for measuring masses of short-lived nuclei.[1)] In 2013, the first MRTOF built at RIKEN was tested online by measuring ^{8}Li ions. The mass excess of ^{8}Li was accurately reported to be 20947.6(15)(34) keV ($\Delta m/m \sim 6.6 \times 10^{-7}$). The mass resolving power achieved at that time was $R_m > 150$k.[2)] In 2020, a next-generation device of similar design has been put into operation at the ZeroDegree spectrometer of RIBF with the goal of measuring very exotic nuclides and their isomers with a higher resolving power.

In the MRTOF reflection chamber, ions are confined and reflected back and forth between a pair of ion reflection mirrors, allowing the ions to have a flight path of up to or beyond one kilometer. In any field-free drift region, more energetic ions have a shorter time-of-flight, but in the reflection region inside the ion mirrors, this can change because of the shape of the potential distribution. It is possible to make more energetic ions penetrate deeper into the mirrors to achieve a longer flight path that compensates for their higher energy and equilibrates the time-of-flight with that of less energetic ions. The better this compensation works, the narrower the final TOF distribution can be as ions with different energies can simultaneously reach the detector.[3)] However, this requires a non-trivial search for complex mirror potentials and those of ion-optical focusing elements located in the central drift tube section. In our case, this would require a search in 11-dimensional parameter space.

In a first-order approach, every possible potential distribution is the generator of a function mapping the TOF of an ion to a kinetic energy TOF(E). In recent offline experiments using the new ZD-MRTOF system, by use of a pulsed drift tube between the ion trap and MRTOF, we measured these response functions in a much wider energy range than done before. This measurement was repeated after changing some voltage of each ion mirror. In this manner, the effect of changing each mirror potential on this function could be studied. This allowed for an improved local search around the present conditions to fulfill the condition $\partial \mathrm{TOF}(E)/\partial E \approx 0$ for a particular number of reflections. The different shapes of the TOF(E) functions have been added in an appropriate manner, which resulted in a new voltage configuration with excellent energy compensation.

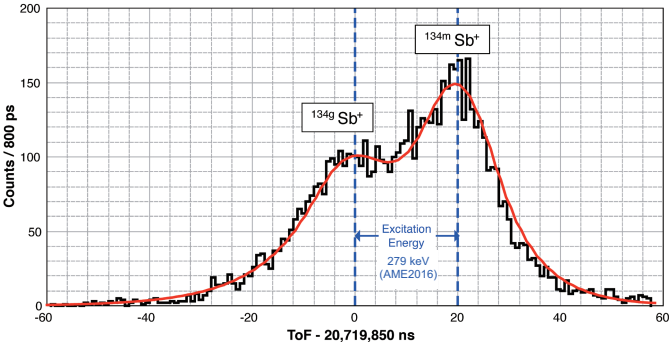

Fig. 1. TOF spectrum of ^{134g}Sb^{+} and ^{134m}Sb^{+} in the online experiment of the ZD-MRTOF system.

In the corresponding offline tests, by using ^{39}K^{+} ions from a thermal ion source to perform the procedure mentioned above, a mass resolving power $R_m \sim 700$k was achieved for the first time at RIBF, with a flight time of ~9 ms after 490 laps.

The first online commissioning experiment of the MRTOF at ZeroDegree terminal was conducted at the end of 2020. Even under online conditons, we were generally able to maintain a mass resolving power in excess of 500k during the commissioning. This high mass resolving power allowed us to demonstrate an isomeric separation of ^{134m,g}Sb^{+}, which has an isomeric state with an excitation energy of 279(1) keV [$T_{1/2}$ = 10.07(5) s] above the ground state [$T_{1/2}$ = 0.78(6) s]. As shown in Fig. 1, we could successfully identify the ground state (^{134g}Sb^{+}) and the isomeric state (^{134m}Sb^{+}) in the TOF spectrum owing to the very high mass resolving power that the ZD-MRTOF system achieved.

*1 Department of Physics, The University of Hong Kong
*2 Wako Nuclear Science Center (WNSC), IPNS, KEK
*3 Institute of Modern Physics, Chinese Academy of Science
*4 RIKEN Nishina Center
*5 Department of Physics, Osaka University
*6 Advanced Science Research Center, JAEA
*7 Department of Physics, Kyushu University
*8 Dep. of Chem. and Biochem., New Mexico State University
*9 Institute of Mass Spectrometry and Atmospheric Environment, Jinan University

References

1) Y. Ito *et al.*, Phys. Rev. C **88**, 011306(R) (2013).
2) P. Schury *et al.*, Nucl. Instrum. Methods Phys. Res. B **335**, 39 (2014).
3) R. N. Wolf *et al.*, Int. J. Mass Spectrom. **313**, 8(2012).

Offline ion source for laser spectroscopy of RI at SLOWRI†

M. Tajima,[*1] A. Takamine,[*1] M. Wada,[*2] and H. Ueno[*1]

The collinear laser spectroscopy of radioactive isotope (RI) beams is a powerful technique used to directly measure the nuclear properties of ground or isomeric states. Isotope shift measurement is planned using RI ion beams supplied from the universal slow RI-beam facility (SLOWRI) at RIBF. The main targets are medium-mass nuclei of refractory elements, for which experimental studies are insufficient. To achieve high precision, it is essential to determine a reference frequency with well-studied isotopes for the planned spectroscopy apparatus to minimize systematic uncertainties. In this work, an ion source combining the laser ablation of solid targets in helium gas and a radio frequency (RF) ion guide system with an RF carpet[1)] was constructed for the reference measurement of isotope shifts.

Figure 1(a) shows a sketch of the ion source. It consists of cylindrical DC electrodes, an RF carpet, a quadrupole ion beam guide, and an RF quadrupole (RFQ). A solid target for laser ablation was fixed on the surface of the cylindrical DC electrodes. Helium gas was continuously introduced into the first chamber via a piezo valve while the second and the third chambers were evacuated. The pressure of the first chamber was measured using a capacitance manometer and stabilized by controlling the piezo valve with proportional-integral-derivative (PID) feedback. A Q-switched Nd:YAG laser (532 nm, ∼5 ns width) was installed outside the chamber. The laser light was focused using a lens, and the light passed through a view port normal to the ablation target surface. The laser power was 25 mJ per pulse at maximum, and it could be varied using a manual attenuator. The spot size was ≤1 mm, which corresponds to a maximum fluence of 3.2 J/cm^2. The lens was moved using XY linear stages remotely controlled via a LabVIEW program on a step-by-step basis such that the laser spot moved randomly on the surface of the target. This ion source system was connected to a test beamline through an insulation flange. The ion source could be biased to 10 kV to extract ion beams to the downstream beamline, which was grounded. A dipole magnet with movable slits was placed in front of and behind the magnet to observe mass spectra.

Figures 1(b) and (c) show the observed mass spectra when solid targets of the refractory elements Zr and W were used for laser ablation, respectively. The ratio of intensity among the isotopes was consistent with natural abundance. The performance of the ion guide

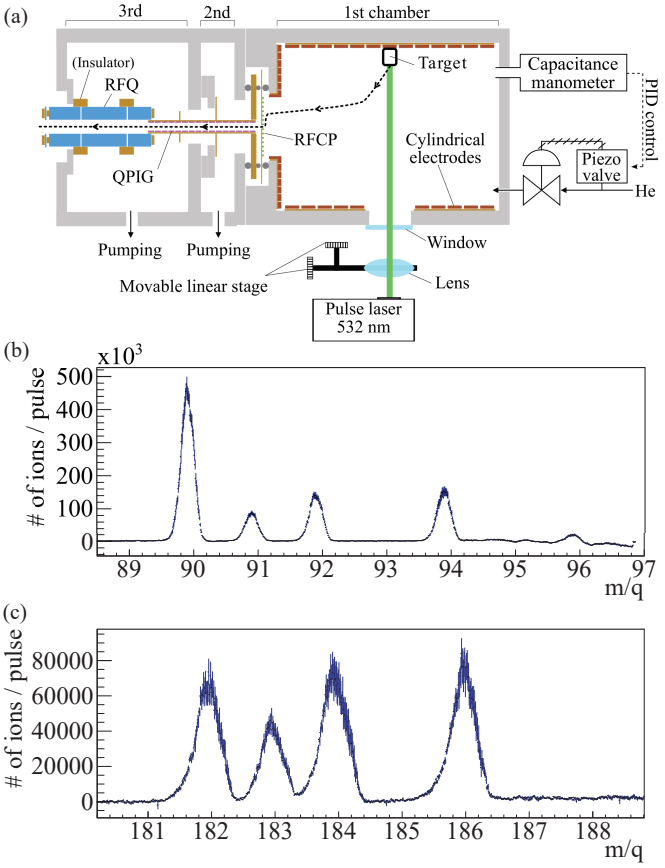

Fig. 1. (a) Sketch of the ion-source system. (b) Mass spectrum of Zr^+. (c) Mass spectrum of W^+.

system was studied separately using a Cs^+ emitter, and the transport efficiency was approximately 60–80%. The laser-intensity threshold of ion formation was 1–1.3 J/cm^2, and weak dependence on the repetition rate of laser ablation was observed. Consequently, 10^5–10^7 singly charged ions per laser pulse, consistent with the natural abundance, were successfully observed for metal targets of Ni, Ag, Zr, Ta, W, and a barium compound (BaF_2). The energy spread of the extracted ions was evaluated to be <1 eV via a comparison of the width of the obtained mass spectra with trajectory simulations assuming various initial temperatures, although direct measurements are needed for conclusive evidence.

Therefore, singly charged ion beams of one selective isotope including refractory elements are available for the reference measurement of collinear laser spectroscopy. Background reduction will be possible using a time gate in coincidence with the pulsed ablation laser.

† Condensed from the article in Nucl. Instrum. Methods Phys. Res. B **486**, 48 (2021)

*1 RIKEN Nishina Center
*2 Wako Nuclear Science Center (WNSC), IPNS, KEK

References

1) M. Wada *et al.*, Nucl. Instrum. Methods Phys. Res. B **204**, 570 (2003).

Temperature and pressure dependence of ion extraction from RF gas cell

D. Hou,[*1,*2,*3] A. Takamine,[*4] S. Iimura,[*4,*5] S. Chen,[*2,*6] Y. Hirayama,[*2] H. Ishiyama,[*4] Y. Ito,[*7] S. Kimura,[*4] J. Liu,[*1] H. Miyatake,[*2] S. Nishimura,[*4] M. Rosenbusch,[*2] P. Schury,[*2] M. Wada,[*2] Y. X. Watanabe,[*2] H. Wollnik,[*8] W. Xian,[*2,*6] and S. Yan[*2,*9]

The SLOWRI facility relies on gas catcher cells to employ the radio-frequency (RF) ion guide method for thermalizing and transporting radioactive ions.[1)] During an online experiment, we studied the pressure and temperature dependence of ion extraction from the gas cell. Molecular impurities in the gas cell can react and exchange charge[2)] with the ions of interest during their transport, and even after extraction, the ions can be neutralized and combined with molecular impurities. Because of the relatively low mobility of molecular impurities, they decrease the overall extraction efficiency of the gas cell. To reduce the amounts of molecular contaminants, we used high-purity helium and a gas purification system and operated the gas cell at very low temperatures. At temperatures below 50 K, most of these molecular impurities are absorbed at the wall of the gas cell.

In this online test setup, secondary beams passed through the ZeroDegree spectrometer and stopped in the gas cell. Subsequently they were extracted from the gas cell and transported to a multi-reflection time-of-flight (MRTOF) mass spectrograph for mass measurements.

The setup, as implemented in the commissioning runs, allowed for cooling the gas cell to ≈180 K. To avoid convoluting the stopping and extraction efficiencies, a pressure regulation system maintains a constant gas density of ≈33 μg/cm^3 for all temperatures. As shown in Fig. 1,

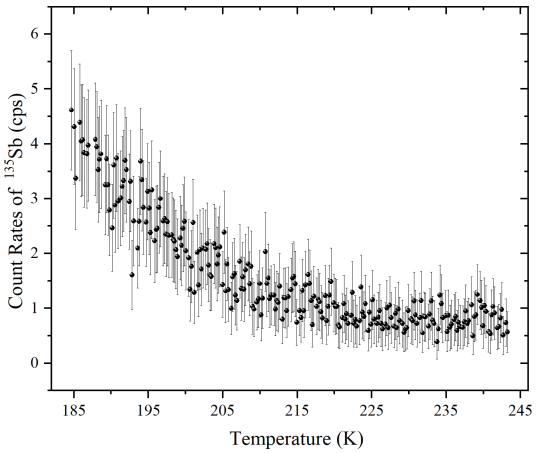

Fig. 1. Rates of ^{135}Sb$^+$ at different temperatures of the gas-cell chamber.

*1 Institute of Modern Physics, Chinese Academy of Sciences
*2 Wako Nuclear Science Center (WNSC), IPNS, KEK
*3 School of Nuclear Science and Technology, Lanzhou University
*4 RIKEN Nishina Center
*5 Department of Physics, Osaka University
*6 Department of Physics, The University of Hongkong
*7 Advanced Science Research Center, JAEA Ibaraki
*8 Dep. of Chem. and Biochem., New Mexico State University
*9 Institute of Mass Spectrometer and Atmospheric Environment, Jinan University

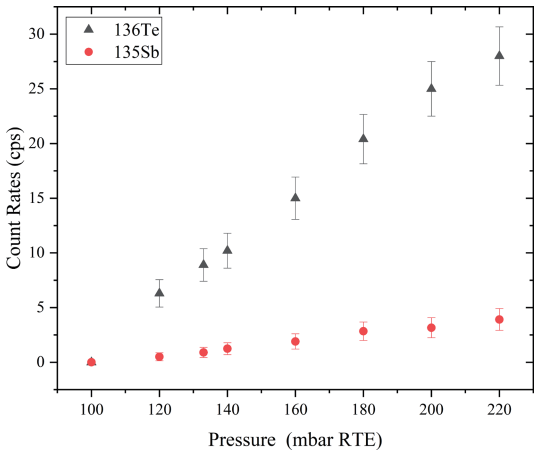

Fig. 2. Rates of ^{135}Sb$^+$ and ^{136}Te$^+$ observed at MRTOF as functions of RTE gas-cell pressure.

the extraction of ^{135}Sb$^+$ increases dramatically as the temperature falls below 210 K, at which some molecular impurities, such as H_2O, SO_2, and Cl_2, start to decrease. As the cryogenic cooling system reaches its lower limit before the extraction efficiency saturates, we intend to implement improvements to allow better cooling prior to the next online campaign.

By varying the gas density, we can probe the stopping efficiency. Figure 2 shows the results of such a measurement, performed with the gas cell at ≈180 K, with the observed rate of ^{136}Te$^+$ and ^{135}Sb$^+$ plotted as functions of room temperature-equivalent (RTE) helium pressure. As one might expect, the stopping fraction increased as the gas density increased. As such, we must consider how to safely operate at the highest possible gas density.

We used LISE^{++} to evaluate the stopping efficiency in the gas cell. With a pressure of 220 mbar RTE, 6.4% of ^{136}Te and 6.5% of ^{135}Sb should be stopped in helium gas, while decreasing the pressure to 133 mbar RTE would result in the reduction of stopping efficiencies to 2.3% and 2.4%, respectively. As shown in Fig. 2, the rates improved by a factor of 3.4 for ^{136}Te and 4.3 for ^{135}Sb, while LISE^{++} indicated that the stopping efficiencies should only increase by a factor of 2.7 from 133 mbar to 220 mbar. The difference likely results from the pressure dependence of the RF ion guide efficiency and ion mobility. Detailed analysis is underway to find an optimum operation condition ahead of the next online experiment.

References

1) M. Wada *et al.*, Nucl. Instrum. Menthods Phys. Res. B **204**, 570 (2003).
2) D. J. Morrissey *et al.*, Nucl. Instrum. Menthods Phys. Res. B **266**, 4822 (2008).

Degrader optimization for ZeroDegree gas cell

S. Chen,[*1,*2] Y. Hirayama,[*2] D. Hou,[*3,*2] S. Iimura,[*4,*5] H. Ishiyama,[*4] Y. Ito,[*6] S. Kimura,[*4] J. Liu,[*3] H. Miyatake,[*2] S. Nishimura,[*4] T. Niwase,[*7,*4,*2] M. Rosenbusch,[*2] P. Schury,[*2] A. Takamine,[*4] M. Wada,[*2] Y. X. Watanabe,[*2] H. Wollnik,[*8] W. Xian,[*1,*2] and S. Yan[*9,*2]

Using a high-quality beam provided by BigRIPS and the ZeroDegree spectrometer, a system combining a gas cell and a multi-reflection time-of-flight (MRTOF) mass spectrograph was set up at F11 to study the masses of exotic nuclei.[1] The first online commissioning was conducted in the winter of 2020 as parasitic experiments during the HiCARI campaign. To achieve the mass measurement in the MRTOF device, the radioactive beams received from ZeroDegree must be stopped in the gas cell, which is 500-mm long and filled with He gas. The typical beam energy behind ZeroDegree is 100–200 MeV/nucleon. To stop such high-energy beams in the He gas, a degrader is essential, and its thickness must be precisely adjusted. Therefore, a movable degrader system was introduced.

Figure 1 shows a sketch of the gas cell with the degrader system. The degrader system contains a rotational flat degrader placed in front of the gas cell and a downstream silicon detector array inside the outer chamber. The flat degrader was coupled to a step motor, which can rotate the degrader plate from 0° to 55° in steps of 0.0072°; therefore, it can finely adjust the effective thickness of the degrader. The downstream silicon detectors contain 15 Si PIN photodiods s3204-09, arranged in a 5×3 array to cover the full range of the beam spot. After losing most of its energy in the flat degrader, part of the beam is stopped in the He gas, while the rest deposits energy in the Si detectors. The signal from the Si detectors was acquired in coincidence with the beam-line detectors of ZeroDegree for particle identification; therefore, optimization can be performed for specific isotopes. The stopping in He gas can be optimized according to the beam energy loss measured by the Si detectors[2] or simply using the beam rate from the Si detectors.

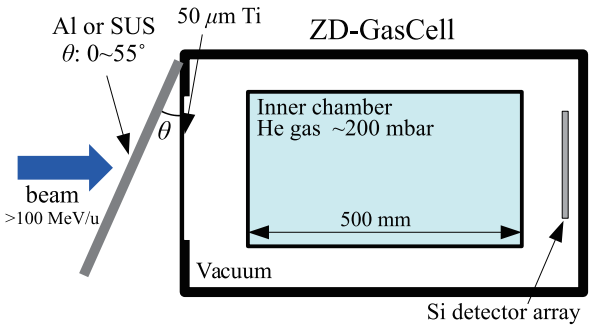

Fig. 1. Sketch of the ZeroDegree gas cell and degrader system.

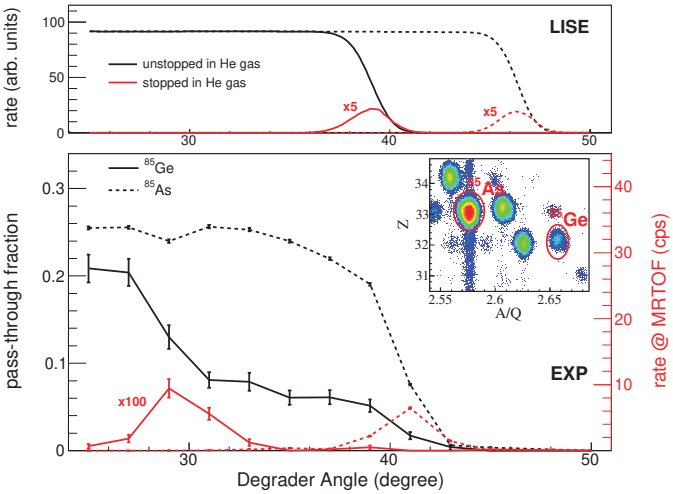

Fig. 2. Degrader optimization for ^{85}Ge (solid) and ^{85}As (dash). The black curve shows the ratio of the rate detected by an Si detector to the rate at F11. Only one Si detector was used in the analysis. The red curve is the rate of isotope identification in the mass spectrum. The inset shows the ZeroDegree particle identification. The upper panel displays the corresponding LISE calculations using the beam energy measured in ZeroDegree.

Figure 2 demonstrates the degrader optimization with a 2.5-mm-thick Al flat degrader for ^{85}Ge and ^{85}As during the commissioning run. The fractions (black), calculated as the beam rate detected in the Si detectors compared with the rate at F11, decrease with increasing degrader angle. The rates of isotopes observed in the MRTOF mass spectrum (red) show peak structures, from which we can determine the optimized degrader angle for each isotope. The LISE calculations well reproduce the measured pattern; however, discrepancies in the absolute angles are observed, which emphasize the importance of such direct measurement in experiments. For low-intensity isotopes (rate in MRTOF as low as 1 count/h), the direct measurement of the rate curve in MRTOF is not feasible. In this case, the fraction curve from Si can still be measured. Combined with the LISE calculation, the optimized degrader angle can be determined in future experiments.

*1 Department of Physics, The University of Hong Kong
*2 Wako Nuclear Science Center (WNSC), IPNS, KEK
*3 Institute of Modern Physics, Chinese Academy of Science
*4 RIKEN Nishina Center
*5 Department of Physics, Osaka University
*6 Advanced Science Research Center, JAEA
*7 Department of Physics, Kyushu University
*8 Department of Chemistry and Biochemistry, New Mexico State University
*9 Institute of Mass Spectrometry and Atmospheric Environment, Jinan University

References

1) M. Wada, RIKEN Proposal NP1912-RIBF176.
2) J. Liu, RIKEN Accel. Prog. Rep. **53**, 133 (2020).

Online extraction efficiency from RF ion guide gas cell at SLOWRI

S. Iimura,[*1,*2,*3] A. Takamine,[*1] D. Hou,[*4,*3,*5] M. Rosenbusch,[*3] M. Wada,[*3] S. Chen,[*3,*6] J. Liu,[*4] W. Xian,[*3,*6] S. Yan,[*7,*3] P. Schury,[*3] S. Kimura,[*1] T. Niwase,[*8,*1,*3] Y. Ito,[*9] T. Sonoda,[*1] T. M. Kojima,[*1] Y. X. Watanabe,[*3] S. Naimi,[*1] S. Michimasa,[*10] S. Nishimura,[*1] A. Odahara,[*2] and H. Ishiyama[*1]

We have been developing a radio-frequency carpet (RFC)–type ion guide[1] gas catcher cell (RFGC) at the SLOWRI. In offline tests, the maximam transport efficiency for the RFGC was more than 80%,[2] where the efficiency was defined as the ratio of ion current extracted from the cell to that corrected at the first-stage RFC. Here, the efficiency does not include factors such as ion survival probability and ion losses due to molecular formation. In order to obtain the "real" efficiency, an online test was performed using radioactive isotopes (RIs) provided by BigRIPS with an energy of several 100 MeV/nucleon as a symbiotic experiment behind the ZeroDegree spectrometer (ZD), in conjunction with the HiCARI campaign.

A multi-reflection time-of-flight (MRTOF) mass spectrometer[3] installed at the downstream of the RFGC was used for particle identification (PID) and mass measurements, as shown in Fig. 1. The RIs partly stop in the RFGC, after passing through a rotational energy degrader. Subsequently, the stopped ions are extracted from the RFGC and transported to the MRTOF system through quadrupole ion guides and flat-type ion trap.

Table 1 presents the preliminary result for the efficiencies for several RI species. After identification at ZD, the total efficiency ($\varepsilon_{\mathrm{total}}$) for each RI was determined as the ratio between the observed count rate after the MRTOF and the count rate before the RFGC. The stopping efficiency ($\varepsilon_{\mathrm{stop}}$) is the fraction of RIs stopped in the RFCG, which was evaluated using LISE^{++} based on the measured energy distribution of each RI. By future application of mono-energetic beam optics,[4] $\varepsilon_{\mathrm{stop}}$ is expected to improve by a factor of more than 5.

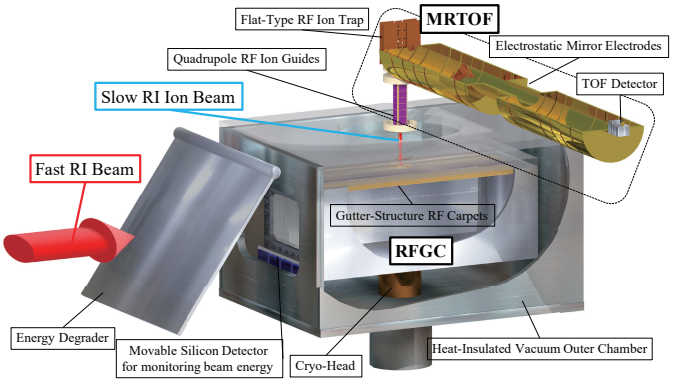

Fig. 1. Schematic view of the experimental setup. The RFGC is 50 cm long. It was operated at a nominal temperature of 180 K and pressurized with helium to 200 mbar room-temperature equivalent.

Table 1. Total efficiencies ($\varepsilon_{\mathrm{total}}$) measured with the detectors on ZD and the MRTOF. Stopping efficiencies ($\varepsilon_{\mathrm{stop}}$) were calculated from LISE^{++} The transport efficiencies ($\varepsilon_{\mathrm{trans}}$) correspond to ion transmission after stopping in the gas cell.

Nuclide (ions)	$\varepsilon_{\mathrm{total}}$	$\varepsilon_{\mathrm{stop}}$	$\varepsilon_{\mathrm{trans}}$
$^{134}Sb^{+}$	1.1%	9.1%	12%
$^{137}Te^{+}$	1.3%	9.2%	14%
$^{88}Se^{+}$	0.33%	3.4%	10%
$^{90}Se^{+}$	0.36%	2.0%	18%
$^{85}As^{+}$	0.16%	3.6%	4%
$^{55}ScOH^{+}$	0.0007%	2.9%	0.02%
$^{48}CaOH^{+}$	0.014%	3.2%	0.44%

The transport efficiency ($\varepsilon_{\mathrm{trans}}$) was obtained to subtract $\varepsilon_{\mathrm{total}}$ from $\varepsilon_{\mathrm{stop}}$. It should be noted that $\varepsilon_{\mathrm{trans}}$ includes transmission not only for RFGC but also for the ion guide, ion trap, and MRTOF. As indicated in Table 1, for many RIs, a reasonable $\varepsilon_{\mathrm{trans}}$ higher than 10% could be obtained. In this situation, $\varepsilon_{\mathrm{trans}}$ can depend on several factors such as the incoming beam intensity contributing to space-charge effects,[5] mass-to-charge ratio sensitive to RF trap stability,[2] and half-life providing decay loss. Another important dependency originates from the chemical properties of the incoming species when impurities are present in the He gas; *e.g.*, $^{55}ScOH^{+}$ was identified. Those molecular formations can be suppressed by further improvement of the cooling performance of the RFGC, based on our experience of the cryogenic gas cell at GARIS II.[6] Further improvement of the gas cell is ongoing.

We have successfully measured the masses of more than 70 nuclides in this experiment and are in the process of further analysis and simulation.

*1 RIKEN Nishina Center
*2 Department of Physics, Osaka University
*3 Wako Nuclear Science Center (WNSC), IPNS, KEK
*4 Institute of Modern Physics, Chinese Academy of Sciences
*5 School of Nuclear Science and Technology, Lanzhou University
*6 Department of Physics, The University of Hong Kong
*7 Institute of Mass Spectrometry and Atmospheric Environment, Jinan University
*8 Department of Physics, Kyushu University
*9 Advanced Science Research Center, JAEA Ibaraki
*10 Center for Nuclear Study, the University of Tokyo

References

1) M. Wada *et al.*, Nucl. Instrum. Methods Phys. Res. B **204**, 570 (2003).
2) A. Takamine *et al.*, RIKEN Accel. Prog. Rep. **53**, 108 (2020).
3) M. Rosenbusch *et al.*, Nucl. Instrum. Methods Phys. Res. B **463**, 184 (2020).
4) S. Chen *et al.*, RIKEN Accel. Prog. Rep. **53**, 100 (2020).
5) A. Takamine *et al.*, Rev. Sci. Instrum. **76**, 103503 (2005).
6) P. Schury *et al.*, Nucl. Instrum. Methods Phys. Res. B **407**, 160 (2017).

Development of MCP timing detector for low-energy heavy ions

T. T. Yeung,[*1,*2] S. Nishimura,[*2] W. Xian,[*1,*3] and H. Ishiyama[*2]

A prototype microchannel plate (MCP) timing detector was developed for correlated measurement of time of flight and decay properties by coupling with a multi-reflection time-of-flight mass spectrograph. The detector consists of a silicon PIN photodiode S3590-19 and an MCP F2223-21SH, as shown in Fig. 1. We investigated the performance of the detector using five types of beams: 2, 3 and 9 MeV ^{197}Au and 0.6 and 3 MeV ^{4}He at the Pelletron accelerator. Three degrader settings were available to reduce the beam intensity and provide various beam energies. The beam was collimated by a 0.2-millimeter-wide hole, degraded by a 2-micrometer-thick mylar foil, or stopped by a 0.5-millimeter-thick aluminum sheet, as shown in Fig. 1.

Energy calibration of a silicon detector for ^{197}Au was conducted by evaluating its dead layer thickness and pulse height defect using the Stopping and Range of Ions in Matter (SRIM) code[1] and assuming the charge state assignment for the multi-peak 9 MeV Au^{5+} spectrum in Fig. 2. From the SRIM results, the entrance window effect and the nuclear collision effect account for 7% and 48%, respectively, of 9 MeV Au. By considering both effects, the calculated dead layer thickness of the silicon detector was 0.266 μm and the energy-response function was obtained.

Based on coincidence of the MCP and silicon detector signals, the detection efficiency of the MCP was evaluated. The MCP efficiency for detecting Au is over 90% down to 2 MeV, as shown in Fig. 3. Pulse height analysis was performed to determine the energy response of the MCP using the offline data produced by a digitizer. The pulse height of the MCP fast amplifier signal was calculated by subtracting the baseline from the maximum of the pulse. The response was sensitive and increased with the beam energy linearly, as shown in Fig. 4. We confirmed that the MCP timing detector could be a complementary option for a timing detector instead of MagneTOF and α-TOF.[2]

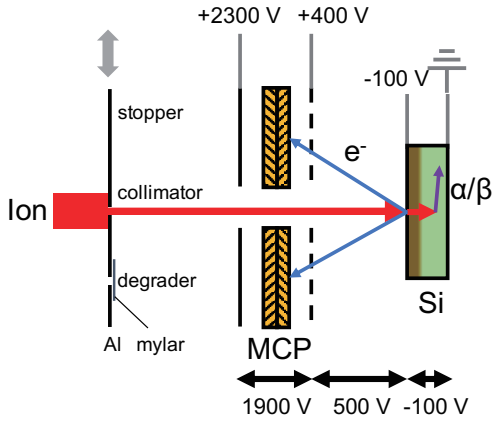

Fig. 1. Schematic of experimental setup, including degrader and MCP timing detector, with voltage settings. Position of aluminum plate is adjustable. Ion beam, secondary electrons, and decay particle are shown. Decay is not in scope of this experiment.

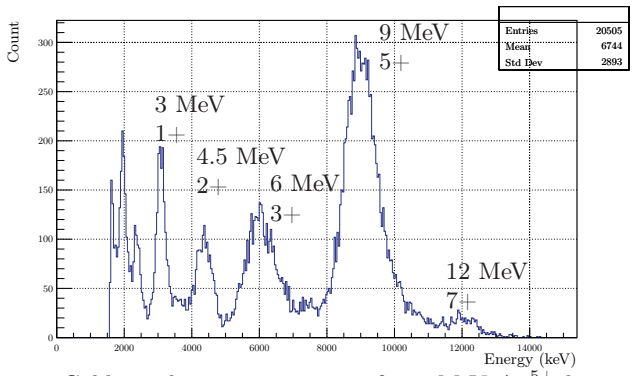

Fig. 2. Calibrated energy spectrum for 9 MeV Au^{5+} beam with labelled energy and charge state.

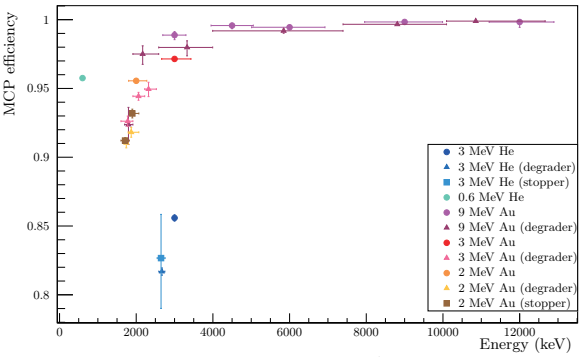

Fig. 3. MCP efficiencies for He and Au against ion energy.

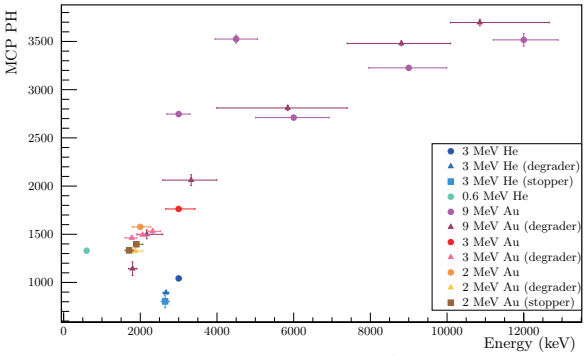

Fig. 4. MCP pulse height for He and Au against ion energy.

*1 Department of Physics, The University of Hong Kong
*2 RIKEN Nishina Center
*3 Wako Nuclear Science Center (WNSC), IPNS, KEK

References

1) J. F. Ziegler *et al.*, Nucl. Instrum. Methods Phys. Res. B **268**, 1818 (2010).
2) T. Niwase *et al.*, Nucl. Instrum. Methods Phys. Res. A **953**, 163198 (2020).

Improvement of kicker system for rare-RI ring

Y. Yamaguchi,[*1] D. Nagae,[*1,*2] S. Naimi,[*1] A. Ozawa,[*1,*3] and M. Wakasugi[*1,*4]

The kicker system at the rare-RI ring (R3) facility has contributed to successful event-by-event measurements. Thus far, three kicker units have been utilized for injecting and ejecting particles using the same field waveform. However, this is not ideal because the top of waveform is not flat (see Fig. 1(a)). It causes an approximately 10% fluctuation in the kick angle within an effective injection duration of 100 ns. In addition, because the ejection duration is the same as the injection duration, it is impossible to eject all nuclides having different revolution times.[1)] In the following, we report a successful improvement in these issues by the addition of a kicker magnet.

Recent R3 experiments are conducted with an injection energy of around 165 MeV/nucleon. Revolution time at R3, which has a circumference of 60.35 m, is approximately 380 ns. It is necessary to make the magnetic field strength negligibly small when particles pass the kicker in the next revolution after injection. Hence, a flat-top with a duration of 100 ns is appropriate considering the fall time of the magnetic field. Furthermore, it is possible to eject all circulated particles in a single ejection duration by lengthening the flat-top to 380 ns or more.

The magnetic field shown in Fig. 1(a) is achieved by

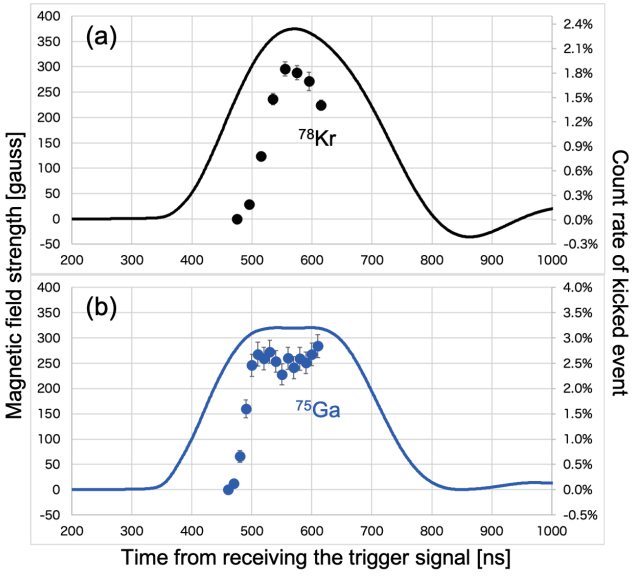

Fig. 1. Black line shows measured magnetic field, whereas blue line shows field experienced by particle (see text). Black and Blue dots indicate kicked events of ^{78}Kr and ^{75}Ga, respectively.

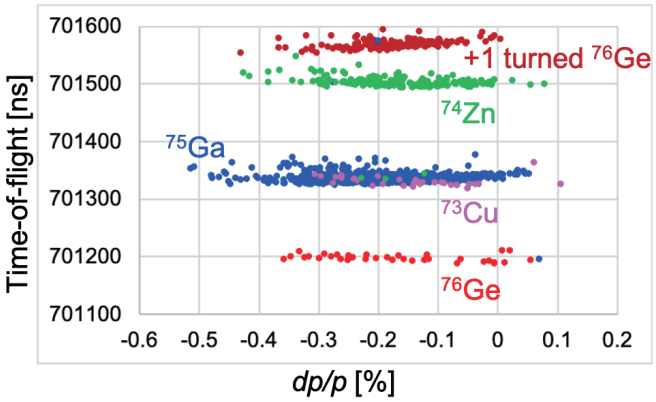

Fig. 2. Time-of-flights of ejected nuclides in single ejection as function of their momentum.

trial and error by adding a capacitor to suppress the reflections.[2)] In this study, two different types of magnetic field waveforms with and without this additional capacitor are produced. When passing through these two different fields, which are generated by two kicker units, a particle experiences a total magnetic field that has a flat-top (see Fig. 1(b)). Each kicker unit can generate a magnetic field twice within 0.7 ms. For injection, two kicker units are used, whereas for ejection, two additional kicker units are needed. To ensure a long flat-top ejection waveform, the delay between the firing of the first two kicker units and the additional two units is fixed to approximately 350 ns.

Blue dots in Fig. 1(b) indicate the kicked ^{75}Ga particles counted by a plastic scintillator with a width of 5 mm installed in the center orbit of the R3. This measurement was performed while changing the kicker trigger timing in 10 ns steps. It can be clearly seen that the count rate is constant compared with the ^{78}Kr case in the range of 100 ns, for which a flat-top has been realized. Kick angle fluctuation on the flat-top is expected to be 1%.

Figure 2 shows the measured flight times of the ejected nuclides as a function of momentum obtained from the position information of the PPAC at BigRIPS-F5. We succeeded in ejecting all injected nuclides in a single ejection. The events of ^{76}Ge that were not ejected in the first kick were ejected in the next kick. Thus, a long flat-top of approximately 400 ns was realized. Consequently, experimental efficiency became at least twice better than that achieved using the previous method, where different ejection timings were needed to eject all particles.

*1 RIKEN Nishina Center
*2 Research Center for SuperHeavy Elements, Kyushu University
*3 Institute of Physics, University of Tsukuba
*4 ICR, Kyoto University

References

1) S. Naimi *et al.*, J. Phys. Conf. Ser. **1643**, 012058 (2020).
2) H. Miura *et al.*, RIKEN Accel. Prog. Rep. **49**, 154 (2016).

Improved position resolution of the beam diagnostics detector for the Rare-RI Ring

G. Hudson-Chang,[*1] S. Naimi,[*1] T. Moriguchi,[*2] S. Suzuki,[*2,*3] M. Hayashi,[*2] N. Kaname,[*2] K. Tomita,[*2] A. Yano,[*2] A. Ozawa,[*2] Y. Abe,[*4] D. Nagae,[*5] and the Rare-RI Ring collaboration

To measure masses of rare isotopes at RIBF using the Rare-RI Ring, it is essential to increase the efficiency by better monitoring the beam condition at the injection into the ring. Therefore, we are developing a large area position-sensitive detector with a thin foil. The principle of the detector operation is based on secondary electrons (SEs) emitted from a thin foil when the beam passes through. The SEs are first accelerated by the acceleration grid and then reflected by the mirror grids potential (see Fig. 1). The beam position is inferred from SEs position measurement with the delay line MCP placed 90° from the foil. To achieve high position resolution the SEs velocity spread should be minimized inside the detector by simply increasing the acceleration voltage. However, increasing the voltage led to undesirable effects such as bending of the grid's wires and electrical discharges. We report here on the improvements introduced to minimize these effects. We tested different versions of the detector during four experiments conducted at HIMAC with a 200 MeV/nucleon ^{84}Kr beam. The details of the experimental setup can be found eslewhere.[1)] The position resolution as well as the accuracy of the detector for each experiment are shown in Fig. 1. In Table 1 are summarized the improvements introduced for each version of the detector as well as the acceleration potential that could be applied. The new wiring method for the grids is based on the method developed in this Ref. 2). With this method, the grids' wires were tighter and higher voltage could be applied resulting in improved resolution. By reducing the thickness of the spacer between the mirrors and acceleration grids, higher voltage up to 7 kV could be applied. This could be understood in the context of the Paschen Curve that related the product of the gas pressure and distance between the grids to the discharge voltage. By a systematic study of different spacer sizes we deduced that reducing the spacer size was necessary for the same vacuum condition. The resolution achieved in this condition was the best resolution ever achieved for large area detector of this type. We also tested the detector with a larger pitch size (2 mm) for a better transparency of the detector. However, it showed the worst performance. To improve further the position resolution we are planning to test a compact version of the same detector.

Table 1. Condition for each experiment (see text)

	Jul. 19	Nov. 19	Oct. 20(1)	Oct. 20(2)
New wiring method	X	O	O	O
Pitch of girds [mm]	1	2	1	1
Mirr Spacer [mm]	8	8	8	6
Acc Spacer [mm]	10	10	10	8
Acc. Potential [kV]	3	4	4	7

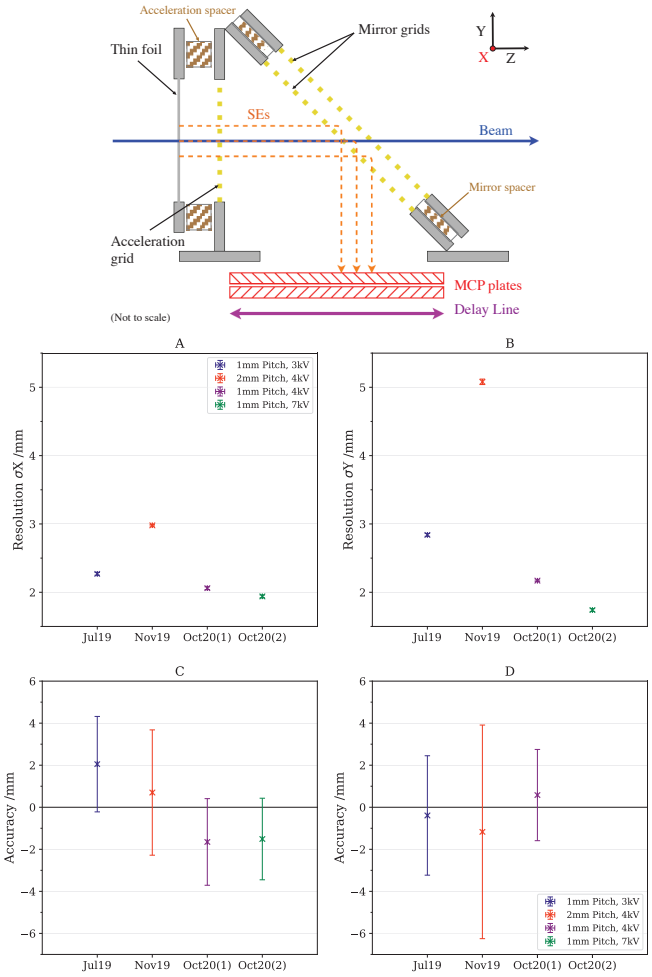

Fig. 1. (top) Schematic side-view of the position-sensitive detector. (bottom) Detector resolution (A&B) and accuracy (C&D) in the horizontal X and vertical Y position from four HIMAC experiments. The accuracy is defined as deviation from expected position. For Oct20(2), the accuracy is not plotted for the Y because a different method was used to optimize the voltage and accuracy could not be estimated.

*1 RIKEN Nishina Center
*2 Department of Physics, University of Tsukuba
*3 IMP, CAS
*4 National Institute of Radiological Sciences (NIRS), QST
*5 Faculty of Sciences, Kyushu University

References
1) R. Crane *et al.*, RIKEN Accel. Prog. Rep. **53**, 117 (2019).
2) O. K. Yoon *et al.*, J. Am. Soc. Mass Spectrom. **18**, 1901 (2007).

Computer server and network for HiCARI experiments

H. Baba,[*1] F. Browne,[*1] P. Doornenbal,[*1] B. Mauss,[*1] B. Moon,[*1] D. Suzuki,[*1] N. Aoi,[*2] S. Iwazaki,[*2] A. Kohda,[*2] Y. Yamamoto,[*2] T. Koiwai,[*3,*1] R. Taniuchi,[*4,*1] and K. Wimmer[*5,*1] for the HiCARI Collaboration

The HiCARI project[1] has been launched at the RIKEN RIBF. To process signals from Ge detectors, the GRETINA data acquisition system (DAQ)[2] is adopted. 100 MHz digitizers acquire information on the energy, timing, and pulse shapes of detectors and send data to data processing nodes. For tracking-type Ge detectors, data processing nodes perform pulse shape analysis (PSA) to obtain position information. Finally, processed data are merged by the event builder node and stored into a RAID storage system. For this DAQ system, computer servers and network equipment were newly installed. In addition, HOKUSAI SS[3] is used as a near-online analysis environment. In this report, we describe the computer server and network for the HiCARI experiment.

Table 1 lists the computer nodes. Five nodes of HP ProLiant DL360 G10 (16 CPU cores) were newly installed. One node is for the event builder; three nodes (48 CPU cores in total) are for the PSA of a triple segmented tracking detector from LBNL Berkeley (LBNL P3), which has 111 signals in total; and the last one is for the data process (DP) of Miniball and clover detectors (152 signals in total). Since PSA is not applied for Miniball and clover detectors, the demand for CPU resources is small. However, owing to the limitation of the GRETINA DAQ software, the number of processes per OS is limited. To optimize the allocation of CPU resources, four virtual machines (VM) are launched using KVM.[4] Three CPU cores are allocated to each VM, and four CPU cores are reserved for the KVM host process. In addition, ten HP ProLiant DL380 G6 (8 CPU cores) were transported from RCNP Osaka. Eight nodes (64 CPU cores in total) are used for the PSA of the RCNP quad-type segmented tracking detector (RCNP Quad). One of them is used for the DAQ controller, and the last one is reserved as a spare node.

Table 1. List of computer nodes.

Function	Model	Unit	Core
DAQ Controller	DL380 G6	1	8
Event Builder	DL360 G10	1	16
PSA for LBNL P3	DL360 G10	3	48
DP for Miniball/Clover	DL360 G10	1	16
PSA for RCNP Quad	DL380 G6	8	64
Spare	DL380 G6	1	8

*1 RIKEN Nishina Center
*2 RCNP, Osaka University
*3 Department of Physics, University of Tokyo
*4 Department of Physics, University of York
*5 IEM-CSIC

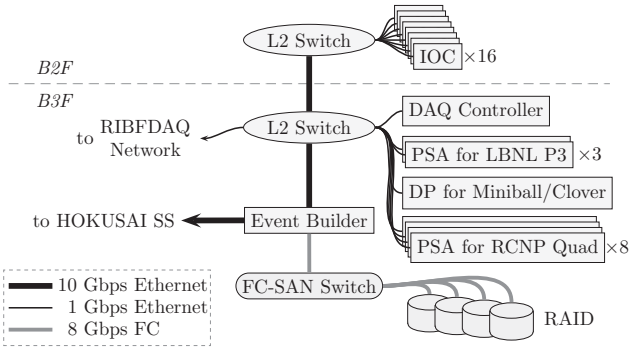

Fig. 1. Network diagram for HiCARI experiments.

A data analysis environment has been prepared in HOKUSAI SS for RIBF experiments. HOKUSAI SS is a private cloud system based on OpenStack.[5] As of January 2021, a total of 80 cores and a disk space of 100 TB has been secured, and it can be expanded upon request. These resources are allocated not only to the HiCARI project, but also to other experimental projects. In 2020, 64 cores out of 80 cores were tentatively allocated to the VM of HiCARI experiments. From 2021, the resource allocation will be optimized according to the usage.

The network diagram for the HiCARI experiment is shown in Fig. 1. Sixty digitizers are installed on the B2F, and sixteen CPU boards (called IOC) send data to the PSA nodes. Processed data are merged by the event builder and stored in the RAID system via an 8-Gbps fibre channel-storage area network (FC-SAN). For now, a total of 160 TB of space has been prepared for the HiCARI project, and 36 TB of data were acquired in 2020. These data were also transferred to the HOKUSAI SS through a 10-Gbps Ethernet connection for near-online analysis.

In summary, the computer server and network equipment were set up for the HiCARI project. They worked stably and successfully acquired data of seven experimental proposals. The equipment reported in this paper will be used for upcoming HiCARI experiments in 2021.

References

1) K. Wimmer *et al.*, in this report.
2) J. T. Anderson *et al.*, IEEE NSS Conference Record **56**, 1751 (2007).
3) HOKUSAI SS, `https://i.riken.jp/data-sci/`.
4) Kernel Virtual Machine (KVM), `https://www.linux-kvm.org/`.
5) OpenStack, `https://www.openstack.org/`.

Development of a high-bandwidth waveform processing system using RFSoC

S. Takeshige,[*1] H. Baba,[*2] K. Kurita,[*1] Y. Togano,[*1] J. Zenihiro,[*3] and Y. Hijikata[*3]

We are developing a real-time digital signal processing unit using a GHz-band flash-type analog-to-digital converter (FADC) to establish the next-generation data acquisition system at RIBF. In experiments using radioactive ion (RI) beams, it is necessary to identify each particle. For this purpose, detectors are installed along the beam line, and signals are acquired on an event-by-event basis. However, as the amount of beams increases, conventional CAMAC/VME ADC/TDC modules become a measurement bottleneck owing to its slow processing rate. For germanium detectors, real-time digital signal processing is applied using 100-MHz FADCs instead of conventional ADC/time-to-digital converter (TDC) modules.[1] However, 100 MHz is insufficient for signals with high-frequency components such as those from plastic scintillators used as beam-line detectors.

The Xilinx radio frwaquency system-on-chip (RFSoC) has been commercially available since 2018. It is a device designed for 5 G communication and integrates an FADC (up to 5 GHz) and field-programmable gate array (FPGA) on one chip. This RFSoC has the potential to perform real-time digital signal processing for high-intensity RI-beam experiments.

In this study, we used the Xilinx ZCU111 evaluation kit[2] (Fig. 1). This kit has 8 channels of ADC inputs, 8 channels of DAC outputs, and 20 channels of general-purpose I/O ports. The specifications of the ADC input are as follows: 100 Ω differential impedance, AC coupling, and 1 Vppd voltage range. The maximum sampling frequency of the ADC is 4.096 GHz, and the resolution is 12 bits.

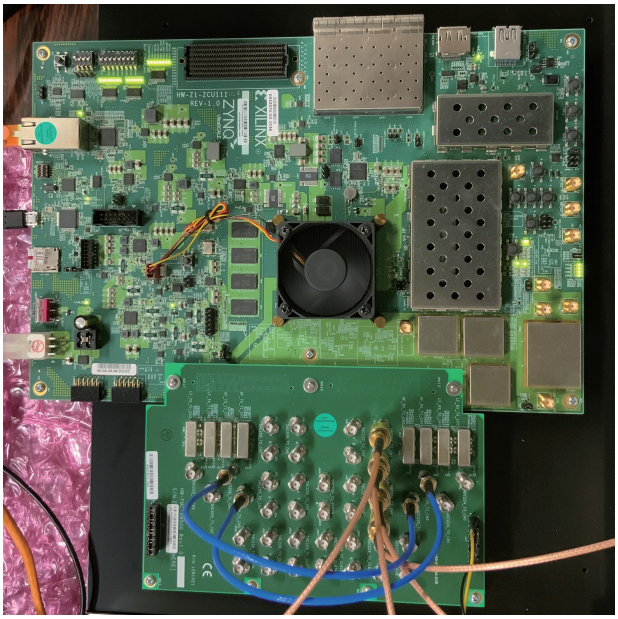

Fig. 1. Xilinx ZCU111 evaluation kit used for development.

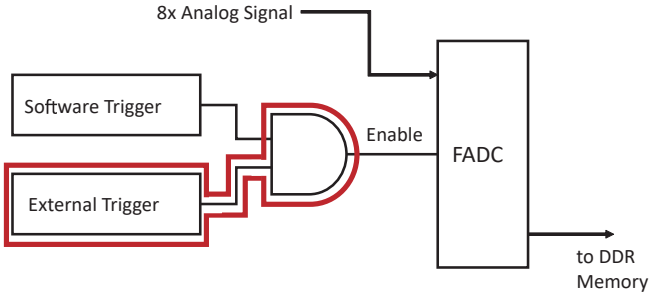

Fig. 2. Block diagram of the implemented external trigger function.The bold line shows the implemented part.

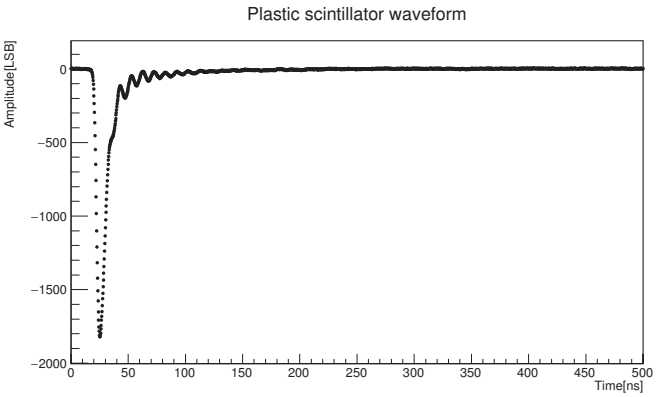

Fig. 3. An example of an acquired plastic scintillator waveform.

As it is not possible to impliment external triggers with sample FPGA firmware provided by Xilinx, we added external trigger function. The block diagram is shown in Fig. 2. When data acquisition is started, a software trigger is enabled. At this time, when an external trigger is issued, digitized data are stored in memory. Finally, data are retrieved by a PC via the network. An example of an acquired plastic scintillator waveform is shown in Fig. 3.

We added an external trigger function to the RFSoC device and confirmed that it works successfully. Basic studies such as the measurement of the timing resolution are in progress.

*1 Department of Physics, Rikkyo University
*2 RIKEN Nishina Center
*3 Department of Physics, Kyoto University

References

1) J. -P. Martin *et al.*, IEEE Trans. Nucl. Sci. **55**, 84 (2008).
2) Xilinx, Zynq UltraScale+ RFSoC ZCU111 Evaluation Kit, `https://japan.xilinx.com/products/boards-and-kits/zcu111.html`.

GPU acceleration of SAMURAI particle tracking simulation

J. Gao[*1,*2]

The possibility of graphical processing unit(GPU) acceleration of the trajectory simulation of particles passing through SAMURAI was evaluated. To obtain A/Z in particle identification plot, information such as the flight path and rigidity obtained from this type of simulation is necessary. Usually, this tracking simulation is the most time-consuming step in the analysis of SAMURAI data.

As with most other steps in nuclear physics data analysis, this particle tracking simulation is performed event by event. Therefore the simulation could be accelerated by distributing the events to large amount of threads of a GPU to process in parallel. In principle, all the event-by-event analysis could be accelerated by parallel computing and could take advantage of a GPU.

Another advantage of a GPU is its special cache structure. In contrast to the linear structured cache in a CPU, the cache in a GPU could have a higher-dimensional layout.[1] Therefore, when interpolating in the magnet field map, the GPU could fetch the neighboring mesh point with fewer cache misses.

In this work, a simplified task is designed to evaluate the performance of trajectory simulation on a CPU and GPU. The standard program used in data analysis takes the position and angle before and after the magnet and provides the rigidity as the output. It iterates several times to obtain a certain rigidity that reproduces the position and angle measured in the experiment. This simplified version takes the position, angle, and rigidity before the magnet and outputs the position and angle after the megnet without any iterations. The CPU version is modified from the code used for the particle identification of SAMURAI11 data.[2]

The program uses a fourth-order Runge-Kutta method to simulate the trajectory of a particle in the SAMURAI magnet. Both the CPU and GPU versions of the program were developed. The test was performed on a server with 4 Intel Xeon Gold 6136 CPUs (each has 12 cores/24 threads), 128 GB memory, and one Nvidia Titan V GPU. The CPU version code is written in Go programming language and optimized using the AVX2 assembly.[3,4] The GPU version is written in C++ and CUDA. 1024000 events were fed into the programs, and each version ran 3 times.

The results are summarized in Table 1. The timer starts immediately after the field map is loaded into the main or GPU memory and the input data are loaded into the main memory, and it stops as soon as the calculation finishes, which means the hard disk I/O time is excluded so that the time of calculation is isolated.

Table 1. Test results of CPU and GPU versions of the simplified simulation. The GPU could accelerate the simulation by a factor of 5 to 13 times approximately.

code	CPU 1	CPU 2	GPU
configuration	32 coroutines	126 coroutines	320×32
test #1	13.292 s	5.277 s	0.999 s
test #2	13.309 s	5.319 s	1.004 s
test #3	13.317 s	5.378 s	1.011 s
average	13.306 s	5.324 s	1.004 s

In Table 1, the CPU 1 code enabled 34 threads and allocated 32 coroutines for simulation. The CPU 2 code enabled all the 128 threads and allocated 126 coroutines for simulation. The GPU version divides the input data into 100 groups, each of which is passed to a device function using a configuration of 320 thread blocks and 32 threads per block. Different groups are processed asynchronously to hide the time of data transfer between the main memory and device memory.

For SAMURAI11 data, it takes 3.15 iterations on average to obtain the rigidity and a maxmium of 5 iterations. For the CPU1 and CPU 2 configurations, the time for simulation should be $13.306 \times 3.15 = 41.91$ s and $5.324 \times 3.15 = 16.77$ s, respectively. If we consider the worst case for the GPU, where each thread block contains an event that need 5 iterations, then the simulation time is $1.004 \times 5 = 5.02$ s, which is 8 or 3 times faster than the CPU version, depending on the number of threads used in the CPU code.

In conclusion, with a reasonable GPU cost and coding effort, the simulation could be made significantly faster.

References

1) CUDA C++ Programming Guide, `docs.nvidia.com/cuda/cuda-c-programming-guide/index.html`
2) J. Gao *et al.*, in this report.
3) Intel 64 and IA-32 Architectures Software Developer's Manual, `software.intel.com/content/www/us/en/develop/articles/intel-sdm.html`
4) A Quick Guide to Go's Assembler, `golang.org/doc/asm`

*1 School of Physics, Peking University
*2 RIKEN Nishina Center

Observation of Rb D1 fluorescence in superfluid helium using picosecond time-resolved detection

Y. Takeuchi,[*1,*2] H. Kuramochi,[*3] K. Ishii,[*4] K. Imamura,[*2] A. Takamine,[*2] M. Doi,[*1,*2] T. Yamamoto,[*1,*2] Y. Matsuo,[*1,*2] Y. Zempo,[*5] T. Tahara,[*4] and H. Ueno[*2]

Our research group is developing a laser spectroscopy technique (OROCHI) for atoms in superfluid helium (He II). When atoms are introduced into He II, the surrounding helium atoms are pushed out by the exchange (Pauli) repulsion force.[1] The resulting vacuum region is called an atomic bubble. Because the shape of the electron orbit of an impurity atom is deformed according to its energy state, the atomic bubble is also deformed following the shape change of the atomic orbit. According to the Franck-Condon principle, the time required for the atomic transition is 10^{-15} s, which is much shorter than the time required for the bubble deformation therefore, it is considered that the bubble is deformed after the transition. The wavelengths of atomic transitions for both absorption and emission in He II are shifted from those in vacuum owing to this deformation cycle.[2] The emission wavelength is considered to change in correspondence with the degree of bubble deformation.

It is estimated that the time required for the bubble deformation is of the order of a few picoseconds, but so far, the relaxation time has not been measured in the time domain in bulk He II. In this study, we aim to determine the relaxation time through time-resolved emission measurements at different wavelengths.

The OROCHI group is conducting a research project in collaboration with the Molecular spectroscopy laboratory to observe the relaxation time of Rb atomic bubbles in He II.[3] Recently, we evaluated the performance of the time-correlated single photon counting (TCSPC) detection system that will be used for photo-detection in the relaxation time measurement. Observations were performed using an avalanche photodiode (APD) and time amplitude converter (TAC) as detectors. So far, our research group has used PMT for laser-induced fluorescence (LIF) photon counting of Rb atoms. This measurement will be the first LIF observation by the TCSPC system.

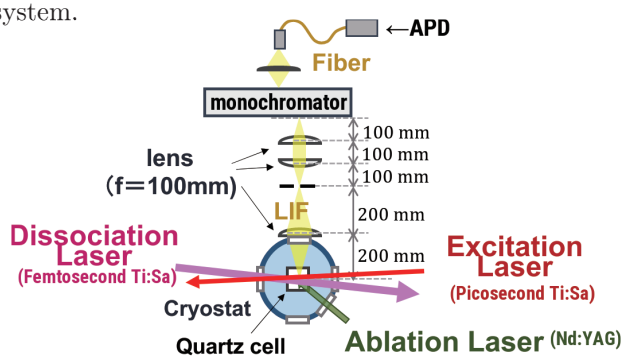

Fig. 1. Experimental setup of LIF detection.

*1 Department of Advanced Sciences, Hosei University
*2 RIKEN Nishina Center
*3 Institute for Molecular Science
*4 Molecular Spectroscopy Laboratory, RIKEN
*5 Department of Computer and Information Science, Hosei University

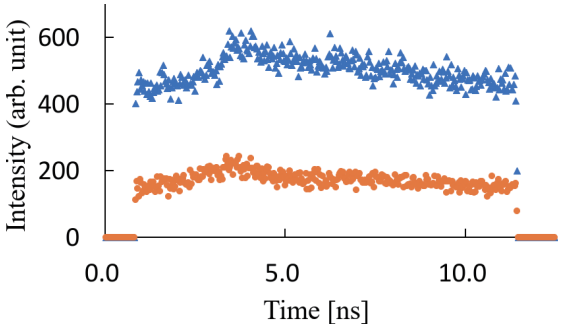

Fig. 2. Observed photon intensity as a function of delay time.

We first confirmed the fluorescence detection of the D1 line of the Rb atom (absorption center wavelength in He II: 778.0 nm). We used a picosecond mode-locked Ti:sapphire laser (laser power: 130 mW, repetition rate: 80 MHz, pulse width: 1.6 ps, center wavelength: 778.2 nm) as an excitation laser, and we observed LIF using the APD and acquired data using a TCSPC module (SPCM, Becker & Hickl GmbH) (Fig. 1). The Rb atoms were supplied by performing laser ablation on the RbCl sample installed above the observation area and laser dissociation to RbCl clusters in He II. The monochromator wavelength was set at 793 nm, which is the center of the emission line.

Figure 2 shows the result of the observation. The data plotted here are the observed photon intensities as a function of delay time. In this figure, the blue triangle is the total detected light when all lasers are turned on, and the orange dot is the scattered light when only the excitation laser is turned on. The fact that the peaks appear at the same position of the horizontal axis indicates that the excitation laser is scattered inside the cryostat and is slightly detected, although the monochromator wavelength is 15 nm longer than that of the excitation laser. The background also contains ambient light from sources other than the laser in the environment. The blue curve has a longer tail. This tail indicates the decay due to the lifetime of the Rb D1 emission. While the excitation pulse interval was 12.5 ns, the fluorescence lifetime was 27 ns therefore, atoms are excited by the next laser pulse before the emission vanishes and LIF photons are piled up. Therefore, the result agreed with the expectation that the spectrum would have the appearance of a sawtooth wave with repeated cycles of decay and rise due to excitation on top of the piled-up signal.

With the current data, the background scattered light is not small, and the setup should be adjusted so that more fluorescence light can be obtained. We are planning to make such improvements and move to the observation of weaker emission on the short-wavelength side.

References

1) B. Tabbert *et al.*, J. Low Temp. Phys. **109**, 653 (1997).
2) Y. Takahashi *et al.*, Phys. Rev. Lett. **71**, 1035 (1993).
3) Y. Takeuchi *et al.*, RIKEN Accel. Prog. Rep. **53**, 130 (2019).

Development of ion trap system for the neutralizer toward production of spin-polarized RI beam using atomic beam magnetic resonance method

K. Imamura,[*1] A. Takamine,[*1] and H. Ueno[*1]

Spin-polarized radioactive isotope (RI) beams have been used for the measurements of nuclear electromagnetic moments and spins to investigate nuclear structure. In many experiments, the polarization of nuclear spin is generated via a projectile fragmentation reaction. Although the reaction mechanisms have been well studied so far, the achievable spin polarization is typically as low as several percentage points.[1)] Laser optical pumping can realize spin polarization of greater than a few tens of percentage points, but the method is element-limited. A highly efficient and universal method for producing spin-polarized RI beams is desired. For this purpose, we are developing a spin-polarized beam production apparatus using the atomic beam magnetic resonance (ABMR) method. In the method, the spin polarization of neutral atomic beams is generated by two-step spin selection using multi-pole magnets and magnetic resonance. The efficient production of a thermal energy neutral RI atomic beam is significantly difficult from a technical perspective, although the ABMR method itself is one of the conventional methods for investigating spin-related nuclear properties of nuclei near the stability region.[2)] To overcome this difficulty, we propose a new ion neutralizer which, combines ion trapping with the laser cooling technique. The main feature of the neutralizer is that it traps and cools RIs produced by nuclear reactions to decrease the beam energy.

In the system, we first prepare laser-cooled ions in a linear Paul trap. RI ions of several eV are introduced to the trap region of the laser-cooled ions and trapped using He buffer gas cooling. The trapped RI ions are sympathetically cooled down through Coulomb interaction between laser-cooled ions and the RI ions. After cooling, a neutralization gas (*e.g.*, N_2, NH_3, and so on) is blown against the RI ions. Subsequently, neutral atoms are produced by charge-exchange interaction. For the efficient extraction of the neutral atoms, we apply a swing field in the beam-propagation direction to move trapped RI ions back and forth prior to the neutralization.

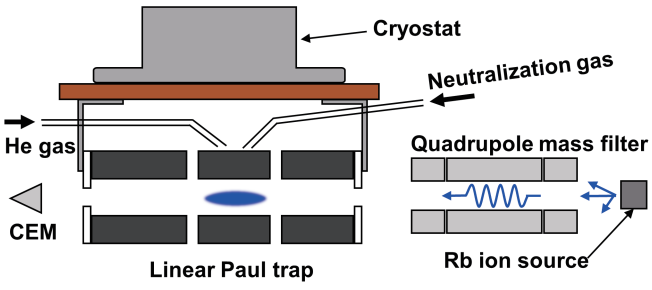

Fig. 1. Schematic diagram of the setup.

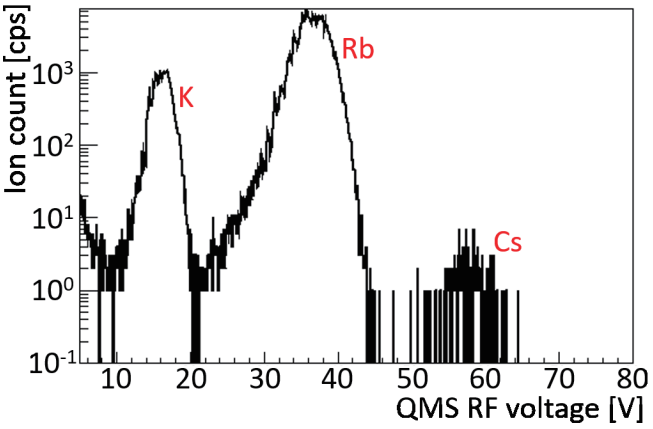

Fig. 2. Mass spectrum obtained downstream of the linear Paul trap.

In order to develop the proposed neutralizer, we initiated an offline R&D experiment using Rb by constructing a linear Paul trap system and quadrupole mass filter (QMF) for selecting ions that are introduced to the trap region. The experimental setup for the R&D experiment is shown in Fig. 1. Rb ions emitted from a surface-ionization ion source were guided to a linear Paul trap after mass selection by a QMF. The electrodes of the trap were assembled at the head of the cryostat, which is used for realizing a sufficient high vacuum to conduct the ion trapping and laser cooling experiment. We achieved a vacuum of $\sim 10^{-8}$ Pa in the current setup. Two gas lines were prepared near the center part of the trap. One is used for introducing He as the buffer gas to perform buffer gas cooling. The other is used for introducing a neutralization gas. A channel electron multiplier (CEM) detector was placed downstream of the trap to detect transported ions.

Toward the Rb ion trap experiment, we conducted an ion transportation test. Figure 2 shows a mass spectrum of the ions transported. The vertical and horizontal axes correspond to ion counts and RF voltages applied to the QMF electrodes, respectively. Three peaks correspond to singly charged K, Rb, and Cs. According to this result, we confirmed that sufficient Rb ions to test ion trapping are guided from the ion source to the trap. We will proceed to the next step of Rb ion trapping. We will then start a neutralization test in the near future.

*1 RIKEN Nishina Center

References

1) K. Asahi *et al.*, Phys. Lett. B **251**, 488 (1990).
2) N. F. Ramsey, *Molecular Beams* (Oxford University Press, New York, 1956).

Status of the J-PARC E16 experiment in 2020

S. Yokkaichi*1 for the J-PARC E16 Collaboration

We proposed the experiment E16[1] to measure the vector meson decays in nuclei in order to investigate the chiral symmetry restoration in dense nuclear matter. The experiment started at the J-PARC Hadron Experimental Facility.

This experiment aims to systematically study the spectral modification of vector mesons in nuclei, particularly the ϕ meson, using the e^+e^- decay channel with statistics that are two orders larger in magnitude than those of the precedent E325[2] experiment performed at KEK-PS. In other words, it aims to accumulate 1×10^5 to 2×10^5 events for each nuclear target (H, C, Cu, and Pb) and deduce the dependence of the spectral modification on the size of matter and meson momentum.

A scientific ("stage-1") approval was granted to the experiment E16 by PAC in March 2007. For the full ("stage-2") approval, a technical design report was submitted to PAC in May 2014 and reviewed for experimental and budgetary feasibility. In the PAC meeting held in July 2017, the stage-2 approval for 320 hours of a commissioning run was granted. In this run, background measurement at the new beamline is required. The construction of High-momentum beamline, where the experiment will be conducted, has been completed by KEK in June 2020.

Our proposed spectrometer has 26 modules. As shown in Fig. 1, a module consists of Lead-glass calorimeter(LG) and Hadron-blind detector (HBD) for electron identification, as well as three-layers of GEM Trackers (GTR) and a single layer of silicon strip detecor (SSD) as the tracking devices. Owing to budget limitations, the commissioning run was started with a limited number of modules.

The first half of the commissioning run, called Run-0a, was successfully performed in June 4–20, 2020, with a configuration of 6(SSD)-6(GTR)-4(HBD)-6(LG) modules.[3] The beam was delayed from February in the original plan, owing to a bureaucratic issue and possibly because of the COVID-19 pandemic, in the Nuclear Regulatory Agency, to issue the permission for the new beamline. As a user beamtime, 159 hours were executed, including 10-hours of downtime in total; each downtime was less than 30 min. (downtimes over 30 min were compensated). Here, "downtime" is due to problems caused by the accelerator or the beamline operation and not by users.

As the design, a primary proton beam with an intensity of 1×10^{10} protons per 2 sec duration (5.2 sec cycle) was delivered to our spectrometer. The interaction rate at the targets (C and Cu) is 10 MHz because the total interaction length of the targets is 0.2%. One of our concerns, GEM breakdown under a high particle rate,

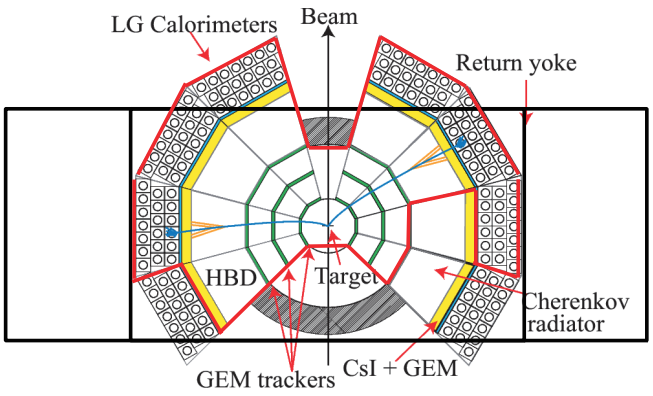

Fig. 1. Plan view of the proposed E16 spectrometer in the eight-module configuration for Run-1. The red lines show the parts that have been constructed as of December 2021, for the commissioning run planned for February 2021 (Run-0b). The SSD located in the innermost layer is not shown.

was not observed in HBD. In GTR, the breakdown of 13 strips was observed in 300-GTR, which caused approximately 11% of dead region in total, but operation was continued. The electron ID performance of HBD and LG were roughly confirmed.

A background study was performed, and the LG single rate was found to be two times as high as the expectation, which is a scaled value of the E325 experiment. However, a factor of two is within the designed margin. The origin of the background will be studied to improve the situation.

As of January 2021, the second half of the commissioning run, Run-0b, is scheduled for February 2021. GTR and HBD were uninstalled from the spectrometer after the Run-0a, and refurbished in J-PARC and RIKEN, respectively. Additionally, two GTR and two HBD modules were newly constructed, and installed in November–December 2020 along with the refurbished ones. Consequently, a 6(SSD)-8(GTR)-6(HBD)-6(LG) were installed, as shown by the red lines in Fig. 1.

After Run-0b, Run-1 (physics run) is planned for autumn 2022. Its approval should be obtained at the J-PARC PAC. We have to update the technical design report for Run-1 based on the result of Run-0 and submit by December 2021, following which discussion will be conducted at the PAC held in January 2022.

*1 RIKEN Nishina Center

References

1) S. Yokkaichi *et al.*, J-PARC proposal No. 16 (`http://j-parc.jp/researcher/Hadron/en/pac_0606/pdf/p16-Yokkaichi_2.pdf`); Y. Komatsu *et al.*, JPS Conf. Proc. **12**, 020005 (2017); S. Ashikaga *et al.*, JPS Conf. Proc. **26**, 024005 (2019).
2) R. Muto *et al.*, Phys. Rev. Lett. **98**, 042501 (2007).
3) S. Yokkaichi, RIKEN Accel. Prog. Rep. **53**, 79 (2020).

Construction of GEM Tracker for J-PARC E16 experiment Run0-a

T. N. Murakami*1 for the J-PARC E16 Collaboration

The J-PARC E16 experiment[1] has started to reveal the relationship between spontaneous chiral symmetry breaking and masses of hadrons. We measure the mass spectrum of the ϕ meson in nuclei using e^+ e^- decays. The momenta of e^+ and e^- are reconstructed from the curvature in a magnetic field; therefore, tracking of the lepton pairs is quite essential. To deal with the expected high-particle rate of 5 kHz/mm^2 and to cover a wide area of 1.1 m^2, we adopted a gas electron multiplier (GEM) as the tracking device. GEM chambers are reported to operate normally even under a 25 kHz/mm^2 particle rate.[2]

We have developed GEM Tracker (GTR), whose GEM foils are manufactured by a Japanese company. Each GEM chamber consists of three different sizes of the chambers; 100 mm × 100 mm (GTR1), 200 mm × 200 mm (GTR2), and 300 mm × 300 mm (GTR3). A GEM chamber consists of three GEM foils and is filled with Ar+CO_2 (70:30) gas. Each chamber enable measuring the positions of charged particles with a resolution of 100 μm.[3] We prepared six modules of GTR for the first commissioning run for E16 (Run0-a) in June 2020. They were placed to cover the same solid acceptance surrounding the target. The process of construction was as follows: In the first step, we selected good GEM foils for stable operation. We measured the leakage current by applying 500-V between the bottom and top electrodes of the GEM foils with a 400 mL/min N_2 gas flow. We required the leakage current to be less than 10 nA/100 cm^2 and the number of discharges to be less than 10/h. The results are summarized in Table 1. After selecting good foils, we assembled them as a GEM chamber. Prior to installation, two steps were performed. First, we tested the chambers for presenting sufficient operation stability and sufficiently high amplification gain of 6000, as required for a position resolution of 100 μm. If there were problems, such as an insufficient gain or impossibility of applying a nominal voltage of 380 V to the GEM electrodes, we disassembled the chamber and exchanged the GEM foils. Second, we transported them to the experimental area, set them on the CFRP frame, as shown in Fig. 1, and tested them again. Here, we checked the operation stability as well as the cable disconnections. Subsequently, we successfully installed the GTR in the spectrometer magnet.

Table 1. Results of leak current test. Approximately 100 GEM foils were checked over 3 months.

size of GEM (mm^2)	good	bad	sum
100 × 100	21	15	36
200 × 200	18	12	30
300 × 300	19	11	30
sum	58	38	96

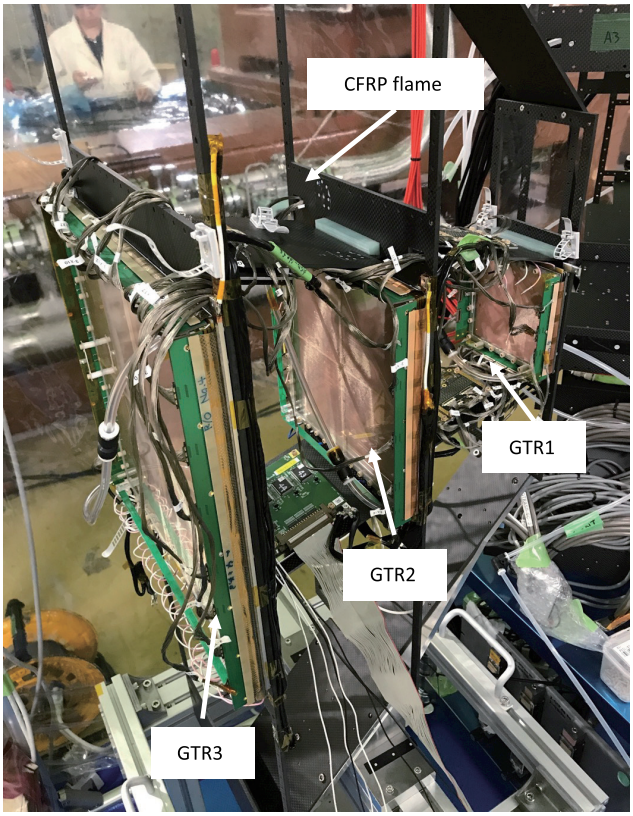

Fig. 1. GEM chambers attached in CFRP frame. This is single module of GTR, and six modules are placed surrounding targets in Run0-a.

References

1) S. Yokkaichi *et al.*, in this report.
2) B. Ketzer *et al.*, Nucl. Instrum. Methods Phys. Res. A **535**, 314 (2004).
3) Y. Komatsu *et al.*, Nucl. Instrum. Methods Phys. Res. A **732**, 241 (2004).

*1 Department of Physics, Graduate School of Science, The University of Tokyo

Performance evaluation of the electron identification system for the J-PARC E16 experiment

S. Nakasuga[*1,*2,*3] for the J-PARC E16 Collaboration

The J-PARC E16 experiment[1] is proposed for measuring the spectral modification of vector mesons in nucleus. Here, we detect electron-positron pairs generated in ϕ meson decays, produced in pA reactions. It is crucial for a successful measurement to separate electrons from huge hadronic backgrounds, especially pions, which are a primary component of those.

For the electron identification, we adopt two-stage detectors comprising hadron blind detectors (HBDs) and lead-glass electro-magnetic calorimeters (LGs). The HBD is a gas-type Cherenkov detector with a CF_4 radiator.[2] Emitted Cherenkov photons are converted into electrons at a CsI photocathode, and these electrons are amplified by a gas-electron multiplier (GEM).[3] The LG is a calorimeter sensitive to EM showers generated by an incident particle in lead-glass. The high-energy electrons generate large showers compared with pions; therefore, the LG is able to distinguish electrons from pions based on the quantity of Cherenkov photons emitted by the showers.

Both detectors were developed independently, and their performances were evaluated separately.[4,5] If particle detection by one detector affects another detector, the combined performance of the system possibly becomes worse than expected from the individual performances. For example, an incident pion may produce knock-on electrons in the CF_4 radiator of the HBD, one of which may have sufficient energy to produce EM showers in the LG, which is installed behind the HBD. These effects are expected to be small; however, experimental validation is necessary.

We performed a beam test for a total performance evaluation of the HBD and LG in the commissioning run of the E16 spectrometer at the high-momentum beamline at J-PARC. As shown in Fig. 1, we constructed a novel setup, which covered the forward acceptance of the E16 spectrometer. The responses of the HBD and the LG were examined for pions, identified by the triple coincidence of scintillation counters and two gas Cherenkov detectors (GCs) positioned in front of the HBD. The primary beam intensity was typically 1×10^9 protons/spill suitable for the readout system of this measurement. We adopted one carbon and two copper targets, whose total thickness was 0.2% interaction length. This was the same configuration as the E16 experiment.

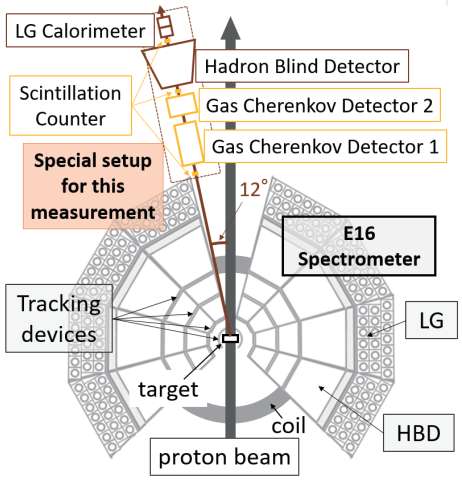

Fig. 1. Experimental setup for evaluating the overall performance of the electron identification system.

The HBD and LG distinguished electrons from pions by applying a threshold to the number of detected photons. We measured the threshold dependence of three quantities: single rejection power of the HBD (SR_{HBD}), that of the LG (SR_{LG}), and total rejection power of the HBD and the LG (TR). Here, the rejection power was defined as the number of total events divided by that of misidentified events. If the correlation between the detectors is negligible, the product of SR_{HBD} and SR_{LG} is expected to be consistent with TR. At the threshold, which will be used in the future experiment, the values of SR_{HBD} and SR_{LG} were determined to be 49 ± 44 and 3.6 ± 0.1, respectively; therefore, the product of these values was 178 ± 16. Compared with the product, the measured value of TR was 174 ± 29. These two values were consistent within their statistical uncertainties; therefore, we concluded that the HBD and LG independently work for pions.

In the coming beamtime in February and June 2021, we plan to study and evaluate the performance minutely with the E16 spectrometer, in terms of rate capability and the response depending on an incident angle and momentum of incoming particles.

*1 Department of Physics, Graduate School of Science, Kyoto University
*2 Advanced Science Research Center, Japan Atomic Energy Agency
*3 RIKEN Nishina Center

References

1) S. Yokkaichi, in this report.
2) W. Anderson *et al.*, Nucl. Instrum. Methods Phys. Res. A **646**, 20–24 (2011).
3) F. Sauli, Nucl. Instrum. Methods Phys. Res. A **386**, 531–534 (1997).
4) K. Kanno *et al.*, Nucl. Instrum. Methods Phys. Res. A **819**, 35–58 (2016).
5) S. Ashikaga, Master's thesis, Kyoto University (2018).

Intermediate silicon tracker for sPHENIX experiment at RHIC

I. Nakagawa,[*1] Y. Akiba,[*1] D. Cacace,[*2] K. Cheng,[*3] T. Hachiya,[*1,*4] S. Hasegawa,[*5] D. Imagawa,[*9] H. Imai,[*9] T. Kondo,[*6] C. Kuo,[*3] H. -S. Li,[*7] R. -S. Lu,[*8] E. Mannel,[*2] C. Miraval,[*2] M. Morita,[*4] Y. Namimoto,[*4] S. Nishimori,[*4] R. Nouicer,[*2] G. Nukazuka,[*1] R. Pisani,[*2] M. Shibata,[*4] C. Shih,[*3] M. Stojanovic,[*7] W. -C. Tang,[*3] and X. Wei[*7]

The INTermediate Tracker (INTT) is the one of three major tracking detectors to be implemented in sPHENIX experiment[1] which is to be launched in 2023 at RHIC. It is consisted of two layers of silicon strip sensors assembled into the barrel structure covering the central region of sPHENIX collision point. Silicon sensors and FPHX readout chips[2] are implemented on high density interconnect (HDI) cables which are glued on top of a 50 cm long cooling stave. The stave as shown in Fig. 1 is made of the carbon fiber reinforced plastics and fabricated in Asuka co.

The mass production of silicon sensors, FPHX chips, and HDI cables have been completed. The stave production is to be completed by the end of February, 2021. A bus extender cable (BEC) and a conversion cable (CC) form series of INTT readout chain together with the HDI cable. The development of the BEC and CC are almost completed[3] and the mass production of these cables are scheduled in JFY2021. Several preproduction INTT ladders (Fig. 2) have been assembled in National Taiwan University and BNL. Once the final tune for the optimization of assembly procedure is over, the mass production of the ladder assembly will be started and expected to be finished in Spring, 2021.

The preparation for testing production ladders has been ongoing at Nara Women's University in both hardware and software. There 3 major items listed below are under development.

(1) **Source test fixture**: The motor driven radiation source scanner of the ladder (Fig. 3)
(2) **FPHX readbacker**: The software application to read back the resisters of FPHX chips.
(3) **Interception board**: The compact circuit board to be inserted between the readout cables which branches out signal traffic without disturbing the data taking. To be used for debugging of any mis-communications between ladder and readout control board.[2]

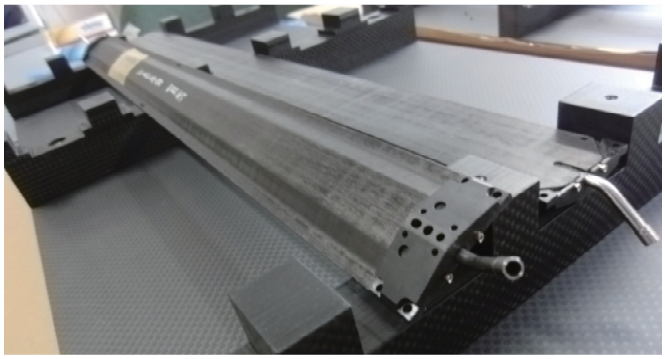

Fig. 1. The CFRP staves for INTT ladder.

Fig. 2. Fully assembled INTT preproduction ladders.

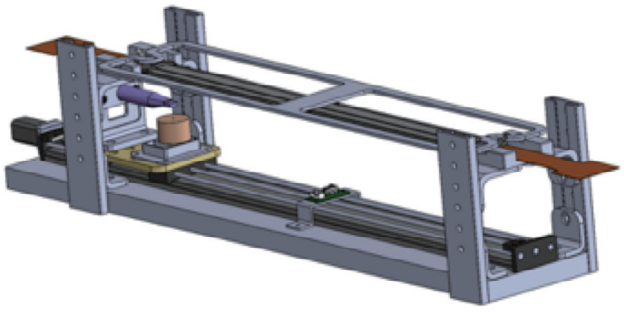

Fig. 3. The fixture for radiation source test of a ladder.

*1 RIKEN Nishina Center
*2 Physics Department, Brookhaven National Laboratory
*3 Department of Physics, National Central University
*4 Department of Mathematical and Physical Science, Nara Women's University
*5 Japan Atomic Energy Agency
*6 Tokyo Metropolitan Industrial Technology Research Institute
*7 Department of Physics and Astronomy, Purdue University
*8 Department of Physics, National Taiwan University
*9 Department of Physics, Rikkyo University

References

1) Conceptual Design Report of sPHENIX (2018).
2) C. Aidala *et al.*, Nucl. Instrum. Methods Phys. Res. A **755**, 44 (2014).
3) T. Hachiya *et al.*, in this report.

Detection efficiency of the INTT test bench for sPHENIX

G. Nukazuka,[*1] Y. Akiba,[*1] D. Cacace,[*2] K. Cheng,[*3] T. Hachiya,[*1,*4] S. Hasegawa,[*5] D. Imagawa,[*6] H. Imai,[*6] T. Kondo,[*7] C. Kuo,[*3] H. -S. Li,[*8] R. -S. Lu,[*9] E. Mannel,[*2] C. Miraval,[*2] M. Morita,[*4] I. Nakagawa,[*1] Y. Namimoto,[*4] S. Nishimori,[*4] R. Nouicer,[*2] R. Pisani,[*2] M. Shibata,[*4] C. Shih,[*3] M. Stojanovic,[*7] W. -C. Tang,[*3] and X. Wei[*8]

sPHENIX[1] will start data acquisition in the Relativistic Heavy Ion Collider at Brookhaven National Laboratory from 2023 to study quark-gluon plasma. The Silicon Intermidiate Trackter (INTT),[2] which is one of the crucial pieces in the detector complex, enables us to perform jet flavor tagging with high precision and low background. INTT inherits the readout electronics from the Forward Silicon Vertex Detector of PHENIX[3] so that R&D can proceed with low cost in a short period.

In a test-beam experiment at Fermilab,[4] we confirmed that the prototype of INTT satisfied the essential specifications for position resolution and timing resolution. Detection efficiency was approximately 96%, although almost 100% was expected. In these measurements, the prototype worked using the internal clock (BCO) of 9.4 MHz while the beam arrived independently from BCO. The lower-than-expected detection efficiency can be due to timing mismatch between the beam and BCO, because of which signals of the silicon module were occasionally not detected.

To test the hypothesis, we implemented an external trigger system using the Nuclear Instrumentation Module (NIM) and Computer Aided Measurement And Control (CAMAC) modules and integrated it into the existing data acquisition system (DAQ) (Fig. 1). The silicon module was set between two trigger scintillators. The transverse dimensions of the scintillators were the same as the active area of the silicon module. One scintillator on the top was set along the silicon module, while the other was rotated by 90° longitudinally to restrict acceptance. Coincidence of signals from the two scintillators is treated as a trigger signal. The DAQ stores the following parameters:

- hit information on the silicon module

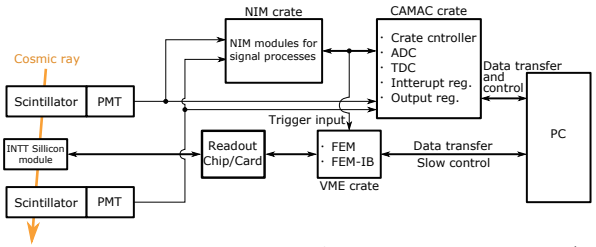

Fig. 1. Overview of the new DAQ system. See Ref. 3) for some of the abbreviations.

*1 RIKEN Nishina Center
*2 Physics Department, Brookhaven National Laboratory
*3 Department of Physics, National Central University
*4 Department of Mathematical and Physical Science, Nara Women's University
*5 Japan Atomic Energy Agency
*6 Department of Physics, Rikkyo University
*7 Tokyo Metropolitan Industrial Technology Research Institute
*8 Department of Physics and Astronomy, Purdue University
*9 Department of Physics, National Taiwan University

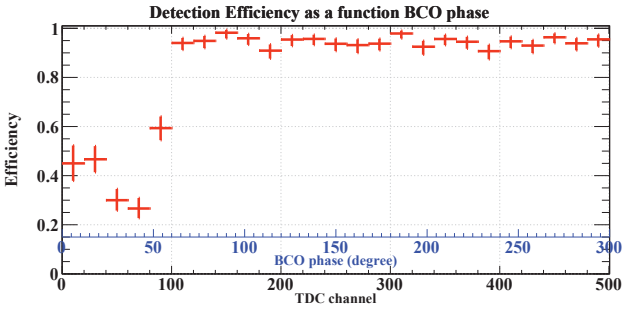

Fig. 2. Detection efficiency as a function of BCO phase with the quality cuts.

- total charge and timing information of the scintillator signals
- the timing difference between the coincidence signal and a BCO pulse, *i.e.*, a phase of BCO.

In the analysis, quality cuts for analog-to-digital converter (ADC) and time-to-digital converter (TDC) distributions of the scintillator signals reject noise-like events. The detection efficiency defined as a ratio of the number of trigger events with INTT hit to the number of the trigger events is calculated after applying the quality cuts as a function of the BCO phase (Fig. 2). Measurement could not be performed for a sixth of the BCO period owing to technical difficulties. A clear drop in efficiency in the first 100 TDC channels was found as expected. The average efficiency excluding and including the dropping region was approximately 94% and 85%, respectively. This low-efficiency condition can be the reason for the 96% efficiency obtained in the test-beam experiments. The efficiency obtained in this study is lower than that in the test-beam experiment because the acceptance restriction was not perfect; consequently cosmic rays could activate the trigger without impingement on the silicon module.

We could also observe a positive correlation between the efficiency and ADC for the bottom scintillator. Requiring higher ADC value to the signal may eliminate cosmic rays, which do not penetrate the silicon sensor. This observation suggests that optimization of the setup can yield a higher detection efficiency.

In summary, we found dependency of the detection efficiency on the BCO phase. It explains the lower efficiency observed in the test-beam experiment. Since RHIC will provide a beam-synced trigger, this timing mismatch cannot be an issue for sPHENIX

References

1) A. Adare *et al.*, sPHENIX proposal (2015).
2) I. Nakagawa *et al.*, in this report.
3) C. Aidala *et al.*, Nucl. Instrum. Methods. Phys. Res. A **755**, 44 (2014).
4) A. Suzuki, Master's thesis, Nara Women's Univ. (2020).

Radiation resistance of bus extender cable for sPHENIX-INTT

H. Imai,[*1,*9] Y. Akiba,[*1] D. Cacace,[*2] K. Cheng,[*3] T. Hachiya,[*1,*4] S. Hasegawa,[*5] D. Imagawa,[*9] T. Kondo,[*6] C. Kuo,[*3] H. -S. Li,[*7] R. -S. Lu,[*8] E. Mannel,[*2] C. Miraval,[*2] M. Morita,[*4] I. Nakagawa,[*1] Y. Namimoto,[*4] S. Nishimori,[*4] R. Nouicer,[*2] G. Nukazuka,[*1] R. Pisani,[*2] M. Shibata,[*4] C. Shih,[*3] M. Stojanovic,[*7] W. -C. Tang,[*3] and X. Wei[*7]

We are developing INTermidate Tracker (INTT), which is a new tracking detector for the sPHENIX experiment at RHIC in BNL, which is a successor of PHENIX. The INTT needs to be designed to transmit approximately 14k signal lines through a very narrow space; therefore any commercial detector available in the market will not fit to interconnect the INTT and the downstream readout controller board (ROC).[1)] Thus, we have been developing a long and high-density cable, which is called "bus extender" for the last four years.

The bus extender cable is a multilayered flexible print cable. Liquid crystal polymer (LCP) and copper foil layers are laminated using an epoxy glue, forming a multilayered structure. The LCP and the glue are made of macromolecule materials; therefore, there is concern for their use under the radiation enviroment because macromolecules are known to be weak against a radiation dose, in geneanl. Thus, the cable needs to demonstrate radiation hardness. We list the following two physical characteristics as indicators of the radiation hardness: 1) loss of flexibility, 2) decrease in the peel strength of the glue. The former can be quantitatively evaluated by measuring Young's modulus. The latter was evaluated by a peel force measurement.

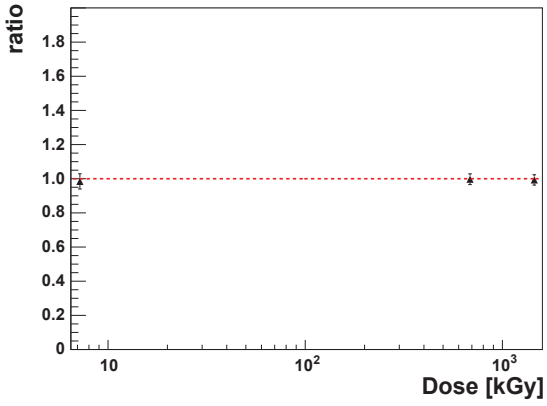

Fig. 1. Ratio of Young's modulus as function of radiation dose.

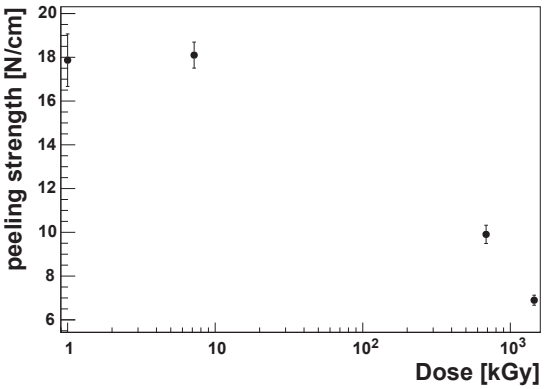

Fig. 2. Peeling strength as function of radiation dose.

Dedicated test samples for the radiation test were fabricated, which have the same layer structure as the bus extender but a smaller size: 40 cm length and 2 cm width each. These test samples are exposed to gamma ray radiation from a ^{60}Co source at a facility in the National Institute of Quantum and Radiological and Technology.

The natural frequency method was employed to measure Young's modulus. The natural frequency can be related with Young's modulus as defined in Eq. (1) where, f is the natural frequency, E is Young's modulus, I is the moment of second-order, A is a cross-section area, ρ is the density, l is the length, and λ is a constant. λ is approximately 1.8 for basic frequency.

$$f = \frac{\lambda^2}{2\pi l^2}\sqrt{\frac{EI}{\rho A}} \tag{1}$$

Figure 1 shows the results of the measurement. The vertical axis shows the ratio of the observed Young's modulus of the samples with and without exposure. The result is constant within the size of the error bars, and thus, there is no indication of loss of flexibility.

Figure 2 shows the radiation dose dependence of the observed peel strength. The peel strength is measured using SHIMAZU MST-I. A clear degradation of the peel strength is observed. However, the degradation is still moderate within the expected radiation dose ∼5 kGy in three of sPHENIX operation. We conclude that the bus extender demonstrates sufficient radiation hardness to be used in the sPHENIX experiment.

*1 RIKEN Nishina Center
*2 Physics Department, Brookhaven National Laboratory
*3 National Central University
*4 Department of Mathematical and Physical Science, Nara Women's University
*5 Japan Atomic Energy Agency
*6 Tokyo Metropolitan Industrial Technology Research Institute
*7 Department of Physics and Astronomy, Purdue University
*8 Department of Physics, National Taiwan University
*9 Department of Physics, Rikkyo University

Reference

1) T. Hachiya *et al.*, in this report.

Electrical and mechanical properties of the bus-extender

M. Morita,[*1] Y. Akiba,[*2] D. Cacace,[*3] K. Cheng,[*4] T. Hachiya,[*2,*1] S. Hasegawa,[*5] D. Imagawa,[*9] H. Imai,[*9] T. Kondo,[*6] C. Kuo,[*4] H. -S. Li,[*7] R. -S. Lu,[*8] E. Mannel,[*3] C. Miraval,[*3] I. Nakagawa,[*2] Y. Namimoto,[*1] S. Nishimori,[*1] R. Nouicer,[*3] G. Nukazuka,[*2] R. Pisani,[*3] M. Shibata,[*1] C. Shih,[*4] M. Stojanovic,[*7] W. -C. Tang,[*4] and X. Wei[*7]

The sPHENIX experiment at the Relativistic Heavy Ion Collider (RHIC) is scheduled to start in 2023 in Brookhaven National Laboratory (BNL). The INTermediate Tracker (INTT)[1] is a silicon sensor strip detector to be implemented in the central rapidity region. The massive raw data generated in INTT need to be transmitted to downstream readout electronics through a quite narrow and curving cabling path for 1.2 m. As there is no commercial cable available, a high-signal-density cable was developed using flexible printed cable technology. The cable is called "bus-extender" and has 62 pairs of 130-µm-width signal lines. The bus extender mainly transmits digital signals. The development of the bus extender is in the final stage.[2]

Owing to the long path length of high-density flexible printed cables, the poor performance of signal transmission of high-frequency data is a major concern. A simulation predicts 30% attenuation for a 200 MHz signal.

An eye diagram is a useful tool to visually inspect the attenuation and distortion of the signal pulse. We measured the eye diagram by overlaying the waveforms of various bit patterns. The transmission efficiency can be evaluated qualitatively by the size of the opening of the eye. Figure 1(a) and (b) show the eye diagram of the low-voltage differential signaling (LVDS) signals before and after passing the bus-extender. From the comparison, the attenuation of the signal is determined as 33%. The result is consistent with the simulation. It is found that the eye opening after the bus-extender is too small to receive the signals at the readout electronics. To solve the problem, we increase the drawing current of the LVDS signals from 2 mA to 8 mA to effectively obtain a sufficiently wider eye opening.

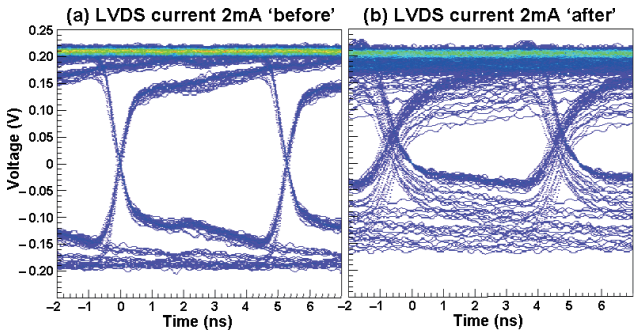

Fig. 1. Eye diagrams (a) before and (b) after the bus-extender in the readout chain.

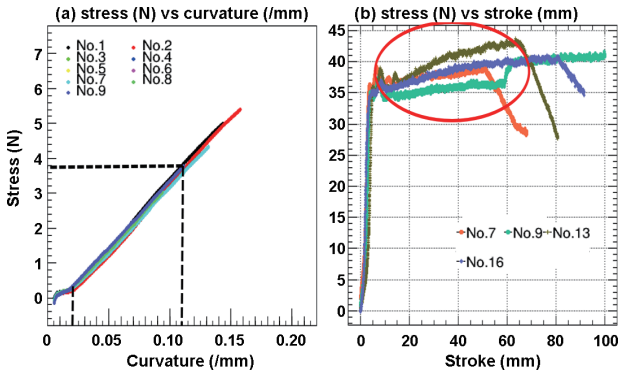

Fig. 2. (a) Stress concerning the U-shaped curvature of test pieces. (b) Peeling strength as a function of the peeled length, evaluated in the region covered by a red circle.

The mechanical properties are also important to assess the long-term stability and radiation hardness. The bus extender needs to survive at least three years of operation in a high-radiation environment. The bus-extender is made using a liquid crystal polymer (LCP) as substrate, instead of a polyimide, which is generally used for flexible cables. LCP is a new material used for high-energy physics experiments. Therefore, we studied its mechanical properties by comparing it with polyimide. In addition, this study provides a baseline to assess the radiation hardness.

We measured two quantities: (1) flexibility and (2) peeling strength between layers of the multilayered cable. Here, the results of the 2-cm-wide specimen used are shown instead of results per unit. The former is measured by bending the cable in the middle by 180° as it forms a "U-shape" inside view. The stress from the cable is recorded for several test samples as a function of curvature and is plotted in Fig. 2(a). The flexibility is evaluated by the slope of a 4 N increase in the curvature region from 0.02 to 0.11/mm. This result is further compared to that from cables exposed to radiation, and no drastic change was found.[3] Therefore, we could obtain the reference value for flexibility. The latter is measured by recording the stress of peeling off the cable as a function of the stroke. The result plotted in Fig. 2(b) shows a peeling strength of 34 to 44 N. This value is twice that of the polyimide.

We plan to start the mass production of bus-extenders in 2021. The continuity of all signal lines will be tested using newly developed test equipment.[4]

*1 Department of Mathematical and Physical Science, Nara Women's University
*2 RIKEN Nishina Center
*3 Physics Department, Brookhaven National Laboratory
*4 Department of Physics, National Central University
*5 Japan Atomic Energy Agency
*6 Tokyo Metropolitan Industrial Technology Research Institute
*7 Department of Physics and Astronomy, Purdue University
*8 Department of Physics, National Taiwan University
*9 Department of Physics, Rikkyo University

References

1) I. Nakagawa *et al.*, in this report.
2) T. Hachiya *et al.*, in this report.
3) H. Imai *et al.*, in this report.
4) D. Imagawa *et al.*, in this report.

Upgrade of the Si-CsI array TiNA for transfer reactions at OEDO

B. Mauss,[*1] J. W. Hwang,[*2,*3] D. Suzuki,[*1] N. Ma,[*2] N. Imai,[*2] M. Dozono,[*2] S. Michimasa,[*2] T. Sumikama,[*1] S. Ota,[*2] C. Iwamoto,[*1] N. Iwasa,[*3] and F. Endo[*3]

TiNA is an array of silicon strip detectors (SSDs) and CsI(Tl) crystals for measuring recoiling particles from transfer reactions.[1] Initially, TiNA had six telescopes in a lamp-shade configuration. Each telescope had a YY1-type single-sided SSD of Micron and two CsI crystals behind the SSD, the total active area of which is 6×5 cm^2. The telescopes were placed 8 to 10 cm away from the reaction point and surrounded the beam axis. They covered a laboratory angle range of 100° to 150°. TiNA has been used in several transfer experiments at RIBF.[2,3]

Upcoming experiments using transfer reactions, however, require a larger solid angle and better resolutions in angle and energy. For instance, for the ^{50}Ca(d,p) experiment at the OEDO beamline, an excitation energy resolution better than 200 keV in σ should be achieved. The upgrade project of TiNA has been launched to fulfill these requirements. In this report, we present the details of the improvements of TiNA and the results of the offline test.

Figure 1 shows the upgraded structure of TiNA. Four more telescopes are introduced to cover a larger solid angle, and they are located between the target and the YY1 telescopes. Each has a 0.3 mm-thick TTT2-type double-sided SSD (DSSD) of Micron and four 25 mm-thick CsI(Tl) crystals. The DSSD covers 97×97 mm^2. The CsI crystals placed behind can measure relatively high-energy charged particles (*e.g.*, protons with $E < 80$ MeV). The angular resolution is improved to be less than 0.5°. Three new trapezoidal CsI crystals are brought in to fully cover the active area of the original YY1 SSD.

A new electronic system for the TTT2 has been established. Since the additional detectors have more than a thousand channels, we employ the General Electronics for TPCs (GET), an integrated system for signal processing including analog to digital converters (ADCs), trigger logic, and amplifiers for detectors with many channels.[4] For the connection between the DSSDs and GET, flexible-printed-circuit (FPC) connectors and circuits for the separation of signals from a DC bias are used. A new scattering chamber housing was prepared as well.

The performance of the GET system to readout the signal from the TTT2 was tested at RIKEN. The test bench consisted of one TTT2 and a standard ^{241}Am α-source installed inside the new TiNA chamber. The detector was fully depleted at -55 V. The GET system consisted of an application-specific integrated circuit (ASIC) and ADC (AsAd) board connected to a total of 256 strips and a reduced version of the Concentration Board (rCoBo). The system was triggered by an internal multiplicity signal of rCoBo. A pulse-shape analysis is performed on the GET digitized signal to extract the energy of particle hits. The resolution obtained on the ^{241}Am α-spectrum is 28 keV (FWHM) for the 5.485 MeV peak. More tests have been performed with the full system using 4 AsAd boards connected to a normal CoBo. It yielded similar results.

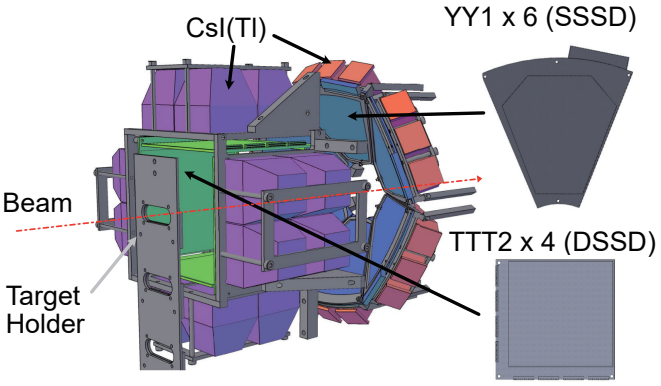

Fig. 1. Schematic drawing of TiNA after upgrade. The YY1-type SSDs and CsI(Tl) crystals of original TiNA are colored with blue and red, respectively. The new TTT2-type DSSDs and CsI(Tl) crystals are colored with green and purple, respectively.

In conclusion, the TiNA array was upgraded by integrating new DSSDs, CsI detectors, and the GET system. The performance was tested using a standard α-source. The results demonstrate the high resolution capabilities allowed by the new design and electronic circuit. This resolution was used to simulate the ^{50}Ca(d,p) reaction. The overall excitation energy resolution is less than 150 keV in σ, which is within the experiment specification. The full system of TiNA will be tested in-beam at the Tandem accelerator of the University of Kyushu in January 2021.

*1 RIKEN Nishina Center
*2 Center for Nuclear Study, the University of Tokyo
*3 Center for Exotic Nuclear Studies, Institute for Basic Science
*4 Department of Physics, Tohoku University

References

1) P. Schrock *et al.*, CNS Annu. Rep. 2016, CNS-REP-**96**, 7 (2017).
2) K. Wimmer *et al.*, CNS Annu. Rep. 2017, CNS-REP-**97**, 7 (2019).
3) N. Imai *et al.*, CNS Annu. Rep. 2018, CNS-REP-**98**, 1 (2020).
4) E. C. Pollacco *et al.*, Nucl. Instrum. Methods Phys. Res. A **887**, 81 (2018).

Heat durability test of molybdenum foil for the new CRIB cryogenic gas target

S. Hayakawa,[*1] N. Ma,[*1] H. Shimizu,[*1] and H. Yamaguchi[*1,*2]

A cryogenic gas target was developed and used for over 10 years[1] for high-intensity low-energy secondary beam productions at CRIB (Center for Nuclear Study RI Beam separator.[2]) The basic design comprises a stainless-steel gas cell with a 80-mm-long vs. ϕ20-mm cylindrical aperture, where the target gas is confined by 2.5-μm-thick Havar foil windows at the beam entrance and exit sides. The gas supply duct and gas cell are cryogenically cooled by liquid nitrogen. A forced gas flow system is employed through the entire gas line to avoid density reduction under high heat deposition caused by beam irradiation. The maximum intensity of the primary beam irradiation is limited by the heat durability of the Havar foil, which is known to be 2 W. Therefore, the gas target is always operated at a sufficiently low heat deposition of the primary beam onto the Havar foil windows to avoid damage.

Currently, we are developing a ^{26}Si RI beam with an intensity of 5×10^4 pps or higher for future measurements of the α-resonant scattering and ^{26}Si(α,p) reaction at CRIB (Exp. No. NP1812-AVF55). The highest beam intensity of ^{26}Si achieved at CRIB is 1.2×10^4 pps[3] with a ^{24}Mg primary beam at 7.5 MeV/nucleon and 0.2 particle μA (pμA), which is limited by the 2-W heat deposition on the Havar windows. The above goal is possible once we achieve the maximum heat deposition of 8 W or higher. To this end, we consider the following design changes: (1) Using a foil material with a higher heat conductivity and/or higher melting point than those of Havar foil; (2) Redesigning the gas cell with a higher cooling performance.

In the previous test experiment (Exp. No. NP1812-AVF55-01), we confirmed the advantages of molybdenum (Mo) and titanium (Ti) over Havar foil. The former has better high-temperature property due to its higher melting point and heat conductivity, and the latter has lower heat deposition because the minimum required vacuum-tight thickness offers smaller energy loss of the beam passing through it. Next, we tested the heat durability of 2- and 3-μm-thick Mo foil mounted on the currently used gas target cell in the Detector Develop Beam Time (Exp. No. DD20-01). The target cell was filled with ^{4}He gas up to 400 Torr, cooled by liquid nitrogen with forced circulation. An ^{16}O beam at 6.8 MeV/nucleon was injected into the gas target with the maximum beam intensity of 1.4 pμA. The time course of the maximum temperature monitored by the thermography is shown in Fig. 1 for different

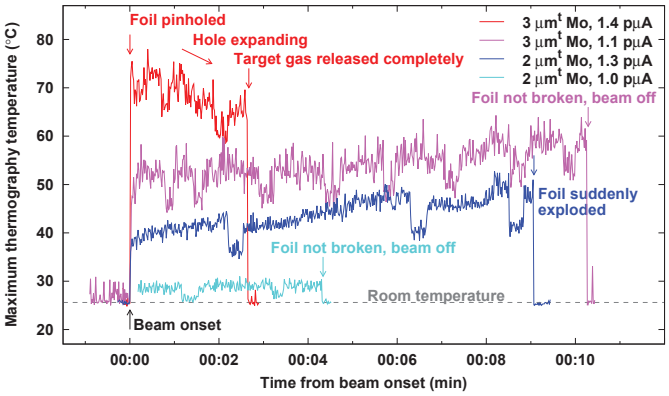

Fig. 1. Time course of maximum temperatures.

foil thicknesses and beam intensities. Note that the read temperature tends to be considerably lower than the expected value because of the limited spatial resolution of the thermography for the beam spot size. For an overall trend, the thicker foil is more easily heated up because of the larger energy loss of the beam particle than the thinner one. We believe that the process of each foil above 1.3 pμA was different; the temperature of the thinner one (blue line) increased gradually and the foil suddenly exploded at some point. In contrast, the thicker one (red line) showed a pinhole created right after the beam injection started, and the read temperature was decreasing as the hole expanded to loose the gas completely at the end. Despite such different trends, the breaking intensity was found to be similar (1.3–1.4 pμA), which can be attributed to the mechanical strength of the thinner foil becoming too weak to hold the gas even at a lower temperature where the thicker foil is still stable (even with a pinhole). We conclude that both the 2- and 3-μm-thick Mo foils can resist a beam intensity of 1.0–1.1 pμA or a heat deposition of 6–7 W at least; thicker foils are preferred for stable operation.

The remaining issue is the more efficient heat release from the Mo foil to the cryogenic gas cell body; this can be achieved by a design change (2). This is important to achieve further heat duration (>8 W) and for a more stable long-duration operation. This will be tested by another Detector Development Beam Time (Exp. No. DD20-02).

*1 Center for Nuclear Study, University of Tokyo
*2 National Astronomical Observatory of Japan

References

1) H. Yamaguchi *et al.*, Nucl. Instrum. Methods Phys. Res. A **589**, 150 (2008).
2) Y. Yanagisawa *et al.*, Nucl. Instrum. Methods Phys. Res. A **539**, 74 (2005).
3) H. S. Jung *et al.*, Phys. Rev. C **85**, 045802 (2012).

Radiation resistivity test of an optical fiber for laser cooling of francium atoms

T. Hayamizu,[*1] K. Nakamura,[*2] T. Aoki,[*3] Y. Kotaka,[*2] H. Nagahama,[*2] S. Nagase,[*2] M. Ohtsuka,[*2,*4] N. Ozawa,[*2] M. Sato,[*3] A. Takamine,[*1] K. S. Tanaka,[*5] H. Haba,[*1] and Y. Sakemi[*2]

Francium is an alkali element in the 7th period, and all its isotopes are radioactive with half-lives of up to 20 min. The application of francium atoms to high-precision spectroscopy for testing fundamental symmetries has been implemented on a vertical beam line of the E7 room at the RI Beam Factory. Francium is produced in the ^{197}Au(^{18}O, xn)$^{215-x}$Fr reaction and finally supplied as laser-cooled atoms into the spectroscopic region. For Fr production, a 7 MeV/nucleon $^{18}O^{6+}$ beam (target current 18 $e\mu$A) propagating through two beryllium foils and helium gas flow is injected into a gold target positioned at the end of the beam line. However, the optical experimental region for spectroscopy is exposed to high radiation from the target, which is placed a few meters away. Therefore, the optical experimental devices should be evaluated for radiation resistivity.

Laser sources were placed in the laser spectroscopy room in the basement of the RIBF building. A titanium-sapphire laser and external cavity diode lasers supplied 718 nm light beams for the laser cooling of Fr atoms. These light beams will be transported to the E7 room via 400 m of optical fiber. The optical fiber consists of a polarization-maintaining optical fiber (Fujikura SM63-PS-U25D) covered by a stainless flexible tube and flame-retardant polyvinyl chloride (Nippon Steel Welding & Enginering PICOFLEC). One of the concerns is radiation damage caused by boron, which has a large capture cross section of neutrons, contained in stress-applied parts of this optical fiber.[1)] We expected the radiation damage to cause two behaviors: transmission power drifting and degradation of light polarizability.

To evaluate the radiation resistivity, we performed a light transmission monitoring test using 40 m of the same model optical fiber wired inside the E7 room, during the Fr production beam time (maximum 7.9 $e\mu$A). A part of the optical fiber (4.5 m) was stuck with plastic masking tape on the vertical flat surface of a steel rack approximately 1.2 m away from the vertical beam line. The ends of the optical fiber were connected to an optical monitoring system set downstairs of the E7 room, where the radiation level is low. A 685 nm, 1 mW light beam from a diode laser was used for the monitoring system. The output light power of the diode laser, and each s- and p-polarized light power from the optical fiber were monitored using power meters. We determined the transmittance T by the power of the s-polarized output light from the optical fiber normalized by the value of the input power monitor. In addition, the radiation dose to the optical fiber was estimated using data from the E7 room monitoring posts. The peak value of the neutron dose rate was 3.7 mSv/hr, and the integrated neutron dose at the monitoring posts over the beam time was 21.6 mSv. Considering only the distance from the target, the expected dose of the optical fiber was several times larger than the dose estimated at the monitoring post.

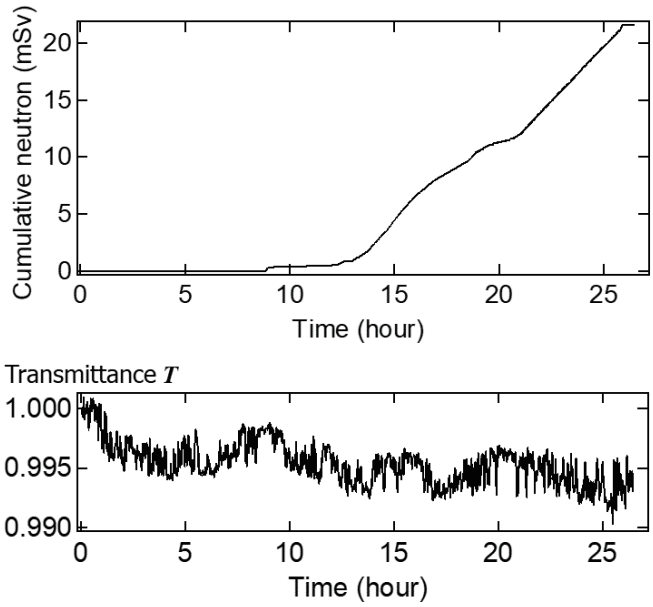

Fig. 1. The upper figure shows the integrated neutron dose at the E7 room monitoring post from the beginning of measurement, and the lower figure shows the optical-fiber transmittance.

The data obtained during the beam time are shown in Fig. 1. Although it is clear that the cumulative neutron dose and the fluctuation of T in Fig. 1 did not correlate, T gradually reduced by less than 1% during 27 h. In order to identify whether this was caused by the irradiation, we carried out followup tests with a low radiation background condition. By checking the optics used in the monitoring system, we found that the coupling efficiency on the fiber couplers may have caused a similar drift. In conclusion, a significant change beyond the measurement accuracy of the transmitted light power and light polarization due to the irradiation was not observed with the current experimental setup. Additional checks using a higher radiation dose are necessary to ensure that this optical fiber can be used for a longer beam time.

*1 RIKEN Nishina Center
*2 Center for Nuclear Study, University of Tokyo
*3 Graduate School of Arts and Science, University of Tokyo
*4 Waseda University Honjo Senior High School
*5 Cyclotron and Radioisotope Center, Tohoku University

Reference
1) S. Karasawa *et al.*, IEEE Trans. Nucl. Sci. **34**, 1105 (1987).

Development of novel detection system for francium ions extracted from online surface ionizer

N. Ozawa,[*1] H. Nagahama,[*2] T. Hayamizu,[*3] K. Nakamura,[*2] M. Sato,[*3,*4] S. Nagase,[*1] Y. Kotaka,[*2] K. Kamakura,[*2] K. S. Tanaka,[*5] M. Otsuka,[*3] T. Aoki,[*3,*4] Y. Ichikawa,[*3,*6] A. Takamine,[*3] H. Haba,[*3] H. Ueno,[*3] and Y. Sakemi[*2]

One of the origins of the matter-antimatter asymmetry in the Universe is considered to be the violation of the charge conjugation and parity symmetries.[1] The existence of a non-zero permanent electric dipole moment (EDM) of an elementary particle is an indicator of symmetry violation.

In particular, electron EDM (eEDM) is enhanced in paramagnetic atoms,[2] up to 10^3 in the case of francium (Fr), which is the heaviest alkali.[3,4] We are currently developing an eEDM measurement system using laser-cooled Fr atoms.

Fr atoms are produced in a surface ionizer via the nuclear fusion-evaporation reaction, ^{197}Au(^{18}O, xn)$^{215-x}$Fr.[5] An ^{18}O primary beam is irradiated onto a solid Au target. A fraction of the produced Fr atoms reach the surface via thermal diffusion, where they are released as ions owing to the surface ionization effect on the Au surface. Using electrodes placed next to the target, the ions are extracted at a 45-degree angle at 1 keV energy. The Fr ion production rate depends on the Au target temperature, which is controlled using an infrared heater installed on the opposite side of the beam irradiation surface of the target.

The Fr yield is monitored by detecting the α particles emitted during their decay using a Si solid state detector (SSD). In previous experiments, because the infrared light from the heater acted as a noise source for the SSD, the heater needed to be stopped for each measurement. However, turning off the heater frequently caused the Fr production to become inefficient, owing to the rapid drop in the Au target temperature.

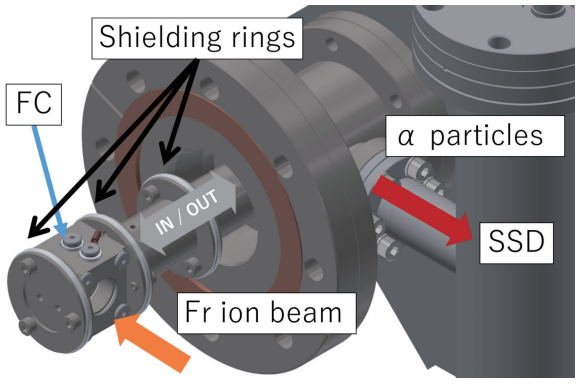

Fig. 1. Developed Fr ion beam detector. Light from infrared heater is shielded by shielding rings.

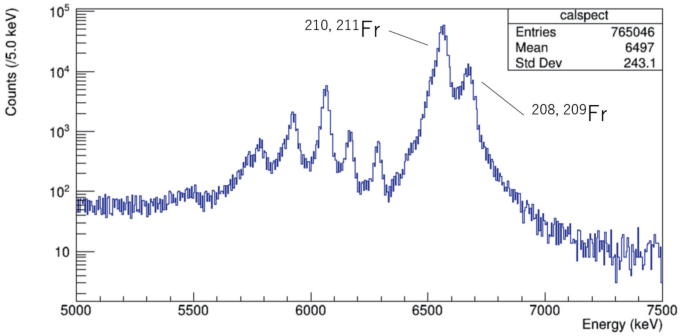

Fig. 2. Typical energy spectrum of α particles emitted during decay of ions captured on FC surface, obtained using the SSD. Labelled peaks within the range of 6.5–6.8 MeV are identified as Fr.

To overcome this problem, we have developed a novel Fr ion detection system that is insensitive to the infrared light of the heater. The detection system, as shown in Fig. 1, consists of an SSD, a Faraday cup (FC), and a moving rod attached to four shielding rings. The extracted Fr ions are first irradiated onto the FC surface, where the beam intensity is observed as electronic current. Subsequently, the FC is moved to the front of the SSD, where the α particles are detected. Throughout the operation, the shielding rings fit to the cylindrical wall of the chamber with a negligible clearance; therefore the light hardly enters the SSD.

In September 2020, an experiment on Fr production was conducted. Figure 2 shows the energy spectrum of the α particles detected by the SSD. The spectrum analysis shows that a ^{210}Fr ion beam of 5×10^6/s was extracted. The Au target was heated to 960°C, and an $^{18}O^{6+}$ beam of 1 particle μA accelerated to 7 MeV/nucleon using an RIKEN AVF cyclotron was used as the primary beam.

Throughout the experiment, the infrared heater had a negligible effect on the SSD. Therefore, the newly developed Fr ion detection system enables beam detection without stopping the infrared heater, which is advantageous for stable production of Fr ions.

*1 Department of Physics, University of Tokyo
*2 Center for Nuclear Study, University of Tokyo
*3 RIKEN Nishina Center
*4 Graduate School of Arts and Sciences, University of Tokyo
*5 Cyclotron and Radioisotope Center, Tohoku University
*6 Department of Physics, Kyushu University

References

1) A. D. Sakharov, Sov. Phys. Usp. **34**, 392 (1991).
2) M. Popeslov *et al.*, Ann. Phys. **318**, 119 (2005).
3) D. Mukherjee *et al.*, J. Phys. Chem. A **113**, 12549 (2009).
4) T. M. R. Byrnes *et al.*, Phys. Rev. A **59**, 3082 (1999).
5) G. Stancari *et al.*, Nucl. Instrum. Methods Phys. Res. A **557**, 390 (2006).

Experiment on hydrogen removal apparatus for helium supply and recovery system

M. Nakamura,[*1] T. Dantsuka,[*1] and H. Okuno[*1]

In the past, the liquid-helium supply and recovery system of the Wako campus have suffered severe damages from hydrogen impurities in the system.[1] To remove this hydrogen from the recovered helium gas, we developed hydrogen removal methods utilized for our system. We found that the silver-zeolite "Ag400" made by "Molecular Products Inc." can be used as the adsorbent, and the applicability of Ag400 for hydrogen removal was confirmed.[2] At that time, we did not install the hydrogen removal apparatus earnestly in our system. However, a new liquid-helium supply system was constructed and operated from 2017 because of the deterioration of the old system.[3] In this system, the newly established hydrogen removal apparatus was installed beforehand. In this study, we examined the amount of hydrogen that can be adsorbed by Ag400, which had not been minutely evaluated until now.

The experimental setup consists of a hydrogen tank, a pressure gauge, a buffer tank, three switch valves, a reaction tank, a data logger, and a vacuum pump. The volume of the buffer tank is approximately 550 cc, and that of the reaction cylinder is approximately 18 cc. These parts are connected as shown in Fig. 1.

The experiment is performed by the following three steps. i) Approximately 20 g of Ag400 is filled in the reaction cylinder. Valve 1 is closed and the whole setup are evacuated. ii) Valve 2 is closed, the valve 1 is released and hydrogen gas is filled to the buffer tank; its pressure reaches 0.4 MPaG. iii) Valves 1 and 3 are closed and valve 2 is released. Hydrogen gas is supplied to the reaction cylinder and adsorption begins. The change of the pressure of the buffer tank is monitored by the pressure gauge and recorded by the data logger.

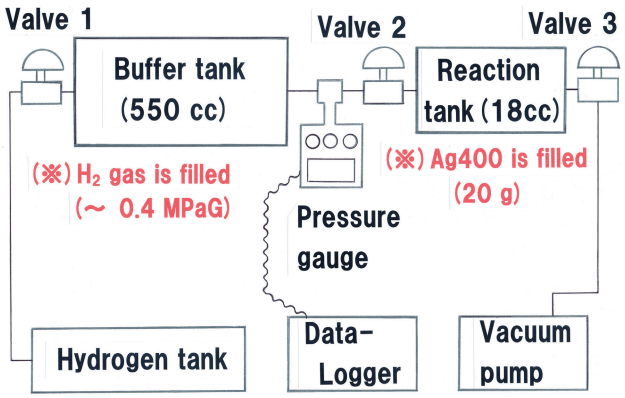

Fig. 1. Experimental setup.

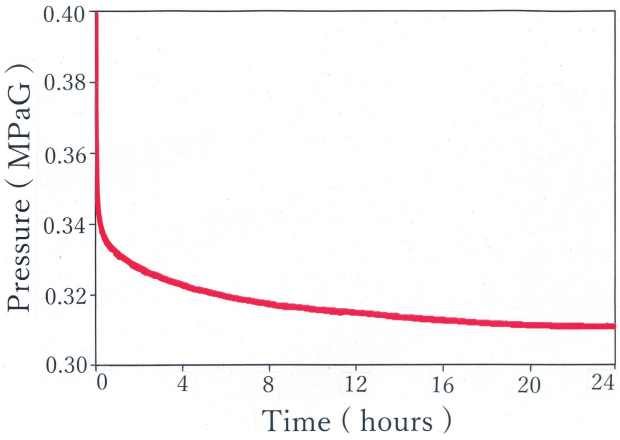

Fig. 2. Change of hydrogen pressure in the buffer tank.

The result of this experiment is shown in Fig. 2. From this figure, it can be observed that the hydrogen pressure in the buffer tank reduced rapidly from 0.4 MPaG to 0.34 MPaG in approximately 30 min after the start of the adsorption reaction. After 12 h, the pressure slowly reduced to 0.32 MPaG. Finally, the hydrogen pressure reduced to approximately 0.31 MPaG and settled at the equilibrium state. This result shows that 20 g of Ag400 can adsorb approximately 500 scc of hydrogen gas throughout the experimental process.

We use approximately 4 kg of Ag400 in the hydrogen removal apparatus in the liquid helium supply and recovery system. Hence, approximately 0.10 Nm^3 of hydrogen impurity gas can be removed by this apparatus. Usually, the concentration of hydrogen contained in recovered helium gas ranges from 0.05 ppm to 1.5 ppm in our system. Therefore, supposing that the recovered helium gas contains 0.1 ppm of hydrogen, our apparatus can purify approximately 1000,000 Nm^3 of recovered helium gas. However, the total volumes of liquid helium supplied in one year in Wako campus were from 180,000 L to 200,000 L.[3] When all this liquid helium is vaporized, approximately 135,000 Nm^3 to 150,000 Nm^3 of helium gas is generated. In this case, we will evaluate that 4 kg of Ag400 can be used approximately 6–7 years for hydrogen removal.

In the next steps, we will evaluate other characteristics of hydrogen removal apparatus containing Ag400.

*1 RIKEN Nishina Center

References
1) K. Ikegami *et al.*, RIKEN Accel. Prog. Rep. **38**, 286 (2005).
2) M. Nakamura *et al.*, RIKEN Accel. Prog. Rep. **41**, 111 (2008).
3) T. Dantsuka *et al.*, RIKEN Accel. Prog. Rep. **53**, 221 (2019).

Safety interlock system for LINAC building

A. Akasiho,[*1] H. Sakamoto,[*1] and K. Tanaka[*1]

An interlock system of the LINAC building toward human safety (LHIS) works for human radiation safety and compliance with radiation lows. Because the previous interlock system was operated for 30 years, it was too complicated to operate and maintain through long-term repeated system improvements and generational changes of developers. Further, a machine protection system (MPS), that is applied to accelerator machine safety, was part of the previous interlock system. This was an operational risk wherein both machine protection and human safety systems were in the same system as it was possible to cause operational conflict. Therefore, the new LHIS was completely separated from MPS.

Figure 1 shows the chart for a new LHIS. In this system, a programmable logic controller (PLC) controls each safety device in the LINAC building directory. The indicator light shows "beam on" or "beam off" at the entrance doors of the irradiation room and the accelerator room, as shown in Fig. 2. The status of the doors are monitored, and then the LHIS determines whether beam irradiation is possible. When the radiation workers enter the irradiation rooms, all take safety keys to recognize the LHIS where the workers are in the room and to inhibit beam irradiation. A radiation monitor generates a signal to the LHIS if it detects an abnormal dose level. Radiation dose level are recorded to radiation monitoring system. An access control PC independent from LHIS and operated by an access management system generate a signal to the LHIS if a worker handles its entry operation during beam irradiation.

Figure 2 shows an operational screen for the LHIS operational PC (LHIS PC) that sends operational commands to PLC as shown in Fig. 1. The schematic diagram of the LINAC building is displayed. The LHIS covers three areas which are accelerator room, irradiation room of the Linac building, and the Connecting building. Each area has its own beam shutter (BS) to stop the beam discretely if an interlock incident occur. Each BS on the accelerator is set on its upstream part to stop a beam before entering the room, as shown in Fig. 2. In the previous systems, a faraday cup, which is applied for accelerator operation, is also commonly applied as BS. The BSs are independent of the faraday cups at LHIS.

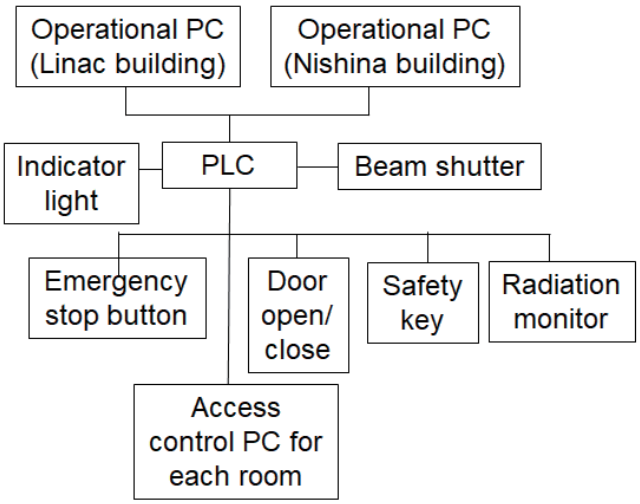

Fig. 1. Conceptual diagram for new LHIS.

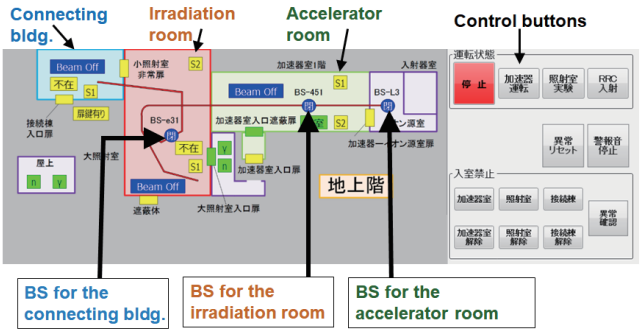

Fig. 2. Part of screen of LHIS PC. Positions of BSs are indicated.

Instructions are issued from the LHIS PC to PLC remotely. The LHIS PCs are set at a radiation control room in the Nishina building and an accelerator operation room in the LINAC building. The position of each operated device such as doors for the accelerator room and the irradiation room is shown in Fig. 2. Green color for the devices shows an acceptable status of a beam irradiation, corresponds to "close" for the door case. A yellow color door shows abnormal status of door "open." All operations for the devices are recorded in the LHIS PCs.

LHIS is handled by the accelerator operators for RILAC. The operators choose a button on the screen for the beam irradiation area. Then LHIS analyzes conditions of the safety devices for accelerator operation and beam irradiation. A BS opens if all statuses are good. If any status is not sufficient, an "abnormal" indication is displayed and the BS does not open. While the BS open, if a door for accelerator or irradiation rooms open, the LHIS status changes to "abnormal" and BS closes.

The LHIS operation was successfully started at October 2019. At 2020, a rotating red light was installed at the entrance of the irradiation room to show the X-ray risk by the RILAC RF cavity.

*1 RIKEN Nishina Center

Computing and network environment at the RIKEN Nishina Center

T. Ichihara,[*1] Y. Watanabe,[*1] and H. Baba[*1]

We operate the Linux cluster systems[1] at the RIKEN Nishina Center (RNC).

Figure 1 shows the current configuration of the Linux servers at the RNC.

We adopted the Scientific Linux (SL), which is a clone of Red Hat Enterprise Linux (RHEL), as the operating system. Since the support of SL 6 was scheduled to be terminated in November 2020,[2] the SL 6 OSes installed in some servers were replaced with SL 7 or CentOS 8. The host *RIBF.RIKEN.JP* is used as the mail server, NFS server of the user home directory, and NIS master server. This is the core server for the RIBF Linux cluster. Mailing list services are also supported.

The hosts *RIBFSMTP1/2* are the mail gateways used for tagging spam mails and isolating virus-infected mails. Since the OSes of *RIBFSMTP1/2* were SL 6, we replaced them by SL 7 in September. The latest version of Sophos Email Protection-Advanced (PMX 6.4.9) was reinstalled. Figure 2 shows the mail trends in December 2020. Approximately 50% of the incoming mails were blocked by the PMX ip-blocker.

A research record server *RIBFDBOX* was installed, and it started operation in April 2015. Since five years have passed, we replaced the research record server *RIBFDBOX* by an HP-DL20G9 server in February 2020. At the same time, the OS and application software were upgraded to CentOS 8.2 and Proself 5, respectively.

The streaming server *RIBFSS* started operation in 2015 with the Wowza Streaming Engine V4.3 software, which can stream Real Time Messaging Protocol (RTMP) protocol. To play streaming videos of the RTMP protocol, the Adobe flash player should be installed in the PC. Since the support of the Adobe flash player for Windows OS and macOS was discontinued at the end of 2020, the operation of the streaming server *RIBFSS* was terminated at the same time.

The data analysis servers *RIBFDATA02/03* are mostly used to store and analyze the experimental data at RIBF. We have replaced the two RAID units (104 TB each) for /rarf/w file system by new ones. Further, the OSes of the *RIBFDATA02/03* were upgraded from SL 6 by SL 7 in September.

We have been operating approximately 70 units of wireless LAN access points in RNC. Almost the entire radiation-controlled area of the East Area of RIKEN Wako campus is covered by wireless LAN for the convenience of experiments and daily work. Six units of new wireless LAN access points (WAPM1266R) were installed in 2020.[3]

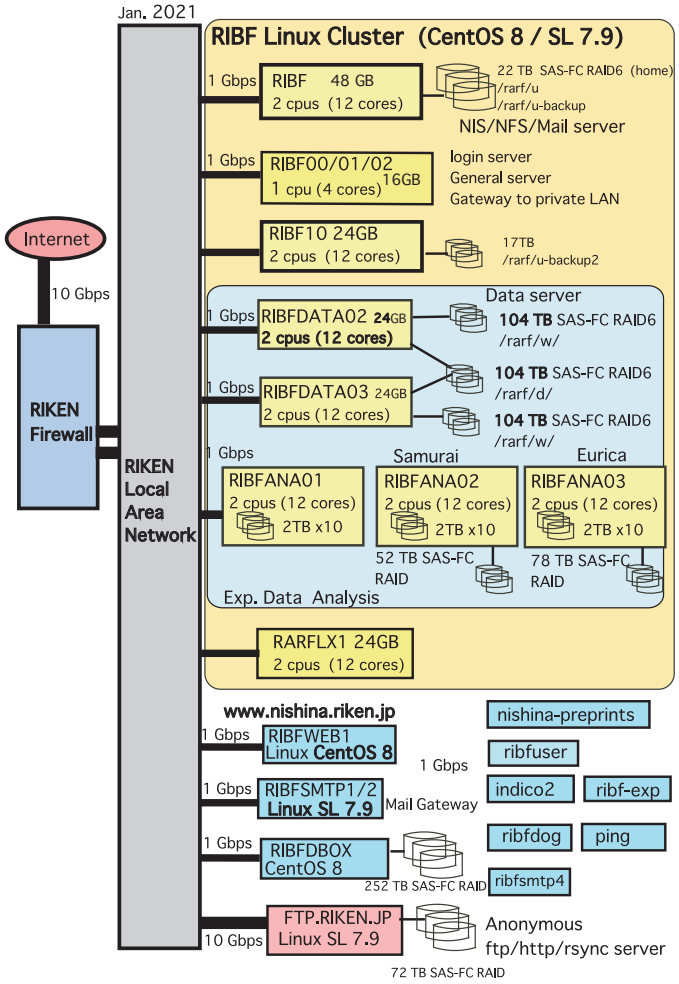

Fig. 1. Configuration of the RIBF Linux cluster.

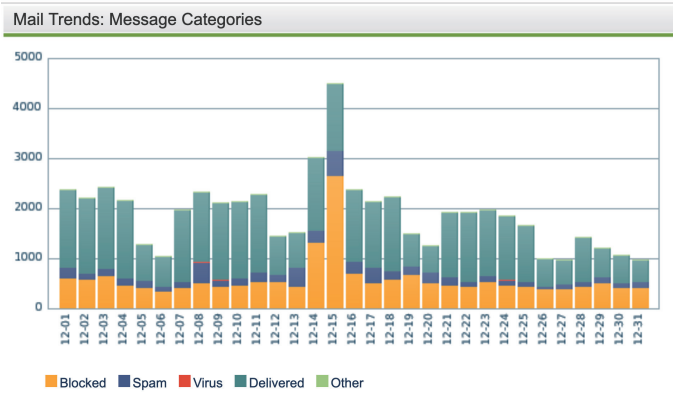

Fig. 2. Mail trends: message categories in December 2020.

References

1) T. Ichihara *et al.*, RIKEN Accel. Prog. Rep. **53**, 136 (2020).
2) `https://scientificlinux.org/downloads/sl-versions/sl6/`.
3) `https://ribf.riken.jp/comp/net/wireless.html`.

*1 RIKEN Nishina Center

CCJ operations in 2020

S. Yokkaichi,[*1] H. En'yo,[*1] T. Ichihara,[*1] W. Nakai,[*1] and Y. Watanabe[*1]

Overview

The RIKEN Computing Center in Japan (CCJ)[1] commenced operations in June 2000 as the largest offsite computing center for the PHENIX[2] experiment being conducted at RHIC. Since then, CCJ has been providing numerous services as a regional computing center in Asia. We have transferred several hundred terabytes of raw data files and nDST[a] files from the RHIC Computing Facility (RCF)[3] to CCJ.

Many analysis and simulation projects are being conducted at CCJ, which are listed on the web page `http://ccjsun.riken.go.jp/ccj/proposals/`. As of December 2020, CCJ has contributed to 44 published papers and 45 doctoral theses.

Computing hardware and software

The network configuration and the computing hardware (nodes) and software (OS, batch queuing systems, database engine, *etc.*) are almost the same as described in the previous APR.[4] We have two login servers, one main server (users' home directory, NIS, DNS, and NTP), and two disk servers, the disk sizes of which are 13 and 26 TB. The main server has an external SAS RAID (21 TB) for the home and work regions of users as well as system usage. Moreover, the server has a RAID with built-in disks (13 TB) that can be used temporarily by users and the system.

We operate 25 computing nodes, of which 16 nodes were purchased in March 2009 and 9 nodes were purchased in March 2011. Thus, in total, 344 ($= 8 \times 16$ nodes $+ 24 \times 9$ nodes) jobs can be processed simultaneously by these computing nodes using a batch queuing system, LSF 9.1.3.[5] Upgrade to LSF 10 is planned in JFY 2021. Table 1 lists the number of malfunctioning SATA or SAS disks in the HP servers, namely, computing nodes and NFS/AFS servers.

One database (postgreSQL[6]) server and one AFS[7] server are operated in order to share the PHENIX computing environment. It should be noted that only the SL5[8] environment is shared by the computing nodes, which have approximately 0.9 TB of library files. We operated two data-transfer servers, which have a 12 TB SATA RAID with built-in disks. This year, another data-transfer server, which has a capacity of 39 TB, was deployed. Data transfer from J-PARC was performed in June during an experiment over 16 days, and 33 TB of raw data were transferred to CCJ. The data were archived in a tape device in Hokusai.[9] In addition, we operate two dedicated servers for the RHICf group[10] and two servers for the J-PARC E16 group[11] in order to keep their dedicated compilation and library environments along with some data.

A server for the test of Docker[12] was deployed to support the sPHENIX/EIC users as well as to develop an OS-independent job submission scheme.

Table 1. Number of malfunctioning HDDs in HP servers during 2011–2020.

Type (Size)	total	20	19	18	17	16	15	14	13	12	11
SATA (1 TB)	192	9	8	16	18	8	14	11	16	20	9
SATA (2 TB)	120	5	10	2	10	2	10	0	2	5	4
SATA (4 TB)	10	0	0	0	–	–	–	–	–	–	–
SAS (146 GB)	38	3	6	3	1	5	3	2	0	1	1
SAS (300 GB)	26	1	2	0	1	0	1	1	0	0	1

Table 2. Tape usage in Hokusai as of December 2020.

user	total	PHENIX official	KEK/ J-PARC	RHICf	user-level archive
size (TB)	921	749	60	3	109

Joint operation with ACCC/HOKUSAI

CCJ and the RIKEN Integrated Cluster of Clusters (RICC) have been jointly operated since July 2009. In April 2015, a new system named "HOKUSAI Greatwave"[13] was launched by RIKEN ACCC,[9] and the joint operation with CCJ continued, with the inclusion of a new hierarchical archive system in which approximately 900 TB of CCJ data are stored. A breakdown of the data is presented in Table 2.

In autumn 2020, ACCC started a system of charging users for their usage of CPU time and storage capacity. Tape usage is not yet charged as of 2020, and a charging policy for the future has not yet been fixed. We are in discussiions with ACCC to set a reasonable fee.

[*1] RIKEN Nishina Center

a) Term for a type of summary data files in PHENIX

References

1) `http://ccjsun.riken.jp/ccj/`.
2) `http://www.phenix.bnl.gov/`.
3) `https://www.racf.bnl.gov/`.
4) S. Yokkaichi *et al.*, RIKEN Accel. Prog. Rep. **53**, 137 (2020).
5) `https://www.ibm.com/docs/en/spectrum-lsf/`.
6) `http://www.postgresql.org/`.
7) `http://www.openafs.org/`.
8) `http://www.scientificlinux.org/`.
9) `http://accc.riken.jp`.
10) Y. Itow *et al.*, arXiv:1409.4860 (Proposal).
11) S. Yokkaichi, in this report.
12) `https://www.docker.com/`.
13) `https://i.riken.jp/supercom/`.

III. RESEARCH ACTIVITIES II
(Material Science and Biology)

1. Atomic and Solid State Physics (Ion)

Control of electrical conductivity in diamond by boron-implantation using an ECR ion source—application of high-temperature and high-pressure annealing

H. Yamazaki,[*1] T. Minamidate,[*2] M. Kidera,[*1] A. Yamamoto,[*3] R. Kato,[*4] and H. Ueno[*1]

Diamond is an excellent electrical insulator with a large band-gap of 5.5 eV. It becomes a semiconductor when doped with a small amount of boron (for p-type) or phosphorus (for n-type). Ekimov *et al.* reported that B-doped diamond, when doped beyond the metal-to-insulator transition at $n_B \sim 3 \times 10^{20}$ B/cm^3, exhibits superconductivity in samples grown by the high-pressure and high-temperature synthesis.[1)] Theoretically, the superconducting critical temperature T_c can be significantly increased by reducing the effects of the disorder in the B-doping processes.[2)] For a higher T_c, more subtle control of doping using CVD and/or MBE methods is required. However, a different method based on ion implantation is also worth investigating, since it enables selective ion-doping in a controlled manner. This has great potential for future device applications.

We attempted to control the electrical conductivity in diamond by using the ion-implantation technique, utilizing RILAC at the RIBF facility. For n- and p-type semiconductors (and possibly superconductors), nitrogen and boron ions were implanted into diamonds, respectively. By varying the beam intensity and irradiation time, the concentration of nitrogen or boron was controlled. Note that it is challenging to obtain the n-type semiconductor, as well as the n-type superconductor, by nitrogen-doping of diamond, since nitrogen behaves as a deep donor in diamond and does not contribute to conductivity.[3)]

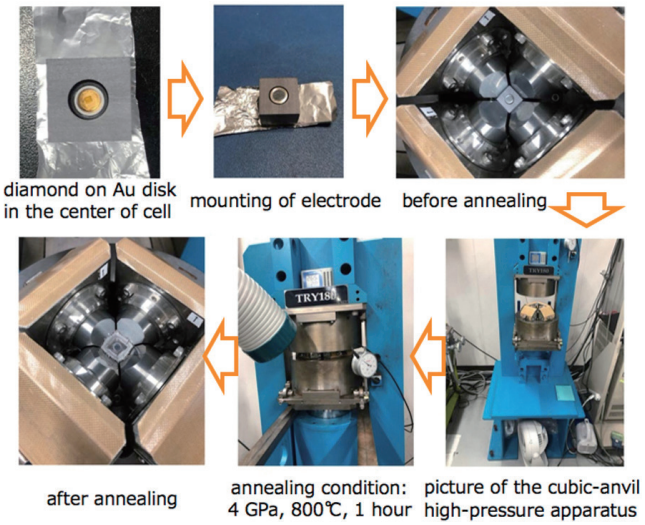

Fig. 1. The process of high-temperature and high-pressure annealing.

*1 RIKEN Nishina Center
*2 Faculty of Science, Tokyo University of Science
*3 Graduate School of Engineering and Science, Shibaura Institute of Technology
*4 Condensed Molecular Materials Laboratory, RIKEN

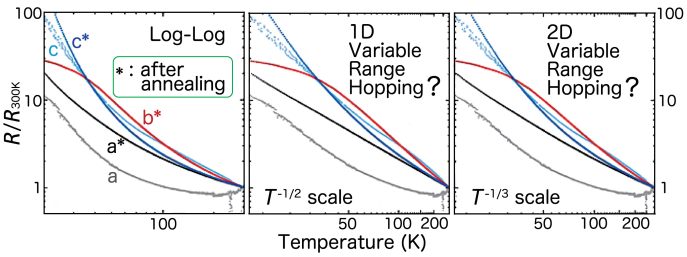

Fig. 2. Temperature dependence of electrical resistivity before and after annealing for B concentrations of (a) 1.8×10^{21}, (b) 1.3×10^{22}, and (c) 6.8×10^{22} B/cm^3. The possibility of the hopping conductivity in carrier-doped semiconductor cannot be denied for these samples.

Fig. 3. Typical appearance of Ib- and IIa-type diamonds.

In this fiscal year, we continued studying boron-implanted diamonds. Boron ions were implanted into diamond crystals (each size is $1 \times 1 \times 0.3$ mm^3) at 5 keV (implantation depth: ~10 nm) by using an ECR ion source.[4)]) Ten samples of different concentrations from $n_B \sim 4.9 \times 10^{20}$ to 6.8×10^{22} B/cm^3 were studied. The magnetization and electrical resistivity measurements showed that the as-implanted diamonds do not exhibit superconducting transitions, even though n_B's are nominally beyond the metal-to-insulator transition at 3×10^{20} B/cm^3. To reduce the lattice damage produced during the implantation, we performed annealing treatments after implantation. The phase diagram of carbon shows that diamond is not stable at low pressures; we annealed the samples at 800°C and 4 GPa for 1 hour. The process of the annealing is shown in Fig. 1. Contrary to our expectations, the annealed samples exhibited no sign of superconductivity (see Fig. 2).

The laser Raman spectra with 632.8 nm excitation indicated that the annealing promoted the NV$^-$ center formation in diamond. To reduce this effect, we are preparing for the boron implantation of IIa-type diamonds (Fig. 3) with nitrogen concentration less than 8 ppm.

References

1) E. A. Ekimov *et al.*, Nature **428**, 542 (2004).
2) T. Shirakawa *et al.*, J. Phys. Soc. Jpn. **76**, 014711 (2007).
3) S. J. Sque *et al.*, Phys. Rev. Lett. **92**, 017402 (2004).
4) M. Kidera *et al.*, Eur. J. Mass Spectrom. **13**, 239 (2007).

Single-event effects in SiC planar and trench power MOSFETs

M. Iwata,[*1] E. Mizuta,[*1] M. Takahashi,[*1] and H. Shindou[*1]

Wide-bandgap semiconductors such as silicon carbide (SiC) have been attracting attention as materials for high-efficiency semiconductor devices. The adoption of SiC power modules has recently progressed in the field of railways and automobiles. In the aerospace industry, the use of SiC devices requires the effects of radiation to be clarified and these issues to be overcome. In this paper, we report the results of radiation tests for SiC power metal-oxide-semiconductor field-effect transistors (MOSFETs).

Two types of commercial n-channel SiC power MOSFETs were used in this experiment, as shown in Fig. 1. The maximum rating for the drain-source breakdown voltage of these devices is 1200 V. Test samples were irradiated with ^{136}Xe ions of 638 MeV perpendicularly at the device surface at room temperature in air using RIKEN RILAC2 in combination with the RIKEN Ring Cyclotron (RRC). During irradiation, the gate voltage, V_{GS}, was set to 0 V. The drain bias voltage, V_{DS}, was initialized at 100 V and increased in 20 V steps. The total fluence at each V_{DS} was 3.0×10^5 ions/cm^2.

Figure 2 shows the current transition of I_{DS} during irradiation up to V_{DS} = 160 V. The leakage current of the planar-type sample started to increase gradually at V_{DS} = 140 V, as shown in Fig. 2(a). This behavior is quite different from that usually observed during heavy-ion irradiation on Si power MOSFETs, where the leakage current abruptly increases by single-event burn-out. The tendency of gradual increase on the planar sample is analogous to the failure modes of SiC Schottky barrier diodes.[1] On the other hand, the leakage current of the trench-type sample increased rapidly at the beginning of irradiation, as shown in Fig. 2(b). In Si trench MOSFETs, a degradation mechanism related to a microdose effect due to heavy-ion irradiation was reported,[2] and we assume that the same effect is caused in the SiC

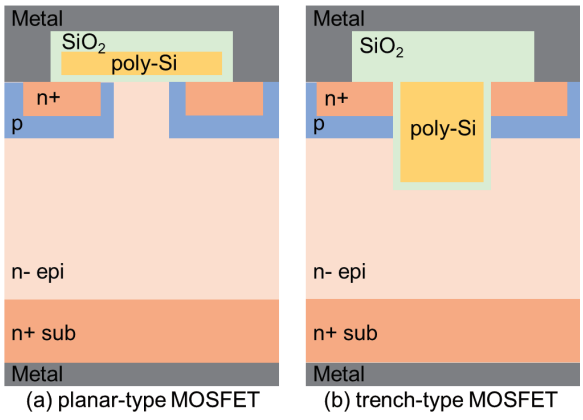

Fig. 1. Cross-sectional structure of the test devices.

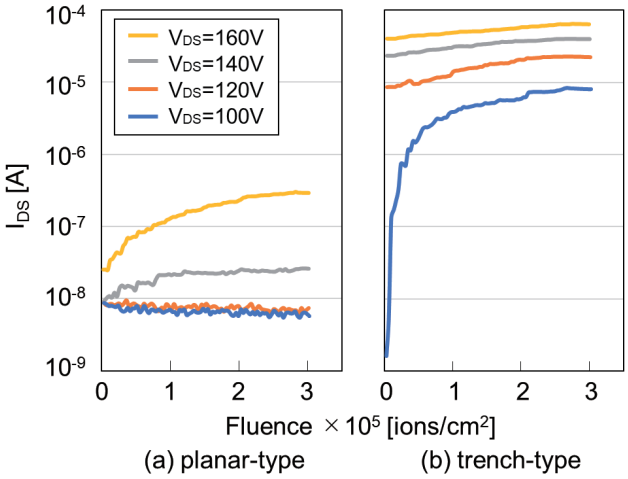

Fig. 2. Result of current monitoring during irradiation.

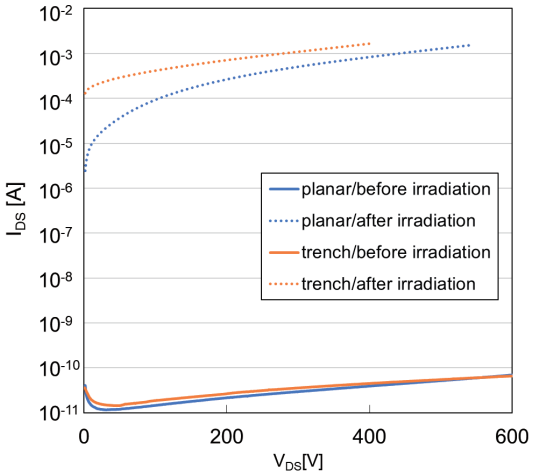

Fig. 3. Result of current monitoring before and after irradiation.

trench-type sample. The trench structure enables the irradiated ions to pass through the gate oxide along the entire length of the channel and generate electron-hole pairs. Trapped holes might exist in the gate oxide because the hole diffusion velocity is less than that of electrons, and they might introduce a large leakage current path immediately after the start of irradiation.

Figure 3 shows the I-V curves of the drain leakage current before and after irradiation. The degradation by irradiation seemed worse in the trench-type sample than in the planar sample.

Because the planar-type SiC MOSFETs did not show the microdose effect and its leakage current after irradiation was less than that of the trench-type sample, the planar gate structure can be considered suitable for use in space.

*1 Research and Development Directorate, Japan Aerospace Exploration Agency

References
1) S. Kuboyama *et al.*, IEEE Trans. Nucl. Sci. **53**, 6 (2006).
2) J. A. Felix *et al.*, IEEE Trans. Nucl. Sci. **54**, 6 (2007).

Profile measurements of dual-microbeams generated by glass capillaries

M. Mori,[*2,*1] T. Ikeda,[*1,*2] and W. -G. Jin[*2]

Tapered glass capillary optics is known to be a simple and reliable microbeam generator for ion/laser beams.[1,2] The DNA of living cells is seriously damaged by not only ion-beam irradiation but also UV light. However, to avoid mis-hitting of a target cell nucleus, a laser sight of a visible micrometer-sized spot is needed prior to the UV microbeam shooting, where the visible light never damages the DNA. We have proposed a dual-microbeam system of visible light + ion beam (produced at Pelletron in RIKEN Nishina Center) and visible + UV light because any quantum beams can be transmitted through the capillary optics. The transmission characteristics and the microbeam profiles of visible laser were investigated until 2017,[3] followed by the similar study for UV microbeams.[4] To realize the system of visible + UV laser, the two microbeam spots should be on the same position. In this report, the displacement between the two spots as a function of possible mis-alignment of the input beam is described, although a laser beam is well-guided by the capillary optics.

Figure 1 shows the setup in Toho University. A UV laser with a wavelength λ = 375 nm from a source (THORLABS L375P70MLD) entered a glass capillary with an outlet diameter of 60 μm, where the capillary was aligned with an accuracy better than the smallest scale of 0.34 mrad in the mirror tuning. The microbeam profile approximately 3-mm downstream of the capillary was obtained as shown in Fig. 2 by a knife-edge method employing a motorized stage (SURUGASEIKI XY620-G-N) and a photodiode (OPHIR PD300) connected to a power meter display. The central sharp peak like an airy disk, which is known in Fraunhofer diffraction for a circular aperture, was used to extract the full width at half maximum (FWHM) as the spot size after Gaussian fitting. A visible light laser (λ = 488 nm) from a source (Photochemical Research Associates Inc. LA15R) also entered the capillary with a half mirror, which was tilted horizontally to emulate the mis-alignment with a

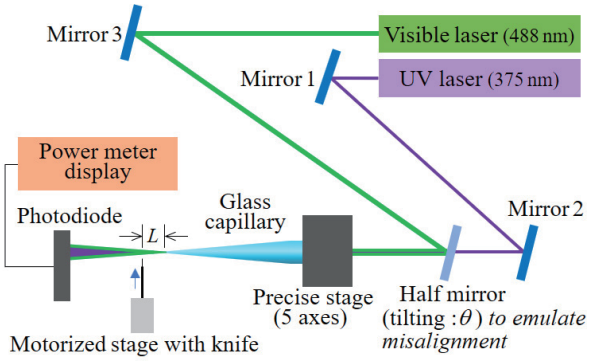

Fig. 1. Experimental setup with a knife-edge method to obtain the beam profiles. The distance $L \sim 3$ mm.

*1 RIKEN Nishina Center
*2 Department of Physics, Toho University

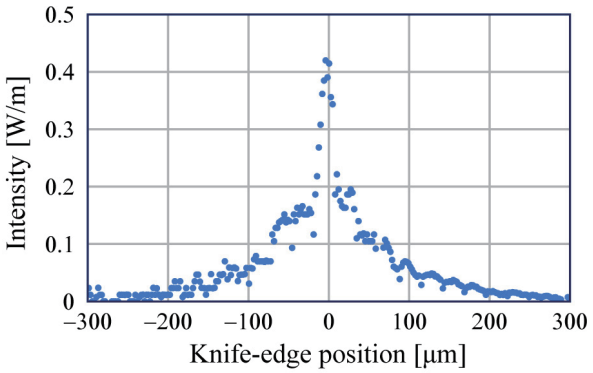

Fig. 2. Horizontal profile of a UV microbeam. The spot size is defined as the FWHM of the central sharp peak.

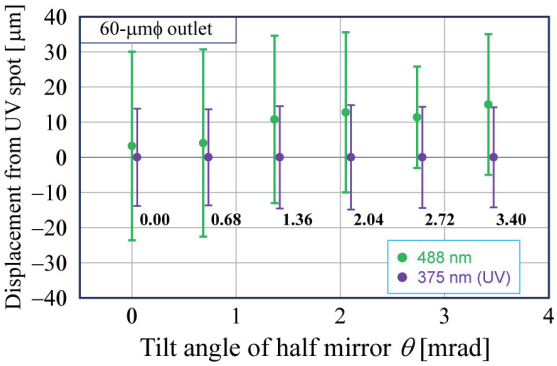

Fig. 3. Displacement of the visible spot from the UV spot as a function of θ, along with the spot sizes.

step of 0.68 mrad. The peak position and the spot size of each laser were measured according to the tilting angle θ, where θ = 0 when the UV and visible laser entered coaxially.

The displacements of the visible laser spot from the UV spot as a function of θ are plotted in Fig. 3. The green and purple symbols show the peak positions of visible and UV lasers, respectively, where the UV peak positions were set to zero. The vertical bars correspond to the spot sizes, which depend on the initial beam divergences. As expected, the UV spot sizes were almost constant. We confirmed that the visible laser peak positions were measured to be constant in the larger θ region ($\geq$1.36). The guiding effect of the laser beam through the capillary optics is clearly proven.[5] However, for UV spot sizes of $\sim$30 μm, the mis-alignment θ should be suppressed to less than 1.36 mrad to obtain the same spot positions so that the mis-hitting in the UV microbeam irradiation is avoided.

References

1) T. Ikeda *et al.*, Appl. Phys. Lett. **89**, 163502 (2006).
2) W. -G. Jin *et al.*, J. Phys. Soc. Jpn. **84**, 114301 (2015).
3) M. Koushima *et al.*, J. Phys. Conf. Ser. **875**, 112004 (2017).
4) S. Kawamura *et al.*, J. Phys. Soc. Jpn. **89**, 055002 (2020).
5) M. Mori *et al.*, RIKEN Accel. Prog. Rep. **53**, 143 (2020).

2. Atomic and Solid State Physics (Muon)

Partial order of conduction electrons in Mn_3CoSi

S. Shamoto,[*1,*2,*3,*4] D. P. Sari,[*5,*3] I. Watanabe,[*3] H. Yamauchi,[*4] and L. -J. Chang[*1]

Unconventional phase transitions have been discovered in various materials.[1] One of them is a phase separation at the tri-critical point of quantum phase transition.[2] Partial magnetic order has been observed in a non-centrosymmetric compound of MnSi near the quantum phase transition under pressure.[3,4] On the search of new unconventional magnetic transition, we discovered the highest-temperature magnetic short-range order (SRO) in a new noncentrosymmetric magnet Mn_3RhSi by the complementary use of muon spin relaxation (HiFi and ARGUS at ISIS), neutron, X-ray scattering, electron diffraction, and magnetization measurements.[5] It has a hyperkagome network of magnetic Mn ions. We think that the unconventional magnetic SRO emerges due to the spatially inhomogeneous order parameter, where the Lifshitz condition is violated by the Dzyalonshinskii-Moriya interaction in a noncentrosymmetric magnet. The intriguing point of the SRO is not limited in the highest-temperature record of magnetic SRO, but also in the observed Q-position different from long-range antiferromagnetic (AF) order Q-position. At present, however, the mechanism is still unknown. To reveal the mechanism, we believe that it is necessary to complete the phase diagram (Fig. 2) by measuring the related family compounds such as Mn_3CoSi ($a = 6.28$ Å) with a different lattice constant resulting in a different bandwidth from that of Mn_3RhSi ($a = 6.47$ Å). The Néel temperature of Mn_3CoSi is about 100 K, whereas that of Mn_3RhSi is 190 K. However, it was unknown which the SRO transition temperature of Mn_3CoSi becomes lower than that of Mn_3RhSi.

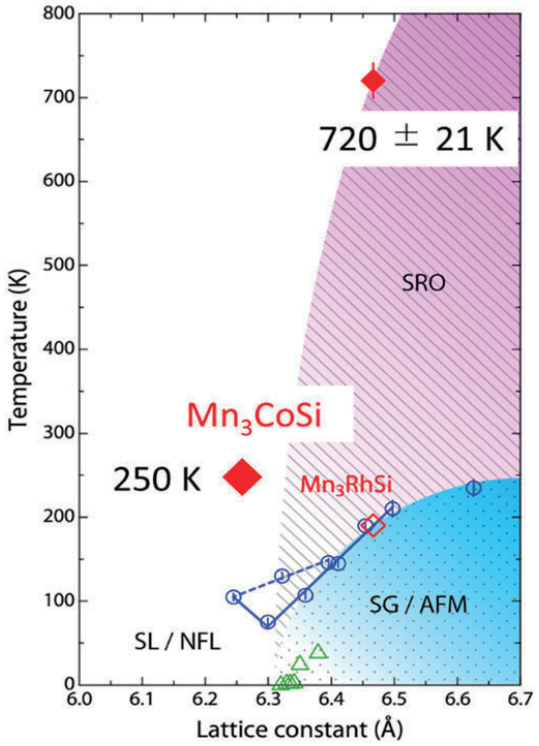

Fig. 2. Phase diagram of β-Mn type structure alloys.

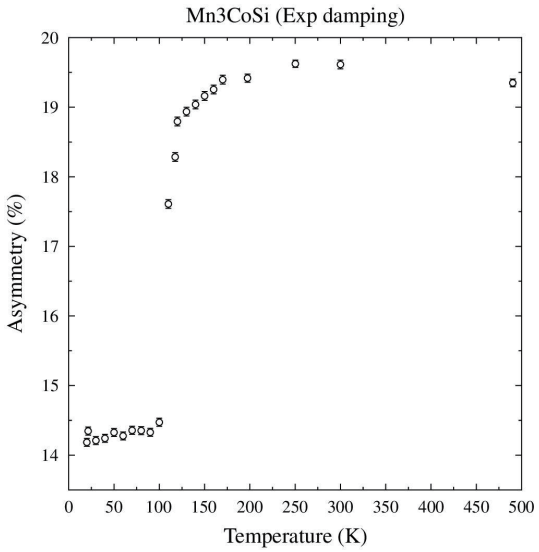

Fig. 1. Temperature dependence of TF μSR asymmetry of Mn_3CoSi.

TF μSR measurement of Mn_3CoSi (RB2070006) successfully showed SRO anomaly above Néel temperature in the asymmetry as shown in Fig. 1. The magnetic SRO of Mn_3CoSi is found to start at about 250 K. From this result, we may conclude that the SRO temperature increases with increasing the lattice constants as shown in Fig. 2. This result suggests that the present world record of SRO temperature may further increase with increasing the lattice constant.

*1 Department of Physics, National Cheng Kung University
*2 Comprehensive Research Organization for Science and Society
*3 RIKEN Nishina Center
*4 Advanced Science Research Center, Japan Atomic Energy Agency
*5 College of Engineering, Shibaura Institute of Technology

References

1) S. Shamoto, J. Phys. Soc. Jpn. **88**, 081008 (2019), arXiv:1905.03905.
2) D. Belitz, T. R. Kirkpatrick, T. Vojta, Rev. Mod. Phys. **77**, 579 (2005).
3) C. Pfleiderer *et al.*, Nature **427**, 227 (2004).
4) Y. J. Uemura *et al.*, Nat. Phys. **3**, 29 (2007).
5) H. Yamauchi, D. P. Sari, I. Watanabe, Y. Yasui, L. -J. Chang, K. Kondo, T. U. Ito, M. Ishikado, M. Hagihara, M. D. Frontzek, S. Chi, J. A. Fernandez-Baca, J. S. Lord, A. Berlie, A. Kotani, S. Mori, S. Shamoto, Commun. Mat. **1**, 43 (2020).

Magnetism and superconductivity in underdoped region of T*-type $La_{1-x/2}Eu_{1-x/2}Sr_xCuO_{4-y}F_y$

M. Takahama,[*1,*2] T. Taniguchi,[*1] D. P. Sari,[*3,*4] I. Watanabe,[*3] and M. Fujita[*1]

In the study of high-transition-temperature cuprates, the doping evolution of magnetism and its relationship with superconductivity are important issues. It had been considered that the superconductivity is induced by carrier doping into Mott insulators.[1] However, the appearance of superconductivity in RE_2CuO_4 (RE = rare earth) without effective carrier doping (undoped superconductivity) was clarified by improving material synthesis and annealing techniques.[2,3] After the discovery of undoped superconductivity, the broad superconducting (SC) phase was reported.[4]

Recently, we succeeded in synthesizing T*-type structured $La_{1-x/2}Eu_{1-x/2}Sr_xCuO_4$ (LESCO) in which the oxygen coordination around a copper ion is five and reported the magnetic and SC properties as functions of Sr concentration.[5,6] Our muon spin rotation/relaxation (μSR) measurement of LESCO revealed the presence of a spin-glass state and the absence of static magnetism in the as-sintered non-SC and high-pressure oxidated SC samples, respectively. Therefore, the short-range magnetic order disappears with the emergence of superconductivity, suggesting competition between the two states. However, as it is challenging to synthesize a single-phase sample of LESCO with a smaller x, the electronic state of the underdoped (UD) region of T*-type cuprates has not been investigated. Thus, we newly synthesized $La_{1-x/2}Eu_{1-x/2}Sr_xCuO_{4-y}F_y$ (LESCOF), in which the hole concentration can be reduced by increasing y while keeping the single-phase T*-type structure. The evidence of low carrier density in both as-sintered and oxidation-annealed LESCO was reported by x-ray absorption spectroscopy measurement,[6] and LESCO with $x \lesssim 0.23$ corresponds to UD $La_{2-x}Sr_xCuO_4$. Therefore, LESCOF with $x = 0.18$ is expected to be located in a more UD region. The magnetism in UD LESCOF was studied by μSR measurements at RIKEN-RAL.

Figure 1(a) shows the temperature dependence of the zero-field μSR time spectra of as-sintered LESCOF with $x = 0.18$ and $y = 0.14$. Exponential-type spectra are observed below ~80 K, and muon spin precession was observed at the lowest temperature of 5.1 K. The appearance of precession suggests the emergence of long-range magnetic order. Furthermore, the temperature at which the spectra change from Gaussian-type to exponential is higher than that in the pristine

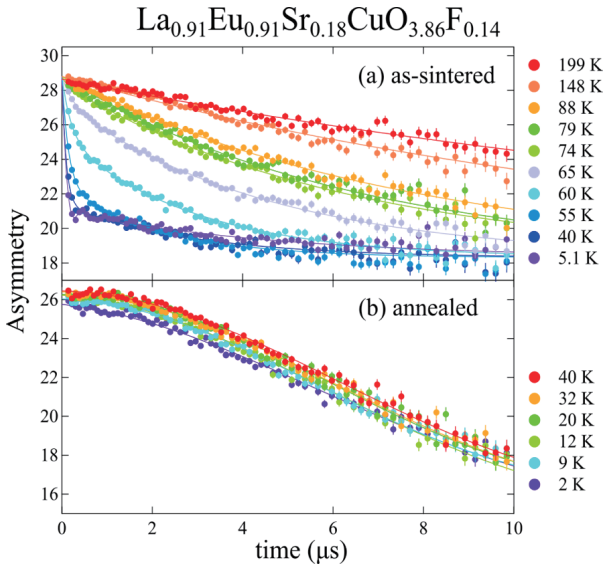

Fig. 1. Zero-field μSR time spectra of (a) as-sintered and (b) oxidation-annealed $La_{1-x/2}Eu_{1-x/2}Sr_xCuO_{4-y}F_y$ with $x = 0.18$ and $y = 0.14$.

LESCOF with $x = 0.18$,[4] indicating the development of static magnetism upon underdoping. On the other hand, the oxidation-annealed SC sample shows no evidence of magnetic order down to 2 K (Fig. 1(b)).

Two characteristic features of magnetism were clarified in the present study. Firstly, a long-range magnetic ordered state exists in the lightly doped sample of as-sintered T*-type LESCOF. Combined with previously reported results,[4] the short-range spin-glass state is replaced by the long-range state upon underdoping, as is the case with other cuprates. Secondly, such an ordered state disappears with annealing in connection with the emergence of superconductivity. Therefore, our results suggest that strong Cu-spin correlations cause the superconductivity in T*-type LESCO, and that the spin fluctuations play an essential role in the mechanism of superconductivity in the lightly hole-doped region.

*1 Institute for Materials Research, Tohoku University
*2 Department of Physics, Tohoku University
*3 RIKEN Nishina Center
*4 College of Engineering, Shibaura Institute of Technology

References
1) N. P. Armitage *et al.*, Rev. Mod. Phys. **82**, 2421 (2010).
2) A. Tsukada *et al.*, Solid State Commun. **133**, 427 (2005).
3) T. Takamatsu *et al.*, Appl. Phys. Express **5**, 073101 (2012).
4) O. Matsumoto *et al.*, Physica C **469**, 924 (2009).
5) S. Asano *et al.*, J. Phys. Soc. Jpn. **88**, 084709 (2019).
6) S. Asano *et al.*, J. Phys. Soc. Jpn. **89**, 075002 (2020).

Spin dynamics in Pyrochlore $Nd_2Mo_2O_7$

L. J. Chang,[*1] D. P . Sari,[*2] M. C. Hatnean,[*3] G. Blalkrishnan,[*3] Y. Yasui,[*4] and I. Watanabe[*5]

$Nd_2Mo_2O_7$ is metallic and exhibits a ferromagnetic transition at a Curie temperature $T_c = 93$ K. In contrast with other Nd-pyrochlore systems, such as $Nd_2Sn_2O_7$ and $Nd_2Zr_2O_7$, where the magnetic moments are localized, $Nd_2Mo_2O_7$ possesses delocalized electrons, which may host novel phenomena associated with the interaction between the localized moments Nd^{3+} and the itinerant moment Mo^{4+}. Particularly, $Nd_2Mo_2O_7$ exhibits unusual spin chirality,[1,2] and possesses a two-in-two-out (AIAO) spin ice spin configuration on Nd^{3+}. Unlike the AIAO magnetic order of Ir^{4+} in $Nd_2Ir_2O_7$, the XY type order of Ru^{4+} in $Nd_2Ru_2O_7$, and Mo^{4+} in $Nd_2Mo_2O_7$ orders along the 001 direction. In $Nd_2Mo_2O_7$, the anomalies appearing at 93 K in both the magnetic and heat capacity is attributed to the Mo^{4+} ordering temperature, whereas the ordering of Nd^{3+} becomes significant below 30 K.[3] Therefore, it is interesting to study the spin dynamics in the delocalized electron system of $Nd_2Mo_2O_7$ and compare them to those of other Nd-pyrochlores by μSR technique. Moreover, applied fields in $Nd_2Mo_2O_7$ may change the ground state of Nd^{3+}.[3] μSR experiments were carried out at ARGUS spectroscopy, RIKEN-RAL, between the temperature ranges of 5–300 K to obtain the information below and above the magnetic transition temperatures of 30 and 93 K. Figure 1(a) shows the zero-field mSR relaxation spectra at 7.5, 35, 95, and 160 K and the fitted curves using the function of $A_1 \exp(-\lambda_1 t) + A_2 \exp(-\lambda_2 t) + A_3$. The plots of the fitted parameters are shown in Fig. 1(b). The initial drop of the muon relaxation below 95 K indicates the magnetic order of the compound, which can also be confirmed by the increasing of the relaxation rate λ_1 in Fig. 1(b).

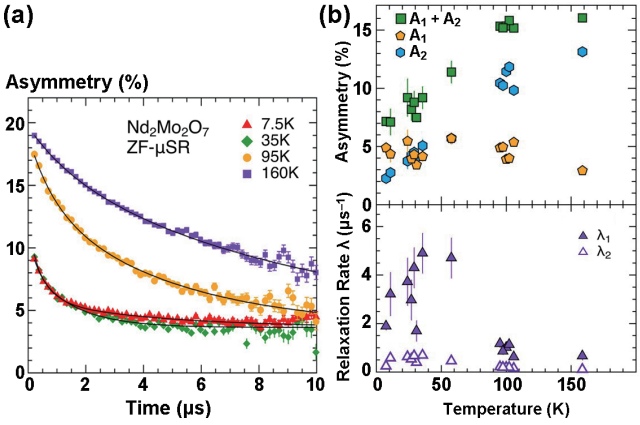

Fig. 1. (a) zero-field μSR relaxation spectra at 7.5, 35, 95, and 160 K and fitted curves using the function of $A_1 \exp(-\lambda_1 t) + A_2 \exp(-\lambda_2 t) + A_3$; (b) plots of the fitted parameters.

*1 Department of Physics, National Cheng Kung University
*2 College of Engineering, Shibaura Institute of Technology
*3 Department of Physics, University of Warwick
*4 Department of Physics, Meiji University
*5 RIKEN Nishina Center

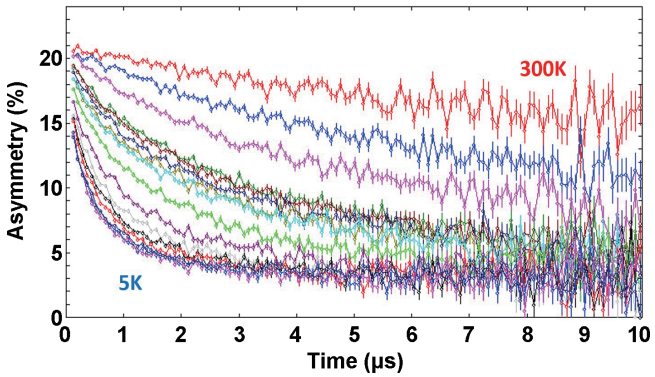

Fig. 2. Temperature-dependence of the asymmetry spectra of muon relaxation signal between 5 and 300 K in the applied field of 4000 G. The spectra can be separated into three different temperature intervals of 30 K and 93 K, the transition temperatures of Nd^{3+} and Mo^{4+} ordering temperatures, respectively.

The initial drop made it impossible to determine the magnetic volume fraction of the AIAO spin structure. However, the transition at 30 K cannot be picked up clearly by muon relaxation. The asymmetry of the slow relaxation parameter exhibits a magnetic anomaly. Longitudinal fields were applied up to 4000 G to evaluate the decoupling of muons on the sites. An applied constant of 4000 G in the temperature-dependent scans was also utilized in the experiments. The transitions at 30 and 93 K can be clarified in the measurements as shown in Fig. 2, in which the relaxations of the spectra are separated to three groups in three different temperature ranges. Proper models have to be proposed to fit these curves and higher fields are necessary to decouple the muon relaxations for further study on this compound.

At 5 K, the significant differences of the asymmetry and muon relaxation have been observed before and after an applied field (not shown in the figure). Similar behaviour does not appear at a higher temperature of 85 K. This hysteresis at 5 K indicates ferromagnetic components at low temperature. In our experiments, this hysteresis even happens in a small applied field of 100 G. The magnetic structure of $Nd_2Mo_2O_7$, had been reported as a spin chirality "umbrella" structure,[4] which is consistent with the observation made in the μSR spectra at low temperatures. This phase occurs below the Nd^{3+} ordering temperature only, and does not exist below the Mo^{4+} ordering temperature between 93 K and 30 K. However, muon precession was not observed in the experiments. We are working on a proper model to fit the spectra below 30 K.

References

1) K. A. Ross *et al.*, Phys. Rev. B **84**, 174442 (2011).
2) A. Maisuradze *et al.*, Phys. Rev. B **92**, 094424 (2015).
3) Y. Yasui *et al.*, J. Phys. Soc. Jpn. **72**, 865 (2003).
4) Y. Taguchi *et al.*, Science **291**, 2573 (2001).

Possible multipolar ordering in spin-orbital-entangled d^2 system on a face-centered-cubic lattice

T. Takayama,[*1,*2] D. P. Sari,[*3,*4] I. Watanabe,[*4] and H. Takagi[*1,*2,*5]

The interplay of strong spin-orbit coupling (SOC) and electron correlation in heavy transition-metal compounds containing $4d$ and $5d$ elements has been revealed to give rise to unprecedented electronic states of matter. In such systems, strong SOC produces spin-orbit-entangled $J_{\rm eff}$ states of d-electrons. The interactions between spin-orbital-entangled objects are distinct from those in spin-only systems, and a plethora of novel electronic phases has been predicted to emerge. In d^2 configurations, SOC yields $J_{\rm eff} = 2$ quintet states. When the $J_{\rm eff} = 2$ states are placed on a face-centered-cubic (FCC) lattice, multipolar ordering phenomena such as charge quadrupolar and magnetic octupole orderings are expected to emerge.[1,2)]

To explore such multipolar orderings of d-electrons, we focused on cubic tungsten halides A_2WCl_6 (A = K, Rb, Cs) with a $5d^2$ configuration of W^{4+} ions. The regular WCl_6 octahedra form an FCC lattice. In these compounds, the magnetic susceptibility $\chi(T)$ shows a Curie-Weiss behavior at high temperatures, and the effective moments are close to the value expected for $J_{\rm eff} = 2$ ($\mu_{\rm eff} \sim 1.22\ \mu_{\rm B}$). K_2WCl_6 displays an anomaly in specific heat $C(T)$ at approximately 180 K, which corresponds to a structural transition from cubic to tetragonal, but no further anomaly was observed at lower temperatures. Rb_2WCl_6 and Cs_2WCl_6 show no pronounced anomaly in $C(T)$ and $\chi(T)$ down to 2 K, although a deviation from the Curie-Weiss behavior is observed at approximately 100 K. The magnetic ground state of these materials is thus not clear yet.

One of the possible ground states is the formation of magnetic octupolar ordering, which has been suggested for d^2 double-perovskite oxides.[3)] In those oxides, although any signature of magnetic dipolar ordering was found in $\chi(T)$ and neutron diffraction, a clear oscillatory signal was observed in muon spin rotation (μSR) measurements, indicating time-reversal-symmetry breaking. The other possibility, especially for K_2WCl_6, is that the structural transition lifts the degeneracy of the $J_{\rm eff} = 2$ quintet and selects the nonmagnetic $J^z_{\rm eff} = 0$ singlet ground state (*i.e.*, charge quadrupole order), which can be regarded as a spin-orbital nematic state in analogy with the $S^z = 0$ spin-nematic state. In this case, the time-reversal-symmetry is retained, and no oscillatory signal is expected in μSR.

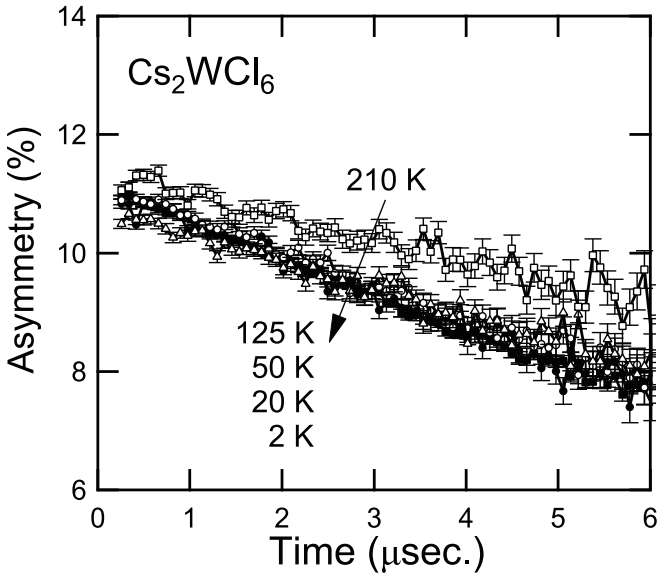

Fig. 1. Zero-field time spectra of muon asymmetry for Cs_2WCl_6 at several temperatures.

In order to investigate the ground states, we performed a μSR measurement on powder samples of A_2WCl_6 (A = K, Rb, Cs) using ARGUS, ISIS. For all the samples, the time dependence of muon asymmetry at low temperatures only shows a monotonic decrease, indicating a nonmagnetic ground state. Figure 1 shows the result for Cs_2WCl_6. The time dependence of muon asymmetry at zero magnetic field did not show any pronounced change down to 2 K. For K_2WCl_6, the relaxation rate λ, obtained by fitting with a Lorentzian curve, shows a kink at approximately 180 K, where a structural transition occurs. No such anomaly was found in Cs_2WCl_6 or Rb_2WCl_6.

This result excludes the presence of magnetic dipolar or octupolar ordering in A_2WCl_6. The question of whether the $J_{\rm eff} = 2$ moments remain fluctuating or form a quadrupolar ordering with a spin-singlet ground state remains open. We expect that the ground states of these compounds can be clarified in combination with other measurements, especially the analysis of low-temperature crystal structures.

*1 Max Planck Institute for Solid State Research
*2 Institute for Functional Matter and Quantum Technologies, University of Stuttgart
*3 Graduate School of Engineering and Science, Shibaura Inst. of Tech.
*4 RIKEN Nishina Center
*5 Department of Physics, University of Tokyo

References

1) G. Chen, L. Balents, Phys. Rev. B **84**, 094420 (2011).
2) S. Voleti *et al.*, Phys. Rev. B **101**, 155118 (2020).
3) D. Maharaj *et al.*, Phys. Rev. Lett. **124**, 087206 (2020).

Successive Transitions in Spin-dimer Compound $Cs_3V_2Cl_9$

H. Kikuchi,[*1,*3] Y. Fujii,[*2] and I. Watanabe[*3]

$A_3M_2X_9$ (A = Cs, Rb : M = transition metal elements: X = Cl, Br) compounds with trigonal space group $P6_3/mmc$ are composed of isolated di-nuclear complexes $[M_2X_9]^{3-}$ and their magnetic properties are explained within an isolated or weakly coupled spin dimer model. Because these spin dimers are arranged in a triangular form, the spin frustration effect is expected to appear when magnetic phase transition occurs via finite interdimer interactions. $Cs_3V_2Cl_9$, one member of the $A_3M_2X_9$ family with magnetic ion V^{3+} ($S = 1$), was previously studied via magnetic susceptibility and inelastic neutron scattering measurement using powder sample[1] and no magnetic ordering was observed above 1.5 K. We recently synthesized a single crystal of $Cs_3V_2Cl_9$ and measured susceptibility $\chi(T)$ and specific heat, and we found successive phase transition at $T_N \approx 4$ K and $T_n \approx 15$ K.[2]

These successive phase transitions are not explained within the framework of the isolated dimer model, and they show the presence of non-negligible interdimer interaction. $\chi(T)$ shows no anomaly at T_n although T_N is accompanied by the cusp-like anomaly of $\chi(T)$. The lower temperature transition is suggested to be an antiferromagnetic transition although the spin structure is not clear. The higher temperature transition is not a mere crystal structure transition because the transition temperature depends on the applied magnetic field.

We measured the μSR of $Cs_3V_2Cl_9$ to clarify the nature of the successive phase transitions. Figure 1 shows the zero-field muon spin relaxation (ZF-μSR) spectra

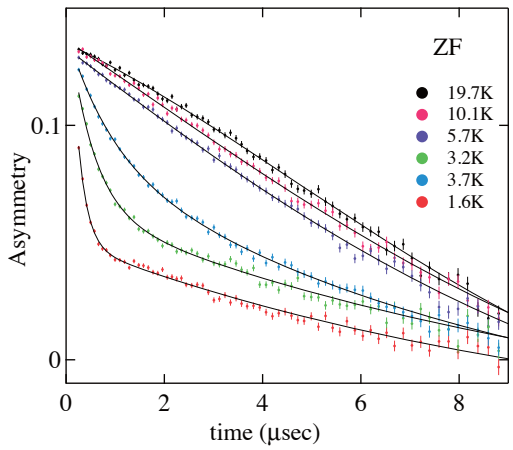

Fig. 1. Temperature dependence of the ZF-μSR spectra of $Cs_3V_2Cl_9$.

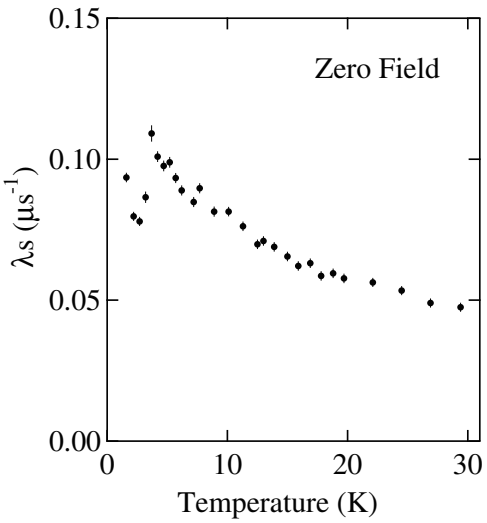

Fig. 2. Temperature dependence of the relaxation rate λ_s.

measured down to 1.6 K. At relatively high temperatures, the spectra follow Gaussian curves. As the temperature decreases, the spectra changes from Gaussian to an exponential curve following $a_s \exp(-\lambda_s t) + a_f \exp(-\lambda_f t)$, where λ_s and λ_f denote slow and fast relaxation rates, and a_s and a_f represent amplitudes of the asymmetry of slow and fast components, respectively. Solid lines in Fig. 1 are fitted results. Figure 2 shows the temperature dependence of λ_s. A distinct peak is observed at around T_N, which confirms that a magnetic long range order occurs at this temperature. No anomaly of lambda is observed at T_n, which indicates that an internal field does not appear. The phase transition at T_n is not accompanied by the internal field, whereas the value of T_n depends on the applied magnetic field. One candidate for the transition at T_n is a spin nematic order wherein quadrupole moments, not magnetic moments, play the role of an order parameter. Because the nematic state does not break the time-reversal symmetry, usual magnetic probes including muon do not detect this transition.[3] Several theoretical studies indicate the occurrence of the nematic order in an $S = 1$ triangular lattice antiferromagnet or spin dimer magnets. The findings obtained by this μSR experiments make it more likely that T_n is the nematic transition.

*1 Department of Applied Physics, University of Fukui
*2 FIR Center, University of Fukui
*3 RIKEN Nishina Center

References

1) B. Leuenberger *et al.*, Inorg. Chem. **25**, 2930 (1986).
2) H. Kikuchi, T. Tanaka, Y. Fujii, A. Matsuo, K. Kindo, Abstract of the 19 International Conference on Magnetism. July 8–13, 2012 Busan, Korea, p. 167.
3) A. Smerald *et al.*, Phys. Rev. B **88**, 184430 (2013).

Magnetism of novel heavy fermion compound $YbCu_4Ni$ investigated by μSR

T. Taniguchi,[*1] K. Osato,[*1,*2] M. Fujita,[*3] D. P. Sari,[*3,*4] and I. Watanabe[*3,*5]

The f-electron systems show many examples of quantum critical phenomena.[1] In previous works, high-quality crystals and advanced experimental methods provided many instances of quantum critical phenomena originating from antiferromagnetism. Recently, quantum critical phenomena that cannot be explained by the self-consistent renormalization (SCR) theory have attracted much attention. However, to study such quantum critical phenomena, actual candidate materials and adequate experimental methods are required.

We focused on $YbCu_4T$ (T = transition metal) because this family exhibits exotic physical phenomena such as the valence transition at zero field and ambient pressure in $YbCu_4In$.[2,3] In $YbCu_4Au$, valence and magnetic transitions are induced by applying a magnetic field.[4] Since the Yb site in this family has three-fold symmetry, this system may show an ordered phase originating from geometrical frustration.

The temperature dependence of the specific heat (C/T) of $YbCu_4Ni$ shows a power-law behavior. This behavior is consistent with the quantum critical phenomena, but the SCR theory cannot explain the temperature dependence of C/T.[5] The purpose of our research is to understand the origin of the power-law behavior of C/T in $YbCu_4Ni$. Magnetism usually plays the vital role of quantum criticality. Thus, we performed muon spin relaxation (μSR) measurements at RIKEN-RAL because μSR is a powerful tool to obtain information on static and dynamic spin correlations.

Figure 1 shows the temperature dependence of the μSR time spectra. To derive the magnetic fluctuation of the f-electron, we applied a longitudinal magnetic field of 100 G. Rapid relaxation was observed at low temperatures below 2 K, indicating the appearance of magnetic fluctuation. However muon spin precession was not observed down to the lowest temperature of 0.4 K. We determined the asymmetry of the spectrum at 0.4 K for the time after ~4 μs as the baseline (~16%). These results suggest the inhomogeneous magnetic field at the muon stopping site even at the lowest measurement temperature.

Here, we discuss the origin of the power-law behavior of C/T from the viewpoint of magnetic fluctuation. As in the case of antiferromagnetism, it is highly possible that the magnetic fluctuation is the cause of the temperature dependence of C/T. There are two possible origins of the magnetic fluctuations: (1) the novel quantum criticality and (2) magnetic inhomogeneity. For the former case, it was theoretically aspect pointed out that a dramatic increase in effective mass should be observed near the quantum critical point, other than that from the antiferromagnetic phase.[6] For example, the temperature dependence of C/T shows logarithmic behavior in β-$YbAlB_4$ even when the valence fluctuation contributed to the physical properties.[7] For the latter case, owing to the distribution of the Kondo temperature originating from the magnetic inhomogeneity, C/T at low temperatures may show a behavior similar to quantum criticality.[8] Since inhomogeneous states such as the spin-glass state may appear because of the geometrical frustration, the latter case is also a candidate scenario. μSR measurements below 0.4 K may provide evidence to clarify the above two possibilities.

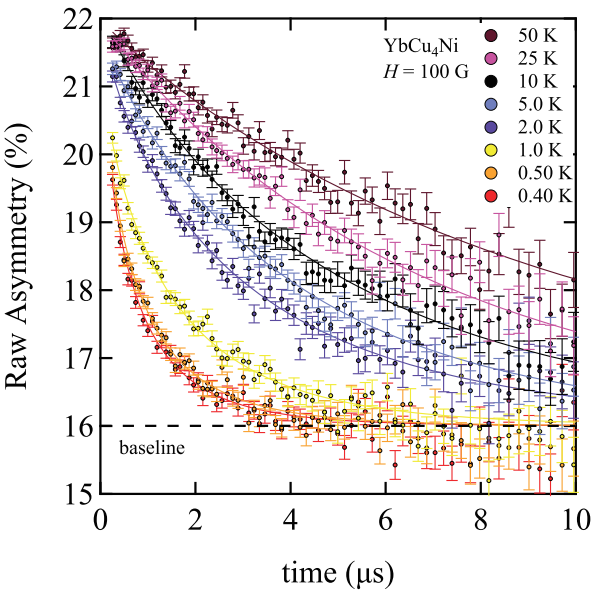

Fig. 1. Temperature dependence of the μSR time spectra of $YbCu_4Ni$ in a longitudinal field of 100 G.

In conclusion, we performed the μSR measurements of $YbCu_4Ni$. At low temperature, the magnetic fluctuation increased. It is highly possible that the power-law behavior of C/T is caused by this fluctuation.

*1 Institute for Materials Research, Tohoku University
*2 Department of Physics, Tohoku University
*3 RIKEN Nishina Center
*4 College of Engineering, Shibaura Institute of Technology
*5 ISIS Pulsed Neutron and Muon Facility, STFC Rutherford Appleton Laboratory

References
1) G. R. Stewart, Rev. Mod. Phys. **56**, 755 (1984).
2) H. Nakamura *et al.*, J. Phys. Soc. Jpn. **59**, 28 (1990).
3) M. Hedo *et al.*, Acta. Phys. Pol. B. **34**, 1193 (2003).
4) S. Wada *et al.*, J. Phys. Condens. Matt. **20**, 175201 (2008).
5) J. G. Sereni *et al.*, Phys. Rev. B. **98**, 094420 (2018).
6) S. Watanabe, K. Miyake, Phys. Rev. Lett. **105**, 186403 (2010).
7) S. Nakatsuji *et al.*, Nat. Phys. **4**, 603 (2008).
8) E. Miranda *et al.*, J. Phys. Condens. Matt. **8**, 9871 (1996).

ZF-μSR measurement to investigate thermal hysteresis of $MgTi_2O_4$ at low temperature

U. Widyaiswari,[*1,*2] N. Hanasaki,[*3] B. Kurniawan,[*2] and I. Watanabe[*1,*2]

We investigated spinel titanate ($MgTi_2O_4$) which has a $3d^1$ electron ($S = 1/2$) within the Ti^{3+} ion and forms a pyrochlore lattice,[1] to explore the magnetic ground state of this strongly correlated system. The lattice of $MgTi_2O_4$ has a cubic structure at room temperature and shows a transition to a tetragonal structure at $T_{st} \simeq 260$ K.[2] This structural phase transition is accompanied by a metal-insulator transition and changes in magnetic properties.[2] Isobe *et al.* proposed a spin-singlet insulator as the ground state, which did not form any magnetic ordering.[2]

Previously, we found that there was no long-range ordered state in $MgTi_2O_4$ down to 6 K through zero-field muon spin resonance (ZF-μSR) measurements. Our preliminary study on $MgTi_2O_4$ showed that thermal hysteresis occurs in the temperature dependence of heat capacity below 3.5 K down to 2.5 K. To investigate the origin of the thermal hysteresis and magnetic properties at a much lower temperature, we extend the ZF-μSR measurement down to 2 K using VARIOX at the RIKEN-RAL Muon Facility in the United Kingdom. ZF-μSR measurements were performed below 30 K with descending temperature (cooling procedure) and ascending temperature (warming procedure) to observe the thermal hysteresis. The time spectra, shown in Fig. 1(a), can be fitted using Eq. (1).

$$A(t) = A_{GKT}(1/3+2/3(1-\Delta^2t^2)\exp(-\Delta^2t^2/2)) + A_L\exp(-\lambda t), \quad (1)$$

where A_{GKT} and A_L are the initial asymmetry from Gaussian and Lorentzian components at $t = 0$, respectively.

The absolute value of the temperature dependence of muon spin relaxation, λ(T), was in good agreement with the previous result[3] and is shown in Fig. 1(b). This result demonstrated that the muon spin relaxation rate does not change significantly indicating the absence of the ordered state down to 2 K. Furthermore, there is no difference in the muon spin relaxation rate measured in the cooling and warming procedures. This indicates that the thermal hysteresis observed in the heat-capacity measurement is beyond the muon-spin time window; therefore, we could not detect such behavior down to 2 K.

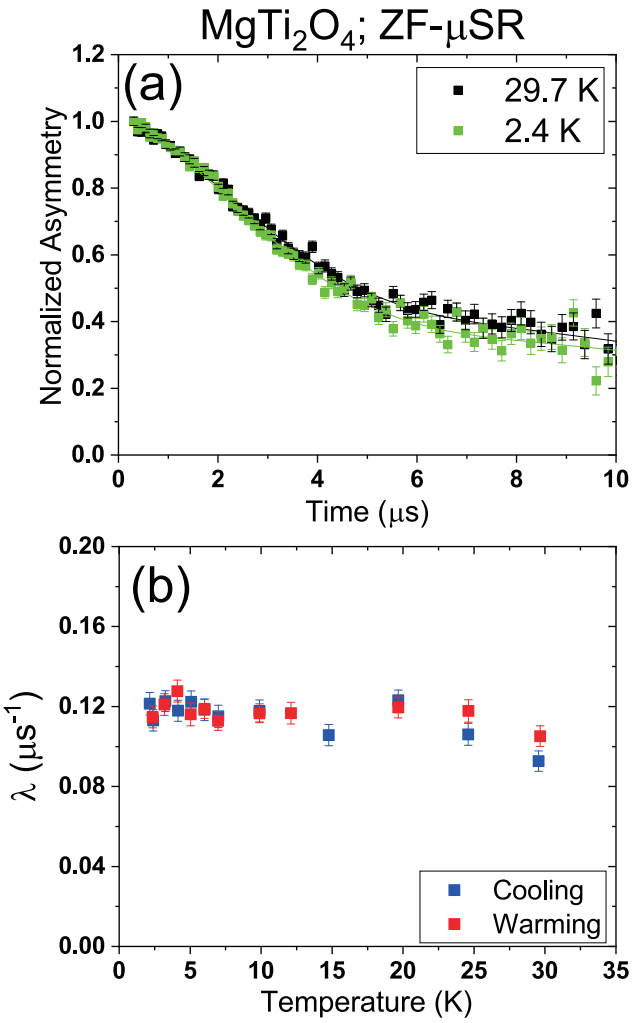

Fig. 1. (a) ZF-μSR time spectra of $MgTi_2O_4$; the solid line is the fitting resulted obtained using Eq. (1). (b) Temperature dependence of the muon spin relaxation rate.

References

1) S. Torigoe *et al.*, Phys. Rev. B **98**, 134443 (2018).
2) M. Isobe, Y. Ueda, J. Phys. Soc. Jpn. **71**, 1848 (2002).
3) U. Widyaiswari *et al.*, RIKEN Accel. Prog. Rep. **53**, 149 (2019).

*1 RIKEN Nishina Center
*2 Department of Physics, Universitas Indonesia
*3 Department of Physics, Osaka University

Observation of Cu spin fluctuations in over-doped regime $La_{2-x}Sr_xCuO_4$ nanoparticles

S. Winarsih,[*1] T. Adachi,[*2] T. Goto,[*2] B. Kurniawan,[*3] B. Soegijono,[*3] and I. Watanabe[*4]

The first observation of exchange anisotropy or exchange bias was reported for cobalt particles capped by cobalt oxide.[1)] The shifted hysteresis loop in field-cooled suggested the occurrence of exchange coupling between the ferromagnetic spin of cobalt with the antiferromagnetic spin of cobalt oxide. For gold nanoparticles encapsulated by butanethiol, clear evidence of magnetism was observed when the size of the gold cluster was 2.2 nm, as studied by muon-spin relaxation (μSR).[2)] The relaxation of muon spins decreased with increasing temperature in the longitudinal field, (LF-μSR), indicating the existence of a magnetic moment. Even though magnetism was clearly observed, this study could not distinguish whether the magnetic moment was located at the encapsulated molecules or inside the gold nanoparticles.

The existence of ferromagnetic spins at the surface was also suggested to lead to the observation of a hysteresis loop at 10 K in CuO nanoparticles.[3)] An anomalously enhanced Curie term at low temperatures in high-T_c superconductor cuprate (HTSC), $La_{2-x}Sr_xCuO_4$, with x = 0.10–0.30, when the particle size was reduced to 113 nm was also linked to the role of the spins at the surface.[4)] This suggests that the surface effect plays an important role in both free-standing nanoparticles, like CuO and $La_{2-x}Sr_xCuO_4$, and nanoparticles capped by molecules, like oxide-coated particles of cobalt and nanogold capped by butanethiol. However, the mechanism of the role of the surface causing the emergence of ferromagnetism in nanoparticles is still an open question.

We aimed to investigate nano-sizing effects in $La_{2-x}Sr_xCuO_4$ because the observation of possible ferromagnetism is a new interesting phenomenon in HTSCs. In the bulk case, a ferromagnetic phase was predicted in the heavily overdoped regime where the superconductance was suppressed.[5,6)] This appearance of ferromagnetism in $La_{2-x}Sr_xCuO_4$ from the underdoped to the overdoped regime is a new question in HTSCs because superconductivity and magnetic ordering are believed to be interconnected.

To synthesize free-standing nanoparticles, the chemical reaction method is believed as one of the best methods because it is a bottom-up method.[7)] A bottom-up method implies spontaneous self-assembly from the atomic level to the nanoparticle level. The detailed synthesis route is reported in our former paper.[8)]

μSR measurements on $La_{2-x}Sr_xCuO_4$ with x = 0.20 and particle size of 46 nm were performed at the RIKEN-RAL Muon Facility, Rutherford-Appleton Laboratory, UK, using a pulsed positive surface muon beam. Figure 1 displays the temperature dependence of the relaxation rate of the muon spins. The relaxation rate starts rapidly increasing below 10 K. This indicates the slowing down of the Cu spin fluctuations below 10 K, which, in turn, suggests that magnetic correlations are developed at low temperatures. Compared to the bulk case, no magnetic correlation was observed even at 0.3 K.[9)]

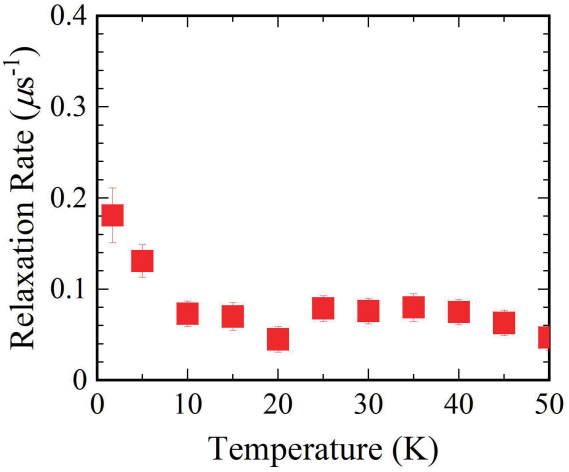

Fig. 1. Temperature dependence of relaxation rate of muon spins, λ, of $La_{2-x}Sr_xCuO_4$ with x = 0.20 and particle size of 46 nm.

Our present result reveals that nano-sizing induces weak magnetism owing to the development of Cu spin fluctuation. Moreover, our magnetization results show that the superconductivity is strongly suppressed in $La_{2-x}Sr_xCuO_4$ nanoparticles. These results suggest an anticorrelation between the magnetic order and the superconductivity and show that the superconductivity in an HTSC is strongly influenced by the magnetic order, which can be explained by the stripe theory. We provided a new insight of studying Cu spin dynamics by investigating the nano-sizing effects in an HTSC, which is typically examined based on the impurity effects on the Cu site.[9–11)]

*1 Department of Physics, Universitas Padjadjaran
*2 Department of Engineering and Applied Sciences, Sophia University
*3 Department of Physics, Universitas Indonesia
*4 RIKEN Nishina Center

References

1) W. H. Meiklejohn, C. P. Bean, Phys. Rev. **102**, 1413 (1956).
2) M. H. Dehn *et al.*, Appl. Phys. Lett. **112**, 053105 (2018).
3) M. S. Seehra, A. Punnoose, Solid State Commun. **128**, 299 (2003).
4) Y. Yin *et al.*, J. Phys. Chem. C **117**, 3028 (2013).
5) A. Kopp *et al.*, Proc. Natl. Acad. Sci. USA **104**, 6123 (2007).
6) J. E. Sonier *et al.*, Proc. Natl. Acad. Sci. USA **107**, 17131 (2010).
7) A. G. Kolhatkar *et al.*, Int. J. Mol. Sci. **14**, 15977 (2013).
8) S. Winarsih *et al.*, Key. Eng. Mater. **966**, 357 (2019).
9) T. Adachi *et al.*, Phys. Rev. B **78**, 134515 (2008).
10) T. Adachi, *et al.*, Phys. Rev B **70**, 060504(R) (2004).
11) Risdiana, *et al.*, Phys. Rev. B **77**, 054516 (2008).

The electron transfer channel in the sugar recognition system assembled on gold nano particles

T. Goto,[*1] T. Hashimoto,[*1] D. P. Sari,[*2] and I. Watanabe[*3]

The recently reported electrochemical sugar recognition system consisting of a gold nano particle (GNP) with a diameter of 12 nm, a ruthenium complex and a phenylboronic acids, attracts much interest because of its high sensitivity for various sugars such as D-glucose or D-fructose. When sugar molecules are "recognized" by the phenylboronic site, the response of electrochemical voltammetry of the ruthenium complex site drastically changes, enabling the system to work as a highly sensitive sugar-sensor.[1,2] In this recognition process, the change in the electronic state at the phenylboronic acids site caused by sugar must be transferred to the ruthenium complex site. The purpose of this study is to find out by LF-μSR technique a channel of the electron transfer from the phenylboronic acid site to the ruthenium complex via gold nano particle. By its finding, we will be given a better understanding of the sugar-recognition mechanism, and also, a possibility to develop a sensor with still higher sensitivity and more functions.

As the present system includes alkyl-chains in the ruthenium complex and the phenylboronic acid site, the injected muons pick up one electron to form a neutral atomic state, which is soon thermalized and bonded to a relatively-reactive site on the chain. The brought-in electrons may show one-dimensional motion along the chain, if the electron transfer channel between the ruthenium complex and the phenylboronic site exists.

This behavior can be detected sensitively by measuring the muon-spin relaxation process, which is caused by the magnetic interaction between the muon spin and the moving electron produced by muon itself. In other words, in place of the attachment of sugar molecules to phenylboronic acid site, one utilizes muon as a trigger to induce a moving electron and also as an observer of it. This method is known as the muon-labelling measurement.

The characteristic dimensionality of the electron motion can be readily studied by measuring LF dependence of μSR relaxation rate λ;[3] for one-dimensional motion, λ is expected to be proportional to $(H_{\rm LF})^{-1/2}$, where $H_{\rm LF}$ is the externally applied field along the muon spin polarization. This method was first applied to the polaron motion in oganic polymer chains,[4] and also successfully to the typical one dimensional system, DNA.[5]

Zero (ZF) and longitudinal (LF) field-μSR measurements at room temperature were performed on a powder sample at RIKEN-RAL Muon Facility using a spin-polarized pulsed surface-muon (μ^+) beam with a momentum of 27 MeV/c. The muon spin depolarization

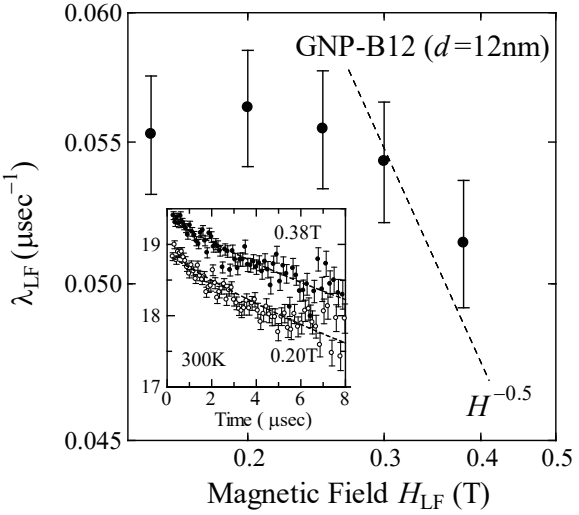

Fig. 1. Temperature dependence of dynamical component of relaxation rate λ under various longitudinal fields $H_{\rm LF}$. The inset shows the typical depolarization curves of the asymmetry (%) with fitted functions. Each curve is vertically shifted for clarity.

data above 0.1 T were analyzed with the function $e^{\lambda\tau}$, where λ is the depolarization rate due to the dynamical spin fluctuation. Note that in this field region, the effect of quasi static nuclear spins or $G_{\rm KT}$, Kubo-Toyabe function is neglected.

The field dependence of λ is shown in Fig. 1. With decreasing $H_{\rm LF}$ from the highest field 0.38 T, λ showed a slight but finite increase until $H_{\rm LF} \cong 0.2$ T, below which λ saturates. An appreciably high depolarization in the totally non-magnetic compound indicates that some muon-triggered moving electron process exists. The observed increase is weaker than expected for the one dimensional diffusion case. This indicates that the contribution from the diffusion process has the lower boundary in the fluctuation spectrum, as is evident from the functional form of $\lambda H_{\rm LF}$ dependence, and in fact is reported for previous report.[4]

In order to confirm that the observed behavior of λ comes from the one-dimensional movement along alkyl-chain, investigation on wider field region or equivalently on wider fluctuation spectrum, including NMR is inevitable, and is now on the progress.

*1 Faculty of Technology and Science, Sophia University
*2 SIT Research Laboratories, Shibaura Institute of Technology
*3 RIKEN Nishina Center

References

1) A. Endo *et al.*, Anal. Methods **6**, 8874 (2014).
2) T. Goto *et al.*, IEEE Trans. Mag. **55**, 2300404 (2019).
3) Risch and Kehr, Phys. Rev. B **46**, 5246 (1992).
4) F. Pratt *et al.*, Phys. Rev. Lett. **79**, 2855 (1997).
5) E. Torikai *et al.*, Hyperfine. Int. **138**, 509 (2001).

Antiferromagnetic ordering of λ-(BEST)$_2$FeCl$_4$ observed by μSR measurement

T. Kobayashi,[*1] D. P. Sari,[*2,*3] K. Koyanagawa,[*1] K. Satoh,[*1] H. Taniguchi,[*1] A. Kawamoto,[*4] and I. Watanabe[*3]

In the organic conductor λ-(BETS)$_2$FeCl$_4$ (see Fig. 1 for BETS), there is a significant strong exchange interaction between the 3*d* electrons of Fe ions, and π electrons of BETS molecules, *i.e.*, π-*d* interaction. This results in exotic properties such as a field-induced superconductivity[1] and a metal-insulator transition with antiferromagnetic (AF) ordering, where 3*d* electrons are paramagnetic even below the AF transition temperature indicated by the heat capacity measurement.[2] To understand these phenomena, a deep understanding of the π-d interaction mechanism is required. As a clue to this, the magnetism of λ-(STF)$_2$FeCl$_4$ has been recently evaluated. As shown in Fig. 1, the STF molecule is a molecule in which part of the selenium in the BETS molecule is replaced by sulphur. Magnetisation, NMR, and Mössbauer measurements showed that λ-(STF)$_2$FeCl$_4$ exhibits AF ordering at 16 K, where both 3*d* and π electrons are ordered, whereas further development of the internal magnetic field owing to the polarized magnetisation of the 3*d* spins was observed below 8 K.[3–5] In addition, μSR measurements demonstrated that the slow precession signals due to the AF order of π-electrons and the fast precession signals due to the polarization of 3*d* spins appear from different temperatures. The magnetic properties that appeared when the BETS molecule was replaced by the STF molecule are thought to be caused by changes in the π-*d* and *d*-*d* interactions. Therefore, to evaluate the relationship between the molecular substitution and the change in the π-*d* interaction, we focused on the substitution from BETS to BEST molecules (see Fig. 1 for BEST). Because the electron density of the outer chalcogen atoms is small, the expansion of the orbitals by the substitution from S to Se is expected to cause steric hindrance and reduce the π-*d* interaction.

According to the reported magnetisation measurement of λ-(BEST)$_2$FeCl$_4$, it exhibits paramagnetic behaviour down to 4 K.[6] However, because the observed spin susceptibility is dominated by 3*d* spins, the magnetism of π spins is almost concealed. To reveal the magnetic order of the 3*d* and π electrons, a microscopic measurement that can sensitively detect the internal field is necessary.

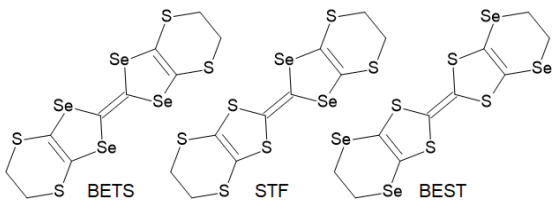

Fig. 1. Structures of donor molecules.

*1 Graduate School of Science and Engineering, Saitama University
*2 College of Engineering, Shibaura Institute of Technology
*3 RIKEN Nishina Center
*4 Graduate School of Science, Hokkaido University

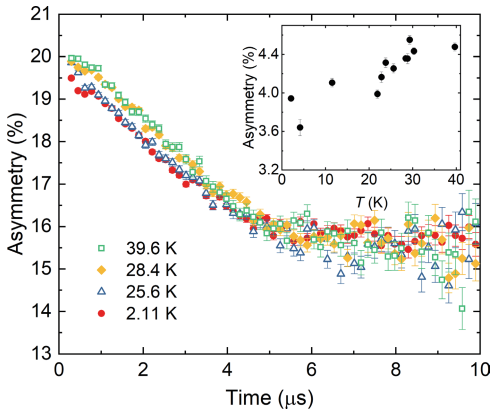

Fig. 2. Zero-field μSR time spectra of λ-(BEST)$_2$FeCl$_4$. Inset: temperature dependence of initial asymmetry.

For this purpose, we performed μSR measurements on λ-(BEST)$_2$FeCl$_4$.

Figure 2 shows the μSR time spectra at several temperatures. We observed that the initial asymmetry changes abruptly between 28.4 K and 25.6 K. The time spectra $A(t)$ are fitted by the stretched exponential function, $A(t) = A\exp[-(\lambda t)^{\beta}] + A_{\rm bg}$, where A and $A_{\rm bg}$ are the asymmetries due to the muons stopped inside the sample and at the sample holder, λ is the relaxation rate, and β is the stretched exponent, respectively. From this analysis, we deduced that the initial asymmetry A indeed decreases below ∼30 K, as shown in the inset of Fig. 2, although its transition temperature is not clear. Because the AF order of π spin was also observed in λ-(BEST)$_2$GaCl$_4$ consisting of nonmagnetic Ga ions, the change in the initial asymmetry observed in λ-(BEST)$_2$FeCl$_4$ can be understood by the AF order. In fact, the disappearance of the paramagnetic EPR signal was observed at 25 K in recent ESR measurements, suggesting an AF transition.

Compared to λ-(STF)$_2$FeCl$_4$, it is interesting to know whether the fast precession signal due to the polarization of 3*d* spins is observed or not. Within our experimental error, no significant spectral change was observed from 25.6 K to 2.11 K, suggesting that only the π spins are magnetically ordered. In λ-(BETS)$_2$FeCl$_4$, unlike λ-(BEST)$_2$GaCl$_4$, the anisotropy of the magnetic susceptibility was observed with AF transition. Therefore, we confirmed that the magnetic state of λ-(BEST)$_2$GaCl$_4$ is different from that of λ-(BETS)$_2$FeCl$_4$ and λ-(STF)$_2$FeCl$_4$. These results provide important clues for the mechanism of π-d interaction.

References

1) S. Uji *et al.*, Nature **410**, 908 (2001).
2) H. Akiba *et al.*, J. Phys. Soc. Jpn. **78**, 033601 (2009).
3) S. Fukuoka *et al.*, J. Phys. Soc. Jpn. **87**, 093705 (2018).
4) T. Minamidate *et al.*, Phys. Rev. B **97**, 104404 (2018).
5) S. Fukuoka *et al.*, Phys. Rev. B **101**, 184402 (2020).
6) H. B. Cui *et al.*, Chem. Lett. **34**, 254 (2005).

Zero-field μSR on the out-of-plane superconductivity of λ-$(BETS)_2GaCl_4$

D. P. Sari,[*1,*2] K. Hiraki,[*3] I. Watanabe,[*1] and Y. Ishii[*1]

λ-$(BETS)_2GaCl_4$ is a quasi-two-dimensional organic metal and it is reported as a high-anisotropic type-II superconductor. It exhibits rich physical properties once we substitute Ga with Fe, Cl with Br, or once we reduce the Se content in the BETS molecule (BETS = $(CH_2)_2S_2Se_2C_6S_2S_2(CH_2)_2$).[1] In the P-T phase diagram, the neighboring phase adjacent to the superconducting (SC) state is the Mott insulating state, which is antiferromagnetically ordered, and separated by a suspicious paramagnetic insulating state with no magnetic ordering down to 0.3 K.[2] A theoretical study based on anisotropic spin fluctuations-mediated superconductivity suggested an anisotropic gap structure with two nodal lines,[3] whereas ^{13}C-NMR study evidenced two types of magnetic fluctuations of the π-electron down to 2 K.[4] There is an urgent requirement for the detailed experimental determination of the SC gap structure. We performed a series of transverse-field (TF) μSR measurement to determine the SC gap structure. First, we found that the SC gap structure of λ-$(BETS)_2GaCl_4$ was unusual as it exhibited both d-wave and s-wave symmetry characteristics.[4,5] Furthermore, considering the study by Powell and McKenzie for entire families of organic superconductors, we plan to confirm whether time reversal symmetry breaking is related to this unusual SC gap structure. Zero-field (ZF) μSR is a powerful tool to detect such breaking symmetry in the SC state.

We recently performed a series of zero-field μSR using aligned single crystals. We prepared ∼130 mg single crystals and oriented them in the same direction. Measurements were performed using the ARGUS spectrometer at the RIKEN-RAL pulse muon facility with a HELIOX cryostat and fly-path setup. The single pulse mode was used to collect 80M events. In a previous report[6] we showed the result when the polarized muon beam direction was nearly perpendicular to the conducting plane. We prepared another sample setup (∼100 mg) to measure with the polarized muon beam direction parallel to the conducting plane. In this report, we compare both measurements to gain information regarding out-of-plane superconductivity.

Figure 1 shows normalized time spectra at several temperatures below and above the critical temperature (T_c ∼ 5.5 K). Open circle curves indicate normalized time spectra with the muon beam direction perpendicular to the conducting plane.[6] Blue solid lines indicate fitting lines using a stretched exponential function $A(t) = A_0 \exp(-(\lambda t)^{\beta})$. At 1.5 K, λ and β values were 0.2281(35) μs^{-1} and 1.123(16), respectively. No temperature dependence was observed between the normal and SC states. Closed circle curves indicate normalized time spectra with the muon beam direction parallel to conducting plane, which reflects the intrinsic behavior of the out-of-plane properties. Although there was no temperature dependence between the normal and SC states, we found that the shape of the spectra was distinct with the open circle spectra showing in-plane properties in λ-$(BETS)_2GaCl_4$. All spectra were best fit by a stretched exponential function. At 1 K, λ and β values were 1.881(21) μs^{-1} and 1.34(2). In-plane properties have a stronger relaxation while the shape is toward a single exponential function. λ-$(BETS)_2GaCl_4$ has high-anisotropy SC properties such as the large ratio of in-plane/out-of-plane upper critical field and transfer integral, $H_{c2||}/H_{c2\perp} > 4$[7] and $t_{||}/t_{\perp} \sim 13$,[3] respectively. Then, the stronger in-plane λ can be related to the antiferromagnetic fluctuations of the π-electron within the conducting plane, which mediates the superconductivity.

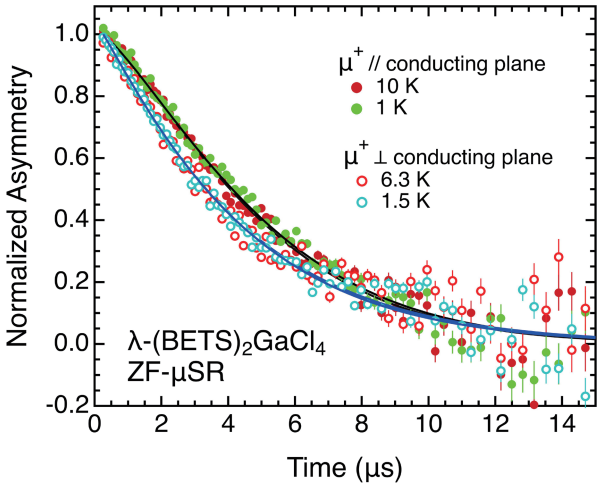

Fig. 1. Normalized ZF-μSR time spectra with the setup of μ^+ injected parallel and perpendicular to the conducting plane. The solid lines represent fitting lines obtained using the stretched exponential function.

These results confirm that the exotic SC state behavior proposed in this material based on TF-μSR could be beyond triplet superconductivity or time-reversal symmetry breaking properties. The next step is to relate this ZF-μSR result with the TF-μSR results using single crystals.

*1 College of Engineering, Shibaura Institute of Technology
*2 RIKEN Nishina Center
*3 Department of Physics, Fukushima Medical University

References
1) H. Kobayashi *et al.*, Chem. Rev. **104**, 5265 (2004).
2) T. Minamidate, RIKEN Accel. Prog. Rep. **51**, 205 (2018).
3) H. Aizawa *et al.*, J. Phys. Soc. Jpn. **87**, 093701 (2018).
4) T. Kobayashi, A. Kawamoto, PRB **96**, 125115 (2017).
5) D. P. Sari, PhD Thesis, Osaka University (2018).
6) D. P. Sari, *et al.*, submitted (2020).
7) D. P. Sari, RIKEN Accel. Prog. Rep. **53**, 155 (2018).
8) M. Tanatar *et al.*, J. Superconductivity **12**, 511 (1999).

Li-ion diffusion in $LiFeSi_xP_{1-x}O_4/C$ with $x = 0$ and 0.03

F. Astuti,[*1] D. P. Sari,[*2,*3] M. Zainuri,[*1] Darminto,[*1] and I. Watanabe[*2]

The primary issue in the use of $LiFePO_4$ in battery applications is its low intrinsic electronic conductivity and lithium-ion diffusion coefficient. Furthermore, there is an urgent need to improve the cycle life and long-term cyclability of $LiFePO_4$.[1)] Several strategies have been considered to enhance the electronic/ionic conductivity and cycle life of $LiFePO_4$, such as carbon coating, reduction of particle size, and element doping.[2)]

Powder samples of $LiFeSi_xP_{1-x}O_4/C$ with $x = 0$ and 0.03 were prepared by a solid-state method. Single-phase samples of $LiFePO_4$ have not been obtained so far. Our study strongly supports that Si doping significantly improves the electrochemical performance of $LiFePO_4$ as reported in Ref. 3). A sample with $x = 0.03$ yielded the highest specific capacity. Further study on Li-ion diffusion is significant for increasing the battery performance. Muon spin relaxation (μSR) is a powerful tool to study Li-ion diffusion.

In order to study the Li-ion diffusion in $LiFeSi_xP_{1-x}O_4/C$ further, we measured zero-field and longitudinal-field μSR (ZF- and LF-μSR, respectively) using the ARGUS spectrometer at the RIKEN-RAL Muon Facility. The ZF-μSR was measured in the temperature range of 5–30 K, and the LF-μSR was measured

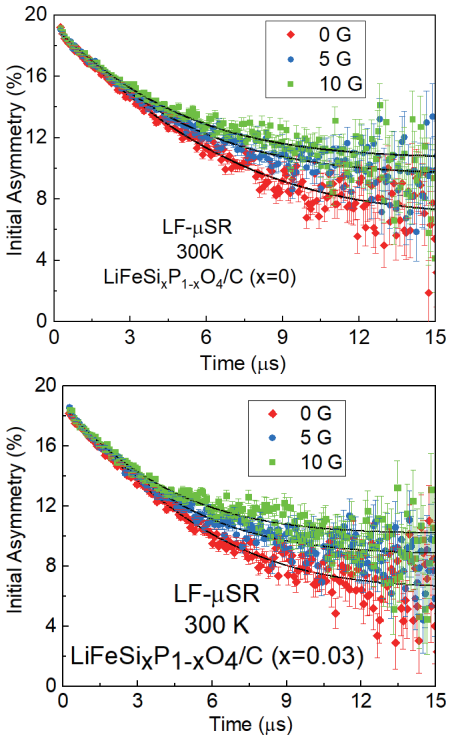

Fig. 1. LF-μSR spectra on of $LiFeSi_xP_{1-x}O_4/C$ with (a) $x = 0$ and (b) $x = 0.03$.

*1 Department of Physics, Institut Teknologi Sepuluh Nopember
*2 RIKEN Nishina Center
*3 Graduate School of Engineering and Science, Shibaura Institute of Technology

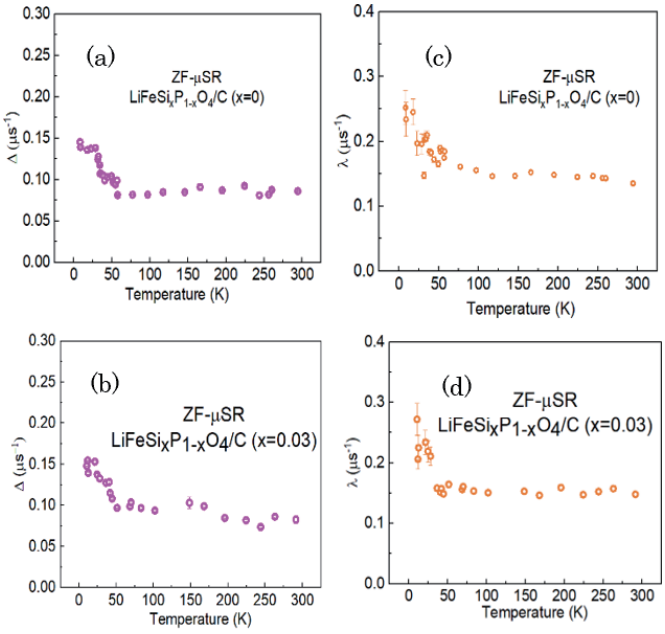

Fig. 2. Temperature dependences of Δ with (a) $x = 0$ and (b) $x = 0.03$ and of λ with (c) $x = 0$ and (d) $x = 0.03$ for $LiFeSi_xP_{1-x}O_4/C$.

at 300 K under low magnetic fields of 5 G and 10 G.

Figure 1 shows the LF-μSR spectra of $LiFeSi_xP_{1-x}O_4/C$ with (a) $x = 0$ and (b) 0.03. The dynamic behavior at 300 K was clearly observed for $LiFeSi_xP_{1-x}O_4/C$ with $x = 0$ and 0.03 because there is only a small "decoupling" effect due to applied LF. The spectra were fitted by an exponentially relaxing dynamic Kubo-Toyabe function.

Based on Fig. 2, the field distribution width (Δ) and field fluctuation (λ) were found to be independent of temperature down to 50 K, whereas Δ and λ increased with temperature decreasing below 50 K for samples with $x = 0$ and $x = 0.03$. There is no abrupt change in Δ or λ in either sample. Following the results in Ref. 4), we obtained the diffusion coefficient as $D_{Li} = (1.598 \pm 0.0033) \times 10^{-10}$ cm^2/s, for $x = 0$ and $D_{Li} = (1.751 \pm 0.0037) \times 10^{-10}$cm^2/s for $x = 0.03$. The present result demonstrates the slight increase of Li-ion diffusion by silicon substitution, which can improve the performance of $LiFePO_4$ cathode materials. Additionally, from the ZF-μSR results, the magnetic transition temperature was detected, starting from the temperature 50 K and close to the estimation of the Neel temperature, T_N, $LiFePO_4$ reported in Ref. 5).

References

1) M. Nishijima *et al.*, Nat. Commun. **5**, 4553 (2014).
2) Z. Xu *et al.*, J. Electrochem. Soc. **163**, A2600 (2016).
3) M. Zainuri *et al.*, Key Eng. Mater. **860**, 75 (2020).
4) M. Månsson *et al.*, J. Phys. Conf. Ser. **551**, 012037 (2014).
5) J. Sugiyama *et al.*, Phys. Rev. B **84**, 054430 (2011).

Measurement of muon spin rotation in muonic hydrogen atom

S. Kanda*1 and K. Ishida*2

A muonic atom is a bound-state consisting of a negative muon and a nucleus. The charge radius of the nucleus can be obtained by measuring the Lamb shift in a muonic atom. In 2010, the Lamb shift of muonic hydrogen (μp) measured at the Paul Scherrer Institute indicated a significantly smaller proton charge radius than previously known from hydrogen spectroscopy and electron-proton scattering.[1)]

In addition to the charge radius, the proton's size is expressed by the Zemach radius, which is defined by convolving the charge and magnetic moment distribution. The Zemach radius is derived from the hyperfine splitting (HFS), in contrast to the charge radius derived from the Lamb shift. For the Zemach radius, the consistency between muonic and electronic measurements has not been fully discussed due to muonic measurements' limited precision. To tackle this problem, we are preparing for laser spectroscopy of the ground-state HFS in μp atoms.[2)]

In the experiment, a circularly polarized laser beam excites μp atoms in the spin-singlet state to the spin-triplet one. However, excited μp atoms are quenched by spin-exchange collisions with protons.[3)] There is no experimental result of this hyperfine quenching rate for μp atoms; therefore, we performed a muon spin rotation (μSR) measurement using a low-density gaseous hydrogen target. Only μp atoms in the spin-triplet state show muon spin precession.

Figure 1 illustrates an experimental setup at Port 4 of the RIKEN-RAL muon facility. A pulsed negative muon beam irradiates hydrogen gas filled in an aluminum vessel. The momentum of the beam was set to 20 MeV/c. The gas pressure was 0.1 atm at room temperature. A transverse magnetic field of 66.7 mT was applied using a Helmholtz coil. Under these conditions, the quenching time of the triplet state and the spin precession period are expected to be 500 ns and 320 ns, respectively. The electrons from the muon decay were counted by a detector consisting of scintillating fibers and silicon photomultipliers (SiPMs). Kalliope front-end electronics[4)] processed the signal from the SiPM, and a multi-hit time-to-digital converter (TDC) recorded the time.

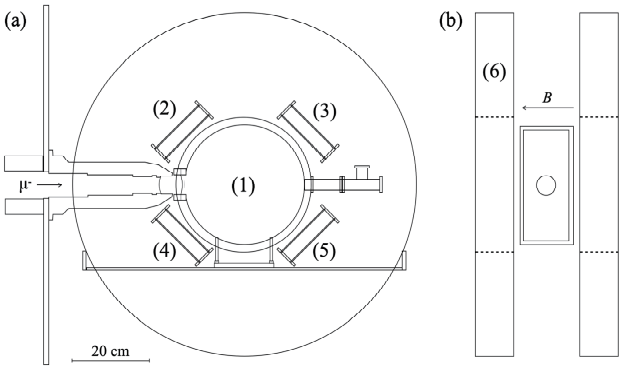

Fig. 1. Experimental setup: (a) cross-sectional view; (b) view from upstream. The numbers in the parentheses denote (1) hydrogen gas contained in an aluminum vessel, (2-5) electron detectors, (6) Helmholtz coils. Note that the electron detectors are not shown in (b).

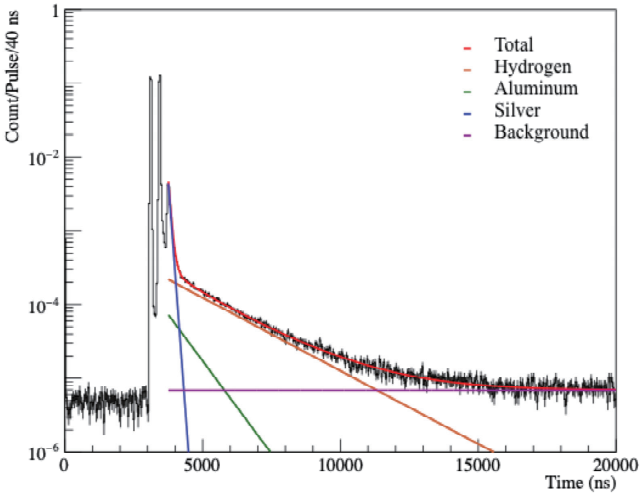

Fig. 2. Decay electron time spectrum with protium gas target at 0.1 atm. A transverse magnetic field of 66.7 mT was applied. Each line corresponds to the respective fitting result. The vertical axis is normalized by the number of beam pulses.

Figure 2 shows a decay electron time spectrum. The spectrum has components corresponding to hydrogen, aluminum, silver, and constant background events. The beam has a double-pulse structure with a 320 ns interval. The first two peaks of the spectrum correspond to prompt electrons. Detailed analysis to extract the μSR asymmetry is in progress.

This experiment was conducted under the user program RB1970003 at the RIKEN-RAL muon facility. This work was supported by Japanese JSPS KAKENHI Grant Numbers 18K13572 and 19H04618.

References

1) R. Pohl *et al.*, Nature **466**, 213 (2010).
2) S. Kanda *et al.*, J. Phys. Conf. Ser. **1138**, 012009 (2018).
3) J. S. Cohen, Phys. Rev. A **43**, 466 (1991).
4) K. M. Kojima *et al.*, J. Phys. Conf. Ser. **551**, 012063 (2014).

*1 Institute of Materials Structure Science, KEK
*2 RIKEN Nishina Center

A LYSO calorimeter prototype for muonic X-ray detection

S. Kanda*1 and K. Ishida*2

The Weinberg angle is an energy-dependent parameter that describes the mixing of electromagnetic and weak interactions. Measurements of the Weinberg angle at various energy scales are important as a precision test of the standard model and a search for new physics. The Weinberg angle can be determined via neutral current interactions. The most precise result was obtained at a low-energy scale by observing the atomic parity violation (APV) in cesium atoms.[1)]

When a nuclear Coulomb potential captures a negative muon, the muon forms an exotic bound state called a muonic atom. An APV experiment using muonic atoms provides a unique opportunity to search for physics beyond the standard model. In the 1990s, several experiments were conducted at the Paul Scherrer Institute.[2)] However, no parity-odd transition was observed because of difficulties in the experiment.

A new experiment using a high-intensity pulsed muon beam and a segmented calorimeter has been proposed to revisit this topic. The process of interest is the transition from the 2S state to the 1S state, which involves a one-photon emission. In the experiment, a segmented calorimeter consisting of Ce: LYSO crystals and silicon photomultipliers (SiPMs) detects X-rays from muonic atoms. The target energy resolution is 10% (FWHM) at 75 keV. As the first stage of the project, a calorimeter prototype was developed and tested at Port4 of the RIKEN-RAL muon facility.

Figure 1 illustrates the experimental setup. Muonic X-rays and decay electrons from a graphite target were detected using the prototype detector. The detector has two layers, each consisting of a 2-cm-square, 3-mm-thick crystal attached to four SiPMs (Hamamatsu S13360-3050CS) with an active area of 3-mm-square. The signals were amplified and shaped using EASIROC-based electronics and recorded with a waveform digitizer using DRS4.

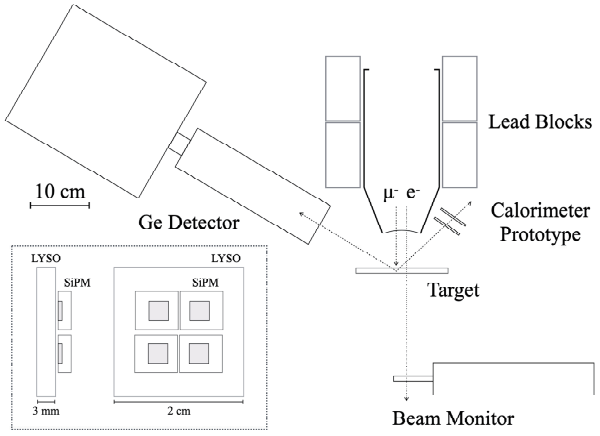

Fig. 1. Experimental setup. The inset shows the structure of the prototype.

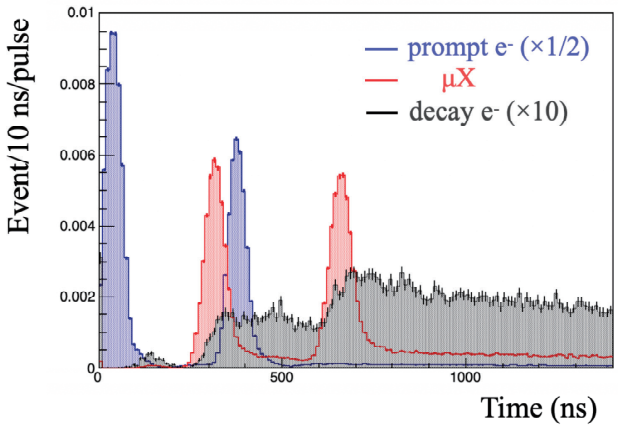

Fig. 2. Electron and X-rays time spectra. The prompt electrons were detected by the beam monitor.

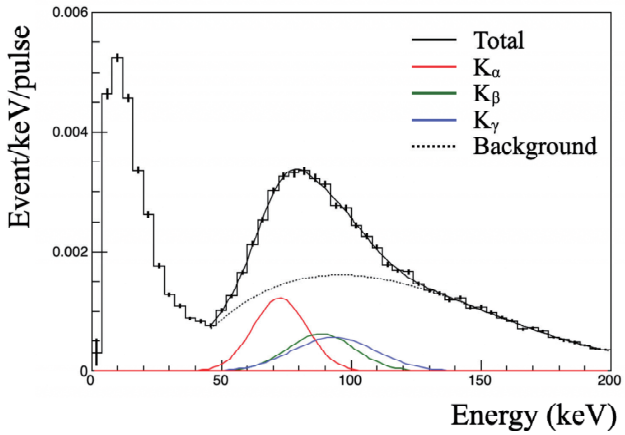

Fig. 3. X-ray energy spectrum obtained by the calorimeter prototype.

Figure 2 shows the time spectra of electrons and X-rays. Since electrons penetrate the two detector layers, the coincidence analysis allowed us to distinguish between electron and X-ray events. Figure 3 shows an energy spectrum of muonic X-rays. The energy was calibrated with the 81 keV line of ^{133}Ba. The peak structure was consistent with K X-rays of muonic carbon atoms. While the prototype demonstrated a sufficient time resolution, there is room for improvement in the energy resolution. A new version with improved light collection efficiency is under fabrication.

The authors thank Dr. Adrian Hillier and Ms. Bethany Hampshire for their kind assistance in preparation for the experimental setup at RAL. This experiment was conducted under the user program RB1970126 at the RIKEN-RAL muon facility. This work was supported by Japanese JSPS KAKENHI Grant Number 19H04618.

References

1) J. Guena *et al.*, Phys. Rev. A **71**, 042108 (2005).
2) K. Kirch *et al.*, Phys. Rev. Lett. **78**, 4363 (1997).

*1 Institute of Materials Structure Science, KEK
*2 RIKEN Nishina Center

3. Radiochemistry and Nuclear Chemistry

Production of ^{266}Bh in the ^{248}Cm(^{23}Na, 5n)^{266}Bh reaction and its decay properties†

H. Haba,[*1] F. Fan,[*2] D. Kaji,[*1] Y. Kasamatsu,[*3] H. Kikunaga,[*4] Y. Komori,[*1] N. Kondo,[*3] H. Kudo,[*5] K. Morimoto,[*1] K. Morita,[*1,*6] M. Murakami,[*7] K. Nishio,[*8] J. P. Omtvedt,[*9] K. Ooe,[*10] Z. Qin,[*2] D. Sato,[*5] N. Sato,[*1] T. K. Sato,[*8] Y. Shigekawa,[*1] A. Shinohara,[*3] M. Takeyama,[*11] T. Tanaka,[*12] A. Toyoshima,[*13] K. Tsukada,[*8] Y. Wakabayashi,[*14] Y. Wang,[*1] S. Wulff,[*9] S. Yamaki,[*1] S. Yano,[*1] Y. Yasuda,[*3] and T. Yokokita[*1]

The decay properties of the neutron-rich and long-lived isotopes ^{267}Bh and ^{266}Bh, which are located around the deformed shell at $Z = 108$ and $N = 162$, were studied in the ^{249}Bk(^{22}Ne, 5;4n)$^{266,\,267}$Bh,[1] ^{209}Bi(^{70}Zn, n)^{278}Nh $\rightarrow$ ^{274}Rg $\rightarrow$ ^{270}Mt $\rightarrow$ ^{266}Bh,[2] ^{243}Am(^{26}Mg, 3n)^{266}Bh,[3] and ^{248}Cm(^{23}Na, 5;4n)$^{266,\,267}$Bh[4] reactions. However, the reported decay properties such as α energies and half-lives of the isotopes are not in good agreement. In this work, we investigated the excitation functions and decay properties of ^{266}Bh and ^{267}Bh via the ^{248}Cm(^{23}Na, 5;4n)$^{266,\,267}$Bh reactions using the GARIS gas-jet and MANON setups.[5]

$^{248}Cm_2O_3$ targets of 256–290 μg/cm^2 thicknesses on 2-μm Ti backing foils were bombarded with a ^{23}Na^{7+} beam extracted from the RIKEN Heavy-Ion LINAC. The beam energies at the middle of the target were 121.2, 125.9, 130.6, and 135.3 MeV. The typical beam intensity was 3 pμA. The evaporation residues (EVRs) of interest were separated in-flight from the beam particles and the majority of the nuclear transfer products by GARIS. At the focal plane of GARIS, the EVRs passed through a Mylar vacuum window foil of 0.7-μm thickness and entered the gas-jet chamber, where the EVRs were thermalized in He gas, attached to KCl aerosol particles, and transported through a Teflon capillary (2.0-mm *i.d.* × 10-m length) to the rotating wheel apparatus MANON for α/SF-spectrometry. In MANON, the aerosol particles were deposited on a Au-coated (5 nm) Mylar foil of 0.5-μm thickness, forty of which were set on the periphery of a rotating wheel. The wheel was stepped to position the foils between 15 pairs of Si PIN photodiodes (Hamamatsu S3204-09). The step intervals of MANON were set to 5.0, 8.5, and 15.0 s.

We searched for time-correlated α-α and α-SF event pairs in a time window of 340 s. Consequently, a total of 23 chains were assigned to ^{266}Bh, its daughter nuclide ^{262}Db, and granddaughter ^{258}Lr, while no chain was assigned to ^{267}Bh. The α-particle energies of ^{266}Bh disperse widely in the range of E_α = 8.62–9.40 MeV. The reported α groups of E_α = 9.29 MeV,[1] E_α = 9.08 and 9.39 MeV,[2] E_α = 9.03 MeV,[3] and E_α = 8.82, 8.84–8.99, and 9.05–9.23 MeV[4] for ^{266}Bh are all within our α-energy range, except for E_α = 9.77 MeV.[2] The half-life of ^{266}Bh was measured to be $T_{1/2} = 10.0^{+2.6}_{-1.7}$ s, which is an order of magnitude longer than the previously reported values of $T_{1/2} \simeq 1$ s[1] and $T_{1/2} = 0.66^{+0.59}_{-0.26}$ s,[3] and 5 times longer than $T_{1/2} = 2.1^{+2.9}_{-0.8}$ s.[2] As shown in Fig. 1, the excitation function for the ^{248}Cm(^{23}Na, 5n)^{266}Bh reaction was measured for the first time, and it indicates a maximum of $\sigma = 57 \pm 14$ pb at 130.6 MeV. The excitation function was reproduced by the statistical model code HIVAP.[6] The upper-limit cross section of $\sigma \leq 14$ pb was also derived for the ^{248}Cm(^{23}Na, 4n)^{267}Bh reaction at 121.2 MeV.

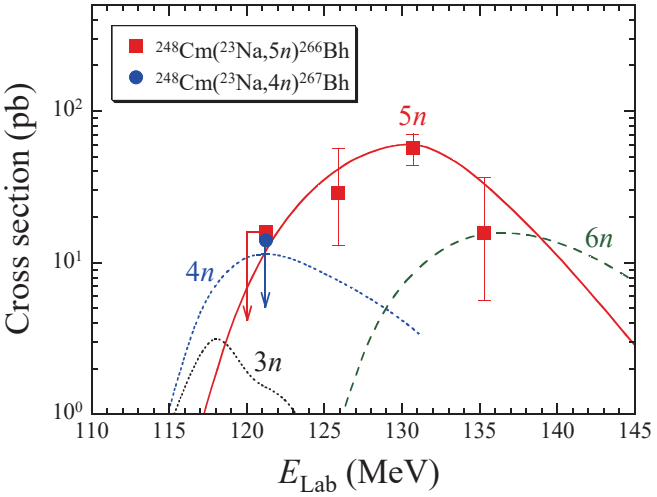

Fig. 1. Cross sections for the ^{248}Cm(^{23}Na, 5;4n)$^{266,\,267}$Bh reactions as a function of the laboratory-frame energy $E_{\rm Lab}$. The curves are the HIVAP calculations[6] for the ^{248}Cm(^{23}Na, $x n$)$^{271-x}$Bh reactions (x = 3–6).

† Condensed from the article in Phys. Rev. C **102**, 024625 (2020)

*1 RIKEN Nishina Center
*2 Institute of Modern Physics, Chinese Academy of Sciences
*3 Graduate School of Science, Osaka University
*4 Research Center for Electron Photon Science, Tohoku University
*5 Department of Chemistry, Niigata University
*6 Department of Physics, Kyushu University
*7 Decommissioning and Radioactive Waste Management Head Office, Japan Atomic Energy Agency
*8 Advanced Science Research Center, Japan Atomic Energy Agency
*9 Department of Chemistry, University of Oslo
*10 Graduate School of Medicine, Osaka University
*11 Faculty of Science, Yamagata University
*12 Department of Nuclear Physics, Research School of Physics, The Australian National University
*13 Institute for Radiation Sciences, Osaka University
*14 Center for Advanced Photonics, RIKEN

References
1) P. A. Wilk *et al.*, Phys. Rev. Lett. **85**, 2697 (2000).
2) K. Morita *et al.*, J. Phys. Soc. Jpn. **81**, 103201 (2012).
3) Z. Qin *et al.*, Nucl. Phys. Rev. **23**, 400 (2006).
4) K. Morita *et al.*, J. Phys. Soc. Jpn. **78**, 064201 (2009).
5) H. Haba *et al.*, Chem. Lett. **38**, 426 (2009).
6) W. Reisdorf, M. Schädel, Z. Phys. A **343**, 47 (1992).

Measurement of the isotopic ratio of Np-236 to Np-237 in Th-232 + Li-7 reaction products by accelerator mass spectrometry

A. Nakajima,,[*1,*2] K. Teranishi,[*1,*3] A. Yokoyama,[*1,*4] A. Sakaguch,[*1,*5] K. Hain,[*6] R. Morita,[*1,*3] A. Seto,[*1,*4] A. Nagai,[*1,*4] D. Mori,[*1] Y. Komori,[*1] T. Yokokita,[*1] Y. Wang,[*1] and H. Haba[*1]

Neptunium-236 can be a useful tracer in the determination of Np-237, an isotope of the minor actinide Np, which exists in tiny quantities in the environment owing to its release from nuclear facilities and nuclear tests. Such determination is of practical use in various earth science fields such as surface material circulation and environmental pollution assessment.[1] The measurement of Np-237 is expected to be quantified by accelerator mass spectrometry (AMS), although an internal standard method for Np needs an appropriate spike. Chemical yield tracers for several elements are available now, but the spike for neptunium has not been developed yet. We aim to devise an efficient method for the production of Np-236 in the ground state of half-life 1.54×10^5 y as a candidate for the spike nuclide, with minimal contamination by Np-237.

In this study, Np-236 tracer production was implemented in the reaction of Th-232 + Li-7 to measure Np-237. The resulting yields of Np-236m and Np-236g were presented in the previous report.[2] The yield in the ground state (6^-) was found to be larger than that in the excited state (1^+) in the studied energy range. This demonstrates that the reaction system adopted is promising. In addition, we have to measure the isotopic ratios of Np-236g to Np-237 in the same nuclear system.

We irradiated Th foil targets with 42 MeV Li-7 ions from the RIKEN AVF cyclotron while integrating the beam current with a Faraday cup in the irradiation course. Chemical procedures were performed to isolate Np atoms from the target. Details of the procedures were described previously.[2]

For the Np-236g and Np-237 measurement, samples for AMS and inductively coupled plasma mass spectrometry (ICP-MS) were prepared through purification with UTEVA resin after waiting for Np-236m to decay out, and they were brought to the VERA facility in the University of Vienna, with which this project is in collaboration.

Figure 1 shows the preliminary isotopic ratios of Np-236g to Np-237 isotopes measured using AMS. The yield of Np-236 was found to be approximately 10 times larger than that of Np-237 in the studied energy range. The figure also shows the ratios calculated under a simple assumption with the nuclear reaction model code EMPIRE2[3] comprising various nuclear models. A large discrepancy is observed between the observation and prediction. It may be due to difficulty in the yield reproduction of used models at the energy region beyond the maximum yield energy for the products. The observation indicates that the reaction system adopted is promising thus far, although the data may need to be modified because of contamination by uranium nuclides and other nuclides with a mass number of 236.

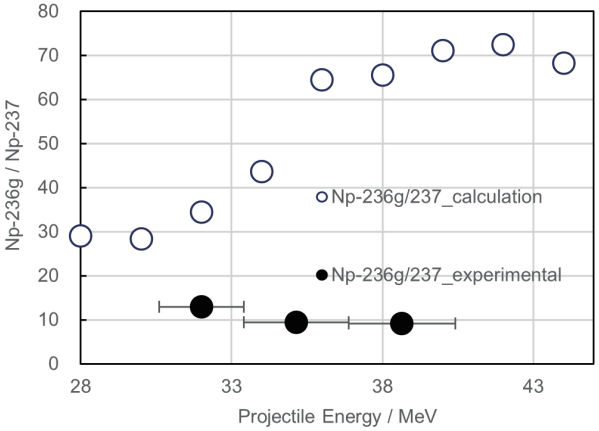

Fig. 1. Preliminary isotopic ratios of Np-236g to Np-237 in the Th-232 + Li-7 reaction system compared with the theoretical prediction. Closed circles represent the observation, while open circles indicate data from calculation.

The analysis of the result is in progress, and additional experiments including mass spectrometry are in planning. We aim to confirm the precision and reproducibility of the data in consideration of the contamination by isobars, which affects the mass measurement and is a major concern.

*1 RIKEN Nishina Center
*2 Master's Program in Chemistry, University of Tsukuba
*3 Graduate School of Natural Science and Technology, Kanazawa University
*4 Institute and College of Science and Engineering, Kanazawa University
*5 Center for Research in Isotopes and Environmental Dynamics, University of Tsukuba
*6 Faculty of Physics, Isotope Physics, University of Vienna

References

1) W. Rund, G. S. Goff, *Radionuclide in the Environment*, edited by D. A. Atwood (Wiley, 2013).
2) Y. Hayakawa *et al.*, RIKEN Accel. Prog. Rep. **53**, 179 (2020).
3) M. Herman *et al.*, Nucl. Data Sheets **108**, 2655 (2007).

Production and photon measurement of ^{229}Pa toward the observation of radiative decay of ^{229m}Th

Y. Shigekawa,[*1] T. Yokokita,[*1] Y. Komori,[*1] and H. Haba[*1]

The first excited state of ^{229}Th (^{229m}Th) has an extremely low excitation energy of ∼8.3 eV (150 nm),[1] which may enable a nuclear clock with unprecedentedly low uncertainty. So far, the radiative half-life of ^{229m}Th, which is an important parameter to develop the nuclear clock, has not yet been determined. To directly observe the radiative decay (γ-ray emission) of ^{229m}Th, the internal conversion (IC) process with a half-life of ∼7 μs[2] must be prohibited by placing ^{229m}Th in the chemical environments where the electron binding energy is higher than the excitation energy of ^{229m}Th. ^{229m}Th doped into fluoride crystals is a candidate for such chemical environments. We are aiming to dope a CaF_2 crystal with ^{229m}Th by doping with ^{229}Pa, which decays to ^{229m}Th by electron capture with a negligibly small recoil energy. Suitable doping can be realized by implanting high-energy ^{229}Pa ions into a crystal and then annealing it. In this study, we developed a method for producing ^{229}Pa ($T_{1/2}$ = 1.5 d) in the ^{232}Th$(p,4n)^{229}$Pa reaction and separating it from the target. We also measured low-energy photons from Pa isotopes on a CaF_2 crystal to evaluate the background toward the future γ-ray measurement of ^{229m}Th.

Two ^{232}Th metallic foils (thickness: 69.07 mg/cm^2, purity: 99.5%) were irradiated with a 30-MeV proton beam having an intensity of 1 μA for 10 h at the RIKEN AVF cyclotron. After the irradiation, we measured γ-ray spectra for the ^{232}Th foils and fractions resulting from the subsequent chemical separation process using a Ge detector.

The chemical separation process for one of the foils was performed as follows. First, we dissolved the foil in 2 mL of 11.3 M HCl plus 300 μL of 1 M HF and heated the solution to dryness. The sample was dissolved in 2 mL of 11.3 M HCl, following which 1.1 g of $Al(NO_3)_3 \cdot 9H_2O$ was added as a masking agent for the remaining F^- ions. After the solution was dried up and dissolved in 2 mL of 11.3 M HCl, the solution was fed into an anion-exchange column (Muromac 1X8, 100–200 mesh, ∼1.0 mL). We poured 10 mL of 11.3 M HCl into the column to elute Th isotopes, Ac isotopes, and some fission products. Next, we added 10 mL of 6 M HCl to elute Zr, following which 5 mL of 8 M HNO_3 was added to elute Zr, Mo, Ru, Sb, and Te isotopes. After we added 1 mL of 11.3 M HCl, Pa isotopes were eluted with 8 mL of 9 M HCl/0.1 M HF. The chemical yield of Pa isotopes in the whole process was 94(2)% (residual Pa isotopes were observed in the 8 M HNO_3 eluate). The radioactivity of chemically separated ^{229}Pa at the end of bombardment was evaluated to be 30(1) MBq, while those of ^{232}Pa, ^{230}Pa ($T_{1/2}$ = 17.4 d), ^{95}Zr ($T_{1/2}$ = 64.03 d), and ^{97}Zr ($T_{1/2}$ = 16.75 h), included as impurities, were 2.18(3), 0.89(4), 0.0054(7), and 0.40(2) MBq, respectively.

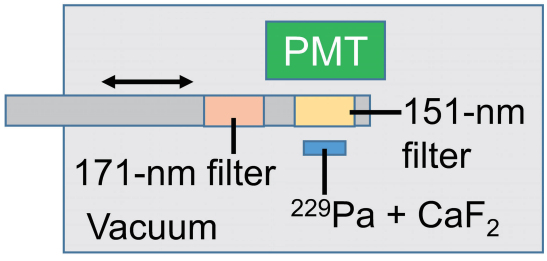

Fig. 1. Setup of the photon measurement of ^{229}Pa.

The ^{229}Pa sample dissolved with 27 M HF was dropped on a CaF_2 crystal, which was then annealed at 900°C for 1 h in a He gas flow (3 L/min). Photons from the crystal were measured with a photomultiplier (PMT, Hamamatsu R10454) in vacuum (Fig. 1). Band-pass filters for the photons of 151 ± 20 and 171 ± 20 nm (eSource Optics) placed between the crystal and the PMT were switched every 5 min. The radioactivities of ^{229}Pa, ^{230}Pa, and ^{232}Pa were 10.7(8), 35(2), and 0.381(8) kBq at the start of the measurement (11 days after the proton irradiation).

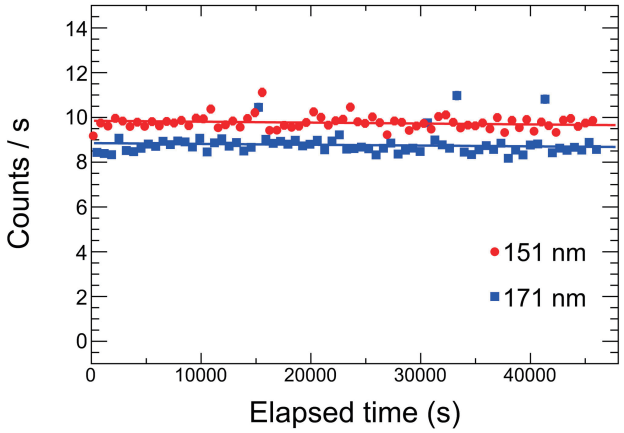

Fig. 2. Count rates of photons as a function of the elapsed time for the 151-nm (red circle) and 171-nm (blue square) filters. Red and blue lines show the decay curves of ^{230}Pa fitted to the data.

As shown in Fig. 2, the count rates of photons for both filters are ∼10 counts per second (cps), which

*1 RIKEN Nishina Center

are much higher than the dark count rate of the PMT (0.96 cps). The detected photons would originate from the Cherenkov radiation caused by the passage of beta particles though the CaF_2 crystal. The long decay time of photons (half-life >7 d) in Fig. 2 indicates that the Cherenkov photons dominantly originate from the beta decay of ^{230}Pa (0.004 photons per beta particle). If we implant 100 kBq of ^{229}Pa into a CaF_2 crystal, anneal it, and start the measurement one day after the proton irradiation, the background photons from ^{232}Pa and ^{230}Pa are estimated to be ∼30 cps, which is much higher than the estimated count rate of γ rays from ^{229m}Th (2 cps). Thus, we plan to perform the mass separation of ^{229}Pa to reduce the amount of ^{232}Pa and ^{230}Pa by a factor of >10 when we implant ^{229}Pa into a CaF2 crystal. Implanting ^{229}Pa into a crystal with an efficiency of 0.1–1% allows us to observe a growth and decay curve of photons of several cps only for the 151-nm filter, resulting in the unambiguous identification of the γ rays from ^{229m}Th.

References

1) B. Seiferle *et al.*, Nature **573**, 243 (2019); A. Yamaguchi *et al.*, Phys. Rev. Lett. **123**, 222501 (2020); T. Sikorsky *et al.*, Phys. Rev. Lett. **125**, 142503 (2020).
2) B. Seiferle *et al.*, Phys. Rev. Lett. **118**, 042501 (2017).

Measurement of extraction time and efficiency of ^{220}Rn ions using a cryogenic RF-carpet gas cell for the chemistry of superheavy elements

Y. Shigekawa,[*1] A. Yamaguchi,[*2] N. Sato,[*1] A. Takamine,[*1] M. Wada,[*3] and H. Haba[*1]

We have been developing a cryogenic RF-carpet gas cell for the gas-phase chemistry of superheavy elements (SHEs) with short half-lives (<5 s) such as ^{283}Cn (Z = 112), ^{284}Nh (Z = 113), and ^{289}Fl (Z = 114).[1] We designed and constructed the gas cell, and measured the transportation efficiency of ions from the surface of the RF carpet to its central hole (>80%) using Cs^+ ions emitted from a Cs ion source.[1] In this work, we measured the extraction time and efficiency of ions to the outlet of the quadrupole ion guide (QPIG) using ^{220}Rn ($T_{1/2}$ = 55.6 s) ions emitted from a ^{224}Ra source with recoil energy from alpha decay.

The ^{224}Ra source (45 kBq) was prepared by collecting ^{224}Ra ions recoiling out of a ^{228}Th source to the surface of a Cu foil (diameter 10 mm).[2] As shown in Fig. 1, ^{220}Rn ions recoiling out of the ^{224}Ra source placed 50 mm from the RF carpet were decelerated by the He buffer gas, extracted from the RF carpet, and transported to an Al foil (thickness 0.8 μm) via QPIG. The number of ^{220}Rn ions on the Al foil was measured by alpha-particle spectrometry using a Si detector. The extraction efficiency against a variety of voltages applied to the RF carpet and QPIG was obtained by dividing the number of ^{220}Rn ions extracted on the Al foil by that emitted from the ^{224}Ra source.

The extraction time measurement was performed by synchronously applying a pulsed voltage to the ^{224}Ra source (55 V, width 2–10 ms) and a pulsed RF voltage to the QPIG (1.6 MHz, 74 V_{pp}, width 2–100 ms). The pulsed voltage to the source creates a pulse of ^{220}Rn ions, which reach the QPIG with some delay. The extraction time can be obtained by searching the pulse

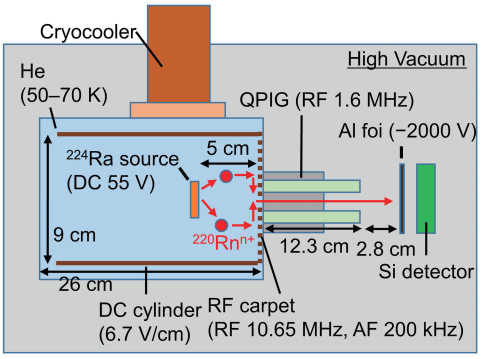

Fig. 1. Setup of the measurement of extraction time and efficiency of ^{220}Rn ions.

*1 RIKEN Nishina Center
*2 Quantum Metrology Laboratory, RIKEN
*3 Wako Nuclear Science Center (WNSC), IPNS, KEK

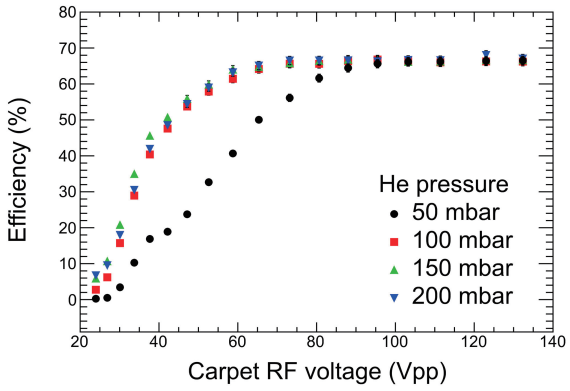

Fig. 2. Extraction efficiency of ^{220}Rn ions as a function of the RF voltage applied to the RF carpet.

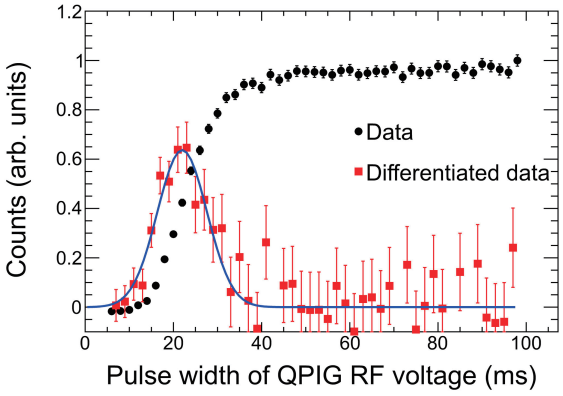

Fig. 3. Counts of ^{220}Rn ions as a function of the pulse RF voltage applied to the QPIG for a He pressure of 100 mbar (black circle). The differentiated data (red square) is fitted with a Gaussian function (blue line).

width of the QPIG RF voltage at which the ^{220}Rn counts increase.

Figure 2 shows the extraction efficiency as a function of the RF voltage applied to the RF carpet, where we find that the maximum efficiency is obtained with an RF voltage of 88 V_{pp} for every He gas pressure (50, 100, 150, and 200 mbar, room temperature equivalent). Similarly, we determined the best values for the audio-frequency voltage of the RF carpet, and the RF and DC voltages of the QPIG. We obtained an extraction efficiency of ~66% even for a He pressure of 200 mbar (Fig. 2), which is higher than the value for the RF-funnel type gas cell (5% at 70 mbar).[3]

Figure 3 shows an example of the results of the ex-

traction time measurement, where the counts of ^{220}Rn ions increase and saturate with an increase in the pulse width of the QPIG RF voltage. The differentiated data was fitted with a Gaussian function, yielding a mean extraction time of 22.0(6) ms for 100 mbar. The mean extraction times for 50, 150, and 200 mbar were determined in the same way as 6.7(4), 30.1(11), and 33.8(9) ms, respectively.

The high extraction efficiency (∼66%) and fast extraction time (<40 ms) indicate that the developed gas cell is applicable to the chemistry of SHEs with half-lives of less than 100 ms at low production rates. We plan to develop a gas chromatographic apparatus connected to the gas cell, and perform online experiments.

References

1) Y. Shigekawa *et al.*, RIKEN Accel. Prog. Rep. **53**, 168 (2020).
2) Y. Shigekawa *et al.*, Rev. Sci. Instrum. **87**, 053508 (2016).
3) C. Droese *et al.*, Nucl. Instrum. Methods Phys. Res. B **338**, 126 (2014).

Anion-exchange behavior of Db in HF/HNO_3 solution

M. Kato,[*1] S. Adachi,[*2] A. Toyoshima,[*3] K. Tsukada,[*4] M. Asai,[*4] T. Yokokita,[*5] Y. Komori,[*5] Y. Wang,[*5] Y. Shigekawa,[*5] D. Mori,[*5] H. Haba,[*5] A. Kashihara,[*2] A. Nakajima,[*2] K. Tokoi,[*6] Y. Suzuki,[*2] K. Nishizuka,[*2] and K. Sueki[*7]

The superheavy elements with atomic number ≥104 are located in the 7th period of the periodic table. Because of the relativistic effects caused by the large positive charge of their atomic nuclei, they are expected to have different chemical properties from those of lighter homologues. However, since these elements have very short half-lives and low production rates, it is difficult to reveal their chemical properties.

The aqueous chemistry of Db was studied in comparison with its lighter homologues Nb and Ta and the pseudohomologue Pa. Previous studies on the aqueous chemistry of the fluoride complex of Db suggested that Db would form $[DbOF_4]^-$ like Nb or $[PaOF_5]^{2-}$ and/or $[PaF_7]^{2-}$ like Pa, but not $[DbF_6]^-$ like Ta.[1,2] However, there was no significant difference in the K_d values between Nb and Pa in the solutions in which Db anion-exchange experiments were performed. Therefore, it was not possible to determine whether Db was similar to Nb or Pa, and it is also difficult to determine the chemical species of the fluoride complex of Db.

In our previous work, we revealed that there is a large difference in the K_d values between Nb and Pa in the mixture solution of HF and 1.0 M HNO_3.[3] The different K_d values for Nb and Pa imply that they have different chemical species. Thus, it is considered that the chemical species of Db can be determined by obtaining the K_d value of Db in this mixed solution and comparing it with those of Nb and Pa. In this study, we performed online anion-exchange experiments of Db in HF/1.0 M HNO_3 mixture solution using automated rapid chemistry apparatus (ARCA) to identify the chemical species of the fluoride complex of Db.

The online anion-exchange chromatography of ^{262}Db, ^{88g}Nb, and ^{170}Ta was performed. The nuclides were produced in the ^{248}Cm(^{19}F, xn), ^{nat}Ge(^{19}F, nx), and ^{nat}Gd(^{19}F, nx) reactions, respectively, at the RIKEN K70 AVF cyclotron. In the ^{262}Db and ^{170}Ta experiments, the products were transported by the He/KCl gas-jet system and were deposited on the collection site of ARCA for 120 s. Subsequently, the products were dissolved in a solution of 14.5 M HF/1.0 M HNO_3. The solution was fed onto the micro chromatographic column (1.6 mm *i.d.* × 7 mm) filled with anion-exchange resin (MCI GEL CA08Y) at a flow rate of 1.0 mL/min. The effluent was collected on two Ta disks as fractions 1 and 2. The remaining products in the column were stripped with a solution of 0.015 M HF/6.0 M HNO_3 and collected on another two Ta disks as fractions 3 and 4.

*1 Master's Program in Education, University of Tsukuba
*2 Graduate School of Science and Tchnology, University of Tsukuba
*3 Institute for Radiation Sciences, Osaka University
*4 Japan Atomic Energy Agency
*5 RIKEN Nishina Center
*6 Graduate School of Science, Osaka University
*7 Faculty of Pure and Applied Sciences, University of Tsukuba

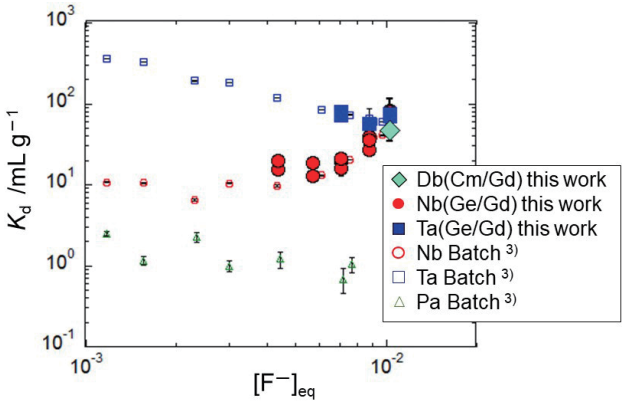

Fig. 1. Distribution coefficients, K_d, of Nb, Ta, Pa, and Db.

These disks were rapidly evaporated to dryness and subjected to α-particle measurements with an automated rapid α/SF detection system.[4] After the measurement, γ-rays of ^{170}Ta were monitored with Ge detectors.

In the ^{88g}Nb and ^{170}Ta experiments, the transported reaction products were deposited on the collection site of ARCA and were dissolved in a solution of 4.4–14.5 M HF/1.0 M HNO_3. Subsequently, the solution was fed onto the microcolumn under the same experimental conditions as those for Db. The effluent fractions were collected in 7 polypropylene(PP) tubes, and the remaining products were collected in another PP tube. These fractions were assayed by γ-ray spectrometry with a Ge detector.

We conducted 350 anion-exchange experiments and observed 5α events from ^{262}Db. Its adsorption probability on the resin was determined by the α counts found in fractions 1–4. The K_d value of Db was determined using the relation between K_d and the adsorption probability (%ads) of Nb and Ta studied in our previous work.[3] Figure 1 shows the K_d values of Nb, Ta, Pa, and Db. The K_d value of Db is close to that of Nb, while it is significantly larger than that of Pa. In our previous study, we found a large difference in the K_d value trends between Nb and Pa. The increase in the K_d value of Nb indicates a change in the chemical species from $[NbOF_4^-]$ to $[NbF_6^-]$. In contrast, the K_d value of Pa decreased monotonically, implying that the Pa species retains its form in this $[F^-]$ region. The present result suggests that Db is similar to the behavior of Nb, and the chemical species of Db chage from fluoro-oxo complex to fluoride like Nb.

In the near future, we will perform further anion-exchange experiments to observe the variation in K_d values of Db and identify the fluoride complex of Db.

References

1) K. Tsukada *et al.*, Radiochim. Acta, **97**, 83 (2009).
2) Y. Kasamatsu *et al.*, Chem Letts, **38**, 1084 (2009).
3) S. Adachi *et al.*, RIKEN Accel. Prog. Rep. **53**, 162 (2020).
4) H. Haba *et al.*, RIKEN Accel. Prog. Rep. **45**, 204 (2012).

Anion exchange of Rf in H_2SO_4 using the batch-type solid-liquid extraction apparatus AMBER

T. Yokokita,[*1] Y. Kasamatsu,[*2] E. Watanabe,[*2] Y. Komori,[*1] Y. Shigekawa,[*1] Y. Wang,[*1] D. Mori,[*1] H. Ninomiya,[*2] S. Hayami,[*2] K. Tonai,[*2] K. Ghosh,[*1] A. Shinohara,[*2] and H. Haba[*1]

The relativistic effect on orbital electrons is relatively more pronounced for heavy elements. In particular, the chemical properties of superheavy elements (SHEs) with atomic number $Z \geq 104$ are expected to deviate from the periodicity of their lighter homologues in the periodic table. Thus, it is important and interesting to investigate the chemical properties of SHEs. So far, ion-exchange experiments on SHEs have been conducted to determine the distribution coefficients (K_d), which are defined as the ratio of the elemental concentrations of the two phases.[1] However, those values at equilibrium have not been obtained in most studies. To obtain the K_d values at equilibrium, the batch-type solid-liquid extraction apparatus called AMBER was developed,[2] and the equilibrium K_d values on the chloride complexation of Rf were successfully obtained in an Aliquat 336/HCl system.[3]

To study the sulfate complexation of Rf, we plan to perform anion-exchange experiments of Rf and its homologous elements. In our previous study, by using AMBER, we obtained the K_d value of Rf in 0.11 M H_2SO_4.[4] The obtained K_d value of Rf is ~10 mL g^{-1}, probably indicating that Rf does not form anionic species or that counter ions of HSO_4^- and SO_4^{2-} inhibit the adsorption of Rf on the anion-exchange resin. In this study, to reduce the effect of counter ions, we performed an anion-exchange experiment of Rf in 0.060 M H_2SO_4, which is lower than 0.11 M.

In the anion exchange of Rf and Hf, we simultaneously produced ^{261}Rf ($T_{1/2}$ = 68 s) and ^{169}Hf ($T_{1/2}$ = 3.24 min) by the bombardment of a mixture of ^{248}Cm and natGd with an ^{18}O beam delivered from the K70 AVF cyclotron at RIKEN. The products were transported to a chemistry room by a He/KCl gas-jet system. The transported products were deposited on the collection site of AMBER's dissolution equipment for 3 min and dissolved with 0.24 mL of 0.060, 0.30, and 0.46 M H_2SO_4. The solution sample was injected into a chemical reaction container containing the anion-exchange resin (MCI GEL CA08Y). After shaking the container with a shaker for 10, 30, and 90 s, only the solution phase was discharged from the container through a PTFE filter with compressed air. The discharged solution was collected in a Ta disk on the round table of an automated rapid α/SF detection system[5] and evaporated quickly to dryness using hot He gas and a halogen heat lamp. Subsequently, the Ta disk was transferred to the position under a Si PIN photodiode detector, and α-particle measurement was performed. After the α-particle measurement, the γ-ray was measured with a Ge detector to monitor ^{169}Hf. We also performed control experiments with 10-s shaking without the resin to determine the standard radioactivity of the solution sample. The K_d values were determined from the radioactivity in the resin and solution phases, the volume of the solution phase, and the mass of the dry resin.

We conducted 390 anion-exchange and 92 control cycles, and observed a total of 73 α events from the decay of ^{261}Rf and its daughter nuclide ^{257}No ($T_{1/2}$ = 24.5 s), including 10 time-correlated α–α correlations. The radioactivity ratios of ^{261}Rf between the resin and solution phases were estimated from the α events. In 0.060 M H_2SO_4, the K_d values of Hf were constant in all the studied time ranges, indicating that equilibrium in the anion exchange of Hf was accomplished within 10 s. Those of Rf were also constant in all the time ranges studied, yielding values of approximately 20 mL g^{-1}. This indicates that Rf is not adsorbed on the resin.

We also obtained the K_d values of Rf, Zr, Hf, and Th in 0.060–0.46 M H_2SO_4. The obtained K_d values of Rf are low ($\leq$25 mL g^{-1}) in the entire studied H_2SO_4 concentration range. In contrast, the K_d values of Zr, Hf, and Th are $\geq$70 mL g^{-1} at 0.060 M H_2SO_4. These results suggest that Rf does not form anionic species and that Zr, Hf, and Th form anionic species in this studied condition. The K_d values at 0.060 M H_2SO_4 follow the order of Zr > Hf $\gg$ Th > Rf, and this sequence is consistent with the trend predicted by theoretical calculation.[6] On the other hand, the sequence of K_d values is Th > Rf > Hf $\geq$ Zr in the cation exchange in the H_2SO_4/HNO_3 system.[7] In the future, we plan to discuss the chemical species of Rf in this studied condition from the obtained anion-exchange behavior of Rf, Zr, Hf, and Th and chemical species of Zr, Hf, and Th.

References
1) Y. Nagame *et al.*, Nucl. Phys. A **944**, 614 (2015).
2) Y. Kasamatsu *et al.*, Radiochim. Acta **103**, 513 (2015).
3) T. Yokokita *et al.*, Dalton Trans. **45**, 18827 (2016).
4) T. Yokokita *et al.*, RIKEN Accel. Prog. Rep. **53**, 165 (2020).
5) H. Haba *et al.*, RIKEN Accel. Prog. Rep. **45**, 204 (2012).
6) V. Pershina *et al.*, Radiochim. Acta **94**, 407 (2006).
7) Z. J. Li *et al.*, Radiochim. Acta **100**, 157 (2012).

*1 RIKEN Nishina Center
*2 Graduate School of Science, Osaka University

Online anion-exchange experiment of Zr in H_2SO_4 for the chemical study of Rf in H_2SO_4

T. Yokokita,[*1] Y. Shigekawa,[*1] Y. Wang,[*1] Y. Komori,[*1] Y. Kasamatsu,[*2] E. Watanabe,[*2] and H. Haba[*1]

The chemical properties of superheavy elements (SHEs) with atomic number $Z \geq 104$ are expected to deviate from the periodicity of their lighter homologues in the periodic table. Thus, chemical studies on SHEs are interesting. These elements are produced at accelerators by using heavy-ion-induced nuclear reactions. The production rates of these elements are low, and their half-lives are short ($T_{1/2} \leq 1$ min). Thus, the chemical studies of SHEs are conducted on a single-atom basis. Therefore, performing, the chemical experiment of SHEs is difficult. Thus far, the chemical properties of SHEs have been discussed by comparing them with those of their homologous elements.[1)]

In the solution chemistry of SHEs, ion exchange and solvent extraction are often performed.[1)] To study the sulfate complexation of Rf, we plan to perform anion-exchange experiments of Rf along with its homologous elements. By using the batch-type solid-liquid extraction apparatus called AMBER[2)], we measured the K_d values of Rf in 0.060–0.46 M H_2SO_4.[3,4)] In our previous study, to obtain the comparison data for Rf, we performed an online anion-exchange experiment of Zr and Hf by using AMBER.[5)] However, the K_d values of Zr had large errors, because the radioactivity of ^{85}Zr was very low. In this work, we re-examined the online anion-exchange behavior of ^{89m}Zr with higher radioactivities.

^{89m}Zr was produced in the ^{89}Y$(d, 2n)^{89m}$Zr reaction by using the K70 AVF cyclotron at RIKEN. The nuclear reaction products were transported to a chemistry room by a He/KCl gas-jet system. The transported products were deposited on the collection site of the AMBER's dissolution equipment for 1 min and were then dissolved with 0.23 mL of 0.060, 0.11, 0.26, 0.30, 0.46, and 0.72 M H_2SO_4. The solution sample was injected into a chemical reaction container containing 1.4–3.8 mg of an anion-exchange resin (Mitsubishi Chemical Co., MCI GEL CA08Y). After shaking the container with a shaker for 10, 30, and 90 s, only the solution phase was discharged from the container by using a PTFE filter with compressed air. The discharged solution was collected in a PP tube, and was assayed by γ-ray spectroscopy. We also performed control experiments with 10, 30, and 90 s shaking without the resin to determine the standard radioactivity of the solution sample. The K_d values were determined from the following equation:

$$K_d = A_r V_s / A_s w_r = (A_c - A_s) V_s / A_s w_r \quad (1)$$

*1 RIKEN Nishina Center
*2 Graduate School of Science, Osaka University

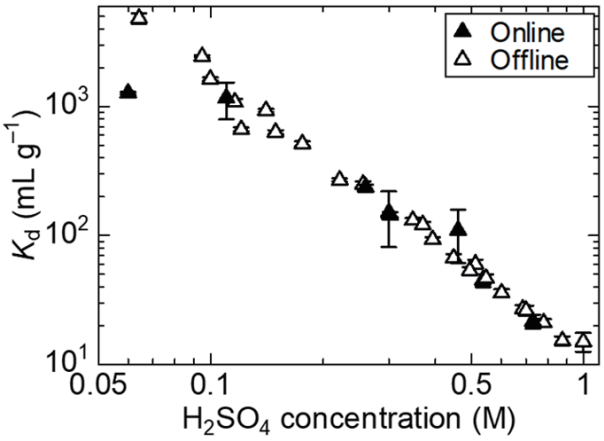

Fig. 1. The K_d values of Zr in anion exchange as a function of H_2SO_4 concentration.

where A_r, A_s, and A_c are radioactivities of the resin, the solution, and the control solution, respectively; V_s is the volume (mL) of the solution; and wr is the mass of the dry resin (g).

Figure 1 shows the H_2SO_4-concentration dependence of the K_d values of Zr in the online and offline experiments. The K_d values of Zr in the online experiment are in agreement with those in the offline experiment within the error range in 0.11–0.72 M H_2SO_4. This indicates that the K_d values of Zr in equilibrium are obtained in the online experiment at these H_2SO_4 concentrations. However, at 0.060 M H_2SO_4 the K_d value of Zr in the online experiment was lower than that in the offline experiment. A probable reason for this disagreement is that the K_d value at this low concentration is too high to be determined with the AMBER system. Another possibility is that the chemical reaction time is not sufficient for the anion-exchange equilibrium. Therefore, it is important to directly investigate the reaction time dependence of the anion-exchange behavior of Rf to confirm the anion-exchange reaction equilibrium of Rf.

From this work, we obtained the comparison data for Rf. We will discuss the sulfate complexation of Rf based on the anion-exchange behavior of Rf, Zr, Hf, and Th in a separate study.[4)]

References

1) A. Türler, V. Pershina., Chem. Rev. **113**, 1273 (2013).
2) Y. Kasamatsu *et al.*, Radiochim. Acta **103**, 513 (2015).
3) T. Yokokita *et al.*, RIKEN Accel. Prog. Rep. **53**, 165 (2020).
4) T. Yokokita *et al.*, in this report.
5) T. Yokokita *et al.*, RIKEN Accel. Prog. Rep. **52**, 187 (2019).

Solvent extraction of Zr and Hf from HCl by Aliquat 336 using a flow-type extraction apparatus toward online chemical studies of element 104, rutherfordium†

Y. Kasamatsu,[*1] N. Kondo,[*1] K. Nakamura,[*1] Y. Kuboki,[*2,*3] H. Ninomiya,[*1] Y. Shigekawa,[*1] E. Watanabe,[*1] Y. Yasuda,[*1] K. Toyomura,[*1] M. Nagase,[*1] T. Yokokita,[*1,*3] Y. Komori,[*1,*3] H. Haba,[*3] T. Yoshimura,[*4] H. Itabashi,[*5] and A. Shinohara[*1]

Chemical studies of the transactinide (superheavy) elements with atomic numbers $Z \geq 104$ are imperative for systematic understanding of all the elements in the periodic table. In particular, the influence of relativistic effects on orbital electrons of superheavy elements could cause their unique chemical properties. For chemical experiments on superheavy elements which can be produced only by nuclear reactions, repetitive or flow-type rapid chemistry apparatus connected with a gas-jet system which rapidly transports the nuclear reaction products from the accelerator room to the chemistry laboratory ("online" experiment) is required. The chemical properties of heavy elements are discussed on the basis of comparison of their behaviors with those of the corresponding homologues.

We plan to apply a flow-type solvent extraction apparatus, having a chemical reaction unit which shortens the time required for equilibrium, to transactinide chemistry in order to obtain equilibrium D values for short-lived transactinide elements. Thus, we developed such a solvent extraction apparatus for the online transactinide chemistry and determined the conditions to rapidly obtain equilibrium D values for Zr and Hf toward the extraction of ^{261}Rf. In addition, we carried out the online extraction experiment as a model experiment for Rf using the developed apparatus.

First of all, we carried out the solvent extraction of Zr and Hf by the conventional shaking (batch) method to obtain the equilibrium D values using ^{88}Zr and ^{175}Hf tracers. The D values were determined from the concentration ratio of the tracers between organic and aqueous solutions.

Then, we developed an online flow-type solvent extraction apparatus: flow Injection Solvent Extraction apparatus for heavy elements (ISE) for rapid solvent extraction and phase separation toward the extraction of 68-s ^{261}Rf. The developed extraction apparatus is equipped with a reactor tube filled with PTFE chips to mix aqueous and organic solutions thoroughly (extraction unit; EU).[1] By this unit, the diffusion length of metal complexes between the aqueous and organic solutions decreases, which is expected to aid the rapid achievement of equilibrium in the extraction reactions.

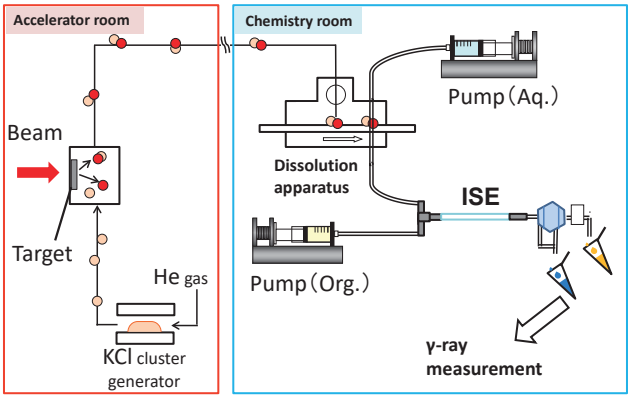

Fig. 1. Schematic diagram of online solvent extraction experiment for heavy elements.

For rapid phase separation between aqueous and organic solutions, a flow-type phase separation unit (PSU) using a PTFE membrane filter (pore size: 0.8 μm) is set downstream of the EU.[2] The online extraction experiment employing the ISE was carried out using the ^{89g,m}Zr and ^{173}Hf nuclides produced at the AVF cyclotron in RCNP as shown schematically in Fig. 1.

The D values obtained with ISE in 7.8 M HCl are clearly lower than the equilibrium D values, suggesting that the equilibrium D values cannot be obtained in 7 M HCl. When the extraction was carried out in 9.3 and 11.2 M HCl using a 30-cm-long EU packed with 250–500 μm PTFE chips, the D values obtained with ISE are all equivalent with the equilibrium values, indicating that the extraction reactions rapidly reach equilibrium state under these conditions. It was also found that the elution of almost all the isotopes from PSU was accomplished within 55 s. Based on this time information, the time taken for extraction and evaporation for α measurements in Rf experiment can be estimated to be <2 min, which is sufficiently fast in comparison with the previous experiment of ^{261}Rf (∼100 s).

A linear relationship was observed between the logarithm of D value and the logarithm of Aliquat 336 concentration for both Zr and Hf, suggesting that the extracted chloride complex determined from the slopes (net charge) could be $[MCl_6]^{2-}$. Similar discussion can be made for Rf, which will help to understand the chloride complexation of Rf.

† Condensed from the article in Solvent Extr. Ion Exch. **38**, 318 (2020)

*1 Graduate School of Science, Osaka University
*2 National Institute of Technology, Ibaraki College
*3 RIKEN Nishina Center
*4 Radioisotope Research Center, Osaka University
*5 Faculty of Engineering, Gunma University

References

1) H. Itabashi, Y. Mesuda, J. Flow Inject. Anal. **20**, 193 (2003).
2) S. Motomizu, M. Oshima, Analyst **112**, 295 (1987).

Cation- and anion-exchange behavior and UV-vis spectroscopy of Zr in HBr for chemical characterization of bromide complexes of Rf

T. Yokokita*1 and H. Haba*1

The chemical properties of superheavy elements (SHEs) with atomic number $Z \geq 104$ deviate from the periodicity of their lighter homologues in the periodic table because of the strong relativistic effects on valence electron shells in these heavy atoms. Therefore, chemical research studies on these elements are intriguing and of great importance. However, the chemical study of these elements is very difficult because the half-lives of these elements are short and the production rates of these elements are low.[1)]

Anion-exchange studies in HF and HCl have been reported for element 104, Rf.[2,3)] The observed adsorption strength on the anion-exchange resin is Zr ≈ Hf > Rf in 1.9–13.9 M HF[2)] and Rf > Zr > Hf in 7.0–9.0 M HCl.[3)] We are interested in the anion-exchange result of Rf in HBr because the adsorption sequence is different between HF and HCl media. There is one report on the bromide complex of Rf.[4)] In this report, the solvent extraction of Rf and its homologous elements were performed. Rf was not extracted from 7.75–9.0 M HBr, while Zr and Hf were extracted. Further study on the bromide complexation of Rf is required to understand the halide complexation of Rf in detail, In this work, cation and anion exchanges of Zr were performed to obtain the comparison data for Rf. The UV-vis spectra of Zr in HBr solution was measured to discuss the ion-exchange behavior of Zr.

The ^{88}Z was produced in the ^{89}Y$(d, 3n)$ reaction using the RIKEN AVF cyclotron; further, ^{88}Zr was purified by an anion-exchange method. The cation- and anion-exchange of Zr were performed by employing the batch method in 1.1–8.8 M HBr, which is the same procedure an in Ref. 5). Further, control experiments without the resin were performed to determine the standard radioactivity of the solution sample. The distribution coefficient (K_d) was obtained according to $K_d = (A_c - A_s)V/A_s w$; here, A_c and A_s denote the radioactivities in the control and exchanged solutions, respectively. V denotes the volume of the solution, and w denotes the weight of the ion-exchange resin.

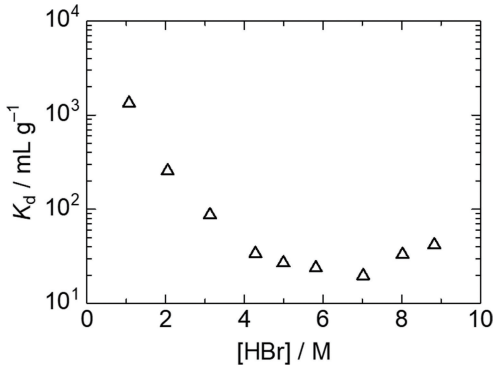

Fig. 1. Variation of the K_d values of Zr on the cation exchange resin as a function of [HBr].

*1 RIKEN Nishina Center

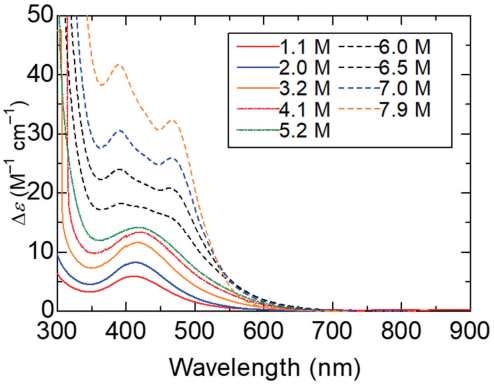

Fig. 2. UV-vis spectra of Zr in 1.1–7.9 M HBr.

The UV-vis spectra of 0.016–0.33 M Zr in the 1.1–7.9 M HBr solution were measured with UV-vis spectrophotometer (JASCO Co., V-730) to obtain the structural information on the Zr species in HBr.

In the anion exchange, the K_d values of Zr are low (< 10 mL g^{-1}) for all [HBr] studied in this work, indicating which implies Zr does not form anionic species at 1.1–8.8 M. This anion-exchange behavior is consistent with that using macro amounts of Zr.[6)] The variation of the K_d values of Zr on the cation exchange resin are shown in Fig. 1. The K_d values decrease with an increase in [HBr] in the range 1.1–7.0 M, and they increase above 7.0 M.

The UV-vis spectra of Zr in HBr solution are shown in Fig. 2. At 1.1–5.2 M, one adsorption band is seen at λ_{max} = 410–421 nm, and its molar adsorption coefficient ($\Delta\varepsilon$) increases with an increase of [HBr]. Above 6.0 M, the UV-vis spectra shows two adsorption bands at λ_{max} = 390–391 and 463–467 nm, and both increase with an increase in [HBr], which indicates that the dominant Zr species is changed. This spectral change at 6.0 M is reasonably reflected on the variation of the K_d values in Fig. 1: bromide complexes are increasingly formed with an increase in [HBr], and above 7.0 M, a different bromide complex is adsorbed on the cation-exchange resin. It is possibility that the oxybromide complex of Zr is protonated and the cationic species of Zr increases.

In the future, we plan to measure the Raman spectra of $ZrBr_4$ in the HBr solution and the mass spectra of the solvent extracted Zr species to determine the Zr species in the HBr solution.

References

1) A. Türler, V. Pershina., Chem. Rev. **113**, 1273 (2013).
2) H. Haba *et al.*, J. Am. Chem. Soc. **126**, 5219 (2004).
3) H. Haba *et al.*, J. Nucl. Radiochem. Sci. **3**, 143 (2002).
4) D. C. Kacher *et al.*, Radiochim. Acta **75**, 127 (1996).
5) T. Yokokita *et al.*, RIKEN Accel. Prog. Rep. **53**, 164 (2020).
6) *Gmelin Handbuch der Anorganishchen Chemie Uranium Suppl.* Vol. D3, edited by R. Warncke (Springer-Verlag, Berlin, Heidelberg, New York, 1982).

Solvent extraction of Fr and Cs with calix[4]arene-bis(benzocrown-6)

Y. Komori*1 and H. Haba*1

Francium (Fr) is the heaviest alkali metal, with the atomic number 87. It is one of the least-studied elements among the naturally occurring elements because all its isotopes are short-lived. The half-life of its longest-lived isotope, ^{223}Fr, is only $T_{1/2}$ = 21.8 min. Owing to experimental difficulties, the chemical properties of Fr have not been studied in detail so far. We aim to clarify the chemical bonding nature of Fr, which is influenced by relativistic effects, through complex formation studies of Fr. For that purpose, we performed solvent extraction experiments on ^{212}Fr ($T_{1/2}$ = 20 min) with several crown ethers and compared the results with those on ^{137}Cs ($T_{1/2}$ = 30.1 y).[1] We found that the distribution ratios (D) of Fr and Cs are almost the same, although the D values of Cs are slightly higher than those of Fr in the extraction with dibenzo-21 crown-7 (DB21C7). Haverlock *et al.* examined the complex formation of Fr^+ with calix[4]arene-bis(benzocrown-6) (BC6B) in 2003.[2] The D values of Fr are almost one order of magnitude higher than those of Cs. Such a large difference is surprising because the ionic radius of Fr (173 pm[3]) is close to that of Cs (167 pm[4]). However, the mechanism for the large difference has not been clarified yet. The higher affinity of BC6B for Fr than for Cs is interesting and important to understand the chemical properties and chemical bonding of Fr. In this work, we reinvestigated the solvent extraction behavior of Fr and Cs with BC6B to confirm the large difference between Fr and Cs.[2]

We used ^{221}Fr ($T_{1/2}$ = 4.8 min) produced as the α-decay daughter of ^{225}Ac ($T_{1/2}$ = 9.9 d). First, we prepared an ^{225}Ac/^{221}Fr generator. 4 MBq of ^{225}Ac was dissolved in 1 mL of 0.01 M HNO_3. It was loaded onto an LN resin column (100–150 μm; φ5 mm × H10 mm). ^{225}Ac was adsorbed on the LN resin, and its daughter nuclide ^{221}Fr was generated inside the column. ^{221}Fr was repetitively eluted with 0.5 mL of 0.01 M HNO_3 after its growth. The yield of ^{221}Fr was ≥98% with one-time elution. 500 Bq of ^{137}Cs dissolved in 5 μL of H_2O was added into the ^{221}Fr solution. The solution was dried up, following which ^{221}Fr and ^{137}Cs were dissolved in 1.4 mL of 10^{-4}–3 M $NaNO_3$ aqueous solutions to achieve ^{221}Fr and ^{137}Cs concentrations of ~10^{-13}–10^{-12} M and ~10^{-10} M, respectively. 700 μL of this aqueous solution was shaken for 5 min together with an equal volume of an organic phase, 1.5×10^{-3} M BC6B in 1,2-dichloroethane. After centrifugation, 500 μL of each phase was subjected to γ-ray spectrometry with Ge detectors to determine the D values as $D = [M^+]_{organic}/[M^+]_{aqueous}$, where M denotes ^{221}Fr or ^{137}Cs. We also investigated the D values of Cs under almost the same experimental condition as Haverlock *et al.*[2] by dissolving ^{221}Fr and ^{137}Cs with 10^{-4}–3 M $NaNO_3$/10^{-4} M $CsNO_3$ aqueous solutions.

The time required for Fr and Cs to reach extraction equilibrium was confirmed to be less than 1 min, which agrees with the results of Haverlock *et al.*[2] Figure 1 shows the D values of Fr and Cs as a function of $NaNO_3$ concentration. Closed symbols indicate the D values from the 10^{-4}–3 M $NaNO_3$ aqueous solutions, and open ones indicate those from 10^{-4}–3 M $NaNO_3$/10^{-4} M $CsNO_3$ aqueous solutions. The D values of Fr and Cs are comparable in both the solutions, although the D values of Cs are slightly higher than those of Fr. These results are reasonable when considering the similar ionic radii of Fr and Cs and our previous results obtained using crown ethers.[1] In the 10^{-4}–3 M $NaNO_3$/10^4 $CsNO_3$ aqueous solutions, however, the D values of both Fr and Cs are smaller by factors of 2 to 14 than those in the 10^{-4}–3 M $NaNO_3$ aqueous solutions. This might be because macro amounts of Cs (10^{-4} M) inhibit the extraction of Fr and Cs, although an excess amount of BC6B exists in the extraction system (the concentration ratio of [Cs]:[BC6B] = 1:15 Note that our D values of Fr from 10^{-4}–3 M $NaNO_3$ aqueous solutions and those of Cs from 10^{-4}–3 M $NaNO_3$/10^{-4} M $CsNO_3$ aqueous solutions are consistent with those reported by Haverlock *et al.*[2] Because Haverlock *et al.*[2] independently obtained the D values of Fr and Cs using the ^{221}Fr tracer and 10^{-4} M $CsNO_3$, respectively, the large difference between the D values of Fr and Cs was observed.

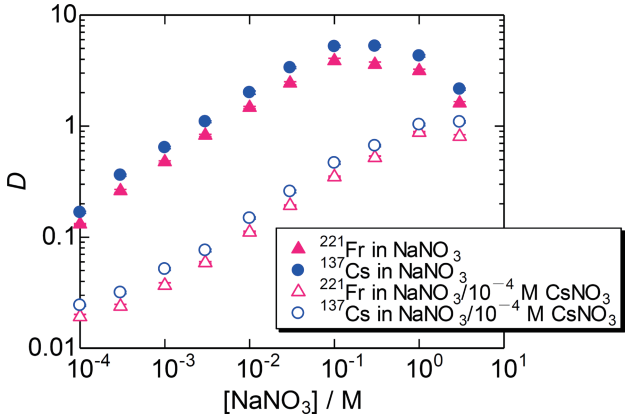

Fig. 1. Variation of D values of Fr and Cs as a function of $NaNO_3$ concentration [$NaNO_3$] in their extraction from 10^{-4}–3 M $NaNO_3$ and 10^{-4}–3 M $NaNO_3$/10^{-4} M $CsNO_3$ aqueous solutions into 1.5×10^{-3} M BC6B in 1,2-dichloroethane.

The slightly higher D values of Cs than those of Fr using BC6B are similar to those using DB21C7.[1] The reason of the order of the D values of Cs > Fr in the extraction with BC6B and DB21C7 is unclear at this moment. Quantum chemistry calculations for Fr as well as Cs are needed to interpret the experimental results and to discuss the electronic state and chemical bonding nature of Fr.

*1 RIKEN Nishina Center

References

1) Y. Komori *et al.*, RIKEN Accel. Prog. Rep. **52**, 185 (2019).
2) T. J. Haverlock *et al.*, J. Am. Chem. Soc. **125**, 1126 (2003).
3) L. H. Delmau *et al.*, J. Phys. Chem. B **117**, 9258 (2013).
4) L. H. Ahrens, Geochim. Cosmochim. Acta **2**, 155 (1952).

Solvent extraction and speciation of astatine species via thin layer chromatography

S. Maruyama,[*1] K. Aoi,[*1] Y. Nagai,[*2] K. Washiyama,[*3] A. Yokoyama,[*2,*4] I. Nishinaka,[*5] Y. Wang,[*4] and H. Haba[*4]

The short path length and high linear energy transfer of α particles are expected to enable targeted alpha therapy for the treatment of cancer. A promising nuclide among various α emitters is ^{211}At with a half-life of 7.21 h, which has gained prominence owing to its appropriate half-life for labelling and drug pharmacokinetics and potential to synthesize labelled compounds as a halogen element. This has motivated several preclinical studies on At chemistry.[1] However, the successive chemical processes for the general use of At chemistry have not been understood well. One of the difficulties in At chemistry is the coexistence of several At species in a sample. For instance, the species of At^-, AtO_3^-, and AtO_4^- are identified in some solutions via thin layer chromatography (TLC).[2] This makes the processes complex, and the species need to be adjusted by varying the redox potential, hydrogen ion concentration, and other factors for appropriate preparation of At solutions.

We aimed to study At species in diisopropyl ether (DIPE) solvent, which was shown to extract cationic species of At in a previous study.[3] Speciation of At was performed via TLC similar to the method in Ref. 2) but in an argon atmosphere, to allow preservation of the species during the drying and development time for the TLC.

In this study, ^{211}At was produced via the ^{209}Bi$(\alpha, 2n)$ reaction at the RIKEN AVF cyclotron and delivered to Kanazawa University. The irradiated Bi target was dissolved in 3 mL of 6 M HNO_3 and mixed with an appropriate amount of H_2O to prepare 1 M HNO_3 solution,

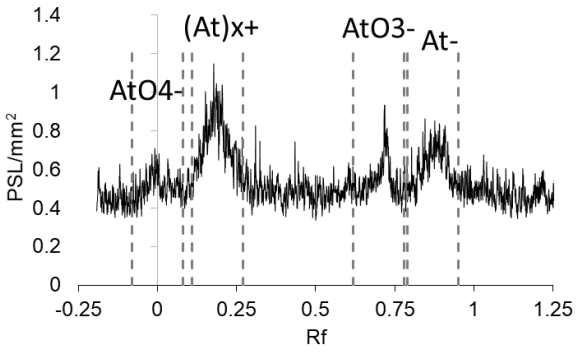

Fig. 1. TLC chromatogram of At species extracted from 9 M HCl.

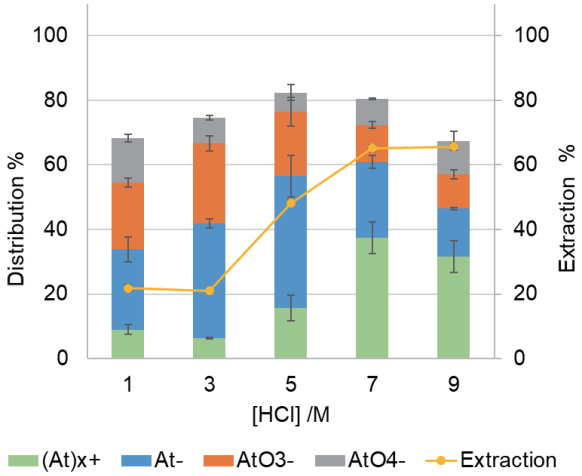

Fig. 2. Distributions of At species extracted to DIPE by TLC and their extraction ratios.

7 mL of which was used to extract the ^{211}At nuclide into 7 mL of dodecane solvent.

Aliquots of the dodecane solution were subjected to back extractions into several solutions of various HCl concentrations ranging from 1 M to 9 M. Approximately 0.5 mL of each HCl solution was subject to solvent extraction with 0.5 mL of DIPE. TLC was performed on 10 μL of each DIPE solution to determine the ^{211}At species.

Figure 1 displays the TLC chromatogram showing a new species at approximately $R_f = 0.2$, which was not found in an open air experiment, in addition to the At^-, AtO_3^-, and AtO_4^-. Figure 2 demonstrates the compositions of the At species, except for the continuum composition deduced from the TLC chromatograms, in Ref. 2), and the At extraction rates dependent on the HCl concentration. The new species increases with the increase in the HCl concentration and the extraction rate. Therefore, the species is considered to be a cation of At based on a previous study.[3]

We are in planning on applying the TLC technique to other extraction systems to identify extracted At species and clarify the mechanism of At extraction. Such information will be useful to construct chemical processes for the general use of At chemistry.

*1 Graduate School of Natural Science and Technology, Kanazawa University
*2 Institute and College of Science and Engineering, Kanazawa University
*3 Fukushima Global Medical Science Center, Fukushima Medical University
*4 RIKEN Nishina Center
*5 Quantum Beam Science Research Directorate, National Institutes for Quantum and Radiological Science and Technology

References

1) F. Guérard, J. -F. Gestin, M. W. Brechbiel, Cancer Biother. Radiopharm. **28**, 1 (2013).
2) I. Nishinaka *et al.*, J. Radioanal. Nucl. Chem. **318**, 897 (2018).
3) T. Taniguchi, Master thesis of Graduate School of Natural Science and Technology, Kanazawa University (2015).

^{99}Ru and ^{57}Fe Mössbauer spectroscopic studies of $Na_2Ru_{1-x}FexO_3$ of sodium-ion battery electrode (2)

K. Hamano,[*1,*2] Y. Kobayashi,[*1,*2] H. Haba,[*2] and H. Ueno[*2]

Sodium-ion batteries have the potential to be the next-generation batteries to replace lithium-ion batteries owing to the abundance of its raw materials. Na_2RuO_3 is a kind of Na-excess layered oxide and is promising as a cathode material for Na-ion batteries.[1)] In this study, we demonstrate the oxidation states and the coordination environments of Ru ions in Na_2RuO_3 after charging and discharging processes via Mössbauer spectroscopy, X-ray diffraction (XRD), and electrochemical analysis.[2)]

A sample of $Na_2Ru_{0.99}Fe_{0.01}O_3$ was prepared *via* a solid-state reaction. Stoichiometric mixtures of RuO_2, $NaHCO_3$, and Fe_2O_3 were pressed and sintered at 850°C for 48 h in an Ar atmosphere. The sample was confirmed to possess a single phase by XRD.[2)] In the electrochemical treatment, a mixture of $Na_2Ru_{0.99}Fe_{0.01}O_3$, acetylene black, and polyvinylidene difluoride as a binder was applied on an Al foil. The Al foil with $Na_2Ru_{0.99}Fe_{0.01}O_3$ and a carbon sheet were used as the cathode and the anode, respectively. As the electrolyte, 1 M $NaBF_4$ solution was used.[1)] These materials were packed in a battery cell and subsequently charged by applying with a DC current of 4 V for 0.5 h. In the XRD pattern after charging, the characteristic peaks of triclinic ilmenite-type $NaRuO_3$ were assigned, in addition to those of honeycomb-type Na_2RuO_3.

For performing ^{99}Ru Mössbauer spectroscopy, the source nuclide ^{99}Rh ($T_{1/2}$ = 16.1 d) was produced by the nuclear reaction of ^{99}Ru$(p,n)^{99}$Rh at the AVF Cyclotron. ^{99}Ru Mössbauer spectra were measured at 5 K in a conventional liquid He cryostat.[3)] The ^{99}Ru Mössbauer spectra of $Na_2Ru_{0.99}Fe_{0.01}O_3$ obtained at 5 K before and after charging are shown in Figs. 1(a) and (b), respectively. The spectrum before charging was fitted by a broadened single line, indicating Ru^{4+} with the isomer shift $\delta = -0.27(1)$ mm/s.[2,3)] The spread of the linewidth was considered to be caused by the doping of Fe atoms. Concurrently, the spectrum measured after charging had a poor quality owing to the small amount of sample packed into the battery cell. However, this spectrum was analyzed to consist of two components having hyperfine magnetic fields (H_{hf}) with quadrupole splitting (ΔE_Q). The red component ($\delta = -0.27(4)$ mm/s, $\Delta E_Q = 0.51(9)$ mm/s, $H_{hf} = 4.7(2)$ T) was consistent with the oxidation state of Ru^{4+} before charging. The blue component ($\delta = -0.01(4)$ mm/s, $\Delta E_Q = 0.07(7)$ mm/s, $H_{hf} = 17.9(9)$ T) presented a larger isomer shift and a larger internal magnetic field. The value of δ indicated that the oxidation state of Ru after charging changed from 4+ to 5+. It is probable that the oxidation number of Ru ions increased as Na^+ ions were removed by charging, and that H_{hf} was generated as the structure changed to a three-dimensional ilmenite structure from a two-dimensional layer structure with a Na^+ deficiency. This speculation is supported by the observation of magnetic splitting in the ^{57}Fe Mössbauer spectrum at low temperatures. The ratio of the area intensity of the blue component was approximately 66%, which is almost consistent with the Coulomb number of the one-electron oxidation reaction under the electrochemical conditions of 4 V for 0.5 h.

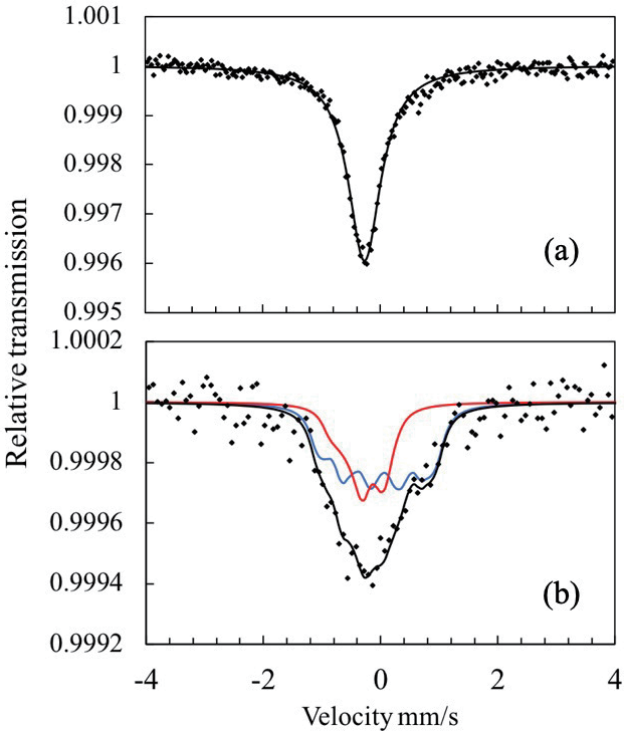

Fig. 1. ^{99}Ru Mössbauer spectra of $Na_2Ru_{0.99}Fe_{0.01}O_3$ (a) before charging and (b) after charging.

References
1) B. M. de Boisse *et al.*, Nat. Commun. **7**, 11397 (2016).
2) K. Hamano *et al.*, RIKEN Accel. Prog. Rep. **53**, 167 (2019).
3) Y. Kobayashi *et al.*, Inorg. Chem. **31**, 4570 (1992).

*1 Dep. of Eng. Sci., University of Electro-Commun
*2 RIKEN Nishina Center

Targeted alpha therapy for thyroid cancer: Radiation-induced toxicity of [^{211}At]NaAt in mice†

Y. Liu,[*2] T. Watabe,[*2,*3] K. Kaneda-Nakashima,[*3,*4] K. Ooe,[*1,*2] Y. Shirakami,[*3] A. Toyoshima,[*1,*3] E. Shimosegawa,[*2] T. Nakano,[*3,*5] A. Shinohara,[*3,*4] and J. Hatazawa[*3,*5]

Radioactive iodine (RAI) therapy is used for the treatment of patients with differentiated thyroid cancer.[1,2] However, a percentage of patients shows insufficient ^{131}I accumulation[3] or low therapeutic effect even with enough ^{131}I accumulation, and some patients suffer from recurrence or metastases and become RAI-refractory during follow-up.[4,5] For these patients, a more effective treatment is required.

Astatine (^{211}At) is a halogen with chemical properties similar to those of iodine, but it emits alpha particles, and we have found that the radiochemical purity of astatide dramatically improves upon treatment with 1% ascorbic acid. Consequently, the uptake of ^{211}At increases in the thyroid gland and thyroid cancer cells.[7] In this study, we evaluated the radiation-induced toxicity of different doses of ^{211}At-NaAt solution at different time points to estimate its time-dependent toxicity.

Methods

The biodistribution of ^{211}At-NaAt was measured in normal ICR mice (n = 12) and the absorbed doses in major organs were calculated.

Groups of ICR mice (n = 60) were injected with 0.1 MBq or 1 MBq of ^{211}At-NaAt using saline as the control group (n = 30). Their body weight and food intake were followed up for 60 days. The blood cell count and serum level of biochemical parameters were measured 3, 7, 15, 29, and 60 days after injection. Histological analyses of major organs with hematoxylin and eosin staining were performed.

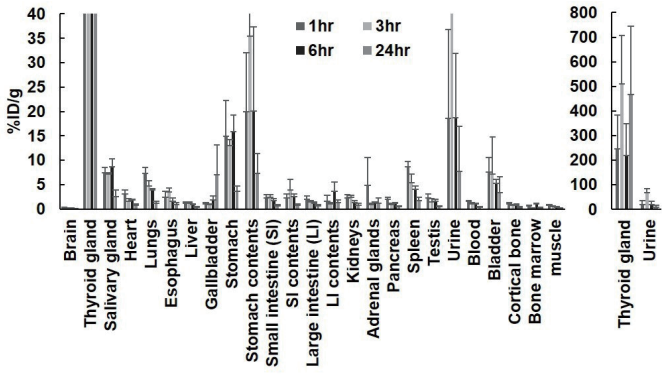

Fig. 1. %ID/g of main organs in normal ICR mice administered with ^{211}At-NaAt solution.

† Condensed from the article in Transl Oncol. **13**, 4 100757 (2020)

*1 RIKEN Nishina Center
*2 Graduate School of Medicine, Osaka University
*3 Institute for Radiation Sciences, Osaka University
*4 Graduate School of Science, Osaka University
*5 Research Center for Nuclear Physics, Osaka University

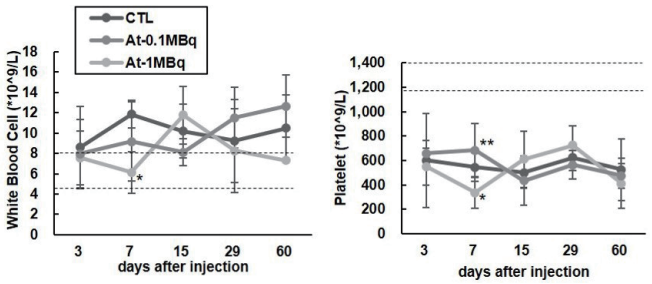

Fig. 2. Evaluation of hematological toxicity in the control, 0.1 MBq, and 1 MBq groups.

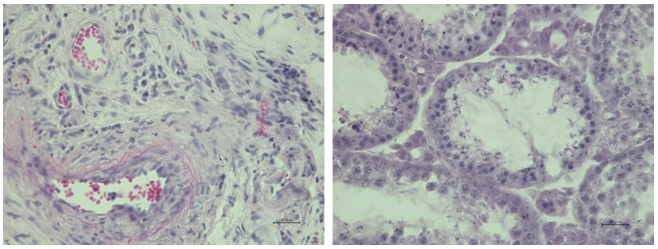

Fig. 3. Histological changes in the thyroid gland (left) and testis (right) evaluated by HE staining in the 1 MBq group on day 29.

Results

Figure 1 revealed a high-absorbed dose in the thyroid gland, stomach, bladder, heart, lungs, spleen, kidneys, and testes. The 0.1 MBq group showed no abnormalities. The 1 MBq group showed decreased body weight and food intake. Figure 2 showed that hematological toxicity was mild and transient. The total cholesterol, albumin, and total protein increased with no signs of recovery, which can be attributed to hypothyroidism. Figure 3 showed atrophy and fibrosis in the thyroid gland and a transient hypospermatogenesis was found in the testis of one mouse on day 29.

Conclusion

High-dose administration of ^{211}At-NaAt showed transient toxicity in the white blood cells and testis without severe hematological or renal toxicity, suggesting its tolerable safety as targeted alpha-therapy for differentiated thyroid cancer in the 1 MBq group.

References

1) H. R. Maxon *et al.*, J. Nucl. Med. **33**, 1132 (1992).
2) Y. K. Maheshwari *et al.*, Cancer. **47**, 664 (1981).
3) L. M. Cobb *et al.*, Radiother. Oncol. **13**, 203 (1988).
4) Y. Jin *et al.*, Crit. Rev. Oncol. Hematol. **125**, 111 (2018).
5) M. Schlumberger *et al.*, Lancet Diabetes Endocrinol. **2**, 356 (2014).
6) M. R. Zalutsky *et al.*, Curr. Pharm. Des. **6**, 1433 (2000).
7) T. Watabe *et al.*, J. Nucl. Med. **60**, 1301 (2019).

Quality confirmation of RIKEN ^{186}Re using bifunctional chelating agents and derivatives

S. Oshikiri,[*1,*2] M. K. -Satake,[*1,*2] H. Kato,[*1,*2] Y. Komori,[*1] K. Suzuki,[*1,*2] T. Kobayashi,[*2] A. Hino,[*2] and H. Haba[*1]

Rhenium-186 (half-life $T_{1/2} = 3.7186$ days) and ^{188}Re ($T_{1/2} = 17.003$ hours) emit beta rays appropriate for targeted radiotherapy use. These radioactive Re isotopes are used according to the tumor size and form radiotheranostic pairs with ^{99m}Tc for radiodiagnosis.[1] However, ^{186}Re has not been investigated as well as ^{188}Re has.[2] One of the possible reasons is that it is difficult to obtain no-carrier-added ^{186}Re through the classical production method of the ^{185}Re$(n,\gamma)^{186}$Re reaction, while no-carrier-added ^{188}Re can be obtained using a ^{188}W/^{188}Re generator.[1,3] At RIKEN, we started to produce no-carrier-added ^{186}Re (RIKEN ^{186}Re) in the ^{186}W$(d,2n)^{186}$Re reaction at the RIKEN AVF cyclotron. In this study, we selected DADT, ECD, MAG3, and DMSA (Fig. 1) as model compounds, which had already been reported in many articles,[4–7] and evaluated radiolabeling efficiencies for these compounds to confirm the quality of RIKEN ^{186}Re, especially in terms of its usefulness as a radioisotope (RI) material for bifunctional chelating agents and derivatives.[8,9]

In this report, the method for DADT radiolabeling is described below as the representative among the model compounds.

Step 1: RIKEN ^{186}Re (3.8 MBq) was dissolved in 0.05 M hydrochloric acid to prepare a ^{186}Re stock solution (138 MBq/mL). The radioactivity of ^{186}Re was determined using a germanium semiconductor detector and a dose calibrator.

Step 2: 2.2 μL of the ^{186}Re stock solution in Step 1 was added to 63.8 μL of saline to prepare a ^{186}Re solution.

Step 3: 3.0 μL of the ^{186}Re solution in Step 2 was mixed with 2.5 μL of DADT (1.0 μg), 1.4 μL of tin (II) dichloride dihydrate (10 μg), and 2.0 μL of L-tartaric acid (200 μg) aqueous solution.

Step 4: The mixture in Step 3 was heated to 99°C and held for 15 min.

Step 5: The radiolabeling yield of ^{186}Re-DADT was determined using the TLC method with a C18 reversed-phase TLC plate (NAGEL RP-18W/UV254) and eluted with acetone and 0.5 M ammonium acetate in a volume ratio of 13:7.

As a result, the radiolabeling yield of ^{186}Re-DADT at the specific radioactivity of 4.3 GBq/mmol was 86%. In Ref. 4), 88% of the radiolabeling yield of ^{188}Re-DADT at the specific radioactivity of 23 GBq/mmol was reported. To compare these results, each activity of ^{186}Re and ^{188}Re was converted to the amount of substance.

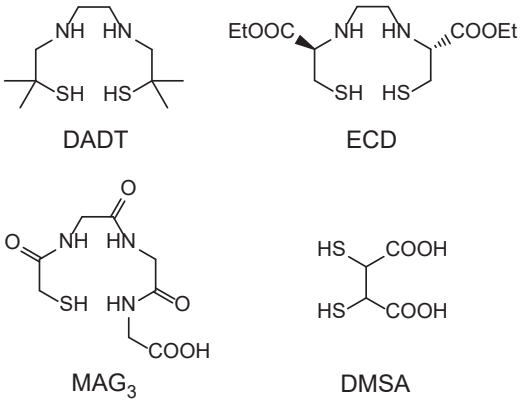

Fig. 1. Chemical structures of DADT, ECD, MAG_3, and DMSA.

Both 4.3 GBq of ^{186}Re and 23 GBq of ^{188}Re correspond to 3.3 nmol. This indicates that the ratio of the amount of DADT to that of $^{186/188}$Re was constant. Therefore, it was regarded that our result of labeling yield corresponded to that of ^{188}Re in Ref. 4). In a previous *in vivo* and *in vitro* evaluation, the radiolabeling of 222-MAMA(*N*-6-Ahx-OEt) with ^{186}Re was performed on 6.1 GBq/mmol.[10] It was suggested that RIKEN ^{186}Re is useful as an RI material for *in vivo* and *in vitro* studies.

Regarding the radiolabeling efficiencies for ECD, MAG_3, and DMSA, the radiolabeling yields were 51%, 46%, and 95%, respectively. It was revealed that these compounds are also able to form ^{186}Re complexes, although these are preliminary results.

In conclusion, our study revealed the availability of RIKEN ^{186}Re for radiolabeling and its feasibility as an RI material with bifunctional chelating agents and derivatives. By optimizing the labeling conditions in the future, RIKEN ^{186}Re is expected to be applied to targeted radiotherapy using bifunctional chelating agents, such as a peptide moiety in their structures.[11]

*1 RIKEN Nishina Center
*2 RI Research Department, FUJIFILM Toyama Chemical Co., Ltd.

References

1) N. Lepareur *et al.*, Front. Med. **6**, 132 (2019).
2) L. Uccelli *et al.*, Molecules **24**, 640 (2019).
3) G. Makris *et al.*, Mol. Imaging Biol. **23**, 52 (2021).
4) J. M. Jeong *et al.*, Nucl. Med. Biol. **28**, 197 (2001).
5) T. -Y. LuO *et al.*, Nucl. Med. Biol. **31**, 671 (2004).
6) G. W. Visser *et al.*, J. Nucl. Med. **34**, 1953 (1993).
7) K. Kothari *et al.*, Appl. Rad. Iso. **51**, 43 (1999).
8) G. Liu *et al.*, Anticancer Agents Med. Chem. **7**, 367 (2007).
9) U. Choudhry *et al.*, Dalton Trans. **3**, 311 (2003).
10) D. W. Demoin *et al.*, Nucl. Med. Biol. **43**, 802 (2016).
11) V. A. Sanders *et al.*, Nucl. Med. Biol. **68–69**, 1 (2019).

Complex formation of Rhenium-186 with lipophilic ligands —Comparison with technetium-99m—

I. O. Umeda,[*1] H. Haba,[*2] Y. Komori,[*2] H. Fujii,[*3] and T. Takahashi[*1]

Technetium-99m is the most used nuclide in diagnostic nuclear medical imaging because the energy of its gamma-ray emission (140 keV) is ideal for imaging using gamma cameras, and it can be produced on demand at medical facilities by using ^{99}Mo/^{99m}Tc generators. Various lesions can be visualized when ^{99m}Tc-labeled radiopharmaceuticals accumulate at the lesion site because of their unique mechanisms. In recent years, radiotheranostics have received considerable attention because radionuclide-targeted treatments are performed based on the imaging of the same target area.[1] Although ^{99m}Tc-radiopharmaceuticals are specialized for diagnostic imaging, their specific lesion accumulation properties are attractive for radiotheranostics. Rhenium, a group 7 congeneric element of technetium, is assumed to have chemical properties similar to those of Tc. ^{186}Re is an ideal radiotheranostic nuclide because it is a beta-emitting nuclide, and it emits gamma-ray associated with beta decay, whose energy is suitable for radionuclide therapy and imaging. Thus far, ^{186}Re has been produced by neutron irradiation in nuclear reactors, and it is difficult to obtain in Japan. At the RIKEN RI beam factory (RIBF), we succeeded in producing no-carrier-added, high-purity ^{186}Re using an accelerator-based ion beam irradiation. ^{99m}Tc-radiopharmaceuticals are complexes of ^{99m}Tc and a variety of ligands. Further rhenium is expected to form complexes as an analog of Tc. Therefore, it is important to evaluate the complex forming ability of Re. In this study, the complex formation of Re with lipophilic ligands was investigated using ^{186}Re produced at RIBF.

Rhenium-186 was produced in the ^{186}W$(d, 2n)^{186}$Re reaction. A 24-MeV deuteron beam delivered from the AVF cyclotron was irradiated onto a $^{186}WO_3$ pellet target (isotope enrichment of ^{186}W: 99.79%; thickness: 580 mg/cm^2). After irradiation, ^{186}Re was purified by chemical separation procedure.[2] The aqueous solution of ^{186}Re-perrhenate in 0.01 M HCl (radioactivity concentration: 83.0 MBq/mL) was supplied. MRP20 (N-(2(1H pyrolylmethyl)) N′-(4-pentene-3-one-2)) ethane-l, 2-diamine), ECD (ethyl cysteinate dimer), and BMEDA (n, n-bis(2-mercaptoethyl)-n′,n′-diethylethylene-diamine) were used as lipophilic chelating ligands. Stannous chloride was used as a reductant and GH (sodium glucoheptonate) was used as a stabilizer for ^{186}Re(V). The formation of ^{186}Re-ligand complexes was evaluated using octanol/water extraction and paper chromatography, and it was developed in methanol or physiological saline.

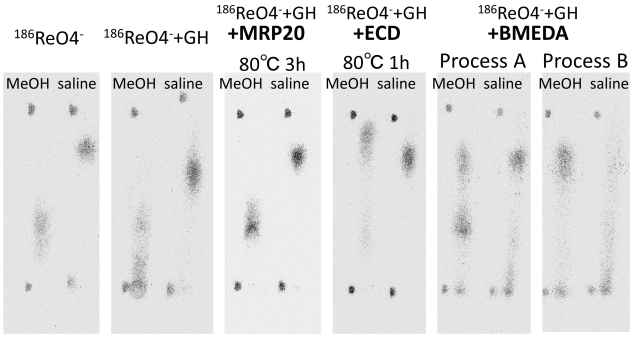

Fig. 1. Profiles of the paper chromatography of the reaction products of ^{186}Re with various lipophilic ligands. Development solution: methanol or physiological saline solution. Detection: Autoradiography using imaging plates.

We have been developing new radiopharmaceuticals by encapsulating various radionuclides in liposomes, which are capable DDS carriers.[3] We used remote loading methods, to achieve a high concentration of radionuclides in liposomes, that is, a ligand exchange reaction across the liposomal membrane using lipophilic and hydrophilic ligands. We successfully prepared ^{99m}Tc- liposomes using MRP20 as a lipophilic ligand. We first examined the reaction between ^{186}Re and MRP20; sit was found that ^{186}Re and MRP20 did not form chelate complexes under the same conditions as ^{99m}Tc. Therefore, the optimal conditions for the reaction of ^{186}Re with lipophilic ligands MRP20, ECD, and BMEDA were investigated. ^{99m}Tc could form stable complexes with each of these three ligands under mild conditions. The complex formation between ^{186}Re and these lipophilic ligands required 10 times more reducing agent, higher reaction temperatures, and longer reaction times than those of ^{99m}Tc. Representative paper chromatography profiles of these reaction products are shown in Fig. 1. ^{186}Re and ECD formed a lipophilic ligand complex that moved close to the solvent front in methanol. In the reaction of ^{186}Re with BMEDA, the products were different depending on the reaction process. The products of process A seemed to contain [$^{186}ReO_4^-$] and the lipophilic complex. ^{186}Re and MRP20 could not form a complex even with these severe conditions, and their chromatogram profiles were almost the same as those of [$^{186}ReO_4^-$]. Based on these results, we speculate that ^{186}Re was more difficult to reduce compared to ^{99m}Tc analogues; further, the reaction rate with ligands was slower than

*1 Kavli IPMU, the University of Tokyo
*2 RIKEN Nishina Center
*3 EPOC, National Cancer Center

that of ^{99m}Tc. ^{186}Re seemed to be re-oxidizing with oxygen from the air back to [$^{186}ReO_4^-$], which may compete with the complex formation and inhibit the reaction.

It is believed that rhenium has similar chemical properties to technetium, and it can be handled in the same manner. However, the results of this study indicate that their chemical properties are very different at least in terms of the ligand-complex formation. Highly concentrated and stable ^{186}Re-labeling compounds are necessary to promote radiotheranostics. The present findings will help establish optimized labeling methods for ^{186}Re.

References

1) K. Herrmann *et al.*, Lancet Oncol. **21**, e146 (2020).
2) N. Shigeta *et al.*, J. Radioanal. Nucl. Chem. **205**, 85 (1996).
3) I. Ogihara-Umeda *et al.*, J. Nucl. Med. **37**, 326 (1996).

Simultaneous imaging of Na^+/K^+ by semiconductor Compton camera GREI

S. Motomura,[*1] I. Kii,[*1,*2] H. Haba,[*3] H. Yakushiji,[*1] Y. Watanabe,[*1] and S. Enomoto[*4]

We have been studying the simultaneous imaging of sodium (Na) and potassium (K) ions that are dynamically controlled in a living body. Na^+ and K^+ are very common cations in body fluids; however, interestingly, they are controlled very differently by some biomolecules. Owing to the different behavior and distribution of Na^+ and K^+, membrane potential can be formed in neurons, and Na^+ can be reabsorbed in the kidneys. Therefore, the imaging of Na^+/K^+ dynamics may be beneficial in inspecting the function of biomolecules.

As summarized in a previous report, we were able to simultaneously take the images of ^{24}NaCl and ^{43}KCl solutions using our imaging apparatus GREI.[1,2] However, we determined some challenges to be addressed in the imaging of ^{24}Na, in addition to the low detection efficiency for the 1369-keV gamma ray. In the gamma-ray energy spectrum of ^{24}Na + ^{43}K (Fig. 1), there is a gamma-ray peak at 1732 keV that corresponds to the double escape peak for the 2754-keV gamma ray of ^{24}Na. This originates from the escape of two 511-keV gamma rays created by the annihilation of the positron that was created by the pair-creation interaction of gamma rays in the gamma-ray detectors. In addition, the $E1+E2 = 1732$ keV events were observed in the $E1$-$E2$ histogram (Fig. 2), where $E1$ and $E2$ represent the detected energies by the front and rear detectors, respectively. Furthermore, the $E1 + E2 =$ 2754 keV events were also observed, although the measurable energy range for each detector was less than 2000 keV in the current GREI system. We inferred that these 1732- and 2754-keV gamma events doubled the dead time of the GREI system. Hence, to realize efficient imaging experiment, we need to further develop a proper method to process the gamma events.

To circumvent the current problem of ^{24}Na, we decided to use ^{22}Na for now. Although ^{22}Na is not suitable for clinical use, owing to its long half-life of 2.6 years, we can use it for preliminary or preclinical experiments. ^{22}Na is a positron emitter and emits two 511-keV gamma-rays and one 1275-keV intrinsic gamma ray.

We performed GREI imaging experiment of ^{22}Na and ^{43}K simultaneously injected in a live mouse. We can use a 511-keV gamma-ray peak to identify ^{22}Na, which is in the optimal imaging efficiency region for GREI (Fig. 3). The $E1$-$E2$ histogram for ^{22}Na + ^{43}K is shown in Fig. 4. Clear lines can be observed for each gamma ray that were all covered by the energy range of GREI. This study is still ongoing, and the results are being prepared to be considered for publication.

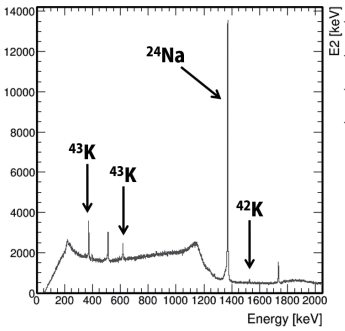

Fig. 1. Gamma-ray energy spectrum of ^{24}Na and ^{43}K measured by GREI.

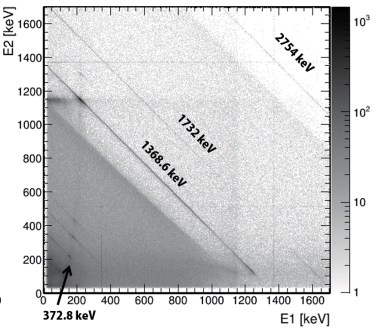

Fig. 2. $E1$-$E2$ histogram of ^{24}Na and ^{43}K.

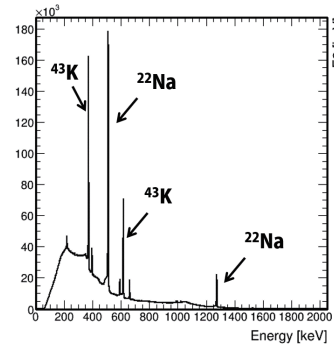

Fig. 3. Gamma-ray energy spectrum of ^{22}Na and ^{43}K measured by GREI.

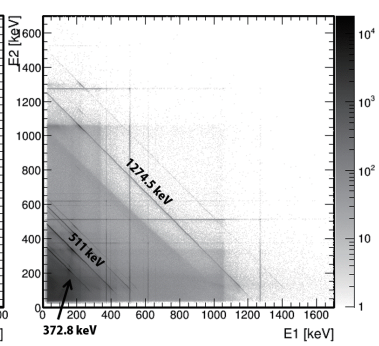

Fig. 4. $E1$-$E2$ histogram of ^{22}Na and ^{43}K.

References

1) S. Motomura *et al.*, J. Anal. At. Spectrom. **28**, 934 (2013).
2) T. Ida *et al.*, Jpn. J. Appl. Phys. **58**, 016002 (2019).

*1 RIKEN Center for Biosystems Dynamics Research
*2 Compass to Healthy Life Research Complex Program, RIKEN
*3 RIKEN Nishina Center for Accelerator-Based Science
*4 RIKEN Center for Life Science Technologies

Development of image reconstruction method for a multiple-isotope PET using ^{44m}Sc†

T. Fukuchi,[*1] M. Shigeta,[*1] H. Haba,[*2] D. Mori,[*2] T. Yokokita,[*2] Y. Komori,[*2] S. Yamamoto,[*3] and Y. Watanabe[*1]

Positron emission tomography (PET) is a powerful tool for radio-tracer imaging in a living biological object. However, conventional PET is useful only for single-tracer imaging because of the energy constancy of annihilation photons, which are utilized for PET imaging. In order to improve PET imaging, we have developed a new small-animal PET system that can be used for multiple-tracer simultaneous imaging. Our PET system, named multiple-isotope PET (MI-PET), detects not only annihilation photons but also prompt γ-rays, which are emitted successively after positrons, using additional γ-ray detectors. Previously, we succeeded in proving the basic principle of MI-PET using a prototype system.[1,2)]

Because of the imperfectness of the prompt γ-ray detection in MI-PET imaging with a pure positron emitter and positron-γ emitter, an image for the pure positron emitter taken by MI-PET is superposed by the positron-γ emitter. Therefore, to create an isolated image of the pure positron emitter, we developed an image reconstruction method based on subtraction between data with the absence (data-D) and presence (data-T) of the prompt γ-ray detection. For this subtraction, the spatial normalization of the prompt γ-ray sensitivity is needed. Therefore, long-period normalization scans of a positron-γ emitter, ^{44m}Sc, was performed using a cylindrical phantom 180 mm in length and 78 mm in diameter. These normalization data were also used for the analysis of the counting-rate dependence of the sensitivity based on its proper decay half-life of 58.6 h. The initial activity of the ^{44m}Sc phantom was 2.45 MBq, and the measurement time was 235 h, which corresponds to approximately 4 half-lives.

To evaluate the practical performance of the developed image reconstruction method, dual-isotope mouse imaging was performed using ^{18}F-FDG and a simple substance, ^{44m}Sc. In this experiment, 1.13-MBq of ^{18}F-FDG and 1.23-MBq of ^{44m}Sc were administered to an 8-week-old normal male mouse by a tail vein injection. After 38 min from administration, a 30-min scan with bed motion was performed under anaesthesia. This animal experiment was performed in accordance with the Principles of Laboratory Animal Care (NIH Publication No. 85-23, revised 1985) and approved by the Institutional Animal Care and Use Committee (IACUC) of RIKEN, Kobe Branch.

Scandium-44m was produced at RIBF *via* the ^{45}Sc$(d, p2n)^{44m}$Sc (for normalization scan) and ^{44}Ca$(d, 2n)^{44m}$Sc (for mouse imaging) reactions with a 24-MeV deuterium beam from the AVF cyclotron, purified by chemical processes at the hot lab, and transported to the RIKEN Center for Biosystems Dynamics Research in Kobe.

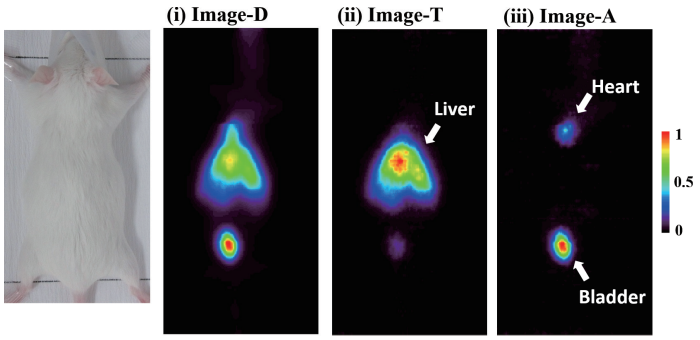

Fig. 1. Photograph (left) and reconstructed images of a mouse administrated with ^{18}F-FDG and ^{44m}Sc. (i) image-D (^{44m}Sc and ^{18}F-FDG), (ii) image-T (^{44m}Sc), and (iii) image-A (^{18}F-FDG).

Table 1. VOI analysis of the mouse. Values are shown in kBq.

	Image-D	Image-T	D-T	Image-A
Heart	31.7	10.2	21.5	23.9
Liver	421.3	427.6	−6.3	0.9
Bladder	69.0	9.2	59.8	77.3

Reconstructed mouse images from data-D (image-D: ^{44m}Sc and ^{18}F-FDG) and data-T (image-T: ^{44m}Sc) as well as an isolated image of the pure-positron emitter (image-A: ^{18}F-FDG) are shown in Fig. 1. From image-T, we can clearly observe ^{44m}Sc accumulation in the liver, whereas from image-A, ^{18}F-FDG accumulated in the heart and urinary bladder. These distributions are reasonable from a physiological viewpoint.

To make a quantitative analysis, 3D volumes of interest (VOIs) were set on the heart, liver, and bladder for image-D, image-T, and image-A. The values of these VOIs and direct subtraction between image-D and image-T (D-T) are listed in Table 1. The D-T activity in the liver was negative. However, activity in the liver of image-A, which has no biological specific accumulation of ^{18}F-FDG, was nearly zero and was comparable with other non-accumulated sections. From this result, we concluded that our newly developed image-A isolation method is useful for practical multiple-isotope imaging using MI-PET.

References
1) T. Fukuchi *et al.*, Med. Phys. **40**(6), 2257 (2017).
2) T. Fukuchi *et al.*, RIKEN Accel. Prog. Rep. **53**, 21 (2020).

† Condensed from the article in Jour. of Inst., (in press) (2021)

*1 RIKEN Center for Biosystems Dynamics Research
*2 RIKEN Nishina Center
*3 Department of Radiological and Medical Laboratory Science, Nagoya University

Double photon emission nuclides for double photon coincidence imaging

H. Takahashi,[*1] M. Uenomachi,[*1] K. Shimazoe,[*1] and H. Haba[*2]

Positron emission tomography (PET) is known as a very high sensitivity imaging method. One reason for this is that it utilizes a coincidence technique, where two detectors are used to identify the event; therefore, a high signal-to-noise ratio is realized. However, PET uses only 511 keV gamma rays. Thus, it cannot be used to distinguish all positron emitters.

Some nuclides successively emit two gamma-ray photons in a very short time. The use of such gamma photons can lead a new type of coincidence imaging method.[1,2)] Recently, we proposed a new concept of time/position correlation type tomography method based on a directionality sensitive gamma camera. For this, we need a nuclide that emits two photons in a relatively short period. Thus far, we have proposed the use of ^{111}In, which emits a 171 keV photon and after the life time of 85 ns, it emits a 245 keV photon. When the measurement system identifies a 171 keV photon, the system waits for a 245 keV photon for approximately 300 ns. If the system recognizes the 245 keV photon, it records two gamma photons and their incident angles, and then, it proceeds to the next measurement. To record angles, an electron tracking type Compton imager can be used for 300–600 keV gamma-ray photons; however, multi-pinhole cameras can be used for low-energy gamma rays. This enables double photon emission computed tomography (DPECT). Although ^{111}In is feasible for measurements, the advantage of the double-photon coincidence method lies in its multi-nuclide capability. Therefore, we are exploring other candidates for double-photon emission nuclides. The gamma ray energies should not be too large since the detection efficiency for high energy gamma rays is limited.

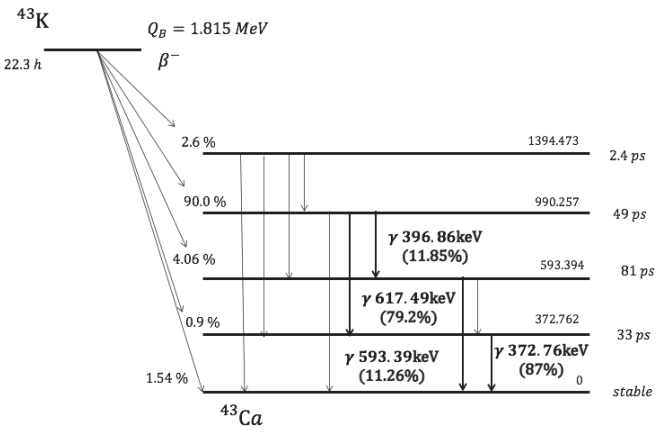

Fig. 1. Decay scheme of ^{43}K.[3)]

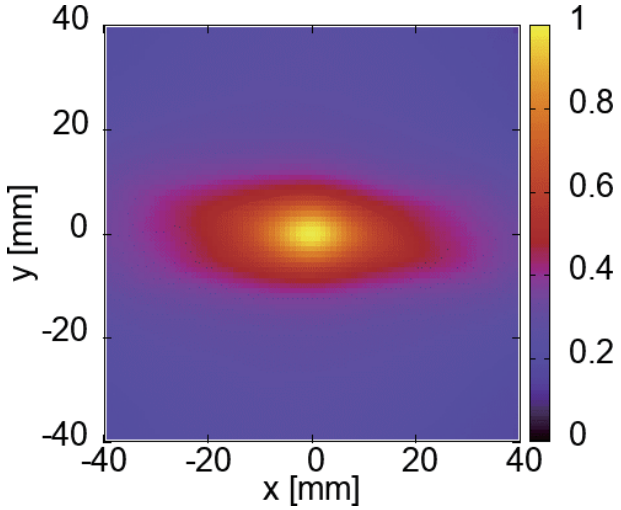

Fig. 2. Single photon Compton image of a ^{43}K source. The color bar shows relative intensity.

For nuclear medicine applications, the half-life of the nuclide should not be too short or too long. The double-photon yield should be large. The gamma-ray energies should not be too large since the detection efficiency for high-energy gamma rays is limited. Further, two photons should be emitted within a short period. Although there are various possibilities for double-photon emission nuclides. they cannot all be used owing to the above requirements. Then we successfully found the following nuclides thus far.

^{43}K is a beta minus nuclide followed by gamma photon emissions. The half-life of the nuclide ^{43}K is 22.3 h, which is a reasonable value. The decay scheme of this nuclide is shown in Fig. 1. It emits three pairs of gamma rays. The first pair is a 617 keV photon (79%) and a 372 keV photon (87%). The second pair is a 397 keV photon (11.9%) and a 593 keV photon (11.3%). Finally, the third pair is a 221 keV photon (4.8%) and a 372 keV photon. The longest life time is 81 ps. Therefore, two gamma-ray photons are observed almost simultaneously in the measurement system. The time resolution is very close to that of positron annihilation. The TOF method can be used to localize the event for this nuclide. As a first step, the single-photon Compton image was obtained as shown in Fig. 2. In this research, ^{43}K was produced at RIKEN for radioisotope imaging.

References

1) M. Uenomachi *et al.*, Nucl. Instrum. Methods Phys. Res. A, **954**, 161682 (2020).
2) K. Shimazoe *et al.*, J. Instrum. **12**, C12055 (2017).
3) A. Dhal *et al.*, EPJ Web Conf. **146**, 10013 (2017).

*1 School of Engineering, University of Tokyo
*2 RIKEN Nishina Center

Production cross sections of ^{225}Ac in the ^{232}Th(^{14}N, $xnyp$) reactions at 116 and 132 MeV/nucleon

X. Yin,[*1] A. Nambu,[*1] Y. Komori,[*1] D. Mori,[*1] S. Oshikiri,[*1,*2] H. Kato,[*1,*2] A. Hino,[*2] and H. Haba[*1]

^{225}Ac ($T_{1/2}$ = 10.0 d) is one of the most promising alpha-particle-emitting radionuclides for targeted radionuclide therapy.[1] However, the current global availability of ^{225}Ac is too small to support large clinical trials, and a stable supply system for ^{225}Ac has not yet been established in Japan even at the basic research scale of 100 MBq. A spallation reaction of ^{232}Th with high-energy protons is expected to be a potential production route for ^{225}Ac.[2] At RIKEN, radionuclides of a large number of elements, called multitracer, have been produced by the spallation of metallic targets such as natTi, natAg, and ^{197}Au irradiated with a 135 MeV/nucleon ^{14}N beam from the RIKEN Ring Cyclotron (RRC).[3] In this work, we investigated the feasibility of ^{225}Ac production via the ^{232}Th(^{14}N, $xnyp$)^{225}Ac reaction for the future domestic supply of ^{225}Ac. We also investigated the production of ^{225}Ra ($T_{1/2}$ = 14.9 d) because it is useful as an ^{225}Ac/^{225}Ra generator to produce high-radionuclidic-purity ^{225}Ac.[2]

A ^{14}N^{7+} beam was extracted from the RRC. Three metallic ^{232}Th foils (69 mg/cm^2), two ^{27}Al plates (415 mg/cm^2), and another three ^{232}Th foils were placed in this order from the upstream side of the beam in the multitracer production chamber.[3] The targets were irradiated for 1 h with a 20-pnA-intensity beam.

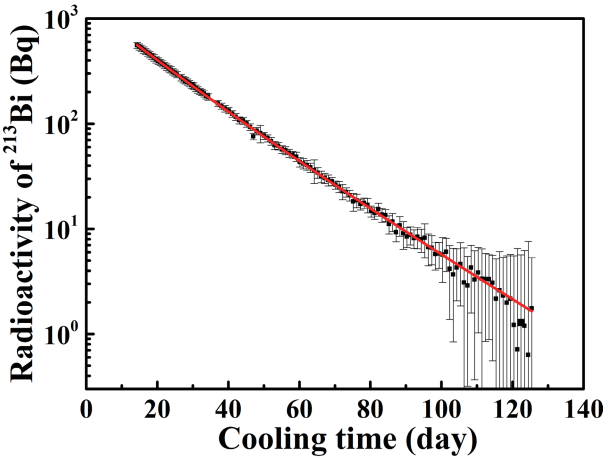

Fig. 1. Radioactive decay curve of the 440.5-keV γ-line of ^{213}Bi on the decay chain of ^{225}Ra $\rightarrow$ ^{225}Ac $\rightarrow$ ^{221}Fr $\rightarrow$ ^{217}At $\rightarrow$ ^{213}Bi $\rightarrow$ $\cdots$. The solid curve indicates the fitting result using the two-body successive decay equation (^{225}Ra $\rightarrow$ ^{225}Ac $\rightarrow$ $\cdots$).

*1 RIKEN Nishina Center
*2 RI Research Department, FUJIFILM Toyama Chemical Co., Ltd.

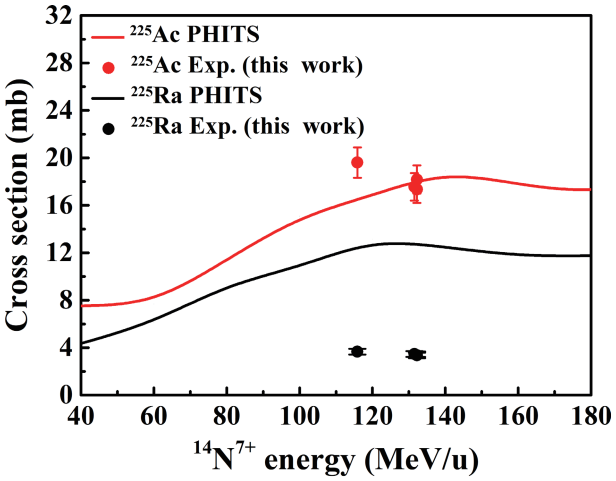

Fig. 2. Cross sections of the ^{232}Th(^{14}N, $xnyp$)^{225}Ac, ^{225}Ra reactions in comparison with the PHITS calculations.

After the irradiation, the second foil of each set of three ^{232}Th foils was subjected to γ-ray spectrometry with Ge detectors to determine the production cross sections of ^{225}Ac and ^{225}Ra. The ^{27}Al plates were used as beam-energy degraders. The beam energies on the measured ^{232}Th targets were calculated to be 132 and 116 MeV/nucleon using the stopping power model[4] in the LISE^{++} program.[5]

The radioactivities of ^{225}Ac and ^{225}Ra at the end of the irradiation were determined by following the activity of ^{213}Bi ($T_{1/2}$ = 45.59 min), which was in radioactive equilibrium as the great granddaughter of ^{225}Ac. Figure 1 shows a typical decay curve of the 440.5-keV γ-line of ^{213}Bi. The two-body successive decay equation (^{225}Ra $\rightarrow$ ^{225}Ac $\rightarrow$ $\cdots$) was applied to fit the decay curve after subtracting the small contribution of the 440.4-keV γ-ray of ^{228}Ac, which originally existed in the ^{232}Th target as the granddaughter of ^{232}Th. Some short-lived parents of ^{225}Ac and ^{225}Ra were produced in the reactions; therefore the measured cross sections of ^{225}Ac and ^{225}Ra are cumulative for electron-capture decay and β^- decay, respectively. The cross sections of the ^{232}Th(^{14}N, $xnyp$)^{225}Ac,^{225}Ra reaction are shown in Fig. 2. The cross sections of ^{225}Ac are larger than those of ^{225}Ra by a factor of 5. The experimental results were compared with those calculated by the Particle and Heavy Ion Transport code System (PHITS).[6] The PHITS code reproduces the cross sections of ^{225}Ac, while it overestimates those of ^{225}Ra by a factor of 4. The production yield of ^{225}Ac was tentatively evaluated to be 3.3 MBq/pμA·h

at 132–80 MeV/nucleon by normalizing the PHITS calculations to the experimental cross sections. Based on our typical experimental conditions (incident beam energy: 132 MeV; beam intensity: 1 pμA; target thickness: 4.5 g/cm^2; irradiation time: 2 d), approximately 150 MBq of ^{225}Ac can be produced at the end of the irradiation. In the near future, we will measure the cross sections of ^{225}Ac and ^{225}Ra at lower energies of 80 and 100 MeV/nucleon to evaluate their yields more reliably.

References

1) G. Maryline *et al.*, Radiochim. Acta **107**, 1065 (2019).
2) A. K. H. Robertson *et al.*, Inorg. Chem. **59**, 12156 (2020).
3) H. Haba *et al.*, Radiochim. Acta **93**, 539 (2005).
4) J. F. Ziegler, J. P. Biersack, U. Littmark, *The Stopping and Range of Ions in Solid* (Pergamon Press, New York, 1985).
5) O. B. Tarasov *et al.*, Nucl. Instrum. Methods Phys. Res. B **266**, 4657 (2008).
6) Y. Iwamoto *et al.*, J. Nucl. Sci. Technol. **54**, 617 (2017).

Cross sections of alpha-particle-induced reactions on ^{nat}Ni: Production of ^{67}Cu†

S. Takács,[*1] M. Aikawa,[*2,*3,*4] H. Haba,[*3] Y. Komori,[*3] F. Ditrói,[*1] Z. Szücs,[*1] M. Saito,[*2,*3] T. Murata,[*2,*3] M. Sakaguchi,[*2,*3] and N. Ukon[*5,*3]

^{67}Cu is considered one of the most promising radioisotopes in targeted radio-immunotherapy. It is a β^--emitter with a mean β^- energy ($E_\beta^- = 141$ keV) that allows treating tumors of size up to approximately 4 mm. Its decay is followed by the emission of low-energy gamma rays suitable for SPECT imaging. Its half-life ($T_{1/2} = 61.83$ h) is optimal for human applications. Among the charged-particle-induced production routes, the ^{64}Ni$(\alpha, \mathrm{p})^{67}$Cu reaction requires much less enriched (expensive) target material for providing a comparable amount of ^{67}Cu activity as compared to proton or deuteron production routes. The available literature data are very different from each other in terms of both shape and amplitude, and only one experiment provided cross-section data above 25 MeV; therefore, we decided to investigate this production route up to 51 MeV.

Experiments were performed at the RIKEN AVF cyclotron. The stacked-foil activation technique and high-resolution γ-ray spectrometry were applied. Pure metallic foils of ^{nat}Ni and ^{nat}Ti from Nilaco Corp., Japan with an average thickness of 5 μm were used. The foils were paired (Ni-Ni, or Ti-Ti) in the stack to handle the recoil effect. Four irradiations were performed using 51.04, 49.42, 40.94, and 26.57 MeV alpha-particle beams. The incident beam energy was measured by the time-of-flight method.[1)] The energy loss of the alpha particles was calculated using the semi-empirical formula of Andersen and Ziegler.[2)] The average beam intensity measured using a Faraday cup was cross checked with the ^{nat}Ti$(\alpha, \mathrm{x})^{51}$Cr monitor reaction.[3)] After a small correction of the measured beam intensities, the re-measured cross-sections for the ^{nat}Ti$(\alpha, \mathrm{x})^{51}$Cr monitor reaction agreed perfectly with their recommended value.[3)] Several series of γ-ray spectra were recorded for each irradiated foil by using a high-resolution HPGe detector-based γ-spectrometer without chemical separation for increasing cooling times to follow the decay of the reaction products. Q-values and decay data were taken from the Q-value calculator[4)] and NuDat 2.7 database[5)] of National Nuclear Data Center, respectively. On the ^{nat}Ni target, ^{67}Cu can be produced only in the ^{64}Ni$(\alpha, \mathrm{p})^{67}$Cu reaction with an alpha-particle beam. The threshold energy of this reaction is $E_{\mathrm{thr}} = 4.93$ MeV.

The deduced isotopic cross sections for the ^{64}Ni$(\alpha, \mathrm{p})^{67}$Cu reaction were normalized to 100% ^{64}Ni isotopic abundance. Additionally, direct and/or cumulative "elemental" activation cross-sections were deduced for the formation of ^{64,61,60}Cu, ^{63,62}Zn, and ^{57,56}Ni radionuclides as possible radio-contaminants. The obtained experimental data were compared with the experimental data available in the literature and the results of the TALYS theoretical model calculation taken from the TENDL-2019[6)] data library.

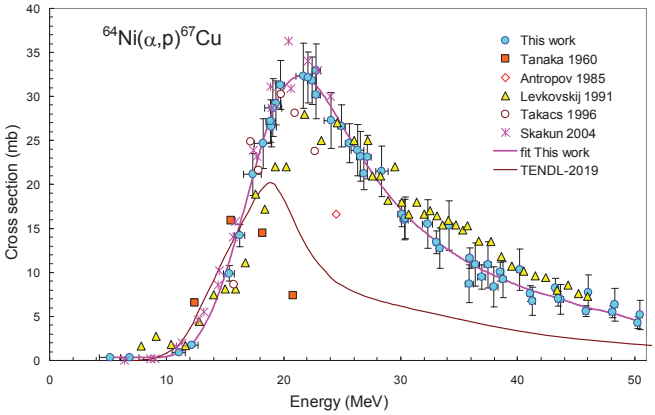

Fig. 1. Excitation function of the ^{64}Ni$(\alpha, \mathrm{p})^{67}$Cu reaction in comparison with previously reported experimental data and the result of the model calculation taken from the TENDL-2019 database.[5)]

Thick target yields were calculated to estimate the expected amount of ^{67}Cu and the possible radiocontamination level of the other co-produced copper radionuclides by using the spline-fitted experimental data in the calculation. It was concluded that the production of ^{67}Cu is possible on a highly enriched ^{64}Ni target for local use only. To reduce the amount of co-produced ^{64}Cu, the bombarding alpha-particle energy should be kept below 30 MeV. During a 24 h-long (30 MeV and 30 μA) irradiation, the estimated end-of-bombardment (EOB) activity of ^{67}Cu is approximately 1 GBq, and the expected activity of the co-produced ^{64}Cu is approximately 0.15%.

This work was conducted in the framework of a common research program between the JSPS and HAS (Contract No: FY2019-2020 and NKM-43/2019).

References

1) T. Watanabe *et al.*, Proc. 5th Int. Part. Accel. Conf. (IPAC2014), (2014), p. 3566.
2) H. H. Andersen, J. F. Ziegler, *Helium Stopping Powers and Ranges in all Elements* (Pergamon, Oxford, 1997).
3) A. Hermanne *et al.*, Nucl. Data Sheets **148**, 338 (2018).
4) NNDC, Q-calc, `https://www.nndc.bnl.gov/qcalc/`.
5) NNDC, NuDat 2.7 database, `http://www.nndc.bnl.gov/nudat2/`.
6) A. J. Koning *et al.*, Nucl. Data Sheets **155**, 1 (2019).

† Condensed from the article in Nucl. Instrum. Methods Phys. Res. B **479**, 125 (2020)

*1 Institute for Nuclear Research, ATOMKI
*2 Graduate School of Biomedical Science and Engineering, Hokkaido University
*3 RIKEN Nishina Center
*4 Faculty of Science, Hokkaido University
*5 Advanced Clinical Research Center, Fukushima Med. Univ.

Production cross sections of ^{68}Ga and radioactive by-products in deuteron-induced reactions on natural zinc†

Ts. Zolbadral,[*1,*2] M. Aikawa,[*1,*3,*2] D. Ichinkhorloo,[*3,*2] Kh. Tegshjargal,[*4] N. Javkhlantugs,[*4] Y. Komori,[*2] and H. Haba[*2]

^{68}Ga ($T_{1/2}$ = 68 min), a positron emitter, is a valuable medical isotope used for positron emission tomography (PET).[1] Charged-particle-induced reactions using cyclotrons are preferable routes for ^{68}Ga production. One of the routes is the deuteron-induced reaction on zinc. Our literature survey revealed three experimental studies on the cross sections of the ^{nat}Zn$(d,x)^{68}$Ga reaction were found,[2–4] and there is a large discrepancy among their experimental data. Therefore, we measured the cross sections of ^{68}Ga via the deuteron-induced reaction on natural zinc. In addition, we measured the cross sections of co-produced radioisotopes to investigate possible radioactive impurities.

The experiment was performed at the AVF cyclotron of RIKEN RI Beam Factory. The stacked-foil activation technique and γ-ray spectrometry were used to measure the activation cross sections. The target was composed of metallic foils of ^{nat}Zn (17.64 mg/cm^2, 99.9% purity, Nilaco Corp., Japan) and ^{nat}Ti (9.13 mg/cm^2, 99.6% purity, Nilaco Corp., Japan) and irradiated for 22 min by a 24-MeV deuteron beam. The incident beam energy was measured using the time-of-flight method. The energy degradation in the stacked target was calculated using the SRIM code.[5] A beam intensity of 96 nA was measured using a Faraday cup.

The γ-ray spectra of the activated foils without chemical separation were measured using a high-resolution high-purity germanium (HPGe) detector. The detector was calibrated using a multiple γ-ray point source. The dead time was kept less than 7% in the measurement. Each foil was measured several times after cooling times ranging from 40 min to 18 d for different half-lives of products.

The cross sections of the ^{nat}Ti$(d,x)^{48}$V monitor reaction were derived to assess the beam parameters. A comparison of the measured cross sections with the recommended values[6] showed that the beam intensity was increased by 6.6% relative to the measured value and corrected to 102.4 nA.

The cross sections of the ^{nat}Zn$(d,x)^{68}$Ga reaction were derived from the measurement of the 1077.34-keV γ-line (I_γ = 3.22%) from the ^{68}Ga decay. The measured excitation function is shown in Fig. 1 in comparison with previous data[2–4] and the theoretical estimation of TENDL-2017.[7]

Our result agrees with the data reported by Šimečková *et al.*[3] and the normalized data for the $(d,2n)$ reaction on ^{68}Zn reported by Gilly *et al.*[4] However, the data reported by Nassiff and Münzel[2] are much lower than the present data in the entire energy range. The TENDL-2017 data overestimate the experimental data around the peak in the energy range of 8–18 MeV. The contribution of the ^{67}Zn$(d,n)^{68}$Ga reaction is small, and the ^{68}Zn$(d,2n)^{68}$Ga reaction is dominant above the threshold energy of 6.1 MeV based on the TENDL-2017 prediction. The production cross sections of co-produced radionuclides ^{65,66,67}Ga, ^{63,65,69m}Zn, ^{61}Cu, and ^{58}Co were also determined. Enriched ^{68}Zn is preferable for the production of ^{68}Ga because radioactive isotopic impurities are not produced below 14.6 MeV, which is the threshold energy of the ^{68}Zn$(d,3n)^{67}$Ga reaction.

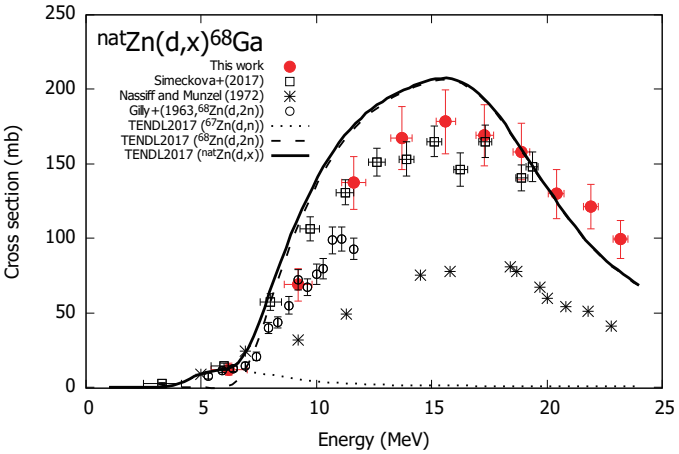

Fig. 1. Excitation function of the ^{nat}Zn$(d,x)^{68}$Ga reaction in comparison with previous data[2–4] and the TENDL-2017 data.[7]

The physical yield of the ^{nat}Zn$(d,x)^{68}$Ga reaction was deduced from the spline-fitted curve of the measured excitation function. The derived yield reaches 2.37 GBq/μAh at 23.2 MeV.

This work is supported by JSPS KAKENHI Grant Number 17K07004. Ts.Z. was granted a scholarship by the M-JEED project (Mongolian-Japan Engineering Education Development Program, J11B16).

References

1) S. R. Banerjee, M. G. Pomper, Appl. Radiat. Isot. **76**, 2 (2013).
2) S. J. Nassiff, H. Münzel, Radiochem. Radioanal. Lett. **12**, 353 (1972).
3) E. Šimečková *et al.*, EPJ Web Conf. **146**, 11034 (2017).
4) L. J. Gilly *et al.*, Phys. Rev. **131**, 1727 (1963).
5) J. F. Ziegler *et al.*, Nucl. Instrum. Methods Phys. Res. B **268**, 1818 (2010).
6) A. Hermanne *et al.*, Nucl. Data Sheets **148**, 338 (2018).
7) A. J. Koning *et al.*, Nucl. Data Sheets **155**, 1 (2019).

† Condensed from the article in Appl. Radiat. Isot. **159**, 109095 (2020)

*1 Graduate School of Biomedical Science and Engineering, Hokkaido University
*2 RIKEN Nishina Center
*3 Faculty of Science, Hokkaido University
*4 School of Engineering and Applied Sciences, National University of Mongolia

Activation cross section measurement of the deuteron-induced reaction on yttrium-89 for zirconium-89 production†

M. Sakaguchi,[*1,*2] M. Aikawa,[*3,*1,*2] M. Saito,[*1] N. Ukon,[*4,*2] Y. Komori,[*2] and H. Haba[*2]

Zirconium-89 ($T_{1/2}$ = 78.41 h) is a positron emitter that is used for positron emission tomography (PET). Its long half-life enables its delivery over long distances and it is suitable for immuno-PET.[1] High-specific activity of the radionuclide can be produced using charged-particle-induced reactions. There are two promising reactions, namely, the ^{89}Y$(p,n)^{89}$Zr and the ^{89}Y$(d,2n)^{89}$Zr reactions. The former has been well investigated and a large amount of experimental data is present. However, there is a lack of research on the latter reactions and the peak amplitudes of the excitation functions are dispersed.[2] Therefore, we performed an experiment of the deuteron-induced reactions on ^{89}Y to measure the production cross sections of ^{89}Zr. Additionally, the cross sections for co-produced radionuclides, ^{88}Zr, ^{90m}Y, ^{88}Y, and ^{87m}Sr, were determined.

The experiment was performed at the RIKEN AVF cyclotron. We adopted well-known and established methods, such as stacked-foil activation technique and high-resolution γ-ray spectrometry. Thin metallic foils of ^{89}Y (purity 99.0%, thickness 25 μm, Goodfellow Co., Ltd., UK) and ^{nat}Ti (purity 99.6%, thickness 20 μm, Nilaco Corp., Japan) were used as the target foils. Their weight and area were measured and the derived thicknessess of ^{89}Y and ^{nat}Ti were 12.7 and 9.1 mg/cm^2, respectively. The foils were then cut into a size of 8 × 8 mm^2. Nine sets of four ^{89}Y and two ^{nat}Ti pieces were stacked as the target. The ^{nat}Ti foils were used for the ^{nat}Ti$(d,x)^{48}$V monitor reaction to assess the thicknesses of the foils and beam parameters. The stacked target in a target holder served as a Faraday cup and it was irradiated by a deuteron beam for 1 h. The average beam intensity of 102.3 nA was measured by the Faraday cup. The incident beam energy of 23.6 ± 0.2 MeV was measured by the TOF method. The energy degradation in the stacked target was calculated using the SRIM code.[3] γ-ray spectra from each irradiated foil without chemical separation were measured using a high-resolution HPGe detector. The foils other than the first one in the same groups were measured to compensate the recoil losses of the products. The efficiency of the detector was calibrated using ^{152}Eu and mixed γ-ray standard sources. Nuclear-decay data were taken from NuDat 2.7.[4]

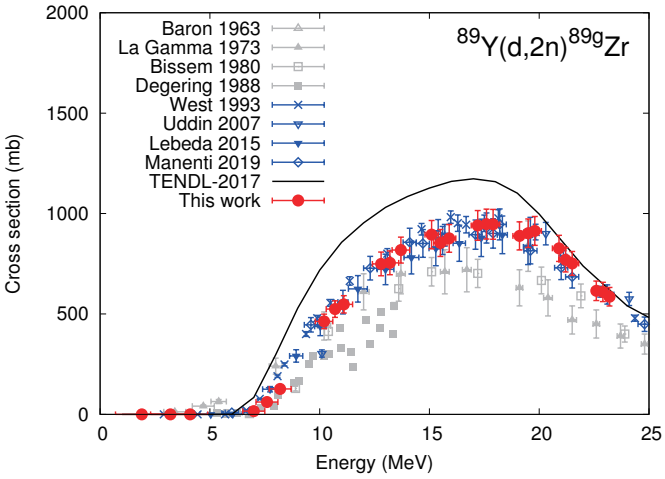

Fig. 1. Cumulative cross sections of the ^{89}Y$(d,2n)^{89g}$Zr reaction in comparison to the previous data[2] and the TENDL-2017 data.[6]

The cross sections of the ^{nat}Ti$(d,x)^{48}$V monitor reaction were derived from the measurements of the γ line at 983.5 keV (I_γ = 99.98%). Based on a comparison with the IAEA recommended values,[5] the thicknesses of the ^{89}Y foils were corrected by +2% within their uncertainty and the measured beam parameters were adopted without any corrections.

The cross sections of the ^{89}Y$(d,2n)^{89g}$Zr reaction were derived using measurements of the 909.2-keV γ line (I_γ = 99.04%) emitted with the decay of ^{89g}Zr. The metastable state ^{89m}Zr ($T_{1/2}$ = 4.161 min) decayed completely during cooling times. The cumulative cross sections were determined, as shown in Fig. 1, with the previous studies and the TENDL-2017 values.[6] Our experimental data were found to be consistent with the latest four works. The TENDL-2017 values were larger than all experimental data in the energy region between 6 and 20 MeV.

This work is supported by the Japan - Hungary Research Cooperative Program, JSPS and HAS, and by JSPS KAKENHI Grant Number 17K07004.

References

1) M. A. Deri *et al.*, Nucl. Med. Biol. **40**, 3 (2013).
2) S. Manenti *et al.*, Nucl. Instrum. Methods Phys. Res. B **458**, 57 (2019) and references therein.
3) J. F. Ziegler *et al.*, SRIM: the Stopping and Range of Ions in Matter (2008).
4) National Nuclear Data Center, The NuDat 2.7 database, `http://www.nndc.bnl.gov/nudat2/`.
5) A. Hermanne *et al.*, Nucl. Data Sheets **148**, 338 (2017).
6) A. J. Koning *et al.*, Nucl. Data Sheets **113**, 2841 (2012).

† Condensed from the article in Nucl. Instrum. Methods Phys. Res. B **472**, 59 (2020)

*1 Graduate School of Biomedical Science and Engineering, Hokkaido University
*2 RIKEN Nishina Center
*3 Faculty of Science, Hokkaido University
*4 Advanced Clinical Research Center, Fukushima Medical University

Excitation functions of deuteron-induced reactions on ^{141}Pr for medical radioisotope production

M. Aikawa,[*1,*2] T. Maehashi,[*3] D. Ichinkhorloo,[*1,*2] Y. Komori,[*2] and H. Haba[*2]

Investigation of the production of medical radioisotopes is indispensable for the development of imaging and therapy. Radioisotopes ^{140}Nd ($T_{1/2}$ = 3.37 d) and ^{142}Pr ($T_{1/2}$ = 19.12 h) are expected for ^{140}Nd/^{140}Pr generator in positron emission tomography (PET)[1] and the treatment for arteriovenous malformations,[2] respectively. Some charged-particle-induced reactions can produce these two radioisotopes. Among them, we focused on deuteron-induced reactions on monoisotopic element ^{141}Pr. In a literature survey, only two experimental studies for these reactions were found[3,4] below 30 MeV and their experimental cross-section data are scattered. Therefore, we performed an experiment to measure the production cross sections of ^{140}Nd and ^{142}Pr to contribute to the development of nuclear medicine.

The experiment was performed at the RIKEN AVF cyclotron. The stacked-foil activation technique and high-resolution γ-ray spectrometry were adopted in the experiment.

The stacked target consisted of pure metallic foils of ^{141}Pr and ^{nat}Ti. The ^{nat}Ti foils were interleaved for the ^{nat}Ti$(d,x)^{48}$V monitor reaction to assess the beam parameters and target thicknesses. The ^{141}Pr (purity: 99%, thickness: 100 μm, size: 25×25 mm^2) and ^{nat}Ti (purity: 99.6%, thickness: 5 μm, size: 50×100 mm^2) foils were purchased from Nilaco Corp., Japan. The surface area and weight of each foil were measured and their thicknesses were determined to be 67.6 and 2.3 mg/cm^2. The foils were cut into a small size of 8×8 mm^2 to fit a target folder. Nine sets of Pr-Ti-Ti foils were stacked into the target folder that served as a Faraday cup.

The stacked target was irradiated with a deuteron beam for 30 min. The beam intensity of 107 nA was measured by the Faraday cup. The incident energy of 24.1 MeV was measured using the time-of-flight method. Energy degradation in the stacked target was calculated using the SRIM code.[5]

γ rays emitted from the irradiated foils were measured using an HPGe detector. The efficiency of the detector was calibrated using a standard γ-ray point source. Each ^{141}Pr foil with the next ^{nat}Ti catcher foil for recoiled products was measured five times after cooling times from 2.2 h to 40.2 d. The dead time was kept below 5.2%. The required nuclear data were retrieved from the NuDat 2.8 online database.[6]

The ^{nat}Ti$(d,x)^{48}$V monitor reaction was used to assess the beam parameters and target thicknesses. The cross sections of the monitor reaction were derived from the measurement of the 983.5-keV γ line. The result was compared with the IAEA recommended values.[7] According to the comparison, the beam intensity was corrected by -7%. The corrected intensity and measured thicknesses were used to deduce the production cross sections.

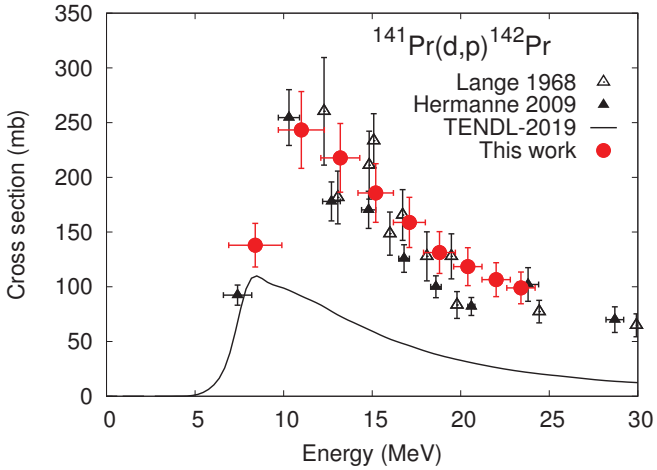

Fig. 1. Cross sections of the ^{141}Pr$(d,p)^{142}$Pr reaction in comparison with the previous data[3,4] and the TENDL-2019 values.[8]

The cross sections of the ^{141}Pr$(d,p)^{142}$Pr reaction were derived from the measurement of the 1575.6-keV γ line (I_γ = 3.7%) with decay of ^{142}Pr. The result is shown in Fig. 1 with the previous studies[3,4] and the TENDL-2019 values.[8] The previous experimental data and their trends are almost consistent with our result within the uncertainties, which are large due to that of the γ-ray intensity ($\Delta I_\gamma / I_\gamma$ = 10.8%). The TENDL-2019 values were found to be smaller than all experimental data.

*1 Faculty of Science, Hokkaido University
*2 RIKEN Nishina Center
*3 School of Science, Hokkaido University

References
1) K. P. Zhernosekov *et al.*, Radiochim. Acta **95**, 319 (2007).
2) S. W. Lee, W. D. Reece, Phys. Med. Biol. **50**, 151 (2005).
3) J. Lange *et al.*, Radiochim. Acta **9**, 66 (1968).
4) A. Hermanne *et al.*, Nucl. Instrum. Methods Phys. Res. B **267**, 727 (2009).
5) J. F. Ziegler *et al.*, SRIM: the Stopping and Range of Ions in Matter (2008).
6) National Nuclear Data Center, The NuDat 2.8 database, http://www.nndc.bnl.gov/nudat2/.
7) A. Hermanne *et al.*, Nucl. Data Sheets **148**, 338 (2017).
8) A. J. Koning *et al.*, Nucl. Data Sheets **155**, 1 (2019).

Production cross sections of medical radioisotope ^{153}Sm in alpha-particle-induced reaction on natural neodymium

M. Sakaguchi,[*1,*2] M. Aikawa,[*3,*2] N. Ukon,[*4,*2] Y. Komori,[*2] H. Haba,[*2] N. Otuka,[*5,*2] and S. Takács[*6]

Samarium-153 ($T_{1/2}$ = 46.3 h) is a beta and gamma emitter that can be applied in radiology. This radionuclide is used for the palliation of metastatic bone cancer as the ethylenediamino-tetrakis-methylenediphosphonic acid (EDTMP) chelate.[1)]

^{153}Sm is typically obtained via the neutron capture reaction on enriched ^{152}Sm in nuclear reactors, but its specific activity is rather low.[2)] For the practical use of ^{153}Sm in radiotherapy, other production routes of ^{153}Sm with relatively high specific activities are required.

This radionuclide can be generated in an alpha-particle-induced reaction on natural neodymium. Only one excitation-function measurement has been reported in the literature for the $^{\rm nat}$Nd$(\alpha,\mathrm{x})^{153}$Sm reaction up to 26.2 MeV.[2)] To confirm the available data and to obtain new data of this reaction, we decided to perform an experiment on the $^{\rm nat}$Nd(α,x) reactions up to 51 MeV.

The experiment was performed at the RIKEN AVF cyclotron. The standard stacked-foil activation technique was adopted for this experiment. The target was composed of twenty-one $^{\rm nat}$Nd foils (purity: 99.0%; thickness: 16.68 mg/cm^2; Goodfellow Co., Ltd., UK) and fourteen $^{\rm nat}$Ti foils (purity: 99.6%; thickness: 2.35 mg/cm^2; Nilaco Corp., Japan). The thicknesses of these foils were derived by measuring their weights and surface areas. The $^{\rm nat}$Ti foils were used for the $^{\rm nat}$Ti$(\alpha,\mathrm{x})^{51}$Cr monitor reaction to assess the initial beam parameters and the energy loss of the beam in the target. The stacked target was irradiated in a target holder, which served as a Faraday-cup, with an alpha-particle beam for 1 h. The primary incident energy and average beam intensity were 51.1 MeV and 172 nA, respectively. Energy degradation through the stacked target was calculated using the SRIM code.[3)]

After a cooling time of approximately 30 min, the target was disassembled, and the gamma-ray spectrometry of the foils was started. The gamma-ray spectra were measured using a high-purity germanium (HPGe) detector (ORTEC GMX30P4-70) without chemical separation and analyzed using the Gamma Studio (SEIKO EG&G) software for each foil.

The cross sections of the $^{\rm nat}$Ti$(\alpha,\mathrm{x})^{51}$Cr monitor reaction were derived from the 320.1-keV gamma-line (I_γ = 9.910%), and the experimental excitation function was compared with the IAEA recommended values.[4)] The thickness of the $^{\rm nat}$Nd foils was adjusted by −1.5% to fit the recommended values and found to be 16.43 mg/cm^2 according to the comparison. The thickness of $^{\rm nat}$Ti foils and the beam parameters were unchanged.

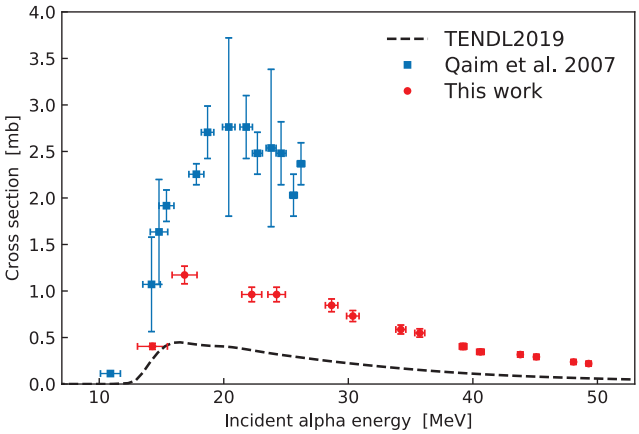

Fig. 1. Excitation function for the $^{\rm nat}$Nd$(\alpha,\mathrm{x})^{153}$Sm reaction compared with previous experimental data[2)] and the TENDL data.[6)]

The excitation function of the $^{\rm nat}$Nd$(\alpha,\mathrm{x})^{153}$Sm reaction was determined using gamma rays with the relatively low energy of 103.18 keV (I_γ = 29.25%). Therefore, the attenuation effect in the metallic Nd foil was considered and calculated from X-ray mass attenuation coefficients.[5)] As a result of the calculation, the net counts of the gamma rays were corrected by +2.1%. Figure 1 shows the corrected cross sections in comparison with the results of a previous study[2)] and the TENDL-2019 data.[6)] The previous data are not consistent with our experimental data and the TENDL data, underestimate both experimental data. The maximum cross section in this work is 1.1 mb, which indicates that this reaction may be unsuitable for the mass production of ^{153}Sm.

This work was supported by JSPS KAKENHI Grant Number 17K07004.

References

1) I. G. Finlay *et al.*, Lancet Oncol. **6**, 392 (2005).
2) S. Qaim *et al.*, Radiochim. Acta **95**, 313 (2007).
3) J. F. Ziegler *et al.*, Nucl. Instrum. Methods Phys. Res. B **268**, 1818 (2010).
4) A. Hermanne *et al.*, Nucl. Data Sheets **148**, 338 (2018).
5) J. H. Hubbell, S. M. Seltzer, X-Ray Mass Attenuation Coefficients, `https://dx.doi.org/10.18434/T4D01F`.
6) A. J. Koning *et al.*, Nucl. Data Sheets **113**, 2841 (2012).

*1 Graduate School of Biomedical Science and Engineering, Hokkaido University
*2 RIKEN Nishina Center
*3 School of Science, Hokkaido University
*4 Advanced Clinical Research Center, Fukushima Medical University
*5 Nuclear Data Section, International Atomic Energy Agency
*6 Institute for Nuclear Research, ATOMKI

Production cross sections of ^{155}Tb in deuteron-induced reactions on natural gadolinium

D. Ichinkhorloo,[*1,*2] M. Aikawa,[*1,*3,*4] Ts. Zolbadral,[*2,*3,*4] Y. Komori,[*3] and H. Haba[*3]

Terbium-155 ($T_{1/2}$ = 5.32 d) can be used for single-photon emission computed tomography (SPECT)[1] and produced through charged-particle-induced reactions. Among the reactions, we focused on the deuteron-induced reaction on natural gadolinium. In a literature survey, three experimental studies on the reaction were found.[2–4] However, some discrepancies could be found among the experimental data. Therefore, we measured the cross sections of the deuteron-induced reaction on natural gadolinium. The result was compared with the previously published experimental data[2–4] and the TENDL-2019 data.[5]

The experiment was performed at the RIKEN AVF cyclotron. We used the stacked-foil activation technique and the high-resolution γ-ray spectrometry to determine the activation cross sections.

The stacked target consisted of 8×8 mm^2 foils cut from a large $^{\rm nat}$Gd foil (25 μm, 50×100 mm^2, 99.9% purity, Nilaco Corp., Japan) and a $^{\rm nat}$Ti foil (5 μm, 50 × 100 mm^2, 99.6% purity, Nilaco Corp., Japan). The isotopic composition of $^{\rm nat}$Gd is ^{152}Gd (0.2%), ^{154}Gd (2.2%), ^{155}Gd (14.8%), ^{156}Gd (20.5%), ^{157}Gd (15.7%), ^{158}Gd (24.8%) and ^{160}Gd (21.8%).

The sizes and weights of the large foils were measured to derive the thicknesses. The thicknesses of the $^{\rm nat}$Gd and $^{\rm nat}$Ti foils were found to be 25.3 and 2.34 mg/cm^2, respectively. The $^{\rm nat}$Ti foils were interleaved for the $^{\rm nat}$Ti$(d,x)^{48}$V monitor reaction to assess beam parameters and target thicknesses. The cut foils were stacked into a target holder, which served as a Faraday cup.

The stacked target was irradiated with the beam for 60 min. An average intensity of 98.1 nA was measured by the Faraday cup. The beam energy was measured by the time-of-flight method.[6] Energy degradation in the stacked target was calculated using the Stopping and Range of Ions in Matter (SRIM) code.[7]

The γ-rays emitted from each irradiated foil were measured using a high-resolution high-purity germanium (HPGe) detector and analyzed using the software Gamma Studio software (SEIKO EG&G).

The total uncertainties (∼10%) were estimated from the square root of the quadratic summation of each component; statistical uncertainty (0.4–1.5%), target thickness (2%), target purity (1%), beam intensity (5%), detector efficiency (6%) and γ-ray intensity (1.3%).

The cross sections of the $^{\rm nat}$Ti$(d,x)^{48}$V monitor reaction were derived using the line at 983.525 keV (I_γ = 99.98%). The derived cross sections were compared with the values recommended by the International Atomic Energy Agency (IAEA).[8] We could obtain good agreements between the results and the recommended values.

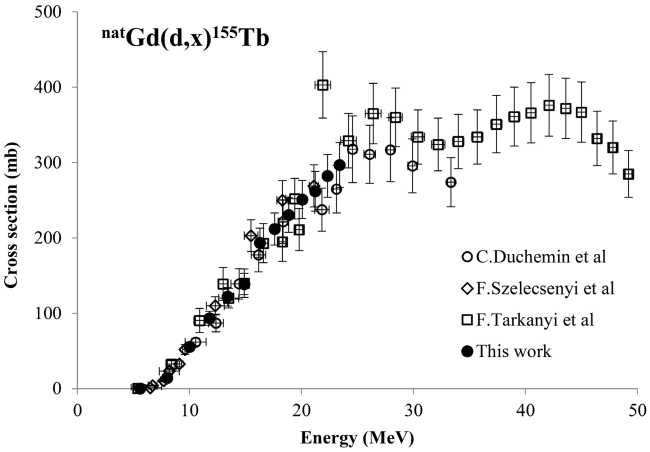

Fig. 1. Excitation function of the $^{\rm nat}$Gd$(d,x)^{155}$Tb reaction along with the previously published data[2–4] and TENDL-2019 data.[5]

The γ line at 105.3 keV (I_γ = 25.1%) emitted with the ^{155}Tb decay was measured to derive the cross sections of the $^{\rm nat}$Gd$(d,x)^{155}$Tb reaction. The measurements were performed after a cooling time of 3 days. The result is presented in Fig. 1 along with the previously published experimental data[2–4] and TENDL-2019 data.[5] Our result shows good agreement with the previous experimental data within the uncertainty, except for one data point at 22 MeV of Tárkányi *et al.*[4] The TENDL-2019 data substantially overestimate all the experimental data in the lower energy region.

In the summary, we performed an experiment to measure the excitation functions of the $^{\rm nat}$Gd$(d,x)^{155}$Tb reaction up to 24.1 MeV at the RIKEN AVF cyclotron. The production cross sections of ^{155}Tb were determined. The result was compared with the experimental data studied published previously and the TENDL data. We good agreement between our result and the previous experimental results.

*1 Faculty of Science, Hokkaido University
*2 Nuclear Research Center, National University of Mongolia
*3 Nishina Center for Accelerator-Based Science, RIKEN
*4 Graduate School of Biomedical Science and Engineering, Hokkaido University

References

1) C. Müller *et al.*, J. Nucl. Med. **53**, 1951 (2012).
2) C. Duchemin *et al.*, Appl. Radiat. Isot. **118**, 281 (2016).
3) F. Szelecsényi *et al.*, J. Radioanal. Nucl. Chem. **307**, 1877 (2016).
4) F. Tárkányi *et al.*, Appl. Radiat. Isot. **83**, 25 (2014).
5) A. J. Koning *et al.*, Nucl. Data Sheets **155**, 1 (2019).
6) T. Watanabe *et al.*, Proc. 5th Int. Part. Accel. Conf. (IPAC 2014), 3566 (2014).
7) J. F. Ziegler *et al.*, SRIM: the Stopping and Range of Ions in Matter, `http://www.srim.org`.
8) A. Hermanne *et al.*, Nucl. Data Sheets. **148**, 338 (2018).

Production cross sections of $^{nat}Er(d,x)^{171}Er$ reactions on natural erbium†

M. U. Khandaker*1,*2 and H. Haba*2

The nuclear reaction cross-sections play a key role in optimization of production parameters for radionuclide of interest via the use of particle accelerators. In this study, the production cross-sections of $^{nat}Er(d,x)^{171}Er$ reaction has been measured by using stacked foil activation technique combined with HPGe gamma-ray spectrometry. ^{171}Er ($T_{1/2}$ = 7.516 h; E_γ = 308.291 keV, $I_\gamma = 64\%$) finds remarkable applications for the development and evaluation of pharmaceutical drug delivery systems via the well-known gamma scintigraphic technique.[1] The measured cross-sections for ^{171}Er also find great significance as a short-lived parent for producing medically important long-lived daughter ^{171}Tm ($T_{1/2}$ = 1.92 y) via the $^{170}Er(d,p)^{171}Er \rightarrow {}^{171}Tm$ process. Note that considering the common drawbacks of (n,γ) production route, several authors[2] studied the production possibility of erbium radionuclides via light-charged particles-induced reactions on several targets. However, since a search of literature shows that the status of deuteron-induced reaction cross-sections on erbium is not satisfactory, further study on such processes may find great significance in various respect.

Under this circumstance, the production cross-sections of $^{nat}Er(d,x)^{171}Er$ nuclear reaction has been measured from threshold up to 23.06 MeV by using the AVF cyclotron of the RIKEN RI Beam Factory, Wako, Japan. Details on the irradiation technique, radioactivity determination, and data evaluation procedures are available in Ref. 3). Owing to the space limitation of this report, we present only the $^{nat}Er(d,x)^{171}Er$ cross sections and the deduced yield in Figs. 1 and 2, respectively. Measured cross sections with an overall uncertainty are listed in Ref. 3). The cross-sections were normalized by using the $^{nat}Ti(d,x)^{48}V$ monitor cross sections recommended by IAEA. Measured data were critically compared with the available literature data, and an overall good agreement was found. However, only partial agreements were obtained with the data extracted from the TENDL-2017 library and EMPIRE-3.2.2 code.

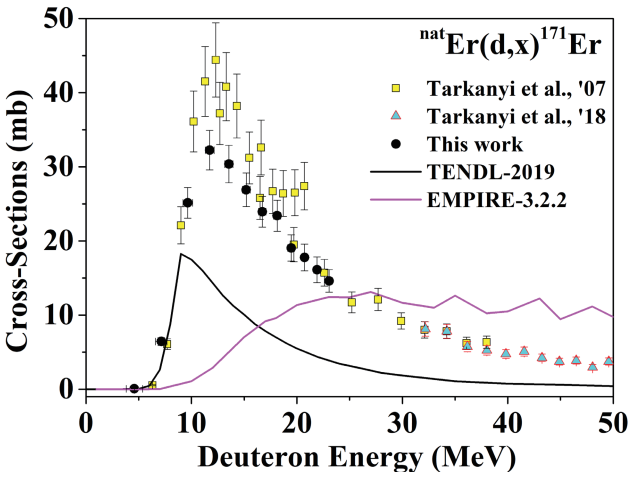

Fig. 1. Excitation function of the $^{nat}Er(d,x)^{171}Er$ reaction.

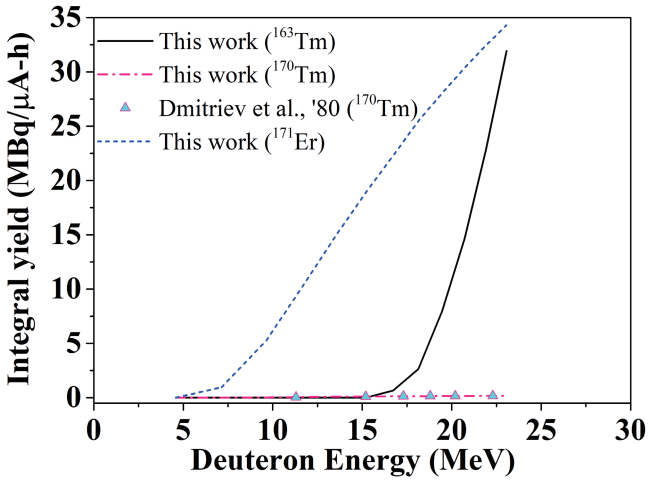

Fig. 2. Thick target integral yields (physical) for $^{163,\,170}Tm$ and ^{171}Er radionuclides.

Realizing the applications of measured radionuclides including $^{nat}Er(d,x)^{171}Er \rightarrow {}^{171}Tm$ in medical and other fields, it is hope that the measured data could play an important role in enrichment of the cross section database that are useful for applications in the medical, industrial and accelerator technologies. The large discrepancy for the $^{170}Er(d,p)^{171}Er$ (E_{thr} = 0.0 MeV) reaction between the model code and the measurement is an important clue to modify the model code.

References

1) A. F. Parr, R. M. Beihn *et al.*, Pharm. Res. **4**, 486 (1987).
2) H. Uusijarvi, P. Bernhardt *et al.*, J. Nucl. Med. **47**, 807 (2006).
3) M. U. Khandaker, H. Haba *et al.*, Nucl. Instrum. Methods Phys. Res. B **470**, 1 (2020).

† Condensed from Nucl. Instrum. Methods Phys. Res. B **470**, 1 (2020)

*1 Centre for Biomedical Physics, Sunway University
*2 RIKEN Nishina Center

Measurement of production cross sections of ^{175}Hf in the ^{nat}Lu(p,x) and ^{nat}Lu(d,x) reactions

Y. Komori,[*1] H. Haba,[*1] M. Aikawa,[*2] M. Saito,[*2] S. Takács,[*3] and F. Ditrói[*3]

The chemical characterization of superheavy elements (SHEs) with atomic number ≤104 is one of the most important and challenging subjects in the field of nuclear chemistry. Prior to chemistry experiments on SHEs, it is important to find suitable chemical systems and experimental conditions using the no-carrier-added radiotracers of their lighter homologues. The long-lived Hf isotope, ^{175}Hf ($T_{1/2}$ = 70 d), is useful for basic studies on element 104, Rf. The ^{175}Hf isotope can be produced in proton- and deuteron-induced reactions on ^{nat}Lu. For efficient and quantitative production of this isotope, excitation functions are necessary to know. However, data are available only for the ^{nat}Lu$(p,x)^{175}$Hf reaction[1] and not for the ^{nat}Lu$(d,x)^{175}$Hf. In this work, we measured the excitation functions for these reactions at RIKEN and the Institute for Nuclear Research (ATOMKI).

The excitation functions were measured using the stacked foil technique. At RIKEN, a target stack that consisted of 9 sets of a ^{nat}Lu foil (99% purity, 27.1 mg/cm^2 thickness), a ^{nat}Ta foil (99.95%, 17.0 mg/cm^2), and 2 ^{nat}Ti foils (≤99.6%, 4.4 mg/cm^2) was irradiated with a 14-MeV proton beam supplied from the RIKEN AVF cyclotron. Another target stack that consisted of 17 sets of a ^{nat}Lu foil (99%, 27.6 mg/cm^2), a ^{nat}Ta foil (99.95%, 17.1 mg/cm^2), and a ^{nat}Ti foil (≤99.6%, 4.4 mg/cm^2) was irradiated with a 24-MeV deuteron beam. At ATOMKI, a target stack that consisted of 17 sets of a ^{nat}Lu foil (99%, 20.7 mg/cm^2), a ^{nat}Ta foil (99.95%, 17.0 mg/cm^2), and 2 ^{nat}Ti foils (≤99.6%, 5.4 mg/cm^2) was irradiated with an 18-MeV proton beam from the MGC-20E cyclotron. Another target stack that consisted of 8 sets of a ^{nat}Lu foil (99%, 20.7 mg/cm^2) and a ^{nat}Ti foil (≤99.6%, 4.4 mg/cm^2) was irradiated with a 10-MeV deuteron beam. The ^{nat}Ta foils were used to determine the excitation functions for the ^{nat}Ta(p,x) and ^{nat}Ta(d,x) reactions. The ^{nat}Ti foils were used to confirm the beam energy and intensity based on the monitor reactions of ^{nat}Ti$(p,x)^{48}$V and ^{nat}Ti$(d,x)^{48}$V. All these target stacks were irradiated with 170–220 nA beam currents for 2 h. After the irradiation, each foil was subjected to γ-ray spectrometry with Ge detectors.

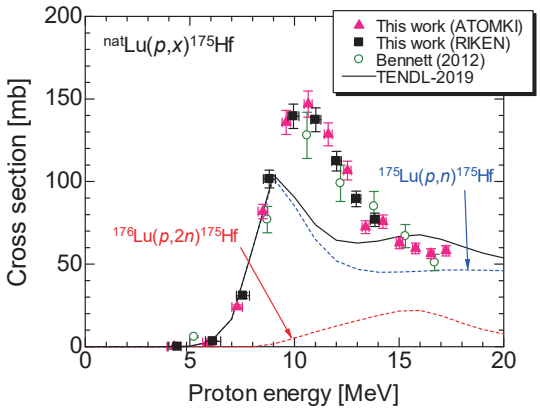

Fig. 1. Excitation function for the ^{nat}Lu$(p,x)^{175}$Hf reaction.

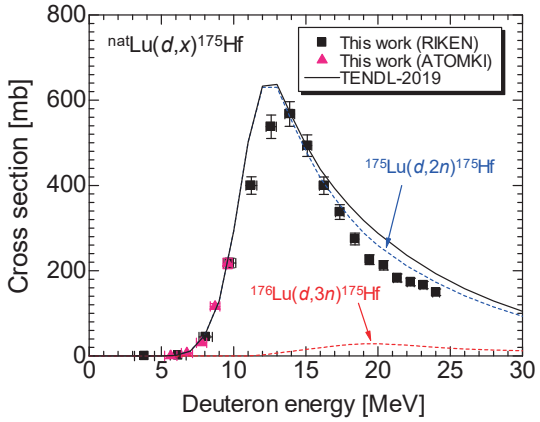

Fig. 2. Excitation function for the ^{nat}Lu$(d,x)^{175}$Hf reaction.

The excitation functions were measured for the ^{nat}Lu$(p,x)^{173,175}$Hf and ^{nat}Lu$(d,x)^{173,175}$Hf, ^{173,174m,174g,176m,177m,177g}Lu reactions. Figures 1 and 2 show the excitation functions for the ^{nat}Lu$(p,x)^{175}$Hf and ^{nat}Lu$(d,x)^{175}$Hf reactions, respectively. For both reactions, our data measured at RIKEN and ATOMKI are consistent with each other. Data of the ^{nat}Lu$(p,x)^{175}$Hf reaction are also consistent with the data previously published by Bennet *et al.*[1] Theoretically predicted cross sections for the ^{nat}Lu$(p,x)^{175}$Hf reaction in the TENDL-2019 library[2] are lower than the experimental ones at 9–14 MeV. The peak energy of the excitation function in the TENDL-2019 is approximately 1.5 MeV lower than the experimental one. For the ^{nat}Lu$(d,x)^{175}$Hf reaction, TENDL-2019 slightly overestimates the cross sections at 10–14 MeV and above 15 MeV. The peak energy in TENDL-2019 is approximately 1 MeV lower than the experimental one. Physical thick-target yields of ^{175}Hf were deduced from the measured excitation functions. The yield of ^{175}Hf in the ^{nat}Lu$(p,x)^{175}$Hf reaction is 0.47 MBq/μA·h in the energy range of 4.2–17.2 MeV, while that in the ^{nat}Lu$(d,x)^{175}$Hf reaction is 2.0 MBq/μA·h in the range of 5.7–24.0 MeV. The yield of the ^{nat}Lu$(d,x)^{175}$Hf reaction is 4 times larger than that of the ^{nat}Lu$(p,x)^{175}$Hf reaction in the energy ranges investigated in this work.

*1 RIKEN Nishina Center
*2 Graduate School of Biomedical Science and Engineering, Hokkaido University
*3 Institute for Nuclear Research, ATOMKI

References

1) M. E. Bennet *et al.*, Nucl. Instrum. Methods Phys. Res. B **276**, 62 (2012).
2) A. J. Koning, D. Rochman, Nucl. Data Sheets **113**, 2841 (2012).

4. Radiation Chemistry and Biology

Selection of high-yield rice mutant induced by heavy-ion beam irradiation

Y. Hayashi,[*1] Y. Shirakawa,[*1] K. Ichinose,[*1] R. Morita,[*1] T. Sato,[*1,*2] and T. Abe[*1]

Improvement in productivity is the main objective of rice breeding. Rice grain yield is determined based on three components: the number of panicles per plant, number of grains per panicle, and grain weight. Among them, the grain weight is a stable varietal character and effective target trait for the mutation breeding of high-yield rice.

We performed mutant selection for achieving high-yield rice from M_2 populations obtained by heavy-ion beams irradiation. M_2 seeds used in this study were derived from irradiated dry rice seeds of 'Nipponbare' (*Oriza Sativa* L.) with C-ion, Ar-ion, and Fe-ion. Liner energy transfer (LET) and irradiation doses are summarized in Table 1. These conditions were the most efficient with the highest mutation rate at each LET in our previous study.[1,2)]

Table 1. Irradiation conditions of heavy-ion beams.

Ion	Energy (MeV/nucleon)	LET (keV/μm)	Dose (Gy)
C	135	30	175
Ar (184)	160	184	20
Ar (290)	95	290	10
Fe	90	650	20

Table 2. Number of lines selected in each generation.

Ion	Planted M_1 line	Surveyed M_1 line	Candidates M_2	Candidates M_3
C	200	113	5	2
Ar (184)	200	121	4	0
Ar (290)	200	122	4	1
Fe	190	106	5	2
Total	790	462	18	5

There were 790 M_1 lines in total and ten plants from each M_1 line were planted in the paddy field. In our previous study on rice, we isolated various mutants of the flowering period, plant height, leaf color, tillering, and weakness by visual evaluation in the paddy field. However, the identification of grain size in the field for mutant selection is not easy and is inefficient. Panicle weight reflects the grain size and fertile grain number, which are two major components of the yield. We adopted the method of measuring the weight of the main panicle from each M_1 plant to select the candidates of the mutant. First, some lines were excluded from panicle weight selection when segregated mutations were observed in the field. We selected 18 candidates based on panicle weight from 462 M_1 lines (Table 2).

Next year, we conducted a yield survey on a small scale to confirm their traits and narrow down the candidates. Thirty M_3 seedlings of each candidate line were planted in a plot (0.9 m wide and 3 m long). 'Nipponbare' was used as control. To avoid the border effect, 8 plants from the inner plot (2.4 m^2) were collected. The panicle weight, spikelet number, seed fertility, and grain weight were investigated on the main culms. The grains from the line with the higher weight were dehulled; the grain width, grain length, and grain thickness were measured using a rice analyzer (RGQ1 10B, SATAKE). However, some lines which had low fertility or low number of grains were not included in the grain size measurement even though their grain weight were high, because the trade-off relationship between the single grain size and grain number should be considered. In addition, lines with large individual differences were excluded. Finally, five lines were selected based on their large grain size. There was a trend for long grains in all 5 candidates (Table 3). Among them, Ar-39 achieved the best results in most components. Our previous study succeeded in discovering novel gene: LIN1 using the long grain mutant induced by Ar-ion irradiation.[3)] The genetic analysis of these candidates to reveal relevant genes is in progress while continuing repeated yield surveys on a large scale.

References
1) Y. Hayashi *et al.*, RIKEN Accel. Prog. Rep. **50**, 27 (2017).
2) Y. Hayashi *et al.*, RIKEN Accel. Prog. Rep. **51**, 238 (2018).
3) R. Morita *et al.*, Molecular Breeding **39**, 135 (2019).

Table 3. Mean ± standard error of yield-related characters and grain size for selected M_3 lines.

Line	Panicle weight (g/one panicle)	Grain number (/panicle)	Seed fertility (%)	Grain weight (g/1,000 grain)	Grain size (mm) Length	Width	Thickness
'Nipponbare'	2.95 ± 0.07	130.4 ± 5.58	87.3 ± 1.86	24.2 ± 0.26	5.02 ± 0.03	2.81 ± 0.02	1.88 ± 0.01
C-98	3.32 ± 0.14	135.6 ± 5.19	85.1 ± 1.44	25.0 ± 0.21	5.08 ± 0.02	2.77 ± 0.02	1.86 ± 0.01
C-190	2.80 ± 0.06	118.0 ± 2.78	83.2 ± 1.70	25.8 ± 0.13	5.18 ± 0.02	2.85 ± 0.02	1.89 ± 0.01
Ar-39	3.63 ± 0.14	148.8 ± 5.70	85.4 ± 0.89	25.7 ± 0.23	5.17 ± 0.02	2.89 ± 0.02	1.89 ± 0.01
Fe-134	3.10 ± 0.11	129.0 ± 3.91	83.5 ± 1.69	25.5 ± 0.17	5.12 ± 0.02	2.85 ± 0.02	1.88 ± 0.01
Fe-153	3.03 ± 0.10	126.6 ± 4.50	83.5 ± 1.48	25.2 ± 0.27	5.08 ± 0.02	2.85 ± 0.02	1.89 ± 0.01

*1 RIKEN Nishina Center
*2 Graduate School of Agricultural Science, Tohoku University

Whole genome sequencing analysis for detecting mutations induced by carbon- and argon-ion irradiations of rice (*Oryza sativa* L.)

R. Morita,[*1] H. Ichida,[*1] Y. Shirakawa,[*1] K. Ichinose,[*1] T. Sato,[*1,*2] and T. Abe[*1]

A mutation analysis with high-throughput sequencing is a powerful tool for characterizing the molecular nature of mutations induced by mutagen at the whole-genome level. We have investigated the mutation effect following heavy ion-beam irradiation of rice (*Oryza sativa* L. cv. Nipponbare), a monocotyledonous model plant, using high-throughput sequencing. In this study, we irradiated C-ion (LET: 30 keV/μm) or Ar-ion (LET: 290 keV/μm) to rice, and investigated numbers and types of mutations induced by both ions at whole-genome level to examine whether the difference in the LET value of the ions influences the numbers and sizes of mutations in rice genome.

We irradiated C-ion (175 Gy, LET: 30 keV/μm) or Ar-ion (10 Gy, LET: 290 keV/μm) to rice (*Oryza sativa* L. cv. Nipponbare) dry seeds. The plants from irradiated seeds (M_1 plants) were grown in a paddy field and self-pollinated to obtain M_2 seeds. Next year, we grew M_2 plants in a paddy field to collect mutant plants with visible phenotypes and harvest M_3 seeds from the each plant. For this study, we selected 11 and 4 mutant plants from C-ion and Ar-ion irradiations, respectively. Genomic DNA extraction for Whole-genome sequence was performed from the leaves of individual M_3 plants. Candidate mutation extraction were performed using "bioinformatics pipeline."[1] We extracted candidate mutations using a combination of the GATK, Pindel, Delly, and Manta programs. GATK adopted the following parameters of (`-stand_call_conf 50 -A Coverage -A RMSMappingQuality -baq CALCULATE_AS_NECESSARY`). Pindel was used following parameters of (`-window_size 1 -report_long_insertions -report_breakpoints -minimum_support_for_event 3 -min_inversion_size 10`). Delly and Manta were run with default parameters. All mutations detected were visually confirmed using Integrated Genomics Viewer (IGV).[2]

We detected 1718 mutations from 11 C-ion-irradiated mutants, and 426 mutations from 4 Ar-ion-irradiated mutants. The average numbers of total mutations in a mutant genome were 156.2 and 106.5 for C-ion and Ar-ion irradiations, respectively. The most abundant mutations induced by both C-ion and Ar-ion irradiation were single-nucleotide variants (SNVs). The average numbers of SNVs in a mutant genome were 123.2 and 86.8 for C-ion and Ar-ion, respectively (Fig. 1). The second most abundant mutations induced by both C-ion and Ar-ion irradiation were small (<100 bp) insertions and deletions (indels). The average numbers of indels in a mutant genome were 31.5 and 16.3 for C-ion and Ar-ion, respectively. There were large deletions

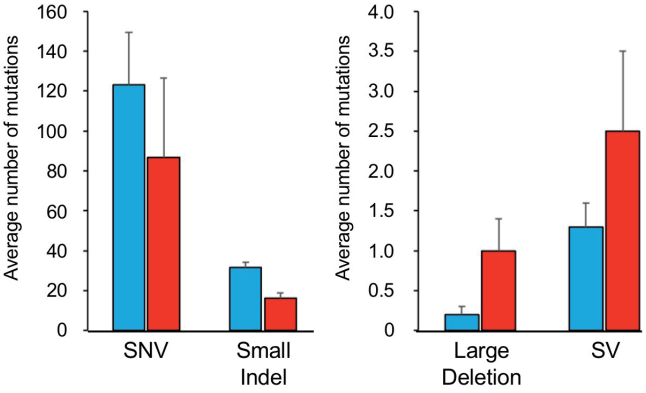

Fig. 1. Average number of SNV, small Indel, Large deletion, and SV induced by C-ion (blue) and Ar-ion (red) irradiations. Error bars indicate standard error.

(≥100 bp) and structural variations (SVs), such as inversion and translocation in a mutant genome derived from both C-ion and Ar-ion irradiations. The average numbers of large deletions and SVs in a mutant genome were 0.2 and 1.3 for C-ion, and 1.0 and 2.5 for Ar-ion, respectively. Comparing the mutations induced by C-ion and Ar-ion, the number of small mutation, such as SNVs and small indels, tended to be higher in the C-ion irradiation than in Ar-ion irradiation. Conversely, the number of both large deletion and SVs tended to be higher in Ar-ion than in C-ion. These tendencies corresponded to the results observed in the irradiation of Arabidopsis seeds.[3] They compared the number of mutations induced by C-ion (LET: 30 keV/μm) or Ar-ion (LET: 290 keV/μm) irradiation using Arabidopsis, a dicotyledonous model plant, at the whole-genome level, and demonstrated that Ar-ions induced rearrangements (including large-deletion and SVs) more frequently than C-ions.[3] They also indicated that Ar-ions induced SNVs less frequently than C-ions. The findings obtained in this study and that of Kazama *et al.* (2017) suggested that C-ion irradiation tends to induce small mutations predominantly, whereas Ar-ion irradiation tends to induce higher number of large deletions and SVs than C-ion irradiations of both rice and Arabidopsis genomes. Because the sample size was not sufficient to compare the numbers of each mutation induced by C-ion and Ar-ion statistically in this study, we plan to increase the sample size to perform a more detailed analysis.

*1 RIKEN Nishina Center
*2 Graduate School of Agricultural Science, Tohoku University

References
1) H. Ichida *et al.*, Plant J. **98**, 301 (2019).
2) J. T. Robinson *et al.*, Nat. Biotechnol. **29**, 24 (2011).
3) Y. Kazama *et al.*, Plant J. **92**, 1020 (2017).

Detection of structural variations in three responsible genes induced by relatively high-LET ion beams in rice

Y. Shirakawa,[*1] R. Morita,[*1] Y. Hayashi,[*1] K. Ichinose,[*1] T. Sato,[*1,*2] and T. Abe[*1]

The molecular characteristics of mutations induced by a heavy-ion beam with a relatively high LET in rice, a model plant of monocotyledonous, has not yet been revealed. In this study, we irradiated dry seeds of rice (*Oryza sativa* L. 'Nipponbare') with Fe- or Ar-ion beams, isolated 3 mutants for which the responsible gene has been clarified, and characterized the structure of the mutated gene using polymerase chain reaction (PCR) analysis.

A *pla1* mutant (Ar7-165, Fig. 1) was isolated from 239 M_1 lines irradiated with Ar ions (7.5 Gy, LET: 289 keV/μm). In this mutant, no PCR amplification occurred when primers designed for amplification of the central area of the *PLA1* gene (primer pairs F4 and R20, F6 and R21, and uF5 and R21, as shown in Fig. 2) were used, suggesting that structural variations (SVs) such as inversion or translocation occurred in the gene (Fig. 2).

A dwarf mutant (Fe15-235, Fig. 1) that showed a defect in gibberellin biosynthesis was isolated from 236 M_1 lines irradiated with Fe ions (15 Gy, LET: 650 keV/μm). We conducted PCR analysis with the primers for gibberellin biosynthesis-related genes and detected a deletion in the region including the 1st to 6th exon of the *OsKS1* gene (Fig. 2). Additional PCR and sequencing analyses revealed that Fe15-235 harbors a 9,843 bp deletion (Chr04: 31018475 - 31028317) in the *OsKS1* gene.

We isolated the *brd1* mutant (WAr30-204), which showed a dwarf phenotype with a defect in brassinosteroid biosynthesis from 242 M_1 lines irradiated with Ar ions generated by the WACAME line[1)] (30 Gy, LET:184 keV/μm). PCR analysis revealed that this mutant harbors a 27 kb deletion involving the entire *OsBRD1* gene (Fig. 2). Another deletion of approximately 5 kb was also detected 18 kb downstream from the 27-kb deletion. It suggested that a complex mutation with large deletions occurred in the *OsBRD1* gene region. Our findings suggest that a heavy-ion beam with a relatively high LET may predominantly induce large deletions or SVs in the responsible gene region in rice. This tendency was also observed in the PCR and sequence analysis for Arabidopsis mutants induced by Ar-ion irradiation on dry seeds[2)] and rice mutants induced by Ar-ion irradiation on imbibed seeds.[3)]

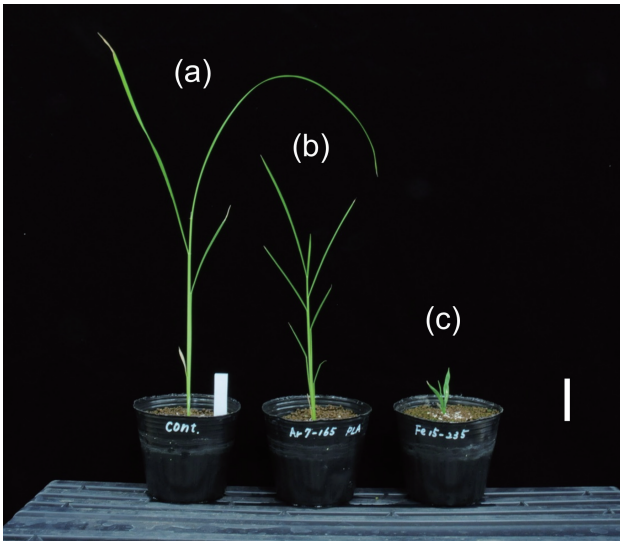

Fig. 1. Morphological comparison of (a) Nipponbare, (b) Ar7-165, and (c) Fe15-235 plants 24 days after sowing. Scale bar = 5 cm.

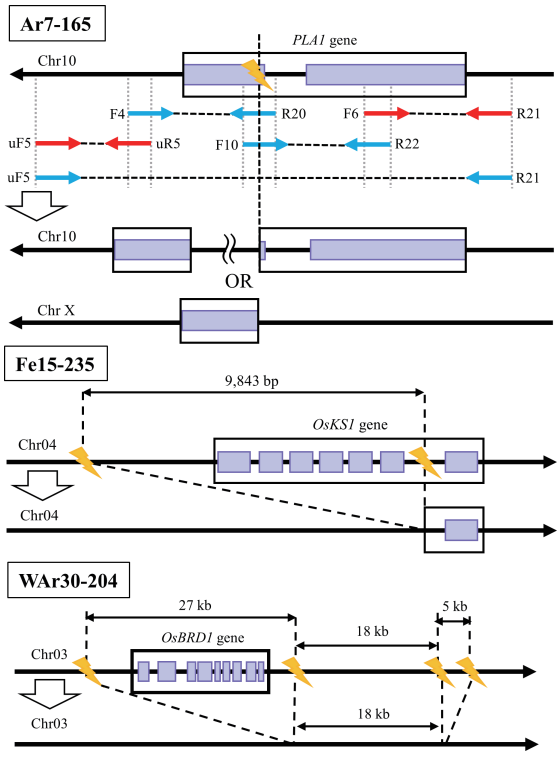

Fig. 2. Schematic representation of mutated genes. Purple boxes indicate protein coding regions (exons), and yellow marks indicate the position of the DNA double-strand breaks induced by heavy-ion beams. In the case of the Ar7-165 mutant, the position of the primers used in PCR are shown. Red arrows indicate primers for which DNA amplification occurs in PCR, whereas blue arrows indicate primers for which DNA amplification did not occur in PCR.

*1 RIKEN Nishina Center
*2 Graduate School of Agricultural Science, Tohoku University

References

1) N. Fukunishi *et al.*, Proc. 13th Heavy Ion Accelerator Technology Conference (HIAT2015), 42 (2016).
2) T. Hirano *et al.*, Mutation Res. **735**, 19 (2012).
3) S. Kogure *et al.*, RIKEN Accel. Prog. Rep. **47**, 289 (2014).

Dose-dependent mutagenic effects of 160-MeV/nucleon-argon beam in *Arabidopsis thaliana*

K. Ishii,[*1] S. Ohbu,[*1] Y. Shirakawa,[*1] and T. Abe[*1]

Heavy-ion beams are used as an effective mutagens that induce localized mutations owing to their high linear energy transfer (LET). We previously reported a dose-dependent mutagenic effect of a 135-MeV/nucleon-carbon beam (30 keV/μm) in *Arabidopsis thaliana* in which the number of mutations per genome was dose-dependently increased in the range of 150–350.[1)] In this study, we investigated the dose-dependent mutagenic effect of a 160-MeV/nucleon-argon beam and its difference to that of a 135-MeV/nucleon beam.

Dry seeds of *Arabidopsis thaliana* (the Col-0 wild-type strain or CS16118 strain, which possesses a heterozygous null mutation in the *APG3* gene for measuring the mutation rate in M_1 generation[2)]) were irradiated with 160-MeV/nucleon-argon ions in doses of 0–120 Gy. The LET of the argon-ion beams was controlled to 188 keV/μm. Survival and mutation rates in M_1 generation were measured as previously described.[2)] Randomly selected ten M_2 plants were harvested from one self-pollinated M_1 plant. Genomic DNA was extracted from a mixture of the leaves of the ten M_2 plants. Five DNA pools were sequenced for each dose using HiSeq X-Ten sequencing systems (Illumina Inc.). The read sequences obtained were input into the mutational analysis pipeline, AMAP, as described previously,[3)] with some modifications. The mutation candidates were detected with GATK (HaplotypeCaller), PINDEL, and BREAKDANCER software. The number of mutations was counted as follows: For small mutations that included single nucleotide substitutions and <100 bp indels (insertions and deletions), each mutation was counted as one. For large mutations, that included ≥100 bp indels and chromosome rearrangements), the number of junctions in each mutant line were counted. Total number of these mutations per DNA pool was envisaged as the number of mutations per genome.

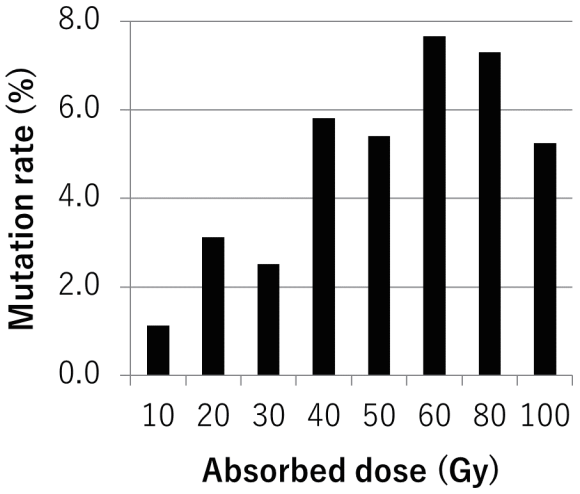

Fig. 1. Mutation rate in M_1 generation after irradiation of 160-MeV/nucleon-argon beam ($n \geq 500$).

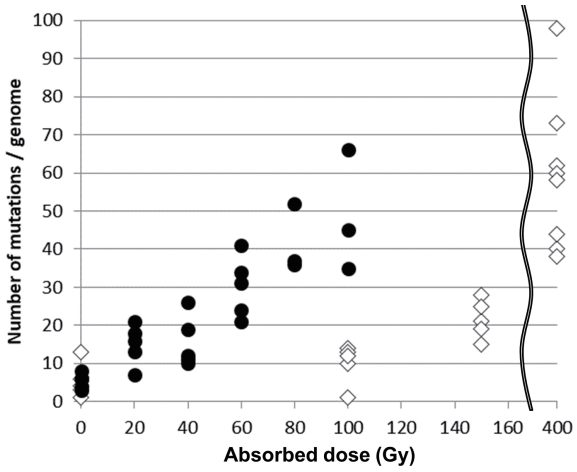

Fig. 2. Number of mutations in M_2 generation induced after irradiation of 188 keV/μm argon-ion beam (black circles) and 30 keV/μm carbon-ion beam (white rhombi).

In the M_1 generation, the average survival rate (flowering rate one month after cultivation[2)]) was 94% at 80 Gy-irradiation and decreased to 74% at 100 Gy-irradiation (data not shown). The mutation rate (appearance ratio of white sector mutation[2)]) indicated an increasing tendency with the increasing dose in the range of 10–80 Gy (Fig. 1). The highest mutation rate was 7.7% at 60 Gy-irradiation, which is as high as that previously reported (7.0% at 400 Gy with 30 keV/μm of LET; $p = 0.54$ by chi-square test).[2)] The decreased mutation rate at 100 Gy-irradiation may reflect the radiation overdose, as seen in the survival rate.

The number of mutations per genome in the M_2 generation after 188 keV/μm argon ion beam irradiation compared to that after 30 keV/μm carbon ion beam irradiation previously reported[1,4)] is shown in Fig. 2. After 400-Gy irradiation of the 30 keV/μm carbon-ion beam, the mutation rate in the M_1 generation was approximately 7%[2)] and the average number of mutations in the M_2 generation was 59 (Fig. 2). In contrast, after the 60-Gy irradiation of the 188 keV/μm argon-ion beam, the mutation rate in the M_1 generation was

*1 RIKEN Nishina Center

7.7% (Fig. 1) but the average number of mutations in the M_2 generation was 29 (Fig. 2). The difference in the average number of mutations in the M_2 generation under between the two irradiation conditions can be attributed to the content of the mutations. Among the number of mutations in the M_2 generation induced by the 30 keV/μm carbon-ion beam, only 4% were derived from large mutations, whereas 32% were obtained by 188 keV/μm argon-ion beam. Further analysis, for example, to compare the number of genes affected by the mutations including inversions that possibly cause the chromosomal position effect of the 30 keV/μm carbon-ion and the 188 keV/μm argon-ion beam may provide insight into the mutagenic characteristics of each beam.

References

1) Ishii *et al.*, RIKEN Accel. Prog. Rep. **52**, 216 (2019).
2) Y. Kazama *et al.*, Plant Biotechnol. **29**, 441 (2012).
3) K. Ishii *et al.*, Genes Genet. Syst. **91**, 229 (2016).
4) Y. Kazama *et al.*, Plant J. **92**, 1020 (2017).

Argon-ion-induced mutant of *Arabidopsis thaliana* exhibiting accelerated leaf chlorosis†

A. Sanjaya,[*1] Y. Kazama,[*2,*3] K. Ishii,[*2] S. Ohbu,[*2] T. Abe,[*2] and M. Fujiwara[*1,*2]

Chloroplast development in leaf tissues is crucial for plant growth and productivity. Plant leaves are composed of the epidermis, which forms the outermost layer, and the mesophyll and vasculature inside. In the model plant *Arabidopsis thaliana*, chloroplasts are distributed in leaf epidermal pavement and guard cells, as well as in mesophyll cells. Despite vast research on the structure and function of leaf chloroplasts, there is limited knowledge about their regulations in the plant life cycle.

To explore possible novel gene functions for leaf chloroplast development, we attempted a forward genetic approach. We created mutants of *A. thaliana* by exposing dry seeds of ecotype Col-0 to accelerated argon ions (290 keV/μm, 50 Gy) at RIBF.[1)] Following two rounds of cultivation and selfing, as well as a macroscopic screening of the M_3 generation of plants, we isolated a new mutant, designated as Ar50-33-pg1.

During seedling development, Ar50-33-pg1 produced slightly pale cotyledons and leaves under standard plant growth conditions (Fig. 1A, B). As the mutant leaves expanded and matured, their chlorosis became prominent (Fig. 1C). This observation of accelerated leaf chlorosis was supported by the chlorophyll measurement of detached leaves through spectrophotometry (data not shown). Furthermore, Ar50-33-pg1 exhibited abnormalities at the reproductive stage, including phenotypes of late flowering, flower longevity, and low seed production (data not shown).

Microscopic examination of expanding leaves of wild-type and Ar50-33-pg1 plants under normal observation conditions revealed that a certain population of mutant epidermal chloroplasts lacked chlorophyll autofluorescence signal (Fig. 2). Meanwhile, mutant mesophyll chloroplasts retained chlorophyll autofluorescence until later stages of leaf senescence. Therefore, the chlorosis leaf phenotype of Ar50-33-pg1 might involve tissue-dependent chloroplast abnormalities between the epidermis and mesophyll.

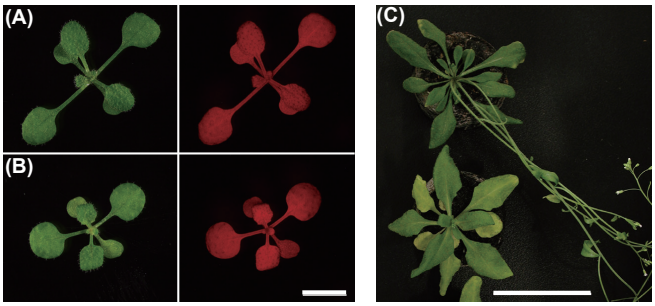

Fig. 1. Growth and morphology of seedlings of *Arabidopsis*. (A) 2-week-old wild-type seedling. (B) 2-week-old Ar50-33-pg1 seedling. In (A) and (B), images of chlorophyll autofluorescence were taken at the same excitation condition by stereofluorescence microscopy. Scale bar = 5 mm. (C) 4-week-old wild-type and Ar50-33-pg1 seedlings. Scale bar = 5 cm.

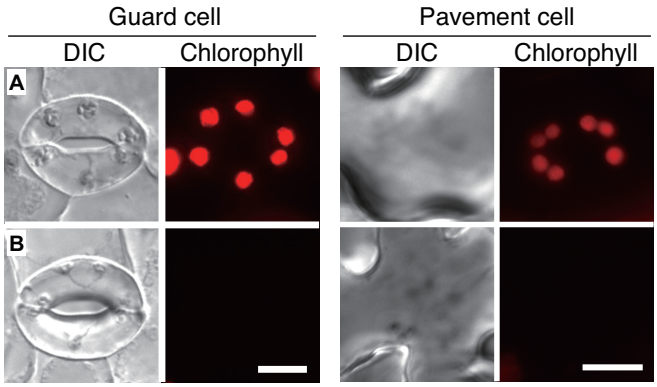

Fig. 2. Fluorescence microscopy of leaf epidermal guard cells and pavement cells of *Arabidopsis*. (A) Wild type. (B) Ar50-33-pg1. Differential interference contrast (DIC) and chlorophyll autofluorescence (colored in red) images of cells from epidermal peels of growing rosette leaves. Scale bar = 10 μm.

Backcrossing and segregation analyses indicated that the chlorotic phenotype of Ar50-33-pg1 is associated with impaired epidermal chloroplasts and is caused by a single nuclear recessive allele. Through whole-genome resequencing, Ar50-33-pg1 was revealed to contain a ~0.9 Mb deletion from position 12621534 to 13561533 in chromosome V, which spans approximately 40 putative or well-characterized protein-coding genes. One of them encoded a known chloroplast membrane-localized, ATP-independent metalloprotease, Ethylene-dependent Gravitropism-deficient and Yellow-green 1 (EGY1).[2)]

Ar50-33-pg1 was then crossed with an *egy1* mutant[3)] in both directions. All F_1 seedlings were similar to both parents in that they commonly exhibited accelerated leaf chlorosis with epidermal chloroplast defects. F_1 plant phenotypes at the reproductive stage were all wild type-like. Therefore, *EGY1* was deemed to be the main causal gene for the impaired chloroplast phenotypes in Ar50-33-pg1.

† Condensed from the article in Plants **10**, 848 (2021)
*1 Department of Biology, Sophia University
*2 RIKEN Nishina Center
*3 Department of Biosciences and Biotechnology, Fukui Prefectural University

References

1) Y. Kazama *et al.*, The Plant J. **92**, 1020 (2017).
2) G. Chen *et al.*, Plant J. **41**, 364 (2005).
3) T. Hirano *et al.*, Mutat. Res. **735**, 19 (2012).

Effect of heavy-ion irradiation on survival rate of *Torenia fournieri*

A. Matsuta,[*1] M. Hatashita,[*2] K. Takagi,[*2] Y. Hayashi,[*3] T. Abe,[*3] K. Murai,[*1] and Y. Kazama[*1,*3]

A heavy-ion beam is a powerful mutagen that has high linear energy transfer (LET). We previously demonstrated that the value of LET affects the size and type of the induced mutations in a model plant *Arabidopsis thaliana*; a C-ion beam with an LET of 30.0 keV/μm predominantly induce small mutations that affect almost single genes, while an Ar-ion beam with an LET of 290 keV/μm can induce chromosomal rearrangements including translocation and large inversions or deletions.[1)] We focus on the induction of chromosomal rearrangements because they can affect multiple genes resulting in the induction of new phenotypic traits that have not been ever observed by single gene mutations.

To investigate such a broad spectrum of phenotypes, we aim at observing the floral phenotypes of *Torenia fournieri* after the irradiation of heavy-ion beams with high LET, because its simple floral structure with colorful petals allows us to observe the change in the phenotypes with high visibility.[2)] Moreover, *T. fournieri* is a useful plant for genetic analysis and molecular biology because of its small genome size ($2n = 18$, 171 Mb), and because of the transformation techniques established.[3,4)] Once an interesting mutant is isolated, mutations including rearrangements responsible for its phenotype can be determined by whole-genome resequencing. Dry seed irradiation and screening of seed propagated mutants needs to be conducted using an inbred strain, to efficiently perform the investigation of the phenotypic mutation spectrum followed by whole-genome resequencing. In this study, prior to performing mutant screening, dose dependence on survival was examined and the effect of LETs on survival was compared.

The inbred line 'Zairai murasaki' was kindly provided by Dr. Nishijima of the National Institute of Floricultural Science. Dry seeds of 'Zairai murasaki' were irradiated with Ar ions with LETs of 184 keV/μm and 290 keV/μm, respectively, at a dose range of 25–200 Gy in the RIKEN RI-beam factory. C-ion beam irradiation with an LET of 50 keV/μm was carried out by the Wakasa Wan Multi-purpose Accelerator with Synchrotron and Tandem at the Wakasa Wan Energy Research Center at a dose range of 100–500 Gy. Irradiated M_1 seeds were surface-sterilized and incubated on 0.7% agar containing 1/2 MS medium supplemented with 3% sucrose at 25°C under long-day conditions (16 h light, 8 h dark). About 30–50 seeds were sown for each irradiation treatment. After 1.5 months, the survival rate (the number of plants having true leaves per total number of germinated plants) was determined.

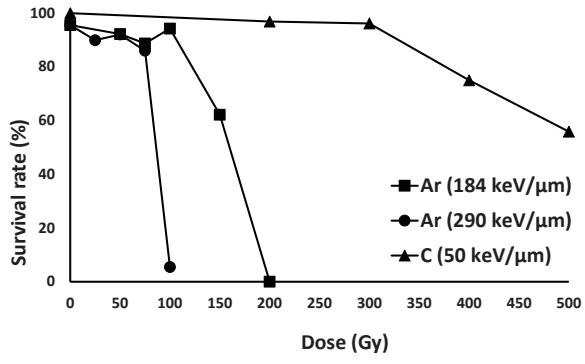

Fig. 1. LET-dependent effect on survival rate in *T. fournieri*.

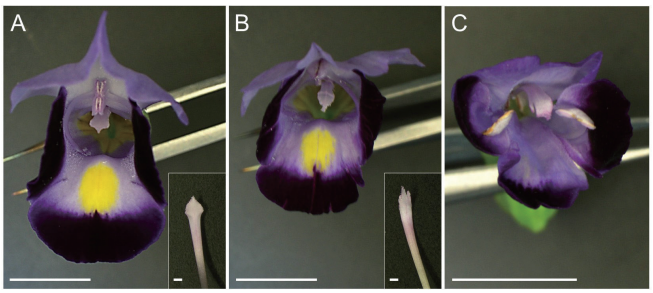

Fig. 2. Photographs of wild-type flower (A); a mutant flower with a rough-edged pistil and petals (B), and a mutant flower without the yellow spot (C). Bars: 1 cm for whole photos, 1 mm for the photos of pistils.

In any LET, survival rates were decreased as the irradiation dose increased (Fig. 1). The effect on survival rate differed among LET values; it increased as LET values increased. The Ar ion beam with the LET of 290 keV/μm was the most effective for the reduction of the survival rates, although the effect of higher values of LET will need to be tested. Based on the rule of thumb that a dose showing around 90% survival is the most effective in mutation induction, the most effective doses on mutation induction were estimated from the current results; 300 Gy, 75 Gy, and 50 Gy for the C ion (50 keV/μm), Ar ion (184 keV/μm), and Ar ion (290 keV/μm), respectively.

Mutant screening is carried out in the M_2 generation because a phenotype caused by recessive mutation is expressed in the M_2 generation. However, we identified two mutants from 30 and 16 M_1 plants after irradiation with LETs of 290 keV/μm and 184 keV/μm, respectively. The former has jagged pistil and petals (Fig. 2B), and the latter has no yellow spot (Fig. 2C). These phenotypes were observed in all flowers produced on the same branch. The detection of mutations responsible for these phenotypes is in progress.

*1 Department of Bioscience and Biotechnology, Fukui Prefectural University
*2 Res. and Develop. Dept., The Wakasa Wan Energy Research Center
*3 RIKEN Nishina Center

References

1) Y. Kazama *et al.*, Plant J. **92**, 1020 (2017).
2) K. Sasaki *et al.*, Plant Biotechnol. **25**, 81 (2008).
3) S. Kikuchi *et al.*, Chromosome Res. **14**, 665 (2006).
4) R. Aida *et al.*, Plant Sci. **153**, 33 (2000).

Behaviors of the Saprophytic *Tricholoma matsutake* Mutants G1 and Ar 59 In Vitro Substrate Cultivation: the former exhibited Morphological Changes while the latter did not†

H. Murata,[*1] T. Yamanaka,[*1] T. Shimokawa,[*1] T. Abe,[*2] H. Ichida,[*2] Y. Hayashi,[*2] and A. Ohta[*1]

Tricholoma matsutake produces a specialty mushroom "*matsutake*" only in a symbiotic association with live trees in the wild, unlike cultivated mushrooms based on wood-decaying fungi. Another ectomycorrhizal mushroom *Lyophyllum shimeji* is commercially cultivated to produce the gourmet mushroom "*shimeji*" using spawn substrates comprising barley and saw dust for a few decades.[1)] The key to successful *L. shimeji* fruiting is that the isolates that can grow as spawn without host plants and easily produce fruiting bodies using a protocol similar to that used for cultivated mushrooms.[1)]

We previously reported *T. matsutake* mutants G1 and Ar 59; the former was isolated after irradiating the wild-type NBRC 33136 (a.k.a., Y1) with γ-rays, and the latter was isolated after irradiating the wild-type with an argon-ion beam.[2)] Both mutants exhibited significantly higher amylase and cellulase activities compared with the wild-type; however, G1 gained more saprophytic traits, and it became lethal rather than symbiotic to *Pinus densiflora* seedlings, whereas Ar 59 remained symbiotic. Because of such phenotypic conversions, we examined if these mutants could exhibit some morphological changes relevant to fruiting body production.

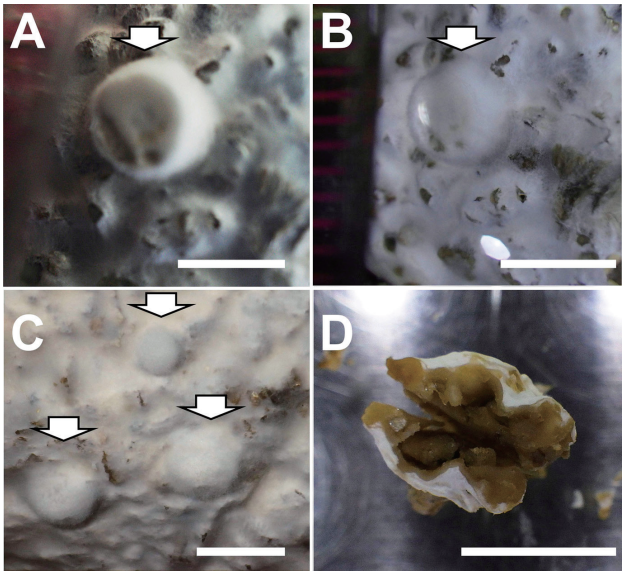

Fig. 1. Morphological changes in *T. matsutake* G1 after substrate cultivation at 23°C for 3 months followed by 16°C for 6 months. (A–C) Lumps arising from the spawn are indicated by arrows. (D) Cross-section of lump indicates tissue differentiation. *Scale bars* 5 mm.

† Condensed partly from the article in Bulletin of FFPRI **19**, 2 153 (2020)

*1 Forest Research and Management Organization
*2 RIKEN Nishina Center

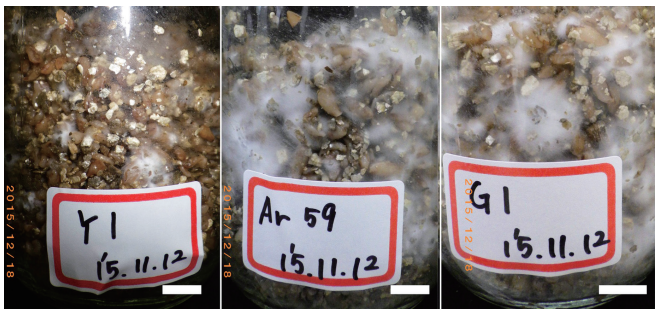

Fig. 2. Mycelial growth of *T. matsutake* NBRC 33136 (= Y1), Ar 59, and G1 after the substrate cultivation for ca. 1 month. *Scale bars* 10 mm.

The *T. matsutake* mutants G1 and Ar 59 and their wild-type NBRC 33136 were separately cultivated with a modified barley-based substrate. G1 developed several tiny (∼5–7 mmϕ) lumps arising from the spawn (Fig. 1A–C). Cross-sections of the lumps indicated that they were not simple aggregates of aerial hyphae but tissue-like, although some uncertainty remains as to whether the lumps are related to fruiting bodies such as a remnant of the inner veil around the pileal margin. The lumps occurred in the G1 spawn in three consecutive independent experiments did not grow into fruiting bodies. Like G1, Ar 59 grew better in the substrate than the wild-type (Fig. 2); however unlike G1, it did not exhibit any morphological changes as observed in NBRC 33136.

The lumps developed in the G1 spawn consecutively in the three independent experiments, and they developed sporadically for nearly 2 years, while other traits of G1 that characterize this mutant, including colony morphology on agar plates, increased degrading enzymatic activities, and harmful effects on plants, were maintained.[2)]

Morphological changes associated with sexual reproduction requires an environment desirable for such vital life cycle events including nutrient availability, temperature, and moisture fluctuations. In the habitat of *T. matsutake*, such moisture and temperature fluctuations occur in the soil and in the atmosphere, even within a single day. To resolve this problem, we are currently inducing mutations in *T. matsutake* G1 by irradiating with heavy-ion beams so that we can obtain mutants that can easily enter the sexual reproduction stage and fruit in artificial cultivation only with substrates. This line of irradiation breeding can eventually yield cultivars of *T. matsutake*.

References

1) A. Ohta, Mycoscience **35**, 147 (1994).
2) H. Murata *et al.*, Botany **97**, 463 (2019).

IV. OPERATION RECORDS

Program Advisory Committee meetings for nuclear physics and for materials and life sciences

H. Ueno,[*1] K. Yoneda,[*1] K. Ishida,[*1] H. Yamazaki,[*1] N. Imai,[*2] Y. X. Watanabe,[*3] K. Yako,[*2] Y. Hirayama,[*3] and M. Iwasaki[*1]

There are two Program Advisory Committees (PACs) that are responsible for reviewing submitted proposals in the fields of nuclear physics (NP-PAC) and materials and life science (ML-PAC). The NP-PAC is co-organized by the RIKEN Nishina Center (RNC), the Center for Nuclear Study (CNS), the University of Tokyo, and the Wako Nuclear Science Center (WNSC), Institute of Particle and Nuclear Studies (IPNS), KEK. The NP-PAC reviews experimental programs at RI Beam Factory (RIBF), whereas the ML-PAC reviews those at the Rutherford Appleton Laboratory (RAL) and RIBF.

NP-PAC

The 21st NP-PAC meeting was held online on December 14–16, 2020 at 9:00 p.m.–2:00 a.m. JST,[1] where 30 proposals were received and reviewed. This was the first online meeting conducted owing to the travel restrictions imposed by COVID-19. The PAC members watched the presentation videos prepared by the applicants in advance, and only conducting a question and answer session with the applicants on the day of the meeting, thus streamlining the meeting. Proposals were evaluated on the basis of five grades: S, A, B, C, and D. Those with a grade of B or higher were approved, of which those with a rating of S or A will be given priority for beamtime allocation. Table 1 summarizes the outcome of the 21st NP-PAC meeting.

The members of the 21st NP-PAC meeting were R. V. F. Janssens (Chair, Univ. of North Carolina), D. Ackermann (GANIL), N. Aoi (Osaka Univ.), M. J. G. Borge (CSIC, Madrid), R. Charity (Washington Univ. in St. Louis), A. O. Macchiavelli (LBNL), G. Martinez-Pinedo (GSI/TU Darmstadt), I. Moore (Univ. of Jyväskylä) D. J. Morrissey (MSU), H. Nakada (Chiba Univ.), A. Obertelli (TU Darmstadt), T. Saito (RIKEN), K. Sekiguchi (Tohoku Univ.), P. J. Woods (Univ. of Edinburgh), A. Vitturi (Univ. of Padova), and X. Zhou (IMP).

ML-PAC

The 20th ML-PAC meeting was held in January 2021.[2] At this meeting, only proposals for the use of the RIBF were solicited, and not proposals for the use of muon beams at RAL owing to the RAL-ISIS long shutdown. All the five submitted RIBF proposals were reviewed. As with the NP-PAC, a face-to-face meeting was avoided, and in consideration of the number of applications, the review was conducted through email. For experimental proposals using RIBF, the same evaluation grade as for NP-PAC was adopted. The outcome of the meeting is summarized in Table 2.

The members of the 20th ML-PAC meeting were A. D. Hillier (Chair, RAL-ISIS), T. Takayanagi (Saitama Univ.) Y. Kobayashi (Univ. of Electro-Communications) Z. Qin (CAS-IMP), and Y. Miyazawa (Yamagata Univ.).

Table 1. Summary of the outcome of the 21st NP-PAC meeting. The sum of the proposals ranked with S and A is listed in the "approval" columns.

	21st NP-PAC (December 14–16, 2020)			
	proposal number		beam time (days)	
	request	approval	request	approval
RILAC (GARIS, ...)	5	2	61.5	15
AVF (CRIB, ...)	7	4	85.5	51
RRC (KISS, ...)	2	1	12.5	6
BigRIPS/ZD	7	3	56.5	16
SHARAQ/OEDO	1	0	7.5	0
SAMURAI	9	4	81.5	32.5
Rare RI Ring	1	0	12	0
(BigRIPS-related	18	7	157.5	48.5)
Total	32	14	317	120.5

Table 2. Summary of the outcome of the 20th ML-PAC meeting. For the RIBF proposals, the sum of the proposals ranked with S and A is listed in the "approval" columns.

	20th ML-PAC (January 2021)			
	proposal number		beam time (days)	
	request	approval	request	approval
RAL	*—no call for proposals—*			
RIBF	5	5	20	17
Total	5	5	20	17

References

1) http://www.nishina.riken.jp/RIBF/NP-PAC/.
2) http://www.nishina.riken.jp/RIBF/ML-PAC/.

*1 RIKEN Nishina Center
*2 Center for Nuclear Study, the University of Tokyo
*3 Wako Nuclear Science Center (WNSC), IPNS, KEK

Electric power status of RIKEN Nishina Center in 2020

E. Ikezawa,[*1] M. Kidera,[*1] Y. Watanabe,[*1] H. Yamasawa,[*1] and O. Kamigaito[*1]

The average hourly electrical power consumption of the RIKEN Nishina Center (RNC) for each day in 2020 is shown in Fig. 1. The total electrical power consumption by RNC in 2020 was 56,549 MWh, which was 1% lower than that in 2019. When the experiment using an argon (^{40}Ar) beam accelerated by the AVF + RRC + IRC was conducted on July 1, 2020, the maximum commercial electrical power supply to the RIKEN Wako campus reached 20.4 MW with a cogeneration system (CGS) output of 6.0 MW. When RI Beam Factory (RIBF) experiments using an uranium (^{238}U) beam were conducted on October 23, 2020, the maximum electrical power consumption of RNC reached 17.5 MW.

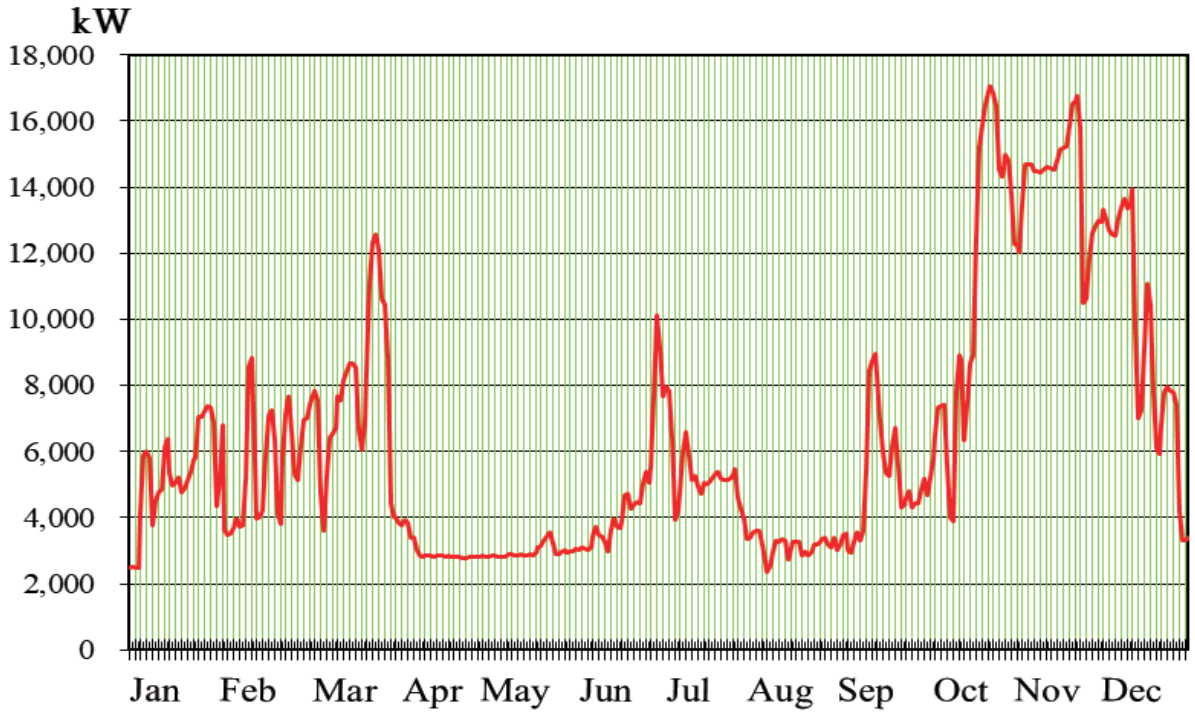

Fig. 1. Average hourly electrical power consumption of RNC for each day in 2020.

*1 RIKEN Nishina Center

RILAC operation

K. Oyamada,[*2] E. Ikezawa,[*1] M. Kase,[*1] T. Nakagawa,[*1] N. Sakamoto,[*1] H. Okuno,[*1] N. Fukunishi,[*1] Y. Watanabe,[*1] M. Komiyama,[*1] A. Uchiyama,[*1] T. Maie,[*1] M. Nagase,[*1] M. Fujimaki,[*1] T. Watanabe,[*1] H. Hasebe,[*1] H. Imao,[*1] K. Ozeki,[*1] K. Suda,[*1] Y. Higurashi,[*1] K. Yamada,[*1] S. Watanabe,[*1] M. Kidera,[*1] T. Nagatomo,[*1] K. Kumagai,[*1] T. Nishi,[*1] T. Ohki,[*2] H. Yamauchi,[*2] M. Tamura,[*2] A. Yusa,[*2] K. Kaneko,[*2] and O. Kamigaito[*1]

The RILAC saw the commissioning of a superconducting RILAC (SRILAC) from January to March 2020. Some statistics regarding the operation of RILAC from January 1 to December 31, 2020 are presented in Table 1. Table 2 lists the beam service times in the standalone mode of RILAC in 2020. The details are described elsewhere in this progress report.

We performed the following maintenance works during the reporting period.

(1) In the radio-frequency(rf) systems, DC high-voltage power supplies were subjected to annual inspection. The major components with mechanical parts were subjected to simple inspection.
(2) The water pumps were subjected to simple inspection. All cooling towers were subjected to monthly inspection.
(3) All turbomolecular pumps were subjected to simple inspection. Cryogenic pumps used for cavities No. 1, No. 2, A1, and A2 were overhauled.
(4) All magnet power supplies were subjected to simple inspection.

We faced the following mechanical problems during the reporting period.

(1) The cooling parts of drift tubes in RILAC cavities No. 2, No. 4, and No. 5 had a coolant leak. We repaired the parts with a repair material.
(2) The plate DC power supply for a tetrode (SIEMENS-RS2012CJ) in the rf amplifier of RILAC No. 5 malfunctioned. It was fixed by replacing the electric parts.
(3) Water was found to have splashed in the rf power feeder of RILAC cavity No. 1 because of leakage from a cooling pipe for the coaxial conductor. We replaced it with new ones.
(4) The water cooling pipe of the RFQ cavity had a water leak. We repaired the cooling pipe with a repair material.
(5) A section of the air-pressure pipe for the contact fingers of the rf shorting plate in RILAC cavity No. 6 had a vacuum leak because of a deteriorated O-ring. We replaced it with a new one.

Table 1. Statistics of RILAC operation from January 1 to December 31, 2020.

Operation time of RILAC	2878.3 h
Mechanical problem	161.3 h
Standalone RILAC	1970.6 h
Injection into RRC	0.0 h
Total beam service time of RILAC	1970.6 h

Table 2. Beam service times of RILAC in the standalone mode in 2020.

Beam course	Total time (h)	%
e11	997.37	50.6
e2	973.23	49.4
Total	1970.60	100.0

*1 RIKEN Nishina Center
*2 SHI Accelerator Service Ltd.

Operation report on the ring cyclotrons in the RIBF accelerator complex

S. Ishikawa,[*1] K. Suda,[*2] T. Dantsuka,[*2] M. Fujimaki,[*2] T. Fujinawa,[*2] N. Fukunishi,[*2] S. Fukuzawa,[*1] M. Hamanaka,[*1] H. Hasebe,[*2] Y. Higurashi,[*2] E. Ikezawa,[*2] H. Imao,[*2] O. Kamigaito,[*2] Y. Kanai,[*2] M. Kase,[*2] M. Kidera,[*2] K. Kobayashi,[*1] M. Komiyama,[*2] R. Koyama,[*1] K. Kumagai,[*2] T. Maie,[*2] T. Nagatomo,[*2] T. Nakagawa,[*2] M. Nakamura,[*2] T. Nakamura,[*1] M. Nishida,[*1] M. Nishimura,[*1] J. Ohnishi,[*2] H. Okuno,[*2] K. Ozeki,[*2] N. Sakamoto,[*2] J. Shibata,[*1] N. Tsukiori,[*1] A. Uchiyama,[*2] S. Watanabe,[*2] T. Watanabe,[*2] Y. Watanabe,[*2] K. Yamada,[*2] K. Yadomi,[*1] and H. Yamasawa[*2]

The operation report of the ring cyclotrons in the RIBF accelerator complex from Jan. to Dec. 2020 is presented. Table 1 presents a summary of the beams accelerated by these cyclotrons. The availability is defined as the ratio of the actual beam service time to the scheduled beam service time, which is an index of the stable Operation of accelerators. In calculating each availability, for beam service times that were completed earlier than scheduled, the scheduled times are identified with the actual times. Multiple experiments supplying identical beams are treated as one and presented in a row. The total actual beam service time was 1639.1 h. The ratio of the beam service times between the experiments conducted in the old facility (RARF) and the new facility (RIBF) was 54:46.

In the RARF, the actual beam service time was 884.5 h, and the availability was 95.7%. In the RIBF, two beam services were carried out. The actual beam service time was 754.6 h, and the availability was 89.8%. Due to the declaration of a state of emergency in relation to the COVID-19 infection, experiments were cancelled for two months from April. Vacuum leak occurred at the RRC resonator No.1 in May, and weld repair was carried out. Due to the repair, all the beam service times scheduled in June were cancelled.

In the ^{238}U beam supply for eight experiments, we achieved a maximum beam intensity of 116 particle nA, which is 1.2 times higher than that of the previous beam service in Nov. 2019. The highest record was obtained due to the upgrade of the RRC resonators[1,2] and the change in gap spacing of the RRC-EDC in 2018, and the relocation of the fRC-EIC in 2020. The beam supply was stopped for 8 days due to the repair of the SRC-EDC and SRC-Resonator 2 (RES2). A septum electrode of the EDC was damaged by a loss of the high intensity beams. After the exchange of the EDC, a beam intensity was reduced to 70 particle nA to prevent EDC damage again. RES2 could not be excited because the contact fingers for the coarse tuning plate was partially burned out by a high RF input power. The damaged contact fingers were exchanged. The beam service time was 510.5 h, and the availability was 81.8%.

In the ^{70}Zn beam supply for three experiments, we recorded the highest beam intensity of 782 particle nA, which is 3.1 times higher than that of the previous beam service in May 2017. The increase of beam intensity was achieved due to the improvement of the oven in the ion source and of the beam tuning based on the beam supply parameters obtained by a scaling of that for ^{238}U. The beam service time was 244.2 h, and the availability was 113.1% because the tuning time was shorter than planned and the experiment was started ahead of schedule.

References

1) K. Yamada *et al.*, RIKEN Accel. Prog. Rep. **52**, 13 (2019).
2) K. Yamada *et al.*, J. Part. Accel. Soc. Jpn. **17**, 159 (2020).

Table 1. Summary of the accelerated beams in 2020.

	Beam particle	Energy (MeV/nucleon)	Acceleration mode	Beam course	Beam intensity (particle nA) Requested	Actual	Beam service time (h) Scheduled	Actual	Availability (%)
RARF	^{12}C	135	AVF-RRC	E5B (Biology)	1	450.0	27.5	9.2	100.0
	^{14}N	135		E3B (RI production)	500	571.0	48.0	49.5	103.2
	^{20}Ne	135		ESB (Biology)	1	270.0	4.0	2.6	100.0
	^{22}Ne	70		E6 (Material)	250	300.0	108.0	107.9	99.9
	^{40}Ar	95		E5A (Material)	1	26.5	84.0	86.1	102.5
	^{56}Fe	90		ESB (Biology)	1	3.5	6.0	2.1	100.0
	^{84}Kr	70		E5A (Material)	1	9.7	240.0	205.8	85.6
	^{4}He	7.25	RILAC2-RRC	A10 (MS)	18300	590.0	33.6	33.6	100.0
	^{136}Xe	10.75		E2B (KEK/KISS) /E3A (Material)	250	325.0	381.0	371.5	97.5
	^{40}Ar	160	AVF-RRC-IRC	E5B (Biology)	1	23.3	23.5	16.2	100.0
RIBF	^{70}Zn	345	RILAC2-RRC -fRC-IRC-SRC	BigRIPS/ZD	>600	782.0	216.0	244.2	113.1
	^{238}U	345		BigRIPS/ZD /Rare-RI Ring	>60	116.3	624.0	510.5	81.8
						Total	1795.6	1639.1	92.9

[*1] SHI Accelerator Service Ltd.
[*2] RIKEN Nishina Center

Operation report on the RIKEN AVF cyclotron for 2020

M. Nishida,[*1] K. Ozeki,[*2] M. Fujimaki,[*2] N. Fukunishi,[*2] S. Fukuzawa,[*1] A. Goto,[*2] H. Hasebe,[*2] M. Hamanaka,[*1] Y. Higurashi,[*2] E. Ikezawa,[*2] H. Imao,[*2] S. Ishikawa,[*1] K. Kamakura,[*3] O. Kamigaito,[*2] M. Kase,[*2] M. Kidera,[*2] K. kobayashi,[*1] M. Komiyama,[*2] Y. Kotaka,[*3] R. Koyama,[*1] K. Kumagai,[*2] T. Maie,[*2] T. Nagatomo,[*2] T. Nakagawa,[*2] T. Nakamura,[*1] M. Nishimura,[*1] J. Ohnishi,[*2] H. Okuno,[*2] Y. Oshiro,[*3] N. Sakamoto,[*2] J. Shibata,[*1] K. Suda,[*2] N. Tsukiori,[*1] A. Uchiyama,[*2] S. Watanabe,[*2] T. Watanabe,[*2] Y. Watanabe,[*2] K. Yadomi,[*1] and K. Yamada[*2]

The yearly report on the operation of the RIKEN AVF cyclotron (denoted as AVF hereafter) for the period January-December 2020 is presented. AVF delivered beams to five courses for stand-alone operations: C01 (machine study), C03 (radioactive isotope (RI) production), C12 (CNS, RI production), E7A (CRIB), and E7B (RI production, student experiment). On the other hand, when AVF was used as an injector of the RIKEN Ring Cyclotron (RRC), beams were delivered to two courses: RRC-RARF and RRC-IRC-E5. Figure 1 shows the experimental apparatuses around AVF.

Thus far, AVF was equipped with three ion sources to deliver various ion beams: the superconducting electron cyclotron resonance ion source (SC ECRIS), Hyper ECRIS, and polarized ion source (PIS, only used for polarized deuterons). However, a GM refrigerator used for cooling the superconducting mirror coils in SC ECRIS had become too old. Therefore, SC ECRIS was replaced with the 18 GHz ECRIS that had been used at RILAC, and beam deliveries from the 18 GHz ECRIS commenced in January.

The yearly operation statistics are presented in Tables 1 and 2. In a total operation time of 2702 h, 1520 h was spent for stand-alone operation, and 1182 h was spent for injection to RRC. Because of the declaration of a state of emergency due to the COVID-19 outbreak, all beam times scheduled for April and May were canceled.

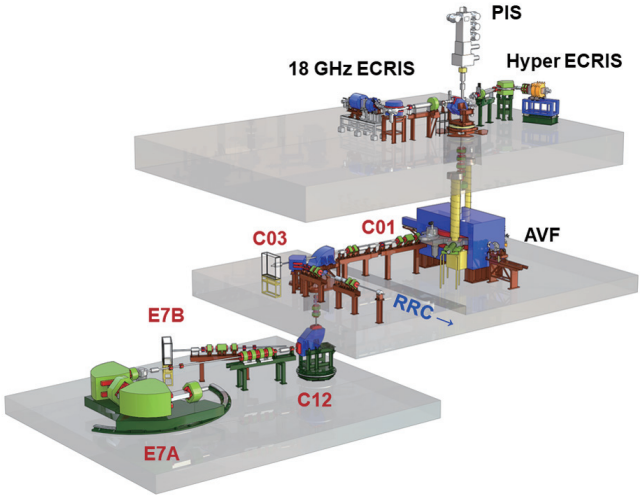

Fig. 1. Overview of the AVF cyclotron with ion sources, each experimental course, and beam transport line to RRC.

[*1] SHI Accelerator Service Ltd.
[*2] RIKEN Nishina Center
[*3] Center for Nuclear Study, the University of Tokyo

This is a main reason why the operation time for stand-alone operation in this year is considerably less than that in the previous year. In addition, an RI production experiment using 30-MeV protons was conducted for the first time in June.

Table 1. Comparison of AVF operation statistics with that in the previous year.

AVF stand-alone operation		2019	2020
Tuning of AVF	[h]	1314	744
Trouble of AVF	[h]	0	1
C01 M. S.	[h]	0	12
C03 exp.	[h]	873	631
C12 exp.	[h]	36	18
E7A exp.	[h]	789	12
E7B exp.	[h]	152	101
Sub total	[h]	3166	1520
AVF operation as injector of RRC		**2019**	**2020**
Tuning of AVF	[h]	117	178
Trouble of AVF	[h]	0	5
RRC-RARF exp.	[h]	320	999
RRC-RIBF exp.	[h]	0	0
Sub total	[h]	437	1182
Total	[h]	3603	2702

Table 2. AVF beam list in 2020.

Particle	Energy (MeV/nucleon)	Course
Stand-alone operation		
p	12.00	C03
p	19.00	C12
p	30.00	C01, C03
d	12.00	C03
α	6.50	E7B
α	7.25	C03, E7B
α	12.50	C03
^{7}Li	6.00	C03
^{16}O	6.80	E7A
^{18}O	7.00	C12
^{19}F	6.30	C03
Operation as injector of RRC		
^{12}C	7.00	RRC-RARF
^{14}N	7.00	RRC-RARF
^{20}Ne	7.00	RRC-RARF
^{22}Ne	3.97	RRC-RARF
^{40}Ar	3.80	RRC-IRC-RARF
^{40}Ar	5.20	RRC-RARF
^{56}Fe	5.00	RRC-RARF
^{84}Kr	3.97	RRC-RARF

Present status of liquid-helium supply and recovery system

T. Dantsuka,[*1] H. Okuno,[*1] M. Nakamura,[*1] S. Tsuruma,[*1] M. Takahashi,[*1] M. Kuroiwa,[*1] M. Ohshima,[*2] H. Miura,[*2] H. Shiraki,[*2] H. Hirai,[*2] K. Kimura,[*2] M. Haneda,[*2] A. Mikami,[*2] M. Nagano,[*2] and H. Hazama[*2]

The liquid-helium supply and recovery system,[1)] which can produce liquid helium at a liquefaction rate of 200 L/h from pure helium gas, has been under stable operation since the beginning of April 2001. However, as operation failure due to deterioration over time has increased in recent years, duplication of the liquefier was conducted in 2017. The new liquefier can produce liquid helium at a liquefaction rate of 220 L/h from pure helium gas. Although the older helium liquefier has been failing since the summer of 2018, with the new helium liquefier, a constant supply of liquid helium can be enabled. The older helium liquefier was repaired in February 2020.

The volumes of liquid helium supplied each year from 2001 to 2019 are illustrated in Fig. 1. From 2001 to 2013, there was a gradual increase in the supplied volume, with two declines observed in 2009 and 2011. In 2014, the supplied volume decreased owing to a system malfunction. However, in 2015, the supplied volume returned to its original value. In 2016, the supplied volume decreased but slightly increased in 2017. In 2018, the supply volume increased significantly. In 2019, we supplied approximately 140,000 L of liquid helium despite the high price of helium gas.

However, the purity of helium gas recovered from the laboratories gradually deteriorated. At present, the impurity concentration in the recovered gas is approximately 1000 ppm. The impurity concentration does not affect the liquefaction operation, but is necessary to observe the progress.

Furthermore, the volume of helium gas recovered from each building in the Wako campus as well as the volume transported to the liquid helium supply and recovery system were measured. The recovery efficiency, which is defined as the ratio of the amount of recovered helium gas to the amount of supplied liquid helium, was calculated. The recovery efficiency for the buildings on the south side of the Wako campus, namely the Cooperation Center building of the Advanced Device Laboratory, Chemistry and Material Physics building, and Nanoscience Joint Laboratory building, increased to approximately 95%.

Reference

1) K. Ikegami *et al.*, RIKEN Accel. Prog. Rep. **34**, 349 (2001).

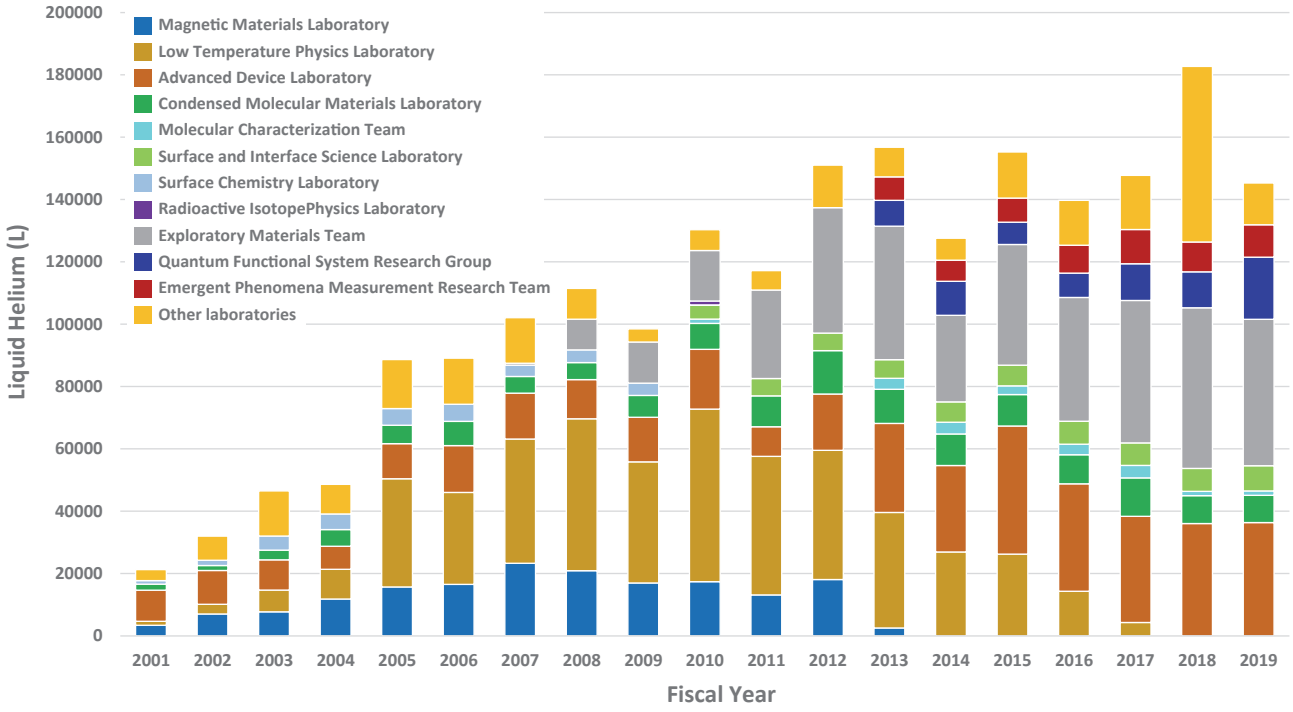

Fig. 1. Volumes of liquid helium supplied to the various laboratories for each fiscal year from 2001 to 2019.

*1 RIKEN Nishina Center
*2 Nippon Air Conditioning Service K.K

Operation of the BigRIPS cryogenic plant

K. Kusaka,[*1] M. Ohtake,[*1] K. Yoshida,[*1] M. Ohshima,[*2] A. Mikami,[*2] H. Hazama,[*2] H. Miura,[*2] H. Shiraki,[*2] H. Hirai,[*2] K. Kimura,[*2] M. Nagano,[*2] H. Shiba,[*2] and S. Okada[*2]

We operated the BigRIPS cryogenic plant for only 2,838 h in 2020 because the spring beam time was cancelled due to the declaration of state of emergency over COVID-19. The operation periods were from March 4 to April 24 and from September 25 to December 21. After the long shutdown of the RIBF facility, we started cooling down the warmed-up superconducting triplet quadrupole (STQ) magnets on October 2.

After successful cooldown operation, we excited STQ1 magnet with stepwise ramping. The STQ1 magnet is an air-core-type superconducting magnet and consists of three quadrupole coils, P1, P2, and P3, and one hexapole coil, SX.[1)] In contrast to the other STQ's case, we excite the coils P1, P2, and P3 separately after cooling down. Before simultaneous excitation of all coils, the coils P1, P3, and SX coils were excited up to their nominal current of 740 A, 628 A, and 32.5 A, respectively. However, when we ramped P2 from 610 A to 620 A, it quenched with a current of 620 A, which is 8 A less than the nominal current. This was the fourth quench of P2, and we consider that it a training quench.

Except for the quenching of P2, we operated the cryogenic system without any trouble. We measured the vibrations of the compressor unit and observed low oil contamination in helium gas during operations. The total operation time of the compressor unit was 75,060 h.

Figure 1 shows the vibration acceleration in the vertical and horizontal directions as a function of the total operation time. We have been measuring the vibrations of the compressor at the high-pressure and low-pressure sides since 2015. Two rapid increases of the vibration acceleration at operation times of 59,000 h and 71,000 h are indicated by arrows. They were caused by the damage of the bearing unit in December 2016[2)] and June 2019.[3)] The vibration acceleration mostly remained below 8 m/s^2 during the operation period. We consider that the exceptionally large value of 10.3 m/s^2 at 74,883 h in the vertical direction at the high-pressure side is due to measurement error.

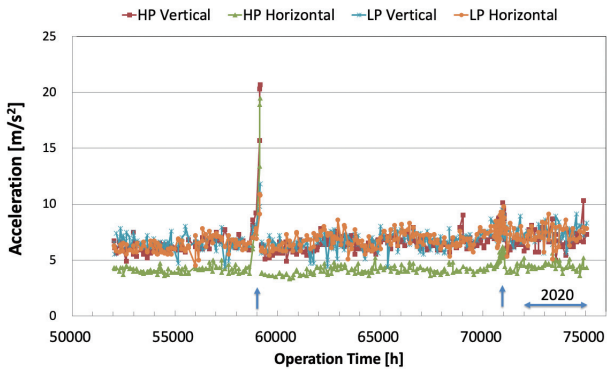

Fig. 1. Vibration acceleration of the compressor unit. The operation period in 2020 is indicated.

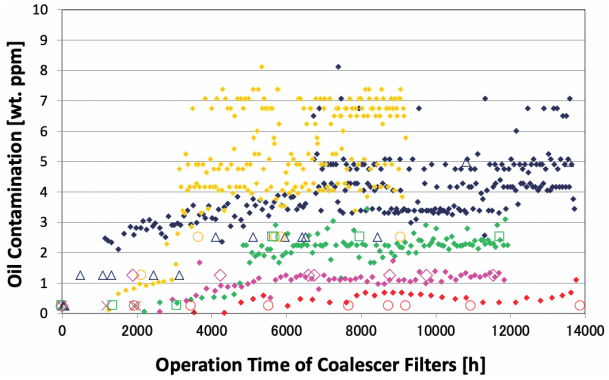

Fig. 2. Oil contamination at the entrance of the third coalescer vessel.

We measured the operation interval of the drain valves of the coalescer vessels in the compressor unit in order to evaluate the oil contamination level. We have replaced coalescer filter elements 5 times since 2008. The operation periods of the replaced filter elements were from August 2008 to July 2010, from September 2010 to July 2012, from September 2012 to July 2014, from September 2014 to July 2016, and from September 2016 to June 2019. Figure 2 shows an estimate of the oil contamination level at the entrance of the third coalescer vessel as a function of the coalescer filter operation time. The navy-blue, green, and yellow diamonds represent the estimates for the first, second, and third elements, respectively. The fourth and the fifth elements are shown with pink and red diamonds, respectively. The oil contamination values measured using the oil check kit are also shown. The open triangles, squares, and circles represent the results for the first, second, and third elements, respectively. The results for the fourth and the fifth elements are indicated by the open diamonds and circles, respectively. The drain valve of the coalescer vessel operated only once in 2020 after the last maintenance in 2019. The operation time and the estimate of the oil contamination level for the current coalescer are 3550 h and 0.05 wt.ppm, respectively, as shown by the brown diamond in Fig. 2.

Both estimations of the oil contamination level are consistent with each other, and the performance efficiency of the fifth set of filter elements seems to be better than that of the others.

*1 RIKEN Nishina Center
*2 Nippon Air Conditioning Services Co., Ltd.

References

1) K. Kusaka *et al.*, IEEE Trans. Appl. Supercond. **18**, 240 (2008).
2) K. Kusaka *et al.*, RIKEN Accel. Prog. Rep. **50**, 285 (2017).
3) K. Kusaka *et al.*, RIKEN Accel. Prog. Rep. **53**, 222 (2019).

Radiation safety management at RIBF

K. Tanaka,[*1] Y. Uwamino,[*1,*2] H. Sakamoto,[*1] R. Hirunuma-Higurashi,[*1] H. Mukai,[*3] A. Akashio,[*1] T. Okayasu,[*1] R. Suzuki,[*4] M. Takekoshi,[*4] T. Sato,[*4] K. Igarashi,[*1] S. Iizuka,[*1] N. Usudate,[*1] and Y. Shioda[*1]

The results of radiation monitoring at RIBF, carried out at the border of the facility and the radiation-controlled area are reported. The residual doses along the accelerator setups are also presented. In 2020, a ^{238}U beam of approximately 345 MeV/nucleon was provided at an intensity of 70 particle nA in October and November. Subsequently, a ^{70}Zn beam of approximately 345 MeV/nucleon of 800 particle nA was used in November and December.

The dose rates at the boundary of the radiation-controlled area were monitored. Neutron and γ-ray monitors were used at three locations: the roofs of the RRC, IRC, and BigRIPS. Figure 1 shows the annual neutron dose at these positions. In 2020, even the highest annual dose of 9 μSv/y at the IRC roof was lower than the legal limit of 5.2 mSv/y. The dose at the IRC roof sensitive to IRC and SRC operation time. In 2020, these operated for only three months. Therefore, the annual dose of the IRC roof was small.

The dose rates at the site boundary, where the legal limit is 1 mSv/y, were monitored by neutron and γ-ray monitors. The detection limits of the neutron monitor were 2 μSv/y and 0.01 μSv/h. The annual dose in 2020 was 3.6 μSv of neutron but less than the hourly detection limits any time after the background correction. The detection limit of the γ-ray monitor was 8 μSv/y. The annual dose of the γ-ray was lower than the limit, which is considerably lower than the legal limit.

The residual radioactivity at the deflectors of the cyclotrons was measured just before maintenance work.

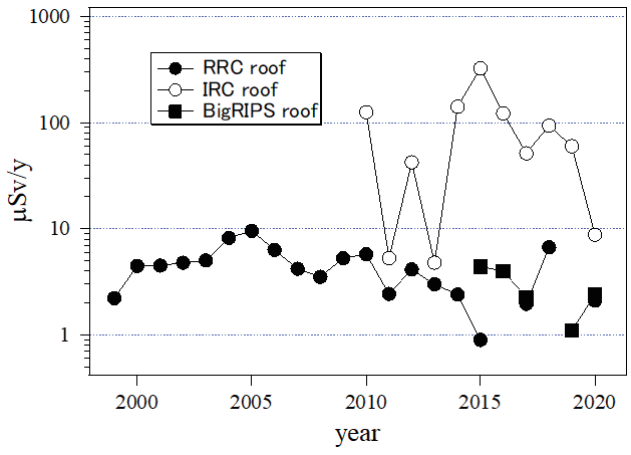

Fig. 1. Radiation dose at the boundary of the radiation-controlled area.

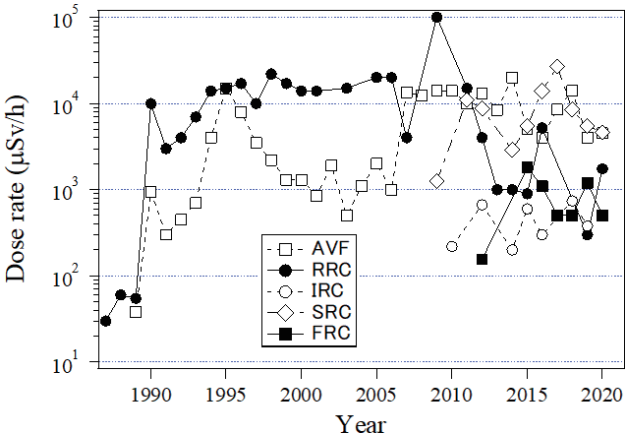

Fig. 2. Dose rates of residual radioactivity at the deflectors of 5 cyclotrons.

The residual dose depends on factors such as the beam intensity, accelerator operation time, and cooling time. The data were obtained from the cyclotrons maintenance works, when the deflectors were accessible. Therefore, the cooling times have not been constant. The dose rates from 1986 are shown in Fig. 2. The dose rates for fRC, IRC, and SRC are shown for the years after 2006, when the RIBF operation started. For AVF, the dose rate increased in 2006 because the radioisotope production was started and the beam intensity increased.

The residual radioactivity along the beam lines was measured after almost every experiment. Figure 3 shows the locations of the measurement points where high residual doses were observed. Table 1 lists the dose rates, beam conditions, and cooling time at the measurement points. The maximum dose was 46 mSv/h at point 23, which is in the vicinity of the beam dump of BigRIPS.

Although the radioactivity in the closed cooling system at BigRIPS is reported annually, it is omitted because the radioactivity was not measured in 2020.

The E-learning module, which can be accessed anytime and from anywhere (even from outside RIKEN), has been used for the re-training of the radiation workers at RIBF. Approximately 580 radiation workers have completed the training in 2020. This is lower than the number in recent years because of the COVID-19 restriction of immigration and etc.

As described above, radiation management to comply with lows and to keep radiation levels as low as possible has been carried out successfully.

*1 RIKEN Nishina Center
*2 Japan Radioisotope Association
*3 Japan Environment Research Corporation
*4 Daiwa Atomic Engineering Corporation

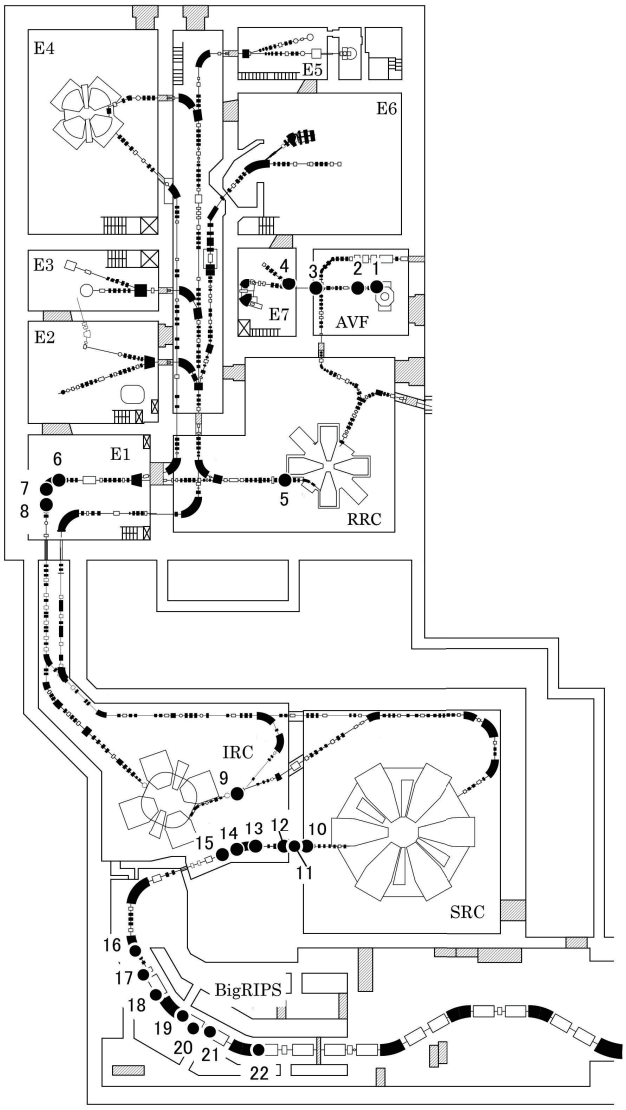

Fig. 3. Layout of the beam lines at RIBF. The measurement locations listed in Table 1 are indicated.

Table 1. Dose rates measured at beam lines in 2020. Points 1–24 indicate the locations where measurements were taken as shown in Fig. 3.

Point	Dose rate (μSv/h)	Date (M/D)	Particle	Energy (A MeV)	Intensity (pnA)	Cooling time (h)
1	100	8/12	α	7.3	10000	554
2	139	8/12	α	7.3	10000	554
3	250	8/12	α	7.3	10000	554
4	100	12/28	α	6.5	10	281
5	188	8/12	C-12	135	2	882
6	4000	12/24	Zn-70	50	990	270
7	2500	12/24	Zn-70	50	990	270
8	110	8/12	Ar-40	66	24	979
9	200	12/24	Zn-70	114	800	270
10	7000	12/24	Zn-70	345	760	271
11	14000	12/24	Zn-70	345	760	271
12	120	12/24	Zn-70	345	760	270
13	150	12/24	Zn-70	345	760	270
14	581	12/24	Zn-70	345	760	270
15	110	12/24	Zn-70	345	760	270
16	130	12/24	Zn-70	345	760	271
17	3300	12/24	Zn-70	345	760	271
18	6000	12/24	Zn-70	345	760	271
19	30000	12/24	Zn-70	345	760	271
20	530	12/24	Zn-70	345	760	271
21	280	12/24	Zn-70	345	760	271
22	230	12/24	Zn-70	345	760	271

Operation of the Pelletron tandem accelerator

T. Ikeda,[*1] M. Hamagaki,[*1] and H. Sato[*1]

Ion beams with an energy range of MeV are available from the tandem accelerator (Pelletron 5SDH-2, 1.7 MV max.) in the Nishina R&D Building, which is managed by the Detector Team of RNC. This accelerator is also registered as joint-use equipment in Wako campus for material analysis. As shown in the configuration of the accelerator and beam lines (Fig. 1), two ion sources are available. One is the RF charge-exchange ion source, called Alphatross, for experiments using He ion beams. The other is the Source of Negative Ions by Cesium Sputtering (SNICS), which can generate almost all other ions. Thus far, ion species of H, He, Li, B, C, N, O, Si, Ti, Ni, Cu, and Au have been accelerated at 0.5–1.7 MV.

There are four beam lines named BL-E/W*nn* (*nn* denotes the bending angle). In 2020, BL-E15 was restarted for a user group in the field of material science to perform the analysis of Rutherford backscattering (RBS) spectrometry. In the west side, BL-W15 (multipurpose line) was used for a micrometer-sized ion beam based on glass capillary optics with an end window. This was for horizontal microbeam irradiation experiments. The irradiation port was developed to have a simple connection to the BL-W15 line. It took a few hours to mount the microbeam port, including the vacuum pumping. At the end of 2020, BL-W30 was under construction for new microbeam irradiation studies of the biological samples in air or solution.

From January 1 to December 31, 2020, the total machine time (MT) including a machine study was only

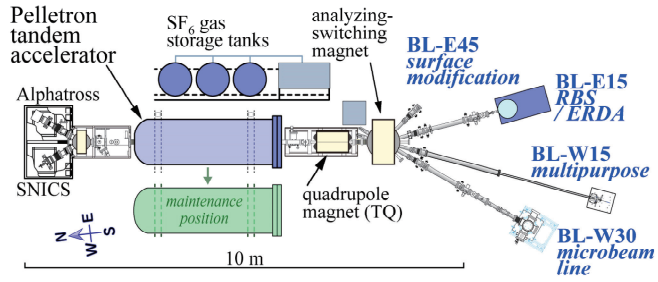

Fig. 1. Pelletron tandem accelerator and beam lines in the Nishina R&D Building.

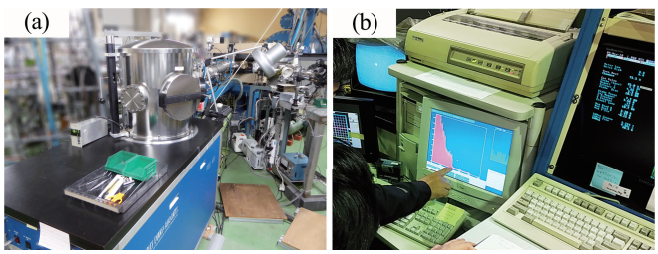

Fig. 2. (a) Apparatus for the RBS spectrometry connected to the Pelletron accelerator. (b) Online analysis.

[*1] RIKEN Nishina Center

Table 1. Beam conditions and experiments conducted in the tandem accelerator.

Ion	Energy [MeV]	Beam current [pnA]	Experiment	Operation time [days]
$^{1}H^{+}$	2.0–3.0	1–120	Irradiation	8
$^{4}He^{2+}$	2.28	0.25–5	RBS	4

Table 2. Approved conditions at the RIKEN Pelletron.

Ion	Maximum Energy	Ion	Maximum Energy
H	3.5 MeV	B	10.2 MeV
He	5.1 MeV	C	12 MeV
Li/Be	6.8 MeV	other	0.6 MeV/nucleon

12 days, where the condition test of the ion sources is not included. In addition to the total MT, development activities were suppressed in 2020.

The ion species accelerated in this year were the light ions H^{+} and He^{2+} with energies ranging from 2.0 to 3.0 MeV, as summarized in Table 1. The RBS experiments always used the energy of 2.28 MeV, following convention. Points 1–6 below list the studies that used the beam lines, along with the number of days of MT. All the studies, including those with zero days of MT, were routine experiments before 2020.

(1) Microbeam performance study with H ions using glass capillaries at BL-W15 and W30[1,2] (7 days)
(2) Microbeam (He ion) irradiation for single cells at BL-W30[3] (0 days)
(3) RBS/ERDA experiments using carbon ions (4 days)
(4) Educational experiment of proton capture by carbon/boron nucleus for Nishina School (0 days)
(5) Development of charged-particle/gamma-ray detector to be used for RIBF experiments (0 days)
(6) Other development using protons (1 day)

The maximum energies of accelerated ions are summarized in Table 2. Since 2019, the regulation of the maximum energy of carbon ions was changed from 7.2 MeV to 11.9 MeV, where $^{12}C^{6+}$ is accelerated with the full voltage of 1.7 MV.

A commercial RBS apparatus (Charles Evans and Associates Model RBS-400) is shown in Fig. 2(a). A goniometer to rotate the sample is fixed inside the chamber, which is in a vacuum level of the order of 10^{-7} Torr. The He^{2+} beam intensity was less than 10 nA. Improvements in the vacuum level and beam intensity are in progress.

References

1) T. Ikeda *et al.*, Nucl. Instrum. Methods Phys. Res. B **470**, 42 (2020).
2) T. Ikeda, Quantum Beam Sci. **4**, 22 (2020).
3) T. Ikeda *et al.*, RIKEN Accel. Prog. Rep. **53**, 215 (2020).

Fee-based activities of the Industrial Application Research Team

A. Yoshida,[*1] T. Kambara,[*1] H. Haba,[*1] A. Nambu,[*1] and D. Mori[*1]

The fee-based activities of the Industrial Application Research Team in 2020, which are the utilization of heavy-ion beams in the industry and the distribution of radioisotopes, are summarized below.

RIKEN Nishina Center allows the use of the AVF cyclotron, RILAC, and RIKEN Ring Cyclotron (RRC) by private companies in Japan for a fee.[1)] At present, the main users are semiconductor companies that irradiate space-use semiconductor devices with Ar, Kr, and Xe ions from the RRC to simulate single-event effects due to the heavy-ion components of cosmic radiation. Proposals for beam utilization are reviewed by a program advisory committee dedicated to industrial use (InPAC). In July 2020, InPAC reviewed and approved via e-mail three proposals that were in continuation to previously approved proposals and held its 10th meeting online, where it reviewed and approved two new proposals. In 2020, six companies executed eleven fee-based beamtimes, seven of which utilized a Kr beam with a total beam time of 153 h and four utilized an Ar beam with a total beam time of 73 h. In response to the users' demand, we are preparing to supply C ions and considering the supply of Xe ions with higher energies.

Since 2007, RIKEN has distributed radioisotopes (RIs) to users in Japan for a fee in collaboration with the Japan Radioisotope Association[2)] (JRIA). The nuclides are ^{65}Zn ($T_{1/2}$ = 244 days), ^{109}Cd ($T_{1/2}$ = 463 days), ^{88}Y ($T_{1/2}$ = 107 days), ^{85}Sr ($T_{1/2}$ = 65 days), and ^{67}Cu ($T_{1/2}$ = 61.8 hours) produced at the AVF cyclotron by the Nuclear Chemistry Research Team. According to a material transfer agreement (MTA) drawn between JRIA and RIKEN, JRIA mediates the transaction of the RIs and distributes them to users. ^{65}Zn and ^{109}Cd are delivered approximately two weeks after the acceptance of an order. ^{85}Sr, ^{88}Y, and ^{67}Cu, which have short half-lives, are not stocked like ^{65}Zn and ^{109}Cd but are instead produced in a scheduled beamtime after an order is accepted. Therefore, they are delivered two months or more after an order. Details can be found in the online ordering system J-RAM[3)] of JRIA.

In 2020, we delivered one shipment of ^{109}Cd with an activity of 10 MBq, three of ^{65}Zn with a total activity of 12 MBq, two of ^{88}Y with a total activity of 2 MBq, and two of ^{85}Sr with a total activity of 3 MBq. The final recipients of the RIs were four universities, one private company, and one medical research center.

Figure 1 shows the yearly trends in the number of orders and the amounts of distributed RIs. Compared with 2019, the amounts of distributed ^{109}Cd, ^{65}Zn, and ^{85}Sr increased, that of distributed ^{67}Cu decreased, and that of distributed ^{88}Y remained the same. During the past 10 years, the demand for long-lived RIs has drastically decreased, whereas that for short-lived RIs is increasing.

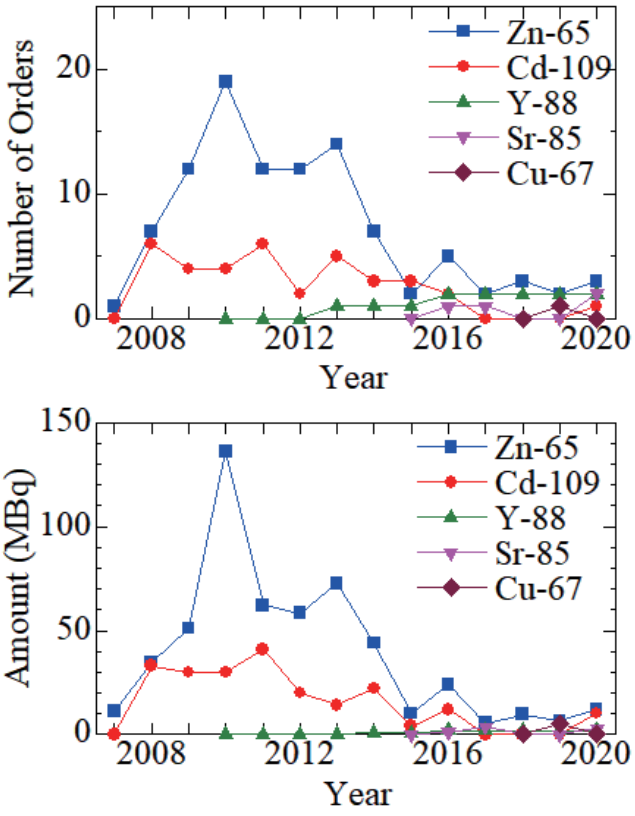

Fig. 1. Number of orders (upper) and amounts (lower) of the RIs distributed yearly from 2007 to 2020. The distribution of ^{88}Y started in 2010, that of ^{85}Sr in 2015, and that of ^{67}Cu in 2018.

References

1) http://ribf.riken.jp/sisetu-kyoyo/ (Japanese).
2) http://www.jrias.or.jp/ (Japanese), http://www.jrias.or.jp/e/ (English).
3) https://j-ram.org (Japanese).

*1 RIKEN Nishina Center

Activity report of the second-term (2014–2021) RIBF Theory Forum

T. Abe,[*1] Y. Aritomo,[*2] W. Horiuchi,[*3] M. Kimura,[*3] H. -Z. Liang,[*4] T. Matsumoto,[*5] F. Minato,[*6] K. Nakazato,[*7] N. Nishimura,[*8] and K. Yoshida[*9]

Preface

Recent advancements in radioactive-isotope (RI) beam technology have opened up the research field of the physics of exotic nuclei. Since the RIBF started operation in 2007, our experimental capabilities have been significantly expanded, including neutron- and proton-rich nuclei as well as superheavies. With increasing experimental data for a vast mass region of the nuclear chart, nuclear structure and reaction theories are expected to play a more important role in interpreting the data and in profoundly understanding atomic nuclei. A mission of the second-term Theory Forum (TF2) is to discuss physics in the future of RIBF. Taking over the discussions in the first-term Theory Forum (TF1) (2006–2014), we have been working through various activities. Although most of the members were renewed, Dr. Y. Utsuno, Dr. K. Ogata, and Dr. S. Wanajo acted as mediators to bridge the activities of TF1 and TF2. We would like to express our gratitude to them. This report summarizes our activities over the last seven years to facilitate handover to the third-term Theory Forum. Because of the limited space in this progress report, details about our activities are provided on a web page.[1)]

Short reports from WGs

TF2 was divided into several working groups (WGs) to discuss physics cases intensively. We also had intergroup discussions regularly. Here, we present short summaries of these activities, which are categorized into three subjects: nuclear astrophysics, the physics of superheavy elements, and the physics of nuclear many-body problems. More details on each subject can be found on the website.

Nuclear astrophysics: r-process, EOS, and nuclear matter

In the field of nuclear astrophysics, discussions were started with two WGs. The primary purpose of the r-process WG was to improve the current theoretical calculations of nuclear properties, including the masses, decay half-lives, neutron-capture reaction rates, and nuclear fission rates for the r-process nucleosynthesis calculations. The possibility of updating these rates used in the nucleosynthesis community was discussed, particularly to reflect the latest results from nuclear theory groups in Japan. A novel mass model based on the Bayesian neural-network method was proposed to assess the model uncertainty and to evaluate the impact of new measurements on the prediction. The significance of direct reaction on the neutron capture rates was investigated through a microscopic approach. Furthermore, we found a compelling difference between the phenomenological fission distributions widely used in the nucleosynthesis calculations and the results obtained using a dynamical model based on the Langevin model in the neutron-rich r-process region. This shows the necessity of considering dynamical fission in the data on systematic fission yields for better r-process calculation.

The equation of state (EOS) and nuclear matter WG aimed to determine the nuclear-physics constraints on the nuclear EOS. The connection between the astrophysical observations and the nuclear properties revealed at RIBF has been explored. We found that we can construct a model that can account for the indication of GW170817 if the symmetry energy at twice the saturation density of nuclear matter is 40–60 MeV. The symmetry energy in this density region can be constrained from the collision experiment of neutron-rich heavy ions measured by the SAMURAI spectrometer at RIBF.

In addition to these activities focusing specifically on theoretical nuclear physics, we organized a series of workshops to bring together nuclear physicists and astrophysicists motivated by the discovery of an r-process event (kilonova) associated with the gravitational-wave detection by the Advanced LIGO–Advanced Virgo from merging neutron stars. The workshops were held at RNC (June 2018), YITP Kyoto University (May 2019), and NAOJ (October 2020).

Superheavy elements

The main purpose of the superheavy element and fission WG (SHE/Fission WS) was to give theoretical suggestions and make proposals for experiments on new superheavy elements conducted at RIBF. A primary interest in the physics of superheavy elements is to synthesize new elements exceeding $Z = 118$, and to produce nuclei at the center of the island of stability located around $Z = 114$ and $N = 184$. For the former, heavier projectiles and stable actinide targets are being promoted. For the latter, there is no available set of stable projectiles and targets because the center of the island of stability is located in the neutron-rich region.

*1 RIKEN Nishina Center
*2 Kindai University
*3 Department of Physics, Hokkaido University
*4 Department of Physics, the University of Tokyo
*5 Department of Physics, Kyushu University
*6 JAEA
*7 Faculty of Arts and Science, Kyushu University
*8 Astrophysical Big Bang Laboratory, RIKEN
*9 Department of Physics, Kyoto University

It is thus desirable to estimate the possibility of new-element synthesis based on the theoretical calculation and to propose new experiments.

To synthesize superheavy elements, we proposed the optimum incident energy and the combination of a target and projectile based on the calculated evaporation-residue cross section. We also calculated the properties of new superheavy elements: lifetime, deformation, nuclear structure, fission barrier height, decay proprieties, etc. We then suggested a new approach to the synthesis of superheavy nuclei.

We (co)organized the RIBF ULIC mini-WS in August 2016 as a kick-off meeting and subsequently held a WS entitled "New developments in superheavy element research" at Kyushu University in July 2018.

Nuclear structure, collective motion, many-body correlations, and halo

The nuclear systems under extreme conditions are expected to reveal new facets associated with the correlations among nucleons. A uniqueness of drip-line nuclei was discussed in view of the nuclear interactions and the strong correlations in a dilute system, such as the multi-neutron halo and its condensation. A possibility of measuring the many-body correlations was also discussed through the nuclear responses and reactions. The connections between the nuclear responses and the EOS of nuclear matter or the reaction (decay) rates relevant to the r-process were investigated.

The true pleasure in nuclear physics is the diversity of research topics. Thus, we realized the importance of offering an opportunity to young colleagues, particularly students and post-docs, where we can frankly discuss nascent plans of physics research. To provide such an environment and to explore important physics for future experiments at RIBF in a variety of research subjects covered in the WG, we decided to organize "Hodan-kai" meetings. In contrast to the style of an ordinary workshop, the Hodan-kai aims to facilitate the exchange of unmatured ideas among young researchers. To concentrate on physics discussions, the venue was a relatively isolated place, and the presentation files are not open to the public.

The first Hodan-kai was held from July 31 to August 2, 2017 and focused mainly on the latest theoretical research on nuclear physics. The second and third meetings were held in February 2019 and 2020, respectively. The topics discussed were extended in the second and third meetings, as listed in Table 1. In the third meeting, in addition to talks given in the regular Hodan-kai style, two "panel discussion" sections consisting of introductory talks by organizers and 5–7 short talks by invited panelists were newly organized to facilitate interaction among the participants. The program and summary of the Hodan-kai are shared on their respective websites.[2–4)]

Table 1. Number of talks by theoretical and experimental nuclear physicists and researchers from other fields, as well as participants in the successive Hodan-kai meetings.

	Date	Theor.	Exp.	Other	Participants
1st	Aug 2017	22	1	0	49
2nd	Feb 2019	6	7	12	42
3rd	Feb 2020	6	7	4	43

Collaboration and Perspective

In addition to the collaborations among the TF2 members, collaborative works with other researchers have been conducted, and further collaborations are expected in the near future. We have already co-authored 4 papers on the experiments performed at RIBF, 2 proposals to the RIBF PAC, 24 papers on the theoretical analysis of the RIBF data, and 30 papers on the physics expected in the future RI beam facilities. Furthermore, 30+ invited talks on the physics of RI beams have been delivered by the TF2 members during this term.

We have been discussing nuclear fission with experimentalists of the Japan Atomic Energy Agency (JAEA). The measurement of nuclear fission processes and the formation of nuclei in the actinide region using the multinucleon transfer reaction have been intensively studied at the tandem facility of JAEA. Through joint research between JAEA and Kindai University, we have published a number of co-authored papers that have advanced the analysis of experimental data and the interpretation of experimental data. Students of Kindai University attended the summer training school at JAEA. These young students are expected to lead the physics of exotic nuclei in the future. This activity will thus be a starting point for further collaborative research in the physics of superheavy nuclei and fission.

The JSPS-NRF-NSFC A3 Foresight Program "Nuclear Physics in the 21st Century" started in 2019. A microscopic understanding of the r-process is one of the main projects, and theoretical collaboration among the A3 countries is key to success. The activities in TF2 would set a foundation for the extended collaboration. A plan for the construction of a microscopic nuclear data library based on nuclear density-functional theory is described in Ref. 5).

References

1) https://www.nishina.riken.jp/RIBF/TheoForum/index.html .
2) 1st Hodan-kai, https://indico2.riken.jp/event/2509/ .
3) 2nd Hodan-kai, https://indico2.riken.jp/event/2864/ .
4) 3rd Hodan-kai, https://indico2.riken.jp/event/3157/ .
5) K. Yoshida, in this report.

V. EVENTS

Symposium on Nuclear Data 2020

H. Otsu on behalf of the SND2020 Local Organizing Committee*1

The Symposium on Nuclear Data 2020 (SND2020) was held on November 26–27, 2020 at the RIBF conference room as an on-site venue, combined with online connections. This symposium originated from the first conference[1] held in 1978 under the auspices of the Japan Atomic Energy Research Institute (JAERI) and Japanese Nuclear Data Committee (Sigma Research Committee) and has been held almost every year since. The Nuclear Data Division (NDD) of the Atomic Energy Society of Japan (AESJ) took over the organization of this symposium in 2006. Since then, the symposium has been organized by an executive committee of the Nuclear Data Division. In practice, it has been hosted in turn by JAEA, domestic universities, or other research institutes every fiscal year.

In 2020, RIKEN Nishina Center hosted the symposium for the first time, in order to plant the seeds for cross-disciplinary research, to promote new collaborations, and to expand the possibility of collaborations. For the effective functioning of the symposium, CNS (U-Tokyo), WSNC (KEK), and the University of Tokyo were asked to co-host the event, and these institutes formed the local organizing committee.

The symposium consisted of 16 invited talks, 2 tutorial lectures, and 26 poster presentations, followed by an RIBF facility tour. The full program and abstracts of the symposium are available on the SND2020 webpage.[2] The invited talks covered recent topics and progress in nuclear data activities and consisted of five sessions: 1) accelerator facilities and nuclear data, 2) fission and heavy-ion nuclear spectroscopy, 3) nuclear reaction, 4) nuclear medicine and pharmacology, and 5) deep learning or machine learning, and its application to nuclear physics and nuclear data. A feature of this year's symposium was the inclusion of a session on machine learning. Machine learning is expected to play an important role in the next decade for nuclear physics and nuclear data, where multiple variables are handled and analyzed from raw or processed data. An introduction to the fundamentals of deep learning was provided including its origins, history of development, and relationship with computing power, The session carefully examined the capabilities of deep learning, examples of common pitfalls, and expectations for the future.

The two tutorial lectures were dedicated to the basic theory and actual operation of nuclear reactors. The lectures aimed to explain how nuclear reactors are established as macroscopic systems, so that even nuclear physics researchers, who usually understand physical phenomena from a microscopic perspective, could understand them. It is uncertain whether the aims were fully achieved, but such efforts are believed to be worthwhile.

Fig. 1. Symposium photo of on-site participants in front and on-line participants on screen.

Poster presentations were held using the break-out room function of the Zoom web meeting tool. This was necessary to prevent cluster outbreaks of COVID-19 that can potentially be introduced by face-to-face discussions. Therefore, not only on-site participants but also online participants presented their posters remotely. The posters themselves were located on the wall at the on-site conference room. Therefore, the on-site participants were able to examine the posters not only during the poster session, but also during coffee breaks.

Figure 1 shows a group photograph of both on-site and online participants of the symposium. Despite the COVID-19 pandemic, which restricted public access, 62 on-site participants visited RIKEN Wako campus. Together with 59 online participants, a total of 121 researchers and students joined the symposium. The Zoom web meeting tool was utilized not only for the poster session but also for several oral presentations. The on-site presentations were distributed via Zoom, and the remote presentations were shown on the screen at the conference room. Therefore, this conference was held in the hybrid model of on-site and remote participation. This model will be followed in the future as well. The next year's symposium will be hosted by J-PARC.

*1 RIKEN Nishina Center

References

1) Proc. the 1978 Seminar on Nuclear Data, https://inis.iaea.org/collection/NCLCollectionStore/_Public/11/537/11537325.pdf.
2) https://indico2.riken.jp/e/snd2020.

The 8th Asia-Pacific Conference on Few-Body Problems in Physics (APFB2020)

E. Hiyama,[*1,*2] A. Tamii,[*3] and S. Ishikawa[4]

The 72th Yamada Conference: The 8th Asia-Pacific Conference on Few-Body Problems in Physics (APFB2020) was held in Kanazawa, Japan on March 1–5, 2021. The purpose of the APFB conference is to encourage PhD students and young researchers in Asian countries to study few-body problems in various physics fields. The 1st APFB conference was held in Tokyo in 1999. Subsequently, we held the following APFB conferences: 2nd APFB, Shanghai, China in 2002; 3rd APFB, Nakhon Ratchasima, Thailand in 2005; 4th APFB, Depok, Indonesia in 2008; 5th APFB, Seoul, Korea in 2011; 6th APFB, Adelaide, Australia in 2014; and 7th APFB, Guilin, China in 2017. The 8th APFB was planned to be conducted in August 2020. However, because of the COVID-19 pandemic, we postponed it to March 1–5, 2021. As the pandemic situation continued well into 2021, we organized the conference in a hybrid format, that is, with participation both online and on-site. The venue for the on-site part of the conference was Bunka hall in Kanazawa, where one large room was prepared for the plenary session and two smaller rooms were prepared for parallel sessions. While maintaining social distancing, we prepared desks and chairs for 60 persons in the plenary-session room and for approximately 20 persons in the other rooms. Moreover, on-site participants were requested to wear masks during the conference, and the consumption of food and drinks was prohibited.

The following topics were covered in APFB2020: few-hadron systems and their interactions, hadron structure and quantum chromodynamics, structure of light nuclei and hypernuclei, relativistic aspects of few-body systems near stability and their interactions, symmetries and symmetry breaking, electroweak interactions

Fig. 1. Conference photograph from the on-site venue.

Fig. 2. Opening address at the on-site venue.

in few-hadron systems, atomic and molecular systems, exotic few-body systems and astrophysics, and methods in few-body systems

This hybrid conference had approximately 300 participants in total, of which 50 participants attended on-site and approximately 250 attended online. We had 160 domestic participants, about 80 participants from other Asian countries, 40 from Europe, and 15 from the U.S.A. All participants from abroad attended online. APFB2020 featured 36 plenary talks, 10 invited talks in parallel sessions, and 90 contributed talks. The most difficult tasks in the hybrid-style conference was to organize a scientific program and to solve network problems. We also needed to address the differences in time zone among Asian countries, Europe, and the U.S.A. Therefore, we split the plenary session into the morning (for the US time zone) and evening (for the European time zone). The parallel sessions were conducted late in the morning and in the early afternoon. In addition, we carefully prepared a reliable network connection, which was expensive. However, we were concerned about poor network connections from presenters. To avoid this difficulty, we asked them to provide recoded talks in advance. As expected, we had to use some of the recoded talks during the conference because of poor connections.

The next international Conference on few-body problems in physics will be held in Beijing, China in 2022. We hope that the conference will be conducted entirely on-site as it would be more efficient to conduct discussions on physics in that manner.

Finally, we would like to acknowledge RIKEN Nishina Center, RCNP, RIKEN iTHEMS, Kyushu University, and Tohoku University as co-host institutes and universities. Furthermore, the conference was hosted by the Yamada Science Foundation through a Grant-in-Aid for Scientific Research on Innovative Areas, titled “Clustering as windows on the hierarchical structure of quantum systems.”

*1 RIKEN Nishina Center
*2 Department of Physics, Tohoku University
*3 RCNP, Osaka University
*4 Science Research Center, Hosei University

Domestic Workshop on Spin Physics

Y. Goto,[*1] for the Local Organizing Committee

24th International Symposium on Spin Physics was scheduled to be held in Matsue City in September 2020 as SPIN2020, but it was postponed to October 2021 because of COVID-19 pandemic and will be held as SPIN2021. Prior to SPIN2021, we held a domestic workshop on spin physics as a satellite workshop of SPIN2021 on February 23rd and 24th, 2021 to discuss future themes of spin physics and related fields, activities of various groups, and prospects for development in Japan, as well as to provide a platform for presentations by young researchers. The workshop language was Japanese.

In the workshop, topics related to spin phenomena in particle and nuclear physics and related fields were discussed. In accordance with the topics to be discussed in SPIN2021, the following topics were reviewed:

- proton radius for the nucleon structure
- RHIC and COMPASS results, three-dimensional parton distribution, and QCD spin physics for the spin structure of hadrons
- physics of the Electron-Ion Collider for future facilities and experiments
- theoretical and experimental reviews for fundamental symmetries and physics beyond the standard model
- polarized electron sources and solid polarized targets
- physics at LEPS for spin physics research using photon, lepton, and hadron probes
- low-energy spin physics in nuclear reactions and nuclei
- applications of spin physics

The workshop also included presentations by young researchers on the understanding of the single-spin asymmetry, nucleon structure studies based on the lattice field theory, theory of the electric-dipole moment, spin-spin correlation in K-pp decay, polarized target of COMPASS, study of three-body nucleon force using a polarized target, and structure analysis of materials by neutron scattering. The presentations and discussions will be published and distributed as conference proceedings.

SPIN2021 is planned to be held in October as a hybrid conference combining on-site and online sessions. The domestic workshop was held at the same venue as that for SPIN2021, the Kunibiki Messe Convention Center in Matsue City. Together with the venue staff, we discussed ideas for the success of the hybrid conference and held the domestic workshop as a test run of SPIN2021. Considering the current situation

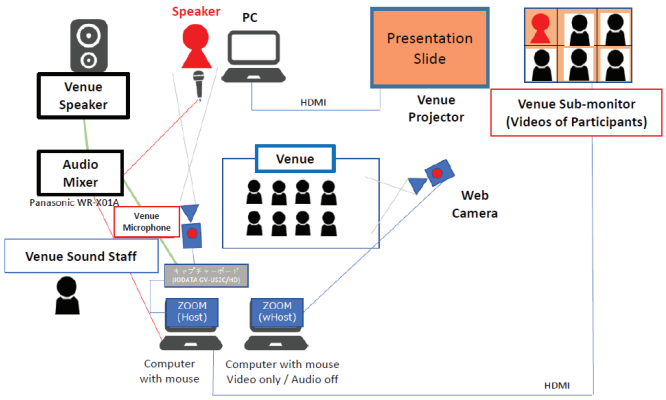

Fig. 1. Setup of the venue for the hybrid conference.

of COVID-19, only the organizing committee participated on-site this time, while the others participated online. The number of on-site participants in the workshop was 7, and the number of online participants was 45.

The on-site portion of the workshop was in the format of a regular research meeting in a conference room, which was distributed via Zoom so that people could participate online. The system shown in Fig. 1 was prepared so that the online participants could participate in the question and answer session in the same way as on-site participants. Some speakers and chairpersons spoke on-site, while others presented online. The speakers at the venue displayed their slides on the projector as in a normal conference, and the operator distributed a split line to Zoom. The online speakers also displayed their slides via Zoom screen sharing.

The workshop was held with financial support from the RIKEN Nishina Center and with great help from the venue staff. The hybrid conference method allowed us to integrate on-site and online discussions and conduct an active workshop. We would like to build on the success of this experience to organize a larger SPIN2021 International Symposium with parallel sessions in addition to the plenary session, welcoming more on-site and online participants from abroad.

*1 RIKEN Nishina Center

VI. ORGANIZATION AND ACTIVITIES OF RIKEN NISHINA CENTER

(Activities, Members, Publications & Presentations)

1. Organization

1.1 Organization Chart as of March 31, 2021 （End of FY2020）

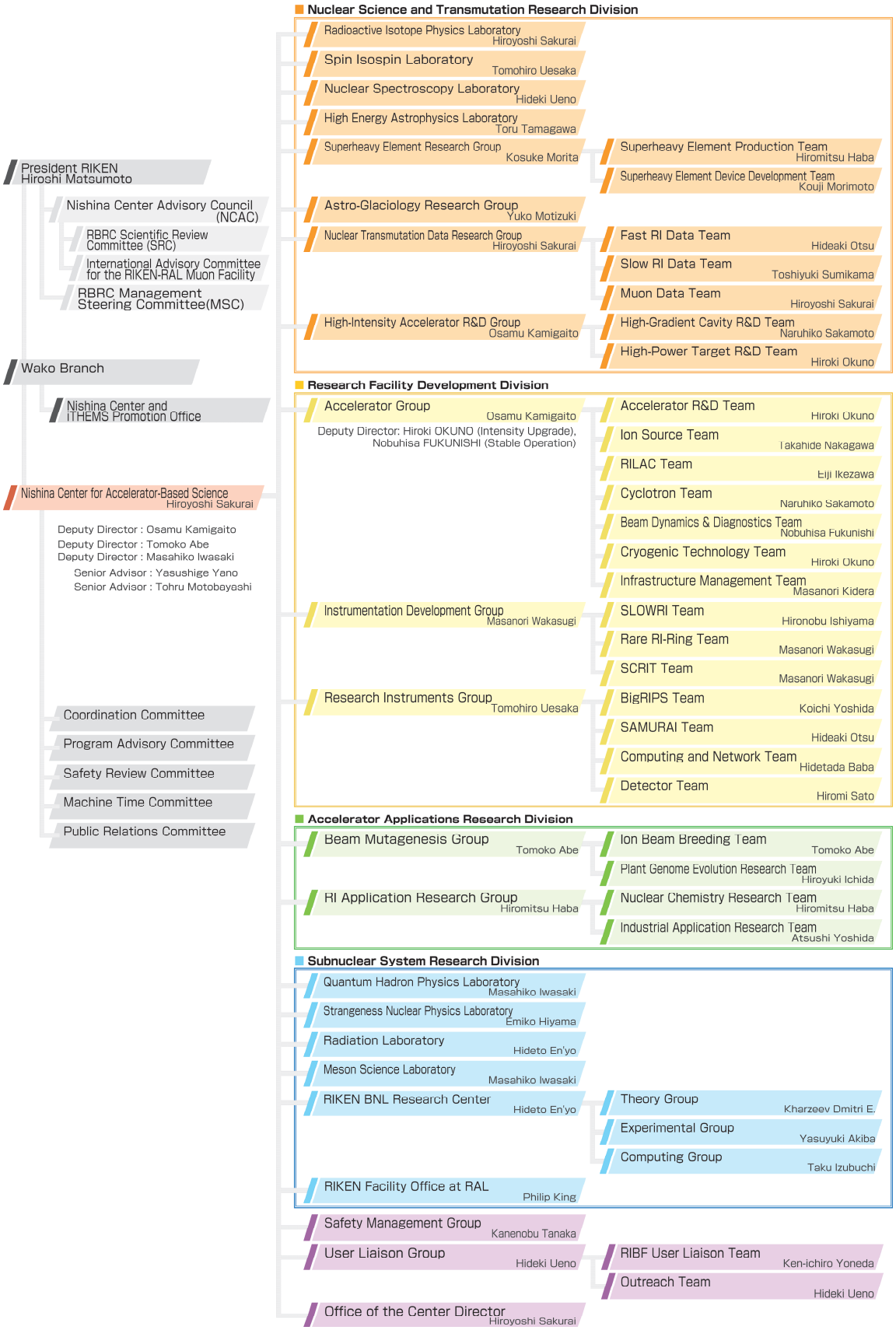

1.2 Topics in FY2020

Year	Date	Topics in Management
2020	Apr. 1	Newly appointed: RNC Director: Hiroyoshi SAKURAI
2020	Oct. 1	Newly appointed: Team Leader of Plant Genome Evolution Research Team: Hiroyuki ICHIDA
2020	Oct. 1	Newly appointed: Team Leader of Infrastructure Management Team: Masanori KIDERA

2. Finances

A transition of the RNC budget for the past four years is shown in following graph.

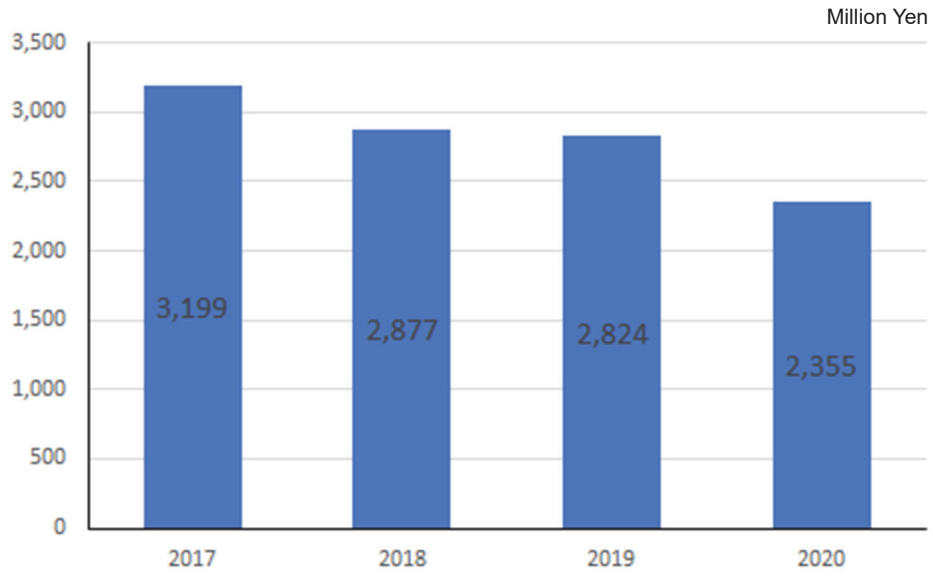

3. Staffing

At the start of FY 2019, there were 142 personnel affiliated with RNC and 419 researchers visiting RNC for research purpose. The following graphs show a breakdown of personnel into six categories as of April 1, 2019, and a transition of the number of each category.

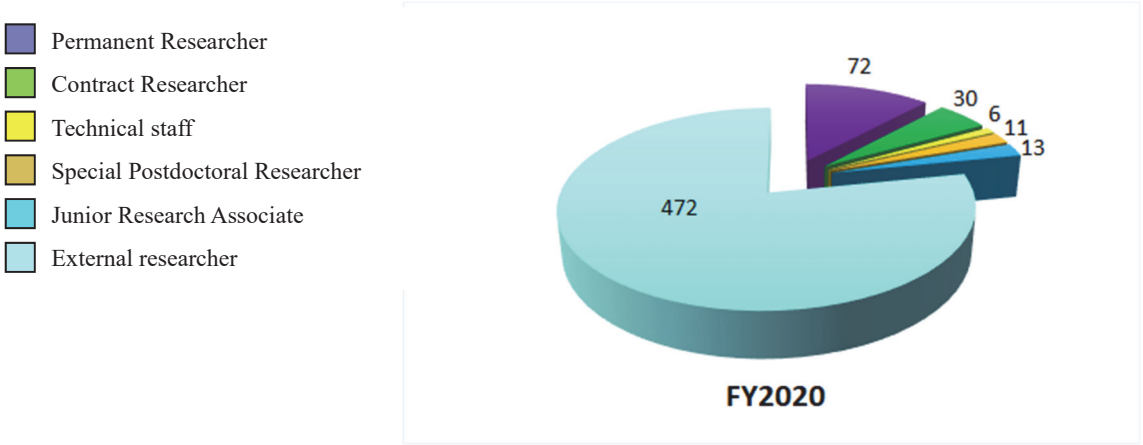

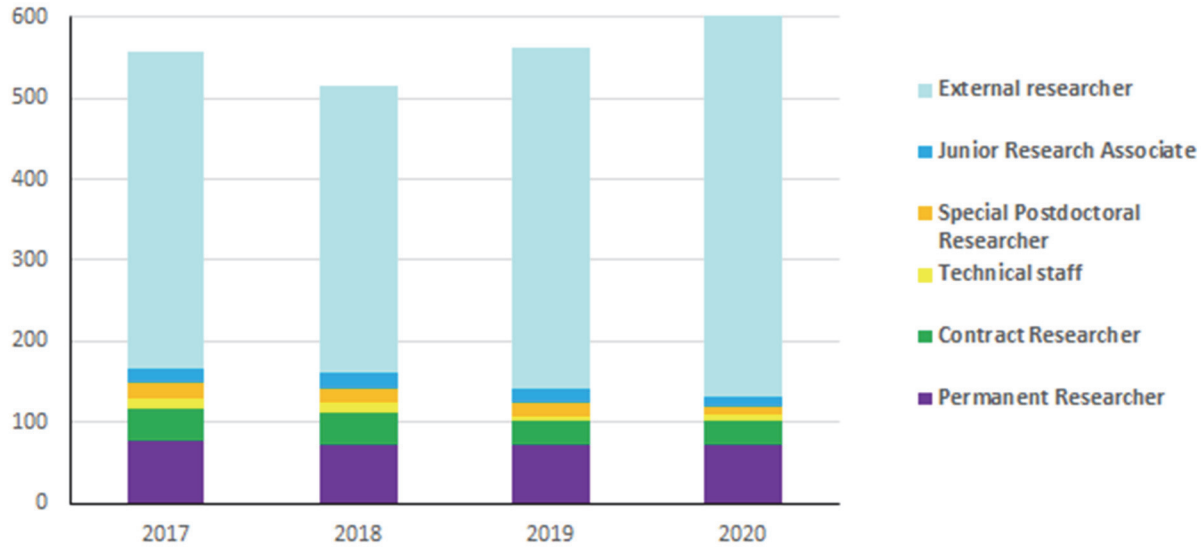

4. Research publication

The number of papers published annually from RNC is shown graphically using the data obtained from Clarivate Analytics' Web of Science Documents.

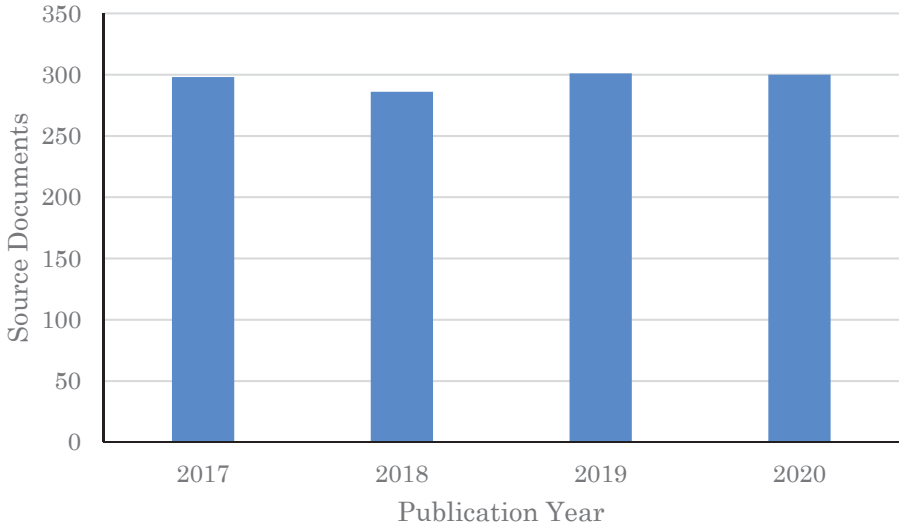

Citation analysis for the past four years

As of April 2021

Indicators \ Year	2017	2018	2019	2020
Total number of papers	298	286	301	300
Percentage of papers in top 10%	16.78	20.63	9.63	1.33
Percentage of papers in top 1%	2.68	4.20	1.00	12.67

5. Management

Headed by the RNC Director Hiroyoshi SAKURAI, the RIKEN Nishina Center for Accelerator-Based Science (RNC) consists of:

- 9 Laboratories
- 10 Groups with 27 Teams
- 2 overseas research centers with 3 Groups

as of the end of FY2020. There are also two 'Partner Institutes' which conduct research in the laboratories set up in RNC. RNC is managed by its Director who takes into consideration the majority decision of the RNC Coordination Committee. The management of RNC is supported by the following committees:

- Program Advisory Committee
- Safety Review Committee
- RIBF Machine Time Committee
- Public Relations Committee

There are also committees to support the President of RIKEN and/or the Director of RNC such as:

- Nishina Center Advisory Council with three subcommittees:
  - RBRC Scientific Review Committee (SRC)
  - International Advisory Committee for the RIKEN-RAL Muon Facility
  - RBRC Management Steering Committee (MSC)

Nishina Center for Accelerator-based Science

Executive Members (as of March 31, 2021)

Hiroyoshi SAKURAI	Director
Osamu KAMIGAITO	Deputy Director (Research Facility Development Division)
Tomoko ABE	Deputy Director (Accelerator Application Division)
Masahiro IWASAKI	Deputy Director (Subnuclear System Research Division)
Yasushige YANO	Senior Advisor
Tohru MOTOBAYASHI	Senior Advisor

RNC Coordination Committee

The following subjects relevant to the RNC management are deliberated under the chairmanship of the RNC Director:

- Establishment of the new organization or reorganization in RNC
- Personnel management of RNC researchers
- Research themes and research budget
- Approval of the Partner Institutes
- Evaluation of the management of RNC and the response to the recommendations by external evaluation

The RNC Coordination Committee is held monthly.

Members (as of March 31, 2021)

Hiroyoshi SAKURAI	Director, RNC; Director, Radioactive Isotope Physics Laboratory and Nuclear Transmutation Data Research Group; Team Leader, Muon Date Team
Osamu KAMIGAITO	Deputy Director, RNC; Director, Accelerator Group and High-Intensity Accelerator R&D Group; Team Leader, Infrastructure Management Team
Tomoko ABE	Deputy Director, RNC; Director, Beam Mutagenesis Group; Team Leader, Ion Beam Breeding Team
Masahiko IWASAKI	Deputy Director, RNC; Director, Meson Science Laboratory
Yasushige YANO	Senior Advisor, RNC
Tohru MOTOBAYASHI	Senior Advisor, RNC
Tomohiro UESAKA	Director, Spin Isospin Laboratory and Research Instruments Group
Hideki UENO	Director, Nuclear Spectroscopy Laboratory and User Liaison Group; Team Leader, Outreach Team
Toru TAMAGAWA	Director, High Energy Astrophysics Laboratory
Emiko HIYAMA	Director, Strangeness Nuclear Physics Laboratory
Yuko MOTIZUKI	Director, Astro-Glaciology Research Group
Kosuke MORITA	Director, Superheavy Element Research Group
Hiroki OKUNO	Deputy Group Director, Accelerator Group; Team Leader, Accelerator R&D Team, Cryogenic Technology Team, and High-Power Target R&D Team
Nobuhisa FUKUNISHI	Deputy Group Director, Accelerator Group; Team Leader, Beam Dynamics & Diagnostics Team
Masanori WAKASUGI	Director, Instrumentation Development Group; Team Leader, Rare RI-Ring Team and SCRIT Team
Hiromitsu HABA	Director, RI Application Research Group; Team Leader, RI Application Team and Superheavy Element Production

	Team
Kanenobu TANAKA	Director, Safety Management Group
Eiji IKEZAWA	Team Leader, RILAC Team
Hideaki OTSU	Team Leader, SAMURAI Team and Fast RI Data Team
Naruhiko SAKAMOTO	Team Leader, Cyclotron Team and High-Gradient Cavity R&D Team
Hiromi SATO	Team Leader, Detector Team
Toshiyuki SUMIKAMA	Team Leader, Slow RI Data Team
Takahide NAKAGAWA	Team Leader, Ion Source Team
Koji MORIMOTO	Team Leader, Superheavy Element Device Development Team
Atsushi YOSHIDA	Team Leader, Industrial Application Research Team
Koichi YOSHIDA	Team Leader, BigRIPS Team
Ken-ichiro YONEDA	Team Leader, RIBF User Liaison Team
Hironobu ISHIYAMA	Team Leader, SLOWRI Team
Hidetada BABA	Team Leader, Computing and Network Team
Hiroyuki Ichida	Team Leader, Plant Genome Evolution Research Team
Masanori Kidera	Team Leader, Infrastructure Management Team
Tsukasa TADA	Vice Chief Scientist, Quantum Hadron Physics Laboratory
Yasushi WATANABE	Deputy Team Leader, RIBF User Liaison Team
Yutaka WATANABE	Deputy Team Leader, Infrastructure Management Team
Hideto EN'YO	Director, RIKEN BNL Research Center; Director, Radiation Laboratory
Yasuyuki AKIBA	Group Leader, Experimental Group, RIKEN BNL Research Center
Taku IZUBUCHI	Group Leader, Computing Group, RIKEN BNL Research Center
Toshiyuki HASHIMOTO	Director, Nishina Center and iTHEMS Promotion Office

Program Advisory Committee

The Program Advisory Committee reviews experimental proposals submitted by researchers and reports the approval/disapproval of the proposals to the RNC Director. The Committee also reports to the RNC Director the available days of operation at RIBF or the Muon Facility at RAL allocated to researchers. The Committee is divided into three categories according to the research field.

- Nuclear Physics Experiments at RIBF (NP-PAC): academic research in nuclear physics
- Materials and Life Science Researches at RNC (ML-PAC): academic research in materials science and life science
- Industrial Program Advisory Committee (In-PAC): non-academic research

Program Advisory Committee for Nuclear Physics Experiments at RI Beam Factory (NP-PAC)

The 21st NP-PAC was held on December 14−16, 2020 at RIBF.

Members (as of March 31, 2021)

Robert V.F. JANSSENS (Chair)	University of North Carolina at Chapel Hill
Dieter ACKERMANN	GANIL
Nori AOI	Osaka University
Maria J.G. BORGE	Consejo Superior de Investigaciones Científicas
Robert CHARITY	Washington University in St. Louis
Augusto O. MACCHIAVELLI	Lawrence Berkeley National Laboratory
Gabriel MARTINEZ-PINEDO	Technische Universität Darmstadt, GSI Helmholtzzentrum für Schwerionenforschung
Iain MOORE	University of Jyväskylä
David J. MORRISSEY	Michigan State University
Hitoshi NAKADA	Chiba University
Alexandre OBERTELLI	Technische Universität Darmstadt
Takehiko SAITO	RIKEN Cluster for Pioneering Research
Kimiko SEKIGUCHI	Tohoku University
Philip J. WOODS	University of Edinburgh
Andrea VITTURI	Universita' di Padova
Xiaohong ZHOU	Institute of Modern Physics, CAS

Program Advisory Committee for Materials and Life Science Researches at RIKEN Nishina Center (ML-PAC)

The ML-PAC of FY2020 was held between January 13 and 20, 2021 via e-mail.

Members (as of March 31, 2021)

Adrian HILLIER (Chair)	ISIS, RAL (UK)
Zhi QIN	Institute of Modern Physics, CAS
Toshiyuki Takayanagi	Saitama University
Yoshio Kobayashi	The University of Electro-Communications
Yutaka Miyazawa	Yamagata University

Industrial Program Advisory Committee (In-PAC)

The 10th In-PAC was held on July 30, 2020 via Web meeting.

Safety Review Committee

The Safety Review Committee is composed of two sub committees, the Safety Review Committee for Accelerator Experiments and the Hot-Lab Safety Review Committee. These Committees review the safety regarding the usage of radiation generating equipment based on the proposal submitted to the RNC Director from the spokesperson of the approved experiment.

Safety Review Committee for Accelerator Experiments

Members (as of March 31, 2021)

Hiromi SATO (Chair)	Team Leader, Detector Team
Kouji MORIMOTO	Team Leader, Superheavy Element Device Development Team
Eiji IKEZAWA	Team Leader, RILAC Team
Hiromitsu HABA	Team Leader, RI Application Team
Atsushi YOSHIDA	Team Leader, Industrial Cooperation Team
Koichi YOSHIDA	Team Leader, BigRIPS Team
Naoki FUKUDA	Technical Scientis, BigRIPS Team
Naruhiko SAKAMOTO	Team Leader, Cyclotron Team
Daisuke SUZUKI	Research Scientist, Radioactive Isotope Physics Laboratory
Masaki SASANO	Senior Research Scientist, Spin Isospin Laboratory
Yuichi ICHIKAWA	Senior Research Scientist, Nuclear Spectroscopy Laboratory

External members

Shinichiro MICHIMASA	Assistant Professor, Center for Nuclear Study, University of Tokyo
Hidetoshi YAMAGUCHI	Lecturer, Center for Nuclear Study, University of Tokyo
Yutaka WATANABE	Associate Professor, High Energy Accelerator Research Organization, KEK

Ex officio members

Kanenobu TANAKA	Director, Safety Management Group
Hisao SAKAMOTO	Technical Scientist, Safety Management Group

Hot-Lab Safety Review Committee

Members (as of March 31, 2020)

Tetsuya OHNISHI (Chair)	Senior Research Scientist, SCRIT Team
Kanenobu TANAKA	Director, Safety Management Group
Hisao SAKAMOTO	Technical Scientist, Safety Management Group
Hiroki MUKAI	Technical Staff I, Safety Management Group
Eriko HIGURASHI	Technical Scientist, Safety Management Group
Hiromitsu HABA	Team Leader, RI Application Team
Kazuya TAKAHASHI	Senior Research Scientist, Nuclear Chemistry Research Team

RIBF Machine Time Committee

Upon request of the RNC Director, the RIBF Machine Time Committee deliberates on the machine time schedule of RIBF and reports the results to the Director.

Members (as of March 31, 2021)

Hideki UENO (Chair)	Director, User Liaison Group and Nuclear Spectroscopy Laboratory
Osamu KAMIGAITO	Director, Accelerator Group
Masanori WAKASUGI	Director, Instrumentation Development Group
Tomohiro UESAKA	Director, Research Instruments Group and Spin Isospin Laboratory
Nobuhisa FUKUNISHI	Deputy Group Director, Accelerator Group
Hiroki OKUNO	Deputy Group Director, Accelerator Group
Shunji Nishimura	Senior Research Scientist, Radioactive Isotope Physics Laboratory
Tomoko ABE	Director, Beam Mutagenesis Group
Hiromitsu HABA	Director, RI Application Research Group
Kanenobu TANAKA	Director, Safety Management Group
Ken-ichiro YONEDA	Team Leader, RIBF User Liaison Team
Kouji MORIMOTO	Team Leader, Superheavy Element Research Device Development Team
Koichi YOSHIDA	Team Leader, BigRIPS Team

External members

Kentaro YAKO	Associate Professor, Center for Nuclear Study, University of Tokyo
Hidetoshi YAMAGUCHI	Lecturer, Center for Nuclear Study, University of Tokyo
Yutaka WATANABE	Associate Professor, High Energy Accelerator Research Organization, KEK

Observers

Hiroyoshi SAKURAI	Director, RNC; Director, Radioactive Isotope Physics Laboratory and Nuclear Transmutation Data Research Group; Team Leader, Muon Date Team
Hideto EN'YO	Director, RIKEN BNL Research Center; Director, Radiation Laboratory
Susumu SHIMOURA	Director, Center for Nuclear Study, University of Tokyo
Michiharu WADA	Director, KEK Wako Nuclear Science Center
Hiroari Miyatake	Professor, High Energy Accelerator Research Organization, KEK
Daisuke Suzuki	Chair, The RIBF Users Executive Committee (RIBF-UEC), Research Scientist, Radioactive Isotope Physics Laboratory)
Kosuke MORITA	Director, Superheavy Element Research Group
Hideaki OTSU	Team Leader, SAMURAI Team
Atsushi YOSHIDA	Team Leader, Industrial Cooperation Team
Tohru MOTOBAYASHI	Senior Advisor, RNC
Hideyuki SAKAI	Senior Advisor, RNC
Yasuhiro SAKEMI	Professor, Center for Nuclear Study, University of Tokyo
Hironobu Ishiyama	Team Leader, SLOWRI Team
Toshiyuki Hashimoto	Director, Nishina Center and iTHEMS Promotion Office
Kazushige FUKUSHIMA	Manager, Nishina Center and iTHEMS Promotion Office

Public Relations Committee

Upon request of the RNC Director, the Public Relations Committee deliberates and coordinates the following matters:

- Creating public relations system for RNC
- Prioritization of the public relations activities for RNC
- Other general and important matters concerning the public relations of RNC

Members (as of March 31, 2021)

Toshiyuki HASHIMOTO (Chair)	Director, Nishina Center and iTHEMS Promotion Office
Osamu KAMIGAITO	Deputy Director, RNC; Director, Accelerator Group
Tomoko ABE	Deputy Director, RNC; Director, Beam Mutagenesis Group
Masahiko IWASAKI	Deputy Director, RNC; Director, Meson Science Laboratory
Tomohiro UESAKA	Director, Spin Isospin Laboratory and Research Instruments Group
Hideki UENO	Director, Nuclear Spectroscopy Laboratory and User Liaison Group
Toru TAMAGAWA	Director, High Energy Astrophysics Laboratory
Emiko HIYAMA	Director, Strangeness Nuclear Physics Laboratory
Kosuke MORITA	Director, Superheavy Element Research Group
Hideto EN'YO	Director, RIKEN BNL Research Center; Director, Radiation Laboratory

RBRC Management Steering Committee (MSC)

RBRC MSC is set up according to the Memorandum of Understanding between RIKEN and BNL concerning the collaboration on the Spin Physics Program at the Relativistic Heavy Ion Collider (RHIC). The 26th and 27th MSC was held on July 16 and August 20, 2019, respectively.

Members (as of March 31, 2021)

Shigeo Koyasu	Executive Director, RIKEN
Hiroyoshi Sakurai	Director, RNC; Director, Radioactive Isotope Physics Laboratory and Nuclear Transmutation Data Research Group; Team Leader, Muon Date Team
Shoji NAGAMIYA	Senior Visiting Scientist, RNC
Robert TRIBBLE	Deputy Director for Science and Technology, BNL
Dmitori DENISOV	Deputy Associate Laboratory Director for High Energy Physics, BNL
Berndt MUELLER	Associate Laboratory Director for Nuclear and Particle Physics, BNL

6. International Collaboration

Country	Partner Institute	Objects	RNC contact person
Austria	Stefan Meyer Institute for Subatomic Physics	Framework	Masahiko IWASAKI, Director, Meson Science Laboratory
China	China Nuclear Physics Society	Creation of the council for China -Japan research collaboration on nuclear physics	Hiroyoshi SAKURAI, Director, Radioactive Isotope Physics Laboratory
	Peking University	Nuclear Science	Hiroyoshi SAKURAI, Director, Radioactive Isotope Physics Laboratory
	Institute of Modern Physics, Chinese Academy of Science	Physics of heavy ions	Hiroyoshi SAKURAI, Director, Radioactive Isotope Physics Laboratory
	School of Nuclear Science and Technology, Lanzhou University	Framework	Masahiko IWASAKI, Director, Meson Science Laboratory
	School of Physics, Nanjing University	Framework	Emiko HIYAMA, Director, Strangeness Nuclear Physics Laboratory
	Department of Physics, Faculty of Science, The University of Hong Kong	Experimental and educational research collaboration in experimental nuclear physics	Hiroyoshi SAKURAI, Director, Radioactive Isotope Physics Laboratory
	School of physics, Nankai University	Framework	Emiko HIYAMA, Director, Strangeness Nuclear Physics Laboratory
	School of Physical Sciences, USTC,	Framework	Masahiko IWASAKI, Director, Meson Science Laboratory
Finland	University of Jyvaskyla	Basic nuclear physics and related instrumentation	Hironobu ISHIYAMA, Team Leader, SLOWRI Team
France	National Institute of Nuclear Physics and Particle Physics (IN2P3)	Physics of heavy ions	Tomohiro UESAKA, Director, Spin Isospin Laboratory
	Normandy University	Framework	Tomohiro UESAKA, Director, Spin Isospin Laboratory
	Commissariat à l'énergie atomique et aux énergies alternatives (CEA, French Alternative Energies and Atomic Energy Commission)・Direction des Sciences de la Matière" (DSM)		Tomohiro UESAKA, Director, Spin Isospin Laboratory
Germany	GSI	Physics of heavy ions and accelerator	Hiroyoshi SAKURAI, Director, Radioactive Isotope Physics Laboratory
	Department of Physics, Technische Universität Darmstadt	Framework	Emiko HIYAMA, Director, Strangeness Nuclear Physics Laboratory
Hungary	The Institute of Nuclear Research of the Hungarian Academy of Sciences (ATOMKI)	Nuclear physics, Atomic Physics	Tomohiro UESAKA, Director, Spin Isospin Laboratory
Indonesia	ITB, UNPAD, ITS, UGM, UI	Material science using muons at the RIKEN-RAL muon facility	Masahiko IWASAKI, Director, Meson Science Laboratory
	Hasanuddin University	Agricultural science and related fields involving heavy-ion beam mutagenesis using Indonesian crops	Tomoko ABE, Director, Beam Mutagenesis Group
Italy	Applied Physics Division, National Institute for New Technologies, Energy and Environment (ENEA)	Framework	Hiroyoshi SAKURAI, Director, Radioactive Isotope Physics Laboratory
	European Center for Theoretical Studies in Nuclear Physics and Related Areas (ECT*)	Theoretical physics	Tetsuo HATSUDA, Director, Quantum Hadron Physics Laboratory
	Istituto Nazionale di Fisica Nucleare (INFN)	Physics of heavy ions	Hiroyoshi SAKURAI, Director, Radioactive Isotope Physics Laboratory

Country	Partner Institute	Objects	RNC contact person
Korea	Seoul National University	Nishina School	Hiroyoshi SAKURAI, Director, Radioactive Isotope Physics Laboratory
	College of Natural Science, Ewha Women's University	Framework	Tomohiro UESAKA, Director, Spin Isospin Laboratory
	College of Natural Sciences, INHA University	Framework	Emiko HIYAMA, Director, Strangeness Nuclear Physics Laboratory
Malaysia	Universiti Sains Malaysia	Muon Science	Masahiko IWASAKI, Director, Meson Science Laboratory
Norway	Faculty of Mathematics and Natural Science, University of Oslo（UiO MN）	Framework	Hiroyoshi SAKURAI, Director, Radioactive Isotope Physics Laboratory
Poland	The Henryk Niewodniczanski Institute of Nuclear Physics, Polish Academy of Sciences(IFPAN)	Framework	Hiroyoshi SAKURAI, Director, Radioactive Isotope Physics Laboratory
Romania	"Horia Hulubei" National Institute of Physics and Nuclear Engineering Bucharest-Magurele, Romania	Framework	Tomohiro UESAKA, Director, Spin Isospin Laboratory
	University of Bucharest	Framework	Tomohiro UESAKA, Director, Spin Isospin Laboratory
Russia	Joint Institute for Nuclear Research (JINR)	Framework	Tomohiro UESAKA, Director, Spin Isospin Laboratory
	Russian Research Center "Kurchatov Institute"	Framework	Hiroyoshi SAKURAI, Director, Radioactive Isotope Physics Laboratory
Switzerland	Paul Scherrer Institute	Improve the performance and reliability of accelerator systems	Osamu KAMIGAITO, Director, Accelerator Group
USA	Columbia University	The development of QCDCQ	Hideto EN'YO, Director, Radiation Laboratory
	Michigan State University	Comprehensive The use of TPC (Time Projection Chamber)	Tomohiro UESAKA, Director, Spin Isospin Laboratory
Vietnam	Vietnam Atomic Energy Commission	Framework	Hiroyoshi SAKURAI, Director, Radioactive Isotope Physics Laboratory
Europe	European Nuclear Science and Application Research2	Framework	Tomohiro UESAKA, Director, Spin Isospin Laboratory
	The European Organization for Nuclear Research (CERN)	R&D and application of micro-pattern gas detectors (MPGD) technology (RD51 Collaboration)	Hideto EN'YO, Director, Radiation Laboratory
	The European Organization for Nuclear Research (CERN)	Collaboration in the ALICE Experiment	Hideto EN'YO, Director, Radiation Laboratory

7. Awards

Awardee, Laboratory / Team	Award	Organization	Date
Tomoki KIMURA, Visiting Scientist at the High Energy Astrophysics Laboratory	The Young Scientists' Prize, the Commendation for Science and Technology for FY2020	Japan Minister of Education, Culture, Sports, Science and Technology	Apr. 7
Masaki NISHIMURA, Student Trainee at Nuclear Spectroscopy Laboratory	The Student Presentation Award of the Physical Society of Japan in the field of experimental/theoretical nuclear physics	The Physical Society of Japan	May. 16
Takashi ICHIHARA, Special Temporary Research Scientist at the Radioactive Isotope Physics Laboratory	The 2020JPCERT/CC Certificate of Gratitude	JPCERT Coordination Center	Aug. 19

Atsumi. SAITO, Student Trainee at the Spin Isospin Laboratory	The A3F-CNSSS Young Scientist Awards	The Center for Nuclear Study, The University of Tokyo (CNS)	Aug. 21
Guo YIXIN, Student Trainee at the Quantum Hadron Physics Laboratory	The A3F-CNSSS Young Scientist Awards	The Center for Nuclear Study, The University of Tokyo (CNS)	Aug. 21
Huang SIWEI, IPA at the Spin Isospin Laboratory	The A3F-CNSSS Young Scientist Awards	The Center for Nuclear Study, The University of Tokyo (CNS)	Aug. 21
Junki TANAKA, Postdoctoral Researcher at the Spin Isospin Laboratory	The A3F-CNSSS Young Scientist Awards	The Center for Nuclear Study, The University of Tokyo (CNS)	Aug. 21
Tomoya NAITO, Student Trainee at the Hadron Quantum Hadron Physics Laboratory	The A3F-CNSSS Young Scientist Awards	The Center for Nuclear Study, The University of Tokyo (CNS)	Aug. 21
Takahiro NISHI, Postdoctoral Researcher at the Accelerator Group	The 17th Annual Meeting Award (the 9th)	The Particle Accelerator Society of Japan	Sep. 2
Kazuma NAKAZAWA, Visiting Scientist at the Strangeness Nuclear Physics Laboratory	The 66th Nishina Memorial Prize for FY2020	Nishina Memorial Foundation	Dec. 4

8. Brief overview of the RI Beam Factory

Intensity of Primary Beams

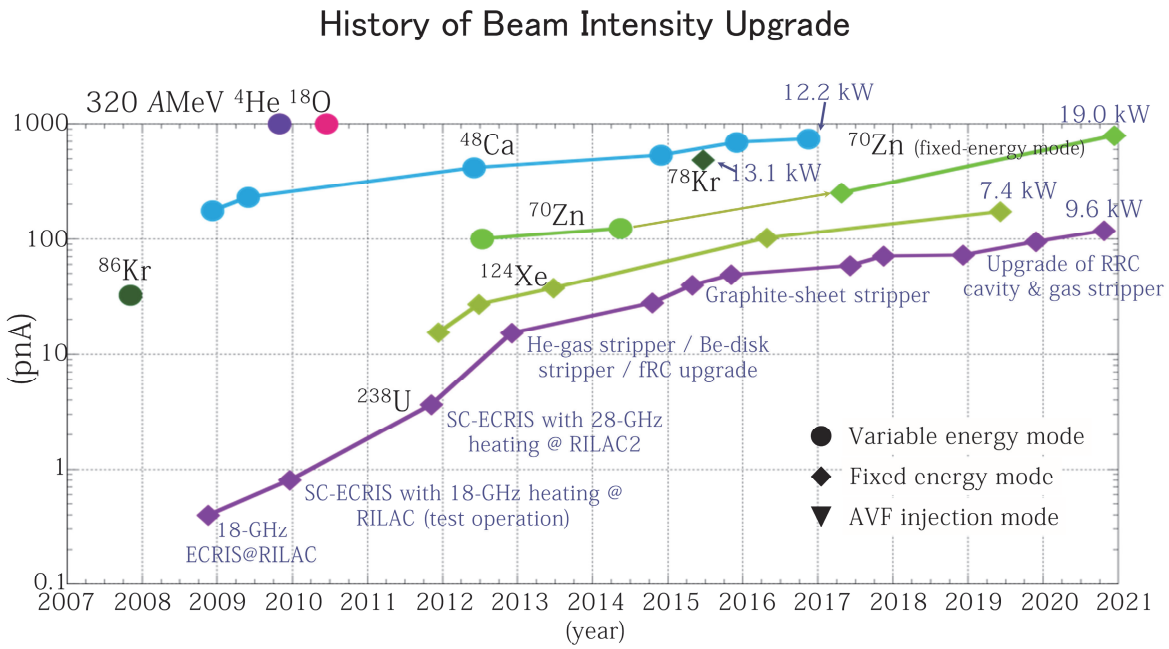

Beam energies of the beams without explicitly indicated are 345 AMeV.

Beamtime for experiments

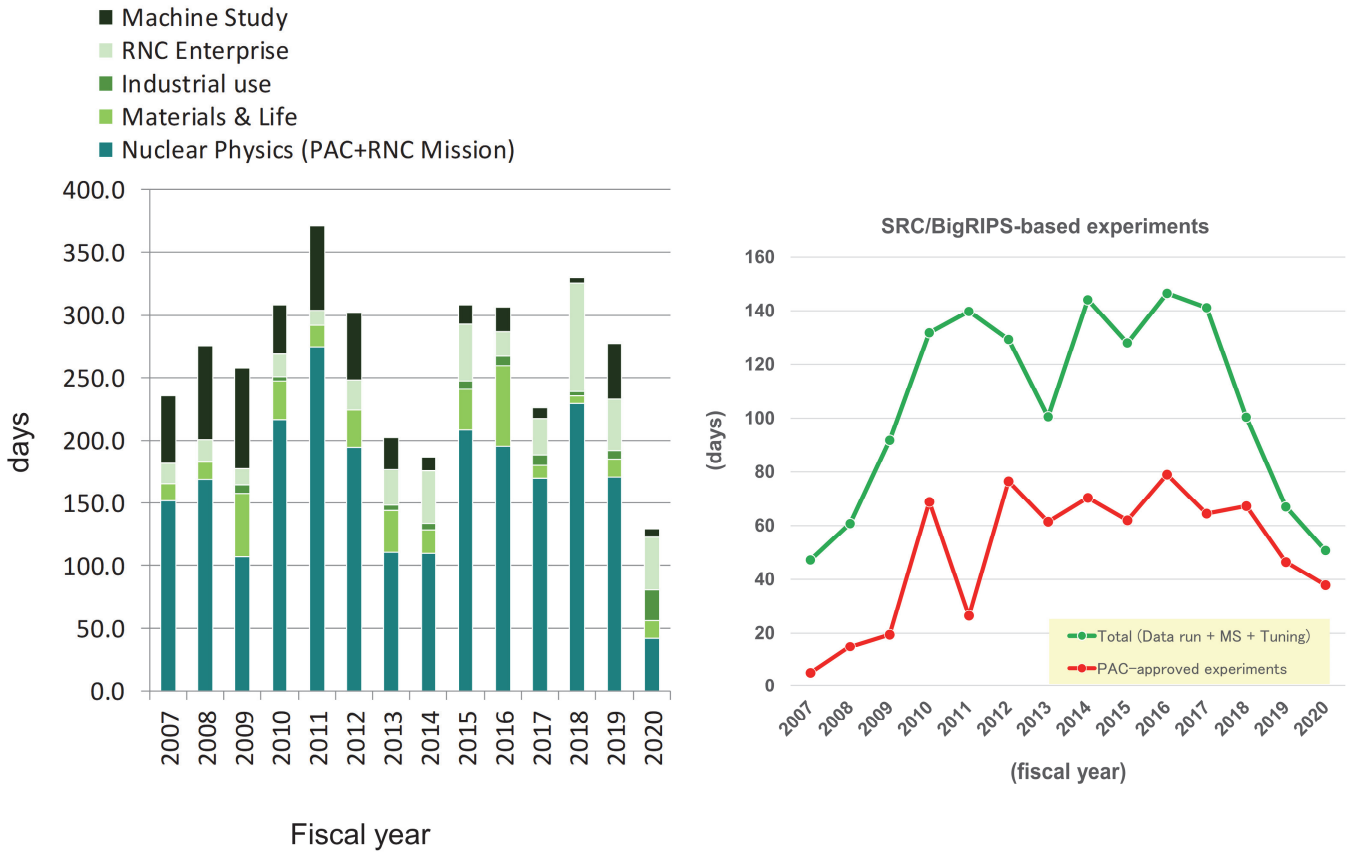

Activities of the Center Director

Meeting Attendance as Ex Officio

International Meetings

[NuPECC associate member]

Online Meeting, October 15–16, 2020. A report of "News from Nishina Center" was given.
Online Meeting, March 5, 2020.

[IUPAP WG9]

No meeting was organized because of COVID-19 pandemic.

Domestic Meetings

[核物理委員会]

仁科センター報告, オンライン開催, 2020 年 6 月 28 日.
仁科センター報告, オンライン開催, 2020 年 9 月 15 日.
仁科センター報告, オンライン開催, 2021 年 1 月 10 日.
仁科センター報告, オンライン開催, 2021 年 3 月 13 日.

[日本原子力産業協会量子放射線利用普及連絡協議会]

第 32 回会合, オンライン開催, 2020 年 11 月 24 日.

List of Publications & Presentations

Publications

[Review Articles]

櫻井博儀他, 「新時代を拓く加速器の『これから』」, Isotope News, 特別号 No. **5** (2021 年 1 月号).

Presentations

[Domestic Conferences/Workshops]

土井琢身, 馬場秀忠, 櫻井博儀（招待講演）, 「理研の物理学研究における研究データ戦略とその事例 ～原子核物理学を中心としたデータ利活用の拡大に挑戦～」, 理研ハッカソン オープンシンポジウム —理研が進めるオープンサイエンスの実践—, オンライン開催, 2021 年 3 月 22 日.

Outreach Activities

櫻井博儀, 「RI ビームファクトリーで進展する元素変換科学」, 核物理委員会×ナレッジキャピタル 超学校 ONLINE スペシャル「21 世紀原子核物理の展望～トップ研究者が語る最前線～」, 2020 年 9 月 27 日.
櫻井博儀, 「『魔法数』の謎を解く」, 理研ニュース **474** (2020 年 12 月).
櫻井博儀, 「有馬朗人先生を偲んで」, 理研ニュース **477** (2021 年 3 月).

Others

[テレビ番組出演]

「ノーベル賞の源流, 仁科芳雄博士」, OHK 岡山放送, 2020 年 12 月 5 日.

Nuclear Science and Transmutation Research Division
Radioactive Isotope Physics Laboratory

1. Abstract

This Laboratory works as one of core research groups conducting programs at the world-premiere heavy-ion accelerator facility of RIKEN "RI Beam Factory (RIBF)." The Laboratory explores exotic nuclear structures and dynamics in exotic nuclei that have never been investigated before, such as those with largely imbalanced proton and neutron numbers. Our aim is to develop new experimental techniques utilizing fast radioactive isotope (RI) beams at RIBF, to discover new phenomena and properties in exotic nuclei. The Laboratory is focusing three major subjects; shell evolution of very neutron-rich nuclei, the r-process path and equation-of-state in asymmetric nuclear matter. The Laboratory has initiated international collaborations for in-beam gamma spectroscopy, decay spectroscopy and heavy-ion induced reactions, and has formed a discussion forum for next generation gamma-ray detectors.

2. Major Research Subjects

(1) Study of structure and dynamics of exotic nuclei through developments of new tools in terms of reaction- and technique-based methodology
(2) Research on EOS in asymmetric nuclear matter via heavy-ion induced reactions
(3) Detector developments for spectroscopy and reaction studies

3. Summary of Research Activity

(1) In-beam gamma spectroscopy

In the medium and heavy mass region explored at RIBF, collective natures of nuclei are one of important subjects, which are obtained through production and observation of high excited and high spin states. To populate such states, heavy-ion induced reactions such as fragmentation, fission are useful. So far, we have developed two-step fragmentation method as an efficient method to identify and populate excited states, and lifetime measurements to deduce transition strength.

Devices utilized for the in-beam gamma spectroscopy are ZeroDegree Spectrometer (ZDS) and a NaI array DALI2. Since the end of 2008, the first spectroscopy on nuclei island-of-inversion region was performed, we have explored step-by-step new and unknown regions in the nuclear chart. The second campaign in 2009 was organized to study background components originating from atomic processes in a heavy target. Neutron-rich nuclei at $N = 20$ to 28 were studied in 2010. In 2011–2013, we conducted experiment programs for Ca-54, Ni-78, neutron-rich nuclei at $N = 82$ and neutron-deficient nuclei at $Z = 50$.

A multitude of data obtained with inelastic, nucleon knock-out, fragmentation channels have been analyzed and published. In 2011–2013, collective natures of Mg-36, 38 and Si-42 were both published in PRL. Excited states firstly observed in Ca-54 were reported in Nature to demonstrate a new nuclear magic number of 34. Fragmentation reaction has been found efficient for nuclei with $A > 100$ and low-lying excited state in Pd-126 has been successfully observed and reported in PRC. In 2019, results of the first spectrosocpy of ^{40}Mg was published in PRL, to demonstrate the exotic structure which is very different from in other neutron-rich Mg isotopes.

To further strengthen the in-beam gamma spectroscopy at RIBF, we have proposed a new setup of MINOS + DALI2 to search for the 1st excited states in even-even neutron-rich nuclei with $Z \sim 20$ to 40. The program was submitted to the PAC 2013 as a new category of proposal, "proposal for scientific program" and was S-ranked. A dedicated collaboration "SEASTAR" has been established as a subset of in-beam gamma collaboration "SUNFLOWER." The three campaigns were organized in 2014, 2015 and 2017 to study very neutron-rich isotopes, and were very productive to access very neutron-rich nuclei such as Ar-52, Ca-56, Ni-78, Kr-100, Zr-110. In 2019, the result of the first spectroscopy of Ni-78 was published in Nature.

A new project of high resolution gamma spectroscopy with fast beams "HiCARI" has been proposed at PAC 2018. MINIBALL and several Ge tracking detectors from Japan, Europe, the USA and Korea are being combined to form an array of germanium detectors. The new setup aims to accelerate researches of the nuclear structure by observing gamma-lines in even-odd nuclei and measuring lifetimes of excited states. The two workshops were organized in 2019, and the machine time of 43.5 days in total was approved at PAC 2019. A part of the HiCARI programs was successfully conducted in 2020. The other HiCARI programs will be performed in 2021.

Concerning a next generation detector, a discussion forum has been established to write up a white paper on tracking germanium detectors and high-efficient crystal detectors such $LaBr_3$ and GAGG.

(2) Decay spectroscopy

Beta- and isomer-spectroscopy is an efficient method for studying nuclear structure, especially for non-yrast levels. We had accumulated experimental techniques at the RIPS facility to investigate nuclear structure in light mass region via beta-gamma and beta-p coincidence. Concerning the medium and heavy mass region available at RIBF, we have developed two position-sensitive active-stoppers, strip-silicon detectors and a cylindrical active stopper called CAITEN, to achieve a low-background measurement by taking correlation between heavy ion stop position and beta-ray emission position. A site of decay-spectroscopy at the new facility of RIBF is the final focal plane of ZDS, where high precision of TOF in particle identification is obtained due to a long flight path from BigRIPS to ZDS.

At the end of 2009, the first decay spectroscopy was organized with a minimum setup of four clover gamma detectors and silicon strip detectors, to study neutron-rich nuclei with $A \sim 110$. The first campaign was found successful and efficient to publish four

letter articles in 2011, two PRL's and two PLB's. One of the PRL papers is associated to the r-process path where half-lives for 18 neutron-rich nuclei were determined for the first time. The other PRL paper reported a finding of deformed magic number 64 in the Zr isotopes.

The success of the first decay-spectroscopy campaign stimulated to form a new large-scale collaboration "EURICA," where a twelve Euroball cluster array is coupled with the silicon-strip detectors to enhance gamma efficiency by a factor of 10. A construction proposal of "EURICA" was approved in the PAC 2011, and the commissioning was successfully organized in spring 2012. Since then, physics runs had been conducted for programs approved to survey nuclei of interest as many as possible, such as Ni-78, Pd-128, Sn-100. The EURICA collaboration finished its physics programs in summer 2016. So far, 54 papers including 14 PRL's and 13 PLB's were published. One of the highlights is discovery of a seniority isomer in Pd-128, of which cascade gamma decay gives the energy of first excited state and robustness of $N = 82$ magic number, and the other is a half-life measurement for 110 neutron-rich nuclei across the $N = 82$ shell gap, which shows implications for the mechanism and universality of the r-process path.

Beta-delayed neutron emission probability of medium and heavy neutron-rich nuclei is important to understand nuclear structure and the r-process path. In 2013, a new collaboration "BRIKEN" has been established to form a He-3 detector array. A present design of the array has neutron efficiency as high as 70% up to 3 MeV. The array was coupled with the AIDA silicon strip system. A construction proposal was approved at the PAC 2013 and three physics proposals have been approved. The commissioning run was conducted in autumn 2016. The major physics runs were conducted in 2017–2020.

The CAITEN detector was successfully tested with fragments produced with a Ca-48 beam in 2010.

(3) Equation-of-state via heavy-ion central collisions

Equation-of-state in asymmetric nuclear matter is one of major subjects in physics of exotic nuclei. Pi-plus and pi-minus yields in central heavy ion collisions at the RIBF energy are considered as one of EOS sensitive observables at the RIBF energy. To observe charged pions, a TPC for the SAMURAI spectrometer is being constructed under an international collaboration "SπRIT," Construction proposal was submitted at the PAC 2012, and physics proposals were approved at the PAC 2012 and 2013. The physics runs were successfully conducted in spring 2016. The data analysis is in progress to produce the first physics results. The first physics paper has been published in 2020.

An international symposium "NuSYM" on nuclear symmetry energy was organized at RIKEN July 2010 to invite researchers in three sub-fields, nuclear structure, nuclear reaction and nuclear astrophysics, and to discuss nuclear symmetry energy together. Since then, the symposium series have been held every year and been useful to encourage theoretical works and to strengthen the collaboration.

(4) Nucleon correlation and cluster in nuclei

Nucleon correlation and cluster in nuclei are matters of central focus in a "beyond mean-field" picture. The relevant programs with in-beam gamma and missing-mass techniques are to depict nucleon condensations and correlations in nuclear media as a function of density as well as temperature. Neutron-halo and –skin nuclei are objects to study dilute neutron matter at the surface. By changing excitation energies in neutron-rich nuclei, clustering phenomena and role of neutrons are to be investigated.

In 2013, two programs were conducted at the SAMURAI spectrometer. One is related to proton-neutron correlation in the C-12 nucleus via p-n knockout reaction with a carbon target. The other is to search for a cluster state in C-16, which was populated via inelastic alpha scattering. The data is being analyzed.

In 2018, a new project based on missing mass spectroscopy was launched to investigate an exotic cluster state in a very proton-rich nucleus. The experiment was organized at GANIL with combination of RIKEN liquid hydrogen target CRYPTA and the MUST2 detector array in 2018.

Members

Director

Hiroyoshi SAKURAI

Research/Technical Scientists

Pieter Christiaan DOORNENBAL (Senior Research Scientist)
Tadaaki ISOBE (Senior Research Scientist)
Akihisa KOHAMA (Senior Research Scientist)
Yoichi NAKAI (Senior Research Scientist)
Shunji NISHIMURA (Senior Research Scientist)
Daisuke SUZUKI (Research Scientist)

Special Postdoctoral Researcher

Browne FRANK

Junior Research Associates

Hideki SHIMIZU (Univ. of Tokyo)
Takuma KOIWAI (Univ. of Tokyo)

International Program Associates

Juan SAIZ LOMAS (Univ. of York)
Xiaohui SUN (Peking Univ.)

Special Temporary Research Scientist

Takashi ICHIHARA

Research Consultants

Akitsu IKEDA
Masayasu ISHIHARA
Kenichi MATSUYANAGI
Hiroyuki MURAKAMI

Senior Visiting Scientists

Koichiro ASAHI (Tokyo Tech)
Shigeru KUBONO (Univ. of Tokyo)
Kengo OGAWA (Chiba Univ.)

Visiting Scientists

Nori AOI (Osaka Univ.)
Giordano CERIZZA (Michigan State Univ.)
Jin-hee CHANG (Michigan State Univ.)
Silvio CHERUBINI (Univ. of Catania)
Martha Liliana CORTES SUA (INFN)
Mitsunori FUKUDA (Osaka Univ.)
Byungsik HONG (Korea Univ.)
Kazuo IEKI (Rikkyo Univ.)
Kei IIDA (Kochi Univ.)
Natsumi IKENO (Tottori Univ.)
Takuji IZUMIKAWA (Niigata Univ.)
Takashi KISHIDA (Aoyama Gakuin Univ.)
Gabor KISS (ATOMKI)
Khiem LE (Vietnam Academy of Sci. and Tech.)
Hiu Ching LEE (The Univ. of Hong Kong)
Giuseppe LORUSSO (Nat'l Phys. Lab.)
Alan MCINTOSH (Texas A & M Univ.)
Yoshiharu MORI (Kyoto Univ.)
Tetsuya MURAKAMI (Kyoto Univ.)
Megumi NIIKURA (Univ. of Tokyo)
Evgueni NIKOLSKI (Kurchatov Inst.)
Daiki NISHIMURA (Tokyo City Univ.)
Takashi OHTSUBO (Niigata Univ.)
Hooi Jin ONG (Osaka Univ.)
Akira ONO (Tohoku Univ.)
Naohiko OTSUKA (IAEA)
Kazuhiro OYAMATSU (Aichi Shukutoku Univ.)
Clementine Angelique Marie-Th SANTAMARIA (Berkeley Lab)
Paer-Anders SOEDERSTROEM (TU Darmstadt)
Maya TAKECHI (Niigata Univ.)
Ryo TANIUCHI (Univ. of York)
Rensheng WANG (Soochow Univ.)
Hiroshi WATANABE (Beihang Univ.)
Kathrin WIMMER (Inst.o de Estructura de la Materia, Consejo Superior de Investigaciones Cientias, CSIC)
Jin WU (Argonne Nat'l Lab.)
Yasutaka YAMAMOTO (Osaka Univ.)

Visiting Technicians

Jorge AGRAMUNT ROS (Valencia city hall)
Hilde DE WITTE (KU Leuven)
Herbert E. HESS (Univ. of Cologne)
Ivan KOJOUHAROV (GSI)

Visiting Researchers

Alejandro ALGORA (JSPS)
Benoit J. C. MAUSS (JSPS)
Byul MOON (Nat'l Res. Foundation)

Student Trainees

Takamichi AOKI (Univ. of Tokyo)
Takumi AOKI (Univ. of Tokyo)
Yusei BANDO (Univ. of Tokyo)
Jonathan BARNEY (Michigan State Univ.)
Linh BUI (Vietnam Atomic Energy Inst.)
Justin B. ESTEE (Michigan State Univ.)
Hiroaki FUKUSHIMA (Rikkyo Univ.)
Shinnosuke KANAYA (Osaka Univ.)
Masanori KANEKO (Kyoto Univ.)
Jiseok KIM (Korea Univ.)
Asahi KOHDA (Osaka Univ.)
Kei KOKUBUN (Univ. of Tokyo)
Shunpei KOYAMA (Univ. of Tokyo)
Jung Woo LEE (Korea Univ.)
Thomas G. PARRY (Univ. of Surrey)
Takeshi SAITO (Univ. of Tokyo)
Hidaka TANABE (Tsukuba Univ.)
Chun Yuen TSANG (Michigan State Univ.)
Phong VI (VNU Univ. of Sci.)
Ryo WAKABAYASHI (Osaka Univ.)
Tik Tsun YEUNG (The Univ. of Hong Kong)
Naoya YOSHIDA (Univ. of Tokyo)

Part-time Workers

Kiyomi ARAI (Research Part-time Worker I)
Mie DOI (Research Part-time Worker I)
Masanori KANEKO (Research Part-time Worker I)
Miki KANOU (Research Part-time Worker I)
Noriko OKAYASU (Research Part-time Worker I)
Tsuneyo SUZUKI (Research Part-time Worker I)
Misuzu KANOU (Research Part-time Worker II)
Eiko MIZUMOTO (Research Part-time Worker II)

List of Publications & Presentations

Publications

[Original Papers]

B. Moon, A. Jungclaus, H. Naïdja, A. Gargano, R. Lozeva, C. -B. Moon, A. Odahara, G. S. Simpson, S. Nishimura, F. Browne, P. Doornenbal, G. Gey, J. Keatings, G. Lorusso, Z. Patel, S. Rice, M. Si, L. Sinclair, P. -A. Söderström, T. Sumikama, J. Taprogge, H. Watanabe, J. Wu, Z. Y. Xu, A. Yagi, D. S. Ahn, H. Baba, F. L. Bello Garrote, S. Bönig, R. Daido, J. M. Daugas, F. Didierjean, F. Drouet, Y. Fang, N. Fukuda, R. Gernhäuser, B. Hong, E. Ideguchi, S. Ilieva, N. Inabe, T. Ishigaki, T. Isobe, H. S. Jung, D. Kameda, I. Kojouharov, T. Komatsubara, T. Kröll, T. Kubo, N. Kurz, Y. K. Kwon, C. S. Lee, P. Lee, Z. Li, A. Montaner-Pizá, S. Morimoto, K. Moschner, D. Mücher, D. Murai, M. Niikura, H. Nishibata, I. Nishizuka, R. Orlandi, H. Sakurai, H. Schaffner, Y. Shimizu, K. Steiger, H. Suzuki, H. Takeda, K. Tshoo, Z. Vajta, A. Wendt, R. Yokoyama, and K. Yoshinaga, "Nuclear structure of Te isotopes beyond neutron magic number $N = 82$,"Phys. Rev. C **103**, 034320 (2021).

M. Juhász, Z. Elekes, D. Sohler, Y. Utsuno, K. Yoshida, T. Otsuka, K. Ogata, P. Doornenbal, A. Obertelli, H. Baba, F. Browne, D. Calvet, F. Château, S. Chen, N. Chiga, A. Corsi, M. L. Cortés, A. Delbart, J. -M. Gheller, A. Giganon, A. Gillibert, C. Hilaire, T. Isobe, T. Kobayashi, Y. Kubota, V. Lapoux, T. Motobayashi, I. Murray, H. Otsu, V. Panin, N. Paul, W. Rodriguez, H. Sakurai, M. Sasano, D. Steppenbeck, L. Stuhl, Y. Sun, Y. Togano, T. Uesaka, K. Wimmer, K. Yoneda, N. Achouri, O. Aktas, T. Aumann, L. Chung, Z. Dombrádi, F. Flavigny, S. Franchoo, I. Gašparić, R. -B. Gerst, J. Gibelin, K. Hahn, D. Kim, T. Koiwai, Y. Kondo, P. Koseoglou, J. Lee, C. Lehr, B. Linh, H. Liu, T. Lokotko, M. MacCormick, K. Moschner, T. Nakamura, S. Park, D. Rossi, E. Sahin, P. -A. Söderström, S. Takeuchi, H. Törnqvist, V. Vaquero, V. Wagner, S. Wang, V. Werner, X. Xu, H. Yamada, D. Yan, Z. Yang, M. Yasuda, and L. Zanetti, "First spectroscopic study of ^{51}Ar by the $(p, 2p)$ reaction," Phys. Lett. B **814**, 136108 (2021).

Y. L. Sun, T. Nakamura, Y. Kondo, Y. Satou, J. Lee, T. Matsumoto, K. Ogata, Y. Kikuchi, N. Aoi, Y. Ichikawa, K. Ieki, M. Ishihara, T. Kobayshi, T. Motobayashi, H. Otsu, H. Sakurai, T. Shimamura, S. Shimoura, T. Shinohara, T. Sugimoto, S. Takeuchi, Y. Togano, and K. Yoneda, "Three-body breakup of ^{6}He and its halo structure," Phys. Lett. B **814**, 136072 (2021).

K. Wimmer, W. Korten, P. Doornenbal, T. Arici, P. Aguilera, A. Algora, T. Ando, H. Baba, B. Blank, A. Boso, S. Chen, A. Corsi, P. Davies, J. P. Delaroche, G. de. Angelis, G. de. France, D. T. Doherty, J. Gerl, R. Gernhäuser, T. Goigoux, M. Girod, D. Jenkins, G. Kiss, S. Koyama, T. Motobayashi, S. Nagamine, M. Niikura, S. Nishimura, A. Obertelli, J. Libert, D. Lubos, T. R. Rodriguez, V. H. Phong, B. Rubio, E. Sahin, T. Y. Saito, H. Sakurai, L. Sinclair, D. Steppenbeck, R. Taniuchi, V. Vaquero, R. Wadsworth, J. Wu, and M. Zielinska, "Shape changes in the mirror nuclei ^{70}Kr and ^{70}Se," Phys. Rev. Lett. **126**, 072501 (2021).

G. Jhang, J. Estee, J. Barney, G. Cerizza, M. Kaneko, J. W. Lee, W. G. Lynch, T. Isobe, M. Kurata-Nishimura, T. Murakami, C. Y. Tsang, M. B. Tsang, R. Wang, D. S. Ahn, L. Atar, T. Aumann, H. Baba, K. Boretzky, J. Brzychczyk, N. Chiga, N. Fukuda, I. Gasparic, B. Hong, A. Horvat, K. Ieki, N. Inabe, Y. J. Kim, T. Kobayashi, Y. Kondo, P. Lasko, H. S. Lee, Y. Leifels, J. Lukasik, J. Manfredi, A. B. McIntosh, P. Morfouace, T. Nakamura, N. Nakatsuka, S. Nishimura, R. Olsen, H. Otsu, P. Pawfowski, K. Pelczar, D. Rossi, H. Sakurai, C. Santamaria, H. Sato, H. Scheit, R. Shane, Y. Shimizu, H. Simon, A. Snoch, A. Sochocka, Z. Sosin, T. Sumikama, H. Suzuki, D. Suzuki, H. Takeda, S. Tangwancharoen, H. Toernqvist, Y. Togano, Z. G. Xiao, S. J. Yennello, J. Yurkon, Y. Zhang, the SπRIT Collaboration M. Colonna, D. Cozma, P. Danielewicz, H. Elfner, N. Ikeno, C. MingKo, J. Mohs, D. Oliinychenko, A. Ono, J. Suae, Y. J. Wang, H. Wolter, J. Xu, Y. X. Zhang, and Z. Zhang, the TMEP Collaboration, "Symmetry energy investigation with pion production from Sn + Sn systems," Phys. Lett. B **813**, 136016 (2021).

S. E. A. Orrigo, B. Rubio, W. Gelletly, P. Aguilera, A. Algora, A. I. Morales, J. Agramunt, D. S. Ahn, P. Ascher, B. Blank, C. Borcea, A. Boso, R. B. Cakirli, J. Chiba, G. De. Angelis, G. De. France, F. Diel, P. Doornenbal, Y. Fujita, N. Fukuda, E. Ganioglu, M. Gerbaux, J. Giovinazzo, S. Go, T. Goigoux, S. Grevy, V. Guadilla, N. Inabe, G. G. Kiss, T. Kubo, S. Kubono, T. Kurtukian-Nieto, D. Lubos, C. Magron, F. Molina, A. Montaner-Piza, D. Napoli, D. Nishimura, S. Nishimura, H. Oikawa, V. H. Phong, H. Sakurai, Y. Shimizu, C. Sidong, P. -A. Söderström, T. Sumikama, H. Suzuki, H. Takeda, Y. Takei, M. Tanaka, J. Wu, and S. Yagi, "β Decay of the very neutron-deficient ^{60}Ge and ^{62}Ge nuclei," Phys. Rev. C **103**, 014324 (2021).

T. Sumikama, N. Fukuda, N. Inabe, D. Kameda, T. Kubo, Y. Shimizu, H. Suzuki, H. Takeda, K. Yoshida, H. Baba, F. Browne, A. M. Bruce, R. Carroll, N. Chiga, R. Daido, F. Didierjean, P. Doornenbal, Y. Fang, G. Gey, E. Ideguchi, T. Isobe, S. Lalkovski, Z. Li, G. Lorusso, R. Lozeva, H. Nishibata, S. Nishimura, I. Nishizuka, A. Odahara, Z. Patel, Z. Podolyák, P. H. Regan, S. Rice, O. J. Roberts, H. Sakurai, G. S. Simpson, L. Sinclair, P. -A. Söderström, M. Tanaka, J. Taprogge, H. Watanabe, V. Werner, O. Wieland, J. Wu, Z. Y. Xu, and A. Yagi, "Observation of new neutron-rich isotopes in the vicinity of ^{110}Zr," Phys. Rev. C **103**, 014614 (2021).

T. Sumikama, D. S. Ahn, N. Fukuda, Y. Shimizu, H. Suzuki, H. Takeda, H. Wang, K. Yoshida, J. Amano, N. Chiga, K. Chikaato, A. Hirayama, N. Inabe, S. Kawase, S. Kubono, M. Matsushita, S. Michimasa, K. Nakano, H. Otsu, H. Sakurai, A. Saito, S. Shimoura, J. Suwa, M. Takechi, S. Takeuchi, Y. Togano, T. Tomai, and Y. Watanabe, "Energy-control and novel particle-identification methods combined with range in a multi-sampling ionization chamber for experiments using slowed-down RI beams," Nucl. Instrum. Methods Phys. Res. A **986**, 164687 (2021).

M. L. Cortés, W. Rodriguez, P. Doornenbal, A. Obertelli, J. D. Holt, J. Menéndez, K. Ogata, A. Schwenk, N. Shimizu, J. Simonis, Y. Utsuno, K. Yoshida, L. Achouri, H. Baba, F. Browne, D. Calvet, F. Château, S. Chen, N. Chiga, A. Corsi, A. Delbart, J. -M. Gheller, A. Giganon, A. Gillibert, C. Hilaire, T. Isobe, T. Kobayashi, Y. Kubota, V. Lapoux, H. N. Liu, T. Motobayashi, I. Murray, H. Otsu, V. Panin, N. Paul, H. Sakurai, M. Sasano, D. Steppenbeck, L. Stuhl, Y. L. Sun, Y. Togano, T. Uesaka, K. Wimmer, K. Yoneda, O. Aktas, T. Aumann, L. X. Chung, F. Flavigny, S. Franchoo, I. Gašparíc, R. -B. Gerst, J. Gibelin, K. I. Hahn, D. Kim, T. Koiwai, Y. Kondo, P. Koseoglou, J. Lee, C. Lehr, B. D. Linh, T. Lokotko, M. MacCormick, K. Moschner, T. Nakamura, S. Y. Park, D. Rossi, E. Sahin, P. -A. Söderström, D. Sohler, S. Takeuchi, H. Toernqvist, V. Vaquero, V. Wagner, S. Wang, V. Werner, X. Xu, H. Yamada, D. Yan, Z. Yang, M. Yasuda, and L. Zanetti, "$N = 32$ shell closure below calcium: Low-lying structure of ^{50}Ar," Phys. Rev. C **102**, 064320 (2020).

A. Jungclaus, J. M. Keatings, G. S. Simpson, H. Naïdja, A. Gargano, S. Nishimura, P. Doornenbal, G. Gey, G. Lorusso, P. -A. Söderström,

T. Sumikama, J. Taprogge, Z. Y. Xu, H. Baba, F. Browne, N. Fukuda, N. Inabe, T. Isobe, H. S. Jung, D. Kameda, G. D. Kim, Y. -K. Kim, I. Kojouharov, T. Kubo, N. Kurz, Y. K. Kwon, Z. Li, H. Sakurai, H. Schaffner, Y. Shimizu, H. Suzuki, H. Takeda, Z. Vajta, H. Watanabe, J. Wu, A. Yagi, K. Yoshinaga, S. Bönig, J. -M. Daugas, R. Gernhäuser, S. Ilieva, T. Kröll, A. Montaner-Piza, K. Moschner, D. Mücher, H. Nishibata, A. Odahara, R. Orlandi, M. Scheck, K. Steiger, and A. Wendt, "Evolution of proton single-particle states in neutron-rich Sb isotopes beyond $N = 82$," Phys. Rev. C **102**, 034324 (2020).

A. Gottardo, G. de Angelis, P. Doornenbal, L. Coraggio, A. Gargano, N. Itaco, K. Kaneko, P. Van Isacker, T. Furumoto, G. Benzoni, J. Lee, H .Liu, M. Matsushita, D. Mengoni, V. Modamio-Hoybjor, S. Momiyama, T. Motobayashi, D. R. Napoli, M. Niikura, E. Sahin, Y. Shiga, H. Sakurai, R. Taniuchi, S. Takeuchi, H. Wang, J. J. Valiente-Dobon, R. Avigo, H. Baba, N. Blasi, F. L. Bello Garrote, F. Browne, F. C. L. Crespi, S. Ceruti, R .Daido, M. -C. Delattre, D. Fang, Zs. Dombradi, T. Isobe, I. Kuti, G. Lorusso, K. Matsui, B. Melon, T. Miyazaki, S. Nishimura, R. Orlandi, Z. Patel, S. Rice, L. Sinclair, P. A. Soderstrom, D .Sohler, T. Sumikama, J. Taprogge, Zs. Vajta, H. Watanabe, O. Wieland, J. Wu, Z. Y. Xu, M. Yalcinkaya, and R. Yokoyama, "Transition strengths in the neutron-rich ^{73,74,75}Ni isotopes," Phys. Rev. C **102**, 014323 (2020).

J. J. Liu, J. Lee, H. Watanabe, S. Nishimura, G. X. Zhang, J. Wu, P. M. Walker, P. H. Regan, P. -A. Söderström, H. Kanaoka, Z. Korkulu, P. S. Lee, A. Yagi, A. C. Dai, F. R. Xu, D. S. Ahn, T. Alharbi, H. Baba, F. Browne, A. M. Bruce, R. J. Carroll, K. Y. Chae, Zs. Dombradi, P. Doornenbal, A. Estrade, N. Fukuda, C. Griffin, E. Ideguchi, N. Inabe, T. Isobe, S. Kanaya, I. Kojouharov, F. G. Kondev, T. Kubo, S. Kubono, N. Kurz, I. Kuti, S. Lalkovski, G. J. Lane, C. S. Lee, E. J. Lee, G. Lorusso, G. Lotay, C. B. Moon, I. Nishizuka, C. R. Nita, A. Odahara, Z. Patel, V. H. Phong, Zs. Podolyak, O. J. Roberts, H. Sakurai, H. Schaffner, C. M. Shand, Y. Shimizu, T. Sumikama, H. Suzuki, H. Takeda, S. Terashima, Zs. Vajta, J. J. Valiente-Dobon, and Z. Y. Xu, "Isomeric and β-decay spectroscopy of decay of ^{173,174}Ho," Phys. Rev. C **102**, 024301 (2020).

F. L. Bello Garrote, E. Sahin, Y. Tsunoda, T. Otsuka, A. Görgen, M. Niikura, S. Nishimura, G. de Angelis, G. Benzoni, A. I. Morales, V. Modamio, Z. Y. Xu, H. Baba, F. Browne, A. M. Bruce, S. Ceruti, F. C. L. Crespi, R. Daido, M. -C. Delattre, P. Doornenbal, Z. Dombradi, Y. Fang, S. Franchoo, G. Gey, A. Gottardo, K. Hadynska-Klek, T. Isobe, P. R. John, H. S. Jung, I. Kojouharov, T. Kubo, N. Kurz, I. Kuti, Z. Li, G. Lorusso, I. Matea, K. Matsui, D. Mengoni, T. Miyazaki, S. Momiyama, P. Morfouace, D. R. Napoli, F. Naqvi, H. Nishibata, A. Odahara, R. Orlandi, Z. Patel, S. Rice, H. Sakurai, H. Schaffner, L. Sinclair, P. -A. Söderström, D. Sohler, I. G. Stefan, T. Sumikama, D. Suzuki, R. Taniuchi, J. Taprogge, Z. Vajta, J. J. Valiente-Dobón, H. Watanabe, V. Werner, J. Wu, A. Yagi, M. Yalcinkaya, R. Yokoyama, and K. Yoshinaga, "β Decay of ^{75}Ni and the systematics of the low-lying level structure of neutron-rich odd-A Cu isotopes," Phys. Rev. C **102**, 034314 (2020).

J. Park, R. Krücken, A. Blazhev, D. Lubos, R. Gernhäuser, M. Lewitowicz, S. Nishimura, D. S. Ahn, H. Baba, B. Blank, P. Boutachkov, F. Browne, I. Čeliković, G.de France, P. Doornenbal, T. Faestermann, Y. Fang, N. Fukuda, J. Giovinazzo, N. Goel, M. Górska, H. Grawe, S. Ilieva, N. Inabe, T. Isobe, A. Jungclaus, D. Kameda, G. D. Kim, Y. -K. Kim, I. Kojouharov, T. Kubo, N. Kurz, Y. K. Kwon, G. Lorusso, K. Moschner, D. Murai, I. Nishizuka, Z. Patel, M. M. Rajabali, S. Rice, H. Sakurai, H. Schaffner, Y. Shimizu, L. Sinclair, P. -A. Söderström, K. Steiger, T. Sumikama, H. Suzuki, H. Takeda, Z. Wang, H. Watanabe, J. Wu, and Z. Y. Xu, "Spectroscopy of ^{99}Cd and ^{101}In from β decay of ^{99}In and ^{101}Sn," Phys. Rev. C **102**, 014304 (2020).

A. Frotscher, M. Gómez-Ramos, A. Obertelli, P. Doornenbal, G. Authelet, H. Baba, D. Calvet, F. Château, S. Chen, A. Corsi, A. Delbart, J. -M. Gheller, A. Giganon, A. Gillibert, T. Isobe, V. Lapoux, M. Matsushita, S. Momiyama, T. Motobayashi, M. Niikura, H. Otsu, N. Paul, C. Péron, A. Peyaud, E. C. Pollacco, J. -Y. Roussé, H. Sakurai, C. Santamaria, M. Sasano, Y. Shiga, N. Shimizu, D. Steppenbeck, S. Takeuchi, R. Taniuchi, T. Uesaka, H. Wang, K. Yoneda, T. Ando, T. Arici, A. Blazhev, F. Browne, A. M. Bruce, R. Carroll, L. X. Chung, M. L. Cortés, M. Dewald, B. Ding, Z. Dombradi, F. Flavigny, S. Franchoo, F. Giacoppo, M. Górska, A. Gottardo, K. Hadynska-Klek, Z. Korkulu, S. Koyama, Y. Kubota, A. Jungclaus, J. Lee, M. Lettmann, B. D. Linh, J. Liu, Z. Liu, C. Lizarazo, C. Louchart, R. Lozeva, K. Matsui, T. Miyazaki, K. Moschner, S. Nagamine, N. Nakatsuka, C. Nita, S. Nishimura, C. R. Nobs, L. Olivier, S. Ota, Z. Patel, Z. Podolyák, M. Rudigier, E. Sahin, T. Y. Saito, C. Shand, P. -A. Söderström, I. G. Stefan, T. Sumikama, D. Suzuki, R. Orlandi, V. Vaquero, Z. Vajta, V. Werner, K. Wimmer, J. Wu, and Z. Xu, "Sequential nature of $(p, 3p)$ two-proton knockout from neutron-rich nuclei," Phys. Rev. Lett. **125**, 012501 (2020).

X. H. Sun, H. Wang, H. Otsu, H. Sakurai, D. S. Ahn, M. Aikawa, N. Fukuda, T. Isobe, S. Kawakami, S. Koyama, T. Kubo, S. Kubono, G. Lorusso, Y. Maeda, A. Makinaga, S Momiyama, K. Nakano, S. Nakayama, M. Niikura, Y. Shiga, P. -A. Soderstrom, H. Suzuki, H. Takeda, S. Takeuchi, R. Taniuchi, Ya. Watanabe, Yu. Watanabe, H. Yamasaki, X. F. Yang, Y. L. Ye, and K. Yoshida, "Spallation and fragmentation cross sections for 168 MeV/nucleon ^{136}Xe ions on proton, deuteron, and carbon targets," Phys. Rev. C **101**, 064623 (2020).

J. W. Lee, G. Jhang, G. Cerizza, J. Barney, J. Estee, T. Isobe, M. Kaneko, M. Kurata-Nishimura, W. G. Lynch, T. Murakami, C. Y. Tsang, M. B. Tsang, R. Wang, B. Hong, A. B. McIntosh, H. Sakurai, C. Santamaria, R. Shane, S. Tangwancharoen, S. J. Yennello, Y. Zhang, For the SπRIT Collaboration "Charged particle track reconstruction with SπRIT time projection chamber," Nucl. Instrum. Methods Phys. Res. A **965**, 163840 (2020).

S. Bagchi, R. Kanungo, Y. K. Tanaka, H. Geissel, P. Doornenbal, W. Horiuchi, G. Hagen, T. Suzuki, N. Tsunoda, D. S. Ahn, H. Baba, K. Behr, F. Browne, S. Chen, M. L. Cortés, A. Estradé, N. Fukuda, M. Holl, K. Itahashi, N. Iwasa, G. R. Jansen, W. G. Jiang, S. Kaur, A. O. Macchiavelli, S. Y. Matsumoto, S. Momiyama, I. Murray, T. Nakamura, S. J. Novario, H. J. Ong, T. Otsuka, T. Papenbrock, S. Paschalis, A. Prochazka, C. Scheidenberger, P. Schrock, Y. Shimizu, D. Steppenbeck, H. Sakurai, D. Suzuki, H. Suzuki, M. Takechi, H. Takeda, S. Takeuchi, R. Taniuchi, K. Wimmer, and K. Yoshida, "Two-neutron halo is unveiled in ^{29}F," Phys. Rev. Lett. **124** 222504 (2020).

K. Wimmer, T. Arici, W. Korten, P. Doornenbal, J. -P. Delaroche, M. Girod, J. Libert, T. R. Rodrigue, P. Aguilera, A. Algora, T. Ando, H. Baba, B. Blank, A. Boso, S. Chen, A. Corsi, P. Davies, G. de. Angelis, G. de. France, D. T. Doherty, J. Gerl, R. Gernhäuser, T. Goigoux, D. Jenkins, G. Kiss, S. Koyama, T. Motobayashi, S. Nagamine, M. Niikura, S. Nishimura, A. Obertelli, D. Lubos, V. H. Phong, B. Rubio, E. Sahin, T. Y. Saito, H. Sakurai, L. Sinclair, D. Steppenbeck, R. Taniuchi, V. Vaquero, R. Wadsworth, J. Wu, and M. Zielinska, "Shape coexistence revealed in the $N = Z$ isotope ^{72}Kr through inelastic scattering." Eur. Phys. J. A **56.6**, 1–12 (2020).

C. Lizarazo, P. -A. Söderström, V. Werner, N. Pietralla, P. M. Walker, G. X. Dong, F. R. Xu, T. R. Rodríguez, F. Browne, P. Doornenbal, S. Nishimura, C. R. Nita, A. Obertelli, T. Ando, T. Arici, G. Authelet, H. Baba, A. Blazhev, A. M. Bruce, D. Calvet, R. J. Caroll, F. Château, S. Chen, L. X. Chung, A. Corsi, M. L. Cortés, A. Delbart, M. Dewald, B. Ding, F. Flavigny, S. Franchoo, J. Gerl, J. -M. Gheller, A. Giganon, A. Gillibert, M. Górska, A. Gottardo, I. Kojouharov, N. Kurz, V. Lapoux, J. Lee, M. Lettmann, B. D. Linh, J. J. Liu, Z. Liu, S. Momiyama, K. Moschner, T. Motobayashi, S. Nagamine, N. Nakatsuka, M. Niikura, C. Nobs, L. Olivier, Z. Patel, N. Paul, Z. Podolyák, J. -Y. Roussé, M. Rudigier, T. Y. Saito, H. Sakurai, C. Santamaria, H. Schaffner, C. Shand, I. Stefan, D. Steppenbeck, R. Taniuchi, T. Uesaka, V. Vaquero, K. Wimmer, and Z. Xu, "Metastable states of 92, 94Se: Identification of an oblate K isomer of ^{94}Se and the ground-state shape transition between $N = 58$ and 60," Phys. Rev. Lett. **124**, 222502 (2020).

J. Wu, S. Nishimura, P. Möller, M. R. Mumpower, R. Lozeva, C. B. Moon, A. Odahara, H. Baba, F. Browne, R. Daido, P. Doornenbal, Y. F. Fang, M. Haroon, T. Isobe, H. S. Jung, G. Lorusso, B. Moon, Z. Patel, S. Rice, H. Sakurai, Y. Shimizu, L. Sinclair, P. -A. Söderström, T. Sumikama, H. Watanabe, Z. Y. Xu, A. Yagi, R. Yokoyama, D. S. Ahn, F. L. Bello Garrote, J. M. Daugas, F. Didierjean, N. Fukuda, N. Inabe, T. Ishigaki, D. Kameda, I. Kojouharov, T. Komatsubara, T. Kubo, N. Kurz, K. Y. Kwon, S. Morimoto, D. Murai, H. Nishibata, H. Schaffner, T. M. Sprouse, H. Suzuki, H. Takeda, M. Tanaka, K. Tshoo, and Y. Wakabayashi, "β-Decay half-lives of 55 neutron-rich isotopes beyond the $N = 82$ shell gap," Phys. Rev. C **101**, 042801 (R) (2020).

J. Ha, T. Sumikama, F. Browne, N. Hinohara, A. M. Bruce, S. Choi, I. Nishizuka, S. Nishimura, P. Doornenbal, G. Lorusso, P. -A. Söderström, H. Watanabe, R. Daido, Z. Patel, S. Rice, L. Sinclair, J. Wu, Z. Y. Xu, A. Yagi, H. Baba, N. Chiga, R. Carroll, F. Didierjean, Y. Fang, N. Fukuda, G. Gey, E. Ideguchi, N. Inabe, T. Isobe, D. Kameda, I. Kojouharov, N. Kurz, T. Kubo, S. Lalkovski, Z. Li, R. Lozeva, H. Nishibata, A. Odahara, Z. Podolyák, P. H. Regan, O. J. Roberts, H. Sakurai, H. Schaffner, G. S. Simpson, H. Suzuki, H. Takeda, M. Tanaka, J. Taprogge, V. Werner, and O. Wieland, "Shape evolution of neutron-rich ^{106,108,110}Mo isotopes in the triaxial degree of freedom," Phys. Rev. C **101**, 044311 (2020).

H. Watanabe, Y. X. Wanatabe, Y. Hirayama, A. N. Andreyev, T. Hashimoto, F. G. Kondev, G. J. Lane, Yu.A. Litinov, J. J. Liu, H. Miyatake, J. Y. Moon, A. I. Morales, M. Mukai, S. Nishimura, T. Niwase, M. Rosenbusch, P. Schury, Y. Shi, M. Wada, and P. M. Walker, "Beta decay of the axially asymmetric ground state of ^{192}Re," Phys. Lett. B **814**, 136088 (2021).

C. Y. Tsang, J. Estee, R. Wang, J. Barney, G. Jhang, W. G. Lynch, Z. Q. Zhang, G. Cerizza, T. Isobe, M. Kaneko, M. Kurata-Nishimura, J. W. Lee, T. Murakami, and M. B. Tsang, the SπRIT Collaboration, "Space charge effects in the SπRIT time projection chamber," Nucl. Instrum. Methods Phys. Res. A **959**, 163477 (2020).

X. Pereira-Lopez, B. Fernandez-Dominguez, F. Delaunay, N. L. Achouri, N. A. Orr, W. N. Catford, M. Assie, S. Bailey, B. Bastin, Y. Blumenfeld, R. Borcea, M. Caamano, L. Caceres, E. Clement, A. Corsi, N. Curtis, Q. Deshayes, F. Farget, M. Fisichella, G. de France, S. Franchoo, M. Freer, J. Gibelin, A. Gillibert, G. F. Grinyer, F. Hammache, O. Kamalou, A. Knapton, T. Kokalova, V. Lapoux, J. A. Lay, B. Le Crom, S. Leblond, J. Lois-Fuentes, F. M. Marques, A. Matta, P. Morfouace, A. M. Moro, T. Otsuka, J. Pancin, L. Perrot, J. Piot, E. Pollacco, D. Ramos, C. Rodriguez-Tajes, T. Roger, F. Rotaru, M. Senoville, N. de Sereville, R. Smith, O. Sorlin, M. Stanoiu, I. Stefan, C. Stodel, D. Suzuki, T. Suzuki, J. C. Thomas, N. Timofeyuk, M. Vandebrouck, J. Walshe, and C. Wheldon, "Low-lying single-particle structure of ^{17}C and the $N = 14$ sub-shell closure," Phys. Lett. B **811**, 135939 (2020).

K. Makiguchi, W. Horiuchi, and A. Kohama, "Utility of antiproton-nucleus scattering for probing nuclear surface density distributions," Phys. Rev. C **102**, 034614 (2020).

N. T. Zhang, X. Y. Wang, D. Tudor, B. Bucher, I. Burducea, H. Chen, Z. J. Chen, D. Chesneanu, A. I. Chilug, L. R. Gasques, D. G. Ghita, C. Gomoiu, K. Hagino, S. Kubono, Y. J. Li, C. J. Lin, W. P. Lin, R. Margineanu, A. Pantelica, I. C. Stefanescu, M. Straticiuc, X. D. Tang, L. Trache, A. S. Umar, W. Y. Xin, S. W. Xu, and Y. Xu, "Constraining the ^{12}C + ^{12}C astrophysical S-factors with the ^{12}C + ^{13}C measurements at very low energies," Phys. Lett. B **801**, 135170 (2020).

N. Iwasa, S. Ishikawa, S. Kubono, T. Sakakibara, K. Kominato, K. Nishio, M. Matsuda, K. Hirose, H. Makii, R. Orlandi, K. Asada, D. Guru, S. Nishimura, S. Hayakawa, and T. Kawabata, "Experimental study of the Γ_{p1}/Γ_{p0} ratios of resonance states in ^{8}Be for deducing the ^{7}Be$(n, p_1)^{7}$Li* reaction rate relevant to the cosmological lithium problem," Phys. Rev. C **103**, 015801 (2021).

[Review Articles]

H. Yamaguchi, D. Kahl, and S. Kubono, "CRIB: The low energy in-flight RI beam separator," Nuclear Physics News (NUPECC) **30**, 21 (2020).

[Proceedings]

K. Nakano, Y. Watanabe, S. Kawase, H. Wang, H. Otsu, H. Sakurai, N. Chiga, J. Suwa, T. Sumikama, S. Takeuchi, T. Nakamura, K. Chikaato, M. Takechi, S. Koyama, D. S. Ahn, H. Baba, S. Chen, M. L. Cortes, P. Doornenbal, N. Fukuda, A. Hirayama, R. Hosoda, T. Isobe, S. Kawakami, Y. Kondo, S. Kubono, Y. Maeda, S. Masuoka, S. Michimasa, I. Murray, R. Nakajima, M. Niikura, T. Ozaki, A. Saito, T. Saito, H. Sato, Y. Shimizu, S. Shimoura, Y. Soudo, P. A. Soderstrom, X. Sun, D. Suzuki, H. Suzuki, H. Takeda, Y.vTogano, T. Tomai, H. Yamada, M. Yasuda, and K. Yoshida, "Isotope-production cross sections of residual nuclei in proton- and deuteron-induced reactions on ^{93}Zr at 50 MeV/u," Proc. Intern. Conf. Nuclear Data for Science and Technology (ND2019), Beijing, China, May 19–24, 2019, Z. Ge *et al*., Eds., p. 20006 (2020).

J. Giovinazzo, T. Goigoux, B. Blank, P. Ascher, M. Gerbaux, S. Grevy, T. Kurtukian-Nieto, C. Magron, P. Doornenbal, N. Fukuda, N. Inabe, G. Kiss, T. Kubo, S. Kubono, S. Nishimura, H. Sakurai, Y. Shimizu, C. Sidong, P. Soderstrom, T. Sumikama, H. Suzuki, H. Takeda, P. Vi, J. Wu, D. Ahn, J. Agramunt, A. Algora, V. Guadilla, A. Montaner-Piza, A. Morales, S. Orrigo, B. Rubio, Y. Fujita, M. Tanaka, W. Gelletly, P. Aguilera, F. Molina, F. Diel, D. Lubos, G. de Angelis, D. Napoli, C. Borcea, A. Boso, R. Cakirli, E. Ganioglu, J. Chiba, D. Nishimura, H. Oikawa, Y. Takei, S. Yagi, K. Wimmer, G. de France, S Go, and B. Brown, "Two-proton radioactivity: the interesting case of ^{67}Kr and further studies," Acta Phys. Pol. B **51**, 577 (2020).

Presentations

[International Conferences/Workshops]

H. Sakurai (invited), "Highlights and future directions of RIBF," Yamada Conference LXXII: The 8th Asia-Pacific Conference on Few-Body Problems in Physics, Kanazawa, Japan, March 1–5, 2021.

H. Sakurai (invited), "Physics of exotic nuclei in a 10-year perspective," Workshop on Frontiers of Nuclear Structure and Nuclear Astrophysics and Toward PKU-UT Joint Research Center on Nuclear Physics, Fragrant Hill Hotel and Online, Beijing, October 14–16, 2020.

P. Doornenbal (invited), "High-resolution in-beam gamma-ray spectroscopy at the RIBF with HiCARI," NUSTAR Annual Meeting 2021, Online, February 22–26, 2021.

D. Suzuki (invited), "Two neutron transfer resonances via alpha scattering," International mini-workshop on physics in resonant reaction induced by low-energy RI beam, Japan, February 22, 2021.

D. Suzuki (invited), "Spectroscopy of light exotic nuclei beyond the proton drip line," Yamada Conference LXXII: The 8th Asia-Pacific Conference on Few-Body Problems in Physics, Kanazawa, Japan, March 1–5, 2021.

K. Asahi (invited), "Electric dipole moment of diamagnetic atom ^{129}Xe as a probe for new physics," Fundamental Sciences and Quantum Technologies using Atomic Systems (FSQT2020) (on-line), Physical Research Laboratory, Navrangpura, Ahmedabad, India, September 28–October 1, 2020.

S. Kubono (invited), "Challenge to explosive hydrogen burning in nuclear physics—study of rp-process and νp-process," NAOJ Workshop on Stellar Alchemy to Galactic Archeology, October 26–29, 2020.

[Domestic Conferences/Workshops]

櫻井博儀（招待講演), 「不安定核ビームが開拓するエキゾチック原子核の物理」, シンポジウム「大強度不安定核ビームが拓く新領域」, 日本物理学会第 76 回年次大会, オンライン開催, 2021 年 3 月 12–15 日.

S. Nishimura (invited), "Frontier of experimental activities relevant to r-process nucleosynthesis at RIBF," KEK Workshop: Beta decay, r process and related weak interaction processes, February 19, 2021.

S. Nishimura (invited), 「不安定核から探るランタノイド元素合成の謎」, NAOJ Workshop: Stellar Alchemy to Galactic Archeology, October 26–29, 2020.

槇口雄仁, 堀内渉, 小濱洋央（口頭発表), 「原子核密度分布に対する反陽子-原子核散乱の有用性」, 日本物理学会 2020 年秋季大会, オンライン開催, 2020 年 9 月 14–17 日.

F. Browne (oral), "Single-particle energies and strengths around ^{55}Sc," FY2020 SPDR Presentation Session, Wako, Japan, January 18, 2021.

[Seminars]

H. Sakurai, "Overview of research activities and plans at RIBF," The C2R2 (CENS, CENuM, RUA, RULIC) Seminar, on-line, CENS, IBS, Korea, October 22, 2020.

K. Asahi, "Electric dipole moment of diamagnetic atom ^{129}Xe as a probe for new physics," ISOLDE Physics Group Seminar, on-line & CERN, Geneva, Switzerland, November 19, 2020.

T. Isobe, 「理研不安定核ビームで探る中性子星の状態方程式」, Physics Seminar, Nara Women's University, Nara, Japan, July 21, 2020.

Awards

Press Releases

「フッ素-29 が「2 中性子ハロー原子核」であることを発見—魔法数 20 の消失と中性子ハロー構造の出現—」, 2020 年 8 月 21 日.

Nuclear Science and Transmutation Research Division
Spin isospin Laboratory

1. Abstract

The Spin Isospin Laboratory pursues research activities putting primary focus on interplay of spin and isospin in exotic nuclei. Understanding nucleosyntheses in the universe, especially those in r- and rp-processes is another big goal of our laboratory.

Investigations on isospin dependences of nuclear equation of state, spin-isospin responses of exotic nuclei, occurrence of various correlations at low-densities, evolution of spin-orbit coupling are main subjects along the line. We are leading a mass measurement project with the Rare RI Ring project, too. Through the experimental studies, we will be able to elucidate a variety of nuclear phenomena in terms of interplay of spin and isospin, which will in turn, lead us to better understanding of our universe.

2. Major Research Subjects

(1) Direct reaction studies of neutron-matter equation of state
(2) Study of spin-isospin responses with RI-beams
(3) R-process nucleosynthesis study with heavy-ion storage ring
(4) Application of spin-polarization technique to RI-beam experiments and other fields
(5) Development of special targets for RI-beam experiments

3. Summary of Research Activity

(1) Direct reaction studies of neutron matter equation of state

Direct reactions induced by light-ions serve as powerful tools to investigate various aspects of nuclei. We are advancing experimental programs to explore equation of state of neutron matter, via light-ion induced reactions with RI-beams.

(1-1) Determination of a neutron skin thickness by proton elastic scattering

A neutron skin thickness is known to have strong relevance to asymmetry terms of nuclear equation of state, especially to a term proportional to density. The ESPRI project aims at determining density distributions in exotic nuclei precisely by proton elastic scattering at 200–300 MeV/nucleon. An experiment for ^{132}Sn that is a flagship in this project has been successfully performed.

(1-2) Asymmetry terms in nuclear incompressibility

Nuclear incompressibility represents stiffness of nuclear matter. Incompressibility of symmetric nuclear matter is determined to be 230 ± 20 MeV, but its isospin dependence still has a large uncertainty at present. A direct approach to the incompressibility of asymmetric nuclear matter is an experimental determination of energies of isoscalar giant monopole resonances (GMR) in heavy nuclei. We have developed, in close collaboration with Center for Nuclear Study (CNS) of University of Tokyo, an active gas target for deuteron inelastic scattering experiments to determine GMR energies. The active gas target has been already tested with oxygen and xenon beams at HIMAC and finally has been applied to a ^{132}Sn experiment at RIBF.

(1-3) Multi-neutron and α-cluster correlations at low densities

Occurrences of multi-neutron and α-cluster correlations are other interesting aspects of nuclear matter and define its low-density behavior. The multi-neutron and α-cluster correlations can be investigated with the large-acceptance SAMURAI spectrometer. The SAMURAI has been already applied to experiments to explore light neutron-rich nuclei close to the dripline. We plan to reinforce experimental capabilities of the SAMURAI by introducing advanced devices such as MINOS (Saclay) and NeuLAND (GSI).

(1-4) Fission barrier heights in neutron-rich heavy nuclei

The symmetry energy has a strong influence on fission barrier heights in neutron-rich nuclei. Knowledge on the fission barrier heights, which is quite poor at present, is quite important for our proper understanding on termination of the r-process. We are planning to perform, in collaboration with the TU Munich group, $(p, 2p)$-delayed fission experiments at the SAMURAI to determine the fission barrier heights in neutron-rich nuclei in Pb region.

(2) Study of spin-isospin responses with RI-beams

The study of spin-isospin responses in nuclei forms one of the important cores of nuclear physics. A variety of collective states, for example isovector giant dipole resonances, isobaric analogue states, Gamow-Teller resonances, have been extensively studied by use of electromagnetic and hadronic reactions from stable targets.

The research opportunities can be largely enhanced with light of availabilities of radioactive isotope (RI) beams and of physics of unstable nuclei. There are three possible directions to proceed. The first direction is studies of spin-isospin responses of unstable nuclei via inverse-kinematics charge exchange reactions. A neutron-detector array WINDS has been constructed, under a collaboration of CNS, Tokyo and RIKEN, for inverse kinematics (p, n) experiments at the RI Beam Factory. We have already applied WINDS to the (p, n) experiments for ^{12}Be, ^{132}Sn and plan to extend this kind of study to other exotic nuclei.

The second direction is studies with RI-beam induced charge exchange reaction. RI-beam induced reactions have unique properties which are missing in stable-beam induced reactions and can be used to reach the yet-to-be-discovered states. We have constructed the SHARAQ spectrometer and the high-resolution beam-line at the RI Beam Factory to pursue the capabilities of RI-beam induced reactions as new probes to nuclei. One of the highlights is an observation of β^+ type isovector spin monopole resonances (IVSMR) in ^{208}Pb and ^{90}Zr via the $(t, {}^3\mathrm{He})$ reaction at 300 MeV/nucleon.

The third direction is studies of neutron- and proton-rich nuclei via stable-beam induced charge exchange reactions, which is conducted under collaboration with Research Center for Nuclear Physics (RCNP), Osaka University. We have performed the double

charge exchange ^{12}C(^{18}O,^{18}Ne) ^{12}Be reaction at 80 MeV/nucleon to investigate structure of a neutron-rich ^{12}Be nucleus. Peaks corresponding to ground and excited levels in ^{12}Be have been clearly observed. Another double charge exchange reaction, (^{12}C,^{12}Be(0^+_2)) are being used to search for double Gamow-Teller resonances.

(3) R-process nucleosynthesis study with heavy-ion storage ring

Most of the r-process nuclei become within reach of experimental studies for the first time at RI Beam Factory at RIKEN. The Rare RI Ring at RIBF is the unique facility with which we can perform mass measurements of r-process nuclei. Construction of the Rare RI Ring started in FY2012 in collaboration with Tsukuba and Saitama Universities. A major part of the ring has been completed and the commissioning run is planned in FY2014.

We are planning to start precise mass measurements of r-process nuclei soon. A series of experiments will start with nuclei in the $A = 80$ region and will be extended to heavier region.

(4) Application of spin-polarization technique to RI-beam experiments and other fields

A technique to produce nuclear polarization by means of electron polarization in photo-excited triplet states of aromatic molecules can open new applications. The technique is called "Tripletd-DNP." A distinguished feature of Triplet-DNP is that it works under a low magnetic field of 0.1–0.7 T and temperature higher than 100 K, which exhibits a striking contrast to standard dynamic nuclear polarization (DNP) techniques working in extreme conditions of several Tesla and sub-Kelvin.

We have constructed a polarized proton target system for use in RI-beam experiments. Recent experimental and theoretical studies have revealed that spin degrees of freedom play a vital role in exotic nuclei. Tensor force effects on the evolution of shell and possible occurrence of *p-n* pairing in the proton-rich region are good examples of manifestations of spin degrees of freedom. Experiments with the target system allow us to explore the spin effects in exotic nuclei. It should be noted that we have recently achieved a proton polarization of 40% at room temperature in a pentacene-d_{14} doped p-terphenyl crystal.

Another interesting application of Triplet-DNP is sensitivity enhancement in NMR spectroscopy of biomolecules. We started a new project to apply the Triplet-DNP technique to study protein-protein interaction via two-dimensional NMR spectroscopy, in close collaboration with biologists and chemists.

(5) Development of special targets for RI-beam experiments

For the research activities shown above, we are developing and hosting special targets for RI-beam experiments listed below:

(a) Polarized proton target (described in (4))
(b) Thin solid hydrogen target
(c) MINOS (developed at Saclay and hosted by the Spin Isospin Laboratory)

Members

Director

Tomohiro UESAKA

Research/Technical Scientists

Masaki SASANO (Senior Research Scientist)
Ken-ichiro YONEDA (Senior Research Scientist)
Sarah NAIMI (Research Scientist)

Research & Development Scientist

Yohei SHIMIZU

Contract Researchers

Takeshi INOUE
Kenichiro TATEISHI

Postdoctoral Researcher

Junki TANAKA

Research Associate

Akane SAKAUE

Junior Research Associates

Tomoya HARADA
Shoichiro MASUOKA

International Program Associates

Siwei HUANG (Peking Univ.)
Alexandra-Ionela STEFANESCU (Univ. of Bucharest)
Ionut-Catalin STEFANESCU (Univ. of Bucharest)

Research Consultants

Harutaka SAKAGUCHI (Osaka Univ.)
Yasuyuki SUZUKI
Kazuko TANABE

Senior Visiting Scientists

Hiroyuki SAGAWA (Univ. of Aizu)
Satoshi ADACHI (Osaka Univ.)
Hidetoshi AKIMUNE (Konan Univ.)
Didier BEAUMEL (Inst. de Phys.Nucl.)
Konstanze BORETZKY (GSI)
Christoph CAESAR (GSI)
Anna CORSI (CEA Saclay)
Zsolt DOMBRADI (ATOMKI)
Zoltan ELEKES (ATOMKI)
Zsolt FULOP (ATOMKI)
Tatsuya FURUNO (Osaka Univ.)
Igor GASPARIC (Rudjer Boskovic Inst.)
Zhuang GE (IMP, CAS)
Alain GILLIBERT (CEA Saclay)
Valdir GUIMARAES (Inst.o de Fisica da Univ. de Sao Paulo)
Zoltan HALASZ (ATOMKI)
Matthias HOLL (TRIUMF)
Kaori KAKI (Shizuoka Univ.)
KAWABATA (Osaka Univ.)
KIKUCHI (NIT, Tokuyama College)
Yosuke KONDO (Tokyo Tech)
Zeren KORKULU (ATOMKI)
Attila KRASZNAHORKAY (ATOMKI)
Dorottya KUNNE SOHLER (ATOMKI)
Istvan KUTI (ATOMKI)
Valerie LAPOUX (Inst.ion CEA-Saclay)
Yury LITVINOV (GSI)
Hongna LIU (TU Darmstadt)
Yohei MATSUDA (Tohoku Univ.)
Kenjiro MIKI (Tohoku Univ.)
Tetsuaki MORIGUCHI (Tsukuba Univ.)
Takashi NAKAMURA (Tokyo Tech)
Alexandre OBERTELLI (TU Darmstadt)
Kazuyuki OGATA (Osaka Univ.)
Emanuel POLLACCO (CEA Saclay)
Kimiko SEKIGUCHI (Tohoku Univ.)
Haik SIMON (GSI)
Laszlo STUHL (ATOMKI)
Baohua SUN (Beihang Univ.)
Shinji SUZUKI (Chinese Academy of Sci.)
Satoru TERASHIMA (Beihang Univ.)
Hans Toshihide TOERNQVIST (TU Darmstadt)
Yasuhiro TOGANO (Rikkyo Univ.)
Takashi WAKUI (QST)
He WANG (Tokyo Tech)
Atomu WATANABE (Tohoku Univ.)
Takayuki YAMAGUCHI (Saitama Univ.)
Nobuhiro YANAI (Kyushu Univ.)
Zaihong YANG (Osaka Univ.)
Juzo ZENIHIRO (Kyoto Univ.)
Yuhu ZHANG (IMP, CAS)

Visiting Technicians

Gilles AUTHELET (CEA)
Denis CALVET (CEA)
Alain DELBART (CEA/CE Saclay)
Jean-Marc GHELLER (CEA)
Arnaud GIGANON (CEA/CE Saclay)
Clement HILAIRE (CEA Saclay)
Daniel KOERPER (GSI)
Cedric PERON (CEA Saclay)
Jean-Yves ROUSSE (CEA)
Olivier TELLIER (CEA Saclay)

Student Trainees

Tomoki ADACHI (Kyushu Univ.)
Paul E. ANDRE (CEA Saclay)
Wenbo DOU (Saitama Univ.)
Naoki EBINA (Tokyo Tech)
Shiyo EN'YO (Kyoto Univ.)
Yuki FUJIKAWA (Kyoto Univ.)
Saiya FUJIWARA (Kyushu Univ.)
Jian GAO (Peking Univ.)
Daiki HAMAKAWA (Saitama Univ.)
Yuya HAMANO (Kyushu Univ.)
Sakumi HARAYAMA (Saitama Univ.)
Mika HAYASHI (Tsukuba Univ.)
Yuto HIJIKATA (Kyoto Univ.)
Kouta HORIKAWA (Tokyo Tech)
Kento INABA (Kyoto Univ.)
Minami INOUE (Tohoku Univ.)
Daisuke KAJIKI (Saitama Univ.)
Koki KAMEYA (Tohoku Univ.)
Naoto KANAME (Tsukuba Univ.)
Masanori KANDA (Saitama Univ.)
Yusuke KAWASHIMA (Kyushu Univ.)
Sho KITAYAMA (Tohoku Univ.)
Shuhei KIYOTAKE (Univ. of Miyazaki)
Taishi KUBO (Kyushu Univ.)
Hayato KUROSAWA (Tohoku Univ.)
Hongfu LI (IMP, CAS)
Pengjie LI (The Univ. of Hong Kong)
Ryu MAEDA (Tohoku Univ.)
Yoshiki MARUTA (Tohoku Univ.)
Tomoki MATSUI (Tokyo Tech)
Riku MATSUMURA (Saitama Univ.)
Shinnosuke NAKAI (Tohoku Univ.)
Mio NISHIMURA (Rikkyo Univ.)
Kotaro NONAKA (Univ. of Miyazaki)
Kyoko NOSAKA (Tohoku Univ.)
Shintaro OKAMOTO (Kyoto Univ.)
Misaki OTSU (Saitama Univ.)
Atsumi SAITO (Tokyo Tech)
Yuko SAITO (Tohoku Univ.)
Shigehito SAKAKI (Kyushu Univ.)
Kosuke SAKANASHI (Osaka Univ.)
Hibiki SEKI (Saitama Univ.)
Naru SHINOZAKI (Saitama Univ.)
Kohei TAKAHASHI (Tokyo Tech)

Keisuke TOMITA (Tsukuba Univ.)
Ryotaro TSUJI (Kyoto Univ.)
Yuta UTSUKI (Tohoku Univ.)
Kohei YAMAMOTO (Tohoku Univ.)
Asahi YANO (Tsukuba Univ.)
Akira YASUDA (Tokyo Tech)
Chieko YONEMURA (Kyushu Univ.)
Yuuki YOSHITOME (Tokyo Tech)

Interns

Maruf ALI (Univ. of Surrey)
George W.G.W. HUDSON-CHANG (Univ. of Surrey)

Assistants

Emiko ISOGAI
Asako TAKAHASHI
Yuri TSUBURAI

List of Publications & Presentations

Publications

[Original Papers]

Y. Kubota, A. Corsi, G. Authelet, H. Baba, C. Caesar, D. Calvet, A. Delbart, M. Dozono, J. Feng, F. Flavigny, J. -M. Gheller, J. Gibelin, A. Giganon, A. Gillibert, K. Hasegawa, T. Isobe, Y. Kanaya, S. Kawakami, D. Kim, Y. Kikuchi, Y. Kiyokawa, M. Kobayashi, N. Kobayashi, T. Kobayashi, Y. Kondo, Z. Korkulu, S. Koyama, V. Lapoux, Y. Maeda, F. M. Marques, T. Motobayashi, T. Miyazaki, T. Nakamura, N. Nakatsuka, Y. Nishio, A. Obertelli, K. Ogata, A. Ohkura, N. A. Orr, S. Ota, H. Otsu, T. Ozaki, V. Panin, S. Paschalis, E. C. Pollacco, S. Reichert, J. -Y. Rousse, A. T. Saito, S. Sakaguchi, M. Sako, C. Santamaria, M. Sasano, H. Sato, M. Shikata, Y. Shimizu, Y. Shindo, L. Stuhl, T. Sumikama, Y. L. Sun, M. Tabata, Y. Togano, J. Tsubota, Z. H. Yang, J. Yasuda, K. Yoneda, J. Zenihiro, and T. Uesaka, "Surface localization of the dineutron in ^{11}Li," Phys. Rev. Lett. **125**, 252501 (2020).

A. Revel, O. Sorlin, F. M. Marqués, Y. Kondo, J. Kahlbow, T. Nakamura, N. A. Orr, F. Nowacki, J. A. Tostevin, C. X. Yuan, N. L. Achouri, H. Al Falou, L. Atar, T. Aumann, H. Baba, K. Boretzky, C. Caesar, D. Calvet, H. Chae, N. Chiga, A. Corsi, H. L. Crawford, F. Delaunay, A. Delbart, Q. Deshayes, Z. Dombrádi, C. A. Douma, Z. Elekes, P. Fallon, I. Gašparić, J. -M. Gheller, J. Gibelin, A. Gillibert, M. N. Harakeh, W. He, A. Hirayama, C. R. Hoffman, M. Holl, A. Horvat, Á. Horváth, J. W. Hwang, T. Isobe, N. Kalantar-Nayestanaki, S. Kawase, S. Kim, K. Kisamori, T. Kobayashi, D. Körper, S. Koyama, I. Kuti, V. Lapoux, S. Lindberg, S. Masuoka, J. Mayer, K. Miki, T. Murakami, M. Najafi, K. Nakano, N. Nakatsuka, T. Nilsson, A. Obertelli, F. de Oliveira Santos, H. Otsu, T. Ozaki, V. Panin, S. Paschalis, D. Rossi, A. T. Saito, T. Saito, M. Sasano, H. Sato, Y. Satou, H. Scheit, F. Schindler, P. Schrock, M. Shikata, Y. Shimizu, H. Simon, D. Sohler, L. Stuhl, S. Takeuchi, M. Tanaka, M. Thoennessen, H. Törnqvist, Y. Togano, T. Tomai, J. Tscheuschner, J. Tsubota, T. Uesaka, Z. Yang, M. Yasuda, and K. Yoneda, "Extending the southern shore of the island of inversion to ^{28}F," Phys. Rev. Lett. **124**, 15, 152502 (2020).

M. Dozono, T. Uesaka, N. Fukuda, M. Ichimura, N. Inabe, S. Kawase, K. Kisamori, Y. Kiyokawa, K. Kobayashi, M. Kobayashi, T. Kubo, Y. Kubota, C. S. Lee, M. Matsushita, S. Michimasa, H. Miya, A. Ohkura, S. Ota, H. Sagawa, S. Sakaguchi, H. Sakai, M. Sasano, S. Shimoura, Y. Shindo, L. Stuhl, H. Suzuki, H. Tabata, M. Takaki, H. Takeda, H. Tokieda, T. Wakasa, K. Yako, Y. Yanagisawa, J. Yasuda, R. Yokoyama, K. Yoshida, and J. Zenihiro, "The parity-transfer (^{16}O, ^{16}F(0^-, g.s.)) reaction as a probe of isovector 0^- states in nuclei," Nucl. Phys. B **962**, 115236 (2021).

N. Itagaki, T. Fukui, J. Tanaka, and Y. Kikuchi, "^{8}He and ^{9}Li cluster structures in light nuclei," Phys. Rev. C **102**, 024332 (2020).

X. Roca-Maza, G. Colo, and H. Sagawa, "Isobaric analog state energy in deformed nuclei: a toy model," Phys. Rev. C **102**, 064303-1–8 (2020).

T. Aumann, C. Barbieri, D. Bazin, C. A. Bertulani, A. Bonaccorso, W. H. Dickhoff, A. Gade, M. Gomez-Ramos, B. P. Kay, A. M. Moro, T. Nakamura, A. Obertelli, K. Ogata, S. Paschalis, and T. Uesaka, "Quenching of single-particle strength from direct reactions with stable and rare-isotope beams," Prog. Part. Nucl. Phys. **118**, 103847 (2021).

S. Yoshida, H. Sagawa, J. Zenihiro, and T. Uesaka, "Trajectory in 2D-plot of isoscalar and isovector densities of ^{48}Ca and ^{208}Pb, and symmetry energy," Phys. Rev. C **102**, 064307-1–12 (2020).

M. Patsyuk, J. Kahlbow, G. Laskaris, M. Duer, V. Lenivenko, E. P. Segarra, T. Atovullaev, G. Johansson, T. Aumann, A. Corsi, O. Hen, M. Kapishin, V. Panin, E. Piasetzky, Kh. Abraamyan, S. Afanasiev, G. Agakishiev, P. Alekseev, E. Atkin, T. Aushev, V. Babkin, V. Balandin, D. Baranov, N. Barbashina, P. Batyuk, S. Bazylev, A. Beck, C. A. Bertulani, D. Blaschke, D. Blau, D. Bogoslovsky, A. Bolozdynya, K. Boretzky, V. Burtsev, M. Buryakov, S. Buzin, A. Chebotov, J. Chen, A. Ciszewski, R. Cruz-Torres, B. Dabrowska, D. Dabrowski, A. Dmitriev, A. Dryablov, P. Dulov, D. Egorov, A. Fediunin, I. Filippov, K. Filippov, D. Finogeev, I. Gabdrakhmanov, A. Galavanov, I. Gasparic, O. Gavrischuk, K. Gertsenberger, V. Golovatyuk, M. Golubeva, F. Guber, Yu. Ivanova, A. Ivashkin, A. Izvestnyy, S. Kakurin, V. Karjavin, N. Karpushkin, R. Kattabekov, V. Kekelidze, S. Khabarov, Yu. Kiryushin, A. Kisiel, V. Kolesnikov, A. Kolozhvari, Yu. Kopylov, I. Korover, L. Kovachev, A. Kovalenko, Yu. Kovalev, A. Kugler, S. Kuklin, E. Kulish, A. Kuznetsov, E. Ladygin, N. Lashmanov, E. Litvinenko, S. Lobastov, B. Löher, Y. -G. Ma, A. Makankin, A. Maksymchyuk, A. Malakhov, I. Mardor, S. Merts, A. Morozov, S. Morozov, G. Musulmanbekov, R. Nagdasev, D. Nikitin, V. Palchik, D. Peresunko, M. Peryt, O. Petukhov, Yu. Petukhov, S. Piyadin, V. Plotnikov, G. Pokatashkin, Yu. Potrebenikov, O. Rogachevsky, V. Rogov, K. Rosłon, D. Rossi, I. Rufanov, P. Rukoyatkin, M. Rumyantsev, D. Sakulin, V. Samsonov, H. Scheit, A. Schmidt, S. Sedykh, I. Selyuzhenkov, P. Senger, S. Sergeev, A. Shchipunov, A. Sheremeteva, M. Shitenkov, V. Shumikhin, A. Shutov, V. Shutov, H. Simon, I. Slepnev, V. Slepnev, I. Slepov, A. Sorin, V. Sosnovtsev, V. Spaskov, T. Starecki, A. Stavinskiy, E. Streletskaya, O. Streltsova, M. Strikhanov, N. Sukhov, D. Suvarieva, J. Tanaka, A. Taranenko, N. Tarasov, O. Tarasov, V. Tarasov, A. Terletsky, O. Teryaev, V. Tcholakov, V. Tikhomirov, A. Timoshenko, N. Topilin, B. Topko, H. Törnqvist, I. Tyapkin, V. Vasendina, A. Vishnevsky, N. Voytishin, V. Wagner, O. Warmusz, I. Yaron, V. Yurevich, N. Zamiatin, Song Zhang, E. Zherebtsova, V. Zhezher, N. Zhigareva,

A. Zinchenko, E. Zubarev, and M. Zuev, "Unperturbed inverse kinematics nucleon knockout measurements with a carbon beam," Nat. Phys. **1-7** (2021).

Z. H. Yang, Y. Kubota A. Corsi, K. Yoshida, X. -X. Sun, J. G. Li, M. Kimura, N. Michel, K. Ogata, C. X. Yuan, Q. Yuan, G. Authelet, H. Baba, C. Caesar,D. Calvet, A. Delbart, M. Dozono, J. Feng, F. Flavigny, J. -M. Gheller, J. Gibelin, A. Giganon, A. Gillibert, K. Hasegawa, T. Isobe, Y. Kanaya, S. Kawakami, D. Kim, Y. Kiyokawa, M. Kobayashi, N. Kobayashi, T. Kobayashi, Y. Kondo, Z. Korkulu, S. Koyama, V. Lapoux, Y. Maeda, F. M. Marques, T. Motobayashi, T. Miyazaki, T. Nakamura, N. Nakatsuka, Y. Nishio, A. Obertelli, A. Ohkura, N. A. Orr, S. Ota, H. Otsu, T. Ozaki, V. Panin, S. Paschalis, E. C. Pollacco, S. Reichert, J. -Y. Rousse, A. T. Saito, S. Sakaguchi, M. Sako, C. Santamaria, M. Sasano, H. Sato, M. Shikata, Y. Shimizu, Y. Shindo, L. Stuhl, T. Sumikama, Y. L. Sun, M. Tabata, Y. Togano, J. Tsubota, F. R. Xu, J. Yasuda, K. Yoneda, J. Zenihiro, S. -G. Zhou, W. Zuo, and T. Uesaka, "Quasi-free neutron knockout reaction reveals a smalls-orbital component in the borromean nucleus ^{17}B," Phys. Rev. Lett. **126**, 082501 (2021).

M. Sasano, H. Sagawa, T. Suzuki, and M. Honma, "Energy-weighted sum rule for Gamow-Teller giant resonances in high spin isomeric states of $N = Z$ nuclei," Phys. Rev. C **103**, 014308-1–10 (2021).

J. Tanaka, Z. Yang, S. Typel, S. Adachi, S. Bai, P. van Beek, D. Beaumel, Y. Fujikawa, J. Han, S. Heil, S. Huang, A. Inoue, Y. Jiang, M. Knösel, N. Kobayashi Y. Kubota, W. Liu, J. Lou, Y. Maeda, Y. Matsuda, K. Miki, S. Nakamura, K. Ogata, V. Panin, H. Scheit, F. Schindler, P. Schrock, D. Symochko, A. Tamii, T. Uesaka, V. Wagner, K. Yoshida, J. Zenihiro, and T. Aumann, "Formation of α clusters in dilute neutron-rich matter," Science **371**, 260–264 (2021).

J. Zenihiro, T. Uesaka, S. Yoshida, and H. Sagawa, "Proton density polarization of the doubly magic ^{40}Ca core in ^{48}Ca and EoS parameters," Prog. Theor. Exp. Phys. **2021**, 023D05 (2021).

S. Takada, K. Tateishi, Y. Wakabayashi, Y. Ikeda, T. Yoshioka, Y. Otake, and T. Uesaka, "Polarized proton spin filter for epithermal neutrons based on dynamic nuclear polarization using photo-excited triplet electron spins PTEP 2020," Prog. Theor. Exp. Phys. **2020**, 123G01 (2020).

D. Wu, C. L. Bai, H. Sagawa, and H. Q. Zhang, "Study of charge radii with neural networks," Phys. Rev. C **102**, 054323-1–7 (2020).

C. Lizarazo, P. -A. Söderström, V. Werner, N. Pietralla, P. M. Walker, G. X. Dong, F. R. Xu, T. R. Rodríguez, F. Browne, P. Doornenbal, S. Nishimura, C. R. Niţă, A. Obertelli, T. Ando, T. Arici, G. Authelet, H. Baba, A. Blazhev, A. M. Bruce, D. Calvet, R. J. Carroll, F. Château, S. Chen, L. X. Chung, A. Corsi, M. L. Cortes, A. Delbart, M. Dewald, B. Ding, F. Flavigny, S. Franchoo, J. Gerl, J. -M. Gheller, A. Giganon, A. Gillibert, M. Górska, A. Gottardo, I. Kojouharov, N. Kurz, V. Lapoux, J. Lee, M. Lettmann, B. D. Linh, J. J. Liu, Z. Liu, S. Momiyama, K. Moschner, T. Motobayashi, S. Nagamine, N. Nakatsuka, M. Niikura, C. Nobs, L. Olivier, Z. Patel, N. Paul, Zs. Podolyák, J. -Y. Rousse, M. Rudigier, T. Y. Saito, H. Sakurai, C. Santamaria, H. Schaffner, C. Shand, I. Stefan, D. Steppenbeck, R. Taniuchi, T. Uesaka, V. Vaquero, K. Wimmer, and Z. Xu, "Metastable states of ^{92,94}Se: identification of an oblate K isomer of ^{94}Se and the ground-state shape transition between $N = 58$ and 60," Phys. Rev. Lett. **124**, 22, 222501 (2020).

A. Frotscher, M. Gómez-Ramos, A. Obertelli, P. Doornenbal, G. Authelet, H. Baba, D. Calvet, F. Château, S. Chen, A. Corsi, A. Delbart, J. -M. Gheller, A. Giganon, A. Gillibert, T. Isobe, V. Lapoux, M. Matsushita, S. Momiyama, T. Motobayashi, M. Niikura, H. Otsu, N. Paul, C. Peron, A. Peyaud, E. C. Pollacco, J. -Y. Rousse, H. Sakurai, C. Santamaria, M. Sasano, Y. Shiga, N. Shimizu, D. Steppenbeck, S. Takeuchi, R. Taniuchi, T. Uesaka, H. Wang, K. Yoneda, T. Ando, T. Arici, A. Blazhev, F. Browne, A. M. Bruce, R. Carroll, L. X. Chung, M. L. Cortes, M. Dewald, B. Ding, Zs. Dombradi, F. Flavigny, S. Franchoo, F. Giacoppo, M. Górska, A. Gottardo, K. Hadyńska-Klęk, Z. Korkulu, S. Koyama, Y. Kubota, A. Jungclaus, J. Lee, M. Lettmann, B. D. Linh, J. Liu, Z. Liu, C. Lizarazo, C. Louchart, R. Lozeva, K. Matsui, T. Miyazaki, K. Moschner, S. Nagamine, N. Nakatsuka, C. Nita, S. Nishimura, C. R. Nobs, L. Olivier, S. Ota, Z. Patel, Zs. Podolyák, M. Rudigier, E. Sahin, T. Y. Saito, C. Shand, P. -A. Söderström, I. G. Stefan, T. Sumikama, D. Suzuki, R. Orlandi, V. Vaquero, Zs. Vajta, V. Werner, K. Wimmer, J. Wu, and Z. Xu, "Sequential nature of $(p, 3p)$ two-proton knockout from neutron-rich nuclei," Phys. Rev. Lett. **1251**, 012501 (2020).

M. M. Juhász, Z. Elekes, D. Sohler, Y. Utsuno, K. Yoshida, T. Otsuka, K. Ogata, P. Doornenbal, A. Obertelli, H. Baba, F. Browne, D. Calvet, F. Château, S. Chen, N. Chiga, A. Corsi, M. L. Cortés, A. Delbart, J. -M. Gheller, A. Giganon, A. Gillibert, C. Hilaire, T. Isobe, T. Kobayashi, Y. Kubotan, V. Lapoux,T. Motobayashi, I. Murray, H. Otsu, V. Panin, N. Paul, W. Rodriguez, H. Sakurai, M. Sasano, D. Steppenbeck, L. Stuhlo, Y. L. Sun, Y. Togano, T. Uesaka, K. Wimmer, K. Yoneda, N. L. Achouri, O. Aktasu, T. Aumann, L. X. Chung, Zs. Dombrádi, F. Flavign, S. Franchoo, I. Gašparic, R. -B. Gerst, J. Gibelin, K. I. Hahn, D. Kim, T. Koiwa, Y. Kondo, P. Koseoglo, J. Lee, C. Lehr, B. D. Linh, H. N. Liu, T. Lokotko, M. MacCormick, K. Moschner, T. Nakamura, S. Y. Park, D. Rossi, E. Sahina, P. -A. Söderström, S. Takeuchia, H. Törnqvist, V. Vaqueroa, V. Wagner, S. Wanga, V. Werner, X. Xu, H. Yamada, D. Yana, Z. Yang, and M. Yasuda, "First spectroscopic study of ^{51}Ar by the $(p, 2p)$ reaction," Phys. Lett. B **814**, 136108 (2021).

W. J. Huang, M. Wang, F. G. Kondev, G. Audi, and S. Naimi, "The AME 2020 atomic mass evaluation (I). Evaluation of input data, andadjustment procedures," Chin. Phys. C **45**, 030002 (2021).

W. J. Huang, M. Wang, F. G. Kondev, G. Audi, and S. Naimi, "The AME 2020 atomic mass evaluation (II). Tables, graphs and references," Chin. Phys. C **45**, 3, 030003 (2021).

N. Itagaki, T. Fukui, J. Tanaka, and Y. Kikuchi, "^{8}He and ^{9}Li cluster structures in light nuclei," Phys. Rev. C **102**, 024332 (2020).

T. L. Tang, T. Uesaka, S. Kawase, D. Beaumel, M. Dozono, T. Fujii, N. Fukuda, T. Fukunaga, A. Galindo-Uribarri, S. H. Hwang, N. Inabe, D. Kameda, T. Kawahara, W. Kim, K. Kisamori, M. Kobayashi, T. Kubo, Y. Kubota, K. Kusaka, C. S. Lee, Y. Maeda, H. Matsubara, S. Michimasa, H. Miya, T. Noro, A. Obertelli, K. Ogata, S. Ota, E. Padilla-Rodal, S. Sakaguchi, H. Sakai, M. Sasano, S. Shimoura, S. S. Stepanyan, H. Suzuki, M. Takaki, H. Takeda, H. Tokieda, T. Wakasa, T. Wakui, K. Yako, Y. Yanagisawa, J. Yasuda, R. Yokoyama, K. Yoshida, K. Yoshida, and J. Zenihiro, "How different is the core of ^{25}F from $^{24}O_{g.s.}$?" Phys. Rev. Lett. **124**, 212502 (2020).

W. Horiuchi, Y. Suzuki, T. Uesaka, and M. Miwa, "Total reaction cross section on a deuteron target and the eclipse effect of the constituent neutron and proton," Phys. Rev. C **102**, 054601 (2020).

M. L. Cortés, W. Rodriguez, P. Doornenbal, A. Obertelli, J. D. Holt, J. Menéndez, K. Ogata, A. Schwenk, N. Shimizu, J. Simonis, Y. Utsuno, K. Yoshida, L. Achouri, H. Baba, F. Browne, D. Calvet, F. Château, S. Chen, N. Chiga, A. Corsi, A. Delbart, J-M. Gheller,

A. Giganon, A. Gillibert, C. Hilaire, T. Isobe, T. Kobayashi, Y. Kubota, V. Lapoux, H. N. Liu, T. Motobayashi, I. Murray, H. Otsu, V. Panin, N. Paul, H. Sakurai, M. Sasano, D. Steppenbeck, L. Stuhl, Y. L. Sun, Y. Togano, T. Uesaka, K. Wimmer, K. Yoneda, O. Aktas, T. Aumann, L. X. Chung, F. Flavigny, S. Franchoo, I. Gašparić, R. -B. Gerst, J. Gibelin, K. I. Hahn, D. Kim, T Koiwai, Y. Kondo, P. Koseoglou, J. Lee, C. Lehr, B. D. Linh, T. Lokotko, M. MacCormick, K. Moschner, T. Nakamura, S. Y. Park, D. Rossi, E. Sahin, P. -A. Söderström, D. Sohler, S. Takeuchi, H. Toernqvist, V. Vaquero, V. Wagner, S. Wang, V. Werner, X. Xu, H. Yamada, D. Yan, Z. Yang, M. Yasuda, and L. Zanetti, "N = 32 shell closure below calcium: Low-lying structure of ^{50}Ar," Phys. Rev. C **102**, 064320 (2020).

D. Nagae, Y. Abe, S. Okada, S. Omika, K. Wakayama, S. Hosoi, S. Suzuki, T. Moriguchi, M. Amano, D. Kamioka, Z. Ge, S. Naimi, F. Suzaki, N. Tadano, R. Igosawa, K. Inomata, H. Arakawa, K. Nishimuro, T. Fujii, T. Mitsui, Y. Yanagisawa, H. Baba, S. Michimasa, S. Ota, G. Lorusso, Yu. A. Litvinov, A. Ozawa, T. Uesaka, T. Yamaguchi, Y. Yamaguchi, and M. Wakasugi, "Development and operation of an electrostatic time-of-flight detector for the Rare RI storage Ring," Nucl. Instrum. Methods Phys. Res. A **986**, 164713 (2021).

Y. Zhang, H. Sagawa, and E. Hiyama, "Hyperon halo structure of C and B Isotopes," Phys. Rev. C **103**, 03432-1–9 (2021).

S. Michimasa, M. Kobayashi, Y. Kiyokawa, S. Ota, R. Yokoyama, D. Nishimura, D. S. Ahn, H. Baba, G. P. A. Berg, M. Dozono, N. Fukuda, T. Furuno, E. Ideguchi, N. Inabe, T. Kawabata, S. Kawase, K. Kisamori, K. Kobayashi, T. Kubo, Y. Kubota, C. S. Lee, M. Matsushita, H. Miya, A. Mizukami, H. Nagakura, H. Oikawa, H. Sakai, Y. Shimizu, A. Stolz, H. Suzuki, M. Takaki, H. Takeda, S. Takeuchi, H. Tokieda, T. Uesaka, K. Yako, Y. Yamaguchi, Y. Yanagisawa, K. Yoshida, and S. Shimoura, "Mapping of a new deformation region around ^{62}Ti," Phys. Rev. Lett. **125**, 12, 122501 (2020).

C. Y. Fu, Y. H. Zhang, M. Wang X. H. Zhou Yu. A. Litvinov, K. Blaum, H. S. Xu, X. Xu, P. Shuai, Y. H. Lam, R. J. Chen, X. L. Yan, X. C. Chen, J. J. He, S. Kubono, M. Z. Sun, X. L. Tu, Y. M. Xing, Q. Zeng, X. Zhou, W. L. Zhan, S. Litvinov, G. Audi, T. Uesaka, T. Yamaguchi, A. Ozawa, B. H. Sun, Y. Sun, and F. R. Xu, "Mass measurements for the $T_z = -2$ fp nuclei ^{40}Ti, ^{44}Cr, ^{46}Mn, ^{48}Fe, ^{50}Co, and ^{52}Ni," Phys. Rev. C **102**, 5, 054311 (2020).

S. Takada, K. Tateishi, Y. Wakabayashi, Y. Ikeda, T. Yoshioka, Y. Otake, and T. Uesaka, "Polarized proton spin filter for epithermal neutron based on dynamic nuclear polarization using photo-excited triplet electron spins," Prog. Theo. Exp. Phys. **2020**, 123G01 (2020).

[Review Articles]

K. Nishimura, H. Kouno, Y. Kawashima, K. Orihashi, S. Fujiwara, K. Tateishi, T. Uesaka, N. Kimizuka, and N. Yanai, "Materials chemistry of triplet dynamic nuclear polarization," Chem. Commum. **56**, 7217–7232 (2020).

[Proceedings]

S. W. Huang, Z. H. Yang, F. M. Marqués, N. L. Achouri, D. S. Ahn, T. Aumann, H. Baba, D. Beaumel, M. Böhmer, K. Boretzky, M. Caamaño, S. Chen, N. Chiga, M. L. Cortés, D. Cortina, P. Doornenbal, C. A. Douma, F. Dufter, J. Feng, B. Fernández-Domínguez, Z. Elekes, U. Forsberg, T. Fujino, N. Fukuda, I. Gašparić, Z. Ge, R. Gernhäuser, J. M. Gheller, J. Gibelin, A. Gillibert, B. M. Godoy, Z. Halász, T. Harada, M. N. Harakeh, A. Hirayama, N. Inabe, T. Isobe, J. Kahlbow, N. Kalantar-Nayestanaki, D. Kim, S. Kim, M. A. Knösel, T. Kobayashi, Y. Kondo, P. Koseoglou, Y. Kubota, I. Kuti, C. Lehr, P. J. Li, Y. Liu, Y. Maeda, S. Masuoka, M. Matsumoto, J. Mayer, H. Miki, M. Miwa, I. Murray, T. Nakamura, A. Obertelli, N. Orr, H. Otsu, V. Panin, S. Park, M. Parlog, S. Paschalis, M. Potlog, S. Reichert, A. Revel, D. Rossi, A. Saito, M. Sasano, H. Sato, H. Scheit, F. Schindler, T. Shimada, Y. Shimizu, S. Shimoura, I. Stefan, S. Storck, L. Stuhl, H. Suzuki, D. Symochko, H. Takeda, S. Takeuchi, J. Tanaka, Y. Togano, T. Tomai, H. T. Törnqvsit, J. Tscheuschner, T. Uesaka, V. Wagner, K. Wimmer, H. Yamada, B. Yang, L. Yang, Y. Yasuda, K. Yoneda, L. Zanetti, J. Zenihiro, T. Elidiano, and C. Lenain, "Experimental study of 4n with ^{8}He(p, 2p) reaction," J. Phys. Conf. Ser. **1643**, 012090 (2020).

V. P. Ladygin, A. V. Averyanov, E. V. Chernykh, Y. V. Gurchin, A. Y. Isupov, D. O. Krivenkov, P. K. Kurilkin, N. B. Ladygina, A. N. Livanov, S. M. Piyadin, S. G. Reznikov, Y. T. Skhomenko, A. A. Terekhin, A. V. Tishevsky, and T. Uesaka, "Angular and energy dependence of A_y, A_{yy} and A_{xx} analyzing powers in dp elastic scattering and dp breakup reaction investigation," Proc. Sci. **LC2019**, 048 (2020).

Z. Yang, J. Tanaka, S. Type, T. Aumann, J. Zenihiro, S. Adachi, S. Bai, P. van Beek, D. Beaumel, Y. Fujikawa, J. Han, S. Heil, S. Huang, A. Inoue, Y. Jia, M. Knösel, N. Kobayashi, Y. Kubota, W. Liu, J. Lou, Y. Maeda, Y. Matsuda, K. Miki, S. Nakamura, K. Ogata, V. Panin, H. Scheit, F. Schindler, P. Schrock, D. Symochko, A. Tamii, T. Uesaka, V. Wagner, and K. Yoshida, "α-Clustering at the surface of Tin isotopes $^{112-124}$Sn studied with (p, $p\alpha$) reaction," JPS Conf. Proc. **31**, 011019 (2020).

P. Koseoglou, V. Werner, N. Pietralla, P. -A. Söderström, P. Doornenbal, A. Obertelli, N. Achouri, H. Baba, F. Browne, D. Calvet, F. Château, S. Chen, N. Chiga, A. Corsi, M. L. Cortés, A. Delbart, J-M. Gheller, A. Giganon, A. Gillibert, C. Hilaire, T. Isobe, T. Kobayashi, Y. Kubota, V. Lapoux, H. Liu, T. Motobayashi, I. Murray, H. Otsu, V. Panin, N. Paul, W. Rodriguez, H. Sakurai, M. Sasano, D. Steppenbeck, L. Stuhl, Y. L. Sun, Y. Togano, T. Uesaka, K. Wimmer, K. Yoneda, O. Aktas, T. Auman, L. X. Chung, F. Flavigny, S. Franchoo, I. Gasparic, R. -B. Gerst, J. Gibelin, K. I. Hahn, D. Kim, T. Koiwai, Y. Kondo, J. Lee, C. Lehr, M. Lettmann, B. D. Linh, T. Lokotko, M. MacCormick, K. Moschner, T. Nakamura, S. Y. Park, D. Rossi, E. Sahin, D. Sohler, S. Takeuchi, H. Toernqvist, V. Vaquero, V. Wagner, S. Wang, X. Xu, H. Yamada, D. Yan, Z. Yang, M. Yasuda, and L. Zanetti, "Spectroscopy of neutron-rich scandium isotopes," J. Phys. Conf. Ser. **1555**, 012026 (2020).

R. Matsumura, H. Otsu, H. Wang, N. Chiga, S. Kawase, K. Nakano, H. Sakurai, M. Shikata, S. Takeuchi, Y. Togano, and for the ImPACT-RIBF Collaboration, "Research for nuclear transmutation of high-radiotoxic nuclide 90Sr via proton- and deuteron-induced reactions," JAEA-Conf. 2021-001(2021).

Presentations

[International Conferences/Workshops]

R. Matsumura, H. Otsu, H. Wang, N. Chiga, S. Kawase, K. Nakano, H. Sakurai, M. Shikata, S. Takeuchi, Y. Togano, and for the ImPACT-RIBF Collaboration, "Nuclear transmutation of high-radiotoxic nuclide ^{90}Sr via proton- and deuteron-induced reactions in inverse

kinematics," A3F-CNS Summer School 2020, オンライン開催, 2020 年 8 月 17–21 日.

K. Nishimura, H. Kouno, Y. Kawashima, K. Orihashi, S. Fujiwara, K. Tateishi, T. Uesaka, N. Kimizuka, and N. Yanai, "Materials chemistry of triplet dynamic nuclear polarization," Chem. Commum. **56**, 7217–7232 (2020).

[Domestic Conferences/Workshops]

松村理久, 大津秀暁, 王赫, 千賀信幸, 川瀬頌一郎, 中野敬太, 櫻井博儀, 四方瑞紀, 武内聡, 栂野泰宏, ImPACT-RIBF Collaboration,「高放射性核種 ^{90}Sr の陽子及び重陽子誘起反応による核変換に向けた研究」, Symposium on Nuclear Data 2020, 埼玉県和光市 (理研仁科センター), 2020 年 11 月 26–27 日.

Nuclear Science and Transmutation Research Division
Nuclear Spectroscopy Laborarory

1. Abstract

The research group has conducted nuclear-physics studies utilizing stopped/slowed-down radioactive-isotope (RI) beams mainly at the RIBF facility. These studies are based on the technique of nuclear spectroscopy such as β-ray-detected NMR (β-NMR), γ-PAD (Perturbed Angular Distribution), laser, and Mössbauer among other methods that takes advantage of intrinsic nuclear properties such as nuclear spins, electromagnetic moments, and decay modes. In particular, techniques and devices for the production of spin-controlled RI beams have been developed and combined to the spectroscopic studies, which enable high-sensitivity measurements of spin precessions/resonances through a change in the angular distribution of radiations. Anomalous nuclear structures and properties of far unstable nuclei are investigated from thus determined spin-related observables. The group also aims to apply such techniques to interdisciplinary fields such as fundamental physics and materials science by exploiting nuclear probes.

2. Major Research Subjects

(1) Nuclear spectroscopy utilizing spin-oriented fast RI beams
(2) Nuclear/Atomic laser spectroscopy & SLOWRI R&D
(3) Application of RI probes to materials science
(4) Fundamental physics: Study of symmetry

3. Summary of Research Activity

(1) Nuclear spectroscopy utilizing spin-oriented fast RI beams

Measurements of static electromagnetic nuclear moments over a substantial region of the nuclear chart have been conducted for structure studies on the nuclei far from the β-decay stability. Utilizing nuclear spin orientation phenomena of RIs created in the projectile-fragmentation reaction, ground- and excited-state electromagnetic nuclear moments been determined by means of the β-ray-detected nuclear magnetic resonance (β-NMR) and the γ-ray time differential perturbed angular distribution (γ-TDPAD) methods. In particular, a new method developed for controlling spin in a system of rare RIs, taking advantage of the mechanism of the two-step projectile fragmentation reaction combined with the momentum-dispersion matching technique, has been developed and employed making fully use of world's highest intensity rare RIBs delivered from BigRIPS for rare isotopes.

(2) Nuclear/Atomic laser spectroscopy & SLOWRI R&D

The group has been conducting system development for nuclear laser spectroscopy from the following two approaches in order to realize experiments for rare isotopes at RIBF. One is collinear laser spectroscopy for a large variety of elements using slowed-down RI beams produced via a projectile-fragmentation reaction, which can be achieved only by the universal low-energy RI-beam delivery system, SLOWRI, under installation in collaboration with the SLOWRI Team. This slowed-down RI-beam scheme enables to perform high-precision laser spectroscopy even with fast-fragmentation-based RIBs without the elemental limitation problematic in the ISOL-based RIBs.

The other approach is a new method utilizing superfluid helium (He II) as a stopping medium of energetic RI beams, in which the characteristic atomic properties of ions surrounded by superfluid helium enables us to perform unique nuclear laser spectroscopy. RI ions trapped in He II are known to exhibit a characteristic excitation spectrum significantly blue-shifted compared with the emission one. Consequently, the background derived from the excitation-laser stray light, which often causes serious problems in measurements, can be drastically reduced.

(3) Application of RI probes to materials science

The application of RI and heavy ion beams as a probe for condensed matter studies is also conducted by the group. The microscopic material dynamics and properties have been investigated through the deduced internal local fields and the spin relaxation of RI probes based on various spectroscopies utilizing RI probes such as β-NMR/NQR spectroscopy, Mössbauer spectroscopy, the γ-ray time differential perturbed angular correlation (γ-TDPAC) spectroscopy. Furthermore, studies on the control of electrical conductivity of diamond by boron and nitrogen implantation are ongoing.

Provided that highly spin-polarized RI probes are produced independently of their element properties and doped into a substance as an impurity, the constituent particle of the substance can be substituted by the same element RI probe without changing the material structure. This scheme provides a new opportunity for materials-science researches, but a key technology, production of element-independent highly spin-polarized RI beams, has not yet been achieved. In this subject, the group has conducted R&D studies to realize an ultra-slow & highly-spin-polarized RI beams, based on the technique of the atomic beam resonance.

(4) Fundamental physics: Study of symmetry

The nuclear spins of stable and unstable isotopes sometimes play important roles in fundamental physics research. New experimental methods and devices have been developed for studies of the violation of time reversal symmetry (T-violation) using spin-polarized nuclei. These experiments aim to detect the small frequency shift in the spin precession arising from new mechanisms beyond the Standard Model.

Members

Director
Hideki UENO

Research/Technical Scientists
Hiroki YAMAZAKI (Senior Research Scientist)
Isao WATANABE (Senior Research Scientist)
Aiko TAKAMINE (Research Scientist)

Research & Development Scientist
Tetsu SONODA

Contract Researcher
Takashi ABE

Special Postdoctoral Researcher
Momo MUKAI

Postdoctoral Researchers
Minori TAJIMA
Kei IMAMURA (CPR)

Research Associate
Aleksey GLADKOV

Senior Visiting Scientists
Yukari MATSUO (Hosei Univ.)
Takaharu OTSUKA (Univ. of Tokyo)

Visiting Scientists
Dimiter L. BALABANSKI (IFIN-HH)
Georgi GEORGIEV (CNRS-IN2P3)
Yuichi ICHIKAWA (Kyushu Univ.)
Yoshio KOBAYASHI (Univ. of Electro-Commun.)
Kenya KUBO (Int'l Christian Univ.)
Kensaku MATSUTA (Osaka Univ.)
Jun MIYAZAKI (Tokyo Denki Univ.)
Takamasa MOMOSE (The Univ. of British Columbia)
Jiro MURATA (Rikkyo Univ.)
Jin NAKAMURA (Univ. of Electro-Commun.)
Hiroki NISHIBATA (Kyushu Univ.)
Tomoya SATO (Tokyo Tech)
Wataru SATO (Kanazawa Univ.)
Andrew E. STUCHBERY (The Australian Nat'l Univ.)
Satoshi TSUTSUI (Japan Synchrotron Radiation Res. Inst.)
Yasuhiro YAMADA (Tokyo Univ. Sci)
Deyan T. YORDANOV (CNRS-IN2P3)
Akihiro YOSHIMI (Okayama Univ.)

Student Trainees
Sai AKIMOTO (Hosei Univ.)
Miru DOI (Hosei Univ.)
Timothy J. GRAY (The Australian Nat'l Univ.)
Kentaro HAMANO (Univ. of Electro-Commun.)
Manami ITO (Hosei Univ.)
Kyouichi IZUOKA (Tokyo Univ. Sci)
Masato KIJI (Univ. of Electro-Commun.)
Masaki NISHIMURA (Hosei Univ.)
Shinichi OKAMURA (Univ. of Ferrara)
Yuika TAKEUCHI (Hosei Univ.)
Satoshi TANAKA (Hosei Univ.)
Kenta TSUBURA (Hosei Univ.)
Takumi YAMAMOTO (Hosei Univ.)
Mio YOSHIDA (Univ. of Electro-Commun.)

Temporary Staffing
Emiko SUGISAKI
Naoko YUASA

Assistant
Izumi YOSHIDA

List of Publications & Presentations

Publications

[Original Papers]

M. Tajima, A. Takamine, M. Wada, and H. Ueno, "Offline ion source for laser spectroscopy of RI at the SLOWRI," Nucl. Instrum. Methods Phys. Res. B **486**, 48–54 (2021).

N. Tsunoda, T. Otsuka, K. Takayanagi, N. Shimizu, T. Suzuki, Y. Utsuno, S. Yoshida, and H. Ueno, "The impact of nuclear shape on the emergence of the neutron dripline," Nature **587**, 66–71 (2020).

M. Mukai, Y. Hirayama, Y. X. Watanabe, S. Schiffmann, J. Ekman, M. Godefroid, P. Schury, Y. Kakiguchi, M. Oyaizu, M. Wada, S. C. Jeong, J. Y. Moon, J. H. Park, H. Ishiyama, S. Kimura, H. Ueno, M. Ahmed, A. Ozawa, H. Watanabe, S. Kanaya, and H. Miyatake, "In-gas-cell laser resonance ionization spectroscopy of ^{196,197,198}Ir," Phys. Rev. C **102**, 054307 (2020).

H. Suzuki, K. Yoshida, N. Fukuda, H. Takeda, Y. Shimizu, D. S. Ahn, T. Sumikama, N. Inabe, T. Komatsubara, H. Sato, Z. Korkulu, K. Kusaka, Y. Yanagisawa, M. Ohtake, H. Ueno, T. Kubo, S. Michimasa, N. Kitamura, K. Kawata, N. Imai, O. B. Tarasov, D. Bazin, J. Nolen, and W. F. Henning, "Experimental studies of the two-step scheme with an intense radioactive ^{132}Sn beam for next-generation production of very neutron-rich nuclei," Phys. Rev. C **102**, 064615 (2020).

Y. Sakemi, T. Aoki, R. Calabrese, H. Haba, K. Harada, T. Hayamizu, Y. Ichikawa, K. Jungmann, A. Kastberg, Y. Kotaka, Y. Matsuda, Y. Matsuo, H. Nagahama, K. Nakamura, M. Otsuka, N. Ozawa1, K. S. Tanaka, A. Uchiyama, H. Ueno, and L. Willmann, "Fundamental physics with cold radioactive atoms," AIP Conf. Proc. **2319**, 080020-1–6 (2021).

H. Watanabe, Y. X. Watanabe, Y. Hirayama, A. N. Andreyev, T. Hashimoto, F. G. Kondev, G. J. Lane, Yu. A. Litvinov, J. J. Liu, H. Miyatake, J. Y. Moon, A. I. Morales, M. Mukai, S. Nishimur, T. Niwase, M. Rosenbusch, P. Schury, Y. Shi, M. Wada, and P. M. Walker, "Beta decay of the axially asymmetric ground state of ^{192}Re," Phys. Lett. B **814**, 136088-1–6 (2020).

P. M. Walker, Y. Hirayama, G. J. Lane, H. Watanabe, G. D. Dracoulis, M. Ahmed, M. Brunet, T. Hashimoto, S. Ishizawa, F. G. Kondev, Yu. A. Litvinov, H. Miyatake, J. Y. Moon, M. Mukai, T. Niwase, J. H. Park, Zs. Podolyák, M. Rosenbusch, P. Schury, M. Wada, X. Y. Watanabe, W. Y. Liang, and F. R. Xu, "Properties of ^{187}Ta revealed through isomeric decay," Phys. Rev. Lett. **125**, 192505-1–5 (2020).

Y. X. Watanabe, M. Ahmed, Y. Hirayama, M. Mukai, J. H. Park, P. Schury, Y. Kakiguchi, S. Kimura, A. Ozawa, M. Oyaizu, M. Wada, H. Miyatake, "Deexcitation γ-ray transitions from the long-lived $I^{\pi} = 13/2^{+}$ metastable state in ^{195}Os," Phys. Rev. C **101**, 041305 (2020).

Y. Hirayama, P. Schury, M. Mukai, H. Choi, S. Imamura, X. Y. Watanabe, M. Wada, H. Watanabe, and H. Miyatake, "Three-dimensional tracking multi-segmented proportional gas counter for β-decay spectroscopy of unstable nuclei," Nucl. Instrum. Methods Phys. Res. A **997**, 165152-1–10 (2021).

Y. Ichikawa, "Nuclear-moment measurements of exotic nuclei using spin-oriented RI beams at RIBF," AIP Conf. Proc. **2319**, 080021 (2021).

Y. Ichikawa, H. Nishibata, Y. Tsunoda, A. Takamine, K. Imamura, T. Fujita, T. Sato, S. Momiyama, Y. Shimizu, D. S. Ahn, K. Asahi, H. Baba, D. L. Balabanski, F. Boulay, J. M. Daugas, T. Egami, N. Fukuda, C. Funayama, T. Furukawa, G. Georgiev, A. Gladkov, N. Inabe, Y. Ishibashi, Y. Kobayashi, S. Kojima, A. Kusoglu, T. Kawaguchi, T. Kawamura, I. Mukul, M. Niikura, T. Nishizaka, A. Odahara, Y. Ohtomo, T. Otsuka, D. Ralet, G. S. Simpson, T. Sumikama, H. Suzuki, H. Takeda, L. C. Tao, Y. Togano, D. Tomonaga, H. Ueno, H. Yamazaki, and X. F. Yang, "Magnetic moment of the isomeric state of ^{75}Cu measured with a highly spin-aligned beam," JPS Conf. Proc. **32**, 010047-1–4 (2020).

S. Bagchi, R. Kanungo, Y. K. Tanaka, H. Geissel, P. Doornenbal, W. Horiuchi, G. Hagen T. Suzuki, N. Tsunoda, D. S. Ahn, H. Baba, K. Behr, F. Browne, S. Chen, M. L. Cortés, A. Estradé, N. Fukuda, M. Holl, K. Itahashi, N. Iwasa, G. R. Jansen, W. G. Jiang, S. Kaur, A. O. Macchiavelli, S. Y. Matsumoto, S. Momiyama, I. Murray, T. Nakamura, S. J. Novario, H. J. Ong, T. Otsuka, T. Papenbrock, S. Paschalis, A. Prochazka, C. Scheidenberger, P. Schrock, Y. Shimizu, D. Steppenbeck, H. Sakurai, D. Suzuki, H. Suzuki, M. Takechi, H. Takeda, S. Takeuchi, R. Taniuchi, K. Wimmer, and K. Yoshida, "Two-neutron halo is unveiled in ^{29}F," Phys. Rev. Lett. **124**, 22250-1–7 (2020).

N. Mărginean, D. Little, Y. Tsunoda, S. Leoni, R. V. F. Janssens, B. Fornal, T. Otsuka, C. Michelagnoli, L. Stan, F. C. L. Crespi, C. Costache, R. Lica, M. Sferrazza, A. Turturica, A. D. Ayangeakaa, K. Auranen, M. Barani, P. C. Bender, S. Bottoni, M. Boromiza, A. Bracco, S. Călinescu, C. M. Campbell, M. P. Carpenter, P. Chowdhnury, M. Ciemała, N. Cieplicka-Oryǹczak, D. Cline, C. Clisu, H. L. Crawford, I. E. Dinescu, J. Dudouet, D. Filipescu, N. Florea, A. M. Forney, S. Fracassetti, A. Gade, I. Gheorghe, A. B. Hayes, I. Harca, J. Henderson, A. Ionescu, Ł. W. Iskra, M. Jentschel, F. Kandzia, Y. H. Kim, F. G. Kondev, G. Korschinek, U. Köster, Krishichayan, M. Krzysiek, T. Lauritsen, J. Li, R. Mărginean, E. A. Maugeri, C. Mihai, R. E. Mihai, A. Mitu, P. Mutti, A. Negret, C. R. Niţă, A. Olăcel, A. Oprea, S. Pascu, C. Petrone, C. Porzio, D. Rhodes, D. Seweryniak, D. Schumann, C. Sotty, S. M. Stolze, R. Şuvăilă, S. Toma, S. Ujeniuc, W. B. Walters, C. Y. Wu, J. Wu, S. Zhu, and S. Ziliani, "Shape coexistence at zero spin in ^{64}Ni driven by the monopole tensor interaction," Phys. Rev. Lett. **125**, 102502-1–7 (2020).

M. M. Juhász, Z. Elekes, D. Sohler, Y. Utsuno, K. Yoshida, T. Otsuka, K. Ogata, P. Doornenbal, A. Obertelli, H. Baba, F. Browne, D. Calvet, F. Château, S. Chen, N. Chiga, A. Corsi, M. L. Cortés, A. Delbart, and L. Zanetti, "First spectroscopic study of ^{51}Ar by the $(p, 2p)$ reaction," Phys. Lett. B **814**, 136108-1–8 (2021).

C. Porzio, C. Michelagnoli, N. Cieplicka-Oryǹczak, M. Sferrazza, S. Leoni, B. Fornal, Y. Tsunoda, T. Otsuka, S. Bottoni, C. Costache, F. C. L. Crespi, Ł. W. Iskra, M. Jentschel, F. Kandzia, Y. -H. Kim, U. Köster, N. Mărginean, C. Mihai, P. Mutti, and A. Turturică, "Detailed low-spin spectroscopy of ^{65}Ni via neutron capture reaction," Phys. Rev. C **102**, 064310-1–13 (2020).

N. Shimizu, Y. Tsunoda, Y. Utsuno, and T. Otsuka, "Variational approach with the superposition of the symmetry-restored quasiparticle vacua for nuclear shell-model calculations," Phys. Rev. C **103**, 014312-1–11 (2021).

F. L. Bello Garrote, E. Sahin, Y. Tsunoda, T. Otsuka, A. Görgen, M. Niikura, S. Nishimura, G. de Angelis, G. Benzoni, A. I. Morales, V. Modamio, Z. Y. Xu, H. Baba, F. Browne, A. M. Bruce, S. Ceruti, F. C. L. Crespi, R. Daido, M. -C. Delattre, P. Doornenbal, Zs. Dombradi, Y. Fang, S. Franchoo, G. Gey, A. Gottardo, K. Hadyńska-Klęk, T. Isobe, P. R. John, H. S. Jung, I. Kojouharov, T. Kubo, N. Kurz, I. Kuti, Z. Li, G. Lorusso, I. Matea, K. Matsui, D. Mengoni, T. Miyazaki, S. Momiyama, P. Morfouace, D. R. Napoli, F. Naqvi, H. Nishibata, A. Odahara, R. Orlandi, Z. Patel, S. Rice, H. Sakurai, H. Schaffner, L. Sinclair, P. -A. Söderström, D. Sohler, I. G. Stefan, T. Sumikama, D. Suzuki, R. Taniuchi, J. Taprogge, Zs. Vajta, J. J. Valiente-Dobón, H. Watanabe, V. Werner, J. Wu, A. Yagi, M. Yalcinkaya, R. Yokoyama, and K. Yoshinaga, "β Decay of ^{75}Ni and the systematics of the low-lying level structure of neutron-rich odd-A Cu isotopes," Phys. Rev. C **102**, 034314-1–13 (2020).

Y. Tsunoda and T. Otsuka, "Triaxial rigidity of ^{166}Er and its Bohr-model realization," Phys. Rev. C **103**, L021303-1–6 (2021).

S. Leoni, B. Fornal, N. Marginean, C. Michelagnoli, J. Wilson, M. Sferrazza, Y. Tsunoda, and T. Otsuka, "Shape-coexistence studies in the ni isotopic chain by using the selectivity of different reaction mechanisms," Acta Phys. Pol. B **51**, 807–815 (2020).

P. -A. Söderström, L. Capponi, E. Açıksöz, T. Otsuka, N. Tsoneva, Y. Tsunoda, D. L. Balabanski, N. Pietralla, G. L. Guardo, D. Lattuada,

H. Lenske, C. Matei, D. Nichita, A. Pappalardo, and T. Petruse, "Electromagnetic character of the competitive $\gamma\gamma/\gamma$-decay from ^{137m}Ba," Nat. Commun. **11**, 3242-1–8 (2020).

Y. Sato, Y. Yamada, Y. Kobayashi, M. K. Kubo, M. Mihara, W. Sato, J. Miyazaki, T. Nagatomo, T. Ando, N. Takahama, K. Some, M. Sato, S. Sato, and A. Kitagawa, "In-beam Mössbauer spectra of ^{57}Mn implanted into lithium aluminium hydride," Appl. Radiat. Isot. **170**, 109582-1–7 (2021).

Y. Yamada, Y. Sato, Y. Kobayashi, T. Ando, N. Takahama, K. Some, M. Sato, M. Mihara, M. K. Kubo, W. Sato, J. Miyazaki, T. Nagatomo, J. Kobayashi, A. Okazawa, S. Sato, A. Kitagawa, "In-beam Mössbauer spectra for ^{57}Mn implanted sulfur hexafluoride," Hyperfine Interact. **241**, 15-1–6 (2020).

Presentations

[International Conferences/Workshops]

A. Takamine (invited), "SLOWRI rf gas catcher development toward symbiotic mass measurement at F11," RIBF User Meeting 2020, online, September 2–10, 2020.

M. Mukai, "In-gas-jet laser spectroscopy of $^{199–202}$Pt, $^{195–198}$Ir, $^{193–198}$Os," SSRI-PNS Collaboration Meeting 2020, online, Japan, September 3, 2020.

H. Ueno (invited), "Nuclear spectroscopy with spin-polarized RI beams," The International School for Strangeness Nuclear Physics 2020 (SNP School 2020), online & J-PARC, Ibaraki, Japan, December 2–5, 2020.

[Domestic Conferences/Workshops]

上野秀樹 (依頼講演), 「高偏極 RI ビームの生成と核・物質科学研究への応用」, 新学術領域研究「宇宙観測検出器と量子ビームの出会い。新たな応用への架け橋。」第 2 回領域研究会, オンライン開催, 2020 年 7 月 27–28 日.

今村慧 (口頭発表), 「RI 原子線磁気共鳴に向けた中性化装置開発」, 新学術領域「宇宙観測検出器と量子ビームの出会い．新たな応用への架け橋. 」第 2 回領域全体会議，オンライン開催, 2020 年 7 月 27–28 日.

飯村俊，高峰愛子，M. Rosenbusch，和田道治，S. Chen，J. Liu，W. Xian，D. Hou，S. Yan，P. Schury，園田哲，小島隆夫，渡辺裕，小田原厚子，石山博恒，「理研 BigRIPS SLOWRI における RF カーペットガスセルの開発」, 日本物学会 2020 年秋季大会, オンライン開催, 2021 年 9 月 14–17 日.

三原基嗣, 松多健策, 福田光順, 若林諒, 沖本直哉, 福留美樹, 泉川卓司, 野口法秀, 生越瑞揮, 大坪隆, 西村太樹, 髙橋弘幸, 菅原奏来, Aleksey Gladkov, 北川敦志, 佐藤眞二, 「短寿命酸素 NMR プローブ核 ^{19}O の物質科学利用」, 日本物学会 2020 年秋季大会, オンライン開催, 2021 年 9 月 14–17 日.

角田佑介, 大塚孝治, 清水則孝, 本間道雄, 宇都野穣, 「モンテカルロ殻模型による $Z = 28$ 近傍の核構造の研究」, 日本物学会 2020 年秋季大会, オンライン開催, 2021 年 9 月 14–17 日.

阿部喬 (口頭発表), "Ab initio description of light nuclei from no-core Monte Carlo shell model," 第 5 回クラスター階層領域研究会, オンライン開催, 2020 年 9 月 24–25 日.

上野秀樹 (依頼講演), 「RI・重イオンビームの学際的利用に向けた研究開発」, 新領域開拓課題 物質階層原理 & ヘテロ界面研究合同年次成果報告会, オンライン開催, 2021 年 2 月 8–9 日.

市川雄一 (招待講演), 「低エネルギースピン物理」, 日本のスピン物理学の展望研究会, 島根県松江市, オンライン開催, 2021 年 2 月 23–24 日.

田島美典, 高峰愛子, 飯村秀紀, 和田道治, H. A. Schuessler, 上野秀樹, 「コリニアレーザー分光による四重極変形度測定を通した原子核構造研究にむけた開発 II」, 日本物学会第 76 回年次大会, オンライン開催, 2021 年 3 月 12–15 日.

小澤直也, 長濱弘季, 早水友洋, 中村圭佑, 佐藤幹, 永瀬慎太郎, 小高康照, 鎌倉恵太, 田中香津生, 大塚未来, 青木貴稔, 市川雄一, 高峰愛子, 羽場宏光, 上野秀樹, 酒見泰寛, 「フランシウム原子の電気双極子能率探索のための表面電離イオン源の開発」, 日本物学会第 76 回年次大会, オンライン開催, 2021 年 3 月 12–15 日.

飯村俊，高峰愛子，M. Rosenbusch，和田道治，S. Chen，D. Hou，J. Liu，W. Xian，S. Yan，P. Schury，木村創大，庭瀬暁隆，伊藤由太，園田哲，小島隆夫，渡辺裕，N. Sara，道正新一郎，西村俊二，小田原厚子，石山博恒，「理研 BigRIPS SLOWRI における RF カーペットガスセルの開発—オンライン実験と質量測定—」, 日本物学会第 76 回年次大会, オンライン開催, 2021 年 3 月 12–15 日.

大谷優里花, 三原基嗣, 松多健策, 福田光順, 若林諒, 沖本直哉, 福留美樹, 木村容子, 高山元, 泉川卓司, 野口法秀, 生越瑞揮, 佐藤弥紗, 高津和哉, 大坪隆, 西村太樹, 髙橋弘幸, 菅原奏来, Aleksey Gladkov, 北川敦志, 佐藤眞二, 百田佐多生, 奥村寛之, 森口哲朗, 小沢顕, 「^{19}O の偏極ビーム生成と固体燃料電池研究への応用」, 日本物学会第 76 回年次大会, オンライン開催, 2021 年 3 月 12–15 日.

清水則孝, 角田佑介, 宇都野穣, 大塚孝治, 「準粒子真空基底によるモンテカルロ殻模型の拡張」, 日本物学会第 76 回年次大会, オンライン開催, 2021 年 3 月 12–15 日.

大塚孝治, 角田佑介, 角田直文, 阿部喬, 清水則孝, P. Van Duppen, 高柳和雄, 鈴木俊夫, 宇都野穣, 上野秀樹, 「原子核物理の再出発」, KEK 理論センター研究会「原子核・ハドロン物理 2020」, オンライン開催, 2020 年 10 月 6 日.

大塚孝治, 「原子核物理の再出発」, ELPH 研究会 C028「電子散乱による原子核研究—原子核の電荷密度・陽子・ 中性子の分布と半径—」, オンライン開催, 2021 年 3 月 18–19 日.

高峰愛子 (招待講演), "Isotope shift measurement project at the SLOWRI facility," ELPH 研究会 C028「電子散乱による原子核研究—原子核の電荷密度・陽子・中性子の分布と半径—」, オンライン開催, 2021 年 3 月 18–19 日.

大塚孝治, 角田直文, 高柳和雄, 清水則孝, 鈴木俊夫, 宇都野穣, 上野秀樹, 「原子核物理の再出発」, "Neutron driplines and shape evolution of atomic nuclei," 第 3 回クラスター階層領域研究会, オンライン開催, 2020 年 5 月 18 日.

[University Lectures]

H. Ueno, "Applied Radiation Engineering," Department of Nuclear Engineering and Management, Graduate School of Engineering, the

University of Tokyo.

H. Yamazaki, “Physics in Daily Life (in Japanese),” General Education Course, Otsuma Women’s University.

A. Takamine, “Exercises in Basic Physics I (in Japanese),” Department of Advanced Sciences, Faculty of Science and Engineering, Hosei University.

A. Takamine, “Exercises in Basic Physics II (in Japanese),” Department of Advanced Sciences, Faculty of Science and Engineering, Hosei University.

Press Releases

新聞等掲載: 「中性子過剰ジルコニウム同位体の励起状態での変形」, フジサンケイビジネスアイ, 2020 年 5 月 22 日.

プレスリリース: 東京大学, 理化学研究所, 日本原子力研究開発機構, 上智大学, 日本大学, 宇都宮大学共同記者発表, 「原子核の存在限界（中性子ドリップライン）の新たなメカニズム －中性子は原子核にいくつ入るか－」, 2020 年 11 月 5 日.

新聞等掲載: 「原子核の最大中性子数決定 －新たなメカニズム提唱－」, 科学新聞, 2020 年 11 月 27 日.

Nuclear Science and Transmutation Research Division
High Energy Astrophysics Laborarory

1. Abstract

In the immediate aftermath of the Big Bang, the beginning of our universe, only hydrogen and helium existed. However, nuclear fusion in the interior of stars and the explosion of supernovae in the universe over 13.8 billion years led to the evolution of a world brimming with the many different elements we have today. By using scientific satellites or balloons to observe X-rays and gamma-rays emitted from celestial objects, we are observing the synthesis of the elements at their actual source. Our goal is to comprehensively elucidate the scenarios for the formation of the elements in the universe, together with our research on sub-atomic physics through the use of an accelerator.

2. Major Research Subjects

(1) History of nucleosynthesis in the universe
(2) Physics in extreme conditions in the universe
(3) Research and development of innovative radiation detectors
(4) Apply radiation technology for human to live in space

3. Summary of Research Activity

High Energy Astrophysics Laboratory started in April 2010. The goal of our research is to reveal the mechanism of nucleosynthesis and the evolution of elements in the universe, and to observe/discover exotic physical phenomena in extremely strong magnetic and/or gravitational fields. We have observed supernova remnants, strongly magnetized neutron stars, pulsars, black holes and galaxies with X-ray astronomical satellites, balloons and ground-based telescopes.

(1) Nucleosynthesis in the universe

(1-1) XRISM

We have contributed to the XRISM (X-ray imaging and spectroscopy mission) mission for the launch in FY2022. XRISM is the recovery mission of the ASTRO-H/Hitomi satellite, which was launched in February 2016 but lost by an accident one month after the launch. Hitomi carried four X-ray and gamma-ray detectors covering the 0.3–600 keV energy range. We, in collaboration with JAXA (Japan Aerospace Exploration Agency), Tokyo Metropolitan University, Kanazawa University, Saitama University, NASA/GSFC etc., contributed to the soft X-ray spectrometer (SXS), which achieves unprecedented energy resolution (<7 eV) in the 0.3–12 keV energy band with a low temperature micro calorimeter. We hoped to use SXS to discover many previously-unknown elemental lines in the universe and to measure the abundance of these elements, but this was not possible with Hitomi. The XRISM satellite carries almost identical X-ray detectors as the Hitomi satellite, and is expected to carry out scientific observations that were not done with the Hitomi mission.

(1-2) MAXI

From April 2018, High Energy Astrophysics Laboratory hosts MAXI (Monitor of All-sky X-ray Image) onboard International Space Station (ISS), which was attached on ISS in 2009. MAXI is a RIKEN-lead project collaborating with JAXA and other universities. Since MAXI scans X-ray all-sky in 90 minutes, many transient objects including neutron star or blackhole binaries are found. All of the data are going to public soon after they are taken, and almost all of the groups in high-energy phenomena rely on the MAXI data. Until the end of 2020, we issued 362 alerts as ATEL (Astronomer's Telegram). To detect counterparts of neutron star merger events (*i.e.* gravitational wave events), we have prepared an automatic searching system and keep watching all-sky.

(2) Extremely strong magnetism and gravity

(2-1) IXPE

We have contributed to the NASA's world-first X-ray polarimeter mission IXPE (Imaging X-ray Polarimeter Explorer). High Energy Astrophysics Laboratory is responsible for providing the gas electron multipliers (GEMs) to the IXPE mission: the GEM is a key device of the X-ray polarimeter and produced based on our patent for space use. The IXPE satellite is scheduled to launched in the second half of 2021. We have already provided the flight qualified GEMs to the project in FY2018, and have contributed to the detector calibrations in FY2019.

By using the IXPE satellite, we aim to proof the strong magnetism of Magnetars, which are one of the species of neutron stars which have ultra-strong magnetic field B > 10^{11} T. In such ultra-strong magnetic field, higher-order diagrams, O(eB/m^2), O(eB/m^2)^2 etc., never ignored in the QED perturbation theory. As the results, we observe newly-emerging phenomenon such as vacuum polarization, vacuum birefringence, etc. If such exotic phenomena are detected, we sure that Magnetars have really ultra-strong magnetic field. In FY2020, we performed a simulation of scientific observations of Magnetars, which are neutron stars with ultra-strong magnetic fields.

(2-2) Astrophysical data analysis

In parallel with the mission development/operations, we are studying gamma-ray binary systems, which are one of the most important astrophysical targets in the MeV gamma-ray band. To reveal a long-standing question of the physical mechanism of efficient particle acceleration in these systems, we focused on the characteristic object LS 5039 and performed the timing analysis in the X-ray band. It resulted in hints of pulsation signals with an about 9-sec period. Though further confirmations are needed considering the

signal detection level, this result suggests that it harbors a strongly magnetized neutron star (magnetar). We proposed a new possibility that the particle acceleration could be related to the strong magnetic field of the magnetar, and have published a paper.

(3) Innovative breakthrough in astrophysics with a small satellite

We are developing technology and acquiring know-how to make space observation, which requires a lot of money, possible with small satellites at low cost. NASA and other space agencies around the world have realized the importance of this opportunities and have started space observation activities using small satellites. NinjaSat is a micro-satellite mission (6U CubeSat; $30 \times 20 \times 10$ cm^3) led by RIKEN in collaboration with universities. NinjaSat will be deployed from the ISS in 2022. Although several science missions have recently been conducted using micro-satellites, NinjaSat is the world's first general purpose CubeSat mission to observe X-ray sources. NinjaSat carries two Xe-filled gas detectors with 2-degree-wide collimators and performs spectroscopy between 2–50 keV and timing obervation with a timing resolution of about 120 μs. Since the effective area is not large (~40 cm^2 at 6 keV), the target of the NinjaSat is a long-term monitoring of bright X-ray sources which are discovered by MAXI etc. In general, bright objects are difficult to observe and a continuous observations for long period is impossible with large satellite missions. The aim of NinjaSat is to perform observations that are difficult to perform on larger missions. For example, NinjaSat observes the time variability of binary neutron stars and binary black holes in conjunction with the ground-based optical, radio and gravitational telescopes. We developed and tested an engineering model of the X-ray detectors in 2020.

(4) Future X-ray and gamma-ray detectors

In collaboration with NASA Goddard Space Flight Center, we have developed and tested a hard X-ray polarimeter with a Time Projection Chamber technique. This TPC polarimeter is one of candidates of the future satellite XPP (X-ray polarimeter Probe mission) planned with an international consortium.

As an successor of the MAXI mission, we are also verifying the principle of a new concept, multiplexing lobster-eye (MuLE) optics, to monitor the entire sky with a wide field-of-view for detecting and immediate reporting transient objects such as a neutron star merger. We puslished a peper on the conceptual design of MuLE, and proved the concept by a simple experiment in 2020.

To explore the MeV gamma-ray sky in the Universe, we are proceeding with the GRAMS project. It utilizes a large-scale liquid argon time projection chamber as a gamma-ray imager and aims to improve the sensitivity in the MeV band, by more than an order of magnitude than before. In a large-scale detector, MeV gamma rays are easily Compton-scattered multiple times and they sometimes escape from the detector before they deposit all energies. Thus, one of the key techniques for the above goal is to establish an algorithm that can reconstruct the incoming gamma-ray energy and direction from such a complex scattering event. We have proposed a new event reconstruction algorithm based on the maximum likelihood, by formulating physical processes in MeV gamma-ray telescopes. It is one of the first algorithms that can also estimate the escape gamma-ray energy. We have confirmed that it works successfully for the multiple scattering events using Geant4 simulations, and have demonstrated a proof of concept of the GRAMS project.

Members

Director

Toru TAMAGAWA

Research/Technical Scientist

Tatehiro MIHARA (Senior Research Scientist)

Special Postdoctoral Researcher

Hiroki YONEDA

Visiting Scientists

Aya BAMBA (Univ. of Tokyo)
Naohisa INADA (NIT, Nara College)
Satoru KATSUDA (Saitama Univ.)
Tomoki KIMURA (Tohoku Univ.)
Kazuki KOMIYA (Tokyo Metropolitan Industrial Tech. Res. Inst.)
Toru MISAWA (Shinshu Univ.)
Ikuyuki MITSUISHI (Nagoya Univ.)
Yujin NAKAGAWA (JAMSTEC)
Toshio NAKANO (JTEC Corporation)
Hirofumi NODA (Osaka Univ.)
Hirokazu ODAKA (Univ. of Tokyo)
Yuki OKURA (NAOJ/Nat'l Inst. of Natural Sci.)
Rohta TAKAHASHI (NIT, Tomakomai College)
Yoko TAKEUCHI (Tokyo Metropolitan Industrial Tech. Res. Inst.)
Yukikatsu TERADA (Saitama Univ.)
Masaki WAKABAYASHI (Jakulin Commercial Company LC)
Shinya YAMADA (Rikkyo Univ.)

Student Trainees

Syoki HAYASHI (Tokyo Univ. Sci)
Naoyuki OTA (Tokyo Univ. Sci)
Tomoshi TAKEDA (Tokyo Univ. Sci)
Marina TSUTSUMI (Tokyo Univ. Sci)
Keisuke UCHIYAMA (Tokyo Univ. Sci)
Yuto YOSHIDA (Tokyo Univ. Sci)

List of Publications & Presentations

Publications

[Original Papers]

Q. Abarr, H. Awaki, M. G. Baring, R. Bose, G. De Geronimo, P. Dowkontt, *et al*., "XL-Calibur—a second-generation balloon-borne hard X-ray polarimetry mission," Astropart. Phys. **126**, 102529 (2021).

S. Yamada, Y. Ichinohe, H. Tatsuno, R. Hayakawa, T. Ohashi, Y. Ishisaki, *et al*., "Broadband high-energy resolution hard X-ray spectroscopy using transition edge sensors at SPring-8," Rev. of Sci. Instrum. **92**, 013103 (2021).

T. Kasuga, H. Odaka, K. Hatauchi, S. Takashima, T. Tamba, Y. Aizawa, *et al*., "Artifact-less coded aperture imaging in the X-ray band with multiple different random patterns," J. Astron. Telesc. Instrum. Syst. **6**, 035002 (2020).

T. Ebisuzaki, H. Katori, J. Makino, A. Noda, H. Shinkai, T. Tamagawa, "INO: Interplanetary network of optical lattice clocks," Int. J. Mod. Phys. D **29**, 1940002 (2020).

R. Sasaki, Y. Tsuboi, W. Iwakiri, S. Nakahira, Y. Maeda, K. Gendreau, *et al*., "The RS CVn-type star GT mus shows most energetic X-ray flares throughout the 2010s," Astrophys. J. **910**, 25 (2020).

Y. L. Tuo, L. Ji, S. S. Tsygankov, T. Mihara, L. M. Song, M. Y. Ge, *et al*., "Insight-HXMT insight into switch of the accretion mode: The case of the X-ray pulsar 4U 1901+03," J. High Energy Astrophys. **27**, 38 (2020).

M. Tominaga, S. Nakahira, M. Shidatsu, M. Oeda, K. Ebisawa, "Discovery of the black hole X-ray binary transient MAXI J1348-630," Astrophys. J. Lett. **899**, L20 (2020).

M. Sugizaki, M. Oeda, N. Kawai, T. Mihara, K. Makishima, and M. Nakajima, "X-ray emission evolution of the galactic ultraluminous X-ray pulsar swift J0243.6 + 6124 during the 2017–2018 outburst observed by the MAXI GSC," Astrophys. J. **896**, 124 (2020).

T. Tamagawa, K. Uchiyama, R. Otsubo, T. Yuasa, Y. Zhou, T. Mihara, *et al*., "Multiplexing lobster-eye optics: a concept for wide-field X-ray monitoring," J. Astron. Telesc. Instrum. Syst. **6**, 025003 (2020).

[Proceedings]

Y. Maeda, Q. Abarr, H. Awaki, M. Baring, R. Bose, D. Braun, *et al*., "XL-Calibur: the next-generation balloon-borne hard X-ray polarimeter," Proc. SPIE **11444**, Space Telescopes and Instrumentation 2020: Ultraviolet to Gamma Ray, 114442X (2021).

K. Uchiyama, T. Tamagawa, T. Mihara, Y. Zhou, Y. Ezoe, M. Numazawa, *et al*., "Source position determination method of multiplexing lobster-eye optics," Proc. SPIE **11444**, Space Telescopes and Instrumentation 2020: Ultraviolet to Gamma Ray, 114447E (2020).

P. Soffitta, P. Attina, L. Baldini, M. Barbanera, W. H. Baumgartner, R. Bellazzini, *et al*., "The imaging X-ray polarimetry explorer (IXPE): technical overview III," Proc. SPIE **11444**, Space Telescopes and Instrumentation 2020: Ultraviolet to Gamma Ray, 1144462 (2020).

T. Takeda, K. Black, T. Enoto, A. Hayato, J. Hill, W. Iwakiri, *et al*., "Development and performance verification of a TPC polarimeter for high energy X-rays," Proc. SPIE **11444**, Space Telescopes and Instrumentation 2020: Ultraviolet to Gamma Ray, 114445Y (2020).

K. Hattori, H. Matsumoto, Q. Abarr, H. Awaki, R. Bose, D. Braun, *et al*., "Current status of the X-ray mirror for the XL-Calibur experiment," Proc. SPIE **11444**, Space Telescopes and Instrumentation 2020: Ultraviolet to Gamma Ray, 114445W (2020).

D. Yonetoku, T. Mihara, A. Doi, T. Sakamoto, K. Tsumura, K. Ioka, *et al*., "High-redshift gamma-ray burst for unraveling the dark ages mission: HiZ-GUNDAM," Proc. SPIE **11444**, Space Telescopes and Instrumentation 2020: Ultraviolet to Gamma Ray, 114442Z (2020).

M. Tashiro, H. Maejima, K. Toda, R. Kelley, L. Reichenthal, L. Hartz, *et al*., "Status of X-ray imaging and spectroscopy mission (XRISM)," Proc. SPIE **11444**, Space Telescopes and Instrumentation 2020: Ultraviolet to Gamma Ray, 1144422 (2020).

T. Enoto, T. Tamagawa, T. Kitaguchi, W. Iwakiri, Y. Kato, M. Numazawa, *et al*., "NinjaSat: an agile CubeSat approach for monitoring of bright X-ray compact objects," Proc. SPIE **11444**, Space Telescopes and Instrumentation 2020: Ultraviolet to Gamma Ray, 114441V (2020).

Y. Takeuchi, K. Komiya, T. Tamagawa, Y. Zhou, "Development and properties of 100 mm-square size LTCC-GEM," J. Phys. Conf. Ser. **1498**, 012011 (2020).

J. Li, T. Sakamoto, M. Serino, D. Yonetoku, T. Sawano, I. Mitsuish, *et al*., "X-ray performance and simulation study of lobster eye optics," Proc. of SPIE **11444**, 114447C (2020).

T. Sawano, D. Yonetoku, M. Arimoto, J. Li, T. Mihara, N. Ogino, "A detection algorithm for faint sources based on 1-d projection for a lobster-eye X-ray imaging system," Proc. SPIE **11444**, Space Telescopes and Instrumentation 2020: Ultraviolet to Gamma Ray, 114445K (2020).

Presentations

[International Conferences/Workshops]

T. Enoto (oral), T. Tamagawa, T. Kitaguchi, W. Iwakiri, Y. Kato, M. Numazawa, *et al*., "NinjaSat: an agile CubeSat approach for monitoring of bright X-ray compact objects," SPIE Astronomical Telescopes + Instrummentation 2020, Online, December 14–18, 2020.

Y. Maeda (oral), Q. Abarr, H. Awaki, M. Baring, R. Bose, D. Braun, *et al*., "XL-Calibur: the next-generation balloon-borne hard X-ray polarimeter," SPIE Astronomical Telescopes + Instrummentation 2020, Online, December 14–18, 2020.

D. Yonetoku (oral), T. Mihara, A. Doi, T. Sakamoto, K. Tsumura, K. Ioka, *et al*., "High-redshift gamma-ray burst for unraveling the Dark Ages Mission: HiZ-GUNDAM," SPIE Astronomical Telescopes + Instrummentation 2020, Online, December 14–18, 2020.

T. Takeda (poster), K. Black, T. Enoto, A. Hayato, J. Hill, W. Iwakiri, *et al*., "Development and performance verification of a TPC polarimeter for high energy X-rays," SPIE Astronomical Telescopes + Instrummentation 2020, Online, December 14–18, 2020.

K. Uchiyama (poster), T. Tamagawa, T. Mihara, Y. Zhou, Y. Ezoe, M. Numazawa, *et al*., "Source position determination method of multiplexing lobster-eye optics," SPIE Astronomical Telescopes + Instrummentation 2020, Online, December 14–18, 2020.

T. Tamagawa (Oral), K. Uchiyama, R. Otsubo, T. Yuasa, Y. Zhou, T. Mihara, *et al*., "New concept for wide-field X-ray monitoring with multiplexing Lobster-eye optics," 43rd COSPAR Scientific Assembly, Online, January 28–February 4, 2021.

[Domestic Conferences/Workshops]

玉川徹 (口頭発表), 北口貴雄, 榎戸輝揚, 内山慶祐, 三石郁之, 山口友洋, 柏倉一斗, 田原譲, 郡司修一, 渡邉瑛里, 寺島政伸, 斎藤耀, 深沢泰司, 水野恒史, 高橋弘充, 内田和海, 山本龍哉, 岩切渉, 林田清, 朝倉一統, Martin Weisskopf, Brian Ramsey, Stephen O'Dell, Paolo Soffitta, Luca Baldini ほか IXPE 衛星チーム, 「X 線偏光観測衛星 IXPE への参加現状 (6)」, 日本天文学会 2021 年春季年会, オンライン, 2021 年 3 月 16–19 日.

三石郁之 (口頭発表), 山口友洋, 柏倉一斗, 瀧川歩, 志村拓馬, 田原譲, 大西崇文, 立花一志, 宮田喜久子, 田村啓輔, 玉川徹, 立花正満, 村島健介, 「X 線偏光観測衛星 IXPE 搭載 X 線望遠鏡用受動型熱制御素子サーマルシールドの開発 (8)」, 日本天文学会 2021 年春季年会, オンライン, 2021 年 3 月 16–19 日.

Y. Ishisaki (口頭発表), R. L. Kelley, H. Akamatsu, H. Awaki, T. G. Bialas, G. V. Brown, M. P. Chiao, E. Costantini, J.-W. den Herder, M. J. Dipirro, M. E. Eckart, Y. Ezoe, C. Ferrigno, R. Fujimoto, A. Furuzawa, S. M. Graham, M. Grim, T. Hayashi, T. Horiuchi, A. Hoshino, Y. Ichinohe, R. Iizuka, M. Ishida, K. Ishikawa, C. A. Kilbourne, S. Kitamoto, M. A. Leutenegger, Y. Maeda, D. McCammon, I. Mitsuishi, M. Mizumoto, T. Ohashi, T. Okajima, S. Paltani, F. S. Porter, K. Sato, T. Sato, M. Sawada, H. Seta, P. J. Shirron, G. A. Sneiderman, Y. Soong, A. E. Szymkowiak, Y. Takei, T. Tamagawa, M. Tsujimoto, Y. Uchida, C. P. de Vries, S. Yamada, N. Y. Yamasaki, S. Yasuda, and N. Yoshioka, 「X 線分光撮像衛星 XRISM 搭載 Resolve の開発の現状 VI」, 日本天文学会 2021 年春季年会, オンライン, 2021 年 3 月 16–19 日.

前田良知 (口頭発表), 石田学, 斎藤芳隆, Abarr Quin, Bose R., Braun D., Dowkontt P., Errando M., Gau E., Guarino V., Hossen A., Lisalda L., Krawczynski H., Pastrani I., Rauch B., Simburger G., West A., 粟木久光, 今村竜太, Baring M., de Geronimo G., Elliot J., Gadson T., Hall K., Harmon K., Heatwole S., Kotsifakis D., Lanzi J., 岡島崇, Peterson Z., Purdy C., Snow C., Stuchlik D., 田村啓輔, Shreeves C., Vincent B., 榎戸輝揚, 北口貴雄, 玉川徹, 眞武寛人, 深沢泰司, 今里郁弥, 今澤遼, 水野恒史, Poon H., 高橋弘充, 内田和海, 内田悠介, 山本龍哉, 楊冲, 古澤彰浩, 郡司修一, 朝倉一統, 服部兼吾, 袴田知宏, 花岡真帆, 林田清, 石倉彩美, 井出峻太郎, 鴨川航, 松本浩典, 松下友亮, 峯田大 晴, 野田博文, 岡崎貴樹, 大出優一, 佐久間翔太郎, 澤上拳明, 常深博米山友景, 善本真梨那, 石橋和紀, Iyer Nirmal K., Mozsi K., Ryde F., Stana T.-A., Pearce M., Kislat F., 宮本明日香, 中庭望, 鈴木瞳, 武尾舞, Spooner S., 宮澤拓也, 武田朋志, 内山慶祐, 吉田勇登, Wulf E., 「硬 X 線偏光観測実験 XL-Calibur 気球実験計画」, 日本天文学会 2021 年春季年会, オンライン, 2021 年 3 月 16–19 日.

沼澤正樹 (口頭発表), 榎戸輝揚, 玉川徹, 北口貴雄, 加藤陽, 三原建弘, 内山慶祐, 武田朋志, 吉田勇登, 大田尚亨, 林昇輝, 佐藤宏樹, 岩切渉, 内山秀樹, Chin-Ping Hu, 高橋弘充, 小高裕和, 丹波翼, 「明るい X 線源の柔軟な観測を狙う超小型 X 線衛星 NinjaSat」, 日本天文学会 2021 年春季年会, オンライン, 2021 年 3 月 16–19 日.

武田朋志 (口頭発表), 玉川徹, 榎戸輝揚, 北口貴雄, 加藤陽, 沼澤正樹, 三原建弘, 岩切渉, 内山秀樹, 内山慶祐, 吉田勇登, 大田尚亨, 林昇輝, 佐藤宏樹, Chin-Ping Hu, 高橋弘充, 小高裕和, 丹波翼, 「超小型 X 線衛星 NinjaSat に搭載のガス X 線検出器の開発 (2)」, 日本天文学会 2021 年春季年会, オンライン, 2021 年 3 月 16–19 日.

吉田勇登 (口頭発表), 玉川徹, 榎戸輝揚, 北口貴雄, 加藤陽, 沼澤正樹, 三原建弘, 岩切渉, 内山秀樹, 内山慶祐, 武田朋志, 大田尚亨, 林昇輝, 佐藤宏樹, Chin-Ping Hu, 高橋弘充, 小高裕和, 丹波翼, 「超小型 X 線衛星 NinjaSat 搭載の高電圧印加/アナログ信号処理基板の開発 (2)」, 日本天文学会 2021 年春季年会, オンライン, 2021 年 3 月 16–19 日.

岩切渉 (口頭発表), 戸枝純哉, 芳野史弥, 井上諒太, 長谷川航平, 坪井陽子, 玉川徹, 榎戸輝揚, 北口貴雄, 加藤陽, 沼澤正樹, 三原建弘, 内山慶祐, 武田朋志, 吉田勇登, 大田尚亨, 林昇輝, 佐藤宏樹, 内山秀樹, Chin-Ping Hu, 高橋弘充, 小高裕和, 丹波翼, 「超小型 X 線衛星 NinjaSat に搭載する小型で軽量な X 線コリメーターの開発」, 日本天文学会 2021 年春季年会, オンライン, 2021 年 3 月 16–19 日.

佐々木亮 (口頭発表), 坪井陽子, 岩切渉, 岡本豊, 北古賀智紀, 河合広樹, 三原建弘, 根來均, 他 MAXI チーム, 「全天 X 線監視装置 MAXI を用いた巨大恒星フレアの統計的研究」, 日本天文学会 2021 年春季年会, オンライン, 2021 年 3 月 16–19 日.

根來均 (口頭発表), 中島基樹, 芹野素子, 三原建弘, 岩切渉, 安達稜, 河合誠之, 小川翔司, 中平聡志, 松岡勝 他 MAXI チーム, 「MAXI/GSC か検出した 2020 年度後半の突発現象—ミニアウトバーストの検出—」, 日本天文学会 2021 年春季年会, オンライン, 2021 年 3 月 16–19 日.

玉川徹 (口頭発表), 榎戸輝揚, 北口貴雄, 加藤陽, 沼澤正樹, 三原建弘, 武田朋志, 吉田勇登, 大田尚亨, 林昇輝, 内山慶祐, 岩切渉, 内山秀樹, 佐藤宏樹, Chin-Ping Hu, 高橋弘充, 小高裕和, 丹波翼, 「超小型 X 線天体観測衛星 NinjaSat」, 日本物理学会第 76 回年次大会, オンライン, 2021 年 3 月 12–15 日.

高橋弘充 (口頭発表), Quin Abarr, 朝倉一統, 粟木久光, Matthew G. Baring, Richard Bose, Dana Braun, Gianluigi de Geronimo, Paul Dowkontt, John Elliot, 榎戸輝揚, Manel Errando, 深沢泰司, 古澤彰浩, Thomas Gadson, Epharaim Gau, Victor Guarino, 郡司修一, 袴田知宏, Kenny Hall, 花岡真帆, Keon Harmon, 服部憲吾, 林田清, L, Scott Heatwole, Arman Hossen, 井出峻太郎, 今里郁弥, 今澤遼, 石橋和紀, 石田学, 石倉彩美, Nirmal Kumar Iyer, Fabian Kislat, Mozsi Kiss, 鴨川航, 北口貴雄, David Kotsifakis, Henric Krawczynski, James Lanzi, Lindsey Lisalda, 前田良知, 松下友亮, 眞武寛人, 松本浩典, 峯田大晴, 宮本明日香, 宮澤拓也, 水野恒史, 中庭望, 野田博文, 大出優一, 岡島崇, 岡崎貴樹, Izabella Pastrani, Mark Pearce, N, Zachary Peterson, Helen Poon, Chris Purdy, Brian Rauch, Felix Ryde, 斎藤芳隆, 佐久間翔太郎, 澤上拳明, Chris Shreeves, Garry Simburger, Carl Snow, Sean Spooner, Theodor-Adrian Stana, David Stuchlik, 鈴木瞳, 武田朋志, 武尾舞, 玉川徹, 田村啓輔, 常深博, 内田和海, 内田悠介, 内山慶祐, Brett Vincent, Andrew West, Eric Wulf, 山本龍哉, 楊冲, 米山友景, 吉田勇登, 善本真梨那, XL-Calibur チーム, 「硬 X 線偏光観測実験 XL-Calibur 気球実験計画の 2022 年フライトへ向けた準備状況」, 日本物理学会第 76 回年次大会, オンライン, 2021 年 3 月 12–15 日.

郡司修一 (口頭発表), 寺島政伸, 渡邉瑛里, 斎藤耀, 水野恒史, 内田和海, 山本龍哉, 深沢泰司, 高橋弘充, 玉川徹, 北口貴雄, 榎戸輝揚, 内山慶祐, 三石郁之, 山口友洋, 柏倉一斗, 田原譲, 林田清, 朝倉一統, 岩切渉, Martin Weisskopf, Brian Ramsey, Stephen O'Dell, Paolo Soffitta, Luca Baldini ほか IXPE 衛星チーム, 「X 線偏光衛星 IXPE の開発の現状」, 日本物理学会第 76 回年次大会, オンラ

イン, 2021 年 3 月 12–15 日.

寺島政伸 (口頭発表), 郡司修一, 渡邉瑛里, 斎藤耀, 水野恒史, 内田和海, 山本龍哉, 深沢泰司, 高橋弘充, 玉川徹, 北口貴雄, 榎戸輝揚, 内山慶祐, 三石郁之, 山口友洋, 柏倉一斗, 田原譲, 林田清, 朝倉一統, 岩切渉, Martin Weisskopf, Brian Ramsey, Stephen O'Dell, Paolo Soffitta, Luca Baldini ほか IXPE 衛星チーム, 「IXPE 衛星による GRB afterglow の偏光観測シミュレーション」, 日本物理学会第 76 回年次大会, オンライン, 2021 年 3 月 12–15 日.

山本あゆ美 (口頭発表), 坂本貴紀, 芹野素子, 李晋, 盛顯捷, 天谷友亮, 米徳大輔, 澤野達哉, 三原建弘, 三石郁之, 「X 線ビームラインを用いたロブスターアイ光学系の性能評価試験」, 日本物理学会第 76 回年次大会, オンライン, 2021 年 3 月 12–15 日.

米田浩基 (口頭発表), 高嶋聡, 小高裕和, 井上芳幸, 辻直美, 一戸悠人, Georgia Karagiorgi, Reshmi Mukherjee, Tsuguo Aramaki, Jonathan Asaadi, Kerstin Perez, GRAMS コラボレーション, 「GRAMS 実験 3: 全体報告・イベント再構成アルゴリズムの開発」, 日本物理学会第 76 回年次大会, オンライン, 2021 年 3 月 12–15 日.

高嶋聡 (口頭発表), 小高裕和, 馬場彩, 米田浩基, 木村眞人, 田中雅士, 寄田浩平, GRAMS コラボレーション, 「GRAMS 実験 4: 液体アルゴン検出器のエネルギー測定性能と宇宙線バックグラウンドの研究」, 日本物理学会第 76 回年次大会, オンライン, 2021 年 3 月 12–15 日.

石崎欣尚 (ポスター発表), Richard L. Kelley, 赤松弘規, 粟木久光, Thomas G. Bialas, Gregory V. Brown, Meng P. Chao, Elisa Costantini, Jan-Willem den Herder, Michael J. Dipirro, Megan E. Ekart, 江副祐一郎, Carlo Ferrigno, 藤本龍一, 古澤彰浩, Steven M. Graham, Martin Grim, 林多佳由, 堀内貴史, 星野晶夫, 一戸悠人, 飯塚亮, 石田学, 石川久美, Caroline A. Kilbourne, 北本俊二, Maurice A. Leutenegger, 三石郁之, 水本岬希, 森英之, 大橋隆哉, 岡島崇, Stephane Paltani, F. Scott Porter, 佐藤浩介, 澤田真理, 瀬田弘美, Peter J. Shirron, Gary J. Sneiderman, Yang Soong, Andrew E. Szymkowiak, 竹井洋, 玉川徹, 辻本匡弘, 内田悠介, Cor P. de Vries, 山田真也, 山崎典子, 安田進, 吉岡奈紗, 「X 線分光撮像衛星 (XRISM) 搭載 Resolve の開発状況」, 第 21 回宇宙科学シンポジウム, オンライン, 2021 年 1 月 6–7 日.

玉川徹,(ポスター発表) 北口貴雄, 榎戸輝揚, 内山慶祐, 三石郁之, 山口友洋, 柏倉一斗, 田原譲, 郡司修一, 渡邉瑛里, 寺島政伸, 斎藤耀, 深沢泰司, 水野恒史, 高橋弘充, 内田和海, 山本龍哉, 岩切渉, 林田清, 朝倉一統, Martin Weisskopf, Brian Ramsey, Stephen O'Dell, Paolo Soffitta, Luca Baldini ほか IXPE 衛星チーム, 「X 線偏光観測衛星 IXPE 開発の現状」, 第 21 回宇宙科学シンポジウム, オンライン, 2021 年 1 月 6–7 日.

三石郁之 (ポスター発表), 山口友洋, 柏倉一斗, 瀧川歩, 田村啓輔, 宮田喜久子, 田原譲, 玉川徹, 大西崇文, 立花一志, 立花正満, 村島健介, 「X 線偏光観測衛星 IXPE 搭載に向けた望遠鏡用サーマルシールドの開発 (2)」, 第 21 回宇宙科学シンポジウム, オンライン, 2021 年 1 月 6–7 日.

郡司修一 (ポスター発表), 寺島政伸, 渡邉瑛里, 斎藤耀, 水野恒史, 内田和海, 山本龍哉, 深沢泰司, 高橋弘充, 玉川徹, 北口貴雄, 榎戸輝揚, 内山慶祐, 三石郁之, 山口友洋, 柏倉一斗, 田原譲, 林田清, 朝倉一統, 岩切渉, Martin Weisskopf, Brian Ramsey, Stephen O'Dell, Paolo Soffitta, Luca Baldini ほか IXPE 衛星チーム, 「日本チームによる IXPE 衛星の偏光観測シミュレーションの現状」, 第 21 回宇宙科学シンポジウム, オンライン, 2021 年 1 月 6–7 日.

三原建弘 (ポスター発表), 根来均, 中平聡志ほか MAXI チーム, 「MAXI の現状」, 第 21 回宇宙科学シンポジウム, オンライン, 2021 年 1 月 6–7 日.

根来均 (ポスター発表), 中島基樹, 芹野素子, 三原建弘, 上野史郎, 冨田洋, 中平聡志, 菅原泰晴, 河合誠之, 吉田篤正, 坂本貴紀, 杉田聡司, 上田佳宏, 坪井陽子, 岩切渉, 山内誠, 山岡和貴, 川室太希, 志達めぐみ, 杉崎睦, 松岡勝, 「2020 年に MAXI が発見した新天体と突発現象」, 第 21 回宇宙科学シンポジウム, オンライン, 2021 年 1 月 6–7 日.

富永愛侑 (ポスター発表), 中平聡志, 志達めぐみ, 大枝幹, 海老沢研, 菅原泰晴, 根来均, 河合誠之, 杉崎睦, 上田佳宏, 三原建弘ほか MAXI チーム, 「ブラックホール X 線新星 MAXI J1348-630 の発見」, 第 21 回宇宙科学シンポジウム, オンライン, 2021 年 1 月 6–7 日.

三原建弘 (ポスター発表) (理研) ほか MAXI チーム, 「MAXI 後期運用 (3) 期間中 (2018-2020) の MAXI の成果: 論文, リンクと概説」, 第 21 回宇宙科学シンポジウム, オンライン, 2021 年 1 月 6–7 日.

米徳大輔 (口頭発表), 三原建弘, 土居明広, 坂本貴紀, 津村耕司, HiZ-GUNDAM WG, 「ガンマ線バーストを用いた初期宇宙・極限時空探査計画 HiZ-GUNDAM」, 第 21 回宇宙科学シンポジウム, オンライン, 2021 年 1 月 6–7 日.

李晋 (ポスター発表), 坂本貴紀, 芹野素子, 澤野達哉, 米徳大輔, 三石郁之, 三原建弘, 「ロブスターアイ光学系の地上試験及びシミュレータによる性能評価」, 第 21 回宇宙科学シンポジウム, オンライン, 2021 年 1 月 6–7 日.

荻野直樹 (ポスター発表), 有元誠, 澤野達哉, 米徳大輔, 平賀純子, 坂本貴紀, 盛顯捷, 谷津陽一, 「HiZ-GUNDAM に向けた CMOS イメージセンサの高速読み出しシステムの開発」, 第 21 回宇宙科学シンポジウム, オンライン, 2021 年 1 月 6–7 日.

澤野達哉 (ポスター発表),, 米徳大輔, 有元誠, 李晋, 三原建弘, 荻野直樹, 坂本貴紀, 芹野素子 「ロブスターアイ光学系による X 線突発天体検出アルゴリズムの研究」, 第 21 回宇宙科学シンポジウム, オンライン, 2021 年 1 月 6–7 日.

武田朋志 (口頭発表)(理科大/理研), 玉川徹, 榎戸輝揚, 北口貴雄, 加藤陽, 沼澤正樹, 三原建弘 (理研), 岩切渉 (中央大), 内山秀樹 (静岡大), 内山慶祐, 吉田勇登 (理科大/理研), 佐藤宏樹 (芝浦工大/理研), Chin-Ping Hu (京都大), 高橋弘充 (広島大), 小高裕和, 「超小型 X 線衛星 NinjaSat に搭載のガス X 線検出器の開発」, 日本天文学会 2020 年秋季年会, オンライン, 2020 年 9 月 8–10 日.

吉田勇登 (理科大/理研), 玉川徹, 榎戸輝揚, 北口貴雄, 加藤陽, 沼澤正樹, 三原建弘 (理研), 岩切渉 (中央大), 内山秀樹 (静岡大), 内山慶祐, 武田朋志 (理科大/理研), 佐藤宏樹 (芝浦工大/理研), Chin-Ping Hu(京都大), 高橋弘充 (広島大), 小高裕和 (東京大) 「超小型 X 線衛星 NinjaSat に搭載の高電圧印加・アナログ信号処理ボードの開発」, 日本天文学会 2020 年秋季年会, オンライン, 2020 年 9 月 8–10 日.

佐藤宏樹 (芝浦工大/理研), 玉川徹, 榎戸輝揚, 北口貴雄, 加藤陽, 沼澤正樹, 三原建弘 (理研), 岩切渉 (中央大), 内山秀樹 (静岡大), 内山慶祐, 武田朋志, 吉田勇登 (理科大/理研), Chin-Ping Hu (京都大), 高橋弘充 (広島大), 小高裕和 (東大) 「超小型 X 線衛星 Ninjasat に搭載の X 線背景放射減衰シールドの最適化」, 日本天文学会 2020 年秋季年会, オンライン, 2020 年 9 月 8–10 日.

畠内康輔, 春日知明, 丹波翼, 高嶋聡, 鈴木寛大, 渡邊泰平, 南木宙斗, 谷本敦, 小高裕和, 馬場彩 (東大), 周圓輝 (理科大/理研), 玉川徹 (理研), 長澤俊作, 峰海里, 高橋忠幸 (東大 Kavli IPMU), 成影典之 (国立天文台), 佐久間翔太郎, 朝倉一統, 林田清 (阪大) 「CMOS イメージセンサを用いた硬 X 線撮像偏光計の開発 III」, 日本天文学会 2020 年秋季年会, オンライン, 2020 年 9 月 8–10 日.

高橋弘充, 内田和海, 内田悠介, 深沢泰司, 水野恒史 (広島大学), 林田清, 松本浩典, 常深博 (大阪大学), 前田良知, 石田学, 斎藤芳隆 (宇宙科学研究所), 宮澤拓也 (沖縄科学技術大学院大学), 粟木久光 (愛媛大学), 石橋和紀 (名古屋大学), 北口貴雄, 玉川徹, 榎戸輝揚 (理化学研究所), 内山慶祐, 武田朋志, 吉田勇登 (東京理科大学), 郡司修一 (山形大学), Henric Krawczynski(ワシントン大学), Fabian Kislat(ニューハンプシャー大学), 岡島崇, 田村啓輔, 林多佳由 (NASA), Mark Pearce(スウェーデン王立工科大学), XL-Calibur チーム「硬 X 線偏光観測実験 XL-Calibur 気球の 2022 年フライトへ向けた準備状況」, 日本天文学会 2020 年秋季年会, オンライン, 2020 年 9 月 8–10 日.

山本龍哉, 水野恒史, 深沢泰司, 高橋弘充, 内田和海 (広島大), 玉川徹, 北口貴雄, 榎戸輝揚 (理研), 三石郁之, 山口友洋, 柏倉一斗, 田原譲 (名古屋大), 郡司修一, 渡邊瑛理, 寺島政伸, 斎藤耀 (山形大), 林田清, 朝倉一統 (大阪大), 内山慶祐 (東理大/理研), 岩切渉 (中央大), Martin Weisskopf, Brian Ramsey, Stephen O 'Dell(NASA/MSFC), Paolo Soffitta(IAPS), Luca Baldini(INFN), 他 IXPE チーム「シミュレーションを用いた IXPE 衛星による広がった天体の軟 X 線偏光解析手法の研究」, 日本天文学会 2020 年秋季年会, オンライン, 2020 年 9 月 8–10 日.

山口友洋, 瀧川歩, 柏倉一斗, 三石郁之, 田原譲, 大西崇文, 立花一志 (名古屋大学), 宮田喜久子 (名城大学), 田村啓輔 (NASA/GSFC, UMBC), 玉川徹 (理研), 立花正満, 村島健介 (株式会社カネカ) 「X 線偏光観測衛星 IXPE 搭載 X 線望遠鏡用受動型熱制御素子サーマルシールドの開発 (7)」, 日本天文学会 2020 年秋季年会, オンライン, 2020 年 9 月 8–10 日.

小高裕和, 高嶋聡 (東京大学), 井上芳幸, 米田浩基, 辻直美 (理研), 一戸悠人 (立教大学), Georgia Kara- giorgi, Reshmi Mukherjee (Columbia 大学), Tsuguo Aramaki (Northeastern 大学/SLAC), GRAMS コラボレーション「GRAMS 計画 1: MeV ガンマ線観測・ダーククマター探索気球実験」, 日本天文学会 2020 年秋季年会, オンライン, 2020 年 9 月 8–10 日.

根來均, 中島基樹, 青木真凜 (日大), 三原建弘, 松岡勝 (理研), 岩切渉, 北古賀智紀, 岡本豊 (中央大), 志達めぐみ (愛媛大), 菅原泰晴 (JAXA), 庭野聖史, 河合誠之 (東工大) 他 MAXI チーム「MAXI/GSC が検出した 2020 年度前半の突発現象: X 線連星系の短期長期活動と増光する矮新星 SS Cyg の検出」, 日本天文学会 2020 年秋季年会, オンライン, 2020 年 9 月 8–10 日.

米田浩基 (理研), 牧島一夫 (Kavli IPMU/東大理/理研), 榎戸輝揚 (理研), Dmitry Khangulyan(立教大), 峰海里 (東大理/Kavli IPMU), 水野恒史 (広島大), 高橋忠幸 (Kavli IPMU/東大理) 「ガンマ線連星 LS 5039 の, NuSTAR 衛星と Fermi 衛星を用いた広帯域スペクトル解析」, 日本天文学会 2020 年秋季年会, オンライン, 2020 年 9 月 8–10 日.

内田悠介 (口頭発表), Quin Abarr, 粟木久光, Richard Bose, Dana Braun, Gialuigi de Geronimo, Paul Dowkontt, 榎戸輝揚, Manel Errando, 深沢泰司, Tom Gadson, Victor Guarino, 郡司修一, Keon Harmon, 林田清, Scott Heatwole, 石田学, Fabian Kislat, Mozsi Kiss, 北口貴雄, Henric Krawczynski, Nirmal Kumar Iyer, Rakhee Kushwah, James Lanzi, Shaorui Li, Lindsey Lisalda, 前田良知, 松本浩典, 宮澤拓也, 水野恒史, 岡島崇, Mark Pearce, Zachary Peterson, Brian Rauch, Felix Ryde, 斎藤芳隆, Theodor-Adrian Stana, David Stuchlik, 高橋弘充, 武田朋志, 玉川徹, 田村啓輔, 常深博, 内田和海, 内山慶祐, Andrew West, Eric A. Wulf, 吉田勇登, XL-Calibur チーム, 「硬 X 線集光偏光系 XL-Calibur 気球実験の準備状況と 0.8 mm 厚 CZT 検出器の性能」, 日本物理学会 2020 年秋季大会, オンライン, 2020 年 9 月 14–17 日.

小高裕和 (口頭発表), 畠内康輔, 春日知明, 渡邊泰平, 丹波翼, 鈴木寛大, 高嶋聡, 南木宙斗, 谷本敦, 馬場彩, 周圓輝, 玉川徹, 長澤俊作, 峰海里, 高橋忠幸, 成影典之, 佐久間翔太郎, 朝倉一統, 林田清, 「CMOS イメージャを用いた X 線偏光撮像システムの開発 V: 開発と性能評価の現状」, 日本物理学会 2020 年秋季大会, オンライン, 2020 年 9 月 14–17 日.

米田浩基 (口頭発表), 牧島一夫, 榎戸輝揚, Dmitry Khangulyan, 峰海里, 水野恒史, 高橋忠幸, 「ガンマ線連星 LS 5039 の MeV ガンマ線放射の起源と, マグネター連星の可能性」, 日本物理学会 2020 年秋季大会, オンライン, 2020 年 9 月 14–17 日.

小高裕和 (口頭発表), 高嶋聡, 井上芳幸, 米田浩基, 辻直美, 一戸悠人, Georgia Karagiorgi, Reshmi Mukherjee, Tsuguo Aramaki, GRAMS コラボレーション, 「GRAMS 実験 1: MeV ガンマ線観測・ダークマター探索気球実験ミッション概要」, 日本物理学会 2020 年秋季大会, オンライン, 2020 年 9 月 14–17 日.

高嶋聡 (口頭発表), 小高裕和, 馬場彩, 米田浩基, 木村眞人, 田中雅士, 寄田浩平, GRAMS コラボレーション, 「GRAMS 実験 2: 液体アルゴン検出器における多重コンプトン散乱イベントの解析」, 日本物理学会 2020 年秋季大会, オンライン, 2020 年 9 月 14–17 日.

米田浩基, 「ガンマ線連星 LS 5039 の MeV ガンマ線放射と, マグネター連星系の可能性」, Pulsar Bi-Monthly Meeting, オンライン, 2020 年 12 月.

[Seminars]

米田浩基, 「ガンマ線連星 LS 5039 のマグネター連星系の可能性: 硬 X 線パルスの兆候と強い MeV ガンマ線放射」, 高エネルギー宇宙物理学研究会 2020, 東京大学宇宙線研, 2020 年 12 月.

Hiroki Yoneda, "Mystery of the strong MeV gamma-ray emission from gamma-ray binary systems—magnetic reconnection close to magnetars in binaries? —," 知の共有ゼミ, 理研, 2020 年 6 月.

Hiroki Yoneda, "The mystery of the MeV gamma-ray emission from gamma-ray binary systems," , ICRR Seminar, オンライン, 2020 年 12 月.

Outreach Activities

三原建弘ほか, 「ISS 20 年, 日本の挑戦の軌跡」, NHK コズミックフロントネクスト 2020 年 12 月 17 日放送.

Nuclear Science and Transmutation Research Division
Superheavy Element Research Group

1. Abstract

The elements with their atomic number $Z > 103$ are called as trans-actinide or superheavy elements. This group has been studying the physical and chemical properties of superheavy elements. They must be produced by artificially for the scientific study utilizing the accelerators in RIBF. Two teams lead the study of the superheavy elements. Superheavy Element Production Team studies various methods of efficient production of the superheavy elements and their physical and chemical properties. Superheavy Element Device Development Team develops the main experimental device, *i.e.*, the gas-filled recoil ion separator, GARIS.

The synthesis of elements having atomic numbers over 119 will be attempted with the aim of establishing nuclear synthesis technology that reaches the "island of stability" where the lifetime of atomic nuclei is expected be prolonged significantly. With the aim of constructing an ultimate nuclear model, maximum utilization will be made of key experimental devices which become fully operational in order to conduct research for the syntheses of element 119 and 120.

2. Major Research Subjects

Superheavy Element Production Team

(1) Searching for new elements
(2) Spectroscopic study of the nucleus of heavy elements
(3) Chemistry of superheavy elements
(4) Study of a reaction mechanism for fusion process Superheavy Element Device Development Team
(5) Maintenance of GARIS, GARIS-II and development of new gas-filled recoil ion separator GARIS-III
(6) Maintenance and development of detector and DAQ system for GARIS, GARIS-II and GARIS-III
(7) Maintenance and development of target system for GARIS, GARIS-II and GARIS-III

3. Summary of Research Activity

(1) Searching for new elements

To expand the periodic table of elements and the nuclear chart, we will search for new elements.

(2) Spectroscopic study of the nucleus of heavy elements

Using the high sensitivity system for detecting the heaviest element, we plan to perform a spectroscopic study of nuclei of the heavy elements.

(3) Chemistry of superheavy elements

Study of chemistry of the trans-actinide (superheavy element) has just started world-wide, making it a new frontier in the field of chemistry. Relativistic effects in chemical property are predicted by many theoretical studies. We will try to develop this new field.

(4) Study of a reaction mechanism for fusion process

Superheavy elements have been produced by complete fusion reaction of two heavy nuclei. However, the reaction mechanism of the fusion process is still not well understood theoretically. When we design an experiment to synthesize nuclei of the superheavy elements, we need to determine a beam-target combination and the most appropriate reaction energy. This is when the theory becomes important. We will try to develop a reaction theory useful in designing an experiment by collaborating with the theorists.

(5) Research highlight

The discovery of a new element is one of the exciting topics both for nuclear physicists and nuclear chemists. The elements with their atomic number $Z > 103$ are called as trans-actinides or superheavy elements. The chemical properties of those elements have not yet been studied in detail. Since those elements do not exist in nature, they must be produced by artificially, by using nuclear reactions for the study of those elements. Because the production rate of atoms of those elements is extremely small, an efficient production and collection are key issues of the superheavy research. In our laboratory, we have been trying to produce new elements, studying the physical and chemical properties of the superheavy elements utilizing the accelerators in RIKEN.

Although the Research Group for Superheavy element has started at April 2013, the Group is a renewal of the Superheay Element Laboratory started at April 2006, based on a research group which belonged to the RIKEN accelerator research facility (RARF), and had studied the productions of the heaviest elements. The main experimental apparatus is a gas-filled recoil ion separator GARIS. The heaviest elements with their atomic numbers, 107 (Bohrium), 108 (Hassium), 109 (Meitnerium), 110 (Darmstadtium), 111 (Roentogenium), and 112 (Copernicium) were discovered as new elements at Helmholtzzentrum fur Schwerionenforschung GmbH (GSI), Germany by using ^{208}Pb or ^{209}Bi based complete fusion reactions, so called "cold fusion" reactions. We have made independent confirmations of the productions of isotopes of 108th, 110th, 111th, and 112th elements by using the same reactions performed at GSI. After these work, we observed an isotope of the 113th element, ^{278}113, in July 2004, in April, 2005, and in August 2012. The isotope, ^{278}113, has both the largest atomic number, ($Z = 113$) and atomic mass number ($A = 278$) which have determined experimentally among the isotopes which have been produced by cold fusion reactions. We could show the world highest sensitivity for production and detection of the superheavy elements by these observations. Our results that related to ^{278}113 has been recognized as a discovery of new element by a Joint Working Party of the International Union of Pure and Applied Chemistry (IUPAC) and International Union

of Pure and Applied Physics (IUPAP). Finally, we named the 113th element as "Nihonium."

We decided to make one more recoil separator GARIS-II, which has an acceptance twice as large as existing GARIS, in order to realize higher sensitivity. The design of GARIS-II has finished in 2008. All fabrication of the separator will be finished at the end of fiscal year 2008. It has been ready for operation after some commissioning works.

Preparatory work for the study of the chemical properties of the superheavy elements has started by using the gas-jet transport system coupled to GARIS. The experiment was quite successful. The background radioactivity of unwanted reaction products has been highly suppressed. Without using the recoil separator upstream the gas-jet transport system, large amount of unwanted radioactivity strongly prevents the unique identification of the event of our interest. This new technique makes clean and clear studies of chemistry of the heaviest elements promising.

The spectroscopic study of the heaviest elements has started by using alpha spectrometry. New isotope, ^{263}Hs (Z = 108), which has the smallest atomic mass number ever observed among the Hassium isotopes, had discovered in the study. New spectroscopic information for ^{264}Hs and its daughters have obtained also. The spectroscopic study of Rutherfordium isotope ^{261}Rf (Z = 104) has done and 1.9-s isomeric state has directly produced for the first time.

Preparatory works for the study of the new superheavy elements with atomic number 119 and 120 have started in 2013. We measured the reaction products of the ^{248}Cm (^{48}Ca, xn)$^{296-x}$Lv (Z = 116) previously studied by Frelov Laboratory of Nuclear Reaction, Russia, and GSI. We observed 5 isotopes in total which tentatively assigned to ^{293}Lv, and ^{292}Lv.

Member

Director

Kosuke MORITA

Nuclear Science and Transmutation Research Division
Superheavy Element Research Group
Superheavy Element Production Team

1. Abstract

The elements with atomic number $Z \geq 104$ are called as trans-actinide or superheavy elements (SHEs). Superheavy Element Production Team investigates synthesis mechanisms of SHEs, nuclear properties of SHE nuclei, and chemical properties of SHEs mainly in collaboration with Superheavy Element Devise Development Team and Nuclear Chemistry Research Team of RIKEN Nishina Center.

2. Major Research Subjects

(1) Search for new superheavy elements
(2) Decay spectroscopy of the heaviest nuclei
(3) Study of reaction mechanisms for production of the heaviest nuclei
(4) Study of chemical properties of the heaviest elements

3. Summary of Research Activity

(1) Search for new superheavy elements

In November, 2016, the 7th period of the periodic table was completed with the official approval of four new elements, nihonium (Nh, atomic number $Z = 113$), moscovium (Mc, $Z = 115$), tennessine (Ts, $Z = 117$), and oganesson (Og, $Z = 118$) by International Union of Pure and Applied Chemistry. We have started to search for new elements to expand the chart of the nuclides toward to the island of stability and the periodic table of the elements toward the 8th period. In January, 2020, RIKEN heavy-ion Linear ACcelerator (RILAC) was upgraded as Superconducting RIKEN heavy-ion Linear ACcelerator (SRILAC). We developed the new gas-filled recoil ion separator GARIS III on the beam line of SRILAC. In June and July, 2020, we conducted the commissioning of the SRILAC + GARIS III setup in the ^{169}Tm + ^{40}Ar, ^{208}Pb + ^{40}Ar, and ^{208}Pb + ^{51}V reactions. Then, we started to search for new element, element 119 in the ^{248}Cm + ^{51}V reaction in October, 2020.

(2) Decay spectroscopy of the heaviest nuclei

In collaboration with KEK, we developed a multi-refection time-of-fight mass spectrograph (MRTOF-MS) equipped with an α-TOF detector on the focal plane of GARIS-II at RRC for decay-correlated mass measurements of low-yield and short-lived SHE isotopes. By correlating measured time-of-flight signals with decay events, it can suppress background events and obtain accurate, high-precision mass and half-life values even in cases of very low event rates. The performance of the system was investigated using the Ra isotopes produced in the ^{159}Tb + ^{51}V reaction.

(3) Study of reaction mechanisms for production of the heaviest nuclei

SHE nuclei have been produced by complete fusion reactions of two heavy nuclei. However, the reaction mechanism of the fusion process is still not well understood both theoretically and experimentally. We measured excitation functions for the quasielastic scattering of the ^{248}Cm + ^{51}V reaction using GARIS III at SRILAC. The result can be utilized to estimate the optimal incident beam energy for production of isotopes of new element 119.

(4) Study of chemical properties of the heaviest elements

Chemical characterization of newly-discovered SHEs is an extremely interesting and challenging subject in modern nuclear and radiochemistry. In collaboration with Nuclear Chemistry Research Team of RIKEN Nishina Center, we are developing SHE production systems as well as rapid single-atom chemistry apparatuses for chemistry studies of SHEs. We installed a gas-jet transport system to the focal plane of GARIS at RILAC. This system is a promising approach for exploring new frontiers in SHE chemistry: the background radiations from unwanted products are strongly suppressed, the intense primary heavy-ion beam is absent in the gas-jet chamber, and hence the high gas-jet extraction yield is attained. Furthermore, the beam-free conditions make it possible to investigate new chemical systems. In 2020, we continued to develop an ultra-rapid gas-chromatograph apparatus at the focal plane of GARIS for the gas chemistry of SHEs. This apparatus consists of an RF carpet gas cell and a cryo-gas-chromatograph column with a Si detector array. For the aqueous chemistry, we developed a flow solvent extraction apparatus which consisted of a continuous dissolution apparatus Membrane DeGasser (MDG), a Flow Solvent Extractor (FSE), and a liquid scintillation detector for α/SF-spectrometry.

Members

Team Leader
Hiromitsu HABA

Research & Development Scientist
Daiya KAJI

Special Postdoctoral Researcher
Tomohiro HAYAMIZU

Visiting Scientists
Marc ASFARI (Inst. Pluridisciplinaire Hubert Curien / Strasbourg Univ.)
Mahananda DASGUPTA (Australian Nat'l Univ.)
Olivier DORVAUX (Strasbourg Univ.)
Benoit Jean-Paul GALL (Strasbourg Univ. / Inst. Pluridisciplinaire Hubert Curien)
Zaiguo GAN (Chinese Academy of Sci.)
Shintaro GO (Kyushu Univ.)
David HINDE (The Australian Nat'l Univ.)
Minghui HUANG (IMP, CAS)
Hiroyuki KOURA (JAEA)
Daisuke NAGAE (Kyushu Univ.)
Satoshi SAKAGUCHI (Kyushu Univ.)
Mirei TAKEYAMA (Yamagata Univ.)
Masaomi TANAKA (Kyushu Univ.)
Taiki TANAKA (The Australian Nat'l Univ.)
Huabin YANG (IMP, CAS)
Zhiyuan ZHANG (IMP, CAS)

Student Trainees
Masato HIGASHI (Kyushu Univ.)
Tamito KAI (Kyushu Univ.)
Kieran KESSACI (IPHC Strasbourg/Strasbourg Univ.)
Ikuto MURAKAMI (Kyushu Univ.)
Taiga MUTO (Kyushu Univ.)
Yuto NAGATA (Kyushu Univ.)
Natsuki NAITO (Kyushu Univ.)
Mako OSADA (Kyushu Univ.)
Taro TOMIMATSU (Kyushu Univ.)

List of Publications & Presentations

Publications

[Original Papers]

H. Haba, F. Fan, D. Kaji, Y. Kasamatsu, H. Kikunaga, Y. Komori, N. Kondo, H. Kudo, K. Morimoto, K. Morita, M. Murakami, K. Nishio, J. P. Omtvedt, K. Ooe, Z. Qin, D. Sato, N. Sato, T. K. Sato, Y. Shigekawa, A. Shinohara, M. Takeyama, T. Tanaka, A. Toyoshima, K. Tsukada, Y. Wakabayashi, Y. Wang, S. Wulff, S. Yamaki, S. Yano, Y. Yasuda, and T. Yokokita, "Production of ^{266}Bh in the ^{248}Cm(^{23}Na, 5n)^{266}Bh reaction and its decay properties," Phys. Rev. C **102**, 024625 (2020).

Y. Kasamatsu, K. Toyomura, H. Haba, T. Yokokita, Y. Shigekawa, A. Kino, Y. Yasuda, Y. Komori, J. Kanaya, M. Huang, M. Murakami, H. Kikunaga, E. Watanabe, T. Yoshimura, K. Morita, T. Mitsugashira, K. Takamiya, T. Ohtsuki, and A. Shinohara, "Co-precipitation behaviour of single atoms of rutherfordium in basic solutions," Nat. Chem. **13**, 226 (2021).

[Review Articles]

羽場宏光, 「元素周期表の新時代 119 番以降の新元素を求めて」, 現代化学 9 月号, No. 594, 43 (2020).

羽場宏光, 「スタニズラオ・カニッツァーロ」, 和光純薬時報, Vol. 88, No. 4, 28 (2020). Vol. 27, pp. 11–14 (2020).

[Proceedings]

T. Niwase, K. Fujita, Y. Yamano, K. Watanabe, D. Kaji, K. Morimoto, H. Haba, T. Hirano, S. Mitsuoka, and K. Morita, "Measurement of fusion barrier distribution in ^{51}V+^{208}Pb system," Proc. 13th Int. Conf. on Nucleus-Nucleus Collisions, JPS Conf. Proc. **32**, 010022 (2020).

Y. Sakemi, T. Aoki, R. Calabrese, H. Haba, K. Harada, T. Hayamizu, Y. Ichikawa, K. Jungmann, A. Kastberg, Y. Kotaka, Y. Matsuda, Y. Matsuo, H. Nagahama, K. Nakamura, M. Otsuka, N. Ozawa, K. Tanaka, A. Uchiyama, H. Ueno, and L. Willmann, "Fundamental physics with cold radioactive atoms," Proc. 14th Asia-Pacific Phys. Conf., AIP Conf. Proc. 2319, 080020 (2021).

Presentations

[International Conferences/Workshops]

H. Haba (invited), "Production and applications of radioisotopes at RIKEN RI beam factory—Search for new elements through diagnosis and therapy of cancer—," Symposium on Nuclear Data 2020, Wako, Japan, November 26–27, 2020.

Y. Komori (poster), H. Haba, M. Aikawa, M. Saito, S. Takács, and F. Ditrói, "Production cross sections of ^{175}Hf in the ^{nat}Lu(p,xn) and ^{nat}Lu(d,xn) reactions," Symposium on Nuclear Data 2020, Wako, Japan, November 26–27, 2020.

T. Hayamizu (oral), H. Haba, K. Nakamura, T. Aoki, H. Nagahama, K. Tanaka, N. Ozawa, M. Ohtsuka, and Y. Sakemi, "Development of ultracold francium atomic sources towards the permanent EDM search," Yamada Conference LXXII: The 8th Asia-Pacific Conference on Few-Body Problems in Physics (APFB2020), Kanazawa, Japan, March 1–5, 2021.

[Domestic Conferences/Workshops]

羽場宏光 (招待講演), 「ラジオアイソトープの製造と応用～新元素の探索からがん治療まで～」, 第 17 回日本加速器学会年会, オンライン, 2020 年 9 月 2–4 日.

寺西翔 (口頭発表), 森田涼雅, 早川優太, 坂口綾, 中島朗久, 小森有希子, 横北卓也, 森大輝, 羽場宏光, 横山明彦, 「^{232}Th+^{7}Li 反応の Np 合成系における不完全融合反応の影響」, 日本放射化学会第 64 回討論会 (2020), オンライン, 2020 年 9 月 9–11 日.

森田涼雅 (口頭発表), 寺西翔, 早川優太, 坂口綾, 中島朗久, 小森有希子, 横北卓也, 森大輝, 羽場宏光, 横山明彦 , 「^{232}Th+^{7}Li 反応における反跳率補正による核分裂断面積測定法の確立」, 日本放射化学会第 64 回討論会 (2020), オンライン, 2020 年 9 月 9–11 日.

庭瀬暁隆 (口頭発表), P. Schury, 和田道治, P. Brionnet, S. Chen, 橋本尚志, 羽場宏光, 平山賀一, D. S. Hou, 飯村俊, 石山博恒, 石澤倫, 伊藤由太, 加治大哉, 木村創大, 小浦寛之, J. J. Liu, 宮武宇也, J. Y. Moon, 森本幸司, 森田浩介, 長江大輔, M. Rosenbusch, 高峰愛子, 渡辺裕, H. Wollnik, W. Xian, S. X. Yan, 「MRTOF+α-TOF による ^{257}Db の直接質量測定」, 日本放射化学会第 64 回討論会 (2020), オンライン, 2020 年 9 月 9–11 日.

重河優大 (口頭発表), 山口敦史, 佐藤望, 高峰愛子, 和田道治, 羽場宏光, 「核化学研究用高周波イオン収集システムの開発」, 日本放射化学会第 64 回討論会 (2020), オンライン, 2020 年 9 月 9–11 日.

加藤瑞穂 (口頭発表), 安達サディア, 豊嶋厚史, 塚田和明, 浅井雅人, 羽場宏光, 横北卓也, 小森有希子, 重河優大, Yang Wang, 森大輝, 柏原歩那, 床井健運, 中島朗久, 鈴木雄介, 西塚魁人, 末木啓介, 「HF/HNO_3 系における Db の陰イオン交換挙動」, 日本放射化学会第 64 回討論会 (2020), オンライン, 2020 年 9 月 9–11 日.

横北卓也 (口頭発表), 笠松良崇, 渡邉瑛介, 小森有希子, 重河優大, 森大輝, 王洋, 二宮秀美, 速水翔, 東内克馬, ゴーシュコースタブ, 篠原厚, 羽場宏光, 「硫酸系における Rf の陰イオン交換: 分配係数の硫酸濃度依存性」, 日本放射化学会第 64 回討論会 (2020), オンライン, 2020 年 9 月 9–11 日.

小森有希子 (ポスター発表), 羽場宏光, 「Calix[4]arene-bis(benzocrown-6) を用いた Fr と Cs の溶媒抽出」, 日本放射化学会第 64 回討論会 (2020), オンライン, 2020 年 9 月 9–11 日.

小森有希子 (ポスター発表), 羽場宏光, 合川正幸, 斎藤萌美, Sándor Takács, Ferenc Ditrói, 「^{nat}Lu(p,xn) および ^{nat}Lu(d,xn) 反応による ^{175}Hf の生成断面積の測定」, 日本放射化学会第 64 回討論会 (2020), オンライン, 2020 年 9 月 9–11 日.

渡邉瑛介 (ポスター発表), 笠松良崇, 横北卓也, 速水翔, 東内克馬, 重河優大, 羽場宏光, 篠原厚, 「Rf の化学研究に向けた ^{89m}Zr の硝酸系でのオンライン陰イオン交換実験」, 日本放射化学会第 64 回討論会 (2020), オンライン, 2020 年 9 月 9–11 日.

小澤直也 (口頭発表), 長濱弘季, 早水友洋, 中村圭佑, 佐藤幹, 永瀬慎太郎, 小高康照, 鎌倉恵太, 田中香津生, 大塚未来, 青木貴稔, 市川雄一, 高峰愛子, 羽場宏光, 上野秀樹, 酒見泰寛, 「フランシウム原子の電気双極子能率探索のための表面電離イオン源の開発」, 日本物理学会第 76 回年次大会（2021 年）, オンライン, 2021 年 3 月 12–15 日.

[Seminars]

早水友洋, Emily Altiere, Eric R. Miller, David J. Jones, Kirk W. Madison, 百瀬孝昌, 「キセノンの $5p^5 6p \leftarrow 5p^6$ 遷移の高分解能 2 光子分光」, 第 6 回精密計測を元に科学技術に変革をもたらす回路技術調査専門委員会, オンライン, 2021 年 3 月 23 日.

Press Releases

原子 1 つの沈殿を調べる! —超重元素ラザホージウムの共沈挙動の実験的観測—, 理化学研究所, 2021 年 2 月 18 日. https://www.riken.jp/press/2021/20210218_1.

Outreach Activities

羽場宏光, 「原子の仕組みとラジオアイソトープの応用〜新元素の探索からがんの治療まで〜」, 令和 2 年度（2020 年度）八王子市生涯学習センター主催市民自由講座, 八王子, 2021 年 3 月 9 日.

Nuclear Science and Transmutation Research Division
Superheavy Element Research Group
Superheavy Element Device Development Team

1. Abstract

A gas-filled recoil ion separator has been used as a main experimental device for the study of superheavy elements. This team is in charge of maintaining, improving, developing, and operating the separators and related devices. In the RIBF facility, three gas-filled recoil ion separators are installed at RILAC and RRC facility. One is GARIS that is designed for a symmetric reaction such as coldfusion reaction, and the other two are developed for an asymmetric reaction such as hot-fusion reaction, GARIS-II and GARIS-III. New elements ^{278}113 were produced by ^{70}Zn + ^{209}Bi reaction using GARIS. Further the new element search is currently in progress by using GARIS-II and GARIS-III.

2. Major Research Subjects

(1) Maintenance of GARIS, GARIS-II and development of new separator GARIS-III
(2) Maintenance and development of detector and DAQ system for superheavy element research
(3) Maintenance and development of target system for GARIS, GARIS-II and GARIS-III

3. Summary of Research Activity

The GARIS-II and III are newly developed which has an acceptance twice as large as existing GARIS, in order to realize higher transmission. A new element search program aiming to element 119 was started using GARIS-II. And new separator GARIS-III was developed and installed into the RILAC experimental hall. After the some commissioning works of GARIS-III, new 119th element search has been started. We will also offer user-support if a researcher wishes to use the devices for his/her own research program.

Members

Team Leader

Kouji MORIMOTO

Research/Technical Scientists

Masaki FUJIMAKI (Senior Technical Scientist)
Daiya KAJI (Technical Scientist)

Postdoctoral Researcher

Pierre BRIONNET

Postdoctoral Researcher

Sota KIMURA

Junior Research Associate

Toshitaka NIWASE

Visiting Scientists

Shin-ichi GOTO (Niigata Univ.)
Eiji IDEGUCHI (Osaka Univ.)
Yuta ITO (JAEA)
Katsuhisa NISHIO (JAEA)
Fuyuki TOKANAI (Yamagata Univ.)

Student Trainees

Satoshi ISHIZAWA (Yamagata Univ.)
Yoshiki TAKAHASHI (Niigata Univ.)
Hiroki TSUNODA (Niigata Univ.)

List of Publications & Presentations

Publications

[Original Papers]

S. Hofmann, S. N. Dmitriev, C. Fahlander, J. M. Gates, J. B. Roberto, and H. Sakai, "On the discovery of new elements (IUPAC/IUPAP Report), —Report of the 2017 Joint Working Group of IUPAC and IUPAP—," Pure Appl. Chem. **92**, 1387 (2020).

[Review Articles]

庭瀬暁隆, 「MRTOF+α-TOF による ^{257}Db の直接質量測定」, 放射化学 **43**, 31 (2021 年 3 月).

Presentations

[International Conferences/Workshops]

K. Morimoto (oral), "Present status and plans of GARIS, GARIS-II and GARIS-III," SSRI-PNS Collaboration Meeting 2020, online, September 3, 2020.

[Domestic Conferences/Workshops]

庭瀬暁隆 (口頭), P. Schury, 和田道治, P. Brionnet, S. Chen, 橋本尚志, 羽場宏光, 平山賀一, D. S. Hou, 飯村俊, 石山博恒, 石澤倫, 伊藤由太, 加治大哉, 木村創大, 小浦寛之, J. Liu, 宮武宇也, J. Y. Moon, 森田浩介, 森本幸司, 長江大輔, M. Rosenbusch, 高峰愛子, 渡辺裕, W. Xian, S. X. Yan, H. Wollnik, 「MRTOF + α-TOF による ^{257}Db の直接質量測定」, 日本放射化学会第 64 回討論会 (2020), オンライン, 2020 年 9 月 9 日–11 日.

庭瀬暁隆 (口頭), 「MRTOF + α-TOF 検出器による（超）重核の精密質量と α 崩壊の相関測定」, 2020 重元素核化学ワークショップ, オンライン, 2021 年 3 月 30 日.

Awards

庭瀬暁隆, 若手優秀発表賞, 日本放射化学会第 64 回討論会 (2020), 令和 2 年度 理研桜舞賞, 理化学研究所.

Others

石澤 倫, 「超重元素探索に用いられる TOF 検出器の検出率向上に関する研究」, 山形大学大学院理工学研究科博士学位論文 (2021).

Toshitaka Niwase, "First direct mass measurement of superheavy nuclide via MRTOF mass spectrograph equipped with an α-TOF detector," Department of Physics, Kyushu University, Doctoral Thesis (2021).

内藤夏樹, 「後方準弾性散乱測定による ^{51}V + ^{248}Cm/^{208}Pb 系の融合障壁分布の 研究」, 九州大学大学院理学研究院修士論文 (2021).

Nuclear Science and Transmutation Research Division
Astro-Glaciology Research Group

1. Summary of Research Activities

Our Astro-Glaciology Research Group promotes both experimental and theoretical studies to open up the new interdisciplinary research field of astro-glaciology, which combines astrophysics, astrochemistry, glaciology, and climate science.

On the experimental side, we measure isotopic and ionic concentrations in ice cores drilled at Dome Fuji station, Antarctica, in collaboration with the National Institute of Polar Research (NIPR, Tokyo). Here, the ice cores are time capsules which preserve atmospheric information of the past. In particular, the ice cores obtained around the Dome Fuji site are very unique, because they contain much more information on the stratosphere than any other ice cores obtained from elsewhere on Earth. This means that we have significant advantages in using Dome Fuji ice cores if we wish to study the Universe, since UV photons, gamma-rays, and highenergy protons emitted by astronomical phenomena affect the stratosphere. Our principal aim is thus to acquire and interpret information preserved in ice cores regarding:

- Signatures of past volcanic eruptions and solar cycles;
- Relationships between climate change and volcanic activity, and climate change and solar activity as well;
- Traces of past supernovae in our galaxy, in order to understand better the rate of galactic supernova explosions.

Moreover, we are promoting experimental projects on:

- Development of an automated laser melting sampler for analyzing ice cores with high depth resolution;
- Development of precise analytical techniques of high sensitivity for analyzing ice cores;
- The evolution of molecules in space.
- The application of analytical methods for measuring isotopes in ice cores to archaeological artifacts;

On the theoretical side, we are simulating numerically:

- Chemical effects of giant solar flares and supernovae on the Earth's atmosphere;
- The explosive and the r-process nucleosynthesis in core-collapse supernovae.

Combining our experimental evidence and theoretical simulations, we are promoting the researches mentioned above. These all will contribute to understanding relationships between the Universe and Earth. In particular, climate change is the most critical issue facing the world in the 21st century. It is also emphasized that the frequency of supernova explosions in our galaxy has not yet been fully understood, and it is the key to understand the r-process nucleosynthesis.

Members

Director
Yuko MOTIZUKI

Special Temporary Research Scientist
Kazuya TAKAHASHI

Senior Research Scientist
Yoichi NAKAI

Technical Staff I
Yu Vin SAHOO

Senior Visiting Scientists
Yasushige YANO
Kunihiko KODERA

Visiting Scientists
Hideharu AKIYOSHI (Nat'l Inst. for Environmental Studies)
Hisashi HAYAKAWA (Nagoya Univ.)
Akira HORI (Kitami Inst. of Tech.)
Kazuho HORIUCHI (Hirosaki Univ.)
Yoshinori IIZUKA (Hokkaido Univ.)
Naoyuki KURITA (Nagoya Univ.)
Hideki MADOKORO (Mitsubushi Heavy Industries, Ltd.)
Hideaki MOTOYAMA (Nat'l Inst. of Polar Res.)

Visiting Technicians
Junya HIROSE (Fusion Tech. Co., Ltd.)
Yuma HASEBE (Denryoku Comp. Ctr., Ltd.)

Assistant
Keiko SUZUKI

Part-time Workers

Satomi NEGISHI (Research Part-time Worker I) Kanako FUJITA (Administrative Part-time Worker I)

List of Publications & Presentations

Publications

[Original Papers]

S. Katsuda, H. Fujiwara, Y. Ishisaki, Y. Maeda, K. Mori, Y. Motizuki, K. Sato, M. S. Tashiro, and Y. Terada, "New measurement of the vertical atmospheric density profile from occultations of the crab nebula with X-Ray astronomy satellites Suzaku and Hitomi," J. Geophys. Res. (Space Physics) **126**, (4) e28886, doi:10.1029/2020JA028886 (2021).

E. Tsantini, T. Minami, M. A. C. Ontiveros, K. Takahashi, and J. C. Melgarejo, "Sulfur isotope analysis to examine the provenance of cinnabar used in wall paintings in the Roman domus Avinyó (Barcelona)," Minerals **11**, (1) 6 (2021).

K. Kitajima, Y. Nakai, W. M. C. Sameera, M. Tsuge, A. Miyazaki, H. Hidaka, A. Kouchi, and N. Watanabe, "Delivery of electrons by proton-hole transfer in ice at 10 K: Role of surface OH radicals," J. Phys. Chem. Lett. **12**, 704 (2021).

A. Miyazaki, N. Watanabe, W. M. C. Sameera, Y. Nakai, M. Tsuge, T. Hama, H. Hidaka, and A. Kouchi, "Photostimulated desorption of OH radicals from amorphous solid water: Evidence for the interaction of visible light with an OH-ice complex," Phys. Rev. A **102**, 052822 (2020).

[Books]

望月優子, 佐藤勝彦, 「シリーズ現代の天文学第 1 巻 人類の住む宇宙 第 2 版」(第 2 刷観測進展にあわせ改訂), pp. 99–144 (「第 3 章 元素の起源」) 岡村定矩他編, 日本評論社, 2020 年 4 月.

望月優子, 佐藤勝彦, 「天文学辞典 (インターネット版)」, 「r 過程」(部分執筆), https://astro-dic.jp/r-process/, 日本天文学会, 2020 年 10 月.

望月優子, 佐藤勝彦, 「天文学辞典 (インターネット版)」, 「s 過程」(部分執筆), https://astro-dic.jp/s-process/, 日本天文学会, 2020 年 10 月.

[Proceedings]

南武志, 高橋和也, 「与呂木古墳から出土した頭蓋骨付着朱の硫黄同位体比分析」, 三木市文化研究資料第 35 集 「与呂木古墳・与呂木 12 号墳—与呂木青葉台団地造成に伴う発掘調査報告書」, 三木市教育委員会, 35–39 (2021).

高橋和也, 南武志, 藤田淳, 池田征弘, 「硫黄同位体比分析による兵庫県の遺跡出土朱の産地推定」, 兵庫県立考古博物館 研究紀要 **13**, 53-–58 (2020).

Presentations

[International Conferences/Workshops]

Y. Motizuki (e-poster), Y. Nakai, K. Takahashi, J. Hirose, Y. V. Sahoo, Y. Yano, M. Yumoto, M. Maruyama, M. Sakashita, K. Kase, and S. Wada, "A novel laser-melting ice-core sampler with high depth resolution and high throughput for discrete ice core analyses," The 11th International Symposium on Polar Science, Online event, November 16-–December 18, 2020.

[Domestic Conferences/Workshops]

中井陽一, 日高宏, 渡部直樹, 「低エネルギーイオンと低温氷表面との反応実験装置開発の現状 2」, 日本物理学会第 76 回年次大会, オンライン発表, 2021 年 3 月 12–15 日.

北島謙生, 中井陽一, W. M. C. Sameera, 宮崎彩音, 柘植雅士, 日高宏, 香内晃, 渡部直樹, 「極低温アモルファス氷への紫外光・電子線同時照射による負の氷透過電流生成」, 原子衝突学会第 45 回年会, オンライン発表, 2020 年 12 月 8–10 日.

高橋和也, 中井陽一, 本山秀明, 望月優子, 「高感度硫黄同位体比分析法を用いた南極ドームふじ基地氷床コアから得られた試料の分析」, 日本分析化学会第 69 回年会, オンライン開催, 2020 年 9 月 16–18 日.

菅澤佳世, 三宅芙沙, 多田悠馬, 堀内一穂, 大谷昴, 笹公和, 高橋努, 松村万寿美, 落合悠太, 高野健太, 望月優子, 高橋和也, 中井陽一, 本山秀明, 松崎浩之, 「約 100 年分のドームふじアイスコア中 ^{10}Be と ^{36}Cl の高分解能測定による BC5480 年宇宙線イベントの調査」, 第 81 回応用物理学会秋季学術講演会, オンライン開催, 2020 年 9 月 8–11 日.

Press Releases

Kazuya Takahashi and Yuko Motizuki, "Sticky tape: A key ingredient for mapping artifact origins," March 9, 2020. https://www.riken.jp/en/news_pubs/research_news/pr/2019/20191126_2/

Nuclear Science and Transmutation Research Division
Nuclear Transmutation Data Research Group

1. Abstract

The nuclear waste problem is an inevitable subject in nuclear physics and nuclear engineering communities. Since the Chicago Pile was established in 1942, nuclear energy has become one of major sources of energy. However, nowadays the nuclear waste produced at nuclear power plants has caused social problems. Minor actinide components of the waste have been studied well as a fuel in fast breeder reactors or ADS. Long-lived fission products (LLFP) in waste, on the other hand, have not been studied extensively. A deep geological disposal has been a policy of several governments, but it is difficult to find out location of the disposal station in terms of security, sociology and politics. To solve the social problem, a scientific effort is necessary for nuclear physics community to find out efficient methods for reduction of nuclear waste radioactivity. In the world-wide situation above, our Group aims to obtain reaction data of LLFP at RIBF and other muon facilities for muon capture data. These data are necessary to design an accelerator-based system for transmutation, and also may lead to a new discovery and invention for peaceful use of nuclear power and the welfare of humanity.

2. Major Research Subjects

The Group is formed by three research teams. The first two Teams, “Fast RI Data Team” and “Slow RI Data Team,” are in charge of proton- and deuteron-induced reaction data of LLFP in inverse kinematics at RIBF. The third Team “Muon Data Team” is to obtain muon capture data of LLFP at muon facilities. All of the teams are focusing to obtain high-quality data which are essentially necessary to establish reliable reaction models. Each team has its own subjects and promotes LLFP reaction programs based on their large experiences, techniques and skills.

3. Summary of Research Activity

In 2014, all the teams polished up experimental strategies, formed collaboration and prepared experiments. Physics runs for spallation reaction were successfully organized at RIBF in 2015–2017. The muon program started at RCNP, Osaka University in spring 2016 and the data for Pd isotopes were successfully obtained in 2017–2019 via in-beam method with DC beams at RCNP, and via activation method with pulsed beams at J-PARC and ISIS-RAL/RIKEN facilities.

The reaction data obtained with both fast and energy-degraded beams at RIBF encouraged the nuclear data group of JAEA, and a new database called “JENDLE/ImPACT-2018” has been released. The new database has been generated by a newly developed reaction model “DEURACS” which treats deuteron-induced reactions. DEURACS reproduces very well cross section data, and much better than other reaction models. A simulation code “PHITS” has been re-coordianted to use the database information.

In December 2018, the Team leader, Hideaki Otsu, was invited to join Technical Meeting of IAEA, entitled “Novel Multidisciplinary Applications with Unstable Ion Beams and Complementary Techniques.” Our activity has been demonstrated and recognized internationally. In November 2020, Hideaki Otsu organized a domestic conference entitled “RIKEN Sympoium on Nuclear Data 2020”.

Member

Director

Hiroyoshi SAKURAI

List of Publications & Presentations

Presentations

[Domestic Conferences/Workshops]

櫻井博儀（招待講演）,「仁科センターの核データ活動」, 理研シンポジウム「2020 年度核データ研究会」, 和光市, 2020 年 11 月 26–27 日.

Nuclear Science and Transmutation Research Division
Nuclear Transmutation Data Research Group
Fast RI Data Team

1. Abstract

Fast RI team aims at obtaining and accumulating the cross section data for long lived fission products (LLFPs) in order to explore the possibility of using accelerator for nuclear transmutation.

LLFPs as nuclear waste have been generated continuously in nuclear power plants for wealth for human lives, while people noticed the way of disposal has not necessarily been established, especially after the Fukushima Daiichi power plant disaster. One of the ways to reduce the amount of LLFP or to recover them as recycled resources is nuclear transmutation technique.

RIBF facility has a property to generate such LLFP as a secondary beam and the beam species are identified by event by event. Utilizing the property, absolute values of the cross section of various reactions on LLFPs are measured and accumulated as a database.

2. Major Research Subjects

(1) Measurement of reaction products by the interaction of LLFPs with proton, deuteron, and photon to explore candidate reactions for the transmutation of LLFPs.
(2) Evaluation of the cross section data for the neutron induced reactions from the obtained data.

3. Summary of Research Activity

(1) Acting as a collaboration hub on many groups which plan to take data using fast RI beams in RIBF facility.
(2) Concentrating on taking data for proton and deuteron induced spallation reactions with inverse kinematics.
(3) Accumulating the cross section data and evaluating them as evaluated nuclear data.
(4) Evaluating cross section of neutron induced reaction on LLFP by collaborating with the nuclear model calculation and evaluation group.

Members

Team Leader

Hideaki OTSU (Concurrent: Team Leader, SAMURAI Team)

Visiting Scientist

Takashi TERANISHI (Kyushu Univ.)

Student Trainee

Koichi GOTO (Kyushu Univ.)

List of Publications & Presentations

Publications

[Original Papers]

X. H. Sun, H. Wang, H. Otsu, H. Sakurai, *et al.*, "Spallation and fragmentation cross sections for 168 MeV/nucleon ^{136}Xe ions on proton, deuteron, and carbon targets," Phys. Rev. C **101**, 064623 (2020).

[Proceedings]

H. Wang, H. Otsu, H. Sakurai, *et al.*, "Spallation reaction study for long-lived fission products in nuclear waste," EPJ Web Conf. **239**, 06003 (2020) (Proc. International Conference on Nuclear Data for Science and Technology (ND2019), Beijing, China, May 19–24, 2019).

K. Nakano, Y. Watanabe, S. Kawase, *et al.*, "Isotope-production cross sections of residual nuclei in proton- and deuteron-induced reactions on ^{93}Zr at 50 MeV/nucleon," EPJ Web Conf. **239**, 20006 (2020) (Proc. International Conference on Nuclear Data for Science and Technology (ND2019), Beijing, China, May 19–24, 2019).

X. Sun, H. Wang, H. Otsu, H. Sakurai, *et al.*, "Cross-section measurement in the reactions of ^{136}Xe on proton, deuteron and carbon" EPJ Web Conf. **239**, 01037 (2020) (Proc. International Conference on Nuclear Data for Science and Technology (ND2019), Beijing, China, May 19–24, 2019).

Presentations

[International Conferences/Workshops]

R. Matsumura, H. Otsu, H. Wang, N. Chiga, *et al.*, "Nuclear transmutation of high-radiotoxic nuclide ^{90}Sr via proton- and deuteron-induced reactions in inverse kinematics," A3F-CNS Summer School 2020, online, August 17–21, 2020.

[Domestic Conferences/Workshops]

松村理久, 大津秀暁, 王赫, 千賀信幸, 他 ImPACT-RIBF Collaboration, 「核分裂生成核種 ^{90}Sr の陽子及び重陽子誘起反応に関する研究」, 日本物理学会第 75 回年次大会, 愛知県名古屋市 (名古屋大学現地開催中止), 2020 年 3 月 16–19 日.

松村理久, 大津秀暁, 王赫, 千賀信幸, 他 ImPACT-RIBF Collaboration, 「高放射性核種 ^{90}Sr の陽子及び重陽子誘起反応による核変換に向けた研究」, Symposium on Nuclear Data 2020, 埼玉県和光市, 2020 年 11 月 26–27 日.

Nuclear Science and Transmutation Research Division
Nuclear Transmutation Data Research Group
Slow RI Data Team

1. Abstract

This team is in charge of the development of low-energy RI beams of long-lived fission fragments (LLFP) from the ^{238}U by means of degrading the energy of beams produced by the BigRIPS fragment separator.

2. Major Research Subjects

Studies of the slowing down and purification of RI beams are the main subjects of the team. Developments of devices used for the slowing down of RI beams are also an important subject.

(1) Study and development of the slowed-down methods for LLFP.
(2) Development of the devices used for the slowing down.
(3) Operation of the BigRIPS separator and supply the low energy LLFP beam to the experiment in which the cross sections of LLFP are measured at the low energy.
(4) Development of the framework to seamlessly handle device, detector, DAQ, and analysis for the easy control of the complicate slowed-down RI beam production and its development.

3. Summary of Research Activity

A new OEDO beam line, designed for the slowed-down RI beams, was constructed under the collaboration with CNS, the University of Tokyo. Our group was responsible for the construction of the infrastructure such as the cooling water and the electrical equipment, and the movement and alignment of existing vacuum chambers, quadrupole magnets. The power supply for the Superconducting Triplet Quadrupoles (STQ) was made, which had a stability also under the low current condition.

Slowed-down ^{93}Zr beams with 20 or 50 MeV/nucleon were successfully developed at June 2016 for the first time. The methods to obtain the narrow energy, position, and angle distribution were developed. The methods of the energy adjustment and the particle identification at 50 MeV/nucleon were developed. The ^{93}Zr and ^{107}Pd beams with 50 MeV/nucleon were produced for the nucleartransmutation experiments using proton or deuteron targets at October 2016. The commissioning experiment of the OEDO beam line was successfully performed at June 2017. The first transmutation experiments using OEDO beam line were performed with ^{93}Zr, ^{107}Pd, and ^{79}Se around 20 MeV/nucleon.

With our developments, the slowed-down RI beams became ready for the transmutation experiments. On the other hand, the procedure to make the slowed-down RI beams became highly specialized. In order to easily produce the slowed-down RI beam, the framework is under the development to seamlessly handle the device, detector, DAQ, and analysis. The procedure of the RI-beam energy control was implemented in the web application.

Members

Team Leader

Toshiyuki SUMIKAMA

Student Trainees

SungHan BAE (Seoul Nat'l Univ.)
Hiroya FUKUDA (Kyushu Univ.)
Misaki SAITSU (Kyushu Univ.)

List of Publications & Presentations

Publications

[Original Papers]

T. Sumikama, D. S. Ahn, N. Fukuda, Y. Shimizu, H. Suzuki, H. Takeda, H. Wang, K. Yoshida, J. Amano, N. Chiga, K. Chikaato, A. Hirayama, N. Inabe, S. Kawase, S. Kubono, M. Matsushita, S. Michimasa, K. Nakano, H. Otsu, and H. Sakurai, "Energy-control and novel particle-identification methods combined with range in a multi-sampling ionization chamber for experiments using slowed-down RI beams," Nucl. Instrum. Methods Phys. Res. A **986**, 164687 (2021).

K. Nakano, Y. Watanabe, S. Kawase, H. Wang, H. Otsu, H. Sakurai, N. Chiga, J. Suwa, T. Sumikama, S. Takeuchi, T. Nakamura, K. Chikaato, M. Takechi, S. Koyama, D. S. Ahn, H. Baba, S. Chen, M. L. Cortes, P. Doornenbal, N. Fukuda, A. Hirayama, R. Hosoda, T. Isobe, S. Kawakami, Y. Kondo, S. Kubono, Y. Maeda, S. Masuoka, S. Michimasa, I. Murray, R. Nakajima, M. Niikura, T. Ozaki, A. Saito, T. Saito, H. Sato, Y. Shimizu, S. Shimoura, Y. Soudo, P. -A. Söderström, X. Sun, D. Suzuki, H. Suzuki, H. Takeda, Y. Togano, T. Tomai, H. Yamada, M. Yasuda, and K. Yoshida, "Isotope-production cross sections of residual nuclei in proton- and deuteron-induced reactions on ^{93}Zr at 50 MeV/nucleon," EPJ Web Conf. **239**, 20006 (2020).

H. Wang, H. Otsu, H. Sakurai, D. S. Ahn, M. Aikawa, T. Ando, S. Araki, S. Chen, N. Chiga, P. Doornenbal, N. Fukuda, T. Isobe, S. Kawakami, S. Kawase, T. Kin, Y. Kondo, S. Koyama, S. Kubono, Y. Maeda, A. Makinaga, M. Matsushita, T. Matsuzaki, S. Michimasa, S. Momiyama, S. Nagamine, T. Nakamura, K. Nakano, M. Niikura, T. Ozaki, A. Saito, T. Saito, Y. Shiga, M. Shikata, Y. Shimizu,

S. Shimoura, T. Sumikama, P. -A. Söderstrom, H. Suzuki, H. Takeda, S. Takeuchi, R. Taniuchi, Y. Togano, J. Tsubota, M. Uesaka, Y. Watanabe, Y. Watanabe, K. Wimmer, T. Yamamoto, and K. Yoshida, "Spallation reaction study for long-lived fission products in nuclear waste," EPJ Web Conf. **239**, 06003 (2020).

J. Ha, T. Sumikama, F. Browne, N. Hinohara, A. M. Bruce, S. Choi, I. Nishizuka, S. Nishimura, P. Doornenbal, G. Lorusso, P. -A. Söderström, H. Watanabe, R. Daido, Z. Patel, S. Rice, L. Sinclair, J. Wu, Z. Y. Xu, A. Yagi, H. Baba, N. Chiga, R. Carroll, F. Didierjean, Y. Fang, N. Fukuda, G. Gey, E. Ideguchi, N. Inabe, T. Isobe, D. Kameda, I. Kojouharov, N. Kurz, T. Kubo, S. Lalkovski, Z. Li, R. Lozeva, H. Nishibata, A. Odahara, Zs. Podolyák, P. H. Regan, O. J. Roberts, H. Sakurai, H. Schaffner, G. S. Simpson, H. Suzuki, H. Takeda, M. Tanaka, J. Taprogge, V. Werner, and O. Wieland, "Shape evolution of neutron-rich ^{106,108,110}Mo isotopes in the triaxial degree of freedom," Phys. Rev. C **101**, 044311 (2020).

T. Sumikama, N. Fukuda, N. Inabe, D. Kameda, T. Kubo, Y. Shimizu, H. Suzuki, H. Takeda, K. Yoshida, H. Baba, F. Browne, A. M. Bruce, R. Carroll, N. Chiga, R. Daido, F. Didierjean, P. Doornenba, Y. Fang, G. Gey, E. Ideguchi, T. Isobe, S. Lalkovski, Z. Li, G. Lorusso, R. Lozeva, H. Nishibata, S. Nishimura, I. Nishizuka, A. Odahara, Z. Patel, Zs. Podolyák, P. H. Regan, S. Rice, O. J. Roberts, H. Sakurai, G. S. Simpson, L. Sinclair, P. -A. Söderström, M. Tanaka, J. Taprogge, H. Watanabe, V. Werner, O. Wieland, J. Wu, Z. Y. Xu, and A. Yagi, "Observation of new neutron-rich isotopes in the vicinity of ^{110}Zr," Phys. Rev. C **103**, 014614 (2021).

Nuclear Science and Transmutation Research Division
Nuclear Transmutation Data Research Group
Muon Data Team

1. Abstract

Dr. Yoshio Nishina observed muons in cosmic rays in 1937. The muon is an elementary particle similar to electron and classified to lepton group. The muon has positive or negative electric charge, and the lifetime is 2.2 μsec. The negative muon (μ^-) is 207 times heavier than the electron and behaves as a "heavy electron" in materials. The negative muon is captured by atomic orbits of nuclei to form a muonic atom and cascades down to the 1 s orbit to make muon nuclear capture. The muon is combined with a proton in the nucleus to convert to a neutron and a neutrino. The muon nuclear capture reaction on a nucleus ($^A_Z N$) with the atomic number Z and mass number A generates the isotopes of $^{A-x}_{Z-1}N(x = 0, 1, 2, 3, 4)$ by emitting some neutrons in the reaction. The phenomenon is called "muon nuclear transmutation." The reaction branching ratio of $^A_Z N(\mu^-, x n \nu)^{A-x}_{Z-1}N$ reactions ($x = 0, 1, 2, 3, 4$) is one of important factors toward various applications with nuclear transmutation technique. From a viewpoint of the nuclear physic, the muon nuclear capture reaction is very unique and interesting. A high-energy compound nuclear state is suddenly generated in the nuclei associated with a weak conversion process of proton to neutron and neutrino. Many experimental results have been so far reported, however, the reaction mechanism itself is not well clarified. The research team aims at obtaining the experimental data to investigate the reaction mechanism of muon nuclear capture, and also at theoretical understanding on the nuclear capture reaction.

2. Major Research Subjects

(1) Experimental clarification on the mechanism of nuclear muon capture reaction
(2) Theoretical understanding on the nuclear muon capture reaction
(3) Interdisciplinary applications with the nuclear transmutation technique

3. Summary of Research Activity

There are two experimental methods to study the muon nuclear capture reaction. The first one is "muon in-beam spectroscopy method." The neutron and γ-ray emissions from the excited states of $^{A-x}_{Z-1}N$ nuclei are prompt events and are observed by the "muon in-beam spectroscopy method" with a DC muon beam. The reaction branching ratio is directly determined by measuring the neutron multiplicity in the reaction. The DC muon beam is available at the MuSIC (Muon Science Innovative Channel) muon facility in the Research Center for Nuclear Physics (RCNP) at Osaka University. The second one is "muon activation method" with the pulsed muon beam. The produced unstable nuclei $^{A-x}_{Z-1}N$ make $\beta^{+/-}$ decays. The γ-rays associated with $\beta^{+/-}$ decays to the daughter nuclei are observed in the experiment. The build-up curve of γ-ray yield at muon beam-on and the decay curve at beam-off are measured. Since the half-lives and decay branching ratios of $\beta^{+/-}$-γ decays are known, the reaction branching ratios to the $^{A-x}_{Z-1}N$ nuclei are determined by the γ-ray yield curves. The pulsed muon beam is available at the RIKEN-RAL Muon Facility in the UK and J-PARC muon facility.

Muon nuclear capture reactions are studied on five isotope-enriched palladium targets ($^{104, 105, 106, 108, 110}$Pd) and five isotope-enriched zirconium targets ($^{90, 91, 92, 94, 96}$Zr) employing two experimental methods. By obtaining the experimental data on the Pd and Zr targets, the reaction mechanism is investigated experimentally, and the results are compared with appropriate theoretical calculations. The ^{107}Pd is classified to a long-lived fission product (LLFP) and is contained in a spent nuclear fuel. The study of muon nuclear capture on the Pd and Zr targets is aiming at exploring a possible reaction path to make the nuclear transmutation of the Pd and Zr metal extracted from the spent nuclear fuel without an isotope separation process. This research was funded by the ImPACT Program of Council for Science, Technology and Innovation (Cabinet Office, Government of Japan).

(1) Experiments with "muon in-beam spectroscopy method"

Muon nuclear capture reactions were investigated on five palladium targets ($^{104, 105, 106, 108, 110}$Pd) by employing the DC muon beam at MuSIC. The γ-ray and neutron in the muon nuclear capture reaction were measured with the time information relative to muon beam arrival. The measured neutron multiplicity gives the reaction branching ratio of $^A_{46}\mathrm{Pd}(\mu^-, x n \nu)^{A-x}_{45}\mathrm{Rh}$ reactions, where $A = 104, 105, 106, 108, 110$ and $x = 0, 1, 2, 3, 4$.

Employing a newly built neutron spectrometer, the neutron was measured to obtain the reaction branching ratios of muon capture reactions on the Pd targets. We have constructed a neutron spectrometer named "Seamine": **S**cintillator **E**nclosure **A**rray for **M**uon **I**nduced **N**eutron **E**mission. The spectrometer consists of 21 liquid scintillation counters, 2 Ge γ-ray detectors, 7 BaF_2 counters. The Pd target, muon beam counters and muon degraders are placed at the center of spectrometer. The neutron counter is a BC-501A liquid scintillation counter with 20 cm diameter and 5 cm depth and is connected to a 5" photo multiplication tube (H4144-01). The total neuron detection efficiency is estimated 5%, where the distance is 4 cm from the target to neutron counters. The Ge γ-ray detectors are placed at 10 cm form the target, and the typical detection efficiency is 0.5% for 200 keV γ-ray. The BaF_2 counters are located beneath the target to detect fast γ-rays emitted from the compound nucleus formed in the reactions. Signals from the liquid scintillation counters are processed in a CAEN V1730B waveform digitizer (16 channel, 14 bit, 500 M samplings/sec.). The neuron-γ discrimination is performed on-line during the experiment, and the detailed data analysis is conducted off-line after the experiment. The neutron energy spectrum is constructed in the digitizer. Signals from Ge detectors are also processed in the digitizer to obtain the energy and time spectrum of γ-rays associated with the reaction. Signals from the BaF_2 counters and muon beam counters are sent to the digitizer to make the fast timing signals.

We have established the muon in-beam spectroscopy method employing the "Seamine" spectrometer. The neutron data analysis

is in progress to obtain the multiplicity, the energy and the TOF spectrum using start signals given by γ-rays detected in the BaF_2 counters. The γ-ray data gives the energy spectrum of prompt γ-rays and muonic X-rays originated from the ^{104,105,106,108,110}Pd targets.

(2) Experiments with "muon activation method" at the RIKEN-RAL Muon Facility

We conducted the experiments on the muon nuclear capture employing the muon activation method at the RIKEN-RAL Muon Facility in the UK. The pulsed muon beam was irradiated on the ^{104,105,106,108,110}Pd targets. The γ-rays were detected by a Ge detector located at the downstream of the Pd targets to maximize the detection efficiency. The build-up and decay curves of γ-ray intensities were measured associated with $\beta^{+/-}$ decays of produced unstable nuclei to daughter nuclei. The γ-ray-yield curves give the absolute radiation activity produced by the reaction, and the reaction branching ratios are determined for ${}^{A}_{46}\mathrm{Pd}(\mu^-, x n \nu)^{A-x}_{45}\mathrm{Rh}$ reactions. The decay curves of γ-rays from the produced nuclei with long half-lives were measured under low γ-ray background at an experimental apparatus built in a separated room. The detailed off-line data analysis is in progress.

(3) Experiments with "muon activation method" at J-PARC muon facility

The experiments employing the muon activation method were performed at J-PARC muon facility. The five isotope-enriched Pd targets (^{104,105,106,108,110}Pd) were irradiated by the pulsed muon beam, and the build-up and decay curves of γ-ray intensities were measured.

In addition to the Pd targets, the experiments on five isotope-enriched Zr target (^{90,91,92,94,96}Zr) were conducted to obtain the reaction branching ratios of ${}^{A}_{40}\mathrm{Zr}(\mu^-, x n \nu)^{A-x}_{39}\mathrm{Y}$ reactions, where $A = 90, 91, 92, 94, 96$. The obtained reaction branching ratios on the Pd and Zr targets are important to understand the reaction mechanism of muon nuclear capture. The ^{93}Zr is one of the LLFP and is contained in a spent nuclear fuel. The experiment on the Zr targets is to explore a possibility to realize the nuclear transmutation of the Zr metal extracted from the spent nuclear fuel.

In order to obtain the reaction branching ratio of ${}^{107}_{46}\mathrm{Pd}(\mu^-, x n \nu)^{107-x}_{45}\mathrm{Rh}$ reactions, the muon activation experiment was performed employing a Pd target containing ^{107}Pd of 15.3%. The γ-ray intensities associated with $\beta^{+/-}$ decays of produced unstable nuclei were measured to obtain the build-up and decay curves. Once the branching ratios of the reactions on the ^{104,105,106,108,110}Pd targets are obtained, these contributions are extracted from the branching-ratio data obtained for the Pd target with ^{107}Pd. The reaction branching ratio of ${}^{107}_{46}\mathrm{Pd}(\mu^-, x n \nu)^{107-x}_{45}\mathrm{Rh}$ reactions is finally determined. The detailed off-line data analysis is in progress.

(4) Comparison with theory

The muon activation method gives the reaction branching ratios. The muon in-beam spectroscopy method gives the neutron multiplicity and the neutron energy spectrum. These experimental results are important to understand the compound nuclear state and neutron emission mechanism. The reaction branching ratios obtained by the muon activation method are compared with the results of neutron multiplicity measurements. The neutron energy spectrum is considered to be reflected by the energy distribution of compound nuclear state and neutron emission mechanism. The experimental results are compared with the appropriate calculations employing the neutron emission mechanisms due to an evaporation, a cascade and a direct emission processes with assuming the energy distribution at compound nuclear state.

Members

Team Leader

Hiroyoshi SAKURAI

Contract Researcher

Teiichiro MATSUZAKI

Part-time Worker

Takeshi SAITO (Research Part-time Worker I)

List of Publications & Presentations

Presentations

[Domestic Conferences/Workshops]

齋藤岳志（招待講演),「ミューオン原子 X 線分光による原子核の荷電分布・荷電半径測定」, ELPH 研究会 C028「電子散乱による原子核研究—原子核の電荷密度・陽子・中性子の分布と半径—」, オンライン, 2021 年 3 月 18–19 日.

Nuclear Science and Transmutation Research Division
High-Intensity Accelerator R&D Group

1. Abstract

The High-Intensity Accelerator R&D group, consisting of two teams, develops elemental technology of high-power accelerators and high-power targets, aiming at future applications to nuclear transmutations of long-lived fission product into short-lived nuclides. The research subjects are superconducting rf cavities for low-velocity ions, design of high-power accelerators, high-power target systems and related technologies.

Nuclear transmutation with high-intensity accelerators is expected to reduce the high-level radioactive wastes and to recycle the precious resources such as rare-earth materials in future. This method is one of the important applications of the ion-accelerator technologies that have been developed at RIKEN for a long time. Under the framework of ImPACT Fujita Program, we have conducted R&D of elemental technology related to the high-power accelerators and high-power targets, from FY2014 to FY2018. We gained a lot of experiences in these R&Ds. Among them, the development of a superconducting rf cavity has become the basis of the upgrade program of the RILAC facility which started in 2016.

2. Major Research Subjects

(1) R&D of elemental technology of high-power accelerators and high-power targets.

3. Summary of Research Activity

(1) A high-gradient rf cavity has been constructed and tested based on the superconducting rf technology.
(2) Several candidates for the high-power target have been proposed and their prototypes have been tested.
(3) A high-current deuteron RFQ has been designed.

Members

Director

Osamu KAMIGAITO (concurrent: Group Director, Accelerator Group)

Nuclear Science and Transmutation Research Division
High-Intensity Accelerator R&D Group
High-Gradient Cavity R&D Team

1. Abstract

We develop new components for accelerators dedicated for low-beta-ions with very high intensity. Specifically, we are designing and constructing a cryomodule for superconducting linac efficient for acceleration of low-beta-ions. In parallel, we try to optimize an rf acceleration system by making computer simulations for acceleration of very high intensity beams.

2. Major Research Subjects

(1) Development of high-gradient cavites for low beta ions
(2) Development of power saving cryomodules

3. Summary of Research Activity

- Development of highly efficient superconducting accelerator modules

Members

Team Leader

Naruhiko SAKAMOTO

Research/Technical Scientists

Kazunari YAMADA
Kazutaka OZEKI
Yutaka WATANABE

Research & Development Scientist

Kenji SUDA

Nuclear Science and Transmutation Research Division
High-Intensity Accelerator R&D Group
High-Power Target R&D Team

1. Abstract

The subjects of this team cover R&D studies with respect to target technology for the transmutation of the LLFPs.

2. Major Research Subjects

(1) Liquid lithium target for production of neutron or muon
(2) Beam window without solid structure

3. Summary of Research Activity

(1) Liquid lithium target for production of neutron or muon (H. Okuno)
(2) Beam window with solid structure (H. Okuno)

Members

Team Leader
Hiroki OKUNO

Special Postdoctoral Researcher
Yasuto MIYAKE

Research Facility Development Division
Accelerator Group

1. Abstract

The Accelerator Group, consisting of seven teams, pursues various upgrade programs on the world-leading heavy-ion accelerator facility, RI Beam Factory (RIBF), to enhance the accelerator performance and operation efficiency. The programs include the R&D of superconducting ECR ion source, charge stripping systems, beam diagnostic devices, radio-frequency systems, control systems, and beam simulation studies. We are also maintaining the large infrastructure to realize effective operation of the RIBF. Moreover, we are actively promoting the applications of the facility to various research fields.

Our primary mission is to supply intense, stable heavy-ion beams for the users through effective operation, maintenance, and upgrade of the RIBF accelerators and related infrastructure. The director members govern the development programs that are not dealt with by a single team, such as intensity upgrade and effective operation. We also discuss the future plans of RIBF along with other laboratories belonging to the RIBF research division.

Various improvements and developments have been carried out for the RIBF accelerators in order to upgrade the beam intensities and stability. Owing to the efforts, for example, we succeeded in accelerating the uranium beam of 117 pnA through SRC in October 2020. This surpassed the long-standing target of 100 pnA, and also means that one of goals of the current mid-term plan of RNC has been achieved. The beam intensity of ^{70}Zn increased to 788 pnA in December 2020, corresponding to the beam power of 19.0 kW.

On the other hand, at the new RILAC facility, which was commissioned at the end of FY2019 with the superconducting booster linac (SRILAC), a superheavy element synthesis experiment was started after the closure of RIKEN due to COVID-19. Despite a problem in one of the superconducting cavities, a high-intensity vanadium beam is being supplied to the users. Construction of a new beam line for the R&D of mass production method of ^{211}At has been also started at the RILAC facility.

An upgrade plan of RIBF for further increasing uranium beam has been continuously discussed. The plan is based on the idea of "charge-stripper ring (CSR)," which is used to improve the overall stripping efficiency of the uranium beam. This device recirculates and re-injects the uranium ions into the charge stripper until the ions have the charge state required for the succeeding acceleration, while the bunch structure is kept with its isometric orbit lengths for all the charge states. We are planning to install two CSRs in the RIBF accelerator chain and the ultimate goal of the uranium beam intensity is 2,000 pnA at the exit of SRC. Initial design study of the first CSR (CSR1) has been almost completed. A pair of quadrupole magnets, that will be used in CSR1, is under fabrication, in order to study the magnetic field in and around the magnets.

2. Major Research Subjects

(1) Intensity upgrade of RIBF accelerators (Okuno)
(2) Effective and stable operation of RIBF accelerators (Fukunishi)
(3) Stable operation of the upgraded RILAC facility
(4) Promotion of the future plan

3. Summary of Research Activity

(1) The maximum intensity of the uranium beam reached 117 pnA at 345 MeV/nucleon, which corresponds to the beam power of 9.6 kW.
(2) The maximum intensity of zinc beam reached 788 pnA, corresponding to 19.0 kW.
(3) The overall beam availability for the RIBF experiments was 90% in 2020.
(4) The new RILAC facility, which was commissioned at the end of FY2019 with the superconducting booster linac (SRILAC), started supplying high-intensity vanadium beam for a superheavy element synthesis experiment.
(5) The large infrastructure was properly maintained based on a well-organized cooperation among the related sections in RIKEN.
(6) An intensity-upgrade plan of the RIBF has been further investigated. Elemental R&D of the first charge-stripper ring (CSR1) is under progress.

Members

Director
Osamu KAMIGAITO

Deputy Directors
Hiroki OKUNO (for intensity upgrade)
Nobuhisa FUKUNISHI (for stable and efficient operation)

Junior Research Associate
Kaori NAKAMURA

Research Part-time Worker I
Akira GOTO
Masayuki KASE

Research Consultants
Tadashi FUJINAWA
Toshiyuki HATTORI (Tokyo Tech)

Visiting Scientists
Eiji KAKO (KEK)
Hirotaka NAKAI (KEK)
Kensei UMEMORI (KEK)
Hiroshi SAKAI (KEK)
Taro KONOMI (KEK)
Noboru SASAO (Okayama Univ.)
Yasutaka IMAI (Okayama Univ.)

Assistant
Karen SAKUMA

Administrative Part-time Worker II
Ryoko UMEZAKI

List of Publications & Presentations

Publications

[Original Papers]

O. Kamigaito, "Circuit-model formulas for external-Q factor of resonant cavities with capacitive and inductive coupling," arXiv:2005.05843 (2020).

Presentations

[International Conferences/Workshops]

O. Kamigaito (invited), "Commissioning of superconducting linac booster for heavy-ion linac at RIKEN," 30th Linear Accelerator Conference (LINAC20), Liverpool, United Kingdom (ONLINE), September 1–4, 2020.

Outreach Activities

"First beam acceleration test successfully performed at SRILAC," RIKEN NEWS No. 470 (8) 2020.

Research Facility Development Division
Accelerator Group
Accelerator R&D Team

1. Abstract

We are developing the key hardware in upgrading the RIBF accelerator complex. Our primary focus and research is charge stripper which plays an essential role in the RIBF accelerator complex. Charge strippers remove many electrons in ions and realize efficient acceleration of heavy ions by greatly enhancing charge state. The intensity of uranium beams is limited by the lifetime of the carbon foil stripper conventionally installed in the acceleration chain. The improvement of stripper lifetimes is essential to increase beam power towards the final goal of RIBF in the future. We are developing the low-Z gas stripper. In general gas stripper is free from the lifetime related problems but gives low equilibrium charge state because of the lack of density effect. Low-Z gas stripper, however, can give as high equilibrium charge state as that in carbon foil because of the suppression of the electron capture process. Another our focus is the upgrade of the world's first superconducting ring cyclotron.

2. Major Research Subjects

(1) Development of charge strippers for high power beams (highly oriented graphite film, low-Z gas)
(2) Upgrade of the superconducting ring cyclotron
(3) Maintenance and R&D of the electrostatic deflection/inflection channels for the beam extraction/injection

3. Summary of Research Activity

(1) Development of charge strippers for high power beams (foil, low-Z gas)

(H. Hasebe, H. Imao, H. Okuno)

We are developing the charge strippers for high intensity heavy ion beams. We are focusing on the developments on highly oriented carbon graphite films and gas strippers including He gas stripper.

(2) Upgrade of the superconducting ring cyclotron

(J. Ohnishi, H. Okuno)

We are focusing on the upgrade of the superconducting ring cyclotron.

(3) Maintenance and R&D of the electrostatic deflection/inflection channels for the beam extraction/injection

(J. Ohnishi, H. Okuno)

We are developing high-performance electrostatic channels for high power beam injection and extraction.

Members

Team Leader

Hiroki OKUNO

Research/Technical Scientists

Hiroshi IMAO (Senior Research Scientist)
Hiroo HASEBE (Technical Scientist)

Special Temporary Technical Scientist

Jun-ichi OHNISHI

Visiting Scientists

Andreas ADELMANN (Paul Sherrer Inst.)
HAYASHIZAKI (Tokyo Tech)

Part-time Worker

Yoshiki SHIKUMA (Research Part-time Worker II)

List of Publications & Presentations

Publications

[Original Papers]

H. Imao, "Charge stripper ring for RIKEN RI beam factory," J. Instrum. **15**, P12036 (2020).

Research Facility Development Division
Accelerator Group
Ion Source Team

1. Abstract

Our aim is to operate and develop the ECR ion sources for the accelerator-complex system of the RI Beam Factory. We focus on further upgrading the performance of the RI Beam Factory through the design and fabrication of a superconducting ECR ion source for production of high-intensity heavy ions.

2. Major Research Subjects

(1) Operation and development of the ECR ion sources
(2) Development of a superconducting ECR heavy-ion source for production of high-intensity heavy ion beams

3. Summary of Research Activity

(1) Operation and development of ECR ion sources

(T. Nakagawa, M. Kidera, Y. Higurashi, T. Nagatomo, Y. Kanai, and H. Haba)

We routinely produce and supply various kinds of heavy ions such as zinc and calcium ions for the super-heavy element search experiment as well as uranium ions for RIBF experiments. We also perform R&D's to meet the requirements for stable supply of high-intensity heavy ion beams.

(2) Development of a superconducting ECR ion source for use in production of a high-intensity heavy ion beam

(T. Nakagawa, J. Ohnishi, M. Kidera, Y. Higurashi, and T. Nagatomo)

The RIBF is required to supply heavy ion beams with very high intensity so as to produce RI's and for super-heavy element search experiment. We have designed and are fabricating an ECR ion source with high magnetic field and high microwave- frequency, since the existing ECR ion sources have their limits in beam intensity. The coils of this ion source are designed to be superconducting for the production of high magnetic field. We are also designing the low-energy beam transport line of the superconducting ECR ion source.

Members

Team Leader

Takahide NAKAGAWA

Research/Technical Scientists

Takashi NAGATOMO (Senior Technical Scientist)
Yoshihide HIGURASHI (Technical Scientist)

Special Temporary Research Scientist

Yasuyuki KANAI

List of Publications & Presentations

Presentations

[International Conferences/Workshops]

T. Nagatomo (poster), "High intense vanadium-beam production to search for new super-heavy element with Z = 119," 24th International Workshop on ECR Ion Sources (ECRIS2020), East Lansing, USA, September 28–30, 2020.

Research Facility Development Division
Accelerator Group
RILAC Team

1. Abstract

The operation and maintenance of the RIKEN Heavy-ion Linac (RILAC) have been carried out. There are two operation modes: one is the stand-alone mode operation and the other is the injection mode operation. The RILAC has been used especially as an injector for the RIKEN RI- Beam Factory accelerator complex. The RILAC is composed of the 28 GHz SC ECR ion source, the frequency-variable RFQ linac, the frequency-variable main linac, and the SC booster linac (SRILAC).

2. Major Research Subjects

(1) The long-term high stability of the RILAC operation.
(2) Improvement of high efficiency of the RILAC operation.

3. Summary of Research Activity

The RILAC was started to supply ion beams for experiments in 1981. Thousands hours are spent in a year for delivering many kinds of heavy-ion beams to various experiments.

The RILAC has two operation modes: one is the stand-alone mode operation delivering low-energy beams directly to experiments and the other is the injection mode operation injecting beams into the RRC. In the first mode, the RILAC supplies a very important beam to the nuclear physics experiment of "the research of super heavy elements." In the second mode, the RILAC plays a very important role as upstream end of the RIBF accelerator complex.

The maintenance of these devices is extremely important in order to keep the log-term high stability and high efficiency of the RILAC beams. Therefore, improvements are always carried out for the purpose of more stable and more efficient operation.

Members

Team Leader
Eiji IKEZAWA

Research/Technical Scientist
Yutaka WATANABE (Senior Technical Scientist)

List of Publications & Presentations

Publications

[Proceedings]

K. Oyamada, E. Ikezawa, T. Ohki, H. Yamauchi, M. Tamura, A. Yusa, K. Kaneko, H. Imao, A. Uchiyama, K. Ozeki, T. Nishi, N. Sakamoto, K. Suda, T. Nagatomo, M. Fujimaki, K. Yamada, T. Watanabe, Y. Watanabe, and O. Kamigaito, "Present status of RILAC," Proceedings of the 17th Annual Meeting of Particle Accelerator Society of Japan, PASJ2020 FRSP06.

Presentations

[Domestic Conferences/Workshops]

小山田和幸, 池沢英二, 大木智則, 山内啓資, 田村匡史, 遊佐陽, 金子健太, 今尾浩士, 内山暁仁, 大関和貴, 西隆博, 坂本成彦, 須田健嗣, 長友傑, 藤巻正樹, 山田一成, 渡邉環, 渡邉裕, 上垣外修一「理研重イオンリニアックの現状報告」, 第 17 回日本加速器学会年会, PASJ2020 FRSP06.

Research Facility Development Division
Accelerator Group
Cyclotron Team

1. Abstract

Together with other teams of Nishina Center accelerator division, maintaining and improving the RIBF cyclotron complex. The accelerator provides high intensity heavy ions. Our mission is to have stable operation of cyclotrons for high power beam operation. Recently stabilization of the rf system is a key issue to provide 10 kW heavy ion beam.

2. Major Research Subjects

(1) RF technology for Cyclotrons
(2) Operation of RIBF cyclotron complex
(3) Maintenance and improvement of RIBF cyclotrons
(4) Single turn operation for polarized deuteron beams
(5) Development of superconducting linac

3. Summary of Research Activity

- Development of the rf system for a reliable operation
- Development of highly stabilized low level rf system
- Development of superconducting linac
- Development of the intermediate-energy polarized deuteron beams.

Members

Team Leader

Naruhiko SAKAMOTO

Research/Technical Scientists

Kazutaka OZEKI (Senior Technical Scientist)
Kenji SUDA (Technical Scientist)

List of Publications & Presentations

Publications

[Proceedings]

西隆博, 内山暁仁, 上垣外修一, 坂本成彦, 長友傑, 福西暢尚, 藤巻正樹, 渡邉環, 渡邉裕, 「理研超伝導線形加速器ビームラインのためのエミッタンス測定及び光学系調整」Proc. PASJ2020, online meeting, THOO08, 116–119 (2020).

N. Sakamoto, M. Fujimaki, E. Ikezawa, H. Imao, O. Kamigaito, T. Nagatomo, T. Nishi, K. Ozeki, K. Suda, A. Uchiyama, T. Watanabe, Y. Watanabe, and K. Yamada, "Commissioning of superconducting-linac booster for RIKEN heavy-ion linac," Proc. PASJ2020, online meeting, FRPP05, 679–683 (2020).

Presentations

[International Conferences/Workshops]

K. Suda, O. Kamigaito, K. Ozeki, N. Sakamoto, K. Yamada, E. Kako, H. Nakai, K. Umemori, H. Hara, A. Miyamoto, K. Sennyyu, and T. Yanagaisawa, ""Compact tuner designed to minimize the intervals of QWRs for RIKEN heavy-ion linac," Tesla Technology Collaboration Meeting 2020 (TTC 2020), Geneva (CERN), Switzerland, February 4–7, 2020.

K. Yamada, "Cryomodule design, assembly and installation utilizing "KOACH" system," Tesla Technology Collaboration Meeting 2020 (TTC 2020), Geneva (CERN), Switzerland, February 4–7, 2020.

N. Sakamoto, K. Yamada, K. Suda, K. Ozeki, O. Kamigaito, Y. Watanabe, H. Imao, T. Nagatomo, E. Ikezawa, K. Kumagai, S. Dantsuka, E. Kako, H. Nakai, and K. Umemori, "Commissioning and operation of RIKEN heavy ion superconducting linac," Tesla Technology Collaboration Meeting 2021 (TTC 2021), online (Hosted by DESY), January 19–21, 2021.

K. Ozeki, "Power coupler issues in CM operation from RIKEN," Tesla Technology Collaboration Meeting 2021 (TTC 2021), online (Hosted by DESY), January 19–21, 2021.

[Domestic Conferences/Workshops]

西隆博, 内山暁仁, 上垣外修一, 坂本成彦, 長友傑, 福西暢尚, 藤巻正樹, 渡邉環, 渡邉裕, 「理研超伝導線形加速器ビームラインのためのエミッタンス測定及び光学系調整」(THOO08), 第 17 回日本加速器学会年会, オンライン開催, 2020 年 9 月 2–4 日.

Others

坂本成彦, 「理研 RIBF における低速重イオン用超伝導線形加速器の開発」, 「加速器」**17**, 70–80 (2020).

Research Facility Development Division
Accelerator Group
Beam Dynamics & Diagnostics Team

1. Abstract

Aiming at stable and efficient operation of the RIBF cascaded cyclotron system, Beam Dynamics and Diagnostics Team developes power supplies, beam instrumentation, computer control and beam dynamic studies. We have successfully increased the beam availability for user experiments to more than 90%. We have also established small-beam-loss operations. The latter strongly contributes to recent high-power operations at RIBF.

2. Major Research Subjects

(1) More efficient and stable operations of the RIBF cascaded cyclotron system
(2) Maintenance and developments of the beam instrumentation
(3) Developments of computer control system for more intelligent and efficient operations
(4) Maintenance and improvements of the magnet power supplies for more stable operations
(5) Upgrade of the existing beam interlock system for high-power beams with few tens of kW

3. Summary of Research Activity

(1) High-intensity heavy-ion beams such as 117-pnA uranium, 173-pnA xenon, 486-pnA krypton, 788-pnA Zinc and 740-pnA calcium beams have been obtained.
(2) The world-first high-T_c SQUID beam current monitor has been developed.
(3) The bending power of the fixed-frequency Ring Cyclotron has been upgraded to 700 MeV.
(4) The world-most-intense V beams are stably supplied to super-heavy-element-search experiments.
(5) The RIBF control system has been operated stably by replacing legacy hardware controllers carried over from our old facility with new ones. Several useful operation tools are also developed.
(6) The dated power supplies exciting the main coils of RIKEN Ring Cyclotron has been upgraded to a new one having a better long-term stability than the old ones.
(7) Developments of automatic beam tuning methods based on recent machine-learning technology and adaptive control are in progress.

Members

Team Leader
Nobuhisa FUKUNISHI

Research/Technical Scientists
Masaki FUJIMAKI (Senior Technical Scientist)
Keiko KUMAGAI (Senior Technical Scientist)
Tamaki WATANABE (Senior Technical Scientist)
Kazunari YAMADA (Senior Technical Scientist)

Technical Scientist
Akito UCHIYAMA (Technical Scientist)

Expert Technician
Misaki KOMIYAMA

Postdoctoral Researcher
Takahiro NISHI

Research Associate
Hiroki FUJII

Visiting Scientists
Shin-ichiro HAYASHI (Hiroshima Int'l Univ.)
Atsushi KAMOSHIDA (Nat'l Instruments Japan Corporation)
Takuya MAEYAMA (Kitasato Univ.)

List of Publications & Presentations

Publications

[Review Articles]

K. Yamada, "Upgrade of the rf system for RIKEN Ring Cyclotron," J. Part. Accel. Soc. Jpn. **17**, 159–168 (2020).
N. Fukunishi, "Performance upgrade and present status of RI Beam Factory accelerator complex," J. Part. Accel. Soc. Jpn. **17**, 236–246 (2020).

[Proceedings]

N. Fukunishi, "Beam intensity upgrade of RIKEN RI Beam Factory," Proceedings of 17th Annual Meeting of Particle Accelerator Society of Japan, 7–12 (2020).

T. Nishi, A. Uchiyama, O. Kamigaito, N. Sakamoto, T. Nagatomo, N. Fukunishi, M. Fujimaki, T. Watanabe, and Y. Watanabe, "Emittance measurement and ion optics tuning for SRILAC beam line," Proceedings of 17th Annual Meeting of Particle Accelerator Society of Japan, 116–119 (2020).

T. Watanabe, T. Toyama, K. Hanamura, H. Imao, A. Uchiyama, K. Ozeki, O. Kamigaito, N. Sakamoto, T. Nishi, N. Fukunishi, K. Yamada, Y. Watanabe, R. Koyama, and A. Kamoshida, "Commissioning of the beam energy and position monitor system for the superconducting RIKEN heavy-ion linac," Proceedings of 17th Annual Meeting of Particle Accelerator Society of Japan, 718–723 (2020).

A. Uchiyama and M. Komiyama, "Introduction of archiver appliance to RILAC control system," Proceedings of 17th Annual Meeting of Particle Accelerator Society of Japan, 739–742 (2020).

T. Watanabe, N. Fukunishi, H. Imao, O. Kamigaito, T. Nishi, T. Ozeki, N. Sakamoto, A. Uchiyama, Y. Watanabe, K. Yamada, T. Toyama, A. Kamoshida, K. Hanamura, and R. Koyama, "Commissioning of the beam energy position monitoring system for the superconducting RIKEN heavy-ion linac," Proceedings of 9th International Beam Instrumentation Conference, 295–302, ISBN:978-3-95450-222-6 (2020).

Presentations

[International Conferences/Workshops]

T. Watanabe (invited), N. Fukunishi, H. Imao, O. Kamigaito, T. Nishi, T. Ozeki, N. Sakamoto, A. Uchiyama, Y. Watanabe, K. Yamada, T. Toyama, A. Kamoshida, K. Hanamura, and R. Koyama, "Commissioning of the beam energy position monitoring system for the superconducting RIKEN heavy-ion linac," 9th International Beam Instrumentation Conference, FRAO04, Santos, Brazil (online), September 14–18, 2020.

[Domestic Conferences/Workshops]

N. Fukunishi (invited), "Beam intensity upgrade of RIKEN RI Beam Factory," 17th Annual Meeting of Particle Accelerator Society of Japan, WEOOP02, Online, September 2–4, 2020.

T. Nishi (oral), A. Uchiyama, O. Kamigaito, N. Sakamoto, T. Nagatomo, N. Fukunishi, M. Fujimaki, T. Watanabe, and Y. Watanabe, "Emittance measurement and ion optics tuning for SRILAC beam line," 17th Annual Meeting of Particle Accelerator Society of Japan, THOO08, Online, September 2–4, 2020.

T. Watanabe (poster), T. Toyama, K. Hanamura, H. Imao, A. Uchiyama, K. Ozeki, O. Kamigaito, N. Sakamoto, T. Nishi, N. Fukunishi, K. Yamada, Y. Watanabe, R. Koyama, and A. Kamoshida, "Commissioning of the beam energy and position monitor system for the superconducting RIKEN heavy-ion linac," 17th Annual Meeting of Particle Accelerator Society of Japan, FRPP20, Online, September 2–4, 2020.

A. Uchiyama (poster) and M. Komiyama, "Introduction of archiver appliance to RILAC control system," 17th Annual Meeting of Particle Accelerator Society of Japan, FRPP26, Online, September 2–4, 2020.

T. Watanabe (invited), "Construction of beam energy position monitoring system using PXI digitizers for the superconducting RIKEN heavy-ion linac," LabVIEW User's Particle Accelerator Community 2020.12.16 Online Conference, Online, December 16, 2020.

Awards

T. Nishi, "Emittance measurement and ion optics tuning for SRILAC beam line," Oral Presentation Awards of 17th Annual Meeting of Particle Accelerator Society of Japan (2020).

Research Facility Development Division
Accelerator Group
Cryogenic Technology Team

1. Abstract

We are operating the cryogenic system for the superconducting ring cyclotron in RIBF. We are operating the helium cryogenic system in the south area of RIKEN Wako campus and delivering the liquid helium to users in RIKEN. We are trying to collect efficiently gas helium after usage of liquid helium.

2. Major Research Subjects

(1) Operation of the cryogenic system for the superconducting ring cyclotron in RIBF.
(2) Operation of the helium cryogenic plant in the south area of Wako campus and delivering the liquid helium to users in Wako campus.

3. Summary of Research Activity

(1) Operation of the cryogenic system for the superconducting ring cyclotron in RIBF (H. Okuno, T. Dantsuka, M. Nakamura, T. Maie).
(2) Operation of the helium cryogenic plant in the south area of Wako campus and delivering the liquid helium to users in Wako campus. (T. Dantsuka, S. Tsuruma, M. Kuroiwa, M. Takahashi, H. Okuno).

Members

Team Leader

Hiroki OKUNO

Research/Technical Scientist

NAKAMURA (Senior Technical Scientist)

Expert Technicians

Tomoyuki DANTSUKA
Takeshi MAIE

Part-time Workers

Mamoru TAKAHASHI (Research Part-time Worker I)
Mayumi KUROIWA (Administrative Part-time Worker II)
Shizuho TSURUMA (Administrative Part-time Worker I)

Research Facility Development Division
Accelerator Group
Infrastructure Management Team

1. Abstract

Our team is in charge of the design, operation, and maintenance of the large-scale infrastructure for the entire RI Beam Factory (RIBF), including cooling water, air conditioning, and electrical equipment, as well as the research and development of their advanced management. In order to operate the RIBF efficiently, it is very important to ensure the sound operation of these infrastructures that lead to the stable functioning of various devices. Another important mission is to coordinate the scheduling of major construction and repair work related to the RIBF so that beamtime runs smoothly.

The recent issue is the aging of infrastructure equipment. In line with these measures, we are making modifications that contribute to the stability of accelerator equipment and energy saving. In addition, infrastructure equipment has many sensors for management, and a huge amount of measurement data from these sensors is archived. We are planning to use this data to build a more advanced management system.

2. Major Research Subjects

(1) Operation, maintenance and monitoring of infrastructure of RI Beam Factory.
(2) Development of advanced management of infrastructure that contributes to accelerator and beam stability.
(3) Coordination of large construction work and modification related to RI Beam Factory.

Members

Team Leader
Masanori KIDERA

Deputy Team Leader
Yutaka WATANABE

Special Temporary Technical Scientist
Shu WATANABE

Special Temporary Employee
Hideyuki YAMASAWA

List of Publications & Presentations

Publications

[Proceedings]

西田稔, 大関和貴, 後藤彰, 大西純一, 大城幸光, 福澤聖児, 濱仲誠, 石川盛, 小林清志, 小山亮, 仲村武志, 西村誠, 柴田順翔, 月居憲俊, 矢冨一慎, 藤巻正樹, 福西暢尚, 長谷部裕雄, 日暮祥英, 今尾浩士, 上垣外修一, 加瀬昌之, 木寺正憲, 込山美咲, 熊谷桂子, 真家武士, 長友傑, 中川孝秀, 奥野広樹, 坂本成彦, 須田健嗣, 内山暁仁, 渡部秀, 渡邉環, 渡邉裕, 山田一成, 鎌倉恵太, 小高康照, 「理研 AVF サイクロトロン運転の現状報告」, “Status report on the operation of RIKEN AVF Cyclotron,” Proc. 17th Annu. Meet. Part. Accel. Soc. Jpn., p. 921, 2020 年 10 月 23 日.

石川盛, 須田健嗣, 福澤聖児, 濱仲誠, 小林清志, 小山亮, 仲村武志, 西田稔, 西村誠, 柴田順翔, 月居憲俊, 矢冨一慎, 段塚知志, 藤巻正樹, 藤縄雅, 福西暢尚, 長谷部裕雄, 日暮祥英, 池沢英二, 今尾浩士, 上垣外修一, 金井保之, 加瀬昌之, 木寺正憲, 込山美咲, 熊谷桂子, 真家武士, 長友傑, 中川孝秀, 中村仁音, 大西純一, 奥野広樹, 大関和貴, 坂本成彦, 内山暁仁, 渡部秀, 渡邉環, 渡邉裕, 山田一成, 山澤秀行, 「理研 RIBF におけるリングサイクロトロンの運転報告」, “Status report of the operation of RIBF ring cyclotrons,” 第 17 回日本加速器学会年会プロシーディングス, web 公開のみ, 2020 年 10 月 21 日. https://www.pasj.jp/web_publish/pasj2020/proceedings/PDF/WESP/WESP03.pdf.

坂本成彦, 藤巻正樹, 池沢英二, 今尾浩士, 上垣外修一, 長友傑, 西隆博, 大関和貴, 須田健嗣, 内山暁仁, 渡邉環, 渡邉裕, 山田一成, 「理研超伝導線型加速器 SRILAC のコミッショニング」, “Commissioning of superconducting-linac booster for RIKEN heavy-ion linac,” 第 17 回日本加速器学会年会プロシーディングス, web 公開のみ, 2020 年 10 月 21 日. https://www.pasj.jp/web_publish/pasj2020/proceedings/PDF/WESP/WESP03.pdf.

渡邉環, 福西暢尚, 今尾浩士, 上垣外修一, 西隆博, 大関和貴, 坂本成彦, 内山暁, 渡邉裕, 山田一成, 外山毅, 鴨志田敦史, 花村幸篤, 小山亮, 「理研超伝導重イオンリニアック用ビームエネルギー・位置モニターシステムのコミッショニング」, “Commissioning of the beam energy position monitoring system for the superconducting RIKEN Heavy-ion LINAC,” Proc. 9th International Beam Instrumentation Conference (IBIC 2020), pp. 295–302 October 30, 2020. http://accelconf.web.cern.ch/ibic2020/papers/frao04.pdf.

渡邉環, 外山毅, 花村幸篤, 今尾浩士, 内山暁, 大関和貴, 上垣外修一, 坂本成彦, 西隆博, 福西暢尚, 山田一成, 渡邉裕, 小山亮, 鴨志田敦史, 「理研超伝導リニアック用ビームエネルギー・位置モニターのコミッショニング」, “Commissioning of the beam energy and position monitor system for the superconducting RIKEN Heavy-ion Linac,” 第 17 回日本加速器学会年会, PASJ2020 FRPP20, pp. 718–723, 2020 年 10 月 23 日. https://www.pasj.jp/web_publish/pasj2020/proceedings/PDF/FRPP/FRPP20.pdf

H. Imao, O. Kamigaito, N. Sakamoto, T. Watanabe, Y. Watanabe, K. Yamada, K. Oyamada, “Non-evaporative getter-based differential pumping system for SRILAC at RIBF,” Proc. 19th International Conference on RF Superconductivity (SRF 2019), web 公開のみ, 2019 年 11 月. http://accelconf.web.cern.ch/srf2019/papers/tup013.pdf.

Research Facility Development Division
Instrumentation Development Group

1. Abstract

This group develops core experimental installations at the RI Beam factory. Three projects are currently going on. SLOWRI is an experimental installations under testing and a common element enabling multiple-use. This will stop high-energy RI beams in a gas-catcher system and re-accelerates up to several-tenth keV, and the high-quality cold RI beam will be delivered to the users. SCRIT is the world first facility for an electron scattering off unstable nuclei, and has been constructed independently of the RIBF main facility. The first physic result was demonstrated in 2017, and the facility is now under upgrading of the electron beam power driving the RI beam production. Rare-RI Ring is an event-by-event operated heavy-ion storage ring aiming at the precision mass measurement for extremely rare exotic nuclei. This is now open for an experimental proposal application, and has already performed PAC-approved experiments, and an improvement for higher precise mass measurement is now going on. A small size heavy-ion storage ring, RUNBA, is R&D machine for technical development of beam recycling aiming at nuclear reaction study for rarely produced isotopes. This is under preparing for construction and the technical development for some key components in the ring are now going on. All instrumentations were designed to maximize the research potential of the world's most intense RI beams, and the exclusive equipment available at the RI Beam Factory makes experimental challenges possible. Technologies and experiences accumulated in this group will be able to provide opportunities of new experimental challenges and the foundation for future developments of RIBF.

2. Major Research Subjects

(1) SCRIT Project
(2) SLOWRI Project
(3) Rear RI Ring Project
(4) RUNBA project (Beam recycling development)

3. Summary of Research Activity

We are developing beam manipulation technology in carrying out above listed project. They are the high-quality slow RI beam production (SCRIT and SLOWRI), the beam cooling and stopping (SCRIT and SLOWRI), and the beam accumulation technology (Rare RI Ring and RUNBA) in a storage ring. The technological knowhow accumulated in our projects will play a significant role in the next generation RIBF. Status and future plan for each project is described in subsections. The electron scattering from ^{132}Xe isotopes has been successfully measured and the nuclear charge density distribution has been obtained in SCRIT. We are upgrading the power of electron beam from RTM, which is the driver for RI production, for going to world-first electron scattering off unstable nuclei. Performance of Rare RI Ring has already been evaluated and successfully started mass-measurements for unknown-mass nuclei in the experiments approved by PAC. Recently, we succeeded in measurement of masses of ^{74,76}Ni, ^{122}Rh, ^{123,124}Pd, and ^{125}Ag for the first time. Since expected performances on a mass resolution and an efficiency has slightly been unachieved, the fast kicker system and the optics tuning system are under improvement. SLOWRI is now under test experiments to establish a slow RI beam production using two types of gas cells. PALIS has been commissioned from 2015, and basic functions such as, for instance, the RI-beam stopping in Ar gas cell and the extraction from the gas cell have beam evaluated. RF carpet gas cell (RFGC) combined with multi-reflection time-of-flight device is now working as a movable mass spectrograph at some facility such as ZeroDegree and GARIS. Detail status and future plans for these projects are described in subsections.

According to the future plans of the Nishina Center, we have started development of a beam re-cycling technique. A circulation of an RI beam in a storage ring equipped by a thin internal target is maintained until that some nuclear reaction occur at the target. In order to establish a beam re-cycling technique, the energy loss has to be compensated and growth of the energy-spread and the emittance have to be corrected by using a re-acceleration system and a beam-cooling or a fast feedback system, respectively. A beam re-cycling technique is supposed to greatly enhance an RI use efficiency in a nuclear physics study. For the development of these novel technique, we will construct a relatively small size of heavy-ion storage ring (RUNBA) connected to ISOL (ERIS) in the SCRIT facility. This is equipped by acceleration devices and beam-cooling devices necessary in our R&D study. It was originally constructed as a beam cooler ring (sLSR) at the Institute for Chemical Research (ICR), Kyoto University more than ten years ago. This ring is re-cycled at RIBF and it has been already moved to RIBF. Technical development for key devices required in RUNBA such as a charge breeder (CB), an energy-dispersion corrector (EDC), angular diffusion corrector (ADC), and an internal target system have been already started under the research cooperation agreement with ICR Kyoto University.

Members

Director
Masanori WAKASUGI

Contract Researcher
Ryo OGAWARA

Visiting Scientists

Yasushi ABE (Nat'l Inst. of Radiological Sci.)
Akira OZAWA (Tsukuba Univ.)
Fumi SUZAKI (JAEA)
Kyo TSUKADA (Kyoto Univ.)

Part-time Worker

Midori TAKEMON (Administrative Part-time Worker I)

List of Publications & Presentations

Publications and presentations are listed in subsections.

Research Facility Development Division
Instrumentation Development Group
SLOWRI Team

1. Abstract

SLOWRI is a universal low-energy RI-beam facility at RIBF that provides a wide variety of short-lived nuclei as high-purity and low-emittance ion beams or stored ions in a trap, including a parasitic operation mode. The SLOWRI team develops and manages the facility and performs high-precision spectroscopy experiments. The construction of the SLOWRI facility began in FY2013 and commissioning work is ongoing. From FY2019, SLOWRI has been started to be co-operated under RNC and WNSC/KEK collaboration.

High-energy radioactive ion beams from the projectile fragment separator BigRIPS are thermalized in a large He gas catcher cell (RFGC) or in a small Ar gas catcher cell (PALIS cell). From these gas cells, the low-energy ion beams will be delivered via mass separators and switchyards to various devices: such as an ion trap, a collinear fast beam apparatus, and a multi-reflection time of flight mass spectrograph. A multi-reflection time-of-flight mass spectrograph (MRTOF) has been also developed.

Two mass measurement projects using MRTOF mass spectrographs have been started: one is for trans uranium elements at the GARIS facility and the other is for r-process nuclides at SLOWRI facility. At GARIS-II, we installed second prototype RFCG combined with MRTOF, which is a medium-sized cryogenic RF-carpet He gas cell. Using second prototype RFGC, more than 80 nuclear masses have been measured including first mass measurements of Md and Es isotopes. In FY2020, we have started mass measurements for neutron rich unstable nuclei using a fission source installed in the second prototype RFGC. At SLOWRI facility, third prototype RFGC has been installed at F11, the downstream of ZeroDegree spectrometer, which is a 50-cm-long RF-carpet-type He gas cell combined with MRTOF. In November and December of FY2020, we have successfully performed the on-line commissioning, symbiotically by using RIs provided for HiCARI campaign. The extraction efficiency in total has been achieved at 1% in maximum and the masses on more than 70 nuclei have been measured using RIs provided with BigRIPS.

Parallelly, the on-line commissioning for PALIS has been continuously performed at F2 of BigRIPS. In FY2020, the extraction of I-emitter Bi Isotopes by the gas flow without a laser ionization has been confirmed from PALIS gas cell.

2. Major Research Subjects

(1) Construction of the stopped and low-energy RI-beam facility, SLOWRI.
(2) Development of a multi-reflection time-of-flight mass spectrograph for precision mass measurements of short-lived nuclei.
(3) Development of collinear laser spectroscopy apparatus.
(4) Development of a parasitic slow RI-beam production method using resonance laser ionization.

3. Summary of Research Activity

(1) Construction of stopped and low-energy RI-beam facility (SLOWRI)

SLOWRI consists of two gas catchers (RF carpet gas cell and PALIS gas cell), mass separators a 50-m-long beam transport line, a beam cooler-buncher, an isobar separator, and a laser system. The RF carpet gas cell (RFGC) will be installed at the exit of the D5 dipole magnet of BigRIPS. The gas catcher contains a large cryogenic He gas cell with a large traveling wave rf-carpet. The PALIS gas cell is installed in the vicinity of the second focal plane slit of BigRIPS. It will provide parasitic RI-beams from those ions lost in the slits during other experiments. In this gas catcher, thermalized RI ions quickly become neutral and will be re-ionized by resonant laser radiations. Off- and on-line commissioning is underway.

Based on test experiments with the prototype setups, the RF-carpet gas cell contains a three stage rf-carpet structure: a gutter rf carpet (1st carpet) for the collection thermal ions in the cell into a small slit, a narrow (about 10 mm) traveling-wave rf-carpet (2nd carpet) for collection of ions from the gutter carpet and for transporting the ions towards the exit, and a small rf carpet for extraction from the gas cell. The off-line test has been completed in FY2019.

A 50-cm-long RFGC, which is a prototype for final version RFGC with 1.5 m length, has been installed at F11 of ZeroDegreee spectrometer of BigRIPS in FY2020. In November and December of 2020, the on-line commissioning has been successfully performed symbiotically using RIs provided with BigRIPS during HiCARI campaign. The extraction efficiency in total has been achieved at 1% in maximum.

(2) Development of a multi-reflection TOF mass spectrograph for short-lived nuclei

The atomic mass is one of the most important quantities of a nucleus and has been studied in various methods since the early days of modern physics. From among many methods we have chosen a multi-reflection time-of-flight (MRTOF) mass spectrometer. Slow RI beams extracted from the RF ion-guide are bunched and injected into the spectrometer with a repetition rate of ~100 Hz. A mass-resolving power of 170,000 has been obtained with a 2 ms flight time for ^{40}K and ^{40}Ca isobaric doublet. This mass-resolving power should allow us to determine ion masses with an accuracy of $\leq 10^{-7}$. A new MRTOF has been assembled in FY2019 to be coupled with the third prototype of RFGC and has been installed at F11 of BigRIPS in FY2020. Mass measurements using RIs provided with BigRIPS during HiCARI campaign have been symbiotically performed. As the result, atomic masses on more than 70 nuclei have been successfully measured. Among them, 11 isotope masses improve the present uncertainty significantly and 3 isotope masses have been measured for the first time.

(3) Development of collinear fast beam apparatus for nuclear charge radii measurements

The root-mean-square charge radii of unstable nuclei have been determined exclusively by isotope shift measurements of the optical transitions of singly charged ions or neutral atoms by laser spectroscopy. Many isotopes of alkali, alkali-earth, and noble-gas elements in addition to several other elements have been measured by collinear laser spectroscopy since these ions all have good optical transitions and are available at conventional ISOL facilities. However, isotopes of other elements, especially refractory and short-lived ones, have not been investigated so far.

In SLOWRI, isotopes of all atomic elements will be provided as well collimated, mono-energetic ion beams. This should expand the range of nuclides available for laser spectroscopy. An off-line mass separator and a collinear fast beam apparatus with a large solid-angle fluorescence detector was built previously. A 617-nm transition of the metastable Ar^+ ion at 20 keV was measured with both collinear and anti-collinear geometry, which allowed determination of the absolute resonant frequency of the transition at rest with a relative accuracy better than 10^{-8}. A new setup is under preparation at the SLOWRI experiment area in collaboration with the Nuclear Spectroscopy Laboratory.

(4) Development of parasitic slow RI-beam production scheme using resonance laser ionization

More than 99.9% of RI ions produced in projectile fission or fragmentation are simply dumped in the first dipole magnet and the slits. A new scheme, named PALIS, meant to rescue such precious RI using a compact gas catcher cell and resonance laser ionization, was proposed as a part of SLOWRI. The thermalized RI ions in a cell filled with Ar gas can be quickly neutralized and transported to the exit of the cell by gas flow. Irradiation of resonance lasers at the exit ionizes neutral RI atoms efficiently and selectively. PALIS has been installed at F2 at the downstream of BigRIPS. and off- and on-line commissioning is under progress.

At F2, due to high radiation from a beam dump, it is not easy to handle ions using electric ion guides. Therefore, a 70-cm-long gas pipe from the Ar gas cell was newly installed to transport RIs to relatively low radiation area thanks for the Ar gas flow. In FY2020, we have confirmed the transportation of RIs through the gas pipe to the relatively low radiation area using -emitting Bi isotopes provided with BigRIPS. In FY2021, an on-line test for resonant laser ionization is planned using α-emitting Bi isotopes.

Members

Team Leader

Hironobu ISHIYAMA

Research/Technical Scientists

Takao KOJIMA (Senior Research Scientist)
Aiko TAKAMINE (Research Scientist)
Tetsu SONODA (Technical Scientist)

Expert Technician

Takeshi MAIE

Junior Research Associate

Shun IIMURA

Visiting Scientists

Hideki IIMURA (JAEA)
Kunihiro OKADA (Sophia Univ.)
Mikael REPONEN (Univ. of Jyvaskyla)
Hans SCHUESSLER (Texas A&M Univ.)
Volker SONNENSCHEIN (Nagoya Univ.)
Minoru TANIGAKI (Kyoto Univ.)
Hideki TOMITA (Nagoya Univ.)
Hermann WOLLNIK (Univ. of Giessen)

List of Publications & Presentations

Publications

[Original Papers]

Y. Hirayama, P. Schury, M. Mukasi, H. Choi, S. Iimura, Y. X. Watanabe, M. Wada, H. Watanabe, and H. Miyatake, "Three-dimentional tracking multi-segmented proportional gas counter for beta-decay spectroscopy of unstable nuclei," Nucl. Instrum. Methods Phys. Res. A **997**, 165152 (2020).

M. Rosenbusch, P. Schury, M. Wada, S. Iimura, Y. Ito, and H. Wollnik, "Accurately accounting for effects on times-of-flight caused by finite field-transition times during the ejection of ions from a storage trap: A study for single-reference TOF and MRTOF mass spectrometry," International Journal of Mass Spectrometry **456**, 116346 (2020).

M. Mukai, Y. Hirayama, P. Schury, Y. X. Watanabe, M. Ahmed, H. Haba, H. Ishiyama, S. C. Jeong, Y. Kakiguchi, S. Kimura, J. Y. Moon, M. Oyaizu, A. Ozawa, J. H. Park, H. Ueno, M. Wada, and H. Miyatake, "Development of a multi-segmented proportional gas counter for β-decay spectroscopy at KISS," Nucl. Instrum. Methods Phys. Res. B **463**, 423–424 (2020).

Y. Hirayama, Y. X. Watanabe, M. Mukai, P. Schury, M. Ahmed, H. Ishiyama, S. C. Jeong, Y. Kakiguchi, S. Kimura, J. Y. Moon, M. Oyaizu, J. H. Park, M. Wada, and H. Miyatake, "Nuclear spectroscopy of r-process nuclei using KEK isotope separation system," Nucl. Instrum. Methods Phys. Res. B**463**, 425–430 (2020).

M. Mukai, Y. Hirayama, Y. X. Watanabe, S. Schiffmann, J. Ekman, M. Godefroid, P. Schury, Y. Kakiguchi, M. Oyaizu, M. Wada, S. C. Jeong, J. Y. Moon, J. H. Park, H. Ishiyama, S. Kimura, H. Ueno, M. Ahmed, A. Ozawa, H. Watanabe, S. Kanaya, and H. Miyatake, "In-gas-cell laser resonance ionization spectroscopy of ^{196,197,198}Ir," Phys. Rev. C **102**, 054307 (2020).

M. Rosenbusch, M. Wada, P. Schury, Y. Ito, H. Ishiyama, S. Ishizawa, Y. Hirayama, S. Kimura, T. M. Kojima, H. Miyatake, J. Y. Moon, T. Niwase, T. Sonoda, A. Takamine, Y. X. Watanabe, and H. Wollnik, "A new multi-reflection time-of-flight mass spectrograph for the SLOWRI facility," Nucl. Instrum. Methods Phys. Res. B **463**, 184–188 (2020).

Presentations

[International Conferences/Workshops]

A. Takamine (invited), "SLOWRI rf gas catcher development toward symbiotic mass measurement," RIBF Users Meeting 2020, on-line, Wako, Japan, September 8–10, 2020.

H. Ishiyama (invited), "Present status of SLOWRI," SSRI-PNS collaboration meeting, on-line, Wako, Japan, September 3, 2020.

[Domestic Conferences/Workshops]

飯村俊, 高峰愛子, M. Rosenbusch, 和田道治, S. Chen, J. Liu, W. Xian, D. Hou, S. Yan, P. Schury, 園田哲, 小島隆夫, 渡辺裕, 小田原厚子, 石山博恒, 「理研 BigRIPS SLOWRI における RF カーペットガスセルの開発～オンライン試験と質量測定」, 日本物理学会第 76 回年次大会, on-line, 2021 年 3 月 12 日.

M. Rosenbush, M. Wada, P. Schury, Y. Hirayama, H. Miyatake, Y. X. Watanabe, S. Iimura, H. Ishiyama, T. Kojima, T. Sonoda, M. Mukai, S. Nishimura, S. Naimi, T. Niwase, A. Takamine, Y. Ito, D. S. Hou, J. Liu, S. Chen, J. Lee, and W. Xian, "New mass measurements of exotic nuclides by the first MRTOF setup at BigRIPS/RIKEN," 日本物理学会第 76 回年次大会, on-line, 2021 年 3 月 12 日.
飯村俊, 高峰愛子, M. Rosenbusch, 和田道治, S. Chen, J. Liu, W. Xian, D. Hou, S. Yan, P. Schury, 園田哲, 小島隆夫, 渡辺裕, 小田原厚子, 石山博恒, 「理研 BigRIPS SLOWRI における RF カーペットガスセルの開発」, 日本物理学会 2020 年秋季大会, 2020 年 9 月 8–11 日.

Research Facility Development Division
Instrumentation Development Group
Rare RI-ring Team

1. Abstract

The aim of Rare-RI Ring (R3) is to measure the masses of short-lived unstable nuclei far from the beta-stability line. In particular, a high-precision mass measurement for nuclei located around the r-process pass (rare-RI) is required in nucleosynthesis point of view. The R3 completed the construction at the end of 2014, and has been performed commissioning experiments several times by 2017. Through the commissioning experiments, we confirmed the high ability of R3 as a storage ring capable of handling one event, and demonstrated that it is possible to perform the time-of-flight Isochronous Mass Spectrometry (IMS) in shorter than 1 ms. We have acquired an adequate efficiency to conduct the mass measurement experiments in the end of 2017. In 2020, a machine study was conducted using upgraded kicker system. We succeeded in extracting all injected nuclides in a single extraction and then the experimental efficiency became at least twice better than that achieved using the previous method, where different extraction timings were needed to extract all nuclides. Furthermore, the systematic uncertainty caused by different kick angles has been eliminated. The open question of the first mass measurement experiment in 2018 will be solved by performing mass measurement experiments utilizing the upgraded kicker system in 2021.

2. Major Research Subjects

(1) Further improvement of experimental efficiency and mass measurement precision
(2) Precision mass measurement for rarely produced isotopes related to r-process

3. Summary of Research Activity

In the commissioning experiments up to 2017, we confirmed the unique performances of R3 and demonstrated the time-of-flight isochronous mass measurement method. The ring structure of R3 was designed with a similar concept of a separate-sector ring cyclotron. It consists of six sectors and straight sections, and each sector consists of four rectangular bending magnets. Two magnets at both ends of each sector are additionally equipped with ten trim coils to form a precise isochronous field. We have realized in forming the precise isochronous field of 5 ppm with wide momentum range of $\Delta p/p = \pm 0.5\%$. Another performance required for R3 is to efficiently seize hold of an opportunity of the mass measurement for rare-RIs produced unpredictably. It was realized by constructing the Isotope-Selectable Self-trigger Injection (ISSI) scheme which pre-identified rare-RI itself triggers the injection kicker magnets. Key device was an ultra-fast response kicker system that has been successfully developed. Full activation of the kicker magnetic field can be completed within the flight time of the rare-RI from an originating point (F3 focal point in BigRIPS) of the trigger signal to the kicker position in R3.

Since R3 accumulates, in principle, only one event, we fabricated high-sensitive beam diagnostic devices in the ring. They should be applicable even for one event circulation. One of them is a cavity type of Schottky pick-up installed in a straight section of R3. The Schottky pick-up successfully monitored a single $^{78}Kr^{36+}$ ion circulation with the measurement time of less than 10 ms in the first commissioning experiment. We also confirmed that it is useful for fine tuning of the isochronous field. Another is a timing monitor, which detects secondary electrons emitted from thin carbon foil placed on the circulation orbit. The thickness of the foil is 50 μg/cm^2. This timing monitor is working well to observe first several tens turns for injected event.

We performed mass measurement in the third commissioning experiment by using unstable nuclei which masses are well-known. The masses of ^{79}As, ^{77}Ga, ^{76}Zn, and ^{75}Cu relative to ^{78}Ge were derived with the accuracy of less than 10 ppm. In addition, we have improved the extraction efficiency to 2% by considering the matching condition between the emittance of injection events and the acceptance of R3. This extraction efficiency was sufficient to conduct the accepted two proposals: mass measurements of Ni isotopes and mass measurements of Sn region.

In the beginning of 2018, we examined the feasibility of these two proposals in detail and decided to proceed with two proposals at the same period. In the beginning of November 2018, we have conducted the first experiment using R3 to measure the masses for ^{74,76}Ni in 4 days. After that, we also measured the masses for ^{122}Rh, ^{123,124}Pd, and ^{125}Ag in 4.5 days at the end of November 2018. These nuclei were successfully extracted from R3 with the efficiency of 1–2%. However, unexpected deviation from the evaluated values of literature remains in the masses obtained by detailed analysis. This open question is thought to be due to the following two reasons. One is that the TOF at R3 is mistaken because the target nuclei were extracted at a slope part of kicker field distribution. The other is that the absolute value of beta or magnetic rigidity determined for each extracted event is incorrect. In order to eliminate the former concern and verify the latter, we have improved the kicker system. This improvement achieves a flat-top of 100 ns for injection and a long flat-top of 350 ns or more for extraction.

A machine study was conducted using the upgraded kicker system in November 2020. We succeeded in extracting all events with different revolution times at once by realizing a long flat-top. Experimental efficiency became at least twice better than that achieved using the previous method, where different extraction timings were needed to extract all nuclides. In addition, it was confirmed that there is a risk that an incorrect mass will be derived when extracted events at a slope part of kicker field distribution, depending on an isochronous condition. On the other hand, the masses could be derived with the expected accuracy when extracted events at a flat-top part of kicker field distribution. Since each proposal mentioned above still has a machine time of several days, we will conduct mass measurement experiments using the upgraded kicker system in 2021 and solve the open question.

Members

Team Leader
Masanori WAKASUGI

Technical Scientist
Yoshitaka YAMAGUCHI (Technical Scientist)

Expert Technician
Takeshi MAIE

List of Publications & Presentations

Publications

[Original Papers]

D. Nagae, Y. Abe, S. Okada, S. Omika, K. Wakayama, S. Hosoi, S. Suzuki, T. Moriguchi, M. Amano, D. Kamioka, Z. Ge, S. Naimi, F. Suzaki, N. Tadano, R. Igosawa, K. Inomata, H. Arakawa, K. Nishimuro, T. Fujii, T. Mitsui, Y. Yanagisawa, H. Baba, S. Michimasa, S. Ota, G. Lorusso, Yu. A. Litvinov, A. Ozawa, T. Uesaka, T. Yamaguchi, Y. Ymaguchi, and M. Wakasugi, "Development and operation of an electrostatic time-of-flight detector for the Rare RI storage Ring," Nucl. Instrum. Methods Phys. Res. A **986**, 164713-1–7 (2020).

S. Suzuki, A. Ozawa, D. Kamioka, Y. Abe, M. Amano, H. Arakawa, Z. Ge, K. Hiraishi, Y. Ichikawa, K. Inomata, A. Kitagawa, T. Kobayashi, H. F. Li, T. Matsumoto, T. Moriguchi, M. Mukai, D. Nagae, S. Naimi, S. Omika, S. Sato, Y. Tajiri, K. Wakayama, and T. Yamaguchi, "Efficiency and timing performance of time-of-flight detector utilizing thin foils and crossed static electric and magnetic fields for mass measurements with Rare-RI Ring facility," Nucl. Instrum. Methods Phys. Res. A **965**, 163807-1–14 (2020).

C. Y. Fu, Y. H. Zhang, M. Wang, X. H. Zhou, Yu. A. Litvinov, K. Blaum, H. S. Xu, X. Xu, P. Shuai, Y. H. Lam, R. J. Chen, X. L. Yan, X. C. Chen, J. J. He, S. Kubono, M. Z. Sun, X. L. Tu, Y. M. Xing, Q. Zeng, X. Zhou, W. L. Zhan, S. Litvinov, G. Audi, T. Uesaka, T. Yamaguchi, A. Ozawa, B. H. Sun, Y. Sun, and F. R. Xu, "Mass measurements for the $T_z = -2$ fp-shell nuclei ^{40}Ti, ^{44}Cr, ^{46}Mn, ^{48}Fe, ^{50}Co, and ^{52}Ni," Phys. Rev. C **102**, 054311-1–11 (2020).

[Proceedings]

S. Naimi, H. F. Li, Y. Abe, Y. Yamaguchi, D. Nagae, F. Suzaki, M. Wakasugi, H. Arakawa, W. Dou, D. Hamakawa, S. Hosoi, Y. Inada, K. Inomata, D. Kajiki, T. Kobayashi, M. Sakaue, K. Yokota, T. Yamaguchi, R. Kagesawa, D. Kamioka, T. Moriguchi, M. Mukai, A. Ozawa, S. Ota, N. Kitamura, S. Masuoka, D. S. Ahn, H. Baba, N. Fukuda, Y. Shimizu, H. Suzuki, H. Takeda, C. Y. Fu, Z. Ge, Q. Wang, M. Wang, Yu. A. Litvinov, G. Lorusso, and T. Uesaka, "Experimental challenges of the first mass measurement campaign at the Rare-RI Ring," J. Phys. Conf. Ser. **1643**, 012058-1–6 (2020).

S. Omika, T. Yamaguchi, N. Tadano, Y. Abe, M. Amano, Z. Ge, D. Kamioka, T. Morigushi, D. Nagae, S. Naimi, A. Ozawa, F. Suzaki, S. Suzuki, T. Suzuki, T. Uesaka, M. Wakasugi, K. Wakayama, and Y. Yamaguchi, "Development of a new in-ring beam monitor in the Rare-RI Ring," Nucl. Instrum. Methods Phys. Res. B **463**, 241–243 (2020).

J. H. Liu, X. Xu, P. Zhang, P. Shuai, X. L. Yan, Y. H. Zhang, M. Wang, Yu. A. Litvinov, H. S. Xu, K. Blaum, T. Bao, H. Chen, X. C. Chen, R. J. Chen, C. Y. Fu, D. W. Liu, W. W. Ge, R. S. Mao, X. W. Ma, M. Z. Sun, X. L. Tu, Y. M. Xing, J. C. Yang, Y. J. Yuan, Q. Zeng, X. Zhou, X. H. Zhou, W. L. Zhan, S. Litvinov, T. Uesaka, Y. Yamaguchi, T. Yamaguchi, A. Ozawa, and B. H. Sun, "Improving the resolving power of isochronous mass spectrometry by employing an in-ring mechanical slit," Nucl. Instrum. Methods Phys. Res. B **463**, 138–142 (2020).

Yu. A. Litvinov, Th. Stoehlker, X. W. Ma, Y. H. Zhang, and T. Yamaguchi, "Nuclear physics research at heavy ion accelerators: Precision studies with stored and cooled exotic nuclei," J. Phys. Conf. Ser. **1401**, 012001-1–9 (2020).

Presentations

[International Conferences/Workshops]

S. Naimi (invited), "Status of R3 and new in-ring detectors," NucAR Workshop, Online, December 7–10, 2020.

S. Naimi (invited), "Development of a large-area position-sensitive detector for the Rare-RI Ring at Riken," TCHoU Workshop, Online, March 29, 2021.

[Domestic Conferences/Workshops]

濱川大貴（口頭発表）,「稀少 RI リングのためのプラスチックシンチレータを用いた位置検出器の開発」, 日本物理学会 2020 年秋季大会, オンライン, 2020 年 9 月 14–17 日.

梶木大輔（口頭発表）,「稀少 RI リングにおける周回周期の測定のためのデルタ線検出器の性能評価」, 日本物理学会 2020 年秋季大会, オンライン, 2020 年 9 月 14–17 日.

[Seminars]

Yu. A. Litvinov (oral), "Heavy-ion storage rings and their use for precision nuclear structure and astrophysics experiments," Seminar on Precision Physics and Fundamental Symmetries, Online, July 2, 2020.

Yu. A. Litvinov (oral), "Combining atomic and nuclear physics in ion storage rings," Online Lectures of the Matter and Cosmos Section (SMuK), Online, March 11, 2021.

Research Facility Development Division
Instrumentation Development Group
SCRIT Team

1. Abstract

The SCRIT Electron Scattering Facility has been constructed at RIKEN RIBF. This aims at investigation of internal nuclear structure for short-lived unstable nuclei by means of electron scattering. SCRIT (Self-Confining RI Ion Target) is a novel method to form internal targets in an electron storage ring. This is a unique method for making electron scattering experiments for unstable nuclei possible. Construction of the facility has been started in 2009. This facility consists of an electron accelerator (RTM), a SCRITequipped electron storage ring (SR2), an electron-beam-driven RI separator (ERIS), and a window-frame spectrometer for electron scattering (WiSES) which consists of a large window-frame dipole magnet, drift chambers and trigger scintillators. Installation of all components in the facility was completed in 2015. After the comprehensive test and tuning, the luminosity was reached to $3 \times 10^{27}/(\mathrm{cm}^2\mathrm{s})$ with the number of injected ions of 3×10^8. In 2016, we successfully completed a measurement of diffraction of scattered electrons from ^{132}Xe nuclei and determined the charge density distribution for the first time. The facility is now under setting up to move the first experiment for unstable nuclei.

2. Major Research Subjects

Development of SCRIT electron scattering technique and measurement of the nuclear charge density distributions of unstable nuclei.

3. Summary of Research Activity

SCRIT is a novel technique to form internal target in an electron storage ring. Positive ions are three dimensionally confined in the electron beam axis by transverse focusing force given by the circulating electron beam and applied electrostatic longitudinal mirror potential. The created ion cloud composed of RI ions injected from outside works as a target for electron scattering. Construction of the SCRIT electron scattering facility has been started in 2009. The electron accelerators RTM and the storage ring SR2 were successfully commissioned in 2010. Typical accumulation current in SR2 is 250–300 mA at the energy range of 120–300 MeV that is required energy range in electron scattering experiment. The SCRIT device was inserted in the straight section of SR2 and connected to an ISOL named ERIS (Electron-beam-driven RI separator for SCRIT) by 20-m long low energy ion transport line. A buncher system based on RFQ linear trap named FRAC (Fringing-RF-field-Activated dc-to-pulse converter) was inserted in the transport line to convert the continuous beam from ERIS to pulsed beam, which is acceptable for SCRIT. The detector system WiSES consisting of a high-resolution magnetic spectrometer, drift chambers and trigger scintillators, was constructed, and it has a solid angle of 100 msr, energy resolution of 10^{-3}, and the scattering angle coverage of 25–55 degrees. A wide range of momentum transfer, 80–300 MeV/c, is covered by changing the electron beam energy from 150 to 300 MeV.

We successfully measured a diffraction pattern in the angular distribution of scattered electron from ^{132}Xe isotope at the electron beam energy of 150 MeV, 200 MeV, and 300 MeV, and derived the nuclear charge distribution by assuming two-parameters Fermi model for the first time. At this time, luminosity was reached to $3 \times 10^{27}/(\mathrm{cm}^2\mathrm{s})$ at maximum and the averaged value was $1.2 \times 10^{27}/(\mathrm{cm}^2\mathrm{s})$ with the number of injected target ions of 3×10^8.

We are now under preparation for going to the experiments for unstable nuclei. There are some key issues for that. They are increasing the intensity of the RI beams from ERIS, efficient DC-to-pulse conversion at FRAC, improving the transmission efficiency from FRAC to SCRIT, and effective suppression of the background in measurement of scattered electrons. RI beam intensity will be improved by upgrading the electron beam power from 10 W to 60 W, increasing the contained amount of U in the target ion source, and some modifications in mechanical structure in the ion source. For upgrading the electron beam power, the RF system of RTM has been maintained intensively, and we will continue the development of RTM. For efficient DC-to-pulse conversion, we established the two-step bunching method, which is time compression at FRAC in combination with pre-bunching at the ion source using grid action. Furthermore, we will improve the conversion efficiency and the transmission efficiency from FRAC to the SCRIT device by cooling the trapped ions using minuscule amounts of a buffer gas. These improvements on FRAC were already confirmed in off-line test. Since one of significant contribution to the background for scattered electron is scattering from massive structural objects around the trapping region originated from halo components of the electron beam, we remodeled the SCRIT electrodes. The vacuum pump system at the SCRIT device has been upgraded to reduce the contribution of residual gases. Luminosity for radioactive Xe isotopes is expected to be more than $10^{26}/(\mathrm{cm}^2\mathrm{s})$ after these improvements. Then, we will be able to start experiments for unstable nuclei. When further upgrading in the RTM power planed to be 3 kW will be achieved, we can extend the measurements to more exotic nuclei.

In 2018, we developed several instruments. One is the introduction of the surface-ionization type ion source at ERIS in order to increase kinds of radioactive beam and to produce high intensity beam. Another development is the upgrading of the drift chamber located in front of the magnetic spectrometer of WiSES to improve the momentum resolution and angular acceptance. These developments help us to realize experiments for unstable nuclei.

In 2019, we installed a newly designed SCRIT electrodes. The main purpose of the replacement was to lower the background during the measurement due to the electron scattering from the SCRIT electrodes itself but not from the ion targets for the experiment. For that purpose, we employed thin metal wires to construct the electrodes rather than metal plates nor blocks. In addition, we modified the inside structure of the SCRIT chamber to symmetrize the electric ground potential affecting the potential curve inside the electrodes.

In 2020, we tested accelerators RTM and SR2 if they bear for long term experiment for 24 hours. Currently, we are adjusting the SR2 accelerator and ion source ERIS to be ready for the real electron scattering measurement of unstable nuclei.

Members

Team Leader
Masanori WAKASUGI

Research/Technical Scientists
Masamitsu WATANABE (Senior Research Scientist)
Tetsuya OHNISHI (Senior Technical Scientist)

Expert Technician
Takeshi MAIE

Junior Research Associate
Hikari WAUKE

Research Consultants
Takashi EMOTO
Toshitada HORI (Hiroshima Univ.)
Masahiro HARA
Shinichi ICHIKAWA

Visiting Scientists
Akitomo ENOKIZONO (Rikkyo Univ.)
Toshimi SUDA (Tohoku Univ.)
Yuki HONDA (Tohoku Univ.)
Shuo WANG (Shandong Univ. (Weihai)

Student Trainees
Taihei AOYAGI (Tohoku Univ.)
Clement V. LEGRIS (Tohoku Univ.)
Taiga GOKE (Tohoku Univ.)
Daisuke TAKI (Tohoku Univ.)
Kazushi ISHIZAKI (Tohoku Univ.)

List of Publications & Presentations

Publications

[Original Papers]

T. Suda, "Electron scattering for exotic nuclei," J. Phys. **1643**, 012159 (2020).

H. Kurasawa, T. Suda, and T. Suzuki, "The mean square radius of the neutron distribution and the skin thickness derived from electron scattering," Prog. Theor. Exp. Phys. **2021**, 013D02 (2021).

Presentations

[International Conferences/Workshops]

H. Wauke (oral), A. Enokizono, T. Suda, T. Tamae, K. Tsukada, T. Ohnishi, M. Wakasugi, and M. Watanabe, "Study of internal structure of unstable nuclei by electron scattering," International School for Strangeness Nuclear Physics 2020, KEK, Tsukuba, Japan, December 3–5, 2020.

[Domestic Conferences/Workshops]

須田利美 (申請代表者), 「シンポジウム: 軽中重核の電弱励起・崩壊と宇宙物理」, 日本物理学会 2020 年秋季大会, オンライン, 2020 年 9 月 14–17 日.

和宇慶ひかり (口頭発表), 石崎一志, 榎園昭智, 大西哲哉, 栗田和好, Clement Legris, 郷家大雅, 須田利美, 高木周, 瀧大祐 玉江忠明, 塚田 暁, 本多佑記, 若杉昌徳, 渡邊正満, 「電子散乱による核内中性子分布半径測定のための前方検出器の開発」, 日本物理学会 2020 年秋季大会, オンライン, 2020 年 9 月 14–17 日.

須田利美 (招待講演), "Electron scattering for structure studies of proton and exotic nuclei," 筑波大学原子核理論セミナー, 2020 年 10 月 23 日.

須田利美 (招待講演), 「陽子のサイズがおかしい？」, 埼玉大学原子核グループセミナー, 埼玉県さいたま市 (埼玉大学), 2021 年 2 月 16 日.

須田利美 (招待講演), 「陽子半径」, 日本のスピン物理学の展望, 島根県松江市, 2021 年 2 月 23–24 日.

Outreach Activities

須田利美 (特別講義), 「陽子のサイズがおかしい？」, 非常勤講師 (対象: 理系 6 クラス, 講義 3 コマ), 埼玉県熊谷市 (埼玉県熊谷高校), 2020 年 12 月 15 日.

須田利美 (集中講義), 「電子散乱による原子核研究」, 埼玉県さいたま市 (埼玉大学理学部物理), 2021 年 2 月 15–17 日.

Research Facility Development Division
Research Instruments Group

1. Abstract

The Research Instruments Group is the driving force at RI Beam Factory (RIBF) for continuous enhancement of activities and competitiveness of experimental research. Consisting of four teams, we are in charge of the operation, maintenance, and improvement of the core research instruments at RIBF, such as the BigRIPS in-flight RI separator, ZeroDegree spectrometer and SAMURAI spectrometer, and the related infrastructure and equipment. We are also in charge of the production and delivery of RI beams using the BigRIPS separator. The group also conducts related experimental research as well as R&D studies on the research instruments.

2. Major Research Subjects

Design, construction, operation, maintenance, and improvement of the core research instruments at RIBF and related R&D studies. Experimental studies on exotic nuclei.

3. Summary of Research Activity

The current research subjects are summarized as follows:

(1) Production and delivery of RI beams and related research
(2) Design, construction, operation, maintenance, and improvement of the core research instruments at RIBF and their related infrastructure and equipment
(3) R&D studies on the core research instruments and their related equipment at RIBF
(4) Experimental research on exotic nuclei using the core research instruments at RIBF

Members

Director

Tomohiro UESAKA

Contract Researcher

Toshiyuki KUBO

Junior Research Associate

Rieko TSUNODA

Senior Visiting Scientist

Toshio KOBAYASHI (Tohoku Univ.)

Student Trainees

Fumitaka ENDO (Tohoku Univ.)
Kosuke ICHIMURA (Tohoku Univ.)
Keisuke SAKUMA (Tohoku Univ.)

Research Facility Development Division
Research Instruments Group
BigRIPS Team

1. Abstract

This team is in charge of design, construction, development and operation of BigRIPS in-flight separator and its related research instruments at RI beam factory (RIBF). They are employed not only for the production of RI beams but also the experimental studies using RI beams.

2. Major Research Subjects

Design, construction, development and operation of BigRIPS in-flight separator, RI-beam transport lines, and their related research instruments.

3. Summary of Research Activity

This team is in charge of design, construction, development and operation of BigRIPS in-flight separator, RI-beam transport lines, and their related research instruments such as ZeroDegree spectrometer at RI beam factory (RIBF). They are employed not only for the production of RI beams but also various kinds of experimental studies using RI beams. The research subjects may be summarized as follows:

(1) General studies on RI-beam production using in-flight scheme.
(2) Studies on ion-optics of in-flight separators, including particle identification of RI beams.
(3) Simulation and optimization of RI-beam production.
(4) Development of beam-line detectors and their data acquisition system.
(5) Experimental studies on production reactions and unstable nuclei.
(6) Experimental studies of the limits of nuclear binding.
(7) Development of superconducting magnets and their helium cryogenic systems.
(8) Development of a high-power production target system.
(9) Development of a high-power beam dump system.
(10) Development of a remote maintenance and remote handling systems.
(11) Operation, maintenance and improvement of BigRIPS separator system, RI-beam transport lines, and their related research instruments such as ZeroDegree spectrometer and so on.
(12) Experimental research using RI beams.

Members

Team Leader

Koichi YOSHIDA

Research/Technical Scientists

Yoshiyuki YANAGISAWA (Senior Research Scientist)
Naohito INABE (Senior Technical Scientist)
Kensuke KUSAKA (Senior Technical Scientist)
Masao OHTAKE (Senior Technical Scientist)
Naoki FUKUDA (Technical Scientist)
Yohei SHIMIZU (Technical Scientist)
Hiroshi SUZUKI (Technical Scientist)
Hiroyuki TAKEDA (Technical Scientist)

Postdoctoral Researcher

Masahiro YOSHIMOTO

Visiting Scientists

Deuk Soon AHN (Korea Basic Sci. Inst.)
Alan Matthew AMTHOR (Bucknell Univ.)
Daniel P. BAZIN (Michigan State Univ.)
Alfredo ESTRADE VAZ (Central Michigan Univ.)
Michael FAMIANO (Western Michigan State Univ.)
Hans GEISSEL (GSI)
Tuomas Arne Santeri GRAHN (Univ. of Jyvaskyla)
Kazuo IEKI (Rikkyo Univ.)
Naohito IWASA (Tohoku Univ.)
Yutaka MIZOI (Univ. of Electro-Commun.)
Sadao MOMOTA (Kochi Univ. Tech.)
David MORRISSEY (Michigan State Univ.)
Mauricio PORTILLO (Michigan State Univ.)
Bradley M. SHERRILL (Michigan State Univ.)
Oleg TARASOV (Michigan State Univ.)

Student Trainee

Shunki ISHIKAWA (Tohoku Univ.)

List of Publications & Presentations

Publications

[Original Papers]

V. Vaquero, A. Jungclaus, T. Aumann, J. Tscheuschner, E. V. Litvinova, J. A. Tostevin, H. Baba, D. S. Ahn, R. Avigo, K. Boretzky, A. Bracco, C. Caesar, F. Camera, S. Chen, V. Derya, P. Doornenbal, J. Endres, N. Fukuda, U. Garg, A. Giaz, M. N. Harakeh, M. Heil, A. Horvat, K. Ieki1, N. Imai, N. Inabe, N. Kalantar-Nayestanaki, N. Kobayashi, Y. Kondo, S. Koyama, T. Kubo, I. Martel, M. Matsushita, B. Million, T. Motobayashi, T. Nakamura, N. Nakatsuka, M. Nishimura, S. Nishimura, S. Ota, H. Otsu, T. Ozaki, M. Petri, R. Reifarth, J. L. Rodríguez-Sánchez, D. Rossi, A. T. Saito, H. Sakurai, D. Savran, H. Scheit, F. Schindler, P. Schrock, D. Semmler, Y. Shiga, M. Shikata, Y. Shimizu, H. Simon, D. Steppenbeck, H. Suzuki, T. Sumikama, D. Symochko, I. Syndikus, H. Takeda, S. Takeuchi, R. Taniuchi1, Y. Togano1, J. Tsubota, H. Wang, O. Wieland, K. Yoneda, J. Zenihiro, and A. Zilges, "Fragmentation of single-particle strength around the doubly magic nucleus ^{132}Sn and the position of the $0f_{5/2}$ proton-hole state in ^{131}In," Phys. Rev. Lett. **124**, 022501 (2020).

M. Tanaka, M. Takechi, A. Homma, M. Fukuda, D. Nishimura, T. Suzuki, Y. Tanaka, T. Moriguchi, D. S. Ahn, A. Aimaganbetov, M. Amano, H. Arakawa, S. Bagchi, K. -H. Behr, N. Burtebayev, K. Chikaato, H. Du, S. Ebata, T. Fujii, N. Fukuda, H. Geissel, T. Hori, W. Horiuchi, S. Hoshino, R. Igosawa, A. Ikeda, N. Inabe, K. Inomata, K. Itahashi, T. Izumikawa, D. Kamioka, N. Kanda, I. Kato, I. Kenzhina, Z. Korkulu, Y. Kuk, K. Kusaka, K. Matsuta, M. Mihara, E. Miyata, D. Nagae, S. Nakamura, M. Nassurlla, K. Nishimuro, K. Nishizuka, K. Ohnishi, M. Ohtake, T. Ohtsubo, S. Omika, H. J. Ong, A. Ozawa, A. Prochazka, H. Sakurai, C. Scheidenberger, Y. Shimizu, T. Sugihara, T. Sumikama, H. Suzuki, S. Suzuki, H. Takeda, Y. K. Tanaka, I. Tanihata, T. Wada, K. Wakayama, S. Yagi, T. Yamaguchi, R. Yanagihara, Y. Yanagisawa, K. Yoshida, and T. K. Zholdybayev, "Swelling of doubly magic ^{48}Ca core in Ca isotopes beyond $N = 28$," Phys. Rev. Lett. **124**, 102501 (2020).

F. Boulay, G. S. Simpson, Y. Ichikawa, S. Kisyov, D. Bucurescu, A. Takamine, D. S. Ahn, K. Asahi, H. Baba, D. L. Balabanski, T. Egami, T. Fujita, N. Fukuda, C. Funayama, T. Furukawa, G. Georgiev, A. Gladkov, M. Hass, K. Imamura, N. Inabe, Y. Ishibashi, T. Kawaguchi, T. Kawamura, W. Kim, Y. Kobayashi, S. Kojima, A. Kusoglu, R. Lozeva, S. Momiyama, I. Mukul, M. Niikura, H. Nishibata, T. Nishizaka, A. Odahara, Y. Ohtomo, D. Ralet, T. Sato, Y. Shimizu, T. Sumikama, H. Suzuki, H. Takeda, L. C. Tao, Y. Togano, D. Tominaga, H. Ueno, H. Yamazaki, X. F. Yang, and J. M. Daugas, "g Factor of the ^{99}Zr ($7/2^+$) isomer: monopole evolution in the shape-coexisting region," Phys. Rev. Lett. **124**, 112501 (2020).

T. L. Tang, T. Uesaka, S. Kawase, D. Beaumel, M. Dozono, T. Fujii, N. Fukuda, T. Fukunaga, A. Galindo-Uribarri, S. H. Hwang, N. Inabe, D. Kameda, T. Kawahara, W. Kim, K. Kisamori, M. Kobayashi, T. Kubo, Y. Kubota, K. Kusaka, C. S. Lee, Y. Maeda, H. Matsubara, S. Michimasa, H. Miya, T. Noro, A. Obertelli, K. Ogata, S. Ota, E. Padilla-Rodal, S. Sakaguchi, H. Sakai, M. Sasano, S. Shimoura, S. S. Stepanyan, H. Suzuki, M. Takaki, H. Takeda, H. Tokieda, T. Wakasa, T. Wakui, K. Yako, Y. Yanagisawa, J. Yasuda, R. Yokoyama, K. Yoshida, K. Yoshida, and J. Zenihiro, "How different is the core of ^{25}F from $^{24}O_{g.s.}$?" Phys. Rev. Lett. **124**, 212502 (2020).

K. J. Cook, T. Nakamura, Y. Kondo, K. Hagino, K. Ogata, A. T. Saito, N. L. Achouri, T. Aumann, H. Baba, F. Delaunay, Q. Deshayes, P. Doornenbal, N. Fukuda, J. Gibelin, J. W. Hwang, N. Inabe, T. Isobe, D. Kameda, D. Kanno, S. Kim, N. Kobayashi, T. Kobayashi, T. Kubo, S. Leblond, J. Lee, F. M. Marqués, R. Minakata, T. Motobayashi, K. Muto, T. Murakami, D. Murai, T. Nakashima, N. Nakatsuka, A. Navin, S. Nishi, S. Ogoshi, N. A. Orr, H. Otsu, H. Sato, Y. Satou, Y. Shimizu, H. Suzuki, K. Takahashi, H. Takeda, S. Takeuchi,1, R. Tanaka, Y. Togano, J. Tsubota, A. G. Tuff, M. Vandebrouck, and K. Yoneda, "Halo structure of the neutron-dripline nucleus ^{19}B," Phys. Rev. Lett. **124**, 212503 (2020).

S. Bagchi, R. Kanungo, Y. K. Tanaka, H. Geissel, P. Doornenbal, W. Horiuchi, G. Hagen, T. Suzuki, N. Tsunoda, D. S. Ahn, H. Baba, K. Behr, F. Browne, S. Chen, M. L. Cortés, A. Estradé, N. Fukuda, M. Holl, K. Itahashi, N. Iwasa, G. R. Jansen, W. G. Jiang, S. Kaur, A. O. Macchiavelli, S. Y. Matsumoto, S. Momiyama, I. Murray, T. Nakamura1, S. J. Novario, H. J. Ong, T. Otsuka, T. Papenbrock, S. Paschalis, A. Prochazka, C. Scheidenberger, P. Schrock, Y. Shimizu, D. Steppenbeck, H. Sakurai, D. Suzuki, H. Suzuki, M. Takechi, H. Takeda, S. Takeuchi, R. Taniuchi, K. Wimmer, and K. Yoshida, "Two-neutron halo is unveiled in ^{29}F," Phys. Rev. Lett. **124**, 222504 (2020).

S. Michimasa, M. Kobayashi, Y. Kiyokawa, S. Ota, R. Yokoyama, D. Nishimura, D. S. Ahn, H. Baba, G. P. A. Berg, M. Dozono, N. Fukuda, T. Furuno, E. Ideguchi, N. Inabe, T. Kawabata, S. Kawase, K. Kisamori, K. Kobayashi, T. Kubo, Y. Kubota, C. S. Lee1, M. Matsushita, H. Miya, A. Mizukami, H. Nagakura, H. Oikawa, H. Sakai, Y. Shimizu, A. Stolz, H. Suzuki, M. Takaki, H. Takeda, S. Takeuchi, H. Tokieda, T. Uesaka, K. Yako, Y. Yamaguchi, Y. Yanagisawa, K. Yoshida, and S. Shimoura, "Mapping of a new deformation region around ^{62}Ti," Phys. Rev. Lett. **125**, 122501 (2020).

G. Jhang, J. Estee, J. Barney, G. Cerizza, M. Kaneko, J. W. Lee, W. G. Lynch, T. Isobe, M. Kurata-Nishimura, T. Murakami, C. Y. Tsang, M. B. Tsang, R. Wang, D. S. Ahn, L. Atar, T. Aumann, H. Baba, K. Boretzky, J. Brzychczyk, N. Chiga, N. Fukuda, I. Gasparic, B. Hong, A. Horvat, K. Ieki, N. Inabe, Y. J. Kim, T. Kobayashi, Y. Kondo, P. Lasko, H. S. Lee, Y. Leifels, J. Łukasik, J. Manfredi, A. B. McIntosh, P. Morfouace, T. Nakamura, N. Nakatsuka, S. Nishimura, R. Olsen, H. Otsu, P. Pawłowski, K. Pelczar, D. Rossi, H. Sakurai, C. Santamaria, H. Sato, H. Scheit, R. Shane, Y. Shimizu, H. Simon, A. Snoch, A. Sochocka, Z. Sosin, T. Sumikama, H. Suzuki, D. Suzuki, H. Takeda, S. Tangwancharoen, H. Toernqvist, Y. Togano, Z. G. Xiao, S. J. Yennello, J. Yurkon, Y. Zhang, the SπRIT Collaboration, M. Colonna, D. Cozma, P. Danielewicz, H. Elfner, N. Ikeno, C. M. Koo, J. Mohs, D. Oliinychenko, A. Ono, J. Su, Y. J. Wang, H. Wolter, J. Xu, Y. -X. Zhang, Z. Zhang, the TMEP collaboration, "Symmetry energy investigation with pion production from Sn + Sn systems," Phys. Lett. B **813**, 136016 (2020).

J. Wu, S. Nishimura, P. Möller, M. R. Mumpower, R. Lozeva, C. B. Moon, A. Odahara, H. Baba, F. Browne, R. Daido, P. Doornenbal, Y. F. Fang, M. Haroon, T. Isobe, H. S. Jung, G. Lorusso, B. Moon, Z. Patel, S. Rice, H. Sakurai, Y. Shimizu, L. Sinclair, P. -A. Söderström, T. Sumikama, H. Watanabe, Z. Y. Xu, A. Yagi, R. Yokoyama, D. S. Ahn, F. L. Bello Garrote, J. M. Daugas, F. Didierjean, N. Fukuda, N. Inabe, T. Ishigaki, D. Kameda, I. Kojouharov, T. Komatsubara, T. Kubo, N. Kurz, K. Y. Kwon, S. Morimoto, D. Murai, H. Nishibata, H. Schaffner, T. M. Sprouse, H. Suzuki, H. Takeda, M. Tanaka, K. Tshoo, and Y. Wakabayashi, "β-Decay half-lives of 55 neutron-rich isotopes beyond the $N = 82$ shell gap," Phys. Rev. C **101**, 042801(R) (2020).

J. Ha, T. Sumikama, F. Browne, N. Hinohara, A. M. Bruce, S. Choi, I. Nishizuka, S. Nishimura, P. Doornenbal, G. Lorusso, P. -A. Söderström, H. Watanabe, R. Daido, Z. Patel, S. Rice, L. Sinclair, J. Wu, Z. Y. Xu, A. Yagi, H. Baba, N. Chiga, R. Carrol, F. Didierjean, Y. Fang, N. Fukuda, G. Gey, E. Ideguchi, N. Inabe, T. Isobe, D. Kameda, I. Kojouharov, N. Kurz, T. Kubo, S. Lalkovski, Z. Li, R. Lozeva, H. Nishibata, A. Odahara, Zs. Podolyák, P. H. Regan, O. J. Roberts, H. Sakurai, H. Schaffner, G. S. Simpson, H. Suzuki, H. Takeda, M. Tanaka, J. Taprogge, V. Werner, and O. Wieland, "Shape evolution of neutron-rich ^{106,108,110}Mo isotopes in the triaxial degree of freedom," Phys. Rev. C **101**, 044311 (2020).

X. H. Sun, H. Wang, H. Otsu, H. Sakurai, D. S. Ahn, M. Aikawa, N. Fukuda, T. Isobe, S. Kawakami, S. Koyama, T. Kubo, S. Kubono, G. Lorusso, Y. Maeda, A. Makinaga, S. Momiyama, K. Nakano, S. Nakayama, M. Niikura, Y. Shiga, P. -A. Söderström, H. Suzuki, H. Takeda, S. Takeuchi, R. Taniuchi, Ya. Watanabe, Yu. Watanabe, H. Yamasaki, X. F. Yang, Y. L. Ye, and K. Yoshida, "Spallation and fragmentation cross sections for 168 MeV/nucleon ^{136}Xe ions on proton, deuteron, and carbon targets," Phys. Rev. C **101**, 064623 (2020).

J. Park, R. Krücken, A. Blazhev, D. Lubos, R. Gernhäuser, M. Lewitowicz, S. Nishimura, D. S. Ahn, H. Baba, B. Blank, P. Boutachkov, F. Browne, I. Čeliković, G. de France, P. Doornenbal, T. Faestermann, Y. Fang, N. Fukuda, J. Giovinazzo, N. Goel, M. Górska, H. Grawe, S. Ilieva, N. Inabe, T. Isobe, A. Jungclaus, D. Kameda, G. D. Kim, Y. -K. Kim, I. Kojouharov, T. Kubo, N. Kurz, Y. K. Kwon, G. Lorusso, K. Moschner, D. Murai, I. Nishizuka, Z. Pate, M. M. Rajabali, S. Rice, H. Sakurai, H. Schaffner, Y. Shimizu, L. Sinclair, P. -A. Söderström, and K. Steiger, "Spectroscopy of ^{99}Cd and ^{101}In from β decays of ^{99}In and ^{101}Sn," Phys. Rev. C **102**, 014304 (2020).

J. J. Liu, J. Lee, H. Watanabe, S. Nishimura, G. X. Zhang, J. Wu, P. M. Walker, P. H. Regan, P. -A. Söderström, H. Kanaoka, Z. Korkulu, P. S. Lee, A. Yagi, A. C. Dai, F. R. Xu, D. S. Ahn, T. Alharbi, H. Baba, F. Browne, A. M. Bruce, R. J. Carroll, K. Y. Chae, Zs. Dombradi, P. Doornenbal, A. Estrade1, N. Fukuda, C. Griffin, E. Ideguchi, N. Inabe, T. Isobe, S. Kanaya, I. Kojouharov, F. G. Kondev, T. Kubo, S. Kubono, N. Kurz, I. Kuti, S. Lalkovski, G. J. Lane, C. S. Lee, E. J. Lee, G. Lorusso, G. Lotay, C. -B. Moon, I. Nishizuka, C. R. Nita, A. Odahara, Z. Patel, V. H. Phong, Zs. Podolyák, O. J. Roberts, H. Sakurai, H. Schaffner, C. M. Shand, Y. Shimizu, T. Sumikama, H. Suzuki, H. Takeda, S. Terashima, Zs. Vajta, J. J. Valiente-Dobón, and Z. Y. Xu, "Isomeric and β-decay spectroscopy of ^{173,174}Ho," Phys. Rev. C **102**, 024301 (2020).

A. Jungclaus, J. M. Keatings, G. S. Simpson, H. Naïdja, A. Gargano, S. Nishimura, P. Doornenbal, G. Gey, G. Lorusso, P. -A. Söderström, T. Sumikama, J. Taprogge, Z. Y. Xu, H. Baba, F. Browne, N. Fukuda, N. Inabe, T. Isobe, H. S. Jung, D. Kameda, G. D. Kim, Y. -K. Kim, I. Kojouharov, T. Kubo, N. Kurz, Y. K. Kwon, Z. Li1, H. Sakurai, H. Schaffner, Y. Shimizu, H. Suzuki, H. Takeda, Z. Vajta1, H. Watanabe, J. Wu1, A. Yagi, K. Yoshinaga, S. Bönig, J. -M. Daugas, R. Gernhäuser, S. Ilieva, T. Kröll, A. Montaner-Piza, K. Moschner, D. Mücher, H. Nishibata, A. Odahara1, R. Orlandi, M. Scheck, K. Steiger, and A. Wendt, "Evolution of proton single-particle states in neutron-rich Sb isotopes beyond N = 82," Phys. Rev. C **102**, 034324 (2020).

H. Suzuki, K. Yoshida, N. Fukuda, H. Takeda, Y. Shimizu, D. S. Ahn, T. Sumikama, N. Inabe, T. Komatsubara, H. Sato, Z. Korkulu, K. Kusaka, Y. Yanagisawa, M. Ohtake, H. Ueno, T. Kubo, S. Michimasa, N. Kitamura, K. Kawata, N. Imai, O. B. Tarasov, D. Bazin, J. Nolen, and W. F. Henning, "Experimental studies of the two-step scheme with an intense radioactive ^{132}Sn beam for next-generation production of very neutron-rich nuclei," Phys. Rev. C **102**, 064615 (2020).

J. Giovinazzo, T. Goigoux, B. Blank, P. Ascher, M. Gerbauxa, S. Grévy, T. Kurtukian-Nieto, C. Magron, P. Doornenbal, N. Fukuda, N. Inabe, G. G. Kiss, T. Kubo, S. Kubono, S. Nishimura, H. Sakurai, Y. Shimizu, C. Sidong, P. -A. Söderström, T. Sumikama, H. Suzuki, H. Takeda, P. Vi, J. Wu, D. S. Ahn, J. Agramunt, A. Algora, V. Guadilla, A. Montaner-Piza, A. I. Morales, S. E. A. Orrigo, B. Rubio, Y. Fujita, M. Tanaka, W. Gelletly, P. Aguilera, F. Molina, F. Diel, D. Lubos, G. de Angelis, D. Napoli, C. Borcea, A. Boso, R. B. Cakirli, E. Ganioglu, J. Chiba, D. Nishimura, H. Oikawa, Y. Takei, S. Yagi, K. Wimmer, G. de France, S. Go, and B. A. Brown, "Two-proton radioactivity: the interesting case of ^{67}Kr and further studies," Acta Physica Polonica B **51**, 577 (2020).

A. Vitéz-Sveiczer, A. Algora, A. I. Morales, B. Rubio, G. G. Kiss, G. de Angelis, F. Recchia, S. Nishimura, J. Agramunt, V. Guadilla, A. Montaner-Pizá, S. E. A. Orrigo, A. Horváth, D. Napoli, S. Lenzi, A. Boso, V. H. Phong, J. Wu, P. -A. Söderström, T. Sumikama, H. Suzuki, H. Takeda, D. S. Ahn, H. Baba, P. Doornenbal, N. Fukuda, N. Inabe, T. Isobe, T. Kubo, S. Kubono, H. Sakurai, Y. Shimizu, S. Chen, B. Blank, P. Ascher, M. Gerbaux, T. Goigoux, J. Giovinazzo, S. Grévy, T. Kurtukián Nieto, C. Magron, W. Gelletly, Zs. Dombrádi, Y. Fujita, M. Tanaka, P. Aguilera, F. Molina, J. Eberth, F. Diell, D. Lubos, C. Borcea, E. Ganioglu, D. Nishimura, H. Oikawa, Y. Takei, S. Yagi, W. Korten, G. de France, P. Davies, J. Liu, J. Lee, T. Lokotko, I. Kojouharov, N. Kurz, and H. Shaffner, "Studying the exotic decay ^{70}Kr → ^{70}Br," Acta Physica Polonica B **51**, 587 (2020).

[Proceedings]

K. Kusaka, "Long term operation of the superconducting triplet quadrupoles with cryocoolers," J. Phys. Conf. Ser. **1559**, 012071 (2020).

Presentations

[International Conferences/Workshops]

N. Fukuda, "Present status of the BigRIPS separator and recent development of RI-beam production," RIBF Users Meeting 2020, Virtual Conference (Zoom), September 09, 2020.

H. Takeda, "RI beam production in RIBF from the perspective of nuclear reaction," JSPS/NRF/NSFC A3 Foresight Program "Nuclear physics in the 21st century" Joint Annual Meeting, Online Conference, November 18, 2020.

N. Fukuda (invited), "Particle identification at BigRIPS separator," Workshop on Techniques and Detectors for Heavy-ion Charge-State Identification in High-acceptance Spectrometers, Virtual Conference (Zoom), December 16–17, 2020.

Research Facility Development Division
Research Instruments Group
SAMURAI Team

1. Abstract

In collaboration with research groups in and outside RIKEN, the team designs, develops and constructs the SAMURAI spectrometer and relevant equipment that are and will be used for reaction experiments using RI beams at RI Beam Factory. The SAMURAI spectrometer consists of a large superconducting dipole magnet and a variety of detectors to measure charged particles and neutrons. After the commissioning experiment in March 2012, the team prepared and conducted, in collaboration with researchers in individual experimental groups, the first series of experiments with SAMURAI in May 2012. Then, several numbers of experiments were well performed until now utilizing the property of SAMURAI. The team also provides a basis for research activities by, for example, organizing collaboration workshops by researchers who are interested in studies or plan to perform experiments with the SAMURAI spectrometer.

2. Major Research Subjects

Design, operation, maintenance and improvement of the SAMURAI spectrometer and its related research instruments. Support and management for SAMURAI-based research programs. Generate future plans for next generation instruments for nuclear reaction studies.

3. Summary of Research Activity

The current research subjects are summarized as follows:

(1) Operation, maintenance and improvement of a large superconducting dipole magnet that is the main component of the SAMURAI spectrometer.
(2) Design, development and construction of various detectors that are used for nuclear reaction experiments using the SAMURAI spectrometer.
(3) Preparation for planning experiments using SAMURAI spectrometer.
(4) Maintenance and improvement of the SAMURAI beam line.
(5) Formation of a collaboration platform called SAMURAI collaboration.
(6) Preparation for next generation spectrometer for nuclear reaction studies.

Members

Team Leader
Hideaki OTSU

Research & Development Scientist
Mizuki NISHIMURA

Junior Research Associate
Takato TOMAI

List of Publications & Presentations

Publications

[Original Papers]

M. M. Juhasz, Z. Elekes, D. Sohler, *et al.*, "First spectroscopic study of ^{51}Ar by the $(p, 2p)$ reaction," Phys. Lett. B **814**, 136108 (2021).

Y. L. Sun, T. Nakamura, Y. Kondo, *et al.*, "Three-body breakup of ^{6}He and its halo structure," Phys. Lett. B **814**, 136072 (2021).

Z. H. Yang, Y. Kubota, A. Corsi, *et al.*, "Quasifree neutron knockout reaction reveals a small *s*-orbital component in the Borromean nucleus ^{17}B," Phys. Rev. Lett. **126**, 082501 (2021).

M. L. Cortes, W. Rodriguez, P. Doornenbal, *et al.*, "$N = 32$ shell closure below calcium: Low-lying structure of ^{50}Ar," Phys. Rev. C **102**, 064320 (2020).

A. Frotscher, M. Gomez-Ramos, A. Obertelli, *et al.*, "Sequential nature of $(p, 3p)$ two-proton knockout from neutron-rich nuclei," Phys. Rev. Lett. **125**, 012501 (2020).

Y. Kubota, A. Corsi, G. Authelet, *et al.*, "Surface localization of the dineutron in ^{11}Li," Phys. Rev. Lett. **125**, 252501 (2020).

T. Lokotko, S. Leblond, J. Lee, *et al.*, "Shell structure of the neutron-rich isotopes ^{69,71,73}Co," Phys. Rev. C **101**, 034314 (2020).

A. Revel, O. Sorlin, F. M. Marqués, *et al.*, "Extending the southern shore of the island of inversion to ^{28}F," Phys. Rev. Lett. **124**, 152502 (2020).

K. J. Cook, T. Nakamura, Y. Kondo, *et al.*, "Halo structure of the neutron-dripline nucleus ^{19}B," Phys. Rev. Lett. **124**, 212503 (2020).

M. L. Cortes, W. Rodriguez, P. Doornenbal, *et al.*, "Shell evolution of $N = 40$ isotones towards ^{60}Ca: First spectroscopy of ^{62}Ti," Phys. Lett. B **800**, 135071 (2020).

Y. L. Sun, A. Obertelli, P. Doornenbal, *et al.*, "Restoration of the natural $E(1/2_1^+)$-$E(3/2_1^+)$ energy splitting in odd-K isotopes towards $N = 40$," Phys. Lett. B **802**, 135215 (2020).

Presentations

[International Conferences/Workshops]

Y. Togano, "Current status and future perspective of SAMURAI at RIBF," RIBF Users Meeting 2020, Online, September 8–10, 2020.

T. Nakamura, "Exploring the extreme of nuclear landscape using radioactive beams," IIT Guwahati and Tokyo Tech-2nd Joint Workshop on Topics in Condensed Matter Physics, High-Energy Physics, Cosmology & Astrophysics, Online, December 15, 17–18, 2020.

T. Nakamura, "Dineutron correlation in neutron-rich nuclei," Tokyo Tech-Uppsala Univ. Joint Symposium, Online, November 16–17, 2020.

SAMURAI International Collaboration Workshop 2020, Online, September 1–4, 2020 (`https://indico2.riken.jp/e/SAMURAIICW2020`).

[Domestic Conferences/Workshops]

中村隆司, 「ダイニュートロンから多中性子クラスターへ」, 日本物学会第 76 回年次大会 シンポジウム「量子クラスターで読み解く物質の階層構造」, , オンライン開催, 2021 年 3 月 12–15 日.

吉留勇起, 「^{25}O の不変質量核分光」, 日本物学会第 76 回年次大会, オンライン開催, 2021 年 3 月 12–15 日.

齊藤敦美, 「クーロンおよび核力分解による ^{6}He の 3 体崩壊」, 日本物学会第 76 回年次大会, オンライン開催, 2021 年 3 月 12–15 日.

海老名直樹, 「陽子準弾性散乱による多中性子クラスター探索実験のための反跳陽子検出器の開発」, 日本物学会第 76 回年次大会, オンライン開催, 2021 年 3 月 12–15 日.

高橋康平, 「中性子過剰核における近距離相関した陽子中性子対探索実験に向けた検出器系の開発」, 日本物学会第 76 回年次大会, オンライン開催, 2021 年 3 月 12–15 日.

栂野泰宏, 「^{52}Ca の電気双極子応答」, 日本物学会第 76 回年次大会, オンライン開催, 2021 年 3 月 12–15 日.

西村未生, 「中性子過剰核の陽子準自由散乱反応測定に向けた CsI(Na) シンチレータの性能評価」, 日本物学会第 76 回年次大会, オンライン開催, 2021 年 3 月 12–15 日.

高橋康平, 「ダイニュートロン相関探索に向けた高分解能中性子検出器 HIME の開発」, 日本物理学会 2020 年秋季大会, オンライン開催, 2020 年 9 月 14–17 日.

王赫, "Development of the detector systems for the recoil protons from the quasi-free scattering of neutron-rich nuclei at SAMURAI at RIBF-I," 日本物理学会 2020 年秋季大会, オンライン開催, 2020 年 9 月 14–17 日.

海老名直樹, 「中性子過剰核の準弾性散乱散乱測定用陽子検出器の開発 II」, 日本物理学会 2020 年秋季大会, オンライン開催, 2020 年 9 月 14–17 日.

齊藤敦美, 「中性子過剰ヘリウム同位体のクーロンおよび核力分解反応」, 日本物理学会 2020 年秋季大会, オンライン開催, 2020 年 9 月 14–17 日.

齊藤敦美, "Coulomb and nuclear breakup of halo nuclei ^{6}He," 第 5 回クラスター階層領域研究会, オンライン, 2020 年 9 月 24–25 日.

大津秀暁, "Cluster structure study on neutron rich nuclei," 第 5 回クラスター階層領域研究会, オンライン, 2020 年 9 月 24–25 日.

堀川晃太 (poster), 「中性子過剰核における短距離相関実験のための反跳陽子検出器の開発」, 日本物学会第 76 回年次大会, オンライン開催, 2021 年 3 月 12–15 日.

松井智輝 (poster), 「多中性子クラスター探索実験のための陽子全エネルギー検出器の開発」, 日本物学会第 76 回年次大会, オンライン開催, 2021 年 3 月 12–15 日.

[Seminars]

T. Nakamura, "Dineutron correlation of exotic nuclei along the neutron drip line," Seminar at Hokkaido University, November 25, 2020.

Awards

A. Saito, A3F-CNSSS20 Award for Young Scientist, 2020.

Doctor Thesis

Atsumi Saito, "Coulomb and nuclear breakup of the Borromean nucleus ^{6}He," Tokyo Institute of Technology, February 2021.

Master Thesis

吉留勇起, 「^{25}O の不変質量核分光」, 東京工業大学理学院.

安田聖, 「ダイニュートロン相関探索実験のための高精細中性子検出器 HIME の開発」, 東京工業大学理学院.

西村未生, 「質量欠損法による中性子過剰核の構造研究に向けた CsI(Na) シンチレータのエネルギー分解能測定」, 立教大学理学研究科.

Bachelor Thesis

堀川晃太, 「中性子過剰核における短距離相関探索実験のための反跳陽子検出器の開発」, 東京工業大学理学院物理学系.

松井智輝, 「多中性子クラスター探索実験のための陽子全エネルギー検出器の開発」, 東京工業大学理学院物理学系.

Research Facility Development Division
Research Instruments Group
Computing and Network Team

1. Abstract

This team is in charge of development, management and operation of the computing and network environment, mail and information servers and data acquisition system and management of the information security of the RIKEN Nishina Center.

2. Major Research Subjects

(1) Development, management and operation of the general computing servers
(2) Development, management and operation of the mail and information servers
(3) Development, management and operation of the data acquisition system
(4) Development, management and operation of the network environment
(5) Management of the information security

3. Summary of Research Activity

This team is in charge of development, management and operation of the computing and network environment, mail and information servers and data acquisition system and management of the information security. The details are described elsewhere in this progress report.

(1) Development, management and operation of the general computing servers

We are operating Linux/Unix NIS/NFS cluster system for the data analysis of the experiments and general computing. This cluster system consists of eight computing servers with 64 CPU cores and totally 200 TB RAID of highly-reliable Fibre-channel interconnection. There are approximately 300 active user accounts on this cluster system (a total of about 800 accounts were registered so far). We are adopting the latest version of the Scientific Linux (X86 64) as the primary operating system, which is widely used in the accelerator research facilities, nuclear physics and high-energy physics communities in the world.

(2) Development, management and operation of the mail and information servers

We are operating RIBF.RIKEN.JP server as a mail/NFS/NIS server. This server is a core server of RIBF Linux cluster system. Postfix has been used for mail transport software and dovecot has been used for imap and pop services. These software packages enable secure and reliable mail delivery. Sophos Email Security and Control (PMX) installed on the mail front-end servers which tags spam mails and isolates virus-infected mails. The probability to identify the spam is approximately 95–99%. We are operating several information servers such as Web servers, Integrated Digital Conference (INDICO) server, Wiki servers, Groupware servers, Wowza streaming servers. We have been operating approximately 70 units of wireless LAN access points in RNC. Almost the entire radiation-controlled area of the East Area of RIKEN Wako campus is covered by wireless LAN for the convenience of experiments and daily work.

(3) Development, management and operation of the data acquisition system

We have developed the standard data-acquisition system named as RIBFDAQ. This system can process up to 40 MB/s data. By using crate-parallel readout from front-end systems such as CAMAC and VME, the dead time could be minimized. To synchronize the independent DAQ systems, the time stamping system has been developed. The resolution and depth of the time stamp are 10 ns and 48 bits, respectively. This time stamping system is very useful for beta decay experiments such as EURICA, BRIKEN and VANDLE projects. One of the important tasks is the DAQ coupling, because detector systems with dedicated DAQ systems are transported to RIBF from foreign facilities. In case of SAMURAI Silicon (NSCL/TUM/WUSTL), the readout system is integrated into RIBFDAQ. The projects of MUST2 (GANIL), MINOS (CEA Saclay), NeuLAND (GSI) and TRB3 (TUM) cases, data from their DAQ systems are transferred to RIBFDAQ and merged online. For SPIRIT (RIKEN/GANIL/CEA Saclay/NSCL), RIBFDAQ is controlled from the NARVAL-GET system that is a large-scale signal processing system for the time projection chamber. EURICA (GSI), BRIKEN (GSI/Univ. Liverpool/IFIC), VANDLE (UTK) and OTPC (U. Warsaw) projects, we adopt the time stamping system to apply individual trigger for each detector system. In this case, data are merged in offline. In addition, we are developing intelligent circuits based on FPGA. General Trigger Operator (GTO) is an intelligent triggering NIM module. Functions of “common trigger management,” “gate and delay generator,” “scaler” are successfully implemented. The trigger system in BigRIPS DAQ is managed by 5 GTO modules. To improve the data readout speed of VME system, we have successfully developed the MPV system which is a parallel readout extension of the VME system. Data readout sequence is completely parallelized that helps to improve the DAQ deadtime. Thanks to the MPV system, now the DAQ system in RIBF is 10 times faster than in 2007. Toward to the next generation DAQ system, I have started to develop a real-time data processing unit based on Xilinx RFSoC that includes FPGA and 4 GHz FADC.

(4) Development, management and operation of the network environment

We have been managing the network environment collaborating with Information Systems Division in RIKEN. All the Ethernet ports of the information wall sockets are capable of the Gigabit Ethernet connection (10/100/1000 BT). In addition, some 10 Gbps networks port has been introduced to RIBF experimental area. Approximately 100 units of wireless LAN access points have been installed to cover the almost entire area of Nishina Center.

(5) Management of the information security

It is essential to take proper information security measures for information assets. We are managing the information security of Nishina Center collaborating with Information Systems Division in RIKEN.

Members

Team Leader

Hidetada BABA

Research/Technical Scientist

Yasushi WATANABE (Senior Research Scientist)

Special Temporary Research Scientist

Takashi ICHIHARA

Visiting Scientist

Shoichiro KAWASE (Kyushu Univ.)

Student Trainee

Shoko TAKESHIGE (Rikkyo Univ.)

List of Publications & Presentations

Presentations

[International Conferences/Workshops]

H.Baba (poster) *et al*., "MPV—Parallel Readout Architecture for the VME data acquisition system," 22nd IEEE Real Time Conference, Virtual, October 12–23, 2020.

[Domestic Conferences/Workshops]

武重祥子 (oral), 馬場秀忠他, 「RFSoC を用いた高帯域波形処理システムの開発」, 日本物理学会第 73 回年次大会, 千葉県野田市 (東京理科大学), 2018 年 3 月 22–25 日.

馬場秀忠 (oral), 「並列化 VME の紹介」, 計測システム研究会 2020@J-PARC, 茨城県東海村 (KEK 東海キャンパス) & オンライン開催, 2020 年 11 月 26–27 日.

Awards

市原卓, 2020 年 JPCERT/CC 感謝, JPCERT コーディネーションセンター, 2020 年 8 月 19 日.

Research Facility Development Division
Research Instruments Group
Detector Team

1. Abstract

This team is in charge of development, fabrication, and operation of various detectors used for nuclear physics experiments at RIBF. Our current main mission is maintenance and improvement of detectors which are used at BigRIPS separator and its succeeding beam lines for beam diagnosis and particle identification of RI beams. We are also engaged in R&D of new detectors that can be used for higher-intensity RI beams. In addition, we are doing the R&D which uses the pelletron accelerator together with other groups.

2. Major Research Subjects

Development, fabrication, and operation of various detectors for nuclear physics experiments, including beam-line detectors which are used for the production and delivery of RI beams (beam diagnosis and particle identification). R&D which uses the pelletron accelerator.

3. Summary of Research Activity

The current research subjects are summarized as follows:

(1) Maintenance and improvement of the beam-line detectors which are used at BigRIPS separator and its succeeding beam lines.
(2) Development of new beam-line detectors with radiation hardness and tolerance for higher counting rates.
(3) Management of the pelletron accelerator and R&D which uses the pelletron.

Members

Team Leader

Hiromi SATO

Research/Technical Scientist

Tokihiro IKEDA (Senior Research Scientist)

Research Consultant

Manabu HAMAGAKI

Visiting Scientist

Takeshi KOIKE (Tohoku University)

Student Trainees

Yuka HIKIMA (Toho University)
Mitsumasa MORI (Toho University)
Keito SANGU (Toho University)

List of Publications & Presentations

Publications

[Original Papers]

A. Revel, O. Sorlin, F. M. Marqués, Y. Kondo, J. Kahlbow, T. Nakamura, N. A. Orr, F. Nowacki, J. A. Tostevin, C. X. Yuan, N. L. Achouri, H. Al Falou, L. Atar, T. Aumann, H. Baba, K. Boretzky, C. Caesar, D. Calvet, H. Chae, N. Chiga, A. Corsi, H. L. Crawford, F. Delaunay, A. Delbart, Q. Deshayes, Z. Dombrádi, C. A. Douma, Z. Elekes, P. Fallon, I. Gašparić, J. -M. Gheller, J. Gibelin, A. Gillibert, M. N. Harakeh, W. He, A. Hirayama, C. R. Hoffman, M. Holl, A. Horvat, Á. Horváth, J. W. Hwang, T. Isobe, N. Kalantar-Nayestanaki, S. Kawase, S. Kim, K. Kisamori, T. Kobayashi, D. Körper, S. Koyama, I. Kuti, V. Lapoux, S. Lindberg, S. Masuoka, J. Mayer, K. Miki, T. Murakami, M. Najafi, K. Nakano, N. Nakatsuka, T. Nilsson, A. Obertelli, F. de Oliveira Santos, H. Otsu, T. Ozaki, V. Panin, S. Paschalis, D. Rossi, A. T. Saito, T. Saito, M. Sasano, H. Sato, Y. Satou, H. Scheit, F. Schindler, P. Schrock, M. Shikata, Y. Shimizu, H. Simon, D. Sohler, L. Stuhl, S. Takeuchi, M. Tanaka, M. Thoennessen, H. Törnqvist, Y. Togano, T. Tomai, J. Tscheuschner, J. Tsubota, T. Uesaka, Z. Yang, M. Yasuda, and K. Yoneda, "Extending the southern shore of the island of inversion to ^{28}F," Phys. Rev. Lett. **124**, 152502 (2020).

K. J. Cook, T. Nakamura, Y. Kondo, K. Hagino, K. Ogata, A. T. Saito, N. L. Achouri T. Aumann, H. Baba, F. Delaunay, Q. Deshayes, P. Doornenbal N. Fukuda, J. Gibelin, J. W. Hwang, N. Inabe, T. Isobe, D. Kameda, D. Kanno, S. Kim, N. Kobayashi, T. Kobayashi, T. Kubo, S. Leblond, J. Lee, F. M. Marqués, R. Minakata, T. Motobayashi, K. Muto, T. Murakami, D. Murai, T. Nakashima, N. Nakatsuka, A. Navin, S. Nishi, S. Ogoshi, N. A. Orr, H. Otsu, H. Sato, Y. Satou, Y. Shimizu, H. Suzuki, K. Takahashi, H. Takeda, S. Takeuchi, R. Tanaka, Y. Togano, J. Tsubota, A. G. Tuff, M. Vandebrouck, and K. Yoneda, "Halo structure of the neutron-dripline nucleus ^{19}B," Phys. Rev. Lett. **124**, 212503 (2020).

G. Jhang, J. Estee, J. Barney, G. Cerizza, M. Kaneko, J. W. Lee, W. G. Lynch, T. Isobe, M. Kurata-Nishimura, T. Murakami, C. Y. Tsang, M. B. Tsang, R. Wang, D. S. Ahn, L. Atar, T. Aumann, H. Baba, K. Boretzky, J. Brzychczyk, N. Chiga, N. Fukuda, I. Gasparic, B. Hong, A. Horvat, K. Ieki, N. Inabe, Y. J. Kim, T. Kobayashi, Y. Kondo, P. Lasko, H. S. Lee, Y. Leifels, J. Lukasik, J. Manfredi, A. B. McIntosh, P. Morfouace, T. Nakamura, N. Nakatsuka, S. Nishimura, R. Olsen, H. Otsu, P. Pawlowski, K. Pelczar, D. Rossi, H. Sakurai, C. Santamaria, H. Sato, H. Scheit, R. Shane, Y. Shimizu, H. Simon, A. Snoch, A. Sochocka, Z. Sosin, T. Sumikama, H. Suzuki, D. Suzuki, H. Takeda, S. Tangwancharoen, H. Toernqvist, Y. Togano, Z. G. Xiao, S. J. Yennello, J. Yurkon, Y. Zhang, the SπRIT Collaboration, M. Colonna, D. Cozma, P. Danielewicz, H. Elfner, N. Ikeno, C. M. Ko, J. Mohs, D. Oliinychenko, A. Ono, J. Suae, Y. J. Wang, H. Wolter, J. Xu, Y. -X. Zhang, Z. Zhang, the TMEP collaboration, "Symmetry energy investigation with pion production from Sn + Sn systems," Phys. Lett. B **813**, 136016 (2021).

Y. Kubota, A. Corsi, G. Authelet, H. Baba, C. Caesar, D. Calvet, A. Delbart, M. Dozono, J. Feng, F. Flavigny, J. -M. Gheller, J. Gibelin, A. Giganon, A. Gillibert, K. Hasegawa, T. Isobe, Y. Kanaya, S. Kawakami, D. Kim, Y. Kikuchi, Y. Kiyokawa, M. Kobayashi, N. Kobayashi, T. Kobayashi, Y. Kondo, Z. Korkulu, S. Koyama, V. Lapoux, Y. Maeda, F. M. Marqués, T. Motobayashi, T. Miyazaki, T. Nakamura, N. Nakatsuka, Y. Nishio, A. Obertelli, K. Ogata, A. Ohkura, N. A. Orr, S. Ota, H. Otsu, T. Ozaki, V. Panin, S. Paschalis, E. C. Pollacco, S. Reichert, J. -Y. Roussé, A. T. Saito, S. Sakaguchi, M. Sako, C. Santamaria, M. Sasano, H. Sato, M. Shikata, Y. Shimizu, Y. Shindo, L. Stuhl, T. Sumikama, Y. L. Sun, M. Tabata, Y. Togano, J. Tsubota, Z. H. Yang, J. Yasuda, K. Yoneda, J. Zenihiro, and T. Uesaka, "Surface localization of the dineutron in ^{11}Li," Phys. Rev. Lett. **125**, 252501 (2020).

H. Suzuki, K. Yoshida, N. Fukuda, H. Takeda, Y. Shimizu, D. S. Ahn, T. Sumikama, N. Inabe, T. Komatsubara, H. Sato, Z. Korkulu, K. Kusaka, Y. Yanagisawa, M. Ohtake, H. Ueno, T. Kubo, S. Michimasa, N. Kitamura, K. Kawata, N. Imai, O. B. Tarasov, D. Bazin, J. Nolen, and W. F. Henning, "Experimental studies of the two-step scheme with an intense radioactive ^{132}Sn beam for next-generation production of very neutron-rich nuclei," Phys. Rev. C **102**, 064615 (2020).

Z. H. Yang, Y. Kubota, A. Corsi, K. Yoshida, X. -X. Sun, J. G. Li, M. Kimura, N. Michel, K. Ogata, C. X. Yuan, Q. Yuan, G. Authelet, H. Baba, C. Caesar, D. Calvet, A. Delbart, M. Dozono, J. Feng, F. Flavigny, J. -M. Gheller, J. Gibelin, A. Giganon, A. Gillibert, K. Hasegawa, T. Isobe, Y. Kanaya, S. Kawakami, D. Kim, Y. Kiyokawa, M. Kobayashi, N. Kobayashi, T. Kobayashi, Y. Kondo, Z. Korkulu, S. Koyama, V. Lapoux, Y. Maeda, F. M. Marqués, T. Motobayashi, T. Miyazaki, T. Nakamura, N. Nakatsuka, Y. Nishio, A. Obertelli, A. Ohkura, N. A. Orr, S. Ota, H. Otsu, T. Ozaki, V. Panin, S. Paschalis, E. C. Pollacco, S. Reichert, J. -Y. Roussé, A. T. Saito, S. Sakaguchi, M. Sako, C. Santamaria, M. Sasano, H. Sato, M. Shikata, Y. Shimizu, Y. Shindo, L. Stuhl, T. Sumikama, Y. L. Sun, M. Tabata, Y. Togano, J. Tsubota, F. R. Xu, J. Yasuda, K. Yoneda, J. Zenihiro, S. -G. Zhou, W. Zuo, and T. Uesaka, "Quasifree neutron knockout reaction reveals a small s-orbital component in the Borromean nucleus ^{17}B," Phys. Rev. Lett. **126**, 082501 (2021).

T. Ikeda, "Applications of microbeams produced by tapered glass capillary optics," Quantum Beam Sci. **4(2)**, 22 (2020).

S. Kawamura, T. Ikeda, and W. -G. Jin, "Transmission characteristic of ultraviolet-laser microbeam with tapered glass capillary optics," J. Phys. Soc. Jpn. **89**, 055002 (2020).

Presentations

[Domestic Conferences/Workshops]

高橋弘幸, 西村太樹, 菅原奏来, 延與紫世, 福田直樹, 原田知也, 土方佑斗, 松村理久, 佐藤広海, 清水陽平, 鈴木宏, 竹田浩之, 田中純貴, 上坂友洋, 宇根千晶, 吉田光一, 銭廣十三 (口頭発表), 「Th ビームの開発に向けたイオンチェンバーの性能評価」, 日本物理学会第 76 回年次大会, オンライン, 2021 年 3 月 12–15 日.

土方佑斗, 銭廣十三, 上坂友洋, 延與紫世, 大田晋輔, 坂口治隆, 佐藤広海, 清水陽平, 菅原奏来, 鈴木宏, 高橋弘幸, 武重祥子, 竹田浩之, 田中純貴, 辻崚太朗, 寺嶋知, 堂園昌伯, 西村俊二, 西村太樹, 馬場秀忠, 原田知也, G, 福田直樹, 松田洋平, 道正新一郎, 山村周, 吉田光一 (口頭発表), 「大強度かつ極めて重い不安定核ビームの粒子識別に向けた Xe ガスシンチレータの開発」, 日本物理学会第 76 回年次大会, オンライン, 2021 年 3 月 12–15 日.

吉留勇起, 近藤洋介, 中村隆司, Nadia Lynda Achouri, Thomas Aumann, 馬場秀忠, Franck Delaunay, Pieter Doornenbal, 福田直樹, Julien Gibelin, Jongwon Hwang, 稲辺尚人, 磯部忠昭, 亀田大輔, 簡野大輝, Sunji Kim, 小林信之, 小林俊雄, 久保敏幸, Sylvain Leblond, Jenny Lee, Miguel Marques, 本林透, 村井大地, 村上哲也, 武藤琴美, 中嶋丈嘉, 中塚徳継, Alahari Navin, 西征爾郎, Nigel Andrew Orr, 大津秀暁, 佐藤広海, 佐藤義輝, 清水陽平, 鈴木宏, 高橋賢人, 竹田浩之, 栂野泰宏, Adam Garry Tuff, Marine Vandebrouck, 米田健一郎 (口頭発表), 「^{25}O の不変質量核分光」, 日本物理学会第 76 回年次大会, オンライン, 2021 年 3 月 12–15 日.

池田時浩 (口頭発表), 「Applications of MeV-ion microbeams produced by tapered glass capillary optics」, 第 21 回「イオンビームによる表面・界面の解析と改質」特別研究会, 京都大学宇治キャンパス&オンライン, 京都, 2020 年 12 月 4–5 日.

引間宥花, 池田時浩, 森光正, 金衛国 (招待講演), 「生物照射のためのガラスキャピラリーマイクロビーム法とスポット径解析」, 原子衝突学会第 45 回年会, オンライン, 2020 年 12 月 8–10 日.

引間宥花, 池田時浩, 森光正, 金衛国 (ポスター), 「生物照射のためのガラスキャピラリーマイクロビーム法とスポット径解析」, 原子衝突学会第 45 回年会, オンライン, 2020 年 12 月 8–10 日.

引間宥花, 池田時浩, 森光正, 金衛国 (口頭発表), 「ガラスキャピラリーによる H^+ マイクロビームの大気中微小標的への照射距離の評価」, 第 63 回放射線化学討論会, オンライン, 2020 年 12 月 12–14 日.

三宮圭人, 池田時浩, 森光正, 引間宥花, 田山優雅, 福田彩実, 山口航平, 金衛国 (口頭発表), 「ガラスキャピラリーにおけるパルスレーザーマイクロビームの透過特性」, 第 63 回放射線化学討論会, オンライン, 2020 年 12 月 12–14 日.

Awards

引間宥花, 「生物照射のためのガラスキャピラリーマイクロビーム法とスポット径解析」, 原子衝突学会第 45 回年会ホットトピック公演.

Accelerator Applications Research Division
Beam Mutagenesis Group

1. Abstract

This group promotes biological applications of ion beams from RI Beam Factory (RIBF). Ion Beam Breeding Team studies various biological effects of fast heavy ions and develops new technology to breed plants and microbes by heavy-ion irradiations. Plant Genome Evolution Research Team studies the effect of chromosomal rearrangements on plant genomes and phenotypes.

2. Major Research Subjects

(1) Biological effects of fast heavy ions
(2) Molecular nature of DNA alterations induced by heavy-ion irradiation
(3) Research and development of heavy-ion breeding
(4) Study on the effect of chromosomal rearrangements on plant genomes and phenotypes

3. Summary of Research Activity

Summary of research activities of the two teams are given in the sections of each team.

Members

Director

Tomoko ABE

Team Leaders

Tomoko ABE

Hiroyuki ICHIDA

Accelerator Applications Research Division
Beam Mutagenesis Group
Ion Beam Breeding Team

1. Abstract

Ion beam breeding team studies various biological effects of fast heavy ions. It also develops new technique to breed plants and microbes by heavy-ion irradiations. Fast heavy ions can produce dense and localized ionizations in matters along their tracks, in contrast to photons (X rays and gamma rays) which produce randomly distributed isolated ionizations. These localized and dense ionization can cause double-strand breaks of DNA which are not easily repaired and result in mutation more effectively than singlestrand breaks. A unique feature of our experimental facility at the RIKEN Ring Cyclotron (RRC) is that we can irradiate living tissues in atmosphere since the delivered heavy-ion beams have energies high enough to penetrate deep in matter. This team utilizes a dedicated beam line (E5B) of the RRC to irradiate microbes, plants and animals with beams ranging from carbon to iron. Its research subjects cover study of ion-beam radiation mutagenesis, genome-wide analyses of mutation, and development of new plants and microbial varieties by heavy-ion irradiation. Thirty-five new varieties have already been brought to the market.

2. Major Research Subjects

(1) Study on the biological effects by heavy-ion irradiation
(2) Study on the molecular nature of DNA alterations induced by heavy-ion irradiation
(3) Innovative applications of heavy-ion beams

3. Summary of Research Activity

We study biological effects of fast heavy ions from the RRC using 135 *A* MeV C, N, Ne ions, 95 *A* MeV Ar ions, 90 *A* MeV Fe ions and from the IRC using 160 *A* MeV Ar ions. We also develop breeding technology of microbes and plants. Main subjects are:

(1) Study on the biological effects by heavy-ion irradiation

Heavy-ion beam deposits a concentrated amount of dose at just before stop with severely changing the linear energy transfer (LET). The peak of LET is achieved at the stopping point and known at the Bragg peak (BP). Adjusting the BP to target malignant cells is well known to be effective for cancer therapy. On the other hand, a uniform dose distribution is a key to the systematic study for heavy-ion mutagenesis, thus to the improvement of the mutation efficiency. Plants and microbes therefore, are irradiated using ions with stable LET. We investigated the effect of LET ranging from 23 to 640 keV/μm, on mutation induction using dry seeds of the model plants *Arabidopsis thaliana* and rice (*Oryza sativa* L.). The most effective LET (LETmax) was 30 keV/μm in *Arabidopsis*. LETmax irradiations showed the same mutation rate as that by chemical mutagens, which typically cause high mutation rate. The LETmax was 23–39 keV/μm in buckwheat, 23–50 keV/μm in rice and 50–70 keV/μm in wheat. By contrast, when LET was 290 keV/μm, the mutation rate was low and the survival rate was greatly reduced in plants. In the case of microbe, filamentous fungus (*Neurospora crassa*), the Ar ions at 290 keV/μm demonstrated higher mutagenic activity than the Fe-ions at 640 keV/μm. Thus, the LET is an important factor to be considered in heavy-ion mutagenesis.

(2) Study on the molecular nature of DNA alterations induced by heavy-ion irradiation

A whole-genome analysis with high-throughput sequencing is a powerful tool used to characterize the nature of induced mutations. We have been using whole genome sequencing to analyze DNA mutations in *Arabidopsis* and rice genomes. C ions with LETmax mainly induced single nucleotide variants (SNVs) and small insertions and deletions (InDels), while the number of large deletions and chromosomal rearrangements was low. However, 290-keV/μm Ar ions showed a different mutation spectrum: SNVs and number of small InDels was low, while the number of large deletions ($\geqq$100 bp) and chromosomal rearrangements was high. Number of mutated gene induced by C-ion and Ar-ion irradiation is less than 10, relatively small, and often only 1 mutation is found near the mapped location. Thus, irradiation with these ions can efficiently generate knockout mutants of a target gene and can be applied to reverse genetics. Mutants of the causative gene of Arabidopsis induced by ion beam irradiation were compared at 30 keV/μm and 290 keV/μm with two typical LETs. The most mutations irradiated with C ion at 30 keV/μm were small deletions (<100 bp). Irradiation with 290-keV/μm C-ion and Ar-ion resulted in the most large-deletions and chromosomal rearrangements, and decreased small deletions.

(3) Innovative application of heavy-ion beams

In 1999, we formed a consortium for ion-beam breeding consisting of 24 groups. In 2020, the consortium grew to 184 groups from Japan and 20 from overseas. Previously, the ion-beam breeding procedures were carried out using mainly flowers and ornamental plants. We have recently put a new non-pungent and tearless onion, 'Smile ball,' on the market along with 'Kiku Meigetsu,' an edible late flowering chrysanthemum. In addition, a new project was launched to expand the cultivation area of this variety of chrysanthemum in Yamagata prefecture. Beneficial variants have been grown for various plant species, such as high yield sea weeds, lipids hyperaccumulating unicellular alga, medicinal plant with high productivity of medicinal ingredient, peanuts without major allergens, oranges with delayed coloring and one-month late harvest, and lettuce with a low browning property as a cut vegetable. As a result of a collaborative study with the University of Hasanuddin, we have selected five useful aromatic rice mutants and increased the percentage of fertile grains from 32% control to over 52%. By broadening the target of heavy-ion breeding extending from flowers

to crops such as grains, the technology will contribute to solving the global problems of food shortage and environmental destruction.

Members

Team Leader

Tomoko ABE

Research/Technical Scientists

Tokihiro IKEDA (Senior Research Scientist)
Masako IZUMI (Senior Research Scientist)
Teruyo TSUKADA (Senior Research Scientist)
Kazuhide TSUNEIZUMI (Senior Research Scientist)
Ryouhei MORITA (Technical Scientist)

Research & Development Scientists

Hiroyuki ICHIDA

Technical Staff I

Yoriko HAYASHI
Yuki SHIRAKAWA

Technical Staff II

Sumie OHBU
Mieko YAMADA

Special Temporary Technical Scientists

Hiroshi ABE
Katsunori ICHINOSE

Research Consultant

Masahiro MII (Chiba Univ.)

Visiting Scientists

Ayumi DEGUCHI (Chiba Univ.)
Makoto FUJIWARA (Sophia Univ.)
Eitaro FUKATSU (Forestry and Forest Products Res. Inst.)
Tomonari HIRANO (Univ. of Miyazaki)
Akiko HOKURA (Tokyo Denki Univ.)
Yutaka MIYAZAWA (Yamagata Univ.)
Kazumitsu MIYOSHI (Chiba Univ.)
Toshikazu MORISHITA (Nat'l Agriculture and Food Res. Org.)
Koji MURAI (Fukui Prefectural Univ.)
Kyosuke NIWA (Tokyo Univ. of Marine Sci. and Tech.)
Norihiro OHTSUBO (Kyoto Prefectural Univ.)
Tadashi SATO (Tohoku Univ.)
Yoichi SATO (Riken Food Co., Ltd.)
Kenichi SUZUKI (Suntory Flowers Co., Ltd.)
Hinako TAKEHISA (Nat'l Agriculture and Food Res. Org.)
Masanori TOMITA (Central Res. Inst. of Electric Power Industry)
Masao WATANABE (Tohoku Univ.)
Takeshi YAMAKI (Riken Vitamin Co., Ltd.)

Visiting Technicians

Yukiko KANAZAWA (Nippon Beet Sugar Manufacturing Co., Ltd.)
Norihide KISHINO (Sanwa Norin Co. Ltd.)
Miho MOGAMIYA (Riken Food Co., Ltd.)
Daisuke SAITO (Riken Food Co., Ltd.)
Takuji YOSHIDA (Takii & Co., Ltd)

Research Fellow

Hironari UCHIDA (Saitama Agricultural Tech. Res. Center)

List of Publications & Presentations

Publications

[Original Papers]

T. Hirano, Y. Sato, K. Ichinose, M. Yamada, Y. Hayashi, N. Fukunishi, and T. Abe, "Mutant induction in gametophytes of *Undaria pinnatifida* (Phaeophyceae) by heavy ion beam irradiation," Phycol. Res. **68**, 63–69 (2019).

N. Fukuda, N. Kitajim, Y. Terada, T. Abe, I. Nakai, and A. Hokura, "Visible cellular distribution of cadmium and zinc in the hyperaccumulator *Arabidopsis halleri* ssp. gemmifera determined by 2-D X-ray fluorescence imaging using high-energy synchrotron radiation," Metallomics **12**, 193–203 (2019).

Y. Oono, H. Ichida, R. Morita, S. Nozawa, K. Satoh, A. Shimizu, T. Abe, H. Kato, and Y. Hase, "Genome sequencing of ion-beam-induced mutants facilitates detection of candidate genes responsible for phenotypes of mutants in rice," Mutat. Res. Fund. Mol. Mech. Mutagen. (2020).

R. Tabassum, T. Dosaka, H. Ichida, R. Morita, Y. Ding, T. Abe, and T. Katsube-Tanaka, "FLOURY ENDOSPERM11-2 encodes plastid HSP70-2 involved with the temperature-dependent chalkiness of rice (*Oryza sativa* L.) grains," Plant J. **103**, 604–616 (2020).

K. Kaya, Y. Kazama, T. Abe, and F. Shiraishi, "Influence of medium components and pH on the production of odd-carbon fatty acids by Aurantiochytrium sp. SA-96," J. Appl. Phycol. **32**, 1597–1606 (2020).

S. Muramatsu, K. Atsuji, K. Yamada, K. Ozasa, H. Suzuki, T. Takeuchi, Y. Hashimoto-Marukawa, Y. Kazama, T. Abe, K. Suzuki, and O. Iwata, "Isolation and characterization of a motility-defective mutant of *Euglena gracilis*," Peer J **8**, e10002 (2020).

H. Murata, S. Nakano, T. Yamanaka, T. Shimokawa, T. Abe, H. Ichida, Y. Hayashi, and K. Tahara, "Argon-ion beam induced mutants of the ectomycorrhizal agaricomycete *Tricholoma matsutake* defective in β-1,4-endoglucanase activity promote the seedling growth of *Pinus densiflora* in vitro," Botany, **99**(3), DOI:10.1139/cjb-2020-0076 (2020).

[Proceedings]

A. M. Okasa, M. Riadi, K. Toriyama, K. Ishii, Y. Hayashi, T. Sato, T. Abe, Trisnawaty, N. J. Panga, and R. Sjahril, "Mutation breeding for improvement of aromatic rice mutant by using ion beam irradiation," IOP Conf. Ser. Earth Environ. Sci. **486**, 012091 (2020).

Presentations

[International Conferences/Workshops]

T. Kashiwabara, N. Kitajima, R. Onuma, N. Fukuda, S. Endo, Y. Terada, T. Abe, A. Hokura, and I. Nakai, "Synchrotron micro-X-ray fluorescence imaging of arsenic in frozen-hydrated sections of a root of *Pteris vittate*," Goldschmidt2020: Global Virtual Conference, online, June 21–26, (2020).

T. Abe (invited), "Development for ion-beam breeding technology over the last two decades in Japan," Virtual Meeting on FAO/IAEA Mutation Breeding Network (MBN) for Asia Pacific Region, online, November 12–13, (2020).

[Domestic Conferences/Workshops]

常泉和秀, 山田美恵子, 一瀬勝紀, 市田裕之, 金禧珍, 萩原篤志, 川田実季, 片山貴士, 崎山一孝, 手塚信弘, 小磯雅彦, 阿部知子, 「シオミズツボワムシの高増殖・大型変異系統の樹立」, 日本農芸化学会 2020 年度大会, 福岡県福岡市 (九州大学), 2020 年 3 月 26 日.

市田裕之, 阿部知子, 「オープンソースな変異タイピング手法の開発とイネをモデルとした概念実証」, 日本育種学会 第 137 回講演会, 東京都文京区 (東京大学), 2020 年 3 月 28 日.

渡邊遙, 大部澄江, 阿部知子, 風間裕介, 「ゲノム編集によるシロイヌナズナへの 758 kb の逆位の導入」, 同上.

A. M. Okasa, M. Riadi, 佐藤雅志, 鳥山欽哉, 石井公太郎, 林依子, 阿部知子, R. Sjahril, "An approach toward isolating early-heading mutants from Tana Toraja local aromatic rice 'Pare Bau' irradiated with heavy ion-beam," 同上.

橋本佳澄, 西浦愛子, 上田純平, 風間裕介, 阿部知子, 市田裕之, 村井耕二, 「2 倍体ヒトツブコムギにおける重イオンビーム照射による超極早生変異体 extra early-flowering 4 の原因遺伝子の同定」, 同上.

森田竜平, 市田裕之, 石井公太郎, 林依子, 安部弘, 白川侑希, 一瀬勝紀, 常泉和秀, 風間智彦, 鳥山欽哉, 佐藤雅志, 阿部知子, 「イネ長粒変異体 lin1 の単離および原因遺伝子同定」, 同上.

石井公太郎, 大部澄江, 白川侑希, 阿部知子, 「全ゲノム変異解析による重イオンビームの高頻度な変異誘発線量区の推定」, 同上.

村井耕二, 風間裕介, 阿部知子, 「2 倍体ヒトツブコムギにおける重イオンビーム突然変異体作出のための最適処理条件」, 同上.

Y. Ding(口頭発表), T. Katsube-Tanaka, H. Ichida, R. Morita, and T. Abe, "Studies on chalkiness of the rice cultivar 'Kinmaze'under heat stress," 日本作物学会第 250 回講演会, オンライン開催, 2020 年 9 月 3–4 日.

蝶野真喜子 (ポスター発表), 藤田雅也, 神山紀子, 松中仁, 氷見英子, 市田裕之, 阿部知子, 川上直人, 「粒の赤みが弱い新規コムギ変異体の農業特性」, 日本育種学会 第 138 回講演会, オンライン開催, 2020 年 10 月 10–11 日.

藤田悠生 (ポスター発表), 市田裕之, 風間智彦, 阿部知子, 鳥山欽哉, 「インディカイネ品種 Lebed に由来する雄性不稔遺伝子とその抑制遺伝子の解析」, 同上.

石井公太郎 (口頭発表), 風間裕介, 浅野円花, 阿部知子, 河野重行, 「Ar・Fe イオンビーム照射によって生じるクロレラ染色体の断片化と染色体再編成」, 同上.

南壮次郎 (口頭発表), 渡邊遥, 大部澄江, 阿部知子, 風間裕介, 「ゲノム編集を用いたシロイヌナズナへの染色体再編成の導入」, 同上.

野村文希 (ポスター発表), 風間裕介, 阿部知子, 村井耕二, 「イオンビーム照射により作出された Ppd-1 欠失『農林 61 号』変異系統の解析」, 第 15 回ムギ類研究会, オンライン開催, 2020 年 12 月 26 日.

橋本佳澄 (ポスター発表), 西浦愛子, 風間裕介, 市田裕之, 阿部知子, 村井耕二, 「重イオンビーム照射によって作出された超極早生コムギ変異体 extra early-flowering 4（exe4）の花成関連遺伝子の発現解析」, 同上.

Awards

佐藤陽一, 斎藤大輔, 最上谷美穂, 令和 2 年度（第 21 回）民間部門農林水産研究開発功績者表彰（農林水産技術会議会長賞民間部門), 「わかめ養殖種苗の優良系統開発と生産条件最適化による普及実用化」, 農林水産会議, 2020 年 11 月 12 日.

Patents

石井重久, 阿部知子, 林依子, サクラ「真和」, 品種登録出願番号 34356, 出願日 2019 年 11 月 27 日.

石井重久, 阿部知子, 林依子, サクラ「真理」, 品種登録出願番号 34356, 出願日 2019 年 11 月 27 日.

石井重久, 阿部知子, 林依子, サクラ「真星」, 品種登録出願番号 34356, 出願日 2020 年 4 月 14 日.

Outreach Activities

We established the "Asagao (morning glory) club" to deepen the understanding of our technology of mutation breeding. The club distributes the morning glory seeds irradiated with C-ion on request, and collects and compiles the observation reports of their growth.

Accelerator Applications Research Division
Beam Mutagenesis Group
Plant Genome Evolution Research Team

1. Abstract

Established in May 2018 and succeed in October 2020, the plant genome evolution research team studies the effect of heavy-ion induced mutations on plant and microbial phenotypes. Chromosome rearrangements including translocations, inversions, and deletions are thought to play an important role in evolution and have a greater potential to achieve large phenotypic changes. However, this potential has not been fully investigated due to the lack of an effective method to induce and analyze complexed mutations. We employ the population genomics approach with robust molecular biology and bioinformatics techniques to characterize genomic mutations in model and non-model plant and microbial species, and create the future of mutation breeding.

2. Major Research Subjects

(1) Study on the effect of chromosomal rearrangements on plant genomes and phenotypes
(2) Genomics-based approach to revolutionize the mutagenesis in model and non-model plants and microbes

3. Summary of Research Activity

(1) Study on the effect of chromosomal rearrangements on plant genomes and phenotypes

We have established an efficient bioinformatics pipeline named AMAP, an automated mutation analysis pipeline, and have used it for genome-wide analysis of chromosome rearrangements and other mutations in various organisms. In Arabidopsis, we isolated a short-petiole mutant, Ar55-as1, from Ar-beam irradiated population at a dose of 50 Gy with an LET of 290 keV/μm. We showed that this mutant has no typical base substitutions, deletions, and insertions that were linked to the mutant's phenotype, but has chromosomal rearrangements in the genome. Genetic linkage analysis showed that the short-petiole phenotype and the presence or absence of the inversion on chromosome 2 was completely linked in M3 generation, indicating that this inversion is responsible for the phenotype. The Ar55-as1 mutant will serve as a good model to investigate the effects on gene expressions by chromosomal rearrangements.

We previously isolated a high oil-production mutant of *Parachlorella kessleri*, a starch and oil-producing unicellular green algae, by C-beam irradiations. The effect on chromosomal rearrangements by Ar- and Fe-beams was quantitatively evaluated by cytological observations and high-throughput sequencing. As the result, Fe-beam irradiation at a dose of 75 Gy caused dramatic increase of fragmented chromosomes: 14 percent of the population had more than 30 chromosomes right after the irradiation and three percent of the population still remained more than 20 chromosomes after four consecutive cultures, although the wild-type *P. kessleri* cells have only seven A- and three B-chromosomes. We performed whole-genome sequencing in two mutants, and the results indicated that one mutant, Fe75-1-3H had chromosomal rearrangements with 10 junction regions, and the other, Ar75-1-2C, had a novel chromosomal terminus by the result from a translocation.

(2) Genomics-based approach to revolutionize the mutagenesis in model and non-model plants and microbes

Recent advances in genome sequencing and bioinformatics technology enabled us to obtain a genome-wide view of the induced mutations in unselected populations. We chose baker's yeast and a legume *Lotus japonicus* as model systems, irradiated different doses of carbon-ion beams to these organisms, and determined the dose-survival correlation. We isolated a semi-dwarf *L. japonicus* mutant, identified the responsible mutation by whole-genome sequencing, and started to characterize the phenotypic traits of this mutant. The semi-dwarf *L. japonicus* mutant is suitable for high-density cultivation in laboratory environment and may serve as an efficient model platform for legume-*Rhizobium* symbiosis.

Members

Team Leader

Tomoko ABE (～2020.09)
Hiroyuki ICHIDA (2020.10～)

Contract Researcher

Kotaro ISHII

Visiting Scientists

Ali FERJANI (Tokyo Gakugei Univ.)
Yusuke KAZAMA (Fukui Prefectural Univ.)

Part-time Worker

Yusaku NISHIMIYA (Administrative Part-time Worker II)

List of Publications & Presentations

Publications

[Original Papers]

Y. Oono, H. Ichida, R. Morita, S. Nozawa, K. Satoh, A. Shimizu, T. Abe, H. Kato, and Y. Hase, "Genome sequencing of ion-beam-induced mutants facilitates detection of candidate genes responsible for phenotypes of mutants in rice," Mutat. Res. Fund. Mol. Mech. Mutagen.**821**, 111691 (2020).

R. Tabassum, T. Dosaka, H. Ichida, R. Morita, Y. Ding, T. Abe, and T. Katsube-Tanaka, "*FLOURY ENDOSPERM11-2* encodes plastid HSP70-2 involved with the temperature-dependent chalkiness of rice (*Oryza sativa* L.) grains," Plant J. **103**, 604–616 (2020).

H. Murata, S. Nakano, T. Yamanaka, T. Shimokawa, T. Abe, H. Ichida, Y. Hayashi, and K. Tahara, "Argon-ion beam induced mutants of the ectomycorrhizal agaricomycete *Tricholoma matsutake* defective in β-1,4-endoglucanase activity promote the seedling growth of *Pinus densiflora* in vitro," Botany **99**, 139–149 (2020). DOI:10.1139/cjb-2020-0076 .

Presentations

[Domestic Conferences/Workshops]

市田裕之, 阿部知子, 「オープンソースな変異タイピング手法の開発とイネをモデルとした概念実証」, 日本育種学会 第 137 回講演会, 東京都文京区 (東京大学), 2020 年 3 月 28 日.

橋本佳澄, 西浦愛子, 上田純平, 風間裕介, 阿部知子, 市田裕之, 村井耕二, 「2 倍体ヒトツブコムギにおける重イオンビーム照射による超極早生変異体 *extra early-flowering 4* の原因遺伝子の同定」, 同上.

森田竜平, 市田裕之, 石井公太郎, 林依子, 安部弘, 白川侑希, 一瀬勝紀, 常泉和秀, 風間智彦, 鳥山欽哉, 佐藤雅志, 阿部知子, 「イネ長粒変異体 *lin1* の単離および原因遺伝子同定」, 同上.

石井公太郎, 大部澄江, 白川侑希, 阿部知子, 「全ゲノム変異解析による重イオンビームの高頻度な変異誘発線量区の推定」, 同上.

Y. Ding (口頭発表), T. Katsube-Tanaka, H. Ichida, R. Morita, and T. Abe, "Studies on chalkiness of the rice cultivar 'Kinmaze' under heat stress," 日本作物学会第 250 回講演会, オンライン開催, 2020 年 9 月 3–4 日.

蝶野真喜子 (ポスター発表), 藤田雅也, 神山紀子, 松中仁, 氷見英子, 市田裕之, 阿部知子, 川上直人, 「粒の赤みが弱い新規コムギ変異体の農業特性」, 日本育種学会 第 138 回講演会, オンライン開催, 2020 年 10 月 10–11 日.

藤田悠生 (ポスター発表), 市田裕之, 風間智彦, 阿部知子, 鳥山欽哉, 「インディカイネ品種 Lebed に由来する雄性不稔遺伝子とその抑制遺伝子の解析」, 同上.

石井公太郎 (口頭発表), 風間裕介, 浅野円花, 阿部知子, 河野重行, 「Ar・Fe イオンビーム照射によって生じるクロレラ染色体の断片化と染色体再編成」, 同上.

橋本佳澄 (ポスター発表), 西浦愛子, 風間裕介, 市田裕之, 阿部知子, 村井耕二, 「重イオンビーム照射によって作出された超極早生コムギ変異体 *extra early-flowering 4*（*exe4*）の花成関連遺伝子の発現解析」, 第 15 回ムギ類研究会, オンライン開催, 2020 年 12 月 26 日.

Accelerator Applications Research Division
RI Application Research Group

1. Abstract

RI Application Research Group promotes industrial applications of radioisotopes (RIs) and ion beams at RIKEN RI Beam Factory (RIBF). Nuclear Chemistry Research Team develops production technologies of useful RIs for application studies in nuclear and radiochemistry. The team also develops technologies of mass spectrometry for trace-element and isotope analyses and apply them to the research fields such as cosmochemistry, environmental science, archaeology, and so on. Industrial Application Research Team promotes industrial applications of the accelerator facility and its related technologies.

2. Major Research Subjects

(1) Research and development of RI production technologies at RIBF
(2) RI application researches
(3) Distribution of RIs produced at RIBF
(4) Development of trace element analyses using accelerator techniques and their applications to geoscience and archaeological research fields
(5) Development of chemical materials for ECR ion sources of the RIBF accelerators
(6) Development of technologies on industrial utilization and novel industrial applications of RIBF
(7) Support of industrial utilization of the heavy-ion beams at RIBF
(8) Support of materials science experiments

3. Summary of Research Activity

See the subsections of Nuclear Chemistry Research Team and Industrial Application Research Team.

Member

Director

Hiromitsu HABA

List of Publications & Presentations

See the subsections of Nuclear Chemistry Research Team and Industrial Application Research Team.

Accelerator Applications Research Division
RI Application Research Group
Nuclear Chemistry Research Team

1. Abstract

The Nuclear Chemistry Research Team develops production technologies of unique radioisotopes (RIs) at RIKEN RI Beam Factory (RIBF) and applies them in the research fields of physics, chemistry, biology, engineering, medicine, pharmaceutical and environmental sciences. The purified RIs such as ^{65}Zn, ^{67}Cu, ^{85}Sr, ^{88}Y, and ^{109}Cd are delivered to universities and institutes through Japan Radioisotope Association. We also develop new technologies of mass spectrometry for the trace-element analyses using accelerator techniques and apply them to the research fields such as cosmochemistry, environmental science, archaeology, and so on. We perform various isotopic analyses on the elements such as S, Pd, and Pb using ICP-MS, TIMS, and IRMS. We also develop chemical materials such as metallic ^{238}U, $^{238}UO_2$, and ^{48}CaO for ECR ion sources of the heavy-ion accelerators at RIBF.

2. Major Research Subjects

(1) Research and development of RI production technologies at RIBF
(2) RI application researches
(3) Development of trace element analyses using accelerator techniques and their applications to geoscience and archaeological research fields
(4) Development of chemical materials for ECR ion sources of the heavy-ion accelerators at RIBF

3. Summary of Research Activity

(1) Research and development of RI production technologies at RIBF and RI application researches

Due to its high sensitivity, the radioactive tracer technique has been successfully applied for investigations of the behavior of elements in the fields of chemistry, biology, engineering, medicine, pharmaceutical and environmental sciences. We have been developing production technologies of useful radioisotopes (RIs) at RIBF and conducting their application studies in collaboration with many researchers in various fields. With 30-MeV proton, 24-MeV deuteron, and 50-MeV alpha beams from the AVF cyclotron, we presently produce about 100 RIs from ^{7}Be to ^{211}At. Among them, ^{65}Zn, ^{67}Cu, ^{85}Sr, ^{88}Y, and ^{109}Cd are delivered to Japan Radioisotope Association for fee-based distribution to the general public in Japan. Our RIs are also distributed to researchers under the Supply Platform of Short-lived Radioisotopes for Fundamental Research, supported by MEXT KAKENHI in FY2016–2021. On the other hand, RIs of a large number of elements are simultaneously produced from metallic targets such as ^{nat}Ti, ^{nat}Ag, ^{nat}Hf, ^{197}Au, and ^{232}Th irradiated with a 135-MeV nucl.$^{-1}$ ^{14}N beam from the RIKEN Ring Cyclotron. These multitracers are also supplied to universities and institutes as collaborative researches.

In 2020, we developed production technologies of RIs such as ^{7}Be, ^{28}Mg, ^{43}K, ^{44m}Sc, ^{44}Ti, ^{48}Cr, ^{186}Re, ^{211}At, ^{212}Pb, ^{224}Ra, ^{225}Ac, and ^{229}Pa which were strongly demanded but lack supply sources in Japan. We also investigated the excitation functions for the ^{nat}V(d, x), ^{nat}Gd(d, x), ^{141}Pr(d, x), and ^{nat}Nd(α, x) reactions to quantitatively produce useful RIs. We used radiotracers of ^{28}Mg, ^{211}At, ^{212}Pb, ^{224}Ra, and ^{229}Pa for application studies in chemistry, ^{44m}Sc, ^{67}Cu, ^{186}Re, ^{211}At, and ^{225}Ac in nuclear medicine, and ^{43}K, ^{48}Cr, ^{186}Re, and ^{211}At in engineering. We also produced ^{65}Zn, ^{85}Sr, ^{88}Y, and ^{109}Cd for our scientific researches on a regular schedule and supplied the surpluses through Japan Radioisotope Association to the general public. In 2020, we accepted 6 orders of ^{65}Zn with a total activity of 33 MBq, 5 orders of ^{85}Sr with 9.7 MBq, 1 order of ^{88}Y with 1 MBq, and 1 order of ^{109}Cd with 10 MBq. We also distributed ^{7}Be (0.45 MBq × 1), ^{88}Zr (1 MBq × 2), ^{95}Nb (1 MBq × 1 and 2 MBq × 1), ^{121m}Te (2 MBq × 1), ^{175}Hf (1 MBq × 2), and ^{211}At (5 MBq × 6, 10 MBq × 1, 18 MBq × 2, 50 MBq × 1, 80 MBq × 1, and 100 MBq × 16) under the Supply Platform of Short-lived Radioisotopes for Fundamental Research.

(2) Superheavy element chemistry

Chemical characterization of newly-discovered superheavy elements (SHEs, atomic number $Z \geq 104$) is an extremely interesting and challenging subject in modern nuclear and radiochemistry. We are developing SHE production systems as well as rapid single-atom chemistry apparatuses at RIBF. Using heavy-ion beams from RILAC and AVF, ^{261}Rf ($Z = 104$), ^{262}Db ($Z = 105$), ^{265}Sg ($Z = 106$), and ^{266}Bh ($Z = 107$) are produced in the ^{248}Cm(^{18}O, $5n$)^{261}Rf, ^{248}Cm(^{19}F, $5n$)^{262}Db, ^{248}Cm(^{22}Ne, $5n$)^{265}Sg, and ^{248}Cm(^{23}Na, $5n$)^{266}Bh reactions, respectively, and their chemical properties are investigated.

We installed a gas-jet transport system to the focal plane of the gas-filled recoil ion separator GARIS at RILAC. This system is a promising approach for exploring new frontiers in SHE chemistry: the background radiations from unwanted products are strongly suppressed, the intense primary heavy-ion beam is absent in the gas-jet chamber, and hence the high gas-jet extraction yield is attained. Furthermore, the beam-free condition makes it possible to investigate new chemical systems. To realize aqueous chemistry studies of Sg and Bh, we have been developing a continuous and rapid solvent extraction apparatus which consists of a continuous dissolution apparatus Membrane DeGasser (MDG), a Flow Solvent Extractor (FSE), and a liquid scintillation detector for α/SF-spectrometry. On the other hand, we produced radiotracers of $^{88, 89m}$Zr, ^{95}Nb, ^{175}Hf, and $^{177, 179}$Ta at the AVF cyclotron and conducted model experiments for aqueous chemistry studies on Rf and Db. We also developed a cryogenic RF-carpet gas cell, which will be placed on the focal plane of GARIS and connected to a gas chromatographic apparatus, for the future gas-phase chemistry of the short-lived SHEs (<3 s).

(3) Development of trace element analyses using accelerator techniques and their applications to geoscience and archaeological research fields

We have been developing the ECR Ion Source Mass Spectrometer (ECRIS-MS) for trace element analyses. We renovated the detection system of ECRIS-MS and evaluated its sensitivity and mass resolution power. We equipped a laser-ablation system with an ion source and a pre-concentration system to achieve high-resolution analyses for noble gases such as Kr and Xe.

Using the conventional ICP-MS, TIMS, IRMS, and so on, we studied Pb and S isotope ratios on cinnabar and asphalt samples from ancient ruins in Japan to elucidate the distribution of goods in the archaic society and to reveal the establishment of the Yamato dynasty in the period from Jomon to Tumulus. We established a sampling technique for pigment without any damages on the artifacts or wall paintings, using a S-free adhesive tape. Then, we applied the technique to the analyses of the pigment from Roman ruins (Avinyó in Barcelona, Spain). We also applied the technique to the analyses of the red-color substances on the artifacts such as Kyoden remains (Izumo-city, Shimane prefecture), Renpeijou-ato (Zentsuji-City, Kagawa prefecture) and so on. We also established the method to identify the source mine of vermilion, using sulfur, mercury and lead isotopic analyses, and we applied this method to investigation of vermilion from three representative tombs (Kofunperiod in Japan)

(4) Development of chemical materials for ECR ion sources of the heavy-ion accelerators at RIBF

In 2020, we prepared $^{238}UO_2$ on a regular schedule for ^{238}U-ion accelerations with the 28-GHz ECR of RILAC II.

Members

Team Leader
Hiromitsu HABA

Research & Development Scientist
Hiroo HASEBE

Contract Researchers
Katsumasa FUJIKI
Yukiko KOMORI

Special Postdoctoral Researcher
Yudai SHIGEKAWA

Postdoctoral Researchers
Yang WANG
Takuya YOKOKITA
Xiaojie YIN

Technical Staff I
Akihiro NAMBU

Special Temporary Research Scientist
Kazuya TAKAHASHI

Research Consultant
Hisaaki KUDO (Niigata Univ.)

Visiting Scientists
Msayuki AIKAWA (Hokkaido Univ.)
Kazuhiko AKIYAMA (Tokyo Metropolitan Univ.)
Takatoshi AOKI (Univ. of Tokyo)
Masato ASAI (JAEA)
Ferenc DITRÓI (ATOMKI)
Osuke FUJIMOTO (Fujifilm Toyama Chemical Co., Ltd.)
Takahiro HIRAKI (Okayama Univ.)
Hayato IKEDA (Tohoku Univ.)
Noriko ISHIOKA (QST)
Masamichi KAJITA (Fujifilm Toyama Chemical Co., Ltd.)
Yoshitaka KASAMATSU (Osaka Univ.)
Hiroshi KATO (Fujifilm Toyama Chemical Co., Ltd.)
Mayeen U. KHANDAKER (Sunway Univ.)
Hidetoshi KIKUNAGA (Tohoku Univ.)
Yoshikatsu KOGA (Nat'l Cancer Center)
Shoko KUBOTA (Fujifilm Toyama Chemical Co., Ltd.)
Takumi KUBOTA (Kyoto Univ.)
Susanta Kumar LAHIRI (Saha Inst. of Nucl. Phys. India)
Takahiko MASUDA (Okayama Univ.)
Toshimitsu MOMOSE (Int'l Univ. of Health and Welfare)
Eri NAKAMURA (Fujifilm Toyama Chemical Co., Ltd.)
Kenichiro OGANE (Int'l Univ. of Health and Welfare)
Miki OHTSUKA (Waseda Univ.)
Kazuhiro OOE (Osaka Univ.)
Shinobu OSHIKIRI (Fujifilm Toyama Chemical Co., Ltd.)
Yasutaka SAITO (Fujifilm Toyama Chemical Co., Ltd.)
Aya SAKAGUCHI (Tsukuba Univ.)
Miho SATAKE (Fujifilm Toyama Chemical Co., Ltd.)
Tetsuya SATO (JAEA)
Yuki SATO (Fujifilm Toyama Chemical Co., Ltd.)
Kenji SHIMAZOE (Univ. of Tokyo)
Keisuke SUEKI (Tsukuba Univ.)
Kentaro SUZUKI (Fujifilm Toyama Chemical Co., Ltd.)
Zoltán SZŰCS (ATOMKI)
Sándor TAKÁCS (ATOMKI)
Hiroyuki TAKAHASHI (Univ. of Tokyo)

Miho TAKAHASHI (Tokyo Univ. of Marine Sci. and Tech.)
Miwako TAKAHASHI (QST)
Yuichi TAKAKU (Inst. for Environmental Sci.)
Hiroki TAKASHIMA (Nat'l Cancer Center)
Kazuo TANAKA (Tohoku Univ.)
Masayoshi TODA (Tokyo Univ. of Marine Sci. and Tech.)
Atsushi TOYOSHIMA (Osaka Univ.)
Kazuaki TSUKADA (JAEA)
Naoyuki UKON (Fukushima Medical Univ.)
Ahmed R. USMAN (Umaru Musa Yar'adua Univ.)
Shigeki WATANABE (QST)
Takahiro YAMADA (Kindai Univ.)
Chunli YANG (Inst. of Modern Phys./Chinese Academy of Sci.)
Akihiko YOKOYAMA (Kanazawa Univ.)
Zenko YOSHIDA (ATOX Co., Ltd.)
Koji YOSHIMURA (Okayama Univ.)

Visiting Technicians

Hideyuki ARAI (Metal Tech. Co. Ltd.)
Hiroshi ARATA (Metal Tech. Co. Ltd.)
Mai FUKUMORI (ATOX Co., Ltd.)
Hidehiro HASHIMOTO (Metal Tech. Co. Ltd.)
Yoshiyuki IIZUKA (ATOX Co., Ltd.)
Akimitsu KANDA (Japan Radioisotope Association)
Shota KIMURA (Japan Radioisotope Association)
Yukiyoshi KON (Osaka Univ.)
Takashi KURIHARA (Metal Tech. Co. Ltd.)
Takahiro MIKAMOTO (Japan Radioisotope Association)
Shingo NAKAMURA (Metal Tech. Co. Ltd.)
Hiroki SHIBAHARA (ATOX Co., Ltd.)
Yuki TAKEMURA (ATOX Co., Ltd.)
Yasutaka TAKEUCHI (ATOX Co., Ltd.)
Shusaku TAZAWA (ATOX Co., Ltd.)
Yuichirou WAKITANI (Japan Radioisotope Association)
Mami YUKI (ATOX Co., Ltd.)

Student Trainees

Kjeld A.A.G. BEEKS (Vienna Univ. of Tech.)
Desheng CHEN (Univ. of Chinese Academy of Sci.)
Shunsuke FUJINO (Kindai Univ.)
Sena HAMAGAMI (Kindai Univ.)
Yukina HANADA (Hokkaido Univ.)
Sho HAYAMI (Osaka Univ.)
Mariko HISAMATSU (Osaka Univ.)
Xuan HOU (Univ. of Tokyo)
Mizuho KATO (Tsukuba Univ.)
Cheonghun KIM (Univ. of Tokyo)
Mizuki KITAJIMA (Univ. of Tokyo)
Takuto MAEHASHI (Hokkaido Univ.)
Kenichi MORI (Kindai Univ.)
Ryoga MORITA (Kanazawa Univ.)
Ayumu NAGAI (Kanazawa Univ.)
Akihisa NAKAJIMA (Tsukuba Univ.)
Ryohei NAKANISHI (Osaka Univ.)
Teruhito NAKASHITA (Univ. of Tokyo)
Koichi OKAI (Okayama Univ.)
Michiya SAKAGUCHI (Hokkaido Univ.)
Motoki SATO (Univ. of Tokyo)
Kei SAWAMURA (Osaka Univ.)
Fumiki SENSUI (Univ. of Tokyo)
Ayano SETO (Kanazawa Univ.)
Kaori SHIRAI (Niigata Univ.)
Hayato SUZUKI (Ibaraki Univ.)
Kakeru TERANISHI (Kanazawa Univ.)
Katsuyuki TOKOI (Osaka Univ.)
Mizuki UENOMACHI (Univ. of Tokyo)
Eisuke WATANABE (Osaka Univ.)
Kazeki YAMANE (Univ. of Tokyo)
Yuki YASUDA (Osaka Univ.)
Zhihong ZHONG (Univ. of Tokyo)

Part-time Workers

Michiko KITAGAWA (Research Part-time Worker I)
Nozomi SATO (Research Part-time Worker I)
Sachiko USUDA (Research Part-time Worker I)
Minako OSANAI (Research Part-time Worker II)

List of Publications & Presentations

Publications

[Original Papers]

A. R. Usman, M. U. Khandaker, H. Haba, N. Otuka, and M. Murakami, "Production cross sections of thulium radioisotopes for alpha-particle induced reactions on holmium," Nucl. Instrum. Methods Phys. Res. B **469**, 42 (2020).

M. U. Khandaker, H. Haba, Y. Komori, and N. Otuka, "Excitation functions of deuteron-induced nuclear reactions on erbium in the energy range of 4–24 MeV," Nucl. Instrum. Methods Phys. Res. B **470**, 1 (2020).

Z. Tsoodol, M. Aikawa, I. Dagvadorj, T. Khishigjargal, N. Javkhlantugs, Y. Komori, and H. Haba, "Production cross sections of ^{68}Ga and radioactive by-products in deuteron-induced reactions on natural zinc," Appl. Radiat. Isot. **159**, 109095 (2020).

M. Saito, M. Aikawa, T. Murata, Y. Komori, H. Haba, S. Takács, F. Ditrói, and Z. Szűcs, "Production cross sections of ^{169}Yb by the proton-induced reaction on ^{169}Tm," Nucl. Instrum. Methods Phys. Res. B **471**, 13 (2020).

M. Sakaguchi, M. Aikawa, M. Saito, N. Ukon, Y. Komori, and H. Haba, "Activation cross section measurement of the deuteron-induced reaction on yttrium-89 for zirconium-89 production," Nucl. Instrum. Methods Phys. Res. B **472**, 59 (2020).

J. Grund, M. Asai, K. Blaum, M. Block, S. Chenmarev, Ch. E. Düllmann, K. Eberhardt, S. Lohse, Y. Nagame, Sz. Nagy, P. Naubereit, J. J. W. van de Laar, F. Schneider, T. K. Sato, N. Sato, D. Simonovski, K. Tsukada, and K. Wendt, "First online operation of TRIGA-TRAP," Nucl. Instrum. Methods Phys. Res. A **972**, 164013 (2020).

Y. Shigekawa, Y. Kasamatsu, Y. Yamakita, Y. Yasuda, E. Watanabe, N. Kondo, H. Haba, and A. Shinohara, "Development of a retarding-field type magnetic bottle spectrometer for studying the internal-conversion process of ^{235m}U," Nucl. Instrum. Methods Phys. Res. A **976**, 164207 (2020).

S. Takács, M. Aikawa, H. Haba, Y. Komori, F. Ditrói, Z. Szűcs, M. Saito, T. Murata, M. Sakaguchi, and N. Ukon, "Cross sections of alpha-particle induced reactions on ^{nat}Ni: Production of ^{67}Cu," Nucl. Instrum. Methods Phys. Res. B **479**, 125 (2020).

H. Haba, F. Fan, D. Kaji, Y. Kasamatsu, H. Kikunaga, Y. Komori, N. Kondo, H. Kudo, K. Morimoto, K. Morita, M. Murakami, K. Nishio, J. P. Omtvedt, K. Ooe, Z. Qin, D. Sato, N. Sato, T. K. Sato, Y. Shigekawa, A. Shinohara, M. Takeyama, T. Tanaka, A. Toyoshima, K. Tsukada, Y. Wakabayashi, Y. Wang, S. Wulff, S. Yamaki, S. Yano, Y. Yasuda, and T. Yokokita, "Production of ^{266}Bh in the ^{248}Cm(^{23}Na, 5n)^{266}Bh reaction and its decay properties," Phys. Rev. C **102**, 024625 (2020).

Y. Ohshima, H. Suzuki, H. Hanaoka, I. Sasaki, S. Watanabe, H. Haba, Y. Arano, Y. Tsushima, and N. S. Ishioka, "Preclinical evaluation of new α-radionuclide therapy targeting LAT1: 2-[^{211}At]astato-α-methyl-L-phenylalanine in tumor-bearing model," Nucl. Med. Biol. **90–91**, 15 (2020).

C. Xu, Y. Wang, T. Zhu, H. Wang, Y. Su, J. Zuo, and J. Han, "Experimental study of tritium activity concentration in cooling water of Heavy Ion Research Facility in Lanzhou," Nucl. Technol. Radiat. Prot. **35**, 304 (2020).

Z. Tsoodol, M. Aikawa, D. Ichinkhorloo, T. Khishigjargal, E. Norov, Y. Komori, H. Haba, S. Takács, F. Ditrói, and Z. Szűcs, "Production cross sections of ^{45}Ti in the deuteron-induced reaction on ^{45}Sc up to 24 MeV," Appl. Radiat. Isot. **168**, 109448 (2021).

Y. Kasamatsu, K. Toyomura, H. Haba, T. Yokokita, Y. Shigekawa, A. Kino, Y. Yasuda, Y. Komori, J. Kanaya, M. Huang, M. Murakami, H. Kikunaga, E. Watanabe, T. Yoshimura, K. Morita, T. Mitsugashira, K. Takamiya, T. Ohtsuki, and A. Shinohara, "Co-precipitation behaviour of single atoms of rutherfordium in basic solutions," Nat. Chem. **13**, 226 (2021).

H. Takashima, Y. Koga, S. Manabe, K. Ohnuki, R. Tsumura, T. Anzai, N. Iwata, Y. Wang, T. Yokokita, Y. Komori, D. Mori, S. Usuda, H. Haba, H. Fujii, Y. Matsumura, and M. Yasunaga, "Radioimmunotherapy with an ^{211}At-labeled anti-tissue factor antibody protected by sodium ascorbate," Cancer Sci. **112**, 1975 (2021).

T. Fukuchi, M. Shigeta, H. Haba, D. Mori, T. Yokokita, Y. Komori, S. Yamamoto, and Y. Watanabe, "Image reconstruction method for multiple-isotope positron emission tomography," J. Instrum. **16**, P01035 (2021).

M. Aikawa, T. Maehashi, D. Ichinkhorloo, S. Ebata, Y. Komori, and H. Haba, "Activation cross sections of deuteron-induced reactions on praseodymium up to 24 MeV," Nucl. Instrum. Methods Phys. Res. B **498**, 23 (2021).

D. Ichinkhorloo, M. Aikawa, Z. Tsoodol, T. Murata, M. Sakaguchi, Y. Komori, T. Yokokita, and H. Haba, "Production cross sections of dysprosium, terbium and gadolinium radioisotopes from the alpha-induced reactions on natural gadolinium up to 50 MeV," Nucl. Instrum. Methods Phys. Res. B **499**, 46 (2021).

E. Tsantini, T. Minami, M. Ángel C. Ontiveros, K. Takahashi, and J. C. Melgarejo, "Sulfur isotope analysis to examine the provenance of cinnabar used in wall paintings in the Roman domus Avinyó (Barcelona)," Mineral. **11**, 6 (2021).

M. K. A. Patwary, T. Kin, K. Aoki, K. Yoshinami, M. Yamaguchi, Y. Watanabe, K. Tsukada, N. Sato, M. Asai, T. K. Sato, Y. Hatsukawa, and S. Nakayama, "Measurement of double-differential thick-target neutron yields of the C(d,n) reaction at 12, 20, and 30 MeV," J. Nucl. Sci. Technol. **58**, 252 (2021).

T. Masuda, T. Watanabe, K. Beeks, H. Fujimoto, T. Hiraki, H. Kaino, S. Kitao, Y. Miyamoto, K. Okai, N. Sasao, M. Seto, T. Schumm, Y. Shigekawa, K. Tamasaku, S. Uetake, A. Yamaguchi, Y. Yoda, A. Yoshimi, and K. Yoshimura, "Absolute x-ray energy measurement using a high-accuracy angle encoder," J. Synchrotron Radiat. **28**, 111 (2021).

藤井博史, 大貫和信, 羽場宏光, 吉本光喜, 安永正浩, 高島大輝, 「生物医学研究施設におけるアルファ線放出核種の放射能測定」, Jpn. Soc. Mol. Imaging (JSMI) Rep. **14**, 3 (2021).

南武志, 高橋和也, 「与呂木古墳から出土した頭蓋骨付着朱の硫黄同位体比分析」, 三木市文化研究資料第 35 集「与呂木古墳・与呂木 12 号墳—与呂木青葉台団地造成に伴う発掘調査報告書—」, pp. 35–39, (2021).

[Review Articles]

海野弘行, 笠松良崇, 重河優大, 羽場宏光, 平木貴宏, 増田孝彦, 山口敦史, 横北卓也, 吉見彰洋, 吉村浩司, 「高輝度 X 線を用いた核共鳴散乱技術による原子核 ^{229}Th アイソマー状態の人工生成」, Isotope News No. 768, 2 (2020).

羽場宏光, 「元素周期表の新時代 119 番以降の新元素を求めて」, 現代化学 9 月号, No. 594, 43 (2020).

羽場宏光, 「スタニズラオ・カニッツァーロ」, 和光純薬時報, Vol. 88, No. 4, 28 (2020).

南武志, 高橋和也, 「清水風遺跡の朱」, 唐古・鍵考古学ミュージアム展示図録, Vol.27, pp. 11–14 (2020).

[Proceedings]

T. Niwase, K. Fujita, Y. Yamano, K. Watanabe, D. Kaji, K. Morimoto, H. Haba, T. Hirano, S. Mitsuoka, and K. Morita, "Measurement of fusion barrier distribution in ^{51}V+^{208}Pb system," Proc. 13th Int. Conf. on Nucleus-Nucleus Collisions, JPS Conf. Proc. **32**, 010022 (2020).

A. R. Usman, M. U. Khandaker, and H. Haba, "Effect of target density uncertainties on extracted experimental cross sections for the ^{nat}Ti(α,x)^{51}Cr,^{46}Sc reactions," Proc. Int. Conf. Nucl. Data Sci. Technol. (ND2019), EPJ Web Conf. **239**, 01011 (2020).

Y. Sakemi, T. Aoki, R. Calabrese, H. Haba, K. Harada, T. Hayamizu, Y. Ichikawa, K. Jungmann, A. Kastberg, Y. Kotaka, Y. Matsuda, Y. Matsuo, H. Nagahama, K. Nakamura, M. Otsuka, N. Ozawa, K. Tanaka, A. Uchiyama, H. Ueno, and L. Willmann, "Fundamental physics with cold radioactive atoms," Proc. 14th Asia-Pacific Phys. Conf., AIP Conf. Proc. 2319, 080020 (2021).

T. Zolbadral, M. Aikawa, D. Ichinkhorloo, K. Tegshjargal, Y. Komori, H. Haba, S. Takács, F. Ditrói, and Z. Szűcs, "Production cross sections of ^{45}Ti via deuteron-induced reaction on ^{45}Sc," Proc. 2019 Symp. Nucl. Data, JAEA-Conf 2020-001, 75 (2020).

M. Saito, M. Aikawa, T. Murata, Y. Komori, H. Haba, S. Takács, F. Ditorói, and Z. Szűcs, "Production of ^{169}Yb by the proton-induced reaction on ^{169}Tm," Proc. 2019 Symp. Nucl. Data, JAEA-Conf 2020-001, 79 (2020).

Presentations

[International Conferences/Workshops]

H. Takashima (poster), Y. Koga, K. Onuki, S. Manabe, R. Tsumura, T. Anzai, N. Iwata, M. Yasunaga, W. Yang, T. Yokokita, Y. Komori, D. Mori, H. Haba, H. Fujii, and Y. Matsumura, "Preclinical evaluation of astatine-211-conjugated anti-tissue factor antibody," American Association for Cancer Research (AACR) Virtual Annual Meeting II, online, June 22–24, 2020.

K. Ooe (poster), T. Watabe, Y. Shirakami, D. Mori, T. Yokokita, Y. Komori, H. Haba, and J. Hatazawa, "Production and separation of theranostic radionuclide Ag-111 from Pd target," Society of Nuclear Medicine and Molecular Imaging (SNMMI) Annual Meeting 2020, online, July 11–14, 2020.

H. Haba (invited), "Production and applications of radioisotopes at RIKEN RI Beam Factory—Search for new elements through diagnosis and therapy of cancer—," Symposium on Nuclear Data 2020, Wako, Japan, November 26–27, 2020.

Y. Komori (poster), H. Haba, M. Aikawa, M. Saito, S. Takács, and F Ditrói, "Production cross sections of ^{175}Hf in the ^{nat}Lu(p,xn) and ^{nat}Lu(d,xn) reactions," Symposium on Nuclear Data 2020, Wako, Japan, November 26–27, 2020.

T. Hayamizu (oral), H. Haba, K. Nakamura, T. Aoki, H. Nagahama, K. Tanaka, N. Ozawa, M. Ohtsuka, and Y. Sakemi, "Development of ultracold francium atomic sources towards the permanent EDM search," Yamada Conference LXXII: The 8th Asia-Pacific Conference on Few-Body Problems in Physics (APFB2020), Kanazawa, Japan, March 1–5, 2021.

[Domestic Conferences/Workshops]

高島大輝 (ポスター発表), 古賀宣勝, 大貫和信, 津村遼, 岩田望, 眞鍋史乃, 羽場宏光, 藤井博史, 安永正浩, 松村保広, 「アルファ線放出核種アスタチン—211 結合抗組織因子抗体の開発」, 第 36 回日本 DDS 学会学術集会, 神戸, 2020 年 8 月 28–29 日.

羽場宏光 (招待講演), 「ラジオアイソトープの製造と応用〜新元素の探索からがん治療まで〜」, 第 17 回日本加速器学会年会, オンライン, 2020 年 9 月 2–4 日.

中島朗久 (口頭発表), 坂口綾, 早川優太, 羽場宏光, 松村夏紀, 寺西翔, 森田涼雅, 横北卓也, 小森有希子, Yang Wang, 森大輝, Karin Hain, 山崎信哉, Jian Zheng, 末木啓介, 横山明彦, 「U+p 及び Th+Li 反応による Np 同位体励起関数の作成」, 日本放射化学会第 64 回討論会 (2020), オンライン, 2020 年 9 月 9–11 日.

寺西翔 (口頭発表), 森田涼雅, 早川優太, 坂口綾, 中島朗久, 小森有希子, 横北卓也, 森大輝, 羽場宏光, 横山明彦, 「^{232}Th+^{7}Li 反応の Np 合成系における不完全融合反応の影響」, 日本放射化学会第 64 回討論会 (2020), オンライン, 2020 年 9 月 9–11 日.

森田涼雅 (口頭発表), 寺西翔, 早川優太, 坂口綾, 中島朗久, 小森有希子, 横北卓也, 森大輝, 羽場宏光, 横山明彦, 「^{232}Th+^{7}Li 反応における反跳率補正による核分裂断面積測定法の確立」, 日本放射化学会第 64 回討論会 (2020), オンライン, 2020 年 9 月 9–11 日.

Xiaojie Yin (口頭発表), 南部明弘, 小森有希子, 森大輝, 羽場宏光, 「Production of ^{225}Ac in the ^{232}Th(^{14}N,xnyp)^{225}Ac reaction」, 日本放射化学会第 64 回討論会 (2020), オンライン, 2020 年 9 月 9–11 日.

庭瀬暁隆 (口頭発表), P. Schury, 和田道治, P. Brionnet, S. Chen, 橋本尚志, 羽場宏光, 平山賀一, D. S. Hou, 飯村俊, 石山博恒, 石澤倫, 伊藤由太, 加治大哉, 木村創大, 小浦寛之, J. J. Liu, 宮武宇也, J. Y. Moon, 森本幸司, 森田浩介, 長江大輔, M. Rosenbusch, 高峰愛子, 渡辺裕, H. Wollnik, W. Xian, S. X. Y an, 「MRTOF+α-TOF による ^{257}Db の直接質量測定」, 日本放射化学会第 64 回討論会 (2020), オンライン, 2020 年 9 月 9–11 日.

重河優大 (口頭発表), 山口敦史, 佐藤望, 高峰愛子, 和田道治, 羽場宏光, 「核化学研究用高周波イオン収集システムの開発」, 日本放射化学会第 64 回討論会 (2020), オンライン, 2020 年 9 月 9–11 日.

重河優大 (口頭発表), 山口敦史, 鈴木健太, 羽場宏光, 平木貴宏, 菊永英寿, 増田孝彦, 西村俊二, 笹尾登, 吉見彰洋, 吉村浩司, 「U-233 の α-γ 同時計数測定による Th-229 の原子核励起状態の半減期の決定」, 日本放射化学会第 64 回討論会 (2020), オンライン, 2020 年 9 月 9–11 日.

加藤瑞穂 (口頭発表), 安達サディア, 豊嶋厚史, 塚田和明, 浅井雅人, 羽場宏光, 横北卓也, 小森有希子, 重河優大, Yang Wang, 森大輝, 柏原歩那, 床井健運, 中島朗久, 鈴木雄介, 西塚魁人, 末木啓介, 「HF/HNO_3 系における Db の陰イオン交換挙動」, 日本放射化学会第 64 回討論会 (2020), オンライン, 2020 年 9 月 9–11 日.

横北卓也 (口頭発表), 笠松良崇, 渡邉瑛介, 小森有希子, 重河優大, 森大輝, 王洋, 二宮秀美, 速水翔, 東内克馬, ゴーシュコースタブ, 篠原厚, 羽場宏光, 「硫酸系における Rf の陰イオン交換：分配係数の硫酸濃度依存性」, 日本放射化学会第 64 回討論会 (2020), オンライン, 2020 年 9 月 9–11 日.

濱野健太郎 (口頭発表), 小林義男, 羽場宏光, 上野秀樹, 「ナトリウム電池電極材料 $Na^2Ru_{1-x}Fe_xO_3$ のメスバウアースペクトル」, 日本放射化学会第 64 回討論会 (2020), オンライン, 2020 年 9 月 9–11 日.

大江一弘 (口頭発表), 渡部直史, 白神宜史, 森大輝, 横北卓也, 小森有希子, 羽場宏光, 畑澤順, 「核医学利用に向けた Ag-111 の加速器による製造と分離精製」, 日本放射化学会第 64 回討論会 (2020), オンライン, 2020 年 9 月 9–11 日.

青井景都 (口頭発表), 新裕貴, 川崎康平, 丸山峻平, 鷲山幸信, 西中一朗, 羽場宏光, 森大輝, Yang Wang, 横山明彦, 「^{211}Rn/^{211}At ジェネレータシステムに必要な ^{207}Po 除去の条件の最適化」, 日本放射化学会第 64 回討論会 (2020), オンライン, 2020 年 9 月 9–11 日.

丸山峻平 (口頭発表), 川崎康平, 青井景都, 東美里, 西中一朗, 鷲山幸信, 羽場宏光, 森大輝, 横山明彦, 「薄層クロマトグラフィーを利用したアスタチン化学種同定による溶媒抽出の最適化」, 日本放射化学会第 64 回討論会 (2020), オンライン, 2020 年 9 月 9–11 日.

小森有希子 (ポスター発表), 羽場宏光, 「Calix[4]arene-bis(benzocrown-6) を用いた Fr と Cs の溶媒抽出」, 日本放射化学会第 64 回討論会 (2020), オンライン, 2020 年 9 月 9–11 日.

小森有希子 (ポスター発表), 羽場宏光, 合川正幸, 斎藤萌美, Sándor Takács, Ferenc Ditrói, 「^{nat}Lu(p,xn) および ^{nat}Lu(d,xn) 反応による ^{175}Hf の生成断面積の測定」, 日本放射化学会第 64 回討論会 (2020), オンライン, 2020 年 9 月 9–11 日.

渡邉瑛介 (ポスター発表), 笠松良崇, 横北卓也, 速水翔, 東内克馬, 重河優大, 羽場宏光, 篠原厚, 「Rf の化学研究に向けた ^{89m}Zr の硝酸系でのオンライン陰イオン交換実験」, 日本放射化学会第 64 回討論会 (2020), オンライン, 2020 年 9 月 9–11 日.

Z. Tsoodol (口頭発表), M. Aikawa, D. Ichinkhorloo, T. Khishigjargal, E. Norov, Y. Komori, H. Haba, S. Takács, F. Ditrói, and Z. Szűcs, "Production cross sections of the medically interesting radionuclide ^{45}Ti in the deuteron-induced reaction on ^{45}Sc," 日本原子力学会

2020 年秋の大会, オンライン, 2020 年 9 月 16 日–18 日.

高橋浩之 (口頭発表), 島添健次, 鎌田圭, 羽場宏光, 百瀬敏光, 「多光子ガンマ線時間・空間相関型イメージング法の開発 1 (概要)」, 2021 年第 68 回応用物理学会春季学術講演会, オンライン, 2021 年 3 月 16–19 日.

鎌田圭 (口頭発表), 金敬鎭, 吉野将生, 島添健次, 高橋美和子, 羽場宏光, 百瀬敏光, 高橋浩之, 吉川彰, 「多光子ガンマ線時間・空間相関型イメージング法の研究 2 (シンチレータ開発)」, 2021 年第 68 回応用物理学会春季学術講演会, オンライン, 2021 年 3 月 16–19 日.

羽場宏光 (口頭発表), 横北卓也, 王洋, 南部明弘, 臼田祥子, 高橋浩之, 島添健次, 鎌田圭, 百瀬敏光, 高橋美和子, 「多光子ガンマ線時間・空間相関型イメージング法の開発 (3) 多光子放出核種生成」, 2021 年第 68 回応用物理学会春季学術講演会, オンライン, 2021 年 3 月 16–19 日.

島添健次 (口頭発表), 上ノ町水紀, 大鐘健一朗, 高橋浩之, 鎌田圭, 吉川彰, 羽場宏光, 百瀬敏光, 高橋美和子, 「多光子ガンマ線時間・空間相関型イメージング法の開発 (システム開発)」, 2021 年第 68 回応用物理学会春季学術講演会, オンライン, 2021 年 3 月 16–19 日.

藤澤豊 (口頭発表), 森大輝, 羽場宏光, 間賀田泰寛, 飯田靖彦, 「Cu-67 標識新規ソマトスタチン誘導体を用いた神経内分泌腫瘍に対する腫瘍抑制効果の評価」, 第 60 回日本核医学会学術総会, 神戸, 2020 年 11 月 12–14 日.

竹村友紀 (口頭発表), 横北卓也, 結城真美, 田沢周作, 羽場宏光, 「TAT のための ^{228}Th/^{224}Ra/^{212}Pb ジェネレータシステム開発に関する基礎検討」, 第 60 回日本核医学会学術総会, 神戸, 2020 年 11 月 12–14 日.

大江一弘 (口頭発表), 渡部直史, 白神宜史, 森大輝, 横北卓也, 小森有希子, 羽場宏光, 畑澤順, 「治療用核種 Ag-111 の Pd 標的からの加速器製造と分離精製」, 第 60 回日本核医学会学術総会, 神戸, 2020 年 11 月 12–14 日.

髙島大輝 (ポスター発表), 古賀宣勝, 大貫和信, 津村遼, 岩田望, 眞鍋史乃, 羽場宏光, 藤井博史, 松村保広, 安永正浩, 「アルファ線放出核種アスタチン-211 結合抗組織因子抗体の前臨床試験」, 第 27 回次世代医工学研究会, オンライン, 2020 年 12 月 7 日.

羽場宏光 (口頭発表), 「ケミカルプローブに利用できる理研 RI」, Chemical Probe 第三回合同セミナー, オンライン, 2020 年 12 月 14 日.

Yin Xiaojie (口頭発表), 「Production of ^{225}Ac in the ^{232}Th(^{14}N,xnyp)^{225}Ac reaction」, Chemical Probe 第三回合同セミナー, オンライン, 2020 年 12 月 14 日.

羽場宏光 (招待講演), 「多光子ガンマ線放出核種の製造」, 科学研究費基盤研究 (S) 「多光子ガンマ線時間/空間相関型断層撮像法の研究」 ワークショップ「多光子ガンマ線検出技術の新展開」, オンライン, 2020 年 12 月 21 日.

岡井晃一 (口頭発表), Kjeld Beeks, 藤本弘之, 羽場宏光, 原秀明, 海野弘之, 笠松良崇, 北尾真司, 小早川大貴, 小無健司, 増田孝彦, 宮本祐樹, 平木貴宏, 笹尾登, Thorsten Schumm, 瀬戸誠, 重河優大, Simon Stellmer, 玉作賢治, 植竹智, 渡部信, 渡部司, 山口敦史, 安田勇輝, 依田芳卓, 吉見彰洋, 吉村浩司, 吉村太彦, 「トリウム 229 アイソマー状態からの真空紫外光観測に向けた Th:CaF_2 結晶の光学特性評価」, 日本物理学会第 76 回年次大会（2021 年）, オンライン, 2021 年 3 月 12–15 日.

小澤直也 (口頭発表), 長濱弘季, 早水友洋, 中村圭佑, 佐藤幹, 永瀬慎太郎, 小高康照, 鎌倉恵太, 田中香津生, 大塚未来, 青木貴稔, 市川雄一, 高峰愛子, 羽場宏光, 上野秀樹, 酒見泰寛, 「フランシウム原子の電気双極子能率探索のための表面電離イオン源の開発」, 日本物理学会第 76 回年次大会（2021 年）, オンライン, 2021 年 3 月 12–15 日.

羽場宏光 (招待講演), 「理研における At-211 の製造分離状況と将来計画」, 放射線科学基盤機構シンポジウム「核医学セラノスティクス：基盤技術から臨床応用まで/Theranostics from radioisotope production technology to clinical application」, オンライン, 2021 年 3 月 18 日.

重河優大 (口頭発表), 「Pa-229 を利用した Th-229m の真空紫外光観測実験の現状」, 2020 重元素核化学ワークショップ, オンライン, 2021 年 3 月 30 日.

Press Releases

原子 1 つの沈殿を調べる! —超重元素ラザホージウムの共沈挙動の実験的観測—, 理化学研究所, 2021 年 2 月 18 日. https://www.riken.jp/press/2021/20210218_1.

Patents

田沢周作, 竹村友紀, 結城真美, 竹内康隆, 芝原裕規, 羽場宏光, 横北卓也, 「目的核種の生成方法」, 特願 2021-037814.

Outreach Activities

羽場宏光, 「原子の仕組みとラジオアイソトープの応用～新元素の探索からがんの治療まで～」, 令和 2 年度（2020 年度）八王子市生涯学習センター主催市民自由講座, 八王子, 2021 年 3 月 9 日.

Accelerator Applications Research Division
RI Application Research Group
Industrial Application Research Team

1. Abstract

Industrial application research team handles non-academic activities at RIBF corresponding mainly to industries.

2. Major Research Subjects

(1) Support of industrial utilization of the RIBF accelerator beam.
(2) Fee-based distribution of radioisotopes produced at RIKEN AVF Cyclotron.

3. Summary of Research Activity

(1) Support of Industrial Utilization of RIBF

RNC promote facility-sharing program "Promotion of applications of high-energy heavy ions and RI beams." In this program, RNC opens a part of the RIBF facility, which includes the AVF cyclotron, RILAC, RIKEN Ring Cyclotron and experimental instruments, to non-academic proposals from users including private companies. The proposals are reviewed by a program advisory committee, industrial PAC (In-PAC). The proposals which have been approved by the In-PAC are allocated with beam times and the users pay RIKEN the beam time fee. The intellectual properties obtained by the use of RIBF belong to the users. In order to encourage the use of RIBF by those who are not familiar with utilization of ion beams, the first two beam times of each proposal can be assigned to trial uses which are free of beam time fee.

In July 2020, the In-PAC met and approved fee-based proposals from private companies; two proposals from new companies and three proposals from continuously using companies. In January 2021, the In-PAC held a mail review and approved three fee-based proposals from continuous users. In 2020, six companies executed eleven fee-based beamtimes, seven of which utilized a Kr beam with a total beam time of 153 h and four utilized, an Ar beam with a total beam time of 73 h.

(2) Fee-based distribution of radioisotopes produced at RIKEN AVF Cyclotron

We have been handling fee-based distribution of radioisotopes since 2007. The radionuclides are ^{65}Zn ($T_{1/2}$ = 244 days), ^{109}Cd (463 days), ^{88}Y (107 days), ^{85}Sr (65 days) and ^{67}Cu (2.58 days) which are produced at the AVF cyclotron by the Nuclear Chemistry Research Team. According to a material transfer agreement (MTA) drawn between Japan Radioisotope Association (JRIA) and RIKEN, JRIA mediates the transaction of the RIs and distributes them to users. Details can be found on the online ordering system J-RAM home page of JRIA.

In 2020, we delivered one shipment of ^{109}Cd with an activity of 10 MBq, three of ^{65}Zn with a total activity of 12 MBq, two of ^{88}Y with a total activity of 2 MBq, and two of ^{85}Sr with a total activity of 3 MBq. The final recipients of the RIs were four universities, one private company, and one medical research center.

Members

Team Leader
Atsushi YOSHIDA

Contract Researcher
Tadashi KAMBARA

Technical Staff I
Akihiro NAMBU

List of Publications & Presentations

Others

Fee-based beamtimes for private companies: Kr beam 153 h, Ar beam 73 h.

Subnuclear System Research Division
Quantum Hadron Physics Laboratory

1. Abstract

Atomic nuclei are made of protons and neutrons bound by the exchange of pion and other mesons. Also, protons and neutrons are made of quarks bound by the exchange of gluons. These strong interactions are governed by the non-Abelian gauge theory called the quantum chromodynamics (QCD). On the basis of theoretical and numerical analyses of QCD, we study the interactions between the nucleons, properties of the dense quark matter realized at the center of neutron stars, and properties of the hot quark-gluon plasma realized in the early Universe. Strong correlations common in QCD and cold atoms are also studied theoretically to unravel the universal features of the strongly interacting many-body systems. Developing perturbative and non-perturbative techniques in quantum field theory and string theory are of great importance not only to solve gauge theories such as QED and QCD, but also to find the theories beyond the standard model of elementary particles. Various theoretical approaches along this line have been attempted.

2. Major Research Subjects

(1) Perturbative and non-perturbative methods in quantum field theories
(2) Quantum computing
(3) Lattice gauge theory
(4) QCD under extreme conditions
(5) Nuclear and atomic many-body problems

3. Summary of Research Activity

(1) Perturbative and non-perturbative methods in quantum field theories

(1-1) Theory of the anomalous magnetic moment of the electron

The anomalous magnetic moment of the electron ae measured in a Penning trap occupies a unique position among high precision measurements of physical constants in the sense that it can be compared directly with the theoretical calculation based on the renormalized quantum electrodynamics (QED) to high orders of perturbation expansion in the fine structure constant α, with an effective parameter α/π. Both numerical and analytic evaluations of ae up to $(\alpha/\pi)^4$ were firmly established. The coefficient of $(\alpha/\pi)^5$ has been obtained recently by an extensive numerical integration. The contributions of hadronic and weak interactions have also been estimated. The sum of all these terms leads to a_e(theory) = 1 159 652 181.606 (11)(12)(229) $\times 10^{-12}$, where the first two uncertainties are from the tenth-order QED term and the hadronic term, respectively. The third and largest uncertainty comes from the current best value of the fine-structure constant derived from the cesium recoil measurement: α^{-1}(Cs) = 137.035 999 046 (27). The discrepancy between a_e (theory) and a_e (experiment) is 2.4σ. Assuming that the standard model is valid so that a_e (theory) = a_e (experiment) holds, we obtained $\alpha^{-1}(a_e)$ = 137.035 999 1496 (13)(14)(330), which is nearly as accurate as α^{-1}(Cs). The uncertainties are from the tenth-order QED term, hadronic term, and the best measurement of a_e, in this order.

(1-2) Transport theory of chiral fermions under external gravity and fluid field

We formulated the kinetic theory of chiral matter in external gravitational fields, based on quantum field theory. The resulting kinetic theory reveals that the Riemann curvature induces non-dissipative transport phenomena of chiral fermions. In particular, we found that the spin-gravity coupling results in the antiparallel flow of the charge current and energy current of fermions, which is never explained in the classical picture. These novel framework and phenomena takes place not only in cosmological systems involving neutrinos but also in chiral matter affected by background fluid, such as quark-gluon plasma, graphene and Dirac/Weyl semimetals. We demonstrated that a temperature gradient and fluid vorticity induce a pressure correction and charge and energy flow in Dirac/Weyl semimetals.

(1-3) Spin transport of massive fermion

We derived the spin kinetic theory under external electromagnetic and gravitational fields. We derived the global equilibrium conditions from the kinetic equations and find that the finite Riemann curvature or an external electromagnetic field is necessary to determine the spin-thermal vorticity coupling. Solving the equation of motion of axial vector part of the Wigner transformed fermion propagator, we evaluated the Pauli-Lubanski vector, which expresses the spin polarization of massive fermions, at the local equilibrium and out of equilibrium. This formula is potentially important of the Λ polarization puzzle found in heavy-ion collisions, which cannot be understood in the calculations based on global equilibrium assumption.

(1-4) Chiral vortical effect in condensed matter systems

We revisited the chiral vortical effect in condensed matter physics, by using the semiclassical wave-packet theory. In high-energy physics, the chiral vortical current is conventionally defined as the Noether current. Such a definition is however improper in the context of condensed matter systems since there potentially exists the contributions of the magnetization current. Indeed we showed that the chiral vortical current is compensated by the magnetization current. Hence the chiral vortical effect cannot be observed in pseudo-relativistic condensed matter systems, such as Dirac/Weyl semimetals. Instead, we demonstrated that the chiral vortical effect is an observable in several nonrelativistic matter, and suggested possible table-top experimental setups.

(1-5) Lorentzian conformal field theories through sine-square deformation

In quantum field theories, symmetry plays an essential and exceptional role. Focusing on some proper symmetry and delving into its meaning have been proven to be one of the most fruitful strategies. We reexamined two-dimensional Lorentzian conformal field theory using the formalism previously developed in a study of sine-square deformation of Euclidean conformal field theory. We

construct three types of Virasoro algebra. One of them reproduces the result by Luscher and Mack, while another type exhibits the divergence in the central charge term. The other leads the continuous spectrum and contains no closed time-like curve in the system.

(2) Quantum computing

(2-1) Hybrid quantum annealing via molecular dynamics

A novel quantum-classical hybrid scheme was proposed to efficiently solve large-scale combinatorial optimization problems. The key concept is to introduce a Hamiltonian dynamics of the classical flux variables associated with the quantum spins of the transverse-field Ising model. Molecular dynamics of the classical fluxes can be used as a powerful preconditioner to sort out the frozen and ambivalent spins for quantum annealers. It was demonstrated that the performance and accuracy of our smooth hybridization are better in comparison to the standard classical algorithms (the tabu search and the simulated annealing) by employing the MAX-CUT and Ising spin-glass problems.

(3) Lattice gauge theory

(3-1) Most charming dibaryon near unitarity

The interaction between Ω_{ccc}–Ω_{ccc} in the S-wave and spin-0 channel was studied from the (2 + 1)-flavor lattice QCD with nearly physical light-quark masses and the relativistic heavy quark action with the physical charm quark mass. The time-dependent HAL QCD method was employed to extract the $\Omega_{ccc}\Omega_{ccc}$ potential from the lattice QCD data of two-baryon spatial correlation, and the scattering observables were calculated. The potential was found to be attractive at mid-range and weakly repulsive at short-range. Taking into account the Coulomb repulsion with the charge form factor of Ω_{ccc} as well, the scattering length $a_0^{\mathrm{C}} \sim= 19$ fm and the effective range $r_{\mathrm{eff}}^{\mathrm{C}} \sim= 0.45$ fm were obtained. The ratio $r_{\mathrm{eff}}^{\mathrm{C}}/a_0^{\mathrm{C}} \sim= -0.024$, whose magnitude is considerably smaller than that of the dineutron (−0.149), indicates that $\Omega_{ccc}\Omega_{ccc}$ is located in the unitary region.

(3-2) d^*(2380) dibaryon from lattice QCD

The $\Delta\Delta$ dibaryon resonance $d^*(2380)$ with $(J^\pi, I) = (3^+, 0)$ was studied from the 3-flavor lattice QCD with heavy pion masses (m_π = 0.68, 0.84, 1.02 GeV). The central $\Delta\Delta$ potential in $^7S_3$ channel obtained by HAL QCD method shows a strong short-range attraction, so that a quasi-bound state corresponding to d*(2380) is formed with the binding energy 25–40 MeV below the $\Delta\Delta$ threshold for the heavy pion masses. The tensor part of the transition potential from $\Delta\Delta$ to NN was also extracted. Although the obtained transition potential is strong at short distances, the decay width of $d^*(2380)$ to NN in the D-wave was found to be kinematically suppressed.

(3-3) Stress tensor around static quark-anti-quark from Yang-Mills gradient flow

The spatial distribution of the stress tensor around the quark-anti-quark pair in SU(3) lattice gauge theory was studied. The YangMills gradient flow plays a crucial role to make the stress tensor well-defined and derivable from the numerical simulations on the lattice. The resultant stress tensor with a decomposition into local principal axes shows, for the first time, the detailed structure of the flux tube along the longitudinal and transverse directions in a gauge invariant manner. The linear confining behavior of the potential at long distances is derived directly from the integral of the local stress tensor.

(4) QCD under extreme conditions

(4-1) Finite density QCD based on complex Langevin method

The complex Langevin method (CLM) is one of a promising approach to overcome the sign problem. The central idea of this approach is that the stochastic quantization does not require the probabilistic interpretation of the Boltzmann weight e^{-S} even when the action takes complex values. Although the equivalence between CLM and the familiar path integral quantization is quite nontrivial, it is pointed out that the probability distribution of the drift term can judge the correctness of the CLM. This enable us to perform lattice simulation of QCD based on CLM in the finite density region in a self-contained manner. We discussed the applicability of the CLM with four-flavor staggered fermions on a $8^3 \times 16$ lattice with quark mass $m = 0.01$. In particular, we focus on the behavior of the eigenvalue distribution of the fermion mass matrix which is closely related to the appearance of the singular drift problem.

(4-2) Non-equilibrium quantum transport of chiral fluids from kinetic theory

We introduced the quantum-field-theory (QFT) derivation of chiral kinetic theory (CKT) from the Wigner-function approach, which manifests side jumps and non-scalar distribution functions associated with Lorentz covariance and incorporates both background fields and collisions. The formalism is utilized to investigate second-order responses of chiral fluids near local equilibrium. Such nonequilibrium anomalous transport is dissipative and affected by interactions. Contributions from both quantum corrections in anomalous hydrodynamic equations (EOM) of motion and those from the CKT and Wigner functions (WF) are considered in a relaxation-time approximation (RTA). Anomalous charged Hall currents engendered by background electric fields and temperature/chemical-potential gradients are obtained. Furthermore, chiral magnetic/vortical effects (CME/CVE) receive viscous corrections as non-equilibrium modifications stemming from the interplay between side jumps, magnetic-moment coupling, and chiral anomaly.

(4-3) Hadron-quark crossover in cold and hot neutron stars

We presented a much improved equation of state for neutron star matter, QHC19, with a smooth crossover from the hadronic regime at lower densities to the quark regime at higher densities. We now use the Togashi *et al*. equation of state, a generalization of the Akmal-Pandharipande-Ravenhall equation of state of uniform nuclear matter, in the entire hadronic regime; the Togashi equation of state consistently describes nonuniform as well as uniform matter, and matter at beta equilibrium without the need for an interpolation between pure neutron and symmetric nuclear matter. We describe the quark matter regime at higher densities with the Nambu-JonaLasinio model, now identifying tight constraints on the phenomenological universal vector repulsion between quarks and the pairing interaction between quarks arising from the requirements of thermodynamic stability and causal propagation of sound. The resultant neutron star properties agree very well with the inferences of the LIGO/Virgo collaboration, from GW170817, of the pressure

versus baryon density, neutron star radii, and tidal deformabilities. The maximum neutron star mass allowed by QHC19 is 2.35 MS, consistent with all neutron star mass determinations.

(4-4) Gluonic energy and momentum distribution at finite temperature

We studied the energy-momentum distribution of the gluons around a static quark at finite temperature on the basis of the effective field theory (EFT) of thermal QCD. Spatial correlations between the Polyakov loop and the energy-momentum tensor were calculated up to the next-to-leading order in EFT. The results were compared with the recent quenched lattice QCD calculation obtained by using the gradient flow formalism. The EFT results and the lattice QCD data agree quite well without any fitting parameters at high temperature above deconfinement. On the other hand, there is a substantial difference near the critical temperature especially in the distribution of the energy density, which indicates some non-perturbative effect.

(5) Nuclear and atomic many-body problems

(5-1) Density functional theory for nuclear structure

The atomic nuclei are composed of protons and neutrons interacting via the nuclear and Coulomb interactions. The density functional theory (DFT) is widely used to calculate the ground-state properties. Nevertheless, because of the lack of knowledge of nuclear interaction in medium (effective interaction), the effective interaction is fitted to experimental data, and it has been attained to develop a high-accuracy one. In contrast, the nucleons have finite charge distributions, while this is not considered in DFT calculation. Because it is indispensable to treat the Coulomb interaction more accurately to achieve high-accuracy nuclear effective interaction, we consider such finite-size effects to nuclear DFT, and we reveal that such effects give a non-negligible contribution to nuclear binding energies. In nuclear structure calculation, both non-relativistic and relativistic schemes of DFT are used, while the connection between them, especially in terms of the effective interaction, is not understood well. To reveal it, we also develop the efficient non-relativistic reduction of the many-body systems.

(5-2) Fundamental problems of density functional theory

The density functional theory (DFT) is one of the powerful methods to calculate ground-state properties of the quantum many-body problems, including atomic nuclei, atoms, molecules, and solids. The accuracy of the DFT depends on the energy density functional (EDF), which contains information on the interaction. We develop a method to calculate EDF for electronic systems purely microscopically using the functional renormalization group. In this method, energy density for so many various densities can be calculated, and eventually, DFT calculation can be performed without fitting energy density to some functional forms. We also develop the relativistic DFT in which the finite-light-speed correction to the Coulomb interaction is also considered to calculate the ground-state properties of super-heavy elements.

(5-3) One-dimensional Bose and Fermi gases with contact interactions

We investigate local quantum field theories for one-dimensional (1D) Bose and Fermi gases with contact interactions, which are closely connected with each other by Girardeau's Bose-Fermi mapping. While the Lagrangian for bosons includes only a two-body interaction, a marginally relevant three-body interaction term is found to be necessary for fermions. Because of this three-body coupling, the three-body contact characterizing a local triad correlation appears in the energy relation for fermions, which is one of the sum rules for a momentum distribution. In addition, we apply in both systems the operator product expansion to derive large-energy and momentum asymptotics of a dynamic structure factor and a single-particle spectral density. These behaviors are universal in the sense that they hold for any 1D scattering length at any temperature. The asymptotics for the Tonks-Girardeau gas, which is a Bose gas with a hardcore repulsion, as well as the Bose-Fermi correspondence in the presence of three-body attractions are also discussed.

(5-4) Mesoscopic spin transport between strongly interacting Fermi gases

We investigate a mesoscopic spin current for strongly interacting Fermi gases through a quantum point contact. Under the situation where spin polarizations in left and right reservoirs are same in magnitude but opposite in sign, we calculate the contribution of quasiparticles to the current by means of the linear response theory and many-body T-matrix approximation. For a small spin-bias regime, the current in the vicinity of the superfluid transition temperature is strongly suppressed due to the formation of pseudogaps. For a large spin-bias regime where the gases become highly polarized, on the other hand, the current is affected by the enhancement of a minority density of states due to Fermi polarons. We also discuss the broadening of a quasiparticle peak associated with an attractive polaron at a large momentum, which is relevant to the enhancement

(5-5) Optical spin conductivity in ultracold quantum gases

Measurement of frequency-resolved spin transport is a subject of much interest in condensed matter physics. Here we show that the optical spin conductivity, which is a small AC response of a spin current, can be measured with existing methods in ultracold atom experiments. We point out that once interatomic interactions are turned on, the optical spin conductivity becomes nontrivial even in clean ultracold atomic gases and thereby can be a probe of generic quantum states of matter. This is a sharp contrast to the optical mass conductivity which becomes trivial in typical cold-atom systems without disorder and lattice potential. For systems with arbitrary spin degrees of freedom, we construct a general formalism of the optical spin conductivity and derive the f-sum rule. To demonstrate the availability of the optical spin conductivity, our formalism is applied to a spin-1/2 Fermi superfluid and a spin-1 Bose-Einstein condensate. It turns out that both superfluids show nontrivial responses that cannot be captured with the Drude conductivity. The application of our proposed method to generic ultracold atomic gases with spin degrees of freedom is feasible.

Members

Director
Masahiko IWASAKI

Vice Chief Scientist
Tsukasa TADA

Research/Technical Scientist
Takumi DOI (Senior Research Scientist)

Senior Scientist
Makiko NIO

Contract Researcher
Dang NGUYEN DINH

Special Postdoctoral Researchers
Matthias W.G. BERWEIN
Kazuya MAMEDA
Shoichiro TSUTSUI

Research Consultant
Takeo INAMI (Inst. of Phys. Vietnamese Academy of Sci. and Tech.)

Visiting Scientists
Shinya AOKI (Kyoto Univ.)
Tatsumi AOYAMA (KEK)
Gergely P. FEJOS (Eotvos Lorand Univ.)
Kenji FUKUSHIMA (Univ. of Tokyo)
Hideki HAMAGAKI (Nagasaki Inst. of Applied Sci.)
Koji HASHIMOTO (Osaka Univ.)
Masashi HAYAKAWA (Nagoya Univ.)
Tomoya HAYATA (Keio Univ.)
Takashi INOUE (Nihon Univ.)
Noriyoshi ISHII (Osaka Univ.)
Yuki KAMIYA (Chinese Academy of Sci.)
Yoichi KAZAMA (Univ. of Tokyo)
Phuc T. LE (Inst. of Fundamental and Applied Sci. Duy Tan Univ.)
Haozhao LIANG (Univ. of Tokyo)
Takaya MIYAMOTO (NEC Corporation)
Kenji MORITA (QST)
Masaki MURATA (Japan Univ. of Economics)
Atsushi NAKAMURA (Osaka Univ.)
Takashi NAKATSUKASA (Tsukuba Univ.)
Hung NGUYEN (Duy Tan Univ.)
Yoji OHASHI (Keio Univ.)
RHINE KUMAR ARAYAKKANDI KEECH (Cochin Univ. of Sci. and Tech.)
Shoichi SASAKI (Tohoku Univ.)
Kenji SASAKI (Kyoto Univ.)
Hiroshi SUZUKI (Kyushu Univ.)
Motoi TACHIBANA (Saga Univ.)
Sachiko TAKEUCHI (The Social Work Research Institute)
Hiroshi TOKI (Osaka Univ.)
Di-Lun YANG (Keio Univ.)

Visiting Researcher
Yuta SEKINO (JSPS)

Student Trainees
Yutaro AKAHOSHI (Kyoto Univ.)
Asahi CHIKAOKA (Univ. of Tokyo)
Yixin GUO (Univ. of Tokyo)
Akira HIRAYAMA (Saitama Univ.)
Xun LIU (Univ. of Tokyo)
Yan LYU (Peking Univ.)
Kotaro MURAKAMI (Kyoto Univ.)
Tomoya NAITO (Univ. of Tokyo)
Hui TONG (Peking Univ.)
Tingyu ZHANG (Univ. of Sci. and Tech. of China)

List of Publications & Presentations

Publications

[Original Papers]

G. Accorto, T. Naito, H. Liang, T. Niksic, and D. Vretenar, "Nuclear energy density functionals from empirical ground-state densities," Phys. Rev. C **103**, 044304 (2021).

T. Hayata, Y. Hidaka, and K. Mameda, "Second order chiral kinetic theory under gravity and antiparallel charge-energy flow," J. High Energy Phys. **2021**, 23 (2021).

N. Itagaki and T. Naito, "Consistent description for cluster dynamics and single-particle correlation," Phys. Rev. C **103**, 044303 (2021).

T. Yokota and T. Naito, "*Ab initio* construction of the energy density functional for electron systems with the functional-renormalization-group-aided density functional theory," Phys. Rev. Res. **3**, L012015 (2021).

Y. Sekino, H. Tajima, and S. Uchino, "Optical spin transport in ultracold quantum gases," arXiv:2103.02418 [cond-mat.quant-gas] (2021).

Y. Lyu, H. Tong, T. Sugiura, S. Aoki, T. Doi, T. Hatsuda, J. Meng, and T. Miyamoto, "Most charming dibaryon near unitarity," arXiv:2102.00181 [hep-lat] (2021).

T. Naito, G. Colò, H. Liang, and X. Roca-Maza, "Second and fourth moments of the charge density and neutron-skin thickness of atomic nuclei," arXiv:2101.07680 [nucl-th] (2021).

Z. Wang, T. Naito, H. Liang, and W. H. Long, "Exploring effects of tensor force and its strength via neutron drops," arXiv:2101.04860 [nucl-th] (2021).

Y. Tanabe, Y. Ito, K. Sugawara, M. Koshino, S. Kimura, T. Naito, I. Johnson, T. Takahashi, and M. Chen, "Dirac Fermion kinetics in three-dimensionally curved graphene," Adv. Mater. **32**, 202005838 (2020).

X. Liu and T. Tada, "Analysis for Lorentzian conformal field theories through sine-square deformation," Prog. Theor. Exp. Phys. **2020**, 061B01225 (2020).

Z. Wang, T. Naito, and H. Liang, "Tensor effects on shell-structure evolution in $N = 82$ isotones and $Z = 50$ isotopes in the relativistic Hartree-Fock theory," arXiv:2012.13143 [nucl-th] (2020).

Y. Sekino and Y. Nishida, "Field theoretical aspects of one-dimensional Bose and Fermi gases with contact interactions," Phys. Rev. A **103**, 043307 (2021).

T. Naito, S. Endo, K. Hagino, and Y. Tanimura, "Are atoms spherical?" arXiv:2009.05955 [physics.atom-ph] (2020).

K. Murakami, Y. Akahoshi, and S. Aoki, "S-wave kaon-nucleon potentials with all-to-all propagators in the HAL QCD method," Prog. Theor. Exp. Phys. **2020**, 093B03 (2020).

H. Irie, H. Liang, T. Doi, S. Gongyo, and T. Hatsuda, "Hybrid quantum annealing via molecular dynamics," Sci. Rep. **11**, 8426 (2021)

Y. Akahoshi, S. Aoki, T. Aoyama, T. Doi, T. Miyamoto, and K. Sasaki, "The HAL QCD potential in $I = 1$ $\pi\pi$ system with the ρ meson bound state," (2020). Prog. Theor. Exp. Phys. **2020**, 073B07 (2020).

Subnuclear System Research Division
Strangeness Nuclear Physics Laboratory

1. Abstract

We proposed accurate calculation method called 'Gaussian Expansion Method using infinitesimally shifted Gaussian lobe basis function.' When one proceeds to four-body systems, calculation of the Hamiltonian matrix elements becomes much laborious. In order to make the four-body calculation tractable even for complicated interactions, the infinitesimally-shifted Gaussian lobe basis function has been proposed. The GEM with the technique of infinitesimally-shifted Gaussians has been applied to various three-, four- and five-body calculations in hypernuclei, the four-nucleon systems, and cold-atom systems. As results, we succeeded in extracting new understandings in various fields.

2. Major Research Subjects

(1) Structure of Hypernuclei and neutron-rich nuclei from the view point of few-body problem
(2) Structure of exotic hadron system
(3) quantum atomic system and ultra cold atomic system
(4) Equation of state for neutron star

3. Summary of Research Activity

(1) We study Λ hypernuclei of C and B isotopes. We calculated Λ binding energies of these Λ hypernuclei and found halo structure in the Λ $1p$ state with extended wave functions. In addition, we propose to measure electric-dipole transition between Λ $1p$ and $1s$ states to see evidence for this hyperon halo structure.
(2) Bound states of double-heavy tetraquark systems are studied in a constituent quark model. We have two bound states for $T = 0$, $J^{\pi} = 1^{+}$ in bbu-bar u-bar system. One is deeply bound state and the other is a shallow bound state. The former state is in good agreement with the result by lattice QCD.
(3) We investigate the miscibility of two kinds of bosons with repulsive interactions. In addition to the known miscible and immiscible phases, we predict a partially miscible phase due to quantum fluctuations. It leads to the formation of mixed bubbles that are similar to quantum liquid droplets found in attractive mixtures and could be observed in experiments.

Members

Director
Emiko HIYAMA

Research/Technical Scientist
Pascal NAIDON (Senior Research Scientist)

Special Postdoctoral Researcher
Tokuro FUKUI

Postdoctoral Researcher
Christiane H. SCHMICKLER

Senior Visiting Scientist
Makoto OKA (JAEA)

Visiting Scientists
Masayuki ASAKAWA (Osaka Univ.)
Kadir Utku CAN (The Univ. of Adelaide)
Jaume CARBONELL (CNRS-IN2P3)
Lorenzo CONTESSI (Hebrew Univ. of Jerusalem)
Jiwei CUI (Xidian Univ.)
Akinobu DOTE (KEK)
Shimpei ENDO (Tohoku Univ.)
Tomokazu FUKUDA (Univ. of Electro-Commun.)
Yasuro FUNAKI (Kanto Gakuin Univ.)
Takenori FURUMOTO (Yokohama Nat'l Univ.)
Philipp GUBLER (JAEA)
Satoru HIRENZAKI (Nara Women's Univ.)
Atsushi HOSAKA (Osaka Univ.)
Jinniu HU (Nankai Univ.)
Tetsuo HYODO (Tokyo Metropolitan Univ.)
Kiyomi IKEDA (Niigata Univ.)
Yoichi IKEDA (Kyushu Univ.)
Masahiro ISAKA (Hosei Univ.)
Souichi ISHIKAWA (Hosei Univ.)
Daisuke JIDO (Tokyo Tech)
Hyun-Chul KIM (Inha Univ.)
Kei KOTAKE (Fukuoka Univ.)
Toshio MOTOBA (Univ. of Electro-Commun.)
Takayuki MYO (Osaka Inst. of Tech.)
Satoshi NAKAMURA (Tohoku Univ.)
Kazuma NAKAZAWA (Gifu Univ.)
Hidekatsu NEMURA (Osaka Univ.)
Jean-Marc RICHARD (Lyon Univ.)
Thomas RIJKEN (Univ. Of Nijmegen)
Shoichi SASAKI (Tohoku Univ.)

Hans-Josef SCHULZE (INFN)
Shoji SHINMURA(Gifu Univ.)
Jirina STONE (Univ. of Tennessee)
Tingting SUN (Zhengzhou Univ.)
Hiroyuki TAJIMA (Univ. of Tokyo)
Hajime TOGASHI (Tohoku Univ.)
Atsushi UMEYA (Nippon Inst. of Tech.)
Shin WATANABE (NIT, Gifu College)
Wolfram WEISE (TU Munich)
Chengjun XIA (Zhejiang Univ.)
Masanobu YAHIRO (Kyushu Univ.)
Ulugbek YAKHSHIEV (Inha Univ.)
Taiichi YAMADA (Kanto Gakuin Univ.)
Yasuo YAMAMOTO (Tsuru Univ.)
Nodoka YAMANAKA (Kennesaw State Univ.)
Takuma YAMASHITA (Tohoku Univ.)
Ying ZHANG (Tianjin Univ.)
Xian-Rong ZHOU (East China Normal Univ.)

Student Trainees

Kongyi HU (Nankai Univ.)
Dongwook LEE (Kyushu Univ.)
Jie LIU (Nanjing Univ.)
Qi MENG (Nanjing Univ.)
Qian WU (Nanjing Univ.)

Part-time Worker

Yoko FUJITA (Administrative Part-time Worker I)

List of Publications & Presentations

Publications

[Original Papers]

Y. Kim, E. Hiyama, M. Oka, and K. Suzuki, "Spectrum of singly heavy baryons from a chiral effective theory of diquarks," Phys. Rev. D **102**, 014004 (2020).

T. -W. Wu, M. -Z. Liu, L. -S. Geng, E. Hiyama, M. P. Valderrama, and W. -L. Wang, "Quadruply charmed dibaryons as heavy quark symmetry partners of the DDK bound state," Eur. Phys. J. **80**, 901 (2020).

Q. Wu, Y. Funaki, E. Hiyama, and H. Zong, "Resonant states of ${}^{9}_{\Lambda}$Be with $\alpha + \alpha + \Lambda$ three-body cluster model," Phys. Rev. C **102**, 054303 (2020).

A. Nay L. Nyaw, K. Nakazawa, *et al*., "Observation of double-strangeness nuclei using nuclear-emulsion technology," Bull. Soc. Photogr. Imag. Jpn. **30**, 2 22–25 (2020).

T. Yamashita, Y. Kino, E. Hiyama, S. Jonsell, and P. Froelich, "Near-threshold production of antihydrogen positive ion in positronium-antihydrogen collision," New J. Phys. **23**, 012001 (2021).

S. H. Hayakawa, K. Nakazawa, *et al*. (J-PARC E07 Collaboration), "Observation of coulomb-assisted nuclear bound state of Ξ^{-}-^{14}N system," Phys. Rev. Lett. **126**, 062501 (2021).

J. Yoshida, K. Nakazawa, *et al*., "CNN-based event classification of alpha-decay events in nuclear emulsion," Nucl. Instrum. Methods Phys. Res. A **989**, 16430 (2021).

N. Yamanaka and E. Hiyama, "Weinberg operator contribution to the nucleon electric dipole moment in the quark model," Phys. Rev. D **103**, 035023 (2021).

Q. Meng, E. Hiyama, A. Hosaka, M. Oka, P. Gubler, K. U. Can, T. T. Takahashi, and H. S. Zong, "Stable double-heavy tetraquarks: Spectrum and structure," Phys. Lett. B **814**, 136095 (2021).

P. Naidon and D. S. Petrov, "Mixed bubbles in Bose-Bose mixtures," Phys. Rev. Lett. **126**, 115301 (2021).

[Proceedings]

J. Carbonell, E. Hiyama, R. Lazauskas, and F. M. Marques, "^{19}B isotope as a ^{17}B-n-n three-body cluster close to unitary limit," J. Phys. Conf. Ser. **1643**, 012120 (2020).

Presentations

[International Conferences/Workshops]

P. Naidon (invited), "A partial mixing of quantum gases," Yamada Conference LXXII: The 8th Asia-Pacific Conference on Few-Body Problems (APFB2020), Kanazawa, Japan, March 1–5, 2021.

P. Naidon (invited), "Mixed bubbles in repulsive Bose-Bose mixtures," The 5th Symposium on Clustering as a Window on the Hierarchical Structure of Quantum Systems, September 24, 2020.

T. Fukui (oral), "Chiral three-body force and shell evolution," Yamada Conference LXXII: The 8th Asia-Pacific Conference on Few-Body Problems in Physics (APFB2020), Kanazawa, Japan, March 1–5, 2021.

C. Schmickler, "Origin of the three-body parameter of the Kartavtsev-Malykh crossover trimer," Yamada Conference LXXII: The 8th Asia-Pacific Conference on Few-Body Problems in Physics (APFB2020), Kamazawa, Japan, March 1–5, 2021.

[Domestic Conferences/Workshops]

P. Naidon (poster), "A new kind of bubble," The 22nd RIKEN Interdisciplinary Exchange Evening, September 25, 2020.

福井徳朗 (口頭発表), 「カイラル相互作用による軽い核のクラスター構造の理解に向けて」, 日本物理学会第 76 回年次大会, オンライン, 2021 年 3 月 12–15 日.

[Seminars & Lectures]

P. Naidon (invited), "Universal few-body physics," 4-Part Lecture at Hokkaido University Nuclear Theory Group, February 16, 2021.
P. Naidon (invited), "Mixed bubbles in repulsive Bose-Bose mixtures," Kindai University, December 16, 2020.
P. Naidon (invited), "Universal few-body physics," 2-Part Lecture at Strange Nuclear Physics School 2020, December 2–5, 2020.
P. Naidon (invited), "QCD-like phase diagram of resonantly interacting SU(3) Fermi gases," Kyushu University, July 10, 2020.

Press Releases

「極低温での新しい量子相 "混合バブル" を予言—混和性・非混和性の中間に存在する部分混和性の発見—」, 2021 年 3 月 22 日.

Subnuclear System Research Division
Radiation Laboratory

1. Abstract

Nucleons, such as protons and neutrons, are a bound state of constituent quarks glued together with gluons. The detail structure of nucleons, however, is not well understood yet. Especially the mechanism to build up the spin of proton, which is 1/2, is a major problem in physics of the strong force. The research goal of Radiation Laboratory is to solve this fundamental question using the world first polarized-proton collider, realized at RHIC in Brookhaven National Laboratory (BNL) in USA. RHIC stands for Relativistic Heavy Ion Collider, aiming also to create Quark Gluon Plasma, the state of Universe just after the Big Bang, and study its property. RIKEN-BNL Research Center (RBRC) also directed by H. En'yo carries our core team at BNL for those exciting researches using the PHENIX detector and its upgraded sPHENIX detector in preparation. We have observed that the proton spin carried by gluons is finite and indeed sizable. We also identified W bosons in the electron/positron decay channel and in the muon decay channel, with which we showed how much anti-quarks carry the proton spin. Other than the activities at RHIC we are preparing and starting new experiments at J-PARC and Fermilab to study the nature of hadron and preparing for the electron-ion collider (EIC). We are also performing technical developments such as novel ion sources, fine-pitch silicon pixel detectors and high-performance trigger electronics.

2. Major Research Subjects

(1) Spin physics with relativistic polarized-proton collisions at RHIC
(2) Study of nuclear matter at high temperature and/or at high density
(3) Technical developments on radiation detectors and accelerators

3. Summary of Research Activity

(1) Experimental study of spin structure of proton using RHIC polarized proton collider

[See also RIKEN-BNL Research Center Experimental Group for the activities at BNL]

The previously published central rapidity neutral and charged pion double spin asymmetries at the highest collision energies at RHIC of 510 GeV have been augmented with the world's first preliminary direct photon results. The direct photon probe also restricts the initial, hard interaction to be predominantly between a quark and a gluon thus further increasing the sensitivity to the gluon spin. It has therefore been considered the golden channel to access the gluon spin, albeit the statistics are limited. Also, the first preliminary jet results have been extracted by PHENIX. The jet measurement is in principle a cleaner probe since no fragmentation functions are involved as in the pion results. All these results will be included in future global fits of all the existing experimental data in the world and will improve the sensitivity of quark and gluon spin contributions to the total spin of the nucleon.

While orbital angular momentum cannot be directly accessed at RHIC, several transverse spin phenomena have been observed which relate to orbital angular momentum and the three-dimensional structure of the nucleon. These phenomena by themselves have become a major field of research as the dynamics of the strong interaction can be studies with these functions. Various single spin asymmetry measurements have been obtained for various rapidities. When moving to central rapidities, these left-right asymmetries are known to be very small for neutral pions. Since then, they have been confirmed to be small also for eta mesons. A substantially improved data set with significantly reduced uncertainties has been recently published in PRD for both final states. For the first time also direct photon single spin asymmetries have been extracted at RHIC. The direct photon asymmetries are again very important here as they are only sensitive to the transverse spin effects in the initial state and not the fragmentation-related effects. Furthermore, it provides sensitivity to a gluon correlation function that is not accessible in other processes. The direct photon results have also been submitted for publication in PRL.

In June of 2017, an electro-magnetic calorimeter was installed in the most forward area of the STAR experiment and took polarized proton collision data for neutral particle production (neutron, photon, neutral pion). The cross-section measurement will give us new inputs to develop high-energy particle-collision models which are essential to understand air-shower from ultra-high energy cosmic rays. The asymmetry measurement will improve the understanding of hadronic collisions at small scales. An unexpectedly large neutral pion asymmetry has been found using this data that may connect to the large pion asymmetries at smaller rapidities and higher transverse momenta. The results have been published in PRL.

At similar rapidities also neutron asymmetries have been observed in the past. While previously only their general magnitude was obtained, using unfolding techniques it was possible to extract the first asymmetries as a function of the neutron transverse moment for proton-proton collisions. These results have been published in PRD and correlated asymmetries, as well as asymmetries in proton-nucleus collisions are being prepared.

Some of us are participating in the Fermilab SeaQuest experiment as a pilot measurement of muon pairs from Drell-Yan process using a 120-GeV unpolarized proton at Fermilab. After finishing unpolarized measurements in 2017 to study the quark spin-orbit effect, a new measurement with a polarized proton target will start in 2021 to study the sea-quark orbit effect of the polarized proton in the target. The first result from the SeaQuest experiment on the asymmetry of the antimatter in the proton has been recently published in Nature.

For many jet related measurements fragmentation functions are necessary to gain spin and or flavor sensitivity. Those are currently extracted by some of us using the KEK-Belle data. In addition to using the fragmentation results with RHIC measurements, they will also provide the basis for most of the key measurements to be performed at the electron-ion collider. In 2020, in improved result for single and di-hadron fragmentation in different event topologies was published in PRD. These measurements are essential to nearly

all nucleon structure measurements at RHIC, semi-inclusive DIS and the EIC.

As the Electron-Ion Collider is becoming a reality, many of us are participating in the various community efforts to define the physics goals of the EIC and how they inform on the choices of collisions energies, luminosities, and detector components. While the accelerator efforts are naturally led by the two main nuclear physics laboratories in the US, BNL and JLAB, a large EIC user group of more than 1200 members from all around the world is working on making the EIC a reality. Within this group, we are participating in various functions from the steering committee, the conference and talks committee to various physics or detector related topical groups. During 2020 the community effort leading to the so-called Yellow Report studied and summarized these physics and detector requirements in detail and the Yellow Report has since been made public on the arXiv.

(2) Experimental study of quark-gluon plasma using RHIC heavy ion collider

[See also RIKEN-BNL Research Center Experimental Group for the activities at BNL]

We have completed several key measurements in the study of quark-gluon plasma at RHIC. As the top of them, we lead the analysis of the first thermal photon measurement in heavy ion collisions. The measurement indicates that the initial temperature reached in the central Au + Au collision at 200 GeV is about 350 MeV, far above the expected transition temperature $T_c \sim 170$ MeV, from hadronic phase to quark-gluon plasma. This work was rewarded by Nishina Memorial Prize given to Y. Akiba in 2011. We also measured direct photons in d + Au and direct photon flow strength v_2 and v_3 in Au + Au

We led measurement of heavy quark (charm and bottom) using VTX, a 4-layer silicon vertex tracker which we jointly constructed with US DOE. The detector was installed in PHENIX in 2011. PHENIX recorded approximately 10 times more data of Au + Au collisions in the 2014 run than the 2011 run. PHENIX recorded high statistics $p + p$ and $p + A$ data in 2015, and the doubled the Au + Au in 2016. PHENIX concluded its data taking in the 2016 run.

The results of the 2011 run were published in Physical Review C (Phys. Rev. C **93**, 034904 (2016)). This is the first publication from VTX. The result showed that the electrons from bottom quark decay is suppressed for $p_T > 4$ GeV/c, but the suppression factor is smaller than that of charm decay electrons for $3 < p_T < 4$ GeV/c. This is the first observation of bottom electron suppression in heavy ion collisions, and the first result that shows the bottom and charm suppression is different. The results of $b \to e$ and $c \to e$ measurement in the 2015 $p + p$ run has been published in Physical Review D99, 092003 (2019). The centrality dependence of the suppression $b \to e$ and $c \to e$ from the 2014 Au + Au data is in preparation. The 2016 run is the final data taking run of PHENIX, and this run doubled the dataset for heavy-flavor measurement with VTX. This year we completed the VTX geometry calibration of the 2016 run.

PHENIX published measurements of flow strength in p + Au, d + Au, and ^{3}He + Au (Nat. Phys. **15**, 214 (2019)). The results provide strong evidence for formation of small droplet of quark gluon plasma in collisions of small systems at RHIC.

In Wako we are operating a cluster computer system (CCJ) specialized to analyze huge data sets taken with the PHENIX detector. It consists of 28 nodes (18 old nodes and 10 new nodes) each of which has two CPUs and 10 sets of local disks for data repository (old node: quad-core CPU, 1 TB disk, new node: six-core CPU, 2 TB disk). There are 264 CPU cores and 380 TB disks in total. This configuration ensures the fastest disk I/O when each job is assigned to the node where the required data sets are stored. It is also important that this scheme does not require an expensive RAID system and network. Through this development we have established a fast and cost-effective solution in analyzing massive data.

The data of 0.9 PByte obtained by the PHENIX experiment is stored in a hierarchical storage system which is a part of HOKUSAI BigWaterfall/SailingShip supercomputer systems operated by the Head Office for Information Systems and Cybersecurity. In addition, we operate a dedicated server for the RHICf group and two servers for the J-PARC E16 group, to keep their dedicated compilation and library environments, and some data.

(3) Study of properties of mesons and exotic hadrons with domestic accelerators

Preparation of the experiment E16 at J-PARC Hadron experimental facility is underway with several Grant-in-Aids. This experiment aims to perform a systematic study of the spectral modification of low-mass vector mesons in nuclei to explore the physics of chiral symmetry breaking and restoration in dense nuclear matter, namely, the mechanism proposed by Nambu to generate most of hadron masses.

The Gas Electron Multiplier (GEM) technology is adopted for the two key detectors, GEM Tracker (GTR) and Hadron-blind Cherenkov detector (HBD). To improve electron-identification performance, lead-glass calorimeters (LG) are used in combination with HBD. We are in the production phase. Read-out electronics and trigger logic modules are also installed and tested. We have been a member of the CERN-RD51 collaboration to acquire the read-out technology for GEM. The MoU for RD51 was extended for the period of 2019–2023.

Due to the budgetary limitation, we aim to install a part of the detectors at the beginning of the experiment, eight modules of a set of GTR, HBD and LG, out of 26 modules in the full installation. J-PARC PAC (Program Advisory Committee) gave us a stage-2 approval in July 2017 to perform commissioning runs (Run 0). Although there is a significant delay from the originally planned date of March 2016, the construction of the beam line by KEK was completed finally in early 2020 to perform this experiment.

We performed the 1st half of commissioning run (Run-0a) in June 2020 successfully, using a primary proton beam with an intensity of 1×10^{10} protons per 2-sec duration of beam spill. This intensity is a designed full intensity of the beam line. The 2nd half, which started in February 2021, was suspended due to the malfunction of the J-PARC MR accelerator and a compensation beam time is allocated in June 2021. Eight modules of GTR, six modules of HBD and six modules of LG are assembled and installed in the E16 spectrometer magnet in January 2021 for this beam time. First physics run is planned in JFY2022, after two more HBDs and two more LG modules are installed.

(4) Detector development for PHENIX experiment

The PHENIX experiment proposes substantial detector upgrades to go along the expected accelerator improvements, including the future electron-ion collider "EIC." The present PHENIX detector is repurposed to the sPHENIX (super PHENIX) detector which reuses the Babar solenoid magnet at SLAC and is covered by the hadronic calorimeter which was not available in the previous RHIC experiments. The sPHENIX was approved for the Project Decision-2/3 (corresponds to DOE's Critical Decision-2/3) in May 2019. We RIKEN group have been developing the one of the tracking devices of sPHENIX detector, so called intermediate tracker (INTT) since 2015. The INTT provides the best timing resolution among the sPHENIX tracking system, in conjunction with a time projection chamber and a MAPS based vertex detectors. The prototype detectors demonstrated satisfactory performance in the efficiency and position resolutions as designed in the last two beam tests at the Fermilab Test Beam Facility (FTBF) using 120 GeV proton beam in March 2018 and June 2019. The production of silicon ladder assembly has been proceeded both in Taiwan Silicon Detector Facility (TSiDF) and BNL since Spring 2021. The INTT barrel assembly will be started in this Summer.

We have been planning to build a forward spectrometer to be added to the sPHENIX detector. With this addition, the detector called fsPHENIX will have hadronic and electromagnetic calorimetry as well as tracking capability in the forward rapidity region. This upgrade makes it possible to study forward jets and hadrons in jets which are of vital importance for the cold QCD program in polarized $p+p$ and $p+A$ collisions at RHIC. The fsPHENIX detector can be further upgraded to the ePHENIX detector to be used for electron-ion collisions at EIC. We are preparing test bench to perform R&D for the forward hadron calorimeter.

As the further investigation of the neutral pion production asymmetry discovered in the RHICf experiment, we started preparation for the next phase of the experiment, namely RHICf-II. The target year of physics data taking is 2024 as a part of either STASR or sPHENIX experiments. The highlight of the upgraded experiment is to adopt a larger acceptance with higher position resolution for the zero-degree calorimeter (ZDC). The detector technology developed for the FoCAL upgrade project of the ALICE experiment at LHC well satisfies the RHICf-II performance requirement. We thus resumed the associated membership of the ALICE collaboration, and the RHICf-II detectors are to be developed together with the ALICE FoCAL collaboration. This new detector technology development is also a part of an essential R&D programs for a ZDC detector for EIC.

Members

Director

Hideto EN'YO

Research/Technical Scientists

Yuji GOTO (Senior Research Scientist)
Itaru NAKAGAWA (Senior Research Scientist)
Seidl RALF (Senior Research Scientist)
Yasushi WATANABE (Senior Research Scientist)
Satoshi YOKKAICHI (Senior Research Scientist)

Contract Researcher

Tomonori TAKAHASHI

Special Postdoctoral Researcher

Koki KANNO

Research Associate

Wataru NAKAI

International Program Associate

Benard MULILO (Korea Univ.)

Senior Visiting Scientist

Toshiaki SHIBATA (Nihon Univ.)

Visiting Scientists

Kazuya AOKI (KEK)
Tatsuya CHUJO (Tsukuba Univ.)
Se Young HAN (Korea Univ.)
Shoichi HASEGAWA (JAEA)
Shunzo KUMANO (KEK)
Tsutomu MIBE (KEK)
Yuhei MORINO (KEK)
Ken-ichi NAKANO (Tokyo Tech)
Megumi NARUKI (Kyoto Univ.)
Kyoichiro OZAWA (KEK)
Susumu SATO (JAEA)
Kenta SHIGAKI (Hiroshima Univ.)
Maya SHIMOMURA (Nara Women's Univ.)
Kiyoshi TANIDA (JAEA)

Student Trainees

Daichi ARIMIZU (Kyoto Univ.)
Sakiko ASHIKAGA (Kyoto Univ.)
Takehito KONDO (Hiroshima Univ.)
Shono KYAN (Tsukuba Univ.)
Miu MORITA (Nara Women's Univ.)
Tomoki MURAKAMI (Univ. of Tokyo)
Satomi NAKASUGA (Kyoto Univ.)
Naoki OGATA (Kyoto Univ.)

Kenta SATO (Nagoya Univ.)
Mika SHIBATA (Nara Women's Univ.)
Yudai TAKAURA (Kyoto Univ.)
Kosuke TSUKUI (Tsukuba Univ.)
Yosuke UEDA (Hiroshima Univ.)

Interns

Daisuke IMAGAWA (Rikkyo Univ.)
Hikaru IMAI (Rikkyo Univ.)

Assistant

Keiko SUZUKI

List of Publications & Presentations

Publications

[Original Papers]

U. A. Acharya *et al*. (PHENIX Collaboration), "Transverse single-spin asymmetries of midrapidity π^0 and η mesons in polarized $p+p$ collisions at $\sqrt{s}$ = 200 GeV," Phys. Rev. D **103**, 5, 052009 (2021).

U. A. Acharya *et al*. (PHENIX Collaboration), "Transverse momentum dependent forward neutron single spin asymmetries in transversely polarized $p+p$ collisions at $\sqrt{s}$ = 200 GeV," Phys. Rev. D **103**, 3, 032007 (2021).

U. A. Acharya *et al*. (PHENIX Collaboration), "Polarization and cross section of midrapidity J/ψ production in $p+p$ collisions at $\sqrt{s}$ = 510 GeV," Phys. Rev. D **102**, 7, 072008 (2020).

U. A. Acharya *et al*. (PHENIX Collaboration), "Production of $b\bar{b}$ at forward rapidity in $p+p$ collisions at $\sqrt{s}$ = 510 GeV," Phys. Rev. D **102**, 9, 092002 (2020).

U. A. Acharya *et al*. (PHENIX Collaboration), "Measurement of jet-medium interactions via direct photon-hadron correlations in Au + Au and d + Au collisions at $\sqrt{s_{NN}}$ = 200 GeV," Phys. Rev. C **102**, 5, 054910 (2020).

U. A. Acharya *et al*. (PHENIX Collaboration), "Measurement of charged pion double spin asymmetries at midrapidity in longitudinally polarized $p+p$ collisions at $\sqrt{s}$ = 510 GeV," Phys. Rev. D **102**, 3, 032001 (2020).

L. Gamberg, Z. Kang, D. Pitonyak, A. Prokudin, N. Sato, and R. Seidl, "Electron-Ion Collider impact study on the tensor charge of the nucleon," Phys. Lett. B **816**, 136255 (2021).

R. Seidl, *et al*. (Belle Collaboration), "Update of inclusive cross sections of single and pairs of identified light charged hadrons," Phys. Rev. D **101**, 092004 (2020).

J. Dove, Y. Goto, *et al*., "The asymmetry of antimatter in the proton," Nature **590**, 561–565 (2021).

Presentations

[International Conferences/Workshops]

K. Kanno (invited), "Experimental study of spectral change of vector mesons in nuclear medium at J-PARC," YITP international workshop on Hadron in Nucleus (HIN2020), Kyoto (YITP), Japan & Online, March 8–10, 2021.

T. N. Takahashi (poster), "Data acquisition system in Run0 of the J-PARC E16 experiment," 22nd IEEE Real Time Conference (RT2020), Online, October 12–23, 2020.

R. Seidl (invited), "PHENIX highlights," RHIC AGS Users Meeting 2020, October 23, 2020.

R. Seidl (invited), "Fragmentation related measurements at Belle," 40th International Conference on High Energy Physics (ICHEP 2020), Prague, July 31, 2020.

Y. Goto, "Physics and detector requirements at zero degree of EIC," Contribution to: Workshop of QCD and Forward Physics at the Future Electron Ion Collider and Cosmic Ray Physics, 59–64 (2020).

K. Sato, Y. Goto, I. Nakagawa, R. Seidl, J. S. Park, M. H. Kim, *et al*., "The energy spectrum of forward photons measured by the RHICf experiment in $\sqrt{s}$ = 510 GeV proton-proton collisions," PoS **ICRC2019**, 413 (2021).

Benard Mulilo, "Transverse momentum dependent forward neutron single spin asymmetry in $p+p$ collisions at 200 GeV," International Workshop on Forward Physics and QCD with LHC, EIC and Cosmic Rays, held at JLAB January 20–23, 2021.

Benard Mulilo, "PHENIX preliminary results of forward neutron transverse single spin asymmetry in $p^{\uparrow}+p$ collisions at $\sqrt{s}$ = 200 GeV," IWHSS2020 Conference, Trieste-Italy, November 16, 2020.

[Domestic Conferences/Workshops]

四日市悟 (招待講演), 「DAQ and circuit in the J-PARC E16 experiment」, 計測システム研究会 2020, 茨城県東海村/オンライン開催, 2020 年 11 月 26–27 日.

中須賀さとみ (口頭発表), 「J-PARC E16 実験のための電子識別検出器の性能評価 II」, 日本物理学会 2020 年 秋季大会, オンライン開催, 2020 年 9 月 14–17 日.

近藤丈仁 (口頭発表), 「J-PARC E16 実験 GEM 飛跡検出器トリガ用信号読出回路の対放電保護」, 日本物理学会 第 76 回 年次大会, オンライン開催, 2021 年 3 月 12–15 日.

村上智紀 (口頭発表), 「J-PARC E16 実験における GEM 飛跡検出器の建設及び実機の性能評価」, 日本物理学会 第 76 回 年次大会, オンライン開催, 2021 年 3 月 12–15 日.

Ralf Seidl (invited), "RHIC and COMPASS results," 「日本のスピン物理学の展望」研究会, 島根県松江市, 2021 年 2 月 23–24 日.

Ralf Seidl (invited), "The electron ion collider as a next generation facility for the study of QCD," KEK 研究会「素粒子・原子核コライダー物理の交点」, オンライン開催, 2020 年 8 月 31 日.

Y. Goto (invited), "FoCal, RHICf-II and EIC," TCHoU Workshop, Online Meeting, March 30, 2021.

後藤雄二（口頭発表）,「PHENIX 実験での縦スピン非対称度測定の最新の結果」, 日本物理学会第 76 回年次大会, オンライン開催, 2021 年 3 月 13 日.

後藤雄二（招待講演）,「Electron-Ion Collider の物理」,「日本のスピン物理学の展望」研究会, 島根県松江市, 2021 年 2 月 23–24 日.

後藤雄二（招待講演）,「EIC 日本グループの議論」, KEK 研究会「素粒子・原子核コライダー物理の交点」, オンライン開催, 2020 年 8 月 31 日.

後藤雄二（口頭発表）,「$\sqrt{s}$ = 510 GeV での縦偏極陽子衝突による荷電パイ中間子の二重スピン非対称度の測定」, 日本物理学会 75 回年次大会, 愛知県名古屋市 (現地開催中止), 2020 年 3 月 17 日.

[Seminars]

Ralf Seidl (invited), "Fragmentation function measurements in Belle," Hiroshima University Nuclear and Particle Physics Seminar, September 3, 2020.

Press Releases

「陽子の中の反物質が持つ大きな非対称性の発見—反クォークの生成過程により物質の成り立ちを探る—」, 東京工業大学, 高エネルギー加速器研究機構, 山形大学, 理化学研究所, 2021 年 2 月 25 日.

Subnuclear System Research Division
Meson Science Laboratory

1. Abstract

Particles like muons, pions, and kaons have finite life times, so they do not exist in natural nuclei or matters. By implanting these particles into nuclei/matters, exotic phenomena in various objects can be studied from new point of view.

For example, kaon is the second lightest meson, which has strange quark as a constituent quark. It is expected that if one embeds mesons into nuclei, the sizes of the nuclei become smaller and one can form a high-density object beyond the normal nuclear density. Study of this object could lead to better understanding of the origin of the mass of the matter, and may reveal the quark degree of freedom beyond the quark-confinement. The other example is the weak interaction in nuclear matter. It can only be studied by the weak decay of hypernuclei, which have Lambda particle in the nuclei.

Muon provides even wider scope of studies, covering condensed matter physics as well as nuclear and atomic physics, and we are trying to extend the application field further into chemical and biological studies. For instance, stopping positively charged muon in a material, we obtain information on the magnetic properties or the local field at the muon trapped site (μSR). Injecting negatively charged muon to hydrogen gas, muonic hydrogen atom (μp) is formed. We are planning to measure μp hyperfine splitting energy to measure proton magnetic radius, which is complementary quantity to the proton charge radius and its puzzle. We are also interested in precision measurement of muon property itself, such as muon anomalous magnetic moment ($g-2$).

In our research, we introduce different kind of impurities into nuclei/matters, and study new states of matter, new phenomena, or the object properties.

2. Major Research Subjects

(1) Study of meson property and interaction in nuclei
(2) Origin of matter mass/quark degree of freedom in nuclei
(3) Condensed matter and material studies with muon
(4) Nuclear and particle physics studies via muonic hydrogen
(5) Development of ultra cold muon beam, and its application from material science to particle physics

3. Summary of Research Activity

(1) Hadron physics at J-PARC, RIKEN-RIBF, GSI and SPring-8

Kaon and pion will shed a new insight to the nuclear physics. The recent discovery of deeply bound pionic atom enables us to investigate the properties of mesons in nuclear matter. At RIKEN-RIBF, we are preparing precise experimental study of the pionic atom. Very lately, we succeeded to discover kaonic nuclear bound state, "K^-pp," at J-PARC. The yield dependence on momentum-transfer shows that observed system is unexpectedly small. We extended our study on $\Lambda(1405)$ that could be K-p bound state. By these experiments, we are studying the KN^- interaction, and clarify the nature of kaon in nuclei. At Spring-8 and at GSI, we are planning to study omega and η' nuclei. By these experiments, we aim to be a world-leading scientific research group using these light meta-stable particles.

(1-1) Deeply bound kaonic nuclei

J-PARC E15 experiment had been performed to explore the simplest kaonic nuclear bound state, "K^-pp." Because of the strong attraction between KN^-, the K^- in nuclei may attract surrounding nucleons, resulting in forming a deeply bound and extremely dense object. Measurement of the kaon properties at such a high-density medium will provide precious information on the origin of hadron masses, if the standard scenario of the hadron-mass-generation mechanism, in which the hadron masses are depends on matter density and energy, is correct. Namely, one may study the chiral symmetry breaking of the universe and its partial restoration in nuclear medium.

The E15 experiment was completed to observe the "K^-pp" bound state by the in-flight ^{3}He(K^-, n) reaction, which allows us the formation via the invariant-mass spectroscopy by detecting decay particles from "K^-pp." For the experiment, we constructed a dedicated spectrometer system at the secondary beam-line, K1.8BR, in the hadron hall of J-PARC.

With the Λpn final states obtained in the first stage experiment, we observed a kinematic anomaly in the Λp invariant mass near the mass threshold of M(K^-pp) (total mass of kaon and two protons) at the lower momentum transfer q region. We conducted a successive experiment to examine the nature of the observed kinematical anomaly in the Λpn final state, and we confirmed the existence of the bound state below the mass threshold of M(K^-pp) at as deep as the binding energy of 40 MeV. The momentum transfer q naturally prefers lower momentum for the bound state formation, but the observed event concentration extended having the form-factor parameter ~400 MeV/c. Based on the PWIA calculation, the data indicated that the "K^-pp" system could be as small as ~0.6 fm. It is astonishingly compact in contrast to the mean nucleon distance ~1.8 fm.

This observed signal shows that ***a meson*** (qq^-) ***forms a quantum state where baryons (qqq) exist as nuclear medium***, *i.e.*, a highly excited novel form of nucleus with a kaon, in which ***the mesonic degree-of-freedom still holds***. This is totally new form of nuclear system, which never been observed before.

(1-2) Precision X-ray measurement of kaonic atom

To study the KN^- interaction at zero energy from the atomic state level shift and width of kaon, we have performed an X-ray spectroscopy of atomic $3d \rightarrow 2p$ transition of negatively charged K-mesons captured by helium atoms. However, our first experiment is insufficient in energy resolution to see the K^--nucleus potential. Aiming to provide a breakthrough from atomic level observation,

we introduce a novel X-ray detector, namely superconducting transition-edge-sensor (TES) microcalorimeter offering unprecedented high energy resolution, being more than one order of magnitude better than that achieved in the past experiments using conventional semiconductor detectors. The experiment J-PARC E62 aims to determine $2p$-level strong interaction shifts of kaonic ^{3}He and ^{4}He atoms by measuring the atomic $3d \rightarrow 2p$ transition X-rays using TES detector with 240 pixels having about 23 mm^2 effective area and the average energy resolution of 7 eV (FWHM) at 6 keV. We carried out the experiment at J-PARC in June 2018 and successfully observed distinct X-ray peaks from both atoms. The data analysis is now ongoing.

Another important X-ray measurement of kaonic atom would be $2p \rightarrow 1s$ transition of kaonic deuteron (K^--d). We have measured same transition of kaonic hydrogen (K^--p), but the width and shift from electro-magnetic (EM) value reflect only isospin average of the $\bar{K}N$ interaction. We can resolve isospin dependence of the strong interaction by the measurements both for K^--p and K^--d. The experiment J-PARC E57 aims at pioneering measurement of the X-rays from K^--d atoms. Prior to full (stage-2) approval of the E57 proposal, we performed a pilot run with hydrogen target in March 2019.

(1-3) Deeply bound pionic atoms and η' mesonic nuclei

We have been working on precision spectroscopy of pionic atoms systematically, which leads to understanding of the non-trivial structure of the vacuum and the origin of hadron masses. The precision data set stringent constraints on the chiral condensate at nuclear medium. We are presently preparing for the precision systematic measurements at RIBF. A pilot experiment performed in 2010 showed a unprecedented results of pionic atom formation spectra with finite reaction angles. The measurement of pionic ^{121}Sn performed in 2014 showed a very good performance of the system. We have been finalizing the data analysis to achieve information on the pion-nucleus interaction based on the pionic atom spectroscopy. At the same time we have been working on a systematic high precision spectroscopy of pionic tin isotopes.

We are also working on spectroscopy of η' mesonic nuclei in GSI/FAIR. Theoretically, peculiarly large mass of η' is attributed to UA(1) symmetry and chiral symmetry breaking. As a result, large binding energy is expected for η' meson bound states in nuclei (η'-mesonic nuclei). From the measurement, we can access information about gluon dynamics in the vacuum via the binding energy and decay width of η'-nuclear bound state. We are preparing for a new experiment using a large solid angle detectors at GSI.

(1-4) $^3_\Lambda$H lifetime puzzle and our approach

Three recent heavy ion experiments (HypHI, STAR, and ALICE) announced surprisingly short lifetime for $^3_\Lambda$H hyper-nucleus's *Mesonic Weak Decay* (MWD), which seems to be inconsistent with the fact that the $^3_\Lambda$H is a very loosely bound system. It is very interesting to study this with a different experimental approach. We proposed a direct measurement of $^3_\Lambda$H MWD lifetime with ~20% resolution at J-PARC hadron facility by using K^- meson beam at 1 GeV/c. As for the feasibility test, we also measure $^4_\Lambda$H lifetime.

A Cylindrical Detector System (CDS) used in J-PARC E15/E31 experiment is employed to capture the delayed π^- as a weak decay product from $^{3,4}_\Lambda$H a calorimeter is installed in the very forward region to tag fast π^0 meson emission at ~0 degree, which ensures that the Λ hyperon production with small recoil momentum. By this selection, we can improve the ratio between $^{3,4}_\Lambda$H and quasi-free Λ and Σ background. A test beam for feasibility study with ^{4}He target has been conditionally approved by J-PARC PAC. We will conduct the experiment and to present the data in short.

(2) Muon science at RIKEN-RAL branch

The research area ranges over particle physics, condensed matter studies, chemistry and life science. Our core activities are based on the RIKEN-RAL Muon Facility located at the Rutherford-Appleton Laboratory (UK), which provides intense pulsed-muon beams. We have variety of important research activities such as particle/nuclear physics studies with muon's spin and condensed matter physics by muon spin rotation/relaxation/resonance (μSR).

(2-1) Condensed matter/materials studies with μSR

We stated to share experimental equipment with those of RAL in order to make organization of RIKEN beam time schedules easier and to enhance the efficiency to carry out RIKEN's experiments. We use shared cryostats and manpower supports available from RAL as well we other experimental areas. Both two μSR spectrometers, ARGUS (Port-2) and CHRNUS (Port-4), are working wel wit maintenance supports provide from RAL. Among our scientific activities on μSR studies from year 2017 to 2020, following studies are most important subjects of material sciences at the RIKEN-RAL muon facility:

(1) Multi magnetic transitions in the Ru-based pyrochlore systems, $R_2Ru_2O_7$.
(2) Magnetic properties of the nano-cluster gold in the border of macro- and micro- scale.
(3) Novel magnetic and superconducting properties of nano-size La-based high-T_c superconducting curates.
(4) Determination of muon positions estimated from density functional theory (DFT) and dipole-field calculations.
(5) Chemical muonic states in DNA molecules.

(2-2) Nuclear and particle physics studies via ultra-cold muon beam and muonic atoms

If we can improve muon beam emittance, timing and energy dispersion (so-called "ultra-cold muon"), then the capability of μSR studies will be drastically improved. The ultra-cold muon beam can stop in a thin foil, multi-layered materials and artificial lattices, so one can apply the μSR techniques to surface and interface science. The development of ultra-cold muon beam is also very important as the source of pencil-like small emittance muon beam for muon $g-2$ measurement.

Ultra-cold muon beam has been produced by laser ionization of muoniums in vacuum (bound system of μ^+ and electron). We are developing two key components, high efficiency muonium generator at room temperature and high intensity ionization laser. The study of muonium generator has been done in collaboration with TRIUMF. In 2013, we demonstrated at least 10 times increase of the muonium emission efficiency by fabricating fine laser drill-holes on the surface of silica aerogel. Further study was done in 2017 with more than 20 aerogel target having different surface conditions. We are analyzing the data to identify which condition most contributed to increasing the muonium emission efficiency. We also developed a high power Lyman-α laser in collaboration with laser

group at RIKEN. In this laser development, we succeeded to synthesize novel laser crystal Nd:YGAG, which has an ideal wavelength property for laser amplification to generate Lyman-α by four-wave mixing in Kr gas cell. We already achieved 10 times increase of Lyman-α generation than before. However, in order to increase the intensity by one more order, we need a larger size crystal. So far we have inhomogeneity problem but we are trying to solve this problem.

A large discrepancy was found recently in the proton charge radius between the new precise value from muonic hydrogen atom at PSI and the values from normal hydrogen spectroscopy and e-p scattering. We are planning a precise measurement of proton Zemach radius (with charge and magnetic distributions combined) using the laser spectroscopy of hyperfine splitting energy in the muonic hydrogen atom. As a key parameter for designing the experiment, we need to know the quench rate of the muonic proton polarization due to collision with surrounding protons, for which only theoretical estimations are available. We first measured the quench rate of muonic deuterium polarization in deuterium gas, which confirmed the long lifetime consistent with the calculation. We also carried out measurement on muonic proton in low pressure hydrogen gas and the analysis is in progress.

Members

Director

Masahiko IWASAKI

Research Scientists

Kenta ITAHASHI (Senior Research Scientist)
Yue MA (Senior Research Scientist)
Haruhiko OUTA (Senior Research Scientist)
Fuminori SAKUMA (Senior Research Scientist)
Isao WATANABE (Senior Research Scientist)

Contract Researcher

Katsuhiko ISHIDA

Junior Research Associates

Shun SEO (Univ. of Tokyo)
Muhamad D. UMAR (Hokkaido Univ.)

International Program Associates

Muhammad H.B. CHE LAH (Univ. Sains Malaysia)
Harison B. ROZAK (Univ. Sains Malaysia)
Suci WINARSIH (Univ. Indonesia)
Utami WIDYAISWARI (Univ. Indonesia)

Research Consultant

Masayasu KAMIMURA

Senior Visiting Scientists

Hiroyuki NOUMI (Osaka Univ.)
Kazuhiro TANAKA (KEK)

Visiting Scientists

Tadashi ADACHI (Sophia Univ.)
Hiroko ARIGA (Hokkaido Univ.)
Retno ASIH (Inst. Teknologi Sepuluh Nopember)
Fahmi ASTUTI (Inst. Teknologi Sepuluh Nopember)
KwangYong CHOI (Chung-Ang Univ.)
Catalina Oana CURCEANU (INFN)
Zyun EZAWA (Tohoku Univ.)
Hiroyuki FUJIOKA (Tokyo Tech)
Masaki FUJITA (Tohoku Univ.)
Shuhei FUKUOKA (Hokkaido Univ.)
Takayuki GOTO (Sophia Univ.)
Maryam HASSANVAND (Isfahan Univ. of Tech.)
Wataru HIGEMOTO (JAEA)
Ko-ichi HIRAKI (Fukushima Medical Univ.)
Satoru HIRENZAKI (Nara Women's Univ.)
Koichi ICHIMURA (Hokkaido Univ.)
Yasuyuki ISHII (Shibaura Inst. of Tech.)
Ryosuke KADONO (KEK)
Takayuki KAWAMATA (Tohoku Univ.)
Seiko KAWAMURA (JAEA)
Hikomitsu KIKUCHI (Univ. of Fukui)
Takuya KOBAYASHI (Saitama Univ.)
Yoji KOIKE (Tohoku Univ.)
Seungwon LEE (Univ. of Toyama)
Kenji MATSUDA (Univ. of Toyama)
Hiroyasu MATSUURA (Univ. of Tokyo)
Mototsugu MIHARA (Osaka Univ.)
Takaaki MINAMIDATE (Tokyo Univ. of Sci)
Yasuhiro MIYAKE (KEK)
Mohamed Ismail MOHAMED-IBRAHIM (Univ. Sains Malaysia)
Takehito NAKANO (Ibaraki Univ.)
Takahiro NAMIKI (Univ. of Toyama)
Katsuhiko NISHIMURA (Univ. of Toyama)
Yasuo NOZUE (Osaka Univ.)
Agustinus NUGROHO (Inst. Teknologi Bandung)
Kazuki OHISHI (Comprehensive Res. Org. for Sci. and Soc.)
Yu OISHI (KEK)
Atsushi OKAZAWA (Univ. of Tokyo)
Dita PUSPITA SARI (Shibaura Inst. of Tech.)
Irwan RAMLI (Univ. Cokroaminoto Palopo)
RISDIANA (Padjadjaran Univ.)
Lusi SAFRIANI (Padjadjaran Univ.)
Naohito SAITO (KEK)
Shinichi SHAMOTO (CROSS)
Ichiro SHIRAKI (Univ. of Yamanashi)
Shukri SULAIMAN (Univ. Sains Malaysia)
Ken SUZUKI (Stefan Meyer Inst.)

Kensuke SUZUKI (Tohoku Univ.)
Takao SUZUKI (Shibaura Inst. of Tech.)
Hiroshi TANIDA (Toyama Prefectural Univ.)
Takanori TANIGUCHI (Tohoku Univ.)
Andrea VACCHI (Udine Univ. (Italy))
Eberhard WIDMANN (Stefan Meyer Inst.)
Zhuan XU (Zhejiang Univ.)
Yasuhiro YAMAGUCHI (JAEA)
Ichihiro YAMAUCHI (Saga Univ.)
Toshimitsu YAMAZAKI (Univ. of Tokyo)
Yukio YASUI (Meiji Univ.)
Masaru YOSOI (Osaka Univ.)
Wan Nurfadhilah B. ZAHARIM (Univ. Sains Malaysia)
Xu-Guang ZHENG (Saga Univ.)
Johann ZMESKAL (Austrian Academy of Sci.)

Student Trainees

Redo Muhammad RAMADHAN (Univ. Indonesia)
Harison B. ROZAK (Univ. Sains Malaysia)
Yuki SAGARA (Shibaura Inst. of Tech.)
Ryo SASAKI (Shibaura Inst. of Tech.)
SUCI WINARSIH (Univ. Indonesia)

Assistants

Kumiko TAKAHASHI
Mitsue YAMAMOTO

List of Publications & Presentations

Publications

[Original Papers]

J. Sugiyama, O. Kenji Forslund, E. Nocerino, N. Matsubar, K. Papadopoulos, Y. Sassa, Stephen P. Cottrell, Adrian D. Hillier, K. Ishida, M. Mansson, and J. H. Brewer, "Lithium diffusion in LiMnPO4 detected with $\mu^{\pm}$SR," Phys. Rev. Research **2**, 033161 (2020).

M. Aramini, C. Milanese, Adrian D. Hillier, A. Girella, C. Horstmann, T. Klassen, K. Ishida, M. Dornheim, and C. Pistidda, "Spectroscopic tool for the investigation of the local chemistry of elements," Nanomaterials **2020**, 10, 1260 (2020).

E. Mocchiutti, A. Adamczak, D. Bakalov, G. Baldazzi, R. Benocci, R. Bertoni, M. Bonesini, V. Bonvicini, H. CabreraMorales, F. Chignoli, M. Clemenza, L. Colace, M. Danailov, P. Danev, A. de Bari, C. DeVecchi, M. DeVincenzi, E. Furlanetto, F. Fuschinod, K. S. Gadedjisso-Tossoua, D. Guffantia, K. Ishida, C. Labanti, V. Maggi, R. Mazza, A. Menegolli, G. Morgante, M. Nastasi, J. Niemela, C. Pizzolotto, A. Pullia, R. Ramponi, L. P. Rignanese, M. Rossella, N. Rossi, M. Stoilov, L. Stoychev, L. Tortora, E. Vallazza, G. Zampa, and A. Vacchi, "First measurement of the temperature dependence of muon transfer rate from muonic hydrogen atoms to oxygen," Phys. Lett. A **384**, 126667 (2020).

C. Pizzolotto, A. Adamczak, D. Bakalov, G. Baldazzi, M. Baruzzo, R. Benocci, R. Bertoni, M. Bonesini, V. Bonvicini, H. Cabrera, D. Cirrincione, M. Citossi, F. Chignoli, M. Clemenza, .Colace,. Danailov, P. Danev, A. de Bari, C. De Vecchi, M. de Vincenzi, E. Fasci, E. Furlanetto,. Fuschino, K. S. Gadedjisso-Tossou, L. Gianfran, D. Guffanti, A. D. Hillier, K. Ishida,. J. C. King, C. Labanti, V. Maggi, R. Mazza, A. Menegolli, E. Mocchiutti, L. Moretti,. Morgante, J. Niemela, B. Patrizi, A. Pirri, A. Pullia, R. Ramponi, L. P. Rignanese, E. Roman,. Rossella, R. Sarkar, A. Sbrizzi,. Stoilov, L. Stoychev, J. J. Suárez-Vargas, G. Toci, L. Tortora, E. Vallazza, M. Vannini, C. Xiao, G. Zampa, and A. Vacchi1, "The FAMU experiment: muonic hydrogen high precision spectroscopy studies," Eur. Phys. J. A **56**, 185 (2020).

J. Beare, G. Beer, J. H. Brewer, T. Iijima, K. Ishida, M. Iwasaki, S. Kamal, K. Kanamori, N. Kawamura, R. Kitamura, S. Li, G. M. Luke, G. M. Marshall, T. Mibe, Y. Miyake, Y. Oishi, K. Olchanski, A. Olin, M. Otani, M. A. Rehman, N. Saito, Y. Sato, K. Shimomura, K. Suzuki, M. Tabata, and H. Yasuda, "Study of muonium emission from laser-ablated silica aerogel," Prog. Theor. Exp. Phys. **2020**, 123C01 (2020).

H. Yamauchi, D. P. Sari, I. Watanabe, Y. Yasui, L. -J. Chang, K. Kondo, T. U. Ito, M. Ishikado, M. Hahara, M. D. Frontzk, C. Chi, J. A. Fernandez-Bac, J. S. Lord, A. Berlie, A. Kotani, S. Mori, and S. Shamoto, "High-temperature short-range order in Mn_3RhSi," Commun. Matter. **1**, 42 (2020).

M. Fujita, K. M. Suzuki, S. Asano, H. Okabe, A. Koda, R. Kadono, and I. Watanabe, "Magnetic behavior of *T'*-type Eu_2CuO_4 revealed by muon spin rotation and relaxation measurements," Phys. Rev. B **102**, 045116 (2020).

R. Kitamura, S. Bae, S. Choi, Y. Fukao, H. Iinuma, K. Ishida, N. Kawamura, B. Kim, Y. Kondo, T. Mibe, Y. Miyake, M. Otani, G. P. Razuvaev, N. Saito, K. Shimomura, and P. Strasser, "Development of negative muonium ion source for muon acceleration," Phys. Rev. Accel. Beams **24**, 033403 (2021).

S. Kanda, Y. Fukao, Y. Ikedo, K. Ishida, M. Iwasaki, D. Kawall, N. Kawamura, K. M. Kojima, N. Kurosawa, Y. Matsuda, T. Mibe, Y. Miyake, S. Nishimura, N. Saito, Y. Sato, S. Seo, K. Shimomura, P. Strasser, K. S. Tanaka, T. Tanaka, H. A. Torii, A. Toyoda, and Y. Ueno, "New precise spectroscopy of the hyperfine structure in muonium with a high-intensity pulsed muon beam," Phys. Lett. B **815**, 136154 (2021).

A. D. Pant, K. Ishida, N. Kawamura, S. Matoba, A. Koda, S. Nishimura, and K. Shimomura, "Study of muonium behavior in n-type silicon for generation of ultra cold muonium in vacuum," Physica B **613**, 412997 (2021).

T. Yamaga *et al*., "Observation of a $\bar{K}NN$ bound state in the ^{3}He(K^-, Λp)n reaction," Phys. Rev. C **102**, 044002 (2020).

[Proceedings]

F. Sakuma *et al*., "$K^- pp$ bound system at J-PARC," AIP Conference Proceedings **2249**, 020005 (2020).

F. Sakuma *et al*., "$\bar{K}$-nuclear bound state at J-PARC," JPS Conf. Proc. **32**, 010088 (2020).

H. Fujioka, K. Itahashi, V. Metag, M. Nanova, and Y. K. Tanaka, "Comment on 'Search for η' bound nuclei in the ^{12}C(γ, p) reaction with simultaneous detection of decay products'," Phys. Rev. Lett. **126**, 019201 (2021).

A. Tani, N. Ikeno, D. Jido, H. Nagahiro, H. Fujioka, K. Itahashi, and S. Hirenzaki, "Structure of double pionic atoms," PTEP 2021, 3, 033D02 (2021).

Presentations

[International Conferences/Workshops]

F. Sakuma (plenary), "Recent results and future prospects of kaonic nuclei at J-PARC," Yamada Conference LXXII: The 8th Asia-Pacific Conference on Few-Body Problems in Physics (APFB2020), Kanazawa, Japan, March 1–5, 2021.

T. Yamaga (invited), "Observation of the K^-pp bound state in J-PARC E15," Hadron in Nucleus 2020 (HIN20), Kyoto, Japan, March 8–10, 2021.

T. Hashimoto (invited), "Kaonic atom experiments at J-PARC," Hadron in Nucleus 2020 (HIN20), Kyoto, Japan, March 8–10, 2021.

Y. Ma (invited), "Towards solving the hypertriton lifetime puzzle with direct lifetime measurement: current status of J-PARC E73 experiment," Hadron in Nucleus 2020 (HIN20), Kyoto, Japan, March 8–10, 2021.

[Domestic Conferences/Workshops]

石田勝彦, 「英国理研 RAL ミュオン施設におけるミュオン利用分析研究の進展」, 第 3 回 文理融合シンポジウム 量子ビームで歴史を探る—加速器が紡ぐ文理融合の地平—, オンライン, 2020 年 9 月 25–26 日.

石田勝彦 (招待講演), 「理研 RAL と J-PARC」, パルス中性子ミュオン発生 40 周年記念シンポジウム, オンライン, 2020 年 12 月 23 日.

石田勝彦, 「理研 RAL での非破壊元素分析」, 第 4 回文理融合シンポジウム 量子ビームで歴史を探る—加速器が紡ぐ文理融合の地平—, オンライン, 2021 年 1 月 28–29 日.

佐久間史典 (口頭発表), 「軽い K 中間子原子核の系統的測定」, 日本物理学会 第 76 回年次大会, オンライン, 2021 年 3 月 12–15 日.

山我拓巳 (口頭発表), 「K^-pp のスピン・パリティ測定と $\overline{K}^0nn$ の探索」, 日本物理学会第 76 回年次大会, オンライン, 2021 年 3 月 12–15 日.

浅野秀光 (口頭発表), 「K^-d 反応の運動量移行と $\pi^\pm\Sigma^\pm$ 不変質量分布の関係」, 日本物理学会 第 76 回年次大会, オンライン, 2021 年 3 月 12–15 日.

橋本直 (口頭発表), 「TES マイクロカロリメータを用いた K 中間子ヘリウム原子 X 線精密分光」, 日本物理学会 第 76 回年次大会, オンライン, 2021 年 3 月 12–15 日.

赤石貴也 (口頭発表), 「K^- ビームを用いたハイパートライトンの寿命直接測定の現状」, 日本物理学会 第 76 回年次大会, オンライン, 2021 年 3 月 12–15 日.

赤石貴也 (口頭発表), 「${}^3_\Lambda$H 寿命直接測定のための PbF_2 カロリメータの性能評価 (2)」, 日本物理学会 2020 年秋季大会, オンライン, 2021 年 3 月 12–15 日.

山我拓巳 (招待講演), "Measurement of spin-spin correlation in K^-pp decay," 日本のスピン物理学の展望, オンライン, 2021 年 2 月 23–24 日.

山我拓巳 (招待講演), 「J-PARC E15 実験における $\bar{K}NN$ 束縛状態の発見と今後の展望」, ELPH 研究会 C029「様々なフレーバー領域で探るクォーク・ハドロン多体系の分光と構造」, 宮城県仙台市 (東北大学電子光理学研究センター), 2020 年 11 月 4–5 日.

Press Releases

正負のミュオンで捉えたイオンの動き 2020 年 8 月 7 日—Li イオンの動きを, 負ミュオンで確認, 正ミュオンで詳細観察—一般財団法人総合科学研究機構 (CROSS) 中性子科学センター杉山 純サイエンスコーディネータ国立研究開発法人理化学研究所 (理研) 仁科加速器科学研究センター石田勝彦協力研究員.

Subnuclear System Research Division
RIKEN BNL Research Center

1. Abstract

The RIKEN BNL Research Center was established in April 1997 at Brookhaven National Laboratory with Professor T. D. Lee of Columbia University as its initial Director. The Center is dedicated to the study of strong interactions, including spin physics, lattice QCD and RHIC physics through the nurturing of a new generation of young physicists. Professor Lee was succeeded by BNL Distinguished Scientist, the former BNL director, N. P. Samios, who served until 2013. The other former BNL director, S. H. Aronson led the Center from 2013. Hideto En'yo succeeded the director position starting from JFY 2017. Support for RBRC was initially for five years and has been renewed four times, and presently extends to March 2023. Theoretical activities in the RBRC Theory and Computing Groups are closely and intimately related to those of the Nuclear Theory, High Energy Theory and Lattice Gauge Theory Groups at BNL. The RBRC Experimental Group jointly works with Radiation Laboratory at Wako RIKEN, the RHIC Spin Group at BNL, the RHIC Spin Physics community, and the PHENIX/sPHENIX collaboration. BNL provides office space, management, computing and administrative support. The Deputy Director of RBRC is D. Morrison (BNL). In May 2021 Y. Hatta (BNL) becomes Theory Group leader, succeeding D. Kharzeev. Y. Akiba (RIKEN) is Experimental Group leader and T. Izubuchi (BNL) is Computing Group leader.

2. Major Research Subjects

Major research subjects of the theory group are

(1) Spin structure of proton
(2) Gluon saturation at small-x
(3) Physics of quark gluon plasma

Major research subjects of the computing group are

(1) Search for new law of physics through tests for Standard Model of particle and nuclear physics
(2) Dynamics of QCD and related theories
(3) Theoretical and algorithmic development for lattice field theories, QCD machine design

Major research subject of the experimental group are

(1) Experimental Studies of the Spin Structure of the Nucleon
(2) Study of Quark-Gluon Plasma at RHIC
(3) sPHENIX detector construction

3. Summary of Research Activity

Summary of Research Activities of the three groups of the Center are given in the sections of each group.

Members

Director

Hideto EN'YO

Deputy Director

David P. MORRISON

Administrative Staff

Kazushige FUKUSHIMA (Administration Manager, Nishina Center and iTHEMS Promotion Office)
Hiroshi ITO (Deputy Administration Manager, Nishina Center and iTHEMS Promotion Office)
Keiko IWANO-OKABE (Deputy Administration Manager, Nishina Center and iTHEMS Promotion Office)
Pamela ESPOSITO (Administrative Assistant)
Maureen MCNEIL-SHEA (Administrative Assistant)

Subnuclear System Research Division
RIKEN BNL Research Center
Theory Group

1. Abstract

The efforts of the RBRC theory group are concentrated on the major topics of interest in High Energy Nuclear Physics, in particular, the physics explored by the RHIC experiment at Brookhaven National Laboratory (BNL). This includes: understanding of the Quark-Gluon Plasma (QGP); the nature of dense quark matter; the initial state in high energy collisions, the Color Glass Condensate and its evolution to QGP through a Glasma; QCD spin physics; physics relevant to the future Electron-Ion Collider at BNL.

2. Major Research Subjects

(1) Heavy Ion Collisions, QCD phase diagram
(2) Perturbative Quantum Chromo-Dynamics (QCD)
(3) Nucleon structure, mass and spin

3. Summary of Research Activity

(1) Phase diagram of QCD

The major goal of RHIC heavy-ion program is to map out the QCD phase diagram at finite temperature and density. Together with collaborations, V. Skokov has determined the location of the Yang-Lee edge singularity in the O(N) model using the functional renormalization group method. This can be applied to the QCD phase diagram to determine the radius of convergence of the fugacity expansion and hence the location of the QCD critical point at finite chemical potential.

(2) QCD at small x

The initial condition of heavy-ion collisions at RHIC is governed by the Color Glass Condensate (CGC) which is the universal form of matter in the high energy (small-x) limit of QCD. The RBRC scientists have made major contributions to this field, and the efforts continue to date. V. Skokov has worked on various aspects of the CGC and their phenomenological consequences. In particular, he has calculated the multiplicity and transverse momentum dependence of the elliptic flow parameter v_2 in proton-nucleus (pA) collisions in the dense-dilute framework of CGC. Together with M. Li, he has also computed the first saturation corrections in pA collisions by solving the real-time classical Yang-Mills equation. Y. Mehtar-Tani and R. Boussarie have proposed a novel formulation of the gluon transverse momentum dependent (TMD) distribution which captures the leading logarithms in both the Bjorken and Regge limits.

(3) Jet and jet quenching

Jets have become an important tool to uncover the transport properties of matter created in heavy-ion collisions and the nontrivial parton structure in the nucleon. These are important goals of the sPHENIX and EIC experiments. Y. Mehtar-Tani has pushed the calculation of jet quenching to higher precision, now up to next-to-next-to-leading order (NNLO) in the opacity expansion. Together with collaborators, he has made concrete prediction of the nuclear modification factor at the LHC based on the state-of-the-art theory of jet quenching. Y. Hatta and collaborators calculated the impact of soft gluon resummation on the azimuthal angular correlation of jets. It has been shown that angular correlations of perturbative origin are numerically significant. They could obscure the primordial correlation due to the nontrivial parton distribution such as the linearly polarized gluon distribution. Y. Hatta and T. Ueda has calculated the gap survival probability in dijet production in proton-proton collisions at the LHC, resumming the nonglobal logarithms without any approximation to the number of colors.

(4) Origin of proton mass

Understanding the origin of proton mass is one of the most important goals of the future Electron-Ion Collider. Y. Hatta and R. Boussarie has developed an OPE-based approach to calculate the cross section of near-threshold electro-production of heavy quarkonia at large photon virtuality. The impact of the gluon condensate, related to the proton mass via the trace anomaly, has been estimated. D. Kharzeev argued that the cross section is dominated by the form factor of the trace of the energy momentum tensor. Based on this, he has extracted the nucleon "mass radius" from the recent experimental data on J/psi production from the Jefferson laboratory. Y. Hatta and Y. Zhao have introduced a parton distribution function associated with the gluon condensate and performed a one-loop calculation with a special attention to the possible zero mode.

(5) Hydrodynamical simulation of heavy-ion collisions

C. Shen has developed a comprehensive dynamical platform to simulate the evolution of fireballs created in heavy-ion collisions based on numerical codes for the viscous hydrodynamic equation. This can be applied to RHIC experiments with a wide range in center-of-mass energy, from the top energy (200 GeV per nucleon) to very low energy (7 GeV per nucleon) relevant to the ongoing Beam Energy Scan II experiment (BES II). This allows him to extract the shear viscosity from the input equation of state and the experimental data on particle multiplicity, *etc*. C. Shen has also studied various aspects of heavy-ion collisions such as Lambda polarization, deutron production and signals of vortex formation.

(6) Quantum information & computing

RBRC theorists also work on quantum computing and quantum information science. Y. Kikuchi discussed how to recover damaged information from Hawking radiation in Hayden-Preskill thought experiment. D. Kharzeev, Y. Kikuchi, and K. Ikeda have studied the real-time dynamics of the topological susceptibility near the critical point of massive Schwinger model and observed a sharp maximum due to critical fluctuations. Their spin Hamiltonian formulation is suitable for future digital quantum simulations.

(7) Beyond the standard model physics in low and high energy nuclear physics

Together with collaborators, J. de Vries has explored possible manifestations of physics beyond the Standard Mode (BSM) in low energy nuclear physics such as neutrinoless double beta decays and the nucleon electric dipole moment. In particular, his group has presented a first estimate of the complete amplitude of neutrinoless double beta decay including a contact term necessary for renormalization in chiral effective theory. J. de Vries also studied the prospect to discover sterile neutrinos at the LHC in the framework of neutrino-extended Standard Model Effective Field Theory.

(8) New connection between the nucleon electric dipole moment and QCD spin physics

One of the plausible operators to induce an electric dipole moment (EDM) in nucleons is the Weinberg operator which is a dimension-6, purely gluonic operator. Y. Hatta has found a novel relation between the nucleon matrix element of the Weinberg operator and certain twist-4 corrections in polarized Deep Inelastic Scattering (DIS) experiment. Based on this observation, he has made a numerical estimate of the EDM which turned out to be smaller than a previous estimate based on the QCD sum rule.

Members

Group Leader

Dmitri KHARZEEV

Deputy Group Leader

Yoshitaka HATTA

RBRC Researchers

Jordy DE VRIES
Yuta KIKUCHI
Yacine MEHTAR-TANI
Chun SHEN
Vladimir SKOKOV

Visiting Scientists

Hiromichi NISHIMURA (Keio Univ.)
Yuya TANIZAKI (North Carolina State Univ.)

List of Publications & Presentations

Publications

[Original Papers]

R. Boussarie and Y. Hatta, "QCD analysis of near-threshold quarkonium leptoproduction at large photon virtualities," Phys. Rev. D **101**, 114004 (2020).

Y. Hatta and Y. Zhao, "Parton distribution function for the gluon condensate," Phys. Rev. D **102**, 034004 (2020).

Y. Hatta, "CP-odd gluonic operators in QCD spin physics," Phys. Rev. D **102**, 094004 (2020).

Y. Hatta, B. Xiao, F. Yuan, and J. Zhou, "Anisotropy in dijet production in exclusive and inclusive processes," Phys. Rev. Lett. **126**, 142001 (2021).

Y. Hatta and T. Ueda, "Non-global logarithms in hadron collisions at $N_c = 3$," Nucl. Phys. B **962**, 115273 (2021).

Y. Hatta, "Nucleon electric dipole moment from polarized deep inelastic scattering," Phys. Lett. B **814**, 136126 (2021).

Y. Hatta and M. Strikman, "ϕ-meson leptoproduction near threshold and the strangeness D-term," Phys. Lett. B **817**, 136295 (2021).

N. Bao and Y. Kikuchi, "Hayden-Preskill decoding from noisy Hawking radiation," J. High Energy Phys. **2021**, 17 (2021).

K. Ikeda, D. Kharzeev, and Y. Kikuchi, "Real-time dynamics of Chern-Simons fluctuations near a critical point," Phys. Rev. D **103**, L071502 (2021).

L. Gao, S. Kaushik, D. Kharzeev, and E. Philip, "Chiral kinetic theory of anomalous transport induced by torsion," arXiv.2010.07123 [cond-mat], (2020).

D. Kharzeev, "The mass radius of the proton," arXiv.2102.00110 [hep-ph] (2021).

M. Buzzegoli and D. Kharzeev, "Anomalous gravitomagnetic moment and non-universality of the axial vortical effect at finite temperature," arXiv.2102.01676 [hep-th] (2021).

D. Kharzeev and E. Levin, "Deep inelastic scattering as a probe of entanglement: confronting experimental data," arXiv.2102.09773 [hep-ph] (2021).

R. Boussarie and Y. Mehtar-Tani, "A novel formulation of the unintegrated gluon distribution for DIS," arXiv.2006.14569 [hep-ph] (2020).

J. Barata, Y. Mehtar-Tani, and A. Soto-Ontoso, "Revisiting transverse momentum broadening in dense QCD media," arXiv.2009.13667 [hep-ph] (2020).

Y. Mehtar-Tani, D. Pablos, and K. Tywoniuk, "Cone size dependence of jet suppression in heavy-ion collisions," arXiv.2101.01742 [hep-ph] (2021).

R. Boussarie and Y. Mehtar-Tani, "Gauge invariance of transverse momentum dependent distributions at small-x," Phys. Rev. D **103**, 094012 (2021).

M. Li and V. Skokov, "First saturation correction in high energy proton-nucleus collisions: I. Time evolution of classical Yang-Mills fields beyond leading order," arXiv.2102.01594 (2021).

T. Altinoluk, N. Armesto, A. Kovner, M. Lublinsky, and V. Skokov, "Angular correlations in pA collisions from CGC: multiplicity and mean transverse momentum dependence of v_2," arXiv.2012.01810 [hep-ph] (2020).

A. Behtash, S. Kamata, M. Martinez, A. Schafer, and V. Skokov, "Transasymptotics and hydrodynamization of the Fokker-Planck equation for gluons," Phys. Rev. D **103**, 056010 (2021).

A. Dumitru and V. Skokov, "An incorrect pre-asymptotic RG flow of scattering amplitudes in QCD towards the unitarity limit," arXiv.2010.03015 [hep-ph] (2020).

A. Connelly, G. Johnson, F. Rennecke, and V. Skokov, "Universal location of the Yang-Lee edge singularity in O(N) theories," Phys. Rev. Lett. **125**, 19 (2020).

C. Cheng and C. Shen, "Exploring theoretical uncertainties in the hydrodynamic description of heavy-ion collisions," arXiv.2103.09848 [nucl-th] (2021).

W. Serenone, J. Barbon, D. Chinellato, M. Lisa, and C. Shen, "Lambda polarization from thermalized jet energy," arXiv.2102.11919 [hep-ph] (2021).

M. Lisa, J. Barbon, D. Chinellato, W. Serenone, C. Shen, J. Takahashi, and G. Torrieri, "Vortex rings from high energy central pA collisions," arXiv.2101.10872 [hep-ph] (2021).

W. Zhao, C. Shen, C. Ko, Q. Liu, and H. Song, "Beam-energy dependence of the production of light nuclei in Au + Au collisions," Phys. Rev. C **102**, 044912 (2020).

D. Oliinychenko, C. Shen, and V. Koch, "Deuteron production in AuAu collisions at $\sqrt{s}$ = 7–200 GeV via pion catalysis," Phys. Rev. C **103**, 034913 (2021).

G. Giacalone, B. Schenke, and C. Shen, "Observable signature of initial state momentum anisotropies in nuclear collisions," Phys. Rev. Lett. **125**, 192391 (2020).

B. Schenke, C. Shen, and P. Tribedy, "Running the gamut of high energy nuclear collisions," Phys. Rev. C **102**, 044905 (2020).

B. Schenke, C. Shen, and D. Teaney, "Transverse momentum fluctuations and their correlation with elliptic flow in nuclear collision," Phys. Rev. C **102**, 034905 (2020).

V. Cirigliano, W. Dekens, J. de Vries, M. Hferichter, and E. Mereghetti, "Towards complete leading-order predictions for neutrinoless double β decay," Phys. Rev. Lett. **126**, 172002 (2021).

J. de Vries, H. Dreiner, J. Gunther, Z. Wang, and G. Zhou, "Long-lived sterile neutrinos at the LHC in effective field theory," J. High Energy Phys. **2021**, 148 (2021).

J. de Vries, A. Gnech, and S. Shain, "Renormalization of CP-violating nuclear forces," Phys. Rev. C **103**, L012501 (2021).

V. Cirigliano, W. Dekens, J. de Vries, M. Hoferichter, and E. Mereghetti, "Determining the leading-rder contact term in neutrinoless double beta decay," arXiv.2102.03371 [nucl-th] (2021).

[Review Articles]

D. Kharzeev and J. Liao, "Chiral magnetic effect reveals the topology of gauge fields in heavy-ion collisions," Nat. Rev. Phys. **3**, 55 (2021).

A. Monnai, B. Schenke, and C. Shen, "QCD equation of state at finite chemical potentials for relativistic nuclear collisions," Int. J. Mod. Phys. A **36**, 2130007 (2021).

C. Shen and L. Yan, "Recent development of hydrodynamic modeling in heavy-ion collisions," Nucl. Sci. Tech. **31**, 122 (2020).

Presentations

[International Conferences/Workshops]

Y. Hatta (invited), "Use of Wigner/GTMD at the EIC," Jet Observables at the Electron-Ion Collider, RIKEN BNL Center Workshop, BNL, July 27–29, 2020.

Y. Hatta (invited), "QCD Wigner distribution," QCD with Electron-Ion Collider, IIT, Bombay, India, January 4–7, 2020.

Y. Hatta (invited), "Quarkonium photo- and lepto-production near threshold," 3rd Proton Mass Workshop, Argonne National Lab, January 14–16, 2021.

Y. Hatta (invited), "Quarkonium production near threshold," Open Questions in Photon-Induced Interactions, CFNS Workshop, April 26–28, 2021.

D. Kharzeev (invited), "Chirality: a theoretical overview," Chirality and Criticality Workshop, INT, Seattle, May 11–22, 2020.

D. Kharzeev (invited), "The Chiral Qubit: quantum computing with Dirac/Weyl semimetals," APS Users Meeting, ANL, August 27–28, 2020.

D. Kharzeev (invited), "Mass radius of the proton," Deep Inelastic Scattering Conference, Stony Brook, April 12–16, 2021.

D. Kharzeev (invited), "Semiclassical description of chiral anomaly with real and synthetic gauge fields," Gravity and Emergent Gauge Fields Workshop, ITP Mainz, April 12–23, 2021.

C. Shen (invited), "Dynamical modeling of the collectivity in pO and OO collisions," Opportunities of OO and pO Collisions at the LHC,

CERN, Febuary 5, 2021.

V. Skokov (invited), "Universality driven analytic structure of QCD crossover," International Workshop "FunQCD: from first principles to effective theories," March 29–April1, 2021.

V. Skokov (invited), "Universality driven analytic structure of QCD crossover," XXXII International (online) Workshop on High Energy Physics, "Hot problems of strong interactions," November 9–13, 2020.

V. Skokov (invited), "Saturation corrections to dilute-dense particle production in the color glass condensate," RHIC&AGS User's Group Meeting, October 22, 2020.

V. Skokov (invited), "Universality driven analytic structure of QCD crossover: radius of convergence in baryon chemical potential," Rice University & University of Illinois at Urbana-Champaign, June 15, 2020.

Y. Kikuchi, "Real-time chiral dynamics from a digital quantum simulation," The 2020 Fall Meeting of the Division of Nuclear Physics of the American Physical Society, October 29–November 1, 2020.

[Seminars]

Y. Hatta, "QCD trace anomaly and proton mass problem," University of Kentucky, October 20, 2020.

Y. Hatta, "Two topics in QCD spin," Kyoto University, November 20, 2020.

Y. Hatta, "Probing the Wigner distribution at the electron-ion collider," Tata Institute of Fundamental Research, July 23, 2020.

D. Kharzeev, "Chiral magnetic effect: from quarks to quantum computers," INT Colloquium, March 18, 2021.

V. Skokov, "Analytic structure of QCD crossover," Seminar Physics Department, Ben-Gurion University of the Negev, April 19, 2021.

C. Shen, "Dynamical modeling of the initial energy-momentum and baryon charge distributions for heavy-ion collisions," LBL HIT Seminar, March 2, 2021.

C. Shen, "Multi-messenger heavy-ion physics," Invited Physics Colloquium, ASU Theoretical Physics Colloquium, March 31, 2021.

C. Shen, "Observable signature of initial state momentum anisotropies in nuclear collisions," Nuclear Seminar, the ALICE Collaboration, December 8, 2020.

C. Shen, "Dynamical modeling of relativistic heavy-ion collision at beam energy scan energies," The 4th RHIC-BES Theory and Experiment Online Seminar, August 25, 2020.

Subnuclear System Research Division
RIKEN BNL Research Center
Experimental Group

1. Abstract

RIKEN BNL Research Center (RBRC) Experimental Group studies the strong interactions (QCD) using RHIC accelerator at Brookhaven National Laboratory, the world first heavy ion collider and polarized $p + p$ collider. We have three major activities: Spin Physics at RHIC, Heavy ion physics at RHIC, and detector upgrades of PHENIX experiment at RHIC.

We study the spin structure of the proton using the polarized proton-proton collisions at RHIC. This program has been promoted by RIKEN's leadership. The first focus of the research is to measure the gluon spin contribution to the proton spin. Recent results from PHENIX π^0 measurement and STAR jet measurement has shown that gluons in the proton carry about 30% of the proton spin. This is a major milestone of RHIC spin program. The second goal of the spin program is to measure the polarization of anti-quarks in the proton using $W \to e$ and $W \to \mu$ decays. The results of $W \to e$ measurement was published in 2016. The final results of $W \to \mu$ was published in 2018.

The aim of Heavy ion physics at RHIC is to re-create Quark Gluon Plasma (QGP), the state of Universe just after the Big Bang. Two important discoveries, jet quenching effect and strong elliptic flows, have established that new state of dense matter is indeed produced in heavy ion collisions at RHIC. We are now studying the property of the matter. Recently, we have measured direct photons in Au + Au collisions for $1 < p_{\mathrm{T}} < 3$ GeV/c, where thermal radiation from hot QGP is expected to dominate. The comparison between the data and theory calculations indicates that the initial temperature of 300 MeV to 600 MeV is achieved. These values are well above the transition temperature to QGP, which is calculated to be approximately 160 MeV by lattice QCD calculations.

We had major roles in detector upgrades of PHENIX experiment, namely, the silicon vertex tracker (VTX) and muon trigger upgrades. Both of the upgrade is now complete. The VTX is the main device to measure heavy quark (charm and bottom) production and the muon trigger is essential for $W \to \mu$ measurement. The results from the first run with VTX detector in 2011 was published. The results show that electrons from bottom quark decay is strongly suppressed at high p_{T}, but the suppression is weaker than that of charm decay electron for $3 < p_{\mathrm{T}} < 4$ GeV/c. We have recorded 10 times as much Au + Au collisions data in each of the 2014 run and 2016 run. The large dataset will produce definitive results on heavy quark production at RHIC.

PHENIX completed its data taking in 2016. We are now working on R&D of intermediate silicon tracker INTT for sPHENIX, a new experiment at RHIC that will be installed in the PHENIX IR.

2. Major Research Subjects

(1) Experimental Studies of the Spin Structure of the Nucleon
(2) Study of Quark-Gluon Plasma at RHIC
(3) sPHENIX INTT detector

3. Summary of Research Activity

We study the strong interactions (QCD) using the RHIC accelerator at Brookhaven National Laboratory, the world first heavy ion collider and polarized $p + p$ collider. We have three major activities: Spin Physics at RHIC, Heavy ion physics at RHIC, and detector upgrades of PHENIX experiment. From 2016, Y. Akiba (Experimental Group Leader) is the Spokesperson of PHENIX experiment.

(1) Experimental study of spin structure of proton using RHIC polarized proton collider

How is the spin of proton formed with 3 quarks and gluons? This is a very fundamental question in Quantum Chromodynamics (QCD), the theory of the strong nuclear forces. The RHIC Spin Project has been established as an international collaboration between RIKEN and Brookhaven National Laboratory (BNL) to solve this problem by colliding two polarized protons for the first time in history. This project also has extended the physics capabilities of RHIC.

The first goal of the Spin Physics program at RHIC is to determine the gluon contribution to proton spin. It is known that the spin of quark accounts for only 25% of proton spin. The remaining 75% should be carried either by the spin of gluons or the orbital angular momentum of quarks and gluons. One of the main goals of the RHIC spin program has been to determine the gluon spin contribution. Before the start of RHIC, there was little experimental constraint on the gluon polarization, ΔG.

PHENIX measures the double helicity asymmetry (A_{LL}) of π^0 production to determine the gluon polarization. Our most recent publication of $\pi^0 A_{LL}$ measurement at 510 GeV shows non-zero value of A_{LL}, indicating that gluons in the proton is polarized. Global analysis shows that approximately 30% of proton spin is carried by gluons.

Figure 1 and Fig. 2 shows most recent spin physics measurement with PHENIX from our group. Figure 1 show the A_{LL} of charged pions in polarized $p + p$ collisions at $\sqrt{s} = 510$ GeV and Fig. 2 shows $A_N(p_T)$ of very forward neutron. These results are published in Physical Review D.

Members of our group also participate in RHICf experiment, a small experiment at RHIC to measure particle production and single spin asymmetry of particles produced at very forward direction. Figure 3 shows $A_N(x_F)$ of very forward π^0 measured by RHICf compared with other experiments, published in Physical Review Letters. This is the first published results of RHICf experiment.

(2) Experimental study of Quark-Gluon Plasma using RHIC heavy-ion collider

The goal of high energy heavy ion physics at RHIC is study of QCD in extreme conditions *i.e.* at very high temperature and at

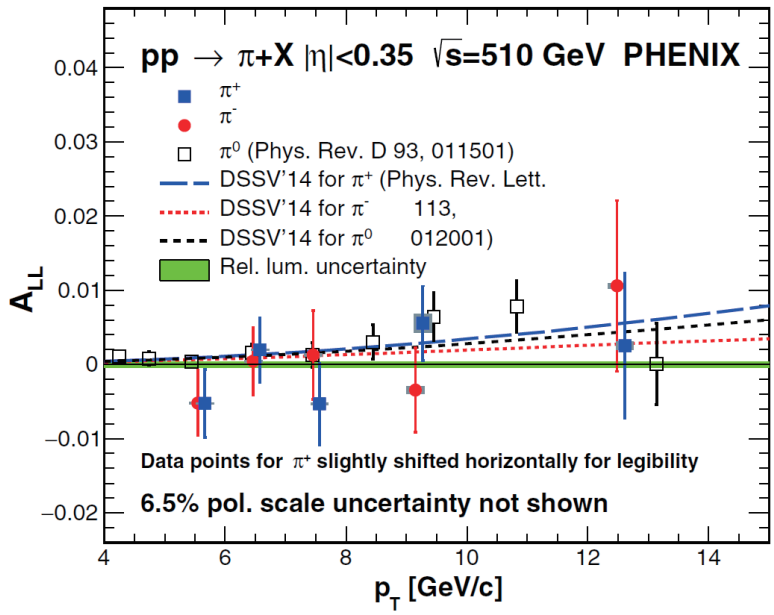

Fig. 1. Double spin asymmetry A_{LL} of charged pions in midrapidity in $p+p$ collisions at $\sqrt{5}$ = 510 GeV compared with theoretical predictions of perturbative QCD. Published in Phys. Rev. D 102, 032001 (2020).

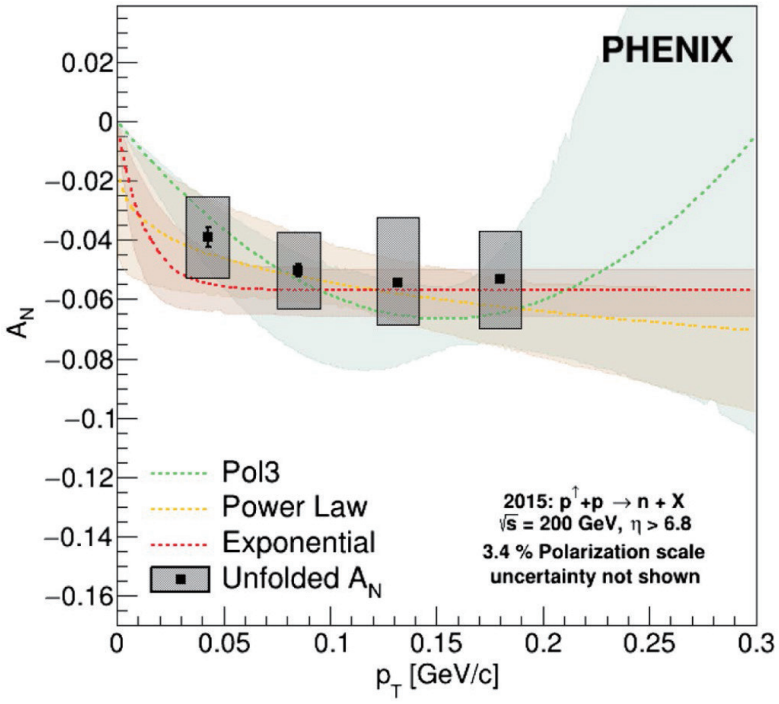

Fig. 2. Pt dependence of single spin asymmetry A_N of very forward neutron in $p+p$. Published in Phys. Rev. D 103, 032007 (2021).

very high energy density. Experimental results from RHIC have established that dense partonic matter is formed in Au + Au collisions at RHIC. The matter is very dense and opaque, and it has almost no viscosity and behaves like a perfect fluid. These conclusions are primarily based on the following two discoveries:

- Strong suppression of high transverse momentum hadrons in central Au + Au collisions (jet quenching)
- Strong elliptic flow

These results are summarized in PHENIX White paper, which has more than 3000 citations to date. The focus of the research in heavy ion physics at RHIC is now to investigate the properties of the matter. RBRC have played the leading roles in some of the most

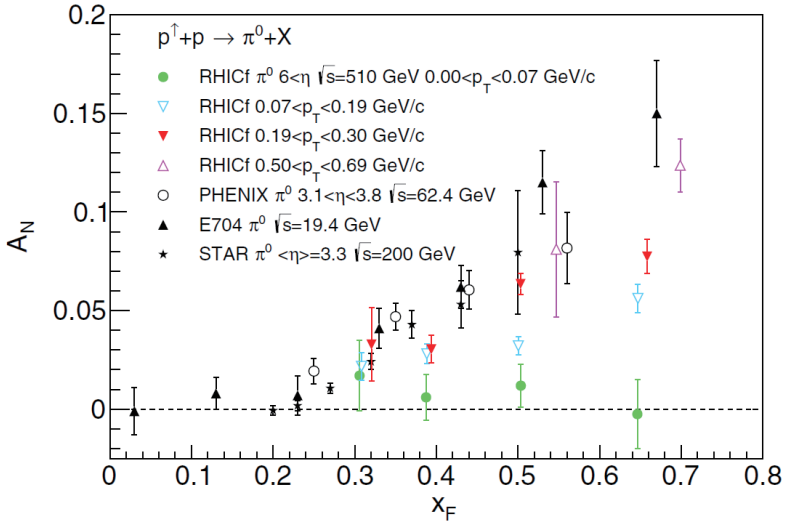

Fig. 3. $A_N(x_F)$ of very forward π^0 measured by RHICf experiment is compared with other data. Published in Phys. Rev. Lett. 124, 252501 (2020).

important results from PHENIX in the study of the matter properties. These include (1) measurements of heavy quark production from the single electrons from heavy flavor decay (2) measurements of J/Ψ production (3) measurements of di-electron continuum and (4) measurements of direct photons.

Our most important result is the measurement of direct photons for $1 < p_T < 5$ GeV/c in $p+p$ and Au + Au through their internal conversion to $e+e^-$ pairs. If the dense partonic matter formed at RHIC is thermalized, it should emit thermal photons. Observation of thermal photon is direct evidence of early thermalization, and we can determine the initial temperature of the matter. It is predicted that thermal photons from QGP phase is the dominant source of direct photons for $1 < p_T < 3$GeV/c at the RHIC energy. We measured the direct photon in this p_T region from measurements of quasi-real virtual photons that decays into low-mass $e+e^-$ pairs. Strong enhancement of direct photon yield in Au + Au over the scaled $p+p$ data has been observed. Several hydrodynamical models can reproduce the central Au + A data within a factor of two. These models assume formation of a hot system with initial temperature of $T_{\rm init}$ = 300 MeV to 600 MeV. This is the first measurement of initial temperature of quark gluon plasma formed at RHIC. Y. Akiba received 2011 Nishina memorial Prize mainly based on this work.

PHENIX experiment recently measured the flow in small collision systems (p + Au, d + Au, and ^{3}He + Au), and observed strong flow in all of these systems. Theoretical models that assume formation of small QGP droplets best describe the data. These results are published in Nature Physics in 2019.

(3) sPHENIX INTT detector

The group had major roles in several PHENIX detector upgrades, namely, the silicon vertex tracker (VTX) and muon trigger upgrades. VTX is a high precision charged particle tracker made of 4 layers of silicon detectors. It is jointly funded by RIKEN and the US DOE. The inner two layers are silicon pixel detectors and the outer two layers are silicon strip detectors. Y. Akiba is the project manager and A. Deshpande is the strip system manager. The VTX detector was completed in November 2010 and subsequently installed in PHENIX. The detector started taking data in the 2011 run. With the new detector, we measure heavy quark (charm and bottom) production in $p+p$, A + A collisions to study the properties of quark-gluon plasma. The final result of the 2011 run was published. The result show that single electrons from bottom quark decay is suppressed, but not as strong as that from charm decay in low p_T region ($3 < p_T < 4$ GeV/c). This is the first measurement of suppression of bottom decay electrons at RHIC and the first observation that bottom suppression is smaller than charm. We have recorded 10 times as much Au + Au collisions data in each of the 2014 run and 2016 run. The large dataset will produce definitive results on heavy quark production at RHIC. A preliminary results on the elliptic flow strength v_2 of $b \to e$ and $c \to e$ has been presented in Quark Matter 2018 conference. The results of bottom/charm ratios in $p+p$ collisions at 200 GeV from the 2015 run was published (Phys. Rev. D 99 092003 (2019)). A paper reporting measurements of the nuclear suppression factor R_{AA} of charm and bottom in Au + Au collisions from the 2014 data is in preparation.

PHENIX completed its data taking in 2016. We are now working on construction of intermediate silicon tracker INTT for sPHENIX, a new experiment at RHIC that will start taking data in 2023. Figure 4 shows snapshot of INTT construction work. INTT consists of 56 ladders of silicon detector. So far approximately 30 ladders are produced. INTT will be completed in JFY2021.

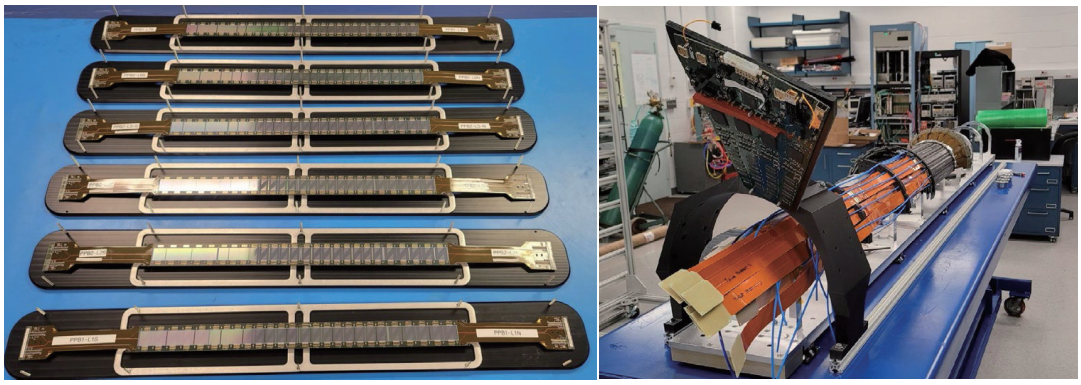

Fig. 4. Left panel shows completed INTT ladders. Right panel shows the test assembly of a half barrel of INTT detector.

Members

Group Leader

Yasuyuki AKIBA

RBRC Researchers

Jan C. BERNAUER
Megan CONNORS
Yuji GOTO
Takashi HACHIYA
Itaru NAKAGAWA
Genki NUKAZUKA
Ralf SEIDL
Atsushi TAKETANI
Takahito TODOROKI
Yasushi WATANABE
Satoshi YOKKAICHI

Special Postdoctoral Researcher

Minho KIM

Special Temporary Research Scientist

Takashi ICHIHARA

Visiting Scientists

Stefan BATHE (Baruch College Univ. of New York)
Gaku MITSUKA (KEK)
Rachid NOUICER (BNL)
Masahiro OKAMURA (BNL)
Takao SAKAGUCHI (BNL)
Takashi SAKO (Univ. of Tokyo)
Milan STOJANOVIC (Purdue Univ.)

Visiting Technician

Li-Hsin HSU (Nat'l Central Univ.)

Student Trainees

Kai-Yu CHENG (Nat'l Central Univ.)
Anthony HODGES (Georgia State Univ.)
Han-Sheng LI (Purdue Univ.)
Lihan LIU (Vanderbilt Univ.)
Xiao RUI (Purdue Univ.)
Cheng Wei SHIH (Nat'l Central Univ.)
Cheuk-Ping WONG (Georgia State Univ.)

List of Publications & Presentations

Publications

[Original Papers]

U. A. Acharya *et al.*, "Transverse sngle-spn asymmetries of midrapidty π^0 and η mesons in polarized $p + p$ collisions at $\sqrt{s} = 200$ GeV," Phys. Rev. D **103**, 052009 (2021).

U. A. Acharya *et al.*, "Transverse momentum dependent forward neutron ssingle spin asymmetries in transversely polarized $p+$ collisions at $\sqrt{s} = 200$ GeV," Phys. Rev. D **103**, 032007 (2021).

U. A. Acharya *et al.*, "Nuclear dependence of the transverse single-spin asymmetry in the production of π^0 and η mesons in U+U collisions at $\sqrt{s_{NN}} = 192$ GeV," Phys. Rev. C **102**, 064905 (2020).

A. Adare *et al.*, "Production of $b\bar{b}$ at forward rapidity in $p + p$ collisions at $\sqrt{s} = 510$ GeV," Phys. Rev. D **102**, 092002 (2020).

U. A. Acharya *et al.*, "Polarization and cross section of J/ψ production in $p + p$ collisions at $\sqrt{s} = 510$ GeV," Phys. Rev. D **102**, 072008 (2020).

M. H. Kim *et al*., "Transverse single-pin aymmetry for very forward neutral pion production in polarized $p+p$ collisions at $\sqrt{s}$ = 510 GeV," Phys. Rev. Lett. **124**, 252501 (2020).

U. A. Acharya *et al*., "Measurement of jet-medium nteractinos via direct photon-hadron correlations in Au + Au and d + Au collisions at $\sqrt{s_{NN}}$ = 200 GeV," Phys. Rev. C **102**, 054910 (2020).

U. A. Acharya *et al*., "Measurement of charged pion double spin asymmetries at midrapidity in longitudinally polarized $p+p$ collisions at $\sqrt{s}$ = 510 GeV," Phys. Rev. D **102**, 032001 (2020).

U. A. Acharya *et al*., "J/ψ nd $\psi(2S)$ production at forward rapidity n $p+p$ collion at $\sqrt{s}$ = 510 GeV," Phys. Rev. D **101**, 052006 (2020).

U. A. Acharya *et al*., "Measurement of J/ψ at forward and backward rapidity in p_p, p + Al, p + Au and ^{3}He + Au collisions at $\sqrt{s_{NN}}$ = 200 GeV," Phys. Rev. C **101**, 014902 (2020).

C. Aidala *et al*., "Nuclear-modification factor of charged hadrons at forward and backward rapidty in p + Al and p + Au collisions at $\sqrt{s_{NN}}$ = 200 GeV," Phys. Rev. C **101**, 034910 (2020).

Presentations

[International Conferences/Workshops]

M. Connors (poster), "Jets modification with two-particle correlations in Au+Au collisions at PHENIX," 10th international conference on Hard and Electromagnetc Probes of High Energy Nuclear Collisions (Hard Probe 2020) (Online) May 31–June 5, 2020.

T. Hachiya (poster), "PHENIX results on quark flavor dependence of low in AuAu colliisions," 10th international conference on Hard and Electromagnetc Probes of High Energy Nuclear Collisions (Hard Probe 2020) (Online) May 31–June 5, 2020.

Press Releases

New research deepens mystery of particle generation in proton collisions, RIKEN, June 23, 2020.

Subnuclear System Research Division
RIKEN BNL Research Center
Computing Group

1. Abstract

The computing group founded in 2011 as a part of the RIKEN BNL Research Center established at Brookhaven National Laboratory in New York, USA, and dedicated to conduct researches and developments for large-scale physics computations important for particle and nuclear physics. The group was forked from the RBRC Theory Group.

The main mission of the group is to provide important numerical information that is indispensable for theoretical interpretation of experimental data from the first principle theories of particle and nuclear physics. Their primary area of research is lattice quantum chromodynamics (QCD), which describes the sub-atomic structures of hadrons, which allow us the ab-initio investigation for strongly interacting quantum field theories beyond perturbative analysis.

The RBRC group and its collaborators have emphasized the necessity and importance of precision calculations, which will precisely check the current understandings of nature, and will have a potential to find a physics beyond the current standard model of fundamental physics. We have therefore adopted techniques that aim to control and reduce any systematic errors. This approach has yielded many reliable results.

The areas of the major activities are R&D for high performance computers, developments for computing algorithms, and researches of particle, nuclear, and lattice theories. Since the inception of RBRC, many breakthroughs and pioneering works has carried out in computational forefronts. These are the use of the domain-wall fermions, which preserve chiral symmetry, a key symmetry for understanding nature of particle nuclear physics, the three generations of QCD devoted supercomputers, pioneering works for QCD calculation for Cabibbo-Kobayashi-Maskawa theory, QCD + QED simulation for isospin breaking, novel algorithm for error reduction in general lattice calculation. Now the chiral quark simulation is performed at the physical up, down quark mass, the precision for many basic quantities reached to accuracy of sub-percent, and the group is aiming for further important and challenging calculations, such as the full and complete calculation of CP violating $K \to \pi\pi$ decay and ε'/ε, or hadronic contributions to muon's anomalous magnetic moment $g-2$. Another focus area is the nucleon's shape, structures, and the motion of quarks and gluon inside nucleon called parton distribution, which provide theoretical guidance to physics for sPHENIX and future Electron Ion Collider (EIC), Hyper Kamiokande, DUNE, or the origin of the current matter rich universe (rather than anti-matter). Towards finite density QCD, they also explore Quantum Computing to overcome the sign problem. The Machine Learning (ML) and Artificial Intelligence (AI) are the new topics some of members are enthusiastically studying lately.

2. Major Research Subjects

(1) Search for new law of physics through tests for Standard Model of particle and nuclear physics, especially in the framework of the Cabibbo-Kobayashi-Maskawa (CKM), hadronic contributions to the muon's anomalous magnetic moment $(g-2)$ for FNAL and J-PARC's experiments, as well as B physics at Belle II and LHCb.
(2) Nuclear Physics and dynamics of QCD or related theories, including study for the structures of nucleons related to physics for Electron Ion Collider (EIC or eRHIC), Hyper Kamiokande, T2K, DUNE.
(3) Theoretical and algorithmic development for lattice field theories, QCD machine (co-)design and code optimization.

3. Summary of Research Activity

In 2011, QCD with Chiral Quarks (QCDCQ), a third-generation lattice QCD computer that is a pre-commercial version of IBM's Blue Gene/Q, was installed as an in-house computing resource at the RBRC. The computer was developed by collaboration among RBRC, Columbia University, the University of Edinburgh, and IBM. Two racks of QCDCQ having a peak computing power of 2×200 TFLOPS are in operation at the RBRC. In addition to the RBRC machine, one rack of QCDCQ is owned by BNL for wider use for scientific computing. In 2013, 1/2 rack of Blue Gene/Q is also installed by US-wide lattice QCD collaboration, USQCD. The group has also used the IBM Blue Gene supercomputers located at Argonne National Laboratory and BNL (NY Blue), and Hokusai and RICC, the super computers at RIKEN (Japan), Fermi National Accelerator Laboratory, the Jefferson Lab, and others. From 2016, the group started to use the institutional cluster both GPU and Intel Knight Landing (KNL) clusters installed at BNL and University of Tokyo extensively.

Such computing power enables the group to perform precise calculations using up, down, and strange quark flavors with proper handling of the important symmetry, called chiral symmetry, that quarks have. The group and its collaborators carried out the first calculation for the direct breaking of CP (Charge Parity) symmetry in the hadronic K meson decay ($K \to \pi\pi$) amplitudes, ε'/ε, which provide a new information to CKM paradigm and its beyond. They also provide the hadronic contribution in muon's anomalous magnetic moment $(g-2)_\mu$. These calculation for ε'/ε, hadronic light-by-light of $(g-2)$, are long waited calculation in theoretical physics delivered for the first time by the group. The $K \to \pi\pi$ result in terms of ε'/ε currently has a large error, and deviates from experimental results by 2.1σ. To collect more information to decide whether this deviation is from the unknown new physics or not, the group continues to improve the calculation in various way to reduce their error. Hadronic light-by-light contribution to $(g-2)_\mu$ is improved by more than two order of magnitudes compared to our previous results. As of 2019 summer, their calculation is among the most precise determination for the $g-2$ hadronic vacuum polarization (HVP), and only one calculation in the world for the hadronic light-by-light (HLbL) contribution at physical point. These $(g-2)_\mu$ calculations provide the first principle theoretical prediction for on-going new experiment at FNAL and also for the planned experiment at J-PARC. Other projects including flavor physics in the framework of the

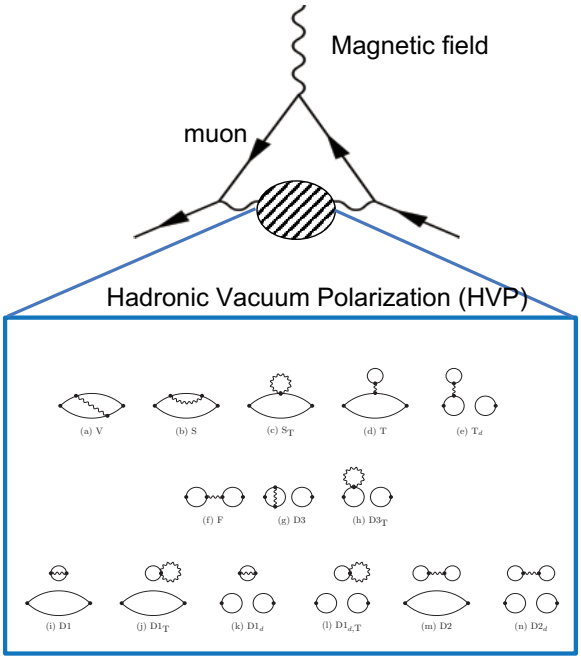

Fig. 1. Feynman diagrams for Lattice QCD computations of Muon's anomalous magnetic moment $(g-2)_\mu$ to take into account for the effects of quark's electric charges. Each diagram, in which the black dots connecting the quark propagators (solid curves) are the electric current emmitting or absorbing photons (wave curves), represents a part of the isospin breaking effects to hadronic vacuum polarization contribution to $(g-2)_\mu$ (top plot).

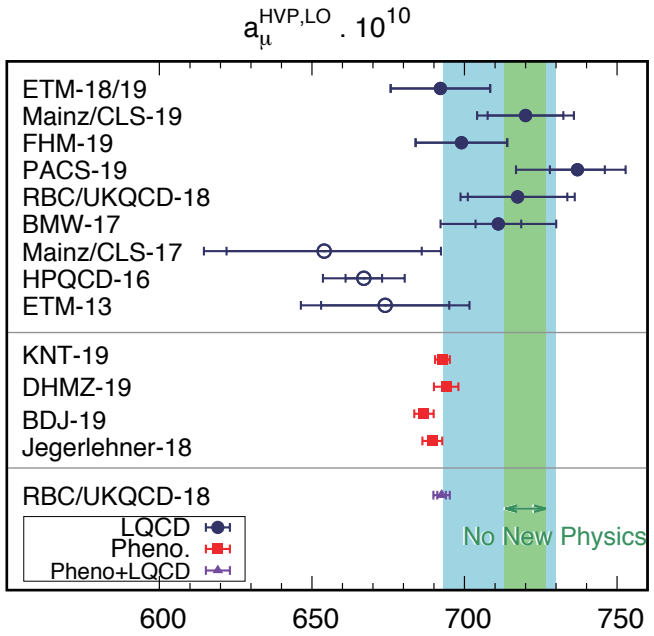

Fig. 2. Current summary of the Hadronic Vacuum Polarization (HVP) contribution for Muon's anomalous magnetic moment $(g-2)_\mu$. Above the upper horizontal line shows various Lattice QCD determinations of HVP while the red results from hadronic decay of electron positron scattering (R-ratio), the green bands is the experimental results of $(g-2)_\mu$ showing a 3–4σ discrepancies.

CKM theory for kaons and B mesons that include the new calculation of b-baryon decay, $\Lambda_b \to p$; the electromagnetic properties of hadrons; the proton's and neutron's form factors and structure function including electric dipole moments; proton decay; nucleon form factors, which are related to the proton spin problem or neutrino-nucleon interaction; Neutron-antineutron oscillations; inclusive hadronic decay of τ leptons; nonperturbative studies for beyond standard model such composite Higgs or dark matter models from strong strongly interacting gauge theories; a few-body nuclear physics and their electromagnetic properties; QCD thermodynamics in finite temperature/density systems such as those produced in heavy-ion collisions at the Relativistic Heavy Ion Collider; Quantum Information, Quantum Computing; and applications of Machine Learning (ML) in field theories.

The RBRC group and its collaborators have emphasized the necessity and importance of precision calculations, which will provide stringent checks for the current understandings of nature, and will have a potential to find physics beyond the current standard model of fundamental physics. We have therefore adopted techniques that aim to control and reduce any systematic errors. This approach has yielded many reliable results, many of basic quantities are now computed within sub-percent accuracies.

The group also delivers several algorithmic breakthroughs, which speed up generic lattice gauge theory computation. These novel technique divides the whole calculation into frequent approximated calculations, and infrequent expensive and accurate calculation using lattice symmetries called All Mode Averaging (AMA), or a compression for memory needs by exploiting the local-coherence of QCD dynamics. Together with another formalism, zMobius fermion, which approximate chiral lattice quark action efficiently, the typical calculation is now improved by a couple of orders of magnitudes, and more than an order of magnitude less memory needs compared to the traditional methods. RBRC group and its collaborators also provide very efficient and generic code optimized to the state-of-arts CPU or GPU, and also improve how to efficiently generate QCD ensemble.

Members

Group Leader
Taku IZUBUCHI

Special Postdoctoral Researchers
Akio TOMIYA

RBRC Researchers

Sergey SYRITSYN
Luchang JIN

Visiting Scientists

Thomas BLUM (Univ. of Connecticut)
Chulwoo JUNG (BNL)
Shigemi OHTA (KEK)
Tomomi ISHIKAWA (Shanghai Jiao-Tong Univ.)
Christoph LEHNER (BNL)
Meifeng LIN (BNL)
Robert MAWHINNEY (Columbia Univ.)
Hiroshi OKI (Nara Women's Univ.)
Christopher KELLY (Columbia Univ.)

List of Publications & Presentations

Publications

[Original Papers]

M. Abramczyk, T. Blum, T. Izubuchi, C. Jung, M. Lin, A. Lytle, S. Ohta, E. Shintani, "Nucleon mass and isovector couplings in 2 + 1-flavor dynamical domain-wall lattice QCD near physical mass," Phys. Rev. D **101**, no.3, 034510 (2020).

T. Izubuchi, L. Jin, C. Kallidonis, N. Karthik, S. Mukherjee, P. Petreczky, C. Shugert, S. Syritsyn, "Valence parton distribution function of pion from fine lattice," Phys. Rev. D **100**, 034516 (2019).

N. H. Christ, X. Feng, L. C. Jin, C. T. Sachrajda, "Finite-volume effects in long-distance processes with massless leptonic propagators," Phys. Rev. D **103**, 014507 (2021).

Y. Li, S. C. Xia, X. Feng, L. C. Jin, C. Liu, "Field sparsening for the construction of the correlation functions in lattice QCD," Phys. Rev. D **103**, 014514 (2021).

C. Y. Seng, X. Feng, M. Gorchtein, L. C. Jin, U. G. Meißner, "New method for calculating electromagnetic effects in semileptonic beta-decays of mesons," J. High Energy Phys. **10**, 179 (2020).

X. Gao, L. Jin, C. Kallidonis, N. Karthik, S. Mukherjee, P. Petreczky, C. Shugert, S. Syritsyn, Y. Zhao, "Valence parton distribution of the pion from lattice QCD: Approaching the continuum limit," Phys. Rev. D **102**, 094513 (2020).

X. Feng, L. C. Jin, Z. Y. Wang, Z. Zhang, "Finite-volume formalism in the $2 \xrightarrow{H_I+H_I} 2$ transition: An application to the lattice QCD calculation of double beta decays," Phys. Rev. D **103**, 034508 (2021).

R. Abdul Khalek *et al.*, "Science Requirements and Detector Concepts for the Electron-Ion Collider: EIC Yellow Report," arXiv:2103.05419 [physics.ins-det].

X. Gao, N. Karthik, S. Mukherjee, P. Petreczky, S. Syritsyn, Y. Zhao, "Pion form factor and charge radius from Lattice QCD at physical point," arXiv:2102.06047 [hep-lat].

X. Gao, N. Karthik, S. Mukherjee, P. Petreczky, S. Syritsyn, Y. Zhao, "Towards studying the structural differences between the pion and its radial excitation," Phys. Rev. D **103**, 094510 (2021).

G. Silvi, S. Paul, C. Alexandrou, S. Krieg, L. Leskovec, *et al*., "P-wave nucleon-pion scattering amplitude in the $\Delta(1232)$ channel from lattice QCD," Phys. Rev. D **103**, 094508 (2021).

M. Yu. Barabanov, M. A. Bedolla, W. K. Brooks, G. D. Cates, C. Chen, *et al*., "Diquark correlations in hadron physics: Origin, impact and evidence," Prog. Part. Nucl. Phys. **116**, 103835 (2021).

M. Engelhardt, J. R. Green, N. Hasan, S. Krieg, S. Meinel, J. Negele, A. Pochinsky, S .Syritsyn, "From Ji to Jaffe-Manohar orbital angular momentum in lattice QCD using a direct derivative method," Phys. Rev. D **102**, 074505 (2020).

G. Rendon, L. Leskovec, S. Meinel, J. Negele, S. Paul, *et al*., "$I = 1/2$ S-wave and P-wave $K\pi$ scattering and the κ and K^* resonances from lattice QCD," Phys. Rev. D **102**, 114520 (2020).

Z. Fan, X. Gao, R. Li, H. -W. Lin, N. Karthik, *et al*., "Isovector parton distribution functions of the proton on a superfine lattice," Phys. Rev. D **102**, 074504 (2020).

H. T. Ding, S. T. Li, Swagato Mukherjee, A. Tomiya, X. D. Wang, Y. Zhang, "Correlated Dirac eigenvalues and axial anomaly in chiral symmetric QCD," Phys. Rev. Lett. **126**, 082001 (2021).

M. Kawaguchi, S. Matsuzaki, A. Tomiya, "Nonperturbative flavor breaking in topological susceptibility at hot QCD criticality," Phys. Lett. B **813**, 136044 (2021).

H. -T. Ding, C. Schmidt, A. Tomiya, X. -D. Wang, "Chiral phase structure of three flavor QCD in a background magnetic field," Phys. Rev. D **102**, 054505 (2020).

B. Chakraborty, M. Honda, T. Izubuchi, Y. Kikuchi and A. Tomiya, "Digital quantum simulation of the Schwinger model with topological term via adiabatic state preparation," arXiv:2001.00485 [hep-lat].

[Review Articles]

T. Aoyama, N. Asmussen, M. Benayoun, J. Bijnens, T. Blum, M. Bruno, I. Caprini, C. M. Carloni Calame, M. Cè and G. Colangelo, *et al.*, "The anomalous magnetic moment of the muon in the Standard Model," Phys. Rept. **887**, 1–166 (2020).

[Books]

Akio Tomiya, "An introduction to machine learning in physics" (in Japanese), Kodansha, March 2021.

K. Hashimoto, A. Tanaka, A. Tomiya, "Deep learning and physics," Springer, February 2021.

[Proceedings]

T. Izubuchi, H. Ohki and S. Syritsyn, "Computing Nucleon Electric Dipole Moment from lattice QCD," PoS **LATTICE2019**, 290 (2020).

M. Bruno, T. Izubuchi, C. Lehner and A. S. Meyer, "Exclusive Channel Study of the Muon HVP," PoS **LATTICE2019**, 239 (2019)

M. Kawaguchi, S. Matsuzaki, A. Tomiya, "Analysis on nonperturbative flavor violation at chiral crossovercriticality in QCD," arXiv:2005.07003 [hep-ph].

A. Tomiya, Y. Nagai, "Gauge covariant neural network for 4 dimensional non-abelian gaugetheory," arXiv:2103.11965 [hep-lat].

M. Kawaguchi, S. Matsuzaki, A. Tomiya, "A new critical endpoint in thermomagnetic QCD," arXiv:2102.05294 [hep-ph].

Y. Nagai, A. Tanaka, A. Tomiya, "Self-learning Monte-Carlo for non-abelian gauge theory withdynamical fermions," arXiv:2010.11900 [hep-lat].

H. -T. Ding, S. -T. Li, A. Tomiya, X. -D. Wang, Y. Zhang, "Chiral properties of (2 + 1)-flavor QCD in strong magnetic fields at zerotemperature," arXiv:2008.00493 [hep-lat].

H. -T. Ding, S. -T. Li, S. Mukherjee, A. Tomiya, X. -D. Wang, "Meson masses in external magnetic fields with HISQ fermions," arXiv:2001.05322 [hep-lat].

Presentations

[International Conferences/Workshops]

L. Jin (invited), "Lattice calculations in muon $g-2$," The Hadron Mass and Structure Forum, online, April 2021.

L. Jin (invited), "Muon $g-2$: hadronic light-by-light contribution and lattice QCD," The Muon $g-2$ Discussion Forum, Peking University, online, April 2021.

L. Jin (invited), "Pion electric polarizability," the χQCD Collaboration Meeting, online, January 2021.

L. Jin (invited), "Lattice calculation of the hadronic light-by-light contribution to the muon magnetic moment," The Hadron Physics Online Forum, online, August 2020.

S. Syritsyn (invited), "Nucleon Form Factors at High Momentum Transfer from Lattice QCD," Nuclear & Particle Theory Seminar, MIT/CTP, March 9, 2020.

A. Tomiya (oral), "Self-learning Monte-Carlo for non-abelian gauge theory withdynamical fermions," APS April Meeting 2020, Virtual, April 18–21, 2020

A. Tomiya (invited), "Self-learning Monte-Carlo for non-abelian gauge theory with dynamical fermions," Workshop on Non-Equilibrium Systems and Machine Learning, Virtual, March 30, 2020.

A. Tomiya (oral), "Quantum computing for QCD phase diagram? Finite chemicalpotential and temperature?" Kickoff Meeting of C2QA Center, Virtual (BNL), October 30, 2020.

A. Tomiya (invited), "Machine learning and theoretical physics," Progress of Particle Physics 2020, Virtual (YITP), September 4, 2020.

A. Tomiya (oral), "Thermal field theory with pure states," Asia-Pacific Symposium for Lattice Field Theory (APLAT 2020), Virtual (KEK), August 6, 2020 (JST).

A. Tomiya (invited), "Applications of machine learning to computational physics," A. I. for Nuclear Physics, Virginia (Jefferson Laboratory), U.S.A., March 3, 2020.

[Domestic Conferences/Workshops]

富谷昭夫 (口頭発表), "Gauge covariant neural network for 4 dimensional non-abelian gaugetheory," 「ゲージ共変なニューラルネットと 4 次元非可換ゲージ理論への応用 (Gauge covariant neural network for 4 dimensional non-abelian gauge theory)」, Deep Learning and Physics, オンライン開催, 2020 年 4 月 8 日 (JST).

富谷昭夫 (口頭発表), 「動的フェルミオンを含む非可換ゲージ理論のための自己学習モンテカルロ法」, 日本物学会第 76 回年次大会, オンライン開催, 2021 年 3 月 12–15 日 (JST).

富谷昭夫 (招待講演), チュートリアル講演「理論物理学における機械学習の応用」, 第 5 回 統計・機械学習若手シンポジウム, オンライン開催, 2020 年 12 月 3–5 日 (JST).

富谷昭夫 (口頭発表), 「ニューラルネットを使った 2 次元イジング模型の相検出」, Deep Learning and Physics 2020, オンライン開催 (大阪大学), 2020 年 11 月 26 日 (JST).

[Seminars]

L. Jin (invited), "Lattice calculations in muon $g-2$," The Theory Seminar at the Department of Physics and Astronomy, University of California, Davis, online, May 2021.

L. Jin (invited), "Lattice calculations in muon $g-2$," The Lunch Seminar at the Institute of Theoretical Physics, Chinese Academy of Sciences, online, April 2021.

L. Jin (invited), "First-principles calculation of electroweak box diagrams from lattice QCD," The Physics Seminar in Hunan University, online, December 2020.

L. Jin (invited), "First-principles calculation of electroweak box diagrams from lattice QCD," The Theory Seminar at the Institute of Modern Physics, Chinese Academy of Sciences, online, July 2020.

L. Jin (invited), "First-principles calculation of electroweak box diagrams from lattice QCD," The BNL Nuclear Theory Seminar, online, May 2020.

L. Jin (invited), "Lattice calculation of the hadronic light-by-light contribution to the muon magnetic moment," The QCD Seminar, online, May 2020.

S. Syritsyn (invited), "From quarks and gluons to nucleons and nuclei," Seminar at IACS (Inst. Adv. Comp. Sci), Stony Brook, Oct 8,

2020.

A. Tomiya (oral), "Gauge covariant neural network for 4 dimensional non-abelian gaugetheory," MIT, online, April 29, 2020.

A. Tomiya (oral), "Applications of machine learning on theoretical physics," Ochanomizu University, online, May 19, 2020.

A. Tomiya (oral), "Gauge covariant neural network for 4 dimensional non-abelian gaugetheory," RIKEN Center for Computational Science (R-CCS), online, April 28, 2020.

A. Tomiya (oral), "Applications of machine learning for theoretical physics," J-PARC, online, March 18, 2020.

A. Tomiya (oral), "Self-learning Monte-Carlo for non-abelian gauge theory withdynamical fermions," Yukawa Institute for Theoretical Physics (YITP), Kyoto Univeristy, online, December 7, 2020.

A. Tomiya (oral), "Applications of machine learning on theoretical physics," Shimane University, online, October 29, 2020

A. Tomiya (oral), "Lattice gauge theory with quantum computers," RIKEN Center for Computational Science (R-CCS), online, June 3, 2020.

A. Tomiya (oral), "Lattice gauge theory with quantum computers," Osaka University, online, May 12, 2020.

Awards

富谷昭夫, 理研基礎科学特別研究員 成果発表会ポスター賞, 2021 年 1 月.

Press Releases

Brookhaven National Laboratory (April 7, 2021), "Background on Brookhaven Lab's Involvement in the Muon g-2 Experiment," https://www.bnl.gov/newsroom/news.php?a=218814 .

CERN Courier (April 14, 2021), "An anomalous moment for the muon," https://cerncourier.com/a/an-anomalous-moment-for-the-muon/ .

UConn Today (May 20, 2021), "UConn Physicists Focus on a Law-Breaking Particle," https://today.uconn.edu/2021/05/uconn-physicists-focus-on-a-law-breaking-particle/ .

Subnuclear System Research Division
RIKEN Facility Office at RAL

1. Abstract

Our core activities are based on the RIKEN-RAL Muon Facility located at the ISIS Neutron & Muon Source at the Rutherford Appleton Laboratory (UK), which provides intense pulsed-muon beams. The RIKEN-RAL Muon Facility is a significant and long-standing collaboration between RIKEN and RAL in muon science—with 2020 being the 30th years of continuous agreements between RIKEN and RAL. The Facility enables muon science throughout Japan and other field—it continues to attract proposals from a wide variety of Japanese universities and institutions (with over 80 groups having now used the facility), and including industrial users such at Toyota, and has been instrumental in establishing scientific links with other Asian universities.

Muons have their own spins with 100% polarization, and can detect local magnetic fields and their fluctuations at muon stopping sites very precisely. The method to study the characteristics of materials by observing time dependent changes of muon spin polarization is called "Muon Spin Rotation, Relaxation and Resonance" (μSR method), and is applied to study electro-magnetic properties of insulating, metallic, magnetic and superconducting systems. Muons reveal static and dynamic properties of the electronic state of materials in the zero-field condition, which is the ideal magnetic condition for research into magnetism. For example, we have carried out μSR investigations on a wide range of materials including frustrated pyrochlore systems, which have variety of exotic ground states of magnetic spins, so the magnetism study of this system using muon is quite unique.

The ultra-cold muon beam can be stopped in thin foil, multi-layered materials and artificial lattices, which enables us to apply the aSR techniques to surface and interface science. The development of an ultra-cold muon beam is also very important as a source of pencil-like small emittance muon beam for muon $g-2$/EDM measurement. We have been developing muonium generators to create more muonium atoms in vacuum even at room temperature to improve beam quality compared with the conventional hot-tungsten muonium generator. We have demonstrated a strong increase in the muonium emission efficiency by fabricating fine laser drill-holes on the surface of silica aerogel. We are also developing a high power Lyman-alpha laser in collaboration with the Advanced Photonics group at RIKEN. The new laser will ionize muoniums 100 times more efficiently for slow muon beam generation.

Over the past 2–3 years, a significant development activity in muon elemental analysis has taken place, proton radius experiments have continued and been developed, and chip irradiation experiments have also continued.

2. Major Research Subjects

(1) Materials science by muon-spin-relaxation method and muon site calculation
(2) Development of elemental analysis using pulsed negative muons
(3) Nuclear and particle physics studies via muonic atoms and ultra-cold muon beam
(4) Other muon applications

3. Summary of Research Activity

(1) Material science at the RIKEN-RAL muon facility

Muons have their own spins with 100% polarization, and can detect local magnetic fields and their fluctuations at muon stopping sites very precisely. The μSR method is applied to studies of newly fabricated materials. Muons enable us to conduct (1) material studies under external zero-field condition, (2) magnetism studies with samples without nuclear spins, and (3) measurements of muon spin relaxation changes at wide temperature range with same detection sensitivity. The detection time range of local field fluctuations by μSR is 10^{-6} to 10^{-11} second, which is an intermediate region between neutron scattering method (10^{-10}–10^{-12}second) and Nuclear Magnetic Resonance (NMR) (longer than 10^{-6} second). At Port-2 and 4 of the RIKEN-RAL Muon Facility, we have been performing μSR researches on strong correlated-electron systems, organic molecules, energy related materials and biological samples to study electron structures, superconductivity, magnetism, molecular structures and crystal structures.

Among our scientific activities on μSR studies from year 2017 to 2020, following subjects of material sciences are most important achievements at the RIKEN-RAL muon facility:

(1) Multi magnetic transitions in the Ru-based pyrochlore systems, $R_2Ru_2O_7$.
(2) Novel magnetic and superconducting properties of nano-size La-based high-T_c superconducting cuprates.
(3) Determination of muon positions estimated from density functional theory (DFT) and dipole-field calculations.
(4) Chemical muonic states in DNA molecules.

Result-1) Doped hole effects on the magnetic properties of corner-shared magnetic moments on pyrochlore systems gave us new interpretations to understand exotic phenomena, like the quantum criticality of magnetic moments and a quasi-magnetic monopole state. Result-2) The same nano-size effect was examined on the La-based high-T_c superconducting oxide changing the electronic state from insulating to superconducting. We confirmed the reduction in the magnetic interaction and the disappearance of the superconducting state leading the increase in the ferromagnetic interaction within the wide-range of the hole concentration. Result-3) Well known and deeply investigated La_2CuO_4 has opened a new scheme of the Cu spin. Taking into account quantum effects to expand the Cu-spin orbital and muon positions, we have succeeded to explain newly found muon sites and hyperfine fields at those sites. Result-4) Chemical states of the muon which attaches to DNA molecules were investigated by the avoided level-crossing muon-spin resonance experiments. In conjunction with DFT calculations, we are trying to reveal the electron motion though the DNA molecule.

We have been continuing to develop muon-science activities in Asian countries. We enhanced international collaborations to organize new μSR experimental groups and to develop muon-site calculation groups using computational method. We are creating

new collaborations with new teams in different countries and also continuing collaborations in μSR experiments on strongly correlated systems with researchers from Taiwan, Indonesia, China, Thailand and Malaysia including graduate students. We are starting to collaborate with the new Chinese muon group who are developing the Chinese Muon Facility and trying to develop more muon activities in the Asian area.

(2) Development of elemental analysis using pulsed negative muons

There has been significant development of elemental analysis using negative muons on Port 4 and Port 1 over the past couple of years. Currently, elemental analysis commonly uses X-ray and electron beams, which accurately measure surfaces. However, a significant advantage of muonic X-rays over those of electronic X-rays is their higher energy due to the mass of the muon. These high energy muonic X-rays are emitted from the bulk of the samples without significant photon self-absorption. The penetration depth of the muons can be varied by controlling the muon momentum, providing data from a thin slice of sample at a given depth. This can be over a centimetre in iron, silver and gold or over 4 cm in less dense materials such as carbon.

Some techniques for elemental analysis are destructive or require the material under investigation to undergo significant treatment and some of the techniques are only sensitive to the surface. Therefore, negative muons offer a unique service in which they can measure inside, beyond the surface layer and completely non-destructively.

The areas of science that have used negative muons for elemental analysis have been very diverse. The largest area is the cultural heritage community as the non-destructive ability is particularly important and will become more so. This community have investigated swords from different eras, coins (Roman gold and silver, Islamic silver and from the Tudor Warship Mary Rose), miniature boats from Sardinia, reliefs on Baptist church gate, Bronze Age tools and cannon balls. In addition, energy materials (Li composition for hydrogen storage), bio-materials (search for iron to potentially help understand Alzheimer's), engineering alloys (manufacturing processes for new materials for jet engines), and functional materials (surface effects in piezo electrics) have also been investigated.

The study was extended to see the difference by isotopes of silver and lead, which may give hint on the source of the material.

(3) Ultra-cold (low energy) muon beam generation and applications

Positive muon beam with thermal energy has been produced by laser ionization of muonium (bound system of μ^+ and electron) emitted from a hot tungsten surface with stopping surface muon beam at Port-3. The method generates a positive muon beam with acceleration energy from several 100 eV to several 10 keV, small beam size (a few mm) and good time resolution (less than 8 nsec). By stopping the ultra-cold muon beam in thin foil, multi-layered materials and artificial lattices, we can precisely measure local magnetic field in the materials, and apply the μSR techniques to surface and interface science. In addition, the ultra-cold muon is very important as the source of pencil-like small emittance muon beam for muon $g-2$/EDM measurement. It is essential to increase the slow muon beam production efficiency by 100 times for these applications. There are three key techniques in ultra-cold muon generation: production of thermal muonium, high intensity Lyman-alpha laser and the ultra-cold muon beam line.

A high-power Lyman-alpha laser was developed in collaboration with the Advanced Photonics group at RIKEN. The new laser system is used at J-PARC U-line and, upon completion, will ionize muoniums 100 times more efficiently for slow muon beam generation. In this development, we succeeded to synthesize novel ceramic-based Nd:YGAG crystal, which realized a highly efficient and stable laser system. However, larger size crystal than presently available is needed for full design power. We are working hard to improve the crystal homogeneity including the option of using material with slightly different composition.

We also succeeded in developing an efficient muonium generator, laser ablated silica aerogel, which emits more muoniums into vacuum even at room temperature. Study has been done at TRIUMF utilizing positron tracking method of muon decay position. We demonstrated in 2013 at least 10 times increase of the muonium emission efficiency by fabricating fine laser drill-holes on the surface of silica aerogel. Further study was carried out in 2017 to find the optimum fabrication that will maximize the muonium emission. From the analysis, we found the emission has large positive correlation with the laser ablated area rather than with any other parameters. We also confirmed the muon polarization in vacuum. An alternative detection method for muonium emission using muonium spin rotation, which will be sensitive even to muoniums near the surface, was tested at RIKEN-RAL in 2018 and was found successful. The study was further applied to the measurement of the temperature dependence.

In RIKEN-RAL Port 3, the ultra-cold muon beam line, which had been designed with hot tungsten, was completely rebuilt to use advantage of the new room temperature silica aerogel target. The equipment was tested with surface muon beam and basic data such as muon stopping in aerogel were taken. A similar target design will be adopted in the ultimate cold muon source planned for muon $g-2$/EDM at J-PARC.

(4) Other fundamental physics studies

A measurement of the proton radius using $2S$-$2P$ transition of muonic hydrogen at PSI revealed that the proton charge radius is surprisingly smaller than the radius measured using normal hydrogen spectroscopy and e-p scattering by more than 5 times their experimental precision. The muonic atom has larger sensitivity to the proton radius because the negative muon orbits closer to the proton, although there is no reason why these measurements can yield inconsistent results if there exists no exotic physics or unidentified phenomenon behind. The cause of the discrepancy is not understood yet, thus a new measurement with independent method is much anticipated.

We proposed the measurement of the proton radius by using the hyperfine splitting of the muonic hydrogen ground state. This hyperfine splitting is sensitive to the Zemach radius, which is a convolution of charge and magnetic-dipole distributions inside proton. We are planning to re-polarize the muonic hydrogen by a circularly polarized excitation laser (excites one of the $F=1$ states and regenerates the muon spin polarization), and detect the recovery of the muon decay-asymmetry along the laser.

Preparation using muon beam is in progress. We measured the muon stopping distribution in low-density hydrogen-gas cell, which

gave us consistent results with beam simulation. Another key is the lifetime of the upper hyperfine state of the muonic hydrogen that will contribute the polarization. We successfully observed the clear muon spin precession of muonic deuterium atom in 2018 for the first time in the world. The measurement with muonic protium was carried out in 2019 and the data is being analyzed.

(5) Other topics

RIKEN and ISIS have signed a new collaboration agreement for the period 2018–2023. This is the fourth in a continuous series of agreements, the first being signed in 1990, resulting in a partnership which will have lasted over 30 years. Under the new agreement, ownership and operation of the facility was passed to ISIS, a refurbishment programme of the facility has started, a user programme for Japanese scientists continued under the partnership between RIKEN and ISIS. The RIKEN-RAL collaboration is regularly highlighted as a good example of UK-Japanese science partnership at the UK-Japan Joint Committee on Science and Technology (chaired by the UK Chief Scientific Advisor to Government and a counterpart from Japan)—for example, Dr. King and Dr. Watanabe presented RIKEN-RAL at the November 2016 meeting of the Committee. The RIKEN-RAL collaboration has also enabled the development of collaborative activity between RIKEN and other Asian universities, *e.g.* through several MoUs with Indonesian and Malaysian universities.

It was very unfortunate that the research activity at RIKEN-RAL had severe restriction in FY2020 due to the COVID-19 pandemic. Almost all the access to RIKEN-RAL by external users had to be stopped. Even though, we managed to carry out several μSR experiments with mailed samples, where the ISIS staff mounted the samples and the external users controlled the experimental sequence remotely.

Members

Director

Philip KING

Senior Research Scientist

Isao WATANABE

Contract Researcher

Katsuhiko ISHIDA

List of Publications & Presentations

Publications

[Original Papers]

R. Kitamura, S. Bae, S. Choi, Y. Fukao, H. Iinuma, K. Ishida, N. Kawamura, B. Kim, Y. Kondo, T. Mibe, Y. Miyake, M. Otani, G. P. Razuvaev, N. Saito, K. Shimomura, and P. Strasser, "Development of negative muonium ion source for muon acceleration," Phys. Rev. Accel. Beams **24**, 033403 (2021).

S. Kanda, Y. Fukao, Y. Ikedo, K. Ishida, M. Iwasaki, D. Kawall, N. Kawamura, K. M. Kojima, N. Kurosawa, Y. Matsuda, T. Mibe, Y. Miyake, S. Nishimura, N. Saito, Y. Sato, S. Seo, K. Shimomura, P. Strasser, K. S. Tanaka, T. Tanaka, H. A. Torii, A. Toyoda, and Y. Ueno, "New precise spectroscopy of the hyperfine structure in muonium with a high-intensity pulsed muon beam," Phys. Lett. B **815**, 136154 (2021).

A. D. Pant, K. Ishida, N. Kawamura, S. Matoba, A. Koda, S. Nishimura, and K. Shimomura, "Study of muonium behavior in n-type silicon for generation of ultra cold muonium in vacuum," Physica B **613**, 412997 (2021).

J. Sugiyama, O. K. Forslund, E. Nocerino, N. Matsubar, K. Papadopoulos, Y. Sassa, S. P. Cottrell, A. D. Hillier, K. Ishida, M. Mansson, and J. H. Brewer, "Lithium diffusion in $LiMnPO_4$ detected with $\mu^{\pm}$SR," Phys. Rev. Res. **2**, 033161 (2020).

M. Aramini, C. Milanese, A. D. Hillier, A. Girella, C. Horstmann, T. Klassen, K. Ishida, M. Dornheim, and C. Pistidda, "Spectroscopic tool for the investigation of the local chemistry of elements," Nanomaterials **2020**, 10, 1260 (2020).

E. Mocchiutti, A. Adamczak, D. Bakalov, G. Baldazzi, R. Benocci, R. Bertoni, M. Bonesini, V. Bonvicini, H. CabreraMorales, F. Chignoli, M. Clemenza, L. Colace, M. Danailov, P. Danev, A. de Bari, C. DeVecchi, M. DeVincenzi, E. Furlanetto, F. Fuschinod, K. S. Gadedjisso-Tossoua, D. Guffantia, K. Ishida, C. Labanti, V. Maggi, R. Mazza, A. Menegolli, G. Morgante, M. Nastasi, J. Niemela, C. Pizzolotto, A. Pullia, R. Ramponi, L. P. Rignanese, M. Rossella, N. Rossi, M. Stoilov, L. Stoychev, L. Tortora, E. Vallazza, G. Zampa, and A. Vacchi, "First measurement of the temperature dependence of muon transfer rate from muonic hydrogen atoms to oxygen," Phys. Lett. A **384**, 126667(2020).

C. Pizzolotto, A. Adamczak, D. Bakalov, G. Baldazzi, M. Baruzzo, R. Benocci, R. Bertoni, M. Bonesini, V. Bonvicini, H. Cabrera, D. Cirrincione, M. Citossi, F. Chignoli, M. Clemenza, L. Colace, M. Danailov, P. Danev, A. de Bari, C. De Vecchi, M. de Vincenzi, E. Fasci, E. Furlanetto, F. Fuschino, K. S. Gadedjisso-Tossou, L. Gianfran, D. Guffanti, A. D. Hillier, K. Ishida, P. J. C. King, C. Labanti, V. Maggi, R. Mazza, A. Menegolli, E. Mocchiutti, L. Moretti, G. Morgante, J. Niemela, B. Patrizi, A. Pirri, A. Pullia, R. Ramponi, L. P. Rignanese, E. Roman, M. Rossella, R. Sarkar, A. Sbrizzi, M. Stoilov, L. Stoychev, J. J. Suárez-Vargas, G. Toci, L. Tortora, E. Vallazza, M. Vannini, C. Xiao, G. Zampa, and A. Vacchi, "The FAMU experiment: muonic hydrogen high precision spectroscopy studies," Eur. Phys. J. A **56**, 185 (2020).

J. Beare, G. Beer, J. H. Brewer, T. Iijima, K. Ishida, M. Iwasaki, S. Kamal, K. Kanamori, N. Kawamura, R. Kitamura, S. Li, G. M. Luke, G. M. Marshall, T. Mibe, Y. Miyake, Y. Oishi, K. Olchanski, A. Olin, M. Otani, M. A. Rehman, N. Saito, Y. Sato, K. Shimomura,

K. Suzuki, M. Tabata, and H. Yasuda, "Study of muonium emission from laser-ablated silica aerogel," Prog. Theor. Exp. Phys. **2020**, 123C01 (2020).

H. Yamauchi, D. P. Sari, I. Watanabe, Y. Yasui, L. -J. Chang, K. Kondo, T. U. Ito, M. Ishikado, M. Hahara, M. D. Frontzk, C. Chi, J. A. Fernandez-Bac, J. S. Lord, A. Berlie, A. Kotani, S. Mori, and S. Shamoto, "High-temperature short-range order in Mn_3RhSi," Commun. Matter. **1**, 42 (2020).

M. Fujita, K. M. Suzuki, S. Asano, H. Okabe, A. Koda, R. Kadono, and I. Watanabe, "Magnetic behavior of *T'*-type Eu_2CuO_4 revealed by muon spin rotation and relaxation measurements," Phys. Rev. B **102**, 045116 (2020).

Presentations

[Domestic Conferences/Workshops]

石田勝彦, 「理研 RAL での非破壊元素分析」, 第 4 回文理融合シンポジウム 量子ビームで歴史を探る—加速器が紡ぐ文理融合の地平—, オンライン, 2021 年 1 月 28–29 日.

石田勝彦 (招待講演), 「理研 RAL と J-PARC」, パルス中性子ミュオン発生 40 周年記念シンポジウム, オンライン, 2020 年 12 月 23 日.

石田勝彦, 「英国理研 RAL ミュオン施設におけるミュオン利用分析研究の進展」, 第 3 回 文理融合シンポジウム 量子ビームで歴史を探る—加速器が紡ぐ文理融合の地平—, オンライン, 2020 年 9 月 25–26 日.

Press Releases

正負のミュオンで捉えたイオンの動き 2020 年 8 月 7 日—Li イオンの動きを, 負ミュオンで確認, 正ミュオンで詳細観察— 一般財団法人総合科学研究機構（CROSS）中性子科学センター・サイエンスコーディネータ 杉山 純国立研究開発法人理化学研究所（理研）仁科加速器科学研究センター・協力研究員石田 勝彦

Safety Management Group

1. Abstract

The RIKEN Nishina Center for Accelerator-Based Science possesses one of the largest accelerator facilities in the world, which consists of two heavy-ion linear accelerators and five cyclotrons. This is the only site in Japan where uranium ions are accelerated. The center also has electron accelerators of microtron and synchrotron storage ring. Our function is to keep the radiation level in and around the facility below the allowable limit and to keep the exposure of workers as low as reasonably achievable. We are also involved in the safety management of the Radioisotope Center, where many types of experiments are performed with sealed and unsealed radioisotopes.

2. Major Research Subjects

(1) Safety management at radiation facilities of Nishina Center for Accelerator-Based Science
(2) Safety management at Radioisotope Center
(3) Radiation shielding design and development of accelerator safety systems

3. Summary of Research Activity

Our most important task is to keep the personnel exposure as low as reasonably achievable, and to prevent an accident. Therefore, we daily patrol the facility, measure the ambient dose rates, maintain the survey meters, shield doors and facilities of exhaust air and wastewater, replenish the protective supplies, and manage the radioactive waste. Advice, supervision and assistance at major accelerator maintenance works are also our task.

Minor improvements of the radiation safety systems were also done. The old type of computer system unit for the radiation monitoring system and the old UPS for radiation management system of the RIBF building were replaced. The old exhaust equipment of hotlabo exhaust system in Nishina building was also replaced.

Members

Director
Kanenobu TANAKA

Research/Technical Scientists
Rieko HIGURASHI (Technical Scientist)
Hisao SAKAMOTO (Technical Scientist)

Expert Technician
Atsuko AKASHIO

Technical Staff I
Hiroki MUKAI

Junior Research Associate
Kenta SUGIHARA

Visiting Scientists
Masayuki HAGIWARA (KEK)
Noriaki NAKAO (Shimizu Corporation)
Toshiya SANAMI (KEK)
Nobuhiro SHIGYO (Kyushu Univ.)
Hiroshi YASHIMA (Kyoto Univ.)

Part-time Workers
Kimie IGARASHI (Administrative Part-time Worker I)
Satomi IIZUKA (Administrative Part-time Worker II)
Yukiko SHIODA (Administrative Part-time Worker II)
Naoko USUDATE (Administrative Part-time Worker II)

Temporary Staffing
Ryuji SUZUKI

Assistant
Tomomi OKAYASU

List of Publications & Presentations

Publications

[Original Papers]

K. Sugihara, N. Shigyo, E. Lee, T. Sanami, and K. Tanaka, "Measurement of thick target neutron yields from 7 MeV/u α incidence on ^{209}Bi," Nucl. Instrum. Method Phys. Res. B **470** (2020).

[Proceedings]

K. Sugihara, N. Shigyo, A. Akashio, and K. Tanaka, "Measurement of neutron energy spectra of 345 MeV/u ^{238}U incidence on a copper target," JAEA-Conf 2020-001, 143–147.

Presentations

[International Conferences/Workshops]

K. Sugihara (poster), Y. Ikeda, T. Kobayashi, K. Fujita, N. Shigyo, K. Tanaka, and Y. Otake, "Study on characteristics of neutron and γ-ray fields at compact neutron source RANS-II facility by simulation by the PHITS code," 2020 Symposium on Nuclear Data, RIKEN Wako Campus, November 26–27, 2020.

User Liaison Group

1. Abstract

The User Liaison Group is a group that provides user support, including various procedures required for accelerator use, in order to promote collaborative-use of the RIBF facilities. The group will provide user support on matters necessary for RIBF experiments, from application to completion. The group will also provide technical support for the dissemination of information on the research results of the RIBF.

The group consists of two teams. The RIBF User Liaison Team provides various supports to visiting RIBF users through the RIBF Users Office. Managing RIBF beam time and organizing the Program Advisory Committee Meetings to review RIBF experimental proposals are also important mission of the Team in order to enhance collaborative-use of the RIBF. The Outreach Team has created various information materials, such as pamphlets, posters, and homepages, to introduce the research activities in the RNC. On the homepage, we provide information on usage of the RIBF facility. The team also participate in science introduction events hosted by public institutions. In addition, the User Liaison Group also takes care of laboratory tours for RIBF visitors from public. The numbers of visitors usually amounts to 2,300 per year.

Members

Director

Hideki UENO

Assistants

Yu NAYA
Midori YAMAMOTO
Tomomi OKAYASU

User Liaison Group
RIBF User Liaison Team

1. Abstract

To enhance synergetic common use of the world-class accelerator facility, the Radioisotope Beam Factory (RIBF), it is necessary to promote a broad range of applications and to maximize the facility's importance. The facilitation and promotion of the RIBF are important missions charged to the team. Important operational activities of the team include: i) the organization of international Program Advisory Committee (PAC) meetings to review experimental proposals submitted by RIBF users, ii) RIBF beam-time operation management, and iii) promotion of facility use by hosting outside users through the RIBF Independent Users program, which is a new-user registration program begun in FY2010 at the RIKEN Nishina Center (RNC) to enhance the synergetic common use of the RIBF. The team opened the RIBF Users Office in the RIBF building in 2010, which is the main point of contact for Independent Users and provides a wide range of services and information.

2. Major Research Subjects

(1) Facilitation of the use of the RIBF
(2) Promotion of the RIBF to interested researchers

3. Summary of Research Activity

(1) Facilitation of the use of the RIBF

The RIBF Users Office, formed by the team in 2010, is a point of contact for user registration through the RIBF Independent User program. This activity includes:

- registration of users as RIBF Independent Users,
- registration of radiation workers at the RIKEN Wako Institute,
- provision of an RIBF User Card (a regular entry permit) and an optically stimulated luminescence dosimeter for each RIBF Independent User, and
- provision of safety training for new registrants regarding working around radiation, accelerator use at the RIBF facility, and information security, which must be completed before they begin RIBF research. The RIBF Users Office is also a point of contact for users regarding RIBF beam-time-related paperwork, which includes:
- contact for beam-time scheduling and safety review of experiments by the In-House Safety Committee, and
- maintaining the above information in a beam-time record database.

In addition, the RIBF Users Office assists RIBF Independent Users with matters related to their visit, such as invitation procedures, visa applications, and the reservation of on-campus accommodation.

(2) Promotion of the RIBF to interested researchers

- The team has organized an international PAC for RIBF experiments; it consists of leading scientists worldwide and reviews proposals in the field of nuclear physics (NP) purely on the basis of their scientific merit and feasibility. The team also assists another PAC meeting for material and life sciences (ML) organized by the RNC Advanced Meson Laboratory. The NP PAC meeting is organized once a year regularly, and the ML PAC meetings are organized once or twice a year.
- The team coordinates beam times for PAC-approved experiments and other development activities. It manages the operating schedule of the RIBF accelerator complex according to the decisions arrived at by the RIBF Machine Time Committee.
- To promote research activities at RIBF, proposals for User Liaison and Industrial Cooperation Group symposia/mini-workshops are solicited broadly both inside and outside of the RNC. The RIBF Users Office assists in the related paperwork.
- The team is the point of contact for the RIBF users' association. It arranges meetings at RNC headquarters for the RIBF User Executive Committee of the users' association.
- The Team conducts publicity activities, such as arranging for RIBF tours, development and improvement of the RNC official web site, and delivery of RNC news via email and the web.

Members

Team Leader
Ken-ichiro YONEDA

Contract Researcher
Tadashi KAMBARA

User Liaison Group
Outreach Team

1. Abstract

The mission of the Outreach Team is to provide various “intangible” technical support for the dissemination of information on the research in RNC. For instance, the team creates brochures introducing the RNC and the RIBF accelerator facility, posters of symposia and the summer school hosted by RNC, the center homepage containing information such as details of RNC and the procedure for the use of the RIBF facility, and images of equipment and facilities available for researchers inside and outside RIKEN, among the others. Furthermore, the team also participates in science introduction events hosted by public institutions.

2. Major Work Contents

The major work contents of the Outreach Team is to promote the publicity of RNC, through the creation of various materials such as brochures, websites, posters, and videos, among the others. The arrangement of tours of the RIBF facility and the exhibition and introduction of the RIBF facility at science events are also conducted independently or in cooperation with RIKEN Public Relations Office.

3. Summary of Work Activity

The specific work contents performed by the team are as follows:

- [Website] The Team creates/manages the RNC official website (`http://www.nishina.riken.jp`), which introduces the organization and its research activities. This website plays an important role in providing information to researchers who visit RNC to conduct his/her own research.
- [Brochures] The Team has produced various brochures introducing the organization and the studies performed at RNC. The brochures named “Your body is made of star scraps” explaining element synthesis in the universe and “Introduction of RIBF Facility” in a cartoon style for children are among them.
- [Posters] Conference/Symposium posters connected with RNC were prepared on the request of organizers. For general purpose, a special poster featuring the nuclear chart has been prepared for distribution. In commemoration of the discovery of nihonium, brochures and posters dedicated to the ceremony were made.
- [RIBF Cyclopedia] In April 2012, the permanent exhibition hall (RIBF Cyclopedia) located at the entrance hall of the RIBF building was set up in cooperation with RIKEN Public Relations Office. Explanatory illustrations on nuclear science, research at RIBF, RIBF history, a 3D nuclear chart built with LEGO blocks, and a 1/6-size GARIS model are displayed to help understanding through visual means. The Team is also working on updating the exhibits.
- [RIBF facility tour] The Team arranges RIBF facility tour for over 2000 visitors per year. The tour is guided by a researcher.
- [Science event participation] In 2010, 2012, 2013, 2015, and 2016, the sub-team opened an exhibition booth of RNC to introduce the latest research activities on the occasion of the “Science Agora” organized by Japan Science and Technology Agency (JST). From time to time, the sub-team was invited to participate in scientific events by MEXT, Wako city, and Nissan global foundation. One attraction targeting children is the hands-on work of assembling “Iron-beads” to create a nuclear chart or a shape of nihonium.

In addition to the above-noted work contents, the Team conducts a variety of works, such as taking pictures of meetings organized by RNC, cooperation in the production of a 3D video to explain the accelerators and the research at RIBF, among the others.

Members

Team Leader
Hideki UENO

Deputy Team Leader
Yasushi WATANABE

Technical Staff I
Narumasa MIYAUCHI

Office of the Center Director

1. Abstract

This office is in place from JFY2018 to conduct works that the Center Director deems necessary for the operation of the research center and the secretarial work related to the research center in general.

2. Major Work Contents

- Nishina Center Monthly Meeting
  The pupose of the meeting is to share information on activities within the Nishina Center with all of the members. The meeting covers introduction of new comers, press-released achievements, announcement of events organized by or related to the Nishina Center, safety issues, and others to be informed to all members. The meeting agenda is distributed to all of the members via mailing-list.
- Conference Support
  Assistant staff members support coherently a large-size conference hosted by the Nishina Center.
- Orientation for new comers to the Nishina Center
  The Orientation is organized once a year to the new comers to give instructions for emergency response, safety in research, computer and network resources and security, and research misconduct prevention.

3. Summary of Work Activity

- Nishina Center Monthly Meeting
  Noriko Asakawa arranged the agenda and Hidetada Baba supported the on-line video system for the meeting.
  - The 157th Meeting on April 2, 2020
    (1) Greetings from newly appointed RNC director
    (2) Introduction of new arrivals and newly appointed members
  - The 158th Meeting on May 13, 2020
    (1) Greetings from the new RNC deputy director (Iwasaki)
    (2) Introduction of newcomers who joined RNC in April and May
    (3) "Swelling of doubly magic ^{48}Ca core in Ca isotopes beyond $N = 28$" (M. Tanaka)
    (4) Coronavirus update
    RIKEN's initiative (Sakurai, the RNC director)
    Remote work from home: tips and problems, issues to be addressed
    (5) Other
  - The 159th Meeting on June 10, 2020
    (1) Report from the RNC director
    Current events
    (2) Introduction of a press release
    "Discovery that a single proton from a fluorine nucleus can have a major effect on the state of the nucleus" (Uesaka)
    (3) Information exchange on corona update
  - The 160th Meeting on July 8, 2020
    (1) Report from the RNC director
    The RNC director reported on the facility visit by M. Ueno, State Minister of MEXT
    revision of the RIKEN rules and the coronavirus update.
    (2) Situation in BNL and Long Island under the COVID-19 Pandemic (I. Nakagawa)
    At the beginning of April, the outbreak of COVID-19 hit New York where BNL is located, which then led to a medical collapse at the epic center, New York City. Living on the outskirts of New York City (nearby BNL), my family and I waited for the right timing to returning to Japan by closely monitoring the situation in NY and Tokyo. With much improvement of the situation in New York lately, we were able to return to Japan safely just recently. BNL is under the process of gradual reopening.
  - The 161st Meeting on September 9, 2020
    (1) Report from the RNC director
    (2) Report from the Nishina Center and iTHEMS Promotion Office
    (3) Website featuring RIKEN-RAL Muon Facility's 30th anniversary
    (4) FY2019 RIKEN Ohbu Award
    Researcher Incentive Award
    Research & Industry Partnership Incentive Award
    (5) Press Release
    (6) Other
  - The 162nd Meeting on October 14, 2020
    (1) Greetings from the newly appointed Team Leaders
    Masanori Kidera (Infrastructure Management Team)

Hiroyuki Ichida (Plant Genome Evolution Research Team)
(2) 2020 JPCERT/CC Certificate of Appreciation
Takashi Ichihara (Radioactive Isotope Physics Laboratory)
(3) Topics on the RIKEN information systems (Baba)
(4) Report from the RNC director
COVID-19
Facility tour
Lecture Presentation (Organizer: Nuclear Physics Committee)
(5) Other

– The 163rd Meeting on November 11, 2020
(1) Report on award
A3F-CNSSS20 Award for young scientist
The 9th Annual Award presented by the Particle Accelerator Society of Japan at the 17th Annual Meeting
(2) Report from the RNC director
Update on COVID-19
Facility tour
(3) Other
e-learning on research ethics (Motobayashi)

– The 164th Meeting on December 9, 2020
(1) On passing of Dr. Akito Arima, former RIKEN President
(2) Introduction of award recipient (Hiyama)
Recipient of the FY2020 Nishina Memorial Prize: Kazuma Nakazawa (Strangeness Nuclear Physics Laboratory)
(3) Report on symposium (Otsu)
SND2020 (Symposium on Nuclear Data) held on November 23–27
(4) On Accelerator Progress Report (Ueno)
(5) Report from the RNC director
Outstanding matters from the old Nishina Laboratory
COVID-19 situation
(6) Other

– The 165th Meeting on January 13, 2021
(1) Introduction of a newcomer (Haba)
Yin Xiaojie Post doctorate Researcher (Nuclear Chemistry Research Team)
(2) Generation of high intensity Zn beam (Higurashi)
(3) Report from the RNC director
New Year's greetings
COVID-19 situation
(4) Other

– The 166th Meeting on February 10, 2021
(1) Press Release
Discovery in neutron pair correlation inside the halo nuclei of Lithium-11—Evidence of dineutron at the surface of neutron-rich nuclei found (Uesaka)
Filling a crucial gap in aquafarming: ion beam breeding to the rescue (Abe)
(2) Report from the RNC director
COVID-19 situation
(3) Other

– The 167th Meeting on March 10, 2021
(1) Introduction of a newcomer (K. Yoshida)
Masahiro Yoshimoto (Postdoctoral Researcher, BigRIPS Team)
(2) Relocation of the third cyclotron (Fukushima)
(3) RIKEN Open Day (Tanaka)
(4) Report from the RNC director
COVID-19 situation
(5) Retirement speech
Eiji Ikezawa (Team Leader, RILAC Team)

- Conference Support
No large size conferences hosted by the Nishina Center were organized.

- Orientation for new comers to the Nishina Center
Due to the COVID-19 pandemic, the Orientation was not organized in 2020.

Members

Director
Hiroyoshi SAKURAI

Research Administrator
Narumasa MIYAUCHI

Assistants
Noriko ASAKAWA
Yu NAYA
Karen SAKUMA
Asako TAKAHASHI
Mitsue YAMAMOTO
Izumi YOSHIDA

Partner Institutions

The RIKEN Nishina Center for Accelerator-Based Science (RNC) has collaborated with universities and research institutes since 2008 under the research partnership agreement. This collaboration framework permits an external institute to develop its own projects at the RIKEN Wako Campus in equal partnership with the RNC. At present, two institutes—the Center for Nuclear Study (CNS), the University of Tokyo and the Wako Nuclear Science Center (WNSC), Institute of Particle and Nuclear Studies (IPNS), High Energy Accelerator Research Organization (KEK)—are conducting joint research under the research partnership agreement.

The CNS and RNC signed the research partnership agreement in 2008. Until then, the CNS had collaborated in joint programs with RIKEN under the "Research Collaboration Agreement on Heavy Ion Physics" (collaboration agreement) signed in 1998. The partnership agreement redefines procedures related to the joint programs while keeping the spirit of the collaboration agreement. The joint programs include experimental nuclear-physics activities using CRIB, SHARAQ, and GRAPE at the RI Beam Factory (RIBF), accelerator development; and activities at RHIC PHENIX.

The KEK-WNSC and RNC signed a research partnership agreement on "Low-Energy Unstable Nuclear Beam Science" in 2011. The joint experimental programs are based on the KEK Isotope Separation System (KISS). The KISS has been available for RIBF users since 2015. The research collaboration agreement for the SLOWRI facility and the multi-reflection time-of-flight (MRTOF) mass spectrograph was then signed in 2019, based on which the SLOWRI Joint Operation Committee has been established for the collaborative use and operation of the SLOWRI facility.

Experimental proposals that request the use of the above-noted devices of the CNS and KEK, together with other key devices at the RIBF, are screened by the Program Advisory Committee for Nuclear Physics experiments at the RIBF (NP-PAC). The NP-PAC meetings are co-hosted by the CNS and KEK.

Matters necessary for the smooth promotion of joint research based on the research partner agreement are determined at the Collaboration Liaison Council. More specific matters related to the execution of collaborative research are discussed at the Collaboration Liaison Committee established under the Liaison Council. In order to enhance the effectiveness of coordination and information sharing on joint research programs, the Joint Researchers Meeting was established in 2020 under the Collaboration Liaison Committee.

Several members of both institutes have also been invited to participate as external members in RNC committees related to the operation of the RIBF, such as the Machine-Time Committee and the Safety Review Committee.

The activities of the CNS and KEK are reported in the succeeding pages.

Partner Institution
Center for Nuclear Study, Graduate School of Science
The University of Tokyo

1. Abstract

The Center for Nuclear Study (CNS) aims to elucidate the nature of nuclear system by producing the characteristic states where the Isospin, Spin and Quark degrees of freedom play central roles. These researches in CNS lead to the understanding of the matter based on common natures of many-body systems in various phases. We also aim at elucidating the explosion phenomena and the evolution of the universe by the direct measurements simulating nuclear reactions in the universe. In order to advance the nuclear science with heavy-ion reactions, we develop AVF upgrade, CRIB and SHARAQ facilities in the large-scale accelerators laboratories RIBF. The OEDO facility has been developed as an upgrade of the SHARAQ, where a RF deflector system has been introduced to obtain a good quality of low-energy beam. A new project for fundamental symmetry using heavy RIs has been starting to install new experimental devices in the RIBF. We promote collaboration programs at RIBF as well as RHIC-PHENIX and ALICE-LHC with scientists in the world, and host international meetings and conferences. We also provide educational opportunities to young scientists in the heavy-ion science through the graduate course as a member of the department of physics in the University of Tokyo and through hosting the international summer school.

2. Major Research Subjects

(1) Accelerator Physics
(2) Nuclear Astrophysics
(3) Nuclear spectroscopy of exotic nuclei
(4) Quark physics
(5) Nuclear Theory
(6) OEDO/SHARAQ project
(7) Exotic Nuclear Reaction
(8) Low Energy Nuclear Reaction Group
(9) Active Target Development
(10) Fundamental Physics

3. Summary of Research Activity

(1) Accelerator physics

One of the major tasks of the accelerator group is the AVF upgrade project that includes development of ion sources, upgrading the AVF cyclotron of RIKEN and the beam transport system to CRIB, E7B, and C12 in the E7 experiment room. In 2020, the operating time of the HyperECR was 1146 hours. The beam extraction system of the HyperECR is developed to realize a high intensity and low emittance beam and the study of mixing gas is started for heavy ionization. The calculation model of injection beam orbit of the AVF cyclotron was completed and the study of the optimization of injection beam orbit was started. For the detailed studies on ion optics of the beamline to CRIB and experiment device of Fr-EDM measurement from AVF cyclotron, the development of 4-dimensional emittance monitor for high power ion beams was started. the prototype was completed and evaluated for performance.

(2) Nuclear astrophysics

The main activity of the nuclear astrophysics group is to study astrophysical reactions and special nuclear structure, such as clusters, using the low-energy RI beam separator CRIB. To produce RI beams at CRIB with higher intensity, a project to improve the heat durability of the cryogenic gas target is in progress. In 2020, we used a high-current oxygen beam to test the heat durability of the gas target. Sealing foils of several materials and copper extention parts were employed in the test, and we found the target can stand for the beam heat much exceeding the previous limit of 2 Watts per foil. The secondary beam development is also on going. A ^{6}He RI beam was first produced at CRIB in March 2021, as the lightest RI beam ever created at CRIB. We successfully produced a ^{6}He beam at the intensity more than 105 pps, which is to be used for the approved ^{6}He + p scattering measurement, as well as other future experiments.

(3) Nuclear structure of exotic nuclei

The NUSPEQ (NUclear SPectroscopy for Extreme Quantum system) group studies exotic structures in high-isospin and/or high-spin states in nuclei. The CNS GRAPE (Gamma-Ray detector Array with Position and Energy sensitivity) is a major apparatus for high-resolution in-beam gamma-ray spectroscopy. Missing mass spectroscopy using the SHARAQ is used for another approach on exotic nuclei. The group plays a major role in the OEDO/SHARAQ project described below. In 2020, analysis of a new measurement of the ^{4}He(^{8}He, ^{8}Be)4n reaction for better statistics and better accuracy has been proceeding.

(4) Quark physics

Main goal of the quark physics group is to understand the properties of hot and dense nuclear matter created by colliding heavy nuclei at relativistic energies. The group has been involved in the PHENIX experiment at Relativistic Heavy Ion Collider (RHIC) at Brookhaven National Laboratory, and the ALICE experiment at Large Hadron Collider (LHC) at CERN. As for ALICE, the group

has involved in the data analyses, which include the measurement of low-mass lepton pairs in Pb-Pb collisions, the measurement of long range two particle correlations in p-Pb collisions, searches for thermal photons in high multiplicity pp and p-Pb collisions and for strangeness dibaryons. The group has involved in the ALICE-TPC upgrade using a Gas Electron Multiplier (GEM), where the group is very active in the development and benchmarking of the online space-charge distortion corrections using machine learning techniques running on the Graphical Processing Unit (GPU).

(5) Nuclear theory

The nuclear theory group participates in a project, "Program for Promoting Researches on the Supercomputer Fugaku" and promotes computational nuclear physics utilizing the Fugaku supercomputer. In FY2020, we proposed a new framework called the "quasi-particle vacua shell model," which is an extension of the Monte Carlo shell model, and promoted its code developments. Based on these methodological developments, we investigated the exotic structure of nuclei, especially neutron-rich Mg isotopes, and discussed the mechanism to determine the neutron drip line. In addition, the nuclear Schiff moments of ^{129}Xe and ^{199}Hg were theoretically evaluated by large-scale shell-model calculations to contribute to the experimental search of time-reversal breaking. In parallel, we promoted the collaborative researches with experimental groups for investigating the exotic structure of unstable nuclei, such as ^{35}S, ^{30}Mg, ^{64}Ni, ^{75}Ni, ^{112}Sn and ^{137}Ba.

(6) OEDO/SHARAQ project

The OEDO/SHARAQ group pursues experimental studies of RI beams by using the high-resolution beamline and the SHARAQ spectrometer. A mass measurement by TOF-$B\rho$ technique for very neutron-rich nuclei successfully reaches titanium isotopes at $N = 40$, ^{62}Ti, of which the report was published in 2020. The experimental study of 0^- strength in nuclei using the parity-tansfer charge exchange (^{16}O, ^{16}F) will be reported soon. As for The OEDO beamline, the results of the first and second experiments for LLFPs will be finalized and reported soon. Since experimental studies using OEDO were newly proposed, we continue developments to improve the performance for coming these beam times, such as the intensity of low-energy RI beams and the suppression of X rays from RF deflector.

(7) Exotic nuclear reaction

The Exotic Nuclear Reaction group studies various exotic reactions induced by beams of unstable nuclei. One subject is inverse-kinematics (p, n) measurement by using the neutron counter array PANDORA. Candidate nuclei to study are high spin isomers such as ^{52}Fe(12^+). Study of the production mechanism of high-spin isomer beams was in progress. Another is search of double Gamow-Teller resonance by a double charge exchange reaction (^{12}C, ^{12}Be). Preparations including the development of MWDCs were ongoing.

(8) Low energy nuclear reaction group

A recoil particle detector for missing mass spectroscopy, named TiNA, had been upgraded under the collaboration with RIKEN and RCNP. The original TiNA consisted of 6 sector telescopes and 12 CsI (Tl) crystals. Four TTT-type (1024 channels) doubly-sided silicon detectors and twenty-two CsI(Tl) were added to make a TiNA2 array. The commissioning experiment of the TiNA2 was conducted at Kyushu University in March 2021. The production cross sections of ^{178m2}Hf were evaluated for the mass production in the future and will be reported soon. The digital signal processing devices for the GRAPE are under development. For the SHARAQ11 experiment which uses a tritium-doped titanium target, the safety devices has been developed with Tohoku University.

(9) Active target development

Three gaseous active target TPCs called CAT-S, CAT-M and GEM-MSTPC are developed and used for the missing mass spectroscopies. The CAT's are employed for the study of equation of state of nuclear matter. The measurement of giant monopole resonance in ^{132}Sn at RIBF with CAT-S and the data analysis is ongoing. The CAT-M was employed for the measurements of the proton inelastic scattering on ^{136}Xe at HIMAC and the proton elastic scattering on ^{132}Sn. The development for the reduction of space charge due to the ion backflow and the reduction of delta-ray background is ongoing. The GEM-MSTPC is employed for the nuclear astrophysics study. The data analysis of (α, p) reaction on ^{18}Ne and ^{22}Mg and the β-decay of ^{16}Ne followed by α emission are ongoing.

(10) Fundamental physics

In order to investigate the origin of matter-antimatter symmetry (CP) violation, we focused on the fact that the permanent electric dipole moment (EDM) of heavy elements such as Francium (Fr) is greatly enhanced by the relativistic effect and octupole deformation of the nucleus. The development of the laser cooled Fr source is in progress at RIBF. In particular, we have established a technique for a high-intensity Fr source by using the nuclear fusion reaction with a surface ionization ion source using a non-contact heating method with an infrared heater. Also the frequency stabilization with an iodine molecule and a high-precision wavemeter are ready at present. Furthermore, by establishing a coexistence trapping technique for two types of Rb isotopes, we have established a co-magnetometer for an accurate EDM measurement.

Members

Director

Susumu SHIMOURA

Scientific Staff

Susumu SHIMOURA (Professor)
Yasuhiro SAKEMI (Professor)
Kentaro YAKO (Associate Professor)
Nobuaki IMAI (Associate Professor)
Taku GUNJI (Associate Professor)
Noritaka SHIMIZU (Project Associate Professor)
Hidetoshi YAMAGUCHI (Lecturer)
Shin'ichiro MICHIMASA (Assistant Professor)
Shinsuke OTA (Assistant Professor)
Hiroki NAGAHAMA (Assistant Professor)

Guest Scientists

Yutaka UTSUNO (Guest Professor)
Daiki NISHIMURA (Guest Associate Professor)
Toshitaka KAJINO (Guest Post Doctoral Associate)
Ikuko HAMAMOTO (Guest Post Doctoral Associate)

Technical Staff

Yasuteru KOTAKA

Techinical Assistant

Masayoshi YAGYU

Project Research Associates

Masanori DOZONO
Seiya HAYAKAWA

Post Doctoral Associates

Daiki SEKIHATA
Keisuke NAKAMURA
Keita KAMAKURA
Nanru MA
Yusuke TSUNODA
Kota YANASE
Thomas William CHILLERY

Assistant Teaching Staff

Yuko SEKIGUCHI
Keita KAWATA
Noritaka KITAMURA
Shumpei KOYAMA

Academic Support Staff

Reiko KOJIMA

Graduate Students

Shoichiro MASUOKA
Hideki SHIMIZU
Rieko TSUNODA
Naoya OZAWA
Shutaro HANAI
Natsuki SHIMIZU
Shintaro NAGASE
Ryotaro KOHARA

Research Student

Jiatai LI

Administration Staff

Noriko SHIMANE
Ikuko YAMAMOTO
Takako ENDO
Yukino KISHI
Aki KOTAKA

List of Publications & Presentations

Publications

[Original Papers]

Z. H. Yang, Y. Kubota, A. Corsi, K. Yoshida, X. -X. Sun, J. G. Li, M. Kimura, N. Michel, K. Ogata, C. X. Yuan, Q. Yuan, G. Authelet, H. Baba, C. Caesar, D. Calvet, A. Delbart, M. Dozono, J. Feng, F. Flavigny, J. -M. Gheller, J. Gibelin, A. Giganon, A. Gillibert, K. Hasegawa, T. Isobe, Y. Kanaya, S. Kawakami, D. Kim, Y. Kiyokawa, M. Kobayashi, N. Kobayashi, T. Kobayashi, Y. Kondo, Z. Korkulu, S. Koyama, V. Lapoux, Y. Maeda, F. M. Marqúes, T. Motobayashi, T. Miyazaki, T. Nakamura, N. Nakatsuka, Y. Nishio, A. Obertelli, A. Ohkura, N. A. Orr, S. Ota, H. Otsu, T. Ozaki, V. Panin, S. Paschalis, E. C. Pollacco, S. Reichert, J. -Y. Roussé, A. T. Saito, S. Sakaguchi, M. Sako, C. Santamaria, M. Sasano, H. Sato, M. Shikata, Y. Shimizu, Y. Shindo, L. Stuhl, T. Sumikama, Y. L. Sun, M. Tabata, Y. Togano, J. Tsubota, F. R. Xu, J. Yasuda, K. Yoneda, J. Zenihiro, S. -G. Zhou, W. Zuo, and T. Uesaka, "Quasifree neutron knockout reaction reveals a small *s*-orbital component in the borromean nucleus ^{17}B," Phys. Rev. Lett. **126**, 082501 (2021).

Y. Kubota, A. Corsi, G. Authelet, H. Baba, C. Caesar, D. Calvet, A. Delbart, M. Dozono, J. Feng, F. Flavigny, J. -M. Gheller, J. Gibelin, A. Giganon, A. Gillibert, K. Hasegawa, T. Isobe, Y. Kanaya, S. Kawakami, D. Kim, Y. Kikuchi, Y. Kiyokawa, M. Kobayashi, N. Kobayashi, T. Kobayashi, Y. Kondo, Z. Korkulu, S. Koyama, V. Lapoux, Y. Maeda, F. M. Marqués, T. Motobayashi, T. Miyazaki, T. Nakamura, N. Nakatsuka, Y. Nishio, A. Obertelli, K. Ogata, A. Ohkura, N. A. Orr, S. Ota, H. Otsu, T. Ozaki, V. Panin, S. Paschalis, E. C. Pollacco, S. Reichert, J. -Y. Roussé, A. T. Saito, S. Sakaguchi, M. Sako, C. Santamaria, M. Sasano, H. Sato, M. Shikata, Y. Shimizu, Y. Shindo, L. Stuhl, T. Sumikama, Y. L. Sun, M. Tabata, Y. Togano, J. Tsubota, Z. H. Yang, J. Yasuda, K. Yoneda, J. Zenihiro, and T. Uesaka, "Surface localization of the dineutron in ^{11}Li," Phys. Rev. Lett. **125**, 252501 (2020).

N. Kitamura, K. Wimmer, N. Shimizu, V. M. Bader, C. Bancroft, D. Barofsky, T. Baugher, D. Bazin, J. S. Berryman, V. Bildstein, A. Gade, N. Imai, T. Kröll, C. Langer, J. Lloyd, E. Lunderberg, G. Perdikakis, F. Recchia, T. Redpath, S. Saenz, D. Smalley, S. R. Stroberg, J. A. Tostevin, N. Tsunoda, Y. Utsuno, D. Weisshaar, and A. Westerberg, "Structure of ^{30}Mg explored via in-beam γ-ray spectroscopy," Phys. Rev. C **102**, 054318 (2020).

S. Momiyama, K. Wimmer, D. Bazin, J. Belarge, P. Bender, B. Elman, A. Gade, K. W. Kemper, N. Kitamura, B. Longfellow, E. Lunderberg, M. Niikura, S. Ota, P. Schrock, J. A. Tostevin, and D. Weisshaar, "Shell structure of ^{43}S and collapse of the $N = 28$ shell closure," Phys. Rev. C **102**, 034325 (2020).

T. Noro, T. Wakasa, T. Ishida, Hidetomo P. Yoshida, M. Dozono, H. Fujimura, K. Fujita, K. Hatanaka, T. Ishikawa, M. Itoh, J. Kamiya, T. Kawabata, Y. Maeda, H. Matsubara, M. Nakamura, H. Sakaguchi, Y. Sakemi, Y. Shimizu, H. Takeda, Y. Tameshige, A. Tamii, K. Tamura, S. Terashima, M. Uchida, Y. Yasuda, and M. Yosoi, "Experimental study of $(p, 2p)$ reactions at 392 MeV on ^{12}C, ^{16}O, ^{40}Ca and ^{208}Pb nuclei leading to low-lying states of residual nuclei," Prog. Theor. Exp. Phys. **2020**, 093D02 (2020).

K. B. Howard, U. Garg, M. Itoh, H. Akimune, M. Fujiwara, T. Furuno, Y. K. Gupta, M. N. Harakeh, K. Inaba, Y. Ishibashi, K. Karasudani, T. Kawabata, A. Kohda, Y. Matsuda, M. Murata, S. Nakamura, J. Okamoto, S. Ota, J. Piekarewicz, A. Sakaue, M.Şenyiğit, M. Tsumura, and Y. Yang, "Compressional-mode resonances in the molybdenum isotopes: Emergence of softness in open-shell nuclei near $A = 90$," Phys. Lett. B **807**, 135608 (2020).

A. Frotscher, M. Gómez-Ramos, A. Obertelli, P. Doornenbal, G. Authelet, H. Baba, D. Calvet, F. Château, S. Chen, A. Corsi, A. Delbart, J. -M. Gheller, A. Giganon, A. Gillibert, T. Isobe, V. Lapoux, M. Matsushita, S. Momiyama, T. Motobayashi, M. Niikura, H. Otsu, N. Paul, C. Péron, A. Peyaud, E. C. Pollacco, J. -Y. Roussé, H. Sakurai, C. Santamaria, M. Sasano, Y. Shiga, N. Shimizu, D. Steppenbeck, S. Takeuchi, R. Taniuchi, T. Uesaka, H. Wang, K. Yoneda, T. Ando, T. Arici, A. Blazhev, F. Browne, A. M. Bruce, R. Carroll, L. X. Chung, M. L. Cortées, M. Dewald, B. Ding, Zs. Dombradi, F. Flavigny, S. Franchoo, F. Giacoppo, M. Górska, A. Gottardo, K. Hadyńska-Klęk, Z. Korkulu, S. Koyama, Y. Kubota, A. Jungclaus, J. Lee, M. Lettmann, B. D. Linh, J. Liu, Z. Liu, C. Lizarazo, C. Louchart, R. Lozeva, K. Matsui, T. Miyazaki, K. Moschner, S. Nagamine, N. Nakatsuka, C. Nita, S. Nishimura, C. R. Nobs, L. Olivier, S. Ota, Z. Patel, Zs. Podolyák, M. Rudigier, E. Sahin, T. Y. Saito, C. Shand, P. -A. Söderström, I. G. Stefan, T. Sumikama, D. Suzuki, R. Orlandi, V. Vaquero, Zs. Vajta, V. Werner, K. Wimmer, J. Wu, and Z. Xu, "Sequential nature of $(p, 3p)$ two-proton knockout from neutron-rich nuclei," Phys. Rev. Lett. **125** 012501 (2020).

A. E. Barzakh, D. Atanasov, A. N. Andreyev, M. Al Monthery, N. A. Althubiti, B. Andel, S. Antalic, K. Blaum, T. E. Cocolios, J. G. Cubiss, P. Van Duppen, T. Day Goodacre, A. de Roubin, G. J. Farooq-Smith, D. V. Fedorov, V. N. Fedosseev, D. A. Fink, L. P. Gaffney, L. Ghys, R. D. Harding, M. Huyse, N. Imai, S. Kreim, D. Lunney, K. M. Lynch, V. Manea, B. A. Marsh, Y. Martinez Palenzuela, P. L. Molkanov, D. Neidherr, M. Rosenbusch, R. E. Rossel, S. Rothe, L. Schweikhard, M. D. Seliverstov, S. Sels, C. Van Beveren, E. Verstraelen, A. Welker, F. Wienholtz, R. N. Wolf, and K. Zuber, "Shape coexistence in ^{187}Au studied by laser spectroscopy," Phys. Rev. C **101**, 064321 (2020).

R. D. Harding, A. N. Andreyev, A. E. Barzakh, D. Atanasov, J. G. Cubiss, P. Van Duppen, M. Al Monthery, N. A. Althubiti, B. Andel, S. Antalic, K. Blaum, T. E. Cocolios, T. Day Goodacre, A. de Roubin, G. J. Farooq-Smith, D. V. Fedorov, V. N. Fedosseev, D. A. Fink, L. P. Gaffney, L. Ghys, D. T. Joss, F. Herfurth, M. Huyse, N. Imai, S. Kreim, D. Lunney, K. M. Lynch, V. Manea, B. A. Marsh, Y. Martinez Palenzuela, P. L. Molkanov, D. Neidherr, R. D. Page, A. Pastore, M. Rosenbusch, R. E. Rossel, S. Rothe, L. Schweikhard, M. D. Seliverstov, S. Sels, C. Van Beveren, E. Verstraelen, A. Welker, F. Wienholtz, R. N. Wolf, and K. Zuber, "Laser-assisted decay spectroscopy for the ground states of ^{180,182}Au," Phys. Rev. C **102**, 024312 (2020).

J. G. Cubiss, A. N. Andreyev, A. E. Barzakh, V. Manea, M. Al Monthery, N. A. Althubiti, B. Andel, S. Antalic, D. Atanasov, K. Blaum, T. E. Cocolios, T. Day Goodacre, A. de Roubin, G. J. Farooq-Smith, D. V. Fedorov, V. N. Fedosseev, D. A. Fink, L. P. Gaffney, L. Ghys, R. D. Harding, F. Herfurth, M. Huyse, N. Imai, D. T. Joss, S. Kreim, D. Lunney, K. M. Lynch, B. A. Marsh, Y. Martinez Palenzuela, P. L. Molkanov, D. Neidherr, G. G. O'Neill, R. D. Page, M. Rosenbusch, R. E. Rossel, S. Rothe, L. Schweikhard, M. D. Seliverstov, S. Sels, A. Stott, C. Van Beveren, P. Van Duppen, E. Verstraelen, A. Welker, F. Wienholtz, R. N. Wolf, and K. Zuber, "Laser-assisted decay spectroscopy and mass spectrometry of ^{178}Au," Phys. Rev. C **102**, 044332 (2020).

T. L. Tang, T. Uesaka, S. Kawase, D. Beaumel, M. Dozono, T. Fujii, N. Fukuda, T. Fukunaga, A. Galindo-Uribarri, S. H. Hwang, N. Inabe, D. Kameda, T. Kawahara, W. Kim, K. Kisamori, M. Kobayashi, T. Kubo, Y. Kubota, K. Kusaka, C. S. Lee, Y. Maeda, H. Matsubara, S. Michimasa, H. Miya, T. Noro, A. Obertelli, K. Ogata, S. Ota, E. Padilla-Rodal, S. Sakaguchi, H. Sakai, M. Sasano, S. Shimoura, S. S. Stepanyan, H. Suzuki, M. Takaki, H. Takeda, H. Tokieda, T. Wakasa, T. Wakui, K. Yako, Y. Yanagisawa, J. Yasuda, R. Yokoyama, K. Yoshida, K. Yoshida, and J. Zenihiro, "How different is the core of ^{25}F from $^{24}O_{g.s.}$," Phys. Rev. Lett. **124**, 212502 (2020).

S. Michimasa, M. Kobayashi, Y. Kiyokawa, S. Ota, R. Yokoyama, D. Nishimura, D. S. Ahn, H. Baba, G. P. A. Berg, M. Dozono, N. Fukuda, T. Furuno, E. Ideguchi, N. Inabe, T. Kawabata, S. Kawase, K. Kisamori, K. Kobayashi, T. Kubo, Y. Kubota, C. S. Lee, M. Matsushita, H. Miya, A. Mizukami, H. Nagakura, H. Oikawa, H. Sakai, Y. Shimizu, A. Stolz, H. Suzuki, M. Takaki, H. Takeda, S. Takeuchi, H. Tokieda, T. Uesaka, K. Yako, Y. Yamaguchi, Y. Yanagisawa, K. Yoshida, and S. Shimoura, "Mapping of a new deformation region around ^{62}Ti," Phys. Rev. Lett. **125**, 122501 (2020).

D. Nagae, Y. Abe, S. Okada, S. Omika, K. Wakayama, S. Hosoi, S. Suzuki, T. Moriguchi M. Amano, D. Kamioka, Z. Ge, S. Naimi, F. Suzaki, N. Tadano, R. Igosawa, K. Inomata H. Arakawa, K. Nishimuro, T. Fujii, T. Mitsui, Y. Yanagisawa, H. Baba, S. Michimasa, S. Ota, G. Lorusso, Yu.A. Litvinov, A. Ozawa, T. Uesaka, T. Yamaguchi, Y. Yamaguchi, and M. Wakasugi, "Development and operation of an electrostatic time-of-flight detector for the Rare RI storage Ring," Nucl. Instrum. Methods Phys. Res. A **986**, 164713 (2021).

H. Suzuki, K. Yoshida, N. Fukuda, H. Takeda, Y. Shimizu, D. S. Ahn, T. Sumikama, N. Inabe, T. Komatsubara, H. Sato, Z. Korkulu, K. Kusaka, Y. Yanagisawa, M. Ohtake, H. Ueno, T. Kubo, S. Michimasa, N. Kitamura, K. Kawata, N. Imai, O. B. Tarasov, D. Bazin, J. Nolen, and W. F. Henning "Experimental studies of the two-step scheme with an intense radioactive ^{132}Sn beam for next-generation production of very neutron-rich nuclei," Phys. Rev. C **102**, 064615 (2020).

T. Sumikama. D. S. Ahn. N. Fukuda, Y. Shimizu, H. Suzuki, H. Takeda, H. Wang, K. Yoshida, J. Amano, N. Chiga, K. Chikaato, A. Hirayama, N. Inabe, S. Kawase, S. Kubono, M. Matsushita, S. Michimasa, K. Nakano, H. Otsu, H. Sakurai, A. Saito, S. Shimoura,

J. Suwa, M. Takechi, S. Takeuchi, Y. Togano, T. Tomai, and Y. Watanabe, "Energy-control and novel particle-identification methods combined with range in a multi-sampling ionization chamber for experiments using slowed-down RI beams," Nucl. Instrum. Methods Phys. Res. A **986**, 164687 (2021).

Y. L. Sun, T. Nakamura, Y. Kondo, Y. Satou, J. Lee, T. Matsumoto, K. Ogata, Y. Kikuchi, N. Aoi, Y. Ichikawa, K. Ieki, M. Ishihara, T. Kobayshi, T. Motobayashi, H. Otsu, H. Sakurai, T. Shimamura, S. Shimoura, T. Shinohara, T. Sugimoto, S. Takeuchi, Y. Togano, and K. Yoneda, "Three-body breakup of ^{6}He and its halo structure," Phys. Lett. B **814**, 136072 (2021).

S. Go, E. Ideguchi, R. Yokoyama, N. Aoi, F. Azaiez, K. Furutaka, Y. Hatsukawa, A. Kimura, K. Kisamori, M. Kobayashi, F. Kitatani, M. Koizumi, H. Harada, I. Matea, S. Michimasa, H. Miya, S. Nakamura, M. Niikura, H. Nishibata, N. Shimizu, S. Shimoura, T. Shizuma, M. Sugawara, D. Suzuki, M. Takaki, Y. Toh, Y. Utsuno, D. Verney, and A. Yagi, "High-spin states in ^{35}S," Phys. Rev. C **103**, 034327 (2021).

G. G. Kiss, M. La Cognata, C. Spitaleri, R. Yarmukhamedov, I. Wiedenhöver, L. T. Baby, S. Cherubini, A. Cvetinović, G. D'Agata, P. Figuera, G. L. Guardo, M. Gulino, S. Hayakawa, I. Indelicato, L. Lamia, M. Lattuada, F. Mudò, S. Palmerini, R. G. Pizzone, G. G. Rapisarda, S. Romano, M. L. Sergi, R. Spartà, O. Trippella, A. Tumino, M. Anastasiou, S. A. Kuvin, N. Rijal, B. Schmidt, S. B. Igamov, S. B. Sakuta, K. I. Tursunmakhatov, Zs. Fülöp, Gy. Gyürky, T. Szücs, Z. Halász, E. Somorjai, Z. Hons, J. Mrázek, R. E. Tribble, and A. M. Mukhamedzhanov, "Astrophysical S-factor for the ^{3}He$(\alpha,\gamma)^{7}$Be reaction via the asymptotic normalization coefficient (ANC) method," Phys. Lett. B **807**, 135606 (2020).

L. Yang, C. J. Lin, Y. X. Zhang, P. W. Wen, H. M. Jia, D. X. Wang, N. R. Ma, F. Yang, F. P. Zhong, S. H. Zhong, and T. P. Luo, "Bayesian analysis on interactions of exotic nuclear systems," Phys. Lett. B **807**, 135540 (2020).

L. Yang, C. J. Lin, H. Yamaguchi, J. Lei, P. W. Wen, M. Mazzocco, N. R. Ma, L. J. Sun, D. X. Wang, G. X. Zhang, K. Abe, S. M. Cha, K. Y. Chae, A. Diaz-Torres, J. L. Ferreira, S. Hayakawa, H. M. Jia, D. Kahl, A. Kim, M. S. Kwag, M. La Commara, R. Navarro Pérez, C. Parascandolo, D. Pierroutsakou, J. Rangel, Y. Sakaguchi, C. Signorini, E. Strano, X. X. Xu, F. Yang, Y. Y. Yang, G. L. Zhang, F. P. Zhong, and J. Lubian, "Insight into the reaction dynamics of proton drip-line nuclear system ^{17}F + ^{58}Ni at near-barrier energies," at near-barrier energies," Phys. Lett. B **813**, 136045 (2021).

N. Iwasa S. Ishikawa, S. Kubono, T. Sakakibara, K. Kominato, K. Nishio, M. Matsuda, K. Hirose, H. Makii, R. Orlandi, K. Asada, D. Guru, S. Nishimura, S. Hayakawa, and T. Kawabata, "Experimental study of the Γ_{p1}/Γ_{p0} ratios of resonance states in ^{8}Be for deducing the ^{7}Be$(n,p_1)^{7}$Li* reaction rate relevant to the cosmological lithium problem," Phys. Rev. C **103**, 015801 (2021).

D. X. Wang, C. J. Lin, L. Yang, N. R. Ma, L. J. Sun, F. Yang, H. M. Jia, F. P. Zhong, and P. W. Wen, "Compact 16-channel integrated charge-sensitive preamplifier module for silicon strip detectors," Nucl. Sci. Tech. **31**, 48 (2020).

Y. J. Yao, C. J. Lin, L. Yang, N. R. Ma, D. X. Wang, G. L. Zhang, G. X. Zhang, H. M. Jia, F. Yang, F. P. Zhong, P. W. Wen, X. B. Qin, and H. M. Zhao, "Relative probabilities of breakup channels in reactions of ^{6,7}Li with ^{209}Bi at energies around and above the Coulomb barrier," Chin. Phys. C **45**, 054104 (2021).

Y. J. Yao, C. J. Lin, L. Yang, N. R. Ma, D. X. Wang, G. L. Zhang, G. X. Zhang, H. M. Jia, and F. Yang, "The effects of beam drifts on elastic scattering measured by the large solid-angle covered detector array," Nucl. Sci. Tech. **32**, Article number:14 (2021).

Shreyasi Acharya *et al.* (ALICE Collaboration), "Production of light-flavor hadrons in pp collisions at $\sqrt{s}$ = 7 and $\sqrt{s}$ = 13 TeV," Eur. Phys. J. C **81**, 256 (2021).

U. A. Acharya *et al.* (PHENIX Collaboration), "Transverse single-spin asymmetries of midrapidity π^0 and η mesons in polarized $p+p$ collisions at $\sqrt{s}$ = 200 GeV," Phys. Rev. D **103**, 052009 (2021).

J. Adolfsson *et al.* (ALICE TPC Collaboration), "The upgrade of the ALICE TPC with GEMs and continuous readout," J. Instrum. **16**, P03022 (2021).

U. A. Acharya *et al.* (PHENIX Collaboration), "Transverse momentum dependent forward neutron single spin asymmetries in transversely polarized $p+p$ collisions at $\sqrt{s}$ = 200 GeV," Phys. Rev. D **103**, 032007 (2021),

Shreyasi Acharya *et al.* (ALICE Collaboration), "Pion-kaon femtoscopy and the lifetime of the hadronic phase in Pb-Pb collisions at $\sqrt{s_{NN}}$ = 2.76 TeV," Phys. Lett. B **813**, 136030 (2021).

Shreyasi Acharya *et al.* (ALICE Collaboration), "Transverse-momentum and event-shape dependence of D-meson flow harmonics in Pb-Pb collisions at $\sqrt{s_{NN}}$ = 5.02 TeV," Phys. Lett. B **813**, 136054 (2021).

Shreyasi Acharya *et al.* (ALICE Collaboration), "Centrality dependence of J/ψ and ψ(2S) production and nuclear modification in p-Pb collisions at $\sqrt{s_{NN}}$ = 8.16 TeV," J. High Energy Phys. **2102**, 002 (2021).

T. Awes *et al.*, "Design and performance of a silicon tungsten calorimeter prototype module and the associated readout," Nucl. Instrum. Methods Phys. Res. A **988**, 164796 (2021).

Shreyasi Acharya *et al.* (ALICE Collaboration), "Unveiling the strong interaction among hadrons at the LHC," Nat. Phys. **588**, 232–238 (2020).

Shreyasi Acharya *et al.* (ALICE Collaboration), "Search for a common baryon source in high-multiplicity pp collisions at the LHC," Phys. Lett. B **811**, 135849 (2020).

U. Acharya *et al.* (PHENIX Collaboration), "Production of π^0 and η mesons in U + U collisions at $\sqrt{s_{NN}}$ = 192 GeV," Phys. Rev. C **102**, 064905 (2020).

Shreyasi Acharya *et al.* (ALICE Collaboration), "Dielectron production in proton-proton and proton-lead collisions at $\sqrt{s_{NN}}$ = 5.02 TeV," Phys. Rev. C **102**, 055204 (2020).

U. Acharya *et al.* (PHENIX Collaboration), "Measurement of jet-medium interactions via direct photon-hadron correlations in Au + Au and d +Au collisions at $\sqrt{s_{NN}}$ = 200 GeV," Phys. Rev. C **102**, 054910 (2020).

Shreyasi Acharya *et al.* (ALICE Collaboration), "Elliptic and triangular flow of (anti)deuterons in Pb-Pb collisions at $\sqrt{s_{NN}}$ = 5.02 TeV," Phys. Rev. C **102**, 055203 (2020).

U. Acharya *et al.* (PHENIX Collaboration), "Production of b-$\bar{b}$ at forward rapidity in $p+p$ collisions at $\sqrt{s}$ = 510 GeV," Phys. Rev. D **102**, 092002 (2020).

U. Acharya *et al.* (PHENIX Collaboration), "Polarization and cross section of midrapidity J/ψ production in $p+p$ collisions at $\sqrt{s}$ = 510 GeV," Phys. Rev. D **102**, 072008 (2020).

Shreyasi Acharya *et al.* (ALICE Collaboration), "J/ψ elliptic and triangular flow in Pb-Pb collisions at $\sqrt{s_{NN}}$ = 5.02 TeV," J. High Energy Phys. **2010**, 141 (2020).

Shreyasi Acharya *et al.* (ALICE Collaboration), "Azimuthal correlations of prompt D mesons with charged particles in pp and p-Pb collisions at $\sqrt{s_{NN}}$ = 5.02 TeV," Eur. Phys. J. C **80**, 979 (2020).

Shreyasi Acharya *et al.* (ALICE Collaboration), "Measurement of isolated photon-hadron correlations in $\sqrt{s_{NN}}$ = 5.02 TeV pp and p-Pb collisions," Phys. Rev. C **102**, 044908 (2020).

Shreyasi Acharya *et al.* (ALICE Collaboration), "Measurement of the low-energy antideuteron inelastic cross section," Phys. Rev. Lett. **125**, 162001 (2020).

Shreyasi Acharya *et al.* (ALICE Collaboration), "J/ψ production as a function of charged-particle multiplicity in p-Pb collisions at $\sqrt{s_{NN}}$ = 8.16 TeV," J. High Energy Phys. **2009**, 162 (2020).

S. Acharya *et al.* (ALICE Collaboration), "(Anti-)deuteron production in pp collisions at $\sqrt{s}$ = 13 TeV," Eur. Phys. J. C **80**, 889 (2020).

Shreyasi Acharya *et al.* (ALICE Collaboration), "Constraining the chiral magnetic effect with charge-dependent azimuthal correlations in Pb-Pb collisions at $\sqrt{s_{NN}}$ = 2.76 and 5.02 TeV," J. High Energy Phys. **2009**, 160 (2020).

Shreyasi Acharya *et al.* (ALICE Collaboration), "Z-boson production in p-Pb collisions at $\sqrt{s_{NN}}$ = 8.16 TeV and Pb-Pb collisions at $\sqrt{s_{NN}}$ = 5.02 TeV," J. High Energy Phys. **2009**, 076 (2020).

Shreyasi Acharya *et al.* (ALICE Collaboration), "Multiplicity dependence of J/ψ production at midrapidity in pp collisions at $\sqrt{s}$ = 13 TeV," Phys. Lett. B **810**, 135758 (2020).

Shreyasi Acharya *et al.* (ALICE Collaboration), "$K^*(892)^0$ and $\phi(1020)$ production at midrapidity in pp collisions at $\sqrt{s}$ = 8 TeV," Phys. Rev. C **102**, 024912 (2020).

Shreyasi Acharya *et al.* (ALICE Collaboration), "Multiplicity dependence of $K^*(892)^0$ and $\phi(1020)$ production in pp collisions at $\sqrt{s}$ = 13 TeV", Phys. Lett. B **807**, 135501 (2020).

Shreyasi Acharya *et al.* (ALICE Collaboration), "Global baryon number conservation encoded in net-proton fluctuations measured in Pb-Pb collisions at $\sqrt{s_{NN}}$ = 2.76 TeV," Phys. Lett. B **807**, 135564 (2020).

U. A. Acharya *et al.* (PHENIX Collaboration), "Measurement of charged pion double spin asymmetries at midrapidity in longitudinally polarized $p+p$ collisions at $\sqrt{s}$ = 510 GeV," Phys. Rev. D **102**, 032001 (2020).

Shreyasi Acharya *et al.* (ALICE Collaboration), "Multiplicity dependence of π, K, and p production in pp collisions at $\sqrt{s}$ = 13 TeV," Eur. Phys. J. C **80**, 693, (2020).

Shreyasi Acharya *et al.* (ALICE Collaboration), "Measurement of nuclear effects on ψ(2S) production in p-Pb collisions at $\sqrt{s_{NN}}$ = 8.16 TeV," J. High Energy Phys. **2007**, 237 (2020).

Shreyasi Acharya *et al.* (ALICE Collaboration), "Probing the effects of strong electromagnetic fields with charge-dependent directed flow in Pb-Pb collisions at the LHC," Phys. Rev. Lett. **125**, 022301 (2020).

U. Acharya *et al.* (PHENIX Collaboration), "Measurement of J/ψ at forward and backward rapidity in $p+p$, $p+$Al, $p+$Au, and ^{3}He + Au collisions at $\sqrt{s_{NN}}$ = 200 GeV," Phys. Rev. C **102**, 014902 (2020).

Shreyasi Acharya *et al.* (ALICE Collaboration), "Production of ω mesons in pp collisions at $\sqrt{s}$ = 7 TeV," Eur. Phys. J. C **80**, 1130 (2020).

Shreyasi Acharya *et al.* (ALICE Collaboration), "Evidence of spin-orbital angular momentum interactions in relativistic heavy-ion collisions," Phys. Rev. Lett. **125**, 012301 (2020).

Shreyasi Acharya *et al.* (ALICE Collaboration), "Non-linear flow modes of identified particles in Pb-Pb collisions at $\sqrt{s_{NN}}$ = 5.02 TeV," J. High Energy Phys. **2006**, 147 (2020).

Shreyasi Acharya *et al.* (ALICE Collaboration), "Investigation of the p-Σ^0 interaction via femtoscopy in pp collisions," Phys. Lett. B **805**, 135419 (2020).

Shreyasi Acharya *et al.* (ALICE Collaboration), "Centrality and transverse momentum dependence of inclusive J/ψ production at midrapidity in Pb-Pb collisions at $\sqrt{s_{NN}}$ = 5.02 TeV," Phys. Lett. B **805**, 135434 (2020).

Shreyasi Acharya *et al.* (ALICE Collaboration), "Measurement of the (anti-)^{3}He elliptic flow in Pb-Pb collisions at $\sqrt{s_{NN}}$ = 5.02 TeV," Phys. Lett. B **805**, 135414 (2020).

Shreyasi Acharya *et al.* (ALICE Collaboration), "Coherent photoproduction of ρ^0 vector mesons in ultra-peripheral Pb-Pb collisions at $\sqrt{s_{NN}}$ = 5.02 TeV," J. High Energy Phys. **2006**, 035 (2020).

Shreyasi Acharya *et al.* (ALICE Collaboration), "Jet-hadron correlations measured relative to the second order event plane in Pb-Pb collisions at $\sqrt{s_{NN}}$ = 2.76 TeV," Phys. Rev. C **101**, 064901 (2020).

Shreyasi Acharya *et al.* (ALICE Collaboration), "Higher harmonic non-linear flow modes of charged hadrons in Pb-Pb collisions at $\sqrt{s_{NN}}$ = 5.02 TeV,"J. High Energy Phys. **2005**, 085 (2020).

Shreyasi Acharya *et al.* (ALICE Collaboration), "Longitudinal and azimuthal evolution of two-particle transverse momentum correlations in Pb-Pb collisions at $\sqrt{s_{NN}}$ = 2.76 TeV,"Phys. Lett. B **804**, 135375 (2020).

Shreyasi Acharya *et al.* (ALICE Collaboration), "Measurement of electrons from semileptonic heavy-flavour hadron decays at midrapidity in pp and Pb-Pb collisions at $\sqrt{s_{NN}}$ = 5.02 TeV," Phys. Lett. B **804**, 135377 (2020).

Shreyasi Acharya *et al.* (ALICE Collaboration), "Production of charged pions, kaons, and (anti-)protons in Pb-Pb and inelastic pp

collisions at $\sqrt{s_{NN}}$ = 5.02 TeV," Phys. Rev. C **101**, 044907 (2020).

Shreyasi Acharya *et al*. (ALICE Collaboration), "Production of (anti-)^{3}He and (anti-)^{3}H in p-Pb collisions at $\sqrt{s_{NN}}$ = 5.02 TeV," Phys. Rev. C **101**, 044906 (2020).

Shreyasi Acharya *et al*. (ALICE Collaboration), "Underlying event properties in pp collisions at $\sqrt{s}$ = 13 TeV," J. High Energy Phys. **2004**, 192 (2020).

Shreyasi Acharya *et al*. (ALICE Collaboration), "Global polarization of $\Lambda\bar{\Lambda}$ hyperons in Pb-Pb collisions at $\sqrt{s_{NN}}$ = 2.76 and 5.02 TeV," Phys. Rev. C **101**, 044611 (2020).

A. Kastberg, B. K. Sahoo, T. Aoki, Y. Sakemi, and B. P. Das, "Analysis of an optical lattice methodology for detection of atomic parity nonconservation," Symmetry **12**, 974 (2020).

N. Shimizu, Y. Tsunoda, Y. Utsuno, and T. Otsuka, "The variational approach with the superposition of the symmetry-restored quasi-particle vacua for nuclear shell-model calculaions," Phys. Rev. C **103**, 014312 (2021).

K. Kaneko, N. Shimizu, T. Mizusaki, and Y. Sun, "Triple enhancement of quasi-SU(3) quadrupole collectivity in strontium-zirconium N Z isotopes," Phys. Lett. B **817**, 136286 (2021).

S. Go, E. Ideguchi, R. Yokoyama, F. Azaiez, N. Aoi, K. Furutaka, Y. Hatsukawa, A. Kimura, K. Kisamori, M. Kobayashi, F. Kitatani, M. Koizumi, H. Harada, I. Matea, S. Michimasa, H. Miya, S. Nakamura, M. Niikura, H. Nishibata, N. Shimizu, S. Shimoura, T. Shizuma, M. Sugawara, D. Suzuki, M. Takaki, Y. Utsuno, Y. Toh, D. Verney, and A. Yagi, "High-spin states in ^{35}S," Phys. Rev. C **103**, 034327 (2021).

N. Kitamura, K. Wimmer, N. Shimizu, V. M. Bader, C. Bancroft, D. Barofsky, T. Baugher, D. Bazin, J. S. Berryman, V. Bildstein, A. Gade, N. Imai, T. Koll, C. Langer, J. Lloyd, E. Lunderberg, G. Perdikakis, F. Recchia, T. Redpath, S. Saenz, D. Smalley, S. R. Stroberg, J. A. Tostevin, N. Tsunoda, Y. Utsuno, D. Weisshaar, and A. Westerberg "Structure of ^{30}Mg explored via in-beam γ-ray spectroscopy," Phys. Rev. C **102**, 054318 (2020).

N. Tsunoda, T. Otsuka, K. Takayanagi, N. Shimizu, T. Suzuki, Y. Utsuno, and H. Ueno, "The impact of nuclear shape on the emergence of the neutron dripline," Nature **587**, 66 (2020).

K. Kaneko, N. Shimizu, T. Mizusaki, Y. Sun, "Quasi-SU(3) coupling of ($1h_{11/2}$, $2f_{7/2}$) across the N = 82 shell gap: Enhanced $E2$ collectivity and shape evolution in Nd isotopes," Phys. Rev. C **103**, L021301 (2021).

N. Shimizu, T. Togashi, and Y. Utsuno, "Gamow-Teller transitions of neutron-rich N = 82 and N = 81 nuclei by shell-model calculations," Prog. Theor. Exp. Phys. **2021**, 033D01 (2021).

K. Yanase and N. Shimizu, "Large-scale shell-model calculations of nuclear Schiff moments of ^{129}Xe and ^{199}Hg," Phys. Rev. C **102**, 065502 (2020).

K. Yanase, "Screening of nucleon electric dipole moments in atomic systems," Phys. Rev. C **103**, 035501 (2021).

P. A. SÖderstrÖm, L. Capponi, E. Açiksöz, T. Otsuka, N. Tsoneva, Y. Tsunoda, D. L. Balabanski, N. Pietralla, G. L. Guardo, D. Lattuada, H. Lenske, C. Matei, D. Nichita, A. Pappalardo, and T. Petruse, "Electromagnetic character of the competitive $\gamma\gamma/\gamma$-decay from ^{137m}Ba,"

N. Mărginean, D. Little, Y. Tsunoda, S. Leoni, R. V. F. Janssens, B. Fornal, T. Otsuka, C. Michelagnoli, L. Stan, F. C. L. Crespi, C. Costache, R. Lica, M. Sferrazza, A. Turturica, A. D. Ayangeakaa, K. Auranen M. Barani, P. C. Bender, S. Bottoni, M. Boromiza, A. Bracco, S. Călinescu, C. M. Campbell, M. P. Carpenter, P. Chowdhury, M. Ciemala, N. Cieplicka-Oryńczak, D. Cline, C. Clisu, H. L. Crawford, I. E. Dinescu, J. Dudouet, D. Filipescu, N. Florea, A. M. Forney, S. Fracassetti, A. Gade, I. Gheorghe, A. B. Hayes, I. Harca, J. Henderson, A. Ionescu, L. W. Iskra, M. Jentschel, F. Kandzia, Y. H. Kim, F. G. Kondev, G. Korschinek, U. Köster, Krishichayan, M. Krzysiek, T. Lauritsen, J. Li, R. Mărginean, E. A. Maugeri, C. Mihai, R. E. Mihai, A. Mitu, P. Mutti, A. Negret, C. R. Niţă, A. Olăcel, A. Oprea, S. Pascu, C. Petrone, C. Porzio, D. Rhodes, D. Seweryniak, D. Schumann, C. Sotty, S. M. Stolze, R. Şuvăilă, S. Toma, S. Ujeniuc, W. B. Walters, C. Y. Wu, J. Wu, S. Zhu, and S. Ziliani, "Shape coexistence at zero spin in 64Ni driven by the monopole tensor interaction," Phys. Rev. Lett. **125**, 102502 (2020).

F. L. Bello Garrote, E. Sahin, Y. Tsunoda, T. Otsuka, A. Görgen, M. Niikura, S. Nishimura, G. de Angelis, G. Benzoni, A. I. Morales, V. Modamio, Z. Y. Xu, H. Baba, F. Browne, A. M. Bruce, S. Ceruti, F. C. L. Crespi, R. Daido, M. -C. Delattre, P. Doornenbal, Zs. Dombradi, Y. Fang, S. Franchoo, G. Gey, A. Gottardo, K. Hadyńska-Klęk, T. Isobe, P. R. John, H. S. Jung, I. Kojouharov, T. Kubo, N. Kurz, I. Kuti, Z. Li, G. Lorusso, I. Matea, K. Matsui, D. Mengoni, T. Miyazaki, S. Momiyama, P. Morfouace, D. R. Napoli, F. Naqvi, H. Nishibata, A. Odahara, R. Orlandi, Z. Pate, S. Rice, H. Sakurai, H. Schaffner, L. Sinclair, P. -A. Söderström, D. Sohler, I. G. Stefan, T. Sumikama, D. Suzuki, R. Taniuchi, J. Taprogge, Zs. Vajta, J. J. Valiente-Dobón, H. Watanabe, V. Werner, J. Wu, A. Yagi, M. Yalcinkaya, R. Yokoyama, and K. Yoshinaga, "β decay of 75Ni and the systematics of the low-lying level structure of neutron-rich odd-A Cu isotopes," Phys. Rev. C **102**, 034314 (2020).

C. Porzio, C. Michelagnoli, N. Cieplicka-Oryńczak, M. Sferrazza, S. Leoni, B. Fornal, Y. Tsunoda, T. Otsuka, S. Bottoni, C. Costache, F. C. L. Crespi, L. W. Iskra, M. Jentschel, F. Kandzia, Y. -H. Kim, U. Köster, N. Mărginean, C. Mihai, P. Mutti, and A. Turturică, "Detailed low-spin spectroscopy of 65Ni via neutron capture reaction," Phys. Rev. C **102**, 064310 (2020).

Y. Tsunoda and T. Otsuka, "Triaxial rigidity of ^{166}Er and its Bohr-model realization," Phys. Rev. C **103**, L021303 (2021).

A. Kundu, Md. S. R. Laskar, R. Palit, R. Raut, S. Santra, N. Shimizu, T. Togashi, E. Ideguchi, H. Pai, S. Ali, F. S. Babra, R. Banik, S. Bhattacharya, B. Das, P. Dey, R. Donthi, A. Goswami, S. Jadhav, G. Mukherjee, B. S. Naidu, L. P. Singh, S. Rajbanshi, H. P. Sharma, S. S. Tiwary, and A. T. Vazhappilly, "New lifetime measurement for the 2_1^+ level of ^{112}Sn by the Doppler shift attenuation method," Phys. Rev. C **103**, 034315 (2021).

[Review Articles]

H. Yamaguchi, D. Kahl, and S. Kubono, "CRIB: the low energy in-flight RI beam separator," Nuclear Physics News International **30**, No. 2, 21–27 (2020).

[Proceedings]

L. Lamia, R. G. Pizzone, M. Mazzocco, S. Hayakawa, M. La Cognata, C. A. Bertulani, S. Cherubini, G. D'Agata, G. L. Guardo, M. Gulino, I. Indelicato, G. G. Rapisarda, S. Romano, M. L. Sergi, R. Spartà, C. Spitaleri, and A. Tumino, J. Phys. Conf. Ser. **1643**, 012096 (2020).

A. Inoue, A. Tamii, P. Chan, S. Hayakawa, N. Kobayashi, Y. Maeda, K. Nonaka, T. Shima, H. Shimizu, D. T. Tran, X. Wang, H. Yamaguchi, L. Yang, and Z. Yang, J. Phys. Conf. Ser. **1643**, 012049 (2020).

H. Yamaguchi, S. Hayakawa, N. Ma, H. Shimizu, L. Yang, D. Kahl, K. Abe, T. Suhara, N. Iwasa, A. Kim, D. Kim, S. Cha, M. Kwag, J. Lee, E. Lee, K. Chae, Y. Wakabayashi, N. Imai, N. Kitamura, P. Lee, J. Moon, K. Lee, C. Akers, H. Jung, N. Duy, L. Khiem, C. Lee, S. Cherubini, M. Gulino, C. Spitaleri, G. Rapisarda, L. Cognata, L. Lamia, S. Romano, A. Coc, N. de Sereville, F. Hammache, G. Kiss, S. Bishop, T. Teranishi, T. Kawabata, Y. Kwon, and D. Binh, J. Phys. Conf. Ser. **1643**, 012069 (2020).

M. Mazzocco, N. Keeley, A. Boiano, C. Boiano, M. L. Commara, A. Lagni, C. Manea, C. Parascandolo, D. Pierroutsakou, C. Signorini, E. Strano, D. Torresi, H. Yamaguchi, D. Kahl, L. Acosta, D. Meo, J. P. Fernandez-Garcia, T. Glodariu, J. Grebosz, A. Guglielmetti, Y. Hirayama, N. Imai, H. Ishiyama, N. Iwasa, S. C. Jeong, H. M. Jia, Y. H. Kim, S. Kimura, S. Kubono, G. L. Rana, C. J. Lin, P. Lotti, G. Marquínez-Duran, I. Martel, H. Miyatake, M. Mukai, T. Nakao, M. Nicoletto, A. Pakou, K. Rusek, Y. Sakaguchi, A. M. Sanchez-Benitez, T. Sava, O. Sgouros, V. Soukeras, F. Soramel, E. Stiliaris, L. Stroe, T. Teranishi, N. Toniolo, Y. Wakabayashi, Y. X. Watanabe, L. Yang, Y. Y. Yang, and H. Q. Zhang, J. Phys. Conf. Ser. **1643**, 012096 (2020).

H. Yamaguchi, S. Hayakawa, L. Yang, H. Shimizu, D. Kahl, T. Suhara, N. Iwasa, S. M. Cha, M. S. Kwag, J. H. Lee, E. J. Lee, K. Y. Chae, A. Kim, D. H. Kim, Y. Wakabayashi, N. Imai, N. Kitamura, P. Lee, J. Y. Moon, K. B. Lee, C. Akers, N. N. Duy, L. H. Khiem, and C. S. Lee, JPS Conf. Proc. **32**, 010055 (2020).

S. Hayakawa, L. Lamia, C. Spitaleri, C. A. Bertulani, S. Q. Hou, M. L. Cognata, M. Mazzocco, R. G. Pizzone, D. Pierroutsakou, S. Romano, M. L. Sergi, and A. Tumino, JPS Conf. Proc. **32**, 010058 (2020).

R. G. Pizzone, G. D'Agata, I. Indelicato, M. L. Cognata, P. Figuera, G. L. Guardo, S. Hayakawa, L. Lamia, M. Lattuada, M. Milin, G. G. Rapisarda, S. Romano, M. L. Sergi, N. Skukan, N. Soic, C. Spitaleri, and A. Tumino, JPS Conf. Proc. **32**, 010062 (2020).

A. Tumino, C. Spitaleri, M. L. Cognata, S. Cherubini, G. L. Guardo, M. Gulino, S. Hayakawa, I. Indelicato, L. Lamia, H. Petrascu, R. G. Pizzone, S. M. R. Puglia, G. G. Rapisarda, S. Romano, M. L. Sergi, R. Sparta, and L. Trache, Proceedings of 13th International Conference on Nucleus-Nucleus, JPS Conf. Proc. **32**, 010059 (2020).

Y. Kotaka, Y. Ohshiro, H. Yamaguchi, N. Imai, Y. Sakemi, S. Shimoura, T. Nagatomo, J. Ohnishi, T. Nakagawa, M. Kase, A. Goto, K. Hatanaka, and H. Muto, "Development of the calculation method of injection beam trajectory of RIKEN AVF Cyclotron with 4D emittance measured by the developed pepper-pot emittance monitor," Proceedings of the 8th International Beam Instrumentation Conference (IBIC2019), JACoW-IBIC2019-TUPP022 (2020).

Y. Sakemi, T. Aoki, R. Calabrese, H. Haba, K. Harada, T. Hayamizu, Y. Ichikawa, K. Jungmann, A. Kastberg, Y. Kotaka, Y. Matsuda, H. Nagahama, K. Nakamura, M. Otsuka, N. Ozawa, K. S. Tanaka, A. Uchiyama, H. Ueno, and L. Willmann, "Fundamental physics with cold radioactive atoms," AIP Conf. Proc. **2319**, 080020 (2021).

Presentations

[International Conferences/Workshops]

N. Imai (invited), "Preparation status of NP1912-SHARAQ18," OEDO/SHARAQ Collabotration Meeting 2020, On-line, September 7, 2020.

S. Michimasa (invited), "Mapping background X-rays from OEDO RFD," OEDO/SHARAQ Collabotration Meeting 2020, On-line, September 7, 2020.

M. Dozono (invited), "Probing exotic structures of highly excited nuclei: OEDO-SHARAQ activities," RIBF User Meeting, On-line, September 8–10, 2020.

S. Michimasa (invited), "Development of energy-degraded RI beam and expansion of nuclear reaction studies," Symposium of Nuclear Data 2020 (hybrid), Saitama, Japan, November 26–27, 2020.

S. Ota (invited), "Study of nuclear matter property via nuclear scattering and reactions," JPS/NRF/NSFC A3 Foresight Program "Nuclear Physics in the 21st Century" Joint Annual Meeting, Huizhou, China and On-line, November 18–19, 2020.

H. Yamaguchi (oral), "Activities at the low-energy RI beam separator CRIB," RIBF Users Meeting 2020 (on-line), Saitama, Japan, Sepember 8–10, 2020.

H. Yamaguchi (oral), "Overview of alpha resonant scattering experiments at CRIB," International mini-workshop on "Physics in resonant reaction induced by low-energy RI beam", Web Meeting Hosted by CNS, the University of Tokyo/IBS Center for Exotic Nuclear Studies/Department of Pure and Applied Physics, Kansai University/Research Center for Nuclear Physics (RCNP), Osaka, Japan, February 22, 2021.

N. R. Ma (oral), "Primary result of $^{14}O + \alpha$ clustering study at CRIB," International mini-workshop on "Physics in resonant reaction induced by low-energy RI beam", Web Meeting Hosted by CNS, the University of Tokyo/IBS Center for Exotic Nuclear Studies/Department of Pure and Applied Physics, Kansai University/Research Center for Nuclear Physics (RCNP), Osaka, Japan, February 22, 2021.

D. Sekihata (oral) for the ALICE Collaboration, "Low-mass dielectron measurements in pp, p-Pb and Pb-Pb collisions with ALICE at the LHC," 10th International Conference on Hard and Electromagnetic Probes of High-Energy Nuclear Collisions, Online, June 2020.

T. Hayamizu (oral), "Development of ultracold francium atomic sources towards the permanent EDM search," Yamada Conference LXXII: The 8th Asia-Pacific Conference on Few-Body Problems in Physics (APFB2020), Kanazawa, Japan, March 4, 2021.

N. Shimizu (oral), "Data-driven approaches in nuclear shell-model calculations," Nuclear Data Symposium 2020 (RIKEN Nishina Cen-

ter), Saitama, Japan, November 27, 2020.

Y. Tsunoda (invited), "Structure of medium-mass nuclei studied by Monte Carlo shell model calculations," The RIBF Users Meeting 2020, Online, September 9, 2020.

Y. Tsunoda (oral), "Nuclear shapes and collective motions in the region of Sm," 12th Symposium on Discovery, Fusion, Creation of New Knowledge by Multidisciplinary Computational Sciences, Online, October 6, 2020.

K. Yanase (oral), "Large-scale shell-model calculations of nuclear Schiff moments of 129Xe and 199Hg," Beyond-the-Standard-Model Physics with Nucleons and Nuclei (INT 20-2b), online, July 23, 2020.

[Domestic Conferences/Workshops]

今井伸明 (招待講演), 「不安定核の中性子捕獲率測定プロジェクト」, 研究会「星の錬金術から銀河考古学へ」, 東京都三鷹市（国立天文台）, 2020 年 10 月 26–29 日.

下浦亨（招待講演）, "Direct reactions as quantum probes of nuclear system," Symposium on "JPS nuclear physics and physical review C," 日本物理学会 2020 年秋季大会, オンライン, 2020 年 9 月 14 日–17 日.

花井周太郎 (口頭発表), 「分割電極型 PPAC(SR-PPAC) における位置較正手法の開発」, 日本物理学会 2020 年秋季大会, on-line, 2020 年 9 月 14 日–17 日.

道正新一郎（口頭発表）, 「中性子過剰 ^{62}Ti 核および近傍核の質量測定」, 日本物理学会 第 76 回年次大会, オンライン講演, 2021 年 3 月 12–15 日.

堂園昌伯（口頭発表）, 「(^{4}He, ^{6}He) 反応による錫同位体の対振動状態の研究」, 日本物理学会 第 76 回年次大会, オンライン講演, 2021 年 3 月 12–15 日.

郡司卓（招待講演）, "ALICE upgrade and physics topics (II)," 第 4 回クラスター階層領域研究会, オンライン講演, 2020 年 5 月 28 日.

関畑大貴（口頭発表）, 「機械学習を用いた ALICE-TPC 検出器内部の空間電荷効果補正」, MPGD & Active 媒質 TPC 研究会 2020, 兵庫県神戸市（神戸大学+オンライン）, 2020 年 12 月.

関畑大貴 for the ALICE Collaboration（口頭発表）, 「機械学習を用いた ALICE-TPC 検出器内部の空間電荷効果補正」, 日本物理学会 第 76 回年次大会, オンライン講演, 2021 年 3 月 12–15 日.

関畑大貴（基調講演）, 「核子対あたり重心系エネルギー 5.02 における中性中間子と直接光子測定」(受賞記念企画公演), 日本物理学会 第 76 回年次大会, オンライン講演, 2021 年 3 月 12–15 日.

関口裕子（口頭発表） for the ALICE Collaboration, 「LHC-ALICE 実験を用いた小さな衝突系における方位角異方性の擬ラピディティ依存性測定」, 日本物理学会 第 76 回年次大会, オンライン講演, 2021 年 3 月 12–15 日.

清水夏樹（口頭発表） for the ALICE Collaboration, 「ALICE 実験における Run2 全統計を用いたエキゾチックハドロン探索」, 日本物理学会 第 76 回年次大会, オンライン講演, 2021 年 3 月 12–15 日.

佐藤幹（口頭発表）, 「高効率フランシウム原子線のための吸着防止コーティング材の評価」, 日本物理学会 第 76 回年次大会, オンライン講演, 2021 年 3 月 12–15 日.

君塚大樹（口頭発表）, 「狭線幅光会合を用いた極低温 Sr_2 分子生成のための高安定な光源開発」, 日本物理学会 第 76 回年次大会, オンライン講演, 2021 年 3 月 12–15 日.

池田英彦（口頭発表）, 「電場の量子センシングに向けた Sr リドベルグ原子の分光」, 日本物理学会 第 76 回年次大会, オンライン講演, 2021 年 3 月 12–15 日.

小澤直也（口頭発表）, 「フランシウム原子の電気双極子能率探索のための表面電離イオン源の開発」, 日本物理学会 第 76 回年次大会, オンライン講演, 2021 年 3 月 12–15 日.

清水則孝（口頭発表）, 「準粒子真空基底によるモンテカルロ殻模型の拡張」, 日本物理学会 第 76 回年次大会, オンライン講演, 2021 年 3 月 12–15 日.

角田佑介（口頭発表）, 「モンテカルロ殻模型による二重ベータ崩壊の核行列要素の計算」, 新学術領域「地下宇宙」2020 年度領域研究会, オンライン講演, 2020 年 6 月 2 日.

角田佑介（口頭発表）, 「モンテカルロ殻模型による二重ベータ崩壊の核行列要素の計算」, 日本物理学会 第 76 回年次大会, オンライン講演, 2021 年 3 月 12–15 日.

柳瀬宏太（口頭発表）, 「原子核殻模型による電気双極子モーメントの精密計算」, 「富岳で加速する素粒子・原子核・宇宙・惑星」シンポジウム, オンライン講演, 2021 年 1 月 28 日.

柳瀬宏太（口頭発表）, 「清水則孝, 原子核殻模型による電気双極子モーメントの精密計算」, 日本物理学会 第 76 回年次大会, オンライン講演, 2021 年 3 月 12–15 日.

[Seminars]

N. Kitamura (oral), "In-beam spectroscopy of ^{30}Mg: structural evolution approaching the island of inversion," CNS Seminar, On-line, July 29, 2020.

S. Koyama (oral), "Spectroscopy of resonance states in light proton-rich nuclei via missing mass method," CNS Seminar, On-line, August 7, 2020.

鎌倉恵太 (oral), 「東大 HyperECR イオン源の現状」, 第 19 回 AVF 合同打ち合わせ, 宮城県仙台市（東北大学）, 2021 年 3 月 10 日.

小高康照 (oral), 「理研 AVF のビーム輸送系最適化の現状」, 第 19 回 AVF 合同打ち合わせ, 宮城県仙台市（東北大学）, 2021 年 3 月 10 日.

Awards

関畑大貴, 第 15 回日本物理学会若手奨励賞 (実験核物理領域).

関畑大貴, 第 27 回原子核談話会新人賞.

Press Releases

道正新一郎, 小林幹, 下浦享, 上坂友洋, 井手口栄治, 西村太樹, 「チタン同位体でおこる新たな安定化現象を発見—質量測定で迫る原子核存在限界」, 2020 年 9 月 16 日.

大塚孝治, 角田直文, 高柳和雄, 清水則孝, 鈴木俊夫, 宇都野穣, 吉田聡太, 上野秀樹, 「原子核の存在限界（中性子ドリップライン）の新たなメカニズム」, 2020 年 11 月 5 日, https://www.s.u-tokyo.ac.jp/ja/press/2020/7074/.

Others

[東京大学理学部ニュース]

道正新一郎, 「質量から探る原子核の秩序と存在限界」, 学部生に伝える研究最前線, 東京大学理学部ニュース 2021 年 1 月号.

Partner Institution
Wako Nuclear Science Center, IPNS (Institute of Particle and Nuclear Studies)
KEK (High Energy Accelerator Research Organization)

1. Abstract

The Wako Nuclear Science Center (WNSC) of KEK aims to promote low-energy nuclear physics and nuclear astrophysics research and interdisciplinary studies using short-lived radioactive nuclei. WNSC operates the KEK Isotope Separation System (KISS), an electro-magnetic isotope separator featuring elemental selectivity from resonance laser ionization in a gas catcher. The KISS facility provides various neutron-rich nuclei via multinucleon transfer reactions. Of particular significance is its provision of nuclei in the vicinity of the neutron magic number $N = 126$. Optical and β-γ spectroscopy have been applied to these neutron-rich nuclear beams for nuclear structure and nuclear astrophysical studies. In addition, several new developments—a rotating target, a donut-shaped gas cell, and an in-jet laser ionization scheme—have been performed to improve the performance of the KISS facility. The WNSC has also developed multi-reflection time of flight mass spectrographs (MRTOF-MS) for precision mass measurements of short-lived nuclei in collaboration with the RIKEN SLOWRI team and the Institute of Basic Science (IBS), Korea. After successful mass measurements combined with the GARIS-II at RILAC, the existing MRTOF-MS setup has been renewed for use with the GARIS-II relocated after the ring cyclotron for high precision mass measurements of superheavy nuclides. Furthermore, additional MRTOF-MS setups have been placed at KISS and F11 of the ZeroDegree Spectrometer for comprehensive mass measurement.

The Wako Nuclear Science Center (WNSC) of KEK aims to promote low-energy nuclear physics and nuclear astrophysics research as well as interdisciplinary studies using short-lived radioactive nuclei. WNSC operates the KEK Isotope Separation System (KISS) which is an electro-magnetic isotope separator featuring elemental selectivity from the use of resonance laser ionization in a gas catcher. The KISS facility provides various neutron-rich nuclei via multinucleon transfer reactions. Of particular significance is its provision of nuclei in the vicinity of the neutron magic number $N = 126$. Optical and β-γ spectroscopy have been applied to these neutron-rich nuclear beams, for nuclear structure and nuclear astrophysical studies. Several new developments—a rotating target, a donut-shaped gas cell, and in-jet laser ionization scheme—have been performed to improve the performance of KISS facility. The WNSC has also developed multi-reflection time of flight mass spectrographs (MRTOF-MS) for precision mass measurements of short-lived nuclei in collaboration with the RIKEN SLOWRI team and the Institute of Basic Science (IBS), Korea. After successful mass measurements in combination with the GARIS-II at RILAC, the existing MRTOF-MS setup has been renewed for use with the GARIS-II relocated after the ring cyclotron for high precision mass measurements of superheavy nuclides, and additional MRTOF-MS setups have been placed at KISS and at F11 of the ZeroDegree Spectrometer for comprehensive mass measurements of more than one thousand nuclides.

2. Major Research Subjects

(1) Production and manipulation of radioactive isotope beams for nuclear experiments.
(2) Explosive nucleosynthesis (r- and rp-process).
(3) Heavy ion reaction mechanism for producing heavy neutron-rich nuclei.
(4) Development of MRTOF mass spectrographs for short-lived nuclei.
(5) Comprehensive mass measurements of short-lived nuclei including superheavy elements.
(6) Development of KISS-II.

3. Summary of Research Activity

The Wako Nuclear Science Center (WNSC) provides low-energy short-lived radioactive ion beams to researchers from universities using the KEK isotope separator system (KISS). Research activities in RIKEN RIBF were restricted due to the COVID-19 pandemic for more than half of the JFY2020. During the governmental "stay home" period, the WNSC researchers worked on writing research papers and technical development at home. Five physics papers were published for the experiments conducted at KISS, including two experiments right before a national state of emergency was declared. A press release was announced on one of the experiments to advertise the KISS uniqueness that can provide low-energy neutron-rich isotopes of refractory elements. These nuclides are essential ones for the study of the origin of gold in the universe.

In late September, a part of the activities was restarted at the laboratory. Modification of the KISS beamline has started to perform decay spectroscopy of pure isobaric or isomeric nuclides by placing the detector array behind a multi-reflection time-of-flight (MRTOF) mass spectrograph. When the modification is completed in JFY2021, simultaneous spectroscopy of multiple species will be realized thanks to the spectrographic future of the MRTOF device and a gamma-ToF detector that is under development.

The WNSC is conducting a campaign of comprehensive mass measurements of all available nuclides at RIKEN RIBF in collaboration with RIKEN's SLOWRI team. A new combined gas cell and MRTOF device were installed in front of the beam dump of the BigRIPS in-flight fragmentation separator. A series of online commissioning experiments were conducted using parasitic beams of the in-beam gamma-ray spectroscopy experiments (HiCARI campaign) in November–December 2020. The energetic radioactive ion beams passing through the upstream experiments' target were guided to the gas cell and converted to trapped ions for precision mass measurements using the MRTOF mass spectrograph.

The total system efficiencies were studied with various elements. While some species were diverse across molecular sidebands (*e.g.*, ScOH), more than 1% efficiencies were obtained for heavier nuclides (*e.g.*, Te and Sb). In sum, the commissioning campaign was highly successful, with more than 70 atomic masses measured with the parasitic beams. The masses of three nuclides (88As,

89As, 112Mo) have been measured for the first time, and eleven other nuclear masses improve the present uncertainty significantly.

The WNSC plans to extend the present KISS facility to investigate the nuclides in the neutron-rich region of uranium using the multi-neutron transfer reactions of actinide targets to study the origin of uranium. The primary studies of the future facility are in progress.

Members

Group Leader
Michiharu WADA

Researchers
Yutaka WATANABE
Peter SCHURY
Sunchan JEONG
Yoshikazu HIRAYAMA
Hiroari MIYATAKE
Marco Rosenbusch

Technical Staff
Yutaka KAKIGUCHI
Michihiro OYAIZU

Visiting Researchers
Hermann WOLLNIK (NMSU)
Jun-young MOON (IBS)
Sidong CHEN (HKU)
Wenduo XIAN (HKU)
Hiroshi WATANABE (Beihan University)
Hyun-suk CHOI (Seoul National University)
Jiajian LIU (HKU)
Shuxiong YAN (Jinan University)
Dongsheng HOU (IMP)

Student Trainees
Toshitaka NIWASE (PhD. Student, Kyushu Univ.)
Shun IIMURA (PhD. Student, Osaka Univ.)

Assistant
Machiko IZAWA

List of Publications & Presentations

Publications

[Original Papers]

H. Watanabe, Y. X. Watanabe, Y. Hirayama, A. N. Andreyev, T. Hashimoto, F. G. Kondev, G. J. Lane, Yu.A. Litvinov, J. J. Liu, H. Miyatake, J. Y. Moon, A. I. Morales, M. Mukai, S. Nishimura, T. Niwase, M. Rosenbusch, P. Schury, Y. Shi, M. Wada, and P. M. Walker, "Beta decay of the axially asymmetric ground state of ^{192}Re," Phys. Lett. B, **814**, 136088 (2021).

S. Kimura, D. Kaji, Y. Ito, H. Miyatake, K. Morimoto, P. Schury, and M. Wada, "Reduction of contaminations originating from primary beam by improving the beam stoppers in GARIS-II," Nucl. Instrum. Methods Phys. Res. A, 164996 (2020).

P. M. Walker, Y. Hirayama, G. J. Lane, H. Watanabe, G. D. Dracoulis, M. Ahmed, M. Brunet, T. Hashimoto, S. Ishizawa, F. G. Kondev, Yu. A. Litvinov, H. Miyatake, J. Y. Moon, M. Mukai, T. Niwase, J. H. Park, Zs. Podolyák, M. Rosenbusch, P. Schury, M. Wada, X. Y. Watanabe, W. Y. Liang, and F. R. Xu, "Properties of ^{187}Ta reveled through isomeric decay," Phys. Rev. Lett. **125**, 192505 (2020).

M. Rosenbusch, P. Schury, M. Wada, S. Iimura, Y. Ito, and H. Wollnik, "Accurately accounting for effects on times-of-flight caused by finite field-transition times during the ejection of ions from a storage trap: A study for single-reference TOF and MRTOF mass spectrometry," Int. J. Mass Spectrom. **456**, 116346 (2020).

M. Mukai, Y. Hirayama, Y. X. Watanabe, S. Schiffmann, J. Ekman, M. Godefroid, P. Schury, Y. Kakiguchi, M. Oyaizu, M. Wada, S. C. Jeong, J. Y. Moon, J. H. Park, H. Ishiyama, S. Kimura, H. Ueno, M. Ahmed, A. Ozawa, H. Watanabe, S. Kanaya, and H. Miyatake, "In-gas-cell laser resonance ionization spectroscopy of ^{196,197,198}Ir," Phys. Rev. C **102**, 054307 (2020).

H. Choi, Y. Hirayama, S. Choi, T. Hashimoto, S. C. Jeong, H. Miyatake, J. Y. Moon, M. Mukai, T. Niwase, M. Oyaizu, M. Rosenbusch, P. Schury, A. Taniguchi, Y. X. Watanabe, and M. Wada, "In-gas-cell laser ionization spectroscopy of ^{194,196}Os isotopes by using a multireflection time-of-flight mass spectrograph," Phys. Rev. C **102**, 034309 (2020).

A. V. Chudinov, M. Rosenbusch, V. I. Kozlovskiy, V. V. Raznikov, P. Schury, M. Wada, and H. Wollnik, "Model independent peak fitting and uncertainty assignment for high-precision time-of-flight mass spectrometry," Analyst **145**, 3401–3406 (2020).

Y. X. Watanabe, M. Ahmed, Y. Hirayama, M. Mukai, J. H. Park, P. Schury, Y. Kakiguchi, S. Kimura, A. Ozawa, M. Oyaizu, M. Wada, and H. Miyatake, "Deexcitation γ-ray transitions from the long-lived $I^{\pi} = 13/2^{+}$ metastable state in ^{195}Os," Phys. Rev. C **101**, 041305(R) (2020).

[Proceedings]

Y. Hirayama, Y. X. Watanabe, M. Mukai, M. Ahmed, H. Ishiyama, S. C. Jeong, Y. Kakiguchi, S. Kimura, J. Y. Moon, M. Oyaizu, J. H. Park, P. Schury, M. Wada, and H. Miyatake, "Nuclear spectroscopy of *r*-process nuclei using KEK isotope separation system," J. Phys. Conf. Ser. **1643**, 012138 (2020).

M. Mazzocco, Y. Hirayama, S. C. Jeong, H. Miyatake, Y. X. Watanabe, *et al*., "Direct processes for the systems ^{7}Be, ^{8}B + ^{208}Pb at Coulomb barrier energies," J. Phys. Conf. Ser. **1643**, 012096 (2020).

J. W. Hwang, H. Miyatake, Y. X. Watanabe, *et al*., "Performance of the OEDO beamline," J. Phys. Conf. Ser. **1643**, 012035 (2020).

Presentations

[International Conferences/Workshops]

Michiharu Wada (invited), "MRTOF development and status @ RIKEN-RIBF," NUSTAR Annual Meeting, Online, February 24, 2021.

[Domestic Conferences/Workshops]

Marco Rosenbusch (口頭発表), "New mass measurements of exotic nuclides by the first MRTOF setup at BigRIPS/RIKEN," 日本物学会第 76 回年次大会, オンライン開催, 2021 年 3 月 12–15 日.

飯村俊 (口頭発表), 「理研 BigRIPS SLOWRI における RF カーペットガスセルの開発—オンライン実験と質量測定—」, 日本物学会第 76 回年次大会, オンライン開催, 2021 年 3 月 12–15 日.

渡邉裕 (招待講演), 「KISS, MRTOF を用いた核分光実験の現状」, 令和 2 年度専門研究会「短寿命 RI を用いた核分光と核物性研究 VII」, オンライン開催, 2021 年 1 月 15 日.

平山賀一, 「KISS での核分光実験/Nuclear spectroscopy at KISS」, 2020 年度核データ研究会, 埼玉県和光市, 2020 年 11 月 26–27 日.

Toshitaka Niwase (口頭発表), "First direct mass measurement of superheavy nuclide via MRTOF-MS +α-TOF," KEK Student Day, Online, November 17, 2020.

和田道治 (招待講演), 「何故, 如何に原子質量を測るのか?」, 日本物理学会 2020 年秋季大会, オンライン開催, 2020 年 9 月 14–17 日.

渡邉寛 (口頭発表), 「非軸対称変形核 ^{192}Re の基底状態からのベータ崩壊」, 日本物理学会 2020 年秋季大会, オンライン開催, 2020 年 9 月 14–17 日.

飯村俊 (口頭発表), 「理研 BigRIPS SLOWRI における RF カーペットガスセルの開発」, 日本物理学会 2020 年秋季大会, オンライン開催, 2020 年 9 月 14–17 日.

[Seminars]

Peter Schury (invited), "Use of multi-reflection time-of-flight mass spectrometry to study SHE," Virtual SHE seminars, Online, January 12, 2021.

Press Releases

「中性子過剰なタンタル核異性体で探る原子核形状の多様性—原子核構造の研究から重元素合成の起源天体解明に迫る—」, 2020 年 11 月 11 日. https://www.kek.jp/ja/press/ipns_pr20201111-2/.

VII. APPENDICES

List of Symposia & Workshops (April 2020—March 2021)

RNC

1	SAMURAI International Collaboration Workshop 2020 https://indico2.riken.jp/event/3429/	online	Sep. 1–4
2	SSRI-PNS Collaboration Meeting 2020 https://indico2.riken.jp/event/3452/	online	Sep. 3–4
3	RIBF Users Meeting 2020 https://indico2.riken.jp/event/3443/	online	Sep. 8–10
4	International Technical Safety Forum（ITSF2020）	RIBF Conf. Hall, RIKEN Wako Campus	Nov. 9–13
5	Symposium on Nuclear Data 2020	RIBF Conf. Hall, RIKEN Wako Campus	Nov. 26–27
6	第 17 回高エネルギーQCD・核子構造勉強会 https://indico2.riken.jp/event/3623/	online	Feb. 5
7	Spin Symposium	Kunibiki Messe, Shimane	Feb. 23–24
8	The 8th Asia-Pacific Conference on Few-Body Problems in Physics (APFB2020)	Kanazawa Bunka Hall	Mar. 1–5

KEK

1	SSRI-PNS Collaboration meeting 2020 https://research.kek.jp/group/wnsc/ssri-pns/	online	Sep. 3–4
2	第 11 回停止・低速 RI ビームを用いた核分光研究会（京大複合研専門研究会「短寿命 RI を用いた核分光と核物性研究VI」同時開催） http://www.rri.kyoto-u.ac.jp/NBMP/kurpro/R1pro.pdf	online	Jan. 16–17

List of Seminars (April 2020—March 2021)

Nuclear Physics Monthly Colloquium

	Not held in 2020		

RIBF Nuclear Physics Seminar

1	Sidong Chen (U. Hong Kong)	Structural evolution of neutron-rich calcium isotopes https://indico2.riken.jp/event/3365/	May 26
2	Junki Tanaka (RIKEN)	Experimental evidence of α clustering in the ground state of stable heavy nuclei https://indico2.riken.jp/event/3441/	Jul. 28
3	Wataru Horiuchi (Hokkaido University)	Utility of antiproton- and deuteron-scattering for studies of unstable nuclei https://indico2.riken.jp/event/3639/	Jan. 21
4	Takumi Yamaga (RIKEN)	Observation of an anti-kaon nuclear bound state, $\bar{K}NN$ https://indico2.riken.jp/event/3650/	
5	Masaomi Tanaka (Kyushu U.)	Swelling of doubly magic ^{48}Ca core in Ca isotopes beyond N = 28 https://indico2.riken.jp/event/3640/	Feb. 9
6	Heather Crawford (Berkeley Lab)	First spectroscopy in ^{40}Mg and the implications for structure near the dripline https://indico2.riken.jp/event/3669/	Feb. 16

Seminar by Each Laboratory

Nuclear Science and Transmutation Research Division

1	Jens Lassen (TRIUMF)	Nuclear Spectroscopy Lab. Seminar (Quantum Beam Application Research B03 Seminar) Radioactive ion beams at TRIUMF using the resonance ionization laser ion source https://indico2.riken.jp/event/3469/"	Sep. 2
2	Yutaka Shikano (Keio U.)	Nuclear Spectroscopy Lab. Seminar (Quantum Beam Application Research B03 Seminar) Fundamentals and applications of weak measurement (弱測定の基礎と応用) https://indico2.riken.jp/event/3662/	Feb. 4

High Energy Astrophysics Lab. Seminar → http://astro.riken.jp/wordpress/?page_id=65

Subnuclear System Research Division

1	Eduardo Grossi (SBU)	Nuclear Physics & RIKEN Theory Seminar (virtual) A mode by mode approach to heavy ion collision	Apr. 10
2	Debasish Banerjee (PNNL)	Nuclear Physics & RIKEN Theory Seminar (virtual) The Color Glass Condensate density matrix: Lindblad evolution, entanglement entropy and Wigner functional	Apr. 17
3	Jianwei Qiu (Jefferson Lab)	Nuclear Physics & RIKEN Theory Seminar (virtual) 3D tomography of parton motion inside hadrons	Apr. 24
4	Andrea Signori (Jlab)	Nuclear Physics & RIKEN Theory Seminar (virtual) Transverse momentum distributions: predictive power and flavor structure	May 1
5	R. Loganayagam (ICTS)	Nuclear Physics & RIKEN Theory Seminar (virtual) Open QFTs from holography	May 8
6	Emilie Huffman (Perimeter Inst)	Nuclear Physics & RIKEN Theory Seminar (virtual) Quantum criticality in fermion-bag inspired Hamiltonian lattice field theories	May 15

7	Fabian Rennecke (BNL)	BNL RIKEN Seminar (virtual) From anomalous correlations to dark matter: the effects of higher topological charge	May 21
8	Sourendu Gupta (TIFR)	Nuclear Physics & RIKEN Theory Seminar (virtual) Why is chemical freezeout at the chiral cross over temperature?	May 22
9	Yuta Sekino (RIKEN)	SNP Seminar Mesoscopic spin transport between strongly interacting Fermi gases	May 27
10	Masafumi Fukuma (Kyoto U.)	BNL RIKEN Seminar (virtual) Sign problem in Monte Carlo simulations and the tempered Lefschetz thimble method	May 28
11	Luchang Jin (U. Conn)	Nuclear Physics & RIKEN Theory Seminar (virtual) First-principles calculation of electroweak box diagrams from lattice QCD	May 29
12	Phiala Shanahan (MIT)	BNL RIKEN Seminar (virtual) From quarks to nuclei: machine learning the structure of matter	Jun. 4
13	Alexander Soloviev (Stony Brook U.)	BNL RIKEN Seminar (virtual) Transport and hydrodynamics in the chiral limit	Jun. 11
14	Gregory Soyez (IPhT)	Nuclear Physics & RIKEN Theory Seminar (virtual) The quest for precision across scales	Jun. 12
15	Shao-Feng Wu (Shanghai U., Yangzhou U.)	Nuclear Physics & RIKEN Theory Seminar (virtual) Deep learning black hole metrics from shear viscosity	Jun. 18
16	Akihiko Monnai (JWU)	Nuclear Physics & RIKEN Theory Seminar (virtual) Prompt, pre-equilibrium, and thermal photons in relativistic nuclear collisions	Jun. 19
17	Munekazu Horikoshi (Osaka City U.)	SNP Seminar Ultracold AMO experiment for quantum few-body and many-body	Jun. 22
18	Mamiya Kawaguchi (Fudan U.)	Nuclear Physics & RIKEN Theory Seminar (virtual) Nonperturbative quark-flavor breaking at chiral crossover criticality in hot QCD	Jun. 25
19	Lukas Weih (ITP)	Nuclear Physics & RIKEN Theory Seminar (virtual) Postmerger gravitational-wave signatures of phase transitions in binary mergers	Jun. 26
20	Chris Greene (Purdue U.)	SNP Seminar Linking Efimov physics, few-fermion universality, and the 3n and 4n systems	Jul. 10
21	Andreas Ipp (TU)	Nuclear Physics & RIKEN Theory Seminar (virtual) Transverse momentum broadening in the Glasma	Jul. 10
22	Asmita Mukherjee (IIT)	Nuclear Physics & RIKEN Theory Seminar (virtual) Probing Gluon Sivers Function in J/ψ production at the Electron-Ion Collider	Jul. 17
23	Xiang Gao, (BNL)	Nuclear Physics & RIKEN Theory Seminar (virtual) Parton distribution functions inside hardron from lattice QCD	Jul. 23
24	Gregory Johnson, (NCSU)	Nuclear Physics & RIKEN Theory Seminar (virtual) Universal location of the Yang-Lee edge singularity in $O(N)$ theories	Jul. 24
25	C.-J. David Lin (National Chiao-Tung U.)	Nuclear Physics & RIKEN Theory Seminar (virtual) Massive Thirring model in $1+1$ dimensions from matrix product states	Jul. 30
26	Zhangbo Kang (UCLA)	Nuclear Physics & RIKEN Theory Seminar (virtual) QCD factorization and resummation in the small-x regime	Jul. 31
27	Sinya Aoki (YITP)	Nuclear Physics & RIKEN Theory Seminar (virtual) Conserved charges in general relativity and its implication on Oppenheimer-Volkoff equation	Aug. 7
28	Vincent Cheung (UC Davis)	Nuclear Physics & RIKEN Theory Seminar (virtual) Quarkonium production and polarization in the color evaporation model	Aug. 13
29	Mithat Unsal (NCSU)	Nuclear Physics & RIKEN Theory Seminar (virtual) Strongly coupled QFT dynamics via TQFT coupling	Aug. 21

30	Pasi Huovinen (Inst. Physics Belgrade)	Nuclear Physics & RIKEN Theory Seminar (virtual) Does eta/s depend on EoS?	Aug. 28
31	Peng Zhang (Renmin University, Beijing)	SNP Seminar Laser control of two-body processes in nuclear and cold-atom systems	Sep. 3
32	Hans-Werner Hammer (TU Darmstadt)	SNP Seminar The lifetime of the hypertriton	Sep. 3
33	Bowen Xiao (CCNU)	Nuclear Physics & RIKEN Theory Seminar (virtual) The curious story of the photon	Sep. 4
34	Vajravelu Ravindran	Nuclear Physics & RIKEN Theory Seminar (virtual) On next to soft corrections to Inclusive cross sections at the colliders	Sep. 11
35	Jesse Stryker (U. Washington)	Nuclear Physics & RIKEN Theory Seminar (virtual) Loop, string, and hadron dynamics in SU(2) Hamiltonian lattice gauge theories	Sep. 18
36	Christian Bierlich (Lund U.)	Nuclear Physics & RIKEN Theory Seminar (virtual) New applications of dipole Monte Carlo implementations	Sep. 25
37	Tetsuo Hyodo (TMU)	SNP Seminar $\Lambda(1405)$ as a hadronic molecule	Sep. 28
38	Aleksi Vuorinen (U. Helsinki)	Nuclear Physics & RIKEN Theory Seminar (virtual) Quark matter cores in massive neutron stars	Oct. 2
39	Yiannis Makris (INFN)	Nuclear Physics & RIKEN Theory Seminar (virtual) Groomed and energy-energy correlation event shapes in DIS	Oct. 9
40	Ying Zhang (Tianjin U., RIKEN)	SNP Seminar Farewell seminars of Ying Zhang and Jinniu Hu Lambda halo structure of C, B and Zr isotopes	Oct. 14
41	Jinniu Hu (Nankai U., RIKEN)	SNP Seminar Farewell seminars of Ying Zhang and Jinniu Hu The mass limit of a neutron star	Oct. 14
42	Chien Yeah Seng (U. Bon)	Nuclear Physics & RIKEN Theory Seminar (virtual) The quest for explaining the top-row CKM unitarity deficit	Oct. 16
43	Volker Koch (LBNL)	Nuclear Physics & RIKEN Theory Seminar (virtual) Correlations, fluctuations and the QCD phase diagram	Oct. 23
44	Servaas Kokkelmans (TU/e)	SNP Seminar Elastic few-body interactions in dilute Bose gases	Oct. 27
45	Isobel Kolbe, (U. Washington)	BNL RIKEN Seminar (virtual) Matter and radiation in the fragmentation region of heavy-ion collisions	Nov. 5
46	Dr Xin An (NC State U.)	Nuclear Physics & RIKEN Theory Seminar (virtual) Deterministic fluctuating hydrodynamics and relativistic heavy-ion collisions	Nov. 6
47	Viljami Leino, (TUM)	Nuclear Physics & RIKEN Theory Seminar (virtual) Heavy quark diffusion constant from the lattice"	Nov. 13
48	Heng-Tong DING (CCNU)	BNL RIKEN Seminar (virtual) Correlated Dirac eigenvalues and axial anomaly in chiral symmetric QCD	Nov. 19
49	Thomas Cohen (Maryland U.)	Nuclear Physics & RIKEN Theory Seminar (virtual) Surprises in large N_c Thermodynamics	Nov. 20
50	Shun Uchino (JAEA)	SNP Seminar Atomtronics	Nov. 26
51	Teppei Kitahara (Nagoya U.)	BNL RIKEN Seminar (virtual) Electroweak effective field theory from massive scattering amplitudes	Dec. 3
52	Aleksey Cherman (U. Minnesota Twin Cities)	Nuclear Physics & RIKEN Theory Seminar (virtual) Higgs-confinement phase transitions with fundamental representation matter	Dec. 4

53	Hidenori Fukaya (Osaka U.)	BNL RIKEN Seminar (virtual) Study of axial U(1) anomaly at high temperature with lattice chiral fermions	Dec. 10
54	Shin Inouye (Osaka City U.)	SNP Seminar Measurement of the variation of electron-to-proton mass ratio using ultracold molecules produced from laser-cooled atoms	Dec. 11
55	Salazar Wong (Stony Brook U.)	BNL RIKEN Seminar (virtual) Gluon imaging using azimuthal correlations in diffractive scattering at the Electron-Ion Collider	Dec. 17
56	Srimoyee Sen (Iowa State U.)	Nuclear Physics & RIKEN Theory Seminar (virtual) Quarkyonic model for neutron stars	Dec. 18
57	Yair Mulian (Jyvaskyla U.)	BNL RIKEN Seminar (virtual) Toward full result for next-to-leading order dijet production in proton-nucleus collisions	Jan. 7
58	Pavel Kovtun (U. Victoria)	Nuclear Physics & RIKEN Theory Seminar (virtual) Relativistic Navier-Stokes equations	Jan. 8
59	Heng-Tong DING (CCNU)	BNL RIKEN Seminar (virtual) Correlated Dirac eigenvalues and axial anomaly in chiral symmetric QCD	Jan. 14
60	Yuichiro Mori (KEK)	BNL RIKEN Seminar (virtual) Weak value and CP violation measurement	Jan. 21
61	Martin Gonzalez-Alonso (U. Valencia)	High-Energy Physics & RIKEN Theory Seminar (virtual) EFT constraints from neutrino oscillation data	Jan. 21
62	Tokuro Fukui (Kyoto U.)	SNP Seminar Many-body effective models with chiral interaction	Jan. 22
63	Varun Vaidya (MIT)	Nuclear Physics & RIKEN Theory Seminar (virtual) Effective Field theory for jet substructure in heavy ion collisions	Jan. 22
64	Ian Balitsky (JLab, ODU)	Nuclear Physics & RIKEN Theory Seminar (virtual) Gauge-invariant TMD factorization for Drell-Yan hadronic tensor at small x	Jan. 29
65	James Halverson (Northeastern)	BNL RIKEN Seminar (virtual) A triangle of influence: Bringing together physics, pure mathematics, and computer science	Feb. 4
66	Andrew Hanlon (BNL)	Nuclear Physics & RIKEN Theory Seminar (virtual) Two-baryon interactions from lattice QCD	Feb. 5
67	Philipp Scior (BNL)	BNL RIKEN Seminar (virtual) Spectral functions from the real-time functional renormalization group	Feb. 18
68	Michael Ramsey-Musolf (U Mass)	High-Energy Physics & RIKEN Theory Seminar (virtual) Was there an electroweak phase transition?"	Feb. 19
69	Konrad Tywoniuk (U. Bergen)	Nuclear Physics & RIKEN Theory Seminar (virtual) Energy loss of QCD jets in heavy-ion collisions	Feb. 24
70	Shimpei Endo (Tohoku U.)	SNP Seminar Are atoms spherical?	Feb. 25
71	Yusuke Tanimura (Tohoku U.)	SNP Seminar How to visualize nuclear many-body correlations?	Feb. 25
72	Mattia Bruno (CERN)	High-Energy Physics & RIKEN Theory Seminar (virtual) Variations on the Maiani-Testa approach and the inverse problem	Feb. 25
73	Peter Schweitzer, (Connecticut U.)	Nuclear Physics & RIKEN Theory Seminar (virtual) The D-term and forces inside hadrons	Feb. 26
74	Paul Caucal (BNL)	BNL RIKEN Seminar (virtual) Pinning down pQCD modifications of in-medium jet evolution with substructure observables	Mar. 4
75	Andreas von Manteuffel (MSU)	High-Energy Physics & RIKEN Theory Seminar (virtual) Mixed EW-QCD two-loop amplitudes for Drell-Yan dilepton production	Mar. 4

76	Yizhuang Liu (U. Regensburg)	Nuclear Physics & RIKEN Theory Seminar (virtual) Quantum anomalous energy and proton mass decomposition	Mar. 5
77	Yuber Perez-Gonzalez (Fermilab, Northwestern)	High-Energy Physics & RIKEN Theory Seminar (virtual) Neutrinos from Primordial Black Holes, an opera in two acts	Mar. 11
78	Raoul Rontsch (CERN)	High-Energy Physics & RIKEN Theory Seminar (virtual) Mixed QCD-electroweak corrections to vector boson production and their impact on the *W*-mass measurement by Raoul Rontsch (CERN)"	Mar. 18
79	Yukinari Sumino (Tohoku U.)	Nuclear Physics & RIKEN Theory Seminar (virtual) Understanding heavy quark-antiquark system by perturbative QCD	Mar. 19
80	Yifei Niu (Lanzhou U.)	SNP Seminar Beyond mean-field description of nuclear weak interaction processes in stars	Mar. 25

QHP Seminar → http://ribf.riken.jp/QHP/seminar.html
SNP Seminar → http://snp.riken.jp/seminar.html
RIKEN/BNL Lunch Time Talk → https://www.bnl.gov/events/

Events (April 2020—March 2021)

RNC

Jul. 1–13	The 14th Industrial Program Advisory Committee (In-PAC)
Jul. 16	The 26th RBRC Management Steering Committee (MSC)
Jul. 30	The 15th Industrial Program Advisory Committee (In-PAC)
Aug.20	The 27th RBRC Management Steering Committee (MSC)
Dec.14–16	The 21st Program Advisory Committee for Nuclear Physics Experiments at RI Beam Factory (NP-PAC)
Dec.19–Jan.13	The 16th Industrial Program Advisory Committee (In-PAC)
Jan.13–20	The 20th Program Advisory Committee for Materials and Life Science Researches at RIKEN Nishina Center (ML-PAC)

CNS

Aug. 17–21	19th CNS International Summer School (CNSSS20) https://indico2.cns.s.u-tokyo.ac.jp/event/102/

Press Releases (April 2020–March 2021)

RNC

May. 15	Extending the southern shore of the island of inversion to ^{28}F	T. Uesaka, H. Otsu, Spin isospin Laboratory, SAMURAI Team
May. 28	"A single proton can make a heck of a difference" —Exploring the limits of existence of neutron-rich nuclei—	T. T. Leung, Spin isospin Laboratory
Jun. 18	Halo structure of the neutron-dripline nucleus ^{19}B	H. Otsu, K. Yoneda, SAMURAI Team, Spin isospin Laboratory
Jun. 23	Left-right asymmetry of π meson production from proton collisions —New discovery reveals the origin of particle production—	Y. Goto, Radiation Laboratory
Jul. 21	High-temperature short-range order in Mn_3RhSi	I. Watanabe, Meson Science Laboratory
Aug. 7	Lithum diffusion in $LiMnPO_4$ detected with $\mu^{\pm}$SR	K. Ishida, Meson Science Laboratory
Aug. 21	Discovery of "two-neutron halo" in fulorine-29 —Magicity loss at 20 and emergence of halo structure—	H. Sakurai, P. Doornenbal, Radioactive Isotope Physics Laboratory
Sep. 16	Mapping of a new deformation region around ^{62}Ti	T. Uesaka, Spin isospin Laboratory
Nov. 5	The impact of nuclear shape on the emergence of the neutron dripline	T. Otsuka, H. Ueno, Nuclear Spectroscopy Laboratory
Nov. 5	Dirac Fermion Kinetics in 3D curved graphene	T. Naito, Quantum Hadron Physics Laboratory
Nov. 11	Properties of ^{187}Ta revealed through isomeric decay	M. Mukai, Nuclear Spectroscopy Laboratory
Dec. 17	A new discovery on dineutron correlation in neutron halo of Lithium-11 —Evidence of surface localization of the dineutron found—	T. Uesaka, Spin isospin Laboratory
Jan. 13	Broadband high-energy resolution hard X-ray spectroscopy using transition edge sensors at Spring-8.	T. Tamagawa, T. Isobe, High Energy Astrophysics Laboratory, Radioactive Isotope Physics Laboratory
Jan. 15	Larger-than-usual rotifer fed to juvenile tuna, successfully produced —"Mega-rotifer" created by a heavy ion beam—	T. Abe, K. Tsuneizumi, Ion Beam Breeding Team
Jan. 21	Alpha particles found at the surface of nuclei of Sn —Unraveling the mystery of the structure of neutron stars and the process of alpha decay—	T. Uesaka, Spin isospin Laboratory
Feb. 18	Co-precipitation behavior of single atoms of rutherfordium in basic solutions	H. Haba, Nuclear Chemistry Research Team
Mar. 22	Prediction of a new quantum phase "mixed bubble" at ultra-low temperatures. —Discovery of quantum partial miscibility between miscibility and immiscibility—	P. Naidon, Strangeness Nuclear Physics Laboratory

KEK

Nov. 11	中性子過剰なタンタル核異性体で探る原子核形状の多様性 —原子核構造の研究から重元素合成の起源天体解明に迫る— https://www.kek.jp/ja/press/ipns_pr20201111-2/	P. M. Walker, Y. Hirayama

List of Preprints (April 2020—March 2021)

RIKEN NC-NP

	Not Applicable	

RIKEN NC-AC

	Not Applicable	

RIKEN MP

	Not Applicable	

RIKEN QHP

418	Partial wave decomposition on the lattice and its applications to the HAL QCD method	T. Miyamoto *et al.*
419	Superfluid phase transitions and effects of thermal pairing fluctuations in asymmetric nuclear matter	H. Tajima *et al.*
420	Non-relativistic expansion of single-nucleon Dirac equation: Comparison between Foldy-Wouthuysen transformation and similarity renormalization group	Y. Guo, H. Liang
421	Coulomb energy density functionals for nuclear systems: Recent studies of coulomb exchange and correlation functionals	T. Naito *et al.*
422	Coexistence of giant Cooper pairs with a bosonic condensate and anomalous behavior of energy gaps in the BCS-BEC crossover of a two-band superfluid Fermi gas	Y. Yerin *et al.*
423	Probing Ω-Ω and p-Ω dibaryons with femtoscopic correlations in relativistic heavy-ion collisions	K. Morita *et al.*
424	How to improve functionals in density functional theory? —Formalism and benchmark calculation—	T. Naito *et al.*
425	Heavy hadronic molecules with pion exchange and quark core couplings: a guide for practitioners	Y. Yamaguchi *et al.*
426	Theoretical study of Nb isotope productions by muon capture reaction on ^{100}Mo	M. Ciccarelli *et al.*
427	Spin-dipole mode in a trapped Fermi gas near unitarity	H. Tajima *et al.*
428	Relativistic density functional theory with finite-light-speed correction for the Coulomb interaction: a non-relativistic-reduction-based approach	T. Naito *et al.*
429	Possible lightest Ξ hypernucleus with modern ΞN interactions	E. Hiyama *et al.*
430	Lattice QCD and baryon-baryon interactions: HAL QCD method	S. Aoki, T. Doi
431	Study of the pion-pion scatterings with a combination of all-to-all propagators and the HAL QCD method	Y. Akahosh *et al.*
432	Exploring the QCD phase diagram at finite density by the complex Langevim method on a $16^3 \times 32$ lattice	S. Tsutsui
433	Emergent discrete 3-form symmetry and domain walls	Y. Hidaka *et al.*
434	BCS-BEC crossover and pairing fluctuations in a two-band superfluid/superconductor: a T-matrix approach	H. Tajima *et al.*
435	$\Lambda\Lambda$ and $N\Xi$ interactions from Lattice QCD near the physical point	K. Sasaki *et al.*
436	Non-relativistic expansion of Dirac equation with spherical scalar and vector potentials by reconstituted Foldy-Wouthuysen transformation	Y. Guo, H. Liang
437	Collisional dynamics of polaronic clouds immersed in a Fermi sea	H. Tajima *et al.*
438	Towards an *ab initio* covariant density functional theory for nuclear structure	S. Shen *et al.*

439	Predictions of nuclear beta-decay half-lives with machine learning and their impact on *r*-process nucleosynthesis	Z. M. Niu *et al.*
440	Goldstino spectrum in an ultracold Bose-Fermi mixture with explicitly broken supersymmetry	H. Tajima *et al.*
441	Quantum kinetic theory for spin transport: general formalism for collisional effects	D.-L. Yang *et al.*
442	Measurement of the Decays $\Lambda_c \to \Sigma\pi\pi$ at Belle	M. Berger *et al*
443	First evidence for $\cos 2\beta > 0$ and resolution of the Cabibbo-Kobayashi-Maskawa quark-mixing unitarity triangle ambiguity	I. Adachi *et al*
444	Measurement of $\cos 2\beta$ in $B^0 \to D^{(*)}h^0$ with $D \to K_S^0\pi^+\pi^-$ decays by a combined time-dependent Dalitz plot analysis of BABAR and Belle data	I. Adachi *et al*
445	Search for the rare decay of $B^+ \to \ell^+\nu_\ell\gamma$ with improved hadronic tagging	M. Gelbet *et al*
446	Search for a light CP-odd Higgs boson and low-mass dark matter at the Belle experiment	I.S. Seong *et al,*
447	Measurement of time-dependent CP violation in $B^0 \to K_S^0\pi^0\pi^0$ decays	Y. Yusa *et al*
448	Search for CP violation with kinematic asymmetries in the $D^0 \to K^+K^-\pi^+ + \pi^-$ decay	J. B. Kim *et al*
449	Observation of transverse $\Lambda/\bar{\Lambda}$ hyperon polarization in $e^+ + e^-$ annihilation at Belle	Y. Guan *et al*
450	Observation of $\Xi(1620)^0$ and evidence for $\Xi(1690)^0$ in $\Xi_c^+ \to \Xi^-\pi^+\pi^+$ decays	M. Sumihama *et al*
451	Measurements of isospin asymmetry and difference of direct CP asymmetries in inclusive $B \to X_s\gamma$ decays	S. Watanuki *et al*
452	First Measurements of absolute branching fractions of the Ξ_c^+ baryon at Belle	Y. B. Li *et al*
453	Observation of $B^+ \to p\bar{\Lambda}K^+K^-$ and $B^+ \to \bar{p}\Lambda K^+K^+$	P.-C. Lu *et al*
454	Search for the $B \to Y(4260)K$, $Y(4260) \to J/\psi\pi^+\pi^-$ decays	R. Garg *et al*
455	Measurements of branching fraction and direct CP asymmetry in $B^\pm \to K_S^0K_S^0K^\pm$ and a search for $B^\pm \to K_S^0K_S^0\pi^\pm$	A. B. Kaliyar *et al*
456	Evidence for the decay $B^0 \to \bar{p}p\pi^0$	B. Pal *et al*
457	Search for $X(3872)$ and $X(3915)$ decay into χ_{c1} in B decays at Belle	V. Bhardwaj *et al*
458	Transverse momentum dependent production cross sections of charged pions, kaons and protons produced in inclusive e^+e^- annihilation at $\sqrt{s} = 10.58$ GeV	R. Seidl *et al*
459	Measurement of branching fraction and final-state asymmetry for the $\bar{B}^0 \to K_S^0K^\mp\pi^\pm$ decay	Y.-T. Lai *et al*
460	Evidence for $B^+ \to h_cK^+$ and observation of $\eta_c(2S) \to p\bar{p}\pi^+\pi^-$	K. Chilikin *et al*
461	Search for $B^0 \to X(3872)\gamma$	P.-C. Chou *et al*
462	First measurements of absolute branching fractions of the Ξ_c^+ baryon at Belle	Y. B. Li *et al*
463	Search for $\Omega(2012) \to K\Xi(1530) \to K\pi\Xi$ at Belle	S. Jia *et al*
464	Measurement of the CKM matrix element $\lvert V_{cb}\rvert$ from $B^0 \to D^{*-}\ell^+\nu_\ell$ at Belle	E. Waheed *et al*
465	Observation of $\tau^- \to \pi^-\nu_\tau e^+e^-$ and search for $\tau^- \to \pi^-\nu_\tau\mu^+\mu^-$	Y. Jin *et al*
466	First measurement of the CKM angle φ_3 with $B^\pm \to D(K_S^0\pi^+\pi^-\pi^0)K^\pm$ decays	P. K. Resmi *et al*
467	Observation of a new structure near 10.75 GeV in the energy dependence of the $e^+e^- \to \Upsilon(nS)\pi^+\pi^-(n = 1,2,3)$ cross sections	R. Mizuk *et al*
468	Azimuthal asymmetries of back-to-back $\pi^\pm - (\pi^0, \eta, \pi^\pm)$ pairs in e^+e^- annihilation	H. Li *et al*
469	Measurements of the branching fractions $\mathcal{B}(B^- \to \bar{\Lambda}_c\Xi_c^{'0})$, $\mathcal{B}(B^- \to \bar{\Lambda}_c\Xi_c(2645)^0)$ and $\mathcal{B}(B^- \to \bar{\Lambda}_c\Xi_c(2790)^0)$	Y. Li *et al*
470	Observation of a vector charmoniumlike state in $e^+e^- \to D_s^+D_{s1}(2356)^- + c.c.$	S. Jia *et al*

471	Measurement of the integrated luminosity of the Phase 2 data of the Belle II experiment	F. Abudinén *et al*
472	Mesoscopic spin transport between strongly interacting Fermi gases	Y. Sekino *et al*
473	Effects of finite nucleon size, vacuum polarization, and electromagnetic spin-orbit interaction on nuclear binding energies and radii in spherical nuclei	T. Naito *et al*
474	The HAL QCD potential in $I=1$ $\pi\pi$ system with the ρ meson bound state	Y. Akahoshi *et al*
475	Analysis for Lorentzian conformal field theories through sine-square deformation	X. Liu, T. Tada
476	Hybrid quantum annealing via molecular dynamics	H. Irie *et al*
477	S-wave kaon-nucleon potentials with all-to-all propagators in the HAL QCD method	K. Murakami *et al*
478	Low-dimensional fluctuations and pseudogap in Gaudin-Yang Fermi gases	H. Tajima *et al*
479	Complex Langevin calculations in QCD at finite density	Y. Ito *et al*
480	Are atoms spherical?	T. Naito *et al*
481	Second and fourth moments of the charge density a Consistent description for cluster dynamics and single-particle correlation nd neutron-skin thickness of atomic nuclei	T. Naito *et al*
482	*Ab initio* construction of the energy density functional for electron systems with the functional-renormalization-group-aided density functional theory	T. Yokota, T. Naito
483	Dirac Fermion kinetics in three-dimensionally curved graphene	Y. Tanabe *et al*
485	Consistent description for cluster dynamics and single-particle correlation	T. Naito *et al*
487	Field theoretical aspects of one-dimensional Bose and Fermi gases with contact interactions	N. Itagaki, T. Naito
488	Second order chiral kinetic theory under gravity and antiparallel charge-energy flow	Y. Sekino, Y. Nishida
489	Tensor effects on shell-structure evolution in $N=82$ isotones and $Z=50$ isotopes in the relativistic Hartree-Fock theory	T, Hayata *et al*
490	Exploring effects of tensor force and its strength via neutron drops	Z. Wang *et al*
491	Most charming dibaryon near unitarity	Z. Wang *et al*
492	Nuclear energy density functionals from empirical ground-state densities	Y. Lyu *et al*
493	Optical spin transport in ultracold quantum gases	G. Accorto *et al*

CNS-REP

99	CNS Annual Report 2019	H. Nagahama

Nishina Center Preprint server (not including Partner Institution) can be found at
http://nishina-preprints.riken.jp/

理化学研究所
埼玉県　和光市　広沢
RIKEN 2021-45
ISSN 0289-842X